ELSEVIER

11TH INTERNATIONAL SYMPOSIUM ON PROCESS SYSTEMS ENGINEERING

PART A

Edited by

I.A. KARIMI AND R. SRINIVASAN

COMPUTER-AIDED CHEMICAL ENGINEERING, 31

PSE 2012

11th INTERNATIONAL SYMPOSIUM ON PROCESS SYSTEMS ENGINEERING

COMPUTER-AIDED CHEMICAL ENGINEERING
Advisory Editor: R. Gani and E.N. Pistikopoulos

Volume 1: Distillation Design in Practice (L.M. Rose)
Volume 2: The Art of Chemical Process Design (G.L. Wells and L.M. Rose)
Volume 3: Computer Programming Examples for Chemical Engineers (G. Ross)
Volume 4: Analysis and Synthesis of Chemical Process Systems (K. Hartmann and K. Kaplick)
Volume 5: Studies in Computer-Aided Modelling. Design and Operation
Part A: Unite Operations (I. Pallai and Z. Fonyó, Editors)
Part B: Systems (I. Pallai and G.E. Veress, Editors)
Volume 6: Neural Networks for Chemical Engineers (A.B. Bulsari, Editor)
Volume 7: Material and Energy Balancing in the Process Industries - From Microscopic Balances to Large Plants (V.V. Veverka and F. Madron)
Volume 8: European Symposium on Computer Aided Process Engineering-10 (S. Pierucci, Editor)
Volume 9: European Symposium on Computer Aided Process Engineering-11 (R. Gani and S.B. Jørgensen, Editors)
Volume 10: European Symposium on Computer Aided Process Engineering-12 (J. Grievink and J. van Schijndel, Editors)
Volume 11: Software Architectures and Tools for Computer Aided Process Engineering (B. Braunschweig and R. Gani, Editors)
Volume 12: Computer Aided Molecular Design: Theory and Practice (L.E.K. Achenie, R. Gani and V. Venkatasubramanian, Editors)
Volume 13: Integrated Design and Simulation of Chemical Processes (A.C. Dimian)
Volume 14: European Symposium on Computer Aided Process Engineering-13 (A. Kraslawski and I. Turunen, Editors)
Volume 15: Process Systems Engineering 2003 (Bingzhen Chen and A.W. Westerberg, Editors)
Volume 16: Dynamic Model Development: Methods, Theory and Applications (S.P. Asprey and S. Macchietto, Editors)
Volume 17: The Integration of Process Design and Control (P. Seferlis and M.C. Georgiadis, Editors)
Volume 18: European Symposium on Computer-Aided Process Engineering-14 (A. Barbosa-Póvoa and H. Matos, Editors)
Volume 19: Computer Aided Property Estimation for Process and Product Design (M. Kontogeorgis and R. Gani, Editors)
Volume 20: European Symposium on Computer-Aided Process Engineering-15 (L. Puigjaner and A. Espuña, Editors)
Volume 21: 16th European Symposium on Computer Aided Process Engineering and 9th International Symposium on Process Systems Engineering (W. Marquardt and C. Pantelides)
Volume 22: Multiscale Modelling of Polymer Properties (M. Laso and E.A. Perpète)
Volume 23: Chemical Product Design: Towards a Perspective through Case Studies (K.M. Ng, R. Gani and K. Dam-Johansen, Editors)
Volume 24: 17th European Symposium on Computer Aided Process Engineering (V. Plesu and P.S. Agachi, Editors)
Volume 25: 18th European Symposium on Computer Aided Process Engineering (B. Braunschweig and X. Joulia, Editors)
Volume 26: 19th European Symposium on Computer Aided Process Engineering (Jacek Je owski and Jan Thullie, Editors)
Volume 27: 10th International Symposium on Process Systems Engineering (Rita Maria de Brito Alves, Claudio Augusto Oller do Nascimento and Evaristo Chalbaud Biscaia, Editors)
Volume 28: 20th European Symposium on Computer Aided Process Engineering (S. Pierucci and G. Buzzi Ferraris, Editors)
Volume 29: 21st European Symposium on Computer Aided Process Engineering (E.N. Pistikopoulos, M.C. Georgiadis and A.C. Kokossis, Editors)
Volume 30: 22nd European Symposium on Computer Aided Process Engineering (David Bogle and Michael Fairweather)

COMPUTER-AIDED CHEMICAL ENGINEERING, 31

11th INTERNATIONAL SYMPOSIUM ON PROCESS SYSTEMS ENGINEERING

PART A

Edited by

Iftekhar A. Karimi
Department of Chemical & Biomolecular Engineering
National University of Singapore, Singapore

Rajagopalan Srinivasan
Department of Chemical & Biomolecular Engineering
National University of Singapore, Singapore

ELSEVIER

Amsterdam – Boston – Heidelberg – London – New York – Oxford
Paris – San Diego – San Francisco – Singapore – Sydney – Tokyo

Elsevier
Radarweg 29, PO Box 211, 1000 AE Amsterdam, The Netherlands
The Boulevard, Langford Lane, Kidlington, Oxford OX5 1GB, UK

First edition 2012

British Library Cataloguing in Publication Data
A catalogue record for this book is available from the British Library

Library of Congress Cataloging-in-Publication Data
A catalog record for this book is available from the Library of Congress

ISBN (Part A): 978-0-444-59507-2
ISBN (Set): 978-0-444-59505-8
ISSN: 1570-794L

Printed and bound in Great Britain

12 13 14 15 16 10 9 8 7 6 5 4 3 2 1

Contents

Highlights on Modeling & Simulation

Highlights on Process & Product Design

Highlights on Process Supervision

Highlights on Process Control

Highlights on Energy

Highlights on Environment & Sustainability

Highlights on Trends in PSE

Highlights on Process Operations

Posters

PART B

Bioprocessing & Biotechnology

Computational Fluid Dynamics

Parameter Estimation

Education

Energy

Enterprise Optimization

Planning & Scheduling

Industrial Applications

Pharmaceutical Systems

Process Design

Process Simulation

Process Monitoring

Process Operations

Product Design

Sustainability & Environment

Water

Oil & Gas

Optimization

Alarms & Sensors

Heat Integration

Distillation

Model Predictive Control

Control Strategies

Modeling and Analysis

Process Synthesis

Biomedical Applications

Preface

The International Symposia on Process Systems Engineering (PSE) have been a triennial tradition since 1982. The series has been organized by the International Organization for Process Systems Engineering with representations from the Asia Pacific Confederation of Chemical Engineering, the European Federation of Chemical Engineering, and the Inter-American Confederation of Chemical Engineering. It has proved to be an attractive global platform for the PSE academics, researchers, and practitioners from all corners of the world for sharing advances in PSE education, research, and application. PSE2012, the 11^{th} in the series, was held in the global village of Singapore during July 15-19, 2012. This 2-part book presents the various plenary, keynote, oral, and poster papers that featured in PSE2012.

While the PSE community continues its focus on understanding, synthesizing, modeling, designing, simulating, analyzing, diagnosing, operating, controlling, managing, and optimizing a host of chemical and related industries using the systems approach, the boundaries of PSE research have expanded considerably over the years. While the early PSE research concerned largely with individual units and plants, the current research spans wide ranges of scales in size (molecules to processing units to plants to global multinational enterprises to global supply chain networks; biological cells to ecological webs) and time (instantaneous molecular interactions to months of plant operation to years of strategic planning). The changes and challenges brought about by the increasing globalization and common global issues of water, energy, sustainability, and environment provided the motivation for the theme of PSE2012: Process Systems Engineering and Decision Support for the Flat World.

PSE2012 involved nearly 340 contributions on modeling, simulation, design, optimization, operations, control, water, energy, environment, sustainability, biosystems, oil and gas, pharmaceuticals, education, industrial applications, and others. Part A includes the plenary, keynote, short oral, and poster contributions, while Part B comprises the full oral presentations.

We are indebted to many from the PSE community, who contributed their invaluable time and effort as members of the three main committees of PSE2012, namely the International Program Committee (IPC), the Local Organizing Committee (LOC), and the Graduate Organizing Committee (GOC). The LOC reviewed nearly 580 initial abstracts and also full-length papers. The IPC members provided at least two timely and critical reviews for each contributed full-length paper. Finally, the GOC led by Naresh Susarla and Mohammad Sadegh Tavallali accomplished the many tedious and challenging tasks required in bringing this book to its current form. We are grateful to the members of all three committees for their voluntary contributions in various capacities.

We hope that this book serves as a useful reference for the PSE community to advance the science and application of Process Systems Engineering.

I A Karimi and Rajagopalan Srinivasan
Chairs, PSE2012

PSE2012 Committees

Symposium Chairs

I A Karimi / R Srinivasan National University of Singapore (NUS)

International Program Committee

L Achenie	Virginia Tech	C Adjiman	Imperial College
R Agrawal	Purdue University	E Almutairi	King Fahd University of Petroleum & Minerals
R M B Alves	University of Sao Paulo	M H Azlan	University of Malaya
B S Babji	ABB Corporate Research	M J Bagajewicz	University of Oklahoma
A Barbosa-Povoa	Universidade Tecnica de Lisboa	P Barton	Massachusetts Institute of Technology
R Batres	Toyohashi University of Technology	M Bhushan	Indian Institute of Technology, Bombay
L T Biegler	Carnegie Mellon University	D Bogle	University College London
P Bongers	Unilever Research	W Budhi Yogi	Bandung Institute of Technology
J Cerda	CONICET-Universidad Nacional del Litoral	C-T Chang	National Cheng Kung University
C-L Chen	National Taiwan University	I-L Chien	National Taiwan University
M A A S Choudhury	Bangladesh University of Engineering and Tehnology	M Doherty	University of California, Santa Barbara
M R Eden	Auburn University	T Edgar	University of Texas, Austin
M M El-Halwagi	Texas A & M University	S Engell	Technische Universitat Dortmund
A Espuna	Universitat Politecnica de Catalunya	X Feng	Xi'an Jiaotong University
C Floudas	Princeton University	D Foo	University Of Nottingham, Malaysia
R Gani	Technical University of Denmark	M Georgiadis	Aristotle University of Thessaloniki
I E Grossmann	Carnegie Mellon University	S K Gupta	Indian Institute of Technology, Kanpur
C Han	Seoul National University	S Hasebe	Kyoto University
G Henning	CONICET-Universidad Nacional del Litoral	G Heyen	University of Liege
M Hirao	University of Tokyo	D B Huang	University of Alberta
H-P Huang	National Taiwan University	D C W Hui	Hong Kong University of Science and Technology
M Ierapetritou	Rutgers University	X Joulia	Procedes Systemes Industriels
N Kaishta	Indian Institute of Technology, Kanpur	J Klemes	University of Pannonia
A Kokossis	National Technical University of Athens	A Kraslawski	Lappeenranta University of Technology
Z Kravanja	University of Maribor	I B Lee	Pohang University of Science and Technology
P Linke	Texas A&M Qatar	A Linninger	University of Illinois at Chicago
S Mahadzir	Universiti Teknologi Petronas	T Majozi	University of Pretoria
Z A Manan	Universiti Teknologi Malaysia	D Manca	Politecnico di Milano

C Maravelias	University of Wisconsin	F Marechal	Ecole polytechnique federale de Lausanne
W Marquardt	Aachener Verfahrenstechnik	H A Matos	Technical University of Lisbon
N Menshutine	Mendeleev University of Chemical Technology of Russia	I Moon	Yonsei university
I M Mujtaba	University of Bradford	C Nascimento	University of Sao Paulo
S Narasimhan	Indian Institute of Technology, Madras	K M Ng	Hong Kong University of Science and Technology
H Nishitani	Nara Institute of Science and Technology	M Noda	Nara Institute of Science and Technology
S Park	Korea Advanced Institute of Science & Technology	S Pierucci	Politecnico di Milano
J M Pinto	Praxair	E Pistikopoulos	Imperial College
V Plesu	University Politehnica of Bucharest	H A Preisig	Norwegian University of Science and Technology
G Reklaitis	Purdue University	J A Romagnoli	Louisiana State University
P K Saha	Indian Institute of Technology, Guwahati	Y Samyudia	Curtin University of Technology
W Seider	University of Pennsylvania	S Shah	GE Oil & Gas
M A Shaik	Indian Institute of Technology, Delhi	D Shin	Myongji University
J Siirola	Sandia National Laboratories	G Sin	Technical University of Denmark
S Skogestad	Norwegian University of Science and Technology	G Stephanopoulos	Massachusetts Institute of Technology
M O Tade	Curtin University of Technology	R Tan	De La Salle University
Y Tsuge	Kyushu University	M Turkay	Koc University
V Venkatasubramanian	Purdue University	S-Q Wang	Zhejiang University
M Wogsri	Chulalongkorn University	D S-H Wong	National Tsing-Hua University
Y Yamashita	Tokyo University of Agriculture and Technology	E S Yoon	Seoul National University
X-G Yuan	Tianjin University	J Zhao	Tsinghua University
K V Dam	Imperial College	E Zondervan	Eindhoven University of Technology

Local Organizing Committee (Singapore)

G P Rangaiah	NUS	M-S Chiu	NUS
D-Y Lee	NUS	P Linga	NUS
A Rajendran	NTU	P Sharratt	ICES
A Adhitya	ICES	BBalagurunathan	ICES
J Eades	Ispahan	S Huang	SUTD

Graduate Organizing Committee (National University of Singapore)

K S Ang	G Krishna
H P Veluswamy	M C Lau
M Kandpal	M Lakshmanan
M S Tavallali	N Susarla
P V Babu	M Sha
S Sharma	Q Su
V K Kamaraju	

I.A. Karimi and Rajagopalan Srinivasan (Editors), Proceedings of the 11th International Symposium on Process Systems Engineering, 15-19 July 2012, Singapore.

A Perspective on Energy and Sustainability

Jeffrey J. Siirola

Purdue University, West Lafayette, Indiana 47907 and Carnegie Mellon University, Pittsburgh, Pennsylvania 15213, USA

Abstract

There is much interest in concepts of sustainability within the chemical industry, especially related to health, safety, and environmental performance, product stewardship, value chain management, efficient use of resources, and mitigation of potential climate change. However, perhaps the greatest sustainability challenges are those associated with energy production and consumption. Energy consumption directly contributes to the majority of carbon dioxide emissions, and recent estimates of future economic growth imply that global energy consumption may more than triple over the coming decades. Since at present carbon capture and sequestration technologies are very expensive, in difficult economic times emphasis will be given first to energy conservation and fuel switching as primary carbon management approaches. A number of current issues will be discussed including economic limitations to implementing energy conservation in retrofit situations, new approaches to the optimal control of energy during process operations, techniques to hasten the utilization of biomass energy sources, and the impacts of shale gas development.

Keywords: carbon management, energy conservation, fuel switching, biomass torrefaction, smart manufacturing

1. Introduction

While contemplating the near and longer term future of the chemical industry, it is instructive to examine the recent past. For the organic chemical industry, it appears that especially for the half-century from 1940 and the advent of synthetic polymers, the industry was driven by substitution and in particular by the substitution by polymeric fibers, films, and plastics for metals, stone, brick, cotton, wool, linen, and paper. As that period of materials substitution matured, the growth rate in the chemical industry instead tended to more closely reflect general economic activity. That activity in turn is related to population size and increases in the standard of living within each region.

The global population has been steadily expanding and has just reached seven billion. However, many projections estimate that over the coming decades it will stabilize, probably at a level just below ten billion. Over the same period, the standard of living as measured by per capita gross economic product, especially in areas currently less well off, is projected to significantly improve largely because of technology. The result of both of these factors is that the global gross economic product is expected to increase by a factor of six-seven over the next five decades. Based on past trends, such an increase would also result in an increased demand for material commodities including the products made by the chemical industry by perhaps a factor of five and an increase

in overall energy demand by more than a factor of three but an electrical energy demand by perhaps a factor of seven. A legitimate concern is raised whether such a magnitude of materials and energy demand increase, even if only approximately accurate, can be sustainably satisfied. That is, can such a demand be satisfied without compromising the ability of future generations to meet their quality of life aspirations?

The current interest in sustainability focuses on a number of areas including environmental protection, health and safety, energy efficiency, product stewardship, industrial ecology, renewable resources, water management, green chemistry, and national security. But perhaps the greatest challenges to sustainability are the issues of climate change and carbon management, and especially those associated with energy production and consumption.

About eighty-five percent of all energy consumed throughout the world today is derived from carbonaceous fossil fuels (natural gas, shale gas, crude oil, coal, lignite, and peat). Coal is the most abundant and the fuel used most for the production of electricity. Oil is the most common source for the production of transportation fuels. Gas is globally the least abundant and is difficult to transport except by pipeline, but is easy to clean, has the greatest energy content per unit of carbon, and traditionally has commanded the highest price.

The present burning of fossil fuels for the production of energy results in the release of carbon dioxide, a portion of which dissolves in the ocean, but the remainder of which adds to the inventory in the atmosphere, currently increasing the CO_2 concentration by a little more than 2ppm per year. Recent atmospheric CO_2 concentrations have exceeded 395ppm compared with the pre-industrial-revolution level of 280ppm. The level is expected to continue to increase at an accelerating rate as annual fossil fuel combustion to meet growing global energy demand continues to grow. There is widespread concern that the increased CO_2 concentration may interfere with nocturnal radiative emission which could lead to increased average temperatures, altered weather patterns, more severe storms, expanded periods and regions of drought, and other manifestations of global climate change. In any event, such a rise in concentration of any atmospheric constituent is in itself a cause for concern.

The present emission of carbon from the combustion of fossil fuel is on the order of 8 billion tons carbon (30 billion tons CO_2) per year. If over the coming decades the global demand for energy more than triples and if the same mix of fossil fuels continues to be burned even with population stabilization, living standard maturity, and a fair amount of energy conservation awareness, these annual emissions could increase to on the order of 30 billion tons carbon (100 billion tons CO_2) per year at which time atmospheric CO_2 concentration could be increasing at something like 7ppm per year to a total concentration between 600 and 700ppm.

Although there may be significant error in these concentration estimates and in the climatic impact of such concentrations, the atmospheric addition of even only a few tons CO_2 per year clearly is not sustainable and as a result policymakers are likely to mandate some kind of fossil fuel combustion restrictions or carbon emission restrictions in the near future. In anticipation of this possibility, a number of reduction and control strategies are being evaluated by governments, research institutions, and companies around the world.

2. Carbon Management

A number of approaches to carbon management have emerged including carbon emissions reduction, carbon capture and permanent storage, and carbon offsetting or recycling. Common carbon capture approaches from flues and other sources of CO_2 include absorption, adsorption, membrane separation, and others. In general, the captured CO_2 is then recovered from the capturing media and then prepared for storage for example as a supercritical liquid in saline aquifers or in depleted oil and gas reservoirs, or adsorbed in coal seams too thin to mine, or dissolved in oceanic waters. Each of the capture methods is sensitive to the CO_2 partial pressure of the source, and each of the storage methods has its own concerns including acidification, stability, leakage, etc. Although the US Government has targets that carbon management should not increase the cost of electricity to consumers by more than 50%, current estimates for base case absorption, recovery, and compression technologies for coal-fired power plants are several times greater than the target. The Carbon Capture Utilization and Storage program was initiated by the US Department of Energy to directly address capture and storage technology and economic performance, risk, and uncertainty in an attempt to accelerate the timeline in which carbon capture and storage could be considered commercially available by a factor of three. Much current research in the component Carbon Capture Simulation Initiative and the National Risk Assessment Partnership is directed to accelerating all phases of carbon capture and storage technology from development through deployment using a framework of science based and valuated performance simulation, technical and financial uncertainty quantification, and risk adjusted decision making.

3. Emissions Reduction

Nevertheless, at the present time, carbon capture and storage appears extremely expensive and no full scale capture systems on commercial power plants have been installed. Therefore, it is expected that first response to any control restrictions or mandates will most likely take the form of engineered emissions reductions. Within the chemical industry these reductions may be approached from several directions. One is energy conservation.

Energy conservation has long been studied within the process systems community. Topics range from simple operational efficiency considerations (turning out unneeded lighting, optimal insulation thickness to minimize heat losses from pipes, proper matching of driver power to machine requirement, etc.) to greater use of energy recovery and reuse (heat exchanger networks, waste incinerators and heat recovery boilers, etc.) to more aggressive conservation consideration during the process design phase (operating condition selection to maximize the opportunities for heat integration especially of latent heats, use of multi-effect configurations in evaporation and distillation, thermally-coupled distillation, process electricity utility and process steam utility cogeneration, etc.). Typical energy savings range from a few percent for operational policies to ten to twenty percent for the incorporation of heat recovery networks to fifty percent or more for multi-effect separations.

Unfortunately, as large as some of these energy savings are, they are most times difficult or impossible to justify economically as retrofit projects, unless other aspects of the project also result in additional manufacturing capacity and additional sales volume potential. Only in these cases does the potential for additional income (in addition to the energy cost savings) offset the capital costs of the energy-conserving process improvement modifications. There have been many studies where it was speculated that a certain rise in energy costs (or perhaps a future energy or carbon tax) alone could justify the new energy conservation capital (calculated from recent equipment cost experience). However, these studies have been almost never borne out, as it is now more widely recognized that chemical plant equipment costs correlate almost exactly with energy (especially crude oil) prices (with a several year delay), and have done so consistently for more than a century. Any study projecting at what future energy price the capital investment for a particular energy-saving technology will finally be justified must carefully consider that the current equipment cost indices will also escalate by a similar ratio. It is because of this effect that energy conserving retrofit projects rarely can be justified in the absence of additional product sales revenue.

4. Smart Manufacturing

However, there is now under consideration a new paradigm called Smart Manufacturing that may also have an important impact on energy conservation. Smart manufacturing is a proposal to use massive amounts of process data and extensive computational resources to enable a dramatically intensified knowledge-enabled chemical process enterprise in which all business and operating actions are executed to achieve significantly enhanced safety, health, environmental, economic, sustainability, and energy performance. Among the concepts included within smart manufacturing especially for energy-intensive industries like the processing industries are greater use of process sensors, much larger stores of process data, the necessary computational infrastructure to allow real-time reconciliation, analysis, and interpretation of process data, and the process modeling and other generation of knowledge needed to make on-line plant-wide optimal control decisions considering the multiple objectives of fitness-for-use, safety, environmental protection, economics, and energy.

In addition to obviously massive computational and IT requirements and installation of many more process sensors, it is anticipated that process engineering modifications will also need to be invented in order to increase the number of control degrees of freedom so that other smart manufacturing objectives and in particular energy consumption may also be optimized in addition to the usual requirements for product fitness-for-use and public safety.

In the present process systems engineering paradigm, it is common practice to design for energy conservation. During process synthesis, lower energy consuming equipment or configuration alternatives can be selected and operating conditions to minimize energy use and maximize heat recovery opportunity can be chosen. However, during actual operation, energy minimization is less often a control objective. Quite to the contrary, if a fitness-for-use specification (for example, product purity) is being missed, it is often the reflux ratio (and energy consumption) that is first increased in an attempt

to return to specification. Likewise, it is to the utility system that control disturbances are rejected (and in doing so generally resulting in increased energy consumption).

One of the aims of the smart manufacturing initiative in the processing industries is to design for and use additional operational degrees of freedom so that with the aid of increased amount of process data and large-scale on-line computational capability, product fitness-for-use goals can be met while at the same time actively optimizing other sustainability objectives including energy minimization. As an example, consider a distillation column fitted with some futuristic additional engineering infrastructure that would allow active sensing and control of phase mixing or approach to flooding (and hence efficiency) on each tray. In such a case, even though the reflux ratio is still used to control product purity, active control of tray efficiency could simultaneously lower that required reflux ratio even though the existing number of trays remains fixed.

5. Fuel Switching

Different carbonaceous fuels have different heats of combustion depending on their composition. The lower heating value heat of combustion (product water remains as a vapor) per carbon atom can readily be estimated from the average "oxidation state" of carbon in the fuel which is turn can be estimated from the molecular formula and considering the constituents in the fuel that will be converted to a mass of water upon combustion. With this scheme, it is readily seen that the heat of combustion per carbon atom of natural gas is about twice that of coal, and that of most liquid hydrocarbon fuels lies about half way in between. This also means that for the same heat production, the amount of CO_2 emissions from burning gas are about half those from burning coal.

That also means that fuel switching will likely be another early approach to carbon emissions reduction. In the US, coal accounts for approximately half of all electricity generation. Although electrical generation is the largest consumer of coal by about an order of magnitude, significant amounts are also burned in heating plants for large institutions (such as universities) and utility boilers (including some in the chemical industry).

In the past, natural gas consumption in the US for electricity generation was limited by both policy and economics. However, policy began to change two decades ago, which has led to many new natural gas electrical generators, especially to meet peaking demand. At the time these new peaking plants first came on line, the available supply of gas could not increase with the result that gas prices rose. This price increase had several effects which included rejection of gas for most base load demand, a much steeper price for peak-hour electricity (leading to more widespread adoption of time-of-day electricity pricing), and decrease use of natural gas as a feedstock in the US chemical industry (except for the production of hydrogen). Under these economic conditions, few users would consider replacing base-load coal even though it has high CO_2 coproduction.

However, high gas prices also encouraged the development of two new production technologies, directional (horizontal) drilling and hydraulic fracturing. These technologies in turn have enabled the exploitation of shale gas, gas contained in

relatively thin and impermeable shale rock formations. Previously, as no extraction technology was known to be practical, shale gas was not even counted among gas reserves. In the US, there are perhaps two dozen shale gas fields, some of them very large. The first to be developed with horizontal drilling and fracturing were so productive, that now official gas reserves in the country have been doubled. This increased production has also fundamentally changed gas pricing structure which has decreased from its historical ratio to the price of both oil and coal on an energy basis by a factor of four. This means natural gas has gone from the most expensive fossil fuel to being the least expensive as well as being the fuel with the greatest combustion energy per unit CO_2 emissions. Natural gas turbines, in addition to being favored for peaking plants is also useful as a backup electricity generation for intermittent wind farms and solar photovoltaic installations because of relative ease in starting and dynamic load following.

With new natural gas economic realities, it may be that a relatively simple carbon emissions reduction technique will be fuel switching of natural gas into existing coal-fired boilers (many pulverized versions of which already have natural gas burners for pilots). Such a conversion requires only minimal capital, but can almost halve carbon emissions (firing a coal-designed boiler with gas results in some derating of output because the ratio of the size of the convective heat section to the radiant heat section is low compared to what it would be in a purpose-designed gas-fired boiler). If low shale-gas-inspired prices continue, the pace of such fuel switching may even accelerate until either gas prices re-equilibrate to some higher value, or virtually all coal firing is eliminated.

A related feature that will further reduce CO_2 emissions from the electricity generation sector is the further installation of natural gas combined cycle (NGCC) technology. This technology combines a very high temperature Brayton cycle gas turbine with a conventional Rankine waste heat bottoming cycle steam turbine and achieves an electrical generation efficiency approaching 60% (compared to 35-40% for coal-fired power plants). This increased electrical generation efficiency combined with the higher heat of combustion per carbon atom means that new NGCC plants could reduce carbon emissions from the coal part of the electric power generation industry by something close to 70% before implementation of capture and storage technology.

6. Biofuel

Another approach to carbon dioxide emissions reduction is the substitution of biofuels for fossil fuels. Biofuels are considered to be carbon neutral, at least after an equal amount of replacement biomass is regrown. Most current biofuels involve conversion of one specific component in the biomass (for example starch or oil) into a specific compound (ethanol or fatty ester methyl ester) typically for use as a liquid fuel for the transportation sector. Much of the remaining energy content in the biomass feedstock is not used.

However, another option which may in fact have a larger and more immediate impact on CO_2 emissions reduction is the direct combustion of biomass in power plants especially as a partial or total replacement for coal. The oxidation state of carbon in

most biomass is about the same as that of the carbon in coal. Per carbon atom, biomass has about the same heat of combustion as coal. However, unlike coal, biomass also carries with it two kinds of water in the form of bulk moisture and in the "hydrate" part of the carbohydrate components starch, cellulose, and hemicellulose. This water not only takes up weight, but its heat of vaporization detracts from the heat of combustion. In addition, it may be difficult to burn bulk biomass in a boiler designed to burn coal. The additional water lowers combustion temperatures which in turn derates boiler capacity. Economizers in boilers designed for coal in particular are undersized when the same boiler burns biomass.

Nevertheless, in regions where significant biomass is available and underutilized including some hardwood and softwood forests and agricultural residues, biomass could be sustainably harvested for coal substitution for electricity production. In addition, some pretreatment technologies, such as the mild form of pyrolysis known as torrefaction, have been proposed which can remove all of the bulk moisture and some of the "hydrate" part of the carbohydrate components producing a dark, relatively dense, hydrophilic, and brittle material that can even be ground and burned in pulverized coal boilers using existing equipment. Depending on the specific nature of the biomass, the torrefaction process can also produce volatile organic coproducts which could be recovered and used to fuel the torrefaction pyrolysis process itself. Torrefied biomass is another way to extract value from the existing coal-fired power generation assets and infrastructure while significantly reducing net carbon dioxide emissions by substituting a carbon neutral fuel for what is now the most CO_2 inefficient fuel.

7. Conclusions

Although there is growing interest in chemical industry sustainability issues such as health, safety, and environmental performance, perhaps the greatest process systems sustainability challenges are those associated with energy production. Energy production directly contributes to the majority of carbon dioxide emissions of growing concern. As presently known carbon capture and sequestration technologies are very expensive, in difficult economic times carbon management emphasis will first take the form of engineered emissions reduction. Emissions reduction by capital retrofit energy conservation techniques have proven to be difficult to economically justify in the absence of increased product sales revenue. Instead, emissions reductions are likely to implemented first by fuel switching especially increasingly plentiful shale gas for coal in electrical power production, and also by increased substitution of whole biomass and especially torrefied biomass for coal which may prove to have a greater environmental impact that the production and use of bioderived transportation fuels. Implementation of the data rich and computing intense smart manufacturing paradigm may also allow energy minimization to be included along with product fitness-for-use objectives in the optimal control of operating chemical facilities.

I.A. Karimi and Rajagopalan Srinivasan (Editors), Proceedings of the 11th International Symposium on Process Systems Engineering, 15-19 July 2012, Singapore.

Optimizing the end-to-end value chain through demand shaping and advanced customer analytics

Brenda Dietrich, Markus Ettl, Roger D. Lederman, Marek Petrik

IBM Research, Yorktown Heights, NY 10598, USA

Abstract

As supply chains become increasingly outsourced, the end-to-end supply network is often spread across multiple enterprises. In addition, increasing focus on lean inventory can often create significant supply/demand imbalances over a multi-enterprise supply chain. This paper discusses a set of integrated analytics for supply/demand synchronization with a new emphasis on customer facing actions called demand shaping. Demand shaping is the ability to sense changing demand patterns, evaluate and optimize an enterprise supply plan to best support market demand and opportunity, and execute a number of demand shaping actions to "steer" demand to align with an optimized plan. First, we describe a multi-enterprise cloud-based data model called the Demand Signal Repository (DSR) that includes a tightly linked end-to-end product dependency structure as well as a trusted source of demand and supply levels across the extended supply chain. Secondly, we present a suite of mathematical optimization models that enable on demand up-selling, alternative-selling and down-selling to better integrate the supply chain horizontally, connecting the interaction of customers, business partners and sales teams to procurement and manufacturing capabilities of a firm. And finally, we describe findings and managerial insights from real-life experiences with demand shaping in a server computer manufacturing environment.

Keywords: Demand shaping, product substitution, configure-to-order, mixed choice models, supply chain visibility.

1. Introduction

In today's competitive and dynamic business environment, companies need to continually evaluate the effectiveness of their supply chain and look for ways to transform business processes to achieve superior customer service and higher profitability. Imbalances between supply and demand are the primary reason for degraded supply chain efficiency, often resulting in delinquent customer orders, missed revenue, and excess inventory. This paper describes a novel supply chain planning and execution process that incorporates demand shaping and profitable demand response to drive better operational efficiency of the supply chain. The proposed methodology aims at finding marketable product alternatives that replace demand on supply-constrained products while minimizing expected stock-out costs for unfilled product demand and holding costs for left-over inventory. While most prior related literature focuses on the concept of Available-To-Promise (ATP) where a scheduling system determines a particular product's availability, this paper proposes a customer-centric approach based on customer choice modeling and demand shaping to dynamically incorporate product substitutions and up-sell opportunities into the supply-demand planning process.

Demand shaping is a demand-driven, customer centric approach to supply chain planning and execution. The aim is to align customer's demand patterns with a firm's supply and capacity constraints through better understanding of customer's preferences which helps influencing customer's demand towards products that the firm can supply easily and profitably. Demand shaping can be accomplished through the levers of price,

promotions, sales incentives, product recommendations, or on the spot upgrades / discounts to enables sales teams to close deals for in-stock products.

The underlying principles of demand shaping are centered on three competencies:

- Customer preference and demand pattern recognition
- Supply capability analysis that provides improved visibility to the sales force on in-stock and out-of-stock products
- Optimal demand shaping based on advanced customer analytics that estimate propensities of customers to purchase alternate products so that the sales force can guide customers to "next-best" product options

Detecting customer preferences and demand patterns relies heavily on predictive analytics and automated gathering of sales data from every customer touch point, including retailer point-of-sales data, channel partner data, and shopping basket or checkout data from e-Commerce sales portals. Such data is often stored in a so-called Demand Signal Repository (DSR), a cross-enterprise database that stores sales data in a format that allows for easy retrieval of information so that a firm can easily query the database to identify what's selling, where, when and how. Supply capability analysis provides timely information on available product supply to identify imbalances between customer demand and available supply. The third competency of optimal demand shaping is to steer customer demand to a preferred set of products that optimizes the firm's profitability and revenue while increasing overall serviceability and customer satisfaction.

In this paper, we propose a methodology for demand shaping based on mathematical models that aim at finding marketable product alternatives in a product portfolio that best utilize inventory surplus and replace demand on supply-constrained products. We explicitly analyze customer expectations in a dynamic setting utilizing a customer choice model that determines how customers evaluate product substitutions if their initial product selection is unavailable. Moreover, we present numerical results that attempt to quantify the business value of demand shaping in a configure-to-order (CTO) supply chain where end products are configured from pluggable components, such as hard disks, microprocessors, video cards, etc., an environment where demand shaping is most effective.

2. Related Literature

The demand shaping approach we discuss in this paper has connections to several problems in related literature streams. Ervolina and Dietrich (2001) describe an application of the implosion technology for order promising in a configure-to-order (CTO) manufacturing environment. Building on this approach, Dietrich et al. (2005) develop a deterministic implosion model that identifies suitable product configurations for an Available-to-Sell process that consume the most surplus inventory and require minimal additional component purchasing costs. Market demand, customer preferences, or product substitution policies are not considered in their model. Chen-Ritzo (2006) studies a similar availability management problem in a CTO supply chain with order configuration uncertainty. Ervolina et al. (2009) employ integer programming to identify marketable product alternatives in a product portfolio that best utilize inventory surplus and replace demand on supply-constrained products. Yunes et al. (2007) apply a

customer migration model in conjunction with mixed-integer programming to determine the optimal product portfolio at John Deere and Company. A customer migration list contains alternative product configuration choices if a customer's preferred product selection is unavailable. Balakrishnan et al. (2005) apply concepts from revenue management to investigate how a firm can maximize profits by shaping demand through dynamic pricing. Liu and van Ryzin (2008) discuss choice-based optimization in the context of network revenue management, and present a static linear programming approximation that relates to the approximate dynamic programming formulation presented in this paper. Dong et al. (2009) employ a stochastic dynamic programming formulation to study inventory control of substitutable products. Finally, Bernstein et al. (2011) present a model of assortment customization, similar to the choice-set manipulation that we model as a possible lever for demand shaping.

3. Customer Choice Model

In addition to the product-level demand patterns that can be derived from sales data collected at customer touch points, demand shaping requires a detailed model of customer decision-making that can be used to predict the success rate of various shaping actions. We model customers' product choices using a discrete-choice framework that casts the likelihood of all possible purchase decisions within a parametric form. Our framework incorporates product attributes, customer characteristics, and additional market signals that may effect customer decisions. The resulting *customer choice model* depicts latent inter-product relationships, and is combined with up-to-date product-level forecasts to give a full picture of demand.

Product demand forecasts and customer choice modeling are integrated into a two-stage decision process for customer purchases. The first stage occurs prior to demand shaping and involves determination of an *unshaped product choice* for each customer. Our assumption is that the distribution of unshaped product choices is, with the exception of some random forecast error, represented accurately by product demand forecasts that are generated through the traditional planning process. We then allow for a second decision stage in which some portion of this forecasted demand is re-allocated by various shaping actions that are applied across the product portfolio. The end result is a *shaped demand* that we expect to observe post-shaping. The customer choice model is used to predict the degree of redistribution that can be achieved through each possible set of shaping actions.

3.1. Representation of Substitution Probabilities

Customer choice analytics support optimization of shaping actions by generating a matrix of *substitution probabilities* to reflect the rate of demand redistribution between product pairs for any potential collection of shaping actions. To start, customers are segmented by a combination of customer characteristics and unshaped product choice. The set Y provides a collection of observable customer profiles, used to group customers by attributes such as, e.g., sales channel, industry segment, length of relationship, etc. For each type $y \in Y$, we obtain at time $t \in T$ an unshaped forecast F_{tyj} of demand for each product j in the product portfolio J. This allows a further segmentation by unshaped product choice, so that shaping actions are targeted at a

segment $s \in Y \times J$, with a forecasted segment size n_{st} equal to the corresponding unshaped forecast. Let $S = Y \times J$ and partition so that S_y contains those segments with customer type *y*.

For each segment s, we operate within a set A_s of admissible shaping actions. An example of a possible shaping action in A_s is to "offer product *i* to segment *s* customers at a 20% discount". As each segment relates to a specific unshaped product choice *j,* actions for that product are intended to redistribute some portion of product *j*'s demand to elsewhere in the portfolio. Since multiple actions may be applied simultaneously, we define an *action profile* $h_s \in H_s \subseteq 2^{A_s}$ to characterize the full set of shaping activities targeted at segment *s*. For each action profile, we provide the optimizer with the following representation of demand redistribution:

$V_s(h_s)$: a |J|-vector of substitution probabilities, such that V_{si} is the proportion of the unshaped demand from segment *s* that is redistributed to product *i* when the action profile h_s is applied.

As a result, we are able to represent the predicted shaped demand for any set of segment-specific action profiles as $\tilde{F}_{ty}(\{h_s\}_{s \in S}) = \sum_{s \in S_y} n_{st} V_s(h_s)$, where $\tilde{F}_{yt}$ itself is a |J|-vector of shaped product demands.

As is often done in the discrete-choice literature (Kök and Fisher 2007), we can decompose the vector $V_s(h_s)$ into the product of a substitution-structure vector $B_s(h_s)$, and a substitution-rate parameter $\delta \in [0,1]$. The parameter δ is an important measure of the overall substitutability between products in the market. In our numerical tests, we will explore the degree to which effective shaping is dependent on a high value of δ. First, we discuss the estimation of $B_s(\cdot)$ from historical orders and customer data.

3.2. Estimation with Mixed Logit Models

For any significant number of products and actions, the large number of required substitution probabilities makes direct estimation of these values prohibitive. Instead, we derive all of the necessary terms from a discrete-choice model containing far fewer parameters. An important element of this model is the ability to accurately represent customer heterogeneity. In particular, substitution patterns reflect the degree to which products draw from overlapping customer pools, which can only be captured meaningfully through a heterogeneous model. To this end, we employ a mixed logit model of demand (McFadden and Train 2000), which extends the standard logit model (McFadden 1974) to incorporate variation in customer preferences.

We fit a demand model for each customer type *y*, using historical orders from the customer set K_y over the time horizon, T_{Hist}. As with the standard logit model, the mixed logit model predicts order probabilities as a function of product attributes. At time *t*, customer *k* has a stochastic valuation of each product *j*, denoted $u_{kjt} = \alpha_k^T x_j + \beta_k z_{kjt} + \varepsilon_{kjt}$, where x_j contains product attributes, z_{kjt} contains information on shaping actions applied at time *t*, $\{\alpha_k, \beta_k\}$ are model parameters to be estimated, and ε_{kjt} is a stochastic error term. In the server environment that we model, attributes in x_j include, e.g., CPU speed, hard drive capacity, hard drive speed, and GB of memory. The second data term, z_{kjt}, contains factors impacting purchasing that may be manipulating through shaping actions. In the simplest case z_{kjt} equals the price p_{kjt}, but this vector can be expanded to encompass quoted order lead-times, marketing intensity, and other relevant factors.

Under the logit assumption that ε_{kjt} are i.i.d. extreme-value distributed, the likelihood of purchase for product *j*, assuming a choice-set J_{kt} of available products, is:

$$L_{kjt|J_{kt}}(\alpha, \beta, x, z) = e^{\alpha_k^T x_j + \beta_k z_{kjt}} / (1 + \sum_{i \in J_{kt}} e^{\alpha_k^T x_i + \beta_k z_{kit}}).$$

Whereas, in the standard logit model, α and β are constant across customers, the mixed logit model allows for these values to vary across the population according to a specified mixing distribution $G_y(\alpha, \beta \mid \theta)$, whose parameters can in turn be estimated. This can be a continuous distribution, i.e. a normal or lognormal distribution, or a discrete distribution, which then gives rise to distinct latent customer segments. In practice, we combine a discrete component of preference variation, which introduces multi-modality into our preference distribution, with a continuous component that is more economical in its use of parameters. The full parameter vector θ is then estimated along with α and β using a maximum likelihood procedure with our historical order set. In this case, simulation must be used to evaluate $E_{G_y}[L_{kjt|J_{kt}}]$, since this quantity no longer has a closed form.

Under the mixed model of demand, customers' unshaped product choices reflect on their personal values of α and β, giving insight into each customer's sensitivity to shaping actions, and the likelihood of accepting specific substitutes. By conditioning the mixing distribution on each customer's unshaped product choice *j* (e.g., Revelt and Train (1999)), or more generally, on their history of product choices, we obtain an individualized mixing distribution, $G_{y|j}$, that is used to assess various targeted action profiles. In particular, we associate, with each action profile h_s, a shaping attribute vector $\tilde{z}(h_s)$ and an alternative product set $\tilde{J}(h_s)$. The likelihood of a segment *s* customer, where this dictates a type *y* and unshaped choice *j,* accepting substitute *i*

when shaping profile h_s is applied, is then provided by the expected value $E_{G_{y|j}}[\, L_{kit|\tilde{J}_{kt}(h_s)}(\alpha, \beta, x, \tilde{z}(h_s))]$.

This quantity is computed to populate the i^{th} entry in $B_s(h_s)$.

4. Demand Shaping Optimization

Having outlined customer behavior and the effects of shaping actions, we turn in this section to a description of the optimization model that selects our recommended shaping actions. The optimization is based on a stochastic view of demand forecasts and is formulated as a Markov decision process. Because of the large size of the model, we solve it using approximate dynamic programming.

As described above, demand is shaped in the context of a manufacturer which purchases and inventories individual components and then uses them to assemble and sell products. The demand is shaped over a sequence of time periods, which is indexed as $t = 1,2,\ldots$. The set of all component types is denoted by C and the set of all products, as above, is denoted by J. The bill of material is represented by U; that is each product $j \in J$ is assembled of $U(j,c)$ components of type c. Components that are not sold are inventoried; the inventory of a component c at time *t* is denoted $I_t(c)$.

The planning horizon is infinite and future returns are discounted by a given discount factor γ. The purchase of each component is subject to a moderate lead-time l, which we assume to be identical across components. The order size cannot be changed once it is placed.

Demand shaping, as considered in this paper, can address two main types of the supply-demand imbalance: 1) deterministic imbalance, and 2) stochastic imbalance. A deterministic imbalance is known in advance of the lead time for most components, but the supply constraints do not allow to fully satisfy the demand. This kind of imbalance typically occurs after an introduction of a new product or during a long-term component shortage and it may be mitigated deterministically in advance. Stochastic imbalance is not known in advance and only becomes known after it is too late to adjust component supply. This kind of imbalance can be caused by an incorrect demand forecast, an unexpected last-minute supply disruption, or incorrect planning.

Deterministic and stochastic imbalances in the supply chain not only have separate causes, but also require different solution approaches. Since a deterministic imbalance is known within the lead-time of most components, the demand can be shaped into other products and the supply can be adjusted accordingly. Since a stochastic imbalance occurs only after it is too late to modify the component supply, it can only be mitigated by keeping appropriate inventories and shaping the excess demand into products that are available in the inventory. The model described here addresses both deterministic and stochastic supply-demand imbalances.

Components are ordered based on a build-to-order supply policy—that is the supply matches the expected demand. This assumption is made to simplify the model; in most actual applications, the orders would be based on the solution of a newsvendor optimization problem. The actual solution that we use is based on approximate dynamic programming and in essence generalizes the news-vendor solution to multiple stages. Since the supply is assumed to match the product demand, we can ignore component supplies in our model. In addition, all unused components are automatically inventoried with no expiration.

We model the customers using the customer-choice model defined above. In particular, the set S represents the customer segments with a forecasted size n_{st} at time t for a segment s. The forecast is assumed to be made at time $t-l$, the latest time when the supply can be adjusted. Because the forecast must be made in advance, we allow for stochastic disturbances Δ_t in demand, which will lead to imbalances between supply and the unshaped demands. As a result, the realized segment size is a random variable N_{st} with mean n_{st}. The realization of this value at time t becomes known only at time $t+1$.

The realized demand disturbances are normally distributed with mean 0. The distribution used in the model can be arbitrary and can be fit to historical data. The variance of this distribution depends on an external stochastic process of demand variability. Here, we consider a single-dimensional model of variability, denoted ϑ. The variability itself evolves as a normally distributed martingale with fixed variance and zero mean. The demand disturbances Δ across the products are usually negatively correlated with a larger variance in individual products than the total demand. We use Δ_ϑ to denote the covariance matrix.

The realized, unshaped customer demand is modified by taking shaping actions from the set H_s; which includes a no-shaping action option. As described above, the probability of a customer from segment s buying a product i after a shaping action h_s is taken is $V_{si}(h_s)$. Applying action profiles $\{h_s\}_{s\in S}$ at time t results in a realized, shaped demand of $\tilde{D}_{ty} = \sum_{s\in S_y} N_{st} V_s(h_s)$. At the start of the horizon, $\tilde{D}_{ty}$ is a random vector, whose realization will depend on realized values of N_{st} for $s \in S_y$.

The inventory of component type c is subject to a per-item holding cost $c_H(c)$. Taking any shaping action h carries a fixed cost $c_S(h)$—such as the cost of advertising—and variable costs $c_V(h)$—such as product discounts—which are a function of the segment size. The marginal profit for a product j is $c_M(j)$. Finally, the customer model assumes no backlogging---all demand that cannot be satisfied is lost. The overall objective is then to minimize the sum of lost sales due to the product being unavailable, the cost of shaping actions, and the holding costs.

We are now ready to formulate the stochastic optimization problem. If desired, we allow for specific action profiles to be applied to only a portion of a segment. As such, our decision variables π_t represent the probability of taking each shaping action h_s at every time step t for each segment s. These probabilities are denoted as $\pi_t(s, h_s)$.

The main optimization problem in demand-shaping is stochastic due to the uncertain nature of the demand forecasts and can be modeled as a Markov decision process (MDP) (Puterman 2005). The Markov state at time t is represented by the inventory of all products, the demand variability, and the demand forecast. Demand forecast evolves stochastically as described above; the demand variability evolves as a martingale. The Bellman optimality condition for a value function $v_t(I_t, \vartheta_t, n_t)$ is as follows:

$$v_t(I_t, \vartheta_t, n_t) = \min_{\pi_1, q_1} E\left[\begin{array}{l} \sum_{c\in C} c_H(c)\cdot I_t(c) + \sum_{j\in J} c_M(j)\cdot \min\{q_t(j), \sum_{y\in Y} \tilde{D}_{tyj}\} + \\ + \sum_{s\in S}\sum_{h\in H} \pi_1(s,h_s)\cdot(c_S(h_s) + c_V(h_s)\cdot N_{s,1}) + \\ + \gamma\cdot v_{t+1}(I_{t+1}, \vartheta_{t+1}, n_{t+1}) \end{array}\right] \quad (1)$$

Here, we use $q_t(j)$ to represent how many products can be build from the available components and $\gamma \in (0,1)$ to represent the discount factor.

The optimization variables in the problem above are constrained as follows. The first constraint ensures that the shaped demands $\tilde{D}$ are based on the shaping action probabilities π:

$$\tilde{D}_{tyj} = \sum_{s\in S_y}\sum_{h_s\in H_s} N_{st}\cdot V_{sj}(h_s)\cdot \pi_t(s,h_s) \quad \text{for all } y\in Y \text{ and } j\in J.$$

The second constraint ensures that the number of the products sold corresponds to the inventory of each component type:

$$q_t(j)\cdot U(j,c) \le I_t(c) \qquad \text{for all } j\in J \text{ and } c\in C.$$

Note that due to the assumption of the supply matching the deterministic demand n, we can assume that the demand with no shaping is 0. This assumption allows us to study the effects of stochastic imbalances alone and can be easily relaxed. There are additional constraints that ensure that the probabilities of shaping actions in each segment sum to 1 and that the inventories are correctly tracked across time periods.

The optimization problem in Eq. (1) is too large to be solved directly because the value function is defined for continuously many states. Instead, we solve the MDP using approximate linear programming, which is a version of approximate dynamic programming (Powell 2008). Normal distributions are approximated by the Gauss-Hermite quadrature. The shaping decisions are then chosen greedily with respect to the approximate value function.

5. Numerical Experiments

In this section, we evaluate the effectiveness of demand shaping, as it is depicted in Sections 3 and 4, in minimizing backlogging costs that result in the presence of unbalanced supply and demand. We simulate a production/sales environment that is modeled on a realistic problem setting taken from IBM's server supply chain. The simulation has two parameters – the demand variability ϑ and the substitution rate δ – that may be altered to create alternative settings. Within this two dimensional space, we compare the expected backlogging costs that arise both with and without shaping to assess the value of shaping optimization, and to highlight its sensitivity to the two control parameters.

The details of our simulation are as follows: we begin with true historical forecasts and realized customer orders from the hard drive options portfolio supporting IBM's System X line of servers. We link the forecasts directly into the above model to populate F, while we use customer and order data to estimate a substitution structure framework B. We assume a baseline level of supply that exactly covers the forecasted demand, but simulate the stochastic process Δ of demand disturbances to induce supply imbalances, with the potential to correct these through shaping. Our product set consists of 16 hard drives, and we model customer decisions on the basis of hard drive capacity, speed, interface type, and – a potential shaping lever - price. We assume that any unfilled demand will result in lost sales, and evaluate supply chain performance by the percentage of sales that are lost. Results are averaged across 15 simulation runs for each setting. Simulations cover a 30 week horizon, with a discount rate $\gamma = 5\%$ and a cost of 1% of unit revenue for holding inventory across periods.

Figure 1 plots the percentage of sales lost across a range of simulation environments. Each curve is generated at a particular δ (i.e. low, moderate, or high substitutability), and ϑ is varied from zero up to a setting with a coefficient of variation of 22.5% for each product demand. The $\delta = 0$ case provides a baseline where no demand can be shaped, and the improvement from this case illustrates the *value of shaping* in each setting.

The directions of performance improvement for our shaping optimization are quite intuitive. As variability is increased, there is a greater inherent mismatch between forecasts and realized demand. This increases lost sales in all settings, but also presents a larger opportunity to increase performance through shaping. As such, the value of shaping, measured by the performance gap from the $\delta = 0$ case, widens with increasing ϑ. In conjunction, shaping actions become more effective as the degree of substitutability between products is increased, so that the value of shaping increases in the direction of δ as well. When both variability and substitutability are high, the impact of shaping can be dramatic. For example, with high variability and $\delta = 1$, we observe a reduction in lost sales from 13.1% down to only 2.4% with shaping.

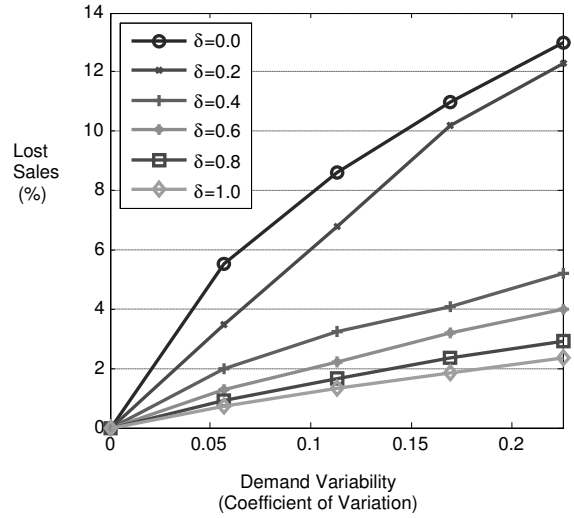

Figure 1: Percentage of sales lost in simulated experiments with demand shaping.

As substitutability is increased from 0, we observe a sharp jump downwards in lost sales resulting from only weak substitutability. For example, in the high variability case, shaping with a conservative substitution rate of δ = 0.4 delivers a relative reduction of 60% in lost sales compared to not shaping. It thus appears, from a product assortment perspective, that only a modest amount of substitutability is needed to successfully implement demand shaping. Interestingly, this result provides something of a demand-side analog to the result of Jordan and Graves (1995) on the steepness of initial returns to production flexibility. A deeper analysis of the interactions between demand shaping and production flexibility may indeed prove worthwhile for future study.

With regards to variability, we observe that the gap in lost sales between each δ curve and the no-shaping curve will increase with ϑ in most cases (the exception is with δ = 0.2, where the gap increases at first, before reaching a threshold where it seems that potential shaping actions are being exploited fully). Despite this trend in performance, it is apparent that additional variability drives a steady increase in lost sales percentage along each curve. Thus, while shaping can soften the deleterious effects of mismatched supply, a comprehensive approach aimed at improved forecast accuracy and/or reduced lead-times is most beneficial. To this end, however, we note that demand shaping will often be the simplest of available measures to implement, and may come at a relatively small cost to the manufacturer. With a strictly supply-side focus, the investment required to achieve a comparable reduction in lost sales can often be prohibitive.

6. Conclusion

In this paper, we have described a mathematical model for demand shaping that aims at finding marketable product alternatives in a product portfolio that best utilize inventory surplus and replace demand on supply-constrained products. We outlined demand shaping actions that improve inventory positions with early and efficient actions to

address surplus materials, and shift demand to available and profitable products through dynamic pricing. Our numerical results showed that more flexible customers are more profitable customers. Market intelligence and data analytics can identify these more flexible customers via market models. For example, a very price-sensitive client may only be presented with two sales recommendations – both of which are alternative-sells or one alternative sell and one down sell. A more price insensitive client may be presented with five dynamic sales recommendations – three are up-sells and two are alternative sells (no down sells). This stratification of clients by price sensitivity and the approach to dynamic sales recommendations will be essential to achieving the business results we have identified.

References

Balakrishnan, A., Y. Xia and B. Zhang. 2005. Shaping Demand to Match Anticipated Supply. In: Proc. Manufacturing & Services Operations Management Conference. Northwestern University.

Bernstein, F., A.G. Kök., L.Xie. 2011. Dynamic assortment customization with limited inventories. Working paper. Fuqua School of Business, Duke University, Durham, NC.

Chen-Ritzo, C.-H. 2006. Availability Management for Configure-to-Order Supply Chain Systems. PhD Dissertation. Pennsylvania State University.

Dietrich, B., D. Connors, T. Ervolina, J.P. Fasano, R. Lougee-Heimer and R. Wittrock. 2005. Applications of Implosion in Manufacturing. In: An, C. and H. Fromm (eds.). Supply Chain Management on Demand. Springer. 97-115.

Dong, L., P. Kouvelis, Z. Tian. 2009. Dynamic pricing and inventory control of substitute products. Manufacturing and Service Operations Management, 11(2), 317-339.

Ervolina, T., M. Ettl, Y.M. Lee and D.J. Peters. 2009. Managing Product Availability in an Assemble-To-Order Supply Chain with Multiple Customer Segments. OR Spectrum, 31, 257-280.

Ervolina, T. and B. Dietrich. 2001. Moving Toward Dynamic Available-to-Promise. In: Gass, S. and Jones. A.T. (eds.) Supply Chain Management Practice and Research: Status and Future Directions. 1-19.

Jordan W., S.C. Graves. 1995. Principles on the benefits of manufacturing process flexibility. Management Science, 41(4), 577-594.

Kök, A.G., M.L. Fisher. 2007. Demand estimation and assortment optimization under substitution: Methodology and application. *Operations Research,* **55**(6), 1001-1021.

Liu, Q., G. van Ryzin. 2008. On the choice-based linear programming model for network revenue management. Manufacturing and Service Operations Management, 10(2), 288-310.

McFadden, D. 1974. Conditional logit analysis of qualitative choice behavior. In: P. Zarembka (ed.), *Frontiers of Econometrics*, Academic Press, New York, NY.

McFadden, D., K. Train. 2000. Mixed MNL models of discrete response. *Journal of Applied Econometrics*, **15**(5), 447-470.

Powell, W. B. 2011. Approximate dynamic programming: Solving the curses of dimensionality. 2nd ed., John Wiley & Sons.

Puterman, M. L. 2005. Markov decision processes: Discrete stochastic dynamic programming. John Wiley & Sons.

Revelt, D., K. Train. 1999. Customer-specific taste parameters and mixed logit: Households' choice of electricity supplier. Working Paper No. E00-274, Department of Economics, University of California, Berkeley, CA.

Yunes, T.H., D. Napolitano, A. Scheller-Wolf and S. Tayur. 2007. Building Efficient Product Portfolios at John Deere and Company. Operations Research 55, 4, 615-629.

I.A. Karimi and Rajagopalan Srinivasan (Editors), Proceedings of the 11th International Symposium on Process Systems Engineering, 15-19 July 2012, Singapore.

Bio-based Value Chains of the Future – An Opportunity for Process Systems Engineering

Wolfgang Marquardt, Andreas Harwardt, Sebastian Recker,
Joern Viell, Anna Voll
AVT–Process Systems Engineering, RWTH Aachen University, 52064 Aachen, Germany

Abstract

This paper argues for a paradigm shift to properly address the requirements of model-based design of future bio-based value chains. Rather than focusing on the process with emphasis on separations and heat integration, the decisions on the molecular level require much more attention. A rough sketch of a systematic sequential and iterative model-based design strategy is presented and illustrated by a few examples related to the manufacturing of future bio-based fuels.

Keywords: Bioeconomy, biofuels, bio-based chemicals, process synthesis, process design, molecular sciences, reaction pathways, reactor synthesis

1. Introduction

Different scenarios have been published recently which predict the depletion of fossil carbon resources for the production of fuels, chemicals and materials in face of the increasing demand of a growing world population. The substitution of fossil by biorenewable carbon feedstock seems to be inevitable to stop the increase of the average surface temperature on our planet by equilibrating global CO_2 binding and release.

The shift from fossil to biorenewable carbon offers a unique opportunity to design new value chains, which are tailored to the feedstock properties while exploring a novel product range (Marquardt et al., 2010). The first opportunity is the exploitation of the rich molecular structure of biomass to the extent possible (Sanders et al., 2007). Rather than breaking its molecular structure into C_1 building blocks, either by gasification to synthesis gas (CO, H_2) or by anaerobic fermentation to a methane-rich gas (CH_4, CO_2, H_2), the synthesis power of nature should be preserved by exploiting and refunctionalizing the native molecular structures in the feedstock into new chemicals, materials and fuels. A second opportunity is the replacement of existing molecular products by novel products of comparable performance in a desired application. Current molecular products contain little oxygen because they are derived from oxygen-free fossil carbon feedstock. In contrast, future bio-based products should contain higher oxygen content to reduce the amount of oxygen to be released during processing as either CO_2 or H_2O. While the former alternative reduces carbon efficiency and contributes to the climate problem, the latter requires large amounts of hydrogen, which has to be produced sustainably.

Such a perspective of the future calls for a radical change in chemical and biochemical catalysis, in the associated process technologies, and in the strategies towards novel molecular and functional products. A holistic systems approach orchestrating experimental and model-based methods and tools across disciplines in a complementary manner offers an enormous potential for sustainable, first-time-right solutions (Bakshi & Fiksel, 2003). Process systems engineering (PSE) is in a perfect position to address

this challenge by *extending its scope* to become a leader in implementing this transition in the next decades. This way, our field can effectively contribute to address the global challenges our society is facing (Glenn & Gordon, 2007).
This contribution will focus on opportunities for *process design and synthesis*. In particular, we will motivate a paradigm shift in process design in Section 2: Rather than taking raw materials, products, reactions and reaction pathways as well as a first process flowsheet for granted, these choices should become part of integrated and rational, ideally model-based decision-making to achieve an optimum in terms of sustainability. Following the PSE tradition, all significant aspects might be cast into an optimization problem which is solved to global optimality. Obviously, model complexity and limitations of numerical optimization methods prevent such a strategy. Rather, decomposition of the multi-faceted design problem is unavoidable to arrive at manageable subproblems. A first sketch of such a strategy is presented in Section 3. A brief outlook on future research needs is finally given in Section 4.

2. Designing bio-based processes – need for a paradigm shift?

Established process design usually starts off when the raw materials and the products have been fixed and a promising reaction pathway has been identified (Douglas, 1988). Stoichiometry and yield of this sequence of reactions fix the material flows from raw materials to target and side products. The given pathway is then translated into a flowsheet consisting of interconnected reactors and unit operations. While flowsheet design is a creative work process largely driven by experience, mass and energy balancing, the choice of suitable unit operations, heat integration or the estimation of cost and expected revenue constitute routine engineering tasks. All these tasks are well-supported by process design software, which is routinely employed in industrial practice. As a consequence of this established approach, process economics is largely determined by the often rational, but typically not model-based selection of the reaction pathway by chemists and the process flowsheet by process engineers. A similar strategy is also followed in process revamping: while aiming, e.g., at an improvement of reaction selectivity and conversion or at the debottlenecking of existing process units the reaction pathway and (basic) flowsheet structure are typically not questioned. Consequently, early design decisions – being often heuristic and experience-based – run at risk to bias the technological development and to miss promising research results in chemistry or process engineering which could enable innovative process concepts.
The history of the Organosolv process for the pretreatment of native biomass as part of future biorefineries can serve as an educating example to underline this argument. Originally invented by chemists as early as 1931 (Kleinert & v. Tayenthal, 1931), this process relies on some aqueous-organic solvent mixture to produce pulp from wood or to fractionate wood into its components lignin, hemicellulose, and cellulose. Despite the continuous improvements to realize environmentally friendly reaction conditions, the concept has been discredited when a pilot plant had to be shut down due to technical and economical deficits in the early 1990s (Hergert, 1998). However, the potential of the Organosolv process as a first step toward the production of bio-based chemicals, materials or fuels from the variety of available lignocellulosic feedstock lead to a revival of this technology. Recent cooperative research has led to an impressing technology readiness level (Michels & Wagemann, 2010), though conceptual process design and model-based analysis have largely been neglected. Consequently, the developed process may still be economically unviable and may face scale-up pitfalls.

Obviously, model-based analysis and scale-up studies carried out prior to building a large-scale pilot plant would reduce the risk of unsatisfactory plant performance which might even jeopardize the success of the biorefinery concept as a whole. Our recent conceptual design study of the Organosolv process has identified significant room for improvement. For example, the energy demand of the costly solvent recovery system can be reduced by heat integration by 89 % (Viell et al., 2012). An economic analysis shows that the improved process can be profitably operated even at capacities well below that of current world-scale plants. Still, our systematic analysis identifies serious deficits inherent to the Organsolv process, such as large solvent streams and a high energy demand of the separation system. While the latter can be tackled by yet not fully exploited heat integration, the efficiency of the Organosolv process is still much lower than that of fossil refinery processes.

Radical improvement might be materialized, if tailored solvents and reaction media are employed to facilitate innovative process concepts off the beaten track. For example, a biphasic aqueous-organic electrolytic solvent system could be chosen to facilitate lignocellulose fractionation solvent recovery in an integrated process (vom Stein et al. 2011). Such a concept encourages integrated reaction and separation in a single unit which constitutes the core of a highly integrated pulping process. Unfortunately, the reaction mechanisms and kinetics of this and related biomass pretreatment processes are not yet adequately understood to support model-based design. Intensive research is required to unveil new promising mechanisms for wood pretreatment, such as chemical disintegration and fractionation by means of ionic liquids (Viell & Marquardt, 2011) or by their mixtures with molecular solvents (Rinaldi, 2011).

This example motivates that an innovative formulation of the process design problem should not only address reaction, separation and recycling strategies on the flowsheet level, but should rather include decision-making on the molecular level (e.g., Bardow et al. (2010)). Such extended design strategies not only require intense collaboration between chemists and process engineers, but also a shift in the research agenda to overcome inherent methodological limitations. For example, complex reaction chemistry and phase behaviour (i.e., organic-aqueous electrolyte mixtures or non-aqueous electrolyte systems with various dissolved macromolecular species) cannot yet be described by available property models at desirable accuracy. Moreover, experiments have to be carried out to allow for quantitative (reaction kinetics) modelling, following for example, the concept of model-based experimental analysis (Marquardt, 2005).

3. Toward an incremental strategy for integrated design of value chains

State-of-the-art process design focuses on the degrees of freedom available after the reaction pathway has largely been fixed. Such an approach will inevitably miss the true potential buried in the reaction (sequence), catalyst systems and reaction solvents. Though integration of chemistry- and process-related decision-making practiced in industry to some extent, systems-oriented methods and tools are largely lacking. Rather, design problems are currently often approached pragmatically, hence, running at risk to miss truly innovative solutions as demonstrated by example in the previous section.

The predicted manifold capacity increase in chemical industries and the advent of bio-based value chains emphasize the necessity to integrate process and molecular level decision-making. Rather than waiting for the “pull” of the evolving bioeconomy and applying established, but inadequate design methodologies, researchers in PSE should shift their attention and develop appropriate methodologies which systematically

address molecular degrees of freedom in addition to those on the process level. Due to the complex nature of biobased raw materials as well as the increasing importance of sustainability, decisions on the most promising reaction steps and pathways, on proper compartmentalization of reactions, on efficient catalysts and reaction solvents, on non-standard (often multi-phase) reactor systems, and on an integration of reaction and separation in either a single multi-functional unit or in non-standard reaction-separation flowsheet structure have to be routinely addressed during design. Such an extended scope of systematic, model-based process design and optimization results in a design problem of unprecedented complexity, because it spans multiple scales from the molecular level to the level of the process, the site or even the complete value chain. Since an "all-in-one" formulation and model-based solution of such a design problem does not seem to be tractable, an incremental strategy is suggested to comprehensively address the requirements of designing future bio-based value chains.

The proposed concept assumes given raw material and target product molecules, though product and raw material design could be integrated into process design. The design problem is addressed here on three levels: the reaction, the device and the flowsheet level. The decision on a reaction pathway on the *reaction level* is based on a material-flow analysis of a set of promising pathways through a network of chemical compounds linking raw materials and target products. The reactions (and material flows) are not yet associated to a "physical" reaction compartment. This decision constitutes the first step of the *device level*, where a reaction kinetic model is used to decide on a network of reaction compartments to refine the yield-based approach employed on the reaction level. At the same time, the number and interconnection of reaction and separation subsystems is determined for specified target split factors and/or recoveries. In a second step, separation system variants are generated and evaluated for feasibility and effort using shortcut methods. This decision making process results in a spatially resolved allocation of the reaction or separation tasks to a device in the spirit of task-based design (Menon et al., 2007), thus proposing a first flowsheet configuration. The realization of the devices in concrete pieces of equipment and their connectivity to a process flowsheet are decided on *the flowsheet level*. Major equipment design parameters are optimized rigorously by minimizing total annualized cost subject to mass and energy balances and rigorous physical property and reaction kinetic models.

On each level, the number of possible alternatives is reduced, while the degree of detail is refined in order to obtain a sustainable process, thus generalizing the process synthesis framework of Marquardt et al. (2008) to reaction-separation processes. Furthermore, the uncertainties on the different levels are addressed systematically by propagating available results to the following more detailed steps. Since assumptions in a previous step may be disproved in a subsequent step, iterations are not only unavoidable but also desirable. The incremental refinement and improvement can be stopped once the postulated design targets are fulfilled.

In the following, the individual design levels and their relations are introduced and sketched from a methodological perspective. They are illustrated in parallel by means of exemplary design problems arising in the context of designing a process for the production of the novel biofuel candidate 2-methyltetrahydrofuran (2-MTHF).

3.1. Reaction level

The objective on the reaction level is to assess possible reaction pathways for the molecular transformation of a given raw material to a desired molecular product from a process perspective. Relevant design decisions are pointed out, including the selection of (a few) favourable pathways for a more detailed analysis regarding energy and raw

material demand, carbon footprint, product yield and selectivity or production cost. Consequently, the reaction level is designed to link the traditional areas of bio-/chemo-catalysis and conceptual process design, thus bridging the disciplinary gap between chemistry and process engineering. This early design stage is characterized by many reaction pathway alternatives and, at the same time, by very little data on reactions and fairly uncertain property predictions. Under these circumstances, the use of established conceptual process design methods is not only very time-consuming, if possible at all, but also not very informative in face of the lack of valid information on reactions, material properties and process performance. To reduce the reaction pathway alternatives to a manageable number, fast screening methodologies are required to accomplish a first crude characterization of the target production process. Even though the analysis of large reaction networks is well established in metabolic pathway analysis (Varma & Palsson, 1994), and the design of reaction networks in the context of chemical synthesis has been discussed for a long time (e.g., Mavrovouniotis & Bonvin (1995) or Broadbelt et al. (2004)), systematic screening strategies for the assessment of reaction pathways in the context of process design are still scarce, but have received some attention recently in the context of biorenewables processing (Cherubini & Stromman, 2010; Pham & El-Halwagi, 2011).

Motivated by metabolic pathway analysis and by the challenges of designing innovative bio-based value chains, a novel reaction scouting method called "Reaction Network Flux Analysis" (or RNFA for short) has been developed to assist model-based selection of promising reaction pathways in the early stage of process design (Besler et al., 2009, Voll & Marquardt, 2011). All relevant reactions are summarized in a network including all known reaction alternatives in the sense of a superstructure such that stoichiometric material balances can be formulated for all the substances to result in a set of linear equations. This basic model can be extended by yield constraints or by selected performance models to predict, for example, the overall product yield, the use of main and auxiliary reactants such as H_2, or the formation of (undesired) by-products such as CO_2 or H_2O. It is also possible to estimate indicators for investment and operating cost or for process sustainability such as carbon or energy efficiencies and environmental impact without having completed the process design process. The promising reaction pathways can be found as the multiple solutions of a mixed-integer optimization problem which minimizes or maximizes a given objective function reflecting multiple selected performance criteria. Finally, the different reaction pathways can be compared according to even additional evaluation criteria. The analysis not only reveals most promising pathways, but also identifies single reaction steps which have tremendous impact on performance and hence require further attention – either in the following investigation on the device level (to reduce uncertainty in the assumptions on yield or selectivity) or in catalysis research (to search for catalyst systems with higher turnover number).

The RNFA methodology has recently been used to evaluate reaction networks for the production of 10 novel biofuel candidates and to compare them to those of more common biofuels like ethanol or butanol (Voll & Marquardt, 2012). Assuming that the same amount of fuel energy should be produced by each pathway, a multi-objective optimization problem accounting for environmental impact and total annualized cost has been solved for each fuel candidate to identify the most competitive fuel product and corresponding reaction pathways. This model-based screening suggests 2-MTHF as a target biofuel and the pathway shown in Fig. 1. Starting from glucose, 2-MTHF can be synthesized via hydroxymethylfurfural (HMF) and levulinic acid (LA) followed by a

sequence of hydrogenation and dehydration reactions (Geilen et al., 2010). According to lab experience, the reaction pathway can be subdivided into two reaction systems, namely A for converting glucose to LA and B synthesizing 2-MTHF from LA. The yield of the acid-catalysed reaction system A limited by decomposition of glucose and HMF to humines. The reaction forming 2-MTHF is catalyzed by a ruthenium-based catalyst with a triphos-ligand and a p-toluene sulfonic acid additive. Selectivity towards 2-MTHF is high at 95%, with pentanol being the major by-product. The aqueous-organic mixture exhibits a miscibility gap, which can be exploited for separation. However, a simple liquid-liquid phase split does not result in the product purity, because the water produced in the dehydration has to be completely removed from 2-MTHF for fuel application.

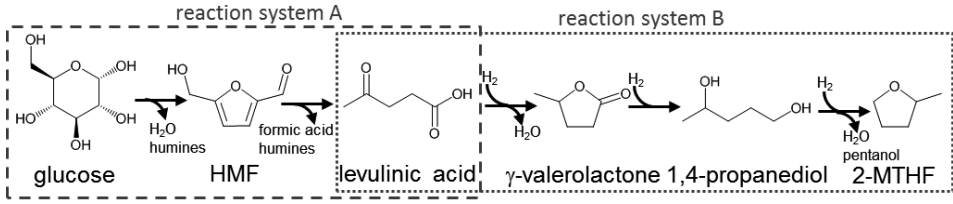

Figure 1: Reaction pathway for the production of 2-methyltetrahydrofuran

3.2. Device level

The goal on the device level is to close the gap between the reaction level and the flowsheet level by evaluating the assumptions made on the reaction level, optimizing the reactions, deciding on reaction compartments, and validating the feasibility of the chosen separation strategies. The result of this step is a network of *devices* which assign an abstract reaction or separation task to a physical compartment without deciding on its technical realization. This is similar to the first steps of the (heuristic) hierarchical framework for conceptual design introduced by Douglas (1988). In particular, the Douglas methodology starts with clustering the reactions of the network into groups of reactions which can take place in the same *reaction device*. Starting from the results obtained on the reaction level, a single or a set of contiguous reaction steps is mapped to an *"elementary process"* (using the terminology of Douglas). The result is a partial decoupling of the reaction pathway into sequences of reactions carried out in individual *reaction devices*, which are possibly structured into *reaction compartments*, and which are typically separated by *separation devices*. While reaction compartments are modeled by well-mixed, homogeneous volume elements, the separation devices are represented by splitters with given target split factors. Although such modular frameworks have been suggested before in process synthesis (Papalexandri & Pistikopoulos (1996) and later work), they either restrict the achievable product composition to reaction equilibrium (Ismail et al., 2001) or they use superstructure-based methods to account for different flowsheet options (Linke & Kokossis, 2003).

For an assessment of the validity of the assumptions on the reaction level regarding reaction yield and selectivity, for the optimal choice the reaction conditions and for the decision on the network of reaction and separation devices, a classical mass-exchange network is used to model the interconnections of the reaction and separation devices. Each reaction device is structured and represented by a network of reaction compartments, which is subject to structural optimization. There are various possible formulations to derive candidate networks of interconnected reaction and separation devices. For example, Peschel et al. (2010) uses the concept of elementary process functions. A fluid element is tracked on its way along a (spatial or temporal) reaction

coordinate. During its travel, the state of the fluid element defined by concentrations, temperature, and pressure, for example, can be manipulated by reaction and heat and mass transfer fluxes. Thus, an optimal state trajectory of the element in thermodynamic state space can be decided. An analysis of this trajectory provides insight into the choice of promising device networks. While largely neglecting the separations, Peschel et al. (2010) decide on the type of reactor system by experience and refine it by a model-based approach. In contrast, we prefer to use nonlinear programming to first decide on the compartment structure of a reaction device embedded in a postulated network of reaction and separation devices (Recker & Marquardt, 2012). This way, reaction device performance can be assessed at an optimal operating point accounting for relevant external (feed and effluent) streams without fixing the type of reactor a priori.

Deciding on the internal structure of each reaction device requires knowledge about the kinetics of the reactions in the relevant part of the pathway including undesired side reactions. Hence, in contrast to the reaction level, a number of decisions regarding molecular transformations have to be fixed to allow postulating a likely reaction mechanism, which is a prerequisite for reaction kinetic modeling. Consequently, reaction solvent selection, catalyst design, reaction kinetic experiments as well as reaction kinetic modeling have to be carried out before the calculations on the device level become possible. The objective used for deciding on the compartment network of the reaction device can be the same as the one employed in RNFA. Then, the results obtained on the device level (for possibly different chemistries) can be abstracted into yields, which may be fed back to the reaction level to repeat the RNFA with refined assumptions to revise the rating of the reaction pathway alternatives.

The described approach has been used to structure the reaction device implementing the elementary process A from glucose to LA in Fig. 1 using reaction kinetics and side reactions of an acid-catalyzed pathway proposed by Girisuta et al. (2007). A single compartment is found to constitute the optimal device structure, because the rates of the side reactions are an order of magnitude slower than those of the main reactions. The elementary process exhibits a yield of 77 %, which is beyond the yields reported in literature (Huber et al., 2006) and assumed in RNFA analysis on the reaction level.

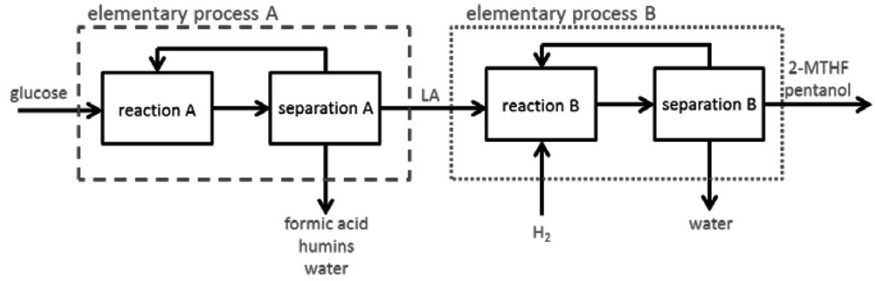

Figure 2: Device network for the production of 2-MTHF

After a device network of the process has been optimized assuming ideal separation (see Fig. 2 for 2-MTHF process), the thermodynamic and economic feasibility of the separations have to be investigated. Candidate separation sequences are constructed (manually) based on insight into the thermodynamic mixture behavior and process specifications. Separation sequence alternatives can efficiently be rated by means of shortcut methods. The separation is always analyzed in combination with the structured reactor device to properly handle the coupling of reaction and separation. Exemplarily, the separation system for elementary process B is designed to separate 2-MTHF from

the reactor effluent containing water, pentanol and 2-MTHF (cf. Fig. 2). Three different flowsheet variants have been created based on a thermodynamic analysis of the mixture and have been screened using the feed pinch shortcut method of Kraemer et al. (2010).

3.3. Flowsheet level

The device structure determined on the device level is the starting point for the development of candidate flowsheets and their rigorous optimization on the flowsheet level. Consequently, the network of separation and reaction devices is refined to a process flowsheet constituting of concrete concrete reactors and unit operations. In particular, the structured reactor device has to be mapped to concrete reactors and the separation sequences have to be detailed with respect to their technical realization. The large number of structural and continuous degrees of freedom cannot be adequately addressed by heuristic rules, process simulation and sensitivity analysis (Barnicki & Siirola, 2004). Therefore, the promising sequences are optimized by means of deterministic mixed-integer optimization minimizing total annualized cost. Each of the separation variants is detailed by a superstructure to capture additional technical detail, for example the number of trays and the feed and sidestream trays in a distillation column (Viswanathan & Grossmann 1990) which is part of the separation sequence. A similar approach could be used to detail the design of the reactor systems.

The mixed-integer optimization problem can robustly be solved by employing the results from shortcut evaluation on the device level for efficient initialization and by its reformulation into a continuous optimization problem (Kraemer et al., 2009). Still, these difficult problems can only be solved if robust formulations and solution strategies are available. For example, the switching from two to three phases on the trays in heteroazeotropic distillation has been tackled successfully only recently (Skiborowski et al., 2012) by tailored sequential and simultaneous optimization strategies. All models used on the flowsheet level rely on rigorous property prediction models in addition to reaction kinetic models. Since model parameters are often not available to predict the behaviour of the complex mixtures arising in biorenewables processing, the missing parameters have to be determined experimentally or need to be estimated by some computational chemistry approach such as molecular dynamics, CosmoRS, group contribution methods or quantitative structure-property relationships.

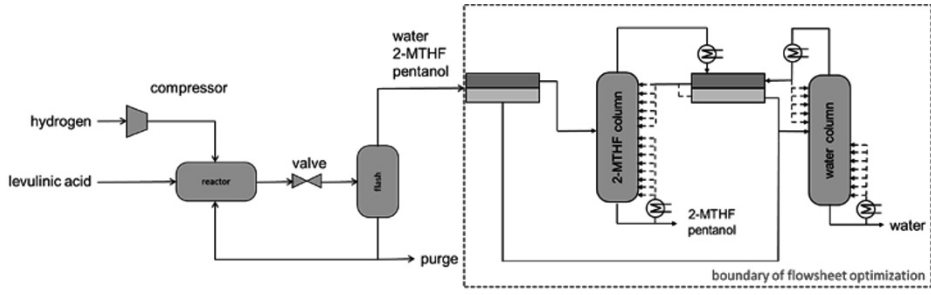

Figure 3: Process flow diagram with superstructure for the optimization of the 2-MTHF purification

The most promising flowsheet variant found on the device level for elementary process B (cf. Fig. 1) consists of two decanters and two distillation columns; the corresponding superstructure is shown in Fig. 3. The vaporous reactor effluent is first condensed and split into two liquid fractions, each of which is fed to a distillation column. In both columns, the product is withdrawn at the bottom at high purity. The composition at the top corresponds to the vapour line of the miscibility gap, which starts at the minimum

boiling heteroazetrope of 2-MTHF and water. Rigorous mixed-integer optimization is used to minimize for total annualized cost by fixing the column designs and the operating point. A total energy demand of about 2.6% of the energy content of the fuel (Geilen et al., 2010) was determined for the cost-optimal design. The cost of separation can further be reduced by heat integration. In particular, recompression of the top vapour can be used to provide the heat of vaporization, which allows for a reduction of 75% in energy demand and of 54% in cost. Hence, the resulting energy demand is an order of magnitude lower than that of bioethanol production (Vane, 2008).

4. Conclusions

This paper presents a first and rough sketch of a process design methodology which extends the scope of traditional PSE from decision-making on the flowsheet to the molecular level in order to address the multiple and often competing objectives of sustainability in the emerging bioeconomy. The extended scope of process design introduces a number of complications, including the need of improved models to predict molecular phenomena, which can be integrated into reactor system and flowsheet design as well as proper formulations of the multi-scale and multi-objective decision-making problem. Since a direct solution of the design problem will not be possible, decomposition and iterative refinement of promising alternatives for the subproblems become mandatory. As always, decomposition runs at risk to miss important interdependencies. This trade-off between the desired holistic treatment and the inevitable decomposition of the design problem as well as the existing limitations of model-based design approaches will constitute the major future research challenges. Interdisciplinary cooperation between PSE and the molecular sciences seems to be a key to success, because truly innovative process solutions are typically initiated on the molecular level. Vice versa, the tradition of quantification in PSE has to offer a lot to the exploratory research in the molecular sciences. In particular, model-based approaches can provide focus and orientation in the discovery process to systematically track down the truly golden “needles in the haystack”.

Acknowledgements

This work was performed as part of the Cluster of Excellence “Tailor-Made Fuels from Biomass”, which is funded by the Excellence Initiative by the German federal and state governments to promote science and research at German universities and by the European Community’s Seventh Framework Programme [FP7/2007-2013] for SYNFLOW under grant agreement n° NMP2-LA-2010-246461.

References

B. R. Bakshi, J. Fiksel, 2003, The quest for sustainability: Challenges for process systems engineering, AIChE Journal, 49, 1350-1358

A. Bardow, K. Steur, J. Gross, 2010, Continuous molecular targeting for integrated process and solvent design, Ind. Eng. Chem. Res.. 49, 2834–2840

A. Besler, A. Harwardt, W. Marquardt, 2009, Reaction networks – A rapid screening method, In: J. Jeszowski, J. Thullie (Eds.) Proc. 19th European Symposium on Computer Aided Process Engineering, Elsevier, 243-248

L. Broadbelt, J. Pfaendtner, 2005, Lexicography of kinetic modeling of complex reaction networks, AIChE Journal, 51, 8, 2112 – 2121

F. Cherubini, A. Stromman, 2010, Production of biofuels and biochemicals from lignocellulosic biomass: Estimation of maximum theoretical yields and efficiencies using matrix algebra, Energy Fuels, 24, 4, 2657–2666

J. M. Douglas, 1988, Conceptual Design of Chemical Processes, McGraw-Hill, New York
F. Geilen, B. Engendahl, A. Harwardt, W. Marquardt, J. Klankermayer, W. Leitner, 2010, Selective and flexible transformation of biomass-derived platform chemicals by a multifunctional catalytic system, Angew. Chem., 49, 5510-5514
B. Girisuta, L. P. B. M. Janssen, H. J. Heeres, 2007, Kinetic study on the acid-catalyzed hydrolysis of cellulose to levulinic acid. Ind. Eng. Chem. Res., 46, 1696-1708
J. C. Glenn, T. J. Gordon, 2007, State of the Future, the Millennium Project. United Nations Publications
H. L. Hergert, 1998, Developments in Organosolv pulping – An overview, In: R. A. Young, M. Akhtar (Eds.), Environmentally Friendly Technologies for the Pulp and Paper Industry, 5-68
G. W. Huber, S. Iborra, A. Corma, 2006, Synthesis of Transportation Fuels from Biomass: Chemistry, Catalysts, and Engineering, Chem. Rev., 106, 4044-4098
S. R. Ismail, P. Proios, E. N. Pistikopoulos, 2001, Modular synthesis framework for combined separation/ reaction systems. AIChE Journal, 47,3, 629-649
T. Kleinert, K. v. Tayenthal, 1931, Über neuere Versuche zur Trennung von Cellulose und Inkrusten verschiedener Hölzer, Angewandte Chemie, 44, 788-791
K. Kraemer, S. Kossack, and W. Marquardt, 2009, Effficient optimization-based design of distillation processes for homogenous azeotropic mixtures. Ind. Eng. Chem. Res., 48, 14, 6749–6764
K. Kraemer, A. Harwardt, M. Skiborowski, S. Mitra, W. Marquardt, 2011, Shortcut-based design of multicomponent heteroazeotropic distillation. Chem. Eng. Res. Design, 89, 8, 1168 – 1189
P. Linke, A. Kokossis, 2003, Attainable reaction and separation processes from a superstructure-based method. AIChE Journal, 49, 6, 1451-1470
W. Marquardt, 2005, Model-based experimental analysis of kinetic phenomena in multi-phase reactive systems, Chem. Eng. Res. Design, 83, 561–573
W. Marquardt, S. Kossack, K. Kraemer, 2008, A framework for the systematic design of hybrid separation processes, Chin. J. Chem. Eng., 16, 3, 333–342
W. Marquardt, A. Harwardt, M. Hechinger, K. Kraemer, J. Viell, A. Voll, 2010, The biorenewables opportunity - toward next generation process and product systems, AIChE Journal, 56, 2228-2235
M. Mavrovouniotis, D. Bonvin, 1995, Towards design of reaction pathways, AIChE Symposium Series, 304, 91, 41-51
A. R. Menon, A. A. Pande, H. J. M. Kramer, P. J. Jansens, J. Grievink, 2007, A task-based synthesis approach toward the design of industrial crystallization process units, Ind. Eng. Chem. Res., 46, 3979-3996
J. Michels, K. Wagemann, 2010, The German lignocellulose feedstock biorefinery project, Biofuels Bioproducts & Biorefining 2010, 4, 263–267
K.P. Papalexandri, E.N. Pistikopoulos, 1996, Generalized modular representation framework for process synthesis. AIChE Journal, 42, 4, 1010-1032
V. Pham, M. El-Halwagi, 2011, Process synthesis and optimization of biorefinery configurations, AIChE Journal, doi: 10.1002/aic.126040
A. Peschel, H. Freund, K. Sundmacher, 2010, Methodology for the design of optimal chemical reactors based on the concept of elementary process function. Ind. Eng. Chem. Res., 49, 10535-10548
S. Recker, W. Marquardt, 2012, A nonlinear programming approach to conceptual design of reaction-separation systems, In: I. D. Lockhart Bogle, M. Fairweather (Eds.), Proc. 22nd European Symposium on Computer Aided Process Engineering, in press
R. Rinaldi, 2011, Instantaneous dissolution of cellulose in organic electrolyte solutions, Chemical Communications, 47, 511-513
J. Sanders, E. Scott, R. Weusthuis, H. Mooibroek, 2007, Bio-refinery as the bio-inspired process to bulk chemicals, Macromolecular Bioscinece, 7, 105-117
M. Skiborowski, A. Harwardt, R. Hannemann, K. Kraemer, W. Marquardt, manuscript in preparation
L. M. Vane, 2008, Separation technologies for the recovery and dehydration of alcohols from fermentation broths. Biofuels, Bioproducts and Biorefining, 2, 6, 553–588.
A. Varma, B. Palsson, 1994, Metabolic Flux Balancing – Basic concepts, scientific and practical use, Bio-Technology 12, 10, 994-998
J. Viell, W. Marquardt, 2011, Disintegration and dissolution kinetics of wood chips in ionic liquids, Holzforschung, 65, 519-525
J. Viell, A. Harwardt, J. Seiler, W. Marquardt, 2012, manuscript in preparation
A. Voll, W. Marquardt, 2011, Reaction network flux analysis: Optimization-based evaluation of reaction pathways for biorenewables processing, AIChE Journal, doi: 10.1002/aic.12704
A. Voll, W. Marquardt, 2012, Benchmarking of next-generation biofuels from a process perspective, Biofuels, Bioprod. Bioref., doi: 10.1002/bbb.1325
T. vom Stein, P.M. Grande, H. Kayser, F. Sibilla, W. Leitner, P. Dominguez de Maria, 2011, From biomass to feedstock: one-step fractionation of lignocellulose components by the selective organic acid-catalyzed depolymerization of hemicellulose in a biphasic system, Green Chemistry, 13, 1772-1777

I.A. Karimi and Rajagopalan Srinivasan (Editors), Proceedings of the 11th International Symposium on Process Systems Engineering, 15-19 July 2012, Singapore.

Process Systems Engineering: Quo Vadis?

G V Rex Reklaitis [a]

[a]*Purdue Univeristy, West Lafayette IN, USA*

Abstract

Process systems engineering, which in content if not in title has a history almost as old as the chemical engineering discipline itself, can rightly be proud of having had a remarkable and sustained impact on the chemical and related industries. Model based methodologies for process design, process control and operations have become firmly imbedded in industrial practice world-wide, with focused teams regularly applying these approaches and tools in virtually all major CPI corporations (Stephanopoulos and Reklaitis, 2011). Within academic environments, instruction in process design and control likewise was firmly embedded as a core part of the chemical engineering curriculum, beginning in the mid 60's. However, in the 90's through the early years after the turn of the century, this core gradually eroded, especially in US universities. While the US ABET criteria continue to emphasize that the chemical engineering curriculum should" enable graduates to design, analyze, and control physical, chemical, and biological processes", many departments gradually lost the in-house capabilities to provide the appropriate process engineering educational experience, have relied on adjunct faculty to meet those critical needs, and in some cases have simply scaled-back in delivering this educational experience. This was on the one hand driven by exciting developments in nanoscale materials and applied biological sciences and growth in associated research funding which stimulated departments to add faculty who could contribute to such efforts. On the other hand, declines in available research funding for PSE methodology from US R&D funding agencies coupled with reduction of industrial support for academic research in PSE areas, at least in part as a result of reduced capital investments within the developed world, caused departments to see PSE faculty candidates as less attractive contributors to the departmental research funding portfolio. Accordingly, faculty numbers in PSE declined while industry demand for engineers trained in PSE was sustained in part as a result of the needs in associated industries such as semiconductors and pharmaceuticals.

However, in the past five years, the rising cost of petroleum and associated increasing cost of transportation fuels and core chemical building blocks, the mounting shortages of potable water in many parts of the world , and the concerns to at least restrain the growth of CO2 in the atmosphere, have driven a resurgence of research in process innovations, such as in technologies to exploit renewable energy sources and in the invention of process pathways towards biologically sourced organic chemical building blocks. In parallel, the healthcare needs of the aging populations of the developed economies and burgeoning healthcare needs of developing economies that required cost-effective solutions, have stimulated research and developments in products and processes for meeting those needs. Most recently, the economic downturn and loss of manufacturing jobs in the developed countries have awakened governments to the importance of advanced manufacturing to their economies both in terms of economic output and in creation of good quality jobs. These factors have impacted demands for PSE trained graduates both from industry and increasingly to staff university departments. It thus seems that the scene has been set for a period of growth in the PSE discipline.

In parallel with these economic drivers, the enabling technologies on which the PSE discipline can build its model-based applications have also seen tremendous growth in capabilities and scope. Four major technology drivers of particular note are massive low cost data storage, cheap and powerful computing, near universal connectivity and innovative multimode man-machine interfaces. The PSE community is already exploiting this growth in power to address large scale process problems. We are seeing applications such as the dynamic grade change optimization of a chemical plant in which the optimization formulation involves some 6+ million differential algebraic equations (Hartwick and Marquardt, 2010) and integrated production planning and scheduling applications involving tens of thousands of discrete variables (Grossmann, 2012). An important and interesting question is where can and will these capabilities take us in the next decade?

It can be predicted with certainty that PSE algorithms and tools will be enhanced to take advantage of computing and data management capabilities. Global optimization and treatment of stochastic decision problems certainly are among the methodology domains of highest potential and need. For instance, such decision problems readily arise in product development pipeline management which involve large scale multi-stage stochastic decision problems of very challenging dimensions (Lainez et al., 2012). Certainly the capabilities to store, manage and access Big Data, developments in which science applications in biology and physics have dominated to date, will allow the PSE community to effectively exploit massive process and product historical data to better model process and product performance but also to better understand and mitigate abnormal process behavior along the lines advanced by Seider and coworkers to extract, characterize and learn from process near misses (Pariyani et al 2012). The management of the information, models and knowledge, which constitute the intellectual capital of an enterprise is another area of great potential. For instance, effective knowledge management over the life cycle of pharmaceuticals is recognized as central to the quality by design process promulgated by the FDA (Junker et al 2011). While the financial and commercial worlds are already exploiting wireless connectivity and highly intuitive graphical interfaces that use visual, tactile and audio inputs and outputs to support real time distributed decision making, there is tremendous promise for applications to real time process management, extending from the plant to the supply chain.

These technologies will also allow considerable expansion of the scope of PSE problems that it will be possible to attack, ranging from design and operation of smart manufacturing systems and enterprise-wide decision support systems to socio-technical systems such as regional power and water distribution grids. Such expansions in temporal and special dimensions will be matched by PSE support for modeling and design synthesis at micro and nano scales in biological and materials applications. It is interesting to speculate whether the PSE community can establish a valued role in these application domains where scientific discovery is the driver but PSE support tools and analysis are needed to support and guide that discovery process. Developments in the discovery, manufacture and delivery of medicines for personalized treatment and developments of innovative chemical pathways to the processing biologically derived feedstocks, both of which require multiscale approaches spanning the molecular to the process scale, seem to offer significant promise challenge.

In this paper we will offer speculations and predictions on such future directions along with opinions on prospects for success and impact. It certainly seems that the PSE area of chemical engineering is on an exciting path towards reestablishing its central role in chemical engineering.

References

I. Grossmann, "Advances in Mathematical Programming Models for Enterprise-wide Optimization", FOCAPO 2012, Savannah, GA, January 8-11, 2012.

A. Hartwich and W. Marquardt, "Dynamic optimization of the load change of a large-scale chemical plant by adaptive single shooting", Comp.& Chem.Engr, 34, 1873–1889 (2010)

J. M. Laínez-Aguirre, E. Schaefer, and G. V. Reklaitis," Challenges and Opportunities in Enterprise-wide Optimization in the Pharmaceutical Industry", FOCAPO 2012, Savannah, GA, January 8-11, 2012.

B. Junker, G. Maheshwari, T. Ranheim, et al., "Design-for-Six-Sigma To Develop a Bioprocess Knowledge Management Framework", PDA J Pharm Sci and Tech 65 140-165 (2011)

A. Pariyani, W. D. Seider, U.G.Oktem and M.Soroush, "Dynamic Risk Analysis Using Alarm Databases to Improve Process Safety and Product Quality: Part I—Data Compaction", AIChE J, 58, 812-825 (2012)

G. Stephanopoulos, and G.V. Reklaitis, "Process systems engineering: From Solvay to modern bio- and nanotechnology. A history of development, successes and prospects for the future", Chem Eng Sci 66, 4272-4306 (2011)

I.A. Karimi and Rajagopalan Srinivasan (Editors), Proceedings of the 11th International Symposium on Process Systems Engineering, 15-19 July 2012, Singapore.

Process Intensification in Water and Wastewater Treatment Systems

Yatin Tayalia[a] and Vijaysai P[b]

[a]*Regional Product Sales Manager – Asia Pacific, GE Power & Water, Singapore*
[b]*Engineering Manager, GE Power & Water, GE ITC Pvt.Ltd. Bangalore, India*

Abstract

Demand for fresh water is continuously growing worldwide and more than half of the world would be under water stress by 2015 [1]. As the gap between available fresh water and demand widens, the current water and wastewater treatment technologies are challenged to treat tougher waters and meet stringent environmental regulations at affordable cost. Conventional treatment technologies have been successful within limits of feed water quality, contaminant removal efficiencies, recoveries and treatment cost. However, to manage this global crisis, a holistic approach to water treatment needs to be adopted to provide a robust and cost effective solution for lot more demanding requirements. This paper focuses on key trends in water treatment technology, from both the component and system design perspective that significantly impact the total solution and ability to meet the overall requirements. Also specific developments in desalination and wastewater treatment technologies like Reverse Osmosis, Ultrafiltration, energy recovery devices and Membrane bioreactors are discussed that have significantly widened the capability envelope. An integrated multi-scale approach to system design leveraging various technologies can provide the viable alternatives and meet this global challenge in sustainable way.

Keywords: Process Intensification in water, Novel water solution, Cost of water, Evolution in water technology

1. Introduction

Water quality and quantity issues are certainly one of the biggest challenges that the world is facing at present. Water consumption is constantly increasing and has increased six times in the last 100 years and is expected to double again by 2050 [1]. Population growth, rapid industrialization and urbanization have been key factors driving increase in consumption. There are 1.2 billion people who live in regions experiencing water scarcity, and the situation is expected to worsen for individuals as well as companies which operate in many emerging economies. To make situation worse, water quality of surface water and aquifers has deteriorated in certain regions due to indiscriminate discharge of wastewater without adequate treatments. Environmental regulations pertaining to water discharge and usage are becoming tighter. Both, drinking and wastewater infrastructure either are ageing or require new development in most part of the world. The multitude of water related issues means water industry has to do more with less.

Traditional water treatment approaches are not able to meet afore mentioned growing needs and there is need to look beyond conventional methods of water treatment [2]. The new approaches should either be able to treat more contaminated water as source, or allow alternative sources of water with increasing salinity at affordable cost, or treat

tougher wastewater to meet discharge standards and to reuse. These should also be able to work without ageing or non-existent infrastructure like point-of-source supply, point of discharge and point-of-use systems. The management of this global crisis requires a holistic approach to water treatment solution that is more robust and cost effective for growing requirements.

Process Intensification is an innovation strategy that has greatly benefitted process industry in making the process more efficient, safer, flexible, smaller, cheaper and more environment-friendly [3]. It defines a holistic approach starting with an analysis of economic constraints followed by the selection or development of a production process.. Process intensification also aims at taking a systemic approach towards performance improvements of each process. In a few words, this strategy aims to "Produce much more with much less" [4] for more sustainable industrial processes. This in the context of water treatment industry could mean reducing energy consumption, increasing recovery, reducing the foot-print, reducing the waste or even generating the value from the waste, more flexible processes that meets varying feed water qualities, shorter time to market, lower lifecycle costs or combination of these objectives.

This paper essentially seeks to address the relevance and realization of process intensification in water and waste water treatment at various levels including development of new materials, equipment design and plant design. It also discusses cases of successfully commercialized technologies that demonstrate the paradigm shift in designing water treatment solutions. Within this context, the process intensification in following five categories is discussed:

(1) Surface Water Treatment
(2) Desalination
(3) Wastewater Treatment and Reuse
(4) Waste to Value
(5) Zero Liquid Discharge

2. Surface Water Treatment

Surface water like river or reservoir water is increasingly used in the production of potable water or industrial process water. Surface water is characterized by high degree of suspended solids and microbial contamination [4]. A conventional surface water treatment plant comprises of a multi-step process based on physico-chemical processes including screen-filtration, ozonisation, coagulation and flocculation, sedimentation, media filtration, and usually disinfection as a last step. The process is fairly complex and each step of this process has to be controlled to get an optimal performance of the overall process. The use of chemicals like ozone, flocculants, hydrogen peroxide, lime and chlorine requires special precautions for safety purposes [5]. As the surface water quality gets further deteriorated, the conventional process is really limited in its ability to meet treated water specifications. Recent advances in Ultra Filtration (UF) have enabled direct filtration of surface water after a course filtration step without cost intensive pretreatment [6, 23].

It is to be noted that conventional media filtration worked on the basic principle of depth filtration while ultrafiltration works on the principle of surface filtration. The term ultrafiltration is used to describe a membrane filter, ideally with a pore size of 100 nanometers or less [6]. This is smaller than bacteria, rejecting virtually all non-dissolved particles on its surface. They have capability to produce 6 log reductions in bacteria and considerable reduction in viruses too.

The UF membrane filtration process provides several advantages such as superior quality of water and ease of operation over the conventional process. Simplicity in the process allows automation to be effective. Furthermore, fluctuations in the demand and changing river water quality can be managed through modular construction, offering higher degree of flexibility. Except for cleaning of membranes, excessive use of chemicals is avoided thus enabling significant reduction in residues and by-products. The ultrafiltration also serves to reduce the risk of biofouling and particulate fouling in subsequent operations such as nano-filtration and reverse osmosis. A more efficient performance of UF is also complemented with the reduced foot print of the plant, which is primarily achieved through elimination of large settling tanks. .

Large plants are most often managed by well trained and qualified engineers, which is seldom the case with decentralized facilities and remote areas [7]. Fully automated UF systems aptly fit into these conditions and their reliability could further be improved through remote monitoring and diagnostics.

Ultrafiltration Plants are also increasingly used for retrofitting existing conventional drinking water plants that demands higher capacity within existing footprint, or as a decentralized water treatment solution

The increased usage of Ultrafiltration for surface water treatment for industrial and municipal applications with above mentioned benefits is a great example of process intensification in water treatment.

3. Desalination

Desalination through membrane processes represents one of the unique successes in water treatment technology and is probably one of the distinct examples today of the success of process intensification in the water industry..

Seawater and saline aquifers account for 97.5% of all water on the Earth. Hence capturing even a tiny fraction could have a huge impact on water scarcity. Until recently, seawater desalination was only limited to desert areas like Middle East but now it has expanded its use in coastal areas owing to all technological developments and decrease in cost [8]. Two basic types of technologies have been widely used to separate salts from ocean water: thermal evaporation and membrane separation [15]. Over the past ten years, seawater desalination using semi-permeable sea water reverse osmosis (SWRO) membranes has gained momentum and currently dominates desalination markets. Membrane treatment process is more efficient, requires less physical space and is less energy consuming than vaporization or distillation [22].

A key factor which has contributed to the noteworthy reduction in seawater desalination costs is the advancement of the SWRO membrane technology [21]. Today's high-productivity membrane elements are designed with higher surface area, enhanced permeability and denser membrane packing. Increasing active membrane leaf surface area and permeability allows it to gain higher flux and hence significant productivity improvement is achieved using the same size (diameter) membrane element. The total active surface area in a membrane element is also increased by increasing the membrane size. Although 8 inch SWRO membrane elements are still the 'standard' size most widely used in full-scale applications, larger 16 inch and 18 inch size SWRO membrane elements have become commercially available over the past three years, and have already found full-scale implementation in SWRO projects worldwide[9]. The above mentioned factors result in significantly reduced footprint, piping, pressure vessels and associated costs [25].

Advances in the technology and equipment allowing the recovery and reuse of energy applied for seawater desalination, have resulted in a reduction of 80% of the energy used for water production over the last 20 years. While few years ago, the majority of the existing seawater desalination plants used Pelton-Wheel based technology to recover energy from the SWRO concentrate, today the pressure exchanger-based energy recovery systems dominate most desalination facility designs. The key feature of this technology is that the residual energy exchange between the concentrate and fresh seawater intake to the SWRO system. . Pressure exchanger technology typically yields 5-15% higher energy recovery savings than the Pelton-Wheel based systems. The specific (per unit of produced potable water) energy of desalination has been reduced from over 20kWh/m3 in the 1970s to below 3 kWh/m3 [10].

Further efficient desalination processes can be achieved through integrated membrane systems. Integrating different membrane technologies for minimizing the limits of the single membrane units and for increasing the efficiency of the overall system offers significant benefits. Feed water to RO systems needs pretreatment to remove inorganic and organic membrane foulants. Conventional pretreatment process is complex and has a high operating cost. There is a growing trend to replace all of this equipment with ultrafiltration. These membrane pre-treatment processes can handle a large variation in raw water quality and still produce water for the RO unit that is of better quality than water produced by the conventional technology [11]. Membrane pretreatment systems are also more compact and have lower operating costs than the conventional processes. Membrane based pretreatment allows RO design to be operated at higher fluxes, more compact membranes (440 ft2 vs. 400 ft2) and significantly reduces the fouling occurrence in RO system thus further making the design more efficient and robust.

Extending the capability of desalination further, integrated systems have been developed to push the recovery up for brackish water systems. High Efficiency Reverse Osmosis (HERO™) is one such proprietary system originally developed to provide ultrapure water to the microelectronics industry [12]. Ultrapure water is critical in a number of industrial applications, such as power generation, semiconductor manufacturing, and pharmaceutical formulation. Besides greater water recovery (95-99% vs. 75% from conventional RO), it also has other advantages like higher quality permeate, higher operating flux (gallons per square foot of membrane per day), and generally lower costs. HERO™ systems are ideally suited for applications with challenging feed water (e.g., with silica content greater than 20 ppm) or in areas with high water costs, limited available water, high water quality requirements, or zero liquid discharge requirements. It produces water that is higher in quality than necessary for potable use.

In HERO™, the membrane process is operated at higher pH thus eliminating microbiological fouling and making membranes self-cleaning. Due to the use of high pH, the hardness of the feed is reduced to less than 0.1mg/litre using hardness and alkalinity removal stage through weak and strong acid cation exchanger upstream. HERO™ does not use anti-scalant chemicals and requires less cleaning and maintenance than conventional RO. HERO™ also has limited self-healing properties, so small problems tend not to cause major system disruptions. In addition, there are the environmental benefits of saving water and energy [12].

Electro-deionization (EDI) is another such technology developed that combines ion-exchange resins, ion-exchange membranes and electric field. This has the capability to make ultrapure water using permeate from RO process [13]. Traditionally, ion exchange has been used to provide ultrapure water in these industries. EDI process can provide very high levels of demineralization and offer the advantage of continuous operation.

Moreover, these are not as mechanically complex as ion-exchange systems, and they require no acid and caustic regeneration, nor waste neutralization. Thus there is no need to store or handle bulk chemicals on the site.
All these technologies are well integrated and now available in pre-engineered packaged plants or even containerized mobile plants. This significantly reduces the footprint, overall cost and it can be installed in very short times to the point that they are used routinely for providing even emergency services.

4. Wastewater Treatment and Reuse

As the regulations and environment compliance parameters are being tightened and as concerns are mounting over the deteriorating quality and quantity of water supply, water reuse is recognized as more viable and sustainable source of water both for municipal and industrial applications [14]. The treatment and reuse of wastewater has two fold advantages as it reduces the quantity of wastewater to be discharged and it reduces the requirement of fresh water.
Reclaimed municipal or industrial wastewater must meet very stringent treatment standards to be acceptable to regulatory agencies and the end-users. In addition to removal of conventional pollutants such as Total Suspended Solids (TSS) and BOD, the elimination of all waterborne pathogens is required, as well as the reduction of nutrients such as total nitrogen and phosphorous . Membrane Bioreactor (MBR) systems provide this high effluent quality in a greatly simplified process. This requires only head works, biological processes, membrane filtration and disinfection to meet the most stringent water quality standards. In comparison, conventional process requires additional primary treatment, secondary clarifiers, enhanced nutrient removal and media filtration. The main advantage of the MBR process is that it reduces for the burden of biomass sedimentation, thus allowing a significantly smaller tank to be used for the bio-treatment process [24]. The operations can be conducted at higher mixed liquor concentrations (commonly 8,000-18,000 mg/l) as compared to conventional systems (around 2000 mg/l); this significantly reduces the footprint required as well as improves the removal of dissolved constituents. MBR designs will require only 30- 50% of the space required for conventional systems designed to meet the even more stringent treatment goals. This improved space efficiency benefits not only for new facilities but allows expansion and upgrade of existing facilities up to 3-5 times existing capacity without additional treatment volume or site footprint.
MBR systems also provide more flexibility in coping with flow rate and feed quality variation as hydraulic retention time (a function of flow rate) can be decoupled from sludge retention time (a function of biological reaction processes and sludge setting rates). They are also simpler, with fewer process components and maintenance requirements. Common maintenance is still required on mechanical components, but operators can now avoid difficulties in operation tied to sludge settling and clarifier sludge blankets. Besides, these can be easily automated and instrumented to measure performance. It allows systems to be remotely operated and monitored, thus significantly reducing operator attendance. The modular nature of the membrane system allows more efficient phasing of facilities. Membrane modules can be delivered on a "just in time" basis, thus reducing the need for large and costly initial construction to meet long-term projections.
The holy grail of reclamation and reuse of water is to capture water directly from non-traditional sources such as industrial or municipal wastewaters and restore it to direct useable quality either for potable or industrial purpose. Since the large part of the cost

of water is pumping, transport and storage, recovering water at or close to the point of use is the most efficient. Decentralized systems allows remote treatment of wastewater, thereby alleviating the need for expanding centralized sewage systems and long distance pipelines, which can be disruptive and costly. However, there has been a historic concern about the robustness, cost and operational effectiveness, creating the need for treatment solutions that deliver reduced complexity and provide affordability for the customer, as well as allow regulators to ensure high operation and maintenance standards. Also, wastewater treatment plants have historically required a significant amount of land to construct the necessary tanks and infrastructure for the required levels of treatment. MBR technology greatly addresses the concerns and makes it ideal choice for decentralized systems.

It offers ability to meet more stringent effluent water quality requirements, space constraints, lower operator involvement, modular expansion characteristics and consistent effluent water quality capabilities. Thus MBR technology meets the Process Intensification Criterions laid out earlier.

5. Waste-to-value

There is a conceptual shift from today's pollution prevention towards resource recovery. For instance, organics (COD) in water can be used as source of methane rather than having them destroyed aerobically by adding fossil energy. The same concept can be applied to nutrients such as phosphorous, nitrogen and potassium. Rather than removing or draining nutrients, we can make products out of them.

Water can be treated through aerobic process (oxidation) which consumes energy, or anaerobic digestion (reduction) which generates energy in the form of methane. Aerobic process consumes 1-2 MJ/kg of COD, while anaerobic digestion delivers about 12 MJ per kg of COD consumed. As the name suggests, anaerobic digestion demands the system to be completely isolated from air (oxygen) and maintain a redox potential of less than -250 mV. Ideally, anaerobic digestion is recommended on higher strength wastewater (COD>3000) whereas the aerobic process is suitable for a lower strength waste.

The waste-to-value concept discussed in this paper focuses on two different schemes both aiming at deriving energy/power from the organics followed by reusable water. The first scheme is applicable for the wastewater with higher COD loading. With necessary pretreatment, the water is fed to the anaerobic digester, followed by optional TSS removal unit, MBR and RO. The biogas thus generated is typically used for generating steam or electricity in gas engines. This integrated approach also seeks to treat the concentrate produced from MBR/RO with the help of waste heat of the flue gas. This strategy is more suitable for high strength wastewater from food and beverage industries. The second scheme is typically more applicable for wastewater laden with higher amount of volatile suspended solids. The water is initially clarifier to separate the solids whereas the supernatant from the clarifier is fed to the MBR. The solids from clarifier and the sludge from the MBR are fed to the anaerobic digester. The biogas from the digester produces captive power driving the entire system towards energy neutral condition.

In addition to the power and water, both the above mentioned integrated solutions can be designed to bring-down the concentration of the nutrients in the treated wastewater below the dischargeable limits. These solutions defeat the notion of wastewater treatment being cost intensive but on the contrary make the economics more attractive for the customer.

The holistic approach to wastewater treatment and shift towards resource recovery again highlights the process intensification trend in wastewater management.

6. Zero Liquid Discharge

Many industries, power plants, oil and gas exploration companies and even municipalities are facing with problems on the disposal of the liquid waste generated by their operations. In most of these plants, the ultimate goal is salt or total dissolved solids (TDS) reduction using economical process and minimization of liquid wastewater. As a result, Zero liquid discharge (ZLD) systems have become more prevalent. The goal of a well-designed system is to minimize the volume of liquid waste that requires treatment while also producing a clean stream suitable for use elsewhere in the plant processes.

Energy companies involved in development of unconventional gases and oil sands are facing severe challenges in managing the wastewater on site. Extraction of gas sources like Coal Bed Methane, Shale rock deposits and tight sand gas deposits requires fracturing to create openings in the deposits. The fracking process is enormously water-intensive, with up to five million gallons of water being required for a single well. Anywhere from 5% to 60% of this water flows back to the surface. In addition, water that is naturally found in the rock formations will flow from the well over the course of its proactive life, which is known as "Produced Water". Besides, in enhanced oil recovery process (EOR) using steam assisted gravity drainage (SAGD), 100% quality steam is injected into the well to heat-up the formation and get the heavy oil to flow. Produced water is highly variable and evolves over time, so a new well will produce smaller volumes of water than an older well. For treatment technology to be effective in produced water market, it must be robust to work efficiently under varying conditions and with variable flow rates. It must be versatile to remove a variety of contaminants and process a wide range of waters. It must be serviceable for easy O&M and most importantly, it must be economical.

In EOR process, huge water demand and ultimate conversion to steam requires the maximum amount of recycle potential from the water. Oil and condensed steam are brought to the surface where the oil is separated, and the condensate, or produced water, is treated and recycled to produce the steam. The traditional de-oiling, softening, filtration, and ion exchange produced water treatment scheme is complex, costly, produces several waste streams requiring disposal, is labor intensive, requires the use of steam generator, and requires vapor/liquid separation systems (to produce the required 100% steam quality for SAGD process). Evaporation through novel evaporators provides an alternate approach to produced water treatment which is simpler, more cost effective, more reliable, and reduces the size and complexity of the steam generation system significantly.

Novel design of evaporators and crystallizers has greatly facilitated the Zero Liquid Discharge solutions even with significantly challenging conditions like in gas fields with significantly reduced complexity and in cost effective way.

7. Integrated System Design Framework

There have been numerous technical advancements in water and wastewater treatment technologies as discussed in sections above. The holistic approach to water management requires evaluation of water treatment solution on various technical, economic, social and environmental parameters. The overall solution is integrated part of larger system that could be an industrial process or residential communities and has the capability to significantly influence it. For example, for industrial process, water and wastewater

treatment solution can influence the choice of technology with regard to water consumption, effluent discharge quality and quantity and overall economics. Likewise, for municipal process, water treatment solution clearly influences the water quality and quantity of the potable water, water tariffs and development in the territory. The evaluation of various options at various levels including using existing water source or desalination or wastewater reuse as an option requires an integrated framework. This framework should provide capability to evaluate the solution on various technical, economic, social and environmental parameters. This requires development of predictive process models for various water treatment unit operations, capability to integrate various unit operations, cost models for CAPEX, OPEX and lifecycle cost analysis, all on one platform. The predictive capability needs to be for specific water quality parameters, product flow rate, system recovery, energy consumption and several other parameters discussed in sections above. Likewise, these models should be able to predict in wide range of operating conditions, account for all the variability in the system, and allow designers to carry out what-if and sensitivity studies [16]. Besides, this also should be able to provide framework for optimization during design as well as operations phase. The choice of water treatment technologies and their capabilities are so numerous that even a knowledge management based decision support tool is required to help design flow-sheet and configuration to reach an optimum solution.
There is huge opportunity from Process Systems Engineering standpoint to develop this integrated framework that allows city planners, industrial process engineers or even residential communities to come up with the optimum solution that works within the constraints defined by them and also meet their overall requirements.

8. Conclusion

The developments of new technologies that follow the process intensification principles are critical to solve the current water and wastewater treatment challenges. This in the context of water treatment industry could mean reducing energy consumption, increasing recovery, reducing the foot-print, generating the value from the waste, more flexible processes that meets varying feed water qualities, shorter time to market, lower lifecycle costs or combination of these objectives. The new processes like membrane based ultrafiltration treatment, seawater desalination processes, membrane bio-reactors are lot more process efficient, safer, flexible, smaller, lower cost and more environment-friendly as compared to conventional processes and have the capability to meet the challenging requirements in the current scenario. The shift in approach towards resource recovery from pollution prevention is a good example of benefits of holistic approach and system level thinking. There is also a need for integrated design framework that allows evaluation of multiple options on economical, technical and environmental parameters, has the capability to integrate advanced and conventional technologies and evaluate various process configurations to design optimum solution.

References

1. GE Reports (2011, April 6), Water Reuse Gains as Urban and Industrial Demand is Set to Double, Retrieved from http://www.gereports.com/water-reuse-gains-as-urban-industrial-demand-is-set-to-double/
2. Roni Kasher (2009), Membrane-based water treatment technologies: Recent achievements,and new challenges for a chemist, *Bulletin of the Israel Chemical Society* (24), 10-18.

3. Charpentier, J.C. (2007), "Modern Chemical Engineering in the Framework of Globalization, Sustainability, and Technical Innovation", *Ind. Eng. Chem. Res.,*(46), 3465-3485.
4. F. Berne and J. Cordonnier, Industrial water treatment, Gulf Publishing Company, 1995.
5. U.S. Environmental Protection Agency, *The Environmental Protection Agency's White Paper on Peroxone* (EPA Guidance Manual, 1999; http://www.epa.gov/ogwdw/mdbp/pdf/alter/chapt_7.pdf
6. G.K. Pearce (2007), The case for UF/MF pretreatment to RO in seawater applications, *Desalination.*(203), 286-295
7. World bank report (2011,Sep), India Rural Water Supply, Retrieved from http://www.worldbank.org.in/WBSITE/EXTERNAL/COUNTRIES/SOUTHASIAEXT/
8. Mark Wilt, Craig Bartels (2005), Optimization of seawater RO systems design, *Desalination* (173), 1-12
9. Membrane Filtration (2008, Aug) Large-diameter RO elements only for large scale plants? http://waterwastewaterasia.com/WWA_archive/JulAug08/32t34.pdf
10. Baltasar Peñate and Lourdes García-Rodríguez, Current trends and future prospects in the design of seawater reverse osmosis desalination technology, *Desalination* (284), 1-8
11. Lauren F. Greenlee, Desmond F. Lawler, Benny D. Freeman, Benoit Marrot, and Philippe Moulin (2009), Reverse osmosis desalination: Water sources,
12. Science Direct, 2011, Expanded licensing agreement enables GE to incorporate HERO systems in more products, *Membrane Technology* (2011), Retrieved from http://www.sciencedirect.com/science/journal/09582118/2011/3
13. Y.Tanaka(2007), Chapter 4 Electro-deionization, *Membrane Science and Technology* (12), 437-460
14. Venkatesh Madyastha, Vijaysai P and Venkatram Mahendraker (2011), Reduced Order Model for Monitoring and Control of a Membrane Bioreactor System via Delayed Measurements, *Water Science & Technology* (64), 1675-1684
15. A.M. Helal, A.M. El-Nashar, E. Al-Katheeri, S. Al-Malek (2003), Optimal design of hybrid RO/MSF desalination plants Part I: Modeling and algorithms, *Desalination,* (154) 43-66
16. GE Water (2012), Winflows Membrane System Design Software, Retrieved from http://gewater.com/winflows.jsp
17. Raymond R. Tan, Dominic Chwan Yee Foo, Kathleen B. Aviso, Denny Kok Sum Ng (2009), The use of graphical pinch analysis for visualizing water footprint constraints in biofuel production, *Applied Energy,*(86), 605-609
18. Alessandra Criscuoli and Enrico Drioli (2007), New Metrics for Evaluating the Performance of Membrane Operations in the Logic of Process Intensification, *Ind. Eng. Chem. Res.*(46), 2268-2271
19. *Global Trends 2015,* NIC 2000-02, National Intelligence Council, Washington, DC, December 2000, p. 27
20. Mark Wilf and Kenneth Klinko (2001), Optimization of Sea Water RO Systems Design, *Desalination*, (138), 299-306.
21. K.V.Reddy and N.Ghaffour (2007), Overview of the cost of desalinated water and costing methodologies , *Desalination*, (205), 340-353
22. Ioannis C. Karagiannis and Petros G Soldatos (2008), Water desalination cost literature: review and assessment , *Desalination*, (223), 448-456
23. Enrico Drioli, Andrzej I. Stankiewicz, and Francesca Macedonio (2011), Membrane engineering in process intensification—An overview, *Journal of Membrane Science*, (380), 1-8
24. Thomas Buer and Jeff Cumin (2010), MBR Module Design and Operation (250), 1073-1077
25. Nikolay Vouchkow (2008), Sea Water Reverse Osmosis Design and Optimization, Advanced Membrane Technologies,

I.A. Karimi and Rajagopalan Srinivasan (Editors), Proceedings of the 11th International Symposium on Process Systems Engineering, 15-19 July 2012, Singapore.

Applications of Technology Roadmapping to Planning and Building Systems for Medicine and Vaccine Manufacturing

Anando A. Chowdhury[a], Michael P. Thien[a]

[a]*Global Science Technology & Commercialization, Merck Manufacturing Division, Merck/MSD, Whitehouse Station, NJ 08889*

Abstract

Health and sustainability are two of the most daunting global challenges facing humankind today. The need to preserve and improve human life in new and more robust ways is at the core of these global challenges. Process systems engineering (PSE) when applied to the manufacturing and distribution of medicines and vaccines has the capacity to impact these global issues for the better, but it must be effective at size scales that span global enterprises and supply chains and time scales that cross multi-year long range planning. Technology roadmapping is a process that has been applied effectively to the identification, selection, acquisition, development, exploitation, and protection of technologies in a variety of industries. We explain how this method combined with PSE can be used to design and enact complex technological change at the size and time scales needed to transform a global manufacturing operation.

Keywords: manufacturing technology roadmap pharmaceuticals vaccines biologics.

1. Introduction

Technology roadmapping is a process that has been applied effectively to the identification, selection, acquisition, development, exploitation, and protection of technologies in a variety of industries. In this paper we describe an approach taken at our company that allows this technique to be used to drive process systems engineering (PSE) activities across a size scale that spans a global manufacturing operation with hundreds of connected supply chains and time scales that cover multiple years into the future. When driven at the global operation level, technology roadmapping provides the only viable way to align thousands of technological, organizational and business model changes to systematically transform and coordinate PSE activities across the organization. This is especially critical in our business sector where our global operations deal with the manufacture and distribution of medicines and vaccines that preserve or improve human life and animal health. We have defined **technology** as a system comprised of scientific/technical knowledge, processes and equipment that is used to accomplish a specific goal. The knowledge encompasses the understanding of fundamental principles and relationships that provide the foundation of the technology. The processes are the procedures, techniques and best practices associated with the technology. The equipment is the physical manifestation of the technology as devices, instruments and machinery. Given this definition, **manufacturing technologies** are combinations of knowledge, process and equipment that transform raw materials into products and deliver them in a useful form to our patients & customers. Additionally, **product configurations** are changes in format to a product that a customer would see

or perceive – for example formulation platforms or packaging configurations that manufacturing technologies enable.

Our approach follows this reasoning in a fairly linear way. Initially we create global operations level systems views, allowing for holistic management and consideration of systems changes. This creates the visual of the larger system that is the subject of transformation and deployment of technologies. Stakeholder maps are created that account for the external and internal constituencies, clearly identifying the key stakeholder groups involved in global systems level transformation. The changing global trends are then mapped inwards from the customer market and societal needs and outwards from the business drivers and requirements from the manufacturer. In this paper, we focus on the some significant shifts in the health and sustainability areas. This stakeholder mapping also allows for the development of key performance indicators (KPIs) for the global system, thus collapsing the trends and drivers identified into workable and measurable goals. These KPIs result in very precise operational definitions around which global operations level changes can be made. During the needs and requirements definition, technology inventories can be created simultaneously by technology subject matter experts that become repositories of internal and external technology efforts and innovations. The two streams of efforts combine when the KPIs, trends and drivers are used to prioritize the technologies in time that are most important. This allows for the initial creation of technology roadmaps. Individual technologies are generally at the single and multi-phase system and process unit level, and thus visualization on roadmaps allow for plant, site and enterprise level integration and planning. Interactions between different global pathways can be analyzed utilizing dependency structure matrix (DSM) analysis. This creates a portfolio of PSE projects that can be managed through maturity by an enterprise-wide technology management process and governance, with information and knowledge being refreshed on an annual basis as the transformation and implementation progresses.

2. Global Operations Level Systems Views

A simple schematic of all the possible pathways of manufacturing possible at the global operations level was created. This is depicted in Exhibit 1 below.

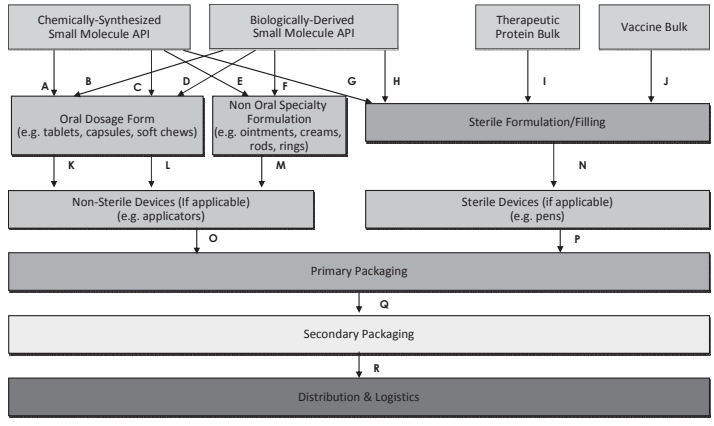

Exhibit 1: Global operations level system view

In this global view, process unit systems up to plant scales can exist within each box, while site and enterprise level integration occurs along pathways defined by connections of different boxes. An example of a pathway is AKOQR, which represents the pathway for a small molecule pharmaceutical oral dosage form. It is clear that from even this view, PSE models for enterprise optimization such as those discussed by Sahinidis (Sahinidis et al, 1989) or Grossman and Biegler (Biegler et al., 1997) can be applied to pathways such as AKOQR, and that the evolution of technologies within any given node of box would inform the variables, constants and coefficients of the models from the current pathways to future pathways. Each processing unit box can be further blown out as necessary, but the overarching scheme allows for taxonomy of future roadmaps for each node and each pathway.

3. Stakeholder maps, trends, drivers and key performance indicators

Having a clear way of representing all the stakeholders of the global operation is incredibly important as it allows for segmentation of needs and ultimate definition of key performance indicators by constituency. A high level stakeholder map from our work is shown in Exhibit 2.

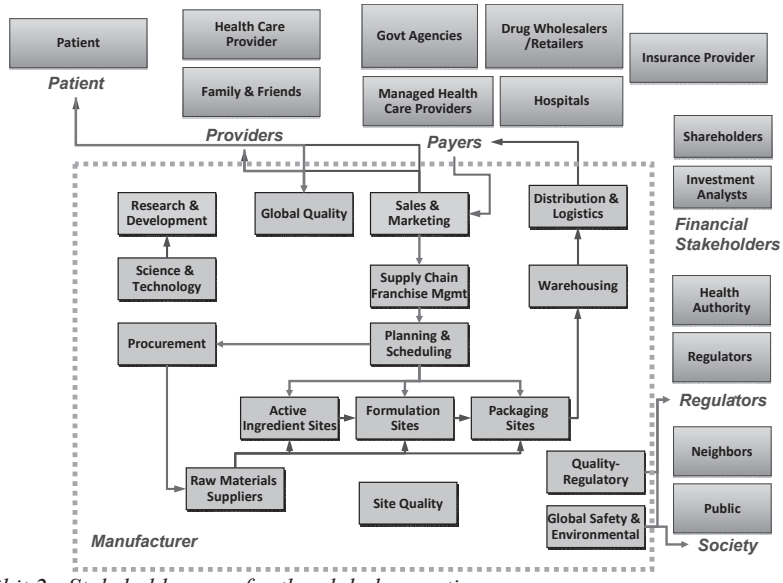

Exhibit 2: Stakeholder map for the global operation

As global operations-level transformation occurs, there are multiple interests that must be met. Patients and consumers must benefit from the appropriate use of our products and services and challenges such as affordability and adherence must be met. Different configurations that allow for convenient and safe use as well as protect the product from human and environmental threats must be introduced. On the other side of the stakeholder map, we serve our society, from the local communities in which we operate to the national and international levels, by supporting and promoting environmental sustainability. This leads to processes designed to be green with respect to emissions and waste and sustainable packaging designs and configurations.

MAJOR PARAMETER		KEY PERFORMANCE PARAMETER	MEASURE DEFINITION	STAKEHOLDER WHO CARES	SAMPLE TRENDS & DRIVERS FOR THE NEXT 5 YEARS
PRODUCT	A winning product fashioned with the customer value drivers in mind and continues to deliver this value consistently.	Safety & Tolerability	The safety profile of the medicine.	Patient, Provider, Payer, Regulator	More potent compounds
		Efficacy	How effective is the medicine in effecting the disease target, generally measured by bioavailability over time.	Patient, Provider, Payer, Regulator	Variety of different dosage forms to achieve delivery optimums
		Features	Attributes that signify the non-biological elements of the product, like integrity and elegance of the medicine, the ease of use of the packaging etc.	Patient, Provider, Payer, Regulator	Increased set of market and customer-specific requirements
PROCESS	Sustainable and profitable business/manufacturing system to create and deliver the product robustly, wherever they are needed while building and leveraging institutional wisdom seamlessly.	Manufacturing Efficiency and Robustness Measures	All the manufacturing parameters that are part of being a world class supplier including inventory stock turns, process capability (CpK), overall equipment effectiveness (OEE), right first time (RFT), on time in full (OTIF), and cycle times.	Manufacturer, Regulator	Need to do substantially better in all manufacturing effectiveness measures
		Standard Cost to Make Product	The manufacturing cost to create a certain number of units of the product.	Manufacturer	Appropriate reductions to assit with affordability of medications for more customers
		Flexibility to Continuously Improve	The measure of how rigid or flexible the process is to learning and then instituting improvements based on that learning.	Manufacturer	The need for flexible process technologies are going
		Sustainability and Environmental Factor	The inherent operational safety and the green-ness or environmental friendliness and sustainability of the process.	Manufacturer, Society, Regulator	Much greater global need for on green sustainable solutions
		Global Access	Increased global access for medicines is important and this parameter represents the technologies ability to be operable in various markets around the globe.	Patient, Society, Manufacturer	Desire to expand access to previously unserved patients and customers
		Scalability and Continuity of Technology from R&D to Manufacturing	This measures the continuity of the technology from bench scale and pilot scale models to manufacturing allowing for knowledge to be built over time and across different products using the same platform.	Manufacturer, Regulator	The need to have and demonstrate continuous learning from development through to manufacturing is vital

Exhibit 3: Stylized stakeholder, KPI, trend and driver mapping

It is important to reflect the needs and requirements of the various stakeholders in precise terms, with operational definitions and maps that can establish precise sub-factors that can be targeted by the global operation for improvement. Exhibit 3 is a generic global operations level stakeholder needs and requirements mapping that shows a stylized representation of the stakeholder, KPI, trend and driver mapping.

4. Technology inventories

While the work of defining key performance indicators are being established for the technologies, parallel work can and should be occurring to gain common and universal enterprise level visibility to all technologies being considered or potentially of interest. An important connection between advances in technology achieved at local levels in the enterprise and the higher level technology strategy should be the development and maintenance of a **technology inventory**. The technology inventories should be a primary reference source whenever an effort to resolve a stakeholder-driven set of needs or requirement via manufacturing technology is undertaken. The inventory serves as one avenue to connect technology advances in manufacturing, research and all manufacturing businesses to the customers and business. Leaders of technical organizations should assign functional areas to have one or more representatives keep the technology inventory current so that it may be a continuously useful tool for technology roadmapping. Local groups in research and manufacturing can have updating the inventory as a standing objective for technologies in their scope of work. We have found that customer field visits, and reports from conferences, visits to partner companies and industrial collaborations may serve as key sources of contributions to the inventory. Individuals within each area of the enterprise should appoint an appropriate function or group of individuals to periodically check to ensure the inventory is kept current, at least, on an annual basis.

5. Technology Management Process

A stylized example of a technology roadmap is shown in Exhibit 4, and does not differ much from conceptual examples presented by Phaal (Phaal, 2004) and other manifestations of roadmaps going back to their initial use in Corning and Motorola in the 1980s. The top of the roadmaps are representations of product or business strategies while the bottom represents investments in the most critical enabling technology projects. The horizontal axis represents multi-year transformation time scales while the dotted line ties from the top to the bottom represent a visually simple way of showing the most critical ties. It is important to note that these roadmap visuals constitute a graphical summary of much more complex and interrelated connections that are best managed through multi-domain matrices as will be discussed in the last section.

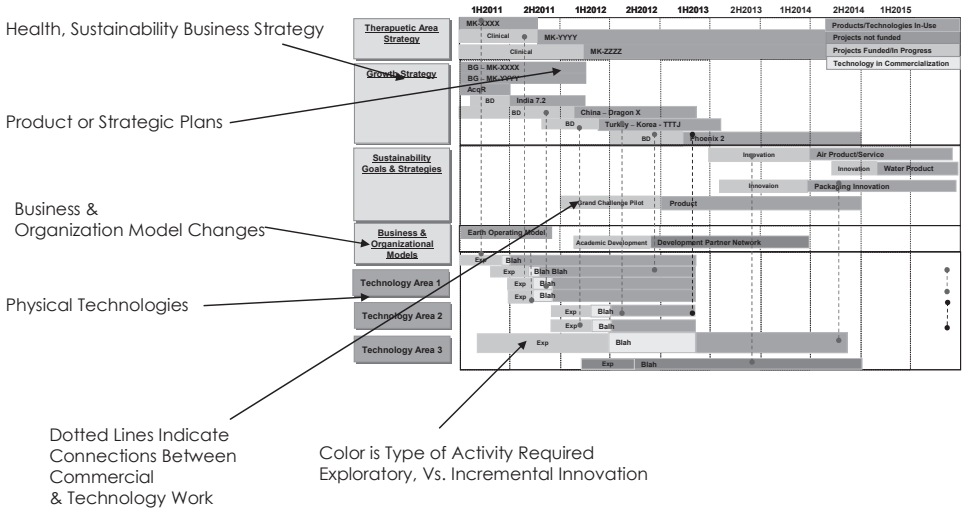

Exhibit 4: Stylized example of a technology roadmap.

The subsystems we have spoken of so far become a part of an integrated technology management process that has these roadmaps at the center, and this concept we have depicted in Exhibit 5. We have chosen to adopt the European Institute of Technology Management (EITM) definition of technology management as that which "addresses the effective identification, selection, acquisition, development, exploitation and protection of technologies (product, process and infrastructural) needed to maintain (and grow) a market position and business performance in accordance with the company's objectives." (Phaal, 2004). This must be managed by an organizational structure that has clear accountabilities and decision rights established. Most importantly, an overarching ability of tracking and responding to process health metrics and realization indicators are extremely important. Each section and its roles are described.

5.1 **F1 – Technology inventory system –** This part of the process ensures that the enterprise can consistently track and update the technologies it has in its inventories from the inside and outside as the business learns more. The sub-process gives access to all technologists to help maintain and access these inventories.

Appropriate guidelines for an intellectual property strategy are embedded in this section.

5.2 **F2 – Product planning system –** Access for the latest product plans for every health area and market are embedded here. The means of transforming these product plans into a way the technology roadmaps can consume and use them are defined in this sub-system.

5.3 **F3 – Customer & business needs/reqts system –** It is critical that a firm link is created between the clinical and marketing portions of the business and the customer need-sensing and translation processes are established so that observations can be translated into business requirements and goals. This sub-system also assures that we stay in touch with the business needs and requirements that are independent of customer needs.

5.4 **P1 – Technology roadmap mgmt –** This part of the system establishes how the enterprise manages the actual roadmaps, including gathering changing information, augmenting investment choices, socializing the recommendations, and making decisions on the overall maps and investments. **T**he maps are made visible and visualized on an ongoing basis.

5.5 **P2 – The gated technology process –** The mapping of technology and technical systems to roadmaps allows for global tracking of technologies at each stage of maturity. This is an important concept as different investment postures need to be taken based on different maturity states of the technologies. A clear map of the decision rights at all levels of the enterprise for progressing technologies through must be created, the broader and more externally facing the technology is, the more challenging decision rights can become. Additionally, the enterprise must account for technologies that "pop in" at a gate, that is acquired from the outside or working with a partner. Each gate should have the standard ways to kill projects as well as clear way to map the overall health of the process.

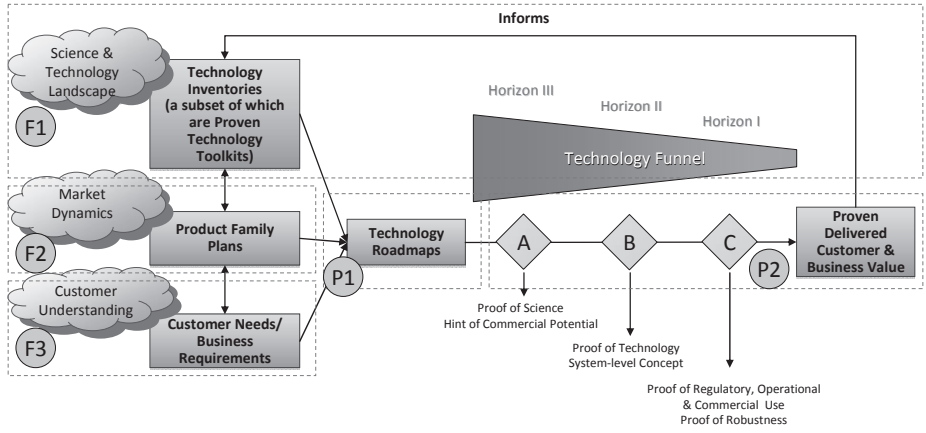

Exhibit 5: Conceptual design of an enterprise level technology management process.

The progression of technologies through the various phases of maturity is critical and linking technology development with the knowledge and capability level of the organization is vital. In this we have proposed using **horizons** of maturity (Cournoyer, 2003, Chowdhury, 2009, Kukura, 2012). **Horizon I** technologies refer to incremental

improvements in currently commercialized or near commercialized technologies. They are implementable in the near term. **Horizon II** technologies are in the middle part of the adoption curve (potential technology), the physical principles have been demonstrated either in our industry or elsewhere - we need to adapt the solution for our needs. These are medium term solutions 2-3 years out. **Horizon III** technologies are much further out and likely the physical principles have not yet been demonstrated. They require some fundamental knowledge work and are a ways from being commercialized. These are longer term solutions.

This maturity level assessment, which is also depicted in Exhibit 5 in the part of the diagram labelled the "technology funnel", can be married up with a needs assessment. As the various stakeholder needs, and for our purposes those that contribute to transforming human health and driving sustainability globally, some will be well articulated (i.e. a problem looking for a solution) and others will not be (i.e. a solution looking for a big way to impact a problem). As we assess transformation at a global operational level, it is important that our efforts have a combination of these types of technologies and these types of defined value drivers. These dual dimensions and the trade space that is created by examining them are represented in Exhibit 6.

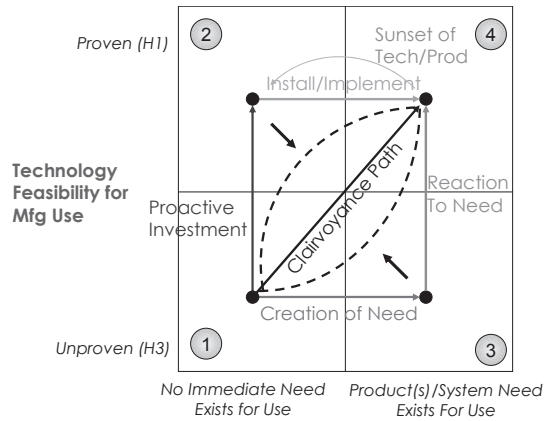

Exhibit 6: Technology Maturity by Extent of Need

In the y-axis, the technology maturity as represented by the different horizons is shown while the extent of known and identifiable need is shown on the x-axis. Theoretically, technologies can traverse from zone 1 to zone 2, where we make proactive investment in a technology without a well articulated need or move from zone 2 to zone 3 where we are implementing a proven technology as a need is articulated. They can theoretically traverse from zone 1 to zone 3 where we work to create a need for an unproven technology or (where most mental models around technology development reside), move from zone 3 to zone 4 where we develop a technology for a particular need. In reality technologies traverse this trade space in multiple and diverse trajectories and at different speeds. They are can start within any zone and can stay within a zone and never go anywhere and die. The idea of technology roadmapping as a means to build large scale systems or transform them essentially looks to solve the most difficult problem of moving technologies from zone 1 to zone 4 in a more methodical, integrated

and predictive way. We represent this concept in the diagram as the "path of clairvoyance". Theoretically, well fashioned roadmaps that are refreshed with technical knowledge would deliver a straight line from zone 1 to zone 4. In reality this is impossible, but this thinking does provide some helpful principles as the enterprise puts in place an overarching technology process.

6. The Technology and PSE portfolio and network management

The final leg of the process is to actually manage the technologies and PSE efforts that are born of the technology roadmaps. One of the key issues around technology management is the lack of visibility of how different efforts touch each other and need information or data from one another to make a larger, more holistic transformation possible. In helping to manage these interdependencies, the concept of the multi-domain matrix (MDM) has been applied (Crawley et al, 2004). A mock version of an MDM is shown in Exhibit 7 for the manufacturing pathway AKOQR discussed in Section 2 that has been applied to our efforts in managing technologies and PSE efforts at an enterprise scale. The MDM is laid out to show relationships within like elements (such as the process to process connections dependency structure matrix (DSM) in the red box, or the operand to operand connections DSM within the blue box or across unlike elements such as operand to initiative, as shown in the area labeled zone 1.

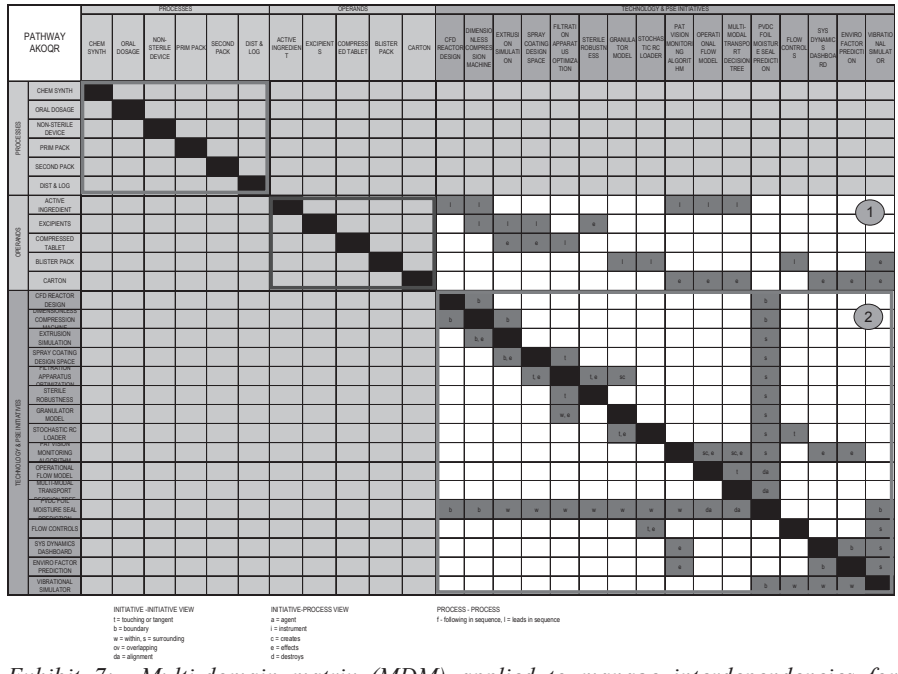

Exhibit 7: Multi-domain matrix (MDM) applied to manage interdependencies for technology and PSE initiatives.

Understanding the relationships between some of the most important potential efforts and the process or operands at the enterprise level is critical to help manage multi-year efforts and to foster the right knowledge sharing and hard connections required as

internal and external resources execute on the portfolio of choices. The cross hairs within the matrix can represent the nature of the connection, e.g. "supporting", "connected" to or "integral". In this mock example, we see that the following projects are in the portfolio: CFD reactor design, dimensionless compression machine, extrusion simulation, spray coating design space, filtration, apparatus optimization, sterile robustness, granulator model, stochastic RC loader, PAT vision monitoring algorithm, operational flow model, multi-modal transport decision tree, monitoring algorithm, PVDC foil moisture seal prediction, flow controls, sys dynamics dashboard, enviro factor prediction, and vibration simulator. First and foremost, the importance of these PSE initiatives and their ability to address multiple needs at the global operational level would not be seen if were not for the roadmapping effort. The MDM analysis brings to light for example that the PAT vision monitoring project as creating datasets that are needed for the system dynamics dashboard or the enviro factor prediction model. These interconnections can then me mapped to intended resource connections through a process called organizational network analysis where people resources are mapped with their current structured technical and data sharing relationships (Cross et al, 2009). This leads to being able to visualize the resource connections between technical resources working on various programs and drive management of needed connections. An actual mapping of technical resource connections working in on the pathway AKOQR is shown in Exhibit 8.

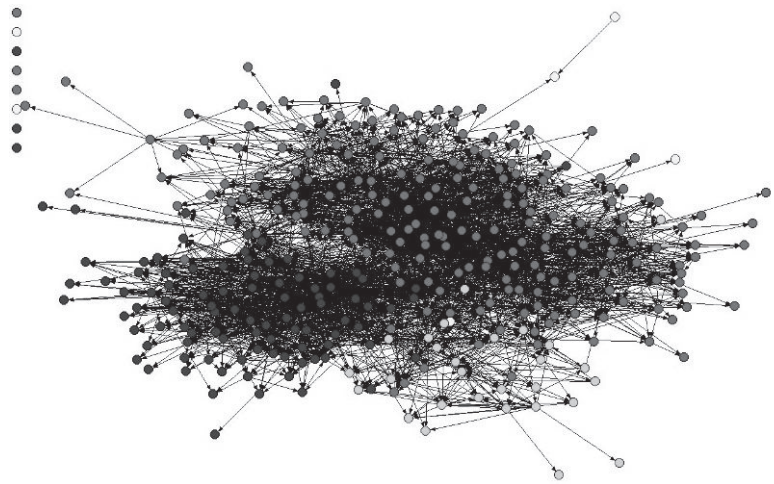

Exhibit 8: Organizational network analysis of connections between technical resources working on technology/PSE initiatives

7. Conclusion

The ability to impact human health and global sustainability requires enterprise transformation at size scales of global operations and time scales that traverse multi-year planning cycles. We have introduced a systematic method that has been pressure tested in our enterprise that combines technology roadmapping, portfolio management, multi-domain matrix and network analysis to methodical management of technology and PSE initiatives in an integrated and interdependent way.

References

Ansel, H.C., Loyd, A.V., and Popovich, N.G. (2005), "Ansel's Pharmaceutical Dosage Forms and Drug Delivery Systems 8th Edition", Lippencott Williams & Wilkins.

Biegler, L.T., Ignacio E.G., and Westerberg. A.W. (1997), "Systematic Methods of Chemical Process Design", Prentice Hall PTR.

Chowdhury, A. (2009), "Technology Strategy Papers 15.965 #1-4, Pharmaceutical Manufacturing Technology Platforms," Individual Paper Assignments for partial fulfillment of requirements of Fellowship, System Design & Management, Massachusetts Institute of Technology.

Cournoyer, R. et al (2003), "Growth Initiatives Technology Framework", Eastman Kodak Company.

Crawley, E., de Weck, O., Eppinger, S., Magee, C., Moses, J., Seering, W., Schindall, J., Wallace, D., and Whitney, D. (2004), "The Influence of Architecture in Engineering Systems", MIT Engineering Systems Division Monograph.

Cross, R., Thomas, R.J., (2009), "Driving Results through Social Networks: How Top Organizations Leverage Networks for Performance and Growth." John Wiley & Sons.

Cross, R., Singer, J., Zehner, D., and Vossen, D. (2009), "Global Pharmaceutical Commercialization Organizational Network Analysis Final Report." Merck Internal Document, Merck & Co., Inc., Whitehouse Station, NJ.

IBM Business Consulting Services (2005), "Transforming Industrialization: A new paradigm for pharmaceutical development."

Kukura, J. (2012), "Strategic Manufacturing Technology Management in the Pharmaceutical Industry", Cornell University Lecture, Policy Analysis and Management in the Pharmaceutical Industry.

Kukura, J., Starbuck, C., and Chowdhury, A. et al (2007), "Merck Commercialization Technical Forum White Paper on a Framework and Guidance for Distinguishing Core and Non‐Core Technologies.", Merck Internal Document, Merck & Co., Inc., Whitehouse Station, NJ.

Moore, G.A. (2002), "Crossing the Chasm: Marketing and Selling Disruptive Products to Mainstream Customers", HarperBusiness Essentials.

Nelson, R.R. (2003), "Physical and Social Technologies and Their Evolution.," Columbia University working paper available from the author, Columbia University.

Phaal, R., Farrukh, C.J.P. and Probert, D.R. (2004), "Technology roadmapping - a planning framework for evolution and revolution." Technological Forecasting and Social Change, 71. pp. 526. ISSN 0040-1625.

Phaal, R., Farrukh, C.J.P., and Probert, D.R. (2004), "A framework for supporting the management of technological knowledge." International Journal of Technology Management, 27. pp. 1-15. ISSN 0267-5730

Phaal, R., Farrukh, C., Mitchell, R. and Probert, D. (2003) "Starting-up roadmapping fast." IEEE Engineering Management Review, 31. pp. 54-60. ISSN 0360-8581

Phaal, R. (2003), "Strategic roadmapping: linking technology resources to business objectives." International Journal of Technology Management, 26. ISSN 0267-5730

Ravasz, E., Somera, A.L., Mongru, D.A., Oltvai, Z.N., Barabási1, A-L., (2002). Hierarchical Organization of Modularity in Metabolic Networks. Science.

Rogers, E.M. (1962), "Diffusion of Innovations", Simon & Schuster.

Sahinidis, N.V., Grossman, I.E., Fornari, R.E., and Chatharthi, M. (1989), "Optimization model for long range planning in the chemical industry", Computers & Chemical Engineering.

I.A. Karimi and Rajagopalan Srinivasan (Editors), Proceedings of the 11th International Symposium on Process Systems Engineering, 15-19 July 2012, Singapore.

Multi-scale Optimization for Advanced Energy Processes

Lorenz T. Biegler[1] and Yi-dong Lang

Department of Chemical Engineering; Carnegie Mellon University; Pittsburgh, PA USA 15213

Abstract

Advanced energy systems demand powerful and systematic optimization strategies for analysis, high performance design and efficient operation. Such processes are modeled through a heterogeneous collection of device-scale and process scale models, which contain distributed and lumped parameter models of varying complexity. This work addresses the integration and optimization of advanced energy models through multi-scale optimization strategies. In particular, we consider the optimal design of advanced energy processes by merging device-scale (e.g., CFD) models with flowsheet simulation models through sophisticated model reduction strategies. Recent developments in surrogate-based optimization have led to a general decomposition framework with multiple scales and convergence guarantees to the overall multi-scale optimum. Here, we sketch two trust region-based algorithms, one requiring gradients from the detailed model and one that is derivative-free; both demonstrate multi-scale optimization of advanced energy processes. Motivated by an advanced Integrated Gasification Combined Cycle (IGCC) process, we present two case studies that include PSA models for carbon capture and CFD models for gasification and combustion.

Keywords: model reduction, nonlinear programming, proper orthogonal decomposition (POD), trust region methods, IGCC power plants, carbon capture

1. Introduction and Motivation

Increasing pressures and awareness of critical energy systems demand powerful and systematic optimization strategies for their design and operation. These demands present a number of challenges, particularly as emerging energy processes incorporate advanced technologies that are described by complex process, nonconventional, multi-scale process models. In this study, we discuss the development of a multi-scale optimization framework that addresses these challenges. This framework is enabled through rapid advances in optimization models and solution strategies over the past decade. Nonlinear optimization algorithms can now solve models with millions of decision variables and constraints. Correspondingly, the computational cost of solving discrete optimization problems has been reduced by *nine orders of magnitude* (Biegler and Grossmann, 2004; Biegler, 2010). These algorithmic advances have been realized through software/design frameworks that integrate these optimization models through nonlinear and mixed-integer nonlinear programs (NLPs, MINLPs). On the other hand, it is essential to note that these benefits arise because these frameworks permit (indeed require) optimization models to be formulated carefully as well-posed, well-conditioned problems with exact first and second derivatives.

[1] biegler@cmu.edu

To extend these tools to multi-scale energy processes, we require the integration of efficient and accurate model reduction strategies within the optimization framework, leading to simple analytic descriptions that we term *reduced order models* (ROMs). Moreover, the development of efficient and accurate model reduction strategies allows the capture of multi-scale, multi-fidelity model behavior within an optimization framework. As described in Chung et al. (2011), these strategies can be applied within a cascaded network that link multi-scale models (from atomic to enterprise scales) along with optimization formulations that provide the "glue" to exploit synergies among these systems through ROMs.

With this goal in mind, a number of important research questions arise. First, how should reduced models be constructed and how do we balance accuracy with computational cost for the model construction phase? Second, does the multi-scale optimization framework converge to the optimum of the original system models? Third, can multi-scale optimization be performed efficiently without frequent recourse to the original models? To motivate these questions and describe our recent research, we consider the advanced IGCC process with carbon capture, shown in Fig. 1.

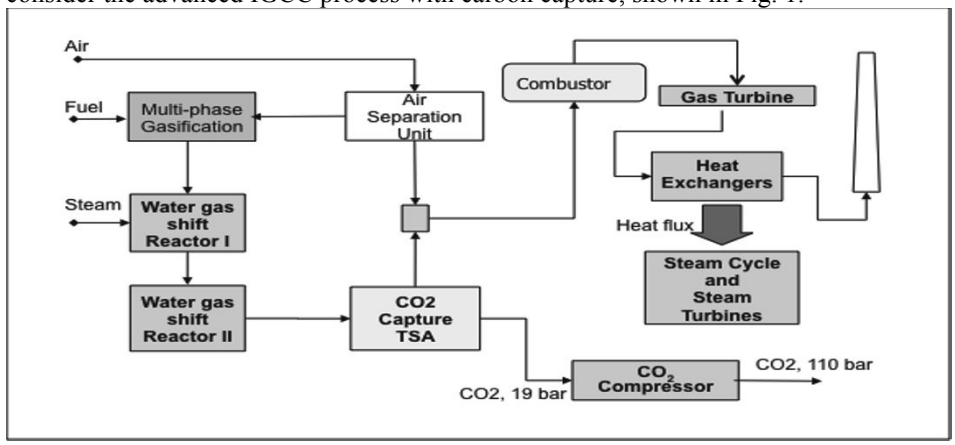

Figure 1. IGCC Flowsheet with Carbon Capture

The advanced IGCC process is described in a detailed case study prepared by TNO (Kessel et al., 1998). The gasifier converts feeds for fuel, water and oxygen into syngas; the effluent CO in the syngas is converted into H_2 and CO_2 in two cascaded water-shift reactors, and the syngas becomes an H_2-rich stream, with 90% of the CO_2 in the stream captured by a temperature-swing adsorption (TSA) unit. The CO_2 is compressed for subsequent storage and sequestration. On the other hand, after mixing with nitrogen and oxygen, the H_2-rich gas enters the combustor of the gas turbine to produce electricity. The energy in the turbine exhaust is recovered by driving the steam turbines in the steam cycle. This process model comprises lumped parameter (algebraic) models for heat exchange and compression, distributed, dynamic (differential-algebraic) models for the TSA unit and distributed, multi-phase (partial differential-algebraic) CFD models for the gasification and combined cycle units. To provide the optimization capability for the overall process model, our strategy converts these heterogeneous (AE, DAE, PDAE) models to equation-based optimization models through model reduction and nonlinear programming. In this way we capture the phenomena of multi-phase flow, particle mechanics, and dynamic operation within the process optimization. In addition, we

describe a framework that allows the optimum of the original, heterogeneous process model to be obtained.

The next section discusses previous model reduction developments, challenges for ROM-based optimization and the extension of these methods for integrated flowsheet optimization with heterogeneous models. The third section describes a ROM-based optimization method that requires gradients from the detailed model. A case study based on the optimization of a pressure swing adsorption (PSA) process demonstrates the performance of this method. In the fourth section we describe a derivative free alternative for ROM-based optimization for the integrated optimization of the IGCC process in Figure 1. Here we develop an optimization strategy based on a trust region framework that guarantees convergence to the rigorous optimum with minimum recourse to detailed models. Conclusions and future work are discussed in the fifth section.

2. Paradigm for Reduced Order Models

Model reduction is a widespread practice that extends over many engineering disciplines, and over several decades. In process systems engineering, early work on model reduction includes the use of reduced models for physical properties that require detailed thermodynamics and transport models (see Leesley and Heyen, 1977; Boston and Britt, 1978, Barrett and Walsh, 1979). These early strategies provide a vision for reduced models that extend beyond physical property models to a wide range of process engineering tasks. In fact, Caballero and Grossmann (2008) applied a related ROM-based strategy for distillation models in flowsheet optimization.

Similarly, in the PDE modeling community, reduced order modeling strategies have been developed and include multi-grid methods, proper orthogonal decomposition (POD) and state-space ROMs based on data-driven modeling and principal component analysis (PCA). To adapt ROMs to process optimization, a typical strategy is to match the ROM to rigorous models at specific points, usually over the course of the optimization path, and to rely on the constructed ROM for gradient information needed for optimization. However, it is well-known that such a strategy cannot be guaranteed to converge to the optimal solution of the detailed model (Biegler, et al., 1985; Brdys, et al., 1987; Gao and Engell, 2005), as gradients from the original model are needed to satisfy optimality conditions. Instead, ROM-based optimization strategies centered on trust region strategies (Conn, Gould, Toint, 2000) provide effective communication between the original model and the ROM, as well as convergence guarantees.

Model reduction strategies coupled with optimization generally cover two approaches. The first approach is based on model reduction that retains most of the structure of original equations but leads to simpler and smaller models. Examples include shortcut models based on physical phenomena, coarsening of discretization (finite difference, element, volume) steps and the use of spectral-based strategies such as POD. The second approach is based on data driven model reduction that leads to the construction of input-output models used in the optimization problem. Issues for the construction of these ROMs include experimental design for model reduction, well-posedness and conditioning of the constructed ROM (known as poisedness) and the choice of basis functions (e.g., specific regression models, artificial neural networks, radial basis functions and Kriging). Often the reduced models from the data-driven approach are used as surrogate models within a derivative-free optimization (DFO) strategy.

Additional requirements arise when adding multiple ROMs within an overall process optimization model. Here, well-conditioned algebraic ROMs need to be incorporated within the optimization framework with exact derivatives provided from the ROMs. This implementation allows the use of equation-based models, fast optimization algorithms and greater robustness in the optimization (e.g., intermediate failures of CFD models are avoided). On the other hand, over the course of the optimization process, ROMs may need to be reconstructed from the original models, often leading to the dominant computational cost. For example, when coupling CFD to flowsheeting models, the former may require CPU hours or days, while the ROM-based flowsheet optimization requires only a few CPU minutes. As a result, recourse to the original model needs to be minimized; this is enabled through the ROM's predictive capability.

Finally, to guarantee convergence of the ROM-based optimization to the optimum of the detailed model, two general trust region frameworks have been developed. The first framework assumes that accurate gradients are available from the detailed model. This allows the ROM to be formulated within a *model NLP,* which is solved within a trust region to generate a search direction for the original model. A key property is that *both* functions and gradients from the original model match the basepoint on the model NLP, i.e.*, first order consistency*. This trust-region framework was developed for unconstrained problems by Alexandrov et al. (1998) and is sketched in Figure 2. They also introduced scaled (i.e., corrected) objective functions in the trust-region subproblem to enforce consistency conditions. Fahl (2000) extended this approach by relaxing the consistency conditions and solving the trust-region subproblem inexactly. Finally, Agarwal and Biegler (2012) extended Alexandrov's approach through a filter trust region approach, which greatly reduces the need for gradients from the detailed model.

The second approach does not require gradients from the detailed model and is based on concepts of trust-region-based DFO methods (Conn, Scheinberg, Vicente, 2009). In the context of unconstrained optimization, convergence to a stationary point requires the ROM to have the *fully linear property,* i.e., $\left\|\nabla f(x) - \nabla f^R(x)\right\| \le \kappa_g \Delta$, where $f(x)$ and $f^R(x)$ are objective functions related to the original and reduced models, respectively, and Δ is the size of the trust region. The trust region then proceeds according to Fig. 4 and requires the trust region Δ to vanish upon convergence. Convergence properties of the trust region method with fully linear and fully quadratic ROMs were developed in Conn, Scheinberg and Vicente (2009). Wild et al. (2008) developed conditions for ROMs constructed with Radial Basis Functions (RBFs) that satisfy the fully linear property and lead to well-conditioned models. March and Willcox (2012) recently extended their approach to Kriging models and demonstrated the effectiveness of this approach over conventional unconstrained methods. More detail on this approach is presented in Section 4.

3. ROM-based Optimization with Detailed Model Gradients

For ROM-based trust region methods we consider the following *constrained* nonlinear programming problem:

$$Min\ f(x),\ s.t.,\ c_E(x) = 0,\ c_I(x) \le 0,\ x_L \le x \le x_U \qquad (1)$$

where the objective and constraint functions $f(x)$, $c_E(x)$, $c_I(x)$ are assumed to be at least twice differentiable functions. At iteration k of the optimization cycle, a ROM is

constructed at x_k, and this is used to build the following ROM-based trust-region subproblem at iteration k:

$$Min\ f^R(x_k + s),\ s.t.,\ c^R_E(x_k + s) = 0,\ c^R_I(x_k + s) \le 0,\ x_L \le x_k + s \le x_U,\ ||s|| \le \Delta_k \qquad (2)$$

where $f^R(x_k + s)$, $c^R_E(x_k + s)$, $c^R_I(x_k + s)$ are the ROM objective and constraint functions and the trust region Δ_k is a (l_∞) box that restricts the step size s.

3.1 ROM-based Algorithm Development

To simplify the construction of ROMs, model functions are derived by using local corrections that correspond to the current iterate k. Additive correction schemes for the objective and constraints of (2) are given by:

Zero Order Correction (ZOC)

$$\tilde{\Phi}^R_k(x) = \Phi^R_k(x) + (\Phi(x_k) - \Phi^R_k(x_k)) \qquad (3)$$

First Order Correction (FOC)

$$\tilde{\Phi}^R_k(x) = \Phi^R_k(x) + (\Phi(x_k) - \Phi^R_k(x_k)) + (\nabla\Phi(x_k) - \nabla\Phi^R_k(x_k))^T(x - x_k) \qquad (4)$$

with $\Phi(x) = f(x), c_i(x)$ and $\Phi^R_k(x) = f^R_k(x), c^R_{i,k}(x) \qquad i \in \{E, I\}.$

Here ZOC matches basepoint functions only, while FOC matches both functions and gradients at the basepoint. In terms of corrected objective and constraint values, subproblem (2) becomes:

$$Min\ \tilde{f}^R_k(x_k + s),\ s.t.\ \tilde{c}^R_{E,k}(x_k + s) = 0,\ \tilde{c}^R_{I,k}(x_k + s) \le 0,\ x^L \le x_k + s \le x^U,\ \| s \|_\infty \le \Delta_k \qquad (5)$$

Subproblem (5) is then solved using only functions and derivatives from the ROM. On the other hand, functions and derivatives from the detailed model are calculated for the construction of the ROM values in (5), using ZOC and FOC. The algorithm proceeds by choosing step sizes that satisfy a sufficient decrease condition for an exact penalty function of problem (5):

$$\psi^R(x_k + s) = \tilde{f}^R_k(x_k + s) + \mu\left[\left\|\tilde{c}^R_{E,k}(x_k + s)\right\| + \sum_j \max(0, \tilde{c}^R_{I,k,j}(x_k + s))\right] \qquad (6)$$

The corresponding decrease of the penalty function of problem (1) leads to the metric:

$$\rho_k = ared / pred = (\psi(x_k + s) - \psi(x_k)) / (\psi^R(x_k + s) - \psi^R(x_k)) \qquad (7)$$

which determines the increase or decrease of the trust region Δ_k. The resulting trust region algorithm is shown in Fig. 2. Note that the algorithm expands or shrinks the trust region based on how well the ROM-based subproblem follows the original problem surface. Also, the algorithm may terminate with $\Delta_k \rightarrow 0$ if ZOC is applied and detailed model gradients are not provided. On the other hand, if FOC is applied, the algorithm is guaranteed to converge with $||s|| \rightarrow 0$ and a stationary point (where the norms of the directional derivatives $||D_s\psi^R(x^*)|| = ||D_s\psi^R(x^*)|| = 0$) is found for the original problem (1). More details of this approach can be found in Agarwal and Biegler (2012). In addition to the algorithm below, Agarwal and Biegler developed a more detailed filter-based trust region algorithm, which is not sensitive to the penalty parameter μ in (6) and leads to faster performance.

3.2 PSA Case Study

The ROM-based trust-region algorithm was applied in Agarwal and Biegler (2012) to optimize a two-bed four-step pressure swing adsorption process with an 85%-15% N_2-CO_2 feed mixture, as shown in Fig. 3. Although this process cannot be applied directly to the IGCC process in Fig. 1, PSA models have a similar structure to the TSA process and the optimization strategy applies in a straightforward way. The operation consists of four distinct operating steps; pressurization, adsorption, depressurization (counter-current), and light reflux (or desorption). We maximize CO_2 recovery subject to a constraint on CO_2 purity and consider five decision variables, high pressure P_h, low pressure P_l, step times t_p and t_a and adsorption feed velocity u_a according to:

$$\begin{aligned} \max \quad & CO_2 \text{ recovery} \\ \text{s.t.} \quad & CO_2 \text{ purity} \geq 50\% \quad 0.1 \text{ m/s} \leq u_a \leq 0.3 \text{ m/s} \\ & 1 \text{ bar} \leq P_h \leq 3 \text{ bar} \quad 0.4 \text{ bar} \leq P_l \leq 1 \text{ bar} \\ & 35 \text{ sec} \leq t_p \leq 150 \text{ sec} \quad 50 \text{ sec} \leq t_a \leq 400 \text{ sec} \end{aligned} \tag{8}$$

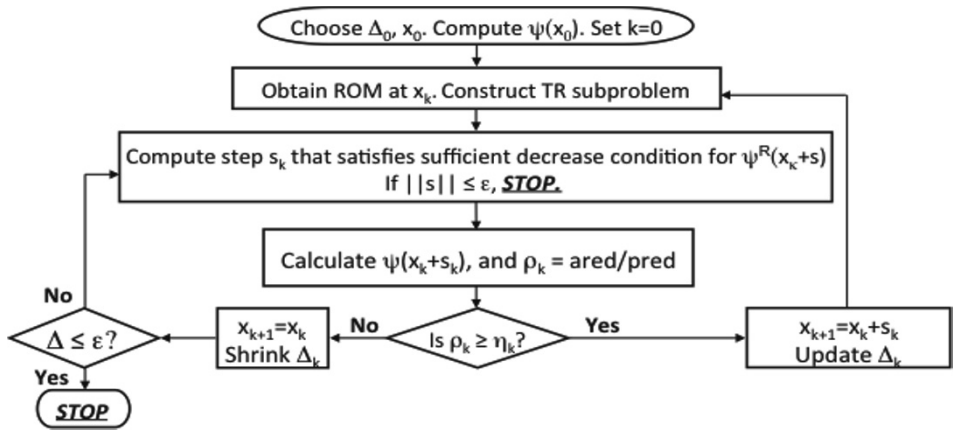

Figure 2. Trust Region Method with Detailed Model Gradients

For the PSA process, the ROM is based on POD applied to the bed equations (as described in Agarwal and Biegler, 2009). The algorithm in Fig. 2 includes the solution of subproblem (5), using the POD-based ROM and IPOPT (Waechter and Biegler, 2006) in an equation-based environment. Also, evaluating the detailed bed models can be done efficiently as part of the generation of the ROM, but here gradient evaluation of the detailed models is done through finite differences. The algorithm requires the solution of 105 trust region subproblems (using IPOPT) and 2.47 CPU h (Intel Quad Core 2.4 GHz processor). It should be noted that if the filter-based trust region algorithm is used, only 51 trust region subproblems and only 1.36 CPU h are required. Moreover, using finite difference gradients we conclude that the algorithm converges to a local optimum. More information on these models and algorithms is given in Agarwal and Biegler (2012).

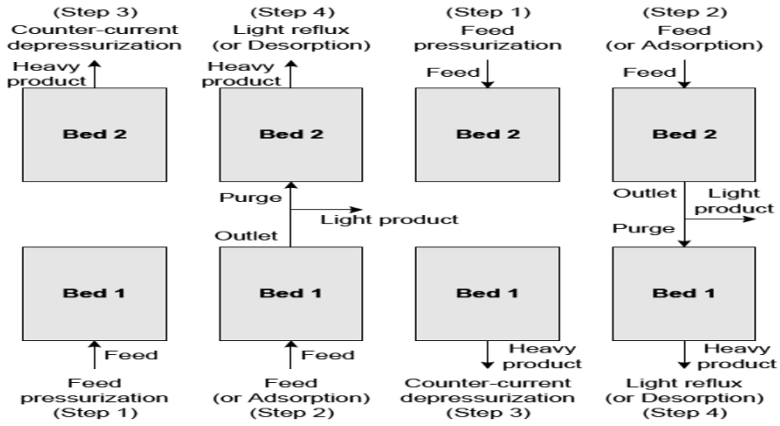

Figure 3: A two-bed four-step PSA cycle

4. ROM-based Optimization without Detailed Model Gradients

Obtaining gradients from detailed CFD models is often prohibitively expensive; hence, the algorithms in Fig. 2 can no longer be used and modifications are needed. In this case convergence guarantees are available if the following properties hold for the ROM. The *fully linear* and *fully quadratic* properties are given by:

$$\left\|\nabla\Phi(x)-\nabla\Phi^R(x)\right\| \le \kappa_g\Delta \text{ and } \left\|\nabla^2\Phi(x)-\nabla^2\Phi^R(x)\right\| \le \kappa_h\Delta, \text{ respectively.}$$

If the *fully linear* property is satisfied, ROM-based trust region algorithms can be constructed that guarantee convergence to a stationary point, satisfying first order optimality conditions. Stronger guarantees for convergence to locally optimal solutions require *fully quadratic* ROMs. Moreover, for ROMs based on radial basis functions (such as Kriging) the fully linear property can be satisfied *only if at least* n+1 *interpolation points lie within the trust region* Δ, where n is the dimension of the degrees of freedom in problem (1).

For fully linear ROMs, a derivative free trust region algorithm was developed and analyzed in Conn et al., 2009) and is sketched in Fig. 4. As with the algorithm in Fig. 2, this algorithm constructs and solves trust region subproblems (such as (5)), updates the trust region based on agreement with the detailed model, and shrinks the trust region if progress is poor. In both cases, frequent recourse is needed to the original detailed model. Moreover, this algorithm has some additional complexities. In particular, note that finding a stationary point for the ROM-based subproblem is *not* sufficient for convergence. Instead, termination of the algorithm occurs if either $\|D_s\psi^R(x^k)\| \rightarrow 0$ or $\Delta_k \rightarrow 0$ *and the ROM remains fully linear*. With a shrinking trust region, the fully linear property therefore needs to be monitored and the ROM needs to be updated. This update step may require more frequent recourse to the original model.

4.1 ROM-based Algorithm Development

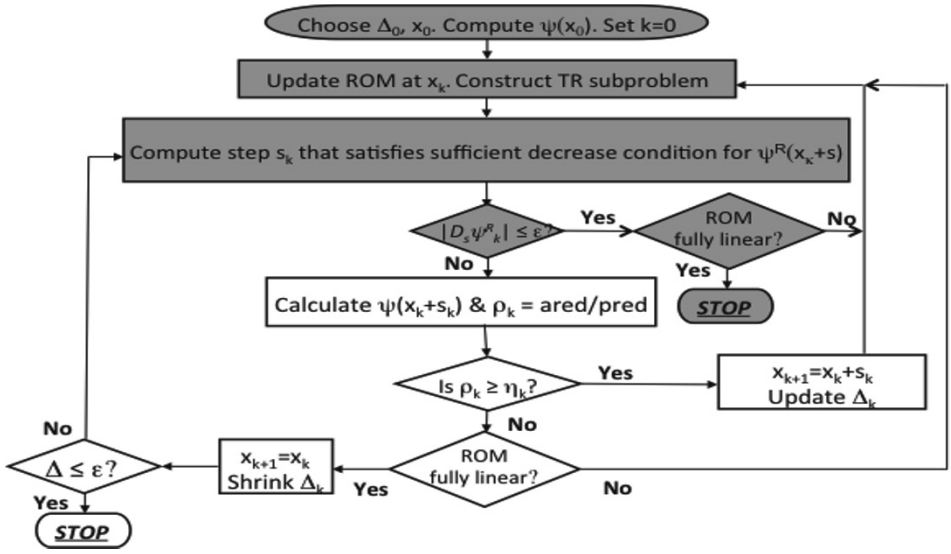

Figure 4. Trust Region Method without Detailed Model Gradients

Now consider the flowsheet optimization problem with heterogeneous models, as illustrated by the IGCC process in Figure 1. Here, it is particularly clear that recourse to the original CFD models during the optimization step is prohibitively expensive. In fact, checking the CFD model at the *solution* of the ROM-based flowsheeting optimization problem may be all that the computing budget allows. To deal with this challenging restriction, we develop ROMs from efficient space-filling experimental designs. We also ensure that ROMs are poised (sampling points are chosen and ROMs are well-posed and well-conditioned). Kriging models with RBFs are a good choice for this. Finally, the ROM-based trust region subproblem (5) comprises the overall flowsheeting model with an initial large trust region, and this subproblem is solved to convergence.

The above characteristics greatly simplify the algorithm in Figure 4. In fact, since the ROM-based model is always fully converged and $\|D_s\psi^R(x^k)\| \le \varepsilon$, only the grayed steps apply and the trust region management steps are bypassed. Moreover, once the ROM-based optimization is determined, the remaining concern is maintaining the fully linear property of the ROM. We propose to address this concern with the following approach:

1. Based on the number and location of sampling points as well as the Lipschitz constants of the original model, determine the smallest value of κ_g that defines a fully linear ROM.
2. Armed with the value of κ_g and a specified tolerance, ε, determine the largest trust region size Δ_{min} that satisfies the convergence criterion.
3. Solve subproblem (5) and locate the number of sampling points within distance Δ_{min} from the solution of (5).
4. If at least n+1 sampling points are within Δ_{min}, convergence is achieved. Else, update the ROMs with additional sampling points and return to step 1.

4.2 ROM-based Process Optimization coupled with CFD Models

We now demonstrate the above approach with the optimization of the advanced IGCC

process shown in Figure 1. In addition to lumped parameter flowsheeting models, the process model contains two CFD models, for the gasifier and combustor. As described in Lang et al. (2009) and Lang et al. (2012), ROMs were developed for both CFD models using Latin Hypercube Sampling for the experimental design and PCA-based reduction of the snapshots of their vector fields at each sampling point. For the combustor ROM, a Kriging model was developed to map the process inputs to the output streams, while an artificial neural network (ANN) ROM was developed for input-output mapping of the gasification unit. Cross-validation on both ROMs showed excellent predictive capabilities over the entire input space. Both output temperatures and compositions were typically predicted with relative errors of less than 1%. Full details of the ROM construction and validation of these models are given in Lang et al. (2009). It is notable that sampling points of the CFD combustor model required over 30 CPU min, while the CFD gasifier model required as much as 20 CPU h. On the other hand, each of the resulting ROMs could be executed within 1 CPU s.

As detailed in Lang et al. (2012), the ROM models were integrated within an equation-based version of the Aspen Plus simulator using the USER3 protocol. This allowed fast, equation-based NLP solvers to be applied directly. For the process optimization, we select four independent variables that relate to the gasifier and the combustor, i.e. fuel distribution, steam and oxygen ratios for the gasifier, and the split fraction that determines the flowrate of the oxidant stream supplied to the combustor. In addition, three independent variables are selected from the process variables in the flowsheet: mass flowrate feeding the water gas shift (WGS) reactors; mass flowrate of the makeup stream recycle within the steam cycle and heat allocation ratio of the high pressure turbine to the medium pressure turbine. The flowsheet optimization problem included ROMs for the for the combustor and gasifier and the objective is to maximize the power generated by the IGCC plant. The problem formulation consists of 3747 variables; solution of the ROM-based optimization problem (9) requires no more than 15 iterations and less than 3 CPU seconds by DMO, the default solver available in Aspen Plus. With an additional $n+1 = 8$ CFD simulations, one can verify the detailed model optimality of these results. The optimization with the ROMs derived from CFD models improves the objective function by a total of 23.22 MWe or 6.8%. This result demonstrates the advantages of process optimization through conversion of ROMs from CFD models into EO process models. With the CFD-derived process models, the process optimization clearly improves the objective function, and provides greater process accuracy. This result shows that ROM-based process modules overcome the prohibitive computational requirements of CFD models and are effective surrogate models for process simulation and optimization.

5. Conclusions and Future Work

Large-scale process optimization of advanced energy systems needs to consider a heterogeneous collection of device-scale and process scale models, with distributed and lumped parameter models of varying complexity. The integrated optimization of these models through multi-scale optimization strategies is enabled by state of the art, equation oriented optimization algorithms along with management of reduced order models. Recent developments in surrogate-based optimization have led to a powerful decomposition framework with multiple scales and convergence guarantees to the overall multi-scale optimum. Here, we also develop an efficient framework that requires infrequent recourse to the original detailed model. Motivated by an advanced IGCC process, we present two case studies that include PSA models for carbon capture and

CFD models for gasification and combustion. In particular, integrated optimization of the IGCC process (including ROMs derived from CFD models) shows that the power output of the process increases by 7% compared to an optimization model that does not consider degrees of freedom in the gasifier and combustion units. This implies that ROM-based flowsheet optimization can significantly increase the efficiency of energy processes. Moreover, the ROM-based optimization framework extends across a wide range of engineering disciplines that include multiple scales and model types. Future work will deal with a detailed analysis of convergence properties for ROM-based trust region methods, particularly with the development and application of fully linear and fully quadratic ROMs. We also plan to improve methods to develop accurate and efficient ROMs from detailed models that arise at device and molecular scales, as well as their integration and validation within multi-scale optimization environments.

References

Agarwal, A., Biegler, L. T., Zitney, S. E. (2009). *Ind. Eng. Chem. Res., 48,* 2327.
Agarwal, A., Biegler, L. T. (2012). *Optim. Eng.,* in press, doi: 10.1007/s11081-011-9164-0
Alexandrov, N. M., Dennis Jr., J. E., Lewis, R. M., Torczon, V. (1998) *Struct. Optim., 15,* 16.
Barrett, A., J.J. Walsh, Comput. Chem. Engng, 3 (1979), p. 397
Biegler, L.T., I.E. Grossmann and A.W. Westerberg, *Comp. Chem. Engr.* 9, 2, p. 201 (1985).
Biegler, L. T., I. E. Grossmann, *Comp. Chem. Eng.* , 28, 8, pp 1169-1192 (2004)
Biegler, L. T. *Nonlinear Programming: Concepts, Algorithms and Applications to Chemical Processes,* SIAM, Philadelphia (2010)
Boston, J. F., H.I. Britt, *Comp. Chem. Eng.*, 2 (1978), p. 109
Brdys, M., P.D. Roberts, *International Journal of Systems Science*, 18, pp. 1305-1322 (1987)
Caballero, J. A. and I. E. Grossmann, *AIChE Journal*, 54, 2633-2649 (2008)
Chung, P. S., M. S. Jhon, L. T. Biegler, *Adv. Chem. Eng*., 40, pp. 59–118 (2011)
Conn, A. R., Gould, N. M., Toint, P. L. (2000). *Trust-region Methods*, *SIAM.* Philadelphia, PA.
Conn, Scheinberg, Vicente, *SIAM J. Opt.,* 20, pp. 387-415, 2009
Fahl, M. (2000). *PhD Thesis.,* Trier Univ.
Gao, W., S. Engell, Comp. Chem. Eng., 29, pp. 1401-1409 (2005)
Kessel, L.B.M. van, J.C.P.L. Saeijs, V. Lalbahadoersing, A.R.J. Arendsen, M. Stavenga, A.B.M. Heesink and H.M.G. Temmink, TNO-Report R98/135 (1998)
Lang, Y-D, A. Malacina, L. T. Biegler, S. Munteanu, J. I. Madsen, S. E. Zitney, *Energy and Fuels,* 23, 1695–1706 (2009)
Lang, Y-D, S. E. Zitney, L. T. Biegler, *Comp. and Chem. Engr.*, 35, pp. 1705 – 1717 (2011)
M.E. Leesley, G. Heyen, Comput. Chem. Engng, 1 (1977), p. 102
March, A. and Willcox, K., AIAA-2010-9198, AIAA/ISSMO Multidisciplinary Analysis and Optimization Conference (2010)
Wächter, A., Biegler, L. T. (2006). *Math. Program., 106,* 25.
Wild, S. M., R. G. Regis, C. A. Shoemaker, *SIAM J.Sci. Comp*. 30, pp. 3197-3219 (2008)

I.A. Karimi and Rajagopalan Srinivasan (Editors), Proceedings of the 11th International Symposium on Process Systems Engineering, 15-19 July 2012, Singapore.

PSE in China: Retrospect and Prospects

Youqi Yang[a] Siwei Cheng[b]

[a]*China National Chemical Information Center,Beijing 100029,China;*
[b]*Research Centre for Virtual Economy, University of Science and Technology of China, Beijing 100049,China;*

Abstract

This is an overview on the developments of Process Systems Engineering (PSE) in China, outlining some viewpoints on future prospects, consisting of four parts:1) Introduction, consisting of progress of the international PSE community and the definitions of PSE from well-known authors;. 2).Retrospect on 20 years of development of PSE in China: Part I describing 5 major PSE contributions: modeling, simulation and optimization for process design and operation; advanced process control and monitoring; process integration for energy conservation and waste reduction; supply chain management for global competition and green PSE for sustainable development, and Part II on problems in development;3).Challenges on future developments for PSE,
4).Future prospects consisting of: two issues: problems in development of PSE in China and future strategies.

Keywords: Process Systems Engineering; Retrospect; Prospects; Overview

1. Introduction

Although the general systems theory could be traced back to the 1930s, system engineering was founded during World War II, when Operation Research (OR) was applied by the Allied Forces to improve logistics. In the 1940s Bell Telephone Laboratory started the large network system theory to meet the requirement of large-scale communication network development. In the 1950s the electronic computer was created and applied in engineering areas, thus providing a sound material basis for systems engineering. In 1954 MIT started offering “systems engineering” as a course, and the well-known book “Engineering Cybernetics” written by H.. S. Tsien（1954） was published in same year. In 1957 the first book titled “Systems Engineering” was published by Goode and Machol (1957).

The development of Process Systems Engineering (PSE) started about 10 years later. The book, “Systems Engineering for the Process Industries”, was published by Williams in 1961. The earliest dynamic process simulator SPEED-UP was developed by Sargent and Westerberg in 1964. In the 1970s PSE began an explosive growth worldwide, along with the rapid growth of the chemical industries, while the first worldwide energy crisis started to challenge energy conservation.

PSE was introduced into China in the late 1970s, several books were written or translated into Chinese (Takamatsu, 1981; Kafarov, 1983; Yang, 1989). Training classes and courses were offered in universities, and teaching-research groups were organized since that time. In 1991 Professor H. S. Tsien recognized as “the father of systems engineering in China”, suggested to Siwei Cheng to organize a PSE society in China. This society was established some 20 years ago as a PSE academic society

covering 11 industries. The major PSE educational and research institutes in main land China is listed on Fig.1.

The Major PSE educational and research institutes in main land China

- Tsinghua University, Institute of PSE in Chemical Engineering Dept.
- Dalian University of Technology, Institute of PSE in School of Chemical Eng.
- East China University of Science and Technology, Eng. Research Center of PSE, sponsored by Ministry of Education
- Qingdao University of Science and Technology, Institute of Computer and Chem. Eng.; Institute of Hi-Tech in Petrochemical Industry
- Tianjing University, Teaching and Research Group of PSE in School of Chem. Eng.
- South China University of Science and Technology, Chem. Eng. Institute in School of Chemistry and Chemical Eng.
- Zhejiang University, The state key laboratory of industrial control technology; National Engineering Research Center for Industrial Automation
- Beijing University of Chemical Technology, School of Chemical Engineering; School of Information Science and Technology
- Wuhan University of Science and Technology, PSE institute of Dept. of Chemical Engineering
- Automation Research and Design Institute of Metallurgical Industry, National Metallurgical Automation Engineering Technology Research Center
- Institute of Process Engineering in Chinese Academy of Science: State Key Lab of Multi-Phase Complex System; Lab for Green Process and Engineering
- Some professors at Beijing University of Petroleum. Xi'an Jiaotong University, Nanjing University of Industry, Nanjing University of Science and Technology are also working involving PSE

Figure1. The list of Major PSE educational and research institutes in main land China

The definition of PSE has witnessed changing since its first definition given by Takamatsu at the first international PSE conference in 1982 (Takamatsu,1983) :
PSE is an academic and technological field related to methodologies for chemical engineering decisions. Such methodologies should be responsible for indicating how to plan, how to design, how to operate, how to control any kind of unit operation, chemical and other production process or chemical industry itself.
This definition emphasized the *multi-scale* concept from the very beginning. Later, Grossmann and Westerberg (2000) extended PSE to chemical supply chains, that is, extended chemical engineering decisions to much larger scope consisting of economics and management. The present authors suggested in 2003 the following definition of PSE:
PSE is a comprehensive science focusing on systems processing mass, energy and information, with its core of studying process system organization, planning, coordination, design, control, operation and management, and aimed at holistic optimization of process system in order to meet the requirements of sustainable development. PSE is broadly applied in industries, such as chemical, pharmaceutical, metallurgical, paper, construction materials, food, etc.

Recently Stephanopoulos and Reklaitis (2011) extended the scope of PSE to (a) processing plants; (b) manufacturing systems producing consumer goods; (c) diagnostic and therapeutic products and processes to treat human diseases;(d) energy production, distribution, and consumption systems; and (e) systems which ensure the quality of environment.

2. Retrospect on 20 years of PSE developments in China

2.1. Contributions of PSE

2.1.1. Simulation and optimization technologies for optimal design and operation of chemical plants

In late 1980s Qingdao Institute of Chemical Technology has developed the second generation Chinese process simulator called "Engineering Chemistry Simulation System, ECSS", which was applied in many design and educational institutes in China. In the new century this technology has been recognized from top leadership of major Chinese petrochemical giants such as Sinopec and PetroChina. For instance, according to report from Sinopec, 3000 people have been trained in 17 enterprises and 8 research/ engineering institutes. 142 plants were simulated in 8 years and 250 million RMB (40MM USD) benefits was gained. (Qi, X., 2007)

An ethylene cracker simulator called EPSOS was developed by corporation between Tsinghua University, Research Institute of Petrochemical Technology under PetroChina and Lanzhou Petrochemical Co. This software is based upon chemical kinetics mechanism model and optimization algorithms, which can predict ethylene yield of the cracker and provide optimal operation guide. (Gao, X., Chen, B., etc.,2010) Operation Training Simulator (OTS) is another area PSE made significant progress in China, most OTS used in China are developed domestically.

2.1.2. Advanced process control and real time monitoring

As China became the world largest iron and steel production country since 1996,the development of process control and monitory technologies in metallurgical industry in China has made significant progresses. For example, the multi-scale close loop hierarchical control system developed by Automation Research and Design Institute of Metallurgical Industry and Baoshan consistent process control system(BPC) are used in China with significant economic benefit. (Sun, G.,2008)

An APC controller based on neural network model predicted control for ethylene cracking furnace was developed at East China University of Science and Technology (Wang, H., Qian, F.. 2011), which can control the outlet temperature from cracking coils keeping the temperature fluctuation range less than 1℃ and the production fluctuation range less than 0.25%.

The Manufacturing Executive System (MES) developed by Zhejiang University, Software Research Institute of Chinese Science Academia and Sinopec is a national key project and the first result SMES 1.0 came out in 2004. As an example, after the installation of SMES in Yanshan Petrochemical Co. the time of material balance calculation of whole enterprise reduced from original 6 days to 6～8 hours, the raw material consume reduced 2% and energy consume reduced about 1%.(Li, D., 2011)

2.1.3. Contributions of process integration for energy conservation

Pinch Technology, as a well-known representative technology of process integration has been broadly promoted in China: energy pinch technology was promoted in 1980s,water

pinch technology in 1990—2000, hydrogen pinch in 2000—2010, cooling water pinch 2010—up to now . In application of those pinch technologies, Chinese scholars have made many progresses (Feng, X.,etc.,2007;Du J., etc..,2010).

2.1.4. Supply chain management technology contributes to increasing competitive capability

Since Sinopec adopting linear programming planning tool PIMS in 35 refineries in 2006 the yield of gasoline/kerosene/diesel increased in 1.03% and the benefit from this is about 291 million RMB per year. In 2007—2010 the application of planning optimization in the deeper integration application phase,19 chemical enterprises and 7 refinery-petrochemical enterprises adopted XPIMS. Not only crude oil for each enterprise but also the intermediates supply for each other's between refinery and chemical plants are also optimized. For instance of Shanghai Petrochemical Co., the benefit from optimization of AGO production planning is about 229 million RMB/a and of naphtha is 187 million RMB.

2.1.5. Green PSE contributes to increasing utilization efficiency of resources and to improving development of ecological industry

EIP is a natural, industrial and social complex, in which the integrations of materials, energy, water and information are all included. PSE provides the theoretical guide for design and construction of EIP in China. (Jin, Y., Arons, J. de. Swaan, 2009)

For example, Tsinghua University was responsible to helping planning and construction of Kaiyang phosphorus-coal chemical eco-industrial basis located in Guiyang,. Through the eco-industry network preliminarily established, the number of product kind is increased to more than 60,total amount of product reached 3 million tons annually and total value of output reach 8000 million RMB per year with average annual growth rate 27.2%. (Hu, S Y., Li, Y., Shen, J., 2003)

2.2. Real problems

The development of simulation and optimization technologies have not satisfied the requirements of industries' growth. Up to now the optimization of chemical process design is still based upon multiple iterations between experience and calculations of simulation tools. Besides, many R/D projects are depending upon big size pilot plants, because the mathematical simulation scale-up methodology has no power to guarantee the results in despite of reduction of pilot experiments.

As we put forwarded "comprehensive integration and holistic optimization" for PSE in order to obtain the whole economic benefit optimal and environment impact minimized results of those large scale petrochemical complexes 12 years ago (Yang, S., Zhou, Z., Hua, B., Chen, S.,1999), but there is seldom expected good results coming out. Application researches of PSE in the strategically important new industries, such as new chemical materials, new energy industry, biochemical industry, clean coal industry, are insufficient.

As mentioned by Klatt, K. U., Marquardt, W., (2009), many good results of PSE only enjoyed published on journals, have not penetrated industrial practice.

The combination of PSE with management science is not close enough. The informatization of process industries needs PSE providing theoretical guide. Another example is the supply chain management of process industry is much lagging behind that of other industries, such as automobile, electronic industries.

3. Challenges for future development of PSE

3.1. Challenges from demands in application

3.1.1. Enterprise-wide operation optimization for cross-country global corporations

The operation of cross-country global corporations depends upon dynamic supply chain management .However, unfortunately the logistic cost of chemical supply chain is the highest among the asset-intensive industries, it cost about 12% of total value of sales, which of pharmaceutical industry and automotive industry is 10% and 9% respectively. The proportion of logistic cost in the net increase value is 43% for petroleum industry; 37% for chemical industry; 30% for paper industry and 28% for automobile industry. (Karimi, I. A. 2009). This is because of the rather low chemical supply chain efficiency.

3.1.2. Challenges of low-carbon sustainable development for process industries

The main tendency of optimization study is extending the scope from internal enterprise to external ecological environment in order to construct a sustainable environment friendly enterprise. Particularly to China, there are following issues should be mentioned: ① Use of renewable resources to replace those fossil resources can play an important role in sustainable development; ② Challenges of clean production: For China, coal as the major primary energy (70% of total energy input) is the main cause of pollution. Therefore the principle task is clean utilization of coal; ③The industrial ecology and eco-industrial parks. In China there are 38 state approved EPI and 319 province approved EPI involving petroleum and chemical industries have been built up to last year. ;④Improving energy efficiency.

3.1.3. Rapid IT progress and emerging development of industrialization and informatization

Since 2010 the chemical industry of China became the largest one in the world. However, the biggest one does not mean the strongest one. So how to turn the large one into strong one is the strategic task in China. Since the new IT innovations commercialized rapidly, such as cloud computation, radio frequency identification (RFID), internet of things are getting popular and will effect on emerging cyber infrastructure. All these progresses will undoubtedly lead to one of the grand challenges of modern PSE.

3.1.4. Small scale production and process intensification

Current production modes are increasingly challenged by decentralization, modularization and miniaturization. Process intensification also tends toward this direction. The micro-chemical technology studies systems within the spatial range of 1—100μm and temporal range of 1—100ms. This kind of systems has many features different from traditional chemical systems(Yang, YQ., 2008): ① The miniaturization of length scale causes significant process intensification: ② Miniaturization brings significant reduction of sample amount required in tests, much faster and more accurate; ③ Inherent safety and good controllability. ④Convenience in scale-up to commercial production of new products; ⑤ Possibility of implementing distributed production mode in chemical industry; ⑥ Pursuing new reaction paths. Combining Micro-chemical Technology with process intensification may create the way of miniaturization of chemical plants. How to design, operate and control this kind of micro-chemical systems is the task of micro scale PSE.

3.1.5. Urbanization causing the need to optimize the infrastructure network of cities

An infrastructure can thus be seen as a complex socio-technical system, the complexity of which is defined by its multi-agent/multi-actor character, the multi-level structure of the system, and the multi-objective optimization. Since PSE field has enabled

tremendous advances in holistic optimization, it is interesting to explore those PSE methods and tools to be applied to infrastructure system design and operations. (Lukszo, Z., etc. 2006).

3.2. Challenges from academic developments

3.2.1. Integration of multi-scale modeling

The simulation scope of PSE is quite different on scales: time scales (10^{-15} to 10^{8} s) and length scales (10^{-9} to 10^{6} m) are used. This large research scope is studied by different disciplines: Atomistic-based simulations such as molecular mechanics (MM), molecular dynamics (MD), and Monte Carlo-based methods (MC) are the area of Computer-Aided Molecular Design (CAMD); for the morphology on scales of 100–1000 nm is the mesoscopic modeling techniques; both of above belong to Computational Chemistry; the scales of 1000nm～10m is the area of Computational Fluid Dynamics (CFD);the scales of 0.1m～10^{4}m is the area of traditional Process System Modeling (PSM), The application ranges of the PSM and CFD methods partly overlap owing to scaling down of the modeled equipment in PSM (Jaworski, Z., Zakzewska, B., 2011).

Each simulation area has its own commercialized tools. As we stressed "comprehensive integration and holistic optimization", the integration approaches of the numerical simulation tools are urgently needed.

3.2.2. Challenges from sustainable development

Simulation and analysis of sustainable development requires extending the scope to include the society−economy−ecology. As Bakshi mentioned (Bakshi, B. R., Fiksel, J., 2003) there are 3 kinds of sustainable business practices that simultaneously benefit both an enterprise and its stakeholders :design for sustainability ,eco-efficient manufacturing and industrial ecology.

3.2.3. The third paradigm of chemical engineering− challenges from product engineering

A classification of chemical products divides all chemical products into three classes: *basic* chemical products (e.g., commodity and specialty chemicals, pharmaceuticals, polymeric materials), *industrial* chemical products (e.g., films, fibers, paper, glass substrates, pastes, creams), and *configured-consumer* chemical products (e.g., light bulbs, hemodialysis devices, labs-on-a-chip). (Seider, W. D., etc. 2009) For *basic* chemical products, emphasis is normally on *process design*, with significant involvement in molecular-structure design – to select the molecules that satisfy customer requirements. Herewith CAMD tools may help a lot. However, for *industrial* and *configured-consumer* products, the key issues probably become to morphology problem. There is no simulation tools and little or no PSE knowledge available for this area.

3.2.4. Nanoscale Process Systems Engineering

With the birth of nano scale process systems engineering, Stephanopoulos (2005) at MIT proposed "nano scale factories" as the next frontier of processing scale and nano scale PSE as the new theory to handle the design, simulation and operation of those active processing systems.,

Yang (2008) pointed out the challenges for PSE. As "molecular factories" is the frontier of next generation manufacturing, traditional PSE is not valid in this area. Nano scale PSE could be realized as a cross-discipline ,where one may find the PSE, system biology, molecular tectonics and molecular computer all fueling the development of nano scale PSE.

4. Future Prospects

4.1. Problems in development of PSE in China

The core competence of PSE used to be related to modeling, simulation and optimization (MSO), methods and tools, which soon became a regular part of chemical engineering studies at the end of the last century. Therefore a risk for PSE is more or less being marginalized. If the PSE community continues limiting efforts to academic research without penetrating industrial practice, PSE is bound to shrink. Risk investment is needed to help transform many good PSE research results into commercial software and routine tools used in industries. This is especially urgent in China.

4.2. Strategies for the future

4.2.1. Upgrade PSE to Multi-scale Product & Process Systems Engineering (MPPSE) to intensify contribution to chemical engineering.

The future challenges in chemical engineering are essentially systems problems, for which PSE could bridge the scales, addressing product design, reaction pathway synthesis as well as equipment and process design in an integrated manner to link user requirements to engineering solution. PSE needs to promote holistic treatment by integrating mature methods/tools from different disciplines into a commercial platform for industrial use, including specialized simulation systems, e.g., for coal-based chemical processes, efficient optimization algorithm packages, etc.

4.2.2. Extend simulation scope — toward virtual plant

Since a plant is accounted as a cost center, cost minimization is the optimization objective. In order to do so, resource and energy/water reduction with quality control is an everyday routine. Should there be a virtual plant based on integration of rigorous models, this would be highly helpful both in operation decision, support and operator training.

4.2.3. Combination with management science — from virtual plant to virtual corporation

Since the headquarter or Strategy Business Unit (SBU) is the benefit center, which accounts every day the net benefits of the whole company dealing with financial flow and financial cost. Therefore, there is a need of combining traditional PSE with management science to simulate the behavior and performance on the corporation level.

If the integrated optimization of a corporation including not only material energy and information flows but also financial flow, the benefit room for the enterprise must be enlarged. The decision support tools are not yet integrated with PSE tools. Once such IT systems were seamlessly integrated with the PSE tools, the competitive power of a corporation would be much improved.

4.2.4. Extend scope of PSE to supply chain — corporation-to-supply-chain optimization

Supply chain management (SCM) extends the enterprise border to enable the enterprise to share information, to cooperate in financial deployment for mutual benefits, and even to establish global manufacturing networks, thus making the enterprise more competitive. Supply chain dynamic optimization avoids, too, *bullwhip effect* and *wave effect*.

4.2.5. Integral simulation of real economy – Virtual Business

Real economy circulation means the entire chain of exchange, production and circulation. The focus of current PSE is production, and the focus of recent e-commerce is exchange (mainly the last exchange). However, virtual business tries to simulate the

whole real economy circulation as a whole by means of advanced information technology together with overall optimization on this basis. Due to extensive use of Internet Protocol Version 6(IPV 6) and network of things the mode of global business will be essentially changed, all presaging the birth of *Virtual Business*.

References

Bakshi,B.R., Fiksel, J., (2003),The Quest for Sustainability: Challenges for Process Systems Engineering, AIChE Journal, 49[6]:1350-1358

Du J., Li X. , Chen, L., Yao,P., (2010),Synthesis of heat integrated mass exchanger networks using step-wise approach based on superstructure, Chinese Journal of Chemical Engineering, 61[10]:2636-2643

Feng, X., Bai, J., Zheng,Z.(2007),On the use of Graphical Method to Determine the Targets of Single-contaminant Regeneration Recycling Water Systems, Chem. Eng. Science, 62 (8) 2127-2138

Gao ,X., Chen, B., He, X., Qiu, T., Li, J., Wang, C., and Zhang, L.,(2008), Multi objective optimization for the periodic operation of the naphtha pyrolysis process, Comput. and Chem. Eng., 32[11] : 2801-2811

Goode, H.,Machol,R.E.,1957, System Engineering, McGraw Hill.

Grossmann, I. E., &Westerberg, A.W. (2000). Research challenges in process systems engineering. AIChE J., 46, 1700–1703.

Hu,SY., Li, Y.,Shen, J.(2003), Integration methodology and applications of Eco-industrial systems(In Chinese), Environment Protection, [1]:16-19

Jin, Y., Arons, J.de.Swaan, (2009), Resource· Energy· Environment· Society —scientific and engineering principles for circular economy, Chemical Industry Press, Beijing.

Karimi,I.A. (2009)., Chemical Logistics—Going Beyond Intra-Plant Excellence Proceedings of 10th Intern.Symposium on PSE—PSE'2009,Elsevier B.V.

Klatt,K.U., Marquardt,W.,(2009), Prospectives for process systems engineering—Personal views from academia and industry, Comp. & Chem. Eng, 33:536-550

Li, DF., (2011) The design and applications of a model driven Manufacture Executive System (MES) for process enterprises, Proceedings of 20 years anniversary conference of PSE, Beijing.

Lukszo, Z., Weijnen, M.P.C., Negenborn,, R.R., Schutter, B. De, Ilić,M., （ 2006 ）, Challenges for process system engineering in infrastructure operation and control, Proceedings of 9th International Symposium on Process Systems Engineering, W. Marquardt, C. Pantelides (Editors) , Elsevier B.V.:95-100

Qi,XZ., (2007),The Status and prospects of informatization construction in Sinopec(in Chinese),Proceedings of 11th annual conference on IT applications in chemical industry CIESC,Xi'ning , China.

Seider, W. D. , Widagdob, S., J.D. Seader, Daniel R. Lewin, (2009), Perspectives on chemical product and process design, Comp. and Chem . Eng., 33 :930–935

Stephanopoulos,N.,Solis, E.O.P. and Stephanopoulos, G.., (2005), Nanoscale process systems engineering: Toward molecular factories, synthetic cells, and adaptive devices, AIChE Jour. 51[7]:1858-1869

Stephanopoulos, G. , Reklaitis, G.V.,(2011).Process systems engineering: From Solvay to modern bio- and nanotechnology. A history of development,successes and prospects for future. Chem. Eng. Science,66:4272-4306

Sun, G.,(2008), The automation technologies for energy conservation in iron and steel industry(In Chinese), Proceedings of annual conference of PSE society of China, Shanghai.

Takamatsu, T. (1983). The nature and role of process systems engineering. Comput. Chem. Engg.,7, 203–218.

Tsien, H. S.,1954, Engineering Cybernetics, McGraw Hill.

Wang, H., Wang, Z., Mei, H., Qian, F.,and Tang, Z.,(2011), Intelligent severity control stabilizes ethylene crackers. Oil and Gas Journal, 109 (6):104-109.

Williams,T.J., 1961, Systems Engineering for the Process Industries, McGraw Hill.

Yang, YQ,1989, Chemical Process Engineering in Practice (In Chinese), Chemical Industry Press, Beijing.

Yang, YQ., (2008), Microscale and nanoscale process systems engineering: Challenge and Progress(In English),The Chinese Journal of Process Engineering, 18, [3] : 616-624,

Yang, S., Zhou, Z., Hua, B., Cheng, SW.,(1999) Comprehensive integration of PSE and management(In Chinese), Modern Chemical Industry(Suppl),:209-214

I.A. Karimi and Rajagopalan Srinivasan (Editors), Proceedings of the 11th International Symposium on Process Systems Engineering, 15-19 July 2012, Singapore.

RECENT DEVELOPMENTS ON PSE EDUCATION AND RESEARCH IN MALAYSIA

Mohd Azlan Hussain[a*], Zainuddin Abdul Manan[b], Norashid Aziz[c]

[a]*Department of Chemical Engineering, Faculty of Engineering,Universiti Malaya, Kuala Lumpur, Malaysia.*

[b]*Process Systems Engineering Centre (PROSPECT), Faculty of Chemical Engineering, Universiti Teknologi Malaysia, 81310 Skudai, Johor, Malaysia.*

[c]*Department of ChemicalEngineering,Faculty of Engineering,Universiti Sains Malaysia, Nibong Tebal, Penang, Malaysia.*

Abstract

Process systems engineering (PSE) is a relatively young area in chemical engineering. The term PSE was used for the first time in the 1961 AICHE symposium series and became more established in Asia in 1982 after the first international symposium in Kyoto, Japan. The development of PSE education and research in Malaysia have taken shape within the last 15 years. PSE has recently evolved into a generic tool for the planning and management of policies as well as resource supply-chain that transcends the process domain. This paper presents the development of PSE education and research in Malaysia. Special highlights are given on the elements of innovation in PSE education and on various research works done by institutions in Malaysia including those that fits the big picture of systems planning and engineering.

Keywords: Chemical Engineering,Process Systems Engineering (PSE), Systems Planning, Engineering education, Malaysia.

1. Introduction

Prof Takamatsu from Kyoto University defined process systems engineering as "...an academic advanced technology field related to methodologies for Chemical Engineering decisions. Such methodologies should be responsible for indicating how to (i) plan (ii) design (iii) operate and (iv) control any kind of unit operation, chemical and other production and chemical industrial processes" [1]. Over the years, this definition has been the basis of many core courses in Chemical Engineering taught in universities around the world including in Malaysia.

The previous definition of Takamatsu falls within the typical and traditional systems engineering concept that is largely confined to the process domain (hence the phrase *process systems engineering)* that is aimed at providing technical solutions for *process industry*. Over the years, systems engineering research has transcended the process industry domain and has, in fact, been used as a tool for the planning and management

[*]azlan@um.edu.my (azlan); zain@cheme.utm.my (zain); chnaziz@eng.usm.my (norashid)

of a nation's policy, resource supply-chain and for facility design and operations [2]. This paper highlights the development of education and research in the field of process systems engineering in Malaysia that fits this big picture of systems engineering that goes beyond the process domain.

2. PSE Education in Malaysia

In Malaysia, the field of Chemical Engineering was introduced in the late 60's at University of Malaya (UM) via the Chemical Technology course, which was established in the Department of Chemistry in 1965. In 1975, Chemical Engineering replaced the Chemical Technology course in University of Malaya [3]. Development of Chemical Engineering programmes with sizable PSE education and R & D elements later took place at Universiti Teknologi Malaysia (UTM), Universiti Kebangsaan Malaysia (UKM), Universiti Sains Malaysia (USM), Universiti Putra Malaysia (UPM), Universiti Teknologi PETRONAS (UTP), Curtin University of Technology and University of Nottingham Malaysia Campus (UNMC).

The area of process systems engineering (PSE) has been widely viewed as the foundation of chemical engineering that provides graduates with the overall, or the systems' perspective to problem solving. This basic foundation in PSE is first introduced in the chemical engineering Material and Energy Balances course. The concept is further strengthened in subsequent courses such as Computational Methods/Computer Programming, Process Simulations and Applications, Chemical Engineering Thermodynamics, Mathematical Methods for Chemical Engineering, Process Dynamics and Control, Reactor Design and Analysis, Product and Process Design and Analysis, Process Integration and Plant Design and Economics.

The Malaysian Chemical Engineering degree is recognised and accredited by the Engineering Accreditation Council (EAC) under the Board of Engineers Malaysia (BEM). As Malaysia is a signatory of the Washington Accord, all engineering degrees in Malaysia including Chemical Engineering is internationally accredited under the Washington Accord. This provides the vital means for benchmarking as well as exposure to international best practices in systems engineering. A few institutions including UM, UKM, UTP and USM have also opted for accreditation by the Institutions of Chemical Engineers of UK (IChemE, UK). USM receives M.Eng accreditation by the IChemE. In order to enhance teaching and learning in PSE, educators in Malaysia have introduced elements of innovations in the PSE modules as highlighted in **Table 1**.

3. Showcase Innovation in PSE Education - Co-operative Problem-Based Learning (CPBL) Approach in Process Control

Extensive innovation in teaching and learning in PSE in Malaysia can be well-exemplified by the successful accomplishments of Mohd-Yusof co-workers from UTM-Process Systems Engineering Centre (PROSPECT) and UTM-Regional Centre on Engineering Education (UTM-RCEE). They introduced, developed and implemented the Co-operative Problem-Based Learning Approach (CPBL) in Process Control and Dynamics Course over a period of ten years. Since the year 2002, teaching and learning in the undergraduate Process Control and Dynamics course at Universiti Teknologi Malaysia has evolved via implementation of tools such as Cooperative Learning (CL),

Problem-based Learning and finally Cooperative Problem-based Learning (CPBL) [4],[5]. CPBL is the integration of CL principles into the PBL cycle to support the implementation of PBL in a typical class setting. Since active learning and solving of practical problems occur in small groups of three to five students before they are taught the necessary concepts, proper support must be given through a functioning learning team. A detailed description of the CPBL framework, and the implementation in the course can be seen Mohd-Yusof et. al. [6].

Table 1: Highlights on the elements of innovation in PSE courses in Malaysia.

PSE-Based Course	Year offered	Elements of Innovation
Introduction to Engineering	1st year	Introduction of principles and applications of engineering and chemical engineering; exposure to, and application of, practical engineering practices through innovative industry and community-related problem-based projects
Material and Energy Balances	1st year	Separation of the material from the energy balance modules to provide more effective learning time for undergraduates
Computational Tools in Chemical Engineering	2nd year	Use of programming tools, simulation software, Matlab/Mathcad and optimization tools/software in Chemical Engineering
Process Control and Dynamics	3rd year	CPBL (see section on innovation in teaching and learning for Process Control an Dynamics Couse)
Product and Process Design/Process Synthesis/Plant Engineering, Process Economics	4th year	Introduction of down-to-earth design concepts and approach through the 7M approach of Chemical Engineering design; use of CPBL. Integration of Process Design and Process Control
Advance Process Control, Process Integration,	4th year & postgraduate	Use of software and patented techniques developed in-house and locally (within Malaysia), and elsewhere.
Design Project	4th year	Industrial visits to process sites related to students projects
Energy Management	4th year (elective) and postgraduate	Job-creation – student are employed as energy auditors to solve problems within the university and present results to the university community.
Industrial Training	3rd year undergraduate, and postgraduate	Integration of undergraduate/postgraduate research projects with industrial training via UNIX (University-Industry Innovation Exchange) programme results in a one year industry-based project.

Efforts to innovate the teaching of the course have brought positive impacts on the students. Research conducted on the implementation of CPBL showed that there were significant increases in students' motivation towards learning the course, as well as their learning strategies and team-based problem solving skills [6]. Consequently, it is not surprising that the final grades for the course also increased significantly. Students' performance in answering the examination questions showed significant improvement in terms of higher class average scores and smaller number of failures (less than 5%) compared to when traditional lectures were used. While grades had improved

tremendously compared to when traditional lectures were given, comparing the different teaching and learning techniques is not the main purpose, knowing that there is a difference in the assessment strategy of the course to ensure constructive alignment. What is vital is that the assessment results show significant learning of the content as well as increased learning motivation and strategies had occurred with CPBL, even when solely measured using written examinations, compared to the dismal grades students used to achieve (at least 30% failures and low average grade) when traditional lectures were

4. Research and Development in PSE in Malaysia

In Malaysia, R & D in systems engineering that exemplifies *the big picture* has begun in earnest over the past few years. The vast majority of the Malaysian institutions however has made noteworthy contributions in the well-established process systems engineering domain of design and synthesis, control and modelling and operations of *processes*. Alongside this, ample progress has been made in the development of holistic and sustainable business model via systems planning and management, facility design and operations within a multi-disciplinary R & D environment beyond the *process* domain. The R & D activities in PSE in Malaysia can be classified under the following sub-areas[2]:

(1) Molecular product design - Design of tailor-made, marketable green products to meet customer requirements.
(2) Facility design, control and operation- Development of models, tools, techniques and products to design, control and operate sustainable facilities and enterprises (process plants and buildings) that are cheaper, safer, cleaner, energy-efficient and operable.
(3) Community, systems and resource planning and management - Development of business models for optimal planning and management of green and smart townships, regions and nations that cover technical and implementation solutions including development of policies and market instruments, educational systems and guidelines as well as development blueprints.

Table 2 highlights the R & D activities in PSE in various institutions in Malaysia.

5. Conclusion

The development of PSE education and research in Malaysia has recently evolved in the direction of a generic tool for systems, policy as well as resource supply-chain planning and management that transcends the process domain. Continuous international benchmarking, networking and world-class R & D works have spurred various innovations in PSE teaching and learning as well as in research.

References

[1] Takamatsu T, Process Systems Engineering, Proceeding of the International Symposium on Process Systems Engineering, Japan, 1982.
[2] Universiti Teknologi Malaysia-Process Systems Engineering Centre (PROSPECT), http://www. Cheme.utm.my/prospect.

[3] Department of Chemical Engineering, Faculty of Engineering, University Malaya.http://engine.um.edu.my/

[4] K. Mohd.-Yusof, Z. Tasir, J. Harun, S. A. Helmi, "Promoting Problem-based Learning (PBL) in Engineering Courses at the Universiti Teknologi Malaysia", Global Journal on Engineering Education, Vol. 9, No. 2, 2005 (page 175 – 184).

[5] Khairiyah Mohd Yusof and S. A. Helmi, "Designing Effective Learning Environment for Cooperative Problem-based Learning (CPBL) for Engineering Courses", ASEE Global Colloquium Proceedings, Paper GC2008-87, Cape Town, South Africa, October 2008.

[6] Khairiyah Mohd-Yusof, Syed Ahmad Helmi, Mohammad-Zamry Jamaluddin and Nor Farida Harun, "Cooperative Problem-based Learning: A Practical Model for Typical Course", International Journal of Emerging Technologies in Learning, Vol. 6, Issue 3, September 2011.

Table 2. Highlights on PSE research and development activities in various Malaysian universities

Institution (Year Established); Group/Centre of Excellences related to PSE	**Current PSE Focus Areas**	**Key Research Themes**
University of Malaya (1975) UMPEDAC www.umpedac.um.edu.my	Process Control, Modeling and Automation	Process Control and Modeling, power electronics, drives, automation and control.
Universiti Teknologi Malaysia (1983); UTM-PROSPECT (Process Systems Engineering Centre), IHE (Institute of Hydrogen Energy) & RCEE (Regional Centre on Engineering Education) www.cheme.utm.my/prospect	Sustainable Systems Planning and Engineering; Hydrogen Energy; Engineering Education	From molecular product design to facility planning and operation and community planning and management; Hydrogen energy and fuel cell energy systems
Universiti Kebangsaan Malaysia (1984); Fuel Cell Institute www.ukm.my/selfuel/	Fuel Cell and Hydrogen Energy	Renewable energy – i.e. solar, hydrogen energy and fuel cell systems
Universiti Sains Malaysia (1992);Process Systems Engineering Group chemical.eng.usm.my/	Process Control and Modeling	Process Control and Modeling, optimization, process integration and intensification.
Universiti Teknologi PETRONAS (1997); Process Systems Engineering Group www.utp.edu.my/index.php?option=com_content&view…	Process Design, Process Integration, Control and Optimisation	Process design and analysis, process integration and control for energy efficiency and environmental protection
Curtin University of Technology (2000); Process Systems Engineering Group http://soes.curtin.edu.my/chemical-engineering/	Sustainable Process Systems and Design	Bioreactor optimization, energy and resource management, optimal pollution prevention and treatment
University of Nottingham (Malaysia) (2000); COE for Green Technologies www.nottingham.edu.my/SPI www.nottingham.edu.my/CEGT	Sustainable Process Integration and Green Technologies	Resource conservation and planning, biorefinery and molecular design

I.A. Karimi and Rajagopalan Srinivasan (Editors), Proceedings of the 11th International Symposium on Process Systems Engineering, 15-19 July 2012, Singapore.

Opportunities for Energy Savings in Azeotropic Separation Processes

I-Lung Chien

Department of Chemical Engineering, National Taiwan University, Taipei 10617, Taiwan.

Abstract

There are various methods in industry which can be used for separating azeotrope. Wise choice of the most effective separation method is very important in saving energy and reducing total annual cost of such processes. In this paper, methods for separating azeotrope via distillation will be overviewed. Industrial applications will be used to demonstrate that large savings of operating energy can be realized by selecting the most effective separation method. Several analytical tools can be used to aid the decision of the selection.

To further save energy of the azeotropic separation processes, several feasible heat integration schemes are explored. These include: feed-effluent heat exchanger, double-effect distillation, and divided-wall column. Industrial examples will be used to illustrate the heat integration applications.

Keywords: Azeotropic Separation, Extractive Distillation, Heterogeneous Azeotropic Distillation, Heat Integration, Divided-Wall Column

1. Introduction

Distillation is the most widely used separation process in chemical industry. In Tyreus (2011), it is estimated that separation processes account for 40-70% of both capital and operating costs in petrochemical processing and that distillation is used to make 90-95% of all separations in the chemical process industry. In Julka, et al. (2009), it is stated that distillation columns and their support facilities can account for about one-third of the total capital cost and more than half of the total energy consumption. Consequently, the design and optimization of the distillation train have a critical impact on the economics of the entire process.

Among all the distillation processes, the mixtures containing azeotrope are most difficult to be separated. Simple distillation cannot be used to achieve complete separation. A recent book by Luyben & Chien (2010) summarizes the feasible ways used in industry to achieve such separation.

Although for a particular azeotropic mixture, there are more than one way to achieve the separation. This paper will address the important issue of how to use analytical tools such as vapor-liquid equilibrium plots, residue curve maps (RCM), and material balance lines to select the most suitable separation method. Two industrial applications will be used to demonstrate that significant energy savings can be realized with proper selection of the most suitable separation method.

To further save energy of the azeotropic separation processes, various heat-integration schemes will be explored. The simplest scheme is via feed-effluent heat exchanger (FEHE) to recover heat from hot product stream. One other ways is to operating two columns in the process at different pressures so that the condenser of the high-pressure column can be combined with the reboiler of the low-pressure column to save energy. This is called the double-effect columns. The other feasible way is to come

up with thermally-coupled (divided-wall) design in the process so that the possible "re-mixing effect" in the column can be eliminated. Another heat-integration method mentioned in open literature is to use vapor recompression scheme so that the vapor from the overhead of a column is compressed as the heat pumping fluid to support energy required for its reboiler in the bottoms of the same column. This is called the internal heat-integrated distillation column (HiDiC). However, this scheme needs to add an expensive compressor to the process thus is not studied in this paper.

2. Azeotropic Separation Processes via Distillation

There are various ways to achieve the separation of azeotrope via distillation. In the following, industrial examples will be used to overview these separation methods.

2.1. Pressure-swing distillation

The distillate stream from a reactive-distillation column to produce *tert*-amyl methyl ether (TAME) is used here as an example (Luyben, 2005). This distillate stream contains several inert C5s and methanol. The purpose is to recover methanol from these C5s and to recycle back to the reactive-distillation column. Let's use iC5-methanol separation as an example to illustrate the concept to achieve the separation. Other inert C5s have the similar property as iC5.

The Txy plots of iC5 and methanol mixture at two different operating pressure are shown in Figure 1. There is difference in azeotropic compositions at these two pressures which permits the use of the design flowsheet in Figure 2 to achieve the separation. The question of how far apart these two azeotropic compositions is very important for determining the competitiveness of this flowsheet versus other separation methods. Large recirculation flow rate will result in larger operating energy as well as large capital cost. From total material and composition balances, it is very easy to estimate the ratio of HP recycle flow rate vs. the fresh feed flow rate.

The usual way for the selection of the operating pressure at LP column is to have a high enough top temperature to permit the use of inexpensive cooling water in the condenser. For the HP column, the decision is usually dependent on the unit price of the steam used in the reboiler. The decision here is to select a high enough pressure but still permit the use of same steam. Other limitation for the HP column is to avoid too high a temperature at reboiler to prevent the forming of oligomer or other problems.

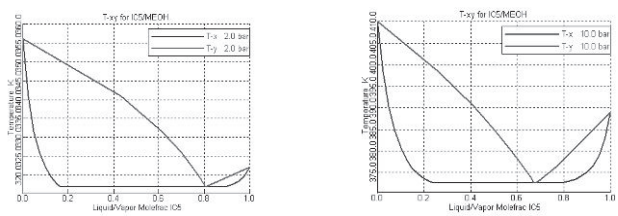

Figure 1. Txy plots of iC5-methanol mixture at two different operating pressures.

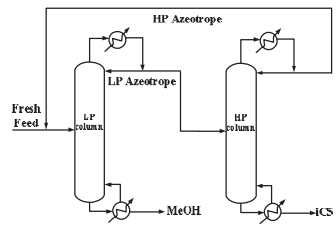

Figure 2. Pressure-swing distillation design flowsheet.

2.2. Heterogeneous Binary Azeotrope Separation

From previous Figure 1, one distinguish characteristics of this mixture can easily be observed. It is found that the azeotrope after condensed to liquid phase can naturally be separated into two liquid phases. The following alternative design flowsheet in Figure 3 takes advantage of the liquid-liquid separation in a decanter to achieve the separation. Note that the methanol-enriched phase can further be separated in a stripper to obtain pure methanol and the iC5-enriched phase can also be separated in another stripper to obtain pure iC5.

Notice that in this design flowsheet the fresh feed is fed into the decanter. The reason is because the feed composition is already in the liquid-liquid splitting region. Luyben & Chien (2010) introduced other applications where the fresh feed can be fed into one of the two strippers. The other choice is the operating pressures of the two strippers. The decision is similar in the pressure-swing distillation to achieve easy vapor-liquid separation and to avoid using more expensive cooling or heating mediums.

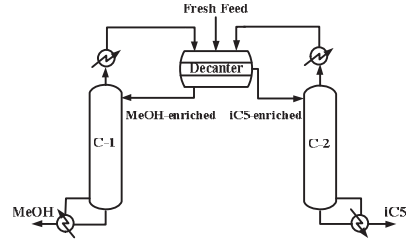

Figure 3. Heterogeneous Binary Azeotrope design flowsheet.

2.3. Heterogeneous Azeotropic Distillation

Another way to separate azeotropic mixture is to add a light entrainer into the system so that an additional azeotrope can be formed that helps in the separation. The most common applications are to form a heterogeneous minimum-temperature azeotrope so that one of the original components can be carried overhead in a distillation column and liquid-liquid splitting in a decanter. Various industrial applications can be found in Chapter 8 of Luyben & Chien (2010). Wu, et al. (2011) illustrated another application where a middle decanter is designed.

Isopropyl alcohol (IPA) dehydration is used here as an example to illustrate the separation principle of this separation system. The residue curve map and liquid-liquid boundary of this system with cyclohexane as an entrainer is shown in Figure 4. The design flowsheet in Figure 5 contains a combined column (served as a pre-concentrator column and also as a recovery column) and another heterogeneous azeotropic distillation column. The conceptual design can be explained by the material balance lines in Figure 4.

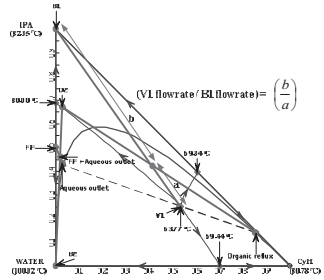

Figure 4. RCM, LLE, and material balance lines of the IPA dehydration system.

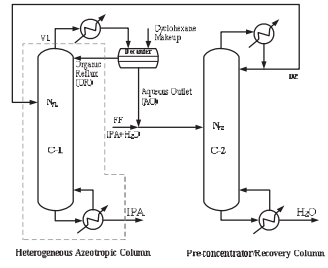

Figure 5. Design flowsheet via heterogeneous azeotropic distillation.

2.4. Extractive Distillation

Another way to separate azeotropic mixture is to add a heavy entrainer into an extractive distillation column so that the relative volatility of the original two components can be greatly enhanced. Thus, one original component can go overhead and the other component will go with the heavy entrainer to the column bottoms. A second entrainer recovery column is designed to separate this stream so that the entrainer can be recycled back to the extractive distillation column. The conceptual design flowsheet of the IPA dehydration system is shown in Figure 6.

The most important decision in this design is to choose a most effective entrainer in order to enhance the relative volatility of the original two components. Chapter 10 in Luyben & Chien (2010) used isovolatility and equivolatility curves to compare candidate entrainers. An even easier plot to generate is shown in Figure 7. In this plot, the starting composition is right at the azeotrope of IPA and water. By gradually adding entrainer into the system, we can calculate the enhancement of relative volatility at various feed ratio. This figure demonstrates that dimethyl sulfoxide (DMSO) is a much more effective entrainer than ethylene glycol (EG) for this separation system.

The way to generate the above plot is very easy by using commercial simulator such as the one from Aspen Technologies, Inc. The way to generate each point in the plot is to use the *Flash2* module in the unit operation library. Without adding entrainer, the relative volatility of a stream at azeotropic composition will be at 1.0. At any other feed ratio, the vapor and liquid composition in equilibrium can be calculated by Aspen Plus under adiabatic flash operating at 1 atm and with negligible vapor flow. Excerpting information about the IPA and water, the relative volatility between these two components can be calculated.

Other factors that affect the entrainer performance are the yx or Txy plots. The yx or Txy plots of the IPA-entrainer pair can be used to determine the ease of separation in the rectifying section of the extractive distillation column. The yx or Txy plots of the water-entrainer pair can be used to determine if the separation in the entrainer recovery column is easy or not. Of course, thermally stable, nontoxic, low price, and other favorable physical properties should also be considered in the entrainer selection.

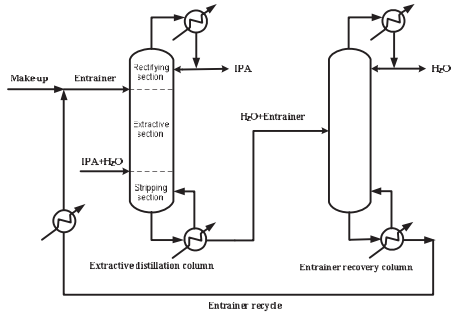

Figure 6. Design flowsheet via extractive distillation.

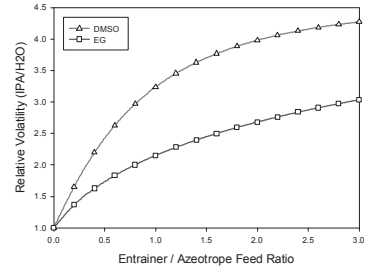

Figure 7. Relative volatility Plots at 1 atm for two heavy entrainers.

2.5. Other Separation Methods

We did not include discussion of other separation methods such as hybrid distillation-adsorption, hybrid distillation-pervaporation in this paper. The main reason is because the efficiency of the separation is highly dependent on the performance of the adsorbent (e.g. molecular sieve) in the adsorption unit or the membrane in the

pervaporation unit. Chapter 14 in Luyben & Chien (2010) showed a hybrid distillation-pervaporation application for the separation of ethanol and water.

Another separation method is to use a reactive intermediate to react away one of the components in the azeotrope in a reactive-distillation (RD) column and then to utilize reverse reaction in another RD column to obtain that component. We also did not include any discussion of this separation method in this paper.

3. Two Industrial Examples via Different Separation Methods

For a particular application, there are usually more than one ways to achieve the separation. In the following, two industrial examples will be used to demonstrate the importance of selecting the most effective separation method in terms of energy savings.

3.1. C5s and Methanol Separation

In previous Sections 2.1 and 2.2, two alternative design flowsheets can be used to achieve the same separation of C5s and methanol. The optimal design flowsheet via pressure-swing distillation in Fig. 2 is obtained in Luyben (2005) while that of the design flowsheet via heterogeneous binary azeotrope in Fig. 3 is obtained in Wu, et al. (2009). In either of the two flowsheets, feed composition and also product specifications are kept the same, thus direct comparison can be made.

Table 1 compares the total annual cost (TAC), the capital and the energy costs of the two alternative design flowsheets. The calculations are based on the cost data in Appendix E of Douglas (1988). From Table 1, it is shown that significant reductions in both the capital and energy costs can be made by choosing the more suitable separation method. Using the design flowsheet in Fig. 3, the capital cost can be cut by 66.2% and the energy cost can be reduced by 81.9%. The main reason for the significant savings is because natural liquid-liquid splitting behavior is utilized in the flowsheet in Fig. 3.

Table 1. TAC and energy cost of C5s and methanol separation.

	Figure 2 design	Figure 3 design
Annualized capital cost (10^6 \$/yr)	1.42	0.48
Annualized energy cost (10^6 \$/yr)	6.92	1.25
TAC (10^6 \$/yr)	8.34	1.73

3.2. Isopropyl Alcohol Dehydration Process

In previous Sections 2.3 and 2.4, two alternative design flowsheets are used to achieve the same separation of IPA and water. The optimal design flowsheet via heterogeneous azeotropic distillation in Fig. 5 is obtained in Arifin & Chien (2007) while via extractive distillation in Fig. 6 is obtained in Arifin & Chien (2008).

Table 2 compares the total annual cost (TAC), the capital and the energy costs of the two alternative design flowsheet. It is observed that 31.2% energy savings can be made by using the design in Figure 6. Significant savings in TAC and the capital cost can also be made by performing the separation via extractive distillation.

The main reason that heterogeneous azeotropic distillation flowsheet is not competitive can be observed from previous Fig. 4. Doing material balance for the heterogeneous azeotropic column indicated in red-dashed envelope in Fig. 5, the flow ratio for the top vapor to the bottoms can be estimated for this column. From Fig. 4, this ratio is approximately to be three. This means large organic reflux flow rate is recycled back to this column as well as large aqueous flow to the entrainer recovery column. These in terms cause large capital and energy costs. This deficiency of using this separation method can easily be found before doing any rigorous simulation.

Table 2. TAC and energy cost of IPA and water separation.

	Figure 5 design	Figure 6 design
Annualized capital cost (10^6 \$/yr)	0.71	0.47
Annualized energy cost (10^6 \$/yr)	0.48	0.33
Entrainer makeup cost (10^6 \$/yr)	nil	nil
TAC (10^6 \$/yr)	1.19	0.80

4. Further Energy Savings via Heat Integration

In this section, other heat-integration methods widely used in industry will be outlined below and applied to azeotropic separation processes.

4.1. Feed-Effluent Heat Exchanger (Economizer)

Since the bottom temperature of a distillation column is at the highest, the simplest method is to utilize this heat to exchange to the feed stream of this column. This is called a feed-effluent heat exchanger (FEHE) design or called an economizer. Implementing this heat-integration method required an additional heat exchanger. The trade off will be the additional investment of this heat exchanger to the savings of the reducing reboiler duty. A typical economizer design for pressure-swing distillation flowsheet is shown in Figure 8. This design concept can also be used in the extractive distillation flowsheet. For the heterogeneous design flowsheet in Fig. 5, the temperature difference between the hot and cold stream is usually not large enough to justify the use of this heat-integration method.

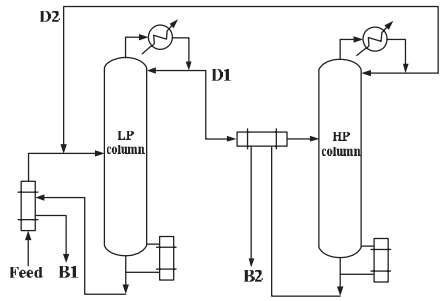

Figure 8. Pressure-swing distillation with two feed-effluent heat exchangers.

4.2. Double-Effect Distillation Columns

This design concept of double-effect distillation is to utilize the heat recovered in a condenser to be used in another reboiler. With this design, a heat exchanger is installed which serves as the condenser for the high-pressure column and also as the reboiler for the low-pressure column. The conceptual design flowsheet of this design with two additional FEHEs is shown in Figure 9. Note that because the heat removal in the condenser should be exactly the same as the heat input in the reboiler, a control degree-of-freedom is lost. Most often, the dynamic and control of this complete heat-integration design will be deteriorated. Another alternative design to trade-off economics/controllability is to install an auxiliary reboiler and/or auxiliary condenser. In this way, partial heat-integration can still be achieved without the lost of one control degree-of-freedom.

This design is not suitable to be used in the flowsheets in Figs. 5 and 6. Although there are also two columns in these two flowsheets, increasing operating pressure in the entrainer recovery column usually will have adverse effect in the ease of separation. For

the extractive distillation system, the bottom temperature may also become too high to prohibit the use of the original heat source.

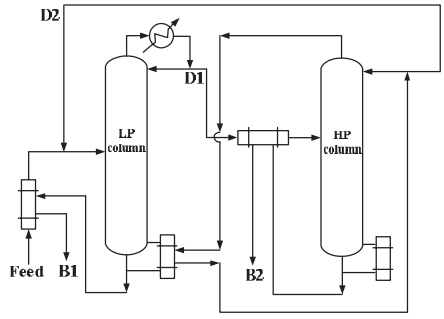

Figure 9. Pressure-swing distillation with two FEHEs and a double-effect arrangement.

4.3. Thermally-Coupled (Divided-Wall) Column

Another method used in industry is to eliminate the remixing effect in a column sequence via thermally coupled two columns. This is also called Petlyuk column or divided-wall column because a special-designed wall can be installed in a column to achieve the same purpose of thermally-coupling two columns together. In this way, besides energy savings the plant site can also be reduced. By observing the four previous separation methods for azeotropes, the extractive distillation column in Fig. 6 exhibited remixing effect in the stripping section of the extractive distillation column. To further save energy of this process, the way is to thermally-coupled the two columns so that the vapor for the extractive distillation column is supplied by a sidedraw from the entrainer recovery column. This design configuration is shown on the left-side of Figure 10. The identical divided-wall column design is illustrated on the right-side of the same figure.

Notice that the number of reboilers of this extractive distillation process is reduced from two to only one. We have studied this design configuration for two chemical systems of IPA-H_2O-DMSO and acetone-methanol-H_2O. The total reboiler duty can always be reduced. However, the total steam cost of this extractive divided-wall column process may not be lower than the original design without divided-wall. The main reason is that the combined reboiler requires a heat medium with higher temperature because a heavy entrainer is used. The question if it is beneficial to use thermally-coupled design can easily be determined by checking the two bottom temperatures in Fig. 6.

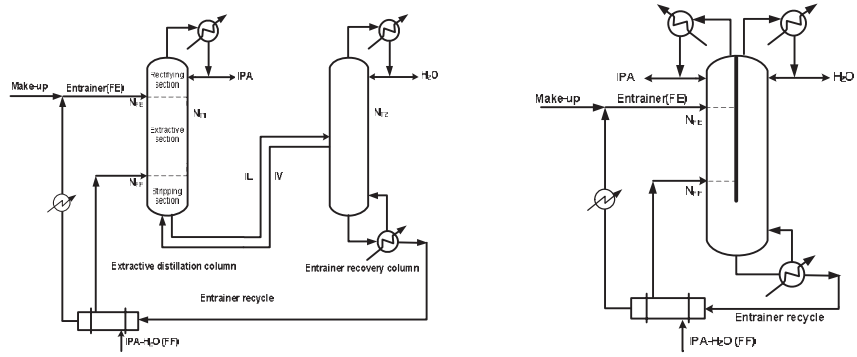

Figure 10. Extractive divided-wall column with FEHE.

5. Conclusions

In this paper, various ways to save operating energy in azeotropic separation process are presented. Two industrial systems illustrated the importance of choosing the most effective separation method. For heterogeneous binary azeotropes, a separation process with a decanter and two strippers should be used to take advantage of the natural liquid-liquid splitting in this system. The disadvantage of the pressure-swing distillation is the necessary recirculation flows of LP and HP azeotropic compositions in the system. This recirculation flow rate can easily be estimated from Txy plots as in Figure 1. The deficiency of the heterogeneous azeotropic distillation presented in this paper is also due to the large recirculation flows in the system. This deficiency can easily be revealed from RCM, LLE, and material balance lines in Figure 4. For extractive distillation process, the key is to select an effective entrainer to greatly enhance the relative volatility of the original two components. This capability can be known with the comparison plot as in Figure 7. Another point needs to be aware is the inherent disadvantage of the heterogeneous azeotropic distillation or extractive distillation of introducing a third component into the system that will appear as impurity in the product streams.

To further save operating energy, FEHE can be used in pressure-swing distillation and extractive distillation systems because of enough temperature difference between the feed and bottoms streams. The double-effect distillation can also be used in pressure-swing distillation process to combine a reboiler and a condenser. However, there is a trade-off between the economics and dynamic controllability. For extractive distillation processes, the thermally-coupled design principle can also be applied to reduce the total reboiler duty. However, the attention should be given to the heat medium used in this system. There are industrial examples where the total steam cost adversely increased by using thermally-coupled design as in Figure 10.

6. Acknowledgment

Research cooperation with Prof. W. L. Luyben on the C5s-methanol separation is gratefully acknowledged. Hard works from my former and current graduate students on the case studies in this paper are also greatly appreciated.

References

S. Arifin & I. L. Chien, 2007, Combined preconcentrator/recovery column design for isopropyl alcohol dehydration process, Ind. Eng. Chem. Res., 46, 2535.

S. Arifin & I. L. Chien, 2008, Design and control of an isopropyl alcohol dehydration process via extractive distillation using dimethyl sulfoxide as an entrainer, Ind. Eng. Chem. Res., 47, 790.

J. M. Douglas, 1988, Conceptual Design of Chemical Processes, McGraw-Hill, New York.

V. Julka, M. Chiplunkar, & L. O'Young, 2009, Selecting entrainers for azeotropic distillation, Chem. Eng. Prog., March, 47.

W. L. Luyben, 2005, Cmoparison of pressure-swing and extractive distillation methods for methanol recovery systems in the TAME reactive-distillation process, Ind. Eng. Chem. Res., 44, 5715.

W. L. Luyben & I. L. Chien, 2010, Design and Control of Distillation Systems for Spearating Azeotropes, Wiley, Hoboken, New Jersey.

B. D. Tyreus, 2011, Distillation–energy conservation and process control, a 35 year perspective, AIChE Annual Meeting, October 16-21, Minneapolis MN, U.S.A.

Y. C. Wu, I. L. Chien, & W. L. Luyben, 2009, Two-stripper/decanter flowsheet for methanol recovery in the TAME reactive-distillation process, Ind. Eng. Chem. Res., 48, 10532.

Y. C. Wu, C. S. Hsu, H. P. Huang, & I. L. Chien, 2011, Design and control of a methyl methacrylate separation process with a middle decanter, Ind. Eng. Chem. Res., 50, 4595.

I.A. Karimi and Rajagopalan Srinivasan (Editors), Proceedings of the 11th International Symposium on Process Systems Engineering, 15-19 July 2012, Singapore.

Process Systems Engineering Approach to Synthesis of Batch Chemical Processes

Thokozani Majozi[a,b]

[a]*Department of Chemical Engineering, University of Pretoria, Pretoria, South Africa*
[b]*Council for Scientific and Industrial Research, Advanced Modelling and Digital Science, Pretoria, South Africa*

Abstract

The problem of batch chemical process synthesis was first posed formally in the seventies. However, it is only in the last 2 decades that significant advances have been made in this regard. The volatility in global market trends that has characterised recent times necessitates that the chemical process of today readily adapts to sudden changes in demand and supply. Unlike their continuous counterparts, batch processes are readily amenable to this situation due to their inherent discreteness of unit operations. Consequently, they continue to remain an obvious choice where competitiveness is paramount. Much credit in understanding and ultimately addressing the idiosyncrasies of batch facilities is attributable to the adoption of a process systems engineering approach in synthesis of these processes. Whilst highlighting challenges that still prevail in this domain, the paper also presents some of the most advanced contributions made in recent years in synthesis of batch facilities. The presentation focuses on scheduling, design, heat integration, as well as water minisation in multipurpose batch processes. Results from various case studies of industrial relevance are presented.

Keywords: Synthesis, Optimisation, Scheduling, Batch, Multipurpose

1. Introduction

The most challenging aspect in optimum synthesis and design of batch chemical processes is the ability to capture the essence of time. This mandates a robust framework which allows accurate treatment of time without steep computational intensity. Early contributions in this regard proposed a discretization of time which is concomitant with enhanced binary dimensions that invariably lead to serious computational difficulties. The mid-nineties were characterised by the introduction of continuous-time frameworks which drastically reduced the binary dimension thereby allowing some of the developments to permeate the practical space. However, the industrial applications of these developments were still limited to very short time horizons which proved insufficient. Very recently, methods that seek to extend the range of time horizons within which these continuous time frameworks could be applied with confidence have been proposed in published literature, albeit at the expense of rigor.

Significant advances in scheduling batch plants followed the work of Kondili et al. (1993), which proposed even discretization of the time horizon. This approach was met with significant computational challenges, due to the extent of the binary dimension. Consequently, Zhang and Sargent (1996) proposed a continuous time formulation based on the concept of the resource task network (RTN) representation. The resulting

formulation led to a MINLP problem later linearized into a large MILP model that was difficult to solve by conventional solvers.
Méndez et al. (2006), Floudas and Lin (2004), Shaik and Floudas (2006) present excellent reviews of the current scheduling techniques based on different time representations and associated challenges. In their review the different models are classified as slot based, event based and precedence based (sequence - based) time representation. In the slot based models (Pinto and Grossmann, 1994, 1995; Lim and Karimi, 2003; Liu and Karimi, 2007, 2008) the time horizon is divided into non-uniform unknown slots with tasks starting and finishing at the same slot. The event based models (Maravelias and Grossmann, 2003; Castro et al., 2004) use uniform unknown events where the time associated with the events is common across all units. On the other hand, the sequence-based or precedence-based representation uses either direct precedence (Méndez and Cerdá, 2000; Hui and Gupta, 2000; Gupta and Karimi, 2003a,b; Liu and Karimi, 2007) or indirect precedence sequencing of pairs of tasks on units (Méndez et al., 2000, 2001; Méndez and Cerdá, 2003, 2004; Ferrer-Nadal et al., 2008).
Another unique contribution in the synthesis of batch plants is the technique based on the so called S-graph framework, which has been reported extensively by Friedler and co-workers (1998, 2002). This framework does not require any presupposition of time points, which renders it truly continuous in time. However, it also experiences challenges in handling Finite Intermediate Storage (FIS) operational policy.
The aforementioned contributions have laid a solid foundation for handling resource conservation problems, like energy optimization and wastewater minimization, in batch chemical plants. Presented in this paper are some of the most recent results in this regard.

2. A brief description of problems addressed

This section gives a brief description of problems addressed in this paper.

Batch process scheduling and synthesis
In its simplest form, the problem of batch process scheduling involves determination of maximum throughput over a given time horizon, or determination of minimum makespan for a given production profile. Both these objectives are achieved through an optimum production schedule, which takes into account the production recipe, the capacity of a unit and the type of tasks the unit can perform, as well as the maximum storage capacity for each material. Although the scheduling problem qualifies as a synthesis problem, since it involves the optimum combination of tasks in the temporal space, the exact synthesis problem is mainly about optimum capacity and number of processing units that satisfy a predefined objective. Figure 1 below shows a typical superstructure used as a basis for the synthesis a minimum capital cost Parahydroxy-Benzoic-Acid (PHBA) facility, whilst Figure 2 shows the optimum design.

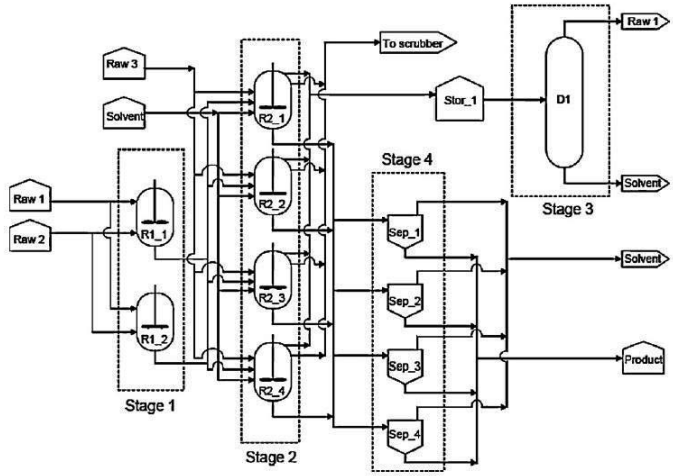

Figure 1: Superstructure for the synthesis of the industrial facility (Pattinson and Majozi, 2010)

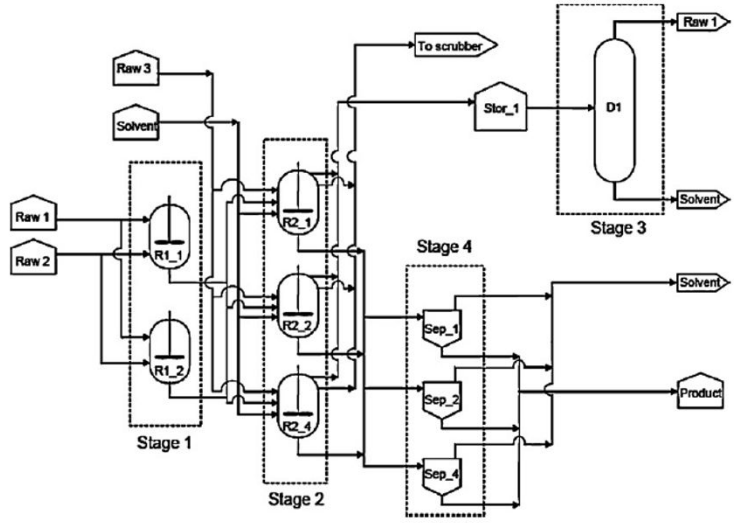

Figure 2: Optimum design (Pattinson and Majozi, 2010)

Energy optimization in batch processes

The problem of energy optimization in batch facilities is fundamentally distinct from a similar problem in continuous processes, due to the inherent time dimension that cannot be readily suppressed. Figure 3 shows a superstructural representation of a typical batch heat integration framework that considers both direct and indirect heat integration. Indirect heat integration involves storage of heat for purposes of bypassing time and utilizing maximum available heat in the process. The work presented in this paper considers one of the most advanced problems in this category, which involves

simultaneous production scheduling and heat integration within a comprehensive framework.

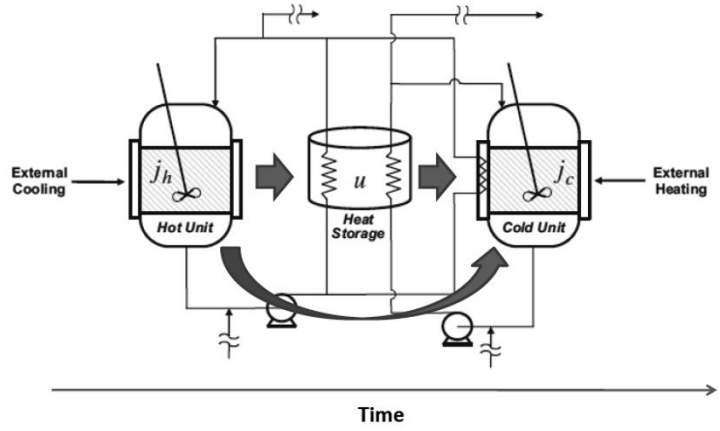

Figure 3: Superstructure for heat integration in batch plants (Stamp and Majozi, 2011)

Water optimization in batch processes

The problem of water optimization in batch processes is similar to the problem of heat integration, except that the source process has to be finished prior to commencement of the sink process. Both cases of direct and indirect water reuse are addressed in this paper. Figure 4 shows a superstructure that forms the basis of most mathematical models that simultaneously address the problem of scheduling and water minimization.

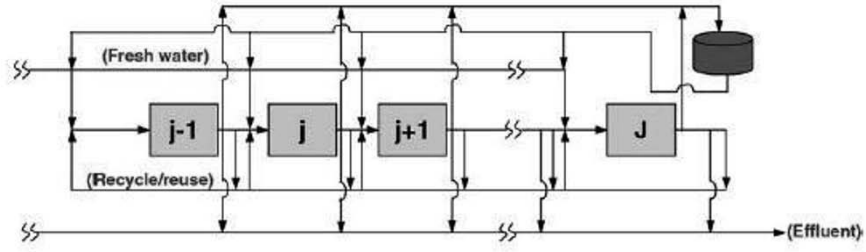

Figure 4: Superstructure for water optimisation in batch plants (Majozi, 2005)

3. Solution procedure

Whilst the paper does not disregard the significance of discrete time formulations, the results presented only consider continuous time formulations.

4. Case study I

Case study I is taken from Susarla et al. (2010). This case study indicates the necessity of non-simultaneous transfer of intermediate into a unit to get a better objective value. This batch plant constitutes six tasks performed in three units and three storages for the

intermediates. The plant produces two products using two different production paths (R1 and R2) as depicted in the STN representation (Figure 5). The processing time for a task, the capacity of the unit to process a task, the storage capacity and the initial inventories for each state are given (Susarla et al., 2010).

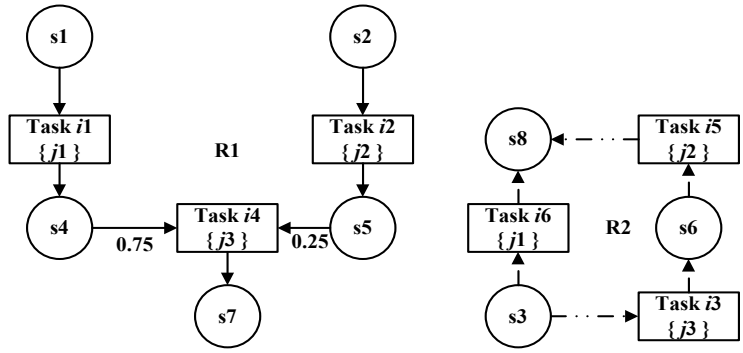

Figure 5: STN representation for case study I

For revenue maximization of the time horizon of 6 h, the models by Maravelias and Grossmann (MG) (2003), Sundaramoorthy and Karimi (SK) (2005) and Shaik and Floudas (SF) (2009) give an optimal solution of $560.The models by Susarla et al. (SLKs) (2010) and the models proposed by Seid and Majozi (SMs) (2011) give a better objective value of $650. The better objective value by SLKs and SMs is because the model allows non-simultaneous material transfers, which means for a task that uses more than one intermediate states, it is possible one state to be stored in a unit that is processing it for a while and wait for the other intermediates to come together to start the task.

In this case task 4 needs state *s*4 and *s*5 to produce *s*7. The 10 kg of *s*5 is produced at 3 h and 30 kg of *s*4 is produced at 4 h (Figure 6). Since *s*5 is produced earlier when compared to *s*4 and there is no enough storage to store *s*5 and later to use together with *s*4, it is required that the state s5 is stored in unit 3 for 1 h and start processing together with *s*4 at 4 h. By doing so we get better revenue since unit 2 transfers the state *s*5 to unit 3 at 3 h and start processing *s*6 at the same time to produce the product state *s*8. The models by SF, SK and MG give sub optimal results since the models do not allow non-simultaneous mass transfer. In this case the state *s*5 produced at 3 h stayed in unit 2 for 1 h until used at 4 h by unit 3; as a result unit 2 is inactive for 1 h. The amount of material processed by each unit, the type of task each unit is conducting and the starting and finishing time of each task are shown in Figure 6.

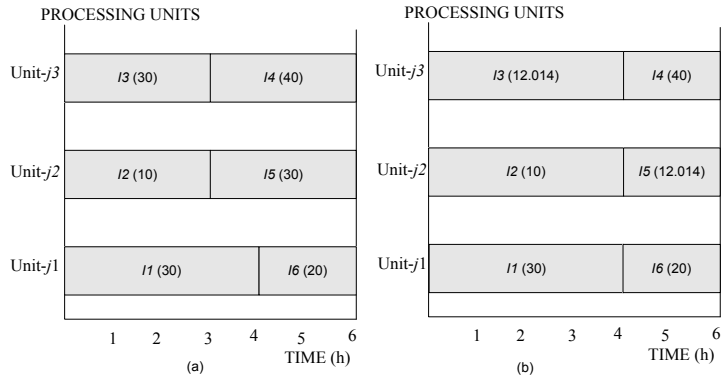

Figure 6: (a) schedule from SLKs and SMs (b) schedule from MG, SK and SF

5. Case study II

This case study has been studied extensively in the literature. It is a simple batch plant requiring only one raw material to get a product as depicted in the STN representation (Figure 7).

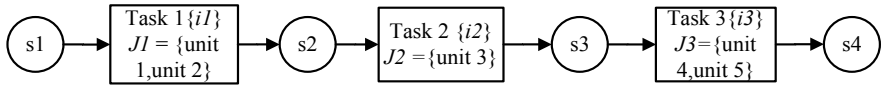

Figure 7: STN representation for case study II

The plant encompasses 5 units and two intermediate storages. The conversion of the raw material into a product is achieved through three sequential processes. The first task can be performed in two units ($j1$and $j2$), the second task can be performed only in unit $j3$ and the third task is suitable for units $j4$ and $j5$. The required data to solve the case study is given (Susarla et al., 2010). The computational performances for the different models are summarised below.

For the time horizon of 10 h, models SMs require 5 slots (p = 6) to get the optimal objective value of 2628.2. Almost all the models get the same optimal objective value in a similar CPU time. For the time horizon of 12 h, the models SMs require 6 slots (p = 7) to get the optimal objective value of 3463.6. These models require 2 slot less when compared to the other models. The models SMs outperform both single grid and multi grid models in terms of CPU time required to get the optimal objective value (0.25 s for SM1and 4.5 s for SM2 vs. 781 s for SLK2, 1492 for SLK1, 585 s SF ($\Delta n = 1$), 11.6 s for SK and 10.3 s for MG). In a case where task need not span over multiple time points SF ($\Delta n = 0$) and SM1 perform better - 1.88 s for SF ($\Delta n = 0$) and 0.25 s for SM1. For the time horizon of 16 h the proposed model SM2 requires 8 slots (p = 9) which is 3 slot less when compared to other models to get the optimal objective value of 5038.2. The models SMs outperform the multi grid models SF and SLKs in terms of CPU time required (75.8 s for SM1 and 60 s for SM2 vs. 10,000 s for SLKs and SF ($\Delta n = 1$)). In this case also the models SMs give a better CPU time when compared to the single grid models (377 s for SK and 2431 s for MG).

For makespan minimization two scenarios are taken with product demands of 2000 mu and 4000 mu. In the first scenario the model SM2 gives better objective value of 27.98 in a specified CPU time of 10,000 s when compared to other models. The model SMs

required 12 slots (p = 13) to get an optimal objective value, which is 4 slots less when compared to the other models. For the second scenario, the model SM2 again gives a better objective value of 53.1 when compared to other models in literature which give objective value of 56.432. The superior performance of the proposed models is due to the reduction of the required time points and does not allow task to span over multiple time points to get a better objective value like in the models of SF and SLKs. The Gantt chart for the time horizon of 12 h is shown in Figure 8.

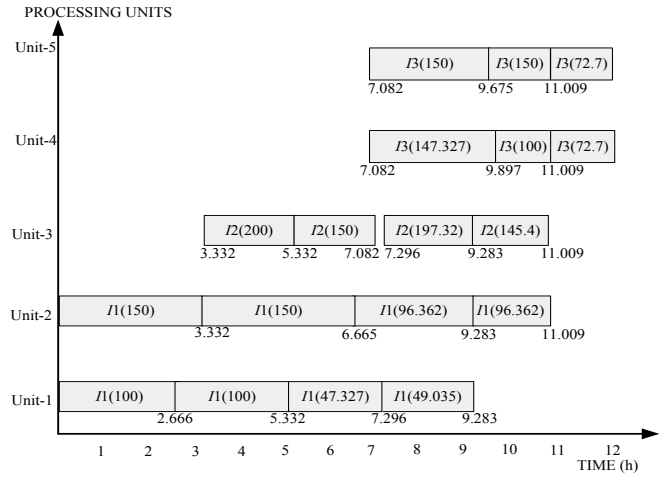

Figure 8: Gantt chart for case study II

6. Conclusion

The results from the various mathematical models on batch chemical process synthesis in published literature have been presented. The paper aims to draw comparisons among various models in terms of performance based on different objective functions. In particular, the paper aims to highlight advances that have been made in the last 2 decades in process systems engineering as applied to synthesis of batch processes.

References

E. Kondili, C.C.Pantelides, R.W.H.Sargent, (1993), A general algorithm for short-term scheduling of batch operations. I. MILP formulation, Comput. Chem. Eng., 17, 211-227

X.Zhang, & R.W.H.Sargent, (1996), The optimal operation of mixed production facilities-a general formulation and some approaches for the solution, Comput. Chem. Eng., 20, 897-904

C.A. Méndez, J. Cerdá, I.E. Grossmann, I. Harjunkoski, M. Fahl, (2006), State of- the-art review of optimization methods for short-term scheduling of batch processes, Comput. Chem. Eng., 30, 913–946

C.A. Floudas, & X. Lin, (2004), Continuous-time versus discrete-time approaches for scheduling of chemical processes: a review. Comput. Chem. Eng., 28, 2109-2129

M.A. Shaik, S.L. Janak, C.A. Floudas, (2006), Continuous-time models for short-term scheduling of multipurpose batch plants: A comparative study, Ind. Eng. Chem. Res., 45, 6190-4209

J.M. Pinto, & I.E. Grossmann, (1994), Optimal cyclic scheduling of multistage continuous multiproduct plants, Comput. Chem. Eng., 18, 797-816

J.M. Pinto, & I.E. Grossmann, (1995), A continuous-time mixed-integer linear programming model for short-term scheduling of multistage batch plants, Ind. Eng. Chem. Res., 34, 3037-3051

M.F. Lim, & I.A. Karimi, (2003), Resource-constrained scheduling of parallel production lines using asynchronous slots, Ind. Eng. Chem. Res., 42, 6832-6842

Y. Liu, & I.A. Karimi, (2007), Novel continuous-time formulations for scheduling multi-stage batch plants with identical parallel units. Comput. Chem. Eng., 31, 1671-1693

Y. Liu, & I.A. Karimi, (2008), Scheduling multistage batch plants with parallel units and no interstage storage. Comput. Chem. Eng., 32, 671-693

C.T. Maravelias, & I.E. Grossmann, (2003), New general continuous-time state-task network formulation for short-term scheduling of multipurpose batch plants, Ind. Eng. Chem. Res., 42, 3056-3074

P. M. Castro, A. P. Barbosa-Povóa, H. A. Matos, A.Q. Novais, (2004), Simple continuous-time formulation for short-term scheduling of batch and continuous processes, Ind. Eng. Chem. Res., 43, 105-118

C.A. Méndez, & J. Cerdá, (2000), Optimal scheduling of a resource-constrained multiproduct batch plant supplying intermediates to nearby end-product facilities, Comput. Chem. Eng., 24, 369-376

C.W. Hui, & A. Gupta, (2000), A novel MILP formulation for short-term scheduling of multi-stage multi-product batch plants, Comput. Chem. Eng., 24, 2705-2717

S. Gupta, & I.A. Karimi, (2003a), Scheduling a two-stage multiproduct process with limited product shelf life in intermediate storage, Ind. Eng. Chem. Res., 42, 490-508

S. Gupta, & I.A. Karimi, (2003b), An improved MILP formulation for scheduling multiproduct, multistage batch plants, Ind. Eng. Chem. Res., 42, 2365-2380

C.A. Méndez, G.P. Henning, J. Cerdá, (2001), An MILP continuous-time approach to short-term scheduling of resource-constrained multistage flowshop batch facilities, Comput. Chem. Eng., 25, 701-711

C.A. Méndez,& J. Cerdá, (2003), An MILP continuous-time framework for short-term scheduling of multipurpose batch processes under different operation strategies, Optim. Eng., 4, 7-22

C.A. Méndez, & J. Cerdá, (2004), Short-term scheduling of multistage batch processes subject to lmited finite resources, Computer Aided Chemical Engineering 15B:984-989

S. Ferrer-Nadal, E. Capón-Garćia, C.A. Méndez, L. Puigjaner, (2008), Material transfer operations in batch scheduling, A critical modeling issue, Ind. Eng. Chem. Res., 47, 7721-7732

N. Susarla, J. Li, I.A. Karimi, (2010), A novel approach to scheduling of multipurpose batch plants using unit slots, AICHE J., 56, 1859-1879

M. Shaik, & C. Floudas, (2009), Novel unified modeling approach for short term scheduling, Ind. Eng. Chem. Res., 48, 2947-2964

R. Seid, & T. Majozi, (2012), A robust mathematical formulation for multipurpose batch plants, Chem. Eng. Sci., 68, 36–53

E. Sanmarti, F. Friedler, L. Puigjaner, (1998), Combinatorial technique for short term scheduling of multipurpose batch plants based on schedule-graph representation, Comput. Chem. Eng., 22, 847-850

E. Sanmarti, T. Holczinger, L. Puigjaner, F. Friedler, (2002), Combinatorial framework for effective scheduling of multipurpose batch plants, AIChE J., 48, 2557-2570

J. Stamp, & T. Majozi (2011), Optimum Heat Storage Design for Heat Integrated Multipurpose Batch Plants, Energy, 36 (8), 5119 – 5131

T. Majozi,(2005), An Effective Technique for Wastewater Minimisation in Batch Processes, J. Clean. Prod., 13(15), 1374-1380

T. Pattinson, & T. Majozi, 2010, Introducing a New Operational Policy: The PIS Operational Policy, Comput. Chem. Eng., 34, 59 – 72

I.A. Karimi and Rajagopalan Srinivasan (Editors), Proceedings of the 11th International Symposium on Process Systems Engineering, 15-19 July 2012, Singapore.

The Role of PSE Community in Meeting Sustainable Freshwater Demand of Tomorrow's World via Desalination

Iqbal M. Mujtaba*

School of Engineering, Design & Technology, University of Bradford, Bradford BD7 1DP, UK. Email: I.M.Mujtaba@Bradford.ac.uk

Abstract

This paper highlights how the Process Systems Engineering (PSE) community and the practitioners of desalination can address sustainable freshwater issue of tomorrow's world via desalination using model based techniques. This paper will focus both on thermal and membrane based desalination techniques but will restrict to only Multistage Flash (MSF) and Reverse Osmosis (RO) processes. State of the art and future challenges in both MSF and RO desalination process will be presented.

Keywords: Freshwater demand, Desalination, MSF, RO, Model based techniques

1. Introduction

Quality water and quality life go hand in hand. The food we eat, the house we live in, the transports we use and the things we cannot do without in 24/7/365 determine our quality of life and require sustainable and steady water supplies (IChemE Technical Roadmap, 2007). Exponential growth in population and improved standards of living (together with water pollution due to industrial use of water) are increasing the freshwater demand and are putting serious strain on the quantity of naturally available freshwater. By the year 2030, the global needs of water would be 6900 billion m^3/day compared to 4500 billion m^3/day required in 2009 (Water Resources Group, 2009). With most of the accessible water around us being saline (94 percent of the world's water), desalination technology is vital for our sustainability.

The commonly used industrial desalination processes can be classified broadly into two groups: (a) thermal processes (b) membrane processes. Although thermal process (mainly MSF) is the oldest and still dominating for large scale production of freshwater, RO process, due to advancement in membrane technology, has been continuously increasing its market share. Numerous researches have been conducted in the past decades to develop more sustainable technological solutions that would meet increasing water demand (Greenlee et al., 2009; Misdan et al., 2011). However, exploitation of the full potential of model based techniques in such solutions can hardly be seen.

Process Systems Engineering (PSE) community makes extensive use of model based techniques in design, operation, control and in designing experiments due to the fact that model based techniques are less expensive compared to any experimental investigation. The yearly event of ***European Symposium on Computer Aided Process Engineering*** (since 1991) and 3-yearly event of ***International Symposium on Process Systems Engineering*** (since 1985) and the ***Computers and Chemical Engineering Journal*** (published by Elsevier since 1979) cover design, operation, control, process integration of many processes but desalination (very limited). Interestingly, most reported literatures on desalination are experimental based and are mostly published in

Desalination Journal (since 1966 by Elsevier) although periodically it publishes some model based research works.
With these in mind, this paper highlights the state of the art in model based techniques and future challenges for the PSE community and the practitioners of desalination to address sustainable freshwater issue of tomorrow's world.

2. State of the Art: MSF Desalination Process

Recently, Mujtaba (2008, 2009) reflected on the state of the art in MSF desalination process. A typical MSF desalination process is shown in Figure 1. Note, many alternative configurations of the MSF process can be generated depending on the way the seawater is fed and brine is recycled (El-Dessouky and Ettouney, 2002).

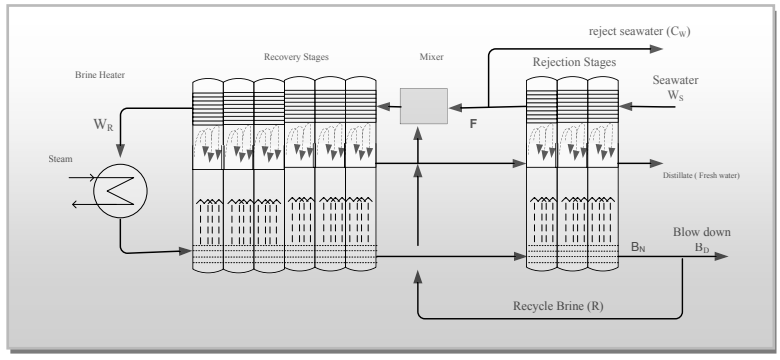

Figure 1: A Typical MSF Desalination Process (adopted from Hawaidi and Mujtaba, 2010)

To date, with a basis of given *fixed or seasonal freshwater demand profile*, *seawater composition*, *seasonal seawater temperature profile* and *fouling profile* the main issues in an MSF process have been to determine the following.

Design parameters: Number of stages, Width and height of the stages, Heat transfer area (number of tubes in the condensers), Materials of construction, Vent line orifice (air and non-condensable), Demister size and materials, inter-stage brine transfer device, Brine heater area, size of freshwater storage tank, etc.

Operation parameters: Steam flow, Top brine temperature, Brine recycle, Seawater rejection and Maintenance schedule.

Cost: Capital, Operating (utilities, cleaning), Pre-treatment and post-treatment (chemicals).

Majority of the experimental or model based study of the past and recent is focused on either to maximise the profitability of operation, or maximise the recovery ratio or maximise the plant performance (GOR – Gained Output Ratio) ratio, or minimise the cost or minimise the external energy input, etc. by optimising design and operating parameters (Rosso et al., 1996; Mussati et al., 2001; Tanvir and Mujtaba, 2008; Hawaidi and Mujtaba, 2010, 2011).

2.1 Steady State and Dynamic Modelling of MSF Desalination Process

Table 1 describes the evolution of steady state MSF process models over the last half century (included only the major developments published in international journals). Table 2 lists the studies using dynamic model. Note, most of these dynamic models are interestingly an extension of the steady state model developed by Helal et al. (1986).

Table 1: Steady State Models for MSF since 1970

Authors, Yr	Type/Description of Model
Mandil & Ghafour, 1970	Approximate Lumped Parameter Model, Constant thermophysical properties
Coleman, 1971	Stage to Stage Model, Linear and simplified TE (boiling point Temperature Elevation) correlation for different temperature range, no fouling/scaling.
Helal et al., 1986	Detailed Stage to Stage Model, Nonlinear TE correlation and other physical properties as function of (Temperature, seawater composition), Temperature loss due to demister included, Heat Transfer Co-efficient (HTC) via polynomial fit (fouling included).
Rosso et al., 1996	Model similar to Helal et al. and carried out different simulation studies. Model validation with plant data
El-Dessouky et al., 1995; El-Dessouky and Ettouney, 2002	Model based on Helal et al. but included: Heat losses to the surroundings, Constant inside/outside tube fouling factors, Pressure drop across demister, Number of tubes in the condenser and tube material, Constant non-equilibrium allowance (measure of stage thermal efficiency).
Mussati et al., 2001	Detailed Stage to Stage Model but with constant thermophysical properties
Tanvir and Mujtaba, 2006, 2008	Model based on Helal et al. (1986) but included NN (Neural Network) based correlation for TE calculation.
Hawaidi and Mujtaba, 2010, 2012	Model based on Helal et al. (1986) but included dynamic brine heater fouling and dynamic seawater temperature profile. Also included dynamic intermediate storage tank to enhance flexibility in operation
Said et al., 2010, 2012	Model based on Helal et al. (1986) but included effect of non-condensable gases (NCGs) and fouling factors on overall HTC. Considered regular (variable) and irregular (variable) water demand
Al-Fulaij et al., 2010, Al-Fulaij, 2011a,b	Rigorous modelling, CFD based demister modelling

Table 2: Use of Dynamic Models in MSF Desalination

Authors, Yr	Purpose/Software
Hussain et al. (1993)	Simulation / SPEEDUP
Maniar & Deshpande (1995)	Control / SPEEDUP
Aly and Marwan (1995)	Simulation
Thomas et al. (1998)	Simulation / SPEEDUP
Mazzotti et al. (2000)	Simulation / LSODA
Shivayyanamath and Tewari (2003)	Startup
Gambier and Badreddin (2004)	Control/MATLAB-SIMULINK
Sowgath (2007)	Simulation / gPROMS
Al-Fulaij et al. (2010, 2011a)	Simulation / gPROMS
Hawaidi and Mujtaba (2011)	Optimisation/ gPROMS
Said et al. (2012)	Optimisation/ gPROMS

2.2 Flexible Scheduling of MSF Desalination Process

Most recently, Tanvir and Mujtaba (2008), Hawaidi and Mujtaba (2010, 2011) observed that, for a fixed or variable freshwater demand, seawater temperature dictates the optimum number of flashing chambers (winter season requiring less number of stages than the summer). This opens up huge opportunities for flexible maintenance and operation schedule throughout the year (without shutting the plant fully for maintenance) and for new way of designing MSF processes.

3. State of the Art: RO Desalination Process

Since 1950s, membrane processes have been rapidly developing and are now surpassing thermal desalination processes (Misdan, et al., 2011). Reverse osmosis is a membrane process commonly used for seawater and brackish water desalination (Figure 2).

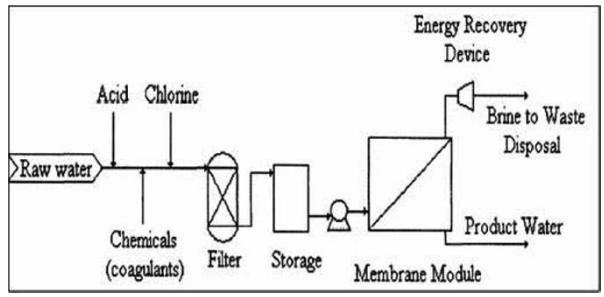

Figure 2. A Typical RO Desalination Process

Table 3: Models for RO membranes since 1958

Authors, Yr	Type/Description of Model
Kedem and Katchalsky, 1958	Model based on irreversible thermodynamics approach and describes the solvent and solute fluxes in terms of pressure and osmotic differences for solvent flux and osmotic variation and average concentration for solute.
Spiegler and Kedem, 1966	Modified Kedem and Katchalsky model and assumed that the solute flux is a combination of diffusion and convection.
Lonsdale et al., 1965	Model assumes that the solvent and solute dissolve in the nonporous and homogeneous surface layers of the membrane.
Sherwood et al., 1967	Modified Lonsdale et al. model and includes pore flow and diffusion of solute and solvent through the membrane.
Michaels, 1968	Analytical Film Theory (FT) model to estimate concentration polarisation (due to build up of solute along the membrane surface)
Sourirajan, 1970	Preferential sorption-capillary flow model - assumes that the separation is due to both surface phenomena (preferential sorption for solvent) and fluid transport through the pores.
Matsuura and Sourirajan, 1981	Modified Sourirajan model and allows characterization and specification of a membrane as a function of pore size distribution along with surface forces.
Song and Yu, 1999	Retained Solute (RS) model to estimate concentration polarisation.
Zhu et al.,1997	Simple model for decay in water flux due to fouling.
Al-Bastaki and Abbas, 2004	Detailed analytical expression to represent decay in water flux due to membrane fouling.
Abbas and Al-Bastaki, 2005	Neural Network based modeling of an RO water desalination process
Wardeh and Morvan, 2008, 2011	CFD model for evaluating fluid flow and concentration polarisations throgh RO membrane channels

3.1 Modelling of RO Desalination Process

Table 3 describes the evolution of RO process models (different component of the process) over the last half century. Kim and Hoek (2005) made a comparative study of different models and found that film theory model accurately predicted experimental permeate flux and salt rejection data. Solution-diffusion model was used in many

membrane applications (Baker, 2004) including desalination (simulation and optimisation by Lu et al., 2007) and Al-Bastaki and Abbas model was used for membrane fouling (used in simulation and optimisation by Sassi and Mujtaba, 2011b). However, Villafafila and Mujtaba (2003) considered simulation and optimisation of RO process using irreversible thermodynamics based transport model.

Most of the dynamic RO models have been obtained by system identification using real data so that they are only valid for a particular plant, working at the selected operating point (Alatiqi et al., 1989; Robertson et al., 1996; Abbas, 2006). There are only few dynamic models based on mass and energy balances and solution-diffusion model available in the literature (Gambier et al., 2007; Bartman et al., 2009).

3.2 Network Optimisation in RO Desalination Process

Generally, the most common arrangements of the membrane modules (Figure 3A) are: a) Series, b) Parallel and c) Tapered arrays. Although applied in RO waste treatment process, El-Halwagi (1992) presented the most comprehensive model based RO network synthesis problem formulation and solution by considering a superstructure configuration (Figure 3B). Zhu et al. (1997) extended El-Halwagi's work by including scheduling aspect and membrane fouling and applied in seawater desalination. See et al. (1999) extended the work of Zhu et al.'s and included membrane cleaning and regeneration. Most recently Sassi and Mujtaba (2011a) considered RO network synthesis problem for a wide range of salinity and seawater temperature.

3.3 Summary

Fritzmann et al. (2007) and Misdan et al. (2011) reviewed the state-of-the-art of RO desalination and have mentioned 'modelling', 'simulation' and 'optimisation' only once or twice in over 100 references (each) with not a single one considering model based techniques. Greenlee et al. (2009) reviewed more than 200 papers on RO desalination and there was only one mention of a model based RO optimisation of Vince et al. (2008). Kim et al. (2009) presented an overview of RO process from Systems Engineering approach and observed that there were only 30 research articles since 1965 which had used model based techniques for simulation and optimisation of RO processes (to some extent). However, only about half of these works included applications in seawater or brackish water desalination.

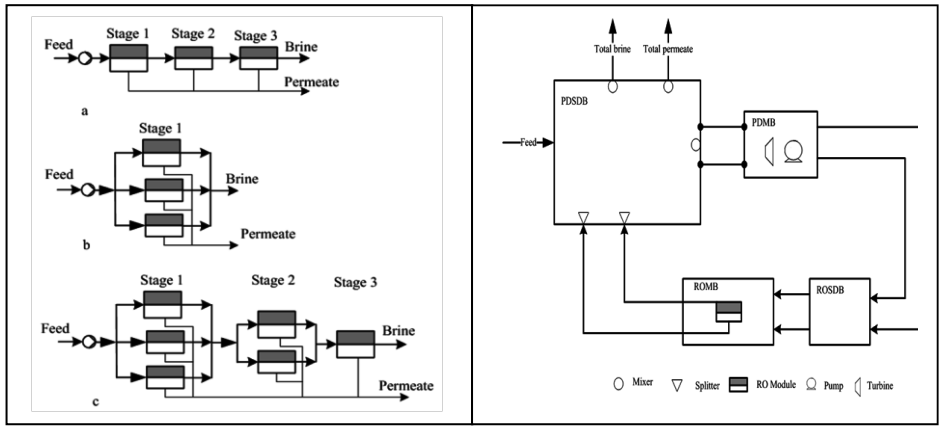

Figure 3: A. Reverse osmosis configuration. a. Series b. Parallel c. Tapered;
B: Superstructure of reverse osmosis configuration (Adapted from El-Halwagi, 1992)

4. State of the Art: Hybrid MSF/RO Desalination Process

Integration of a seawater RO unit with an MSF distiller provides the opportunity to blend the products of the two processes. Such arrangement allows operating the RO unit with relatively high TDS (total dissolved solids) and thus reduces the replacement rate of the membranes (Hamed, 2005). Although the discussions on hybrid MSF/RO date back to 80s, Helal et al. (2003, 2004a,b) and Marcovecchio et al. (2005) presented the detailed model based feasibility studies of hybrid MSF/RO desalination process. Several ways of connecting the RO with MSF process have been considered.

5. State of the Art: Use of Renewable Energy in MSF and RO Process

Rizzuti et al. (2006) edited a book comprising 26 research articles from around the world on desalination coupled to renewable energies (solar and wind), however, with only two articles considering model based MSF process (Bogle et al., 2006) and hybrid MSF/RO process (Fois et al., 2006). Mathioulakis et al. (2007) showed possible combinations of renewable energies to be used in MSF and RO processes (Figure 4) but no model based techniques have been discussed. Model based simulation of renewable energy driven desalination systems has been provided by Koroneos et al. (2007).

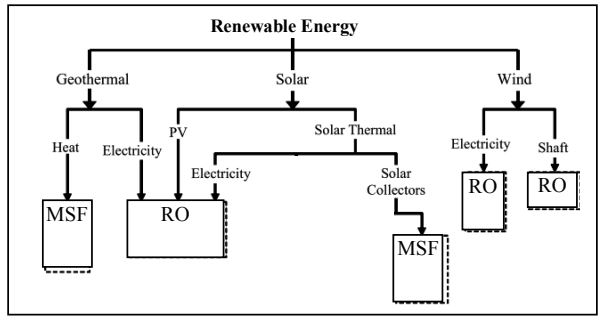

Figure 4: Technological combinations of the renewable energies and desalination methods

6. State of the Art & Future Challenge: Environmental Impact Modelling

Due to increasing environmental legislation (EL), the activities in the area of assessment and quantification of environmental impact (EI) are gaining importance in desalination processes. Sommariva et al. (2004), for the first time, attempted to establish model based relations between the improvement in plant efficiency (PE) and EI in thermal desalination system. Vince et al. (2008a) provided a simple model based LCA (Life Cycle Analysis) tool to provide help at the decision making stage for designing, operating and choosing an appropriate process to minimise EI. Mujtaba (2009) summarised some of the major work since 1999 on quantifying EI in MSF process. In most cases, EI issues are dealt in a reactive mode where EI from an existing process is assessed and, based on the current EL, the operations are adjusted. The preventive mode requires that new design and operations are achieved based on a set/desired EI targets (Vince et al., 2008a). While trial and error based on experimental studies is time consuming and expensive, studying these via model based techniques are less time consuming and inexpensive and remains a future challenge.

7. Opportunities for the PSE Community

Based on the discussions presented in earlier sections, Figure 5 summarised the state of the art in MSF and RO desalination processes. Clearly, the engagement of the PSE community in this very important sector is far away from expectation. Figure 5 also summarises the area of opportunities for the PSE community to be engaged in tackling the world's water crisis of the future by using model based techniques. Development of economically and environmentally efficient desalination processes is the future challenge. This can be achieved by better design, operation and control and model based techniques and the PSE community can play a significant role in this.

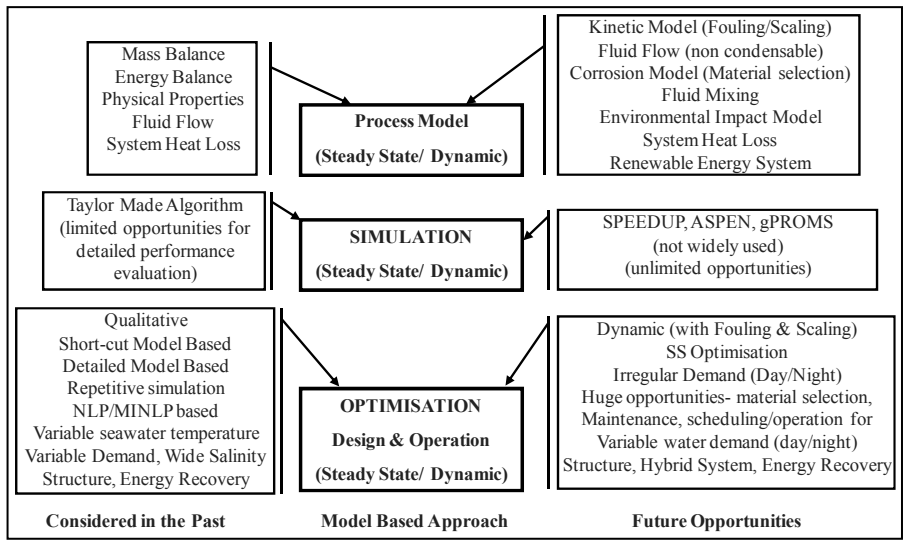

Figure 5: State of the Art and Future opportunities for PSE Community in Desalination

References

A. Abbas (2006), *Desalination*, 194, 268–280
A. Abbas and N. Al-Bastaki (2005), *Chemical Engineering Journal*, 114, 139–143
N. Al-Bastaki, and A. Abbas, A. (2004), *Chemical Engineering and Processing,* 43(4)**,** 555-558.
I. Alatiqi, A. Ghabris, and S. Ebrahim (1989), *Desalination*, 75, 119–140
H.F. Al-Fulaij (2011a), *PhD Thesis*, University College London, UK.
H.F. Al-Fulaij, A. Cipollina, H. Ettouney, D. Bogle, (2011b) *Desalination*, 281, 404–412
H.F. Al-Fulaij, A. Cipollina, D. Bogle, H. Ettouney (2010), *Desalin. Water Treat*.18, 46–60.
N.H. Aly and M.A. Marwan. (1995), *Desalination*, 101, 287-293
J.S. Baker, and L.Y. Dudley, (1998), *Desalination,* 118(1-3)**,** 81-89.
A.R. Bartman, P.D. Christofides, and Y. Cohen (2009), *Ind. Eng. Chem. Res*., 48, 6126–6136
I.D.L. Bogle et al. (2006), *Solar Desalination for the 21st Century*, Eds. L. Rizzuti et al., Spinger.
A.K. Coleman (1971), *Desalination*, 9, 315-331.
H.T. El-Dessouky, and H.M. Ettouney, (2002), *Fundamentals of salt water desalination*, Amsterdam, Elsevier Science Ltd.
H. El-Dessouky, H.I. Shaban, H. Al-Ramadan, *Desalination*, 103, 271-287, 1995
M.M. E1-Halwagi (1992), *AIChE J.*, 38(8), 1185- 1198.
E. Fois et al. (2006), In *Solar Desalination for the 21st Century*, Eds. L. Rizzuti et al., Spinger.
C. Fritzmann, J. Lowenberg, T. Wintgens, and T. Melin, (2007), *Desalination,* 216**:** 1-76.
A. Gambier and E. Badreddin (2004), *Desalination*, 166, 191-204
A. Gambier, A. Krasnik, E. Badreddin (2007), *Proceedings of the 2007 American Control Conference*, New York City, USA, July 11-13, 2007, FrA19.3, 4854-485

L. F. Greenlee et al. (2009), *Water Research.* 43, 2317–2348.
O.A. Hamed (2005), *Desalination*, 186, 207–214
E.A.M. Hawaidi and I.M. Mujtaba (2010), *Chemical Engineering Journal*, 165, 545–553
E.A.M. Hawaidi and I. M. Mujtaba (2011), *Ind. Eng. Chem. Res.*, *50* (18), 10604–10614
A. M. Helal, M.S. Medani, M.A. Soliman and J.R. Flower (1986), *comput. chem. eng*., 10, 327.
A.M. Helal, A.M. El-Nashar, E.S. Al-Katheeri and S.A. Al-Malek (2003), *Desalination*, 154, 66.
A.M. Helal, A.M. El-Nashar, E.S. Al-Katheeri and S.A. Al-Malek (2004a), *Desalination*, 160, 13.
A.M. Helal, A.M. El-Nashar, E.S. Al-Katheeri and S.A. Al-Malek (2004b), *Desalination*, 169, 43
A. Hussain et al. (1993), *Desalination*, 92, 21-41
O. Kedem, and A. Katchalsky, A. (1958), *Biochim Biophys Acta,* 1000**:** 413-30.
C. Koroneos, A. Dompros, G. Roumbas (2007), *Journal of Cleaner Production*, 15, 449-464.
S. Kim, and E.M.V. Hoek, (2005), *Desalination,* 186(1-3): 111-128.
Y.M. Kim, S.J. Kim, Y.S. Kim, S. Lee, I.S. Kim, J.H. Kim (2009), *Desalination* 238, 312–332
H.K. Lonsdale, U. Merten and R.L. Riley (1965), *Appl. Polym. Sci*., 9,1341.
Y.Y. Lu, Y.D. Hu, X.L. Zhang, L.Y. Wu and Q.Z. Liu (2007), *J. Membr. Sci*., 287, 219–229.
M.A. Mandil and E.E.A. Ghafour (1970), *chem. eng. sci* , 25, 611-621.
V.M. Maniar and P.B. Deshpande, *J. Proc. Cont.*, 6, 49-66, 1995
M.G. Marcovecchio et al. (2005). *Desalination*, 182, 111-122.
E. Mathioulakis, V. Belessiotis, E. Delyannis (2007), *Desalination*, 203, 346–365
T. Matsuura, and S. Sourirajan, S. (1981), *Ind. Eng. Chem. Process Des. Dev.*, 20, 273.
M. Mazzotti et al. (2000), *Desalination*, 127, 207-218
A.S. Michaels, (1968), *Chem. Eng. Prog.,* 64**,** 31−43.
N. Misdan, W.J. Lau and A.F. Ismail (2011), *Desalination*, doi:10.1016/j.desal.2011.11.001
I.M. Mujtaba (2008), Keynote lecture, CAPE FORUM 2008, February, Thessaloniki, Greece.
I.M. Mujtaba (2009), In *Dynamic Process Modelling*, Eds. Georgiadis et al., Vol 7, Wiley-VCH
S.F. Mussati, P.A. Aguirre and N.J. Scenna (2001), *Desalination*, 138, 341-347.
L. Rizzuti et al. (2006), *Solar Desalination for the 21st Century*, Spinger.
M. Rosso, A. Beltmmini, M. Mazzotti, and M. Morbidelli (1996), *Desalination*, 108, 365-374
M.W. Robertson et al. (1996), *Desalination*, 104, 59-68
S.A. Said, I.M. Mujtaba and M. Emtir (2010), In *Computer Aided Chemical Engineering- 28*, S. Pierucci and G. Buzzi Ferraris (Editors)., Vol 28, 25-30, Elsevier
S.A. Said, I.M. Mujtaba and M. Emtir (2012), *Proceedings of the 9th International conference on Computational Management*; 18-20 April 2012, London
K.M. Sassi and I.M. Mujtaba (2011a). *Chemical Engineering Transactions*, 25, 1055-1060.
K.M. Sassi and I.M. Mujtaba (2011b), *Chemical Engineering Journal*, 171, 582–593
H.J. See, V.S. Vassiliadis and D.I. Wilson (1999), *Desalination,* 125(1-3): 37-54.
T. Sherwood, P. Brian, R. Fisher, and L. Dresner, (1965), *Ind. Eng, Chem. Fundam.*, 4, 113
S. Shivayyanamath, P.K. Tewari (2003), *Desalination* 155, 277-286
C. Sommariva, H. Hogg and K. Callister (2004), *Desalination*, 167, 439-444
L.F. Song and S.C. Yu (1999), *AIChE Journal,* 45(5), 921-928.
S. Sourirajan (1970), *Reverse Osmosis*, Logos Press*,* London.
M.T. Sowgath (2007), *PhD Thesis*, University of Bradford, UK.
K.S. Spiegler and O. Kedem, (1966), *Desalination,* 1(4)**,** 311-326.
M.S. Tanvir and I.M. Mujtaba (2006), *Desalination*, 195, 251–272
M.S. Tanvir and I.M. Mujtaba (2008), *Desalination,* 222, 419–430
Technical Roadmap, Section 3.5, pp24, IChemE, 2007.
P.J. Thomas, S. Bhattacharyya, A. Patra, A. and G.P. Rao, (1998), *Comput. Chem. Eng*, 22, 1515
A. Villafafila and I.M. Mujtaba (2003). *Desalination*, 155, 1–13.
F. Vince, E. Aoustin, P. Breant and F. Marechal (2008a). *Desalination*, 220, 37–56.
F. Vince, F. Marechal, E. Aoustin, P. Breant (2008). *Desalination* 222 (1–3), 96–118.
S. Wardeh, H.P. Morvan (2008), *Chemical Engineering Research and Design*, 86, 1107–1116.
S. Wardeh, H.P. Morvan (2011), *Chem. Prod. Proc. Modeling*. 6 (2), 1–28
2030 Water Resources Group (2009), *Charting Our Water Future - Economic frameworks to inform decision-making*.
M.J. Zhu, M.M. El-Halwagi, and M. AlAhmad, (1997), *J. Membrane Science,* 129(2), 161-174.

I.A. Karimi and Rajagopalan Srinivasan (Editors), Proceedings of the 11th International Symposium on Process Systems Engineering, 15-19 July 2012, Singapore.

LNG Processing: From Liquefaction to Storage

Chonghun Han and Youngsub Lim

School of Chemical and Biological Engineering, Institute of Chemical Processes, Seoul National University, San 56-1, Shillim-dong, Kwanak-gu, Seoul 151-742, Korea

Abstract

Development of LNG technology has responded to expanding LNG demand. LNG worldwide consumption is expected to increase continuously for the following two or three decades. The LNG value chain includes pretreatment, liquefaction process, shipping and storage of LNG. This paper addresses the process and development of LNG liquefaction plant and receiving terminals. In addition, the role of process systems engineering in the LNG industry is reviewed with future challenges as the concluding remarks.

Keywords: LNG, liquefaction, terminal, BOG

1. Introduction

The rapid growth of Earth population coupled with the industrialization of undeveloped countries has dramatically increased the global energy demand. In the GAS(Golden Age of Gas) Scenario, global primary natural gas demand increases from 3.1 tcm (trillion cubic meters) in 2008 to 5.1 tcm in 2035 – an increase of 62% - the average rate of increase being nearly 2% per year. The reason for this continuous increase of natural gas demand largely arises from its cleanness and economic feasibility. The lower C/H ratio and lower carbon emissions compared to oil and coal, along with reduced emissions of SOx, NOx and particulates, make natural gas a very environmentally attractive option. Furthermore, the costs of processes based on natural gas such as power generation are much lower than those for coal or oil.

Although the usage of LNG (Liquefied Natural Gas) has been increased and its importance as an energy source has been emphasized, the systematic approach to LNG value chain in academia is insufficient rather than other processes. The fundamental of LNG value chain lies in the practical use of phase change of liquefaction and regasification process. That is, it is essentially important to ponder on how to liquefy natural gas into LNG more efficiently in natural gas liquefaction plant and how to regasify LNG into natural gas more safely and effectively in the terminal. The academic approach of process design and operation derived from process systems engineering can give a reasonable solution in this area.

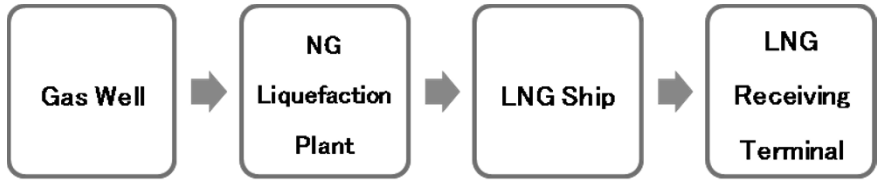

Figure 1 LNG Value Chain

The LNG value chain is well described in Figure 1. The natural gas is extracted from gas field and then transferred to the natural gas liquefaction plant. Them, natural gas is cooled and liquefied to LNG at the plant. LNG is shipped in LNG ship and transported to LNG storage tanks in LNG receiving terminals. At the terminal, it is vaporized to natural gas and sent to end users via pipeline system. The essential reason to utilize LNG value chain is placed on its massive volume shrinkage occurring in liquefaction process, which enables to deliver natural gas to remote demand regions economically rather than PNG (Pipe Natural Gas) which uses pipeline system. In other words, the volume of natural gas is reduced by 1/600 when liquefied, which improves its transportability via LNG ship.

2. Natural Gas Liquefaction

2.1. Liquefaction process

Liquefaction plant is composed of 3 major processes including pretreatment section, liquefaction section and post-treatment section. Pretreatment secion includes acid gas removal unit, dehydration unit and mercury treatment unit. Figure 2 depicts the block diagram of a typical liquefaction plant.

Mercury removal unit is needed to reduce the mercury level in the feed gas usually by adsorption through an activated carbon bed. Failure to reduce mercury levels may result in mechanical failure of downstream plant and equipment made from Aluminium. The role of acid gas removal unit is to remove carbon dioxide from the feed gas stream to less than 50 ppmv to prevent freezing out and blockage in the downstream liquefaction unit. H_2S is a toxic, poisonous gas, which cannot be tolerated in gases that may be used for domestic fuels. In presence of water, H_2S is extremely corrosive and can cause premature failure of valves, pipelind, and pressure vessels. Most pipeline specifications limit H_2S content to about 4 ppm. Water vapor is probably the most undesirable impurity found in untreated natural gas. Water content can affect long-distance transmission of natural gas and can form hydrates that may plug the pipeline and other equipment. Water content also decreases the heating value of natural gas.

Post-treatment section is mainly fractionation unit, which separates the natural gas liquids (NGL) into methane, ethane, propane and other heavy hydrocarbons. Fractionation unit is not needed when dealing with lean natural gas feed.

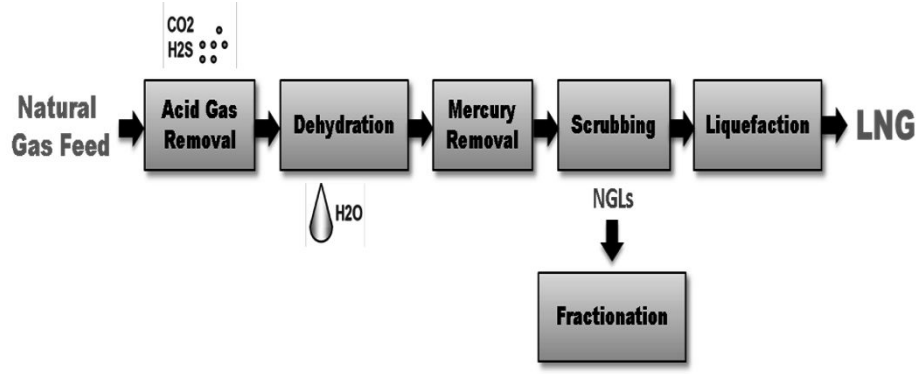

Figure 2 Block diagram of a typical liquefaction plant

2.2. Development of liquefaction processes

LNG industry started with the need of natural gas peak shaving. Cascade cycle wa used in the beginning. Later, mixed refrigerant concept was introduced. Phillips Petroleum invented the cascade liquefaction cycle. This cycle utilizes three refrigerants; propane, ethylene and methane. Air Products applied the mixed refrigerant cycle in the Libya Marsa El Brega LNG Plant in 1970.

For many years, propane precooled mixed refrigerant (C3MR) process developed by Shell and APCI (Air Products and Chemicals International) has remained the dominant liquefaction cycle in the LNG industry. The train capacity with Air Products' main cryogenic heat exchanger (MCHE) is up to 5 million tons per annum (MTPA). Natural gas and the mixed refrigerant are precooled by propane refrigerant cycle to -30°C and then liquefied to around -150°C by thermal contact with mixed refrigerant which mainly consists of methne, ethane, propane and nitrogen in main cryogenic heat exchanger (MCHE).

Recent improvents of the mixed refrigerant cycle, the AP-X^{TM}, can increase train capcity beyong 10 MTPA. Final sub-cooling is not done in the MCHE part and the temperature exiting the exchanger is about -115°C. Final stage of sub-cooling is done using a nitrogen expander loop. However, the AP-X N_2 refrigeration process would not be optimized to perform all three refrigeration system : precooling, liquefaction and subcooling. Many variables such as the number of expanders, pressure and temperature levels must be optimized for process efficiency.

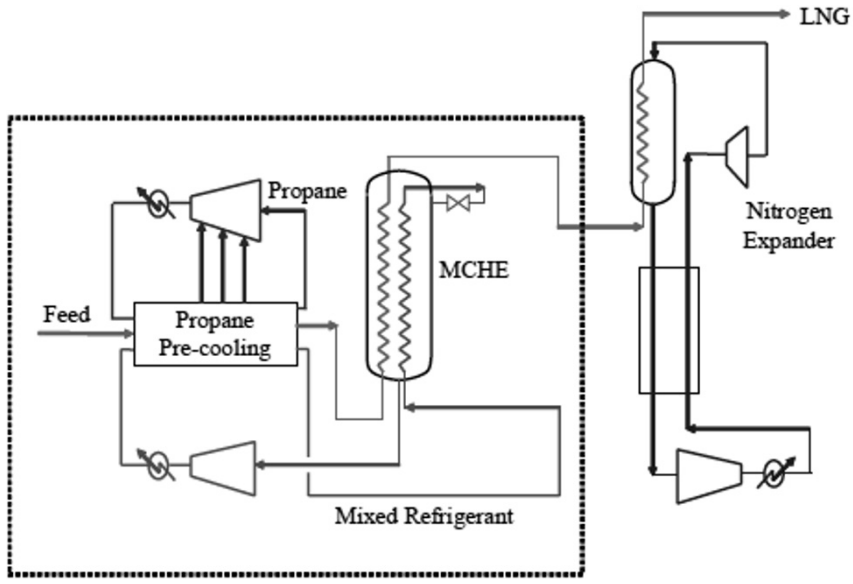

Figure 3 AP-X^{TM} Process

Other developments in recent years include the double mixed refrigerant cycles developed by Shell. Shell also developed the Parallel MR cycle which utilizes the split casing propane compressor arrangement.

New energy-saving developments across the LNG value chain include the use of cryogenic liquid expanders and new concepts including floating LNG plants. Land-based LNG plants must be solved at the debottlenecking: increased capacity, extended

life and operational improvements. Because of environmental issues including global warming, low the CO2 emissions and the treatment of sour gases and impurities are serious problems that cannot be ignored. An LNG liquefaction plant on a floating platform is similar to an onshore LNG plant but has some important differences. The motion of the LNG vessel by the sea conditions is a key issue. Development of new liquefaction process for safety caused flammable component is a problem awaiting solution.

The reverse brayton cycle and the single MR cycle are the most remarked process as a FLNG liquefaction process. The reverse brayton cycle has an object in minimization of flammable inventory for process safety. On the other hand, the single MR cycle is more efficient than the reverse brayton cycle form the power consumption point of view. It is necessary to consider which system is suitable. LNG vessel design and operating scenarios following the sea conditions are also short of study and research.

2.3. LNG Plant R&D Center in Korea

The Korean government initiated LNG Plant R&D program to acquire own technology in the liquefaction process of natural gas according to the Plant Technology Advancement Program in the Ministry of Land, Transport and Maritime Affairs. The main goals are to establish own license through the liquefaction process development and the basic designing of the commercial liquefaction plant. Test-bed construction is in successful progress with a roadmap of base construction for overseas entry in 2014.

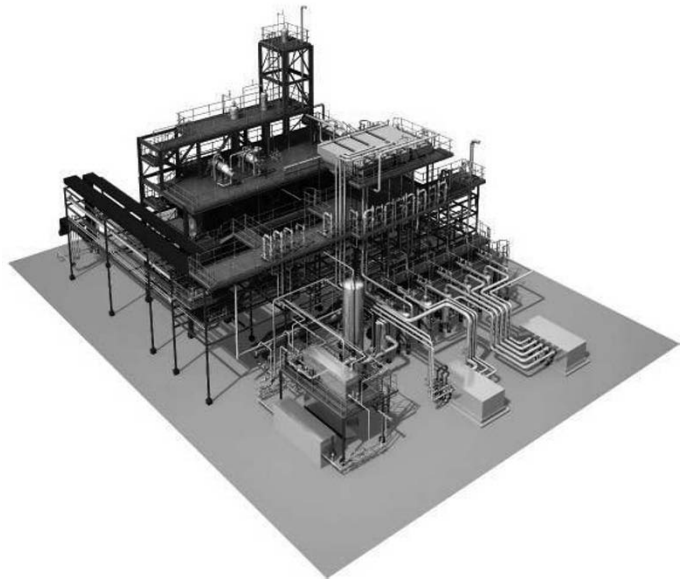

Figure 4 Bird's-eye view of the test bed constructed in Korea

3. LNG Storage and Regasification

The role of LNG receiving terminals in LNG value chain is for LNG storage and sending natural gas to end users as depicted in Figure 1. It generally includes a pipeline, LNG storage tanks, compressors, vaporizers, pumps and so on. LNG is transferred to the storage tank through the unloading pipeline from the LNG carrier ship. Stored LNG is transported to vaporizer process using a pump in the storage tank. Through the vaporization process, the natural gas is supplied to end user.

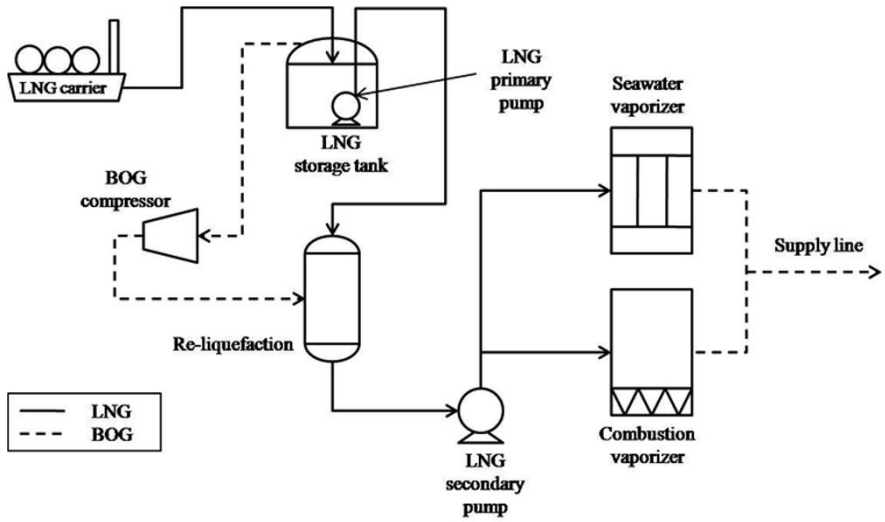

Figure 5 Schematic diagram of LNG receiving terminal (Park et al., 2010)

The LNG unloading operation consists of recirculation, depressurization and unloading. Before LNG unloading, the unloading pipeline needs to be kept cryogenic state to prevent warming of the pipeline. In the recirculation stage, a small amount of LNG from the storage tank circulates continuously through the pipeline to keep the pipeline cool. In the depressurization stage, the pressure of the pipeline is lowered to the appropriate pressure to transfer LNG from the carrier to the storage tank. After unloading stage, the operation move to the first stage of recirculation.

On unloading and storing LNG, the vapor continuously evaporates from LNG because of absorbed heat in the storage tank and in the cryogenic pipelines. This vapor is called boil-off gas (BOG). It can cause a physical damage in the LNG facilities for sudden volume expansion by 600 times. Over-treatment of the BOG causes consumption of excess energy. Hence, proper BOG handling is required for an energy saving. Usual BOG handling methods for LNG receiving terminals include recondensation and direct compression. BOG from the storage tank is compressed to around 10 bar through a BOG compressor and mixed with enough send-out LNG, which is pumped in the recondenser to obtain a liquid mixture. The liquid mixture is compressed to supply pressure in high-pressure (HP) pump and vaporized by seawater. If the LNG rate required in demands is insufficient to condense all of the BOG, it cannot be condensed in the recondenser. The remaining BOG in the recondenser is compressed to the pipeline pressure through the HP compressor and is directly transported to the pipeline mixed with the natural gas (Park et al., 2010). Because the operation of the HP

compressor requires considerable energy, it is desirable to minimize the operation of the HP compressor.

4. Process systems engineering in LNG processing

Many authors have worked on design, modeling, simulation, optimization and monitoring of LNG processing.

Wu and Zhu intoduced method for synthesizing integrated refrigeration system combining mathematical optimization techniques and engineering knowledge. The system includes the refrigeration cycle and heat integration. (Wu and Zhu, 2002) Del Nogal et al. used genetic algorithm to simultaneously solve optimal design of mixed refrigerant cycles. Their consideration of multistage refrigerant compression and application of stochastic optimization algorithm showed better performance compared to previously published works. (Del Nogal et al., 2008) Group of Michelsen et al. showed dynamic modeling and simulation of the TEALARC LNG process, selection of controlled variables of regulatory control layer as linear combination of measurements using self-optimizing control principles, and impact of process design decision on operability and control of the LNG process (Michelsen et al., 2010a, Michelsen et al., 2010b, Michelsen et al., 2010c). Natarajan and Srinivasan published their work on multi-model based process condition minitoring of offshore oil and gas production process. Online fault detection and identifiaction were performed. (Natarajan and Srinivasan, 2010)

Some researches on the LNG receiving terminals have been focused on analyzing the operation of a specific facility in the LNG receiving terminal Lee et al. suggested a reliable unloading operation procedure for a mixed operation of above-ground and in-ground storage tank (Lee et al., 2010). Shin et al. studied on the optimal operation of the BOG compressor at the Pyeoungtaek LNG receiving terminal using industrial data (Shin et al., 2007). Liu et al. proposed the optimal design of a process for the multi-stage recondensation of the BOG based on a thermodynamic analysis (Liu et al., 2010). Studies on optimal operating conditions for a regasification facility have been performed by Dharmadhikari S. (Dharmadhikari, 2004). Park et al. studied on the approach to minimize the cost in terminal operation according to the variation of LNG demand (Park et al., 2010).

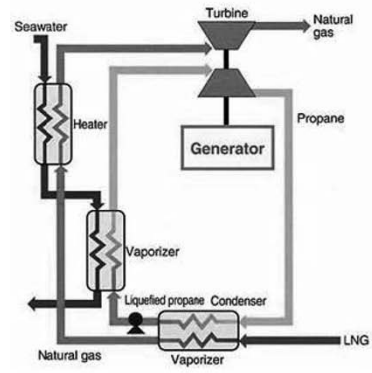

Figure 6 Power generation using LNG cold energy (Otsuka, 2006)

Researches on the utilization of the cold energy of the LNG stream have received attention. Various studies have been proposed a power generation plant using cold energy applied to power cycle as shown Figure 6. Liu and You developed the mathematical model to predict the total heat exergy of LNG stream (Liu and You 1999). The LNG cold energy has been conventionally used for air separation, power generation, and other application. (Otsuka, 2006) Recently, the industry has focused on process integration in industrial complex for LNG cold energy, ethane extraction using LNG cold energy and carbon dioxide liquefaction using the LNG cold energy for utilization of the LNG cold energy.

5. Future challenges

Future growth in LNG industry appears to be marked by an increasing interest in developing remote offshore gas fields. Offshore plants on fixed platforms, Floating Production Storage and Offloading (FPSO) vessels developed for oil production in deep water and Floating Storage and Regasification Unit (FSRU) are the main targets. Challenges for FLNG include weight and space limits, flammable components, corrosion and motion of vessels.

Gas-to-liquids technologies are also improving recently with the need for monetizing significant reserves of non-associated and stranded natural gas. It is also expected that energy efficiency improvements to limit CO_2 emissions is required in LNG value chain design. New design using combined cycle and cogeneration is therefore important.

The main purpose of LNG value chain enhancement has been to increase the LNG production capacity over the last decade. While the limitation of each process unit, such as the maximum capacity of the cold-box, is a major cause of the existing process capacity, the main topic of process research has been the optimization of LNG plants recently. For process systems engineers, hydraulic modeling and dynamic modeling of the cold-box is a field of interest. Integration of refrigeration design with power systems is another challenging issue. Proper driver selection can significantly increase the performance and decrease the capital and operating costs. In the case of FLNG, the steady-state process model is quite similar to land-based LNG process, but the dynamic model shows different behavior from land-based due to the sea condition. Analysis of hydraulic behavior using CFD and vessel design has been achieved recently. The dynamic modeling and simulation of the whole FLNG process is necessary. The unit arrangement which is suitable for installing on board and the development of operating system are the important topics of FLNG research for safety.

6. Conclusion

Worldwide liquefied natural gas consumption will increase steadily, especially in Asian countries. The LNG value chain includes the liquefaction, shipping and storage. Starting from the cascade cycles of liquefaction process, utilization of mixed refrigerants made the train capacity grow up to 5 MTPA and more. Nowadays, dual mixed refrigerant loop or AP-X^{TM} are able to handle up to 10 MTPA production. The LNG receiving terminal is designed for LNG storage and regasification. During the unloading procedure, efficient BOG handling is required for safety and energy saving. Numerous works on design, modeling, optimization, control, operation and monitoring of the LNG processing have been published. Future challenges include the floating liquefaction plants, floating storage and regasification units, gas-to-liquids technology and combined cycles.

Acknowledgment

This research was supported by the second phase of the Brain Korea 21 Program in 2012, Institute of Chemical Processes in Seoul National University, Strategic Technology Development and Energy Efficiency & Resources Development of the Korea Institute of Energy Technology Evaluation and Planning (KETEP) grant funded by the Ministry of Knowledge Economy (MKE) and grant from the LNG Plant R&D Center funded by the Ministry of Land, Transportation and Maritime Affairs (MLTM) of the Korean government.

References

F. Del Nogal, J. Kim, S. Perry, R. Smith, 2008, Optimal Design of Mixed Refrigerant Cycles, Industrial & Engineering Chemistry Research, 47, 8724-8740.

S. Dharmadhikari, 2004, Optimize LNG Vaporizers, Hydrocarbon Processing, 83(10), 95-9.

C. Lee, Y. Lim, C. Park, C. Han, 2010, Optimal Unloading Procedure for a Mixed Operation of Above-ground and In-ground LNG Storage Tank using Dynamic Simulation, *2nd Annual Gas Processing Symposium*, Doha, Qatar, January 11-14.

C. Liu, J. Zhang, Q Xu, J Gossage, 2010, Thermodynamic-Analysis-Based Design and Operation of Boil-Off Gas Flare Minmization at LNG Receiving Terminals, Industrial & Engineering Chemistry Research, 49(16), 7412-20.

H. Liu, L. You, 1999, Characteristics and applications of the cold heat exergy of liquefied natural gas, Energy Conversion and Management, 40(14), 1515-25.

F. A. Michelsen, I. J. Halvorsen, B. F. Lund, 2010, The Impact of Process Design Decisions on Operability and Control of an LNG Process, Journal of Natural Gas Science and Engineering, 183-191.

F. A. Michelsen, I. J. Halvorsen, B. F. Lund, P. E. Wahl, 2010, Modeling and Simulation for Control of the TEALARC Liquified Natural Gas Process, Industrial & Engineering Chemistry Research, 49, 7389-7397.

F. A. Michelsen, B. F. Lund, I. J. Halvorsen, 2010, Selection of Optimal, Controlled Variables for the TEALARC LNG Process, Industrial & Engineering Chemistry Research, 49, 8624-8632.

S. Natarajan, R. Srinivasan, 2010, Multi-model Based Process Condition Monitoring of Offshore Oil and Gas Production Process, Chemical Engineering Research and Design, 88, 572-591.

T. Otsuka, 2006, Evolution of an LNG terminal: Senboku terminal of Osaka gas, 23rd World Gas Conference, Amsterdam.

C. Park, C. Lee, Y. Lim, S. Lee, C. Han, 2010, Optimization of Recirculation Operating in Liquefied Natural Gas Receiving Terminal, J. Taiwan Inst. Chem. Eng., 41(4), 482-491.

M. Shin, D. Shin, S. Choi, E. Yoon, C. Han, 2007, Optimization of the operation of boil-off gas compressors at a liquified natural gas gasification plant, Industrial & Engineering Chemistry Research, 46(20), 6540-5.

G. Wu, X. Zhu, 2002, Design of Integrated Refrigeration Systems, Industrial & Engineering Chemistry Research, 41, 553-571.

I.A. Karimi and Rajagopalan Srinivasan (Editors), Proceedings of the 11th International Symposium on Process Systems Engineering, 15-19 July 2012, Singapore.

Research Challenges in Alarm Management for Safe and Stable Plant Operations in Chemical Process Industries

Masaru Noda[a]

[a]*Nara Institute of Science and Technology, 8916-5 Takayama, Ikoma 630-0192, Japan*

Abstract

Industrial plan alarm systems form an essential part of the operator interfaces for automatically monitoring plant state deviations and for attracting plant operators' attention to changes that require their intervention. To design effective plant alarm systems, it is essential to evaluate their performances. In this presentation, I introduce two methods for evaluating plant alarm systems. The first is the data-based evaluation method that refers to operation and alarm event data in a plant. It uses event correlation analysis to detect statistical similarities among time series data of discrete alarm and operation events. Grouping correlated events on the basis of their degrees of similarity makes it easier to consider countermeasures for reducing frequently generated alarms than merely analyzing individual alarm and operation events. The second is a model-based evaluation method, where an operator model is used to mimic humans' fault detection and identification behaviors. Analyzing simulated fault detection and identification tracks after all assumed malfunctions have occurred in a plant makes it possible to evaluate alarm system performance without human-subject-based experiments. Case study results demonstrated the usefulness of these methods for safe and stable plant operations in the chemical process industries.

Keywords: plant alarm system, event correlation analysis, operator model, behavior simulation, ethylene plant

1. Introduction

An alarm system is a core element in almost all operator interfaces of industrial plants, including oil refineries, power stations, and chemical plants. The progress with distributed control systems (DCSs) in the chemical industry has made it possible to install many alarms easily and inexpensively. Figure 1 shows statistics compiled by the Society of Chemical Engineering of Japan in 2005 indicating that typical Japanese chemical plants had 200 alarms per day and per operator. While most alarms help operators detect abnormalities and identify their causes, some are unnecessary. A poor alarm system might cause floods of alarms and nuisance alarms, which would reduce the ability of operators to cope with abnormalities at plants because critical alarms would be buried under many unnecessary alarms (Nimmo, 2002, Alford, 2005).

The Engineering Equipment and Materials Users' Association (EEMUA, 2007) defined the primary function of an alarm system as directing the operator's attention toward plant conditions requiring timely assessment or action. To achieve this, every alarm should have a defined response and adequate time should be allowed for the operator to carry out this response. The International Society of Automation (ISA, 2009) suggested a standard alarm-management lifecycle covering alarm-system specifications, design, implementation, operation, monitoring, maintenance, and change

activities from initial conception through to decommissioning. The lifecycle model recommends continuously monitoring and assessing operation data to rationalize alarm systems.

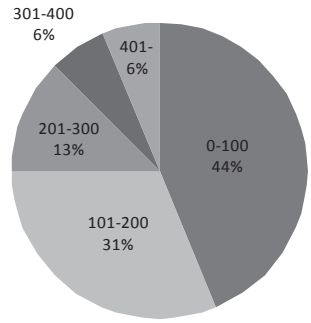

Fig. 1 Generated alarms per day and per operator in Japanese chemical plants (Society of Chemical Engineering of Japan, 2005)

The "top-ten worst alarm method" has been widely used in the Japanese chemical industry to reduce the number of unnecessary alarms. It is used to collect data from the event logs of alarms during operation, and it creates a list of frequently generated alarms. Although this method can effectively reduce the number of alarms triggered at an early stage, it is less effective at reducing them as the proportion of the worst ten alarms decreases. Because the ratio of each alarm in the top-ten worst alarm list is very small in the latter case, effectively further reducing the number of unnecessary alarms becomes difficult.

Kondaveeti *et al*. (2009) proposed the High Density Alarm Plot (HDAP) and the Alarm Similarity Color Map (ASCM) to assess the performance of alarm systems in terms of effectively reducing the number of nuisance alarms. HDAP visualizes the time various alarms occurred, which facilitated the identification of periods when the plant was unstable. ASCM orders alarms in accordance with their degree of Jaccard similarity (Lesot *et al.*, 2009) with other alarms to identify redundant alarms. However, these visualization tools cannot tell whether individual alarms have a defined response, because they only focus on alarms in the operation data.

In 2008, the Japan Society for Promotion of Science established an alarm management workshop comprising members from 29 universities and different firms from the chemical, petrochemical, oil refinery, electrical equipment, electronics, and other industries. The workshop aims to develop new alarm management technology to operate plants safely and sustainably. This paper introduces two methods for evaluating plant alarm systems developed in the workshop, i.e., a model-based evaluation method and a data-based evaluation method.

2. Alarm system evaluation by event correlation analysis

2.1. Event correlation analysis

Nishiguchi and Takai (2010) proposed a method for data-based evaluation that referred to not only alarm event data but also operation event data in the operation data of plants. The operation data recorded in DCS consist of the times of occurrences and the tag names of alarms or operations as listed in Table 1, which we call "events" hereinafter.

Table 1 Example of operation data

Date/Time	Event	Type
2011/01/01 00:08:53	Event 1	Alarm
2011/01/01 00:09:36	Event 2	Operation
2011/01/01 00:11:42	Event 3	Alarm
2011/01/01 00:25:52	Event 1	Alarm
2011/01/01 00:30:34	Event 2	Operation

The operation data are converted into sequential event data $s_i(k)$ by using Eq. (1). When event i occurs between $(k\text{-}1)\Delta t$ and $k\Delta t$, $s_i(k) = 1$, otherwise $s_i(k) = 0$. Here, Δt is the time-window size and k denotes the discrete time.

$$s_i(k) = \begin{cases} 1 \text{ if event } i \text{ occurs between } (k-1)\Delta t \text{ and } k\Delta t \\ 0 \text{ otherwise} \end{cases} \tag{1}$$

The cross correlation function, $c_{ij}(m)$, between $s_i(k)$ and $s_j(k)$ for time lag m is calculated with Eq. (2). Here, K is the maximum time period for lag and T is the time period for complete operation data.

$$c_{ij}(m) = \begin{cases} \sum_{k=1}^{T/\Delta t - m} s_i(k) s_j(k+m) & (0 \le m \le K/\Delta t) \\ c_{ji}(-m) & (-K/\Delta t \le m < 0) \end{cases} \tag{2}$$

Here, we assumed that two events, i and j, are independent of each other. If probability p_{ij} that two events, i and j, will occur simultaneously is very small, the probability distribution that two events will occur simultaneously is approximated by the Poisson distribution. The total probability that two events will occur simultaneously more than c_{ij}^* times, which is the maximum value of the cross correlation function with time lag m is given by Eq. (3), where λ is the expected value of c_{ij} (Mannila and Rusakov, 2001).

$$P(c_{ij}(m) \ge c_{ij}^* \,|\, -K/\Delta t \le m \le K/\Delta t) \cong 1 - \left(\sum_{l=0}^{c_{ij}^*-1} \frac{e^{-\lambda} \lambda^l}{l!} \right)^{2K+1} \tag{3}$$

Finally, the similarity, S_{ij}, between two events, i and j, is calculated with Eq. (4) (Nishiguchi and Takai, 2010).

$$S_{ij} = 1 - P(c_{ij}(m) \ge c_{ij}^* \,|\, -K/\Delta t \le m \le K/\Delta t) \tag{4}$$

If a high degree of similarity between two events is not detected, the time window is doubled in size and is used to reconvert the log data of two events into sequential binary data using (Kurata *et al.*, 2011). The time window continues to be expanded and similarity continues to be recalculated until either a high degree of similarity is detected or the time window becomes larger than the maximum pre-determined size.

A larger similarity means a stronger dependence or closer relationship between the two events. After similarities are calculated between all combinations of any two events in the plant log data, all events are classified into groups with a hierarchical method for clustering. The following four types of nuisance alarms and operations can be found by analyzing the results obtained from clustering.

(1) ***Sequential alarms***: These are when a group contains multiple alarm events that occur sequentially. Changing the alarm settings of sequential alarms may effectively reduce the number of times they occur.

(2) ***Routine operations***: These can be when a group includes many operation events and operation events in the same group appear frequently in the event log data. These operation events can be reduced by automating routine operations using a programmable logic controller.

(3) ***Alarms without corresponding operations***: These can be when a group contains only alarm events and operation events are not included in the same group. As every alarm should have a defined response (EEMUA, 2009), these may be unnecessary and should be eliminated.

(4) ***Alarms after operation***: Operations can cause alarm events to occur after all operation events in a group. These are unnecessary because they are not meaningful or actionable.

2.2. Alarm system evaluation of ethylene plant

Idemitsu Kosan Co. Ltd. started operations at the ethylene plant of their Chiba complex in 1985. Figure 2 is an overview of the ethylene plant, which is operated by two board operators using DCS. The plant log data gathered in one month included 914 types of alarm events and 857 types of operation events, and a total of 51640 events was generated. Figure 3 shows the points at which 1771 types of alarm and operation events occurred.

Fig. 2 Ethylene plant in Idemitsu Kosan Chiba complex. (Higuchi *et al.*, 2009)

Event correlation analysis was applied to the operation data obtained from the ethylene plant (Noda *et al.*, 2012). By using the hierarchical method of clustering, 1771 types of alarms and operation events were classified into 588 groups. Figure 4 is a similarity color map of events in the top 10 worst groups, where the alarm and operation events are ordered in accordance with the group Nos. The red indicates that two events have a high degree of similarity.

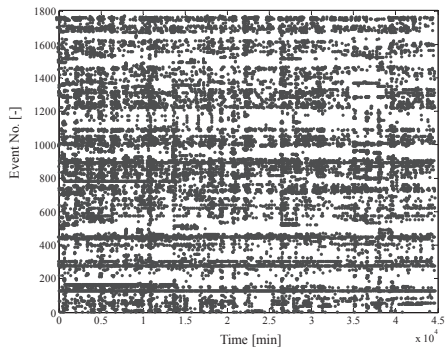

Fig. 3 Operation data of ethylene plant

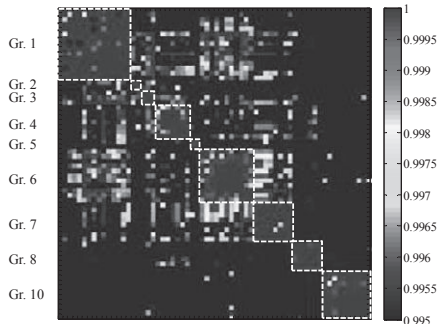

Fig. 4 Similarity color map

The top group contains five types of alarm events and ten types of operation events, and the total number of events in the group accounted for 5.8% of all generated events at the ethylene plant. Although the total number of events in the worst 10 groups accounted for 32.4% of all generated events at the plant, this included only 4.2% of alarm and operation event types. Evaluation results shows that we could effectively identify unnecessary alarms and operations within a large amount of event data by using the method, which should be helpful for reducing the number of unnecessary alarms and operations in other industrial chemical plants.

3. Alarm system evaluation by a virtual subject

3.1. Operator Model

An operator model can be used as a virtual subject in evaluating alarm systems by analyzing their performance during fault detection and identification (FDI) under a set of assumed malfunctions. This evaluation method using a virtual subject makes it possible to check alarm system performance without needing operation data provided by human operators so that the alarm system satisfies the specifications determined by the philosophy, identification, and rationalization stages in the alarm management lifecycle.

The model human processor (Card *et al.*, 1983) explicitly describes human perception, cognition, execution, and memory. The operator model (Liu *et al.*, 2010) shown in Fig. 5 for evaluating alarm systems was built by referring to this processor. In every scenario under abnormal situations, the operator model's main tasks are monitoring plant status with alarms and identifying causes of failure.

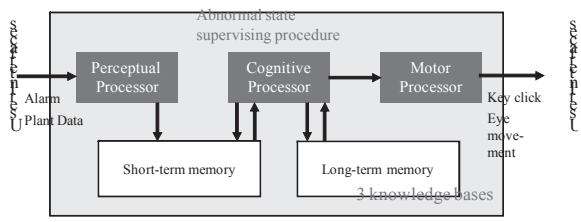

Fig.5 Structure of operator model (Liu *et al.*, 2010)

Human behavior during FDI process is classified into physical and mental subtasks. The latter includes perception, cognition, short-term memory, and long-term memory activities, respective examples of which are reading an alarm message, remembering a previous alarm, searching for a symptom in the knowledge base, and rejecting a cause of failure. An FDI track is an information-flow diagram composed of these subtasks. The FDI track from detecting an alarm to successfully identifying a cause of failure is generated automatically in accordance with the supervising procedure for failure-cause identification in the operator model.

3.2. Numerical example

The boiler plant in Fig. 6 produces 80 tons of superheated steam per hour at 485 ºC. As normal fluctuations, the steam load of the boiler plant randomly changes between 77.9 and 82.4 t/h. Figure 7 shows the overview a graphic panel of DCS. Abnormality propagation diagrams were drawn up for each of the 11 malfunctions assumed in the boiler plant listed in Table 2.

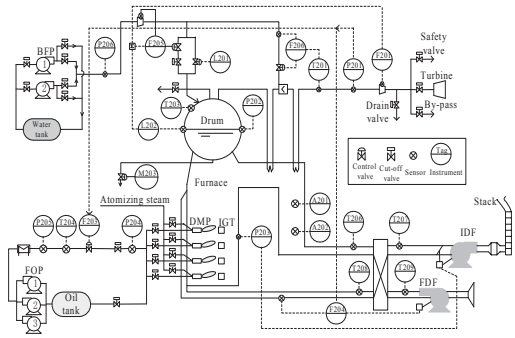

Fig. 6 Boiler plant process flow diagram

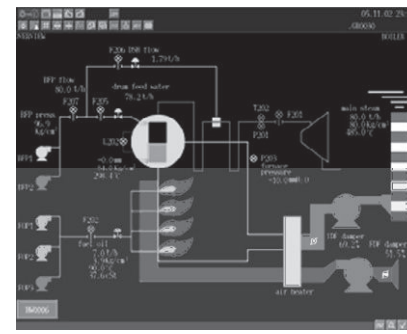

Fig. 7 Overview of graphic pannel of DCS

Table 2 Assumed malfunctions in the boiler plant

Malfunction	Description
1	FDF (forced draft fan) degradation
2	FOP (fuel oil pump) failure
3	Fuel leak
4	Burner's fire extinction
5	O_2 sensor failure
6	Oil heater failure
7	Water tube leak
8	P204 sensor failure
9	Turbine trip
10	BFP (boiler feed pump) trip
11	IDF (induced draft fan) trip

In the case study, we evaluated the actual alarm system of the boiler plant simulator using the following five criteria:

(1) Number of alarms triggered within 10 min of the malfunction
(2) Number of different kinds of alarms triggered within 10 min.
(3) Time the first alarm was triggered after the malfunction
(4) Elapsed time of the FDI process after the first alarm
(5) Total elapsed time of the FDI process after the malfunction

Table 3 shows the evaluation results for the alarm system. The number of alarms triggered within 10 min (Criterion (1)) remained at a low level for most malfunctions, while for an FOP failure malfunction (Mal-2) the number increased to 66 and was still more than 10 for a turbine trip (Mal-9). However, fewer than 10 different kinds of alarms (Criterion (2)) were triggered. The time the virtual subject needed to identify the malfunction (Criterion (5)) was short for most malfunctions, i.e., the subject was able to find the cause of a malfunction fairly quickly. An important alarm was triggered that enabled the operator to judge quickly that a water tube leak (Mal-7) had occurred, and useful alarms that enabled a turbine trip (Mal-9) to be identified were triggered in a timely manner.

Table 3 Alarm system evaluation results by virtual subject

	Malfunction										
Criteria	1	2	3	4	5	6	7	8	9	10	11
(1)	6	66	3	4	2	6	1	8	21	1	2
(2)	5	1	3	4	2	5	1	7	8	1	2
(3)	6	9	24	2	20	13	88	2	6	5	14
(4)	6	4	39	4	213	3	215	81	11	2	6
(5)	12	13	64	6	233	15	303	83	17	8	20

Units for criteria (3), (4), and (5) are in seconds.

4. Conclusion

This presentation introduced quantitative evaluation methods based on operation data and an operator model to rationalize plant alarm systems. Applying an event correlation analysis to operation data of the ethylene plant verified its effectiveness in identifying nuisance alarms and repeating operations occurring within the context of a large amount of event data. The behavior simulation by the virtual subject makes it possible to locate weak points in alarm systems and improve them from the viewpoint of operator workload without human-subject-based experiments. Case study results demonstrated that these two methods can be used to support alarm system design and evaluation. Future work will include using the evaluation results described in this paper to develop a method for redesigning alarm systems.

References

Alford, J. S., K. Kindervater, R. Stankovich, 2005, Alarm Management for Regulated Industries, *Chemical Engineering Progress*, 101, 25-30

Card, S. K., T. P. Moran, and A. Newell, 1983, The Psychology of Human-Computer Interaction, Lawrence Erlbaum Associates, London

Engineering Equipment and Material Users' Association (EEMUA), 2007, Alarm Systems - A Guide to Design, Management and Procurement, EEMUA Publication No.191 2nd Edition, EEMUA, London

Higuchi, F., I. Yamamoto, T. Takai, M. Noda, and H. Nishitani, 2009, Use of Event Correlation Analysis to Reduce Number of Alarms, *Proc. of PSE2009*, 1251-1256

International Society of Automation (ISA), 2009, Management of Alarm Systems for the Process Industries (ANSI/ISA-18.2-2009), ISA, Research Triangle Park, NC

Kondaveeti, S. R., S. L. Shah, and I. Izadi, 2009, Application of multivariate statistics for efficient alarm heneration, *Proc. of the 7th IFAC Symposium of Fault Detection, Supervision and Safety of Technical Processes*, 657-662

Kurata, K., M. Noda, Y. Kikuchi, and M. Hirao, 2011, Extension of Event Correlation Analysis for Rationalization of Plant Alarm Systems (in Japanese), *Kagaku Kogaku Ronbunshu*, 37, 338-343

Lesot, M. J., M. Rifqi, and H. Benhadda, 2009, Similarity measures for binary and numerical data: a survey, *Int. J. Knowledge Engineering and Soft Data Paradigms*, 1, 63-84

Liu, X., M. Noda, and H. Nishitani, 2010, Evaluation of Plant Alarm Systems by Behavior Simulation using a Virtual subject, *Computers & Chemical Engineering*, 34, 374-386

Mannila, H., D. Rusakov, 2001, Decomposition of Event Sequences into Independent Components, *Proc. of 2001 SIAM International Conferences on Data Mining*

Nimmo, I., 2002, Consider Human Factors in Alarm Management, *Chemical Engineering Progress*, 98, 30-38

Nishiguchi, J., and T. Takai, 2010, IPL2 and 3 performance improvement method for process safety using event correlation analysis. *Computers & Chemical Engineering*, 34, 2007-2013

Noda, M., T. Takai, and F. Higuchi, 2012, Operation Analysis of Ethylene Plant by Event Correlation Analysis of Operation Log Data, *Proc.of FOCAPO2012*

Society of Chemical Engineering of Japan, 2005, Report of the Questionnaire Survey of Plant Operations and Skill Transferes (In Japanese)

I.A. Karimi and Rajagopalan Srinivasan (Editors), Proceedings of the 11th International Symposium on Process Systems Engineering, 15-19 July 2012, Singapore.

Uncertainty propagation in condensate stabilization column

M. Askarian[a,b], R. Zarghami[a], F.Jalali[a], N.Mostoufi[a]

[a]*School of Chemical Engineering, College of Engineering, University of Tehran, PO Box 11155-4563, Tehran, Iran*
[b]*Pars Oil and Gas Company, PO Box 141471311, Tehran, Iran*

Abstract

Uncertainties, present in any engineering calculations would impact on decision making. In this work, uncertainty propagation in the simulation of condensate stabilization column in gas refinery is performed by Monte Carlo (MC) and Latin hypercube sampling (LHS) methods. Furthermore, a novel approach of building a statistical emulator of a simulation model for uncertainty analysis is presented. The results showed that the emulator is enormously more efficient than conventional approaches and the LHS is superior to MC due to its convergence in small sampling size.

Keywords: Uncertainty, Emulator, Monte Carlo, Latin Hypercube Sampling, Condensate Stabilization Column

1. Introduction

Process systems typically involve significant uncertainty in their design and operation. Based on the nature of the source of uncertainty in a process, a suitable classification can be proposed as: (i) model-inherent uncertainty which includes kinetic constants, physical properties, transfer coefficients; (ii) process-inherent uncertainty including flow rate, temperature variations and stream quality fluctuations; (iii) external uncertainty including feed stream availability, product demands, prices and environmental conditions; and (iv) discrete uncertainty for equipment availability and other random discrete events [1]. The existence of uncertainty transforms conventional deterministic concepts to stochastic problems, the solution of which remains challenging.

Uncertainty propagation is the computation of the uncertainty in the outputs which is induced by the uncertainty in its inputs. Different techniques have been developed to handle this issue include: (i) random sampling techniques such as Monte Carlo (MC), Latin hypercube (LH) and orthogonal array (OA). Use of MC in uncertainty analysis was introduced by Helton [2]. Iman and Conover took into account the correlation among variables in sampling techniques [3, 4]. Seaholm proposed applying LHS in order to limit the number of runs and account the interaction of model parameters [5]. Applying OA sampling was introduced by Koehler [6]. However, these conventional techniques typically require a large number of runs that demand heavy computation [7, 8]. (ii) emulators as surrogates model including response surface methodology, artificial neural network method, adaptive regression spline, radial basis function approximation and Kriging method. These approaches construct simple and fast approximations of complex computer analyses to minimize the computational expense of runs [9]

In this work, a stabilization column in gas refinery was studied. The purpose of this column (has 13 trays, re-boiler and reflux) is separation of light cuts (C^1-C^4) from C^{5+}. This process decreases vapor pressure of condensate (C^{5+}) to provide feasibility of its export; thus Reid Vapor Pressure (RVP) is considered an important index for the quality of product. Uncertain parameters that would impact on quality and quantity of product are assumed to be process-inherent type. Uncertainty propagation would be studied by three methods; Monte Carlo, Latin hypercube sampling, and Kriging method. Based on the sampling size for each method, their efficiency would be compared. This study would be done by two categories of data: historical data of plant and simulation results.

2. Uncertainty propagation

The conventional approach of expressing non-deterministic parameters is probability distribution or its statistics such as the mean and standard deviation. In the present work, the feed flow rate to stabilization column, steam flow rate of the re-boiler, temperature and pressure of column were treated as uncertain parameters and were assumed to be the sole sources of uncertainty in the stabilizing process. All the remaining parameters and inputs were treated as deterministic quantities. Using historical data of the plant, statistics (mean values and standard deviation) of probability distribution functions for inputs were obtained and showed at Table 1. The impact of these uncertain parameters on quality (RVP and specific gravity of condensate) and quantity (flow rate of condensate and gas) of product was studied.

Table 1: Input uncertain parameters of condensate stabilization column based on historical data

	feed flow rate (m^3/h)	Steam flow rate of re-boiler (Kg/h)	Pressure of column(bar g)	Temperature of column (°C)
Mean	86.2772	4351.8361	6.8970	88.9035
Std	7.374	364.911	0.020	4.354

2.1. Monte Carlo Sampling

In the Monte Carlo simulations, each uncertain parameter was treated as a random variable. Thus random values were generated between 0 and 1, and then multiplied by the available number of historical data. The calculated number indicated random scenario and corresponding inputs (feed flow rate to stabilization column, steam flow rate of the re-boiler, temperature and pressure of column were) were drawn from historical data. In this way, the correlation between parameters is considered inherently. For this scenario, experimental response (RVP, SG and flow rate of condensate and gas) could be drawn from historical data; in addition, simulation response was obtained for each random scenario. In order to study uncertainty propagation, the same procedure was repeated to achieve response distribution (for both experiment and simulation). When stable statistics for response distribution were achieved, the results would be reliable. The computational tractability of Monte Carlo method depends heavily on the number of random variables and complexity of the model [10].

2.2. Latin Hypercube Sampling

The approach of uncertainty propagation by LHS is the same as MC, the only difference is the strategy for generating random values. LHS ensures that all the portions of the uncertain parameters are represented [10]. Consider the case where it is required to

sample *N* points from M uncertain parameters; LHS partitions the parameter space into an N^M grid of bins, with N bins along each axis. Then, the sample points are distributed such that all one-dimensional projections of the samples yield one sample per bin [11].

2.3. Emulator

For obtaining response distribution through the simulator, large number of runs should be taken. To deal with this problem, emulator (response surface model taken based on limited number of run) could be constructed sufficiently accurate to replace the original simulator. The emulator attempts to reduce the number of simulations required for an adequate estimation of uncertainty propagation [7]. This emulator is then used instead of simulation code, facilitating uncertainty quantification (by predicting output from a model at untried inputs), design space exploration, optimization, and reliability analysis [9].

Kriging model as an emulator postulates a combination of a linear model and departures of the form [11]:

$$\hat{y}(x) = \sum_{j=1}^{k} \beta_j y_j(x) + Z(x) \quad (1)$$

Where $\hat{y}(x)$ is an approximate model of y (x), β is the regression factor, and Z(x) is assumed to be a realization of a stochastic process with mean value of zero and spatial correlation function (e.g. exponential, generalized exponential, Gaussian, linear, spherical, cubic spline) given by:

$$\mathrm{Cov}[Z(x_i),Z(x_j)]=\sigma^2 R(x_i,x_j) \quad (2)$$

Where σ^2 is the variance and R is the correlation. Subsequently, Kiging model is generalized to polynomial.

Since approximation models interpolate the sample data, additional validation points are collected for each example to assess the accuracy of each approximation model over the region of interest. For each set of validation points, root mean square error (RMSE) is computed as:

$$RMSE = \sqrt{\frac{\sum_{i=1}^{n}(y_i-\hat{y}_i)^2}{n}} \quad (3)$$

DACE (Design and Analysis of Computer Experiments) software is used to construct Kriging model [11]. The best Kriging model was obtained by zero order polynomial and exponential correlation (RMSE= 0.08) for RVP that is illustrated in Figure 1. Other output parameters would be presented in future works of the authors.

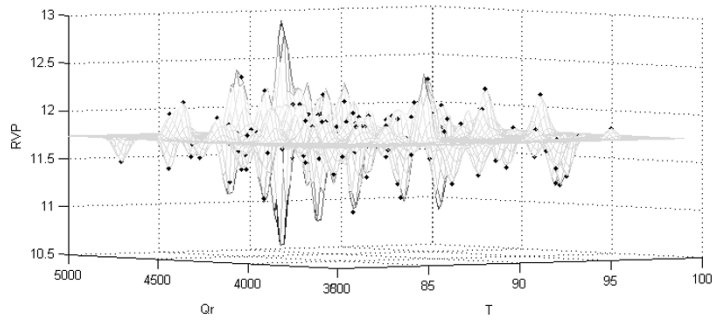

Fig 1: Kriging model for RVP treated by uncertain parameter T_{column} and $Q_{reboiler}$, RMSE=0.08 (bold point is sample point and curve demonstrate untried points)

3. Results

MC, LHS sampling and Kriging method were applied and uncertainty propagation was investigated for output parameters (RVP, SG, Condensate flow rate, and Gas flow rate) of the condensate stabilization column. Figure 2 shows the mean value of experimental RVP for different sample sizes. The data points for the MC, LHS, and Kriging methods have been slightly shifted along the horizontal axis to facilitate viewing of the data. As this figure shows, by getting 300 samples, the mean of RVP predicted by Kriging is converged. Since LHS generates more even distribution of sample points in the parameter space than typically generated with MC, LHS tends to converge in smaller sampling sizes in comparing with MC. On the other hand, the Kriging method by applying stochastic process (Z(x)) appears to be better. In addition it seems three methods converge to same mean value.

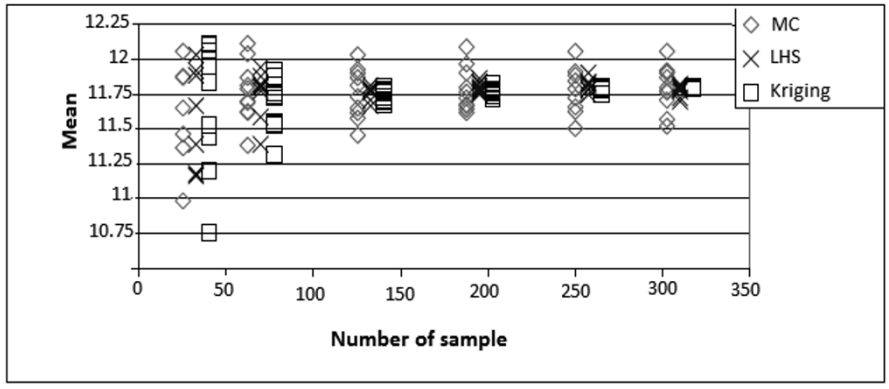

Fig 2: Mean value of RVP for different sample numbers each have eight replicas

However, MC requires more sampling sizes to obtain stable statistics. Propagation of uncertainties to output could be deduced by LHS and Kriging. This result is presented in Table 2. The standard deviation of each parameter obtained from experimental data is larger than that obtained by simulation. It could be caused by external-uncertainty sources (such as an environmental condition) that reflect on data inherently.

Table 2: Propagation of uncertainties to output

		Reid VP of condensate	Specific Gravity of condensate	Condensate flow rate (m^3/h)	Gas flow rate (Nm^3/h)
Experiment	**Mean**	11.760	0.738	33.083	2808.367
	std	0.257	0.002	20.625	640.807
Simulation	**Mean**	11.980	0.731	40.120	2901.231
	std	0.198	0.001	13.540	508.231

4. Conclusion

LHS provides an attractive alternative approach to Monte Carlo by reducing the number of runs required to converge statistics of response variables. However, Kriging method has the advantage of generating a set of samples that more precisely reflect the shape of a sampled distribution than random (Monte Carlo, Latin Hypercube) samples.

Acknowledgement

This research is supported by Pars Oil and Gas Company. Special thanks are directed to Mr.Amir Niko, Mr.Valinejad and Ms.Jafarpour for their guidance.

Reference:

[1] M.G. Ierapetritou, J. Acevedo and E.N.Pistikopoulos, 1996, “An Optimization Approach For Process Engineering Problems Under Uncertainty”, Comp. & Chem. Eng., 20, 703-709

[2] J.C. Halemane, I.E. Grossman, 1983, “Optimal Process Design Under Uncertainty”, ALCHE J. 29(3) 425-433

[3] R.L. Iman, W.J. Conover, 1980, “Small Sample Sensitivity Analysis Techniques for Computer Models,With an Application to Risk Assessment”, Commun, Stats. Theor Meth. A9(17) 1749-1874

[4] R.L. Iman, W.J. Conover, 1982, “A Distribution-free Approch to Including Rank Correlation Among Input Variables”, Commun, Stats. Simulat. Comput. 11(3) 311-334

[5] Susan K. Seaholm, Eugene Ackerman, Shu-Chen Wu, 1988, “ Latin hypercube Sampling and the Sensitivity Analysis of a Monte Carlo Epidemic Model” International Journal of Bio-Medical Computing, 23(1-2) 97-112

[6] Koehler, Owen, 1996, “Handbook of Statistics, Computer Experiments”, Elsevier science, NewYork, P261-308

[7] S. Balakrishnan, M. Ierapetritou;P.G. Georgopoulos, 2001, “Coping with Uncertainty in the Description of Complex Kinetic Mechanisms”, AIChE Annual Meeting, Reno

[8] Brian D.Phenix, Joanna L.Dinaro, Menner A.Tatang, Jefferson W.Tester, Jack B.Howard, and Gregory J.Mcrae, 1998, “Incorporation of Parametric Uncertainty into Complex Kinetic Mechanisms: Application to Hydrogen Oxidation in Supercritical Water", Combustion and Flame 112: 132-146

[9] Timothy W. Simpson, Dennis K. J. Lin, Wei Chen, 2001, “Sampling Strategies for Computer Experiments: Design and Analysis”, International Journal of Reliability and Application

[10] M.D. McKay, W.J. Conover, R.J. Beckman, 1979, “A Comparison of Three Methods For Selecting Values of Input Variables in the Analysis of Output from a Computer Code”, Technometrics, vol.21, no.2

[11] Søren N. Lophaven, Hans Bruun Nielsen, Jacob Søndergaard, 2002, “DACE A MATLAB Kriging Toolbox, Informatics and Mathematical Modeling

I.A. Karimi and Rajagopalan Srinivasan (Editors), Proceedings of the 11th International Symposium on Process Systems Engineering, 15-19 July 2012, Singapore.

A multi-scale model of naphtha pyrolysis process

Lei Zhang,[a] Bingzhen Chen*,[a] Tong Qiu[a]

[a]*Department of Chemical Engineering, Tsinghua University, Beijing, 100084, China*[*]

Abstract

Continuing demand for ethylene, propylene and butadiene makes the naphtha pyrolysis process occupying an important position in the chemical industry. For the accurate prediction of the product yields of given naphtha pyrolysis, it is crucial to establish the naphtha pyrolysis model based on the detailed reaction mechanism. Even though this subject is extensively studied, there are still some remaining unsolved issues in the existing models resulting in a less satisfied accuracy of predicting the product yields. Current challenges include: the detailed reaction mechanism involving a lot of kinetic parameters that are hard to obtain and need to be estimated based on the experimental or real data; a lack of effective method on mapping the feed from commercial indices, such as ASTM boiling curve and PINA fractions, to the conventional components; inefficient method of controlling the scale of the model meeting the required prediction accuracy. This paper develops a multi-scale model of industrial cracker to meet the challenges mentioned above. Here the multi-scale model of the pyrolysis process has been illustrated in detail from microscopic scale to mesoscopic and macroscopic ones. The established multi-scale model has been tested in the plant. Calculated results of the product yields match well with data collected from the plant with satisfied prediction accuracy. Also, based on the established model, an improvement of the performance of an industrial naphtha pyrolysis furnace will be obtained through simulation analysis.

Keywords: multi-scale model, naphtha pyrolysis, radical reaction model, Shannon's maximum entropy theory.

1. Introduction

Naphtha pyrolysis process occupys an important position in the chemical industry. To meet the demands from science and engineering on the depth of revealing the characteristics of a system, a mathematical model may involve relations of properties at different scales of the system (A. Yang, 2009), called multi-scale model. The multi-scale model often consists of nonlinear equations and differential equations that are not easy to solve. And the communication of information between scales is the key factor in the multi-scale model (A. Lucia, 2010).

Reaction network is the kernel part of the multi-scale modeling and nowadays the detailed reaction model is widely used in the simulation of pyrolysis process. Many reasearchers have studied the radical reaction model in depth and described the generation of radical reaction model in detail (E. Ranzi, 2005; R. Fournet, 2001; D. Depeyre, 1991; Z. Belohlav, 2003). Even though this subject is extensively studied, there are still some remaining unsolved issues in the existing models resulting in a less satisfied accuracy of predicting the product yields. Current challenges includes: the detailed reaction mechanism involving a lot of kinetic parameters that are hard to obtain

[*]Corresponding author. Tel.:+86 10 62784572; fax: +86 10 62770304; Email address: dcecbz@tsinghua.edu.cn (B. Chen).

and need to be estimated based on the experimental or real data; a lack of effective method on mapping the feed from commercial indices, such as ASTM boiling curve and PINA fractions, to the conventional components that results in a less satisfied prediction accuracy; ineffcient method of controlling the scale of the model meeting the required prediction accuracy. To meet the challenges mentioned above, a multi-scale model of industrial cracker was developed in this paper, the reaction model contains 125 species and 2424 reactions.

2. Establishment of multi-scale model

2.1. macroscopic scale – process model

Generally speaking, the aspect ratio of tubular reactor for naphtha is greater than 100, so it can be treated as one-dimension reactor. One-dimensional reactor model is used in some commercial steam cracking software, e.g. SPYRO, CRACKER,and COILSIM. The hydrocarbon in the reactor is supposed to be ideal gas, and the reactor is a PFR (Plug Flow Reactor) without axial dispersion and radial temperature and concentration difference. According to the assumptions above, Xu Qiang (Xu, Q., 2001) proposed a process model of pyrolysis:

$$\frac{dN_m}{dL} = \frac{S}{V}\sum_i \upsilon_{im}\, r_i = f_N(T, P, N_m) \tag{1}$$

$$\frac{dP}{dL} = -\frac{f \cdot E(L) \cdot G^2}{5.07 \times \rho \cdot D_i \times 10^4} = f_P(T, P, N_m) \tag{2}$$

$$\frac{dT}{dL} = \frac{k\pi D_o(-\frac{1}{2}\sqrt{\theta_2 - \theta_1} + \frac{1}{2}\sqrt{\theta_1 - \theta_2 + \theta_3} - T) - \sum_m \Delta H_{fm}^0 \cdot \frac{dN_m}{dL}}{\sum_m C_{pm} \cdot N_m + C_{\mathrm{pH_2O}}\, N_{\mathrm{H_2O}}} = f_{\mathrm{T}}(T, P, N_m) \tag{3}$$

In equation (1) N_m is the concentration of substance m and L is the corresponding reactor tube length, S is the reactor tube flow passage area, V is the volumetric flow rate, υ_{im} is the reaction stoichiometric coefficient, r_i is the reaction rate for reactrion i. In equation (2) P is the pressure at length L, f is the Fanning friction factor, E(L) is the equivalent length, G is the mass flow rate, ρ is the density, D_i is the inner diameter of the reactor. In equation (3) T is the temperature at length L, k is the heat transfer coefficient, D_o is the outer diameter of the reactor, $\theta_1, \theta_2, \theta_3$ are variables in solving external wall temperature, ΔH_{fm}^0 is the formation enthalpy of substance m, C_{pm} is the heat capacity of substance m.

2.2. Mesoscopic scale – reaction model

Reaction model of pyrolysis plays an important role in optimization of production process and process improvement. In equation (1) of process model r_i is the reaction rate equation. For radical reaction A+B→C:

$$r_i = d[C]/dt = k[A][B] \tag{4}$$

So the process model is communicated with reaction model through equation (1). and the multi-scale model can be solved by solving the ordinary differential equations (1-4).

The radical reaction model is proposed by Rice and Herzfeld in 1934. Initiation, propagation and termination reactions are included in a detailed radical reaction model. A detailed radical reaction model can be established based on the four types of reactions above.

Dente proposed the generation of radical reaction model based on large number of experimental data (R. Fournet, 2001). And RMG software as the reaction network

generator was developed (W. Green., 2007). Also graph theory can be used to generate a detailed reaction network (Broadbelt, L. J., 1994, 1996).

2.3. Microscopic scale – radical properties and reaction kinetic parameters

In equation (4) $k = AT^n \exp(-E/RT)$ is the reaction rate constant. Pre-exponential factor A, activation energy E, and heat capacity C_p, enthalpy ΔH in equation (3) are constants that need to be settled. Here, for the key reactions, transition state theory (P. Willems, 1988) can be used to establish a more accurate model.

In addition, thousands of reactions and substances are in the radical reaction model, so the constants are hard to obtain, so quantum chemistry is used to calculate the constants not available.

3. The information communications between different scales

The emphasis of the establishment of the multi-scale model is the information communications between different scales. The relationship of different scales is shown in figure 1.

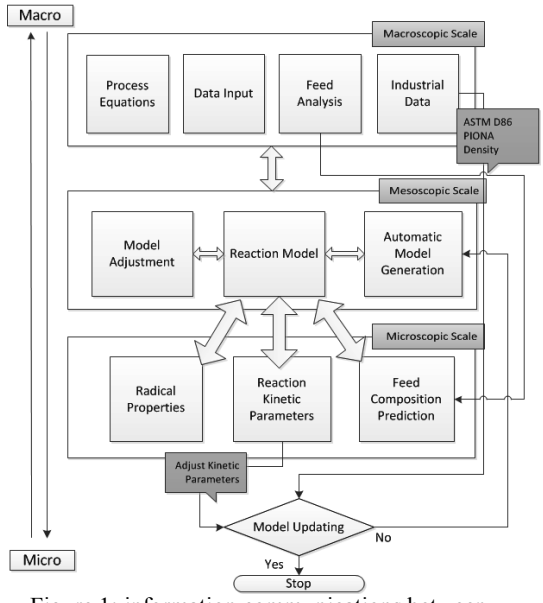

Figure 1: information communications between different scales

3.1. Relationship between macroscopic scale and microscopic scale – feed composition prediction

The input data are important for the pyrolysis simulation, but only ASTM D86, PIONA, and density etc. of the feed property are obtained from industry data. If detailed reaction model is used for the simulation, the feed properties need to be translated into detailed feed information. Shannon's entropy theory is used in the prediction of detailed feed information (K. Geem, 2007). The feed properties prediction problem could be formulated as an optimization problem (L. Zhang, 2012) based on Shannon maximum principle where the objective function max S(x) is Shannon's entropy shown as equation (5), and the relationships between the properties of each substance and mixture properties are the constraints. The calculated results using Shannon's entropy theory are shown in figure 2.

$$\max \quad S(x) = -\sum_{i=1}^{n} x_i \ln x_i \tag{5}$$

3.2. Relationship between macroscopic scale and mesoscopic scale – control of reaction network scale

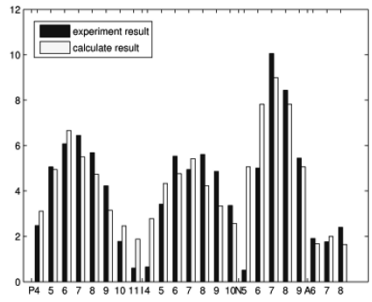

Figure 2: comparision between experimental and calculated results for the feed composition

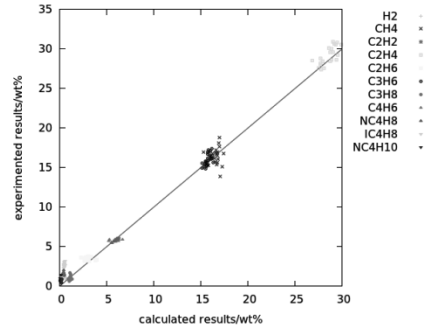

Figure 3: comparision calculated and industrial product yields using the multi-scale modeling

Large number of reactions in the reaction model caused it difficult to solve. So it is necessary to simplify the reaction model on the premise of accuracy. In order to establish an appropriate model that can represent the pyrolysis process, a criterion for controlling characteristics and scale of the radical reaction model based on the difference of industry data and calculate result is derived as follows:

Vajda (S. Vajda, 1985) proposed PCA for the reduction of reaction network. The objective condition for constructing a minimal reaction set:

$$Q(\alpha) = \sum_{j=1}^{q} \sum_{i=1}^{m} \left[(y_{i,j}(\alpha) - y_{i,j}(\alpha^0)) / y_{i,j}(\alpha^0) \right]^2 \tag{6}$$

$y_{i,j}(\alpha) = y_i(t_j, \alpha)$, $\alpha_i = \ln k_i$ in equation (6), k is the rate constant of reaction i, m is the number of substance in the model, and q is the number of selected time points.

According to PCA and perturbation method, the equation (7) can be derived.

$$\sum_i \lambda_i (\ln t) \le mq\xi^2 \tag{7}$$

Where λ_i are the eigenvalues obtained from PCA, $t = k_i / k_i^0$, ξ is the error of calculation result of each product (L. Zhang, 2011).

Equation (7) is considered as a criterion for controlling characteristics and scale of the radical reaction model based on the difference of industry data and calculated result. The right side of equation (7) is known from the macroscopic level, and the eigenvalues can be obtained from the mesoscopic level. So the reaction model can be adjusted to a minimum set of reactions based on equation (7). Besides, the most important reactions in the model can be found using equation (7) for the model adjustment. Therefore, the information transfer between macroscopic scale and mesoscopic scale is the most important issue for model reduction.

3.3. The integration of multi-scale models

Communications of information between different scales as shown in figure 1 are crucial for the establishment of the multi-scale model. The established multi-scale model has been tested in the plant. As the multi-scale model shows the nature of the pyrolysis process, so its simulation results agree well with the industrial data. The calculated product yields for all 22 industrial cases of naphtha pyrolysis match well with that collected from the plant, as shown in figure 3 , which demonstrates the advantage of the proposed model in enhancing the prediction accuracy.

4. Conclusions

In this work a multi-scale model of naphtha pyrolysis process from macroscopic scale to microscopic scale was established and the communication of information between different scales was studied in detail. It has been shown that the modeling results agree well with the industrial data, which demonstrates the advantage of the proposed model in enhancing the prediction accuracy. The proposed multi-scale modeling approach to the naphtha pyrolysis process would be expected to be implemented in modeling of other chemical pyrolysis processes.

Acknowledgments

The authors gratefully acknowledge the financial support from PetroChina Company limeted (Grant No. 20102000079).

References

A. Lucia, 2010, “Multi-scale methods and complex processes : A survey and look ahead”, Comput. Chem. Eng., vol. 34, 1467-1475.

A. Yang and W. Marquardt, 2009, “An ontological conceptualization of multiscale models”, Comput. Chem. Eng., vol. 33, 822-837.

Broadbelt, L. J., Stark, S. M., and Klein, M. T. 1994, “Computer generated reaction networks: on-the-fly generation of species, reactions and rates”, Ind. Eng. Chem. Res., 33, 790-799.

Broadbelt, L. J., Stark, S. M., and Klein, M. T. 1996, “Computer generated reaction modeling: decomposition and encoding algorithms for determining species uniqueness”, Comput. Chem. Eng., 20, 113-129.

D. Depeyre and C. Flicoteaux, 1991, “Modeling of Thermal Steam Cracking of n-Hexadecane”, Ind.Eng.Chem.Res, vol. 30, 1116-1130.

E. Ranzi, A. Frassoldati, S. Granata, and T. Faravelli, 2005, “Wide-Range Kinetic Modeling Study of the Pyrolysis , Partial Oxidation , and Combustion of Heavy n-Alkanes”, Ind. Eng. Chem. Res, vol. 44, 5170-5183.

K Geem, D. Hudebine, M. Franc, J. Verstraete, and G. Marin, 2007, “Molecular reconstruction of naphtha steam cracking feedstocks based on commercial indices,” Comput. Chem. Eng., 31, 1020-1034.

L. Zhang, B. Chen, 2012, “Applications of shannon’s entropy theory to naphtha pyrolysis simulation”, Chem. Eng. Technol., 35, 281-286

L. Zhang, B. Chen, T. Qiu, 2011, “Reaction network model reduction based on PCA”, CIESC Journal (in Chinese), 1, 137-141

P. Willems and G. Froment, 1988, “Kinetic Modeling of the Thermal Cracking of Hydrocarbons. 1. Calculation of Frequency Factors”, Ind. Eng. Chem. Res, vol. 27, 1959-1966.

P. Willems, 1988, “Kinetic modeling of the thermal cracking of hydrocarbons. 2. Calculation of activation energies”, Ind. Eng. Chem. Res, vol. 27, 1966-1971.

R. Fournet, F. Battin-Leclerc, P. Glaude, B. Judenherc, V. Warth, G. Come, G. Scacchi, A. Ristori, G. Pengloan, P. Dagaut, and M. Cathonnet, 2001, “The gas-phase oxidation of n-hexadecane”, International Journal of Chemical Kinetics, vol. 33, 574-586.

R. Fournet, F. Battin-Leclerc, P. Glaude, B. Judenherc, V. Warth, G.M. Come, G. Scacchi, A. Ristori, G. Pengloan, P. Dagaut, and M. Cathonnet, 2001, “The gas-phase oxidation of n-hexadecane”, International Journal of Chemical Kinetics, vol. 33, 574-586.

S. Vajda, 1985, “Principal component analysis of kinetic models”, International Journal of Chemical Kinetics, 14, 55-81.

W. Green. 2007, “Predictive kinetics: A new approach for the 21st century”, Advances in Chem. Eng., 32, 1-51.

Xu, Q., Chen, B. Z., He, X. R., 2001, "Simulation for Naphtha Pyrolysis in Clear Radiation Tube of SRT-IV Cracking Furnace", Comput. and Appl. Chem. (in Chinese), 18(3), 223-228

Z. Belohlav, 2003, “The kinetic model of thermal cracking for olefins production”, Chemical Engineering and Processing, vol. 42, 461-473.

I.A. Karimi and Rajagopalan Srinivasan (Editors), Proceedings of the 11th International Symposium on Process Systems Engineering, 15-19 July 2012, Singapore.

Simulation and Optimization of Saponification Process in Propylene Oxide Plant

Li Xia [a], Xiaoyan Sun [a], you Li [b], Shuguang Xiang [a]

[a] *The Hi-Tech Institute for Petroleum and Chemical Industry，Qingdao University of Science and Technology，Qingdao，266042，Shandong，China*
[b] *China Petroleum Engineering&Construction corporation (CPECC) East-China Design Branch ，Qingdao，266071，Shandong，China*

Abstract

By combining Electrolyte NRTL and the NRTL activity coefficient model, and using the reaction kinetics of propylene chlorohydrins (PC) saponification and propylene oxide (PO) hydrolysis, the simulation of the saponification process in propylene oxide plant is accomplished. In order to reduce the Chemical Oxygen Demand (COD) of wastewater and improve the yield for propylene oxide, the effects of several conditions for the COD of wastewater are studied. The simulation results showed that the yield for propylene oxide has increased 0.47% and the COD of wastewater has reduced 371 mg/l in the case of the optimum condition. Moreover, the unit operation models and thermodynamic models used here had been proved accurately and reliably to simulate the saponification system. So the optimized operating conditions could provide the theoretical basis to the operation of propylene oxide plant.
Keywords: Propylene oxide, Chlorohydrination, Saponification reaction, Simulation

1. Introduction

Propylene oxides are one of the important intermediates in the petroleum and chemical industry. Today, it is produced industrially using multistep manufacturing processes, namely, the antiquated chlorohydrin process and the peroxidation process (Berndt, et al., 2003).In the chlorohydrin process, a large volume of wastewater which contains organic compounds is generated (Steltenpohl & Graczová, 2008). There is an enhanced environmental stress caused by these organic compounds. The COD of wastewater is very important guide posts. It not only directly reflects the status of propylene chlorohydrins saponification and propylene oxide hydrolysis, but also affects the wastewater treatment system. Adopting the suitable operating conditions and reducing the COD of wastewater is crucial.

In this study, a COD-based optimization of the saponification process is presented that develops a detailed simulation model and obtains the optimum operating conditions and equipment configuration.

2. Process Description

The saponification process is shown schematically in Fig. 1. The saponification column from the feed stage is a packed bed and the lower half of the column is a multistage column. The type of multistage part is a sieve tray, and the packed bed is packed irregularly with 4 meters height of ceramic pall rings.

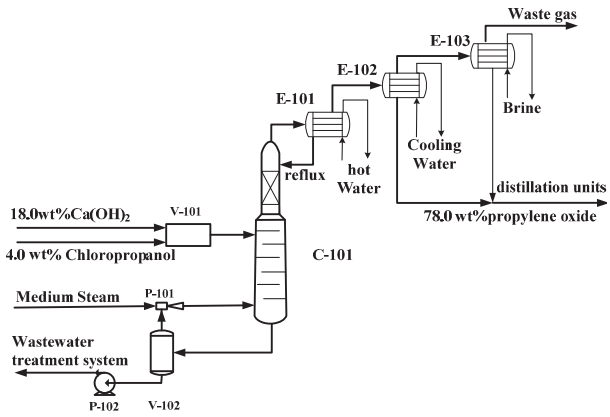

Fig. 1. Process diagram of Saponification Process in Propylene Oxide Plant

2.1. Reaction Kinetics

Choosing the optimal operating conditions for saponification process requires the kinetic parameters for the above reactions involved in the process. In a paper (Carrà, et al., 1979), a kinetic of the reaction involved in the manufacturing of propylene oxide from chlorohydrin have been given in table 1.

Table1. Kinetic parameters for the saponification and hydrolysis reaction

Reaction	Adopted kinetic model	A_i	E_i (kcal/mole)
saponification	$r_{PC} = k_1[PC], k_1 = A_1 \times e^{-E_1/RT}$	$3.02\times10^{9}s^{-1}$	15.86
hydrolysis	$r_{PO} = k_2[PC]\cdot[OH^{-1}], k_1 = A_2 \times e^{-E_2/RT}$	$2.68\times10^{8}mol^{-1}s^{-1}$	16.253

note: A_i :preexponential factors; E_i :activation energy;[OH^{-1}]:OH^{-1} concentration; r:reaction rates; [PC]:propylene chlorohydrins concentration; [PO]:propylene oxide concentration.

2.2. Exchangers, pumps, separators, reactive distillation column models

The saponification process, shown in Figure 1, is modeled using ASPEN PLUS. Standard equipment modules are used for modeling exchangers, pumps, separators, reactive distillation column, etc., given in table 2. Every model is constructed and solved by the sequential modular approach.

2.3. Simulation results

Finally, the material and energy balance for a saponification process is computed in the model. The simulation results are analyzed and compared with actual plant operation data, given in table 3. The results showed that the simulation proposed in this paper is suitable and can be applied to process optimization.

3. Process Optimization

Since the hydrolysis reaction lowers the yields, propylene oxide must be removed as quickly as possible from the reaction environment. For these reasons, the production of propylene oxide is mainly performed in saponification column, and propylene oxide is flashed out with the stream to shorten the contact time and to prevent hydrolysis.

Table2. Modeling in the saponification process

equipment	model in ASPEN PLUS	configuration(mm) diameter×height	thermodynamic model	reaction kinetics
V-101	RPLug	Φ800×1000	Electrolyte NRTL	S. CARRA et al.[5]
pipelines(from V-101 to C-101)	RPLug	Φ300×13800	Electrolyte NRTL	S. CARRA et al.[5]
V-102	Flash2	-	Electrolyte NRTL	-
C-101	RadFrac	Φ2200/3600×25292	Electrolyte NRTL	S. CARRA et al.[5]
E-101/102/103	Heater+Flash2	-	NRTL	-
P-101	Mixer	-	NRTL	-
P-102	Pump	-	Electrolyte NRTL	-

Table3. Comparison of the Simulation Results and the Actual Operating Data

conditions	simulation results	actual operating data
The dilute PC solution flow rate, kmol/h	20837.7	20837.7
$Ca(OH)_2$ solution flow rate , kmol/h	4097.2	4097.2
Top temperature of saponification column, ℃	90.0	92.7
bottom temperature of saponification column, ℃	99.8	100.5
product flow rate (78wt% propylene oxide), kmol/h	274.4	-
The yield for propylene oxide, %	95.87	95.80
The COD of wastewater, mg/l	1218.0	1300.0

3.1. Optimization conditions

On initial analysis, it quickly became apparent that the COD of wastewater were heavily dependent on hydrolysis reaction and separation of the saponification column. To reduce the COD of wastewater, several factors, shown in Table 4, are taken into account separately.

Table4. Optimization decisions regarding saponification

	actual condition	Boundary
Saponification column pressure, kPaA	97.0	67.0~107.0
The number of trays for saponification column	9	9~13
The height of weir, mm	80.0	70.0~110.0
The fresh steam injection rate, 10^3kg/h	23.0	20.0~24.0
The mole ratio of OH^{-1} to the sum of PC and HCl	1.3	1.1~1.5
The saponification reaction temperature, K	349.6	344.6~354.6

3.2. Optimization Results and Discussion

In Figure 2 and Figure 3, the effects of the conditions, shown in Table 4, for the COD of wastewater are studied ordinal. The optimal conditions are determined via a COD-based optimization calculation that minimized the COD of wastewater.

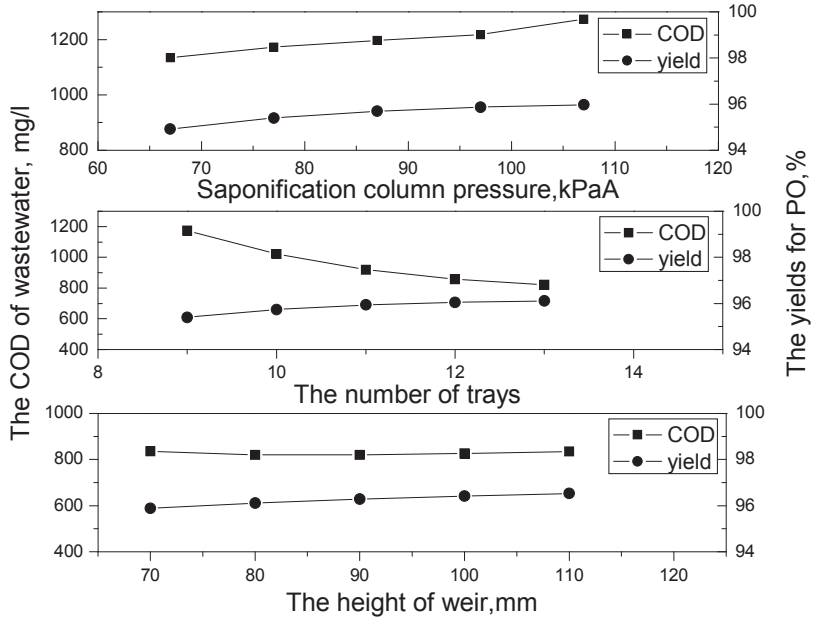

Fig. 2. Top:Trend of saponification column pressure vs the COD and yields. Middle:Trend of the number of trays vs the COD and yields. Bottom: Trend of the height of weir vs the COD and yields.

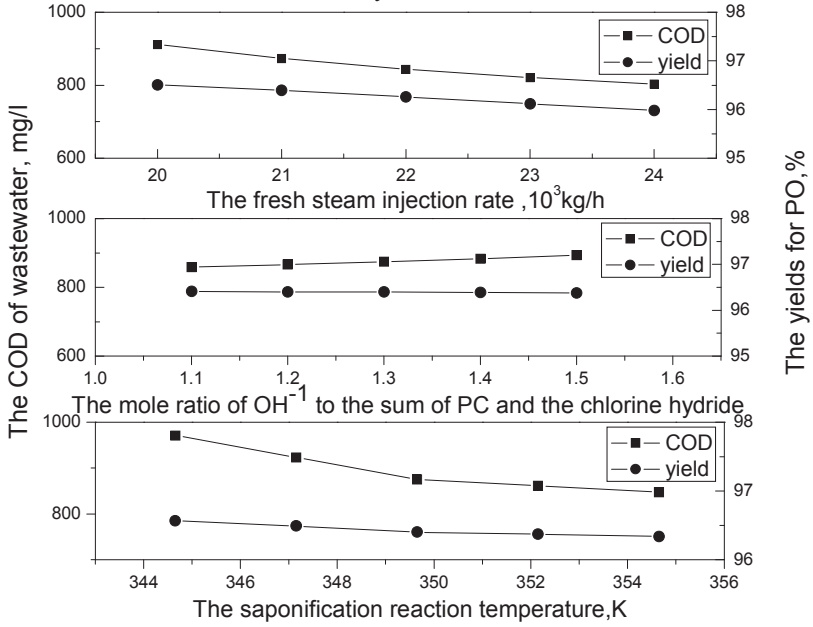

Fig. 3. Top: Trend of the fresh steam injection rate vs the COD and yields. Middle: Trend of the mole ratio of OH^{-1} to the sum of propylene chlorohydrins and chlorine hydride vs the COD and yields. Bottom: Trend of the saponification reaction temperature vs the COD and yields.

Optimization is accomplished which directs appropriate changes in the independent variables to the executive system (H. Martin Rodriguez, et al., 2010). Boundary constraints on the independent variables, shown in Table 5, are checked before performing the computations in the ASPEN PLUS.

Process optimization requires consideration of many trade-offs as a whole. In addition to minimizing the COD of wastewater, the actual situation of the propylene oxide plant must be taken into account: ⑴ Because of restriction of its pumped vacuum system, the lowest of saponification column pressure is 77 kPa(A);⑵ Although increasing the steam consumption can lower the COD of wastewater, fresh steam is 21000kg/h from the economic point of view.

Finally, the optimum conditions are obtained as follows: (1) saponification column pressure is 77kPa(A); (2) the number of trays is 13; (3) the height of weir is 80mm; (4) fresh steam is 21000kg/h; (5) mole ratio of OH^{-1} to the sum of propylene chlorohydrins and chlorine hydride is 1.1; (6) the saponification reaction temperature is 354.6K.

4. Conclusions

During the course of the operation optimization described in this article, the yield for propylene oxide has increased 0.47% and the COD of wastewater has reduced 371 mg/l. In addition to delivering an optimal operation, the project proved that:

- Equipment configuration decisions, such as the height of weir of trays and the volume of the saponification mixer, should be taken into account.
- Models are sufficiently accurate to be able to reflect the effects of small changes in operating condition, for example, saponification column pressure.
- The methods used in this optimization are suitably general and can be applied to any process plant. They are available via commercially-available simulation and modeling tools.

Acknowledgment

Financial support of National Natural Science Foundation, China (Project 21176127), for this work is gratefully acknowledged.

References

Berndt, T., O. Böge, et al., 2003, From Atmospheric Research to an Industrial Process:The Formation of Propylene Oxide, Ind. Eng. Chem. Res.,42,12, 2870-2873.

Steltenpohl, P. and E. Graczová, 2008, Vapor−Liquid Equilibria of Selected Components in Propylene Oxide Production, J. Chem. Eng. Data, 53,7, 1579-1582.

Carrà, S., E. Santacesaria, et al., 1979, Synthesis of propylene oxide from propylene chlorohydrins-I: kinetic aspects of the process, Chem. Eng. Sci., 34,9, 1123-1132.

Carrà, S., M. Morbidelli, et al., 1979, Synthesis of propylene oxide from propylene chlorohydrins-II: Modeling of the distillation with chemical reaction unit, Chem. Eng. Sci.,34,9, 1133-1140.

H. Martin Rodriguez, A. Cano, et al., december 2010, Improve engineering via whole plant design optimization, Hydrocarbon Process., Int. Ed., 43-49.

I.A. Karimi and Rajagopalan Srinivasan (Editors), Proceedings of the 11th International Symposium on Process Systems Engineering, 15-19 July 2012, Singapore.

Simulation Studies and Sensitivity Analysis of Methyl Tert-butyl Ether Reactive Distillation

Sudibyo, M.N. Murat and *N.Aziz

School of Chemical Engineering, Engineering Campus, Universiti Sains Malaysia, 14300 Nibong Tebal, Seberang Perai Selatan, Penang, Malaysia.
**E-mail: chnaziz@eng.usm.my*

Abstract

Methyl Tert-butyl Ether (MTBE) is an important chemical used as an octane booster in gasoline to replace tetra ethyl lead. Maximum production of the MTBE can be achieved using reactive distillation (RD) process that is operated at the optimum operating conditions and column configuration. However, optimizing the column configuration such as tray or catalyst location is experimentally expensive. Therefore, a reliable model of the MTBE reactive distillation is important to find the optimum conditions for MTBE production. In this work, continuous RD processes is simulated based on dynamic model using Aspen Dynamics. The model is then further used in Simulink for the singular value decomposition (SVD) analysis in order to select the best input-output pair for the control implementation. Finally, the step test is conducted in order to observe the sensitivity of the MTBE process toward changes of selected input variables. The results show that the model obtained from the Aspen produced a comparable result with the literature. The results also show that the tray temperature number 3 and 8 are the most sensitive output variables toward changes of reflux flowrate and reboiler duty.

Keywords: Reactive distillation; Dynamic simulation; MTBE, sensitivity analysis

1. Introduction

Separation and reaction processes can be combined in one unit process which is called as reactive distillation (RD). It has been used in several industries especially for the process which have reversible reaction [Sharma and Singh, 2010]. RD can reduce the capital investment, because two process steps can be carried out in the same device [Higler et al., 1999; Taylor and Krishna, 2000; Murat et al., 2003; Mohammed, 2009]. However, it is still difficult to bring a new reactive distillation column into industrial applications because of the complexities in design, synthesis and operability of RD, which is resulting from the interaction of reaction and distillation. [Satyanarayana and Saha, 2005]. Here, MTBE is considered because it is an important chemical that is used as solvent, chemical reagent and antiknock additive to improve octane number of gasoline [Sharma & Singh, 2010]. MTBE can be efficiently produced using RD; with isobutene conversion up to 99 % can be achieved [Taylor and Krishna, 2000].

The purpose of RD control is to maintain the product purity and conversion at a desired value or specified range. However, to control the conversion directly is a difficult task and expensive to be applied in industry. Thus, MTBE purity can be controlled by controlling tray temperature because the MTBE purity can be correlated with tray temperature [Taylor and Krishna, 2000]. Many researchers have modeled or simulated the MTBE RD process using either first principle model or various commercial software such as HYSIS and Aspen [Higler et al., 1999; Taylor and

Krishna, 2000; Murat et al., 2003; Satyanarayana and Saha, 2005; López-Arenas et al., 2006; Mohammed, 2009;]. However, those who used the commercial software were aim for the steady state model. In this work, the industrial RD dynamic process model is developed using Aspen Dynamics which is more feasible to be used for design and verification of process control schemes and safety studies.

At the same time, the SVD analysis and the step test are also carried out in order to evaluate the controllability and sensitivity of the process [Pearson, 2003]. The work is carried out in Simulink and interfacing with Aspen.

2. Description of the MTBE Column

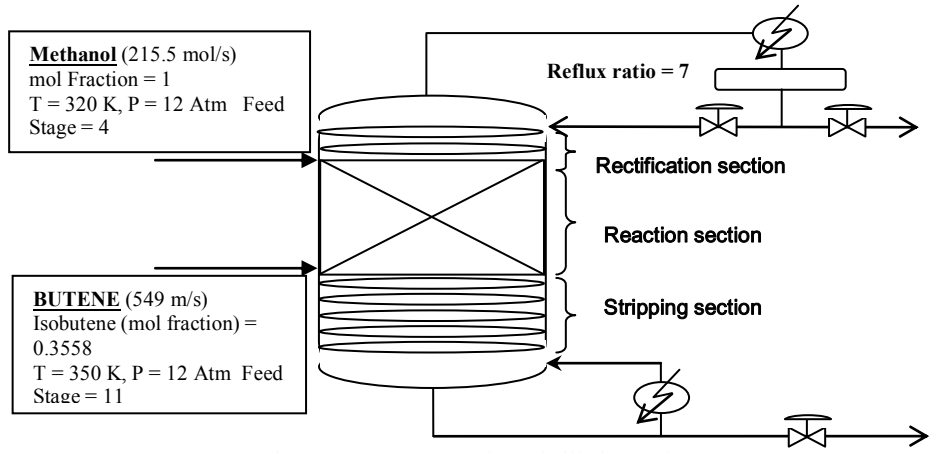

Figure 1. MTBE Reactive Distillation Column

Table 1. Tray and Packed Column Specification [Higler *et al.,* 1999]

Packed column specification		Tray specification		
Parameters	Reaction Section	Parameters	Rectifying Section	Stripping Section
Column Diameter	6 m	Column Diameter	5.95 m	5.019 m
Total column area	28.27 m^2	Total tray area	24.58 m^2	19.78 m^2
Packing height	0.7 m	Number of pass	4	4
Packing size	¼ in	Active area	19.21 m^2	15.32 m^2
Nominal size	0.00635 m	Total hole area	2.12 m^2	1.52 m^2
Packing factor	5249.34	Downcomer area	2.68	2.23

MTBE reactive distillation column consists of three sections: rectification, reaction and stripping as shown in Fig. 1. For this case study, the RD column has 17 stages, including a total condenser and a partial reboiler as given in Fig. 1 [Higler *et al.*, 1999]. The tray and packed column specifications and operation conditions are given in Table 1. The specification used here is similar to the specification used by Higler *et al.* [1999], except the number of passes, the pressure column and location of feed stages are different. In this work, 4 passes and 12 atm of pressure column while Higler *et al.* [1999] have used 5 passes and 11 atm. Meanwhile, the feed, methanol and butane, are fed at stages 4 and 11, respectively (being optimized) in order to get the maximum value of isobutene conversion.

2.1. MTBE Reaction Scheme

The most promising technique of producing MTBE is from methanol and isobutene, where the liquid-phase reaction is catalyzed by ion exchange resin (heterogeneous reaction). The reaction scheme is:

$$i\text{-}C_4H_8 + CH_3\text{-}OH \rightleftharpoons C_5H_{12}O \quad (1)$$

Chemical equilibrium constant for reaction (1) as used in the Aspen is:

$$ln\ k_{eq} = ln\ k_{eq0} + \alpha[(1/T) - (1/T^*)] + \beta\ ln\ (T/T') + \sigma(T - T^*) + \delta\ (T^2 - T^{*2}) + \varepsilon(T^3 - T^{*3}) + \theta(T^4 - T^{*4}) \quad (2)$$

where α is -1.49277 x 10^3, β is -7.74002, γ is 5.07563 x 10^{-1}, δ is -9.12739 x 10^{-4} , ε is 1.10649 x 10^{-6} , θ is -6.27996 x 10^{-10} , T* = 298.315 K , *keq0* = 284 [Murat et al., 2003].

3. Results and Discussion

3.1. Modeling of Reactive Distillation

The results obtained from the RD dynamic model using Aspen dynamics were compared with data available in literature and tabulated in Table 2. From the table, it is found that the simulation results obtained are comparable to the published results which verify that the proposed Aspen Dynamics model is capable to simulate the MTBE reactive distillation process. The small differences observed in the result obtained are due to some different specifications (as mentioned earlier) used in the simulation. The isobutene conversion can reach 99.82% using reactive distillation and which is in a good agreement with the value reported in the literature [Taylor and Krishna, 2000].

Table 2. Model Comparison

	Nijhuis *et al.* 1993	Murat *et al.,* 2003	This Work
i -butene conversion	98.5%	99.5%	99.82%
MTBE Purity	98%	98.6%	95.04%
Software	Aspen	Fortran 90	Aspen Dynamics

3.2. Singular value decomposition (SVD) analysis

Here, the most suitable tray temperature to be paired as controlled variable in respect of manipulated variable changes (reflux flowrate and reboiler duty) was determined using SVD analysis technique. The SVD test was conducted by changing the inputs of manipulated variable with the step magnitude of +0.1% from nominal input value [Luyben , 2006; Imam and Aziz, 2011]. The SVD analysis was performed by SVD command in Matlab which calculated the left singular vectors from SVD analysis result (U_{SVD}) as shown on Fig. 2. From Fig. 2, tray number 3 and 8 show the largest magnitude which signifies that they are the most sensitive trays temperature towards the changes of reflux flowrate and the reboiler duty, respectively.

3.3. Step Test Study

3.3.1. Effect of Reflux Flowrate

The study was performed by introducing several step-tests with different magnitude of manipulated variable (reflux flowrate) and the response on tray temperature (tray number 3) is observed. Fig. 3 shows the effect of reflux flowrate changes on the temperature of tray number 3 and MTBE purity. From Fig. 3a, it is show that the temperature of tray number 3 is decreasing when the reflux flowrate is increasing. The

changes in the reflux flowrate produce an asymmetric form of the output response thus signify that the reactive column is a nonlinear process. The changing of reflux flowrate also affected the MTBE purity as shown in Fig. 3b, where the MTBE purity decrease as the reflux flowrate increase.

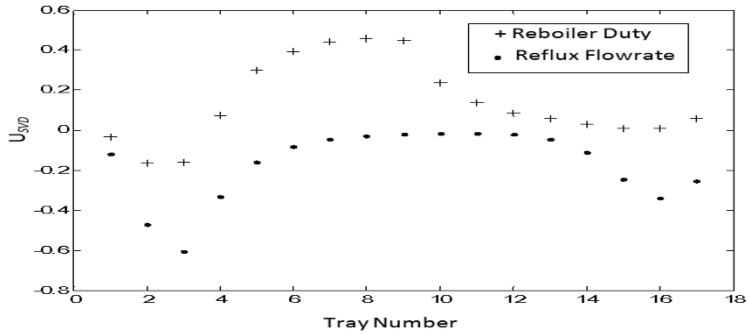

Figure 2. U_{SVD} versus tray number

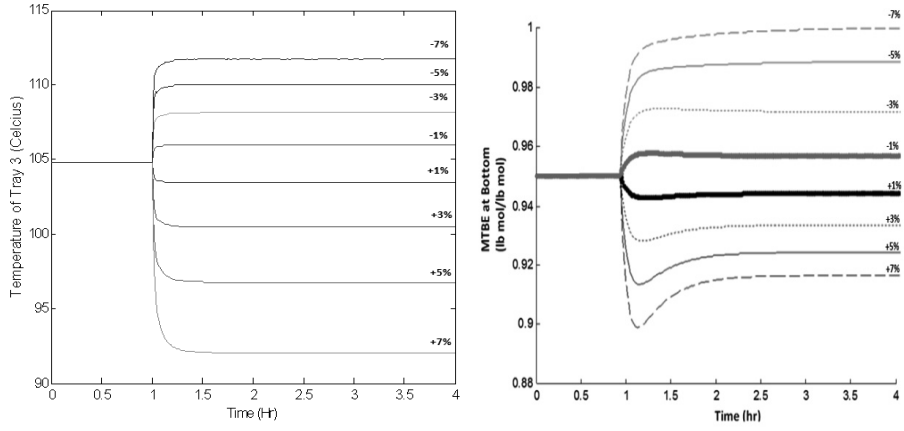

(a) (b)

Figure 3. Effect of reflux flowrate change on (a) 3rd tray temperature (b) MTBE Purity

3.3.2. Effect of Reboiler Duty

The result of step-test on reboiler duty towards the temperature of tray number 8 is shown in Fig. 4. From the figure, the changes in the reflux flowrate produce an asymmetric form on the output response thus again proved that the reactive column is a nonlinear process. Meanwhile, the effect of reboiler duty change on the MTBE purity in the bottom product is shown in Fig. 4a, where the MTBE purity increases as the reboiler duty increases.

4. Conclusion

The dynamic model of MTBE RD has been developed using Aspen Dynamics which has been validated using data available from literature. The singular value decomposition (SVD) analysis show that the tray temperature number 3 and 8 are the most sensitive toward changes of reflux flowrate and reboiler duty. Finally, the step

test results show that MTBE RD is a nonlinear process hence need nonlinear controller to control MTBE reactive distillation.

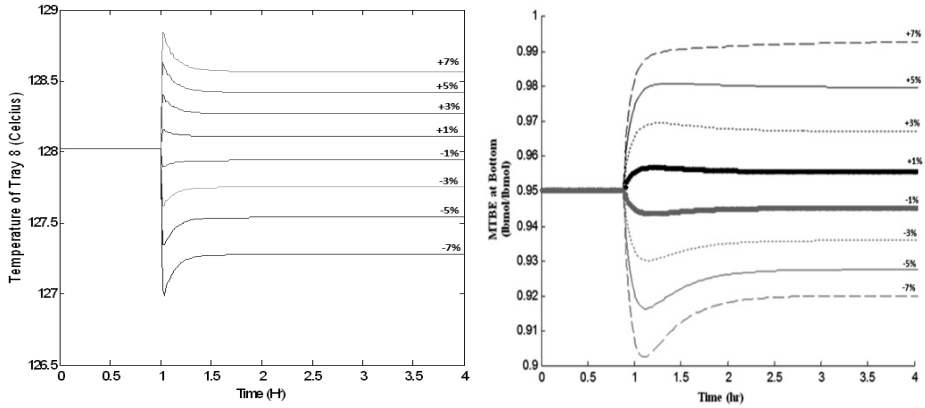

(a) (b)

Figure 4. Effect reboiler duty change on (a) 8th tray temperature (b) MTBE Purity

Acknowledgement

The financial support from Universiti Sains Malaysia through Research University (RU) Grant and Graduate Assistant (GA) to the first author are greatly acknowledged.

References

A.P. Higler, R. Taylor and R. Krishna, 1999, The influence of mass transfer and mixing on the performance of a tray column for reactive distillation, Chem. Eng. Science, 54, 2873-2881.

H. Lin and P.L. Douglas, 2000, Dynamic Simulation and Control of an MTBE Catalytic Distillation Column. Dev. Chem. Eng. Mineral Process, 8(3/4), 375-399.

I.M. Iqbal and N. Aziz, 2011, Comparison of Various Wiener Model Identification Approach in Modelling Nonlinear Process, IEEE Proceedings of the 3rd Conference on Data Mining and Optimization (DMO 2011), 134-140.

M.N. Murat, A.R. Mohamed and S. Bhatia, 2003, Modelling of reactive distillation column: Methyl Tertiary Butyl Ether (MTBE) simulation studies, IIUM Engineering Journal, 4.

N. Sharma and K.Singh, 2010, Control of Reactive Distillation Column: A Review, Int. J. Chemical Reactor Eng., 8, R5.

R.K. Pearson, 2003, Selecting Nonlinear model structures for computer control,Journal of process control, 13,1-26.

R. Taylor and R. Krishna, 2000, Review: Modelling reactive distillation, Chem. Eng. Science, 55, 5183-5229.

S.A. Nijhuis, F.P.J.M. Kerkhof, and A.N.S. Mak, 1993, Multiple steady states during reactive distillation of methyl tert-butyl ether, Ind. and Eng. Chemistry Res., 32, 2767-2774.

T. López-Arenas, S. Eduardo and R. Gani, 2006, Static/dynamic analysis and controllability issues in reactive distillation columns, Computer Aided Chemical Engineering, 21, 1323-1328.

T. Satyanarayana and P. Saha, 2005, Modeling and Control Structure Selection for Reactive Distillation Process using Aspen Custom Modeler, CHEMCON – 05, New Delhi.

W. L. Luyben, 2006, Evaluation of criteria for selecting temperature control trays in distillation columns, Journal of Process Control, 16, 115–134.

Z. M. Mohammed, 2009, Mathematical Modeling and Simulation for Production of MTBE by Reactive Distillation, MSc Thesis, Chemical Eng. Department, Univ. of Technology, Kingdom of Saudi Arabia.

I.A. Karimi and Rajagopalan Srinivasan (Editors), Proceedings of the 11th International Symposium on Process Systems Engineering, 15-19 July 2012, Singapore.

Optimal Design of HMX recrystallization process using supercritical carbon dioxide as antisolvent

Sungho Kim,[a] Shin Je Lee,[a] Hyoun-Soo Kim,[b] Youn-Woo Lee,[a] Jong Min Lee*[a]

[a]*School of Chemical and Biological Engineering, Institute of Chemical Process, Seoul National University, 1 Gwanak-ro, Gwanak-gu, Seoul, 151-744, Republic of Korea*
[b]*High Explosives Team, Agency for Defense Development, 462, Jochiwon-gil, Yuseng-gu, Daejeon 305-600, Republic of Korea*

Abstract

This work studies optimization of a Cyclotetramethylenetetranitramine (HMX) recrystallization process by precipitation. HMX is a powerful and relatively insensitive explosive. Since the shape and particle size are important properties for explosive materials, there have been many efforts to control those properties. Due to their vulnerability to heat and impact traditional methods like milling and solution-based recrystallization are inapplicable. Gas Anti-Solvent (GAS) process with supercritical carbon dioxide as an antisolvent does not have such safety issues and can produce particles with required shape and size distribution. This process, however, has been tested mostly in laboratory scale semi-batch reactors. The main purpose of this study is to develop a process flowsheet model for large-scale GAS processes and determine optimal process economics. The proposed process consists of a reactor, a separator, and recycle of carbon dioxide. An optimal operating point is also determined.

Keywords: Gas antisolvent, supercritical fluid, process optimization.

1. Introduction

Explosives with high energy density require increased performance and stability, and their physical properties are determined by crystal size, shape, and uniformity. Even in recent years, many crystals are produced by conventional milling or recrystallization from solution. Though these processes provide economical, easy, and conventional ways to product powder from the bulk material, heat or impact during the processing can cause unexpected accidents like explosion. Moreover, the conventional processes are known to be ineffective for the control of physical properties.

Gas Anti-Solvent (GAS) process can be considered as an alternative for recrystallization due to its capability to control the particle size distribution (PSD) of the product. It can also satisfy the required quality using various process variables such as antisolvent inlet flow rate and temperature [1]. Furthermore, GAS process is much safer than traditional techniques such as milling.

Experimental studies have shown that several variables like antisolvent addition rate, temperature and agitation speed play a key role in determining PSD. A population balance model is presented to predict PSD for general GAS processes [2]. A GAS process for recrystallization of beclometasone dipropionate using carbon dioxide as antisolvent and acetone as a solvent is analyzed with Muhrer's model [3].

These studies are focused on laboratory-scale reactors, and no studies have been reported for modeling and optimization for an integrated GAS process towards large-scale productions. Since GAS processes using supercritical fluids require large amounts of energy, economic optimization of the process is also necessary.

This work provides a conceptual design and a steady-state optimal operating condition for large-scale recrystallization of Cyclotetramethylenetetranitramine (HMX) where acetone is used as a solvent for HMX and supercritical carbon dioxide as the antisolvent. The proposed model is a scaled-up version of the currently operating laboratory-scale process.

2. GAS process

For scale up of the experiment to a large-scale process, not only the reactor itself but also the entire process including peripheral equipment and necessary unit operations must be specified first. Figure 1 shows a lab-scale GAS process reactor with feeding and separator units in Seoul National University. The process consists of three operations; reaction, separation, and recycle of used carbon dioxide. The process is operated in a fed-batch mode. In the followings , major unit operation steps in the lab-scale process are described.

Figure 1. A lab-scale GAS process including feeding and separator units.

2.1. Reactor

Figure 2 shows reaction steps for a batch cycle. HMX is first dissolved in acetone for recrystallization. The solution is loaded in the reactor before a batch cycle begins. Each batch cycle starts once supercritical carbon dioxide (antisolvent) is fed into the reactor. As carbon dioxide being fed, rapid expansion of solution occurs and the volume of solution and pressure inside the reactor are increased. After carbon dioxide feeding is completed, the mixture stays in the reactor for a few minutes for thermal equilibrium and then outlet flow valve is opened for the product flow to move out to the separator.

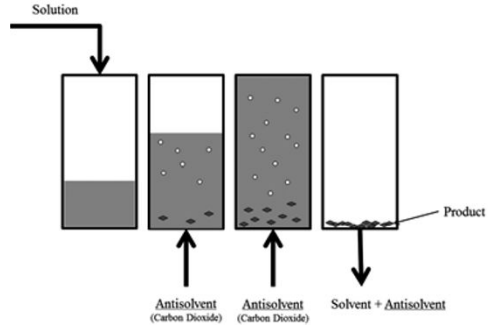

Figure 2. Reaction steps of GAS process in a cycle.

2.2. Separator

In the separation unit, solid HMX is separated first. A fabric filter is installed in the pipe to collect solid HMX in the outlet flow. The filter is removed after each batch cycle to collect solid HMX. Mixture of carbon dioxide and acetone is easily separated because these materials are insoluble and their boiling points differ significantly. Carbon dioxide is recovered from top of the separator and acetone is recovered from the bottom. A small amount of energy is used to minimize the amount of acetone in the top flow.

2.3. Recycle

Used carbon dioxide is recycled to reduce the carbon dioxide emission. Separated carbon dioxide is recompressed and brought back to the reactor inlet stream condition. The carbon dioxide contained in the acetone needs to be recovered before compression. In order to reduce the burden of each unit, compression and cooling are done by two compressors and two coolers, respectively.

3. Base-case design and optimization of the entire process

The three processing units mentioned above are combined and created as a process flowsheet. Aspen Plus V7.2 is used as the flowsheet simulator, and Figure 3 shows the flowsheet and calculation results.

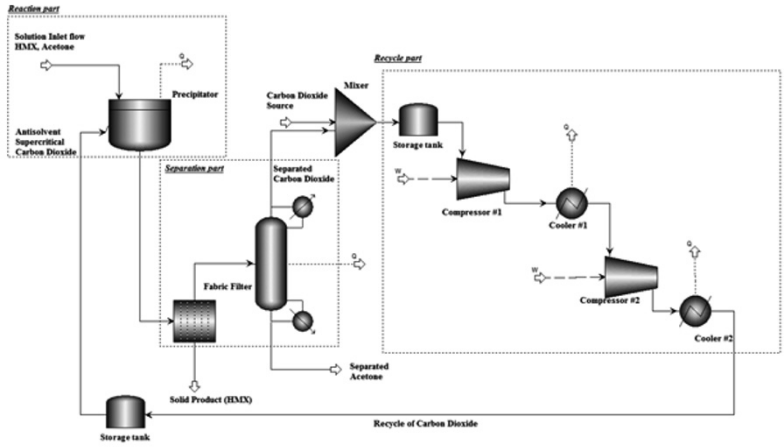

Figure 3. Process flowsheet of GAS process

Material and energy balances are calculated for 5000 ton/year production rate of HMX. UNIQ-RK EOS was chosen as a thermodynamic model. Steady state operation is presumed and dynamic operation for control of PSD of HMX is not considered in this step. Pressure drops in the fabric filter and cooler are neglected.

A batch reactor model is used to simulate the reactor. The reactor is operated at constant temperature of 30℃ and the temperature is controlled by the water jacket. Heat duty of water jacket is estimated by comparing the conditions of inlet and outlet flows. This assumption is valid because no chemical reaction occurs in the process. Batch cycle time of the reactor is one hour and the amount of antisolvent (carbon dioxide) feed

per cycle is 5 times bigger than the amount of HMX-acetone solution to increase the product yield. HMX-acetone solution is at standard temperature and pressure condition (101.325 kPa, 25℃). The condition of the antisolvent are chosen as 10000 kPa and 35℃ [4].

A fabric filter is installed to collect HMX product. Default simulation mode and parameters are used because PSD is not considered in the reactor. Hence, all the solid materials were assumed to be recovered from solvent flow.

For separation of CO_2 and acetone a flash drum is added. For implementation, the Sep2 model in Aspen Plus was employed because this can specify the mole-fraction of each substream and can compute the corresponding pressure and temperature condition. The Sep2 model is useful when the split ratio of each component is the key factor, while details of the separation are not important. Mole fraction of acetone in the bottom product is set to be above 0.999 and in the top product is set to be below 0.001 to avoid condensation of acetone in the recycle flow.

Compression and cooling set-points were specified as the inlet condition of the antisolvent for the reactor, e.g., 10000 kPa and 35 ℃. Storage tanks are also installed on each side of recycle part to store the recycled carbon dioxide between each batch cycle. Properties in the storage tank are assumed to be the same as the recompressed carbon dioxide stream.

Optimal operating points for compressor and coolers were also determined. Optimizer of Aspen HYSYS V7.2 is used for optimization. The objective function is to minimize the sum of heat duties of compressor and cooler. The optimization variables are the ΔP of compressor #1 and ΔT of cooler #1. Efficiency of each unit are was set to be a proper value less than 100% to have convergence. By solving this optimization problem, the optimal operating point and heat duties of each unit were estimated as shown in Tables 1 and 2.

Table 1. Optimal operating points of each unit.

	Compressor #1	Cooler #1	Compressor #2	Cooler #2
ΔP (kPa)	1748		7735	
Pressure Ratio	4.3		4.5	
ΔT (℃)		-42.41		-128.4

Table 2. Heat duty of each process unit.

	Reactor jacket	Solvent separator	Compressor #1	Cooler #1	Compressor #2	Cooler #2
Heat duty (Btu/hr)	7.30×10^4	2.14×10^4	4.17×10^5	1.85×10^6	4.96×10^6	1.27×10^7

It is shown that the cooling process requires most of the energy and thus will contribute to the increased operating cost. In this work carbon dioxide is designed to be fully recycled for environmental consideration, but for economic optimization the recycle ratio of carbon dioxide can be another manipulated variable for reducing operating cost. If carbon dioxide is not fully recycled for each cycle and the additional carbon dioxide for replenishment is increased, reduction of operating cost may be achievable. Detailed analysis for the optimal tradeoff will be done in the future work.

4. Concluding Remark

This work provides a base-case design for an integrated GAS process towards large-scale production of HMX and a steady-state optimal operating point for minimization of energy use. A rigorous population balance model will be incorporated into the reactor model to provide a more rigorous solution to optimal process economics and dynamics of the particle size distributions.

5. Acknowledgement

This work was financially supported by Agency for Defense Development of South Korea

References

[1] P. M. Gallagher, 1991, Gas Anti-Solvent (GAS) Recrystallization: Application to Particle Design, in Particle Design via Crystallization, AIChE symposium.
[2] G. Muhrer and C. Lin, 2002, Modeling the Gas Antisolvent Recrystallization Process, Industrial & Engineering Chemistry Research.
[3] S. Dodds and J. A. Wood, 2007, Modeling of the Gas-Antisolvent (GAS) Process for Crystallization of Beclomethasone Dipropionate Using Carbon Dioxide, Industrial & Engineering Chemistry Research.
[4] B. M. Lee, 2011, Preparation of Micronized β-HMX Using Supercritical Carbon Dioxide as Antisolvent, Industrial & Engineering Chemistry Research.

I.A. Karimi and Rajagopalan Srinivasan (Editors), Proceedings of the 11th International Symposium on Process Systems Engineering, 15-19 July 2012, Singapore.

Thermal integration of a hot process stream on distillation columns through a side-reboiler

Qinglin Chen*, Zhiqiang Wei, Shengyuan Wu, Bingjian Zhang

School of Chemistry and Chemical Engineering/Key Lab of Low-carbon Chemistry & Energy Conservation of Guangdong Province, Sun Yat-Sen University, Guangzhou 510275, China

Abstract

This paper presents a novel procedure to effectively integrate a hot process stream on a distillation column. The original value of the side-reboiler heat duty is identified through a comparison of the available heat duty of the hot process stream with the required heat duty of the side-reboiler. A benzene-toluene column is used to demonstrate the performance of the procedure. The results obtained demonstrate that the available heat duty of the hot process stream, the place location, heat duty of the side-reboiler, and stage number modification for the column could be identified by using the proposed procedure in a relatively simple and reliable way.

Keywords: distillation column, thermal integration, side reboiler, process streams.

1. Introduction

Integrating a hot process stream on distillation columns through side-reboilers is important for either designing an energy-efficient distillation column or improving the energy-use efficiency of chemical processes (Bandyopadhyay, 2007). In practical, when the available heat duty ($Q_{ava,hs}$), and the inlet temperature ($T_{in,hs}$) of the hot process stream are specified, a challenge for improving energy-use efficiency is how to effectively integrate the hot process stream with a specific distillation column through side-reboilers. Some approaches for thermal integration of distillation systems have been reported in the literature (Sobočan, 2002; Gadalla, 2003; Cabrera-Ruiz, 2011). Unfortunately, the key issues related to integration of the hot process stream on columns have not been fully addressed up to now. Thus, a novel procedure aimed to effectively integrate the hot process stream on distillation columns is proposed in this paper. Based on the procedure, the available heat duty of the hot process stream, the location and heat duty of the side-reboiler, stage number modification for the column could be easily and effectively identified. A benzene-toluene column is used to demonstrate the performance of the procedure.

2. Available heat duty of a hot process stream

The outlet temperature ($T_{out,hs}$) and the available heat duty of a hot process stream are calculated through Eqs. (1) and (2), respectively.

$$\Delta T = \frac{\left(T_{in,bs} - T_{out,ss}\right) - \left(T_{out,bs} - T_{in,ss}\right)}{\ln \dfrac{T_{in,bs} - T_{out,ss}}{T_{out,bs} - T_{in,ss}}} \tag{1}$$

* Correspondence author; email: chqlin@mail.sysu.edu.cn.

$$Q_{ava,bs} = CP_{bs} \cdot (T_{out,bs} - T_{in,bs}) \quad (2)$$

Where CP represents heat capacity flowrate, $\triangle T$ is the temperature difference for heat exchanging. The subscripts *in, out, hs* and *ss* represent the inlet temperature, outlet temperature, hot process stream and side-reboiled stream, respectively. In calculating the value of $T_{\text{out,hs}}$, $\triangle T$ is assumed to be 10 K, as the minimum temperature difference.

The arranging location ($N_{\text{side-re},i}$) and required heat duty ($Q_{\text{side-re},i}$) of the side-reboiler are identified through exergy grand composite curve (EGCC) and avoidable exergy destruction curve (AEDC), as proposed by our group (Wei, 2012). Thus, the inlet and outlet temperatures of the side-reboiled stream are identified, and the available heat duty of the hot process stream is calculated through Eqs. (1) and (2). With the value of $Q_{\text{ava,hs},i}$ and $Q_{\text{side-re},i}$, one can conclude whether the heat duty of the hot process stream is sufficient or not for setting a side-reboiler, as is presented in Fig. 1.

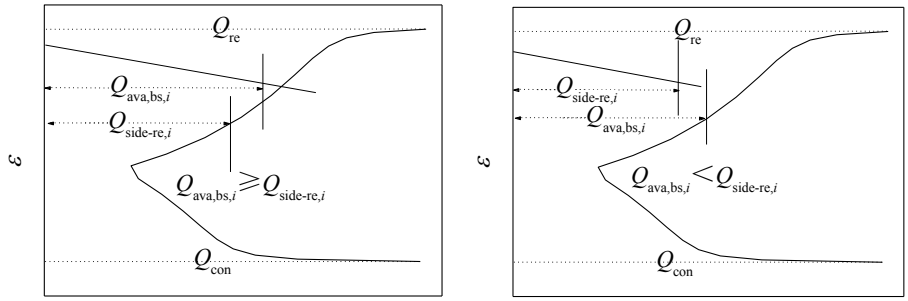

Fig. 1 Schematic of $Q_{\text{ava,hs},0}$ and $Q_{\text{side-re},0}$

As shown in Fig. 1a, the value of $Q_{\text{ava,hs},i}$ is greater than $Q_{\text{side-re},i}$, which suggests that $Q_{\text{ava,hs},i}$ is sufficient for setting a side-reboiler, and the heat duty has a surplus. Then, $Q_{\text{side-re},i}$ and $N_{\text{side-re},i}$ are identified as the original values of the side-reboiler heat duty and location. While in Fig. 1b, $Q_{\text{ava,hs},i}$ is smaller than $Q_{\text{side-re},i}$, which means that $Q_{\text{ava,hs},i}$ is not sufficient for arranging a side-reboiler. In this case, the original value of the side-reboiler heat duty should be reconsidered. In general, the value should be fallen among $Q_{\text{ava,hs},i}$ and $Q_{\text{side-re},i}$. Therefore, stage number between these two boundary values is determined and the corresponding available heat duty $Q_{\text{ava,hs},j}$ is calculated. The maximum value of $Q_{\text{ava,hs},j}$ is treated as the original value of the side-reboiler heat duty, and the corresponding stage is used to arrange the side-reboiler.

3. Calculation procedure

The calculation procedure, illustrates in Fig 2, can effectively integrate the hot process stream with a specific distillation column through arranging a side-reboiler.

1) Identify the optimum feed stage $N_{F,\text{opt}}$ and the optimum reflux ratio $R_{0,\text{ opt}}$.
2) Identify the location $N_{\text{side-re},i}$ and the duty $Q_{\text{side-re},i}$ of a side-reboiler through EGCC and AEDC.
3) Identify the inlet and outlet temperature of the side-reboiled stream, $T_{\text{in,ss},i}$ and $T_{\text{out,ss},i}$.
4) With the values of $T_{\text{in,ss},i}$, $T_{\text{out,ss},i}$ $T_{\text{in,hs},i}$ and CP_{hs}, calculate the outlet temperature of the hot process stream $T_{\text{out,hs},i}$ and the available heat duty $Q_{\text{ava,hs},i}$.
5) If $Q_{\text{ava,hs},i}$ is equal to or greater than $Q_{\text{side-re},i}$, $N_{\text{side-re},i}$ and $Q_{\text{side-re},i}$ are used as the

original values of the location and heat duty for arranging a side-reboiler.
6) Determine the new reflux ratio R_i' after the side-reboiler arranged.

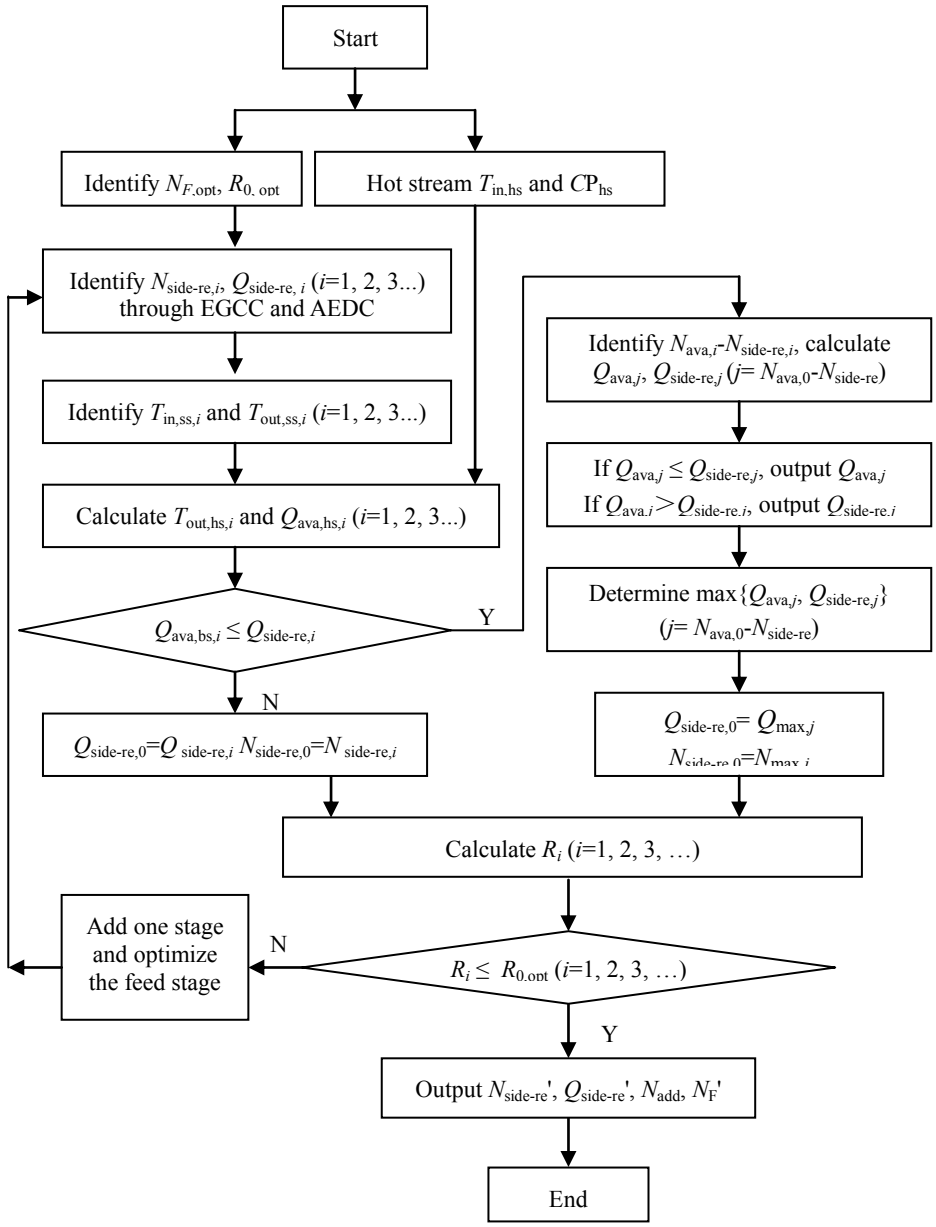

Fig. 2 Calculation procedure to integrate the hot process stream on a distillation column

7) If R_i' is not larger than $R_{0,opt}$, adjust the stage number is unnecessary, and information of the side-reboiler $N_{side\text{-}re}$', $Q_{side\text{-}re}$' can be output and the procedure is ended.
8) If R_i' is greater than $R_{0,opt}$, add one stage to the column, and optimize the feed stage.
9) Return to the second step, recalculate until R_i' is not greater than $R_{0,opt}$, output the information of the side-reboiler $N_{side\text{-}re}$', $Q_{side\text{-}re}$', N_{add}, N_F' and the procedure is ended.

10) If $Q_{ava,hs,i}$ is smaller than $Q_{side\text{-}re,i}$, identify the stages between $N_{ava,i}$ and $N_{side\text{-}re,i}$, and calculate the $Q_{ava,hs,j}$ and $Q_{side\text{-}re,j}$ values for these stages, where the EGCC enthalpy values are treated as the corresponding $Q_{side\text{-}re,j}$ to identify the values of $T_{in,ss,j}$ and $T_{out,ss,j}$.
11) If $Q_{ava,hs,j}$ is not larger than $Q_{side\text{-}re,j}$, the output parameter to the next step is $Q_{ava,hs,j}$, while for $Q_{ava,hs,j}$ is greater than $Q_{side\text{-}re,j}$, the value of $Q_{side\text{-}re,j}$ is taken as an output result to the next step.
12) Determine the maximum value of the results $\{Q_{ava,j}, Q_{side\text{-}re,j}\ (j= N_{ava,0}\text{-}N_{side\text{-}re})\}$, and the original values of the location and heat duty of the side-reboiler are the maximum value $Q_{max,j}$ and the corresponding stage $N_{max,j}$.
13) Repeat the steps 6-9 and output information of the side-reboiler $N_{side\text{-}re}'$, $Q_{side\text{-}re}'$, N_{add}, N_F', and the procedure is ended.

A benzene-toluene column is used to demonstrate the performance of the calculation procedure, and specifications of the column are listed in Table 1. The heat capacity flowrate of the hot process stream is set as 25 kW/K, and the inlet temperature is 393 K.

Table 1 Feed, product, and column specifications

Feed properties		Column characteristics		Feed molar fractions	benzene	0.50
Molar flow kmol/h	100	Stage number	25		toluene	0.50
Temperature K	365	Feed number	12	Column specifications	$x_{D,benzene}$	0.99
Pressure MPa	0.1	Condenser	total		$x_{B,toluene}$	0.99

Table 2 Information for determining the avaliable heat duty of the hot process stream

N_{add}	$N_{side\text{-}re,i}$	$T_{in,ss}$ / K	$T_{out,ss}$ / K	$T_{out,hs}'$ / K	$Q_{side\text{-}re,i}$ / kW	$Q_{ava,hs,i}$ / kW
0	17	375.5	378.0	382.0	495	285
	16	373.0	375.5	378.0	395	380
	15	370.0	373.0	374.0	295	470
1	18	375.5	378.0	382.0	485	285
	17	373.0	376.0	378.0	390	375
	16	370.0	373.0	374.5	290	460
2	19	376.0	378.0	382.0	460	280
	18	373.0	376.0	378.0	360	370

The detailed results of arranging a side-reboiler on the benzene-toluene column are listed in Table 2 and Table 3. It can be seen that in the base case, a 495 kW heat duty is needed on the 17th stage, and only 285 kW heat duty is available. The value of $Q_{ava,hs,i}$ is lower than $Q_{side\text{-}re,i}$. Then, the stages between $Q_{ava,hs,i}$ and $Q_{side\text{-}re,i}$ are identified as the 15th and 16th stages. For the 16th stage, the output heat duty for the side-reboiler is 380 kW, and the heat duty determined in the 15th stage is 295 kW. This means that the 16th stage and a 380 kW heat duty should be identified as the original values for the side-reboiler. The modified reflux ratio is larger than that of the base one, which indicates that one stage should be added, and a new iteration is started. The final results are obtained after three iterations, and the outlet temperature of the hot process stream is 378 K and the available heat duty of the hot process stream is 370 kW. In arranging a side-reboiler, two stages should be added. The feed stage is the 13th stage, the placing location is the 18th stage, and the heat duty is 360 kW.

Table 3 Information of arranging a side-reboiler on the benzene-toluene column

Iteration	R	$N_{F,i}$	$N_{\text{side-re},i}$	$Q_{\text{side-re},i}$ / kW	$N_{\text{add},i}$
Base case	1.66	12	---	---	---
1	1.76	12	16	380	0
2	1.72	13	17	375	1
3	1.65	13	18	360	2

4. Conclusions

A novel procedure is proposed to integrate the hot process stream on a distillation column. According to the procedure, the available heat duty of the hot process stream is calculated, and the original value of the side-reboiler heat duty is identified through a comparison of the available heat duty of the hot process stream with the required heat duty of the side-reboiler. A benzene-toluene column is used to demonstrate the performance of the procedure. The results indicate that the available heat duty of the hot process stream and information of the side-reboiler (i.e. the location and heat duty of the side-reboiler, stage number modification for the column) are related to each other. The procedure proposed can effectively integrate the hot process stream on a distillation column in a relatively simple and systematic way.

Acknowledgement

The authors gratefully acknowledge the financial support from the National Natural Science Foundation of China (No. 20906016, 21076233) and the Major Science and Technology R&D Program of Guangdong Province (No. 2010A080801003).

References

G. Sobočan, P. Glavič, 2002, A simple method for systematic synthesis of thermally integrated distillation sequences, Chem. Eng. J., 89, 1, 155-172

J. Cabrera-Ruiz, A. Jiménez-Gutiérrez, J. G. Segovia-Hernández, 2011, Assessment of the implementation of heat-integrated distillation columns for the separation of ternary mixtures, Chem. Eng. Res. Des., 50, 4, 2176-2181

M. Gadalla, M. Jobson, R. Smith, 2003, Optimization of existing heat-integrated refinery distillation systems, Chem. Eng. Res. Des., 81, A1, 147-152

S. Bandyopadhyay, 2007, Thermal integration of a distillation column through side-excahngers, Chem. Eng. Res. Des., 85, A1, 155-166

Z. Q Wei, S. Y. Wu, B. J. Zhang, Q. L. Chen, 2012, An exergy grand composite curve based procedure for side-exchanger arrangement on distillation columns. 11th International Symposia on Process Systems Engineering.

I.A. Karimi and Rajagopalan Srinivasan (Editors), Proceedings of the 11th International Symposium on Process Systems Engineering, 15-19 July 2012, Singapore.

Forecasting Naphtha Price Crack Using Multiple Regression Analysis

Chaeeun Sung[a], Hweeung Kwon[a], Jinsuk Lee[b], Haesub Yoon[b], Il Moon[a]

[a] *Department of Chemical and Biomolecular Engineering, Yonsei University, 50 Yonsei-ro, Seodaemun-gu, Seoul 120-749, Korea*

[b] *SamsungTotal Corporation 411, Dokgot-ri, Daesan-eup Seosan*-si, *Chungcheongnam-do 356-711, Korea*

Corresponding Author's E-mail: sce0214@yonsei.ac.kr

Abstract

The price of naphtha depends on that of crude oil as naphtha is produced by refining crude oil. Naphtha plays an important role as one of basic petrochemicals for downstream products. Large fluctuation of naphtha price has been intensified along with recent political unrest of Middle East Asia and the growing naphtha demand in developing countries. Thus forecasting naphtha price is becoming more uncertain. The development of models for forecasting naphtha crack (price difference between naphtha and crude oil) will help minimize any loss from naphtha price variations. This study is concerned with the derivation of a set of major parameters affecting naphtha prices and the identification of the most dominating factors. We proposed a model for forecasting naphtha crack based on statistical approach and multiple regression analysis, and R^2 was 0.651. .Naphtha price depends mainly on Asia supply and demand of naphtha as well as naphtha substitute and margin. Actual and predicted variations of naphtha crack were also analyzed. The proposed modeling approach can be extended to forecast prices of other downstream chemicals such as LPG and NGL.

Keywords: Naphtha crack, Multiple regression model, Statistical approach, Forecasting

1. Introduction

In recent years, uncertainty of naphtha price forecasting has increase due to expanding price variability of naphtha affected various factors such as supply and demand, prices, margin of naphtha and petrochemical products, global economy and the operational rate of oil company. Forecasting naphtha crack has been regarded as one of the most important thing of purchasing naphtha. Thus, various models have been depicted to provide the naphtha buyers with more precise predictions.

Several studies for price forecasting have been published. Artificial neural networks (ANN) have been referring to forecasting price. B.R. Szkuta et al. (1999) study the System Marginal Price short-term forecasting using artificial neural networks. P. Pai (2005) presents a hybrid model of the autoregressive integrated moving average (ARIMA) and the support vector machines (SVMs). This model is higher evaluated than the prediction performance of the single ARIMA model and single SVMs model. W. Zhang (2010) researches forecasting agricultural and livestock products price using statistical approach.

In this paper, we develop the multiple regression model to forecasting naphtha crack considering more than 20 factors. This paper shows part of these factors, supply and demand of naphtha, margin, and naphtha substitute. This model verified by comparing actual naphtha crack and predicted naphtha crack from January 2011 to November 2011. Finally, we analyze the percentage of the correct predicted variation of naphtha crack.

2. Problem statement

2.1 Data normalization

The actual data was normalized in this work from 0 to 1 in order to standardize unit and range

$$D_{nor} = \frac{D - D_{min}}{D_{max} - D_{min}} \quad (1)$$

where D_{nor} is the normalized data, D is the actual data, D_{min} is the minimum value of the normalized data, and D_{max} is the maximum value of the normalized data.

2.2 Data preparation

Among the various major factors, we select the three factors, supply and demand, margin and naphtha substitute. These are not the only factors influencing naphtha crack. The major factors were used as independent variables in forecasting naphtha crack. Monthly data for major factors are collected from 2008 to 2010 except from October 2008 to March 2009 to avoid unusual economic effect, Lehman Brothers collapse

Table 1. The major factors from 2008 to 2010

Date	Naphtha crack ($/mt)	Supply/ Demand (mt/month)	Margin ($/mt)	Naphtha substitute ($/mt)	Date	Naphtha crack ($/mt)	Supply/ Demand (mt/month)	Margin ($/mt)	Naphtha substitute ($/mt)
Jan-08	41.760	1545000	146.867	6.205	Oct-09	-22.187	1515000	120.668	-28.261
Feb-08	25.974	1463000	154.385	-52.986	Nov-09	-2.692	1481000	119.573	-1.150
Mar-08	-13.974	1501000	171.540	-52.092	Dec-09	30.952	1586000	121.677	45.012
Apr-08	-35.386	1373000	194.698	-82.716	Jan-10	37.742	1571000	147.853	76.163
May-08	-62.668	1455000	211.831	-106.592	Feb-10	19.538	1438000	147.949	64.250
Jun-08	-40.362	1469000	211.885	-165.369	Mar-10	21.987	1405000	200.023	3.750
Jul-08	-53.882	1537000	158.885	-141.883	Apr-10	-10.251	1430000	179.259	3.750
Aug-08	-20.111	1546000	177.856	-136.538	May-10	8.391	1522000	169.018	-44.103
Sep-08	-31.760	1309000	179.613	-72.432	Jun-10	-9.454	1413000	170.609	-23.944
Apr-09	-140.008	1404000	126.375	-60.000	Jul-10	-34.687	1505000	164.643	-25.840
May-09	-197.908	1490000	178.928	-120.855	Aug-10	-12.185	1496000	128.349	-17.600
Jun-09	-101.827	1426000	173.518	-93.648	Sep-10	-7.097	1425000	100.680	7.013
Jul-09	-31.295	1486000	144.537	-67.293	Oct-10	14.215	1443000	121.843	24.800
Aug-09	21.201	1548000	167.900	-79.118	Nov-10	24.593	1496000	129.176	96.100
Sep-09	-3.973	1477000	112.430	-36.670	Dec-10	36.381	1607000	145.223	163.413

4. Modeling

The general model of multiple regressions is given

$$y = \beta_0 + \beta_1 x_1 + \beta_2 x_2 + \cdots + \beta_p x_p + \varepsilon \quad (2)$$

where y is the predicted trend, $x_1, x_2, \cdots x_p$ are the influence factors of predicted trend, $\beta_0, \beta_1 \cdots \beta_p$ are the regression coefficients, and ε is the residual variable.
In this paper, naphtha crack (C) was assumed as function of supply and demand of naphtha (S), margin (M) and naphtha substitute (N). According to the three major factors, we establish the following multiple regression model equation

$$C = f(S, M, N) = \beta_0 + \beta_1 S + \beta_2 M + \beta_3 N + \varepsilon \quad (3)$$

5. Results

Table 2 shows that correlation coefficients between the naphtha crack and three major factors.

Table 2. Pearson correlation and significance values to naphtha crack

	Pearson Correlation	**Significance**
Supply/Demand (S)	.792	.000
Margin (M)	.358	.026
Naphtha substitute (N)	-.452	.006

Significance values of major factors to naphtha crack are less than the significance level 5%. It means that major factors have very strong correlations with naphtha crack.

Table 3. Coefficients and R^2 in model

Model	**Unstandardized Coefficients**		**Standardized Coefficients**	**Significance**	**R^2**
	β	**Std. Error**	**Beta**		
Constant	.211	.298		.484	.651
Supply/Demand (S)	.404	.076	.734	.000	
Margin (M)	.477	.375	.154	.215	
Naphtha substitute (N)	-.033	.141	-.032	.818	

This table explain the values of multiple regression model. Supply and demand of naphtha is less than the significance level 5% shows that this factor has a large impact on naphtha crack rather than other two factors. From R^2 of this model, we know that 65.1 % of the variations in naphtha crack can be explained by the three major factors.

The regression coefficients of multiple regression model is obtained from β of unstandardized coefficients.

$$C = 0.211 + 0.404S + 0.477M - 0.33N \quad (4)$$

Using this model, actual and predicted variations of the naphtha crack from January 2008 to December 2010 are investigated 48.3%. (The data are not shown) We forecast this model by forecasting naphtha crack from January 2011 to November 2011. Fig. 1 shows actual naphtha crack and predicted naphtha crack from January 2011 to November.

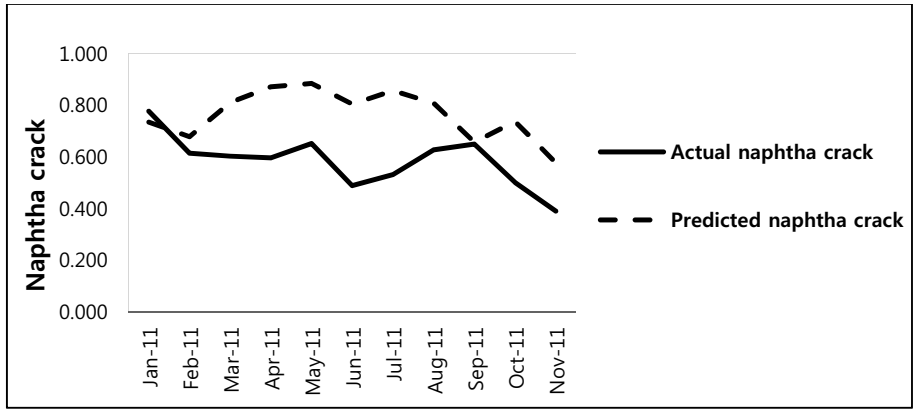

Figure 1. Time series plot of actual naphtha crack and predicted naphtha crack.

In forecasting of naphtha crack, it is important variation more than exactly naphtha crack data. Table 4 shows actual and predicted variations of naphtha crack. From prediction result in table 4, we obtain the percentage of the correct predicted variation. The variation of naphtha crack obtained from the difference between that month and previous month. If both actual and predicted variations of the naphtha crack have the same sign, it indicates that it means that the prediction is same. Owing to 5 same predictions out of total 10 months in table 4, the correct predicted variation is 50%

Table 4. Actual and predicted variations of naphtha crack

Date	Actual naphtha crack variation	Predicted naphtha crack variation	Prediction result
Jan-11	-0.162	-0.057	Same
Feb-11	-0.012	0.133	Different
Mar-11	-0.006	0.061	Different
Apr-11	0.056	0.013	Same
May-11	-0.163	-0.079	Same
Jun-11	0.043	0.052	Same
Jul-11	0.096	-0.048	Different
Aug-11	0.022	-0.151	Different
Sep-11	-0.149	0.079	Different
Oct-11	-0.111	-0.159	Same

6. Conclusion

In this study, we develop the multiple regression models to forecasting naphtha crack. Three major factors influencing naphtha crack have correlation with naphtha crack. Among the major factors, supply and demand of naphtha have strong impact on naphtha crack. From multiple regression models, we could forecast future naphtha crack and analysis the percentage of the correct predicted variation. Through this study, we could more consider major factors influencing naphtha crack for obtaining higher R^2 in model and the percentage of the correct predicted variation.

6. References

B.R. Szkuta, L.A. Sanabria, T.S. Dillon, 1999, Electricity Price Short-Term Forecasting Using Artificial Neural Networks, IEEE Transactions on Power Systems, Vol.14, 854-857

P. Pai, C. Lin, 2005, A hybrid ARIMA and support vector mahines model in stock price forecasting, The International Journal of Management Science, Vol.33, 497-505

W. Zhang, H. Chen, M. Wang, 2010, A forecast model of agricultural and livestock products price, Mechanics and materials 20-23, 1109-1114

A. Ghaffari, S. Zare, 2009, A novel algorithm for prediction of crude oil price variation based on soft computing, Energy economics 31, 4, 531-536

P. Visetsripong, P. Sooraksa, P. Luenam, 2008, Naphtha's Price Forecasting using Neuro-fuzzy System, Society of Instrument and Control Engineers Annual Conference, 659-663

Kim, J., Lee, Y., Moon, .I., 2008, Optimization of a hydrogen supply chain under demand uncertainty, International Journal of Hydrogen Energy, Vol.33, Issue 18, 4715-4729

Kim, J., Moon, .I., 2008, Strategic design of hydrogen infrastructure considering cost and safety using multiobjective optimization, International Journal of Hydrogen Energy, Vol.33, Issue 21, 5887-5896

Kim, J., Moon, .I., 2008, The role of hydrogen in the road transportation sector for a sustainable energy system: a case study of Korea, International Journal of Hydrogen Energy, Vol. 33, No.24, 7326-7337

I.A. Karimi and Rajagopalan Srinivasan (Editors), Proceedings of the 11th International Symposium on Process Systems Engineering, 15-19 July 2012, Singapore.

Model-based development of optimal reaction concepts for plant wide process intensification

Andreas Peschel,[a] *Andreas Jörke*,[b] *Hannsjörg Freund*,[a] *Kai Sundmacher*[a,b]

[a]*Max Planck Institute for Dynamics of Complex Technical Systems, 39106 Magdeburg, Germany.* [b]*Process Systems Engineering, Otto-von-Guericke University, 39106 Magdeburg, Germany*

Abstract

In order to design optimal chemical reactors, the interaction between reactor and process needs to be considered. In this contribution we propose a new method for the design of optimal reactors in the overall process framework by simultaneous determination of the best reaction concept and optimization of the process design parameters. The reaction concept is apparatus independent and optimal state space profiles for composition and temperature are provided along the reaction coordinate.
The oxygen based production of ethylene oxide, one of the most important bulk chemicals, is considered as an example. Here, advanced cooling and distributed dosing of oxygen is identified as best reaction concept from an economical and technological point of view. Applying this innovative reaction concept, the production costs of an average sized plant are reduced by 1.35 Mio \$/a, and the CO_2 emissions are decreased by $2.7 \cdot 10^4$ t/a compared to an optimized reference case. This general method provides a first step towards more economical and greener processes.

Keywords: Reactor, design, optimization, ethylene oxide, process intensification.

1. Introduction and methodological approach

Since selectivity and conversion in the reactor determines the effort of the downstream purification process, the reaction concept offers a large potential to enhance the energy and raw material efficiency of today's chemical processes. To identify the best reaction concept from a process point of view, the interaction between reactor and process needs to be taken into account; otherwise suboptimal reactors are placed in the process. Only a simultaneous optimization of the reaction concept and the plant operation gives rise to the reaction concept that results in the maximum improvement of the overall process. In order to identify the most promising reaction concept, the elementary process functions approach is used to describe the reaction module [1, 2]. Within this approach, optimal profiles of the heat flux and component dosing/removal fluxes are realized in order to obtain the best reaction conditions over the entire residence time and process intensification options are considered by modeling the physico-chemical phenomena. This method constitutes a symbiosis of process intensification and process systems engineering methods as can be seen from the objectives and methods of both disciplines [3].

2. Example process: Oxygen based ethylene oxide synthesis

Ethylene oxide (EO) is one of the most important bulk chemicals and already small improvements in the reactor results in large savings in the running expenses of the process. Due to the undesired total oxidation of ethylene to CO_2 in the reactor and the energy intensive downstream purification process, the EO process is one of the main producers of CO_2 within the chemical industry.

For the synthesis of EO, the oxygen based process is state-of-the-art. However, few publications consider the optimization of the oxygen based EO process and, in particular, the optimal reaction concept has never been determined so far. An earlier publication on the air based EO process [4] shows significant potential for a better reaction concept for the EO synthesis, but the reaction concept was not determined within the overall process. The flowsheet of the oxygen based ethylene oxide process is shown in Fig. 1. Downstream of the reaction section, the produced EO is absorbed using water. Further downstream, part of the CO_2 is removed by absorption in hot potassium carbonate, before the fresh feed is added to the recycle stream.

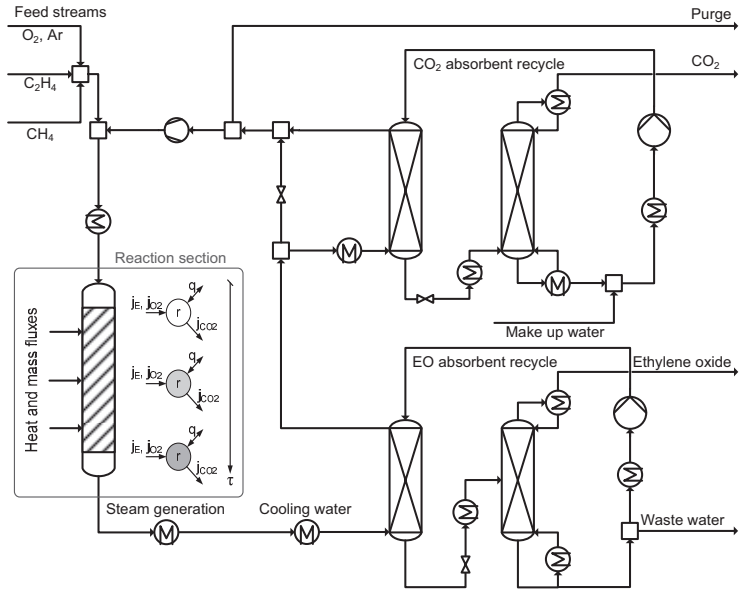

Figure 1: Flowsheet of the oxygen based ethylene oxide process

The overall objective of this work is the minimization of the EO production costs by optimizing the reaction concept and the plant operation simultaneously. Thereby, all raw material (ethylene, oxygen, methane) and utility costs (electricity, steam, cooling water) are taken into account using the most currently available cost data [5].

3. Modeling

The overall process according to Fig. 1 is modeled using a detailed model of the reaction section, tailored models for the EO and CO_2 absorption sections, and short-cut models for the additional process units. This paper is an excerpt of a more comprehensive paper [5], where all model equations are given, the optimization problems are stated, the modeling assumptions are discussed, and a sensitivity analysis is performed to investigate the influence of uncertainties.

3.1. Reaction section

The reaction module is modeled according to the elementary process function approach [1, 2]. Here, a fluid element is tracked and optimal flux profiles are determined in order to obtain the best reaction conditions for this fluid element over its entire residence time. Exemplarily, the component mass balance for the tracked fluid element is given below (n_i=amount in fluid element, a_i=exchange area, j_i=dosing flux, ρ=catalyst density, ε=void fraction, V_{gas}=gas volume of fluid element, r=reaction rate, NR=# of reactions).

$$\frac{dn_i}{dt} = a_i j_i + \rho_{cat} \frac{1-\varepsilon}{\varepsilon} V_{gas} \sum_{j=1}^{NR} \upsilon_{ij} r_j$$

The dosing fluxes j_i are used to manipulate the concentration profile in an optimal manner along the reaction coordinate and they constitute an optimization function in the intensified reaction concepts discussed in Section 4. Different reaction concepts including advanced cooling and distributed dosing of reactants and in-situ removal of CO_2 are considered. The optimal profiles for these fluxes are obtained by solving a dynamic optimization problem, which is constrained by the complete process model for the reaction section and downstream purification. The model of the reaction module consists of the component balances, the energy balance, bounds for the temperature region of the catalyst, a lower limit for the obtained space time yield of 1 mol/(m^3s), the reaction kinetics [7], and intrinsic bounds imposed by the explosion limits of the mixture.

Due to the explosion hazard inside the reactor, the reaction mixture must stay outside the explosive region all along the reaction coordinate. For this purpose, a new model based on literature data for the explosive region, which is developed in [5], is included into the optimization. This model rigorously accounts for the influence of the individual flammable gases (ethylene, methane, ethylene oxide) [8] including the non-idealities arising from the composition [9], as well as the pressure [10, 11] and temperature dependency of the explosive region. A detailed model of the explosive region allows for the optimal manipulation of the composition along the reaction coordinate in order to improve the reactor performance but always keeping clear of the explosive region.

3.2. Downstream process

The downstream process consists of an EO absorption section and a CO_2 separation section. In the former, EO is separated from the gases by physical absorption in water. The absorber is modeled using the Kremser equation and the desorber is described using two flash tanks. The produced EO has a purity of 95% and is send to further distillation to remove the light components. In order to separate the CO_2 from the recycle gas, a hot potassium carbonate solution with piperazine as promoter is used. The chemical equilibrium of this chemisorption is modeled taking all 6 equilibrium reactions and all 10 intermediate species into account [12]. The physical solubility of all gas components are modeled using Henry's law combined with a specialized approach to describe the physical solubility of CO_2 in the potassium carbonate solution. The additional process units (pumps, compressors, heat exchangers, mixers, and splitters) are modeled using common short-cut models as proposed in the literature [13]. Ideal heat integration is assumed in order to determine the minimal utility consumption of the process.

4. Results

Depending on the investigated reaction concept the heat flux (q) as well as the mass fluxes of oxygen (j_{O2}), ethylene (j_E), and CO_2 (j_{CO2}) into or out of the fluid element are optimized along the reaction coordinate. In addition, the feed streams, the reaction pressure, the residence time in the reactor, the temperature of the absorbers and desorbers, the absorbents stream of water and potassium carbonate solution, the split fractions of each splitter are degrees of freedom to be simultaneously optimized to the reaction concept. The optimization problem is constrained by the overall process model including the detailed description of the reaction section and of the downstream process. The distributed balance equations of the reaction section are discretized using orthogonal collocation on finite elements and the overall process model is implemented in *AMPL* yielding a large scale NLP problem which is solved using the state-of-the-art solver *CONOPT*.

The optimization results of all investigated reaction concepts are summarized in Fig. 2. In the reference case (case 1), the reaction conditions are assumed to be isothermal and

no components are dosed in order to manipulate the concentration profiles in the reaction section. This reaction concept refers to the industrially used tube bundle reactor with very effective cooling. The EO production costs of the optimized reference case are 656.3 $/t, which is in good agreement to the published production costs of the oxygen based EO process [5].

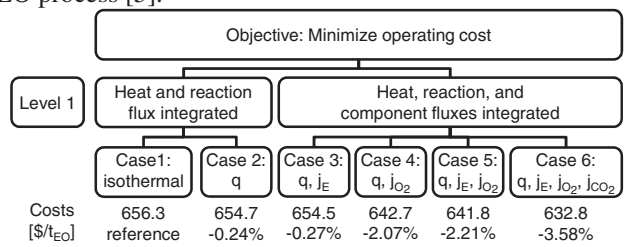

Figure 2: Results overview

Obtaining an optimal temperature profile in the reactor (case 2) as well as optimal cooling combined with distributed dosing of ethylene (case 3), show only small potential for the reduction of the running expenses. However, distributed dosing of oxygen combined with an optimal heat flux profile (case 4) reduces the running expenses of the process by more than 2%. Such a cost reduction refers to annual savings in the order of 1.35 Mio $/a for an average plant capacity of 100 kt/a.

The combined dosing of ethylene and oxygen in combination with in-situ removal of CO2 (case 6) are investigated in order to determine the maximum potential of an optimal reaction concept for the overall process improvement. Even if such an in-situ removal cannot be realized at the moment, the maximum potential of such a case is helpful for guiding further research and development activities. In addition, the combined dosing of ethylene and oxygen (case 5) performs only slightly better than case 4. Since the combined dosing oxygen and ethylene suffers from safety hazards, distributed oxygen dosing combined with an advanced cooling strategy (case 4) is the most promising option from a technical and economic point of view and investigated in more detail. The obtained profiles in the reactor of the reference case (case 1) and the selected case (case 4) are shown in Fig. 3.

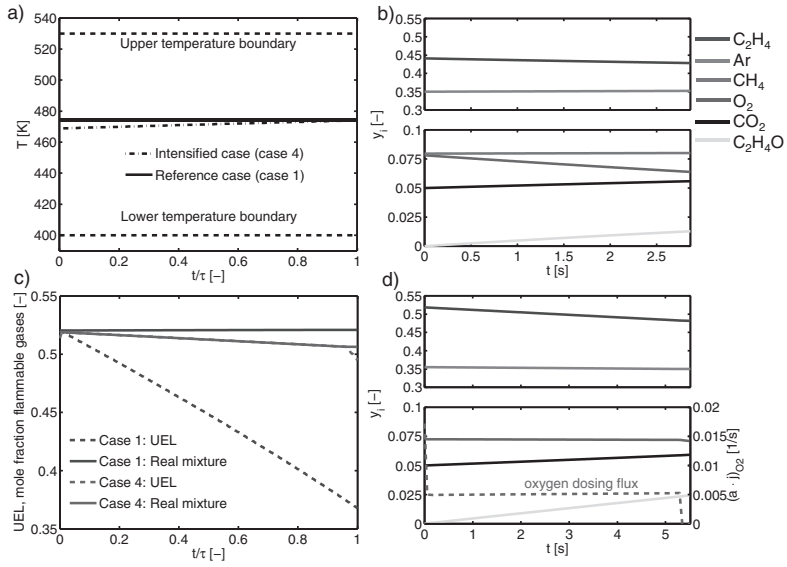

Figure 3: Detailed profile comparison. a) Temperature profiles b) Mole fraction profiles (case 1) c) Explosion limits d) Mole fraction profiles (case 4)

The optimal temperature profile slightly increases (Fig. 3a). By comparing the composition in the reactor (Fig. 3b and Fig. 3d) it can be noted that the ethylene level and the ethylene oxide outlet mole fraction are considerably higher in the intensified case. This leads to a major reduction of the gas recycle stream of 47.4%, which gives rise to smaller apparatuses and lower energy consumption of the overall process. The steam consumption is reduced by 7.0%, the cooling water by 6.9%, and the electricity consumption by 46.3%. In addition, no methane is required in the intensified case to keep the gas composition out of the explosive region. This simplifies the overall process design and control significantly. By dosing oxygen and controlling the temperature profile of the reactor, the composition in the reactor can be kept at the upper explosion limit all along the reaction coordinate, but the mixture is never explosive (refer to Fig. 3c). In the reference case, the composition at the reactor inlet is at the explosion limit, but oxygen depletes and the margin from the explosive region increases. Thereby, the composition falls short of the optimal reaction conditions, which results in a lower process performance. The total CO_2 emissions associated with the purge stream and the utility consumption is reduced by 8.0%, which refers to a reduction of the annual CO_2 emission of $2.7 \cdot 10^4$ t/a for an average sized EO plant.

5. Conclusion

The method proves to be able to determine the optimal reaction concept from an overall process point of view giving rise to a better process performance. The reaction kinetics and complex intrinsic bounds such as explosion limits are directly considered in the model of the reaction section, yielding an accurate model from the thermodynamic and reaction engineering point of view. Based on the determined reaction concept, an optimal tailor-made reactor for this process can be designed [2, 3]. The obtained results proof that the optimal reaction concepts offers significant potential to intensify the overall process; the significant reductions of the production costs, recycle flow rate, and CO_2 emissions give rise to a new generation of more economical and more sustainable chemical processes.

6. Acknowledgments

The authors gratefully acknowledge financial support by BASF SE.

References

[1] H. Freund, K. Sundmacher. Chem. Eng. Process., 2051–2060 (47), 2008.
[2] A. Peschel, H. Freund, K. Sundmacher. Ind. Eng. Chem. Res., 10535–10548 (49), 2010.
[3] J.A. Moulijn, A. Stankiewicz, J. Grievink, A. Górak. Comput. Chem. Eng., 3–11 (32), 2008.
[4] A. Peschel, F. Karst, H. Freund, K. Sundmacher. Chem. Eng. Sci., 6453–6469 (66), 2011.
[5] Nexant-Inc. Ethylene Oxide/Ethylene Glycol. PERP Program 04/05–5, 2006.
[6] A. Peschel, A. Jörke, H. Freund, K. Sundmacher. Chem. Eng. J., submitted.
[7] L. Gan, H. Wang, B. Zhu, S. Xu, Z. Wang. Chem. Ind. Eng., 969–972 (52), 2001.
[8] M. Molnárné, T. Schendler, V. Schröder. Safety Characteristic Data. Volume 2: Explosion Regions of Gas Mixtures. Wirtschaftsverlag NW, Bremerhaven, 2008.
[9] M. Klaubert. PhD thesis, University of Paderborn, Germany, 1998.
[10] F. van den Schoor, F. Verplaetsen. J. Hazard. Mater., 1–9 (128), 2006.
[11] F. van den Schoor, F. Verplaetsen. Int. J. Hydrogen Energ., 2548–2552 (32), 2007.
[12] J.T. Cullinane, G.T. Rochelle. Chem. Eng. Sci., 3619–3630 (59), 2004.
[13] L.T. Biegler, I.E. Grossmann, A.W. Westerberg. Systematic Methods of Chemical Process Design. Prentice Hall, Upper Saddle River, 1999.

I.A. Karimi and Rajagopalan Srinivasan (Editors), Proceedings of the 11th International Symposium on Process Systems Engineering, 15-19 July 2012, Singapore.

Hierarchical simulation of integrated chemical processes with a web based modeling tool

Robert Kraus, Victor Alejandro Merchan, Harvey Arellano-Garcia, Günter Wozny

Chair of Process Dynamics and Operation, Berlin Institute of Technology, Sekr. KWT-9, Straße des 17. Juni 135, D-10623 Berlin, Germany

Abstract

A novel approach for the systematic and hierarchical derivation of process models is presented. Model candidates for different unit phenomena are collected and rated on the basis of the model structure, origin and the modeler's belief. The process model is created as a superstructure with the competing partial models. Thereby, it is possible to determine the best possible combination through optimization with respect to different objective functions. The systematic procedure has been implemented into the online web modeling platform MOSAIC. Based on the superstructure, optimization code for the state-of-the art optimization and simulation software can automatically be created. Based on two case studies, the new approach is demonstrated, namely a process model for the hydroformylation of long-chain olefins and a model for the pressure drop in packed columns with foaming components.

Keywords: model discrimination, integer optimization, code generation.

1. Introduction into hierarchical simulation

As illustrated in Fig. 1, the equation system for a complete chemical process is a combination of different models, which fully describe the different phenomena of all process units, for instance, the pressure drop of a packed column, or a chemical reaction network. These models can be more or less complex and rigorous. The selection and connection of these elementary models is mostly done without the knowledge, which combination of all sub-models is able to describe the whole system in the best possible way. It is possible that the selected models explain single phenomena's very well, but when they are combined, they may fail. Furthermore, it is not known then, if a combination of less complex and more robust models is able to describe the unit with the same accuracy and less effort. Thus, with the possibility to exchange single equations and systems, it is now possible to create a process as a superstructure of different model combinations and to determine the optimal structure through integer optimization with respect to different objective functions, which mainly depend on the designated use of the model.

The approach is implemented and based on the web modeling platform MOSAIC[*], which is an in-house development. It has all the features, which are needed to realize the new modeling approach. The users can in fact work together online. All the models and measurements are centrally stored in libraries. The modeling with MOSAIC is highly modular and each equation and equation system can be reused, shared and exchanged.

[*] www.mosaic-modeling.de.

Generally, MOSAIC is a system-independent simulation and modeling platform where the user can work online through a Java-web applet. Working groups from different departments, who are working in different locations and different software, can use MOSAIC as a common modeling platform. Based on the Models stored in the MOSAIC database, a complete program code can be created for the preferred modeling and simulation environment as for example in Matlab, GAMS, Aspen Custom Modeler, gPROMS and many more as described by Kuntsche et al. (2011). In a second database, measurements are systematically stored, which can be directly connected to the models. Hence, MOSAIC can help to support the collaboration of the modeler and the experimenter. Moreover, the reuse of all elements in a different context and other projects is possible because of its modular structure.

The modeling process in MOSAIC is very close to the structure of a written mathematical model in a publication, which consists mainly of a variable notation, model equations, and descriptions. In MOSAIC, the first modeling step is to define a new, or select an existing, mathematical notation. In this notation, all used base names, superscripts, subscripts and indices have to be defined and described. The consistency of the model is checked and verified in each step against a notation. For the next step, the model equations are created. This can be done with Latex code or via the Microsoft Word Formula editor. Each equation is stored separately as an equation object and can be used in more than one model. The complete equation systems are created by combining the equations and already existing equation systems. The last step is the evaluation of the created equation system, where the values of the variables and parameters are specified and thus the system can be solved or exported to other simulation environments. A description is compulsory for each step and model element, which guaranties a consistent documentation through the whole project.

All modeling elements, such as the notation, the equations and equation systems, are

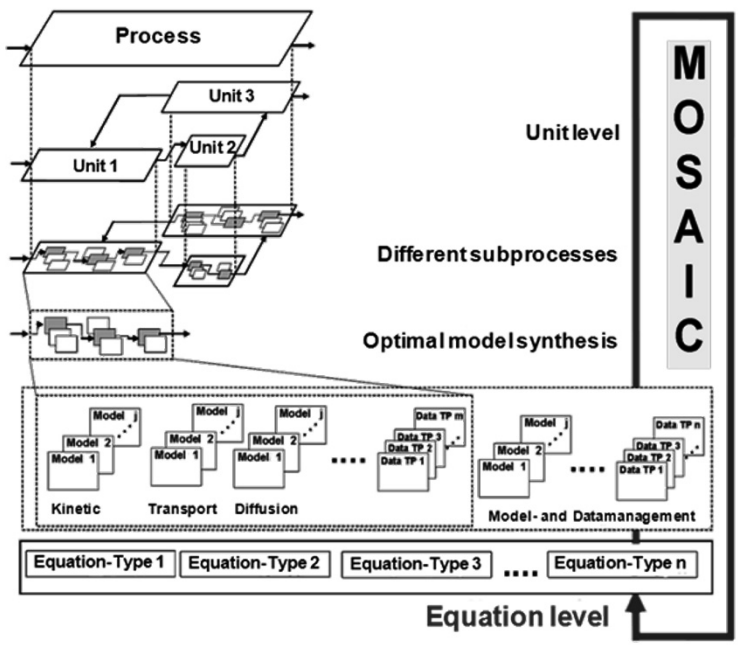

Fig. 1: Hierarchical modeling

stored separately as single objects. Each element can be used in different applications and with a different context. A connection of all elements is always possible, also between different users. This is realized with connectors, which are defined by the user and enable MOSAIC to connect the equation systems between working groups with different notations. The variables in the equations are directly translated and integrated in the corresponding system. In this way, models or even single equations can be easily reused for new purposes. There is no need to enter the same equations more than once. If a model from a publication is already included into the MOSAIC database, it can be directly used together with the knowledge, that it was already tested and the source of errors is minimized.
The connection of modeling and experimental work can be a difficult and error prone task. It can be time consuming for the modeler to follow the changes of the plant setup and to keep his model up to date. The association of measurements to the model variables can be incorrect, or not even possible, if the documentation of the plant was not probably maintained. As a solution, a systematic and central data management module is provided by MOSAIC. It can be directly accessed by the experimenter through an intuitive graphical user interface. It is mandatory to supply a piping and instrumentation diagram for each plant, which has to be updated for every change in the configuration. In this way, a clear identification of the measurement locations in the plant is always guarantied and all changes are well documented and stored. The modeler has the possibility to access all this information directly. It is also possible to connect the model with the measurements by assigning the system variables to measuring points in the plant. Different sets of measurements can be selected by specifying the time scope, which can also have an open end. In this way, values added by the experimenter, are automatically included and added to the model or optimization statement.

2. Workflow for hierarchical modeling in MOSAIC

The workflow and the process of hierarchical modeling are illustrated in Fig. 2 and it consists of two major parts. First, an abstract model of the process is created in MOSAIC, which includes all model candidates and possible combinations. All available partial models are collected, which have been developed by the project participants during a constant process and are stored in the model database. Over the project time, the models are altered and changed. Our policy is to include all versions; otherwise possible informations are lost by simple misjudgment. Based on this collection, the single units and the process are modeled, which is a combination of different models with different degrees of complexity.
The second step is the optimization of the model combination. Program code for state-of-the-art optimization languages such as GAMS, AMPL or Matlab can automatically be created. The superstructure for the MINLP optimization is already stored in the abstract model description. The objective function has to be specified and mainly depends on the designated use. There is mostly a trade-off between the model accuracy and complexity. When the optimization is finished, the optimal model combination is stored in MOSAIC for future use. Finally, the optimal model structure can be exported to the needed simulation environment. In case that new partial models, or measurements are updated, or the objective function changes, the optimization has to be readapted or even repeated. Thus, the hierarchical modeling systematic represents a continuous process.

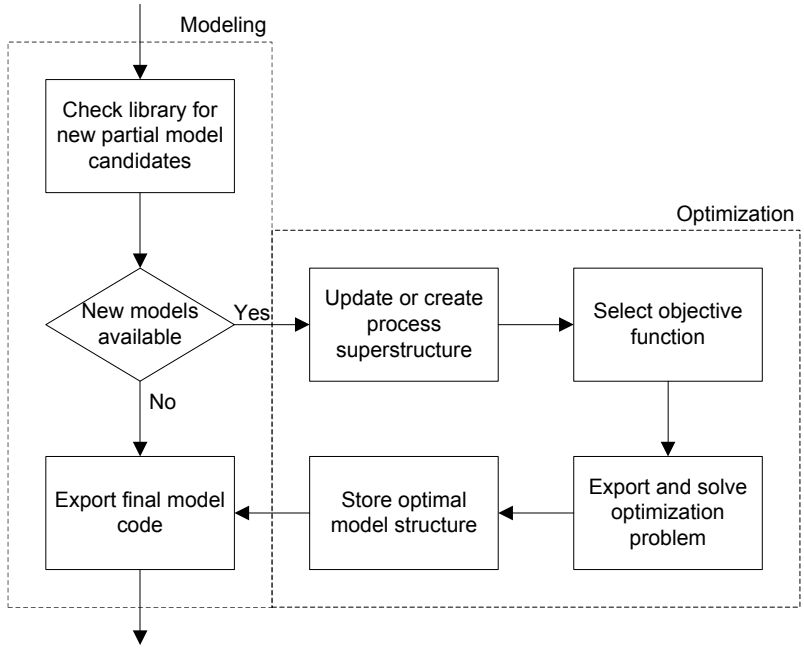

Fig. 2: Hierachical modeling workflow

3. Case studies

The hierarchical modeling systematic is applied to two case studies. In the research project „Integrated Chemical Processes in Liquid Multiphase Systems[*]“, fourteen groups, located at three different universities are working together. The goal is to investigate the hydroformylation of long-chain olefins. Each group is working on different particular aspects of the process. For instance, one of the subprojects concerns the reaction network, where different theories and models are developed with different degrees of complexity. Consequently, the result is a variety of models in different research groups, which have to be selected and properly combined for a complete process model. With MOSAIC, the groups can share their work. Models from the literature and the different user will be combined in a superstructure and based on the algorithm for the hierarchical simulation, the most suitable model combination can finally be determined.

The second case study is the modeling of the pressure drop in packed columns with foaming components. Foam can cause severe problems in distillation and absorption columns and is one of the most frequent malfunctions (Kister, 2003). The main problems are an increased pressure drop and a lower separation efficiency, which leads to a reduced capacity of the separation unit. Up to now, it is not possible to derive a model, which is based on physical parameter of the system like density and viscosity. The hierarchical modeling approach is used to extend existing models for non foaming systems from the literature. In this work, models where used, which have been described in Bravo (1985), Rocha (1993), Billet (1999), Engel (2001), Olujic (2003) and Mackowiak (2010). Therewith, we have a basis of different correlations available

[*] http://www.inprompt.tu-berlin.de.

with different degrees of complexity and accuracy. The next step is the development of different approaches to include the formation of foam and to describe it with a calculated correction factor. A superstructure of the classic literature models for the non foaming area and the new models for the correction factor is created with the aid of MOSAIC. The different model combinations are verified by comparing them to measurements in a packed column for different systems and the optimal model combination is determined by model discrimination. A big advantage is the possibility to determine the parameter for new foaming systems. It is not necessary to run experiments in column, the results of a foam test cell will be then sufficient.

4. Conclusion

A new concept of hierarchical modeling is introduced together with the workflow for a constant improvement of the process model structure. The new methods are implemented in the web simulation environment MOSAIC. Partial models in the database are rated by the user or by MOSAIC on the basis of the model structure, parameter, and degree of nonlinearity. Two case studies show the benefit of the new approach based on a systematic selection and discrimination of models. It is shown how simulations and measurements from different users can be combined and stored over the whole project period. The program keeps track of the development of the partial models and takes all major development steps into consideration. The optimal model combination is then determined depending on the designated use. As a result, an optimized model is available, which can be automatically exported to any equation based simulation environment.

Acknowledgements

This work is part of the Collaborative Research Centre "Integrated Chemical Processes in Liquid Multiphase Systems" coordinated by the Technische Universität Berlin. Financial support by the Deutsche Forschungsgemeinschaft (DFG) is gratefully acknowledged (TRR 63).

References

R. Billet and M. Schultes, 1999, Prediction of mass transfer columns with dumped and arranged packings, Trans IChemE, vol. 77, pp. 498–504.

J. L. Bravo, A. J. Rocha, and J. R. Fair, 1985, Mass transfer in gauze packings, Hydrocarbon Processing, pp. 91–95

G. Buzzi-Ferraris and F. Manenti, 2009, Kinetic models analysis, Chemical Engineering Science, vol. 64, pp. 1061-1074

V. Engel, J. Stichlmair, and W. Geipel, 2001, Fluid Dynamics of Packings for Gas-Liquid Contactors, Chemical Engineering & Technology, vol. 24, pp. 459–462

H. Z. Kister, 2003, What Caused Tower Malfunctions in the Last 50 Years?, Chemical Engineering Research and Design, vol. 81 (1), pp. 5-26

S. Kuntsche, T. Barz, R. Kraus, H. Arellano-Garcia and G. Wozny, 2011, MOSAIC a web-based modeling environment for code generation, Computers & Chemical Engineering, vol. 35, pp. 2257-2273

J. Mackowiak, 2010, Fluid Dynamics of Packed Columns, Springer

Z. Olujic, A. F. Seibert, B. Kaibel, H. Jansen, T. Rietfort, and E. Zich, 2003, Performance characteristics of a new high capacity structured packing, Chemical Engineering and Processing, vol. 42, pp. 55–60

A. J. Rocha, J. L. Bravo, and J. R. Fair, 1993, Distillation columns containing structured packings: a comprehensive model for their performance. 1. Hydraulic models, Industrial & Engineering Chemistry Research, vol. 32, pp. 641–651

I.A. Karimi and Rajagopalan Srinivasan (Editors), Proceedings of the 11th International Symposium on Process Systems Engineering, 15-19 July 2012, Singapore.

Modeling and Simulation of a Catalytic Distillation Process for Production of Ethylene Glycol Monobutyl Ether

W. Z. An [a,*] ,X. Meng[a], D. W. Bi[b] and J. M. Zhu[b]

([a] Department of Chemical Engineering, Ocean University of China, Qingdao 266100; Shandong;China;
[b] Liaoning Oxiranchem Group; Liaoyang 111003; Liaoning; China)

Abstract

The production of ethylene glycol monobutyl ether (EGMBE) from ethylene oxide (EO) and n-butanol was studied in a catalytic distillation (CD) column using a base catalyst immobilized in a structured packing. A pilot plant CD packed column been built up for experimental investigations and a steady-state mathematical model was developed to investigate the basic laws of the CD column. The results revealed that the CD process offers potential advantages for EGMBE production, and a 99% conversion of EO and 91% selectivity of EGMBE could be achieved simultaneously that was otherwise not possible with the traditional reactors.
Keywords: Catalytic distillation; Ethylene Glycol Monobutyl Ether; Ethylene oxide;

1. Introduction

Ethylene glycol monobutyl ether (EGMBE) is an environmentally friendly EO-based solvent and widely used in industries. Traditionally, the route (process) for producing EGMBE consists of two separate unit operations, i.e., synthesis reaction and distillation separations are carried out separately and sequentially(Sulzer technical review, 2001). The disadvantages existed for these traditional processes are obvious, such as a low selectivity of desired product, the high energy consumption, as well as the severe corrosion problem due to the use with homogeneous catalysts. In order to overcome these disadvantages, a catalytic distillation (CD) process, which has been proven to be a very high efficiency process(Malone & Doherty, 2000) was developed at Liaonin Oxiranchem Group in China. In this research a steady-state equilibrium model was developed to investigate the basic laws of the CD process and to obtain the suitable operating parameters. Simulations results for the CD process were discussed and compared with experimental data as well.

2. Process characteristic

2.1. Chemical systems and reaction kinetics

EGMBE is produced commercially by reacting EO with n-butanol($C_4H_{10}O$), i.e., ethoxylation of n-butanol, in the presence of a base or acid catalyst. Based on ethoxylation reaction mechanism (An et al., 2008), the reaction can conveniently be expressed as the following irreversible, consecutive and competing reactions:
Main reaction:

* Corresponding author: awzhong@ouc.edu.cn
Supported by the National Natural Science Foundation of China (20976172).

$C_2H_4O + C_4H_{10}O \rightarrow C_6H_{14}O_2$ (EGMBE) (1)

Undesired side reaction:

$C_2H_4O + C_6H_{14}O_2 \rightarrow C_8H_{18}O_3$ (DEGMBE) (2)

It is noted that the chemical systems exists a large volatility difference between reactants and products. The normal boiling points of the four components is ranged as follows: ethylene oxide 283.6 K; n-butanol 390.81 K; EGMBE 444.47 K; DEGMBE 504.15 K. The difference ensures a rapid separation of EGMBE from reaction zone, which prevents further reaction to yield DEGME, and therefore the selectivity of EGMBE should be improved. The reaction heats of the two reactions are -104.2 and -100.4 kJ· (mol EO)$^{-1}$, respectively, which are considered highly exothermic. The reaction heat of system can also be utilized directly for distillation, thus a natural heat integration can be achieved. Consequently, CD technique is suitable for the studied system.

The rate equations of the two reactions obtained previously in our laboratory by using a sold alkali catalyst can be described by the first order power law with respect to EO and n-butanol as follows(An et al., 2008):

$$r_1 = k_1 C_{cat} C_{EO} C_{C_4H_{10}O} \tag{4}$$

$$r_2 = k_2 C_{cat} C_{EO} C_{C_6H_{12}O_2} \tag{5}$$

The kinetic study has revealed that the two reactions have the approximately same rate constant based on the mechanism of ethoxylation(Serio et al., 2005, An et al., 2008)which are given by the following Arrhenius forms.

$$k_1 = k_2 = 7.2318 \times 10^6 \exp(-63016 / RT) \tag{6}$$

2.2. Phase equilibrium data

Since the presented CD column is operated at low-to-moderate pressures (<0.3Mpa), the vapor phase can be reasonably considered as ideal, thus the vapor-liquid equilibrium constant could be calculated with the liquid phase activity coefficient and the vapor pressure of the pure components. In this work, the Antoine equation is used for the calculation of the saturation vapor pressures of the pure components and the UNIFAC method is employed for description liquid phase non-ideality of the system. The data of the binary interaction parameters for UNIFAC for the pure component are summarized in Table 1.

2.3. Catalytic distillation column configuration

Figure 1 shows a sketch of the CD pilot column bulit in our laboratory. The CD column (100 mm in diameter, 6 m of the overall height, 20 kg/h of bottom product flowrate) was equipped with a total condenser and partial reboiler and consisted of two parts: a reaction section and a stripping section. The stripping section of the column was filled with non-catalytic structured packing, while in the reaction section a base catalyst was immobilized in a structured packing. The geometrical data and HETP of the two types of packings were determined experimentally and given in Figure 1. The mass of dry catalyst per meter of catalytic packing has been determined experimentally to $m_{cat,dry}$ =0.205 kg $_{cat,\ dry}$/$m_{packing}$, whereas the activity of the catalyst has been measured to c_{cat}=0.78 eq/$kg_{cat,dry}$. Due to the nature of EO (a toxic and explosive gas and should not be released into the environment), sampling along the current set-up CD column was

forbidden, and therefore only temperature was measured using thermometers mounted at six different place of column from top to bottom as shown in Figure 1.

Table 1 Parameters for UNIFAC model

Groups		CH_3	CH_2	CH_2O	OH
v_k^i	n-butanol	1	3	0	1
	EO	0	1	1	0
	EGMBE	1	4	1	1
	DEGMBE	1	5	2	1
R_k		0.901	0.674	0.9183	1.000
Q_k		0.848	0.540	0.780	1.200
a_{jk}	CH_3	0	0	251.5	986.5
	CH_2	0	0	251.5	986.5
	CH_2O	83.36	83.36	0	237.7
	OH	156.4	156.4	28.06	0

In the operation of the CD column, n-butanol is supplied to the top of the column, while EO feed is partitioned to two streams which are supplied to the middle and bottom of reaction zone respectively. The motivation for adopting the feed mode is to reduce the concentration of EO in reaction zone since a low concentration of EO is benefit to prevent the generation of more byproducts.

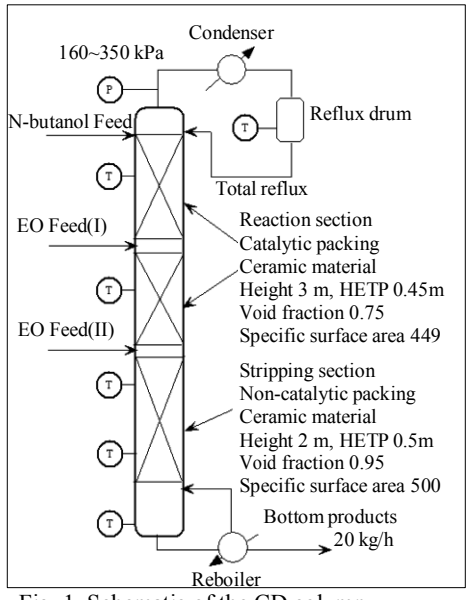

Fig. 1 Schematic of the CD column

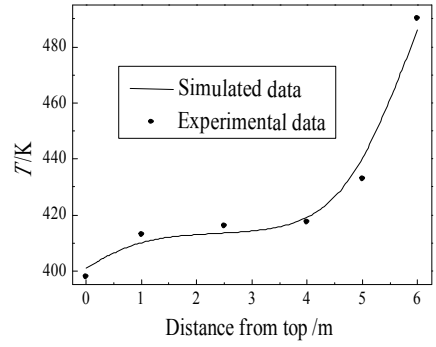

Fig. 2 Temperature profiles along the column

3. Modeling of CD column

In the open literatures there are two types of models for reactive/catalytic distillation, the equilibrium model and non-equilibrium (rate-based) model (Malone &Doherty,

2000; Taylor & Krishna,2000). Although some authors concluded a non-equilibrium model describes better the performance of a reactive distillation process(Peng et al., 2002), it requires accurate estimations of mass transfer coefficients, binary diffusion coefficients, surface tensions values, etc., and as these estimations are a big challenge. Based on these, an equilibrium model, which has been extensively applied for modeling various reactive/catalytic columns (Malone &Doherty, 2000), is adopted in this study to investigate the basic law of a new CD process Future works will attempt to incorporate more complex modeling method in this framework.

The modeling approaches to various CD column have been reported elsewhere (for a review, see Malone &Doherty, 2000), which were developed based on mass and heat balances, vapour-liquid equilibrium and the chemical kinetics on every stage of the reactive distillation column. In the present study Newton's method is used for solving the model equations and a computation program has been formulated using C++ programming language.

4. Results and discussions

4.1. Suitable operating conditions

Based on the model approach described above, detailed simulations are carried out to investigate the influence of selected operating parameters (pressure, boilup ratio, and feed ratio) on the process performance (conversion and selectivity). From both the simulation studies and our current pilot experiments of CD column, the suggested operational parameters of the CD process are summarized in Table 2. From the simulation results it was found that, although the reactants are fed to the column in a nearly stoichiometric ration, it is due to the distillation effect so that unconverted n-butanol is always recycled into the reaction section and EGMBE product is separated for the reaction section simultaneously, thus resulting in the reactive section n-boutanol is in tremendous stoichiometric excess (n-boutanol /EO>300). It is concluded that CD technology not only obtains a high EO conversion but also a high EGMBE selectivity. This seems to contradict with the commonly accepted premise in reaction engineering based on the batch and flow reactors that a higher conversion is always accompanied by a lower selectivity to its intermediate product. However, a higher conversion with a higher selectivity is possible for CD process because of its function of an internally recycled flow reactor (Malone &Doherty, 2000).

Table 2 The suggested operating parameters

Parameters	*Value*	*Parameters*	*Value*
Column pressure, kPa	*200*	*Conversion of EO, %*	*>99.0*
Molar feed ratio of EO to n-butanol	*1.05*	*Selectivity to EGMBE, %*	*91.73*
Bottom rate, kmol/h	*0.178*	*Yield of EGMBE, %*	*91.73*
Boil-up ratio	*10*	*Condenser duty, kW*	*36924*
Mole fraction of EGMBE in bottom	*0.917*	*Reboiler duty, kW*	*27320*

4.2. Model validation

In order to investigate the reliability of simulation, the calculated bottom concentration and temperature profiles along the column are compared with experimental results. Under the given operating conditions as shown in Table 2, the temperature profiles of the six temperature measuring points configured in the CD

column were measured as shown in Figure 2. It can be seen that the agreement between simulated data and experimental data is very good, since the temperature profiles correlate well with an average relative error of 1.22%. Table 3 gives the comparisons of calculated product composition in the bottom stream with experimental results analyzed using gas chromatograph. The agreement between simulation and experiment for both processes is satisfactory. The results presented here demonstrate clearly that the model developed in this paper could predict the steady-stage behavior of this CD process well.

Table 3 The comparison of simulated data and experimental data

Items	*Simulation values*	*Experimental data*
Molar fraction of n-butanol in bottom stream	*0.0413*	*0.0440*
Molar fraction of EO in bottom stream	*1.6843e-10*	*0*
Molar fraction of EGBME in bottom stream	*0.9173*	*0.9118*
Molar fraction of DEGMBE in bottom stream	*0.0410*	*0.0442*
Selectivity of EGMBE, %	*91.73*	*91.18*

5. Conclusion

The production of ethylene glycol monobutyl ether (EGMBE) from ethylene oxide (EO) and n-butanol was studied in a catalytic distillation (CD) column. From both the simulation studies and our current pilot experiments showed that the use of a catalytic distillation offered potential advantages compared with conventional processes. The CD column allowed the use a moderate operation pressure and a lower molar feed ratio of n-butanlo to EO. The reaction heat released can be completely utilized in distillation. The key component EO can be converted completely and a selectivity of 91% toward the desired product EGMBE can be achieved, which is otherwise not possible with conventional processes. The industrial significance of this study lies in the fact that the understanding of the process has been made clearer. The provided results have served as useful guidelines for improving the plant design and operation without need of expensive test runs.

References

J. Peng, S.Lextrait, T.F.Edgar,&R.B. Eldridge, 2002, A comparison of steady-state equilibrium and rate-based models for packed reactive distillation columns. Ind. Eng. Chem. Res., 41: 735-2744

M. D. Serio,R.Tesser, A. Dimiccoli, &E. Santacesaria,2005,Comparison of different reactor types used in the manufacture of ethoxylated, propoxylated products. Ind. Eng. Chem. Res., 44(25): 9482-9489.

M.F. Malone & M.F.Doherty, 2000, Reactive distillation. Ind. Eng. Chem. Res.,39, 3953-3957

R.Taylor, &R. Krishna, 2000, Modelling reactive distillation. Chem.Eng.Sci., 55: 5183-5229.

Sulzer technical review, 2001, A New Technical Solution for Glycol Ether Production. 4: 14-17

W.Z. An, F. L. Dong, Z. B. Liu, & J.M. Zhu, 2008, Kinetics of n-butanol ethoxylation. Journal of Chemical Engineering of Chinese Universities, 22, 4, 612-617

.

I.A. Karimi and Rajagopalan Srinivasan (Editors), Proceedings of the 11th International Symposium on Process Systems Engineering, 15-19 July 2012, Singapore.

Use of reactive distillation for triacetin production from crude glycerol: Simulation and performance analysis

Pimpatthar Siricharnsakunchai, Lida Simasatitkul, Apinan Soottitantawat, Amornchai Arpornwichanop*

Department of Chemical Engineering, Faculty of Engineering, Chulalongkorn University, Bangkok,10330, Thailand
* *Corresponding author (e-mail: Amornchai.a@chula.ac.th)*

Abstract

This study is focused on the use of crude glycerol from biodiesel production to produce triacetin via esterification reaction with acetic acid by using a reactive distillation. In general, a composition of crude glycerol consisting mostly glycerol and methanol varies with biodiesel feedstock and processes. Simulation studies are performed to investigate the effect of using crude glycerol with different fractions of methanol on triacetin production. Three process configurations are considered: (i) direct feed of crude glycerol to reactive distillation, (ii) separation of crude glycerol coupled with reactive distillation and (iii) reactive separation of crude glycerol coupled with reactive distillation.

Keywords: Triacetin production, Crude glycerol, Reactive distillation, Esterification.

1. Introduction

In a conventional process of biodiesel production, glycerol is generated as by-product. Increases in the demand and production of biodiesel enlarge an amount of glycerol produced. Efficient utilization of crude glycerol could lead to significant economic and environmental benefits.

In general, crude glycerol contains mostly glycerol (60-70 wt.%) and other contaminants such as methanol and soap (Thompson and He, 2006), so that the cost of crude glycerol is low. The composition of crude glycerol varies with raw materials and catalyst used for biodiesel production and post-reaction cleanup processes such as acidulation and demethylization (Bohon et al., 2010). To purify crude glycerol for food, pharmaceutical or cosmetics industries, further processing steps such as filtration, chemical additions, fractional vacuum distillation, bleaching and deodorization are required. These purification processes are costly and economically infeasible for small and medium-scale biodiesel producers. To date, a number of studies have been being explored to find useful applications for glycerol via combustion, anaerobic digestion, thermo-chemical process and biological conversion. In addition, glycerol can be used as a raw material to produce high value-added products such as hydrogen, propylene glycol, acetol and 1,3-propanediol.

This study investigates the use of glycerol to produce triacetin, an important chemical used as a plasticizer and a solvent (Wolfson et al., 2009), via esterification with acetic acid. Since the esterification reaction is limited by chemical equilibrium, a reactive distillation is implemented to improve the conversion of glycerol. Crude glycerol with different ratios of methanol is considered and three different process configurations for

Table 1. Kinetic constants for esterification of glycerol and acetic acid

Reaction	$k_{0,i}$ (L mol^{-1}s^{-1})	Ea$_i$ (cal kmol^{-1})	$k_{0,-i}$ (L mol^{-1}s^{-1})	Ea_{-i} (cal kmol^{-1})
1	5.24×10^{-4}	616.8	8.56×10^{-4}	-3864.4
2	9.69×10^{-5}	-1462.3	2.16×10	8701.1
3	6.26×10^{-2}	4964.1	1.86	5137.5

triacetin production are studied.

2. Process Description

In general, triacetin can be produced by the liquid-phase esterification of glycerol and acetic acid in a conventional process consisting of a continuous stirred tank reactor followed by a series of distillation columns. This causes a low conversion of glycerol and high energy consumption. A reactive distillation is potentially an attractive process as reaction and separation tasks can be carried out in a single unit. To analyze the triacetin production process, simulations of a reactive distillation are performed using the RADFRAC module of Aspen Plus. The UNIFAC method is employed to predict thermodynamic properties of substances in the system. The kinetics of esterification of glycerol and acetic acid in the liquid phase proposed by Maria-Isabel et al. (2009) are used as follows:

Glycerol + Acetic Acid ↔ Monoacetin + Water

$$r_1 = k_1 C_{\text{glycerol}} C_{\text{acetic acid}} - k_{-1} C_{\text{mono acetin}} C_{\text{H2O}} \quad (1)$$

Monoacetine + Acetic Acid ↔ Diacetin + Water

$$r_2 = k_2 C_{\text{monoacetine}} C_{\text{acetic acid}} - k_{-2} C_{\text{diacetin}} C_{\text{H2O}} \quad (2)$$

Diacetin + Acetic Acid ↔ Triacetin + Water

$$r_3 = k_3 C_{\text{diacetin}} C_{\text{acetic acid}} - k_{-3} C_{\text{triacetin}} C_{\text{H2O}} \quad (3)$$

Table 1 shows the kinetic constants of the esterification reaction for triacetin production.

2.1. System I: Direct feed of crude glycerol to reactive distillation

In general, a composition of crude glycerol obtained depends on biodiesel feedstock and production process. However, crude glycerol consists of mainly glycerol and methanol. Fig. 1 shows the schematic of a reactive distillation for triacetin production. Acetic acid and crude glycerol at the ratio of 6 are fed to the stage 3 and 2 of the reactive distillation column having a total stage of 17. The column is operated at atmospheric pressure and reflux ratio of 2 and the bottom product is removed at flow rate of 5 kmol/h. The temperature of feed streams is 298 K. Flow rate of crude glycerol is 5 kmol/h

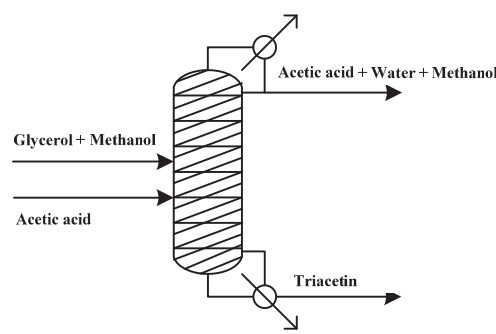

Fig. 1. Direct feed of crude glycerol to reactive distillation.

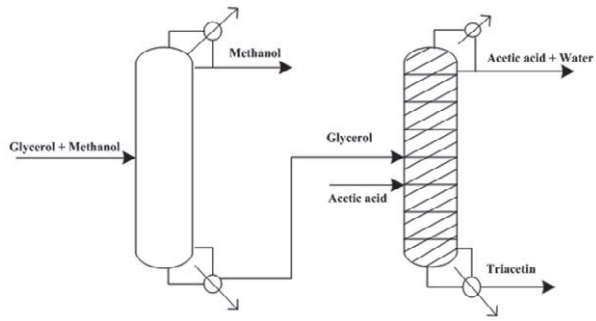

Fig. 2. Separation of crude glycerol coupled with reactive distillation.

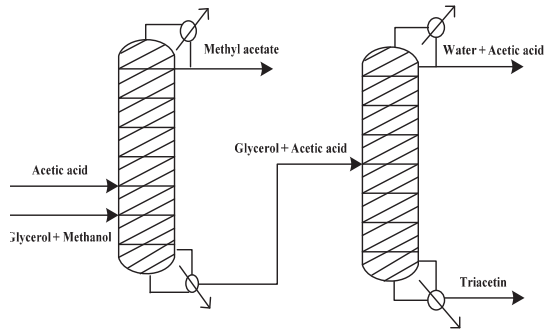

Fig. 3. Reactive separation of crude glycerol coupled with reactive distillation.

2.2. System II: Separation of crude glycerol coupled with reactive distillation

In this process configuration, crude glycerol is first purified to remove methanol using a conventional distillation and pure glycerol is then fed to a reactive distillation to produce triacetin. Crude glycerol is fed to the distillation column at stage 2 (Table 2). The distillation column is operated at reflux ratio of 0.1 and the bottom flow rate is fixed at 5 kmol/h. Pure glycerol obtained and acetic acid are introduced to the reactive distillation at stage 2 and 3, respectively. Reflux ratio of the reactive distillation is 2.3 and the bottom product rate is 5 kmol/h. The acetic acid to glycerol ratio is fixed at 6.

2.3. System III: Reactive separation of crude glycerol coupled with reactive distillation

Two reactive distillations are applied for triacetin production. The first reactive distillation column is used to separate methanol from crude glycerol by reacting with acetic acid via esterification to produce methyl acetate (Song et al., 1998). It consists of a total stage of 38 and is operated at reflux ratio of 2.8 (Table 3). With this process design, crude glycerol can be purified and a valuable product (methyl acetate) is obtained at the same time. The second reactive distillation is employed to convert glycerol to triacetin as mentioned above.

3. Simulation Results

3.1. Direct feed of crude glycerol to reactive distillation

The results show that the fraction of methanol in crude glycerol has a slight effect on the conversion of glycerol. When crude glycerol with 30 wt.% of methanol is used for triacetin production, the triacetin yield of 99.85% is obtained. However, the purity of triacetin obtained reduces when methanol content in crude glycerol increases. Further,

Table 2. Feed conditions and specifications in case of separation of crude glycerol coupled with reactive distillation (System II)

Feed Conditions		Column specifications			
		Distillation column		Reactive distillation column	
Temperature (K)	298	Total stages	10	Total stages	17
Pressure (bar)	1	Pressure (bar)	1	Pressure (bar)	1
Flow rate (kmol/h)		Reflux ratio	0.1	Reflux ratio	2.3
1) acetic acid	30	Bottom rate (kmol/h)	5	Bottom rate (kmol/h)	5
2) glycerol	5	Feed location		Feed location	
Mole fraction		1) glycerol + methanol	2	1) glycerol	2
1) glycerol + methanol	1			2) acetic acid	3

Table 3. Feed conditions and specifications in case of reactive separation of crude glycerol coupled with reactive distillation (System III)

Feed Conditions		Column specifications			
		First reactive distillation		Second reactive distillation	
Temperature (K)	323	Total stages	38	Total stages	17
Pressure (bar)	1	Pressure (bar)	1	Pressure (bar)	1
Flow rate (kmol/h)		Reflux ratio	2.8	Reflux ratio	2
1) acetic acid	280	Bottom rate (kmol/h)	510	Bottom rate (kmol/h)	250
2) glycerol + methanol	280	Feed location		Feed location	
		1) acetic acid	3	1) acetic acid	3
Mole fraction		2) glycerol + methanol	36	2) glycerol + acetic acid	2
1) acetic acid	1				
2) glycerol + methanol	1				

the total energy consumptions of condenser and reboiler decrease with increasing the content of methanol.

3.2. Separation of crude glycerol coupled with reactive distillation

It is found that adding a purification unit to crude glycerol can improve the triacetin production; high conversion of glycerol is achieved even crude glycerol is used. However, the yield of triacetin is reduced to 92.5% in case of using crude glycerol with 30 wt.% of methanol. Increased fraction of methanol in glycerol decreases the molar fraction of triacetin at the bottom stream of the reactive distillation and water at the distillate stream; however, the fraction of acetic acid increases. When crude glycerol with 30 wt.% of methanol is used, the purity of triacetin product is 84%, higher than that the crude glycerol is directly employed for triacetin production. Considering the energy consumption of the system, it is found that the condenser and reboiler duties decrease with increasing the percentage of methanol in crude glycerol. The requirement of energy for this process configuration is more than that for the system I as one more conventional distillation is needed for purifying crude glycerol.

3.3. Reactive separation of crude glycerol coupled with reactive distillation

Considering the first reactive distillation for methyl acetate production, the molar fraction of methyl acetate in the distillate stream increases with the increased amount of methanol in crude glycerol. At 30 wt.% of methanol in crude glycerol, the molar fraction of methyl acetate obtained is 95%. High pure glycerol with slight acetic acid is fed to the second reactive distillation for triacetin production. The molar fraction of triacetin reduces when increasing the percentage of methanol in crude glycerol. The

conversion of glycerol decreases slightly and the yield of triacetin reduces to 99.85% when methanol in crude glycerol is 30 wt.%. It is also found that this process design consumes the highest energy, compared with other ones due to the reactive separation process of crude glycerol to generate methyl acetate causes high energy requirement.

4. Conclusions

This study investigates the potential of using crude glycerol derived from biodiesel production to produce triacetin via an esterification process. Reactive distillation is used to improve the performance of triacetin production. Three process designs: (i) direct feed of crude glycerol to reactive distillation, (ii) separation of crude glycerol coupled with reactive distillation and (iii) reactive separation of crude glycerol coupled with reactive distillation, are proposed. An increase of methanol content in crude glycerol decreases the purity of triacetin product. The conversion of glycerol and yield of triacetin obtained by using crude glycerol are slightly lower than those using pure glycerol. Removal of methanol from crude glycerol before being fed to the reactive distillation causes the highest purity of triacetin when crude glycerol with high methanol content is used. The two productions of methy acetate via a reactive separation of crude glycerol and triacetin via a reactive distillation require the highest energy consumption compared with other process designs.

5. Acknowledgement

Support from the 90th Anniversary of Chulalongkorn University Fund (Ratchadaphiseksomphot Endowment Fund) and the Computational Process Engineering Research Group, the Special Task Force for Activating Research (STAR), Chulalongkorn University Centenary Academic Development Project is gratefully acknowledged.

References

M.D. Bohon, B.A. Metzger, W.P. Linak, C.J. King, W.L. Roberts, 2010, Glycerol combustion and emissions, Proceedings of the Combustion Institute.

G. Maria-Isabel, B. Jordi, S. Romain, R. Jean-Michel, E.P. Alexandra, 2009, From residual to useful oil: Revalorization of glycerine from the biodiesel synthesis, Bioresource Technology 100, 3775-3778.

J.C. Thompson, B. He, 2006, Characterization of crude glycerol from biodiesel production from multiple feedstocks, Applied Engineering in Agriculture 22, 261-265.

W. Song, G. Venimadhavan, J.M. Manning, M.F. Malone, M.F. Doherty, 1998, Measurement of residue curve maps and heterogeneous kinetics in methyl acetate synthesis, Industrial Engineering and Chemical Research 37, 1917-1928.

A. Wolfson, A. Atyya, C. Dlugy, D. Tavor, 2009, Glycerol triacetate as solvent and acyl donor in the production of isoamyl acetate with Candida antarctica lipase, Bioprocess and biosystems engineering 33, 363–366.

I.A. Karimi and Rajagopalan Srinivasan (Editors), Proceedings of the 11th International Symposium on Process Systems Engineering, 15-19 July 2012, Singapore.

Dynamic modeling of direct contact membrane distillation processes

Badr Bin Ashoor[a,b], Hassan Fath[b], Wolfgang Marquardt[a] , Adel Mhamdi[a]

[a]*Lehrstuhl für Prozesstechnik, RWTH Aachen, D-52056 Aachen, Germany*
[b]*Masdar Institute, P.O.Box 54224 Abu Dhabi, United Arab Emirates*

Abstract

Membrane distillation (MD) for desalination is an emerging thermally driven process exhibiting various advantages in comparison with traditional processes. Most of the MD configuration processes have been modeled as steady-state one-dimensional systems using empirical heat and mass transfer equations. Stationary two-dimensional MD models have been considered only in very few studies. In this work, a dynamic model of a direct contact membrane distillation (DCMD) process in plate-and-frame configuration is developed. It aims at giving insight into the underlying coupled physico-chemical phenomena at a level of detail. The model is implemented in the modeling package gPROMS. Numerical simulations are conducted for different operational parameters at the module inlets such as the feed and permeate temperature or feed and permeate flow rate. The results are compared with experimental data published in the literature.

Keywords: direct contact membrane distillation. plate-and-frame configuration. dynamic two-dimensional model. heat and mass transfer. numerical simulation

1. Introduction

Membrane distillation (MD) is a non-isothermal process known for less than fifty years. The first paper was published in 1967 by Findly [1]. MD was considered first as a process that would operate with minimum external energy requirements. The large vapor space required by a conventional distillation column is replaced in MD by the pore volume of a microporous membrane. As a result, the MD process equipment can be much smaller. Membrane distillation may be operated in several configurations [2,3]. In this work, we focus on direct contact MD (DCMD), although the approach may be easily extended to other configurations. Today, we see an enormous number of publications dealing with experimental and modeling issues of MD [4].

In MD, both mass and heat transfer occur simultaneously and both temperature and concentration polarization effects should be taken into consideration. Most modeling works in literature on DCMD processes usually focus on the mass transfer resistance of vapor across a membrane attributed to the membrane characteristics (i.e. pore size, porosity and tortuosity) and heat transfer resistances to obtain the mean temperature on the membrane surface [5]. The concentration polarization phenomena are usually ignored to simplify the calculation procedure. Only few publications use stationary one- or two-dimensional heat-transfer equation to simulate a particular application more accurately. Although many semi-empirical models have been developed, a detailed model for temperature polarization on flat-plate MD processes is still lacking. In this study, we develop a dynamic two-dimensional flat-plate mathematical model for DCMD processes, in order to obtain the temperature and concentration distributions in

the channels and the local mass flux at the membrane surfaces. The availability of such a model for simultaneous energy and mass balances will be an important basis for the analysis, design and optimization of DCMD processes for saline water desalination.

2. Dynamic modeling of a plate-and-frame direct contact MD module

The DCMD to be considered in this study is a flat-sheet membrane module (Figure 1). The module has two adiabatic impermeable walls with the flat-sheet membrane in between. The membrane has two hydrophobic walls permeable for water vapor but impermeable for liquid water.

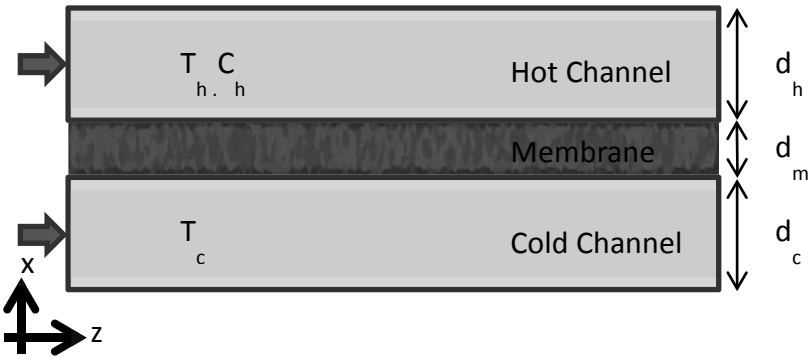

Figure 1. Schematic diagram of a DCMD module in rectangular coordinates.

The work focuses on modeling the heat and mass transport in two spatial dimensions through the three parts of the DCMD module, i.e. membrane, feed and permeate channels. . The model is implemented in the modeling package gPROMS. This allows implementing the model equations in a modular and hierarchical way, such that it is very easy to adapt the model to different plant configurations or operating conditions. Moreover, the model can be used without much effort for parameter estimation, design or optimization studies. In the following subsections, we describe the main equations and assumptions used in the model.

2.1. Vapor transport through the membrane pores

The mass transfer driving force across the membrane is the difference in saturated pressure on both membrane surfaces due to the temperature gradient. Depending on a comparison between the mean free path and pore diameter, there are some models that can be used to describe the mass flux across the hydrophobic porous membrane [6]: the Knudsen diffusion model (due to the larger mean free path of vapor molecules than the membrane pore size), Poiseuille flow model (due to the momentum transfer to the supported membrane) and molecular diffusion model (due to the concentration gradient across the membrane). If the mean free path is: much larger than the pore size, molecule-wall collisions become more important and the gas transport is described using the Knudsen diffusion model. If it is much smaller than the pore size, the molecule motion due to the pressure gradient (i.e. saturated pressure difference across the membrane) becomes the major transport phenomenon and is described using the Poiseuille flow model.

The vapour flux density j across the hydrophobic membrane, can be computed from

$$j = C_m \Delta P^{sat} = C_m (\gamma(X) P_h^{sat} - P_c^{sat}), \quad (1)$$

where P_h^{sat} and P_c^{sat} are the saturated pressure of pure water on the hot and cold channel, respectively. They can be determined from corresponding saturation temperatures using the Antoine equation. The coefficient $\gamma(X)$ accounts for influence of the salt (mole fraction X) in the feed on the saturation pressure. P_h^{sat} and P_c^{sat}.
The membrane coefficient C_m in (1) can be estimated by a weighted sum (via parameters θ_k and θ_p) of the Knudsen diffusion and the Poiseuille (viscous) flow models [6], i.e.

$$C_m = 1.06\,\theta_k \frac{\varepsilon\tau}{\tau\delta_m}\left(\frac{M_w}{RT_m}\right)^{1/2} + 0.125\,\theta_p\,\frac{\varepsilon r^2}{\tau\delta_m}\,\frac{M_w P_m}{\eta_v RT_m} \tag{2}$$

The parameters ε , τ and δ_m are the porosity, tortuosity and thickness of the membrane, respectively. M_w is the molecular weight of water, R is the gas constant. T_m is the mean temperature in the membrane ($i.e.$ $(T_h + T_c)/2$). It is related to the mean saturated pressure P_m by the Antoine equation for water, i.e. log10 $(P_m) = A - B/(T_m + C)$.
The heat flux density at the membrane interface between the liquid and the vapor is

$$q_i = j\,\Delta H + k_m\,\frac{T_h - T_c}{\delta_m}, \tag{3}$$

where ΔH is the latent heat of vaporization and k_m the thermal conductivity of the porous membrane. It can be calculated from

$$k_m = \varepsilon\,k_g(T) + (1 - \varepsilon)\,k_s\,, \tag{4}$$

where k_s is the solid membrane thermal conductivity and $k_g(T)$ the temperature-dependent gas pore thermal conductivity.

2.2. Heat and mass transport in the feed and cold channels

Under appropriate assumptions, the general balance equations for mass and energy reduce to the following equations for the distributions of temperature T and salt concentration C_s in each of the hot and cold channels:

$$\rho C_p \frac{\partial T(x,z)}{\partial t} + \rho C_p u(x)\frac{\partial T(x,z)}{\partial z} = k\left(\frac{\partial^2 T(x,z)}{\partial x^2} + \frac{\partial^2 T(x,z)}{\partial z^2}\right), \tag{5}$$

$$\rho \frac{\partial C_s(x,z)}{\partial t} + \rho u(x)\frac{\partial C_s(x,z)}{\partial z} = D\left(\frac{\partial^2 C_s(x,z)}{\partial x^2} + \frac{\partial^2 C_s(x,z)}{\partial z^2}\right). \tag{6}$$

Here ρ, k, C_p, and D are density, thermal conductivity, heat capacity of the fluid and diffusion coefficient, respectively. We assume, for simplicity, a constant or parabolic velocity profile $u(x)$ in the channels. In the permeate channel there is only pure water, such that the mass balance equation (6) is not needed in the model.

2.3. The boundary and initial conditions

At the inlet of the channels, we assume given values for temperature and concentration, T_{in} and $C_{s,in}$ i.e. $T(x,0) = T_{in}$ and $C_s(x,0) = C_{s,in}$. The channel walls are assumed impermeable and adiabatic, so that the corresponding mass and heat fluxes are zero. At the outlet, we use usual outlet conditions.
The boundary conditions in equation

$$k(T)\frac{\partial T(d,z)}{\partial x} = q_i(z)\,,\; D\,\frac{\partial C_s(d,z)}{\partial x} = j(z) \tag{8}$$

link the models for the channels and the membrane. They are obtained via mass and energy balances for the interfaces between liquid and vapor on both sides of the

membrane. d is the channel height, j and q_i are the mass and heat fluxes at the interface given in Eqs. (1) and (3), respectively.

3. Case study

A case study from literature has been investigated. All the data used in our simulations like geometry, physical properties and operating conditions can be found in [5]. Numerical simulations have been conducted for different operational parameters at the module inlets such as the feed and permeate temperature or feed and permeate flow rate. Compared with the stationary experimental data in [5], the computed mass flux densities are in good agreement with the measurements. By varying some of the parameters, we may assess their effects on the trans-membrane flux. For instance, by varying the feed temperature, we observe, as shown in Figure 2, a monotone increase of the MD flux with the increase of the difference between the feed water temperature and the permeate side temperature (ΔT) . This is due to the increase of the vapor pressure of the feed (the driving force) which increase the trans-membrane flux, although the temperature polarization will increase with the increase of the feed temperature. The trans-membrane flux also increases with the flow rate as also shown in Figure 2. The effect of an increasing flow rate is to increase the convective heat transfer coefficient at the feed side of the membrane, to reduce the velocity and temperature boundary layers and to reduce the temperature and concentration polarization effects, thus increasing the trans-membrane flux.

The temperature polarization phenomena dominate the production of water flux in DCMD process. It increases along the flow direction at the feed side which leads to the reduction of the trans-membrane flux. The temperature polarization ratio, which is defined as the ratio of the membrane surface temperature and the bulk feed temperature, increases along the flowing direction at the hot feed side and reduces the temperature difference between the hot and the cold side resulting in reduction of the water flux.

In Figure 3, we plot the temperature distribution at the interface between the hot channel and the membrane along the flow direction at different times. The inlet temperature to the hot channel is 45°C. We observe that after some time, a stationary profile is reached.

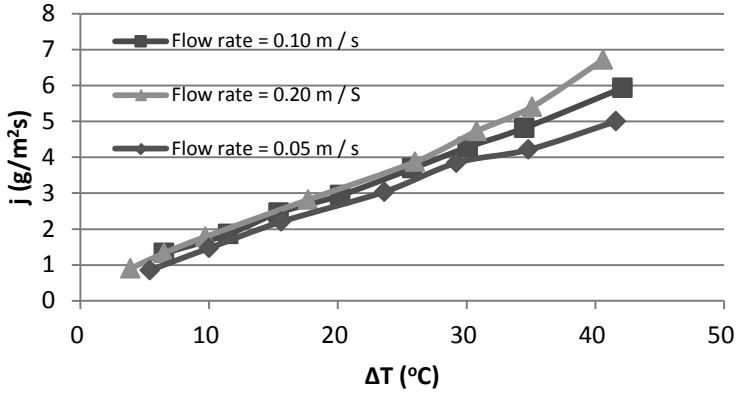

Figure 2. Transmembrane flux increases with increasing ΔT for different flow rates.

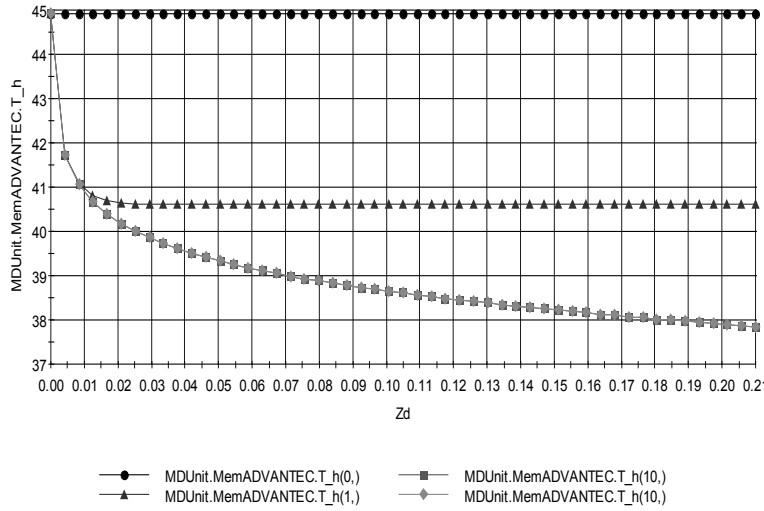

Figure 3. Temperature distribution at the interface hot channel/membrane along the flow direction as a function of time.

4. Conclusions

A dynamic two-dimensional model was developed, describing the flow in the plate-and-frame countercurrent DCMD system. The model has the capabilities of predicting the temperature polarization profile and pure water production. The model is implemented using the modeling package gPROMS.

In our future work, we will on the one hand continue our efforts in enhancing the dynamic model. On the other hand, an experimental setup will be constructed. It will enable us to perform dedicated experiments for the purpose of model validation.

Acknowledgements

The first author would like to thank Masdar Institute for financial support.

References

[1] Findely M.E., Vaporization through porous membranes, 1967, 6, Ind. & Eng. Chem. Process Des. Dev. and ev. 226-237

[2] Lawson K.W., D.R. Lloyd, Review membrane distillation, 1997, 124, J. Membr. Sci. 1-25

[3] El-Bourawi M.S., A framework for better understanding membrane distillation separation process, 2006, 285, J. Membr. Sci. 4-29

[4] Khayet M., Membranes and theoretical modeling of membrane distillation: a review, Adv. in Colloid and Interface Sci., Volume 164, Issues 1–2, 11 May 2011, Pages 56-88

[5] Chen T, Ho C, Yeh H. Theoretical modeling and experimental analysis of direct contact membrane distillation. J Membr Sci 2009;330:279–87.

[6] Schofield R.W., Fane A.G., and Fell C.G.D. 1990, Gas and vapor transport through microporous membrane, J. Membr. Sci 53-159

I.A. Karimi and Rajagopalan Srinivasan (Editors), Proceedings of the 11th International Symposium on Process Systems Engineering, 15-19 July 2012, Singapore.

2-D Population Balance Modelling of Nucleation and Growth of Needle-shape Crystals

A.V. Bekker, T.S. Li, and I. Livk

CSIRO Process Science and Engineering, Minerals Down Under Flagship
PO Box 7229, Karawara WA 6152, Australia

Abstract

Population balance equation models are widely accepted for simulating various particulate processes including crystallization. In this work, a dynamic 2-D population balance equation crystallization model was solved using a finite element method-based numerical algorithm with adaptive mesh and time step for three different cases: i) constant crystal growth rate, ii) constant crystal growth and nucleation rates, and iii) nonlinear crystallization kinetics. The model results obtained for the three different cases clearly demonstrate consistency of the newly developed numerical algorithm for solving 2-D population balance models of crystallization systems that produce crystals with the variable aspect ratio.

Keywords: crystallization modelling, multidimensional population balance equation, crystal aspect ratio, 2-D secondary nucleation, multidimensional crystal growth, FEM.

1. Introduction

A population balance equation (PBE) approach has been widely accepted for modelling particulate processes in various industrial applications including crystallization. In many crystallization applications, the product crystal size distribution (CSD) is a crucial quality parameter, which also makes it a focal point of process modelling. CSD of the crystallization product has been traditionally characterised using a single size dimension, which is the characteristic crystal diameter. The disadvantage of a 1-D description of crystal size is that it can not capture a changing crystal shape. During crystallization, crystals often experience significant changes to their aspect ratio, which requires a two-dimensional population balance model in order to describe the crystal size distribution with respect to the crystal length and width. With the advent of advanced sensing techniques (Bekker, 2011; Khanam, 2011) the crystal size can now be characterised in multiple dimensions. Different approaches for modelling the evolution of multidimensional crystal size, based on fixed mesh high-resolution algorithms, have been reported in literature by various authors (Gunawan, 2004; Sato *et al*., 2008). In this work, we present the development of a finite element method-based solution algorithm, with adaptive mesh and time step, of a 2-D population balance equation-based model to describe the evolution of the size distribution of needle-shape crystals. Secondary nucleation and crystal growth mechanisms are taken into account in the model.

2. 2-D PBE Model Incorporating Crystal Growth and Nucleation Kinetics

For crystals with high aspect ratio, defined as the ratio between crystal length and width, the crystal shape can be approximated as a rectangular prism of length L and equal width and height W, as shown in Fig.1. The volume of crystals can be calculated as $V=LW^2$.

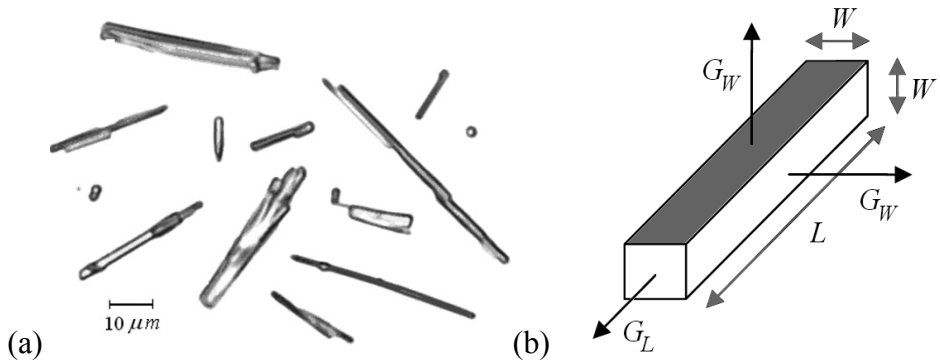

Figure 1. High aspect ratio crystals: (a) an optical microscope image, and (b) a 2-D rectangular approximation of a 3-D needle-shape crystal.

With crystal faces exhibiting different crystal growth rates, due to different supersaturation dependences of the respective growth rate equations, the crystal aspect ratio changes during the crystallization process. Similarly, seed and nuclei crystals can also exhibit a distribution of aspect ratios, which are in general different for the two types of crystals. A 2-D population balance equation model, developed previously for crystal breakage (Sato *et al*., 2008), is adapted in this work to model crystallization with simultaneous supersaturation-dependent 2-D secondary nucleation and crystal growth The resulting dynamic 2-D model can be stated as:

$$\begin{cases} \dfrac{\partial n}{\partial t} + G_W \dfrac{\partial n}{\partial W} + G_L \dfrac{\partial n}{\partial L} = B_u\, n_n(W,L), \quad W \in [0, W_{\max}],\ L \in [0, L_{\max}],\ t \in [t_0, t_{\text{end}}]; \\ \dfrac{d\sigma}{dt} = -\alpha B_u\, \mu_{21}(n_n) - 2\alpha G_W \mu_{11}(n) - \alpha G_L \mu_{20}(n), \\ G_W = k_W \sigma^2,\ G_L = k_L \sigma^4,\ B_u = k_n \sigma^2 \mu_{21}(n),\ \mu_{ij}(n) = \int_0^{L_{\max}} \int_0^{W_{\max}} W^i L^j\, n\, dW\, dL\,, \\ n\big|_{\substack{(0,0)-(W_{\max},0) \\ (0,0)-(0,L_{\max})}} = 0, \quad \left.\dfrac{\partial n}{\partial L}\right|_{\substack{(W_{\max},0)-(W_{\max},L_{\max}) \\ (0,L_{\max})-(W_{\max},L_{\max})}} = 0,\ n\big|_{t=0} = n_0(W,L), \qquad \sigma\big|_{t=0} = \sigma_0\,. \end{cases} \tag{1}$$

were n is the number density, σ is the relative supersaturation, t is time, L and W are the crystal length and width, n_0 and n_n are the initial and nuclei CSDs, respectively, σ_0 is the initial relative supersaturation, G_L and G_W are the crystal length and width growth rates, respectively, B_u is the secondary nucleation rate, α is the crystal density, k_L, and k_W are the length and width growth rate constants, respectively, k_n is the nucleation rate constant, and μ_{ij} is the *i-j* cross-moment of the crystal size distribution.

Solving the above dynamic crystallization model enables prediction of the evolution of crystal size distribution and supersaturation in an isothermal batch crystallizer. The two crystal growth rates are assumed to be independent of crystal size. This spatially-homogenous model describes the population of crystals distributed in a two dimensional domain with the crystal length and crystal width as internal coordinates.

3. A Constant Crystal Growth Rate Case

The 2-D nonlinear dynamic model of Eq. 1, is solved numerically for the case of constant crystal growth rates; $G_W = G_L$ = const., and no nucleation; $B_u = 0$. The seed crystals are described by a 2-D Gaussian CSD as

$$n_0(W,L) = \frac{1}{\pi \delta_W \delta_L} e^{-\left(\frac{W-W_S}{\delta_W}\right)^2 - \left(\frac{L-L_S}{\delta_L}\right)^2} \quad (2)$$

where δ_W=0.4 μm, δ_L=10 μm are the aspect ratio dispersion coefficients in the width and length directions, respectively. The average seed width, W_S, and the average seed length, L_S, equal to 2 and 20 μm, respectively. As shown in Fig. 2 for the case of constant growth rates, the maximum of the initial CSD travels along the diagonal of the *L-W* plane with a translation distance that is equal to $\Delta=(t-t_0)\sqrt{(G_W^2+G_L^2)}$. The Gaussian shape of the initial crystal number density is closely preserved, as expected for the case with the zero nucleation rate. Generally, the larger the value of the ratio, $\Delta/\min(\delta_W,\delta_L)$, and the higher the dispersion ratio, δ_L/δ_W, deviates from unity, the more difficult it is to numerically solve the model in Eq.1. High values of $\Delta/\min(\delta_W,\delta_L)$=100 and δ_L/δ_W=25 were used to demonstrate the ability of the FEM with adaptive mesh and time step to preserve CSD shape.

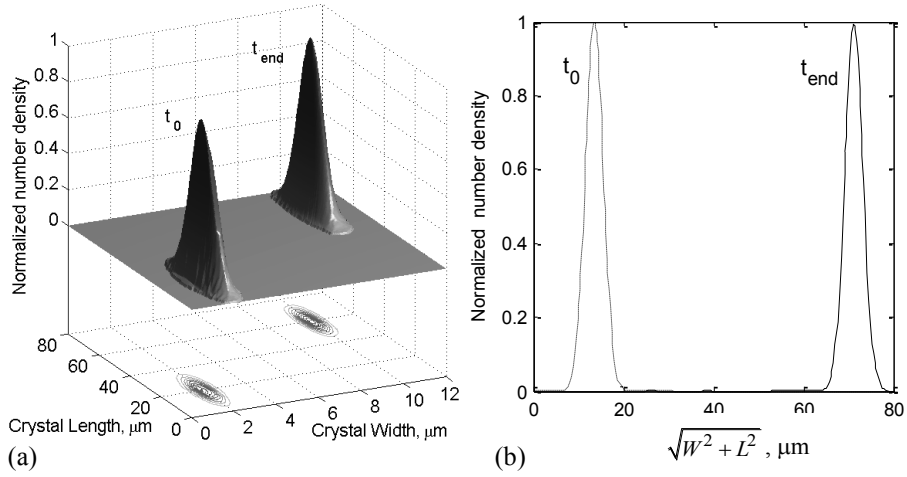

Figure 2. Initial and final normalized number density distributions of needle-shape crystals with the dispersion coefficient ratio, δ_L/δ_W, of 25 for the growth only case: (a) 2-D normalized number density, and (b) 1-D diagonal cross section of the 2-D normalized number density.

4. A Constant Nucleation and Crystal Growth Rate Case

For the case of constant nucleation and crystal growth kinetics; $G_W = G_L = G_0$ = const., and B_u = const., the 2-D dynamic model of Eq.1, with the seed crystals of Eq.2, was solved numerically using the following Gaussian size distribution of nuclei

$$n_n(W,L) = \frac{1}{\pi \delta_W \delta_L} e^{-\left(\frac{W-W_n}{\delta_W}\right)^2 - \left(\frac{L-L_n}{\delta_L}\right)^2} \quad (3)$$

An average width of nuclei, W_n, of 2 μm, and average length, L_n, of 20 μm were used in numerical experiments. Although this nuclei size is not realistic for most practical

problems, it was chosen here to demonstrate the principle, which is general and independent of nuclei size. At the same time, an average width of seed crystals, W_S, was 4 μm, and average length, L_S, 30 μm. The same dispersion coefficients of δ_W=0.4 μm and δ_L=10μm were used for both the nuclei and seed crystal size distributions.

Similar to the pure crystal growth case, in the nucleation-growth case the maximum in the initial seed CSD is shifted diagonally on the *L-W* plane, as shown in Fig. 3 (a). At the same time, nuclei of a smaller size than the seed start appearing and grow along the *L-W* direction. The number density resulting from nuclei forms a saddle-like shape with a constant height. As expected, the initial maximum of the seed number density is correctly preserved during crystallization, as shown in Fig.3 (b) with the 1-D cross sections of the initial and final 2-D normalized number densities compared. Also, the predicted increase in the total number of crystals accurately matches the increase in estimated based on the constant nucleation rate multiplied by the crystallization time. Note, however, that the cross section plane presented in this case in Fig.3 (b) is not exactly the same plane as that presented in Fig. 2(b).

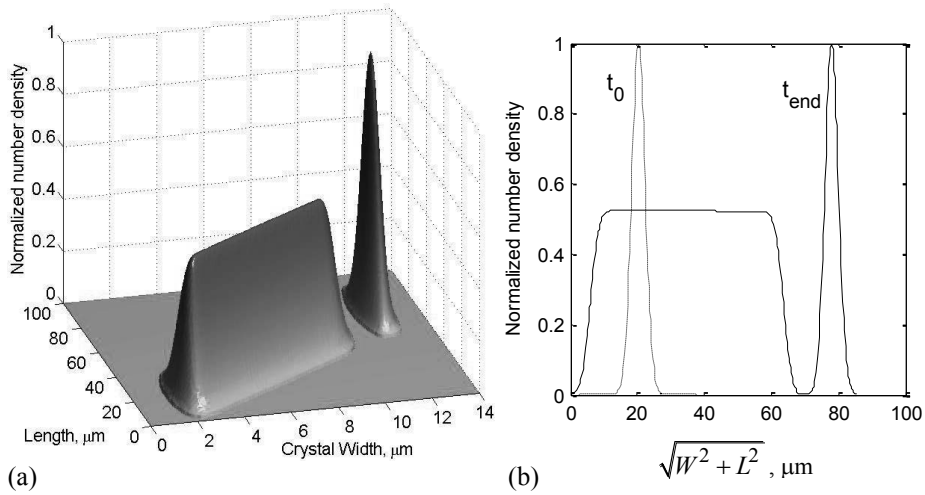

Figure 3. Normalized number density distributions of crystals with seed and nuclei dispersion coefficient ratio, δ_L/δ_W, of 25 for the constant nucleation and growth case: (a) final 2-D normalized number density, (b) initial and final 1-D diagonal cross section of the 2-D number density.

5. A Nonlinear Crystallization Kinetics Case

To test the numerical algorithm for a fully nonlinear kinetic case the number density was coupled with a decreasing supersaturation profile, which lead to decreasing crystal growth and nucleation rates. The statement of Eq.1 was run with the same parameters for the seed and nuclei distribution as those used in the nucleation-growth constant kinetics case. As shown in Fig. 4(a), the final CSD predicted for the nonlinear crystallization kinetic case differs from the one obtained for the constant nucleation-growth kinetic case. However, the maximum and the shape of the CSD of the seed crystals are accurately preserved by the numerical solution, as illustrated in Fig. 4(b). Due to decreasing supersaturation in this case, the travel distance of the maximum in the seed crystal CSD along the diagonal is smaller than in the previous two cases.

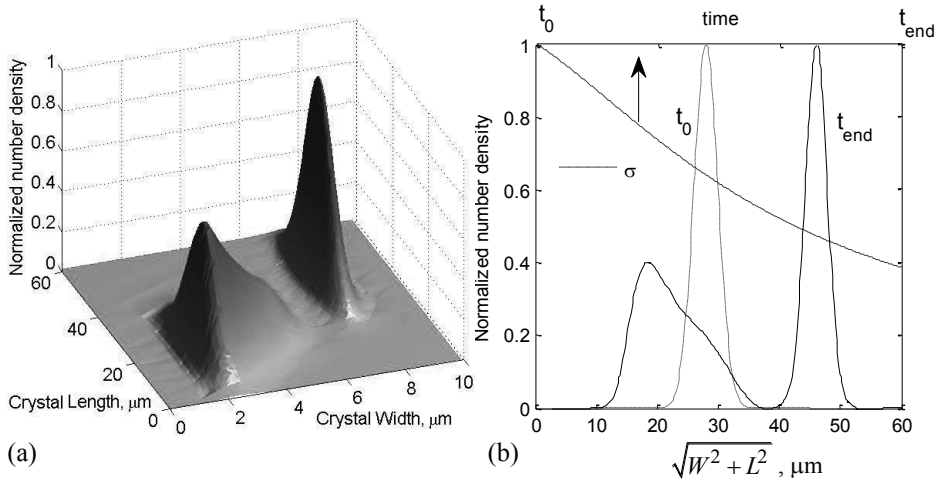

Figure 4. Normalized number density distributions of crystals with seed and nuclei dispersion coefficient ratio, δ_L/δ_W, of 25 for the nonlinear kinetics case: (a) final 2-D number density, and (b) initial and final 1-D diagonal cross section of the 2-D number density shown with the corresponding supersaturation profile.

As shown in Fig. 4(b), the left-hand side part of the normalised number density distribution, the appearance of which is due to the onset of nuclei, exhibits a pyramid-like local maximum forming a shape that differs significantly to the saddle-like shape shown in Fig. 3(b) for the constant nucleation-growth case. Also, in the nonlinear case the height of the pyramid local maximum is lower than the height of the saddle. The results presented in Fig. 4 provide a qualitative demonstration of consistency of the numerical solution of the nonlinear model of Eq.1.

6. Conclusions

A 2-D population balance equation model was solved using a finite element method-based numerical algorithm with adaptive mesh and time step for three different crystallization cases: i) constant crystal growth rate, ii) constant crystal growth and nucleation rates, and iii) nonlinear crystallization kinetics.

The model results obtained for the three different cases clearly demonstrate consistency of the newly developed FEM-based numerical approach for solving dynamic 2-D population balance models of crystallization systems with crystals of variable aspect ratio.

References

A.V. Bekker, J. McShane, D. Bedell and I. Livk, 2011, Image Analysis-based Sizing of Oxalate Crystals, Proceedings of the Chemeca 2011, Sydney, Australia, 18-21 September 2011.

R. Gunawan, I. Fusman and R.D. Braatz, 2004, High Resolution Algorithms for Multidimensional Population Balance Equations, AIChE Journal, 50, 11, 2738-2749.

T. Khanam, M.N. Rahman, A. Rajendran, V. Kariwala, and A.K. Asundi, 2011, Accurate Size Measurement of Needle-shaped Particles Using Digital Holography, Chemical Engineering Science, 66, 12, 2699-2706.

K. Sato, H. Nagai, K. Hasegawa, K. Tomori, H.J.M. Kramer and P.J. Jansens, 2008, Two-Dimensional Population Balance Model with Breakage of High Aspect Ratio Crystals for Batch Crystallization, Chemical Engineering Science, 63, 12, 3271-3278.

I.A. Karimi and Rajagopalan Srinivasan (Editors), Proceedings of the 11th International Symposium on Process Systems Engineering, 15-19 July 2012, Singapore.

Dynamic analysis of reaction kinetics of carton packaging pyrolysis

Larissa M. Alvarenga[a], Thiago P. Xavier[b], Marcos Antonio S. Barrozo[b], Marcelo S. Bacelos[a], Taisa S. Lira[a]

[a] *Departamento de Engenharias e Computação, Programa de Pós-graduação em Energia, Universidade Federal do Espírito Santo,, Rod. BR 101 Norte, km. 60, Bairro Litorâneo, CEP 29932-540, São Mateus- ES, Brazil, email:marcelobacelos@ceunes.ufes.br*

[b] *Programa de Pós-graduação em Engenharia Química, Universidade Federal de Uberlândia, Av. João Naves de Ávila, 2121, Bloco 1K do Campus Santa Mônica, CEP 38408-100, Uberlândia-MG, Brazil*

Abstract

As reported in the literature, the post-consumption carton packaging has been recycled using different process. Pyrolysis can be a promising technology to be used for recovering the aluminum from polyethylene and generating products with high heating value. In this research paper, by using thermogravimetric analysis (TGA), a kinetic study on pyrolysis reactions was performed. Furthermore, the activation energy of pyrolysis reaction was estimated using the methodology proposed by Ozawa (1965).

Keywords: pyrolysis, carton packaging, thermogravimetric analysis.

1. Introduction

A modern solid waste commonly found in urban areas is the post-consumption carton packaging, composed of 75% paper, 20% polyethylene and 5% aluminum. Recycling is one of the alternatives for recovering the long-life packaging. The recycling starts in the paper industry where recycling fibers can be recovered by repulping process. The polyethylene and aluminum separated in a hydropulper can be recovered in three different ways: energy generation from paraffinic oil, recovery of aluminum in pyrolysis ovens, recovery of polyethylene and aluminum by plasma technology, and the processing of the mixtures of polyethylene and metal to obtain high-end plastic lumber products. Among these technologies, pyrolysis highlights to be a good alternative either to separate aluminum from polyethylene or to generate products with high heating value. In the literature, few studies have done on the pyrolysis of carton packaging wastes (de Marco et al., 2009; Korkmaz et al., 2009). Thus, this research aims at analyzing the reaction kinetics of carton-packaging components pyrolysis using thermogravimetric analysis.

2. Methodology

2.1. Thermogravimetric Analysis.

The data were obtained using a thermogravimetric analyzer, TGA-60 (Shimadzu). Table 1 presents operating conditions and sample characteristics used in this research and those reported in the literature.

Table 1: Operating conditions, physical properties, methods and models used.

References	Operating Conditions, physical properties, method and models
Present research	- Continuous flow of nitrogen gas at a rate of 50 mL min^{-1}; - Samples of 6 mg and sieve diameter smaller than 1 mm; - Densities: carton packaging (1.3234g.cm^{-3}), cardboard (1.4893g.cm^{-3}) and polyethylene (0.9414g.cm^{-3}). - Dynamic tests: 25 to 600 °C; heating rates: 5, 10, 20 and 50 °C min^{-1}; - Kinetic model used: Ozawa (1965).
Paik and Kar (2009)	- Continuous flow of nitrogen gas at a rate of 200mL min^{-1} - Average particle diameter: ~20, ~10, ~1μm < 500 nm - Dynamic tests: 40 to 600ºC at heating rates of 5, 10 and 15 ºC/min^{-1} - Kinetic model used: Friedman (Li et al.,1998), Freeman–Carroll (Li et al.,1998), Kissinger (Li and Huang,1999), Kim–Park (1995) and Flynn–Wall (Li and Huang, 1999).
Volker and Rieckman (2002)	- Continuous flow of helium gas at a rate of 1.7 l h^{-1}; - Initial sample masses of 1, 3, 20, 37 and 54 mg and bulk density of 400 and 550 kg m^{-3}; - Dynamic tests performed at heating rates: 0.14, 3, 41 and 105 K min^{-1}. - Kinetic model used is not isoconversional.
Wu and Chang (2001)	- Continuous flow of nitrogen gas at a rate of 50 mL min^{-1}; - Samples of 6±0.5 mg and diameter smaller than 1 mm; - The same properties of this present research. - Dynamic tests performed at heating rates: 5.2, 12.8 and 21.8 K min^{-1}. - Kinetic model used: Friedman (1965).

2.2. Kinetic model

Table 2 shows the set of equations describing the kinetic model used.

Table 2: Kinetic model used for estimating the activation energy.

Conversion of solids

$$X = \frac{m_0 - m}{m_0} \quad (1)$$

m is the solid mass for a given time and m_0 is the initial mass of solid.

Temperature

$$T = T_0 + \beta t \quad (2)$$

β (dT/dt) is the heating rate and T_0 is the initial temperature.

Rate of conversion

$$\frac{dX}{dt} = f(X) \times k(T) \quad (3)$$

f is the conversion function, k is a reaction rate constant.

Arrhenius equation

$$k(T) = Ae^{\frac{-Ea}{RT}} \quad (4)$$

E_a is the activation energy, R is the ideal gas constant, A is the pre-exponential factor and T is the temperature of the sample.

Obtaining Ozawa's model

Based on equations (1), (3) and (4), the expression for degree of solid transformation as function of temperature can be calculated:

$$\frac{dX}{f(X)} = \frac{A}{\beta} e^{\frac{-Ea}{RT}} dT \quad (5)$$

By integrating the Eq.5 from T_0 (corresponding to X_0) to temperature inflection (T_m) (corresponding to X_m), the following equation is obtained:

$$g(X) = \int_{X_0}^{X_m} \frac{dX}{f(X)} = \frac{A}{\beta} \int_{T_0}^{T_m} e^{\frac{-Ea}{RT}} dT \quad (6)$$

Because of the complexity of the pyrolysis reaction, the form of the function $f(X)$ can be simplified assuming that the reaction follows a first order kinetics:

$$f(X) = (1 - X) \quad (7)$$

Ozawa (1965) used an empirical approximation to the integral of Equation 6, which resulted in the following equation:

$$\ln \beta = -1.0518\left[E_a / RT\right] + \left[\ln\left(k_0 E_a / R\right) - \ln g(X) - 5.3305\right] \quad (8)$$

Therefore, a plot of ln β versus $1/T$ should result in a straight line with slope -1.0518 E_a/R, with R = 8.314J/mol.K

3. Results and Discussion

Figures 1a-c show the curves of the rate of mass loss (DTG) as a function of temperature and heating rate, for carton packaging, cardboard and polyethylene, respectively. Comparing the DTG curves for different components, it can be observed that, in general, there are three steps of carton packaging devolatilization.

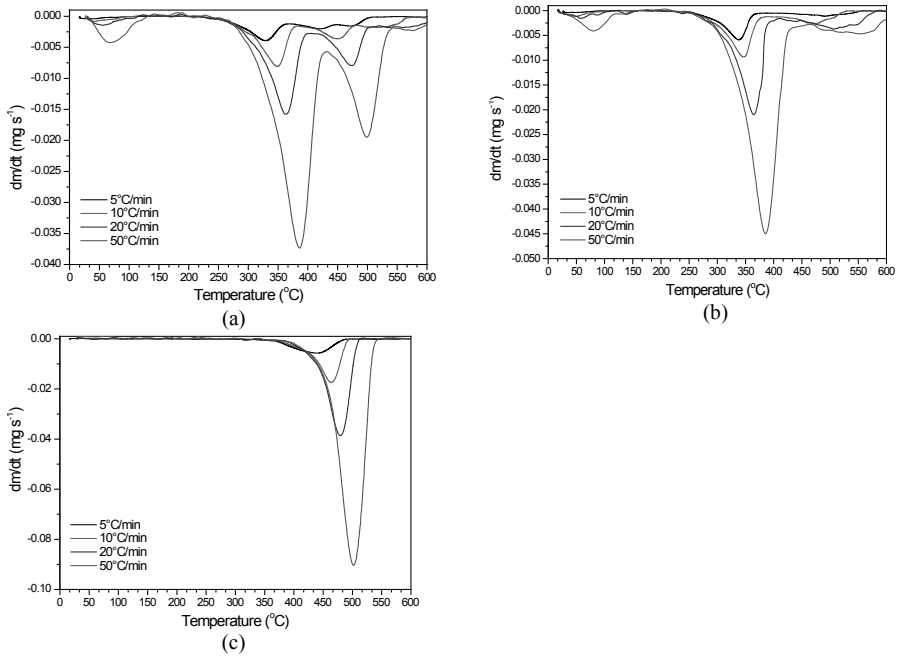

Figure 1: Rate of mass loss as function of reaction temperature and heating rate. (a) Carton packaging, (b) cardboard and (c) polyethylene.

In Figure 1a-b, at low temperatures (T<100°C), the first step is characterized by the significant moisture loss. The second step can be perfectly correlated with the cardboard devolatilization, which occurs at temperatures ranging from 300 to 420°C. Then, the third step it can be associated with the polyethylene devolatilization, occurring in the range of 400 to 550ºC, as shown in Figures 1a and 1c. In addition, in Figure 1a-b, a devolatilization step is also observed at temperature range of 500 to 600°C. This may be probably indexed to either the dye used in manufacturing of both the carton packaging and cardboard or aluminum decomposition. However, the peaks showed in figures 1a-b cannot be related to the decomposition of aluminum as this component is not subject to devolatilization. These findings are in agreement to those reported recently by Korkmaz et al. (2009). These authors verified that only coal and aluminum are the wastes from decomposition of carton packages. Moreover, it can be verified in Figures 1a-c that, for higher temperatures (T>350ºC), as heating rate is increased, the main peaks of mass loss are noticeable. These probably are due to the change in the decomposition mechanism.

Figures 2a-c show the linear regression data for pyrolysis of carton packaging, cardboard and polyethylene using the method proposed by Ozawa (1965), as described in Table 2. For carton packaging, in a range of 10-50% conversion, it can be seen in Figure 2a that the linear fits show approximately the same slop. As well, it is presented a similar behavior of linear fits for cardboard and polyethylene, as shown in figure 2b-c,

in a range of 10-60% and 10-40% conversion, respectively. Such a parallelism of linear fits indicates an analogous kinetic behavior, suggesting that the activation energies are probably similar and the mechanism of reaction can be most likely described and represented by one global step.

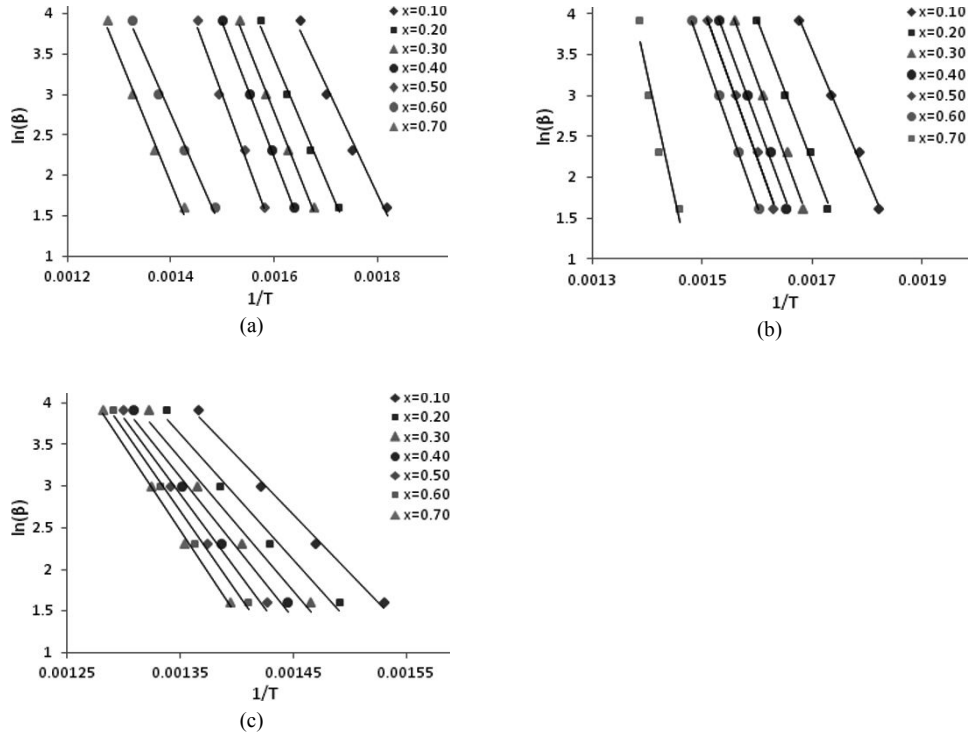

Figure 2: Graph of Ozawa for pyrolysis. (a) carton packaging, (b) cardboard and (c) polyethylene.

However, for higher conversion values, as that 60-70% for carton packaging and 70% for cardboard, a different slopping line is achieved as compared to others, indicating that there is a change in the reaction mechanisms. In addition, for the polyethylene, the lines of the linear fits present comparable behavior for each conversion value achieved, as shown in Figure 2c. Consequently, this leads to similar values of activation energies attained as shown in Table 3.

The Table 3 shows activation energy data (E_a) for each conversion attained in the pyrolysis of carton packaging, cardboard and polyethylene, respectively. For all conversion ranges, the linear fits show highly significant correlation coefficients ($0.93 \leq R^2 \leq 1.0$) and reasonably low values of RMSE ($0.02 \leq \text{RMSE} \leq 0.23$, root-mean-square error). The comparison between E_a averages obtained to those of Literature shows that data are in the same order of magnitude to those of Paik and Kar (2009), Volker and Rieckmann (2002) and Wu and Chang (2001), as shown in Table 3 and 4, even considering either different methods, operating conditions or material physical properties used (see Table 1).

Table 3: Activation energy obtained by the Ozawa's model (1965).

Carton Packaging				Cardboard			Polyethylene		
X	E_a ($kJ.mol^{-1}$)	R^2	RMSE	E_a ($kJ.mol^{-1}$)	R^2	RMSE	E_a ($kJ.mol^{-1}$)	R^2	RMSE
0.1	106.85	0.98	0.11	123.61	0.99	0.06	110.58	0.99	0.08
0.2	119.22	0.99	0.07	138.62	0.99	0.06	118.52	0.98	0.11
0.3	127.17	1.00	0.05	142.62	0.99	0.06	126.36	0.98	0.13
0.4	131.41	1.00	0.02	144.91	0.99	0.07	133.95	0.98	0.13
0.5	136.88	0.99	0.08	148.80	1.00	0.05	144.03	0.98	0.12
0.6	113.21	0.99	0.09	150.65	1.00	0.02	153.82	0.99	0.09
0.7	122.46	0.99	0.09	239.92	0.93	0.22	162.45	1.00	0.05
Mean	**122.46**			**155.59**			**135.67**		
S.D	10.41			38.24			18.84		

Table 4: Activation energy from data obtained by Literature

References	Paik and Kar (2009), for Polyethelene	Volker and Rieckmann (2002), for cardboard	Wu and Chang (2001), for carton packaging
E_a ($kJ.mol^{-1}$)	232.5	244.0	150.0

Conclusions

Based on analysis established in this research the following conclusions can be drawn:

- The carton packaging pyrolysis follows three steps characterized by moisture loss, cardboard and polyethylene devolatilization, respectively.
- For conversion values ranging from 20 to 60%, the pyrolysis reaction probably follows a similar mechanism and can be represented by one global step.
- Considering the high correlation coefficients of linear fit of Ozawa (1965)'model to the experimental data, it can be stated that such a model can be used for satisfactorily estimating the activation energy of pyrolysis reactions of carton packaging, cardboard and polyethylene.

Acknowledgments

The authors wish to express their gratitude to CNPq and FAPES for financial support to carry out this research and, especially, to CAPES for MSc scholarship of L. M. Alvarenga. We also thank to Tetra Pak for providing the samples.

References

KORKMAZ, A.; YANIK, J.; BREBU, M.; VASILE, C., 2009, Pyrolysis of the tetra pak, Waste Management, Vol 29, p. 2836-2841.

OZAWA, T., 1965, A new method of analyzing thermogravimetric data, Bulletin of the Chemical Society of Japan, Vol. 38, p. 1881-1886.

PAIK, P.; KAR, K. K., 2009, Thermal degradation kinetics and estimation of lifetime of polyethylene particles: Effects of particle size", Materials Chemistry and Physics, Vol 113, p. 953-961.

VÖLKER, S.; RIECKMANN, Th. 2002, Thermokinetic investigation of cellulose pyrolysis - impact of initial and final mass on kinetic results", Journal of Analytical and Applied Pyrolysis, Vol 62, p. 165-177.

WU, C.; CHANG, H., 2001, Pyrolysis of tetra pack in municipal solid waste. J. Chem. Technol. Biotechnol., Vol 76, p. 779–792.

de MARCO, I., CABALLERO, B.M., LOPEZ, A., LARESGOITI, M.F., TORRES, A. CHOMON, M.J., 2009, Pyrolysis of the rejects of a waste packaging separation and classification plant, J. Anal. Appl. Pyrolysis 85, 384–391.

I.A. Karimi and Rajagopalan Srinivasan (Editors), Proceedings of the 11th International Symposium on Process Systems Engineering, 15-19 July 2012, Singapore.

A simultaneous synthesis method for combined heat and mass exchange networks

Linlin Liu[a],Jian Du[a*],Mahmoud M.El-Halwagi[b,c],José María Ponce-Ortega[d],Pingjing Yao[a]
[a] *Chemical Engineering Department,Dalian University of Technology,Dalian 116024,China*
[b] *Chemical Engineering Department, Texas A&M University, College Station 77843, TX, USA*
[c] *Adjunct faculty at the Chemical and Materials Engineering Department, King Abdulaziz University, Jeddah, Saudi Arabia,*
[d] *Chemical Engineering Department, Universidad Michoacana de San Nicolás de Hidalgo, Morelia, Mich 58060, Mexico*

Abstract

Mass-exchange operations are highly impacted by heating and cooling. Therefore, there is a natural coupling between the problems of synthesizing mass exchange networks (MENs) and heat exchange networks (HENs). The objective of this paper is to introduce a systematic method for the simultaneous synthesis of combined mass- and heat-exchange networks (CM&HEN). The proposed method is based on a novel approach that integrates the pseudo-T-H diagram approach (PTHDA) for HEN synthesis, with the mass pinch technology (MPT) for MEN synthesis. The applicability of the proposed approach is shown through an example problem, where a significant reduction in the total annual cost is obtained.

Keywords: mass exchange network; heat exchange network; combined mass- and heat-exchange network; simultaneous synthesis.

1. Introduction

Significant conservation of natural resource (mass and energy) can be achieved through the design of MENs and HENs. Because the performance of mass-exchange operations depends on the operating conditions including temperature, there is an important coupling between the synthesis of MENs and HENs. Therefore, systematic methods should be used.

For the simultaneous synthesis of combined mass- and heat-exchange networks (CM&HENs). The design challenges include the need to screen mass-separating agents while accounting for their operating conditions and linking the mass-exchange operations with heat integration among process streams, the rich streams, and the mass-separating agents

Srinivas and El-Halwagi (1994) introduced the problem of combined heat and reactive mass exchange networks and developed a procedure based on optimizing individual mass-exchange temperatures in isothermal unit. Isafiade and Fraser (2007, 2009) presented two approaches for the synthesis of CM&HEN using the mass pinch technology and mathematical programming. Iterative approaches were used to solve the problem. The iterative approach simplifies the solution but does not guarantee the identification of the optimal solution. Du et al. (2010) presented a superstructure based method for the CM&HEN synthesis problem; however, the type of stream for the HEN (hot/cold) is predefined, and this way some potential solutions are eliminated yielding suboptimal solutions.

This paper proposes a new approach for the simultaneous synthesis of CM&HEN considering the multidimensional optimization issue. The proposed approach combines

the mass pinch technology (El-Halwagi and Manousiouthakis, 1989) and the pseudo-T-H diagram (Xiao et al., 2006) methods. The proposed approach considers explicitly the relationships between the MEN and HEN since the synthesis stage eliminating the drawbacks of previously reported methods.

2. Problem Statement

The problem addressed in this paper for the synthesis of CM&HEN can be described as follows: Given are a set of streams that are rich in transferable components, a set of mass-separating agents or lean streams (e.g., solvent streams) that can be used to remove the transferable components, and a set of hot/cold utilities. The task is to synthesize a CM&HEN that considers the tradeoffs between mass transfer and heat exchange at the same time with the objective of minimizing the total annual cost.

To practically solve the CM&HEN synthesis problem, the following assumptions applied for dilute systems are considered (Srinivas and El-Halwagi, 1994): the stream mass flow rates remain constant throughout the network; the mass exchange units operate isothermally; the mass transfer is related to the lean stream temperatures; the coefficient a_n in the equilibrium relationship shown by equation (1) is a monotonic function of temperature.

$$y_n^* = a_n x_n + b_n \qquad (1) \qquad\qquad y_n^* = a_n (x_n + \varepsilon_n) + b_n \qquad (2)$$

In equation (1), y_n^* is the rich stream equilibrium concentration, x_n is the lean stream concentration, and T_n^* is the mass transfer temperature. The minimum concentration difference ε_n ($\varepsilon_n > 0$) is introduced in equation (2) to avoid zero driving forces.

3. Proposed Method

3.1. Method outline

Mass pinch technology and pseudo T-H diagram approach are based on thermodynamic analysis, and both have been used effectively for MEN and HEN synthesis. The simultaneous synthesis method proposed in this paper integrates these two methods to establish a mathematical model for the overall CM&HEN synthesis and optimization. In CM&HEN, HEN provides suitable temperatures for MEN while MEN provides streams for HEN. Therefore, CM&HEN is not merely a simple linkage of single MEN and HEN. This paper follows the coupling approach proposed by Srinivas and El-Halwagi (1994), where the mass exchange temperature for each lean stream remains constant during the mass exchange, and the heat exchange only exists at the two sides of MEN(i.e., pre- and post-mass exchange). To address the simultaneous problem, a synthesis/optimization strategy is explained and detailed in the next section.

3.2. Synthesis and optimization strategy

During the simultaneous synthesis and optimization of CM&HEN, the mass transfer temperatures and the stream flow rates are the linking parameters between the MEN and the HEN, therefore the key point for the simultaneous CM&HEN synthesis problem is to consider the interactions between these variables. It is worth noting that some methods are not suited to satisfy these requirements, because they need to represent the HEN before the optimization. The present paper uses the PTHDA method for the HEN synthesis to avoid the previous complication.

The PTHDA method considers as variables a list of heat transfer temperature difference contribution values T_C for each corresponding stream. These T_Cs may be optimized in a feasible range. Consequently, the PTHDA method does not require identifying and

distinguishing the different types of variables. Based on this feature, the HEN optimization can be coupled with the MEN synthesis by giving every potential hot/cold stream a variable position and identifying it during the optimization process. Hence, it is assumed that there are *i* MEN synthesis variables and at most *j* HEN synthesis variables. When a set of optimization variables are given, all cold/hot streams related can be determined and the treatment of these variables can be represented through the matrix $\boldsymbol{Z}$ as follows:

$$Z=\begin{bmatrix} z_{11}=\text{-1or0}or1 & & & \\ & z_{22}=\text{-1or0}or1 & & \\ & & \cdots & \\ & & & z_{jj}=\text{-1or0}or1 \end{bmatrix}$$

Three types of values can be observed along the diagonal: '-1' means it is a hot stream, '1' means it is a cold stream and '0' means the stream does not exist. The result of Matrix $\boldsymbol{Z}$ dot product with the HEN variables matrix $T_C=\left[T_{C1},\ T_{C2},\ \ldots,\ T_{Cj}\right]$ is an expression of variables and streams that exchange heat in the HEN. A value of 0 indicates no corresponding streams, non-zero means there is a corresponding streams and the absolute value is the temperature difference contribution value.

This strategy is robust and can be particularly applied to the cases of complex operating units whose hot and cold streams are hard to be determined.

3.3. Objective function

Based on the MPT and the PTHDA, and a sub-network coupling, this paper establishes a minimum total annual cost through a mathematical model for the CM&HEN synthesis. The total annual cost shown in equation (3) is a combination for the costs associated to the sub-MEN and the sub-HEN. For the MEN side, the operating cost considers the use of external lean streams and the capital cost is related to the mass exchanger units. For the HEN, the costs are the requirement of hot/cold utility and the fixed costs of the heat exchanger units. The following is the expression for the total annualized cost:

$$\min \sum_{p}\sum_{m}\sum_{n} N_{mnp}\cdot C_{stage}+\sum_{n} L_{l,n}\cdot C_{l,n}+\sum_{i} CF_{cui}+\sum_{j} CF_{huj}+\sum_{k}\sum_{i}\sum_{j} CF_{ijk}$$

$$+\sum_{i} C_{cui}\cdot A_{cui}^{B_{cui}}+\sum_{j} C_{huj}\cdot A_{huj}^{B_{huj}}+\sum_{k}\sum_{i}\sum_{j} C_{ijk}\cdot A_{lijk}^{B_{ijk}}+\sum_{i} C_{cui}\cdot q_{cui}+\sum_{j} C_{huj}\cdot q_{huj} \quad (3)$$

4. Case study

This example was taken from Srinivas and El-Halwagi (1994), Isafiade and Fraser (2007), it involves two H_2S-rich gas streams (R_1, R_2), one process lean stream S_1 and one external lean stream S_2. The cost and stream data are listed in Tables 1-3. Notice that each process stream has a certain target temperatures except S_2. The equilibrium relationships for H_2S in lean stream S_1 and S_2 are shown in equations (4) and (5), respectively. Besides, four external hot and cold streams listing in Table 4 are considered in this case study.

$$S_1: m_1=(5.86807\times10^{-8})\times10^{0.01024\times T_1^*} \quad (4)\qquad S_2: m_2=(9.386\times10^{-10})\times10^{0.0215\times T_1^*} \quad (5)$$

First, the HEN optimization variables–the temperature difference contribution values, are determined. There are at most two hot/cold streams that can be generated from S_1, one at most from S_2, thus 7 temperature difference contribution variables in total are required by adding 4 external hot/cold streams.

Table 1. Process parameters for the example

Operating time	8600 $h \cdot a^{-1}$	Cost of S_2	0.001 $\$ \cdot kg^{-1}$
Column capital cost	4552 $\$ \cdot stage^{-1} \cdot a^{-1}$	Hot utility (HU)	120 $\$ \cdot kW^{-1} \cdot a^{-1}$
Annualizationfactor	0.2	Cold utility 1 (CU_1)	10 $\$ \cdot kW^{-1} \cdot a^{-1}$
Heat exchanger cost	$30000+750A^{0.81}$	Cold utility 2 (CU_2)	30 $\$ \cdot kW^{-1} \cdot a^{-1}$
Annualization factor	0.2	Heat transfer film coefficient	0.2 $kW \cdot m^{-2} \cdot K^{-1}$

Table 2. Streams data for the example

R_i	G_i/kg·s^{-1}	Y_i^s	Y_i^t	S_j	L_j^{up}/kg·s^{-1}	X_j^s	X_j^t
R_1	104	8.83×10^{-4}	5.00×10^{-6}	S_1	40	0.07557	≤0.115
R_2	442	7.00×10^{-4}	5.00×10^{-6}	S_2	∞	0.001	≤0.01

Table 3. Thermal data for the streams in the example

Streams	T^s/K	T^t/K	T^{low}/K	T^{up}/K	Cp/kJ·kg^{-1}·K^{-1}
R_1	298	298	288	313	1.00
R_2	298	298	288	313	1.00
S_1	368	368	279	368	2.50
S_2	310	-	280	330	2.40
HU	453	452	-	-	-
CU_1	288	298	-	-	-
CU_2	278	283	-	-	-

Table 4. Extra stream data

Streams	FCp/ kW·K^{-1}	T^s /K	T^t/K	h/ kW·m^{-2}·K^{-1}
H_1	10.0	448	318	0.2
H_2	40.0	398	338	0.2
C_1	20.0	293	428	0.2
C_2	15.0	313	385	0.2

The results obtained through the proposed approach are represented in Table 5. It is worth noting that the lean streams S_1 and S_2 appear in the optimal solution, and that the number of the mass separation stages is 26. This produces a higher cost of the MEN than the one previously literature reported (Isafiade and Fraser, 2007), which only involves S_2 and 26 column stages. However, the associated cost for the HEN is 39.6% lower, yielding a reduction for the TAC of the CM&HEN of 2.14%lower than the solution reported in Isafiade and Fraser (2007). In literature, the optimal mass exchange temperature of S1 is 286K, then one hot stream (368K-286K) and one cold stream (286K-368K) with a total heat exchange load of 414 kJ are generated. While in this paper, S_1 and S_2 take part in the mass exchange, and optimal mass exchange temperature of $S_1$is equal to its start and target temperatures, meanwhile there is no target temperature constrain for S_2, finally only one hot stream is formed and its temperatures changes from 310K to 280.8 K with a heat load of 103.7kJ.

Table 5.Results comparison

Options	T_1^*/K	T_2^*/K	L_1/kg·s^{-1}	x_1^{out}	L_2/kg·s^{-1}	x_2^{out}	TAC of MEN /10^3\$·a^{-1}	TAC of HEN /10^3\$·a^{-1}	TAC of Combined networks /10^3\$·a^{-1}
Literature	286	-	10.1	0.1150	0	-	54.6	295.4	350.0
This paper	368	280.8	39.4	0.0853	1.48	0.01	164.2	178.3	342.5

Figure.1 presents the optimal combined network obtained. There are 4 mass exchanger units and 7 heat exchanger units including one heater and two coolers in the structure, stream H_3 in the HEN is the only hot stream generated from S2.

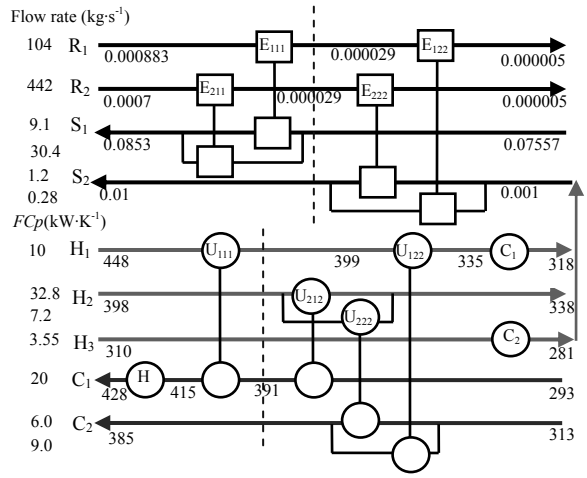

Fig.1 The optimal overall CM&HEN

5. Conclusion

This paper proposes a novel simultaneous synthesis strategy for the synthesis of CM&HEN. Concepts of MPT and PTHDA are adopted and integrated for MEN and HEN integration. An optimization formulation is developed to minimize the total annual cost of the MEN and the HEN while optimizing the selection of the mass-separating agents, the operating temperature of each mass-separating agent, and the assignment of heating and cooling duties. An example was presented to show the applicability and effectiveness of the proposed method with comparison to published results.

6. Acknowledge

The authors gratefully acknowledge the financial support from Natural Science Foundation of China (No. 20976022) and China Scholarship Council. Mahmoud El-Halwagi is thankful to funding from King Abdulaziz University. JoséMaría Ponce-Ortega appreciates funding from CONACyT.

References

A. J. Isafiade, D. M.Fraser, 2007. Optimization of combined heat and mass exchanger networks using pinch technology. Asia-Pacific Journal of Chemical Engineering, 2, 6, 554–565.

A. J. Isafiade, D. M.Fraser, 2009. Interval based MINLP superstructure synthesis of combined heat and mass exchanger networks. Chemical Engineering Research and Design, 87, 11, 1536-1542.

B. K. Srinivas, M. M. El-Halwagi, 1994. Synthesis of combined heat and reactive mass exchange networks . Chemical Engineering Science, 49, 13, 2059–2074.

J. Du, X. F. Li, L. Chen, P. J. Yao, 2010. Simultaneous synthesis of combined mass and heat exchanger networks. 5th International Symposium on Design, Operation and Control of Chemical Processes(PSE Asia 2010), Singapore.

M. M. El-Halwagi, V. Manousiouthakis, 1989. Synthesis of mass exchange networks. AIChE Journal, 35, 8, 1233-1244.

W.Xiao, P. J.Yao, X.Luo, W. Roetzel, 2006. A new and efficient NLP formulation for synthesizing large scale multi-stream heat exchanger networks.Journal of Chinese Institute of Chemical Engineers, 37, 4, 383-394.

I.A. Karimi and Rajagopalan Srinivasan (Editors), Proceedings of the 11th International Symposium on Process Systems Engineering, 15-19 July 2012, Singapore.

A New Method To Determine The Optimum Heat Exchanger Network Approach Temperature

Sharifah Rafidah Wan Alwi,[a] Zainuddin Abdul Manan[a], Sun Kheen Nam[a]

[a]*Process Systems Engineering Centre (PROSPECT), Faculty of Chemical Engineering, Universiti Teknologi Malaysia, 81310 Skudai, Johor, Malaysia.*

Abstract

Supertargeting is a widely used procedure to determine the optimum approach temperature (ΔT_{min}) for heat exchanger networks (HEN). It involves plotting the sum of HEN capital and operating costs, and finding the minimum total cost at an optimum ΔT_{min}. The capital and operating costs are determined from the heat transfer area and the minimum utility targets obtained from the temperature (T) vs enthalpy (H) plot of composited process streams (composite curves (CC)). S*upertargeting* using CC has two key limitations. Firstly, the HEN area calculations are drastically simplified through the assumption that CC segments are pseudo-single hot and cold streams exchanging heat via only one heat exchanger that is governed by a single cost correlation. Secondly, the current *Supertargeting* approach of considering only one hot and one cold utility levels at highest and lowest temperatures respectively is simplistic at best since a plant typically uses multiple levels of utilities. These limitations may lead to a very crude estimation of the total HEN cost and the corresponding ΔT_{min}. This work presents the Stream Temperature vs. Enthalpy Plot *Supertargeting* (STEPS) method that overcomes the aforementioned ΔT_{min} targeting limitations. Multiple utility levels, various heat exchanger types and streams individual heat transfer coefficients can be considered using STEPS. Application of STEPS on two case studies shows that the conventional *supertargeting* method can lead to up to 50% error in the total cost target and poor ΔT_{min} estimation.

Keywords: Pinch Analysis, Streams Temperature Versus Enthalpy Plots (STEP), multiple utilities, supertargeting, Heat Exchanger Network.

1. Introduction

Pinch Analysis has been a well-established tool for the design of maximum heat recovery networks in process plants. Among the important steps in Pinch Analysis is the determination of the optimum approach temperature for heat exchange (ΔT_{min}) to obtain the minimum total annual heat exchanger network (HEN) cost. The total annual HEN cost is affected by the trade-off between HEN capital and the operating costs. Ahmad and Linnhoff [1] introduced *supertargeting*, as a technique to determine the optimum ΔT_{min} that leads to the minimum total cost for HENs based on the composite curves.

Hall *et al*. [2] later developed a method which allows capital cost targets to consider different heat exchanger specifications such as materials of construction, pressure ratings and equipment types. This paper demonstrates that capital cost targets for HEN with different heat exchanger specifications can be predicted with good accuracy using individual stream temperature versus enthalpy plot (STEP). In a later research, Jegede and Polley [3] examined the effects of variations in heat exchanger

specifications on the network cost, and based on this, they developed a general procedure for predicting HEN total cost prior to design. Shenoy *et al*. [4] proposed a methodology to determine the optimum load for multiple utilities considering the cost tradeoffs in energy and capital for HENs. Akbarnia *et al*. [5] developed a method that considered piping costs and include the correlation for estimating piping costs for each stream based on the piping size, materials of construction and pressure rating.

The traditional supertargeting method has two major limitations. Firstly, the HEN area calculations are drastically simplified through the assumption that composite curve (CC) segments are pseudo-single hot and cold streams exchanging heat via only one heat exchanger that is governed by a single cost correlation. Traditionally, a composite stream is also assumed to have a single heat transfer coefficient even though it may consist of many streams, each with unique heat transfer coefficient and set of stream properties. Secondly, the current *Supertargeting* approach of considering only one hot and one cold utility levels at the highest and lowest temperatures respectively is simplistic at best since a plant typically uses multiple levels of utilities. These limitations may lead to a very crude estimation of the total HEN cost and the corresponding ΔT_{min}. These assumptions and limitations may lead to the total HEN cost to be grossly over or underestimated, and the wrong optimum ΔT_{min} selected. This work proposes the new Stream Temperature vs. Enthalpy Plot Supertargeting (STEPS) approach that overcomes all these limitations.

2. Methodology

2.1. Step 1: Data Extraction

The first step is hot and cold streams data extraction. The data required for analysis are primarily heat capacity flowrate, streams supply and target temperatures, and individual heat transfer coefficients, h. **Table 1** shows the extracted stream data for example 1 (Wan Alwi and Manan, 2010).

Table 1: Stream data for example 1 (Wan Alwi and Manan, 2010)

Stream	Supply Temp., T_s (°C)	Target Temp., T_t (°C)	Heat Capacity Flowrate, FCp, (kW/°C)	Enthalpy, ΔH (kW)	Shifted Supply Temp., T_s' (°C)	Shifted Target Temp., T_t' (°C)	Heat transfer coefficient, h, (kW/m^2°C)
Hot 1	300	160	3	-420	290	150	1.3
Hot 2	230	120	7	-770	220	110	1.1
Hot 3	160	60	2	-200	150	50	1.2
Cold 1	40	230	2	380	50	240	1.2
Cold 2	100	230	4	520	110	240	1.2
Cold 3	230	300	3	210	240	310	1.2

2.2. Step 2: Setting the Minimum Utility Targets by Using STEP

The next step is setting the minimum utility targets. In this step, Streams Temperature vs. Enthalpy Plot (STEP) by Wan Alwi and Manan [6] is used to determine the minimum utility targets instead of the traditional composite curves. For more details on STEP construction, readers are referred to Wan Alwi and Manan [6]. The construction of STEP is performed for ΔT_{min} values from 5 to 50°C.

2.3. Step 3: Targeting Multiple Utilities Using the Balanced STEP

Four types of utilities have been included into STEP and drawn as the balanced STEP. The utilities added are cooling water (CW), tempered water (TW), high pressure steam (HPS) and hot oil. The supply temperatures used for the utilities are the closest feasible temperatures relative to the process temperatures. Note that, the supertargeting technique based on composite curves introduced by Khorasany and Fesanghary [7] does not consider multiple utility levels.

2.4. Step 4: Utilities Cost Calculation

The hot and cold utilities determined from **Step 3** are then used to calculate the utility costs.

2.5. Step 5: Area Calculation For Each STEP Segment

The next step is to calculate the area of each heat exchanger. This can be done by observing each segment of STEP. The area for each STEP segment (A_k) can be calculated by using Equation (1). Note that for each composite curves' segment, the area may be calculated from a 'composite', as opposed to an individual stream match. This may lead to the wrong area and capital cost estimations. **Figure 1** shows each heat exchanger match for STEP at ΔT_{min} of 20°C.

$$A_k = \frac{Q_k}{\Delta T_{LMK}}\left(\frac{1}{h_{h,k}} + \frac{1}{h_{c,k}}\right) \quad (1)$$

Where A_k is in m^2, Q_k is the heat transferred (kW), $h_{h,k}$ and $h_{c,k}$ are heat transfer coefficients for hot and cold streams, ΔT_{LMK} is the log-mean temperature difference (K).

2.6. Step 6: Capital Cost Calculation

The double-pipe heat exchanger is assumed to be used for all STEP segments. The capital costs for networks with ΔT_{min} values between 5°C to 50°C are estimated based on the cost correllations from Seider *et al.* [8].

2.7 Step 7: Supertargeting by Constructing Trade-Off Diagram to Determine the Optimum ΔT_{min}

This step involves determining the utility and capital costs for ΔT_{min} values between 5 and 50 ºC. The costs of utilities as well as capital are added together at each ΔT_{min} to obtain the total cost. **Figure 2** shows that the optimum ΔT_{min} obtained is 5 ºC.

3. Case Study 1

The new STEPS method is applied on a Case Study 1 from Linnhoff *et al*. [9]. The results obtained using STEPS are compared with those obtained using the traditional approach. Supertargeting based on composite curves and STEPS both result in an optimum ΔT_{min} of less than 10°C. **Table 2** shows the difference between the total costs obtained via CC supertargeting as well as via STEPS. Note that STEPS result in higher total costs of up to 8.67%.

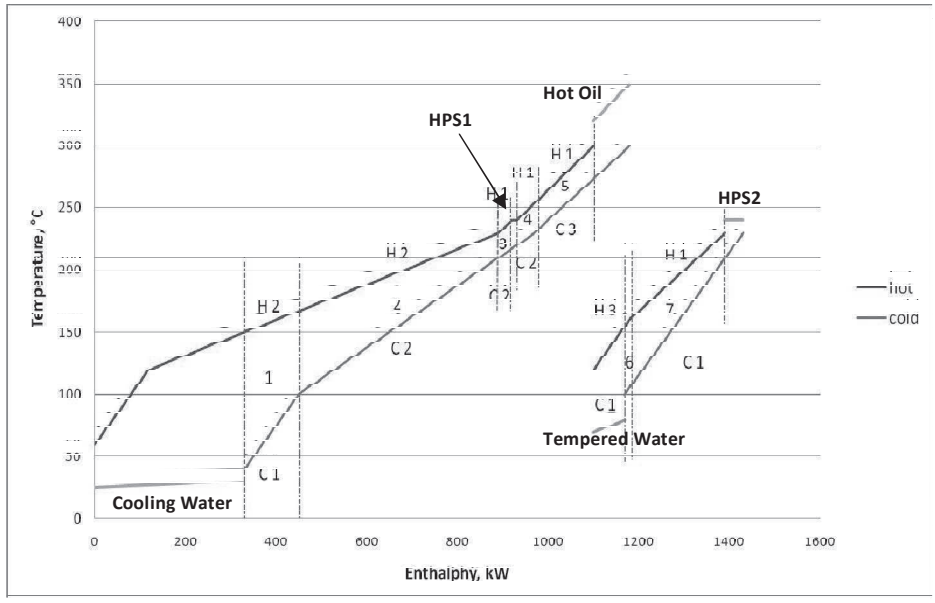

Figure 1: Stream matches for STEP at ΔT_{min} of 20°C (example 1).

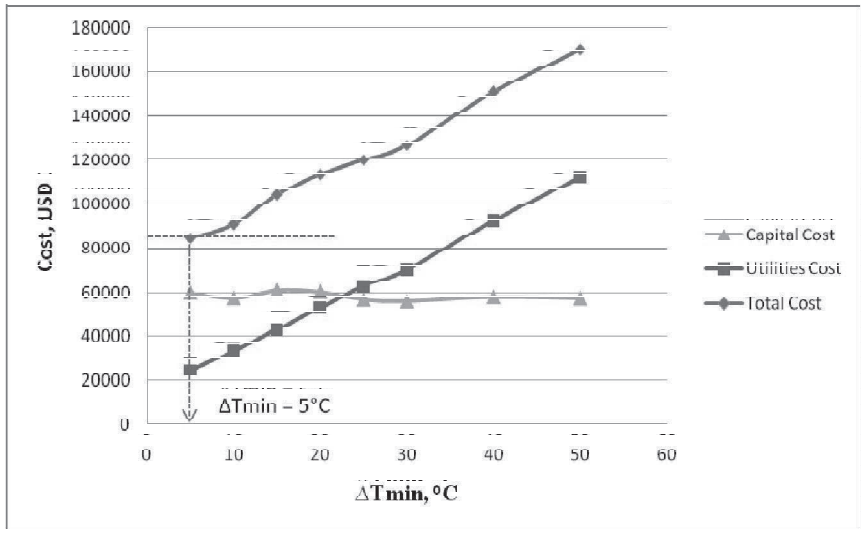

Figure 2: STEP Supertargeting - double-pipe heat exchanger is used for all STEP segments (example 1).

Table 2: Percentage total cost deviations between CC and STEP supertargeting (Case Study 1)

ΔT_{min}, °C	Total Cost, USD/ Yr		Percentage Difference, %
	Composite Curve	STEP	
10	97,755	91,107	6.80
20	104,508	113,572	8.67
30	121,015	126,835	4.81
40	140,534	150,785	7.29
50	159,739	169,877	6.35

4. Conclusion

Supertargeting using CC may lead to inaccurate optimum ΔT_{min} as well as the minimum total cost determination. For the case study considered, an error of up to almost 10% was observed for 6 streams. It is predicted that if there are more composited streams, the error will be bigger. The use of 'composite' to calculate HEN area is the major limitation of the previous methods. The new STEPS method allows the individual heat exchanger capital and utility costs to be considered, leading to an exact total HEN cost calculation. For exact computations of the HEN area, utility costs, the optimum total cost and the optimum ΔT_{min}, supertargeting should be based on the STEP method instead of composite curves.

4. Acknowledgment

The authors would like to thank MOHE (Ministry of Higher Education) Malaysia and UTM for providing the research fund for this project.

References

[1] S. Ahmad, B. Linnhoff, and R. Smith, 1990, Cost Optimum Heat Exchanger Networks-2. Targets and Design for Detailed Capital Cost Models, Computer and Chemical Engineering, 14(7): 751-767.

[2] S. G. Hall, S. Ahmad and R. Smith, 1990, Capital Cost Targets For Heat Exchanger Networks Comprising Mixed Materials Of Construction, Pressure Ratings And Exchanger Types, Computer and Chemical Engineering, Vol. 14, No. 3, pp. 319-335, 1990.

[3] F. 0. Jegede and G. T. Polley, 1992, Capital Cost Targets For Networks With Non-Uniform Heat Exchanger Specifications, Computer and Chemical Engineering, Vol. 16, No. 5, pp. 477-495

[4] U. V. Shenoy, A. Sinha and S. Bandyopadhyay, 1998, Multiple Utilities Targeting For Heat Exchanger Networks, Institution of Chemical Engineers Trans IChemE, Vol 76, Part A.

[5] M. Akbarnia, M. Amidpour and A. Shadaram, 2009, A New Approach In Pinch Technology Considering Piping Costs In Total Cost Targeting For Heat Exchanger Network, Chemical Engineering Research and Design 87 (2009) 357–365.

[6] S. R. Wan Alwi and Z. A. Manan, 2010, STEP - A New Graphical Tool for Simultaneous Targeting and Design of a Heat Exchanger Network, Chemical Engineering Journal, 162, 106–121.

[7] R. Mohammadhasani Khorasanya and M. Fesangharyb, 2009, A Novel Approach for Synthesis of Cost-Optimal Heat Exchanger Networks, Computers and Chemical Engineering, 33, 1363-1370.

[8] W. D. Seider, J. D. Seader and D. R. Lewin, 2010, Product and Process Design Principles-Synthesis, Analysis, and Evaluation. (3rd ed.), John Wiley & Sons (Asia) Pte Ltd.

[9] B. Linnhoff, D. Townsend, D. Boland, G. Hewitt, B. Thomas, A. Guy and R. Marshland, 1982, User Guide on Process Integration for the Efficient Use of Energy (Institute of Chemical Engineers, UK).

I.A. Karimi and Rajagopalan Srinivasan (Editors), Proceedings of the 11th International Symposium on Process Systems Engineering, 15-19 July 2012, Singapore.

Product Driven Process Design Method

Peter M.M. Bongers[a,b], Cristhian Almeida-Rivera[b]

[a]*Chemical Engineering and Chemistry, Eindhoven University of Technology, POBox 513, 5600 MB Eindhoven, peter.bongers@unilever.com*
[b]*Unilever Research and Development, Oliver van Noortlaan 120, POBox 114, 3130 AC Vlaardingen, The Netherlands.*

Abstract

In the last ten years much more processes are being reported to be designed through a process synthesis approach. It has been recognized during those years that (i) processes for structured products are more difficult to design through process synthesis; (ii) process synthesis is disconnected from product development. In a response to those shortfalls a number of authors have described that the gaps need to be filled, however no methodology extension has been proposed.

In this work, we will present extensions to the conceptual process synthesis methodology to include (structured) product design. The whole design methodology spans from how the new product can enlighten the consumer, financial and supply chain boundary conditions, through an optimal flowsheet able to produce the desired product cost effectively. A real case study will be used to illustrate the applicability and scope of the proposed methodology

Keywords: process synthesis, structured products, product development

1. Introduction

All leading fast moving consumer goods companies are rapidly transforming from general manufacturing hubs of loosely connected products to companies delivering health, wellness and nutrition. Manufacturing in a responsible and sustainable way products within strategic areas important for the company imposes technical challenges to work on and requires the development of R&D capabilities. Finding and creating business opportunities to be brought successfully to the market [1] is the response of leading companies to the rapidly changing environment, characterized by slim profit margins and fierce competitiveness. The stage–gate model is a project management tool to effectively manage such initiatives or projects (e.g., new product development, process improvement, business change) throughout companies. Each project is divided into stages separated by gates. At each gate, the continuation of the project is decided. Typically the proceed/re-cycle/stop decision is made by a steering committee. Cooper [2,3] distinguishes five stages: (1) Scoping; (2) Build business case; (3) Development; (4) Testing and validation; (5) Launch. As seen in Figure 1.

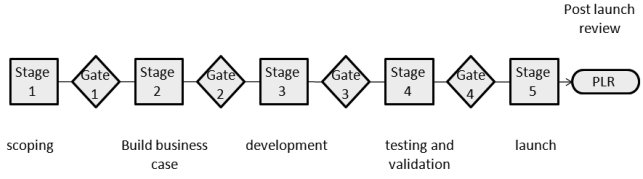

Figure 1 Stage-gate model

The stage-gate model has the clear aim of delivering the right product with all associated benefits at a short time to market and at a reduced manufacturing

expenditure. A key activity in this innovation process (stage-gate model) is the actual creation of the conversion or manufacturing system.
This creative activity referred to as process synthesis (PS), accounts for a cost of 2% of the total design costs and allows fixing 80% of the combined capital and operational costs [4]. In contrast to its relevance, PS is normally carried out by copying existing processes or scaling-up lab scale non-optimized protocols. Our challenge is addressing the PS problem from a systems engineering perspective and proposing a structured approach. Process Synthesis takes place in all conceptual process engineering steps within the innovation process and includes the selection of desired process unit operations, their interconnections and a preliminary design and cost estimation of the major units with key dimensions and operating conditions. Although the definition of PS might suggest a straight-forward and viable activity, the synthesis is complicated by the nontrivial tasks of: (i) identifying and sequencing the physical and chemical tasks to achieve specific transformations; (ii) selecting feasible types of unit operations to perform these tasks; (iii) finding ranges of operating conditions per unit operation; (iv) establishing connectivity between units with respect to mass and energy streams; (v) selecting suitable equipment options and dimensioning; and (vi) control the process operations. Moreover, the synthesis activity increases in complexity due to the combinatorial explosion of potential options. The number of possible combinations can easily run into many thousands [4]. The PS methodology is regarded in this context as a way to beat the problem complexity.

2. A Product-driven Process Synthesis (PDPS) Approach in Foods

It is now well-established by industry and academia that chemical industry focus has shifted from a process- centred orientation to a product-centred one [5]. During the last decades we have experienced how the commodity chemical business is gradually releasing its dominating role towards higher-added value products, such as specialty chemicals and consumer products. This trend is further reflected in the increasing number of scientific publications addressing product and process design [5-8], textbooks [9] and undergraduate/graduate courses in chemical process design [10;11]. In [11] Process Synthesis, for (structured) products is mapped on the stage-gate model as shown in Figure 2.

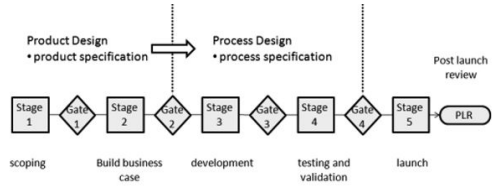

Figure 2 Product-Process design work flow according to [60]

Stretching the boundaries of the synthesis activity towards products has brought challenges for the chemical and process engineers. Those refreshing problems need the development of novel methods and tools, involving areas like the fundamental understanding of the product-process interactions, multi-level modelling of consumer products, property models for products with internal micro-structure, prediction of consumer liking and its dependence on ingredients and processes, etc.
Despite the maturity of most process synthesis approaches for chemical products, they fall short when it comes to extending its scope and applicability to food products. This drawback of current approaches is derived from the intrinsic differences between bulk

chemicals and food products, and include for the case of structure food products: (i) food products are typically structured products where the performance is determined by the internal microstructure of the product (Figure 3); (ii) unit operations are quite different, involving less reaction and separation tasks and more mixing and preservation; (iii) food processes are generally multi product processes, where a same production line can accommodate the manufacturing of different products with different properties; and (iv) cleaning is an essential and non-negotiable task within the operational policy.

Thus, in contrast to bulk chemicals, structured products are characterized not only by the level of each ingredient (i.e. composition, purity, physical state, temperature, pressure, etc.), but also by the relative spatial arrangement of each ingredient and performance behaviour. All these features are responsible for the exclusive attributes of structured products (e.g. creaminess of an ice-cream, spoonability of a mayonnaise, spreadability of a margarine, etc).

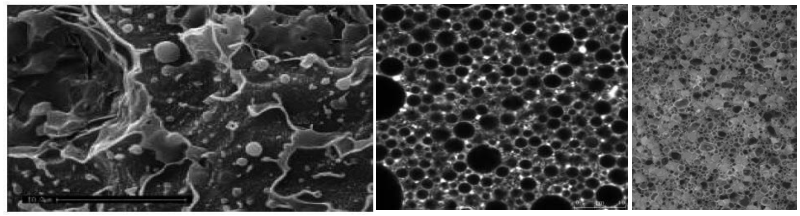

Figure 3. Lamellar structured hair conditioner [5] (left); confocal micrograph of a full-fat O/W emulsion (center); microscope photograph of an ice-cream matrix (right)

Aiming at a more structured approach towards the synthesis of product and processes in the food and drink sector, we proposed a methodology termed product-driven process synthesis (PDPS). This approach exploits the synergy of combining product and process synthesis workstreams and is based on the systems engineering strategy. Thus, it is supported by decomposing the problem into a hierarchy of design levels of increasing refinement (Table 1), where complex and emerging decisions are made to proceed from one level to another.

Table 1. Description of each level of the PDPS approach

Level	Generic description
0	**Framing level**. We embed the design into the overall project. Description of the background of the project and the business context, overall supply chain considerations (product portfolio, demand profiles, regional spread, …)
1	**Consumer wants**. We obtain the consumer wants (consumer likings, focus groups, interviews) in qualitative descriptions and translate them into quantifiable product attributes.
2	**Products.** We identify potential products that meet the consumer wants and map the quantifiable product attributes onto the product properties, which are measurable.
3	**Input-output level.** We make a complete specification of the output. We choose inputs (ingredients) and the descriptors of the output (microstructure, flavour profile and microbiological status). We determine performance parameters such as quality, economic potential, hygienic considerations, flexibility, pumpability, availability...

Table 1 (cont). Description of each level of the PDPS approach

4	**Task network**. We define the fundamental tasks needed to go from input to output, taken from a cluster of tasks and its subgroup. Furthermore, tasks that require a certain sequence or that belong together without any doubt are grouped, to reduce the number of sequencing possibilities. Then, a network is made from the selected tasks and clusters.
5	**Mechanism and operational window**. We select mechanism and principles that can be used to perform a task. This step includes the driving forces and kinetics. Furthermore, the operational window of the problem (time, P, pH, shear, T, etc.) is defined.
6	**Multi product integration**. The outcomes of steps 3 –5 for the different products are compared to look for overlap and possibilities to combine the production.
7	**Equipment selection and design**. The operating units are selected. Integration possibilities (e.g. by combining tasks with the same driving force that are close together in task network) and controllability should be considered. The operational window from step 6 is compared to the operating boundaries of the unit. Then, the final design of the units (only of the key dimension) and final flowchart are made.
8	**Multi product-equipment integration**. We optimise the interaction of the various unit operations in the flowsheet (plant-wide control). Multi-stage scheduling of the multiple products is applied, fed by the run-strategy based on the product demand and portfolio.

Moreover, each level in the PDPS methodology features the same, uniform sequence of activities (scope and knowledge » generate alternatives » analyze performance of alternatives » evaluate and select » report) [12].

The input of the PDPS methodology is a complete and comprehensive specification of the potential raw materials along with any other requirements the process needs to fulfill (e.g. the capacity requirements, cost requirements, hygiene standards, etc).

The method is fed by consumer preference studies and business relevance involving the desired product throughout the whole innovation process (stage-gate model (Figure 4)). In the scoping stage, more effort is put in the "product" design, moving through the gates to the testing and validation stage, more emphasis is put on the "process" design (not neglecting the reality checks with the consumer). This is indicated in bold in Figure 4. Moving through the stage-gate model, the PDPS levels are executed iteratively a number of times. In each iteration, the level of detail will (need to) be increased. For some of the levels, this only means a check if the environment has been changed, and if so, do we need to adapt the product/process.

The output of a process synthesis exercise is a flowsheet structure, along with unit interconnections, operating conditions and key dimensions of key equipment units. Additionally, controllability, reliability and flexibility of the proposed process are accounted for within the methodology. Recent efforts in the development of PDPS methodologies have been focusing on broadening the design scope to consumer preferences, product attributes, process variables and supply chain considerations [12].

The applicability and scope of the proposed methodology has been demonstrated using industrial cases as examples. These case studies include the synthesis of a novel freezing equipment for the production of ice-cream, a novel process for the production of ice-cream premix, a novel process for the production of low-fat starch-free mayonnaise and a bouillon cube manufacturing process.

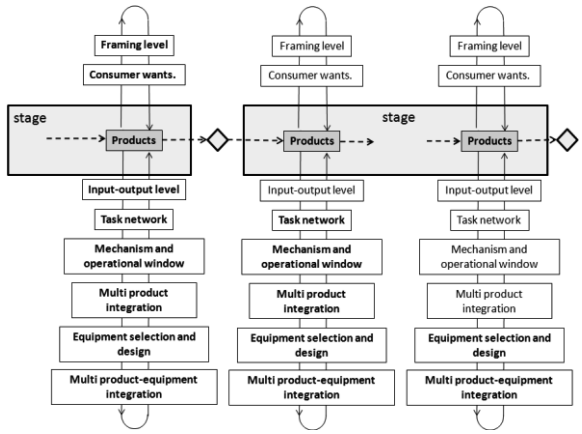

Figure 1. Product Driven Process Synthesis

3. Conclusions

In this contribution we present our approach towards product-driven process synthesis. The proposed methodology is composed of 9 levels of increasing degree of complexity and where complex and emerging decisions are made to proceed from one level to another. The whole methodology spans from how the new product can enlighten the consumer, financial and supply chain boundary conditions, through an optimal flowsheet able to produce the desired product cost effectively. The methodology's applicability and scope have been demonstrated using industrial cases as examples. A model-based strategy was implemented at various levels of the methodology, stressing the relevance of modelling towards more time- and cost-effective process synthesis.

4. References

[1] Verloop, J. (2004). Insight in Innovation - Managing Innovation by Understanding the Laws of Innovation. Amsterdam, Elsevier
[2] Cooper, R.G. (1990). Stage-gate systems: a new tool for managing new products. Business Horizons, p.44-54.
[3] Cooper, R.G. (1996). Overhauling the new product process. Industrial Marketing Management. 25, p.465-482
[4] Douglas, J. (1988). Conceptual design of chemical process. USA, McGraw-Hill
[5] Hill, M. (2004). Product and Process Design for Structured Products. AIChE Journal, 50(8),1656-1661
[6] Gani, R. (2004). Chemical product design: challenges and opportunities. Computers and Chemical Engineering, 28,2441-2457
[7] Edwards, M. F. (2006). Product engineering: Some challenges for Chemical Engineers. Transactions of the Institute of Chemical Engineers - Part A, 84(A4),255-260
[8] Wibowo, C. and Ng, K. M. (2002). Product-Centered Processing: Manufacture of Chemical-Based Consumer Products. AIChE Journal, 48(6),1212-1230
[9] Cussler, E. L. and Moggridge, G. D. (2001). Chemical Product Design. New York, Cambridge Series in Chemical Engineering
[10] Moggridge, G. D. and Cussler, E. L. (2000). An Introduction to Chemical Product Design. Transactions of the Institute of Chemical Engineers - Part A, 78,5-11
[11] Seider, W.D., Seader, J.D., Lewin, D.R., Widagdo, S. (2009) Product and Process Design Principles. Wiley press.
[12] Bongers, P., Almeida-Rivera, C. (2009). Product Driven Process Synthesis Methodology. Computer-Aided Chemical Engineering, 26, 231-236

I.A. Karimi and Rajagopalan Srinivasan (Editors), Proceedings of the 11th International Symposium on Process Systems Engineering, 15-19 July 2012, Singapore.

Sensitivity of Process Design due to Uncertainties in Property Estimates

Amol Hukkerikar[a], Mark Jones[a], Bent Sarup[b], Jens Abildskov[a], Gürkan Sin[a], and Rafiqul Gani[a]
[a] *CAPEC, Department of Chemical and Biochemical Engineering, Technical University of Denmark, DK-2800, Kgs.Lyngby, Denmark.*
[b] *Vegetable Oil Technology Business Unit, Alfa Laval Copenhagen A/S, Maskinvej 5, DK-2860, Søborg, Denmark.*

Abstract
The objective of this paper is to present a systematic methodology for performing analysis of sensitivity of process design due to uncertainties in property estimates. The methodology provides the following results: a) list of properties with critical importance on design; b) acceptable levels of accuracy for different thermo-physical property prediction models; and c) design variables versus properties relationships. The application of the methodology is illustrated through a case study of an extractive distillation process and sensitivity analysis of designs of various unit operations found in chemical processes. Among others vapour pressure accuracy for azeotropic mixtures is critical and needs to be measured or estimated with a ±0.25% accuracy to satisfy acceptable safety levels in design.

Keywords: Process design, sensitivity analysis, uncertainty, property prediction.

1. Introduction
The accuracy and reliability of the process design depends largely on the accurate physical and thermodynamic data and property models employed (Whiting, 1996). Since experimental values of many of the needed pure component and mixture properties cannot be expected to be measured, they must therefore be estimated. Also, process design involving new molecules/mixtures require their properties to be predicted through a suitable model. In such cases, it is important to know the uncertainties of the estimated property values that arise due to uncertainties in the regressed parameters of the selected property model (Hukkerikar et al., 2012). With this information, it is possible to answer the following two questions: (i) what is the effect of uncertainties in the property estimates on the design, and, (ii) which properties are the most sensitive from a process design point of view? These questions, once answered, can provide useful and critical insights into reliability of process design and eventually suggestions for further improvement.
In this paper we present a systematic methodology to establish the sensitivities of process design due to uncertainties in property estimates and to evaluate their effects on the final design; to list the properties based on their sensitivities; to establish acceptable levels of accuracy for different thermo-physical property prediction models; and to provide relationships between design variables and properties.

2. Methodology
The main steps of the systematic methodology for performing the sensitivity analysis for process design are shown in Figure 1.

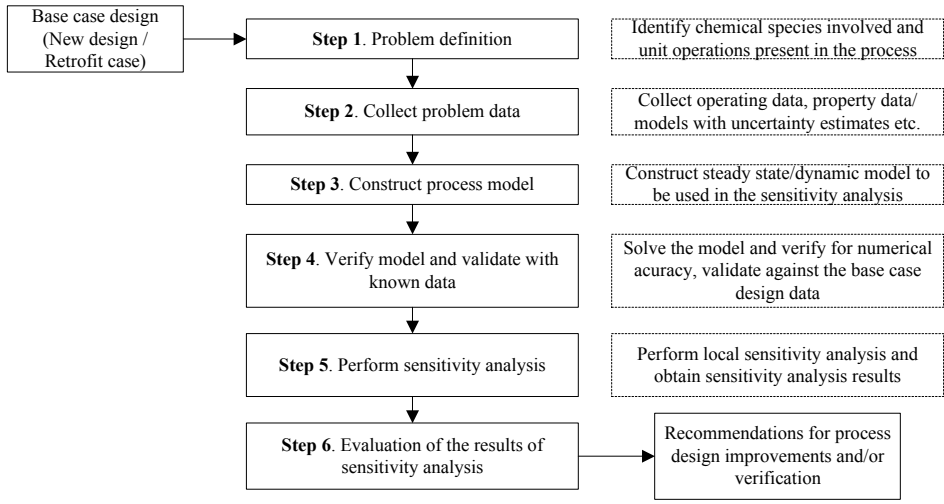

Figure 1. Methodology for performing the sensitivity analysis for process design

2.1. Step 1: Problem definition

In this step, the process (base case) for which sensitivity analysis is to be performed is defined. Information such as the chemical species involved, the unit operations present in the process is also defined.

2.2. Step 2: Collect problem data

The problem data is collected in this step. This includes operating data of the process, desired specifications, kinetics data (if reactions are involved), data related to economic evaluation, equipment data, property data and models of concerned properties together with uncertainties of the predicted property values.

2.3. Step 3: Construct process model

The objective of this step is to construct a model for the process under study so that the effects of change in property estimates can be analysed. The model may be steady state and/or dynamic, depending on the problem definition. Note that the property models belong to the constitutive equations that are part of the process model.

2.4. Step 4: Verify model and validate with known data

The process model is solved. The obtained simulation results are verified for numerical accuracy and validated against base case design data.

2.5. Step 5: Perform sensitivity analysis

Local sensitivity analysis (one-factor-at-a-time approach) is employed. The local sensitivity is the sensitivity of the model output when only one input factor (for example, vapor pressure) is perturbed at a time while keeping all other input factors fixed at their base case design values. The obtained sensitivity analysis results are represented in the form of plots showing relationships between design variables and the properties involved. The y-axis represents the deviation (expressed as relative error in %) of the design variables from its base case design value and the x-axis represents the expected prediction error (in %) in the properties.

2.6. Step 6: Evaluation of the results of sensitivity analysis

The objective of this step is to analyze the relationships between design variables and properties and evaluate the impact of uncertainties in the predicted properties on the design. This involves: (i) examining the slope of plot of design variable versus property

prediction error and identifying the most sensitive properties (a large slope implies that sensitivity of the design variable is high and the uncertainties in the property estimates are significant); (ii) analyzing the possible consequences (such as, effect on capital and operating cost) of property errors on the process design; and (iii) establishing an acceptable level of accuracy for property models based on the maximum allowable deviation (as specified by the user) in the design variable from its base case design value. The analysis carried out in step 6 can be used as an input to a process design tool for improvement in the design. The application of the methodology is illustrated using a case study of process design of extractive distillation.

3. Case Study: Sensitivity of extractive distillation design

3.1. Step 1: Problem definition

It is required to perform sensitivity analysis for design of an extractive distillation process (employed to separate acetone from methanol using water as an entrainer; to obtain a product of at least 99.4% of acetone) subject to uncertainties in the property estimates. Uncertainty estimates of property models are available.

3.2. Step 2: Collect problem data

The operating data of the extractive distillation process is collected from Gil et.al. (2009). The involved single value pure component properties and temperature-dependent properties are collected from the SIMSCI library available in PRO/II®. The UNIQUAC model is employed to calculate the liquid phase activity coefficients while the vapor phase is assumed to behave as an ideal gas.

3.3. Step 3: Construct process model

A steady state simulation model of the extractive distillation process is constructed in PRO/II®. The pure component properties involved in the design calculations are: (i) vapor pressure (P^s), (ii) critical temperature (T_c), (iii) heat of vaporization (H_{vap}), (iv) liquid density (ρ), (v) liquid viscosity (μ), (vi) surface tension (σ), and (vii) activity coefficient (γ). The design variables considered for sensitivity analysis are: (i) number of stages (N), (ii) reflux ratio (R), (iii) binary feed stage (N_f), (iv) entrainer stage (N_s), (v) column diameter (D), and (vi) reboiler (Q_r) and condenser (Q_c) heat duties.

3.4. Step 4: Verify model and validate with known data

The model is solved in PRO/II® and the obtained results are compared and validated against the results given by Gil et.al. (2009). A good match is obtained.

3.5. Step 5: Perform sensitivity analysis

The results of sensitivity analysis for selected design variables with respect to uncertainties in the selected predicted properties are shown in Figure 2. When necessary, chain rule is applied to obtain relationships between the design variables and the properties analysed. For example, to obtain sensitivity of N_s with respect to uncertainties in the predicted P^s, the following chain rule is applied: $[\partial R/\partial P^s]*[\partial N_s/\partial R] = [\partial N_s/\partial P^s]$. In Figure 2, the results are reported for only those simulations in which a converged solution satisfying the desired product purity is obtained from PRO/II®.

3.6. Step 6: Evaluation of the results of sensitivity analysis

Figure 2(a)-2(c) shows that even small errors in the predicted P^s of acetone and water may result in significant uncertainty in the design. The uncertainty (in terms of average relative error) of predicted P^s of acetone from DIPPR correlation used in PRO/II® is ±0.25%. This level of accuracy of P^s is found to have significant impact on the calculation of R, N and N_s (up to 20% deviation from base case). If this level of uncertainty in R, N and N_s is not acceptable then user needs to collect a higher accuracy

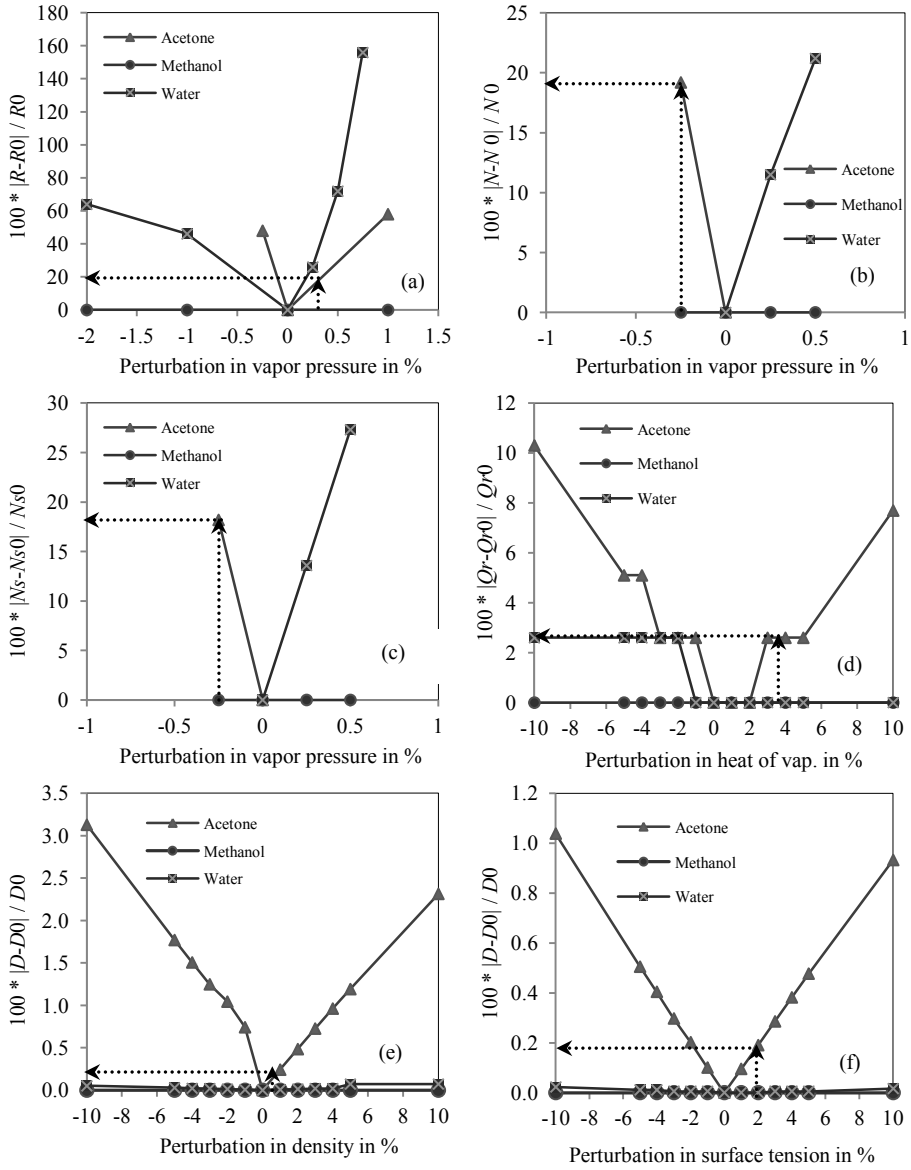

Figure 2. Sensitivity of *R, N, N_s, Q_r,* and *D* with respect to uncertainties in the predicted property values. *R0*, *N0*, N_s0, Q_r0, and *D0* represent the base case values and zero point on the x-axis represents the base case design.

data for P^s and use this data in regression to obtain improved model for P^s with desired accuracy level (i.e. error less than ±0.25%). The uncertainty of predicted H_{vap}, ρ, and σ of acetone from DIPPR correlation used in PRO/II® is ±3.44%, ±0.38%, and ±1.77% respectively. It can be seen from Figure 2(d) that accurate predictions of H_{vap} of acetone is important to reduce the uncertainty in calculation of Q_r. The sensitivities of *D* to prediction errors in ρ and σ are shown in Figures 2(e)-2(f). From Figures 2(a)-2(f), it can be seen that the most sensitive properties are P^s of acetone and water and H_{vap} of acetone. For this case study, process design without the consideration of uncertainties of

the predicted P^s and H_{vap} of acetone and P^s of water may lead to following consequences: (i) an overestimate (+ve or –ve) of R (which is undesirable from an operation point of view); (ii) an overestimate (+ve or –ve) of N and N_s resulting in an inefficient operation; and (iii) an overestimate (+ve or –ve) of Q_r and hence waste of utilities. This information serves as input for a process design tool to carry out further improvements. The uncertainty of design variables R, N, N_s, Q_r and D due to given uncertainties in predicted P^s, H_{vap}, and ρ is 20.0%, 18.0%, 17%, 2.5% and 0.20% respectively. The sensitivity of process design of several other unit operations have also been analysed. The results are summarized in Table 1.

Table 1. Results for sensitivity analysis of process design of unit operations analysed

Unit operation (chemical system involved)	Reference for problem data / required task	Properties inolved in the analysis	Variables considered for sensitivity analysis / most important properties (ranked)
Short-path evaporator (Glycerol + Mono-, Di-, and Tri-glyceride)	Sales-Cruz & Gani (2006) / separate glycerol from the mixture	P^s, T_c, P_c, H_{vap}, μ, specific heat (C_p), acentric factor (ω), and γ	Distillate (glycerol) flow rate / P^s of glycerol, γ of glycerol, ω of di-glyceride, P_c of di-glyceride C_p of glycerol and di-glyceride, T_c of glycerol, H_{vap} of di-glyceride.
Batch distillation (Multicomponent mixture of A, B, C, and D)	ICAS-MoT® / separate A from the mixture	Relative volatality ($\alpha = P^s/P^s_{ref}$)	Purity of A in the distillate / α of component A
Flash process (methanol and water)	ICAS-MoT® / Separate methanol from the mixture	P^s, T_c (used in the correlation for H_{vap}), and ρ	Product (methanol) flow rate / T_c of methanol, P^s of methanol, ρ of methanol Volume of the flash tank / T_c of methanol, ρ of methanol

4. Conclusions

In this work, a systematic methodology to analyze the sensitivity of process design due to uncertainties in property estimates is presented. The application of the methodology is highlighted through several examples. The results of the sensitivity analysis helps to establish relationships between design variables and properties; allows evaluation of the impact of uncertainties in the property estimates on the process design; and helps to identify the most sensitive properties from a process design point of view, thereby, contributing to better-informed and reliable design solutions. Our current and future work is focussed on evaluation of effect of uncertainties of predicted mixture properties (such as, liquid activity coefficient) on the process design.

References

W.B. Whiting, 1996, Journal of Chemical & Engineering Data, 41, 935-941.

A.S. Hukkerikar. B. Sarup, A. Ten Kate, J. Abildskov, G. Sin, and R. Gani, 2012, Fluid Phase Equilibria, 321, 25-43.

Integrated Computer Aided System (ICAS version 14.0), Department of Chemical Engineering, Technical University of Denmark, Lyngby, Denmark, 2010.

I.D. Gil, D.C. Botia, P. Ortiz, and O.F. Sanchez, 2009, Industrial Engineering and Chemical Research, 48, 4858-4865.

M. Sales-Cruz and R. Gani, 2006, Chemical Engineering Research and Design, 84, 583-594.

I.A. Karimi and Rajagopalan Srinivasan (Editors), Proceedings of the 11th International Symposium on Process Systems Engineering, 15-19 July 2012, Singapore.

An integrated quantitative index of stable steady state points in chemical process design

Hangzhou Wang, Bingzhen Chen *, Tong Qiu, Xiaorong He, Jinsong Zhao

Department of Chemical Engineering, Tsinghua University, Beijing 100084, China

Abstract

In order to design inherently safer chemical processes, researchers proposed many methods and strategies, many quantitative indices have been developed to describe the potential hazard and dangerous of different reaction routes and reactants. Because in emergency situation the disturbance may be so large that the system can not return back to the steady state points. For considering both situations under small and large disturbances, this paper proposed a quantitative index (QI), in which disturbance range index (RI) and convergence speed index (SI) were integrated, considering both capability of resistance to disturbances and speed to return to steady state point. Based on the integrated index, this paper proposed an approach for designing a more stable chemical process that can maintain stable within larger region to resist the disturbance and has shorter time to approach to the original stable steady state operation point when disturbance is encountered. The approach is applied to methyl methacrylate polymerization process and a multi-objective optimization problem considering both economic and stability factors were conducted and a Pareto set is obtained.
Keywords: inherently safer; process design; quantitative index; multi-objective optimization

1. Introduction

The concept of inherently safer design was proposed by Kletz, the main concept is that avoids hazards instead of controlling them. Also Kletz proposed many methods and strategies for engineering such designs in practice. Hendershot reviewed the development of inherently safer design strategies in chemical processes. Stability describes the behavior of a system when a disturbance is encountered. Because of the complexity and non-linearity of chemical processes, a system may have multiple steady states and the stabilities of these operating points are different even in the same reaction route. Uppal, Balakotaiah, Yuan and Razon theoretically analyzed the multiple steady state solutions of reactors. Flores-Tlacuahuac, Katariya and Mancusi analyzed more complex chemical processes. Seider also studied multiple steady state solutions of reactors. In the existing related works, only Meel proposed a quantitative index to describe the instability of unstable points. In authors' previous paper a universal quantitative index based on the time for convergence to a stable point under a given small disturbance is introduced. However, even stable steady state operation points have different stabilities from one to another, so it is important to develop a quantitative index of stability for these steady state points. Such an index would play an important role in comparing the stabilities of given operating points or optimizing the process operation conditions.

2. Process design approach

Because in emergency situation the disturbance may be so large that the system can not return back to the steady state points. For considering both situations under small and large disturbances in dynamic model of chemical process

$$\begin{cases} \dfrac{d\mathbf{x}}{dt} = \mathbf{F}(\mathbf{x}) \\ \mathbf{x}(0) = \mathbf{x}^* + \Delta\mathbf{x} \end{cases}$$

Where x* is the steady state solution, $\Delta\mathbf{x}$ is the disturbance. The Jacobian matrix of $\mathbf{F(x)}$ is $\mathbf{F_x}$, and the eigenvalue of $\mathbf{F_x}$ is λ_i. We define disturbance range index

$$RI = \frac{\max(\Delta x^+) + \max(\Delta x^-)}{x^*}$$

where $\Delta x^+ \le x^*$, $\Delta x^- \le x^*$, Δx^+ and Δx^- are positive and negative disturbances of focused variable, respectively. We also define convergence speed index

$$SI = \left| \frac{\prod_{i=1}^{n} \lambda_i}{\sum_{i=1}^{n} \prod_{j=1, j\neq i}^{n} \lambda_i} \right|$$

After normalized RI and SI, we define a quantitative index

$$QI = \min(RI, SI)$$

QI considers both capability of resistance to disturbances and speed to return to steady state point. Based on the integrated index, this paper proposed an approach for designing a more stable chemical process that can maintain stable within larger region to resist the disturbance and has shorter time to approach to the original stable steady state operation point when disturbance is encountered. The detailed steps of this approach are illustrated as follows:

(1) Solve the steady state solution of the dynamic model of chemical process.
(2) Judge the stability of these solutions and distinguish the stability of these solutions, divided the solution curve into parts with different stabilities (stable and unstable).
(3) Calculate RI, the larger RI is the larger convergence range does.
(4) Calculate SI, the larger SI is the faster convergence speed does.
(5) Calculate QI, and QI is better when it is larger.
(6) Use QI for multi-objective process operation optimization.

The approach is applied to methyl methacrylate polymerization reactor process, and a multi-objective optimization problem considering both economic and stability factors was conducted, a Pareto set is obtained. The optimization results provide information that is very important for guiding process design and operation.

3. Case study

Methyl methacrylate (MMA) is an important chemical product and an MMA polymerization reactor is shown in Fig. 1 below.

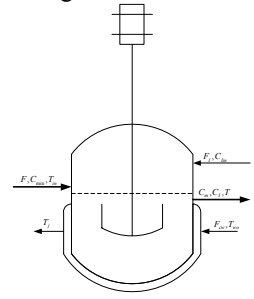

Figure 1 Polymerization reactor flow sheet

For free-radical polymerization, the following elementary reactions are postulated:

Initiation	$I \xrightarrow{k_D} 2R \quad M+R \xrightarrow{k_1} P_1$
Propagation	$P_i + M \xrightarrow{k_p} P_{i+1}$
Monomer transfer	$P_i + M \xrightarrow{k_{fm}} P_i + D_i$
Addition termination	$P_i + P_j \xrightarrow{k_{td}} D_{i+j}$

Disproportionation termination $P_i + P_j \xrightarrow{k_{td}} D_i + D_j$

where I, P, M, R, and D stand for initiator, polymer, monomer, radicals and dead polymer, respectively. The mathematical model for this reactor is given by:

$$\frac{dC_m}{dt} = -(k_p + k_{fm})C_m P_0 + \frac{F(C_{min} - C_m)}{V}$$
$$\frac{dC_I}{dt} = -k_I C_I + \frac{F_I C_{Iin} - FC_I}{V}$$
$$\frac{dT}{dt} = \frac{-\Delta H k_p C_m}{\rho C_p} P_0 - \frac{UA}{\rho C_p V}(T - T_j) + \frac{F(T_{in} - T)}{V}$$
$$\frac{dD_0}{dt} = (0.5k_{tc} + k_{td})P_0^2 + k_{fm} C_m P_0 - \frac{FD_0}{V}$$
$$\frac{dD_1}{dt} = M_m(k_p + k_{fm})C_m P_0 - \frac{FD_1}{V}$$
$$\frac{dT_j}{dt} = \frac{F_{cw}(T_{w0} - T_j)}{V_0} + \frac{UA(T - T_j)}{\rho_w C_{pw} V_0}$$

where

$$P_0 = \sqrt{\frac{2f^* C_I k_I}{k_{td} + k_{tc}}}$$
$$k_r = A_r e^{\frac{-E_r}{RT}}, \quad r=p, fm, I, td, tc$$

The parameter values of the model are listed below in Tab. 1.

Table 1. Parameters for the MMA polymerization reactor

Parameter	Value	Unit	Parameter	Value	Unit
F	1.0	m^3/h	M_m	100.12	kg/kmol
F_I	0.0032	m^3/h	f^*	0.58	—
F_{cw}	0.1588	m^3/h	R	8.314	kJ/(kmol K)
C_{min}	6.4678	$kmol/m^3$	$-\Delta H$	57800	kJ/kmol
C_{Iin}	8.0	$kmol/m^3$	E_p	1.8283*10^4	kJ/kmol
T_{in}	350	K	E_I	1.2877*10^5	kJ/kmol
T_{w0}	293.2	K	E_{fm}	7.4478*10^4	kJ/kmol
U	720	kJ/(h K m^2)	E_{tc}	2.9442*10^3	kJ/kmol
A	2.0	m^2	E_{td}	2.9442*10^3	kJ/kmol
V	0.1	m^3	A_p	1.77*10^9	m^3/(kmol h)
V_0	0.02	m^3	A_I	3.792*10^18	1/h
ρ	866	kg/m^3	A_{fm}	1.0067*10^15	m^3/(kmol h)
ρ_w	1000	kg/m^3	A_{tc}	3.8228*10^10	m^3/(kmol h)
C_p	2.0	kJ/(kg K)	A_{td}	3.1457*10^11	m^3/(kmol h)
C_{pw}	4.2	kJ(kg K)			

The steady state operation points for this model are shown in Fig. 2. It can be seen that monomer concentration changes with effluent value, and there are multiple steady states in this process.

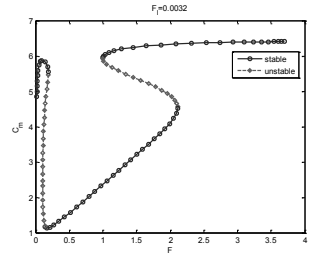

Figure 2 Changes in monomer concentration and temperature with effluent value

Changes in RI, SI and QI with effluent in part 1, 2 and 3 are shown in Fig. 3, 4 and 5.

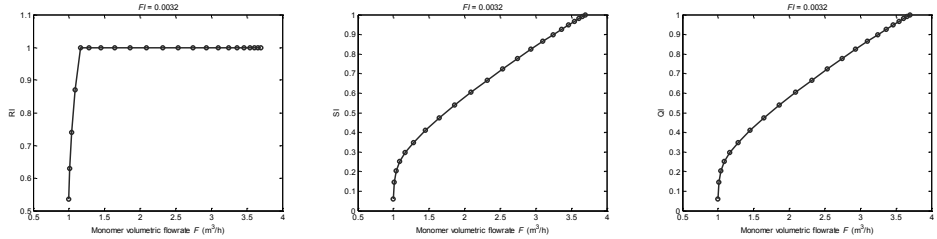

(a) RI with effluent (b) SI with effluent (c) QI with effluent

Figure 3 Changes in RI, SI and QI with effluent(Part 1)

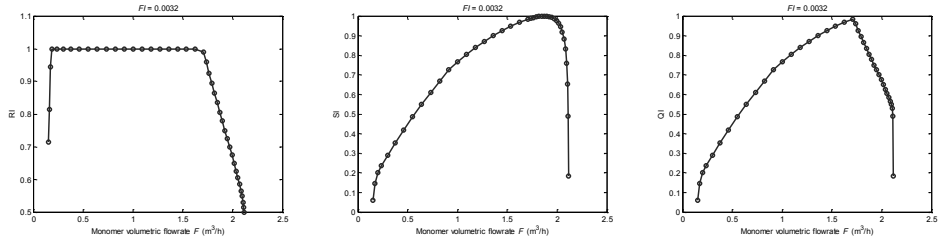

(a) RI with effluent (b) SI with effluent (c) QI with effluent

Figure 4 Changes in RI, SI and QI with effluent(Part 2)

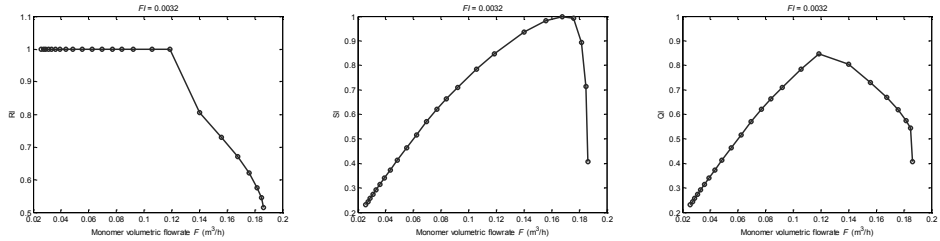

(a) RI with effluent (b) SI with effluent (c) QI with effluent

Figure 5 Changes in RI, SI and QI with effluent(Part 3)

When economy and inherent safety are considered as the main factors in chemical process design, the concentration of monomer indicates the reaction efficiency, and it could indicate process economy. The proposed quantitative stability index could indicate the inherent safety of the reaction. Consequently selecting operation points is a multi-objective (monomer concentration and quantitative stability index) optimization problem. The optimization result is a Pareto set, shown in Fig. 6.

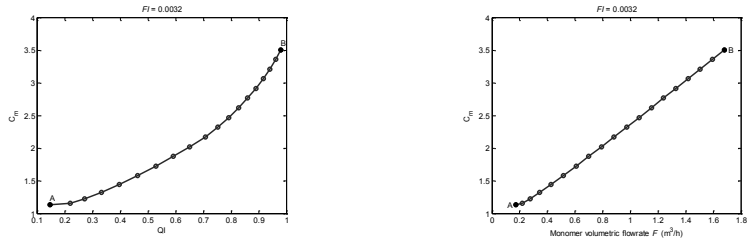

(a) Changes in concentration and quantitative stability indices (b) Changes in concentration with effluent value

Figure 6 Optimization result for the multi-objective: economy and stability (Pareto sets)

Point A is the maximum economic operation point where the monomer with the highest reaction efficiency and point B is the maximum inherent safety point where the convergence time is shortest when a disturbance is encountered and the resistance range of disturbance is the largest at the same time. These values of are listed in Tab. 2.

Table 2. Values of operating points A and B

Points	F	Cm	QI
A	0.173	1.132	0.146
B	1.679	3.505	0.979

In process design the final operation point would be determined from the optimized Pareto set according to the detailed economical and safety requirement.

4. Conclusion

From this study, conclusions can be drawn:

(1) Stability is an important factor in design of an inherently safer chemical process.
(2) Quantitative stability index is useful in multi-objective optimization problem when stability was considered as one of the objectives.

5. Acknowledgements

The authors gratefully acknowledge financial support from National Basic Research Program of China (Grant No. 2012CB720500).

References

V. Balakotaiah, D. Luss, 1984, Global Analysis of the Multiplicity Features of Multi-Reaction Lumped-Parameter Systems. Chemical Engineering Science, 39, 5, 865-881.
E. Gazi, W. D. Seider, L. H. Ungar, 1996, Verification of controllers in the presence of uncertainty: Application to styrene polymerization. Industrial & Engineering Chemistry Research, 35, 7, 2277-2287.
K. S. Gritton, J. D. Seader, W. J. Lin, 2001, Global homotopy continuation procedures for seeking all roots of a nonlinear equation. Computers & Chemical Engineering, 25, 7/8, 1003-1019.
D. C. Hendershot, 2006, An overview of inherently safer design. Process Safety Progress, 25, 2, 98-107.
F. Jalali, J. D. Seader, S. Khaleghi, 2008, Global solution approaches in equilibrium and stability analysis using homotopy continuation in the complex domain. Computers and Chemical Engineering, 32, 10, 2333-2345.
A. Katariya, K. Moudgalya, S. Mahajani, 2006, Nonlinear dynamic effects in reactive distillation for synthesis of TAME. Industrial and Engineering Chemistry Research, 45, 12, 4233-4242.
T. Kletz, 1978, What you don't have, can't leak. Chemistry and Industry, 6, 287-292.
A. Meel, W. D. Seider, M. Soroush, 2006, Game theoretic approach to multiobjective designs: Focus on inherent safety. AIChE Journal, 52, 1, 228-246.
L. F. Razon, 2006, Stabilization of a CSTR in an oscillatory state by varying the thermal characteristics of the reactor vessel. International Journal of Chemical Reactor Engineering, 4, 1320-1329.
W. D. Seider, D. D. Brengel, A. M. Provost, S. Widagdo, 1990, Nonlinear-Analysis in Process Design - Why Overdesign to Avoid Complex Nonlinearities. Industrial and Engineering Chemistry Research, 29, 5, 805-818.
A. K. Trevor, 2003, Inherently Safer Design-Its Scope and Future. Institution of Chemical Engineers Trans IChemE, 81, Part B, 401-405.
H. Z. Wang, Z. H. Yuan, B. Z. Chen, X. R. He, J. S. Zhao, T. Qiu, 2011, Analysis of the stability and controllability of chemical processes. Computers & Chemical Engineering, 35, 6, 1101-1109.
Z. H. Yuan, H. Z. Wang, B. Z. Chen, J. S. Zhao, 2009, Operating zone segregation of chemical reaction systems based on stability and non-minimum phase behavior analysis. Chemical Engineering Journal, 155, 1-2, 304-311.
Q. P. Yuan, Z. M. Qian, 2003, The Study on Static Bifurcation Behavior of the Immobilized Yeast Spherical Beads for Ethanol Production, Journal of Chemical Engineering of Chinese Universities, 17, 5, 527-533.

I.A. Karimi and Rajagopalan Srinivasan (Editors), Proceedings of the 11th International Symposium on Process Systems Engineering, 15-19 July 2012, Singapore.

Applicability of product-driven process synthesis to separation processes in food

Lena Jankowiak[a], Atze J. van der Goot[a], Olivera Trifunovic[b], Peter M.M. Bongers[b], Remko M. Boom[a]

[a]*Laboratory of Food Engineering, Wageningen University, P.O. Box 8129, 6700 EV Wageningen, The Netherlands*
[b]*Unilever Research, P.O. Box 114, 3130 AC Vlaardingen, the Netherlands*

Abstract

The demand for more sustainable processing in the food industry is rising but requires structured methodologies to support the fast implementation of new economic and sustainable processes. Product-driven process synthesis (PDPS) is a recently established methodology facilitating the rapid development of feasible process alternatives for structured products, such as in mayonnaise, ice-cream, or margarine.
Here, we present the application of the PDPS methodology to valorize okara, which is a by-product from soy milk production. It is produced in large amounts, but its use as food or feed is not fully exploited. Besides fibers, protein, and fat, it contains substantial amounts of isoflavones, which are high value components. This paper evaluates the PDPS-methodology for the design of an economic and sustainable process for the production of isoflavones from okara. The main challenge is to adapt the method in such a way that it is able to deal with a complex matrix as starting material. Therefore, the PDPS methodology may require extension. Nevertheless, it promises to be a useful tool also for fractionation of food materials.

Keywords: Product-driven process synthesis, separation, okara, isoflavones.

1. Introduction

During the last decade, conventional product design and process design have been combined into product-oriented process synthesis. An important component of this methodology is aimed at the generation and screening of alternative flow sheets. Conceptualization retards the fixation of a flow sheet, which reduces the risks of irreversible mistakes during the design of a process. However, the process synthesis methodologies have to be updated concomitantly due to the dynamics within the industry, such as a shifting product portfolio, new economic situations, new regulations, and sustainability concerns [1].
Process synthesis has been developed mainly for chemical products until the similarities between complex chemical consumer goods and structured food products were recognized [2-6]. The latter explains the growing interest of the food industry to translate conceptual design methodologies from the chemical sector into the food sector. Therefore, Bongers and Almeida-Rivera (2009) suggested a new methodology combining product and process synthesis based on the systems engineering strategy. This methodology, called product-driven process synthesis (PDPS), eases the complexity of the problem by dividing the problem into several hierarchically ordered

levels. Each level requires important and complex decisions, which allows the user to strategically go from one level to the next one [7, 8].
In this paper we describe in which way PDPS should be further developed to make it applicable for separation processes in food. Refinery of biomaterials is now increasingly important and the separation of high value components is a method to improve the economic potential of bio refinery processes. Okara, a by-product of the soy milk industry, is used as a case study.

2. Applications of PDPS in the food industry

Food microstructure largely determines the properties and, consequently, the consumer acceptance of a food. Contrary to chemical products, spatial distribution of the foods' ingredients is a key attribute of the product, because it largely determines texture, sensory, flavor, and mechanical properties [8, 9].
The PDPS methodology is divided into several levels as described in detail by Bongers and Almeida-Rivera (2009) [8]. The core of the methodology is in levels 1 to 3. Level 1 describes the input and output, level 2 asks for the development of the task network, and level 3 describes the mechanisms and operational window. The most recent application of PDPS is described by Gupta and Bongers (2011) [10]. The authors redesigned a bouillon cube production process by applying PDPS resulting in improved structure of the product, shorter cooling times, and reduction of redundant ingredients. Other examples of structured food products, where the PDPS approaches were practical, are mayonnaise, dressings, and ice-cream [8, 9]. Such food products have one thing in common: they are made by combining single ingredients, and the production process has to consider the interplay of ingredients to obtain the desired end product with the preferred attributes and microstructure.

3. Applicability of PDPS for a separation process

Hostrup et al. (1999) presented an integrated approach of product design and separation process synthesis for chemical processes [11]. The authors used an optimization-based approach combining mathematical modeling with heuristics to design a solvent and a separation process simultaneously. One of the key success factors was the availability of thermodynamic data of the system. However, such approach is difficult to realize for structured food products, since detailed thermodynamic models are generally not available for complex food systems.
The use of PDPS to design a separation process is more complex than for the design of a final structured product. This can be demonstrated by comparing a case in which a three component product is formed, and in which such a product is separated into its building blocks. First, we show how the PDPS methodology works in case a product contains three hypothetical ingredients: A, B and C. In level 1 the input stream and output stream are defined. Thus, the input has to contain component A, component B, and component C. The process can be modified according to the order in which the ingredients are added, but the output is in any case a mixture of component A, B, and C. In the case of a separation process the output is not as straightforward. If the input consists of a structure ABC, the output greatly depends on the process, and the input can result in at least two options for the output. Assuming the main interest is in component A, the options are the following: ABC = A+B+C or ABC = A+BC

The first option can also be obtained by two more options:
ABC = C+AB ➔ C+A+B or ABC = B+AC ➔ B+A+C
The more components the starting material contains, the higher the number of options that should be considered when defining the input and output, and sequences of separation in the task network. The existence of more possibilities for the input/output level is not the only challenge. In case of separation, a component will never be completely separated and will contain certain impurities (e.g. A+*A*BC or A*BC*+BC). Many ratios and combinations of components are possible, which complicates building task networks if limited experimental results are available, and information about the thermodynamics on the process and components is incomplete.

4. Case study: Separation of isoflavones from okara

In contrast to previous approaches where a microstructure had to be established, the starting material in the following case is a structured by-product of the food industry (okara), which has to be decomposed to produce a single ingredient to fully utilize the economic potential of okara.
Being the insoluble part after water extraction of the soybeans, okara contains predominantly insoluble fibers. Additionally, depending on soybean variety and processing conditions, okara contains isoflavones, often present in a range of 0.1-0.2% (db) [12-14]. Isoflavones are minor components belonging to a group of polyphenols and having a high potential economic value due to suspected health benefits [15, 16].
The value of the end product, the isoflavones, can be estimated by comparison to similar, commercially available products. Information about available margins for the process can be obtained by comparing the input value of okara and the output values. Those calculations showed that the economic potential is highest if the output consists of isoflavones in powder form of high purity (>70%).
Further design rules were defined and comprise the following:

- To avoid production of further unutilized waste
- The process should be sustainable regarding energy, water, and chemical usage
- The isoflavone mixture should have a certain purity, be in powder form, food-grade, and microbiological stable

As far as we are aware of, okara is not used as a starting material for isoflavone production yet. Therefore, experiments have to be performed to support decision making during process synthesis.

4.1. Level 1 Input and output

A major difference to the conventional application of PDPS appeared already when the input and output were defined. At this level, the process is only represented with a black box with an incoming stream (input) and an outgoing stream (output).
The only certainty at this stage is the input, namely okara. Moisture content and major components of the material were measured to further characterize the input (Tab.1).

Table 1 Characterization of okara

Moisture (%)	Carbohydrates (% db)		Proteins (% db)	Fat (% db)	Isoflavones (%db)
	Sugars (%)	Uronic acid (%)			
81 ± 0.5	47.5 ± 3.3	6.1 ± 0.2	32.0 ± 0.4	14.6 ± 0.03	0.12 ± 0.01

The output can be twofold. The isoflavones should either be separated in a way that the residual material can still be used, for example as animal feed, thus having the same composition as before only absent of isoflavones. The other option involves separation of several components, which could allow the use of other components as a food ingredient (e.g. soy protein isolate).
The black box representing the process is now evaluated in more detail in the following step, the task network level, as will be described in the following section.

4.2. Level 2 Task network

The basic class of task is defined as separation. We define it as the separation of isoflavones from the rest of the matrix (Fig.1).

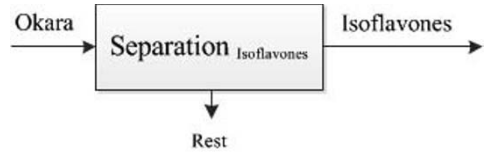

Figure 1 Class of task: separation of isoflavones from okara

To be more specific, a task network could look like in Fig. 2 including some more fundamental tasks.

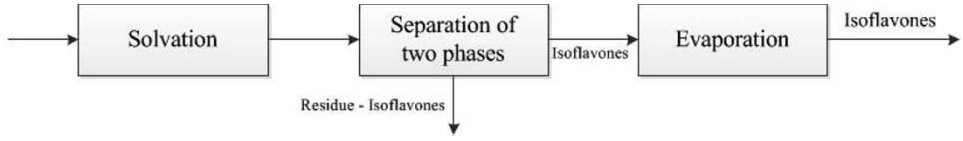

Figure 2 Example of a task network for separation of isoflavones from okara

Okara is a fibrous material, and the isoflavones are in relatively low concentrations present compared to other components. It is assumed that some sort of liquid is available for the disclosure of the isoflavones from the fibrous matrix. Solvation means in this case dissolution of okara in a liquid. Then the liquid, which we assume contains all the isoflavones after some time, has to be separated from the rest of the matrix. Last but not least, one of our design rules says that a dry powder is required. Thus, concentration and solidification (e.g. through evaporation) will be necessary, very likely as the last step of the process. However, at an early stage, there are many possible task networks, and Fig. 2 is only one example. A conservative estimation of the number of possibilities is 12, considering different sequences of separation of the components of okara. This increased number requires insight in the behavior of the materials, and thus, the involvement of experimental experience at an earlier stage compared to the PDPS for a structured product. Experiments are needed to narrow down the possibilities and refine or substitute those fundamental tasks. Thus, an ongoing alternating process between design and experiments seems to be required to reach the final process design.
The PDPS methodology, however, supports and guides the user to be aware of all possibilities and to allow motivated decisions. It becomes even more important to apply a structured approach, and systematically go through different options, when the system becomes more complex.

To summarize, it is possible to apply PDPS to separation processes in the food industry The case discussed above differs from previous cases (mayonnaise, ice-cream, or bouillons) primarily in the fact that there is no existing process describing the separation of isoflavones from okara. Moreover, a separation process can lead to more outcomes than a structuring process and uncertainty in the compositions of the streams. That is why the method needs further development in describing how and when the design process should interact with experimental work to limit the number of possible process design and task networks.

5. Conclusion

Product-driven process synthesis is a useful tool for product and process development in the food industry. The complexity associated with highly structured products can be captured systematically by combining existing product design methodologies with process synthesis. Furthermore, the breakdown of the problem into several levels, and refinement in each level as the design progresses, helps to tackle the problem strategically.
Since the need for a more sustainable use of resources rapidly increases, PDPS is now also used to upgrade a structured by-product of the food industry. Applying the PDPS methodology to an already existing structured food product may require some extensions of the methodology due to the fact that a structure has to be decomposed instead of built. Nevertheless, PDPS is also useful for fractionation of food material even though it requires some further developments, including a continuous information exchange between experimental work and design.

Acknowledgment

The financial support of the Institute for Sustainable Process Technology (ISPT), the Netherlands, is gratefully acknowledged.

References

[1] S.D. Barnicki and J.J. Siirola, Comput. Chem. Eng., 28 (2004)
[2] G.D. Moggridge and E.L. Cussler, Chem. Eng. Res. Des., 78 (2000)
[3] C. Wibowo and K.M. Ng, Aiche J., 47 (2001)
[4] C. Wibowo and K.A. Ng, Aiche J., 48 (2002)
[5] B. Harjo, C. Wibowo and K.M. Ng, Chem. Eng. Res. Des., 82 (2004)
[6] M. Hill, Comput. Chem. Eng., 33 (2009)
[7] J.M. Douglas, Aiche J., 31 (1985)
[8] P.M.M. Bongers and C. Almeida-Rivera, Comput.-Aided Chem. Eng. (2009) 231-236
[9] F.M. Meeuse, J. Grievink, P.J.T. Verheijen and M.L.M. vander Stappen, Aiche Symp. Ser. (2000) 324-328
[10] S. Gupta and P. Bongers, Chem. Eng. Process., 50 (2011)
[11] M. Hostrup, P.M. Harper and R. Gani, Comput. Chem. Eng., 23 (1999)
[12] C.J.C. Jackson, J.P. Dini, C. Lavandier, H.P.V. Rupasinghe, H. Faulkner, V. Poysa, D. Buzzell and S. DeGrandis, Process Biochem., 37 (2002)
[13] V.E.A. Rinaldi, P.K.W. Ng and M.R. Bennink, Cereal Chem., 77 (2000)
[14] H. Wang and P.A. Murphy, J. Agric. Food Chem., 42 (1994)
[15] M.J. Messina, V. Persky, K.D.R. Setchell and S. Barnes, Nutr. Cancer, 21 (1994)
[16] K.D.R. Setchell and A. Cassidy, J. Nutr., 129 (1999)

I.A. Karimi and Rajagopalan Srinivasan (Editors), Proceedings of the 11th International Symposium on Process Systems Engineering, 15-19 July 2012, Singapore.

Simultaneous optimization of hydrogen network with desulfurization processes embedded

Li Zhou, Zuwei Liao, Jingdai Wang, Bingbo Jiang, Yongrong Yang*

Department of Chemical and Biochemical Engineering, Zhejiang University, Zhejiang, China

Abstract

In refineries, hydrogen purification techniques include hydrocarbon removal units and hydrogen sulfide (H_2S) removal units. Hydrocarbon removal units such as membrane separation and pressure swing adsorption (PSA) are frequently employed in the hydrogen network integration (HNI) study. However, the possibility of integrating H_2S removal units into HNI study has been overlooked until recently. In the present work, an improved modeling and optimization approach has been developed to integrate H_2S removal units into HNI. By introducing a desulfurization ratio, $R_{ds_{pl,i}}$, simplified mass exchange network (MEN) is incorporated into hydrogen distribution network. Total annual cost (TAC) is employed as the optimizing object to investigate the tradeoffs between hydrogen distribution network cost and MEN cost. A practical case study is used to illustrate the application and effectiveness of the proposed method.

Key words: hydrogen network; H_2S removal network; desulfurization ratio; total annual cost; optimization.

1. Introduction

Hydrogen network integration has been extensively explored and the studies carried out can simply be classified into two major categories: 1) Pinch analysis approaches, 2) Mathematical programming approaches based on superstructures. The first graphical hydrogen pinch analysis approach was developed by Alves [1,2], who proposed a hydrogen surplus diagram in the purity versus flowrate coordinate system. Later, another coordinate system, the purity versus impurity load system, was employed by Agrawal and Shenoy [3] and Bandyopadhyay [4]. Liao et al. [5] presented a new algebraic method addressing the relationship between pinch simplification and the mathematical model. Recently, pinch analysis for placing purifiers has been improved: optimal placements were obtained for both remove ratio specified [6] and tail gas purity specified [7] purifier models. Pinch analysis methods are useful in giving design targets, while mathematical programming methods are powerful in detailed design. Hallale [8] proposed a MINLP optimization approach. Liao [9] developed a systematic approach for the integration of hydrogen network with purifiers. Considering the life cycle of hydrogenation catalysts, Xuan et al [10] extended the problem formula to cope with the multi-period operation problems. Recently, Jia [11] considered the multi-component effect of hydrogen streams by integrating flash calculations, which made the obtained result more feasible.

However, the incorporation of H_2S removal units into multi-component HNI remains unexplored. In the present work, we aim to develop a systematic optimizing approach that incorporates desulfurization processes with HNI. Desulfurization ratio, $R_{ds_{pl,i}}$, is introduced to connect hydrogen network and the hydrogen sulfide removal network. Total annual cost (TAC) is employed to learn the trade-offs between hydrogen distribution network cost and MEN cost and a real world case study is illustrated.

2. Novel modeling and optimization approach

State-space superstructure [12] is modified in the present work to capture the feature of our desulfurization processes embedded hydrogen network. To be more specific, the hydrogen network in

* Corresponding author. Email: yangyr@zju.edu.cn Fax: + 86 571 87951227

this work is demonstrated as a system of four interconnected blocks as shown in Fig. 1: 1) Hydrogen distribution section; 2) hydrocarbon removal section, where the hydrocarbons get removed and hydrogen concentration of relevant streams get upgraded. 3). Desulfurization section, where the H2S contaminant gets partially removed from the process stream. 4). Compressor section, where the pressure level of streams get upgraded. It's worth noting that the inlets of the purifiers as well as the compressors can serve as hydrogen sinks, while the outlets are considered as hydrogen sources.

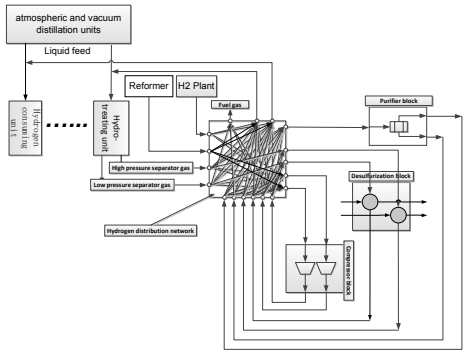

Fig. 1 State-space representation of hydrogen network.

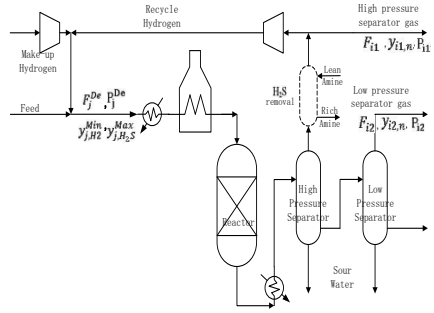

Fig. 2 Schematic diagram of a typical hydrotreating unit.

Fig. 2 represents a typical hydro-treating unit. As is shown, H_2S removal units are optionally installed to remove the overloaded hydrogen sulfide from the HP separator purges in order to reuse the hydrogen. However, there is also reuse potential in the LP separator gases. Though the hydrogen concentrations of these gas streams from LP separator are relatively lower than that of the gas streams from HP separators, while the H_2S concentrations are higher, those streams could be further reused after properly handled with purifiers. In order to hit the ultra-high efficient of hydrogen usage, desulfurization unit is introduced as mass exchange network and incorporated into the hydrogen network integration. It should be stress out that the present work only concerns half of the MEN design, i.e. the distribution of the rich streams and simple design of the desulfurization column.

The inlet and outlet flowrate of the desulfurization column are assumed to be identical:

$$F^{in}_{ds_{pl,i}} = F^{out}_{ds_{pl,i}} \qquad \forall\, pl \in PL, i \epsilon I \tag{1}$$

For the desulfurization column design, the theoretical number of trays N_T is analytically calculated by making use of the Kremser equation [13].

If $A \neq 1$:

$$N_T = \frac{\log\left[\left(y^{in} - mx^{in} - c\right)/\left(y^{out} - mx^{in} - c\right)(1 - 1/A) + 1/A\right]}{\log A} \tag{2}$$

If $A = 1$:

$$N_T = \frac{(y^{in} - y^{out})}{(y^{out} - mx^{in} - c)} \tag{3}$$

where $A = \frac{L}{mG}$, which is the ratio of the operating line slope to the equilibrium line slope, and is called the absorption factor. In this work, the absorption factor is simply assumed to be 1.

As tradeoffs exist between hydrogen distribution network cost and the MEN cost. The more hydrogen sulfide gets removed in the MEN, the more hydrogen can be reused in the hydrogen distribution

network, while the cost of the MEN will increase and the cost of the hydrogen distribution network will decrease. Consequently, the desulfurization ratio, $R_{ds_{pl,i'}}$, is selected as an optimizable variable to investigate the tradeoffs.

$$y_{ds_{pl,i}}^{out} = \left(1 - R_{ds_{pl,i}}\right) y_{ds_{pl,i}}^{in} \qquad \forall\, pl \in PL, i\epsilon I \tag{4}$$

$$1 \le R_{ds_{pl,i}} \le 1 \qquad \forall\, pl \in PL, i\epsilon I \tag{5}$$

Then the following equation can be deduced:

$$N_{T,ds_{pl,i}} = \frac{\left[y_{ds_{pl,i}}^{in} - (1-R_{ds_{pl,i}}) y_{ds_{pl,i}}^{in}\right]}{\left[(1-R_{ds_{pl,i}}) y_{ds_{pl,i}}^{in} - mx^{in} - c\right]} \qquad \forall\, pl \in PL, i\epsilon I \tag{6}$$

The capital cost of a desulfurization column in the present work is simply assumed to be \$4552 per year per stage [14].

$$C_{ds_{pl,i}} = 4552 N_{T,ds_{pl,i}} \qquad \forall pl \in PL,\ \ i \in I \tag{7}$$

As the modeling of other blocks had been widely investigated in HNI study, we will not give a detailed description here subject to the limited space.

3. Case study

A case study with two hydrogen producers and five hydrogen consumers is presented to illustrate the application of the methodology developed. The base case hydrogen network including the placement of the existing pipes and compressors is shown in Fig. 3. Table 1 shows the physical pipe distances between the units, while the inlet stream hydrogen constraints and impurity constraints are illustrated in Table 2.

Table 1 Piping distances between the units for base case.

Source	Sink				
	PE	GHT	G/DHT	PP	DHT
HPlant	400	1900	200	2400	900
RF	1100	1200	900	1700	200
G/DHT	600	2100	0	2600	1100
DHT	1300	1000	1100	1500	0
PSA	1300	1000	900	1500	0

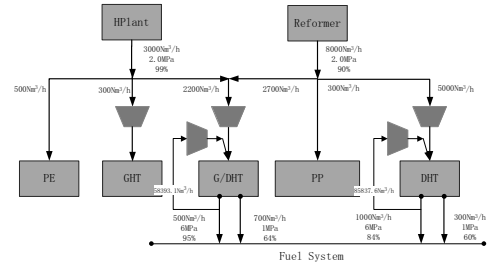

Fig. 3 The existing hydrogen network in the base case.

Table 2 Inlet stream concentration constraints of each hydrogen consumers.

	PE	GHT	G/DHT	PP	DHT
$y_{j,H2}^{Min}$	86%	86%	86%	86%	84%
$y_{j,H2S}^{Max}$	0	0	0.0044	0	0.0045

It is worth noting that there is an idled PSA plant with feed and residual pressure specified at 2 MPa and 0.2 MPa which is not shown in the base case diagram. Since the hydrogen concentration of LP off-gases is not high enough for directly reuse and yet there's recovery potential, the idled PSA plant is considered to be put into use. The recovery ratio and product hydrogen purity of the PSA unit are at 0.9 and 99% respectively. The prices of hydrogen produced by hydrogen plant and catalyst reformer are 0.893 RMB/Nm^3 and 2.054 RMB/ Nm^3 respectively. Electricity costs 0.75 RMB/kw·h, and fuel costs 0.02369 RMB/MJ. The capital cost is annualized in 5 years, with 5% interest rate per year.

As shown in Fig. 3, four purge streams of hydrogen consumers with high hydrogen concentration are released as fuel gas, due to its high content of hydrogen sulfide. In order to take good use of the hydrogen in these streams, desulfurization columns are considered.

The MINLP problem is solved in GAMS software using Baron as solver. The optimal flowsheet from the MINLP optimization is shown in Fig. 4. The optimal result involves two new desulfurization columns, an additional compressor and several pipes, as represented by dashed lines. In the optimum result scheme, the HP purge stream of DHT unit is sent to mix with the HP purge stream of G/DHT unit, and desulfurized in DSH_1. 64.4% of the outlet stream from DSH_1 is sent to the recycle hydrogen compressor of G/DHT unit and reused. While the LP purge stream of G/DHT is sent to mix with the LP purge stream of DHT unit, and desulfurized in DSL_2, the outlet stream is recompressed to 2MPa and then sent to PSA unit. The product from the PSA unit is sent to the make-up hydrogen compressor of DHT unit and reused, while the residual stream served as fuel gas. The optimized desulfurization ratio $R_{ds_{pl,i}}$ and theoretical plate number N_T of each desulfurization column are demonstrated in Table 3. With these new equipments, 82.8% of the purge streams are recovered and reused, contributing to the reduction of 2070.909 Nm^3/h on the hydrogen plant production, thus ￥7.67 million in TAC is saved. It should be noted that the capital cost of PSA is not included in this case. Detailed comparison is illustrated in Table 4. Comparing to the operating cost being saved (9.783 million/a), the additional capital cost (2.113 million/a) is acceptable.

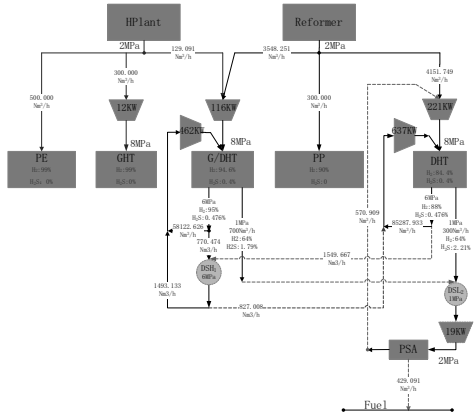

Table3 Optimized design parameter for desulfurization towers.

	DSH_1	DSL_2
$R_{ds_{pl,i}}$	0.814	0.828
$N_{T,ds_{pl,i}}$	5.247	5.020

Fig. 4 Optimum retrofitted hydrogen network.

Table 4 Cost breakdown for the optimal solution of base case.

Existing network	**Optimized network**
Operating cost/RMB·a^{-1}:	**Operating cost/RMB·a^{-1}:**
HPlant: 2.250×10^7(3000$Nm^3\cdot h^{-1}$)	HPlant: 6.968×10^6(929.091 $Nm^3\cdot h^{-1}$)
RF: 1.380×10^8(8000 $Nm^3\cdot h^{-1}$)	RF: 1.380×10^8(8000 $Nm^3\cdot h^{-1}$)
Electricity: 1.047×10^7	Electricity: 1.087×10^7
Fuel: -5.252×10^6	Fuel: -3.996×10^5
	Desulfurization: 4.786×10^5

	Capital cost/RMB·a^{-1}:
	DS tower: 1.660×10^{6}
	Compressor: 3.896×10^{5}
	Piping: 0.636×10^{5}
Total annual cost: 1.657×10^{8}	**Total annual cost: 1.580×10^{8}**

4. Conclusions

A new modeling and optimization methodology has been developed to investigate the combination of these two systems. The desulfurization ratio, $R_{ds_{pl,i}}$, is employed to incorporate H_2S removal units into hydrogen distribution networks. The optimization of the case study demonstrates an ultra-high efficient hydrogen usage compared to the original network. The technique can fully account for not only the trade-offs between HNI and MEN, but also the trade-offs between operating cost and investment cost.

References

1. Alves, J. J., 1999. Analysis and design of refinery hydrogen distribution systems. Ph.D. thesis, UMIST, UK, Manchester.
2. Alves, J. J., Towler, G. P., 2002. Analysis of refinery hydrogen distribution systems. Ind Eng Chem Res 41(23), 5759-5769.
3. Agrawal, V., Shenoy, U. V., 2006. Unified conceptual approach to targeting and design of water and hydrogen networks. AIChE J 52(3), 1071-1082.
4. Bandyopadhyay, S., 2006. Source composite curve for waste reduction. Chem Eng J 125(2), 99-110.
5. Liao, Z. W., Rong, G., Wang, J. D., Yang, Y. R., 2011. Rigorous algorithmic targeting methods for hydrogen networks—part Ⅰ: systems with no hydrogen purification. Chem Eng Sci 66(5), 813-820.
6. Liao, Z. W., Rong, G., Wang, J. D., Yang, Y. R., 2011. Rigorous algorithmic targeting methods for hydrogen networks—part Ⅱ: systems with one hydrogen purification unit. Chem Eng Sci 66(5), 821-833.
7. Zhang, Q., Feng, X., Liu, G. L., Chu K. H., 2011. A novel graphical method for the integration of hydrogen distribution systems with purification reuse. Chem Eng Sci 66(4), 797-809.
8. Hallale, N., Liu, F., 2001. Refinery hydrogen management for clean fuels production. Adv Environ Res 6(1), 81-98.
9. Liao Z. W., Wang, J. D., Yang, Y. R., Rong, G., 2010. Integrating purifiers in refinery hydrogen networks: a retrofit case study. J of Clean Prod 18(3), 233-241.
10. Xuan, J., Liao, Z. W., Rong, G., Yang, Y. R., 2010. Hydrogen network retrofit design in refinery based on stochastic programming. CIESC J 61(2), 398-404.
11. Jia, N., Zhang, N., 2011. Multi-component optimization for refinery hydrogen networks. Energy 36(8), 4663-4670.
12. Bagajewicz, M. J., Manousiouthakis, V., 1992. Mass/heat-exchange network representation of distillation networks. AIChE J 38(11), 1769-1800.
13. Treybal, R. E., 1981. Mass transfer operations. 3rd ed. New York, McGraw-Hill.
14. Peters, M. S., Timmerhaus, K. D., 1990. Plant design and economics for chemical engineers, 4th ed. Singapore, McGraw-Hill.

I.A. Karimi and Rajagopalan Srinivasan (Editors), Proceedings of the 11th International Symposium on Process Systems Engineering, 15-19 July 2012, Singapore.

A Systematic Methodology for Design of Emulsion Based Chemical Products

Michele Mattei, Georgios M. Kontogeorgis, Rafiqul Gani

Department of Chemical and Biochemical Egineering, Technical University of Denmark, Søltofts Plads, Building 229, DK-2800 Kongens Lyngby, Denmark

Abstract

A systematic methodology for emulsion based chemical product design is presented. The methodology employs a model-based product synthesis/design stage and a model-experiment based further refinement and/or validation stage. In this paper only the first stage is presented. The methodology employs a hierarchical approach starting with the identification of the needs to be satisfied by the emulsified product and then building up the formulation by adding one-by-one the different classes of chemicals. A structured database together with dedicated property prediction models and evaluation criteria are employed to obtain a list of formulations that satisfy constraints representing the desired needs (target properties). Through a conceptual case study dealing with the design of a sunscreen lotion, the application of this new methodology is illustrated.

Keywords: Emulsions, Formulation, Model-base Method, Product Design, Sunscreen.

1. Emulsion Based Chemical Product Design – An Introduction

The goal of chemical product design is to find a product that exhibits a set of desirable or specified behavior[1]. A chemical product design problem can be summarized as follows: given a set of desired (target) properties, establish a list of chemical formulations satisfying these targets and then choose from them the most appropriate candidate to be verified experimentally[2]. Cussler and Moggridge[3] recommend a four step systematic methodology to solve this kind of problems: define customer needs; generate ideas to fulfill these requirements; select the most advantageous option among those generated; and finally manufacture the product. The chemical product of interest can be a single chemical or a mixture/blend; a formulated product is a mixture that contains different chemicals, active ingredients as well as additives. Cussler and Moggridge[3] distinguish between commodities (pure chemicals), chemical devices (where the attention is on selection and manufacture), molecular products (where focus is on active ingredients at the molecular level) and microstructured products (where the most important part is the structure of the product itself). The term "microstructure" refers to a chemical organization on the scale of micrometers, which belongs to the colloidal domain and incorporates polymer solutions, foams, gels as well as emulsions. The performances of such products are related not only to the presence of active ingredients and additives in the formulation, but also to the product's structural and material properties[4]. A common way to design these structured products is through trial-and-error approaches as predictive mathematical models needed to describe the relationships between product behavior and its performance need to be developed first[5].
A modified procedure[6], which is applicable to the design of emulsified formulated products, is presented in this paper. These emulsified products have a large use in the food and cosmetic industries and are described as mixtures of two normally immiscible liquids (representing the continuous and the dispersed phases), kinetically stabilized by

so called "emulsifiers" that mainly lie on the surface between the two phases. Active ingredients and additives are usually dissolved in the continuous and/or dispersed phases according to the needs of the product. Property models and databases have been developed to support the product (emulsified formulations) design methodology.

2. A Systematic Methodology for Emulsified Product Design

The steps of the modified methodology (Stage-1) for the design of emulsified chemical products are listed in Table 1. Except for Step 1, where consumer assessments are converted into target properties to be used in following steps, and Step 7, where the composition of the formulated product is determined; each step is responsible for the selection of one or more ingredients of the product satisfying one class of needs. To implement the methodology, a database[7] of ingredients, additives, and solvents has been created together with a library of developed/tested property models and a knowledge base of emulsified products and their need-property relations.

Table 1: Step-by-step methodology (Stage-1) in tabular form with necessary inputs for each step, action performed and outputs generated.

Step	Input	Performed Action	Output
Step 1	Information about the product	Understanding of needs, translation into target properties in terms of constraints to match	List of main needs, secondary needs and target properties with boundaries
Step 2	List of main needs	Find chemicals suitable as active ingredient, select the most advantageous	Candidate active ingredient
Step 3	Candidate active ingredient	Find chemicals suitable as dispersed phase solvents, select the most advantageous	Candidate dispersed phase solvent
Step 4	Candidate active ingredient and dispersed phase solvent	Find chemicals suitable as continuous phase solvents, select the most advantageous	Candidate continuous phase solvent
Step 5	Candidate active ingredient dispersed and continuous phase solvents	Find chemicals suitable as emulsifiers, select the most advantageous	Candidate emulsifier
Step 6	List of secondary needs, candidate dispersed and continuous phase solvents	Find chemicals suitable as additives, select the most advantageous	Candidate additives
Step 7	List of constraints on target properties, all ingredients	Find overall composition of selected ingredients	Product to be experimentally verified (Stage-2)

3. A Conceptual Case Study – A Sunscreen Lotion

A sunscreen lotion has been chosen as a conceptual case study to highlight the application of the emulsified product design methodology. This type of product can also be found as a single-phase liquid formulation[6]. However, as an emulsified formulation the product has advantages, such as, with respect to sensorial properties and cost, because of the presence of water in high concentration.

3.1. Problem Definition (Step 1)

From the knowledge base, it is found that consumers want a sunscreen lotion to protect from sunburns and UV radiations (risk of skin cancer and other diseases), to prevent from skin aging, to be water-proof, to have good sensorial properties (color, odor, *etc*.), good stability, low toxicity, easily spray able, and to have a low price. The protection from sunburns and UV radiations are identified as the main need, while the other consumer assessments are classified as secondary needs. This last distinction is crucial when translating consumer needs into target properties. The main needs are satisfied by active ingredients, while secondary needs are matched through appropriate additives as well as through the identification of the most advantageous overall composition of the formulation.

The above needs are converted to the following properties and their corresponding target values based on the information in the knowledge base[6]: properties needed to satisfy low toxicity ($LC_{50} > 3.16$); easy spray ability (kinematic viscosity, $\nu < 75$ cS; and molar volume, 20 kmol/l $< V <$ 50 kmol/l); protection from sunburn and radiation (UV absorbity; filtering); product stability (emulsion properties of surfactant-water mixtures); liquid product (miscibility in water; solubility).

3.2. Identification of Active Ingredients (Step 2)

The main need of a sunscreen lotion is to protect from sunburns and UV radiations. This is achieved by providing protection from both UV-A and UV-B rays. Two UV absorbers are selected in terms of their ability to block one type of UV radiation. In addition, a physical barrier for radiations (UV filter) is added in order to enhance the effectiveness of the formulated product. According to the legislation for sunscreens in EU[8], only 18 chemicals (also available in our database) are found to be suitable. The maximum allowed concentration of the active ingredients are also set at this point, through the knowledge base. From among the 18 UV absorbers[9] and their LC_{50} values, Avobenzone (CAS number 70356-09-1) is chosen as the UV-A absorber, Octyl Salicylate (CAS 118-60-5) as the UV-B absorber and Zinc Oxide (CAS 1314-13-2) as the UV filter.

3.3. Identification of Dispersed Phase Solvent (Step 3)

As the selected active ingredients (AIs) are solid at standard conditions; a suitable solvent is therefore needed to dissolve them, forming a homogeneous liquid phase. According to the database, Zinc Oxide is an insoluble pigment that can only be finely dispersed in the formulation, while the selected UV absorbers are oil-soluble. This is verified through their calculated (with property model from the model library) total Hildebrand solubility parameters (19.4 and 20.4 $MPa^{1/2}$, respectively). A search of the solvent database (from our CAMD-tool) revealed more than 100 chemicals that potentially are applicable as the dispersed phase solvent. Additionally, the solubility is verified by considering (also predicted with models from model library) the Hansen solubility parameters (dispersive, polar and hydrogen-bonding). Solvents matching the following target values of dispersive, polar and hydrogen bonding contribution, respectively, are identified for Avobenzene (0.57, 0.26 and 0.17); and for Octyl

Salicylate (0.49, 0.21 and 0.3). Only 6 chemicals are found to match these targets. Based on effectiveness (in terms of their expected solubility of active ingredients), toxicity and cost, Butyl Acetate (CAS 123-86-4) is chosen as the most appropriate dispersed phase solvent.

3.4. Identification of Continuous Phase Solvent (Step 4)

The identification of the continuous phase solvent is carried out by considering those chemicals that are not likely to dissolve the AIs or be miscible with the dispersed phase solvent. This is achieved by comparing the Hildebrand solubility parameters of the AIs and the solvent, and, checking for stability of the liquid phase (using models from model library). Note that the selected AIs are known to be only oil-soluble and are not miscible with water. Therefore, water is chosen as the most suitable continuous phase solvent. The total Hildebrand solubility parameter of water (δ^T = 48 $MPa^{1/2}$) confirms that the AIs and the dispersed phase solvent would not be miscible with it. Moreover, water is cheap, non-toxic and environmentally friendly.

3.5. Identification of the Emulsifier (Step 5)

The key-player in the formation of an emulsion is the emulsifier, which is often a surfactant. Since an oil-in-water emulsion is needed, the selected emulsifier needs to ensure the formation of this type of emulsion (indicated by a Hydrophilic-Lipophilic Balance value: HLB > 12) and ensure the stability of the desired emulsion for a wide range of temperature. Note that a sunscreen lotion is expected to be exposed to a range of temperatures and it must be stable under these conditions. Accordingly, Octyl Esaethylene Oxide (CAS 27252-75-1) has been identified (from our database of emulsifiers) as the most suitable emulsifier for this product. Its HLB value is 13.4[10], its cloud point (maximum temperature of use) is 73°C[11], and since it is a non-ionic surfactant, it is not affected by the presence of electrolytes in solution. If HLB and cloud point data are not available, they are predicted with models from the model library.

3.6. Identification of Additives (Step 6)

Additives are usually added to enhance the quality of the product, that is, to satisfy the secondary needs. Prevention from skin aging, stability and odor is improved by adding appropriate additives to the formulation. An antioxidant, a preservative and an aroma are needed, respectively and the choice of oil-soluble chemicals would ensure that these properties would not be affected by contact with water (note that the selected AIs are only oil-soluble). Because of the presence of dispersed Zinc Oxide in the formulation, color needs to be white. For this case study, α-Tocopherol (CAS 59-02-9), Heptylparaben (CAS 1085-12-7) and *laevo*-Menthol (CAS 2216-51-5) have been selected based on the available properties in the database. Selection of feasible candidates has been made based on their available prices.

3.7. Identification of Overall Composition (Step 7)

In this last step, the overall composition of the formulated product based on cost and subject to the property constraints (see Step 1) is determined. Also, solubility issues as well as constraints imposed by legislation[8] on use of the AIs are considered. The formulation toxicity parameter, molar volume and cost are calculated using an ideal mixing rule, weighted in terms of the composition of the chemicals in the mixture, as,

$$\zeta = \sum_{i=1}^{NC} x_i \zeta_i \quad (1)$$

Where ζ is a mixture property, x_i is the molar fraction of compound i in the formulation, and ζ_i the corresponding pure compound property.

Formulation viscosity, however, is calculated through a non-linear model[12].

$$\eta_r = 1 + \frac{2\left[5\lambda - 5\left((\lambda-1)\varphi^{7/3}\right)\right]}{4(\lambda-1) - 5(5\lambda-2)\varphi + 42\lambda\varphi^{5/3} - 5(5\lambda-2)\varphi^{7/3} + 4(\lambda-1)\varphi^{10/3}}\varphi \quad (2)$$

Where η_r is the relative viscosity, λ represents the ratio of viscosities of dispersed phase and continuous phase and φ is the dispersed phase volume fraction.
A candidate composition representing the desired sunscreen emulsified product is given in Table 2. This mixture satisfies the critical micelle concentration (calculated with model from the model library) needed to ensure stable emulsions.

Table 2: Candidate overall composition (weight percentage) for a sunscreen emulsion

Active Ingredients	Avobenzone	0.99%	Emulsifier	Octyl Esaethylene Oxide	0.09%
	Octyl Salycilate	1.22%			
	Zinc Oxide	8.56%	Additives	α-Tocopherol	0.34%
Disp. Phase Solvent	Butyl Acetate	32.4%		Heptylparaben	0.59%
Cont. Phase Solvent	Water	54.9%		laevo-Menthol	0.91%

4. Conclusions and Future Work

The work-flow for a systematic methodology for emulsion based chemical product design has been presented and its application has been highlighted through a conceptual case study from the health-care industry. The methodology is generic in the sense that other similar products can also be designed once the needs-property relations are established. Application range is enhanced through addition of data to the database and/or property models in the model library (details of these models can be obtained from the authors). Uncertainties in prediction of the composition of the formulated product are likely, and therefore, a final stage of verification by experiments is necessary. The work-flow of the methodology will now be implemented into the "The Virtual Process-Product Design Laboratory"[13] software to allow virtual (formulation) design and verification of emulsified products. In this way design and development of these products can be made less costly and introduced to the market earlier, while using the experimental resources only for verification of the product.

References

1. Gani R.; Comput. Chem. Eng., 2004; 28 (12): 2441-2457.
2. Gani R.; Chem. Eng. Res. Des., 2004; 82(A11): 1494-1504
3. Cussler E.L., Moggridge G.D., Chemical Product Design. Cambridge Univ Press; 2011.
4. Smith B.V., Ierapepritou M.G.; Comput. Chem. Eng., 2000; 34: 857-865.
5. Wibowo C., Ng K.M.; AIChE J.,, 2002; 48 (6): 1212-1230.
6. Conte E., Gani R., Cheng Y.S., Ng K.M.; AIChE J., 2011; 58(1), 173-189.
7. Nielsen T.L. et al.; J. Chem. Eng. Data, 2001; 46: 1041-1044.
8. Regulation (EC) No 1223-2009 of the European Parliament and of the Council of 30 November 2009 on Cosmetic Products
9. Couteau C., Chammas R., El-Boury S., Choquenet B., Paparis E., Coiffard L.J.M.; Journal of Dermatological Science, 2009; 50, 159-161.
10. Chen M.L., Wang Z.W., Duan H.J.; Journal of Dispersion Science and Technology, 2009; 30(10): 1481-1485.
11. Ren Y. et al.; Journal of Colloid and Interface Science, 2011; 358(1): 202-207.
12. Choi S.J., Schowalter W.R.; Physics of Fluids, 1975; 18(4): 420-427.
13. Conte E., Gani R., Malik T.I.; Fluid Phase Eq., 2011; 302: 294-304.

I.A. Karimi and Rajagopalan Srinivasan (Editors), Proceedings of the 11th International Symposium on Process Systems Engineering, 15-19 July 2012, Singapore.

Molecular Design using Three-Dimensional Signature Descriptors

Robert H. Herring[a], Rudolfs Namikis[a], Nishanth G. Chemmangattuvalappil[a,b], Christopher B. Roberts[a], Mario R. Eden[a]

[a]*Department of Chemical Engineering, Auburn University, USA*
[b]*Department of Chemical and Environmental Eng., University of Nottingham, Malaysia*

Abstract

Integrated process and product design is a useful approach for identifying globally optimal solutions to increasingly demanding problems. Property based process and product design methods are convenient since both sides of the problem can easily be expressed in terms of molecular properties. Property clustering, a technique for tracking stream properties or functionalities through conserved quantities, allows for interpretation of process performance as a function of properties. The molecular signature descriptor is quite effective in this approach as any topological index, which enumerates molecular information for use in QSPRs, can be derived from the molecular signature. Previous works on application of the signature descriptor have been limited to use with topological indices. This contribution outlines an algorithm for including topographical, or three-dimensional, information with the signature descriptor and how to apply this information in the reverse problem formulation (RPF) methodology.

Keywords: Molecular Design, Topographical Descriptors, Molecular Signatures.

1. Theoretical Background

1.1. Topographical Descriptors

A topographic index is a form of 3D molecular characterization that attributes a molecule with a unique number, thus giving a quantitative reference to shape. The advantage of this technique is that topographic indices can enumerate the spatial orientation of a molecule, which might not be fully captured in the conventional 2D methods of developing QSAR/QSPRs. This would be useful for modelling ligand-receptor type interactions and has even been shown to have strong correlations to several physicochemical properties [1]. Most geometrical descriptors are calculated directly using the (x,y,z) coordinates of the atoms in the molecule and others are derived from these coordinates, e.g. inter-atomic distances or distances from an origin. The information content of topographical descriptors typically allows more discrimination power than topological descriptors for similar molecular structures. It is often necessary to include connectivity information in the form of adjacency matrices, molecular graphs, or molecular signatures in this case since topographic indices do not include this data [1]. Another shortcoming of these descriptors is the necessity for geometry optimization, with the global conformational minima overshadowed by several local conformational minima of slightly different energy values. Overall, this remains an effective method of accounting for the shape of a molecular structure, and can even be used to address electrostatic properties in a 3D context [2]. The topographical descriptors utilized in this study are the 3D Wiener index [3,4] and the Van der Waals volume [5].

1.2. Molecular Signatures

The molecular signature descriptor is a representation of the extended valence sequence of the atoms in a molecule [6]. This descriptor is ideal for the RPF approach because of its low degeneracy and ability to capture enough structural information to derive almost any other index, topological [7,8] and now topographical, necessary for a quality QSPR. Another convenient feature of the signature descriptor is the coloring function, which can be tailored to include useful information about the atoms involved. Graph theory [9] is applied to the concept of molecular signatures to ensure that only feasible and complete solution structures are generated. If G is a molecular graph and x is an atom of G, the atomic signature of height h of x is a canonical representation of the sub-graph of G containing all atoms that are at a distance h from x. If k is a constant, ${}^{h}\alpha_G$ is the vector of occurrences of atomic signature of height h and $TI(root({}^{h}\Sigma))$ is the vector of TI values calculated for each root of atomic signature, then:

$$TI(G) = k \cdot {}^{h}\alpha_G \cdot TI(root({}^{h}\Sigma)) \tag{1}$$

1.3. Reverse Problem Formulation (RPF) Technique and Property Operators

The conventional approach to process and molecular design has been to treat both problems separately. Decisions on which components to use are typically made before the design process and are limited to qualitative intuition based on previous experience. The reverse problem formulation allows these two design aspects to be treated simultaneously, which can likely result in a more optimal solution [10]. The strength of this approach is that process design is not tied to any specific molecular components, which allows for a more thorough search for optimal process conditions, and the molecular design aspect considers a wider range of candidate structures. This method essentially creates two reverse problems that can easily communicate through the use of property operators, which are functions of the original properties forced to obey linear mixing rules. The normalized property operator, Ω_{js} is obtained by dividing it by a reference value [11]. If $\psi_j(P_{js})$ is the property operator of the j^{th} property P_{js} of stream s, x_s is the fractional contribution, N_s is the number of streams, then:

$$\Omega_{js} = \frac{\sum_{s=1}^{N_s} x_s \psi_j(P_{js})}{\psi_j^{ref}} \tag{2}$$

2. Signature Descriptors for Molecular Design

2.1. General Problem Statement and Solution Procedure

Design the molecules with the best dominant property which also satisfy the set of property constraints that are identified during the process design.

Stepwise Solution Procedure:

- The property targets for the input molecules to provide the optimum process performance will be calculated using eq. (2).
- Identify QSAR/QSPR/GC (Group Contribution) models that can predict the properties corresponding to the optimum performance.
- Identify the height of molecular signatures corresponding to TI used in QSPR models that matches the diameter (D) of the target molecule as described in section 2.3

- Based on the structural constraints and transformation techniques explained in section 2.3, identify the signatures and generate candidate molecules from signatures based on the algorithm by Faulon *et al*. [12].

2.2. Topographical Indices in Reverse Problem Formulation

The topographical indices applied in this case, 3D Wiener index and Van der Waals volume, can both be derived from the geometric distance matrix. The geometric distance matrix of a molecular graph (G) is a real symmetric nxn matrix, where n represents the number of vertices in the chosen graph or sub-graph. Each entry in this matrix represents the Euclidean distance between two vertices $v_i(G)$ and $v_j(G)$. These values are calculated as shown below:

$$d_{ij} = \sqrt{(x_i - x_j)^2 + (y_i - y_j)^2 + (z_i - z_j)^2} \tag{3}$$

The geometric distance matrix can be used to calculate the 3D Wiener index through a simple summation of values in the upper or lower triangular matrix. The Van der Waals volume of a molecular graph can be calculated by treating each atomic coordinate as the center of a sphere, with the appropriate Van der Waals radius defined by signature coloring, while accounting for sphere overlapping. If r_i and r_j are the Van der Waals radii of two bonded atoms in a molecular graph and n is the total number of vertices in this graph then the volume can be calculated as shown:

$$V = \frac{4}{3}\sum_{i=1}^{n}\pi r_i^3 - \frac{1}{2}\sum_{i\neq j}^{n}\frac{\pi(r_i + r_j - d_{ij})^2(d_{ij}^2 - 2d_{ij}r_j - 3r_j^2 + 2d_{ij}r_i + 6r_i r_j - 3r_i^2)}{12d_{ij}} \tag{4}$$

Starting geometries for each signature were obtained from a stochastic conformational search, utilizing the xSS100 script in BOSS (biochemical and organic simulation system) [13]. The Cartesian coordinates for each vertex of the molecular graph were calculated from gas phase geometry optimizations, utilizing the semi-empirical quantum mechanical model formulation called Austin Model 1 (AM1) [14]. This method was chosen as suitable for small to medium alkane structures because it generates accurate geometries at a fraction of the time required for most ab initio methods.

2.3. Problem Formulation

If θ is the property function of property P, the property operator corresponding to P is estimated as follows:

$$\theta = f(TI) \tag{5}$$

$$TI = \sum_{i=1}^{N} {}^{h}\alpha_i \cdot TI(root({}^{h}\Sigma)) = \sum_{i=1}^{N} {}^{h}\alpha_i L_i \tag{6}$$

$$\Omega(P) = \sum_{i=1}^{N} x_i L_i \tag{7}$$

The dominant property, being expressed in terms of the occurrences of atomic signatures, can be optimized subject to the property constraints. If Ω_j is the property operator corresponding to the dominant property and Ω_{ij} is the normalized property operator of molecule i, an optimization problem can be formulated as follows:

$$Max / Min\ \Omega_j \tag{8}$$

$$\Omega_j^{\min} \le \Omega_j \le \Omega_j^{\max} \tag{9}$$

The geometry matrix can be generated for each signature. In the next step, the diameter and vertex number of the signatures are identified. The diameter (D) of the signature is the largest distance between all pairs of atoms in the signature. The vertex number is the number of vertices in the subgraph. The height of the signature will be decided based on the type of target molecule.

$$\sum n \le Max(D) \tag{10}$$

If eq. (10) is satisfied, generate the geometry matrix from the signature with maximum vertex value. Since all atoms in the molecule, which this signature is part of, are described in the signature, the geometry matrix will be exactly the same as the molecule. Subsequent studies will include derivation of topographic indices from signature combinations.

3. Case Study – Design of Alkyl Substituent for Rice Plant Fungicide

Application of the molecular signature descriptor in accounting for topological, topographical and information indices is illustrated through the optimal substituent selection for dialkyldithiolanylidenemalonate (DD). DD has been shown to have eradicant and protectant activity against rice blast disease. Uchida [15] enumerated the effectiveness of this fungicide in terms of affinity ($\log(V_E)$), mobility ($\log(\mu)$) and retention ($\log(R/(100\text{-}R))$). These three attributes have been linearly related to the lipophilicity ($\log(P_{oct/wat})$) of the chosen substituents. A QSPR was developed [16] to model $\log(P)$ as a function of several different descriptors. Index values are calculated only for the substituent regions of the fungicide and the summation of property values for the two substituents are constrained to values shown in Table 1. Raman and Maranas [17] previously visited this problem while correlating $\log(P)$ values to the first order molecular connectivity index. The same upper and lower bounds on mobility and retention are applied in this study, while the objective function is to maximize substituent affinity to the rice plant.

Table 1. Property Constraints

Property	Upper Bound	Lower Bound
Retention, $\log(R/100\text{-}R)$	-2.04	-2.48
Mobility, $\log(\mu)$	0.3	-0.3
Affinity, $\log(V_E)$	Maximum	

Property models utilized in this study are shown in Table 2. The information content (IC) indices infer a measure of molecular symmetry, and this formulation was originally introduced by Shannon [18]. Another information theoretical invariant utilized in the $\log(P)$ QSPR is the complementary information content (CIC) index [19]. Some of the descriptors, with large structure references, used in the hydrophobicity QSPR were found to be unnecessary based on the height of the solution signature. This case study, formulated as an MILP optimization problem, was solved using a simplex algorithm.

Table 2. Property Models

Property	Property Model
Retention	$\log(R/100-R)=0.72*\log(P)-1.93$
Mobility	$\log(\mu)=-0.64*\log(P)+1.95$
Affinity	$\log(V_E)=0.53*\log(P)-0.24$
Hydrophobicity	$\log(P)=-5.60+0.19(P_{10})-1.46(IC_0)+1.09(CIC_2)-0.77(CIC_3)-1.36({}^{6}\chi^{b})$ $+5.34({}^{0}\chi^{v})-3.41({}^{1}\chi^{v})+0.55({}^{4}\chi^{v})-0.41({}^{3}\chi^{v}_{C})+1.10(V_W)-0.17({}^{3D}W)$

Using height two atomic signatures for acyclic alkanes, of which there are 65, the optimal DD-substituents which satisfy the criteria for this study are found to be ethyl and sec-butyl. This solution was also found in the original case study [17], thus lending credibility to the developed methodology. It should be noted that in this specific case the inclusion of topographical descriptors did not result in a different solution. For alternate studies in which the contribution of three dimensional descriptors might have a more pronounced effect, this technique could lead to unique solutions which were previously unrealized. Overall, use of the signature descriptor as a platform on which to derive any topostructural and information indices is effective within the reverse problem formulation method.

4. Conclusions

The concept of molecular signature descriptors has been extended to include the use of 3D-descriptors. This extension enables us to make use of both 2D and 3D descriptor based QSPR models on the same platform to solve molecular design problems. In the next step, the algorithm will be modified to define three dimensional descriptors as a function of more than one signature building block.

References

[1] R. Todeschini and V. Consonni (2008), Handbook of Molecular Descriptors: Descriptors from Molecular Geometry, 1004
[2] P. Mezey (2008), J. Math. Chem., 45(2)
[3] B. Bogdanov, S. Nikolić, and N.Trinajstic (1989), J. Math. Chem., 3, 299
[4] Y. Malysheva, Y. Papulov, M. Vinogradova, A. Botov, V. Smolyakov (1998), J. Struct. Chem, 39(3)
[5] A. Bondi (1964), J. of Phys. Chem., 68, 441
[6] D.P. Visco Jr., R.S. Pophale, M.D. Rintoul, J.L. Faulon (2002), J. Mol. Graph Model 20
[7] J.L. Faulon, D.P. Visco Jr., R.S. Pophale (2003), J. Chem. Inf. Compt. Sci., 43, 707
[8] N. G. Chemmangattuvalippil, C.C. Solvason, S. Bommareddy, M.R. Eden (2010),Comp. Chem.Eng.,34, 2062
[9] N. Trinajstic (1992), Chemical Graph Theory, 2nd Edition, CRC press, Boca Raton, FL
[10] M.R. Eden, S.B. Jorgensen, R. Gani and M.M. El-Halwagi (2004), Chem. Eng. Process, 43
[11] M.D. Shelley and M.M. El-Halwagi (2000), Comput. Chem. Eng., 24
[12] J.L. Faulon, C.J.Churchwell, D.P. Visco Jr. (2003), J.Chem. Inf. Compt. Sci., 43, 721
[13] W.L. Jorgensen and J. Tirado-Rives (2005), J. Comput. Chem., 26, 1689
[14] M. Dewar, E. Zoebisch, E. Healy, J. Stewart (1985), J. Am. Chem. Soc., 107
[15] M. Uchida (1980), Pesticide Biochemistry and Physiology, 14, 249
[16] S. Basak, B. Gute and G. Grunwald (1996), J. Chem. Inf. Comput. Sci., 36, 1054
[17] V. Raman and C. Maranas (1998), Comp. Chem. Eng., 22, 747
[18] C. Shannon (1948), Bell Sys. Tech. J., 27, 379
[19] S. Basak and V. Magnuson (1983), Arzneim.-Forsch./Drug Res., 33, 501

I.A. Karimi and Rajagopalan Srinivasan (Editors), Proceedings of the 11th International Symposium on Process Systems Engineering, 15-19 July 2012, Singapore.

Optimization design of RO system for water purification

Yanyue Lu,[a] Anping Liao,[a] Yangdong Hu[b]

[a]*Key Laboratory of Chemical and Biological Transforming Process, College of Chemistry and Chemical engineering, Guangxi University for Nationalities, 188, East Daxue Road Nanning, Guangxi, 530006, China*
[b]*College of Chemistry and Chemical Engineering, Ocean University of China, Qingdao, 266003, China*

Abstract

A mathematical model of reverse osmosis (RO) membrane system is presented. The membrane system can be used to product multiple freshwater with different salinity from seawater. Based on the system model, the mathematical programming method is used to optimizing design the RO water purification system, the objective function is to minimize the total annualized cost of the RO system. The cost equation relating the capital and operating cost to the design variables, as well as the structural variables have been introduced in the mathematical programming model. As a results, the various freshwater with different concentration can be supplied simultaneously, it can lead to significant capital cost and energy saving and provide income from the multiple freshwater sales.

Keywords: reverse osmosis, membrane, seawater desalination, optimization design.

1. Introduction

The seawater and brackish desalination is the main source for supplying fresh water in the regions suffering from the scarcity of natural fresh water supplies (Wade, 2001). Reverse osmosis (RO) is the major technologies for large-size plants for desalinating water. The interest in RO is that it is able to meet varying feed water concentration and varying production water quantity and quality requirement through change system construction and operation condition. These characteristic have made the design of RO process more flexible (Marcovecchio, 2005). Considerable efforts for the research of the optimum RO system design have been made. El-Halwagi (1992, 1997) investigated the synthesis of RO networks which involve multiple feed streams for waste reduction. Based on the state-space approach, a structural representation of RO networks has been introduced. Voros et al. (1997) simplified the El-Halwagi's representation by reducing the distribution boxes to junctions.

In this work, a mathematical model of reverse osmosis (RO) membrane system is presented. The membrane system can be used to product multiple freshwater with different salinity from seawater. Based on the system model, the mathematical programming method is used to optimizing design the RO system for water purification. The design results would determine the optimal system structure and operating conditions, and the optimal streams distribution. At the same time, the most appropriately choice of the types of membrane elements in each stages and the optimal number of membrane elements in each pressure vessel (PV) also be given.

2. RO unit model

It is necessary to adopt the appropriate modeling equations that can satisfactorily predict the membrane performance with reasonable computational complexity. The solution diffusion model is the one most commonly used in RO system design. The model is mainly based on two parameters: the water permeability, A, and the solute transport parameter, B. The values for these two parameters are usually specified by membrane manufactures. According to the model, the pure water flux, J_w (kg/m^2.s), and the salt flux, J_s (kg/m^2.s), can be calculated as follow:

$$J_w = A\left[\left(P_f - P_p - \frac{\Delta P_f}{2}\right) - \left(\pi_w - \pi_p\right)\right] \times 10^6 \tag{1}$$

$$J_s = B\left(C_w - C_p\right) \tag{2}$$

$$V_w = \frac{J_w + J_s}{\rho_p} \tag{3}$$

$$Q_p = 3600 \times V_w \times S_m \times m \tag{4}$$

where V_w is the permeate velocity. ρ_p denotes the density of the permeate. S_m is the membrane area. m is the number of the membrane element, it is a continuous variable.

The arrays of pressure vessels (PV) with 1 up to 8 membrane elements per PV consist of a RO stage. In this paper, the optimal PV structure has been researched. Four different types of spiral wound FilmTec reverse osmosis membrane elements have been considered. According to its performance characteristics and the design requirements of a specific desalination application, the optimum selection of types of the membrane element employed in each PV can be determined by the following equations:

$$\sum_{k=1}^{4} Z_k \le 1 \tag{5}$$

$$L_1 \times \left(1 - \sum_{k=1}^{4} Z_k\right) \le Q_{ROf} - x_c \le U_1 \times \sum_{k=1}^{4} Z_k - \varepsilon \tag{6}$$

$$Q_p = \sum_{k=1}^{4} Q_{p,k} \tag{7}$$

$$Q_{p,k} \le U_2 \times Z_k \tag{8}$$

$$m_k \le U_3 \times Z_k \tag{9}$$

where Z_k is the binary variable. It takes the value of 1 when the kth element type is utilized in the PV. L_1 and U_1, are the arbitrary small and large number, respectively. x_c denote the small positive number. Q_{Rof} is the feed flow rate entering a RO stage. For the Eq. (6), when Q_{ROf} takes some value which is larger than x_c, it means the RO stage is presence and one element type should be chosen. Q_p is the permeate flow rate of pressure vessel. While $Q_{p,k}$ denote the permeate flow rate of pressure vessel when the kth element type is utilized in this PV. U_2 and U_3 are large enough positive number so that $Q_{p,k}$ and m_k are not restricted if $Z_k = 1$. By this way the module type and number of stage are chosen simultaneously when the optimization design is performed.

3. RO network representation

Several RO system configurations were investigated (Marcovecchio, 2005) which are common in seawater and brackish desalination applications. In order to describe the possible RO configuration, a simplified superstructure is presented, which incorporates

all the feasible process flow in the RO desalination system with multiple-product output. As shown in Fig. 1, a RO network consists of N_{ps} pressurization stages and N_{RO} reverse osmosis stages. In this configuration, there are three sets of stream nodes employed: N_{ps} mixing junctions, N_{RO} reverse osmosis junctions, N_p outlet junctions of product streams. The junction of N_{ps+1} indicated the brine stream leaving the network. It is assumed that seawater only enter the RO system from stage 1. The mixing streams pressurized by high pressure (HP) pump or not are connected to the corresponding reverse osmosis stages. The RO stages consist of multiple parallel reverse osmosis pressure vessels operating at the same conditions. The mathematical model that describes the superstructure is presented as follow.

$$Q_{ps,1} = Q_f + \sum_{j=1}^{N_{RO}} Q_{ROb,j} \times x_{b,1,j} + \sum_{j=1}^{N_{RO}} Q_{ROp,j} \times x_{p,1,j} \tag{10}$$

$$Q_{ps,1} \times C_{ps,1} = Q_f \times C_f + \sum_{j=1}^{N_{RO}} Q_{ROb,j} \times x_{b,1,j} \times C_{ROb,j} + \sum_{j=1}^{N_{RO}} Q_{ROp,j} \times x_{p,1,j} \times C_{ROp,j} \tag{11}$$

$$Q_{ps,i} = \sum_{j=1}^{N_{RO}} Q_{ROb,j} \times x_{b,i,j} + \sum_{j=1}^{N_{RO}} Q_{ROP,j} \times x_{p,i,j} \qquad i = 2,3,\ldots,N_{ps} \tag{12}$$

$$Q_{ps,i} \times C_{ps,i} = \sum_{j=1}^{N_{RO}} Q_{ROb,j} \times x_{b,i,j} \times C_{ROb,j} + \sum_{j=1}^{N_{RO}} Q_{ROp,j} \times x_{p,i,j} \times C_{ROp,j} \qquad i = 2,3,\ldots,N_{ps} \tag{13}$$

where $Q_{ps,i}$, $C_{ps,i}$ denote the flow rate and concentration of the ith pressurization stage, respectively. $Q_{ROb,j}$, $C_{ROb,j}$ denote the brine flow rate and concentration of the jth RO stage, $Q_{ROp,j}$, $C_{ROp,j}$ denote the permeate flow rate and concentration of the jth RO stage, respectively. $x_{b,i,j}$, $x_{p,i,j}$ indicate the stream split ratios of the brine and permeate, respectively. The values determine the flow rates of brine and permeate leaving the jth RO stage and being linked to the ith pressurization stage.

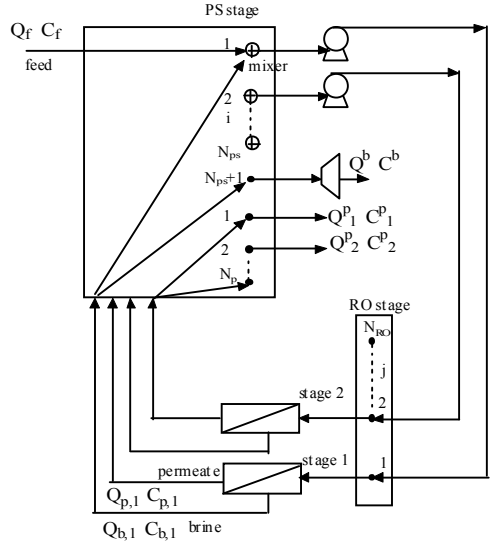

Fig. 1 The representation of the RO network via the superstructure

All the streams connected to the ith pressurization stage firstly mix in the mixer. The outlet pressure from the mixer is the smallest feed pressure. The stream split ratios and the logical expression of stream mixing are employed in this paper, these techniques reduced the number of binary variable and the solving space, therefore the mathematical model may be easily handled.
The overall material balances for the RO network and a set of product quantity and quality constraints concerning the minimum desirable product flow rate, and the maximum allowable product concentration are also needed in the system model.

4. Solution methodology

The optimization design problem is formulated as a mixed-integer nonlinear programming (MINLP) for minimizing the total annualized cost subject to thermodynamic, technical, and flexibility constraints. The MINLP can be solved using the software GAMS. This procedure is carried out by introducing an excessive number of units as an initial guess, while at the optimum certain design variables, such as stream split ratios, are either set to zero or to a value that indicate the absence or presence of the specific stage. Several starting points are used to obtain the best possible solution.

5. Illustrative example

The proposed methodology for RO system optimization design has been applied to deals with the desalination of seawater. In this example, there are three kinds of freshwater required, which subject to different permeate quantity and quality constraints. The minimum desirable product flow rate for these outlets are 200 m^3/h, 100 m^3/h, 50 m^3/h, while the corresponding maximum allowed salt concentration are 100 ppm, 300 ppm, 500 ppm, respectively. Four different types of FilmTec reverse osmosis membrane elements from DOW have been included in the design studies of the current work. They are the low energy, high productivity element SW30XLE-400, the high rejection, high productivity element SW30HR-380, the high rejection, fouling resistant element SW30HR-320, and the high productivity, high rejection brackish RO element BW30-400.
The results of the RO system optimization design were presented in Table 1. The two-stage RO configuration with brine re-processing was employed in design (shown as Fig. 2). This scheme supplies three kinds of freshwater. The first freshwater come from the permeate of stage 1 ($x_{p,5,1}$=0.828) which concentration is lower, while the third freshwater come from the permeate of stage 2 ($x_{p,7,2}$=0.46). The second freshwater consist of partial permeate coming from stage 1 ($x_{p,6,1}$=0.172) and stage 2 ($x_{p,6,2}$=0.54). The total annualized cost of the system is $1,397,600 per year.

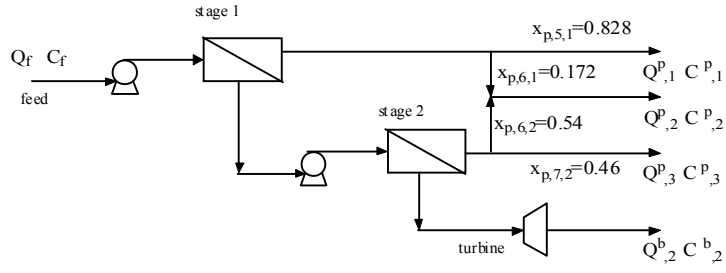

Fig. 2 The optimal RO configuration with multiple-product outlet

6. Conclusions

For a RO system of seawater desalination with multiple-product requirement, the design objective is to identify the most cost effective RO network configuration, the optimal streams distribution and operating conditions, and the optimal arrangement of the membrane elements. A process synthesis method has been applied to the optimal design of RO system with multiple freshwater outlets. The design task has been formulated as an MINLP which minimizes the total annualized cost of the RO system. As a results, in this RO system, the various freshwater with different concentration can be supplied simultaneously, it can lead to significant capital cost and energy saving and provide income from the multiple freshwater sales. A desalination case demonstrated that the design method can meet the requirement for multiple freshwater at the lowest cost.

Table 1 Design and optimization results for the study case

Process flow	two-stage RO system, show as Fig. 2
Seawater feed flow, Q_f (m^3/h)	588
Flow rate of the first freshwater, Q^p_1 (m^3/h)	200
Salt concentration of the first freshwater, C^p_1 (ppm)	100
Flow rate of the second freshwater, Q^p_2 (m^3/h)	100
Salt concentration of the second freshwater, C^p_2 (ppm)	300
Flow rate of the third freshwater, Q^p_3 (m^3/h)	50
Salt concentration of the third freshwater, C^p_3 (ppm)	430
Membrane type in stage 1	SW30HR-320
Number of elements per PV in stage 1	3
Number of PV in stage 1	81
Operating pressure in stage1, P_1 (Mpa)	8.2
Membrane type in stage 2	SW30XLE-400
Number of elements per PV in stage 2	4
Number of PV in stage 2	53
Operating pressure in stage2, P_2 (Mpa)	8.3
The overall system recovery	59%
The total annualized cost, ($)	1,397,600

Acknowledgements

This work was financially supported by the Education Department of Guangxi, China (200812MS084), Project of the Science and Technology Department of Guangxi, China ((No.0992028-13).

References

N.M. Wade, 2001, Distillation Plant Development and Cost Update, Desalination, 136, 3-12.

M.G. Marcovecchio, P.A. Aguirre, 2005, Global Optimal Design of Reverse Osmosis Networks for Seawater Desalination: Modeling and Algorithm, Desalination, 184, 259-271.

M.M. El-Halwagi, 1992, Synthesis of Reverse Osmosis Networks for Waste Reduction, AICHE J, 38, 1185-1198.

M. Zhu, M.M. El-Halwagi, 1997, Optimal Design and Scheduling of Flexible Reverse Osmosis Networks, Journal of membrane science, 129, 161-174.

N.G. Voros, Z.B. Maroulis, 1997, Short-cut Structural Design of Reverse Osmosis Desalination Plants, Journal of membrane science, 127, 47-68.

I.A. Karimi and Rajagopalan Srinivasan (Editors), Proceedings of the 11th International Symposium on Process Systems Engineering, 15-19 July 2012, Singapore.

Retrofit of Heat Exchanger Networks Including the Detailed Equipment Design

Mauro A. S. S. Ravagnani, Aline P. Silva

Chemical Engineering Department – State University of Maringá
Av. Colombo, 5790 – Maringá - CEP 87020900 – Brazil
ravag@deq.uem.br

Abstract

Many studies and methodologies were proposed to minimize the utilities consumption, the number of heat transfer equipment and effluent emissions by synthesizing Heat Exchanger Networks (HEN). Most of these formulations have been developed to the synthesis of new plants. Industrial processes in operation, however, can often be made more energy-efficient and sustainable by a retrofit. In the present paper, a methodology for the retrofit of HEN considering simultaneously the possibilities of reuse of exchangers for different junctions and the inclusion of new units is proposed, both considering the detailed heat exchangers design using TEMA standards. The developed methodology is based on a superstructure simultaneous optimisation model for the HEN synthesis considering stream splitting, with an additional constraint of including all the existent equipment among the possibilities of heat exchanges. The superstructure takes into account the operational and capital costs, by maximizing the recovery of energy and minimizing the installation costs. In the object function the total cost is composed by the costs of utilities used in the HEN and the new equipment. The problem was solved using Particle Swarm Optimization (PSO).

Keywords: heat exchanger networks, retrofit, Particle Swarm Optimization, detailed design, shell and tube heat exchangers.

1. Introduction

Heat exchanger networks (HEN) synthesis is an important field in process systems engineering, and has been the subject of considerable research efforts over the last five decades. Many studies and methodologies were proposed to minimize the utilities consumption, the number of heat transfer equipment and effluent emissions. Most of these formulations have been developed to the synthesis of new plants. Industrial processes in operation, however, can often be made more energy-efficient and sustainable by a retrofit. As a task considerably more arduous than the grassroots design, the retrofit of heat exchanger networks presents a less intense progress. This can be explained because the process must suffer structural modification, considering the reuse of existing heat exchanger equipment and the inclusion of new ones, resulting in increases in process fixed costs. The detailed design of the equipment is also a

subject that can influence in the final cost and in the environmental impact caused by the emissions.

Papers relating retrofit in HEN was first published in the middle of the 1980, using thermodynamic concepts (Tjoe and Linnhoff, 1986, Asante and Zhu, 1996, Nordman e Berntsson, 2009 a,b). Mathematical methods were also proposed (Ciric and Floudas, 1989, Yee and Grosmman, 1990, Ciric and Floudas, 1990, Yee and Grosmman, 1991, Singh and Castillo, 2002, Bjork and Nordman, 2005). Some authors used thermodynamic concepts jointly with Mathematical Programming (Zhu and Asante, 1999, Nie and Zhu, 1999, Panjeh Shahi et al. 2008).

In the present paper it was developed a methodology for the retrofit of HEN including the detailed design of the heat exchangers. A new network is proposed using all the existent equipment. The method is based on the superstructure proposed by Yee and Grossmann (1990).

2. Development

The proposed methodology for the retrofit of HEN consider simultaneously the possibilities of reuse of exchangers for different junctions and the inclusion of new units is proposed, both considering the detailed heat exchangers design using TEMA standards. The developed methodology is based on a superstructure simultaneous optimization model for the HEN synthesis considering stream splitting, with an additional constraint of including all the existent equipment among the possibilities of heat exchanges. This superstructure takes into account the operational and capital costs, by maximizing the recovery of energy and minimizing the installation costs. The object function takes in account the total cost composed by the cost of the utilities used in the HEN and the cost of the new equipment. The heat exchangers are designed using the methodology presented in Ravagnani and Caballero (2007). The standards of TEMA are used, jointly with the Bell-Delaware method for the shell side. The design method is included in the HEN retrofit procedure. The problem was solved using Particle Swarm Optimization (PSO) presented in Ravagnani et al. (2009).

The problem can be formulated as the minimization of the total cost (the summation of the cost of including new heat exchangers and the cost of utilities).

3. Example

An example is used to show the applicability of the developed methodology, presented by Castillo et al. (1998). The current HEN has three heat exchangers (5.69 m^2, 2.55 m^2 and 0.41 m^2, respectively), six heaters and five coolers. Hot and cold utilities consumption are, respectively, 3,100 kW and 4,375 kW. Stream data as well as the cost for additional equipment and the parameters used for PSO are presented in Table 1. Figure 1 shows the existent HEN. The problem is solved using the proposed methodology and the new

HEN is achieved, with sixe heat exchangers (three new and the three old ones, reused), five coolers and no heaters. The stopping criteria used is a fixed number of iterations. Table 2 present the detailed design of the new heat exchangers. Figure 2 present the new HEN and Table 3 show the final costs for the network. Computational effort (@Pentium IV 1.70 GHz) was approximately 600 minutes.

4. Conclusions

In this paper it is proposed a new methodology for the retrofit of HEN. The final network has the minimum cost, considering area and utilities, considering all the existent heat exchangers. The method is based on a superstructure proposed by Yee and Grossmann (1990) and the heat exchangers are designed using the procedure proposed by Ravagnani et al. (2009). The optimisation problem is solved using the PSO algorithm. One example was presented to show the applicability of the proposed methodology.

Results shown that the proposed methodology is very interesting, allowing achieving optimal HEN using all the existent heat exchangers. Computational effort is acceptable, considering the constraints of including all the existent heat exchangers with the detailed design using the Bell-Delaware method.

References

Z. Asante, N. D. K. e Zhu, X. X. (1996). An automated approach for heat exchanger network retrofit featuring minimal topology modifications. *Computers & Chemical Engineering*. 20: S7–S12.

Bjork, K. e Nordman, R. (2005). Solving large-scale retrofit heat exchanger network synthesis problems. *Chemical Engineering and Processing*. 44: 869-876.

Castillo, E., Acevedo, L. e Reververi, A. (1998). Cleaner Production of Nitric Acid by Heat Transfer Optimization: A Case Study. *Chemical & Biochemical Engineering*. 12: 157 – 165**.**

Ciric, A. R., e Floudas, C. A. (1989). A Retrofit Approach for Heat Exchanger Networks. *Computers & Chemical Engineering.* 13(6): 703-715.

Ciric, A. R. e Floudas, C. A. (1990). A Mixed Integer Nonlinear Programming Model for Retrofitting Heat-Exchanger Networks. *Industrial & Engineering Chemistry Research*. 29: 239-251.

Nie, X., R. e Zhu, X. (1999). Heat Exchanger Network Retrofit Considering Pressure Drop and Heat-Transfer Enhancement. *AIChE Journal*. 45(6): 1239-1254.

Nordman, R. e Berntsson, T. (2009a). Use of advanced composite curves for assessing cost-effective HEN retrofit I: Theory and concepts. *Applied Thermal Engineering*. 29: 275–281.

Nordman, R. e Berntsson, T. (2009b). Use of advanced composite curves for assessing cost-effective HEN retrofit II. Case studies. *Applied Thermal Engineering*. 29: 282–289.

Panjeh Shahi, M. H., Ghasemian Langeroudi, E., Tahouni, N. (2008). Retrofit of ammonia plant for improving energy efficiency., *Energy*. 33: 46–64.

Ravagnani, M. A. S. S., and Caballero, J. A. (2007). A MINLP Model For The Rigorous Design Of Shell And Tube Heat Exchangers Using The Tema Standards. *Chemical Engineering Research and Design.* n. 85(A10): 1–13.

Ravagnani, M. A. S. S., Silva, A. P., Biscaia Jr, E. C. e Caballero, J. A. (2009). Optimal Design of Shell-and-Tube Heat Exchangers Using Particle Swarm Optimization. *Industrial & Engineering Chemistry Research.* 48 (6): 2927-2935.

Singh, H. e Castillo, F. (2002). Process life cycle solutions for the case of automated heat exchanger network retrofit. *Applied Thermal Engineering*. 22: 949-958.
Tjoe, T.N. e Linnhoff, B. (1986). Using Pinch Technology for Process Retrofit. *Chemical Engineering*. 28: 47 - 60.
Yee, T. F. e Grossmann, I. E. (1990). Simultaneous Optimization Models for Heat Integration – II Heat Exchanger Network Synthesis. *Computers & Chemical Engineerin*. 14(10): 1165-1184.
Yee, T., F. e Grossmann, I. E. (1991). A Screening and Optimization Approach for the Retrofit of Heat-Exchanger Networks. *Industrial & Engineering Chemistry Research*. 30(1): 146-162.
Zhu, X. X. e Asante, N. D. K. (1999). Diagnosis and Optimization Approach for Heat Exchanger Network Retrofit. *AIChE Journal*. 45(7): 1488-1503.

Table 1 – Inlet data

Stream	*Tin (K)*	*Tout (K)*	*m (kg/s)*	*μ (kg/ms)*	*ρ (kg/m3)*	*Cp (J/kgK)*	*κ (W/mK)*	*ΔP (kPa)*	r_d *(W/mK)*
H1	1113	313	2.033	2.4 E-4	634	2454	0.114	68.95	1.7 E-4
H2	349	318	1.909	2.4 E-4	634	2454	0.114	68.95	1.7 E-4
H3	323	313	0.315	2.4 E-4	634	2454	0.114	68.95	1.7 E-4
H4	453	350	0.249	2.4 E-4	634	2454	0.114	68.95	1.7 E-4
H5	453	452	119.28	2.4 E-4	634	2454	0.114	68.95	1.7 E-4
H6	363	318	1.249	2.4 E-4	634	2454	0.114	68.95	1.7 E-4
C1	297	298	134.39	2.4 E-4	634	2454	0.114	68.95	1.7 E-4
C2	298	343	0.219	2.4 E-4	634	2454	0.114	68.95	1.7 E-4
C3	308	395	1.519	2.4 E-4	634	2454	0.114	68.95	1.7 E-4
C4	363	453	0.248	2.4 E-4	634	2454	0.114	68.95	1.7 E-4
C5	453	454	1051.79	2.4 E-4	634	2454	0.114	68.95	1.7 E-4
UQ	503	503							
UF	293	313							

Area cost = $9094 + 485A^{0.81}$, A em m^2
Pumping cost= $0.7\ (\Delta P_t m_t/\rho_t + \Delta P_s m_s/\rho_s)$, ΔP em Pa, m em kg/s e ρ em kg/m^3
Hot utility cost = 110 $/kW ano
Cold utility cost = 15 $/kW ano
c1 = c2 = 1.0 w = 0.65 Npt = 30

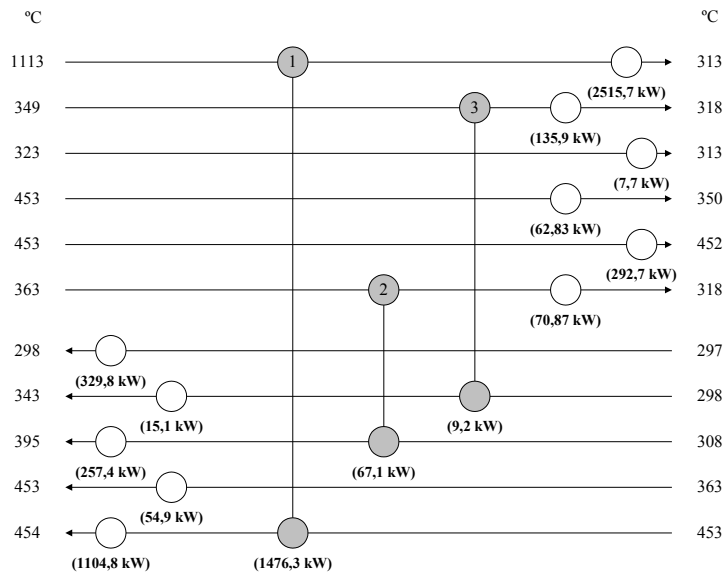

Figure 1 – Actual HEN

Table 2 – New equipment details

	E4	*E5*	*E6*
L (m)	*2.438*	*2.438*	*2.438*
D_c (m)	*0.686*	*0.205*	*0.205*
N_t	*349*	*16*	*14*
d_{ex} (m)	*0.0254*	*0.0191*	*0.0254*
d_{in} (m)	*0.0225*	*0.0122*	*0.0170*
ΔP_t (kPa)	*16587.14*	*63668.32*	*67854.25*
ΔP_c (kPa)	*33.29*	*3.58*	*3.91*
r_d (m^2 KW)	*3.396E-03*	*1.171E-02*	*7.710E-04*
Arrangement	*Triangular*	*triangular*	*triangular*
Hot fluid	*Shell*	*Tube*	*Tube*
Area (m^2)	*6.80*	*0.23*	*0.27*
Cost ($/year)	11,382.53	*9,241.48*	*9,261.94*

Table 3 – Comparison of the global cost

	Cost ($/year) Actual HEN	Cost ($/year) New HEN
HU	193,820	0
CU	46,290	21,240
Area	----------	29,886
Total	240,110	51,126

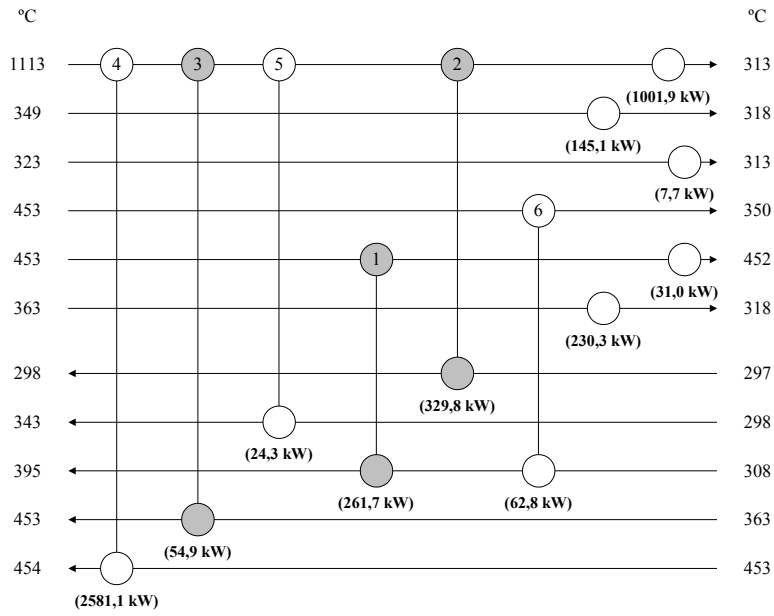

Figure 2 – Final HEN configuration

I.A. Karimi and Rajagopalan Srinivasan (Editors), Proceedings of the 11th International Symposium on Process Systems Engineering, 15-19 July 2012, Singapore.

Production of Cylohexane from Hydrogenation of Benzene using Microreactor Technology

Emmanuel A. Dada,[a] Luke Achenie[b]

[a]*ChemProcess Technologies, LLC, P.O. Box 3046, League City, TX 77573, USA*
[b]*Dept of Chemical Engineering, Virginia Polytechnic Institute & State University, Blacksburg, VA 24061, USA*

Abstract

Cyclohexane is generally used as an intermediate chemical where about 54 percent of its production is used in the production of adipic acid for nylon-6/6, 39 percent for caprolactam for nylon-6, and 7 percent for miscellaneous including solvents, insecticides and plasticizers. The demand for nylon (and hence cyclohexane) in engineering thermoplastics in resins and films is growing at about 6% annually. The production of cyclohexane from hydrogenation of benzene and hydrogen is a highly exothermic reaction where the reactor temperature control is very critical. Consequently, in most conventional commercial cyclohexane processes, multi-stage reactors involving recycling of cyclohexane, inter-reactor cooling to allow efficient removal of the heat of hydrogenation, and staged addition of the benzene feed are employed.

To address the temperature control problem more efficiently, we have taken advantage of the efficient and rapid heat removal characteristics of a microreactor system; our design offers more than two orders of magnitude better temperature removal and control than conventional reactors.. Our design also achieved minimal benzene, methylcyclopentane and other impurities (by-products) in the product thus having less impact on the environment compared with the conventional process. This paper suggests a general microreactor technology framework for the production of cyclohexane and other similar commodity chemicals. The framework is economical and leads to a safer route than the conventional technology.

Keywords: cyclohexane, microreactor, hydrogenation, safe, economical

1. Introduction

Cyclohexane is generally used as an intermediate chemical. Specifically 54 percent of what is produced is used in the production of adipic acid for nylon-6/6, 39 percent for caprolactam for nylon-6, and 7 percent for products including solvents, insecticides and plasticizers. The demand for nylon (and hence cyclohexane) in engineering thermoplastics in resins and films is growing at about 6% annually. Engineering thermoplastics are noted for their outstanding properties of high tensile strength, excellent abrasion, and chemical resistance and heat resistant. They have particular and growing demand in performing mechanical duties that traditionally relied on metal parts. The total world annual capacity of cyclohexane is about 1,800 million gallons of

which the U.S. capacity is about 600 million gallons with the U.S. annual production of Chevron-Phillips of 205 million gallons. Cyclohexane growth rate is estimated to average about 2 percent annually. The demand for cyclohexane in Japan has decreased due to a new production route to adipic acid that employs cyclohexene rather than cyclohexane.

Both patents and technical literature on conventional production of cyclohexane from hydrogenation of benzene have been reviewed. The available processes are very similar but differ by the choice of catalysts to ensure high degree of hydrogenation in order to meet product specifications. The major by-products of hydrogenation of benzene to cyclohexane are n-hexane, methyl-cyclopentane, methyl-cyclohexane, methyl-pentane, n-pentane, and methane. The control of the reactor's temperature and maintaining it at a desired level minimizes by-products formation. One of the major problems encountered in the production of cyclohexane is the deactivation of the reactor's catalyst bed by the CO in the hydrogen source necessitating a pre-treatment reactor unit (methanator) that converts the CO to methane and water before the hydrogen is fed into the main reactor. In the literature, a sensitivity analysis on the temperature control was carried out to investigate the best phase to carry out the reaction. Although most production of cyclohexane is carried out in the vapor phase, there are claims in the open literature that the mixed-vapor (liquid and gas mixture) phase gives the best reactor temperature control. However, when the temperatures and pressures are carefully chosen with the right catalyst, a liquid phase reaction minimizes by-products and gives a good reactor temperature control.

2. Reactor design for Production of Cyclohexane

The design of the reactor is the key to the production of cyclohexane where the temperature control of this highly exothermic reaction is an important determinant in the reactor configuration. We have carried out extensive literature search on many of the industrial processes and found out that most of the processes for the production of cyclohexane were carried out in the vapor phase. Table 2.1 shows the reactor operating conditions for different phases (liquid, liquid + vapor, and vapor). Our results are consistent with the studies reported by John McKetta and William Cunningham, 1978. Although most industrial processes for the production of cyclohexane are carried out in the vapor phase, McKetta and Cunningham suggested that a mixed phase (liquid + vapor) has the advantage of considerable flexibility. In view of these facts we chose to design the reactor for a mixed phase. The operating conditions (temperature of about 200 °C, and pressure of about 40 atms) that we selected for the mixed phase reactor design are very similar to the IFP (US patent 3,202,723). At these operating conditions, the principal side reaction of isomerization of cyclohexane to methyl cyclopentane is minimized.

The mixed phase presents a great challenge for the reactor design; we modeled the mixed phase as separate liquid and vapor phases and applied different kinetics equations to each phase. The work of Konyukhov, et al., appears to be one of the best referenced liquid phase kinetics studies of hydrogenation of benzene to cyclohexane. Likewise the work of Kehoe and Butt appears to be the most relevant vapor phase kinetics studies of hydrogenation of benzene to cyclohexane. Specifically these two pieces of work have

reconciled the many variations of the literature kinetics results in the liquid and vapor phases respectively. Therefore we employed these findings in our preliminary reactor design. In particular, Kehoe and Butt have shown that for a commercial nickel on kieselguhr, Harshaw Ni-0104 P, supplied as a powder and containing 58% wt Ni, equation 2.1 is applicable. Our preliminary reactor design and key results are

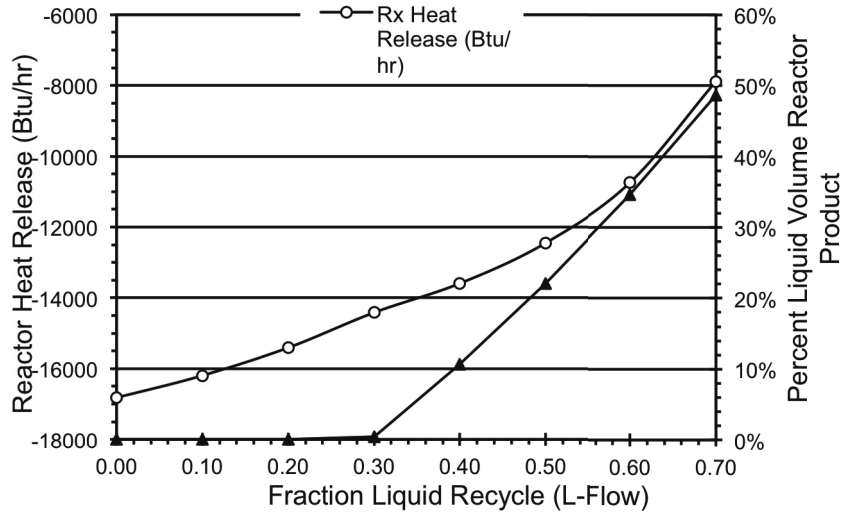

Figure 2.1 Impact of Liquid Recycle on Reactor Heat and Reactor Liquid

Table 2.1 Reactor Operating Conditions

Temperature (F)	Pressure (Psia)	H_2/C_6H_6 (HBR)	Reactor Phase
350 – 500	250 – 500	≥3.5	Vapor
350 – 500	350 – 500	3.05 – 3.5	Vapor + Liquid
350 – 400	≥2500	3.05 – 3.2	Liquid

presented in Figure 2.1.

$$Rate = \{\nu K P_B P_{H2} exp[-(Q+E)/RT]\}/\{1 + K P_B exp(-Q/RT)\} \quad (2.1)$$

Here $\nu = 0.1774$ mol/g catalyst s Torr, $K = 0.000008905$ Torr^{-1} (or 8.905 X10^{-6} Torr^{-1}), $Q = -8.26$ kcal/mol (Heat of adsorption), $E = 12.29$ kcal/mol (activation energy), $P_B =$ Partial Pressure Benzene, Torr, $P_{H2} =$ Partial Pressure Hydrogen, Torr, $T =$ Temperature, deg K, $R = 1.987$ cal/gmol K (gas constant), Torr = (101.325/760) kN/m^2.

3. Process Improvement (i.e. Optimization) Studies

We carried out space-time yield analysis and "optimized" relevant process parameters for the design of the microreactor. The key results are presented here.

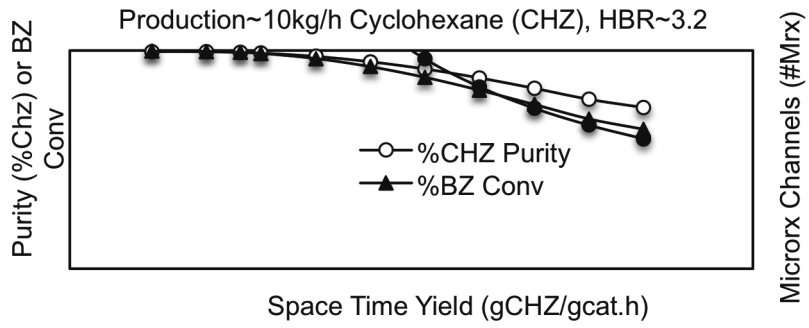

Figure 3.1 Space Time yield vs. Product Purity (3.2 H_2/C6H6 feed ratio)

3.1 Impact of Space Time Yield on product Purity

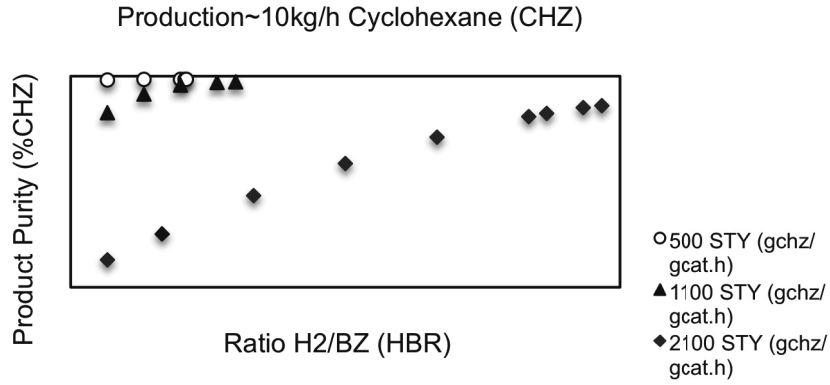

Figure 3.2 Impact of hydrogen to benzene feed ratio (HBR) on Product Purity

As shown in Figure 3.1, a reactor with space-time yield of 600 g Cyclohexane (CHZ)/g cat.h or less is needed to achieve 99wt% or more product purity. For the production of 10 kg/hr of cyclohexane, about 200 or more channels are needed to deliver 99 wt% product purity at hydrogen to benzene feed ratio of 3.2. Each channel is assumed to be of dimensions 500 micron x 500 micron x 6 in.

3.2 Impact of Hydrogen-Benzene Ratio on Product Purity

Figure 3.2 shows that for all space-time yields increasing the hydrogen-benzene ratio will result in higher product purity. As expected, a reactor with moderate to large volume (e.g. 500 - 800 g CHZ/g cat.h (STY) yields high purity product (>99wt %) with moderate amount of hydrogen (3.2- 4.0 HBR). Also, a reactor with small volume (1100-2100 g CHZ/g cat.h STY) will need moderate to large amount of hydrogen (>4.5 HBR) to attain the same product purity.

4. Results and Discussion

In this paper we have presented the design of a microchannel catalytic reactor system for production of cyclohexane from hydrogenation of benzene. The microreactors operate at a combined space-time yield of 500g cyclohexane/g cat.h and at 3.2 molar ratio of hydrogen to benzene. The proposed process involves large and rapid heat transfer, and we have shown that microreactors have promising application for better control and safety because of their large surface to volume ratio better than the conventional reactors.

References

Amend, William J., 1943, "Catalytic Oxidation", US Patent 2316543 assigned to DuPontClement, Thonon, 1965, "Process for the Catalytic Hydrogenation of Aromatic Hydrocarbons", US patent 3,202,723, assigned to Institut Francais du Petrole.

Felix, Albert; Roques, Yves, 2004, "Method of making adipic acid", US patent 6822117 assigned to Rhodia, Fiber And Resin Intermediates (Courbevoie, FR)

John McKetta and William Cunningham, 1978, Vol. 14 of Encyclopedia of Chemical Processing and Design.

Kehoe and Butt, 1972, "Kinetics of Benzene Hydrogenation by Supported Nickel at Low Temperature", Journal of Applied Chem. Biotechnol. 22, 23-30

Kirk-Othmer Encyclopedia of Chemical Technology, 1980, Vol. 12, John Wiley & Sons.

Konyukhov, et al., 1987, "Kinetics of Liquid-Phase Hydrogenation of Benzene on Palladium Catalyst and Hydrogenation of Toluene on Palladium and Catalysts", Kinetika, Vol. 28, No 2, pp. 360-365

Sanderson, John Ronald, et al., 2003, " Manufacture of cyclohexane from benzene and a hydrogen source containing impurities", US patent application # 20030114723

Srinivas, Darba; Chavan, Suhas; Ratnasamy, Paul, 2003, "Process for the preparation of adipic acid", US Patent 6521789 assigned to Council of Scientific and Industrial Research (New Delhi, IN)

Ullmann's Encyclopedia of Industrial Chemistry, 2005

I.A. Karimi and Rajagopalan Srinivasan (Editors), Proceedings of the 11th International Symposium on Process Systems Engineering, 15-19 July 2012, Singapore.

Synthesis Framework of Biorefinery Systems for Lignocellulosic Biorenewables

Wenkai Li[a], Ramadoss Karthik[b], I A Karimi[b], Wong Pui Kwan[c]

[a] *Graduate School of International Management, International University of Japan, Niigata, Japan 949-7277*
[b] *Department of Chemical and Biomolecular Engineering, National University of Singapore, 4 Engineering Drive 4, Singapore 117576*
[c] *Institute of Chemical and Engineering Sciences, Agency for Science, Technology and Research (A*STAR), No. 1, Pesek Road, Jurong Island, Singapore 627833*

Abstract

In this paper, we present a mathematical framework to design an economically attractive and environmentally friendly biorefinery. We embed various biomass feedstocks, conversion technologies, and products into a novel superstructure of alternative configurations for a general biorefinery. To obtain the optimal configuration and design of the biorefinery, we model each technology block using simplified mass, resource, and energy balance equations. These form the basis for the mathematical model.
Keywords: lignocellulose, biorefinery, process synthesis.

1. Introduction

The world is actively looking for sustainable alternatives to meet increasing energy and product demands. This is amid growing concerns of global warming, fast depletion of petroleum resources, expected increase in crude oil price due to rapid demand growth from China and India, and unstable oil supply due to the turmoil in the Middle East. Although the replacement of carbon-based economy is receiving considerable attention nowadays, mankind's reliance on carbon will continue for the foreseeable future. As the only carbon-rich material source, biorenewables processed in biorefineries are very likely to be the only viable alternative to fossil resources for the production of chemicals and transportation fuels. The development of biorefineries will be "the key for the access to an integrated production of food, feed, chemicals, materials, goods, and fuels of the future" (National Research Council, 2000). Several major research projects are underway worldwide on the development and demonstration of biorefineries. These include BIOCORE in EU, DEFRA in UK, and VACL in Singapore.

2. Literature Review

Based on the types of feedstocks used, Kamm and Kamm (2004) categorize biorefineries into three major systems: the whole-crop biorefinery, the green biorefinery and the lignocellulose feedstock (LCF) biorefinery. LCF biorefinery is considered as the most promising one because of its abundance, renewability, lack of competition with food/crop, and ability to contribute to significant CO_2 emission reduction. Most existing literature study either single product (mostly bioethanol) with some by-products or a single main product (mostly bioethanol) together with 1 or 2 value-added products from the LCF biorefinery. Little research has focused on producing high value-added products where bulk chemicals such as bioethanol are not the main products.

Kamm and Kamm (2006) highlight existing works relevant to process, raw material, product, and technology options. However, a study that integrates all these components using a modeling and optimization approach based on mathematical programming does not exist. Here, we aim to bridge these knowledge gaps by systematically and intelligently proposing and evaluating possible alternatives for a biorefinery configuration.

The attractive future prospects for biorefineries are accompanied by several unique and challenging characteristics. Such challenges mainly include supply chain design and management (decentralized raw material sources, low transport densities, etc.), process design and development (e.g. lack of models and critical data, heterogeneity and complexity of biomass sources and conversion technologies) and intelligent decision making (e.g. uncertainty in markets and prices). Furthermore, in most scenarios, successful process synthesis strategies for conventional refineries do not work for biorefineries. Thus, biorefinery synthesis using advanced systems engineering approaches requires substantial research to design and manage economically viable and environmentally benign biorefineries. Ideally, a holistic lignocellulosic biorefinery should integrate the three major aspects shown in Figure 1.

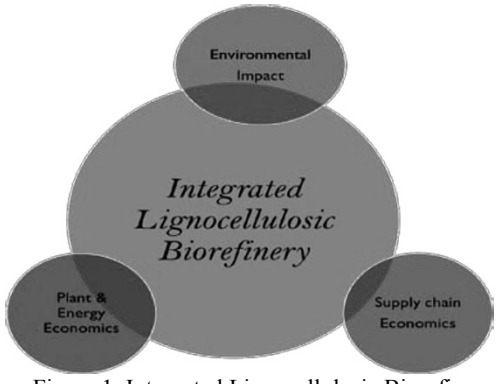

Figure 1. Integrated Lignocellulosic Biorefinery

3. Superstructure for a General Biorefinery

Biomass has a complex composition and can be processed to a plethora of products. Starting from the pre-treatment unit, numerous processing routes and products can exist. We have explored a variety of plausible and promising options for the conversion of cellulose, lignin, and C5 sugars into a slate of potential products using different technologies. The goal was to gather as many "potentially synergistic" alternatives as possible for products, technologies, and processes into a grand pool from which we can synthesize novel, non-intuitive, and best options. We have developed a superstructure (Figure 2) of various alternative configurations for a general VACL biorefinery system. Such a superstructure can enable an objective, systematic, and smart examination of various alternatives through a modeling and optimization approach based on mathematical programming.

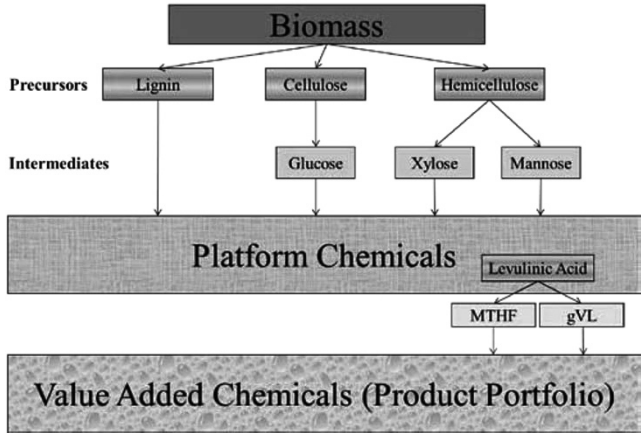

Figure 2. Superstructure For A General Biorefinery

Figure 2 is based on three precursors, namely lignin, cellulose, and

hemicellulose; three intermediate chemicals, namely glucose, xylose, and mannose; and several platform chemicals. Key value-added chemicals from each platform chemical are also identified according to their market importance. Processing routes applying different technologies connecting the precursors, intermediates, platform chemicals, and final value-added chemicals are also identified. The platform chemicals and their derivatives are mainly selected from three major reports in the literature, namely the US DoE Report, the BREW Project report and the FROPTOP white paper. Clearly, the collected pool of options and possibilities is huge and interconnected, making the determination of the optimal configuration of a VACL biorefinery a formidable task.

4. Mathematical Formulation

All operations in the biorefinery are modeled using basic equations. The parameters and values used are based on yearly operation. Some notations are adopted from Oh and Karimi (2004) and Hugo and Pistikopoulos (2005).

4.1. Material Balances

Let m denote all materials (raw materials, products, and utilities) involved in the biorefinery, s denote source, c denote consumer and t denote fiscal year. Let IM_u and OM_u denote sets of input and output materials of unit u respectively and U denote set of all units in the biorefinery. Two special units are used in our model: *Src*, which represents the source of raw materials, and *Market*, which represents the sink of products. The life time of the biorefinery is assumed to be T years. Let f_{msu} denote the flow of material m from unit s to unit u.

As data available in most of the literature are usually based on a primary material to characterize the unit operation, we identify a primary material π_u to be used as the reference for further calculation. The actual consumption/production level of material m can be calculated from the consumption/production level of the primary material π_u.

$$\sum_{m\in OM_s} f_{msu} + \sum_{m\in IM_c} f_{muc} = \rho_{mu}\left(\sum_{\pi_u\in OM_s} f_{\pi_u su} + \sum_{\pi_u\in IM_c} f_{\pi_u uc}\right), u\in U, m\in IM_u \cup OM_u \tag{1}$$

, where ρ_{mu} is the amount of material m needed to process one unit of π_u in unit u.

In addition to the above constraint, the supply of raw materials is limited by its availability in the market, the manufacture of products is limited by its demand in the market, the operation capacity of a unit is restricted by its technological limits, and emissions from the biorefinery should not exceed regulatory limits.

4.2. Environmental Impact Assessment

4.2.1. Goal and Scope

We apply the popular 'cradle-to-gate' approach, in which downstream processing is neglected, to assess the environmental impact of the biorefinery. We employ Eco-indicator 99 score as the environmental performance indicator. The eleven impact categories proposed by Eco-indicator 99 are considered, which are further aggregated into three damage categories.

4.2.2. Inventory Analysis

Let D_{eu} denote the value of impact category e for unit u. Let V denote set of environmental burdens, E denote set of impact categories, W denote set of raw materials and R_u denote set of utilities consumed by unit u. Parameters df_{ve} and ω_{vm} give the damage factor of substance v contributing to impact category e and the amount of substance v generated per unit flow of material m respectively.

$$D_{eu}=\sum_{v\in V}\left[df_{ve}\left(\sum_{\pi_u\in OM_s\in s}f_{\pi_u su}+\sum_{\pi_u\in IM_c\in c}f_{\pi_u uc}\right)\left(\omega_{v\pi_u}+\sum_{m\in W\cup R_u}\omega_{vm}\rho_{mu}\right)\right] \quad (2)$$

4.2.3. Impact Assessment

Let L_{ed} denote set of impact categories e that belong to damage category d and D denote set of damage categories. The values of the impact categories are first normalized and then aggregated into a single Eco-Indicator 99 score using a normalization factor η_d and a weighting factor Ψ_d:

$$Eco\text{-}indicator\ 99=\sum_{d\in D}\left(\Psi_d\eta_d\sum_{e\in L_{ed}}\sum_{u\in U}D_{eu}\right) \quad (3)$$

4.3. Economics

We assume linear relationships between the flow rate of the primary material π_u and both the operation cost $OPEX_{ut}$ and capital investment $CAPEX_{ut}$ of unit u in fiscal year t. All investment costs for unit u are made at the first fiscal year. Also the total capital investment of the biorefinery should not exceed budgetary constraints.

The purchase cost of input materials RC_{ut} of unit u in year t is given by:

$$RC_{ut}=(1+ir)^t\sum_{m\in IM_u}\sum_{m\in OM_s\in s}CIF_{msu}f_{msu},u\in U,t\in T \quad (4)$$

, where ir is the inflation rate and CIF_{msu} is the cost of purchase, insurance, freight, and waste treatment of raw material m from supplier s to unit u.

The cost of utilities UC_{ut} consumed by unit u in year t is given by:

$$UC_{ut}=(1+ir)^t\sum_{r\in R_u}CIF_{r,Src,u}\rho_{ru}\left(\sum_{\pi_u\in OM_s\in s}f_{\pi_u su}+\sum_{\pi_u\in IM_c\in c}f_{\pi_u uc}\right),u\in U,t\in T \quad (5)$$

The selling rate of output materials SR_{ut} of unit u in year t is given by:

$$SR_{ut}=\sum_{m\in OM_u}\sum_{m\in IM_c\in c}P_{muc}f_{muc},u\in U,t\in T \quad (6)$$

, where P_{muc} is the price of product sold from unit u to unit c.

Assuming that the life times of all units start at t=1 and end at t=T, the total capital expenditure CE_{ut} for unit u in year t is given by:

$$CE_{ut}=CAPEX_{ut}+OHC_{ut}-SV_{ut},u\in U,t\in T \quad (7)$$

, where OHC_{ut} is the unit overhead costs and SV_{ut} is the estimated salvage value of the unit at the end of the unit life time. SV_{ut} takes value of zero except at t=T.

The cash flow CF_{ut} of unit u in year t is given by:

$$CF_{ut}=\begin{cases}(SR_{ut}-RC_{ut}-OPEX_{ut}-UC_{ut})(1-TR_{ut})-CE_{ut} & \forall SR_{ut}-RC_{ut}-OPEX_{ut}-UC_{ut}\geq 0\\ (SR_{ut}-RC_{ut}-OPEX_{ut}-UC_{ut})-CE_{ut} & \forall SR_{ut}-RC_{ut}-OPEX_{ut}-UC_{ut}<0\end{cases},u\in U,t\in T \quad (8)$$

, where TR_{ut} is the corporate tax for unit u in year t.

The NPV (Net Present Value) of the biorefinery is given by:

$$NPV=\sum_{u\in U}\sum_{t}\frac{CF_{ut}}{(1+\phi)^t} \quad (9)$$

, where ϕ is the annual interest rate.

4.3.1. Multi-Objective Function

Two objectives, economic (expressed as *NPV*) and environmental (expressed as Eco-Indicator 99 score), are used in VACL biorefinery optimization model:

$$min\begin{pmatrix} -NPV \\ Eco\text{-}Indicator\ 99 \end{pmatrix} \tag{10}$$

Conclusions

We highlighted the need for continued research on the development of biorefineries and the importance of using advanced systems engineering methods to design sustainable biorefineries. We proposed a novel superstructure of various alternative configurations for a general biorefinery, and a general mathematical model to obtain the optimal design and configuration of a biorefinery. Key challenges in the implementation of this novel superstructure are its inherent complexity and unavailability of detailed data for chemicals and processes. We are currently in the process of generating necessary data for the various pathways in the superstructure, development of solution methodology, and testing with appropriate case studies.

References

[1] Biobased Industrial Products, Priorities for Research and Commercialization, National Research Council, National Academic Press, Washington, D.C., 2000.
[2] B. Kamm and M. Kamm, Appl. Microbiol. Biotechnol., No. 64 (2004), 137.
[3] B. Kamm, P.R. Gruber, M. Kamm (eds.), Biorefineries – Industrial Processes and Products, Vols 1 & 2, Wiley-VCH, Weinheim, Germany, 2006.
[4] T. Werpy and G. Petersen (eds.), Top Value Added Chemicals from Biomass Volume I: Results of Screening for Potential Candidates from Sugars and Synthesis Gas, Pacific Northwest National Laboratory and the National Renewable Energy Laboratory, Department of Energy (DoE), USA, 2004.
[5] M.K. Patel (ed.), Medium and Long-term Opportunities and Risks of the Biotechnological Production of Bulk Chemicals from Renewable Resources – The Potential of White Biotechnology – The BREW Report, Utrecht, Netherlands, 2006.
[6] W. Skibar, G. Grogan, J. McDonald and M. Pitts (eds.), UK Expertise for Exploitation of Biomass-Based Platform Chemicals, FROPTOP programme, UK, 2010.
[7] H.C. Oh and I.A. Karimi, Ind. Eng. Chem. Res., No. 43 (2004), 3364.
[8] A. Hugo. and E.N. Pistikopoulos, Journal of Cleaner Production, No. 13 (2005), 1471.

I.A. Karimi and Rajagopalan Srinivasan (Editors), Proceedings of the 11th International Symposium on Process Systems Engineering, 15-19 July 2012, Singapore.

Heat-integrated reactive distillation for biodiesel production from Jatropha oil

Samaporn Phuenduang,[a] Porntida Chatsirisook,[a] Lida Simasatitkul,[a] Woranee Paengjuntuek,[b] Amornchai Arpornwichanop[a,*]

[a] *Department of Chemical Engineering, Faculty of Engineering, Chulalongkorn University, Bangkok 10330, Thailand*
[b] *Department of Chemical Engineering, Faculty of Engineering, Thammasat University, Patumthani 12120, Thailand*
[*] *e-mail: Amornchai.a@chula.ac.th*

Abstract

Minimizing the biodiesel production cost by using inexpensive and inedible feedstock like Jatropha oil is more practical as it is readily available and also not competes with edible oils. However, Jatropha oil contains high free fatty acid content, which causes operational problems in biodiesel production via alkaline-based transesterification reaction. This study aims to design a biodiesel production process from Jatropha oil. A hydrolysis reactor is applied to convert triglyceride in Jatropha oil to fatty acid. The fatty acid obtained then reacts with methanol to produce methyl ester (biodiesel product) using an esterification process. A reactive distillation is employed to intensify reaction and separation tasks for the esterification process. In order to minimize energy consumption, the heat integration of a reactive distillation process is considered. The simulation result using a flowsheet simulator indicates that the heat-integrated reactive distillation can improve the biodiesel production by minimizing the energy requirements, compared with a conventional process.

Keywords: Reactive distillation, Heat integration, Biodiesel production, Jatropha oil

1. Introduction

Biodiesel, a clean renewable fuel, has been considered the best candidate for a petroleum diesel substitute because it can be used in any compression ignition engine without the need for modification (Leung et al., 2010). In general, biodiesel can be produced from natural resources such as vegetable oils, animal fats and algae. A high consumption of edible oils in the world results in a shortage of feedstock for biodiesel production. Alternatively, the use of inedible oils, which are unsuitable for human consumption because of some toxic components in the oils, is an interesting option.

Jatropha curcas is a potential resource for biodiesel production as it contains a high fraction of oils (30-40 wt.%). However, a high amount of free fatty acids (FFAs) in Jatropha oil affects a transesterification process using alkaline catalyst to generate biodiesel. FFAs can react with the alkaline catalyst and form soap, causing a difficulty in the purification of biodiesel product. Accordingly, the development of an efficient process for biodiesel production from oils with high free fatty acid content is required. A two-step biodiesel production has been proposed to deal with such a problem. The first step involves a hydrolysis process where triglycerides in oil are hydrolyzed with water to produce fatty acids and glycerol, whereas all the fatty acids react with methanol via esterification reaction to generate methyl oleate (biodiesel product) and water in the

second step (Chen et al., 2010). However, since the esterification is an equilibrium reaction, the conversion of fatty acid is limited. To improve the performance of biodiesel production, the application of a reactive distillation (RD) in which reaction and separation tasks are carried out in a single unit is an attractive option (Kiss et al., 2008).

This study is focused on the production of biodiesel from Jatropha oil. The two-step method consisting of hydrolysis and esterification sections is studied based on a reactive distillation technology. Process heat integration is considered to improve the energy usage of the biodiesel process.

2. Biodiesel production from Jatropha oil

Since oleic acid is a major component of Jatropha oil, triolein is used to represent a triglyceride in this study. Fig. (1) shows a conventional process for biodiesel production from Jatropha oil. Triolein is first treated with water to produce fatty acid and glycerol (Eq. 1). Fatty acid obtained then reacts with methanol to obtain methyl oleate, biodiesel product, and water (Eq. 2).

$$\begin{array}{l} CH_2-OCOR \\ CH-OCOR \\ CH_2-OCOR \end{array} + 3H2O \leftrightarrows 3RCOOH + \begin{array}{l} CH_2-OH \\ CH-OH \\ CH_2-OH \end{array} \quad (1)$$

(Triolein) (Water) (Oleic acid) (Glycerol)

$$RCOOH + CH_3OH \leftrightarrows RCOOCH_3 + H_2O \quad (2)$$

(Oleic acid) (Methanol) (Methyl oleate) (Water)

The hydrolysis reaction occurs at pressure of 11 MPa and temperature of 563K and reaches equilibrium condition (Chen et al., 2010). The kinetic of esterification (Eq. 2) proposed by Jain and Sharma (2010) is used. The UNIFAC model is selected to estimate thermodynamic properties and simulations are performed using Aspen Plus flowsheet simulator.

A heat integrated reactive distillation process to produce biodiesel is showed in Fig. 2. The esterification reaction of oleic acid and methanol is carried out in a reactive distillation column. The bottom product of the reactive distillation is sent to a conventional distillation to separate methanol from a biodiesel product. The biodiesel product stream is used to preheat methanol and oleic acid feed streams before entering the reactive distillation column.

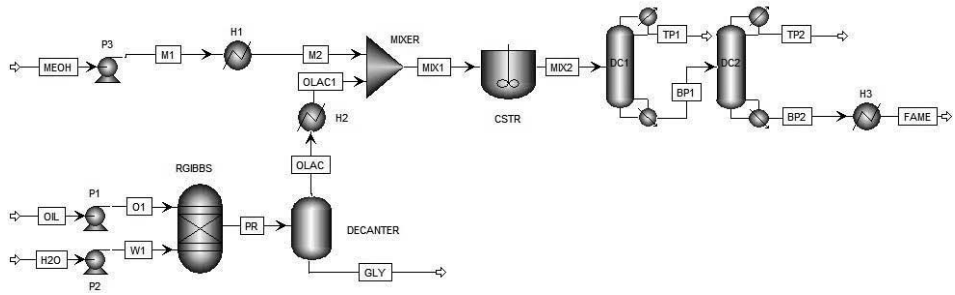

Fig. 1. Conventional process for biodiesel production.

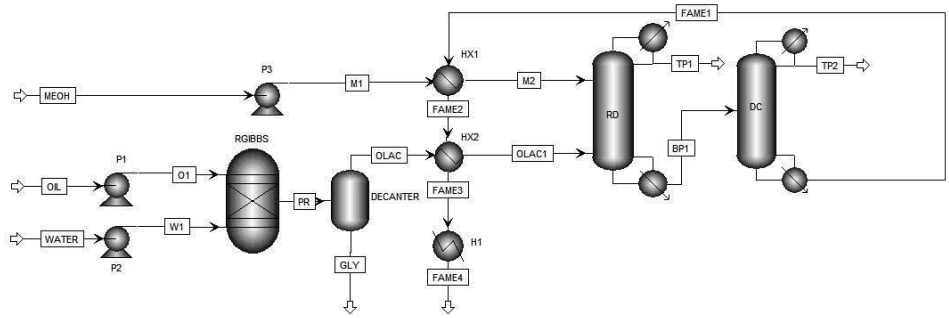

Fig. 2. Heat integrated reactive distillation process for biodiesel production.

Table 1. Specifications and operating conditions for a conventional biodiesel process

Reactor	Hydrolysis	Esterification
Total mole flow (kmol/h)	183.99	496.33
Conversion (mol%)	99.99 (oil)	95.79 (acid)
Heat duty (kW)	2347.75	-3938.16
Temperature (K)	563.15	343.15
Pressure (MPa)	11	0.101325
Decanter		
Temperature (K)	433.15	
Pressure (MPa)	0.101325	
Heat duty (kW)	-4284.97	
Distillation column (DC)	DC 1	DC 2
Stages	25	15
Feed stage	10	6
Distillate to feed mole ratio	0.5	0.3
Reflux ratio	0.6	0.5
Condenser duty (kW)	-3856.32	-1252.39
Reboiler duty (kW)	4794.24	1465.21
Top stage pressure (MPa)	0.101325	0.101325
Biodiesel purity (mol%)	44.39	63.41

3. Simulation results

To perform the simulation of a biodiesel production via a conventional process, the hydrolysis of triolein and the esterification of oleic acid are carried out in equilibrium (RGIBBS) and continuous (CSTR) reactors, respectively. A 46 kmol/h stream of triolein is fed to the equilibrium reactor and reacts with 138 kmol/h of water. Oleic acid and glycerol are generated at the flow rates of 137.94 and 42.88 kmol/h. Then, the oleic acid and methanol are mixed before entering a continuous reactor where the esterificaion reactor is occurred. The reaction product is sent to distillation columns (DC1 and DC2) to purify the methyl oleate product, which is cooled down to temperature of 25 ^{o}C. Table 1 shows the process specifications and conditions of the conventional biodiesel process. Under the standard conditions, the purity of methyl oleate obtained is 63.41 mol%. The overall heat requirement of the conventional process is 25,937 kW.

Table 2. Specifications and operating conditions for a reactive distillation biodiesel process

	RD	DC
Stages	15	15
Molar reflux ratio	0.2	0.5
Methanol feed stage	4	-
Oleic acid feed stage	12	-
BP feed stage	-	7
Reactive stages	2-14	-
Distillate rate (kmol/h)	291.07	80
Condenser duty (kW)	-3799.77	-2970.43
Bottom rate (kmol/h)	200	120
Reboiler duty (kW)	309.57	9656.77
Fatty acid conversion (mol%)	99.99	-
Biodiesel purity (mol%)	68.85	99.80

Table 3. Comparison of energy requirement for different biodiesel processes

	Conventional process	Reactive distillation (RD) process	Heat integrated RD process
Reactor			
Hydrolysis	2347.75	2347.75	2347.75
Esterification	-3938.16	-	-
Distillation column			
Condenser duty	-5108	-2970.43	-2970.43
Reboiler duty	6259.45	9656.77	9656.77
Reactive distillation column			
Condenser duty	-	-3799.77	-3799.77
Reboiler duty	-	309.57	309.57
Additional power			
Pump	245.36	245.36	245.36
Cooler	-2155.16	-7772.61	-1886.68
Heater	5883.87	5883.87	-
Total energy consumption	25937	32986.13	21216.33

Next, the performance of a reactive distillation process to produce biodiesel is presented. The hydrolysis section is similar to the conventional process but the difference is in the esterification section where a reactive distillation is employed. Oleic acid (137.94 kmol/h) and methanol (350 kmol/h) from the hydrolysis section are sent to a reactive distillation at the stage 4 and 12, respectively. The reactive distillation is operated at relatively low molar reflux ratio of 0.2 because the methyl oleate product has much more higher boiling point than methanol and water, so that the separation of these substances can be easily performed. The methyl oleate product is removed at the bottom of the reactive distillation and then sent to a purification section. The purity of methyl oleate obtained is 99.80 mol%. The total energy consumption is 32,986.13 kW, which is higher than the conventional process. Table 2 shows the specification and operating conditions of reactive and conventional distillation columns.

To improve the energy usage, a heat integration of the reactive distillation process for biodiesel production is considered. The methyl oleate product is used as a heat source for preheating the oleic acid and methanol feeds (Fig. 2). Table 3 shows a comparison

of the total energy requirements of biodiesel processes with different configurations. It can be seen that the heat integrated reactive distillation process requires the lowest energy consumptions. The heating and cooling requirements are significantly reduced by 35.7% and 20% when compared with a reactive distillation process without heat integration and a conventional process, respectively.

4. Conclusions

This study presents a biodiesel production using Jatropha oil as feedstock. A two-step biodiesel process consisting of hydrolysis and esterification steps has been studied. A reactive distillation is proposed to improve the performance of the esterification process. In addition, a heat integration of the reactive distillation process is considered for an efficient energy usage. The major benefits of the proposed biodiesel process include increased productivity, reduced investment cost and minimum energy requirement. The results show that the heat integrated reactive distillation can save the energy consumption by 20%, compared with a conventional biodiesel process.

5. Acknowledgement

Support from the Computational Process Engineering Research Group, the Special Task Force for Activating Research (STAR), Chulalongkorn University Centenary Academic Development Project is gratefully acknowledged.

References

C.H. Chen, W.H. Chen, C.M. Chang, S.M. Lai, C.H. Tu 2010, Biodiesel production from supercritical carbon dioxide extracted Jatropha oil using subcritical hydrolysis and supercritical methylation, Journal of Supercritical Fluids 52, 228-234

S. Jain and M.P. Sharma, 2010, Kinetics of acid base catalyzed transesterification of *Jatropha curcas* oil, Bioresource Technology 101, 7701-7706

A.A. Kiss, A.C. Dimian, G. Rothenberg, 2008, Biodiesel by Catalytic Reactive Distillation Powered by Metal Oxides, Energy & Fuels 22, 598-604

D. Leung, X. Wu, M. Leung, 2010**,** A review on biodiesel production using catalyzed transesterification, Applied Energy 87, 1083-1095

I.A. Karimi and Rajagopalan Srinivasan (Editors), Proceedings of the 11th International Symposium on Process Systems Engineering, 15-19 July 2012, Singapore.

Functional modeling applied to HAZOP automation

José Luis de la Mata,[a] Manuel Rodríguez[a]

[a]*Technical University of Madrid, José Gutiérrez Abascal 2, 28006 Madrid, Spain*

Abstract

In this paper we present a new tool to perform guided HAZOP analyses. This tool uses a functional model of the process that merges its functional and its structural information in a natural way. The functional modeling technique used is called D-higraphs. This tool solves some of the problems and drawbacks of other existing methodologies for the automation of HAZOPs. The applicability and easy understanding of the proposed methodology is shown in an industrial case.

Keywords: Functional modeling; HAZOP; Risk assessment.

1. Introduction

Currently, due to economical optimization of process plants, they are working at extreme conditions of pressure and temperature. This situation makes them more likely to fail and, even worse, the consequences of accidents are more severe. In addition, the Chemical Industry is facing tighter regulations and a growing attention of the media towards industrial accidents. Of course, we have also to consider the economical losses associated to accidents in terms of shutdowns, reparations, compensations and fines.

In the design stage of the process plant, Process Hazard Analyses (PHA) are carried out to identify potential sources of accidents and propose some solutions that enhance the safety of the plant. One of the most used of all of the existing PHA techniques is the Hazard and Operability Study (HAZOP) (Zhao et al., 2005). However, this approach consumes a lot of effort, time and, hence, money.

For these reasons, in the last two decades a lot of effort has been devoted to the implementation of tools and methodologies that can lead to the automation of these studies. In this work we present a new tool based on a functional modeling technique called D-higraphs. This approach takes into account in a natural way the structure as well as the functionality of the system (process and control system).

2. D-higraphs: merging function and structure

2.1. Dualization: from Higraphs to D-higraphs

Higraphs were first presented by Harel (1987) and they are a general kind of diagramming that can be understood as a combination and extension of Graphs, Euler/Venn diagrams and the Cartesian Product. They are well suited to specify complex concurrent systems but not process systems.

However, they can be adapted to process specification by the dualization of their properties and relations. This dualization has led to D-higraphs that were first presented in Rodríguez & Sanz (2009). Higraphs and D-higraphs consist of blobs and edges connecting them.

It should be noted that the term ‘dualization’ is used in a different way than the one used in Dual-Graphs or Digraphs; it is only applied to the properties and not to the elements.

2.2. Elements of a D-higraph

A basic blob and its elements are depicted in the left-hand-side of Fig. 1 and the different types of edges are shown in the center of Fig. 1. Blobs represent functions (transitions) that are performed by an ACTOR producing state/s 2 if the state/s 1 is enabled and if the *condition* is true. Edges represent flows of mass, energy, or information, which are responsible of all the interactions in a process system (Lind, 1994). Mass, energy and information edges are depicted differently, but the type of flow does not affect the behavior of the model, it is a just a visual aid.

Disjoint blobs imply an AND relation (both transitions between states take place) while orthogonal blobs represent an OR relation (only one of the transitions takes place). The main properties are:

- *Blob connection*. An edge always links two blobs. Under certain conditions, one of the blobs cannot be represented (elliptic blob), but it exists.
- *Blob inclusion*. Blobs can be included inside of other blobs (Venn diagram inclusion). This means that the inner blob performs a function that is necessary for the function of the outer blob (representation of functions hierarchy).
- *Blob partition*. A blob can be partitioned into orthogonal components, establishing an OR condition between the partitions.

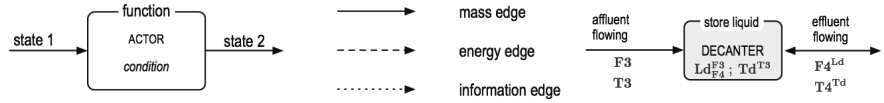

Fig. 1. Basic blob, types of edges, and three layer D-higraph.

2.3. Causality and qualitative reasoning

The main objective of D-higraphs is not only the representation of knowledge about process systems. De la Mata & Rodríguez (2010a,b) provide a series of causation rules relating two events that allow us to track the evolution and propagation of failures across the system. This rules combined with sensor data of the plant enables the possibility of performing FDI analysis using D-higraph models.

However, certain analyses require the use of deviations and not only failures, like HAZOP studies. In a certain way, we need to simulate qualitatively the system in order to propagate these deviations. The description of a system is made in three different layers (Kuipers, 1984):

1. *Structural description*: variables that characterize the system, such as flow (F), pressure (P), temperature (T), composition (x), energy (E), information (I), level (L), valve opening (A), etc. The symbols in brackets will be used in D-higraphs.
2. *Behavioral description*: potential behavior of the system as a network. The M^+ and M^- constraints (Kuipers, 1986) provide this information and they we will use the following compacted compacted notation:

$$Z^{X_1,X_2\ldots X_n}_{Y_1,Y_2\ldots Y_m} \quad \Leftrightarrow \quad M^+(X_i,Z) \wedge M^-(Y_i,Z) \quad \forall i,j \qquad \text{(Eq. 1)}$$

3. *Functional description*: purpose of a structural component of connections; provided by the D-higraphs layout.

The three layers of this representation are shown in the right-hand-side of Fig. 1, where there is a physical device (DECANTER) whose main purpose is to *store liquid*. The decanter has two characteristic variables: level (Ld) and temperature (Td). Ld is affected by the inflow F3 with variations of the same sign (an increment of F3 increases Ld) and by the outflow F4 in the opposite way. In the same way, the flow F4 is affected by the level of the decanter in the same direction (see Eq. 1).

3. D-higraphs environment and HAZOP Assistant

D-higraphs are developed using the environment shown in Fig. 2. The models are implemented using a graphic tool Álvarez (2010). This tool has as input the P&ID of the process and it uses a D-higraphs built in template. Once the model has been developed, it is loaded into the expert system. The HAZOP study is performed feeding the deviations to the reasoning engine. The result of the analysis, a causal tree, is provided to the user and they can be fed back to the modeling tool in order to make changes into the process and/or D-higraph.

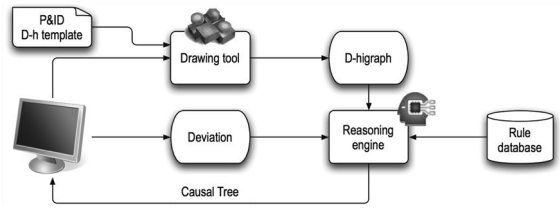

Fig. 2. D-higraphs environment.

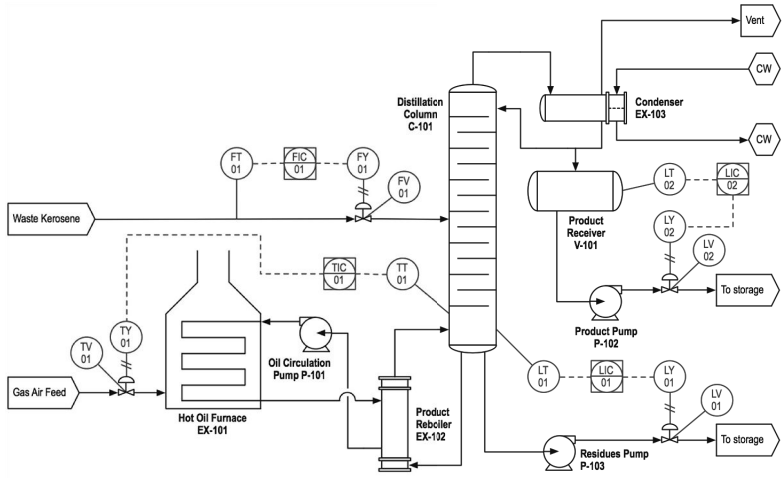

Fig. 3. Kerosene recovery unit.

4. Kerosene recovery unit (case study)

The kerosene recovery unit shown in Fig. 3 is part of a proposal of DOP Refineries Ltd. for the construction of a refinery for the recovery of kerosene from the waste kerosene solvent returned from auto engine repairers. This process and its conventional HAZOP analysis is taken from the "Hazardous Industry Planning Advisory Paper No. 8" (2011).

4.1. Functional decomposition

The main goal of the unit is to recover the kerosene from the waste kerosene solvent. To that end, the system can be decomposed into its subsystems, which perform the necessary subfunctions and subgoals, in the following way: (1) Feed section: provide a constant feed flow, (2) Distillation column: separate the kerosene, (3) Reflux section: provide reflux to the column and remove the recovered kerosene, and (4) Reboiler section: provide energy to the column.

This decomposition can be continued until the desired level of detail. The D-higraph is developed using this decomposition and the P&I diagram. However, in this paper we only show a part of the overall D-higraph due to space constraints. See Fig. 4 for the D-higraph of the reboiler section.

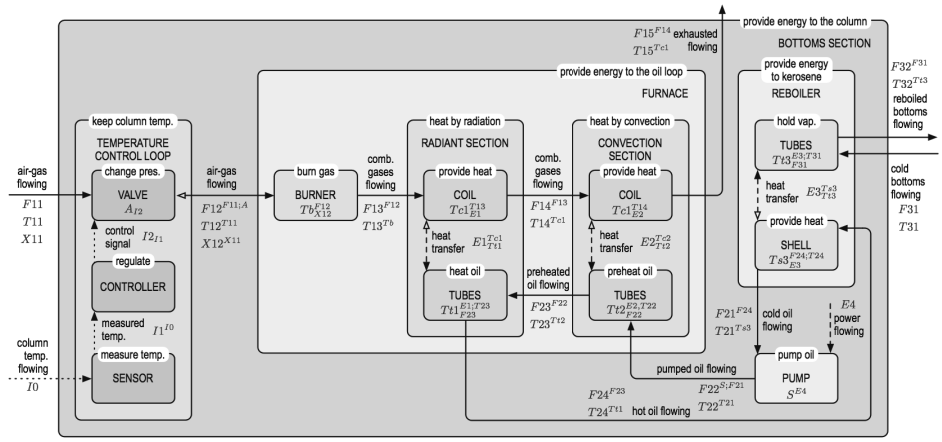

Fig. 4. Reboiler section D-higraph.

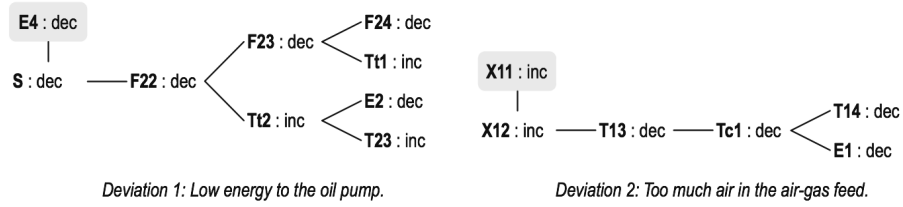

Fig. 5. Consequences trees for the deviations considered.

4.2. Deviation 1: Low energy to the oil pump.

This deviation consists of the variable "power flowing" to the oil pump (E4) and the guide- word "less of". Its consequences tree (with depth 4) are show in Fig. 5. This tree can be expanded to cover all of the D-higraph. The conclusions that can be obtained are: (1) The temperature of the oil can be to high and end in its degradation, (2) the temperature of the reboiled flow would decrease, and (3) the temperature of the exhausted would increase, which means that we are wasting energy.

4.3. Deviation 2: Too much air in the air-gas feed.

This deviation consists of the variable "air-gas composition" (X11) and the guide-word "more of". The consequences tree for this deviation (with depth 4) are shown in Fig. 5. Again, this tree can be expanded to drawn these consequences: (1) low temperature of the oil in its loop, and (2) low temperature of the reboiled flow.

Of course, in both deviations, the trees can be expanded to cover all of the process, only the depth of the tree has to be changed. With this, the analysis can cover all of the plant and not only the node under consideration.

5. Comparison with other methodologies

Conventional HAZOP studies are systematic and a logical way of performing PHA. However, 70% of the time they require is devoted to routine deviations (Venkatasubramanian et al., 2000). The automation of the procedure saves time and hence money. Automating HAZOP, the team can spend their time in analyzing the deviations, causes, consequences and the possible solutions and not in obtaining them. Another advantage of automated HAZOPs is that no nodes are left unexplored. The proposed assistant only needs a model (a D-higraph) of the process and not a model for each node of the HAZOP analysis, like the MFM HAZOP assistant (Rossing et al., 2010). The rule database is also common for all of the process because it is related to the relations between the elements of the model and not to the process itself, like HAZOPExpert (Venkatasubramanian et al., 2000), however, HAZOPExpert is able to deal with batch processes. Another advantage of this approach, when compared with the MFM methodology, is that the conclusions of the study can be directly mapped to the devices and equipment of the process. This is a consequence of the functional and structural integration.

6. Conclusions and further work

We have presented a tool that allows us to perform guided HAZOP studies. This tool uses a functional model, D-higraph, that merges functional and structural information about the process under analysis. This tool has been applied to an industrial case to show its applicability and to compare it with other existing tools. The resulting analyses are more complete, easier to perform and directly related to the process due to the integration of functions and structures. Future work will be devoted to the development of a "translator" between P&IDs and D-higraphs, so the models can be obtained from the diagrams by adding additional information. Further work will also include the integration of this tool with quantitative information and models.

References

Álvarez, M. E. 2010. Diagnosis de fallos en procesos químicos mediante modelos D-higraph. Final Project. Department of Chemical Engineering, Technical University of Madrid.

CLIPS. 2011. CLIPS, A Tool for Building Expert Systems. http://clipsrules.sourceforge.net

De la Mata, J. L., Rodríguez, M. 2010a. Abnormal situation diagnosis using D-higraphs. Proc. of the 20th European Symposium on Computer Aided Process Engineering, pp. 1477-1482.

De la Mata, J. L., Rodríguez, M. 2010b. D-higraphs. ASLab Report. http://www.aslab.org

Department of Planning, State of New South Wales, Australia. 2011. Hazardous Industry Planning Advisory Paper No. 8. HAZOP Guidelines.

Harel, D. 1987. Statecharts: A visual formalism for complex systems. Sci. Comput. Program., 8.

Kuipers, B. 1984. Commonsense reasoning about causality. Artificial Intelligence, 24.

Kuipers, B. 1986. Qualitative simulation. Artifiial Intelligence, 29.

Lind, M. 1994. Modeling goals and functions of complex Industrial plant. Applied Artificial Intelligence, 8 (2).

Lind, M. 2005. Modeling goals and functions of control and safety systems. NKS Report.

Rodríguez, M., Sanz, R. 2009. Development of integrated functional-structural models. Computer Aided Process Engineering, 27.

Rossing, N. L., Lind, M., Jensen, N., Jorgensen, S. B. 2010. A functional HAZOP methodology. Computers and Chemical Engineering, 34 (2).

Venkatasubramanian, V., Zhao, C., Viswanathan, S. 2000. Intelligent systems for HAZOP analysis of complex process plants. Computers and Chemical Engineering, 24 (9-10).

Zhao, C., Bhushan, M, & Venkatasubramanian, V. 2005. PHASuite: An Automated HAZOP Analysis Tool for Chemical Processes. Process Safety and Environment Protection, 83 (6).

I.A. Karimi and Rajagopalan Srinivasan (Editors), Proceedings of the 11th International Symposium on Process Systems Engineering, 15-19 July 2012, Singapore.

Dynamic Flexibility Analysis with Differential Quadratures

Vincentius Surya Kurnia Adi, Chuei-Tin Chang

National Cheng Kung University, University Road 1, Tainan 701, Taiwan

Abstract

Realistic chemical processes are often operated in the presence of complex and uncertain system dynamics. Obviously, flexibility analysis comes into play in designing such systems. In order to build the mixed-integer nonlinear program (MINLP) for computing the flexibility index, the Karush-Kuhn-Tucker (KKT) conditions must be derived from the system model and this model usually consists of a set of differential-algebraic equations (DAEs). A common approach for this task is to replace these DAEs with equality constraints by using a numerical discretization technique. In the present study, the *differential quadratures* (DQs) are adopted to approximate the derivatives in the original system model. The time horizon is discretized at the roots of a Chebyshev polynomial for optimally mimicking the transient profiles of control and state variables. Finally, a novel concept of *temporal flexibility* is also proposed in this paper and a simple system is used to demonstrate its usefulness. All results obtained in case studies show that the proposed approach is convenient and effective for assessing realistic issues in operating complex dynamic chemical processes.

Keywords: dynamic flexibility analysis, temporal flexibility, chemical process design, differential quadrature.

1. Introduction

Dealing with uncertainty is one of the problems in operating the chemical plants. The uncertainties can be considered as variation either in the external parameters (such as the quality of the feed streams, the product demands, and the environmental conditions, etc.), or the internal parameters (such as the heat transfer coefficients, the reaction rate constants, and other physical properties). A satisfactory level of flexibility should be allocated so as to ensure feasible operation over a specified range of every uncertain parameter. Methods for systematic flexibility analysis in the synthesis and design of chemical processes have been developed in the literature (Bansal et al., 1998; Swaney and Grossmann, 1985; Zhou et al., 2009). As suggested by Swaney and Grossmann (1985), a chemical process can be described with the following constraints

$$\mathbf{h}(\mathbf{d},\mathbf{z},\mathbf{x},\boldsymbol{\theta}) = 0 \tag{1}$$

$$\mathbf{g}(\mathbf{d},\mathbf{z},\mathbf{x},\boldsymbol{\theta}) \le 0 \tag{2}$$

where $\dim\{\mathbf{h}\} = \dim\{\mathbf{x}\}$. In eqs. (1) and (2), $\mathbf{h}$ is the vector of equations, i.e., mass and energy balances, and $\mathbf{g}$ is the vector of inequalities, i.e., design specifications or physical operating limits. The variable $\mathbf{d}$ is the vector of design variables, $\mathbf{x}$ is the vector of state variables, $\mathbf{z}$ is the vector of the control variables, and $\boldsymbol{\theta}$ is the vector of the uncertain parameters. Since the state variables in eq. (2) can be implicitly eliminated with eq. (1), the above model can be reduced to

$$\mathbf{g}(\mathbf{d},\mathbf{z},\mathbf{x}(\mathbf{d},\mathbf{z},\boldsymbol{\theta}),\boldsymbol{\theta}) = \mathbf{f}(\mathbf{d},\mathbf{z},\boldsymbol{\theta}) \le 0 \tag{3}$$

Given a set of nominal parameter values $\boldsymbol{\theta}^N$ and the corresponding expected deviations in the positive and negative directions ($\Delta\boldsymbol{\theta}^+$ and $\Delta\boldsymbol{\theta}^-$), the space of uncertain parameters can be expressed as

$$\mathbf{T} = (\boldsymbol{\theta} \mid \boldsymbol{\theta}^N - \Delta\boldsymbol{\theta}^- \le \boldsymbol{\theta} \le \boldsymbol{\theta}^N + \Delta\boldsymbol{\theta}^+) \tag{4}$$

A scalar flexibility index can be formulated to quantify the ability of such processes to operate at points other than the nominal point of operation (Swaney and Grossmann, 1985). This flexibility index F represents the largest deviation that the design can accommodate while remaining feasible. $F \quad 1$ clearly indicates that the flexibility target is satisfied.

A modified formulation for the *dynamic flexibility index* was proposed by Dimitriadis and Pistikopoulos, (1995). To perform flexibility analysis on a dynamic system, the following optimization must be solved

$$\begin{aligned} & F = \max \delta \\ & s.t. \max_{(t)\in\mathbf{T}(\delta)} \min_{\mathbf{z}(t)\in\mathbf{Z}(t)} \max_{t\in[0,H]} \mathbf{g}(\mathbf{d},\mathbf{z}(t),\mathbf{x}(t),\boldsymbol{\theta}(t),t) \le 0 \\ & \quad \mathbf{h}(\mathbf{d},\mathbf{z}(t),\mathbf{x}(t),\dot{\mathbf{x}}(t),\boldsymbol{\theta}(t)) = 0,\ \mathbf{x}(0) = \mathbf{x}^0 \\ & \quad \mathbf{T}(\delta) = (\boldsymbol{\theta}(t) \mid \boldsymbol{\theta}^N(t) - \delta\Delta\boldsymbol{\theta}^-(t) \le \boldsymbol{\theta}(t) \le \boldsymbol{\theta}^N(t) + \delta\Delta\boldsymbol{\theta}^+(t)) \end{aligned} \tag{5}$$

The differential quadrature technique (Bellman *et al*., 1972; Quan and Chang, 1989) is used in this study to convert the differential equations in the above model into algebraic ones. It was suggested that Chebyshev polynomial approximation should be applied for discretization of time horizon (Chen, 1996). Therefore, the main issue to be addressed here is mainly concerned with the applicability of DQ in dynamic flexibility analysis for batch processes. The solution procedures can be implemented on GAMS platform to determine the dynamic flexibility F.

The scope of aforementioned dynamic flexibility index obviously covers the entire operation horizon. In practice, there is also a need to determine a "short-term" flexibility index for the purpose of assessing the effectiveness of quick responses. Thus, the concept of *temporal flexibility* is developed in this work. Let us assume that the general dynamic uncertainty space is defined as below,

$$\boldsymbol{\theta}(t)^{\mathrm{N}} - \delta\Delta\boldsymbol{\theta}^-(t) \le \boldsymbol{\theta}(t) \le \boldsymbol{\theta}(t)^{\mathrm{N}} + \delta\Delta\boldsymbol{\theta}^+(t); \quad t_0 \le t \le t_1 \tag{6}$$

For these expected disturbances within an expected time interval $[t_0,t_1]$, one can define the *net* positive and negative deviations as

$$\int_{t=t_0}^{t=t_1} \Delta\boldsymbol{\theta}(t)^- dt = \Delta\boldsymbol{\theta}^-_{temp}, \quad \int_{t=t_0}^{t=t_1} \Delta\boldsymbol{\theta}(t)^+ dt = \Delta\boldsymbol{\theta}^+_{temp} \tag{7}$$

thus

$$\int_{t=0}^{t=t} \boldsymbol{\theta}(t)^{\mathrm{N}} dt - \delta_{temp} \int_{t=t_0}^{t=t_1} \Delta\boldsymbol{\theta}(t)^- dt \le \int_{t=0}^{t=t} \boldsymbol{\theta}(t) dt \le \int_{t=0}^{t=t} \boldsymbol{\theta}(t)^{\mathrm{N}} dt + \delta_{temp} \int_{t=t_0}^{t=t_1} \Delta\boldsymbol{\theta}(t)^+ dt \tag{8}$$

Or in an alternative form

$$\overset{\mathrm{N}}{}_{temp} - \delta_{temp}\Delta\ \overset{-}{}_{temp} \le \ _{temp}(t) \le \ \overset{\mathrm{N}}{}_{temp} + \delta_{temp}\Delta\ \overset{+}{}_{temp} \tag{9}$$

Eq. (9) are then imposed together with eq. (5) to calculate the temporal flexibility index for the entire time horizon.

2. Applications

Two examples are first presented in the sequel to demonstrate the applicability of differential quadratures in solving the dynamic flexibility model. Another example is then followed to illustrate the proposed temporal flexibility concept.

2.1. Example 1

Let us consider an exothermic first-order reaction (A B) in a jacketed batch reactor (Dimitriadis and Pistikopoulos, 1995). The mathematical model is given below in eqs. (10) - (15), while the parameter values can be obtained from Zhou et al. (2009). The heat of reaction, ΔH_r, is assumed to vary between –72500 and –82500 J/mol with nominal value of –77500 J/mol. The cooling water flow rate, F_{cw}, can be adjusted to satisfy operational constraints and end-time specifications and be regarded as the control variable.

$$\frac{\mathrm{d}N_\mathrm{A}}{\mathrm{d}t} = -kN_\mathrm{A};\ N_\mathrm{A}(0) = 20000 \text{ mol} \tag{10}$$

$$\frac{\mathrm{d}N_\mathrm{B}}{\mathrm{d}t} = kN_\mathrm{A};\ N_B(0) = 0 \tag{11}$$

$$C_p(N_\mathrm{A} + N_\mathrm{B})\frac{\mathrm{d}T}{\mathrm{d}t} = kN_A(-\Delta H_r) - Q_{cw} \tag{12}$$

The final reactant conversion must exceed 95%, i.e.

$$\frac{N_A(t=H)}{N_A(t=0)} \le 0.05 \tag{13}$$

The temperature in the reactor cannot exceed a maximum of 400 K at any time during operation,

$$T(t) \le 400 \text{ K},\ 0 \le t \le H \tag{14}$$

The temperature of the reacting mixture at the end of the operation must not exceed 308 K so that discharge and cleaning operations can take place,

$$T(t=H) \le 308 \text{ K} \tag{15}$$

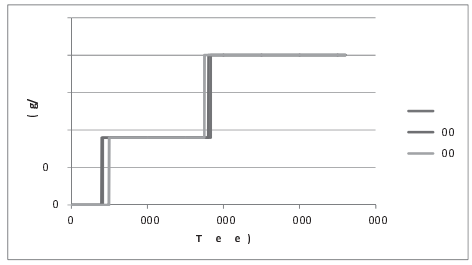

Figure 1. Cooling water flow rate vs. time at the critical point in Example 1; interval 5, 100, 500 s; nodes number = 5

According to Dimitriadis and Pistikopoulos (1995), the initial reaction temperature is fixed at 298 K. The time profile of the cooling water flow rate in 2-h batch cycle is presented in Fig. 1. The dynamic flexibility index and the critical value of the uncertain parameter for different nodes number and a fixed horizon are also presented in Table 1. It can be seen that the node number of differential quadrature method slightly affects the numerical results due to the stepwise nature of the problem. Higher node number can

increase accuracy but the improvement is not significant (see Table 1). N = 5 should be sufficient for adequate accuracy.

Table 1. Dynamic flexibility index and the critical uncertain parameter in Example 1

Node Number	5	10	15
FI ( )	0.7721	0.7783	0.7788
ΔH_r J/mol	82863	81748	81387

2.2. Example 2

Let us consider the following polymerization reaction that produces a polyol lubricant:

$$C_4H_9OH + (n+1)C_3H_6O \rightarrow C_4H_9(OC_3H_6)nOCH_2CHOHCH_3 + \text{heat}$$

The system description and the model parameters can be found in Zhou et al. (2009). To consider the effect of the uncertain parameters, a 10% uncertainty in the activation energy is introduced as it is assumed that the activation energy is inaccurately measured. The reactor temperature profile for 33.3 h with different interval lengths and fixed node number can be found in Fig. 2. The corresponding dynamic flexibility indices can be found in Table 2. From Fig. 2, it can be seen that the profile associated with 5-min intervals has better detail than those corresponding to the 100-min and 500-min intervals. The resulting dynamic flexibility index obtained for 5-min intervals is also significantly higher.

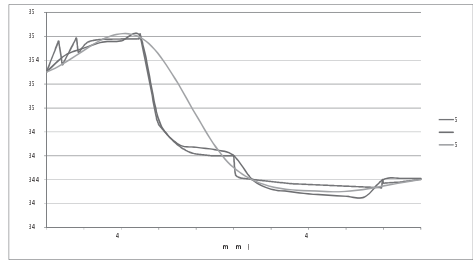

Figure 2. Reactor temperature in Example 2 (node number = 5)

Table 2. Dynamic flexibility indices in Example 2

Interval (min)	5	100	500
FI ( )	0.8	0.6743	0.5063

2.3. Example 3

To illustrate the proposed temporal flexibility concept, the simple tank in Fig. 3 is analyzed. The dynamic model of this system can be written as

$$A\frac{dh}{dt} = \theta(t) - k\sqrt{h} \tag{16}$$

The model parameters are $\theta(t)^N$ = 0.5 m^3/min, h_{low} = 0m, h_{up} = 10 m, h_{ss} = 5 m, A = 5 m^2, k= $\frac{\sqrt{5}}{10}$, H=2500 min.

The disturbance condition is described that from steady state condition, the inlet flow stops at t = 1500 min, and return back to normal after 250 min. For tank area A = 5 m^2, the temporary dynamic flexibility $_{temp}$ is found to be 0.4. From the result, it can be

concluded that the tank does not have enough flexibility to hold up such flow cut. By optimizing the volume of the tank, in this term is by changing A, it is suggested that A should be increased to be 12.5 m^2 and the corresponding $_{temp}$ is 1. It can be evaluated in Fig. 3 that water level of A = 5 m^2 is quickly dried out after 100 min, while water level of A = 12.5 m^2 has 250 min time period before it is empty, and after 250 min the inlet flow returns back to normal.

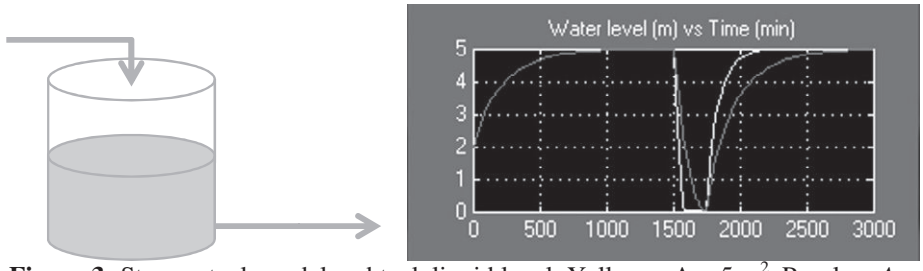

Figure 3: Storage tank model and tank liquid level; Yellow – A = 5 m^2, Purple – A = 12.5 m^2

3. Conclusions

Differential quadrature technique is successfully implemented in computing the dynamic flexibility indices. It is suggested that the node number and the interval length should both be small enough to achieve high accuracy and calculation robustness. The presented approach has been successfully implemented in two examples. Finally, a temporal flexibility concept is also proposed in this work for assessing the need for quick responses.

References

V. Bansal, J. D. Perkins, and E. N. Pistikopoulos, 1998, Flexibility Analysis and Design of Dynamic Processes with Stochastic Parameters, Comput. Chem. Eng., 22, S817

R. Bellman, B. G. Kashef, and J. Casti, 1972, Differential Quadrature: A Technique for The Rapid Solution of Nonlinear Partial Differential Equations, J. Comput. Phys., 10, 40

W. Chen, 1996, Differential Quadrature Method and its Applications in Engineering – Applying Special Matrix Product to Nonlinear Computations and Analysis, PhD Thesis, Shanghai Jiao Tong University, P.R.C.

V. D. Dimitriadis, and E. N. Pistikopoulos, 1995, Flexibility Analysis of Dynamic Systems, Ind. Eng. Chem. Res., 34, 4451

J. R. Quan, and C. T. Chang, 1989, New Insights in Solving Distributed System Equations by The Quadrature Methods – I, Comput. Chem. Eng., 13, 779

J. R. Quan, and C. T. Chang, 1989, New Insights in Solving Distributed System Equations by The Quadrature Methods – II, Comput. Chem. Eng., 13, 1017

R. E. Swaney, and I.E. Grossmann, 1985, An Index for Operational Flexibility in Chemical Process Design. Part I: Formulation and Theory, AIChE. J., 31, 621

R. E. Swaney, and I. E. Grossmann, 1985, An Index for Operational Flexibility in Chemical Process Design. Part II: Computational Algorithms, AIChE. J., 31, 631

H. Zhou, X. X. Li, Y. Qian, Y. Chen, and A. Kraslawski, 2009, Optimizing the Initial Conditions to Improve the Dynamic Flexibility of Batch Processes, Ind. Eng. Chem. Res., 48, 6321

I.A. Karimi and Rajagopalan Srinivasan (Editors), Proceedings of the 11th International Symposium on Process Systems Engineering, 15-19 July 2012, Singapore.

A Method of Designing Plant Alarm Systems with Hierarchical Cause-Effect Model

Takashi Hamaguchi,[a] Kazuhiro Takeda,[b] Masaru Noda,[c] Naoki Kimura[d]

[a] *Graduate School of Engineering, Nagoya Institute of Technology, Gokiso Showa-ku Nagoya, 466-8555, Japan*
[b] *Faculty of Engineering, Shizuoka University, 3-5-1 Johoku Hamamatsu, 432-8561, Japan*
[c] *Graduate School of Information Science, Nara Institute of Science and Technology, 8916-5 Takayama Ikoma, 630-0192, Japan*
[d] *Faculty of Engineering, Kyushu University, 744 Motooka Fukuoka, 819-0395, Japan*

Abstract

Plant alarm systems are important because they enable safe and reliable operations at chemical plants. Takeda *et al*. proposed a method of designing alarm systems for plants based on a plant cause-effect (CE) model. We propose a method of designing alarm systems for plants with a hierarchical CE model to improve the selection of fault origins to distinguish them with the systems and a procedure for designing the systems.

Keywords: Plant alarm system, fault origins, alarm source variables, hierarchical CE model

1. Introduction

Plant alarm systems are important because they enable safe and reliable operations at chemical plants. These alarm systems notify operators through warning tones, warning lights, and messages when the values for process variables move from normal to abnormal ranges. Poorly designed alarm systems cause nuisance, standing, and flooding alarms, and can even result in incidents or accidents. Therefore, new regulations and guidelines for plant safety have been established in the U.S.A. and Europe. The International Society of Automation (ISA, 2009) in the U.S.A. requires strict risk management through plant life cycles, which consists of design, operation, and management phases. The Engineering Equipment and Materials User's Association (EMMUA, 2007) in Europe requires that the philosophy, objectives, and functions of alarm systems be clearly developed, and inadequate alarms be eliminated. However, they have not described any methods of designing alarm systems. Therefore, a systematic method of designing plant alarm systems is needed to detect faults or abnormalities at plants, and to alert, inform and guide the operator during plant upset. Takeda *et al*. (2010) proposed a new method of selecting alarm source variables using a cause-effect (CE) model. They proposed a process of selecting fault origins to distinguish them by using alarm systems based on the grades of fault origins using a risk matrix with their frequencies and impacts of effects. However, it is not an easy task to determine grades in large-scale plants. When alarm systems cannot distinguish origins, this method cannot present useful information to enable problems to be reviewed. We therefore propose a method of designing plant alarm systems with a hierarchical CE model to improve the selection of fault origins to distinguish them by using alarm systems.

2. Hierarchical CE Model

2.1. Structure of Hierarchical CE Model

There is an overview of the method of designing a plant alarm system with the hierarchical CE model in Fig. 1. This model is generated by information from the CE model and it consists of a primitive variable layer, a strongly-connected component layer that enables variable selection of alarm sources, and a group unit layer that enables selection of fault origins.

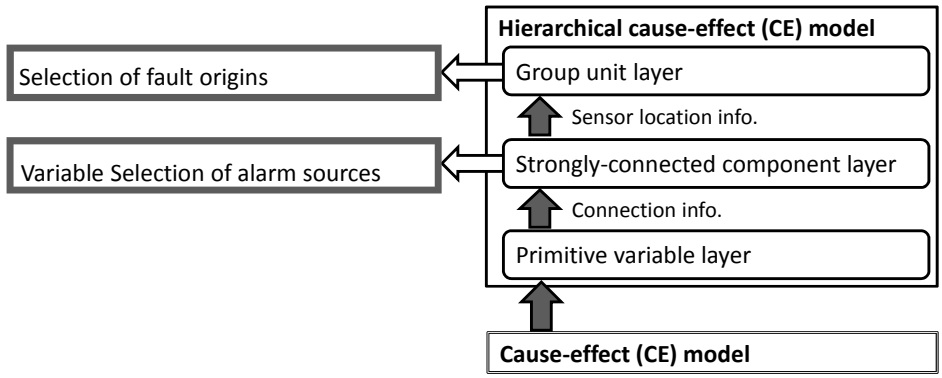

Fig. 1 Overview of method of designing plant alarm system with hierarchical CE model

2.2. CE model and primitive variable layer

Iri et al. (1979) proposed that the structure of a system be represented by a "signed directed graph (SDG)" and its state by "patterns". The SDG in this paper is called a CE model. The CE model is a diagram for the propagation of abnormalities that shows the propagation process for abnormalities after a fault has occurred. The model is based on the material and energy balances of the plant that could be constructed from the plant topology. Consequently, it is easy to maintain the CE model. The state of the system is expressed in terms of the signs "0", "+", and "-", according to the values of the state variables, such as process variables and manipulated variables, which correspond to normal, higher than normal, and lower than normal. The group of signs corresponding to all the state variables is defined as the pattern.

The CE model is composed of nodes and directed branches with a sign. The nodes in the model represent state variables in the plant. The branches represent the directed influence between state variables and each branch is assigned the sign "+" if it represents a positive influence (reinforcement) and the sign "-" if it represents a negative influence (suppression). Let $\boldsymbol{M}$ be a set of all measured variables of state variables and m be the element of $\boldsymbol{M}$. Let $\boldsymbol{N}$ be a set of all unmeasured variables of state variables and n be the element of $\boldsymbol{N}$. Nodes that carry a sign other than "0" are known as "valid nodes", while branches for which the product of the signs on the initial and terminal nodes is the same as the sign of the branch are known as "consistent branches". There are virtually no real systems in which all the state variables are measured. Nodes of a CE model corresponding to the measured state variables are known as "observed nodes" and those corresponding to the unmeasured state variables are known as

"unobserved nodes". In this paper, *s* is an observed node and ***S*** is a set of all observed nodes.

The example plant in Fig. 2(a) is represented as the CE model in Fig. 2(b). Raw material in this plant is fed from outside the boundary to tank 1. Product is discharged to outside the boundary through tank 2. Part of the product is recycled to tank 1. In this paper, *P*, *F*, *L*, and *V* are state variables for pressure, flow rate, liquid level, and valve position. All state variables without *P*1 and *P*2 can be measured. Unobserved nodes are represented by circles with a single line and observed nodes are represented by circles with double lines. Branches with "+" are represented by solid arrows, whereas branches with "-" are represented by dashed arrow. The solid arrow *L*1 to *F*2 represents an enhancing relationship, viz., increasing (or decreasing) *L*1 has a direct effect on increasing (or decreasing) *F*2.

A primitive variable layer is generated from information from the CE model. The primitive variable layer is used to modify the CE model for the alarm system. The primitive variable layer in this example is identical to the CE model in Fig. 2 (b)

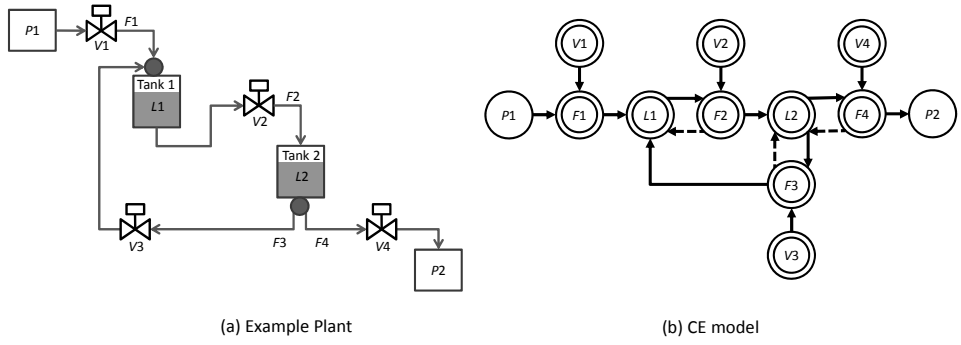

Fig. 2 Example plant and CE model

2.3. Strongly-connected component layer

Strongly-connected components are generated from the connection information in the primitive variable layer in a strongly-connected component layer. When the effect of a fault propagates to a strongly-connected component, then the effect propagates to all variables and loops in the strongly-connected component. Therefore, we selected strongly-connected components as minimal elements for setting fault origins. Fig. 3 has a strongly-connected component layer, which is generated from the primitive variable layer shown in Fig. 2 (b). Strongly-connected components are divided into group unobserved components, which only consist of unobserved nodes, and observed components, which contain some observed nodes. Unobserved components are represented by the rectangles with a single green line and observed components are represented by the rectangles with double green lines.

2.4. Group unit layer

Let ***C*** be a set of fault origins to be distinguished by using the alarm system and *c* be an element of ***C***. Therefore, ***C*** is a subset of all assumed fault origins in the plant. It is assumed that ***C*** could be obtained by process hazard analysis (PHA), like that in the HAZard and Operability (HAZOP) study.

Strongly-connected components in this layer are divided into group units x and y according to the information on their connections and sensor locations. The group unit layer is used to divide $\boldsymbol{C}$ into a subset for each unit x and y to select the fault origins to be distinguished by using the alarm system. Fault origins up to one can be set in group unit x, whereas no fault origins can be set in group unit y. Let $\boldsymbol{X}$ be a set of group unit x. When strongly-connected components can connect from upper strongly-connected components until an observed component is reached by direct branches, then the group of strongly-connected components belongs to group unit x. If a terminal strongly-connected component is an observed component, then the group of strongly-connected components belongs to group unit y. The elements c of $\boldsymbol{C}$ are divided into each group unit.

The group unit layer of the example plant is shown in Fig. 4. Group unit x is represented by the rectangles with double red lines and y is represented by the rectangles with the single blue line. There are six group units x and one group unit y in the example plant. Up to one fault origin can be selected in each group unit x.

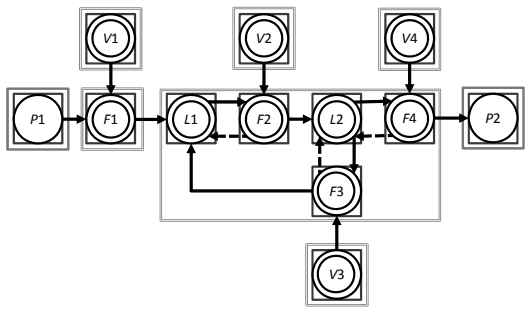

Fig. 3 Strongly-connected layer in example plant

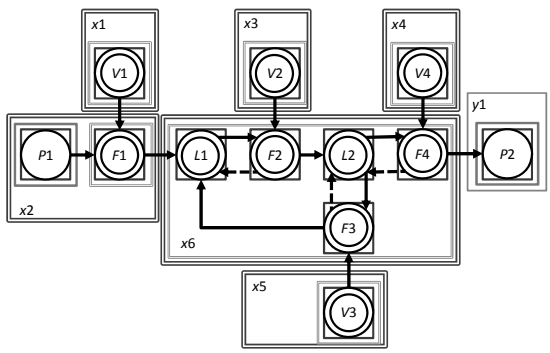

Fig. 4 Group unit layer in example plant

3. Design of Plant Alarm System using Hierarchical Cause-Effect Model

The design of the alarm system is defined in this paper as the selection of alarm source variables from $\boldsymbol{M}$ to distinguish the fault origins of $\boldsymbol{X}$.

The origin of a failure is represented by origin pair z of a node and its sign. Shiozaki *et al*. (1984) proposed the idea of a "consistent rooted tree". If all the branches on an elementary path can be made consistent with either "+" or "-" for unobserved nodes on

the path, then the path is defined as a "consistent path". If there are consistent paths from a node on the CE model to all the valid observed nodes on it, the tree composed of the node and these consistent paths is defined as a consistent rooted tree, and the node is defined as a "root". A consistent rooted tree is also considered to be a representation for the state of propagation of a failure. There may be two or more candidates for the origin of the failure. Therefore, a set of z as candidates for the origin of the failure is defined as candidate pair set $\boldsymbol{Z}$. A set of candidate pairs, which is not a proper subset of all the other sets of candidate pairs for all observed patterns on all observed node $\boldsymbol{S}$, is defined as the greatest set of candidate pairs. Two or more greatest pairs are generally given by the branch and bound method (Shibata and Matsuyama, 1989). If two or more elements of $\boldsymbol{X}$ are not involved in any greatest sets of candidate pairs, then all elements of $\boldsymbol{X}$ can be distinguished in any abnormal situations.

Let $\boldsymbol{A}$ be a set of alarm source variables to distinguish fault origins, which is grouped as group unit x. Set $\boldsymbol{A}$ of alarm source variables can be selected from $\boldsymbol{S}$ as follows. It is assumed that a CE model of the objective plant and the hierarchical CE model have been given.

1. **Determine $\boldsymbol{X}$ of the objective plant**: List up all the fault origins to be distinguished by the alarm system in the objective plant, and map the fault origins to adequate pairs of nodes and the signs of the CE model of the objective plant.
2. **Select alarm source variables**: Select alarm source variables that can distinguish all the elements of $\boldsymbol{X}$. Let $\boldsymbol{Q}$ be a power set of $\boldsymbol{S}$ without an empty set. Calculate a set of greatest sets of candidate pairs when all elements of $\boldsymbol{Q}$ are made into a set of alarm source variables.
3. **Determine monitoring ranges**: Select a fault origin from each group unit x. The monitoring ranges of alarm source variables are adjusted using a dynamic simulator. This step has been omitted from this paper.

4. Conclusion

We proposed a method of designing alarm systems for plants with a hierarchical CE model to improve the selection of fault origins to distinguish them with the systems and a procedure for designing the systems.

References

EEMUA, 2007, ALARM SYSTEMS – A Guide to Design, Management, and Procurement Publication No.191 2nd edn., London

M. Iri, K. Aoki, E. O'shima, and H. Matsuyama, 1979, An Algorithm for Diagnosis of System Failures in the Chemical Process, Comput. Chem. Eng. 3, 489-493

ISA, 2009, Management of Alarms Systems for the Process Industries, North Carolina

J. Shiozaki, B. Shibata, H. Matsuyama, and E. O'shima, 1989, Fault Diagnosis of Chemical Process utilizing Signed Directed Graphs Improvement by using Temporal Information, IEEE Trans. Ind. Electron., 36, 469-474

B. Shibata, and H. Matsuyama, 1989, Evaluation of the Accuracy of the Fault Diagnosis System Based on the Signed Directed Graph, Kagaku Kougaku Ronbunshu, 15, 395-402

K. Takeda, T. Hamaguchi, and M. Noda, 2010, Plant Alarm System Design based on Cause-Effect Model, Kagaku Kougaku Ronbunshu, 36, 136-142

I.A. Karimi and Rajagopalan Srinivasan (Editors), Proceedings of the 11th International Symposium on Process Systems Engineering, 15-19 July 2012, Singapore.

Computer Aided Assessment of Occupationally Healthier Processes during Research and Development Stage

Santha Pandian[a], Mimi H.Hassim[a*], Markku Hurme[b]

[a]*Universiti Teknologi Malaysia, Department of Chemical Engineering, 81310, UTM Johor Bahru, Malaysia*
[b]*Aalto University, Department of Biotechnology and Chemical Technology, P.O. Box 16100, FIN-00076 Aalto, Finland*
*Corresponding email: mimi@cheme.utm.my

Abstract

Each year more people die from occupational related diseases than are killed in industrial accidents. Therefore it is critical to start considering health aspect early when developing a new chemical process. In this paper, computer aided tool for assessing inherent occupational health is proposed for chemical process research and development stage. The method was developed based on the reaction chemistry data, which is the only data available at this stage. Three types of approaches were formulated to calculate the route index value using additive type, average type and worst case type calculations. The tool can be used to rank the alternative chemical synthesis routes by their health properties as well as characterize the hazard level of single process. Finally the tool was applied to six process routes for methyl methacrylate production for demonstration.

Keywords: inherent occupational health, computer aided tool, process design, R&D, CAPE

1. Introduction

Occupational health is the promotion and maintenance of the highest degree of physical, mental and social well-being of workers in all occupations by preventing departures from health, controlling risks and the adaptation of work to people, and people to their jobs (ILO/WHO, 1950). Occupational health hazards are generally more difficult to manage than safety hazards. The causes and consequences of poor safety at work are immediate and often relatively easy to deal with. Meanwhile work-related causes of ill health are more difficult to assess. It often takes some time for health symptoms to develop; therefore the connection between cause, in this case occupational exposure, and worker health effect is less obvious.

In recent years, occupational health issues have become more common and known. In principle it is better to identify health hazards when the proposed plant is still 'on paper'. As the project progresses, the process modifications will be more difficult and more costly and the opportunity to apply inherently healthy design features will become smaller (Hassim and Edwards, 2006).

2. Occupational Health Assessment Methods

There are several methods available for occupational health assessment during design stage. Among the earliest ones is the Occupational Health Hazard Index (OHHI) (Johnson, 2001), which intends to assess and rank chemical synthesis routes in the R&D

stage. The method has several disadvantages including poor assessment of fugitive emissions, which is too brief that the accuracy is questionable. INSET Toolkit (INSIDE Project, 2001) is a comprehensive method which covers assessment of all safety, health and environment (SHE) as well as other feasibility factors. The toolkit however is highly complex besides requiring massive detailed information. Even reading the instruction manual is demanding. Later, Hassim and Edwards (2006) introduced an improved method from the OHHI called the Process Route Healthiness Index (PRHI). However similar to the OHHI, PRHI also suffers from being quite complicated despite claiming for R&D application. The most recent method is by Hassim and Hurme (2010), called the Inherent Occupational Heath Index (IOHI). The method was designed carefully by taking into account all the parameters for health assessment but limited to only those information available in the R&D stage.

All the methods discussed above were created based on manual calculations. This somehow makes them less attractive as industries prefer tools which are simple and swift (Gupta and Edwards, 2002). Besides, most design work is done using CAPE tools now. Therefore, the aim of this research is to develop a computer-aided tool that will assist users in making chemistry pathway selection based on the health hazard level of process candidates using the IOHI method. Such tools are needed since in the R&D stage, large number of routes needs to be screened within a limited time. Computerized tool also avoids incorrect assessment results due to mistakes done in manual calculations.

3. The Inherent Occupational Health Index

Inherent Occupational Health Index (IOHI) comprises of two indexes; Index for Physical and Process Hazards (I_{PPH}) that represents the possibility for workers being exposed to chemicals and Index for Health Hazards (I_{HH}) that characterizes the impacts on health due to the exposure (Hassim and Hurme, 2010). The IOHI for each process route is calculated as a sum of the two indexes:

$$I_{IOHI} = I_{PPH} + I_{HH} \quad [1]$$

The I_{PPH} consists of six subindexes; process mode (I_{PM}), pressure (I_P), and temperature (I_T), materials phase (I_{MS}), boiling point (I_V), and corrosiveness (I_C). For the I_{HH}, two subindexes are included; exposure limit (I_{EL}) and R-phrase (I_R). Each subindex has a range of penalties; a higher penalty represents a higher tendency for exposures or a more severe health impact. Summary of the subindexes and their penalties for the I_{PPH} and I_{HH} are in Hassim and Hurme (2010). The IOHI is reaction-step oriented. Therefore a whole reaction step is considered as one entity. The formula for calculating the IOHI as in Eq. (1) is for each reaction step or here called as subprocess. The index value for a route (may consist of ≥ 1 subprocess) can be calculated using three types of calculation, which are additive type, average type and worst case type. The difference between these evaluations is described by Hassim and Hurme (2010) and is demonstrated in this paper by a case study.

4. Development of Systematic Computer Aided IOHI Tool

A systematic computer-aided tool for inherent occupational health assessment has been developed based on the IOHI using Microsoft Excel. All the subindexes considered in the assessment, penalties system, index formulation etc. are similar to the manual based IOHI (Hassim and Hurme, 2010), therefore will not be elaborated here. The difference

is in the effort of computerizing the IOHI evaluation. An electronic database has been created which consist of 1625 as shown in Fig.1. The database provides chemical properties required for the IOHI calculation, which are the material phase, boiling point, corrositivity, R-phrases value and exposure limit (EL). The first four data were obtained from individual Material Safety Data Sheet (MSDS) provided by ScienceLab. Meanwhile the EL value is the Permissible Exposure Limit (PEL) 8-hour data taken from Schedule 1-Malaysian Regulation.

The proposed tool is very straightforward where the user has to input process related data only i.e. operating pressure, temperature and process mode. Prior to that, user needs to select the chemicals involved in the subprocess from the database. Then the tool will automatically calculate the IOHI value for each subprocess based on the formulation that has been specified using the logical functions in Excel. Once the IOHI for each subprocesses of a routes are calculated, the tool will then calculate the route index value using three approaches i.e additive, average, and worst case type calculation. The tool also is able to characterize the hazard level of process route as either Safe, Moderately Safe, Moderately Hazardous or Hazardous. The details on how the standard for the categorization was developed are described by Hassim and Hurme (2010). To illustrate the proposed approach, an industrial case study on the production of methyl methacrylate (MMA) was used.

5. Case Study on Methyl Methacrylate

The computer aided IOHI tool is demonstrated by a case study of six alternative routes for methyl methacrylate (MMA) manufacture. The routes are:

1. Acetone cyanohydrin based route (ACH)
2. Ethylene via propionaldehyde based route (C2/PA)
3. Ethylene via methyl propionate based route (C2/MP)
4. Propylene based route (C3)
5. Isobutylene based route (i-C4)
6. Tertiary butyl alcohol based route (TBA)

Among these six routes, ACH is the most common and widely used in industries. Details of the routes are in Hassim and Hurme (2010).

5.1. The Index Calculation

Each subprocesses of MMA alternative synthesis routes is assessed for their health properties using the proposed tool. The IOHI index calculations, including the penalties received by each subindex, are summarized by the tool to further ease hazards assessment process. Here only summary of ACH routes is shown (see Fig. 2) due to the space limitation. The index value for the whole route is then calculated using three approaches of additive type, average type and worst case type calculations and presented in Tables 1and 2. Besides tables of results, the tool also generates graphs for each calculation type; the I_{PPH} and I_{HH} as well as the total IOHI values. However due to the limited space, only the IOHI graph for additive calculation is shown here (Fig. 3).

Material	R-Phrases	Boiling Point (°C)	Corrosivity	PEL		Material State	Solid
				8 hrs time weighted	Ceiling limit airborne		
				ppm	ppm		
Acetaldehyde	R12 R36/37/38 R40	21	Stainless Steel	20.00	50.00	Liquid	
Acetamide	R40	223	Non-corrosive in glass	2.07	6.21	Solid	Crystalline Solid
Acetic acid	R10 R35	118.1	Stainless Steel	10.00	30.00	Liquid	
Acetic anhydride	R10 R20/22 R34	139.9	Stainless Steel	5.00	15.00	Liquid	
Acetone	R11 R36	56.2	Stainless Steel	500.00	1500.00	Liquid	

Fig. 1 Overview of the electronic database

Route/Step	I_{PPH}						I_{HH}		I_{IOHI}
	I_{PM}	I_{MS}	I_V	I_P	I_C	I_T	I_{EL}	I_R	
ACH									
2	1	2	2	0	1	0	3	4	13
3		3	0	1	2	1	4	4	15
4		3	1	1	2	1	4	4	16
Total	1	8	3	2	5	2	11	12	44

Fig. 2 Summary of IOHI index calculations for the ACH route

5.2. Results and Discussions

5.2.1. Additive type calculation

The typical way of calculating the process route index is based on the additive method. Based on Table 1 and Fig. 3, it can be seen that the C2/PA and C3 routes have the highest index value compared to the others. This is due to the largest number of subprocesses they have. Additive calculation does affected a lot by the number of subprocess a route has. This somehow indicates that a more complex route (with more subprocesses) has a probability to pose greater hazards due to e.g. the presence of more chemicals etc.

5.2.2. Average type calculation

The average of the IOHI can be calculated for each route to eliminate the influence of the number of subprocess on the final index value (Hassim and Hurme, 2010). Now the results are almost opposite from the additive based approach (see Table 1). Also based on the average IOHI value, the hazard level of a route is determined automatically by the tool; all routes are categorized as moderately hazardous based on the standard developed by Hassim and Hurme (2010).

5.2.3. Worst case type calculation

In the worst case type approach, the highest penalty of each subindex is taken to represent the worst potential hazard of a process. This is to avoid the same 'worst chemical' in different subprocess to be penalized repeatedly (Hassim and Hurme, 2010). Table 2 presents the results obtained based on this approach.

It can be observed from Tables 1 and 2 that all the three calculations give different results as the idea is to provide different perspectives in inherent hazards assessment. However upon a need to integrate the findings, it can be summarized that C2/MP and TBA are the more healthier ones whereas C2/PA and C3 are the least healthier routes among the process candidates for manufacturing MMA.

All the results obtained are similar to those calculated using the manual based IOHI. This is not surprising since the computer aided IOHI tool was developed based on the manual IOHI. Therefore details of the results for all the three calculation types are not discussed here, but are in Hassim and Hurme (2010). Furthermore, the aim of this paper is not to introduce totally a new index but an effort to develop a computer aided tool for the existing IOHI method.

6. Conclusion

This study introduces a computer-aided tool for inherent occupational health assessment of chemical processes in the R&D stage. The tool was developed based on the IOHI but the assessment now becomes so much faster, easier and attractive with the computer tool. Electronic chemical properties database was also constructed for 1625 chemicals. The tool is powerful that it does not only allows swift calculation of the IOHI, but also

Table 1. The Inherent Occupational Health Index for MMA routes (Additive and Average)

Route	No. of steps	Add I_{PPH}	Add I_{HH}	Add I_{IOHI}	Avg I_{PPH}	Avg I_{HH}	Average I_{IOHI}	Status
ACH	3	21	23	44	7.00	7.67	14.67	Moderately hazardous
C2/PA	4	29	28	57	7.25	7.00	14.25	Moderately hazardous
C2/MP	3	25	15	40	8.33	5.00	13.33	Moderately hazardous
C3	4	31	26	57	7.75	6.50	14.25	Moderately hazardous
i-C4	3	23	20	43	7.67	6.67	14.33	Moderately hazardous
TBA	3	21	20	41	7.00	6.67	13.67	Moderately hazardous

Add: Additive-type calculation, Avg: Average-type calculation

Table 2. The Inherent Occupational Health Index values for MMA routes (worst case-type)

Route	Max I_{PPH}	Max I_{HH}	Max I_{IOHI}
ACH	10	8	18
C2/PA	11	8	19
C2/MP	11	6	17
C3	13	7	20
i-C4	11	7	18
TBA	9	7	16

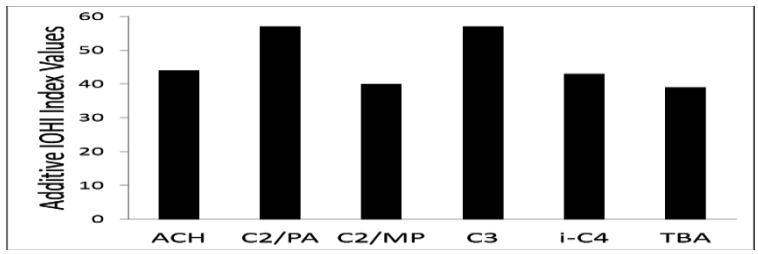

Fig. 3 The IOHI index values for MMA routes (additive-type calculation)

providing users with a summary of results for alternative process routes in terms of tables and graphs, which further ease the hazards assessment process. Furthermore a hazard level of single process can also be determined by the tool.

References

J.P. Gupta, D.W. Edwards, 2002, Inherently Safer Design: Present and Future, Process Saf. Environ. Protect. 80(3) p. 115-125.

M.H. Hassim, D.W. Edwards, 2006, Development of a Methodology for Assessing Inherent Occupational Health Hazards, Process Saf. Environ. Protect. 84(B5) p.378-390.

M.H. Hassim, M. Hurme, 2010, Inherent Occupational Health Assessment During Process Research and Development Stage, J.Loss Prev. Proc. Ind. 23(1) p.127-138.

ILO/WHO, 1950, Joint ILO/WHO Committee on Industrial Hygiene: Report of the First Meeting, ILO, Geneva.

INSIDE Project, 2001, The INSET Toolkit, http://www.aeat-safety-and-risk.com/html/inside.html

V.S. Johnson, 2001, Occupational Health Hazard Index for Proposed Chemical Plant, MSc Thesis, Loughborough University, Loughborough, UK.

I.A. Karimi and Rajagopalan Srinivasan (Editors), Proceedings of the 11th International Symposium on Process Systems Engineering, 15-19 July 2012, Singapore.

A Performance Assessment Method for Feedback Control Loops in Chemical Processes with Distribution Outputs

Jose Munoz and Junghui Chen

Department of Chemical Engineering, Chung-Yuan Christian University, Chung-Li, Taiwan 320, Republic of China

Abstract

Distributions of output quality variables are important in many chemical processes because they significantly affect the product quality and the process performance. A performance assessment method is proposed for feedback control loops in chemical processes with distribution outputs. The method assesses the ability of control loops to minimize the fluctuations in distribution outputs. Presently, due to long delays in obtaining measurements of distribution outputs, fluctuations in distribution outputs are controlled by a non-distribution variable. The non-distribution variable is a process variable that describes the conditions of a chemical process operation. To date, there has been no established method of estimating probability density distribution function (PDF) of a distribution from measured values of non-distribution controlled variable. In this paper, an algorithm is developed to estimate the PDF. An indicator of the performance assessment is defined in terms of the variance of the PDF of the over-all distribution output. This indicator can be used to compare various PDFs of different control loops to determine which control loop yields the optimal PDF.
Keywords: Control loop performance, distribution outputs, feedback control, monitoring and diagnosis

1. Introduction

There are certain chemical processes wherein the controlled variable of interest does not yield a single-value when measured but a distribution consisting of myriad of values. This distribution either gives a description of the quality of the end-product or serves as an indicator of the process operational efficiency. In polymerization, the controlled variable of interest is the molecular weight distribution (MWD) and this represents the different concentrations of polymers of varying molecular weights. It determines the end-use properties of product polymers, such as thermal properties, stress-strain properties, impact resistance, strength and hardness (Crowley & Choi, 1998; Takamatsu, et al., 1988). Clearly, control of process outputs in the form of distribution of values referred to in this paper as distribution outputs is important in producing high quality products and in running efficient plant operations.

Presently, distribution outputs are controlled by a non-distribution variable which is a single-valued variable, and the non-distribution variable has a significant relationship with the distribution output. This non-distribution controlled variable can be measured immediately and independently of the distribution output measurement. In the indirect method of controlling the distribution output, the non-distribution variable can be a process variable describing the conditions of operation. Some polymerization studies show that the first and second moments of MWD are kept within certain ranges as temperature is controlled to lie within a fixed range. The indirect method of controlling

the distribution output is implemented because the direct measurement of output distribution incurs very long delay.

Literature review reveals that there have been some studies done on performance assessment of single-input-single-output and multi-input-multi-output control loops whose controlled variables are non-distribution variables (Desborough & Harris, 1997; Harris, 1989; Harris et al. 1996; Huang et al. 1997). To date, no study has been documented on performance assessment of feedback control loops involving chemical processes with distribution outputs whose control objective is to minimize distribution output fluctuations. This may be due to the absence of a known or established: 1) clear methodology on building a process model used to approximate an actual chemical process, and 2) an acceptable indicator of over-all distribution output fluctuation. In this paper, a method for assessing the performance of feedback control loops used in chemical processes with distribution output is proposed. It can be used to compare the performance of different controllers using non-distribution variables for the distribution process. An algorithm is also developed for analyzing the effects of various control laws, including controller structures and controlled variables, on the resulting distribution outputs. Finally, an indicator of the performance assessment is defined in terms of the variance of the PDF of the over-all distribution output.

2. Modeling of Chemical Processes with Distribution Outputs

Assume that the chemical process with distribution outputs can be represented by a system of nonlinear differential shown as

$$\begin{bmatrix} \dfrac{d\mathbf{s}}{dt} \\ \dfrac{d\boldsymbol{\gamma}}{dt} \end{bmatrix} = \begin{bmatrix} \mathbf{f}_1(\mathbf{s},\boldsymbol{\gamma},u,\boldsymbol{\varepsilon}) \\ \mathbf{f}_2(\mathbf{s},\boldsymbol{\gamma},u,\boldsymbol{\varepsilon}) \end{bmatrix} \tag{1}$$

$\mathbf{s}$ represents the vector of n_s non-distribution state variables and $\boldsymbol{\gamma}$, the vector of N distribution variables at several y locations on the distribution output. For example, location y may refer to a particular molecular weight, crystal or bubble size. u is the control input and $\boldsymbol{\varepsilon}$ is the vector of n_d disturbance variables. $\mathbf{f}_1(\mathbf{s},\boldsymbol{\gamma},u,\boldsymbol{\varepsilon})$ and $\mathbf{f}_2(\mathbf{s},\boldsymbol{\gamma},u,\boldsymbol{\varepsilon})$ are nonlinear functions of $\mathbf{s}$, $\boldsymbol{\gamma}$, u and $\boldsymbol{\varepsilon}$. By means of a Taylor series expansion and the discretization, the distribution process can be represented as

$$\begin{bmatrix} \bar{\mathbf{s}}_{k+1} \\ \bar{\boldsymbol{\gamma}}_{k+1} \end{bmatrix} = \begin{bmatrix} \mathbf{A}_{11} & \mathbf{A}_{12} \\ \mathbf{A}_{21} & \mathbf{A}_{22} \end{bmatrix} \begin{bmatrix} \bar{\mathbf{s}}_k \\ \bar{\boldsymbol{\gamma}}_k \end{bmatrix} + \begin{bmatrix} \mathbf{b}_1 \\ \mathbf{b}_2 \end{bmatrix} \bar{u}_{k-1} + \begin{bmatrix} \mathbf{K}_1 \\ \mathbf{K}_2 \end{bmatrix} \bar{\boldsymbol{\varepsilon}}_k \tag{2}$$

The distribution function $\bar{\boldsymbol{\gamma}}_{k+1}$ is often approximated by a linear combination of m basis functions (Yue et al., 2008). The state space model can be rewritten as

$$\begin{bmatrix} \bar{\mathbf{s}}_{k+1} \\ \bar{\mathbf{v}}_{k+1} \end{bmatrix} = \begin{bmatrix} \mathbf{A}_{11} & \mathbf{A}_{12} \\ \bar{\mathbf{A}}_{21} & \bar{\mathbf{A}}_{22} \end{bmatrix} \begin{bmatrix} \bar{\mathbf{s}}_k \\ \bar{\mathbf{v}}_k \end{bmatrix} + \begin{bmatrix} \mathbf{b}_1 \\ \bar{\mathbf{b}}_2 \end{bmatrix} \bar{u}_k + \begin{bmatrix} \mathbf{K}_1 \\ \bar{\mathbf{K}}_2 \end{bmatrix} \bar{\boldsymbol{\varepsilon}}_k \tag{3}$$

$$\bar{\boldsymbol{\gamma}}_k(\mathbf{y}) = \mathbf{C}(\mathbf{y})\bar{\mathbf{v}}_k$$

3. PDF of the Individual Distribution Values

The fluctuations caused by the control input and disturbances on the non-distribution variables $\bar{\mathbf{s}}$ are obtained and the effects of these fluctuations on the distribution

variables $\bar{\mathbf{v}}$ are evaluated. The transfer function relating the non-distribution variables $\bar{\mathbf{s}}$ to the control input $\bar{u}$ and the disturbance variables $\bar{\boldsymbol{\varepsilon}}$ is found to be

$$\bar{\mathbf{s}}_k = \mathbf{G}_{u,s}\left(z^{-1}\right)\bar{u}_k + \mathbf{G}_{d,s}\left(z^{-1}\right)\bar{\boldsymbol{\varepsilon}}_k \tag{4}$$

The transfer function relating the distribution variables $\bar{\mathbf{v}}$ to the control input $\bar{u}$ and the disturbance variables $\bar{\boldsymbol{\varepsilon}}$ is found to be

$$\bar{\mathbf{v}}_k = \mathbf{G}_{u,v}\left(z^{-1}\right)\bar{u}_k + \mathbf{G}_{d,v}\left(z^{-1}\right)\bar{\boldsymbol{\varepsilon}}_k \tag{5}$$

The derivation of the PDF of each distribution value depends on the non-distribution variable used in the control loop. In the method shown for the assessment of the control loops, the key idea is to determine how a given control law can be rewritten to be expressed in terms of disturbance variables. Let $\bar{s}_l$ be one of the non-distribution variables in $\bar{\mathbf{s}}$, which is taken to be the controlled variable, and the control law be expressed as

$$\bar{u}_k = -G_c\left(z^{-1}\right)\bar{s}_{k,l} \tag{6}$$

Eqn (6) is substituted in Eqn (4) to get a transfer function relating $\bar{u}_k$ to disturbance variables. The transfer function in $\bar{u}_k$ is substituted in Eqn (5) to get a transfer function, which is substituted into Eqn (3) to get $\mathbf{H}_{v,l}\left(z^{-1}\right)$, a transfer function relating individual distribution values to disturbance variables. Each distribution value is computed from the disturbance variables by

$$\bar{\gamma}_k\left(y_l\right) = \mathbf{H}_{v,l}\left(z^{-1}\right)\bar{\boldsymbol{\varepsilon}}_k = \sum_{j=1}^{n_d} H_{v,l,j}\left(z^{-1}\right)\bar{\varepsilon}_{k,j} \tag{7}$$

Each distribution value follows a normal distribution with mean zero and with variance calculated by

$$\sigma_{l,v}^2 = \sum_{j=1}^{n_d}\sum_{p=1}^{\infty}\sigma_j^2 h_{v,l,j,p}^2 \tag{8}$$

4. PDF of the Distribution Output

In a sample considered for constructing PDF of the over-all distribution output, there is no need to make a distinction on which distribution value an observation value comes from. All the values are lumped together to form a PDF for the entire distribution output. Each of N deviation distribution values $\bar{\gamma}\left(y_l\right)$ is considered as a random variable which follows a Gaussian distribution with a zero mean and a variance σ_l^2 computed, so PDF of the over-all distribution output is constructed from the average of PDFs of all the distribution values as shown below

$$\Pr(e) = \frac{1}{N\sqrt{2\pi}}\sum_{l=1}^{N}\frac{1}{\sigma_l}\exp\left[-\frac{e^2}{2\sigma_l^2}\right] \tag{9}$$

In Eqn (9), the random deviation of any distribution value from its set-point is referred to as e and only one PDF can be constructed for a given control law with its specified control parameter values. By varying the control law or the values of the control parameters, various PDF can be constructed; obviously, the control loop yielding the PDF with the smallest variance is the most effective controller.

5. Case Study

The proposed performance assessment method is used to evaluate the performance of temperature control loops using a proportional controller for different controller gains in free radical solution polymerization of styrene. A process variable, temperature, is used as a controlled variable. Due to the space limitation, the mathematical model is listed here and readers can refer to Schmidt & Ray (1981). Most of the parameter values are taken from Hidalgo & Brosilow (1990). The operating conditions are taken from Tatiraju et al. (1999).

The model has the vector of three non-distribution state variables $\mathbf{s} = [C_I \;\; C_M \;\; T]$ (initiator concentration, monomer concentration and temperature) and the vector of $N = 200$ distribution variables at several chain length locations on the MWD output $\boldsymbol{\gamma} = \left[C_{M_2} \;\; C_{M_{2+\Delta n}} \;\; C_{M_{2+2\Delta n}} \;\; C_{M_{2+3\Delta n}} \;\; \cdots \;\; C_{M_{n,\max}} \right]^T$. Q is the heating rate which is the control input, and the vector of two disturbance variables (inlet initiator concentration and inlet temperature) is $\boldsymbol{\varepsilon} = \left[C_{I,i} \;\; T_I \right]^T$. The MWD function $\bar{\gamma}(y)$ is approximated by a linear combination of $m = 35$ B spline cubic wavelet functions. For a temperature proportional controller, the control law is given by

$$\bar{Q}_k = K_p \bar{T}_{k-1} = K_p z^{-1} \bar{T}_k \tag{10}$$

Eqn (10) is substituted into the transfer function relating temperature T to the control input Q and disturbance variable inlet initiator concentration $C_{I,i}$ s and inlet feed temperature T_I to get

$$\bar{T}_k = \left[G_{T,C}\left(z^{-1}\right) \;\; G_{T,T}\left(z^{-1}\right) \right] \begin{bmatrix} C_{I,i,k} \\ T_{I,k} \end{bmatrix} = \mathbf{G}_T\left(z^{-1}\right) \bar{\boldsymbol{\varepsilon}}_k \tag{11}$$

Eqn (11) shows the relationship between the disturbances and the fluctuations in temperatures for a proportional controller with a specified gain. The disturbances, namely fluctuations in inlet initiator concentration and inlet feed temperature, are assumed to follow a Gaussian distribution with mean zero and standard deviations of 0.06 and 20. The PDF of temperature is based on two controller gains namely -0.8 and -0.08 respectively. Since it assumes that controlling fluctuations in MWD are indirectly done by controlling temperature fluctuations, it is speculated that the MWD fluctuations under the controller with higher gain would be smaller than those with a smaller gain. The overall PDF can be calculated using Eqn (9) shown in Figure 1 and 2. It is found that most of the deviations are very close to zero and that only certain distribution values deviate significantly from the target distribution and the performance for the controller gain of -0.8 is better. Using the proposed method, the conclusion can indeed be obtained and plots of PDFs for overall MWD fluctuations can be obtained together with the variance of the PDF. The PDF curve for the overall MWD fluctuation will be narrower and the variance smaller when the controller has higher gain.

6. Conclusions

The feasibility of using the proposed performance assessment method for feedback control loops in chemical processes with distribution outputs is shown. The proposed method assesses the performance of control loops on the ability to minimize fluctuations of distribution outputs. The control loops indirectly control distribution outputs by a non-distribution variable, so the method uses a state space process model to determine the effects of various control laws on the probability density distribution

function (PDF) of the resulting distribution outputs. Results show that the proposed method is effective in assessing the control loop performance.

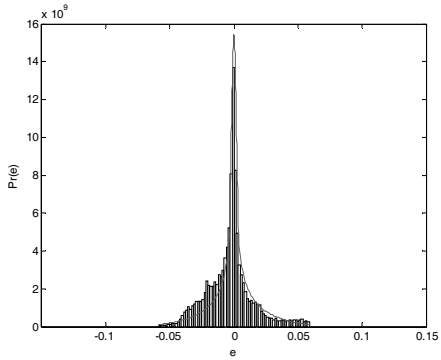

Figure 1 PDF of Distribution Output K=-0.8

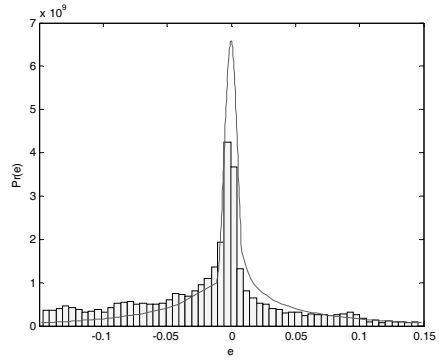

Figure 2 PDF of Distribution Output K=-0.08

References

T.J. Crowley, Y.K. Choi, 1998, Experimental Studies on Optimal Molecular Weight Distribution in a Batch Free Radical Polymerization Process, Chem. Eng. Science, 53, 2769-2790.

T. Takamatsu, S. Shioya, and Y. Okada, 1988, Molecular Weight Distribution Control in a Batch Polymerization Recator, Ind. Eng. Chem. Res., 27, 93-99.

L Desborough, T.J. Harris, 1997, Performance Assessment Measures for Univariate Feedback Control, Canadian J. Chem. Eng., 70, 1186-1197.

T.J. Harris, 1989, Assessment of Control Loop Peformance, Canadian J. Chem. Eng., 67, 856-861.

T.J. Harris, F. Boudreau, and J.F. MacGregor, 1996, Performance Assessment of Multivariable FeedBack Controllers, Automatica,12, 1505-1518.

B. Huang, S.L. Shah, and E.K. Kwok, 1997, Good, Bad or Optimal? Performance Assessment of Multivariable Processes, Automatica, 31, 1175-1183.

H. Yue, H. Wang, and J.F. Zhang, 2008, Shaping of Molecular Weight by Iterative Learning PDF Control Strategies, Proc.IMechE, 227, 639-653.

A.D. Schmidt, W.H. Ray, 1981, The Dynamic Behaviour of Continuous Polymerization Reactors-I, Chem. Eng. Science, 36, 1401-1410.

P.M. Hidalgo, C.B. Brosilow, 1990, Nonlinear Model Predictive Control of Styrene Polymerization at Unstable Operating Points, Comp. Chem. Eng., 4, 481-494.

S. Tatiraju, M. Soroush, and B.A. Ogunnaike, 1999, Multirate Nonlinear State Estimation with Application to a Polymerization Reactor, AIChE J., 45, 769-780.

I.A. Karimi and Rajagopalan Srinivasan (Editors), Proceedings of the 11th International Symposium on Process Systems Engineering, 15-19 July 2012, Singapore

Fault Diagnosis based on *DPCA* and *CA*

Celina Rea, Ruben Morales-Menendez [*], Juan C. Tudón Martínez, Ricardo A. Ramírez Mendoza, Luis E. Garza Castañon

Tecnológico de Monterrey, Campus Monterrey, Av. Eugenio Garza Sada 2501, Col. Tecnológico, 64,849 Monterrey NL, México

Abstract

A comparison of two fault detection methods based in process history data is presented. The selected methods are Dynamic Principal Component Analysis (*DPCA*) and Correspondence Analysis (*CA*). The study is validated with experimental databases taken from an industrial process. The performance of methods is compared using the Receiver Operating Characteristics (*ROC*) graph with respect to several tuning parameters. The diagnosis step for both methods was implemented through Contribution Plots. The effects of each parameter are discussed and some guidelines for using these methods are proposed.

1. Motivation

Industrial process have grown in integration and complexity. Monitoring only by humans is risky and sometimes impossible. Faults are always present, early Fault Detection and Isolation (*FDI*) systems can help operators to avoid abnormal event progression. *DPCA* and *CA* are two techniques based on statistical models coming from experimental data that can be used for fault diagnosis, Detroja et al. (2006b). These approaches are well known in some domains; but, there are several questions in the fault diagnosis. A *ROC* graph is a technique for visualizing, organizing and selecting classifiers based on their performance. *ROC* graph has been extended for use in diagnostic systems. In the published research works, the number of data for model's learning the model, sampling rate, number of principal components/axes, thresholds have not been studied under same experimental databases.

2. Fundamentals

A brief comparative review of both *DPCA* and *CA* approaches is presented focus in modelling, detection and diagnosis.

Modeling for both DPCA and CA. Both methods need a statistical model of the process under normal operating conditions. The data set need be scaled to zero mean and unit variance. *CA* requires n_t observations for p variables having a form of $\mathscr{X}(t) = [X_1(t) \ \ldots X_p(t)\ ]_{(n_t \times p)}$; while *DPCA* additionally includes some past observations (i.e. w-time delay) $\mathscr{X}(t) = [X_1(t) \ \ldots \ X_1(t-w) \ \ldots \ X_p(t) \ \ldots \ X_p(t-w)]_{(n_t \times (p \cdot [w+1]))}$. Based on $\mathscr{X}(t)$ matrix, two subspaces are built. The Principal Subspace captures major faults in the process, and the Residual Subspace considers minor faults and correlation rupture. A SCREE test, determines the number of principal and residual components (axes). By plotting the eigenvalues (singular values) of $\mathscr{X}(t)$ for *DPCA* (*CA*), the principal components (axes) are the first k components (axes) before the inflection point is located, while

[*] rmm@itesm.mx

the remainders are the residuals components (axes). Even *DPCA* and *CA* models cannot be compared. The representation given by *CA* would appear to be better able to capture inter-relationships between variables and samples, Detroja et al. (2006a). Fig. 1 (left) summarizes the model's learning for both methods.

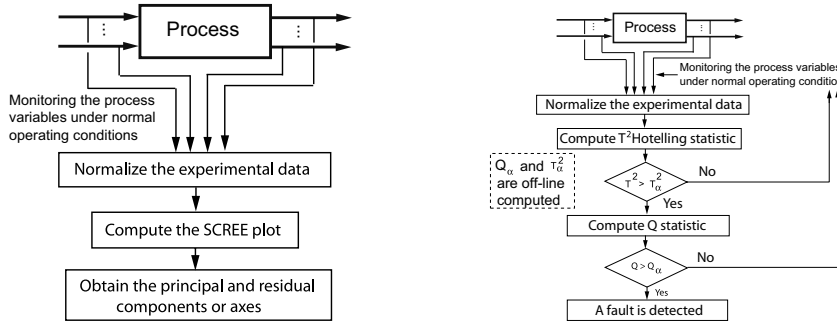

Figure 1. Model's learning algorithm (left) and online detection (right) for DPCA *&* CA.

Detection for DPCA. The variables must be normalized, $\mathscr{X}_S$. Based on the correlation matrix $\mathscr{R}$, the eigenvalues λ_i and eigenvectors $\mathscr{V}_i$ are obtained. The eigenvalues must be organized in decreasing order. The eigenvectors form two matrices: $\mathscr{V}_{[1,k]}$ which is the principal component transformation and $\mathscr{V}_{[k+1,p\cdot[w+1]]}$, known as residual transformation matrix. The projections to the subspaces are based on a linear transformation with no correlation between them. Mapping from multivariate approach to a scalar demands two statistics: T^2 Hotelling and Q statistics. The T^2 measures the deviation of variables in a data set from their mean values. Hotelling T^2 chart is based on the concept of statistical distance and it monitors the change in the mean vector T^2 statistic is obtained by $T^2_{\mathscr{X}_{S_i}}$; a normal operating point can be established as $T^2_\alpha = (n_t-1)F_\alpha(k,n_t-k)/(kn_t-k)$ F_α-distribution with k and n_t-k degrees of freedom, $\alpha = 0.95$. If $T^2 > T^2_\alpha$ a fault is detected. Q statistic will detect changes on the residual directions. The Q statistic is obtained as $Q_{\mathscr{X}_{S_i}} = \mathscr{X}_{S_i} G \mathscr{X}^T_{S_i}$. The threshold for normal operating conditions is given by $Q_\alpha = \theta_1 \left[h_o C_\alpha \sqrt{2\theta_2}/\theta_1 + 1 + \theta_2 h_0(h_0-1)\theta_1^2\right]^{\frac{1}{h_0}}$ If $Q_{\mathscr{X}_{S_i}} > Q_\alpha$ a fault is detected.

Detection for CA. *CA* is an optimization problem with $\mathscr{P} = \mathscr{D}_r^{-1/2}[(1/g)\mathscr{X} - rc^T]\mathscr{D}_c^{-1/2}$ and $\mathscr{A}\mathscr{D}_\mu\mathscr{B}^T = SVD(\mathscr{P})$. For choosing the principal and residual axes, a SCREE plot can be made with the singular values obtained in $\mathscr{D}_\mu$. The Greenacre's criteria was used for selection of k principal axis. The coordinates of the row and column profile points for the new principal axis can be computed by projecting on $\mathscr{A}$ and $\mathscr{B}$, with only the first k columns retained, with $\mathscr{F} = \mathscr{D}_r^{-1/2}\mathscr{A}\mathscr{D}_\mu$ and $\mathscr{G} = \mathscr{D}_c^{-1/2}\mathscr{B}\mathscr{D}_\mu^T$. Matrix $\mathscr{F}$ gives the new row coordinates for the row cloud. Using a new measurement vector $X = [X_1 \ \ldots \ X_m]^T$, the row sum is given by $r = \sum_{i=1}^p X_i$ and the new row score is $f = [r^{-1}x^T\mathscr{G}\mathscr{D}_\mu^{-1}]^T$. The T^2 statistic for *CA* is defined as $T_i^2 = f^T\mathscr{D}_\mu^{-2}f$, where $\mathscr{D}_\mu$ contains the first k-largest singular values. The threshold is computed through T^2_α. For residual axes, Q statistic

allows to detect any significant deviation. Considering $Q_i = Res^T Res$, and the control limit as $Q_\alpha = \mu_Q \pm C_\alpha * \sigma_Q$ where C_α is a confidence limit of 95% according to its normal deviation $\mathcal{N}(\mu_Q, \sigma_Q)$. Fig. 1 (right) shows the scheme for online detection.

Diagnosis for both *DPCA* and *CA*. The T^2 statistic gives a variable which is calculated by using all variables; it shows the changes that occurred in all variables. The T^2 chart does not give information on which variable or variables is faulty. Miller et al. (1998) introduced a method for determining the contribution of each of the p variables in the T^2 computation. Scores of the *PC* are used for monitoring in T^2 chart; upon a faulty signal, first the contribution of each variable in the normalized scores is computed. Then total contributions of each variable are determined and plotted. The plot that shows the contribution of each variable in T^2 chart at time k is called the variable contribution plot, Kosebalaban and Cinar (2001). When T^2 value at time k is above the upper control limit, the variable contribution are calculated and plotted to diagnose the variable(s) that caused the fault alarm in multivariate T^2 chart. The variables with higher contribution, are isolated as the most probable fault: $Cont_i = Z_i^2 / \sum_{j=1}^{n_t} Z_j^2$ where $Z = R_{\gamma_r}$ is a generated residual for *DPCA*. *CA* method cannot diagnose the fault neither; for this purpose, a contribution plot base on the residuals of the Q statistic are used, $Z = Res$. The contribution plots can be plotted over time when a faulty signal alarms, the change in contribution of process variables gives more information about the root cause of the faulty condition at that time period.

3. Experimental Setup

An industrial Heat Exchanger (*HE*) was the test-bed for this research. The *HE* uses steam vapor for heating water. The operating point is 70% of steam vapor flow (FT_2), 38% of water flow (FT_1), and the input water temperature (TT_1) was at 23^{o}C, which give an outlet water temperature (TT_2) of 34^{o}C. More than 20 experimental tests were done. For each sensor an abrupt fault as a bias of $\{ \pm 5, \pm 6, \pm 8 \}\ \sigma$ of the signal were implemented Prakash et al. (2002). Also, the number of data were 200, 500,..., 5000, and the sampling rate: 1,2,...,10.

4. Analysis of the Tuning Parameters.

Number of Principal Components (PC)/axes. Data compression is an important aspect of multivariate statistical tools. SCREE plot indicates the percentage of accumulated information variation versus the components/axes. The components/axes, when the slope of the plot does not change, defines the number of *PC*/axes. Figure 2 (A) shows the percentage accumulated variation information versus the number of components for *DPCA*, and versus number of axes for *CA* is shown in Fig. 2 (B). Each plot includes databases with 100, 200, 500 and 1,000 data vectors. For *DPCA*, 5 *PC* describe 92-94 % of the information; 6 or more components do not contribute significantly. The number of data vector of process variables do not impact in the curve behavior. For *CA* the number of data affects the curve: 100-200 data have lower percentage accumulated variation than 500-1000 data vectors for 1 or 2 axes. After 3 axes there is not difference. According to *Greenacre* criteria, Greenacre and Blasius (1995), three axes are recommended.

Thresholds. A False Negative (*FN*) is when there is a fault, but it is not detected; while a False Positive (*FP*) is when there is no fault, but one is detected. True Positive (*TP*) is when there is a fault, and it is detected; while, True Negative (TN) is when there is no

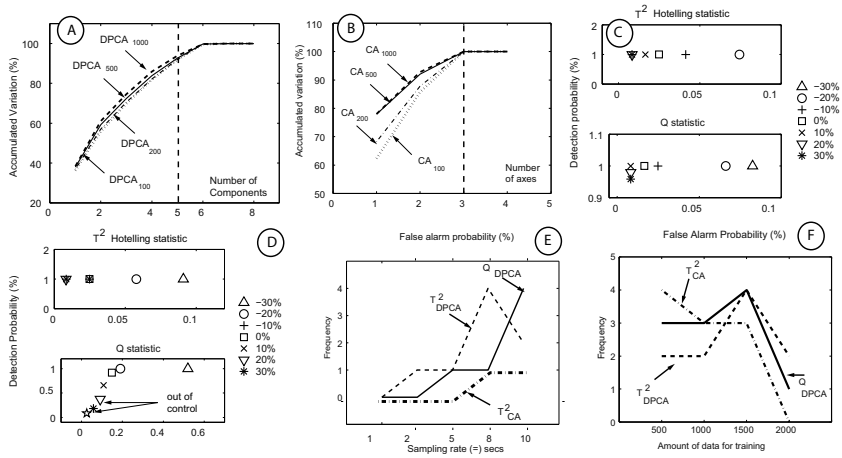

Figure 2. Average variation accumulated versus components for DPCA *(A), and versus number of axes for* CA *(B).* ROC *curves for outlet water temperature (TT_2) transmitter using* DPCA *(C), and for outlet water temperature (TT_2) transmitter* CA *(D). Frequency of errors for different sampling time (E) and for different number of training data (F).*

fault and no fault is detected. The sum of *TP* and *FN* are the total faulty cases (*TFC*) and the sum of *TN* and *FP* are total healthy cases (*THC*). The probability of detection $P_d = \frac{TP}{TFC}$ while the probability of false alarms $P_{fa} = \frac{FP}{THC}$. For every condition, when $[(P_d > 0.9)$ and $(P_{fa} < 0.1)]$, an optimum is achieved by having a good compromise between right detection and minimum false alarms. *ROC* curves show a relation between opportune detection probability P_d versus false alarms probability P_{fa}. Table 1 summarizes the performance of $[(P_d > 0.9)$ and $(P_{fa} < 0.1)]$ criteria for faults sensors. *DPCA* shows successful results; while, *CA* exhibits some troubles mainly with *Q* statistics. Fig. 2 (C and D) shows *ROC* curves, where the thresholds were modified in different percentage. Fig. 2 (C) shows that *DPCA* is successful for both statistics. However, Fig. 2 (D) shows that for *CA* only T^2 statistics works well. *Q* statistics for *CA*, is only based on the residuals axes, which does not capture the variation of the residual per axes, Table 1.

Sampling rate. The process variables were sampled at 1, 2, 5, 8 or 10 s. Fig. 2 (E) shows the number of times that the $[(P_d > 0.9)$ and $(P_{fa} < 0.1)]$ criteria was violated for each statistics for different sampling rate. There is a good performance for both methods when sampling rate is 1 or 2 s; however, the probabilities for missing detections or increasing false alarms grows up for sampling times greater than 5 s. The *Q* statistic for *CA* was avoided because its low performance.

Number of Training Data. Fig. 2 (F) shows the number of times that the $[(P_d > 0.9)$ and $(P_{fa} < 0.1)]$ criteria was violated for each statistics for the number of training data. The number of data is a key issue for learning a statistical model. It can be seen that after 1,500 training data (25 min, 1 s sampling rate) both methods improve their performance.

Table 1. Average performance for different sensors based on ROC *curves.*

Sensor Transmitter	Number Tests	*DPCA-*T^2	*DPCA-Q*	*CA-*T^2	*CA-Q*
TT_2	11	100	100	100	9.09
FT_1	15	100	86.67	40	6.67
FT_2	12	91.67	100	91.67	91.67
TT_1	11	81.82	90.91	81.82	0

Diagnosis. There is a good performance with *DPCA* for the 4 faulty sensors, while *CA* shows 90.9% performance when a fault occurs in (TT_2) and 46.6% if the fault is in (FT_1). Contributions of 4 variables were compared to the same statistic and choose the variables corresponding to the relatively large contributions as the possible causes for faults. Instead of comparing the absolute contribution and the corresponding control limit, the use of the relative contribution is more convenient way to identify faulty variables Choi and Lee (2005).

5. Conclusions

Given experimental data a multivariate statistical model can be learned. SCREE plot and the *Greenacre* criteria guide the complexity of the model based on the minimum number of components/axes. The statistical model for *CA* is more sensible to the number of data than the model for *DPCA*; but, defined the minimum number of components/axes, the number of data does not have influence. The *ROC* graphs are a useful tool for visualizing and evaluating fault detection algorithms. A detection probability ($P_d > 0.9$) and false alarm probability ($P_{fa} < 0.1$.) is a good criteria for choosing the sampling rate, number of data and thresholds. Sampling rate was the most important parameter. Based on *ROC* graphs, *DPCA* outperforms *CA* in fault detection, because the Q statistics does not work well. Diagnosis could be implemented in both methods through contribution plots.

References

Choi, S., Lee, I., 2005. Multiblock PLS-based Localized Process Diagnosis . J of Process Control 15 (3), 295–306.

Detroja, K., Gudi, R., Patwardhan, S., 2006a. Fault Diagnosis using Correspondence Analysis: Implementation Issues and Analysis. In: IEEE Int Conf on Ind Tech. pp. 1374 – 1379.

Detroja, K., Gudi, R., Patwardhan, S., Roy, K., 2006b. Fault Detection and Isolation Using Correspondence Analysis . Ind Eng Chem Res 45, 223 – 235.

Greenacre, M., Blasius, J., 1995. Correspondence Analysis in the Social Sciences. A Press.

Kosebalaban, F., Cinar, A., 2001. Integration of Multivariate SPM and FDD by Parity Space Technique for a Food Pasteurization Process. Computers and Chemical Eng 25, 473–491.

Miller, P., Swanson, R., Heckler, C., 1998. Contribution Plots: A Missing Link in Multivariate Quality Control . Appl. Math. and Comp. 8, 775–792.

Prakash, J., Patwardhan, S., Narasimhan, S., 2002. A Supervisory Approach to Fault-Tolerant Control of Linear Multivariable Systems. Ind. Eng. Chem. Res. 41, 2270–2281.

I.A. Karimi and Rajagopalan Srinivasan (Editors), Proceedings of the 11th International Symposium on Process Systems Engineering, 15-19 July 2012, Singapore.

Design Method of Alarm System for Identifying Possible Malfunctions in a Plant Based on Cause-Effect Model

Makoto Kato[a], Kazuhiro Takeda[b], Masaru Noda[ac], Yasunori Kikuchi[a], Masahiko Hirao[a]

[a]*Department of Chemical System Engineering, University of Tokyo, 7-3-1 Hongo, Bunkyo-ku, Tokyo 113-8656, Japan*
[b]*Department of Material Science and Chemical Engineering, Shizuoka Univeristy, 3-5-1 Johoku, Naka-ku, Hamamatsu, Shizuoka 432-8561, Japan*
[c]*Graduate School of Information Science, Nara Institue of Science and Technology, 8916-5 Takayama-cho, Ikoma 630-0192, Japan*

Abstract

A new alarm system design method is proposed, in which it is assumed that the sign patterns and alarm sequences generated by the alarm system are invariant for each possible plant malfunction in a plant. The proposed method gives the most sets yet provided of plant malfunctions that operators can distinguish using the alarm system. We applied the proposed method to select alarm variables for a simple chemical plant. Results showed that the method provides more alarm variable combinations that can identify possible malfunctions than a previously used method.

Keywords: Plant Alarm System, Design, Cause-Effect Model, Malfunction

1. Introduction

Plant alarm systems form one of the core elements of operator interfaces for automatically monitoring plant state deviations and for alerting plant operators to changes that require their attention in industrial plants such as chemical plants, oil refineries, and power stations. Designing an efficient alarm system that helps operators to quickly identify the causes of abnormalities and respond to abnormal situations is vital to achieve safe and stable plant operations.

Distributed control systems (DCS), which are widely used in chemical industries, utilize control instruments that have process variables (PVs) and manipulated variables (MVs). Plant alarm systems make use of these variables and issue warnings when PV or MV values exceed allowable alarm limits to a degree that is undesirable or potentially unsafe. When a plant situation becomes abnormal, alarm information is reported in the form of flashing icons or buzzing sounds and a text list describing related alarm information appears on an alarm summary panel.

In 2009, the Engineering Equipment and Materials Users' Association (EEMUA) published comprehensive guidelines for the development, procurement, operation, maintenance, and management of industrial alarm systems. While the guidelines mentioned, for example, the key design principle that every alarm (or combination of alarms) presented to the operators should have a response clearly defined by the alarm's designer, some of the design methodologies mentioned in it, such as the selection of alarm variables, are still only conceptual in nature.

Luo *et al.* (2007) proposed a method for selecting a set of alarm variables on the basis of an abnormality propagation diagram that denotes the relations between failure causes and detectable symptoms for all assumed plant malfunctions. The method selects the variables by referring to the number of possible malfunctions that could generate the symptoms. This is because the smaller the number of possible malfunctions that could generate a symptom, the fewer malfunctions an operator needs to check for. However, the method does not theoretically guarantee that operators will be able to identify all malfunctions assumed in the plant by using selected alarm variables.

Takeda *et al.* (2010) proposed using a cause-effect model to derive sets of plant alarm variables for identifying assumed plant malfunctions. The alarm system they designed is theoretically guaranteed to be able to statistically identify all assumed plant malfunctions. However, the number of malfunctions that operators using the system can identify is limited because the method it employs assumes that operators will utilize only alarm variable combinations generated by the system for identifying them.

In this study, we propose a new alarm system design method, in which we assume that the pattern of signs and the sequence of alarms generated by the system are invariant for each possible malfunction. The method gives more plant malfunction sets that operators using an alarm system can identify than have heretofore been provided.

2. Cause-effect model

A cause-effect model is an abnormality propagation diagram that shows the propagation process of abnormalities after malfunctions occur. The signed directed graph in Fig. 1 is used to describe a cause-effect model, where process variables and their causal relations are denoted by nodes and directed braches, respectively (Iri *et al.*, 1979). Node signs are defined as follows:

\+ Positive deviation of process variable from normal condition
0 Process variable is in normal condition
− Negative deviation of process variable from normal condition

The solid and dotted branches in the cause-effect model represent positive (+) and negative (−) influences between two nodes, respectively. A possible plant malfunction is defined by pairs of a state variable and its sign. The cause-effect model of the process is derived by a Hazard and Operability Study or Process Hazard Analysis. In this paper, it is assumed that the cause-effect model of the object plant is given in advance.

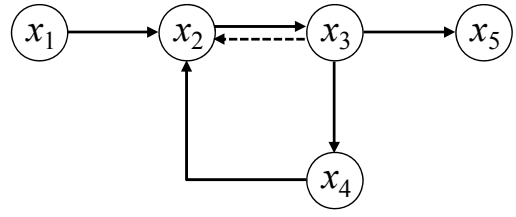

Fig. 1 Example of cause-effect model

3. Alarm variable selection method

3.1. Problem definition

In this paper, the alarm system design problem is how to determine all alarm variable sets that are able to distinguish the true malfunction among all assumed plant malfunctions. Following assumptions are introduced in the method:

- Total number of alarm variables is given
- Multiple malfunctions don't occur simultaneously

3.2. Alarm variable selection method

All measured variables in the cause-effect model can be treated as alarm variables. The proposed method uses the following steps to determine all alarm variable sets that are able to distinguish the true malfunction among all possible plant malfunctions.

Step 1: Generate all alarm variable permutations by selecting measured process variables, where the total number of alarm variables is given.

Step 2: Generate all permutations of pairs of alarm variables and signs by assigning three signs, i.e., "+", "0", and "−", to each alarm variable in all alarm variable permutations. These permutations are called "alarm generation patterns" hereafter.

Step 3: Find directed single paths from the first alarm to each alarm in the alarm generation pattern on which node signs corresponding to alarm variables and signs of directed branches along the directed single path are consistent with each other. If no feasible directed single paths are found, eliminate the alarm generation pattern because there is inconsistency between the pattern and the cause-effect model. Execute the consistency check for all alarm generation patterns with the cause-effect model.

Step 4: Find all assumed malfunctions that can generate the pair of the first alarm and its sign of the alarm generation pattern. If two or more assumed malfunctions that satisfy the above conditions are found, eliminate this pattern because it is not able to distinguish one true malfunction among all assumed plant malfunctions. Eliminate all alarm generation patterns where the first alarm is caused by two or more assumed malfunctions.

Step 5: Derive all alarm variable combinations that are able to identify all assumed plant malfunctions.

4. Case study

4.1. Example process

The proposed method was applied to the alarm system design problem of the simple reaction process with a recycle loop in Fig. 2 (Takeda *et al,* 2010), where P, F, L, and V are state variables of pressure, flow rate, liquid level, and valve position, respectively. All state variables except for P1 and P2 are measured process variables. Therefore, the set of measured process variables is S = {F1, F2, F3, F4, L1, L2, V1, V2, V3, V4}.

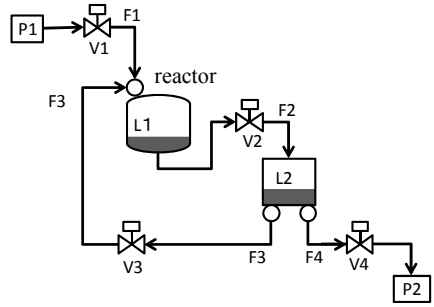

Fig. 2 Example process

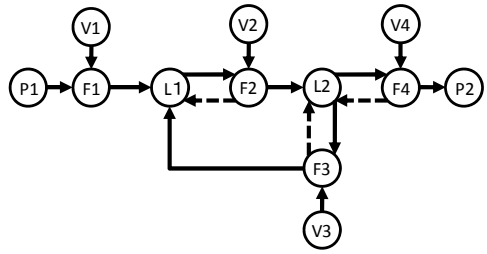

Fig. 3 Cause-effect model

Figure 3 shows the cause-effect model of the objective process. For example, the liquid level of reactor L1 increases when the pressure of feed P1 becomes abnormally high. The following six malfunctions are assumed to occur in the plant.

P1[+]	High feed pressure
P1[−]	Low feed pressure
F2[+]	Leakage from the pipe between reactor and buffer tank
F2[−]	Blockage in the pipe between reactor and buffer tank
V4[+]	Valve stiction at high valve position
V4[−]	Valve stiction at low valve position

The alarm system design problem is how to derive all combinations of alarm variables from S = {F1, F2, F3, F4, L1, L2, V1, V2, V3, V4} that are able to distinguish all assumed malfunctions C = {P1[+], P1[−], F2[+], F2[−], V4[+], V4[−]}.

4.2. Results and discussion

Table 1 shows all alarm variable combinations derived by the proposed method that are able to distinguish all assumed malfunctions for a total of three alarm variables. The table also shows all alarm variable combinations derived by a previously used method. The proposed method found 18 combinations.

5. Conclusion

We have proposed a new alarm system design method in which we assume that the pattern of signs and the sequence of alarms are invariant for each possible malfunction. Theoretical analysis showed that our method is especially effective for isolating the root causes of malfunctions that have corresponding nodes in the connected cause-effect graph.

References

Engineering Equipment & Material Users' Association (EEMUA), ALARM SYSTEMS-A Guide to Design, Management and Procurement, EEMUA Publication No.191 2nd Edition, EEMUA, London (2007)

M. Iri, K. Aoki, E, O'shima, and H. Matsuyama; "An algorithm for diagnosis of system failures in the chemical process," *Comp. Chem. Eng.*, **3(1-4),** 489-493 (1979)

Y. Luo, L. Xiwei, M. Noda, and H. Nishitani, Systematic Design Approach for Plant Alarm Systems, *Journal of Chemical Engineering of Japan*, **40(9)**, 765-772 (2007)

K. Takeda, T. Hamaguchi, and M. Noda; "Plant Alarm System Design based on Cause-Effect Model," *Kagaku Kogaku Ronbunshu*, **36(2)**, 136-142 (2010)

Table 1 Possible alarm variable combinations when total number of alarms is three

Combination of alarm variables
F1, V4, F2
F1, V4, F3
F1, V4, F4
F1, V4, L2
F1, F2, F3
F1, F2, F4
F1, F2, L1
F1, F2, L2
F1, F3, F4
F1, F4, L2
F2, F3, L1
F2, F4, L1
F2, L1, L2
F2, V4, L1
F4, L1, L2
F3, F4, L1
F3, V4, L1
V4, L1, L2

I.A. Karimi and Rajagopalan Srinivasan (Editors), Proceedings of the 11th International Symposium on Process Systems Engineering, 15-19 July 2012, Singapore.

Real-time application of CAPE-OPEN for PTA process monitoring and optimization*

Xiaorui Zhao[a,b], Pengfei Jiang[a], Xi Chen[a], Jun Zhao[a], Zhijiang Shao[a]

[a]*State Key Laboratory of Industrial Control Technology, Institute of Industrial Control, Zhejiang University, 38 Zheda Road, Hangzhou 310027, China*
[b]*Department of Mechanical and Industrial Engineering, University of Illinois at Chicago, Chicago 60607, United States*

Abstract

A computer-aided process engineering (CAPE)-OPEN-based open-architecture application was implemented for the online Purified Terephthalic Acid (PTA) process monitoring and optimization. The framework incorporates independent Process Modeling Components (PMC) that comply with the CAPE-OPEN 1.0 standard: *p*-xylene (PX) oxidation unit operation model, the nonlinear algebraic/nonlinear programming (NLA/NLP) interior point optimizer (IPOPT) solver, as well as the physical properties and the equilibrium calculation engine. All components are seamlessly integrated into the Process Modeling Environment (PME) for process simulation and optimization. The key reaction kinetic constants were estimated using a sequential subproblem strategy and then encapsulated through an *ICapeUnit* interface, with the selective operational parameters exposed for the operation and maintenance requirements. The reactor model can be solved by IPOPT within less than a second through the *ICapeMINLP* interface using an ordinary desktop computer. The convergence reliability in successfully solving the model for a wide-range of operation conditions was subsequently investigated. Based on the developed CAPE-OPEN model, a *de-facto* "Soft-sensing and Optimization System for p-xylene (PX) and acetic acid (HAC) Consumption in the PTA Process" was implemented and successfully used at the Sinopec Yangzi Petrochemical Company in Nanjing, China. The system provides real-time consumption calculation, product quality prediction, and operational guidance for operators. The CAPE-OPEN conceptual design can be applied in industrial settings for real-time applications.

Keywords: CAPE-OPEN, Purified Terephthalic Acid Process, PX Oxidation Reactor, Open Architecture, Real-time Simulation and Optimization

1. Introduction

Purified Terephthalic Acid (PTA) is the important raw material of polyester fibers, polyethylene terephthalate (PET), and insulated paint (Wang, 2005). The current manufacturing method for PTA is based on *p*-xylene (PX) oxidation, which is well known for its highly complex reaction kinetics, thermodynamics, and mass-transfer characteristics.

Environment and safety regulations, as well as growing demand on product quality and increasingly competitive markets, necessitate the continuous improvement of chemical processes in minimal time at minimal cost (Marquadt, 1996). A useful tool based on a

*This work was supported by the 973 Program of China(2012CB720500) and the NSF Program of China(21006086). E-mail address: zjshao@iipc.zju.edu.cn

rigorous model is needed in the process industry to provide operational guidance for production applications. Fortunately, with the rapid development of the computer-aided process engineering (CAPE) technology, the mechanism of PTA manufacture has become well understood and translated into a simulation flowsheet.

In the current work, the PX oxidation kinetics-based continuous stirred-tank reactor (CSTR) model is rewritten and is made CAPE-OPEN compliant. The core kinetic parameters are estimated and encapsulated on a binary level, and the end-users can only access the operational conditions. The reformed model is combined with a CAPE-OPEN compliant numeric algorithm interior point optimizer (IPOPT) and thus can solve itself under a sequential modular (SM) simulation mode. The validated model is then embedded into a PTA manufacturing process steady-state simulation in Aspen Plus as a substitute for the Aspen CSTR model. The validated model is further utilized in an open-architecture simulation and optimization platform being run at the Sinopec Yangzi Petrochemical Company in Nanjing, China. A Microsoft component object model (COM) middleware technology keeps the key model parameters invisible, thereby guaranteeing confidentiality (Banks, 2005).

1.1. PTA Process Introduction

The procedure for the PTA manufacturing process consists of two steps, namely, oxidation and purification. During the oxidation step, the PX oxidation reaction takes place in the liquid phase and is catalyzed by a Co-Mn-Br system at the 150°C to 210°C temperature range, producing crude terephthalic acid (TA).

The reactor unit has four inputs (two for the liquid and oxygen input streams, and two from the cycle loop streams) and two outputs. The vapor phase output of the reactor is passed to the next three-level condenser to feed the subsequent reaction, and the liquid phase output is sent to the crystallizer to be reoxidized.

1.2. PX Oxidation Reactor Model

PX oxidation follows a catalyzed reaction chain (Figure 1) of methyl oxidation to produce the final product, TA.

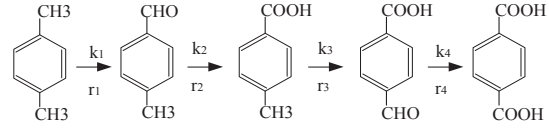

Figure 1. PX oxidation route

The vapor/liquid phase reactants in the tank are assumed to be well-mixed. The main reactions occur in the liquid phase, while the combustion in the gas phase produces side products and releases the CO and CO_2 tail gas. The mathematical model of the PX oxidation unit can be divided into four parts, namely, the reaction kinetics, material balance, physical property and equilibrium calculation, and connectivity equations. The reaction kinetics follows the simplified LHHW (Langmuir-Hinshelwood Hougen-Watson) kinetic equations.

1.3. Kinetic Parameter Estimation

To obtain the rigorous reactor model, the reaction kinetic factors (the K factors in the kinetic factor in LHHW equations) must be precisely estimated. The objective function for estimation is developed using the seven guide concentration variables from the field, namely, TA production, 4-carboxybenzaldehyde (CBA) concentration, acetic acid (HAC) consumption, as well as O_2, CO, CO_2, and crystallizer O_2 tail gases. The objective function is optimized under five typical steady-state operating conditions.

The estimation problem is formulated as formula (1). It has 21,718 variables, and is highly nonlinear. The traditional DMO solver available in Aspen Plus cannot solve the problem easily, especially when the initial values of the optimization variables are far from the optimum.

$$\begin{aligned} &min \sum_{i=1}^{5}\sum_{j=1}^{7}\varphi_{i,j}(y_{i,j}^{pred}-y_{i,j}^{meas})^2 \\ &s.t.\ f(x,y,k)=0 \\ &\quad k=[k_1,k_2,...,k_p] \\ &\quad lb_p \le k_p \le ub_p \\ &\quad p=1,2,...,10 \end{aligned} \tag{1}$$

The authors proposed a sequential subproblem programming strategy for data reconciliation and parameter estimation using multiple datasets (Zhang and Shao et al., 2010). A series of subproblems was constructed based on the objective and the model parameters. The solutions of each subproblem are a good initial estimation of the optimum of the next one. The optimum of the original parameter estimation problem can be derived by solving the series of subproblems.

1.4. Software Interface Implementation

CAPE-OPEN interfaces are used for the simulation under the SM and equation-oriented (EO) modes. The framework is shown in Figure 2.

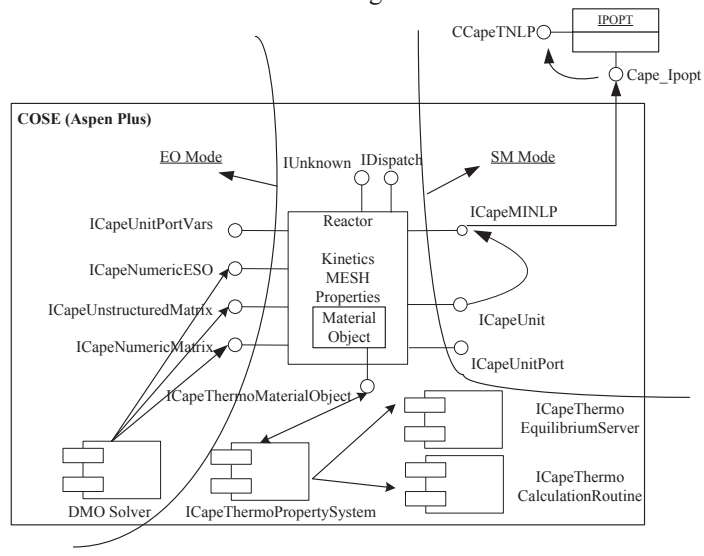

Figure 2. CAPE-OPEN PX oxidation reactor interface implementation

Under the SM mode, each operation unit (OU) should have a self-contained solver and a valid access into the solver to be self-solvable. In the current work, the main *ICapeUnit* interface is generated under the SM mode using the Unit Operation Wizard developed by the CAPE-OPEN Laboratories Network (Co-LaN). The COM-based dynamically linked library component is generated, in which all interfaces are wrapped and used by the simulator **(**Pérez et al., 2005**)**.

The access to the internal property system is provided by a container object, defined as the *ICapeThermoMaterialObject*, which is associated with each port of the OU, has access to the property package server installed within the process PME. The property

component has two functionalities, namely, the physical property and the equilibrium calculation.

The IPOPT solver is adopted to numerically solve the reactor model. IPOPT is a powerful nonlinear programming algorithm developed by the Carnegie Mellon University. It is compatible with the CAPE-OPEN standard through a wrapper (Lang and Biegler, 2005). In the *ICapeUnit_Calculate* routine, the model is defined by an *ICapeMINLP* interface. The wrapper converts the CO-based *ICapeMINLP* model into a nonlinear programming (NLP) problem, which can be solved by the IPOPT solver.

Four EO interfaces are further implemented for the support of any CAPE-OPEN compliant PMEs, which redefine the model into an equation set object (ESO). The EO interfaces contain a mathematical model (through *ICapeNumericESO*), as well as first-order derivatives (through *ICapeNumericUnstructuredMatrix* and *ICapeNumericMatrix*) and stream connectivity mapping information (through *ICapeUnitPortVars*). The validity of the interfaces has been successfully tested in the Aspen Plus simulator under the EO mode.

2. Rigorous Model Validation

The CAPE-OPEN unit is embedded into the PX oxidation section of the PTA manufacturing process to validate the model on a statistical level, and the online operational data are used to determine the accuracy and stability of the model.

The input stream data of the CAPE-OPEN simulation are obtained and processed based on the historical datasets from April to October, 2009 at the PTA manufacturing plant of Sinopec. Five index variables are selected as the key indicators of the production quality (Table 1).

Table 1. Relative errors between real-time process data & CAPE-OPEN simulation

Monthly relative error (%) / Components	Apr.	May	Jun.	Jul.	Aug	Sep.	Oct.
4-CBA	4.66	4.63	5.37	3.47	4.21	4.88	3.76
O_2	1.27	0.91	0.98	1.03	1.17	0.99	0.80
CO	1.73	1.50	1.35	1.81	1.57	1.49	1.19
CO_2	1.44	1.00	0.91	1.05	1.09	1.27	0.91
O_2 after crystallization	3.88	3.20	3.15	3.63	3.55	4.16	3.25

In Table 1, 4-CBA is the most important indicator of the quality of production of the entire process; however, 4-CBA concentration cannot be obtained as an online measurement. The offline sampling and analysis require at least four hours. Meanwhile, the tail gas concentrations are used to estimate the real-time material consumption, which cannot be directly measured either. The CAPE-OPEN model, as a soft sensor, can precisely predict the index variables, the maximum relative errors of which can be bounded within 5.4% through seven months period.

Given its wide-range accuracy and robustness, the CAPE-OPEN model is applied into the field for the online sensing, monitoring, and optimization platform.

3. Online Process Monitoring and Modeling Platform Deployment

Based on the developed CAPE-OPEN model, a *de-facto* "Soft-sensing and Optimization System for PX and HAC Consumption in the PTA Process" was implemented and successfully used at the Sinopec Yangzi Petrochemical Company. As illustrated in Figure 3, the simulation platform fetches streams and operational data from the Honeywell PHD historical data server. The simulation results are sent to the monitoring software for visualization and optimization. Operational instructions are then sent back

to the operators, and all production conditions are visualized by ProcessX, a software package developed by Zhejiang University and Viacontrol Inc. The proposed system provides real-time consumption calculation, product quality prediction, and operation guidance for the operators.

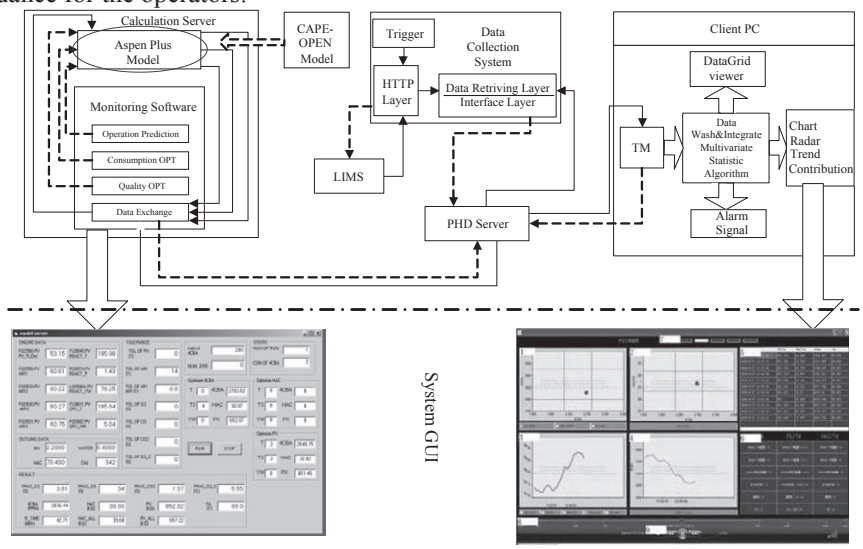

Figure 3. Soft-sensing and optimization system for PX and HAC consumption in the PTA process

4. Conclusion

This paper reports on a CAPE-OPEN solution to process simulation and optimization. Based on an open-architecture prototype, the process simulation has been divided into independent components, of which the PX oxidation reactor core unit of the PTA manufacturing process is developed and applied. The openness and transplant ability of the model are hence demonstrated. The CAPE-OPEN model encapsulates the important kinetic factors to guarantee confidentiality. The online soft-sensing and production quality prediction capability of the CAPE-OPEN conceptual design prove that it can be applied in industrial settings for real-time applications.

References

P. S. Banks, K. A. Irons, M .R. Woodman, 2005, Interoperability of Process Simulation software, Oil and Gas Science and Technology, 60, 4, 607–616

W. Chen, Z. Shao, K. Wang, X. Chen, L. T. Biegler, 2010, Convergence Depth Control for Interior Point Methods, AIChE Journal, 56, 12, 3146–3161

Y. Lang, L. T. Biegler, 2005, Large-scale Nonlinear Programming with a CAPE-OPEN Compliant Interface, Chemical Engineering Research and Design, 83, 718–223

W. Marquardt, 1996, Trends in Computer-Aided Process Modeling, Computers Chemical Engineering, 20(6/7), 591–609

V. L. Pérez, A. O. Domancich, G. E. Vazquez, N. B. Brignole, 2005, A CAPE-OPEN Compliant Simulation Module for an Ammonia Reactor Unit, 2nd Mercosur Congress on Chemical Engineering

L. Wang, 2005, Modeling, Control and Optimization Research on PX Oxidation Process, Doctorate Thesis, Zhejiang University, Hangzhou, China

Z. Zhang, Z. Shao, P. Jiang, X. Chen, Y. Zhao, J. Qian, 2010, Sequential Sub-problem Programming Strategies for Data Reconciliation and Parameter Estimation with Multiple Data Sets, Proceedings of the 49th IEEE Conference on Decision and Control, Atlanta

I.A. Karimi and Rajagopalan Srinivasan (Editors), Proceedings of the 11th International Symposium on Process Systems Engineering, 15-19 July 2012, Singapore.

Towards Holistic Decision Support Systems: Including Human and Organizational Performances in the Loop

Simone Colombo, Salman Nazir, Davide Manca

Politecnico di Milano, Piazza Leonardo da Vinci 32, 20133 Milan, Italy

Abstract

A fundamental challenge and opportunity for risk and operational managers to improve significantly their activity is to adopt a holistic approach to decision-making by grounding their decisions on the effective knowledge, experience and capabilities of operators and their organization. The paper explains why accounting for human and organizational factors is fundamental to strengthen decisions and why doing it in an experimental fashion is the way forward. Further, it is explained that leveraging on human and organizational factors, instead of appealing mainly to the technological ones, opens opportunities to improving decisions and save resources. The manuscript presents an example stemming from a use case developed with one major company of the Oil & Gas sector.

Keywords: Holistic decision-making; Human & organizational factors; Human performance; Process automation; Safety engineering

1. Introduction

Making decisions in complex, safety-critical systems is all but an easy task to accomplish, especially when the decisions relate to Health, Safety and Environmental (HSE) issues. Key Performance Indicators (KPI) used at corporate level, (*e.g.*, *CCPS Guide, 2007*), to depict what the corporate safety level is, to identify what the criticalities are, and, above all, to decide what to improve, *i.e.* where to focus resources, very seldom, for not saying ever, are grounded and traced back to human- and organizational-related parameters reflecting the actual capabilities of the system to respond to critical situations. The reason is threefold: (i) the inherent difficulty to envisaging all the possible alternatives including systematically Human and Organizational Factors (HOF) (*Colombo et al., 2008*), *i.e.* identifying scenarios that might unfold, and enabling even to highlight HOF weaknesses, (ii) the difficulty to estimate the consequences each alternative might bring about (*Manca and Brambilla, 2010*), and (iii) the complexity to verify the consistency between the envisaged scenarios and both (a) the effective resilience of the organizational set-up in place at plant level (*Hollnagel et al., 2006; Costella et al., 2009*), and (b) the effective capabilities of the workforce that has to cope with the unexpected event.

2. Holistic vs. reductionist approach – including systematically HOF

A decision-making process, to be effective, and possibly even efficient, has to be grounded on "pictures" that reflect the entire spectrum of possible alternatives, *i.e.* possible scenarios/stories that might occur, achieved by considering the productive system in a holistic way, *i.e.* as composed by Human, Technological (both hardware and software), and Organizational (HTO) elements tightly interweaved to make the whole.

Typically, for reasons we are going to investigate here to avoid bringing us too far apart from our track, safety analyses are externalized to consultancy companies. New standards, even for safety-related equipment, *e.g.*, *IEC 61508*, do not explicitly prescribe how to calculate the achieved safety but provide just guidelines on "how to", the consequences being that a multitude of safety analyses techniques are used by practitioners, and even approached differently by different industries (*Garrick, 1988*), thus making a (cross-) comparison and the use of their outcomes difficult and demanding (*Rouvroye and van den Bliek, 2002*). This is a further struggle on top of an already delicate, sometime controversial and certainly intensive task that has potentially huge social implications, *i.e.* might bring to major accidents. But this is not all as when it comes to HOF the situation is even worse as many, not all commonly known, accepted and widely used, techniques are applied by practitioners to incorporate HOF in Quantitative Risk Assessment (QRA) (*Skogdalen and Vinnem, 2011a*), whose outcomes are typically the basis for risk managers to make their decisions. And this in the best cases, *i.e.* when HOF techniques are used, because on average it is not so (*Skogdalen and Vinnem, 2011b*), particularly when not explicitly enforced by law.

3. The importance to move to an experimental approach

From the aforementioned context, it should be clear how much important is to verify the realism and completeness of the envisaged scenarios whether they are to be used as a basis for decision-making by risk managers and, more broadly, by operational managers. Further, given the increasing complexity of HTO systems due to the intensification, optimization, and automation processes that are swiftly transforming the (process) industry, relying on an "at-the-desk" verification of the identified scenarios made by expert(s), is not anymore sufficient and an experimental approach becomes necessary. Why? The reason is straightforward: envisaging scenarios in complex industrial settings where HTO factors are tightly interweaved it is a task too complex to be left just to the imagination of analysts; especially when it comes to the identification of HOF-related potential shortcomings. From the research performed in the Virthualis project we came to the conclusion that the verification session requires the support of visually immersive, real-time simulation tools that allow immerging people in Virtual Environments (VE) and experience critical, abnormal working conditions, as they would be in reality. In short, it requires the use of a Plant Simulator (PS). This way it is possible to leveraging not just on people's imagination but also on people's emotions and see how the HTO system behaves lively and effectively while facing the evolution of complex, risky situations. Consequently, the experience of people and the resilience of the organization are built-in the envisaged scenarios that become safer and more effective to use for decision-making purposes.

4. Performance assessment

4.1. Decision-making in process plants

Since the late 80's of last century it was understood that "even in the case of continuous processes monitored from a control room, the operator activity cannot be isolated from the one of the team surrounding him: roundsmen, supervisors, etc." (*De Keyser, 1986*), thus starting to introduce the idea of collective control (*Vidal et al., 2009*). This tells us one simple thing: whatever might be the automation level, *i.e.* the unmanning level, the communication and coordination between the Control Room Operator (CROP) and the Field Operator(s) (FOP), is fundamental to manage the process.

On the aforementioned ground, the Virthualis project was created and brought to the creation of what lately we baptized as PS. And it was following a strand the Virthualis experience has triggered that a piece of software capable to track human beings during operation in VE, with the ultimate goal of supporting decision-making, was created (*Colombo et al., 2011*). This tool, called Performex®, has been conceived and created even capitalizing the experience accumulated in the Virthualis project while performing experiments with field operators of two major companies in the Oil & Gas sector. Performex® is currently fully embedded in a PS used for conducting live experiments.

4.2. Performex® as a decision-making support tool

Performex® enables tracking automatically a set of defined performance indicators according to the four categories of the taxonomy adopted in the Virthualis project, namely (1) Situation Awareness (SA), (2) Decision-Making (DM), (3) Task Management (TM), and (4) Team Communication (TC). Each category has its own elements. SA elements are: (1) Recognition (data Collection), (2) Understanding, and (3) Anticipation. DM elements are: (1) Options Selection, (2) Communication of Options & Intentions, and (3) Options re-evaluation. TM elements are: (1) Planning and Preparation, (2) Tasks Prioritization, (3) Resources Usage. TC elements are: (1) Coping Interruptions, (2) Making Enquiries (info pull), (3) Sending Information (info push).

The number of identified Human Performance Indicators (HPI) is then twelve (12) and each of them has specific behavioral markers measured. As an example, the SA1, which represents the ability of "Recognition" in the SA phase, is measured in terms of different variables, such as (a) time used to reach the state (normally measured as the time elapsed between the system readiness for the operator to perform a specific action and the actual time when the action is performed – if it is performed, else it is "∞"); (b) Number of cues required/checked before reaching the state of recognition; (c) Coherency check.

Each specific HPI is context dependent. This is why the value of the SA1 might vary, even significantly, from one context to another, exactly as it happens when recording the intermediate racing time during a car or ski racing (which clearly depends on the specific raceway). Similarly, even the specific HPI measured depends on the specific task performed in the specific context. However, within the same context, it has to be clearly the same, *i.e.* the benchmark for both teams and individuals.

5. An industrial use case

This section briefly presents the use case developed in cooperation with a major company operating in the Oil & Gas market.

5.1. The decision-making problem

Gas-processing plants daily face the "unavoidable" issue of gas leaks. Gas leaks in the plant might be coarsely separated into small (0.5 kg/s), medium (5 kg/s) and large leakages (50 kg/s). Contrary to intuition, small leakages are the most concerning ones as when a large leak takes place, the decision is straightforward, *i.e.* shutdown the plant, while when a small leak occurs it might turn out to be a big trouble as it is hard to detect (especially in harsh weather conditions) and might create gas clouds that might explode, thus damaging the plant and the surroundings (major accident). Further, the task, in the mind of operators, is strongly traded-off by two contrasting factors: their personal safety and that of colleagues, and the cost of a shutdown (in the order of millions €/day).

Then the decision-making problem for managers is whether installing an automatism to activate the Emergency Shutdown (ESD) system or keeping the ESD system manually

activated by human beings. Fortunately, the management experience on automation systems was extremely high, probably one of the highest one may find, as the plant, where the experiments were made, is highly automated and highly unmanned and the management already knew the limitations and risks the automation might bring about.

5.2. The risk analysis

A preliminary risk analysis was conducted to (a) figure out the spectrum of possible alternatives, *i.e.* stories and type of human failures, (b) identify the conditions to better design the experiments, and (c) to verify the outcomes of the risk analysis already in the hands of the company (and not surprisingly outsourced to an external consultant).

According to the company procedure, the activities of the operators to manage the leak were divided in three phases, namely (1) control room activities with potential involvement of field operator(s) (not involved in case of large leaks), (2) identification and reach of the leak area, (3) shutdown or recovery actions.

Phase 1 produced 3,446 different possible scenarios, *i.e.* different stories for the control room (including the management of spurious signals). Phase 2 produced 56,814 different scenarios (from calling the FOP to asking him/her to identify the leak position). Phase 3 produced 180,951 different scenarios. All these scenarios were then split according to the leak size, *i.e.* small-, medium- and large-related.

Phase 1 comprises (a) 1,416 scenarios for large leaks with 97% probability of shutdown by the CROP, (b) 1,078 scenarios for medium leaks with 40% probability of shutdown by CROP, (c) 952 scenarios for small leaks with 1.4% probability of shutdown by CROP. Phase 2 scenarios are 18,938 evenly shared amongst the three types of leaks. Phase 3 scenarios are (a) 287 scenarios for large leaks with 100% probability to end up with a shutdown, (b) 736 scenarios for medium leaks with 52% probability to conclude with a shutdown, (c) 179,928 scenarios for small leaks with negligible probability to end up with a shutdown.

For each scenario, it was calculated a probability of occurrence and the time required to develop it. This work allowed creating a correlation between the shutdown times and their probability of occurrence. The identified shutdown times span from a fist of seconds for large leaks, independently on whether the shutdown is performed by the CROP or by the FOP, to 22 minutes for small leaks.

5.3. The experiments

Experiments were performed in a PS of the specific plant section with real operators.

From the safety analysis (the one in the hands of the company) the intervention time, *i.e.* the time elapsed from the alarm to the resolution by operators (either shutdown or remedy), was a sharp value estimated in 7 minutes (not clear how). The company thought the decision-making parameter for installing the automatism for the ESD system was the verification of the intervention time. This is why the experiments performed were initially conducted having in mind the verification of the intervention time. Nevertheless, on the way, they allowed to go well beyond and highlight, *i.e.* measuring, strong weaknesses in the organizational elements and, specifically, in the DM capabilities of teams. The decision-making then shifted the attention from the verification of the intervention time highlighted in the safety analyses (by external consultants), to the verification of the realisms and completeness of the scenarios identified. During the verification, the attention focused on the identification of the opportunities to improve the HOF elements of the system, instead of being focused on the Technological ones, thus allowing moving forward and improving the gas leak management activity at the only cost of the simulator and time used to test the scenarios.

6. Conclusions

Adopting both a holistic and experimental approach to decision-making enables plant and corporate managers to make safer and more robust decisions. Specifically, using an experimental approach to grounding decisions on both the effective capabilities of operators and the resilience of the organization, allows to better shape competences on real operational needs and, more broadly, unveiling the huge opportunities given by the improvements in HOF. Opportunities that might allow to save an enormous amount of time and resources, while being safer, by avoiding to unbalancing the decisions towards the adoption of unnecessary, very expensive and potentially risky automation solutions.

References

CCPS Guide, 2007, "Process Safety Leading and Lagging Metrics", Centre for Chemical Process Safety, www.aiche.org/ccps

Colombo S., M. Demichela, 2008, "The systematic integration of human factors into safety analyses: An integrated engineering approach", Reliability Engineering & System Safety, Volume 93, Issue 12, Pages 1911-1921, doi:10.1016/j.ress.2008.03.029

Colombo S., D. Manca, S. Brambilla, R. Totaro and R. Galvagni, 2011, "Towards the Automatic Measurement of Human Performance in Virtual Environement for Industrial Safety", "Proceedings of the ASME 2011 World Conference on Innovative Virtual Reality WINVR 2011, June 27-29, Milano, Italy.

Costella M. F., T. A. Saurin, L. B. de Macedo Guimarães, 2009, "A method for assessing health and safety management systems from the resilience engineering perspective", Safety Science, Volume 47, Issue 8, Pages 1056-1067, doi:10.1016/j.ssci.2008.11.006

De Keyser V., 1986, "Technical Assistance to the Operator in Case of Incident: Some Lines of Thought", Intelligenti Decision Support in Process Environments, NATO ASI Series, Volume 21, Pages 229-253, Springer Verlag, ISBN 3-540-13922-2 / 0-387-13922-2

Garrick B. J., 1988, "The approach to risk analysis in three industries: nuclear power, space systems, and chemical process", Reliability Engineering and System Safety, Volume 23, Issue 3, Pages 195-205, doi:10.1016/0951-8320(88)90109-3

Hollnagel E., D. Woods, N. Leveson, Editors , 2006, "Resilience Engineering: Concepts and Precepts", Ashgate, London, ISBN: 978-0-7546-4641-9

IEC 61508, 2000, "Funcitonal safety of electrical/electronic/programmable electronic safety-related systems", Bureau Centrral de la Commission Electronique International, Genève

Manca D., S. Brambilla, 2010, "Complexity and uncertainty in the assessment of the Viareggio LPG railway accident", Journal of Loss Prevention in the Process Industries, Volume 23, Issue 5, Pages 668-679, doi:10.1016/j.jlp.2010.07.007

Rouvroye J. L., E. G. van den Bliek, 2002, "Comparing Safety Analyses Techniques", Reliability Engineernig and System Safety, Volume 75, Issue 3, Pages 289-294, doi:10.1016/S0951-8320(01)00116-8

Skogdalen J. E., J. E. Vinnem, 2011a, "Quantitative Risk Analysis of Oil and Gas Drilling, Using Deepwater Horizon as Case Study ", Reliability Engineering and System Safety, In Press, doi:10.1016/j.ress.2011.12.002

Skogdalen J. E., J. E. Vinnem, 2011b, "Quantitative risk analysis offshore—Human and organizational factors", Reliability Engineering and System Safety, Volume 96, Issue 4, Pages 468-479, doi:10.1016/j.ress.2010.12.013

Vidal M. C. R., P. V. R. Carvalho, M. S. Santos, I. J. L. dos Santos, 2009, "Collective work and resilience of complex systems", Journal of Loss Prevention in the Process Industries, Volume 22, Issue 4, Pages 516-527, doi:10.1016/j.jlp.2009.04.005

I.A. Karimi and Rajagopalan Srinivasan (Editors), Proceedings of the 11th International Symposium on Process Systems Engineering, 15-19 July 2012, Singapore.

Sensor Location for water systems: A Stochastic Design Approach

Mercedes Carnero,[a] José Hernández,[a] Mabel Sánchez[b]

[a]*Facultad de IngenieriaUNRC, Campus Universitario, 5800 Río Cuarto, Argentina*
[b]*Planta Piloto de Ingeniería Química (UNS- CONICET) Camino La Carrindanga Km 7, (8000) Bahía Blanca, Argentina.*

Abstract

The optimal design of sensor networks consists in selecting the type, number and location of sensors that provide the required quantity and quality of process information by optimizing an appropriate objective. The problem is multimodal and involves many binary variables, therefore a huge combinatorial optimization problem results. In this work, the design for water systems is addressed using metaheuristics. A strategy that combines the advantages of Tabu Search and Estimation of Distribution Algorithms is devised, which is able to solve high scale designs since it can be executed in parallel.

Keywords: Sensor Network design, Combinatorial Optimization, Estimation of distribution algorithms.

1. Introduction

A reliable and complete knowledge of the current system state is essential for implementing monitoring, regulatory and supervisory control, real time optimization, planning and scheduling, and fault diagnosis tasks. The quality and availability of variable estimates strongly depend on the sensor network (SN) installed in the system, the data reconciliation packages used to enhance the precision of estimates during its operation, and the SN maintenance tasks.

The problem of selecting a set of variables to be measured, which is optimal with respect to some specified criteria and simultaneously provides the quantity and quality of information required from the system, is called the sensor network design problem (SNDP). In practice it is necessary to satisfy constraints only on a subset of key variable estimates, therefore a general SNDP arises without knowing in advance the cardinality of the optimal sensor set.

In SND the important decision to be made with regard to each variable is whether to measure it or not. In the first case the sensor is selected from a set of available instruments with certain features, i.e. cost, precision, failure rate, etc. To mathematically formulate these decisions, binary variables are employed which indicate the presence or absence of sensors. The problem is usually multimodal and involves many binary variables, therefore a huge combinatorial optimization problem subject to constraints should be solved.

Different deterministic and stochastic strategies have been presented to address the solution of the SNDP. For the sake of brevity, only some metaheuristics are briefly review in this work given that it is devoted to present a contribution on this particular subject. A metaheuristic is an iterative master process that guides and modifies the operations of subordinates heuristics to efficiently produce high quality solutions.

Regarding the design of general SNs, Benqlilou et al. (2004) applied GAs to solve the design and retrofit of reliable SNs using the GA toolbox of MATLAB program.

Gerkens and Heyen (2005) proposed two ways of parallelizing the GA, namely the global parallelization and the distributed GA, and concluded that the second one is more efficient. Carnero et al. (2005) developed a hybrid procedure based on GAs (HGA) to minimize the instrumentation cost subject to precision constraints on key variables. They used a structured population in the form of neighbourhoods and a local optimizer of the best current solutions, which provide a good balance between the algorithm capabilities of exploration and exploitation. Recently, Gerkens and Heyen (2008) proposed a general approach for designing the cheapest SN able to detect and locate a set of specified faults.

In recent years applications of Tabu Search (TS) metaheuristic for the solution of chemical engineering problems have appeared. Within the framework of TS, a Strategic Oscillation Technique around the feasibility boundary (SO-TS) was reported for solving the SNDP by Carnero et al. (2005). This strategy efficiently searches the solution space, significantly reducing the number of required calls to the evaluation function in comparison with HGA and the Classic TS.

There exist other population-based methodologies that have demonstrated a rewarding performance for solving vehicle routing, knapsack and scheduling problems, and constitute attractive alternatives to GAs. In this regard, Estimation of Distribution Algorithms (EDAs) (Emmendorfer and Pozo, 2009) offers a novel evolutionary paradigm. Within the framework of EDAs approach, Population Based Incremental Learning Algorithms (PBIL) are devised (Baluja, 1994), which introduce the concepts of competitive learning to direct the search. Carnero et al. (2009) presented an efficient strategy for the design of SNs based on PBIL, and implemented a parallel procedure. The comparison between SO-TS and PBIL strategies for solving SNDPs indicates that the first one strongly depends on the structure of the initial solution. If a good starting point is provided it produces a high quality solution with a low computational effort. In contrast, PBIL is more robust. It is capable of making replicas of the best solutions starting from lower quality initial points at the expense of an increment of the computational time. As PBIL can be naturally run in parallel, the total elapsed time can be reduced for a given number of calls. Taking into account this analysis, a new procedure is proposed that combines the advantages of both approaches.

The rest of the paper is structured as follows. In Section 2 a particular design problem, that is, the minimum cost SNDP subject to precision and estimability constraints, is briefly introduced. The new strategy is described in Section 3. Its rewarding performance for the location of sensors in water systems is shown in Section 4 by different case studies of incremental size. A Conclusion section ends this work.

2. Sensor Network Design Problem

The minimum cost SNDP that satisfies precision and estimability constraints for a set of key variable estimates is formulated in Eq. (1), where **q** is an n dimensional vector of binary variables such that: $q_i = 1$, if variable i is measured and $q_i = 0$ otherwise; $\mathbf{c}^{\mathbf{T}}$ is the cost vector; is the standard deviation of the j-th variable estimate after a data reconciliation procedure is applied and E_k stands for the degree of estimability of variable k (Bagajewicz and Sánchez,1999). For this formulation E_k is set equal to one, consequently only a variable classification procedure run is needed to check its feasibility. Furthermore S_J and S_K are the set of key process variables with requirements in precision and estimability respectively, and n is the total number of measurable variables. It is assumed that a linear algebraic model represents process operation and measurements are subject to non-correlated normally-distributed random errors. For the

sake of simplicity no instruments' localization restrictions are imposed and it is assumed that there is only one potential measuring device for each measurable variable.

$$
\begin{aligned}
&\textit{Min} && \mathbf{c}^{\mathrm{T}}\mathbf{q} \\
&\textit{s.t.} && \\
& && \hat{\sigma}_j(\mathbf{q}) \le \sigma_j^*(\mathbf{q}) && \forall\ j \in S_J \\
& && E_k(\mathbf{q}) \ge 1 && \forall\ k \in S_K \\
& && \mathbf{q} \in \{0,1\}^n
\end{aligned}
\tag{1}
$$

3. Stochastic Approach

Estimation of Distribution Algorithms are Evolutionary Algorithms that work with a population (P) of candidate solutions. At first an initial P is generated and their members are evaluated using the objective function. Those with better function values are selected to build a probabilistic model of P, and a new set of points is sampled from the model. The process is iterated until a termination criterion is fulfilled.

Therefore EDAs' approach is based on the evolution of a probabilistic model of the solution space. The potential solutions included in P are assumed as realizations of multivariate random variables, whose joint probability distribution can be estimated and updated. If independent variables are considered, the product of their marginal distributions constitutes the joint distribution of all variables, which is the simplest estimation model. This assumption may originate convergence problems for complex systems. To overcome this limitation of simplest EDAs, like PBIL, the use of more complex factorization models, i.e. Bayesian Network learning, the incorporation of niching techniques, and the hybridization with local search mechanisms are reported.

In this work the core of the solution strategy is constituted by the PBIL. The technique explicitly maintains statistics about the search space and uses them to direct its exploration. A real valued probability vector **p** is created, which reveals high quality solution vectors with high probability when sampled. A parallel implementation of PBIL that allows *NPBIL* instances being executed independently is applied. After the *NPBIL* Ps evolve one iteration, their **p** vectors are related by different mechanisms before sampling, in such a way the relevant information from each sub-P is exchanged with the others.

The previous solution scheme performs well for medium scale problems, but exhibits limitations for large ones. In these cases the identification of constructive blocks of high quality solutions and their maintenance during the evolution turn out more relevant. In this work high dimensional problems are addressed by incorporating to the EDAs a local search algorithm, such as SO-TS, that allows taking into account specific process knowledge during the search. This procedure works in a controlled way in certain regions of the search space, which are selected using a metric that groups solutions of structural similarity using a clustering technique. The local search should be performed in a controlled fashion because the number of its calls to the evaluation function has a linear dependence with the problem size. The pseudocode of the proposed algorithm is presented below**.** Each sub-P is characterized by the following variables: PBIL.**p** is the probability vector, PBIL.**V** is its matrix of solutions, PBIL.$\mathbf{V_b}$ contains the best solution in PBIL.**V**.

Initiate PBILs
for *i*=1 to *MaxGenerations*
  for *k*=1 to *NPBIL*
    $PBIL_k$.**V**=*sample*($PBIL_k$.**p**)
    $PBIL_k$.*fit*=*fitness*($PBIL_k$.**V**)
    $PBIL_k$.$\mathbf{V_b}$=best individual in $PBIL_k$.**V**
    if $PBIL_k$ is not tabu and *randnumber*< *pso*
      Divide $PBIL_k$.**V** in *t* clusters
      Apply SO to one indivual/cluster
      Set $PBIL_k$ tabu for *ptabu* iterations
    endif
    Update probability vector $PBIL_k$.**p** with learning rate *LR*
    Update tabu list
  endfor
  if *randnumber*<*Pinteracion*
    Modify **p** vectors by crossover operator
  endif
endfor
Get **SolOut** by applying SO to best individual along all PBILs
Return(**SolOut**)

4. Application Examples

In this section, application results of the proposed methodology to water systems of incremental size are reported. The analysis of results is based on the solution quality and variability, the procedure robustness and its scalability behavior to tackle the SNDP for large scale plants.

Three process flowsheets (Cases 1 - 3) of dimension: 11 units - 28 streams, 19 units - 52 streams, and 47 units – 82 streams, respectively, are considered. The standard deviation of flowmeters is assumed as 2.5%, 2% and 2% of the corresponding true flowrates for Cases 1 – 3, respectively. For the sake of brevity, instrumentation costs, which are different for each case of study, are not provided. Table 1 shows the complexity of the set of constraints imposed on each Case, and Table 2 reports the parameter settings. The next table presents the best solutions of Cases 1-3 for 40 runs of the algorithm. The same values are obtained for all the runs. The average times of each run are 1, 5.8 and 9 minutes for Cases 1 – 3 when the procedure is executed in a PENTIUM (R) 2.4 GHz, 1GB RAM using MatLab Release 14.

Table 1. Set of constraints for Cases 1-3

Case	Constraints
1	$E \geq 1$ for streams 3 8 9 17 20 21 24 25 $\sigma_3^* = 2.23$ $\sigma_8^* = 3.28$ $\sigma_{21}^* = 1.74$ $\sigma_{24}^* = 0.93$
2	$E \geq 1$ for streams 2 5 15 29 31 32 38 39 40 44-52 $\sigma_{15}^* = 12410$ $\sigma_{31}^* = 13750$ $\sigma_{32}^* = 126$ $\sigma_{40}^* = 1378$ $\sigma_{44}^* = 568$ $\sigma_{45}^* = 595$ $\sigma_{46}^* = 716$ $\sigma_{47}^* = 546$ $\sigma_{49}^* = 1442$
3	$E \geq 1$ for streams 4 11 21 24 30 32 35 39 43 44 52 58 60 68 75 80 81 $\sigma_{11}^* = 1423$, $\sigma_{35}^* = 172$, $\sigma_{39}^* = 1422$, $\sigma_{58}^* = 27$, $\sigma_{60}^* = 579$, $\sigma_{81}^* = 425$

Table 2. Parameter Setting

Parameter	Value	Parameter	Value
# PBIL	4	*Ptabu*	25
PBIL_Size	12	*t*	3
LR	0.1	*Pso*	0.05
Pinteraction	0.7	*# Maxiter*	120
# MaxGeneration	200		

Table 3. Results

Case	Optimal Solution	Estimated deviation	cost
1	1,2,4,7,9-11,13-24	$\hat{\sigma}_3$ =2.16 , $\hat{\sigma}_8$ =2.54, $\hat{\sigma}_{21}$ =1.5, $\hat{\sigma}_{24}$ =0.92	1297.39
2	10,16,31-33,35,37,39- 41, 43-48,50- 52	$\hat{\sigma}_{15}$ =2510, $\hat{\sigma}_{31}$ =916, $\hat{\sigma}_{32}$ =84, $\hat{\sigma}_{40}$ =919, $\hat{\sigma}_{44}$ =379, $\hat{\sigma}_{45}$ =397, $\hat{\sigma}_{46}$ =478, $\hat{\sigma}_{47}$ =364, $\hat{\sigma}_{49}$ =566	1154.34
3	1,2,5,15,21,22,25,28,31,33-35,37,44-46,49-51,53-55,60-63,67,68,72-77,79,80-82	$\hat{\sigma}_{11}$ =698, $\hat{\sigma}_{35}$ =172, $\hat{\sigma}_{39}$ =978, $\hat{\sigma}_{58}$ =22, $\hat{\sigma}_{60}$ =443, $\hat{\sigma}_{81}$ =419	107377.00

5. Conclusions

In this work a new methodology, which combines the advantages of SO-TS and EDAs for solving the SNDP is presented. The strategy is robust, produces high quality solutions, and is able to solve high dimensional problems since it can be executed in parallel. The scalability analysis indicates the SO-TS should work in a controlled fashion to avoid an increase of the computational time. The methodology has been successfully applied to the design of SNs of distribution water systems.

References

M. Bagajewicz, M. Sánchez, 1999, Cost Optimal Design and Upgrade of Non-Redundant and Redundant Linear Sensor Networks, AIChE J., 45, 9, 1927-1938.

S. Baluja, 1994, Population-based incremental learning: A method for integrating genetic search based function optimization and competitive learning, Technical Report, CMU, Pittsburgh, USA.

C. Benqlilou, M. Graells, E. Musulin, L. Puigjaner, 2004, Design and Retrofit of Reliable Sensor Networks, Ind. Eng. Chem. Res., 43, 25, 8026-8036.

M. Carnero, J. Hernández, M. Sánchez, J. Bandoni, 2005, On the Solution of the Instrumentation Selection Problem, Ind. Eng. Chem. Res., 44, 2, 358-367.

M. Carnero, J. Hernández, M. Sánchez, 2005, Optimal Sensor Network Design and Upgrade using Tabu Search, Comp. Aided Chem. Eng., 20, 1447-1452.

M. Carnero, J. Hernandez, M. Sanchez, 2009, Design of Sensor Networks for Chemical Plants based on Metaheuristics ALGORITHMS , 2, 1, 259-281.

L. Emmendorfer, A. Ramirez Pozo, 2009, Effective Linkage Learning Using Low – Order Statistics and Clustering. IEEE Transactions on evolutionary Computation, 13, 6, 1233-1246.

C. Gerkens, G. Heyen, 2005, Use of Parallel Computers in Rational Design of Redundant Sensor Networks, Comput. Chem. Eng., 29, 6, 1379-1387.

C. Gerkens, G. Heyen, 2008, Sensor placement for fault detection and localization. Computer Aided Chemical Engineering, 25, 355-360.

I.A. Karimi and Rajagopalan Srinivasan (Editors), Proceedings of the 11th International Symposium on Process Systems Engineering, 15-19 July 2012, Singapore.

Quantitative Risk Analysis of New Energy Stations by CFD-Based Explosion Simulation

Seungkyu Dan[a], Hyunmin Kim[a], Dongil Shin[b], En Sup Yoon[a]

[a]*Seoul National University, 1 Gwanak-ro, Gwanak-gu, Seoul 151-742, Korea*
[b]*Myongji University, Nam-dong, Cheoin-gu, Gyeonggi-do, 449-728, Korea*

Abstract

In this research, we compared the safety of mixture fuel which is composed of 20% new energy and 80% existing gas against existing fuel in the perspective of explosion risk that would be the biggest concern in the operation of new-energy stations. The new mixture will be used in the existing station in Korea without any changing the structure. The explosion risk was analyzed and compared by three representative models: empirical model, phenomenological model, and a CFD-based model, in increased model complexity and computational efforts. Overpressures of explosion of mixture and existing fuel, respectively, showed similar results, in all three models. Thus, it seems like there is no additional risk in using mixture at the existing refueling facilities. CFD-based explosion simulation was useful in finding out the exact overpressure distribution and installation of prevention equipment if necessary. The final results are being adopted as part of new safety regulations for the new and existing mixture stations to be operated in Korea.

Keywords: Explosion Simulation; Quantitative Risk Analysis; Gas Explosion Modeling; HCNG Mixture Fuel; DME-LPG Mixture Fuel

1. Introduction

Since the environmental pollution problems and climate issues related to ever-increasing energy use have been emerging all over the world, developing efficient renewable and/or alternative energy sources are considered as top-priority research agenda [BP, 2009]. Among them, DME (dimethyl ether) has emerged as an attractive, promising, alternative clean fuel for transportation, power generation and household. Korean Government, with the leading role of KOGAS, is promoting commercial introduction of this new clean energy, DME. This research has been conducted as part of the KOGAS's core technology development activities covering from DME synthesis from feedstock, such as natural gas, through utilization of DME as fuel by end users.

Also CNG, one of alternative energy, is used by fuel of bus in Korea. And it is going to be used with hydrogen to prevent the exhaustion of natural gas and air pollution after combustion.

Using the new mixtures still deal with inflammable gas. Therefore, when dealing with new mixtures at the conventional filling stations, safety managements do not become an automatically solved issue. Since the severe accident at Bucheon LPG filling station [Park et al., 2006], operation, expansion and construction of LPG stations are heavily regulated and controlled in Korea. Thus, converting and operating conventional filling stations into new energy stations must be thoroughly analyzed and studied to get the acceptance and approval by local communities and government authorities. The development of a strategy for improving gas explosion models is also highly desirable

[Jiang et al., 2001] as the use of gas as energy sources is expected to grow in near future.

2. Comparison of explosion simulation models

We need an accurate assessment about possible accidents to reduce the loss caused by overpressure shaped by gas explosion. There are many models ranging from calculations using a simple expression to complex numerical formulas using CFD. The more accurate the simulation results, the better confidence we may have in expecting the real situations and the real risk and enforcing the results out of the analysis. However, selecting and using appropriate models for the problem is important as the information requirements and efforts to run the models increase with its model accuracy. The estimation of the explosion risk have been conducted by following three approaches: Empirical models are based on correlations obtained from analysis of experimental data; and phenomenological models are simplified physical models, which is using simple computer software based on emprical correlations, which seek to represent only the essential physics of explosions; and using computer simulation program based on Computational Fluid Dynamics (CFD) models find numerical solutions to the partial differential equations governing the explosion process [Lea, 2002].

2.1. Empirical Model

Empirical models are based on correlations obtained from analysis of experimental data. Among these models, the TNT equivalency model is a representative empirical model and it is very simple and easy to use. TNT equivalency model is based on the assumption that gas explosion is similarly to an explosive of high efficiency. There are many differences between gas explosion and solid explosion, but using the utility factor helps correcting the gap. Eqs. 1 and 2 below calculate overpressure from the explosion effect of TNT. The calculation of scaled distance is necessary to obtain the overpressure out of the calculation from Eq. 1.

$$W = \frac{\eta M E_c}{E_{TNT}} \tag{1}$$

$$Z_G = \frac{R_G}{W^{1/3}} \tag{2}$$

where W is the equivalent mass of TNT (kg or lb), η is an empirical explosion efficiency (unitless), M is the mass of hydrocarbon (kg or lb), E_c is the heat of combustion of flammable gas (kJ/kg or Btu/lb), and E_{TNT} is the heat of combusition of TNT (4437-4765 kJ/kg or 1943-2049 Btu/lb) [CCPS, 1999].

2.2. Phenomenological Model

Phenomenological models are simplified physical models, which seek to represent only the essential physics of explosions. It is made by simplication of the geometry, and it considers a simplified condition for the simulation: wind, temperature, atmospheric pressure, etc. PHAST, which has been selected as the phenomenological model for our research, is a general tool for consequency analysis examining the progress of a chemical process incident from initial release through formation of a cloud or pool to final dispersion; calculating concentration, fire radiation, toxicity and explosion overpressure. PHAST is a comprehensive hazard analysis package, applicable to all stages of design and operation across a range of process and chemical industry sectors.

The VCE in the PHAST is calculating the overpressure based on TNT Equivalency model and is calculated by below Eqs. 3. [DNV, 2007].

$$\log P_0 = 0.2518 (\log z)^2 - 2.0225 (\log z) + 5.8095 \quad (3)$$

2.3. Simulation Based on the CFD Model

Computer simulation programs based on CFD (Computational Fluid Dynamics) models solve patial differential equations, based on Navier-Stokes equations that govern the fliud flow, to calculate the phenomena controlling the explosion process. CFD simulations can offer insight into the flow behavior in situations where it is impractical or impossible to carry out experiments. Its use is being widely accepted for risk analysis of explosion or dispersion.

The using equations in each model are based on Navier-Stokes equation but there are some different ways for calculating results.

In this research, we utilized FLACS (FLame ACceleration Simulator) made by Gexcon in Norway, which is a tool for dispersion and explosion simulations based on CFD [Gexcon, 2010]. CFD-based complicated models are widely acknowledged for enabling to show the necessary accuracy required for the adoption of simulation results for detailed safety reviews and corresponding upgraded design of refilling stations.

For the comparion of aforementioned three models and the proper risk control, we need to predict and estimate exact damages of existing and new energy refueling facilities' explosion by running the simulation for a 3D structure of the refilling station.

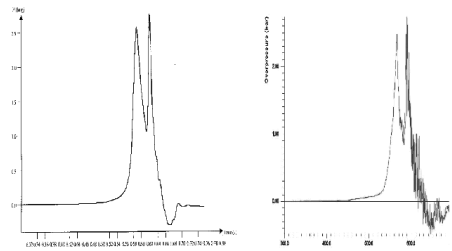

Figure 1: Comparison of Overpressure by Propane Explosion for FLACS and Experiment [Gexcon, 2010]

3. Explosion scenario

DME-LPG refilling stations will begin operating by setting two types of tank. One type of tank is added as new tank which can store 5 ton of DME-LPG mixture gas, and it is located nearby an existing LPG tank. Another way is using an existing tank which can store 40 ton of DME-LPG. Installing tanks is separated by three types: one is pressurized on the ground, another is a refrigeration method on the ground, and the other is pressurized under the ground. Among them, the pressurized tank on the ground was selected as the representative case in this research.

Once a release occurs caused by any accidents, flammable gases are shaped around the refuelling facility. After the release, fire or explosion could happen if an ignition is follwed by that accident, too. Between fire and explosion, we focused on the overpressure hazard out of the explosion.

In the case of CNG or HCNG, because the state of stored fuel is gas, the possible explosion by flammable gas is vapor cloud explosion, and BLEVE is not occurred. Instead of BLEVE, it is possible that the tank is ruptured physically.

4. Results

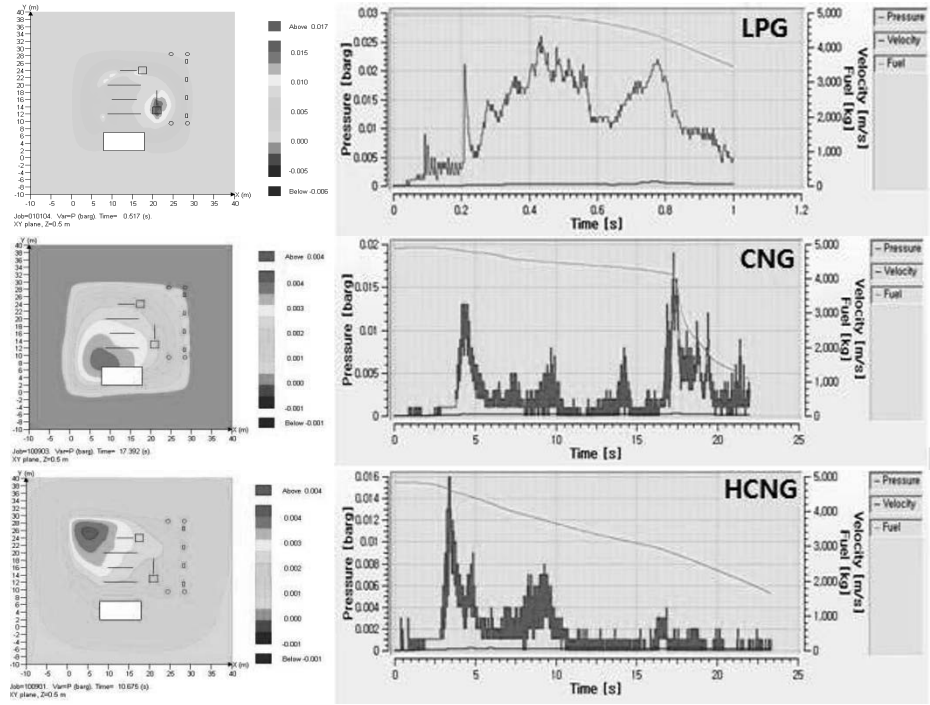

Figure 2: The results of explosion simulation by FLACS

Table 1: Summary of Results (DME-LPG)

Overpressure	**TNT Equivalency Model**	**PHAST**		**FLACS (VCE)**
		VCE	**BLEVE**	
5 ton LPG	5.8 bar at 10 m	1 bar at 10 m	18 bar at 10 m	0.026 bar at 0.43sec after the ignition
	0.13 bar at 50 m	0.4 bar at 50 m	0.1 bar at 50 m	
5 ton DME-LPG	5.3 bar at 10 m	1 bar at 10 m	18 bar at 10 m	
	0.11 bar at 50 m	0.39 bar at 50 m	0.09 bar at 50 m	
40 ton LPG	Over 10 bar at 10 m	1 bar at 10 m	18 bar at 10 m	
	0.76 bar at 50 m	1 bar at 50 m	0.4 bar at 50 m	
40 ton DME-LPG	Over 10 bar at 10 m	1 bar at 10 m	18 bar at 10 m	
	0.70 bar at 50 m	1 bar at 50 m	0.38 bar at 50 m	

Table 2: Summary of Results (HCNG)

Overpressure	**TNT Equivalency Model**	**PHAST** (VCE)	**FLACS (VCE)**
5 ton CNG	Over 10 bar at 10 m	1 bar at 10 m	0.019 at 17sec after the ignition
	0.4 bar at 50 m	0.87 bar at 50 m	
5 ton HCNG	Over 10 bar at 10 m	1 bar at 10 m	0.016 at 0.34sec after the ignition
	0.42 bar at 50 m	0.97 bar at 50 m	
40 ton CNG	Over 10 bar at 10 m	1 bar at 10 m	
	1.79 bar at 50 m	0.87 bar at 100 m	
40 ton HCNG	Over 10 bar at 10 m	1 bar at 10 m	

	1.9 bar at 50 m	0.97 bar at 100 m	

Results of simulations by three models were summarized as Table 1 and Table 2. In the case of LPG and DME-LPG, compared against the TNT equivalency model, PHAST results show a little lower value near to the ignition, but it shows a little bigger value far from the ignition. The FLACS was simulated only for VCE, and comparison of its BLEVE results is still being prepared. In the results of CNG and HCNG, although the results of simulation about hcng mixture is a little higher than the cng, its values are almost same.

5. Conclusions

This study has analyzed and compared the results of explosion risk prediction by three representative models for estimation of explosion consequence, such as the TNT equivalency model, PHAST, and FLACS. First, the three models were used and compared in the explosion risk prediction for the conventional LPG station. When the overpressures of gas explosion for both LPG and DME-LPG mixtures are calculated, there was less difference between the simple TNT equivalency model and PHAST simulation requiring more parameters. Overpressure plots of LPG and DME-LPG mixtures relative to distance were similar to each other. Likewise, in the case of the CNG and HCNG mixtures, the calculated results show almost same overpressure of explosion. So when the HCNG mixtures using in the CNG filling station, it is expected that almost no additional risk.

CFD-based complicated models only showed the necessary accuracy required for the adoption of the simulation results for safety reviews and corresponding upgrade design of refilling stations. Even though some experimental data are available for the explosion characteristics of DME [Mogi and Horiguchi, 2009], we needed to simulate it for the given 3D structure of the recharging station to get the precise view of the explosion consequence. We compared the difference of current LPG station with the one using DME-LPG mixture from the obtained result and investigated how we can reduce the explosion risk effectively, including installation of additional devices for protection. The final results are being adopted as part of new safety regulations for the DME-LPG stations to be operated in Korea.

Also, we are coding a model of explosion by matlab, but it is not perfom properly. So it is required to revise some code to make accurate results of explosion using our model.

References

BP Statistical Review of World Energy 2009, http://www.bp.com/productlanding.do?cate goryId=6929&contentId=7044622

Center for Chemical Process Safety (CCPS), 1999, Guidelines for Chemical Process Quantitative Risk Analysis, 2nd Ed., American Institute of Chemical Engineers.

DNV. Phast User Manual, 2007 (http://www.dnv.com/services/software/products/safeti/ safetihazardanalysis/phast.asp).

Gexcon, 2010, FLACS v9.0 User's Manual (www.gexcon.com).

Lea, C. J. A, 2002, Review of the State-of-the-Art in Gas Explosion Modelling, Health & Safety Laboratory.

Mogi, T. and Horiguchi, S. , 2009, Explosion and detonation characteristics of dimethyl ether, J. Hazardous Materials, 164, 114-119.

Park, K., Mannan, M. S., Jo, Y.-D., Kim, J.-Y., Keren, N. and Wang, Y., 2006, Incident analysis of Bucheon LPG filling station pool fire and BLEVE, J. Hazardous Materials, 137(1), 62-67.

Jiang, J., Liu, Z. G. and Kim, A. K. , 2001, Comparison of blast prediction models for vapor cloud explosion, National Research Council Canada Report, NRCC-44715.

I.A. Karimi and Rajagopalan Srinivasan (Editors), Proceedings of the 11th International Symposium on Process Systems Engineering, 15-19 July 2012, Singapore

Knowledge-based attributes generation for data-driven fault diagnosis in process systems

Yoshiyuki Yamashita *

Department of Chemical Engineering; Tokyo University of Agriculture and Technology; Tokyo 184-8588, Japan

Abstract

Data-driven approaches to fault detection and isolation are widely used for various process systems. The purpose of this paper is to present a new method to improve the performance of fault diagnosis of chemical plant. This method combines simple process knowledge with data-driven diagnosis by introducing new feature variables. Simple method to create new feature variables is proposed. The proposed method was applied to diagnosis of the Tennessee Eastman plant simulation benchmark problem. Fault diagnosis performance on the extended feature sets are compared with the performance on the original dataset. The result shows that addition of new attributes is effective to improve the accuracy of the diagnosis.

Keywords: Fault Detection, Fault Diagnosis, Process Monitoring, Process Knowledge

1. Introduction

Fault diagnosis is of great importance in monitoring of today's industrial chemical plants. Plenty of methods have been reported for fault diagnosis of chemical plants. The methods can be categorized into data-driven, analytical and knowledge-based approaches (Venkatasubramanian et al., 2003a). In industrial plant, data-driven approaches to fault diagnosis are widely used (Venkatasubramanian et al., 2003c). Chemical engineers usually have plenty of knowledge about the target systems. Dimensionless numbers and balance equations are examples of typical tools to extend the description ability of the phenomena. These kind of knowledge must be very useful for fault detection and isolation of process systems, but they have not been used in pure data-driven approaches.

Addition and selection of attribute variables are crucial to obtain good diagnosis result in data-based approaches. It requires engineer's expertise to add and select variables. A systematic methodology to generate new valuable attributes based on the process knowledge is proposed in this paper. Several heuristic rules to add knowledge to the dataset are presented. To examine the appropriateness of this methodology, it was applied to a simulated industrial chemical plant benchmark problem (Downs & Vogel, 1993; Lyman & Georgakis, 1995; Ciang et al., 2001). After generating some new attribute variables, a data-based fault diagnosis method, a decision tree inducer, was applied to the extended dataset. The diagnosis performance on the extended dataset was compared with that on the original dataset. The result shows that addition of new attributes is very effective to improve the accuracy of the diagnosis.

*yama_pse@cc.tuat.ac.jp

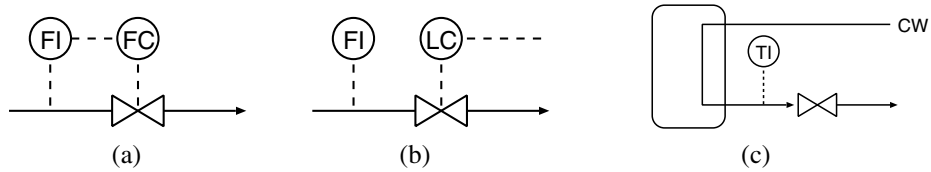

Figure 1. Flowrate and temperature measurement with MV

2. Method

2.1. Addition of Attributes

Chemical Engineer has plenty of knowledge about the target plant. In usual data-based approach for fault diagnosis, these kind of knowledge is not used at all. Model-based approaches for fault diagnosis have been also proposed. But they are not widely used because it usually require time consuming task to develop knowledge model of a plant. In this paper, a simple and easy method to utilize process knowledge for data-based fault diagnosis of a chemical plant is proposed.

The idea of the proposed method is to extend features based on process knowledge. Many kinds of process knowledge can be used for this purpose. Due to the page limit, only two example heuristics to add new features are described here.

1) Flowrate in a Control Loop: Let's think about flowrate measurement through a control valve first. The manipulated variable (MV) of the valve should directly connected to its flowrate for any types of controllers including flow, level and temperature controllers. Therefore, the ratio of flowrate and the MV would provide useful information to diagnose the loop. Typical example configuration of this case are shown in Fig. 1(a) and (b).

2) Temperature in a Control Loop: Temperature measurement of utility flow is considered next. The MV of the valve should closely connected to its outlet temperature. Under the assumption of constant operation, if the utility is a cooling water (CW) as shown in Fig. 1(c), the outlet temperature will decrease as the increase of MV. If the utility is a steam, the outlet temperature will increase as the increase of MV. The ratio of the outlet temperature and the MV would provide useful information to diagnose the line. If the utility flowrate is measured, MV can be replaced by the flowrate.

2.2. Data-based fault diagnosis

After adding extended attributes to the dataset, any usual data-driven fault diagnosis can be applied to the dataset. Various kind of data-driven methods have been proposed for the fault diagnosis of chemical plant (Venkatasubramanian et al., 2003c). Some methods may not suitable for this purpose because they are vulnerable to the increase of the number of attribute variables.

Among various techniques, an well known learning algorithm C4.5 decision-tree inducer is utilized here (Quinlan, 1993). It generates a decision tree from a set of given examples based on the gain ratio of information entropy. In the case study of this paper, Java Implementation of the C4.5 algorithm (known as J48) was applied (Wtten et al., 2011).

Although a problem of fault detection is not treated in this paper, similar idea will also be applied to improve the performance of fault detection on a plant.

Table 1. Selected list of measured, manipulated and extended variables

Variable	Description
XMEAS(1)	A Feed
XMEAS(2)	D Feed
XMEAS(3)	E Feed
XMEAS(4)	Total Feed
XMEAS(10)	Purge Rate
XMEAS(14)	Product Sep Underflow
XMEAS(17)	Stripper Underflow
XMEAS(18)	Stripper Temperature
XMEAS(19)	Stripper Steam Flow
XMEAS(21)	Reactor CW Out Temp
XMEAS(22)	Sep. CW Out Temp
XMV(1)	D Feed Flow
XMV(2)	E Feed Flow
XMV(3)	A Feed Flow
XMV(4)	Total Feed Flow
XMV(5)	Compressor Recycle Valve
XMV(6)	Purge Valve

Variable	Description
XMV(7)	Separator pot liquid flow
XMV(8)	Stripper liquid product flow
XMV(9)	Stripper steam valve
XMV(10)	Reactor CW flow
XMV(11)	Condenser CW flow
XADD(1)	XMEAS(2)/XMV(1)
XADD(2)	XMEAS(3)/XMV(2)
XADD(3)	XMEAS(1)/XMV(3)
XADD(4)	XMEAS(4)/XMV(4)
XADD(5)	XMEAS(10)/XMV(6)
XADD(6)	XMEAS(14)/XMV(7)
XADD(7)	XMEAS(17)/XMV(8)
XADD(8)	XMEAS(19)/XMV(9)
XADD(9)	XMEAS(21)/XMV(10)
XADD(10)	XMEAS(22)/XMV(11)
XADD(11)	XMEAS(18)/XMV(9)
XADD(12)	XMEAS(18)/XMEAS(19)

3. Case Study

3.1. Tennessee Eastman Process

The proposed methodology is tested on the Tennessee Eastman Process (TEP). TEP is a well known benchmark chemical process for fault identification and diagnosis (Downs & Vogel, 1993). Plenty of fault diagnosis methods have been applied to TEP. The process has 41 measured and 12 manipulated variables. Selected list of measured and manipulated variables are shown in Table 1.

The original simulation code is open-loop unstable and should be operated with appropriate control structures. Among various control strategies, decentralized control scheme proposed by Lyman & Georgakis (1995) is used in this study (Lyman & Georgakis, 1995; Ciang et al., 2001).

TEP contains 21 preprogrammed faults as shown in Table 2. For each single fault, training and test datasets are prepared, containing respectively 480 and 800 observations of 3 minutes sampling. Each of the dataset is a matrix consisting of variables XMEAS(1) through XMEAS(41) and XMV(1) through XMV(12).

3.2. Results

At first, 12 new feature variables XADD(1) through XADD(12) are introduced as shown in Table 1 by using heuristics described in the previous section. Here, the last 4 variables are for temperature measurements and the others are for flowrate measurements. These 12 attributes are added to both the training and the test datasets. A decision tree to diagnose all the 21 faults was generated by using the C4.5 algorithm on the extended training dataset. Table 2 summarizes the evaluation result of the trained tree on the test dataset

Table 2. Process faults and diagnosis result

			Diagnosis Accuracy[%]		
Fault	Description	Type	original	extended	Δ
IDV(1)	A/C Feed Ratio, B Comp. Const	Step	98.25	92.88	−5.37
IDV(2)	B Composition, A/C Ratio Const	Step	94.63	93.50	−1.13
IDV(3)	D Feed Temperature	Step	14.63	19.75	5.12
IDV(4)	Reactor CW Inlet Temperature	Step	84.63	82.75	−1.88
IDV(5)	Condenser CW Inlet Temperature	Step	59.75	52.13	−7.62
IDV(6)	A Feed Loss	Step	99.50	99.88	0.38
IDV(7)	C Header Pressure Loss	Step	97.63	100.00	2.37
IDV(8)	A/C Feed Ratio, B Comp. Const	Random	35.00	49.25	**14.25**
IDV(9)	B Composition, A/C Ratio Const	Random	12.25	14.63	2.38
IDV(10)	D Feed Temperature	Random	36.00	39.50	3.50
IDV(11)	Reactor CW Inlet Temperature	Random	66.00	66.50	0.50
IDV(12)	Condenser CW Inlet Temperature	Random	50.88	51.50	0.62
IDV(13)	Reaction Kinetics	Drift	20.00	29.25	**9.25**
IDV(14)	Reactor CW Valve	Sticking	96.00	96.00	0.00
IDV(15)	Condenser CW Valve	Sticking	16.25	13.50	−2.75
IDV(16)	Unknown		33.00	60.25	**27.25**
IDV(17)	Unknown		80.63	84.75	4.12
IDV(18)	Unknown		84.75	82.00	−2.75
IDV(19)	Unknown		59.88	56.75	−3.13
IDV(20)	Unknown		48.38	47.88	−0.5
IDV(21)	Feed Valve was fixed at const	Constant	17.13	24.63	7.50
total			57.39	59.87	2.48

for each fault. In this table, the diagnosis accuracy is defined as the number of correctly identified samples against all the fault samples.

For comparison, evaluation results of a tree trained by the original dataset are also shown in the same table. To clarify the improvement of the extended dataset against the original dataset, the differences of these two diagnosis accuracy are also shown in the last column (Δ). When the value Δ becomes positive, the diagnosis accuracy of the extended dataset is better than that of the original dataset. In total, the diagnosis accuracy was increased 2.48% on the extended dataset. As shown in the table, diagnosis accuracy of IDV(8), IDV(13) and IDV(16) are especially improved. For other faults, the diagnosis accuracy of the extended datasets showed better or worse than that of the original dataset, but the differences between the two datasets are relatively small.

Based on the analysis of the decision tree on the extended dataset, it was found that additional attributes are well utilized in the tree. For example, IDV(6) and IDV(8) can be diagnosed by the value of XADD(3) only. IDV(7) and IDV(18) can be diagnosed by using only the 3 values XADD(3), XADD(4) and XADD(5). On the contrary, the tree generated by the original dataset does not have such a simple structure to diagnose these faults. As the result, the tree on the extended dataset can diagnose IDV(6) abd UDV(7) almost perfectly, and it can diagnose IDV(8) much better than the tree on the original

dataset. For other cases, it is not simple to interpret each result because the decision tree has 830 leaves and the extended attributes are highly integrated in the tree. The tree became a little bit compact and precise by adding extended attributes, while the tree on the original dataset has 856 leaves.

4. Conclusions

Data-driven fault diagnosis of chemical plants have been investigated by many researchers for various plants. Most of them did not use any process knowledge or had difficulty to describe process knowledge. In this paper, a simple method to use process knowledge for data-driven fault diagnosis of chemical plants was proposed. Focused on control valves, which are the most common manipulated variables, two heuristics to add new attribute variables were presented. The original dataset of a plant operation can be easily extended by these heuristics. Based on the extended features dataset, the performance of a data-driven fault diagnosis is improved.

The method was applied to the diagnosis of the Tennessee Eastman process. The proposed heuristics provided twelve new attribute variables for the diagnosis of the plant. Twenty-one faults of the extended dataset was diagnosed by using the C4.5 inductive learning algorithm. The result showed large improvements on the diagnosis accuracy of faults IDV(8), IDV(13) and IDV(16). The result of this application shows effectiveness of the proposed diagnosis method. Investigation of another heuristics and the combination of the extended dataset with another learning method would be interesting.

5. Acknowledgements

This work was supported by Grant-in-Aid for Scientific Research (C) 23560522 from the Ministry of Education, Culture, Sports, Science and Technology, Japan.

References

V. Venkatasubramanian, R. Rengaswamy, K. Yin and S. N. Kavuri, (2003a), A review of process fault detection and diagnosis: Part I, Quantitative model-based methods, *Comput. Chem. Eng.*, **27**, 293–312

V. Venkatasubramanian, R. Rengaswamy, N. Kavuri and K. Yin, (2003b), A review of process fault detection and diagnosis: Part III, Process history based methods, *Comput. Chem. Eng.*, **27**, 327–346

J. J. Downs and E. F. Vogel, (1993), A plant-wide industrial process control problem, *Comput. Chem. Eng.*, **17**, 245–255

P. R. Lyman and C. Georgakis, (1995), Plant-wide control of the Tenessee Eastman process, *Comput. Chem. Eng.*, **19**, 321–331

L. H. Chiang, E. L. Russel and R. D. Braatz, (2001), Fault Detection and Diagnosis in Industrial Systems, Springer, London

J. R. Quinlan, (1993), C4.5: Program for machine Learning, Morgan kaufmann, San Mateo, CA

I. H. Witten, E. Frank and M. A. Hall, (2011), Data Mining: Practical machine learning tools and techniques, 3rd ed., Morgan Kaufmann, Boston, MA

I.A. Karimi and Rajagopalan Srinivasan (Editors), Proceedings of the 11th International Symposium on Process Systems Engineering, 15-19 July 2012, Singapore.

Pattern Recognition using Multivariable Time Series for Fault Detection in a Thermoeletric Unit

Otacílio José Pereira,[a] Luciana de Almeida Pacheco,[b] Sérgio Sá Barreto,[b] Weliton Emanuel,[a] Cristiano Hora de Oliveira Fontes,[a] Carlos Arthur M. Teixeira Cavalcante [a]

[a] *Universidade Federal da Bahia, Escola Politécnica, Rua Aristides Nóvis, 02, Federação, Salvador, BA, CEP 40210-630, Brasil*
[b] *Petróleo Brasileiro S.A. (BA), TIC-BA, Av. ACM, 1113, EDIBA, Itaigara, Salvador, BA, CEP 41856-90, Brasil*

Abstract

This paper presents a methodology for recognition of operating patterns of a gas turbine in a thermoelectric power plant (Brazilian Oil Company). Patterns related to the normal starts (without failure) and starts with failure (trip) were recognized. The process data were obtained from the plant information management system (PIMS) and techniques of data mining suitable for multivariable time series were adopted with emphasis on similarity metrics, linear scan and clustering, among others. The recognized patterns represent important and useful results to support the development of dynamic system for the monitoring and predicting the probability of failure in the equipment.

Keywords: Data mining, Multivariate Time Series, Gas Turbines.

1. Introduction

The advance of information technology (IT) provided the storage and handling of large amount of data. This led to development of methods associated to the Knowledge Discovery in Databases (KDD) and Data Mining (DM) that use data to obtain useful knowledge, adding value to businesses in strategic sectors such as ecommerce, medicine and economy ([1], [2]).

In engineering, the improvements in the technology of instrumentation, control and automation, together with the advance in IT, also built a scenario of high availability of data in industrial plants. While these technologies for data acquisition have been consolidated, the analysis of this information with the appropriate knowledge generation is still an active field of research [3].

In many situations related to industrial plants, data (or objects) are represented by time series that express the dynamics of a given process variable, collected directly from the PIMS [4]. When the object contains more than one time series and the knowledge to be extracted is related to an integrated behavior of these series, there is a problem of pattern recognition in multivariate series. This problem is more complex than the traditional case (static data or univariate time series ([5], [6])) and therefore requires specific techniques ([7-11]).

This paper presents a methodology for the acquisition of knowledge, represented by patterns of operation, from data of an industrial plant. More specifically, patterns of failure in a gas turbine of commercial scale are recognized following a systematic procedure. The turbine represents the main equipment of a thermoelectric unit belonging to the industrial park of the Brazilian Oil Company (Brazil).

The next section presents the industrial unit and the gas turbine. Sections 3 and 4 present and discuss the methodology and results.

2. Application Scenario

The industrial unit analyzed in this work is the Thermoeletric Power Plant Rômulo Almeida (TPP-RA) that is part of the Brazilian Oil Company (Figure 1). It comprises a cogeneration unit that operates in combined cycle producing steam and electricity, with natural gas as raw material.

(a) (b)

Figure 1 – (a) UTE-RA [12] e (b) illustration of a gas turbine RB211-G62 DF [13]

The TPP-RA has three gas turbines (GT) Rolls Royce RB211-G62 DF[13], each one coupled to an electric generator of 27 MW, in conjunction with other equipments to drive a total generation capacity of 137 MW of energy and production of 260.3 t/h steam. Trips may occur in the turbines ([14]) and can be caused by some factors such as surge, vibration and temperature dispersion. This work focused on the recognition of patterns of failure during the starting of the turbine caused by temperature dispersion. This trip occurs when the temperature of one of the 17 temperature sensors, distributed radially after the combustion chamber, reaches a temperature value of $\pm$ 150°C different from the average of the others [13].

3. The methodology

The main process variables associated with the turbine operation comprise the flow of natural gas, inlet temperature of the natural gas and temperature of the exhaust gases. The procedure developed is illustrated in Figure 2 and have the following steps:

1. Generation of samples. Occurrences of normal starts and starts with trip caused by temperature dispersion were chronologically identified through operation reports during the period between 2008 and 2010. Two groups were established, namely, one group with 18 objects associated to starts with trip and another group with 57 objects associated to normal starts. This step was supported by the linear scan algorithm [6] which enabled the automatic capture of samples of starting events of the turbine directly from the database.
2. Analysis of similarity within and between groups. This step involved the quantification of the level of homogeneity within each group (starts with and without trip) and the distinction between them. The quantification of similarity between multivariable time series ([7-11]) was used instead of the commonly approaches applied in the univariate case ([5], [6]) in which the euclidean distance, for example, can be used directly. In this paper we used the SPCA (Similarity Factor Principal

Component Analysis) [10] as a measure of similarity which provides a dimensionless index determined from the angles between the principal components of each object.

3. Clustering and pattern recognition. Inspired in the Fuzzy C-Means ([5], [8], [15]), an algorithm suitable for the clustering of multivariable time series and also based on optimization was developed. This algorithm provided different groups of normal starting of the turbine, the degree of membership of each object to each one of these groups and the centers or patterns of each group (or cluster).

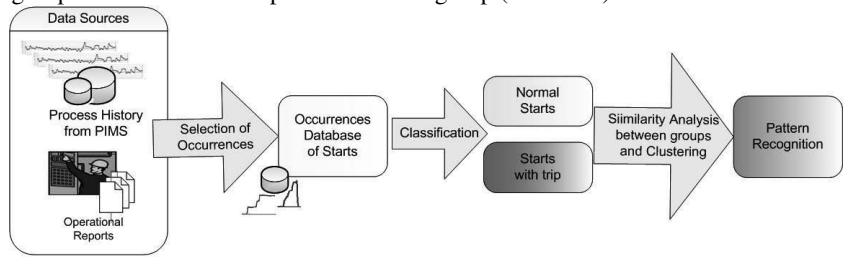

Figure 2 – Overview of the methodology

4. Results

In the analysis of similarity between the two groups (starts with and without trip), some combinations of the three process variables previously selected (flow of natural gas, gas natural inlet temperature and gases exhaust temperature) were tested, considering also the univariate case. The alternative of object with the three variables provided better homogeneity inside the group of starts with trip and better polarization between the two groups of normal starts.

The clustering algorithm was based on these three variables and on the SPCA index to measure the similarity between objects. The algorithm identified two patterns (N1 and N2) for the normal starts group. Despite the homogeneity and the small number of objects in the group of starts with trip, only one pattern was considered. Therefore, the mean object of this cluster was taken as the pattern of trip. Figure 3a presents one of the patterns of normal starts (N2) and Figure 3b, the pattern of trip (T1). Figure 3c ilustrate the distance between the patterns, also based on the SPCA index.

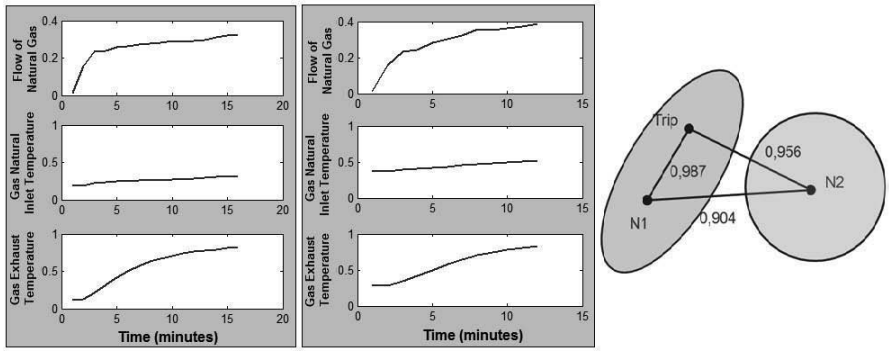

(a) (b) (c)

Figure 3 – (a) One of the patterns of normal start (N2); (b) The pattern of trip (T1) and (c) Distance between patterns

In Figure 4a, the pattern N2 is used as reference and the distances of all objects to this pattern are presented. As expected, the objects belonging to the group N2 are very similar to the pattern of N2. Figure 4b shows the degree of membership of each object of normal starting to the pattern of N2 and a polarized distribution is verified. There are few objects in the center of y-axis which attests that there is little ambiguity or uncertainty in the clustering process.

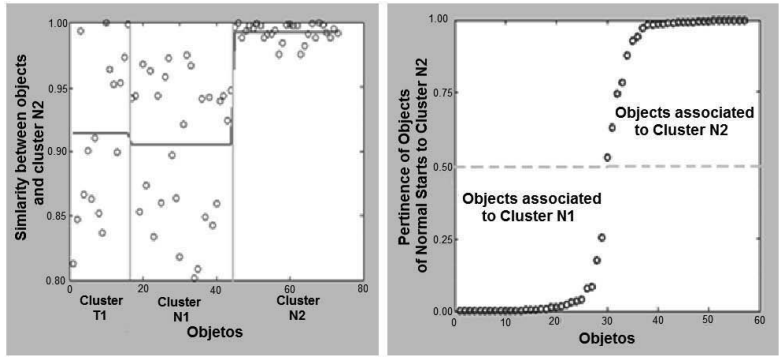

(a) (b)

Figure 4 – (a) Distances of objects to the cluster N2 (b) Objects belonging to cluster N2

Figure 5 shows the gas flow curve in a starting with trip occurrence. Using the moving-window approach [3], the distances between the flow curves of the turbine and each one of the patterns (T1, N1 and N2) are presented. The proximity of the event of failure leads to a rapprochement between the flow curve and the patterns of T1 and N2. This means that the occurrence is closer to the patterns of starting with trip or normal starting N1 and is far from the pattern of N2. It suggests that the pattern N2 represents a safer alternative to starting the turbine.

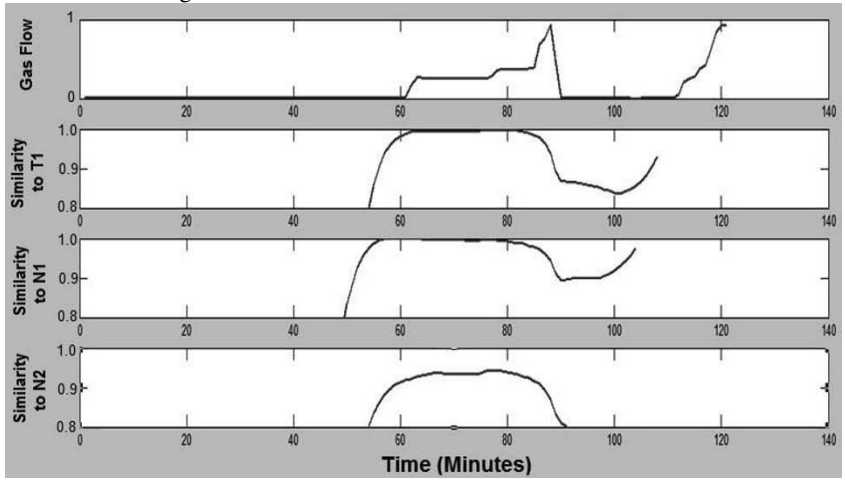

Figure 5 – Dynamic behavior of distances between one starting with trip and the patterns of T1, N1 and N2

5. Conclusion

This paper presents a procedure for recognition of operating patterns in gas turbines in order to provide support to implement a system for fault prediction. In the case studied, techniques based on data mining suitable for multivariate time series allowed the identification of two patterns of normal starts One of them is more distance from the fault pattern and is associated to a safest starting of the turbine.

The solution developed is flexible and portable. Despite its application on the pattern recognition associated to one kind of failure, the tools and techniques employed can be easily adjusted to treat other problems. Other types of failures can be investigated if data and operation reports are available.

References

[1] U.M. Fayyad, G.Piatetsky, P. Smyth, R. Uthurusamy, 1996, Advances in Knowledge Discovery and Data Mining. California: American Association for Artificial Intelligence e MIT Press.

[2] G. Piatetsky, 2007, Data mining and knowledge discovery 1996 to 2005: overcoming the hype and moving from "universty" to "business" and "analystics", Data Mining Knowledge Discovery, 15, 99-105.

[3] A.Singhal, D.E.Seborg, 2002, Pattern Matching in Multivariate Time Series Databases Using a Moving-Window Approach, Industrial and Engineering Chemistry Research, 41, 3822-3838.

[4] F. B. Carvalho, B. S. Torres, M. O. Fonseca, C Seixas Filho, 2003, Sistemas PIMS – Conceituação, Usos e Benefícios, VII Seminário de Automação de Processos da Associação Brasileira de Metalurgia e Materiais – ABM, Santos/SP.

[5] T.W. Liao, 2005, Clustering of time series data - a survey, Science Direct. Pattern Recognition, 38, 1857 – 1874.

[6] M. Vlachos, 2005, A practical Time-Series Tutorial with MATLAB, European Conference on Machine Learning.

[7] H.P.Kriegel, K.M.Borgwardt, P. Kroger, A.Pryakhim, M.Schubert, A.Zimek, 2007, Future Trends in data mining, Data Mining Knowledge Discovery, 15, 87-97.

[8] G.Gan, C. Ma, J. Wu, 2007, Data clustering : theory, algorithms, and applications.ASA-SIAM series on statisticsand applied probability.

[9] X.Wang, A.Wirth, L.Wang, 2007, Structure-based statistical features and multivariate time series clustering, Seventh IEEE Conference on Data Mining, 351-360.

[10] K. Yang, C.Shahabi, 2004, A PCA-based Similarity Measure for Multivariate Time Series, Second ACM International Workshop on Multimedia Databases, ACM-MMDB 2004, Washington, DC, USA, November 13, 2004.

[11] A.Singhal, D.E.Seborg, 2005, Clustering Multivariate Time-series Data, Journal of Chemometrics, 19, 427-438.

[12] S. T. Sá Barreto, 2009, Desenvolvimento de Metodologia para Atualização em Tempo Real de Modelos Matemáticos de Processos Decisõrios. Dissertação de Mestrado em Mecatrônica – PPGM, UFBA, Salvador.

[13] Rolls-Royce. Trainning Manuals of the Gas Turbine RB 211-G62 DF, 2010.

[14] H. I. H. Saravanamutoo, G. F. C. Rogers, H. Cohen, 1996, Gas Turbine Theory. 5.ed. Dorchester: Prentice Hall.`

[15] F. Hoppner, R. Klawonn, R. Kruse, T. Runker, 1999, Fuzzy Cluster Analysis, *Wiley, Chichester*.

I.A. Karimi and Rajagopalan Srinivasan (Editors), Proceedings of the 11th International Symposium on Process Systems Engineering, 15-19 July 2012, Singapore.

Compressive Strength Prediction of Concrete Recycled Aggregates made from Ceramic Tiles using Feedforward Artificial Neural Network (FANN)

Chan Chee Kin,[a] Mashitah Mat Don,[b] Ahmad, Z[c]

[a,b,c]*School of Chemical Engineering, Engineering Campus, Universiti Sains Malaysia, 14300 Nibong Tebal, Seberang Perai Selatan, Penang, Malaysia*

Abstract

In this paper, Feed forward Artificial Neural Network (FANN) model has been used to predict concrete compressive strengths made from ceramics tiles. Multiple regression analysis (MRA) was used to compare the results obtained from FANN. Both models are trained and tested using the available test data of 72 different concrete mix using recycled aggregates derived from homogenous ceramic tiles. The data are arranged in a format of inputs parameters for fine and coarse aggregates that cover the percentage of replacement, water/cement ratio, compacting factor, curing time of 7 and 14 days respectively. The output considered was the compressive strength for curing time of 28 days of the recycle concrete. The r^2 value for fine aggregates was 80% for MRA and 88 % for FANN respectively. In coarse aggregates, the r^2 value was 64 % for MRA and 74 % for FANN respectively. The results showed that FANN is a suitable tool for predicting compressive strength values for different concrete mixtures.

Keywords: **Neural Network Modeling, Concrete Compressive Strength, Multiple Regression Analysis, Ceramic Tiles, Feed Forward Artificial Neural Network**

1. Introduction

Malaysia as a developing country has a very active construction industry. As the construction industry continues to grow, it will generate a large amount of construction wastes which causes significant impacts on the environment. Hassan *et al.* [1] reported that on average, 28.34% of total generated solid wastes came from industrial and construction industry in the central and southern region of Malaysia. These wastes, among which were dependable on many factors, including the stage of construction, type of construction work and practices on site. Instead of dumping it in landfills and dumpsite, recycling and reuses of such wastes is an urgent need for environmental and social benefits. Moreover, conventional crushed stone aggregates reserves are depleting fast. This in turn jeopardized the principle of sustainability and received increasing opposition from environmentalist. Sani *et al.* [2] suggested that recycling of construction wastes could reduce the volume of wastes produced. As a result, the usage of inorganic construction waste will lead to sustainable concrete design and a greener environment. Rao *et al.* [3] reported that recycled aggregate concrete (RAC) have reduction of strength however it should be noted that the extent of reduction is related to the parameters such as type of concrete used, the replacement ratio, water/cement (w/c) ratio and the moisture condition of the recycled aggregates. Previously, Katz [4] found that at a high w/c ratio, the strength of RAC is comparable to that of reference concrete even at a replacement of 75%. The usage of ceramic tile wastes as course aggregates

was first reported by Kaloo in 1995 [5]. He found that crushed tiles concrete had a lower density, higher compressive and flexural strength. However, studies on the use of crushed ceramic tiles as a construction material is scarce [6], though it could provide enormous economical and environmental benefit to the society in general.

It is well recognized that the prediction of concrete strength is important in the modern concrete construction and engineering judgement. Various methods were proposed for predicting the concrete strength. The purpose of this paper is to present a comparison of FANN and MRA while exploring the usage of bootstrap sampling for resampling the limited data for training, testing and validation purposes.

2. Methodology

2.1. Feedforward Artificial Neural Network (FANN)

FANN is an information processing technique that can provide meaningful answers even when the data to be processed include errors or are incomplete, and can process information extremely rapidly when applied to solve real world problems. This FANN architecture considers all neurons of input and output layers in one structure. Prediction results by this architecture could show good results with some test data sets, which has not been used in the training process. n assessing the developed models, mean SSE (MSSE), mean absolute percentage error (MAPE) and the regression of coefficient (r^2) was also calculated to find its accuracy on the unseen validation data is used as the performance criterion. The model is shown as follows:

$$\hat{y}(t) = f[u1(t), u2(t), u3(t), u4(t), u5(t)] \quad (1)$$

where *u1(t)* is the percentage replacement, *u2(t)* is the water/cement ratio, *u3(t)* is the compacting factor, *u4(t)* and *u5(t)* is the compressive strength for curing time of 7 and 14 days respectively. $\hat{y}(t)$ is the predicted process output which is the compressive strength of curing time of 28 days. The model with the smaller MSSE and MAPE and the largest r^2 is considered to be the best where accurately predict the compressive strength of the concrete.

2.2 Multiple Regression Analysis (MRA)

MRA is also known as Ordinary Least Square (OLS) and it assumes that a vector of regression parameters, , can be used to determine the system output y, from n measured variables x, through a linear model of the following form:

$$y = x_1\theta_1 + x_{22} + \ldots + x_n\theta_n$$

By using MRA, the model parameter, , can be estimated through the following equation:

$$\hat{\theta} = (X^T X)^{-1} X^T Y) \quad (3)$$

where X is the matrix of input variable data and Y is a matrix (or a vector in a single output case) output variable data. For this MLR analysis, X will be the prediction output of the individual networks on the training and testing data and Y is the actual process

output on the training and testing data. Once the model parameters are estimated, it can be applied to the unseen validation data.

2.3 Description of data

Homogenous ceramic tiles were collected from 5 construction sites in the state of Perak and Penang, Malaysia. The tiles were broken manually using a hammer and then fed into a jaw crusher (Model: Retsch BB-200) to acquire aggregates of mesh size 20 mm (Plate 1 and 2). Other materials including ordinary portland cement (OPC), locally available river sand (specific gravity 1.73) and natural crushed stone aggregates of maximum size 20 mm (specific gravity 1.62) were also used for the production of concrete block. In the case of homogenous ceramic tiles waste aggregates, five concrete mixes were prepared by varying the content of ceramic tiles coarse aggregates from 20% to 100%. The concrete block were then demoulded and cured under water at 27° ± 2°C until the test age. The samples were demoulded 24 hours after casting and cured. The blocks were then tested for compression strength at different curing time in days (7, 14 and 28 days). In this study, the percentage of placement, the water/cement (W/C) ratio, compacting factor, and compressive strength at 7 and 14 days were used as inputs and the values of the compressive strength for curing time of 28 days was used as an outputs for fine and coarse aggregates respectively. Herein, all the data were divided into 3 categories which are training, testing and validation data because "early stopping" criteria were used in the neural network training. Then, all data are resampled through bootstrap re-sampling approach to make it 72 data in each category.

3. Result and Discussion

3.1 Feedforward Artificial Neural Network (FANN)

FANN structure with 10 hidden nodes was used in fine and coarse aggregate model respectively. Note that all the results in this study are based on scaled data but afterwards being re-scaled to get the real physical data of compressive strength which is in MPa for all figures. The performance values for the predicted results of the compressive strength were presented in **Table 1**. It can be seen from the table that the MAPE and MSSE were lower. This means that the predicted results were closer to the experimental data. The results of testing phase shows that the FANN was capable of generalizing between input variables and the output and reasonably good predictions.

Table 1: Result for the compressive strength for curing time of 28 days using FANN

Performance values	Coarse Aggregates	Fine Aggregates
$\mathbf{r^2}$	0.74	0.88
MAPE	0.39	0.05
MSSE	0.74	0.38

This proved that the experimental results with the predicted ANN results were all in good agreement. The ANN can learn any relationship, linear or non-linear, as long as there are sufficient large numbers of neurons in the hidden layer. Another remarkable advantage of the ANN is the capability of modelling data of multiple data of multiple inputs and multiple outputs. **Figure 1** supported the previous statement where the actual and predicted output for validation data is reasonably closed respectively.

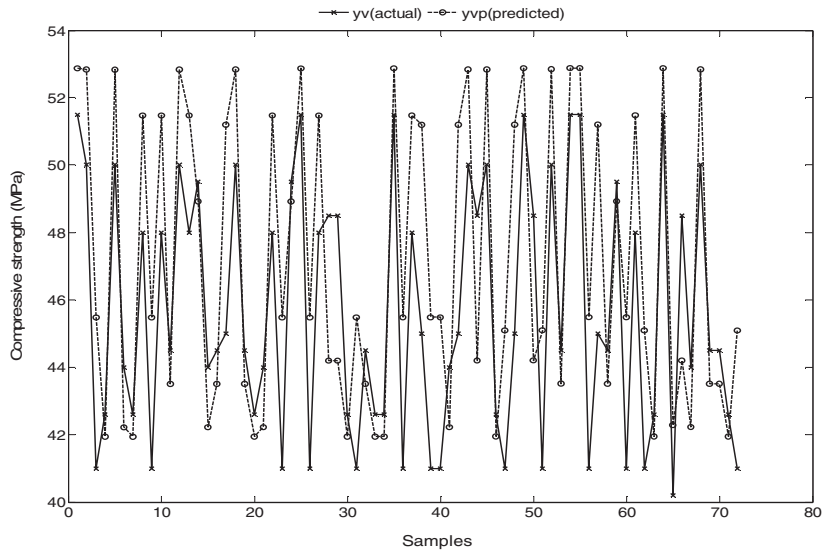

Figure 1: Predicted and measured value of 28 days compressive strength for FANN using coarse aggregates

3.2 Multiple Regression Analysis

Experimental results were satisfactory and gave good agreement to the model used, with the correlation regression coefficient (r^2) values at 0.9128 and 0.9541 respectively. **Table 2** shows the performance values for the predicted results of the compressive strength using the MRA. The MRA is the simplest method for modelling compressive strength. It does not need too complicated computation and all parameters can be tested statically. The MRA has a capability of producing a confidence interval for prediction. However, the MRA cannot be used to model the data with multiple outputs. It is clearly shown in **Figure 2** that MRA is slightly suffered in predicting the compressive strength for fine and coarse aggregates. The actual and predicted values for both outputs are quite different.

Table 2: Results for the compressive strength for curing time of 28 days using MRA

Performance values	Coarse Aggregates	Fine Aggregates
$\mathbf{r^2}$	0.64	0.80
MAPE	0.18	0.04
MSSE	0.64	0.40

4.0 Conclusion

A comparative analysis of two alternative approaches for modelling compressive strength, which are feedforward artificial neural network (FANN) and multiple regression analysis (MRA) has been presented in the present study. It is found that neural network is particularly suitable for learning nonlinear functional relationships and multiple outputs and input relationships which are unknown or cannot be specified

whereas the MRA is suitable for modelling functional relationships which can be specified. This suggests that the FANN is a useful tool for compressive strength of concrete mixture analysis.

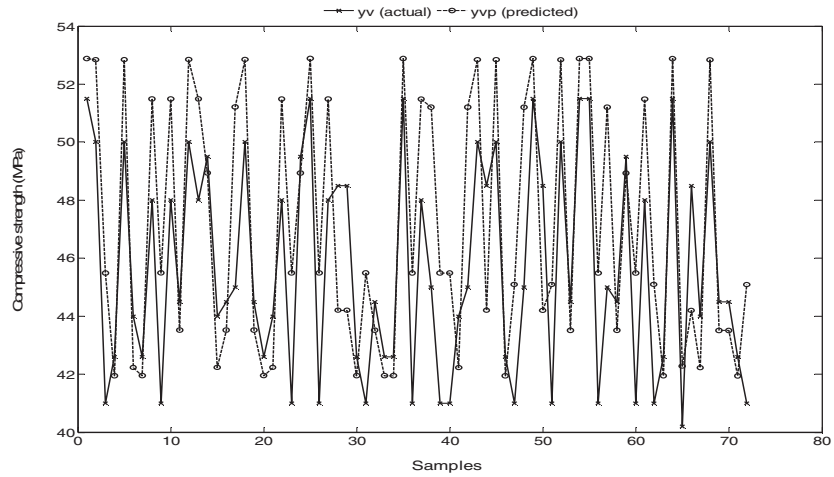

Figure 2 : Predicted and measured value of 28 days compressive strength for MRA using coarse aggregates

5.0 Acknowledgement

The authors are grateful to the Construction Industry and Development Board of Malaysia (CIDB) and Construction Research Institute of Malaysia (CREAM) (Account No.: 6050116) and Universiti Sains Malaysia (USM) for providing the facilities to carry out this study.

References

[1] M.N. Hassan, M.K. Yusoff, M.N.A. Sulaiman, R.A. Rahman, 1998, Issues and problems of solid waste management in Malaysia. Proceedings on national review on environmental quality management in Malaysia: towards the next two decades, Hasan et al. Eds. Institute for Environmental and Development (LESTARI), Universiti Kebangsaan Malaysia.

[2] D. Sani, G. Moriconi, G. Fava, V. Corinaldesi, 2005, Leaching and mechanical behaviour of concrete manufactured with recycled aggregates. Waste Manage., 25, 177-182.

[3] A. Rao, K.N. Jha, S. Misra, 2007, Use of aggregates from recycled construction and demolition waste in concrete, Resour. Conserv. Recycl. 50, 71-81.

[4] A. Katz, 2003, Properties of concrete made with recycled aggregate from partially hydrated old concrete, Cem. Concr. Res. 33, 703-711.

[5] A.R. Khaloo, 1995, Crushed tile coarse aggregate concrete, Cem. Concre. Aggregate 17, 119-125.

[6] C.S. Poon, D. Chan, 2007, Effects of contaminants on the properties of concrete paving blocks prepared with recycled concrete aggregates, Constr. Build. Mater. 21, 164-175.

I.A. Karimi and Rajagopalan Srinivasan (Editors), Proceedings of the 11th International Symposium on Process Systems Engineering, 15-19 July 2012, Singapore.

Control of integrated unit operations

José A. Chinea-Herranz, Manuel Rodríguez [a]

[a] *Autonomous System Laboratory, Universidad Politécnica de Madrid, José Gutierrez Abascal 2, Madrid 28006, Spain.*

Abstract

As a thermal separation method, distillation is one of the most important technologies in the chemical industry. Given its importance, it is no surprise that increasing efforts have been made in reducing its energy inefficiencies. A great deal of research is focused in the design and optimization of the Divided-Wall Column. Its applications are still reduced due to distrust of its controllability. Previous references studied the decentralized control of DWC but still few papers deal about Model Predictive Control. In this work we present a decentralized control of both a DWC column along with its equivalent MPC schema.

Keywords: Process Control, Thermally coupled distillation, Model Predictive Control.

1. Main Text

Basically, in every production process some of the chemicals go through at least one distillation column on their way from raw species to final product. Distillation is and will remain the main separation method in the chemical industry (there are more than 50,000 columns in operation around the world). Despite its flexibility and widespread use, distillation is very energy demanding. It can generate more than 50% of plant operating costs and it is the responsible of 3% of the energy usage in the U.S. (notice that the thermodynamic efficiency of a distillation column is between 5-20%). In order to reduce this drawback new approaches and configurations have appeared.

The divided-wall column (DWC, the name is given because the middle part of the column is split into two sections by a wall) is an important example of process intensification and integration. DWC is very appealing to the chemical industry, with Montz and BASF as the leading companies. Kenig et al. state that there are more than 125 industrial applications nowadays and if the exponential trend continues there will be more than 350 by 2015 [1].

DWC can separate three or more components in one vessel using a single condenser and reboiler, hence reducing capital and operating costs compared to conventional two-column sequences. In fact, DWC can save up to 30% in the capital invested and up to 40% in the energy costs, particularly for close boiling species. DWC is considered to be on the path for energy conservation and green house gases emissions decrease.

DWC is not widespread due to distrust of its controllability. Its control is more difficult than the control of a conventional schema with two columns for the separation of ternary mixtures because there is more interaction among control loops. Besides, the absence of controllability could mean the absence of the energy savings if the optimal operation is not accomplished. The remaining of the paper is organized as follows. Section two discusses thermally coupled distillation columns, making emphasis in DWC columns. Section three presents the control strategies used in the paper. Section four applies decentralized (PID controllers) control and MPC to a ternary system separation. Finally, section five draws conclusions and introduces further work.

2. Energy integration in distillation

Distillation systems have evolved from direct, indirect or distributed column sequences to thermally coupled systems and eventually to Petlyuk configurations [2] and DWC schemes (Fig. 1). Intermediate steps in this path include systems with heat pumps, prefractionators and side-stripers or side-rectifiers. The Petlyuk configuration and the DWC were aimed at the reduction of thermodynamic losses due to mixing streams, especially at the feed tray location.

DWC has more degrees of freedom (DOF) compared to a binary distillation column. This entails a complex design, but also presents extended optimization capabilities. If 3 product specifications are taken into account, DWC has 7 DOF's: distillate and bottoms flowrate, reflux ratio, reboiler duty, side-stream flowrate and vapor and liquid internal split ratios. 5 DOF's are used to stabilize 2 levels and 3 compositions while the remaining 2 DOF's are used for optimization purposes. Traditionally, liquid split ratio ($\alpha_L=L_P/L_M$) and vapor split ratio ($\alpha_V=V_P/V_M$) are optimization variables (Fig. 1c). Vapor split ratio is usually fixed during the design stage because it is given by the pressure drop across both sides of the wall, which in turn depends on the stage type and geometry. The liquid split ratio is used as a control variable during operation by manipulating the flowrates leaving the bottom tray of the rectifying section.

The optimal design is given by the number of stages in the different sections of the DWC. The number of stages at both sides of the wall is usually the same but approaches with different number of plates have been reported. Olujic et al. presents a review on the different design approaches of DWC [3].

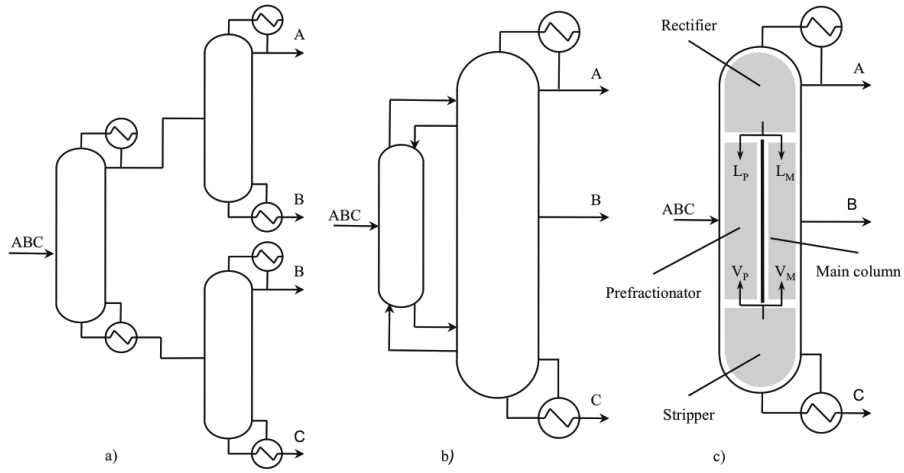

Figure 1. Evolution from a distributed sequence (a) to a Petlyuk configuration (b) and eventually to the DWC (c)

3. Control strategies for Divided-Wall Columns

Past and recent distrust on DWC controllability and flexibility is mainly due to the complex design of a control strategy. Maintaining product specifications while rejecting disturbances and loop interaction are the key concerns together with achieving significant energy savings. Otherwise, DWC advantages might disappear.

Early references on DWC control were focused mainly on decentralized control. The first approaches extended PID control structures of traditional distillation columns by including liquid or even vapor split ratio among the manipulated variables. Wolff & Skogestad [4] demonstrated that three-point control structures were feasible using PID controllers. Mutalib and Smith reported the first experimental application of decentralized control using temperature profile instead of composition measurements [5, 6]. Puigjaner et al. follow a research line in which multiple decentralized control studies are compared by using transfer functions obtained from shortcut modeling and dynamic matrix control is applied to DWC [7-9]. Kim [10] and Adrian [11] are among the first to use model predictive control but their approach is either experimental or shortcut modeling based. DWC has been also applied to complex distillation systems. Wang extended DWC to azeotropic distillation [12], while other references deal with extractive and reactive DWC [13, 14].

4. Process studied

The separation of n-pentane, n-hexane and n-heptane is carried out in a DWC. The rectifying, prefractionator and stripping sections have respectively 7, 12 and 10 stages. The number of stages at both sides of the wall is the same. The feeding stage and side-stream withdraw are located at stage 12 in the prefractionator and main column respectively. The feed is assumed to be 180 kmol/h of a mixture 0.4/0.2/0.4 (C5/C6/C7) in mole fraction at 300 K and product specifications are set at 98%. The operation values are calculated to minimize the reboiler duty. The minimum energy consumption occurs at a liquid split ratio of 0.33 and a vapor split ratio of 0.625. The resulting reflux and boilup ratios are 2.521 and 3.445 respectively. The steady state simulations are performed in Aspen Plus using the rigorous Radfrac model with a Chao-Seader property package. Sizing rules for reflux drum, bottoms and trays are taken from Luyben [15].

4.1. Decentralized control

The main advantage of decentralized control lies in its simple design and tuning. As less time and effort is needed on its development, it might be convenient for simple applications. However, PID ability to reduce interaction among control loops is reduced and as a result settling times and oscillation might compromise stable operation.

In decentralized control, the choice of variable pairings plays a fundamental role in the performance of the system. There are numerous references dealing with the best pairing. Variable pairing depends highly on the chemical system studied, the design and the product specification level. Nevertheless, the best result is traditionally associated to the strategy L/S/V-D/B, meaning that distillate, side-stream and bottoms specifications are controlled by reflux, side-stream and bottoms rate respectively while condenser drum and bottoms levels are maintained by distillate and bottoms rates respectively.

A special reference must be done on a paper by Luyben & Lin applying a four composition PID control scheme [16], which is eventually extended to temperature profile control [17]. Luyben's control scheme minimizes indirectly energy consumption by maintaining heavy component concentration on top of the prefractionator at a minimum value. It is widely accepted that any minimal amount of heaviest component going out the top of the prefractionator causes an irreversible decrease on the side stream purity [4]. The same idea applies if the lightest component crosses the dividing wall at the bottom of the prefractionator, however the influence on product specification is not so important as this component will be present mainly in the vapor phase. As L/S/V-D/B gives the best performance according to most of the references and Luyben's control scheme accomplishes and indirect energy optimization, both

approaches will be used. A PI controller is designed for each control loop, tuning parameters are shown in Table 1.

Table 1. Summary of tunning parameters for decentralized control

	Proportional gain	Integral time	Set point (mole frac.)
Distillate composition control	7.144	63.36	0.98
Side-stream composition control	121.37	38.28	0.98
Bottoms composition control	4.745	35.64	0.98
Prefractionator composition control	0.379	29.04	0.004

4.2. Model Predictive Control (MPC)

There are few applications of MPC to integrated unit operation and especially to DWC. Some references highlight the enhanced performance of MPC while for others PID control gives better results. Relevant experience on the superiority of MPC is still limited. Theoretical and experimental comparisons between MPC and PID controllers should be done for a variety of chemical systems so as to reach a heuristic solution.

MPC present enhanced performance reducing oscillations, loop interactions and settling times. Besides the ability to include optimization constraints allows for the safety improvement. Nevertheless, MPC present several disadvantages: 1) it entails larger development cost and time, 2) it requires a deep knowledge of the process and 3) it requires the availability of a dynamic model representing the main features of the unit operation. The performance of MPC is directly proportional on the accuracy of the dynamic model and the adequate tuning of its parameters.

MPC control of the dynamic model for the DWC is carried out in Matlab with the MPC Toolbox. The step responses obtained from Aspen Dynamics are transformed to the Plant Model using the Systems Identification Toolbox. An ARX linear parametric model is found to represent the plant responses adequately.

The MPC controller is tuned using the Tunning Advisor available in the MPC Toolbox. The Integrated Square Error function is used as the performance function for tuning.

4.3. Performance comparison

The decentralized control scheme has been tested to ±10% disturbances in feed flowrate, temperature and composition as well as a simultaneous set point change in all product purities from 98 to 98.5% (mole frac.). Loop interaction is clearly demonstrated with the set point change experiment (Fig. 2 left). MPC performance is compared to decentralized control by carrying out the same simultaneous set point change.

The results are shown in Fig. 2 and clearly demonstrate the advantage of MPC in eliminating loop interaction and oscillations. Settling times for distillate and bottoms purity are significantly lower. For sidestream purity and prefractionator vapour composition the decentralized control scheme presents lower settling times.

5. Conclusions

In this paper the control of a DWC has been presented applying MPC as well as decentralized control. MPC superiority in eliminating loop coupling has been demonstrated comparing it to a decentralized control scheme. The same comparison has to be done with a decentralized control with decoupling strategies. In this case the development cost and time must be taken into account to compare both strategies

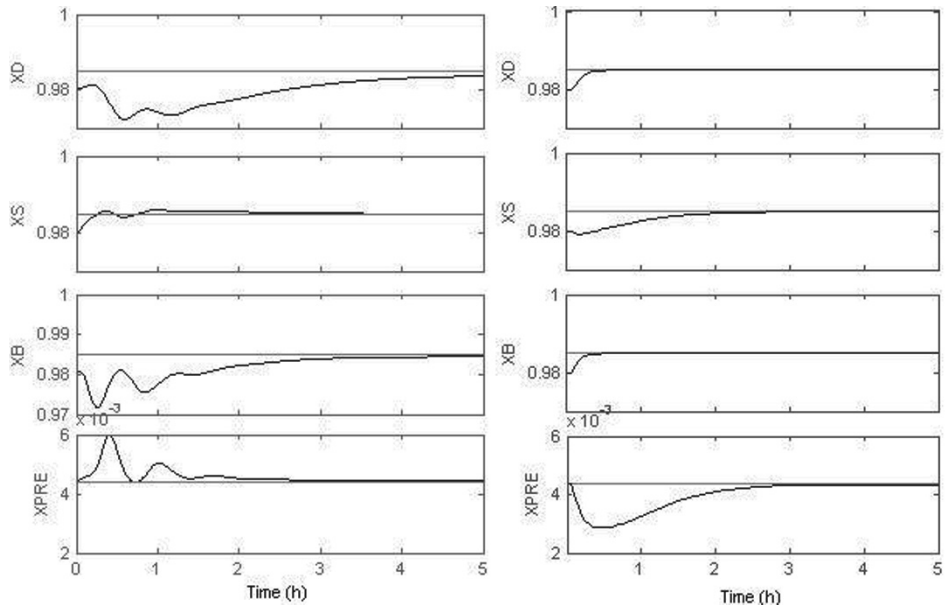

Figure 2. Set point increment of product purities from 98 to 98.5% for a decentralized control (left) and MPC scheme (right)

The industrial application of decentralized or model predictive schemes must be based on temperature profile control to avoid using composition analyzers, which in most of the cases are expensive and present slow responses.
The study of control strategies will be extended to complex schemes such as Kaibel columns, double-wall distillation columns (Sargent arrangements) or Agrawal columns.

References

[1] E. Y. Kenig, O. Yildirim, A. A. Kiss, Sep. Purif. Technol., 80 (2011) 403.
[2] F. B. Petlyuk, V. M. Platonov, V. M. Slavinskii, Int. Chem. Eng. 5 (1965) 555.
[3] Z. Olujic´, I. Dejanović, L. Matijasević, Chem. Eng. Process., 49 (2010) 559.
[4] E. A. Wolff, S. Skogestad, Ind. Eng. Chem. Res., 34 (1995) 2094.
[5] M. Mutalib, M. Smith, Trans. IChemE. 76 Part A (1998) 308.
[6] M. Mutalib, M. Smith, Trans. IChemE. 76 Part A (1998) 319.
[7] L. Puigjaner, M. Serra, A. Espuña, Chem. Eng. Process., 38 (1999) 549.
[8] L. Puigjaner, M. Serra, A. Espuña, Ind. Eng. Chem. Res., 42 (2003) 1773.
[9] L. Puigjaner, M. Serra, A. Espuña, M. Perrier, Comput. Chem. Eng. 25 (2001) 859.
[10] Y. H. Kim, Chem Eng J., 85 (2002) 289.
[11] T. Adrian, H. Schoenmakers, M. Boll, Chem. Eng. Process., 43 (2004), 347.
[12] S. Wang, C. Lee, S. Jang, S. Shieh, J. Process Control, 18 (2008) 45.
[13] C. C. Bravo-Bravo, J. G. Segovia-Hernández, C. Gutiérrez-Antonio, A. L. Duran, A. Bonilla-Petriciolet, A. Briones-Ramírez, Ind. Eng. Chem. Res., 49 (2010) 3672.
[14] A. A. Kiss, H. Pragt, C. van Strien, Chem. Eng. Commun., 196 (2009) 1366.
[15] W. L. Luyben, Distillation design and control using Aspen^{TM} simulation. Bethlehem, Pennsylvania. 2006.
[16] W. L. Luyben, H. Lin, Ind. Eng. Chem. Res., 48 (2009) 6034.
[17] W. L. Luyben, H. Lin, Ind. Eng. Chem. Res., 49 (2010) 189.

I.A. Karimi and Rajagopalan Srinivasan (Editors), Proceedings of the 11th International Symposium on Process Systems Engineering, 15-19 July 2012, Singapore.

Nonlinear Control Strategies for a Micro-Aerobic, Fermentation Process

Emily Liew Wan Teng and Yudi Samyudia

Department of Chemical Engineering, Curtin University, CDT 250, 98009 Miri, Sarawak, Malaysia

Abstract

In this paper, we propose a new strategy to control the yield and productivity of the fermentation process by viewing the fermentation process as a multi-scale process, where the mixing conditions in terms of aeration rate and stirrer speed are considered in studying the bioreactor dynamics. The inclusion of mixing for bioreactor control would allow us to influence the metabolic activities of microorganisms through the distribution of nutrients to the microbial cells. The engagement of both mixing and biological processes, however, would lead to a very complex dynamics of the bioreactor. As a result, the control strategy with a direct use of a nonlinear model will be implemented. Two different modeling techniques to capture the mixing dynamics, namely data-based and kinetics hybrid modeling are proposed. The validated nonlinear models are used in determining the optimal aeration rate and stirrer speed to maintain the desired productivity and yield of the fermentation process for different disturbance scenarios via extensive simulation studies.

Keywords: bioreactor control, mixing, nonlinear model, micro-aerobic fermentation

1. Introduction

A micro-aerobic fermentation process for ethanol production is a complex multi-scale process constituting the dynamic interactions between the microbial cells and the governing environment. The kinetics is the result of microbial metabolic activities at the cellular level within its environmental conditions (i.e. mixing, pH, temperature). The process performance is measured by its productivity and yield, whereby a control system is often used to achieve (and/or maintain) its desired performance. Previous work in controlling this fermentation process (e.g. Schügerl and Bellgardt, 2000; Lane, Schwarz and Evans, 2002; Castillo-Toledo, González-Alvarez and Luna-Gutiérrez, 1999; Cardello and San, 1988;) was mainly focused on the macro bioreactor conditions such as pH, temperature, etc while assuming an ideal mixing condition so that the lumped kinetics models, i.e. Monod type, could be used. The interactions of the microenvironment (i.e. mixing conditions, cellular dynamics) around the microbial cells are not taken into account. In this work, we consider the mixing conditions in developing a new control strategy for the fermentation process. By viewing the process as a multi-scale in nature it would therefore allow us to have additional manipulated variables from which new control strategies for the bioreactor can be developed. It is, however, not easy to get the kinetics model that describes the inhomogeneous conditions of the microorganisms. The aim of the present work is therefore to develop different mathematical models for bioreactor control design by capturing the mixing mechanism within the bioreactor. By analyzing the dynamic behavior of the non-ideally mixed fermentation process, two new manipulated variables, i.e. aeration rate (*AR*) and stirrer speed (*SS*), could be exploited to control the bioreactor's performance, i.e. yield

and productivity. Using these manipulated variables, a nonlinear model-based controller is then designed, where the two different models are compared for the controller design. The closed-loop performances are evaluated for different disturbance scenarios and different models.

2. Modeling and Controller Design

Two process models, i.e. data-based model and kinetics hybrid model, are developed where the mixing phenomena are included via *AR* and *SS*. The data-based model is developed based on linear regression technique to sets of experiment data of *AR, SS*, productivity and yield. The kinetics hybrid model is developed based on Herbert's concept of endogenous metabolism, which is combined with the macro-scale bioreactor model. Herbert's concept is chosen especially in fermentation processes because it could describe the kinetics of the process thoroughly (Starzak et al., 1994). Both data-based model and kinetics hybrid models are developed based on experimental conditions of *AR* (1.0-1.5LPM) and *SS* (150-250rpm).

2.1. Data-Based Model

Suppose that the process yield or productivity is a function of the levels of *AR* (or x_1) and *SS* (or x_2):

$$y = f(x_1, x_2) + \varepsilon \tag{1}$$

where ε represents the error in the response y, i.e. Yield (Y) or Productivity (P). If the expected response is a quadratic function, by applying the regression technique, the data-based model of the fermentation process is obtained as:

$$Y = -29.32 + 42.34 * AR + 0.15 * SS + 0.15 * AR * SS - 26.00 * AR^2 \tag{2}$$

$$P = 0.77 - 0.59 * AR - 0.004 * SS + 0.004 * AR * SS \tag{3}$$

2.2. Kinetics Hybrid Model

A general model of the continuous bioreactor model is given as:

Biomass formation: $dX = -DX + r_x$ (4)

Substrate consumption: $dS = D(S_0 - S) - r_s$ (5)

Product formation: $dP = -DP + r_p$ (6)

where S_0 is the initial substrate concentration (kg/m^3) of the medium, S is the final substrate concentration (kg/m^3) of the medium, P is the final product concentration (kg/m^3) of the medium and X is the final biomass concentration (kg/m^3) of the medium.

According to the Herbert's concept, it is assumed that the observed rate of biomass formation comprised of the growth rate and the rate of endogenous metabolism:

$$r_x = (r_x)_{growth} + (r_x)_{end} \tag{7}$$

$$(r_x)_{growth} = \frac{k_1 XS}{k_2 + S} \exp(-k_5 P) \tag{8}$$

It is also assumed that the rates of substrate consumption and product formation are proportional to the biomass growth rate:

$$r_s = (r_s)_{growth} = -k_3 (r_x)_{growth} \tag{9}$$

$$r_p = (r_p)_{growth} = k_4 (r_x)_{growth} \tag{10}$$

The rate of growth due to endogenous metabolism by a linear dependence is given by:

$$(r_x)_{end} = -k_6 X \tag{11}$$

In order to obtain the relationships of k_1 to k_6 with *AR* and *SS*, the regression analysis is applied, whereby experimental data such as substrate and product concentrations, yield

and productivity values will be utilized. By taking *AR* and *SS* into account in the general expression of linear regression, we get:

$$\text{Variable} = \beta_1 + \beta_2 \frac{(r - \bar{r})}{\Delta r} + \beta_3 \frac{(R - \bar{R})}{\Delta R} \tag{12}$$

where "Variable" represents k_1 to k_6, r and R denote the variables taken into account, i.e. *AR* and *SS*, whereas $\bar{r}$ and $\bar{R}$ represent the baseline values for *AR* and *SS*. β_1, β_2 and β_3 values will be obtained through least squared technique. All of these equations signify the kinetic model and it is of interest to investigate whether *AR* and SS can be described without the use of mass transfer coefficient for oxygen and carbon dioxide stripping. Based on the experiment data, the optimum values of β_1, β_2 and β_3 are obtained so that the developed kinetic model is given as:

$$k_1 = 1.4085 - 0.2852X_1 + 0.3692X_2 \tag{13}$$

$$k_2 = 0.0010 \tag{14}$$

$$k_3 = 0.6631 - 0.0.148X_1 + 0.0220X_2 \tag{15}$$

$$k_4 = 0.1040 + 0.0.142X_1 + 0.0128X_2 \tag{16}$$

$$k_5 = 0.7558 - 0.1019X_1 + 0.0211X_2 \tag{17}$$

$$k_6 = 0.0143 - 0.0001X_1 - 0.0019X_2 \tag{18}$$

where $X_1 = (AR - 1.25)/0.25$ and $X_2 = (SS - 200)/50$. Combining equations (13-18) with the continuous bioreactor model of (4-11), we obtain a kinetics hybrid model of the fermentation process.

2.3. Controller Design

To design the controller for the fermentation process, an optimization approach of (Firmansyah and Samyudia, 2010) is employed, where an explicit non-linear model is required in the form of:

$$y_t = f(y_{t-1}, u_{t-1}, \theta) \tag{19}$$

where y_t and y_{t-1} are the current and past predicted outputs; u_{t-1} is the past inputs; Θ is the process parameters. Equation (19) will be used in solving a constrained or unconstrained nonlinear optimization problem that minimizes the following objective function:

$$\Delta u_t^* = \arg\{\min_{\Delta u_t} (\Delta y_t - e_t)^2 + (\Delta u_t)^2\} \tag{20}$$

Subject to:

$$\Delta y_t = y_t - y_{mt} \tag{21}$$

$$u_{\min} \le u_t \le u_{\max} \tag{22}$$

$$\Delta u_{\min} \le \Delta u_t \le \Delta u_{\max} \tag{23}$$

where y_{mt} are the current measurements of the outputs; $u_t = u_{t-1} + \Delta u_t^*$ are the optimal inputs and e_t is the current error trajectory defined as:

$$e_t = k \int_0^T (y_{sp} - y_{mt}) dt \tag{24}$$

y_{sp} is the set point of the outputs and k is the tuning parameter for desired closed-loop responses. Note that when there are no constraints, i.e. (22) and (23) do not exist so the optimal solution for the nonlinear optimization will have an explicit form as follows:

$$\Delta u_t^* = -[\Delta y_t - k \int_0^T (y_{sp} - y_{m_t}) dt] \tag{25}$$

which is a PI type controller, but the gain is adjusted using the nonlinear model of (19).

3. Simulation Results

The control design objective is to maintain the yield and productivity in the face of disturbances in the feed substrate concentration, S_o and dilution rate, D. The measured yield and productivity will be calculated from the measured biomass, product and substrate concentrations. Table 1 summarizes the steady state conditions for all the input, output and disturbance variables whereas the two scenarios of disturbance step change of $\pm$10% and $\pm$ 30% around their operating conditions are considered. In the closed-loop analysis, we implement the nonlinear controller designed using either the data-based or the hybrid kinetics model to control both yield and productivity in the fermentation process. We compare their performances in the face of the two disturbance scenarios.

Table 11: Summary of Steady State Conditions for All Variables

Description	**Steady State Conditions**
Yield	21.15%
Productivity	0.15g/L.hr ($4.17\text{x}10^{-5}$kg/m^3.s)
Biomass Concentration	30g/L solution (30kg/m^3 solution)
Substrate Concentration	48g/L solution (48kg/m^3 solution)
Product Concentration	5.2g/L solution (5.2kg/m^3 solution)
AR	1.43LPM ($2.38\text{x}10^{-5}$m^3/s)
SS	250rpm (4.17rps)

Fig. 1 shows that both controllers are able to keep the controlled variable in their set-point values, by manipulating both *AR* and *SS*. A step change of +10% is made in S_0 and D at time t=20 hr (72,000s), i.e. both S_0 and D values are changed instantaneously to a new value. From Fig. 1, it can be seen that both controllers perform well, whereby there are not much oscillations observed in the closed-loop dynamics of the yield. More dynamics are observed for the productivity. The kinetics hybrid model controller shows slight oscillations with a higher overshoot, and requires a longer settling time. The use of the simple data-based controller is sufficient to control the bioreactor for this disturbance scenario.

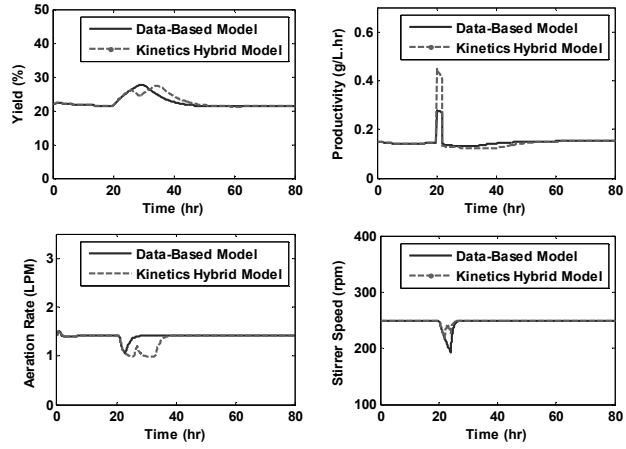

Figure 1: Closed-Loop Responses for 10% Disturbance Scenario.

Our investigation is continued for a larger disturbance scenario exciting more nonlinearity and dynamics of the process. The step perturbation is increased to $\pm$30% from the steady state conditions of S_0 and D. Fig. 2 shows the closed-loop responses for both data-based and kinetics hybrid model-based controllers for the 30% disturbance

change. Both control strategies are able to maintain the controlled variables in the set point values. However, the kinetics hybrid model controller performs much better than the data-based model controller. This could be seen for all the input and output variables. Besides, a higher overshoot can be observed for yield and productivity. Note that the manipulated variables *AR* and *SS* hit their upper limits indicating nonlinear dynamics of the process.

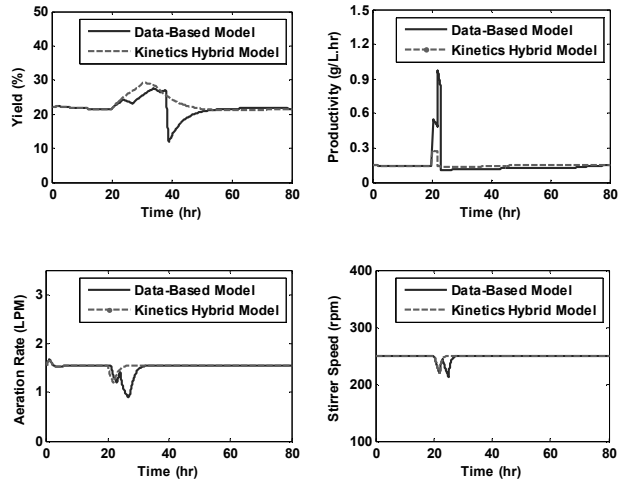

Figure 2: Closed-Loop Responses for 30% Disturbance Scenario

4. Conclusion

A new model-based control design for non-ideally mixed fermentation process has been presented in this paper. Models with different complexity are compared for the controller design. The disturbances of the inlet substrate concentration, S_0 and dilution rate, D, are simulated to study its effectiveness for bioreactor control. Our study revealed that the choice of the nonlinear controller would depend on the expected disturbances on the process. For a relatively small disturbance scenario, the data-based controller should be sufficient; however, for a significantly large disturbance, the kinetics hybrid model-based controller is preferable.

References

B. Castillo-Toledo, V. González-Alvarez and J.A. Luna-Gutiérrez, 1999, Nonlinear robust control of a batch fermentation. Chem. Eng. Technol., vol. 22, pp.675-682.

E.W.T. Liew, J. Nandong and Y. Samyudia, 2010, Optimization of fermentation process using a multi-scale kinetics model, Proc. 5th International Symposium on Design, Operation and Control of Chemical Processes (PSE Asia 2010), pp. 1174-1183, ISBN.978-981-08-6395-1.

G.L. Lane, M.P. Schwarz and G.M. Evans, 2002, Predicting gas-liquid flow in a mechanically stirred tank. Applied Mathematical Modelling, vol. 26, pp.223-235.

K. Schügerl and K.H. Bellgardt, 2000, Bioreaction Engineering, Modeling and Control, Springer-Verlag Berline Heidelberg, New York.

R.J. Cardello and K.Y. San, 1988, The design of controllers for batch bioreactors. Biotechnology and Bioengineering, vol. 32, pp.519-526.

S. Starzak, M. Krzystek, L. Nowicki and H. Michalski, 1994, Macroapproach kinetics of ethanol fermentation by *Saccharomyces cerevisiae*: experimental studies and mathematical modelling. The Chemical Engineering Journal, vol. 54, pp. 221-240.

T. Firmansyah and Y. Samyudia, 2010, Robust Nonlinear Control Systems Design, Lambert Academic Publishing.

I.A. Karimi and Rajagopalan Srinivasan (Editors), Proceedings of the 11th International Symposium on Process Systems Engineering, 15-19 July 2012, Singapore.

Real Time Model Predictive Control of a Four Tank Interacting Storage System

B.Rajasekhara Reddy, Prabirkumar Saha

Department of Chemical Engineering, IIT Guwahati, Assam 781039, INDIA

Abstract

In this paper, two Model Predictive Control algorithms *viz*., Linear and Nonlinear Dynamic Matrix controller (DMC) have been implemented on a four tank interacting liquid storage system. The process is a Two Input Two Output (TITO) nonlinear system and is equipped with data acquisition facility. A mechanisic dynamic model of the process has been developed based on the mass balance equations and model parameters are estimated using experimental data. The performance of the predictive controllers (DMC and NLDMC) have been evaluated through both simulation and experimental studies.

Keywords: Four Tank Interacting Liquid Storage System, Model Predictive Control, Dynamic Matrix Control, Real Time Control.

1. Introduction

Model Predictive Controllers (MPC) have been an attractive research theme by control engineers for decades, however, their use in the real-time control application has been quite limited. Dynamic Matrix Controller (DMC) is a type of MPC which has perhaps been the only MPC that has been applied in the Advanced Process Control (APC) technique in the industrial application (Bequette 2003). Application of other MPCs, especially nonlinear MPCs, would be quite a challenge for control engineers. This research group is actively involved in the investigation for typical bottlenecks which are responsible for hindrance to the comprehensive success of real-time MPC applications. Significance of this work is the development of a complete protocol package (C++ based) for real-time implementation of MPC. This protocol is portable across other process systems with minimum changes required. Customized Object Oriented Program (OOP) can be generated for a nonlinear MPC and readily implemented for any process with minimum or no changes in the main protocol. Initial success has been reported in this work with real-time nonlinear MPC application. Further research is going on for more elaborate study on this issue.

In this paper, DMC and NLDMC have been implemented for a complex and interacting chemical process *viz*., four tank interacting liquid storage system (Patra and Saha, 2012). The process has four interconnected tanks among which two are interacting. The development of model of the process and control laws thereof have been discussed in the subsequent sections. Successful implementation of these control techniques in real-time application would encourage one to try other complex MPC strategies too.

2. Model of Four Tank Liquid Storage System

Fig. 1 demonstrates the four tank liquid storage system. The process consists of four similar sized overflow type cylindrical tanks whose maximum possible level is 25 cm.

Tank 1 and 3 are placed at same height and they are interconnected. Thus they have interacting mutual behaviour. Tank 2 and Tank 1 are in series, whereas Tank 4 and Tank 3 are in series. The tanks are fitted with level measuring transducers that send a signal of 4-20 mA on a linear scale against liquid level. Two metering pumps are also there to feed the tanks at a maximum possible flow rate of 30 L/min. The pumps can be regulated using 4-20 mA signal. The online data is acquired through ADAM 4022T (Advantech® Co. Ltd.) data acquisition card.

Thus the process has two inputs F_1 and F_2 through two pumps. These inputs are bifurcated to serve the Tanks 1 & 4 and Tanks 2 & 3 respectively. Let m and n be the fractions of F_1 and F_2 which are respectively fed to Tanks 1 and 3. Non-interacting outlets of the tanks *viz*., F_{o1}, F_{o2}, F_{o3}, and F_{o4} are proportional to the square roots of their respective liquid heights of the tanks. Interacting outlet of Tank 1 or 3, *viz*. F_{o5} is proportional to the square root of the difference of heights of liquid in Tanks 1 & 3. The direction of flow F_{o5} is dependent upon the liquid height in the tanks 1 & 3. The flow will take place from higher level to the lower level.

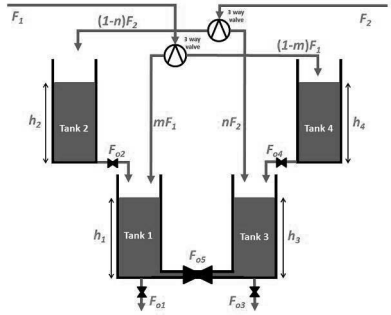

Fig. 1: Four tank storage system

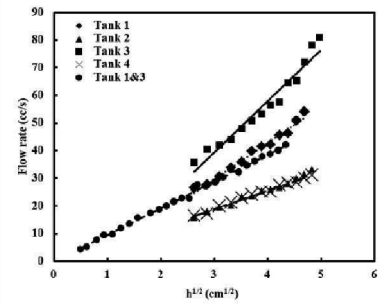

Fig. 2: Data for model parameters c_1-c_5

The model can be developed based on first principles of material balance theory. The relevant ordinary differential equations are summerized as follows:

$$\alpha\frac{dh_1}{dt} = mF_1 + c_2\sqrt{h_2} - fc_5\sqrt{|h_1 - h_3|} - c_1\sqrt{h_1} \quad (1)$$

$$\alpha\frac{dh_2}{dt} = (1-n)F_2 - c_2\sqrt{h_2} \quad (2)$$

$$\alpha\frac{dh_3}{dt} = nF_2 + c_4\sqrt{h_4} + fc_5\sqrt{|h_1 - h_3|} - c_3\sqrt{h_3} \quad (3)$$

$$\alpha\frac{dh_4}{dt} = (1-m)F_1 - c_4\sqrt{h_4} \quad (4)$$

where α is the cross sectional area of the tank(s), c_1-c_5 are the valve constants, $f = 1$ if $h_1 > h_3$ and $f = (-1)$ if $h_1 < h_3$. The diameter of the tank is 9.2 cm and hence the cross sectional area is 66.48 cm^2. In order to estimate the valve constants, various steady state conditions were generated in those tanks and the corresponding flow rates and level measurements were recorded, as plotted in Fig. 2. The figure demonstrates steady state flow rates against the square roots of their corresponding liquid heights in the tank. A linear regression analysis would yield the following values of valve constants: c_1=10.62; c_2=14.53; c_3=6.48; c_4=6.377; c_5=9.613. It is also assumed that both inputs of

the system are equally divided and fed into their respective tanks. Hence, m=n=0.5 for this study.

3. Derivation of DMC controller for Liquid Storage System

The DMC can be designed as per the procedure cited by Bequette (2003). With control horizon of 1 and no weights on control move, the feedback gain matrix for DMC is

$$K = \left(S_f^T S_f\right)^{-1} S_f^T \tag{5}$$

Where S_f is matrix containing step response coefficient. Since deviation variable is used for all manipulated inputs and controlled outputs, the unforced error vector would be $P \times 1$ vector $\left(\bar{h}_{i,sp} - \bar{h}_{is}\right)$ where P is the prediction horizon, $\bar{h}_{i,sp}$ is the setpoint vector. The DMC control law would be

$$F_i = F_{is} + K_j\left(\bar{h}_{j,sp} - \bar{h}_{js}\right) \tag{6}$$

Here $F_{is}, i = 1,2$ are values of flow inputs at steady state, $h_{js}, j \in 1,4$ are liquid levels of tanks 1-4 at steady state, K_j are corresponding feedback gain matrices of DMC. In order to formulate the S_f matrix, step response curves were generated for levels in tanks by introducing small step inputs to F_1 and F_2 at their respective steady state conditions *i.e.* F_{1s} and F_{2s}.

4. Derivation of Nonlinear DMC

Unlike DMC, where step response coefficients are fixed for the entire operation, the nonlinear DMC is operated on the basis of stepwise linearization and re-calculation of step responses at each sampling instant (Gattu and Zafiriou, 1992). For simulation study, the nonlinear meachanistic model, *i.e.* eq. (1) to (4), can be linearized analytically; whereas for real-time control study, numerical derivative can be used if the confidence on the process model is not established. In the present case, analytical linearization is done for both simulation and experimental studies. Using mathematical identity, $|x| \approx \frac{2x}{\pi}\tan^{-1}(kx)$, eqs.(1) to (4) can be linearized as

$$\begin{bmatrix} \frac{dh_1}{dt} \\ \frac{dh_2}{dt} \\ \frac{dh_3}{dt} \\ \frac{dh_4}{dt} \end{bmatrix} = \begin{bmatrix} \left(\frac{-c_1}{2\alpha\sqrt{h_{1s}}} - \frac{c}{\alpha}\right) & \left(\frac{c_2}{2\alpha\sqrt{h_{2s}}}\right) & \left(\frac{c}{\alpha}\right) & 0 \\ 0 & \left(\frac{-c_2}{2\alpha\sqrt{h_{2s}}}\right) & 0 & 0 \\ \left(\frac{c}{\alpha}\right) & 0 & \left(\frac{-c_3}{2\alpha\sqrt{h_{3s}}} - \frac{c}{\alpha}\right) & \left(\frac{c_4}{2\alpha\sqrt{h_{4s}}}\right) \\ 0 & 0 & 0 & \left(\frac{-c_4}{2\alpha\sqrt{h_{4s}}}\right) \end{bmatrix} \begin{bmatrix} h_1 \\ h_2 \\ h_3 \\ h_4 \end{bmatrix} + \begin{bmatrix} \frac{m}{\alpha} & 0 \\ 0 & \frac{1-n}{\alpha} \\ 0 & \frac{n}{\alpha} \\ \frac{1-m}{\alpha} & 0 \end{bmatrix} \begin{bmatrix} F_1 \\ F_2 \end{bmatrix} = A \begin{bmatrix} h_1 \\ h_2 \\ h_3 \\ h_4 \end{bmatrix} + B \begin{bmatrix} F_1 \\ F_2 \end{bmatrix} \tag{7}$$

where,

$$c = fc_5 \left\{ \frac{1}{\pi\sqrt{|h_{1s} - h_{3s}|}} \right\} \left\{ \tan^{-1}(k|h_{1s} - h_{3s}|) \frac{k|h_{1s} - h_{3s}|}{1 + (k|h_{1s} - h_{3s}|)^2} \right\} \quad (8)$$

With a sampling period of T and identity matrix I, The state space matrices in eq. (7) is discretized as

$$\Phi = e^{AT} \quad (9)$$

$$\Gamma = A^{-1}(e^{AT} - I)B \quad (10)$$

$$e^{AT} = \sum_{n=0}^{\infty} \frac{(AT)^n}{n!} \quad (11)$$

The step response coefficients can be updated as

$$S_f = \sum_{j=1}^{i} C\Phi^{j-1}\Gamma \; ; i \in 1, P \quad (12)$$

The performance of nonlinear DMC is evaluated through simulation and experimental studies as described in the following section.

5. Results and Discussion

Both the simulation and experimental studies were carried out in a PC with Intel® Core™ 2 Duo CPU P8600 @2.40GHz processor using Windows 7 (64bit) operating system. All the codes have been written in Microsoft® Visual C++(.NET 2003). In this report, the results have been limited to SISO operations only. The level of the Tank 3 has been controlled using pump 1. The prediction and control horizons of DMC has been taken to be 20 and 1 respectively whereas weight on control action is 10.

5.1. Simulation Studies

The Fig.3 shows the simulation results on performance of both DMC and nonlinear DMC.

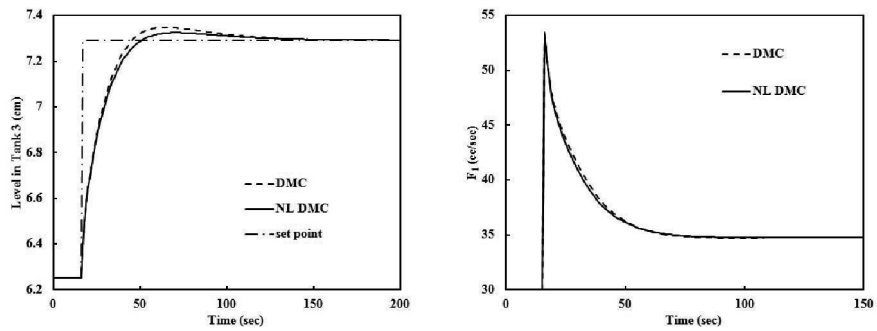

(a) Controlled output (b) Manipulated input

Fig. 3: Closed loop response of level in Tank 3 through simulation

The DMC yields marginally larger overshoot than the nonlinear DMC. The IAE values of DMC and NLDMC performances are 11.49 and 10.99 respectively. However, the IAE values do not show real efficacy of the NLDMC. The merit of the nonlinear controller should be evaluated rather qualitatively than quantitative manner. The profile of manipulated input is almost same for bothe DMC and NLDMC. Not much of advantage is observed by using nonlinear version of DMC.

5.2. Real Time Experimental Studies

The Fig.4 shows the performance of both DMC and nonlinear DMC for real-time control studies on the four tank system.

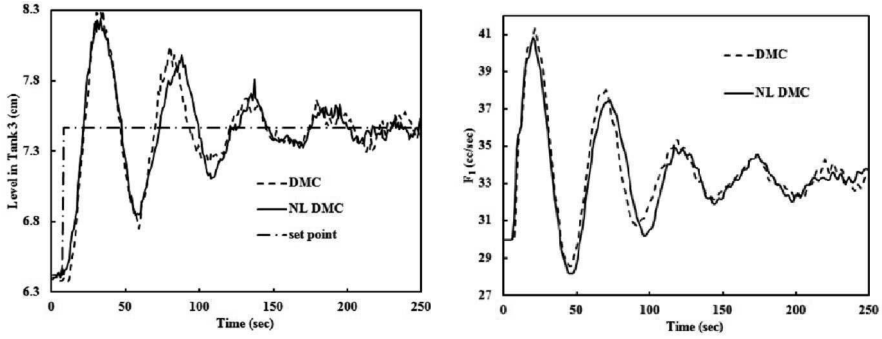

(a) Controlled output (b) Manipulated input

Fig. 4: Real-time closed loop control of level in Tank 3

Unfortunately the performance of NLDMC cannot be claimed to be improved one, though the ISE values show slight improvement (ISE_{DMC}=27.18 and ISE_{NLDMC}=24.27). The unsatisfactory improvement of NLDMC over DMC can be attributed to the physical limitation for actuation by metering pump. It has been observed that full fledged flow would lead to overflow of the tank. This fact compels the operator to put tight and narrow constraint on F_1, thereby limiting the process operation within a fairly linear zone of operation. This problem can be solved by suitable alteration in the process (*e.g.* making bypass line for release of excess water) so that one can employ full range of manipulation and obtain satisfactory improvement of NLDMC over DMC. Moreoever, the analytical linearization of mechanistic model doesn't accurately match with the actual derivative of the process, a numerical derivative could be better option.

6. Conclusion

Two basic structures of model predictive controllers, *viz*., DMC and nonlinear DMC have been employed for controlling a four tank interacting liquid storage system through both simulation and real-time control application. Substantial improvement in controller performance by incorporating nonlinear component hasn't been observed. This limitation can be attributed to the physical limitation for actuation by metering pump. Further modification in the process and/or incorporating numerical derivative would enhance the chance of better performance with nonlinear control application on four-tank system. This paper has been limited only to SISO application, however, MIMO application is under progress which would be reported elsewhere in future.

References

B. W. Bequette, 2003, Process Control-Modelling Desing and Simulation (Prentice Hall, India 2003).

G. Gattu and E. Zafiriou, 1992, Nonlinear Quadratic Dynamic Matrix Control with State Estimation, Ind. Eng. Chem. Res., 31, 4, 1096-1104

S. Patra and P. Saha, 2012, Modeling and Control of a Complex Interacting Process, Advanced Materials Research, 403-408, 3758-3762

I.A. Karimi and Rajagopalan Srinivasan (Editors), Proceedings of the 11th International Symposium on Process Systems Engineering, 15-19 July 2012, Singapore

Approximate Dynamic Programming based control for Water Gas Shift reactor

Sudhakar M Sridharakumar Narasimhan * Niket S Kaisare
Department of Chemical Engineering, IIT Madras, Chennai-36, India.

Abstract

The Water Gas Shift (WGS) reactor is an important component in a fuel processing system. It is necessary to maintain low CO levels during steady state and transient operation of fuel processing system when used onboard in a vehicle. The WGS reactor plays an important role in this regard. The focus of this paper is a model based controller for the regulation of CO level in the presence of the possible disturbances from upstream temperature and flow rate. The use of model based controllers such as nonlinear Model Predictive Control (nMPC) suffers from large computational load. On the other hand Approximate Dynamic Programming (ADP) based controller will result in better performance with lower computational load. In this paper, a non-adiabatic WGS reactor modeled by hyperbolic partial differential equations is considered. The performance of the ADP is illustrated through numerical simulations.

Keywords: Water Gas Shift reactor, Approximate Dynamic Programming, Disturbance rejection

1. Introduction

The Water Gas Shift (WGS) reactor is one of the important reactors in fuel processing system for reducing the carbon monoxide (CO) levels in the reformate which is subsequently required for a PEM Fuel cell. The WGS reaction is mildly exothermic whose conversion is limited by equilibrium temperature. Hence, the reaction is usually carried out in two stages: A high temperature followed by low temperature shift reactor. Alternatively, the WGS reaction could be carried out in a compact, coupled reactor-heat exchanger device, which provides an "optimal" temperature profile to promote the equilibrium-limited WGS reaction [Kim et al. (2005); Baier and Kolb (2007)]. In this paper we have used counter-current reactor with the reactant flowing through one channel and coolant flowing through the other channel.

During the transient operation, the WGS reactor can encounter several disturbances, such as change in the upstream reactant flow rate, temperature and composition. Efficient control of WGS reactor is therefore essential to minimize the effect of the disturbances on CO conversion. Varigonda et al. (2004) have designed Linear Quadratic Regulator (LQR) based control for the nonlinear plant by using a linear model which is linearized at three different operating points to address the nonlinear nature of the plant. Wright and Edgar (1994) have used nMPC for the control of fixed bed WGS reactor and the performance was observed to be superior to that of linear or adaptive controllers. Ling and Edgar (1997) have used model based fuzzy gain scheduling which uses several linear models partitioned in the state space. Nevertheless, all these efforts conclude that use of nonlinear model would have better performance over other approximations with the

*sridharkrn@iitm.ac.in

limitation on excessive online computational load. This paper illustrates the potential of using Approximate Dynamic Programming (ADP) strategy for the control of a coupled WGS reactor resulting in a significant reduction of computational cost.

2. Mathematical model and simulation of WGS Reactor

A 1-D transient model of parallel plate reactor-heat exchanger device is considered. The reactor has the following dimensions with length (l) : 50 mm, breadth (b) :40 mm and height (h): 0.5 mm. The model consists of the following equations for species balance, and energy balances for reacting and coolant streams:

$$\frac{\partial Y_i}{\partial t} = -v_r \frac{\partial Y_i}{\partial x} - \frac{\rho_{cat} r_i}{C} \text{ where } i = \text{CO, } \text{CO}_2\text{, } \text{H}_2\text{, } \text{H}_2\text{O, } \text{N}_2 \tag{1}$$

$$\frac{\partial T_r}{\partial t} = -v_r \frac{\partial T_r}{\partial x} + \frac{Ub}{CAc_{p,r}}(T_c - T_r) + \frac{\rho_{cat} r(-\Delta H_r)}{Cc_{p,r}} \tag{2}$$

$$\frac{\partial T_c}{\partial t} = v_c \frac{\partial T_c}{\partial x} - \frac{Ub}{A\rho_{air} c_{p,air}}(T_c - T_r) \tag{3}$$

where C is the total concentration, U is the overall heat transfer coefficient and Y represents the mole fraction. Note that the axial dispersion and wall conduction have been neglected in the above expressions, resulting in a set of hyperbolic PDEs. The WGS reaction considered is $\text{CO} + \text{H}_2\text{O} \rightarrow \text{CO}_2 + \text{H}_2$; $\Delta H_r = -48.4$ kJ/mol and the kinetics of the WGS reaction is given by (Ref Kim et al. (2005))

$$r = kP_{\text{CO}}P_{\text{H}_2\text{O}}\left(1 - \frac{P_{\text{CO}_2}P_{\text{H}_2}}{KP_{\text{CO}}P_{\text{H}_2\text{O}}}\right), \ \frac{\text{mol}}{\text{g}_{\text{cat}}\ \text{s}} \tag{4}$$

with $k = 0.00225\exp(\frac{-50{,}000}{RT})$ and $K = 9.543 \times 10^{-3}\exp(\frac{39{,}876}{RT})$.

The values of ρ_{cat}, ρ_{air}, $c_{p,air}$, $c_{p,r}$ and U are taken to be 10^3 kg/m^3, 0.883 kg/m^3, 1009 J/kg K, 34 J/mol K and 37 W/m^2 K respectively. The inlet to the reactor is assumed to be of constant composition (mole fraction) typical to that of reformer outlet ($\text{CO} : 0.06$, $\text{CO}_2 : 0.1$, $\text{H}_2 : 0.29$, $\text{H}_2\text{O} : 0.25$, $\text{N}_2 : 0.30$). The inlet steady state reactant temperature and inlet air temperature are 700 K and 450 K respectively. We assume negligible pressure drop in the reactor and the operating pressure is 303 kPa.

3. Online Control using Approximate Dynamic Programming (ADP)

The control objective is to regulate the CO conversion to steady state value using available manipulated inputs in the presence of disturbances. The disturbance considered are changes in inlet reactant flow rate and temperature with inlet air flow rate and inlet steam flow rate considered as manipulated variables. The control problem becomes non-square with two manipulated variables and single control variable (conversion). An additional constraint is that the inlet steam can only be added and not removed from the inlet reactant stream. In order to simplify the analysis, we assume that steam flow rate is linearly related to the inlet air flow rate as long as the steam flow rate is greater than the corresponding nominal steady state flow rate. Hence, in this analysis, the only manipulated variable is the inlet air flow rate and the steam flow rate is a piece wise linear function of the air flow rate.

Model predictive control is a well established model based control technique which depends on open loop model prediction and online optimization at every sampling time step. The typical objective function solved online at k^{th} sampling instant considering infinite horizon prediction length is given by,

$$J(x_k) = \min_{u(k,\ k+1,\ldots)} \sum_{i=k}^{i=\infty} \left(Q(y_{i+1} - y_{sp})^2 + R\Delta U_i^2 \right) \tag{5}$$

where y_{sp} is the desired CO conversion. Since the infinite-horizon control problem is not tractable, a finite horizon nMPC is implemented with prediction horizon p = 25 and input horizon m = 1 and the results are shown in figure 1 for two different disturbances (disturbance 1: 20% step down in inlet temperature and disturbance 2: 20% step down in inlet temperature and inlet flow rate). The computational requirement for 2.5 seconds of closed loop simulation is around 3413.10 seconds and 3303.91 seconds for disturbance 1 and 2 respectively.

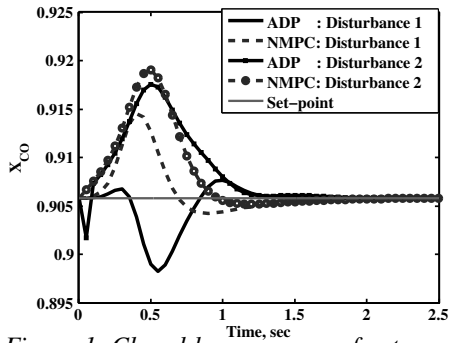

Figure 1. Closed loop response for two disturbances given by ADP and nMPC with $p = 25$ and $m = 1$

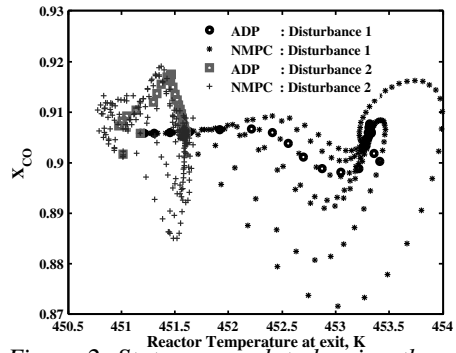

Figure 2. State space plot showing the path traced by the ADP in the operating region

As seen above, the computational requirement for the implementation of nMPC is significant as an open loop, multi-step nonlinear optimization problem has to be solved at every sampling instant. Dynamic Programming (DP) provides an alternate way of solving the infinite-horizon optimization described in equation 5 by solving the following equivalent one-stage problem:

$$J(x_k) = \min_{u_k}(\phi(x_k, u_k) + J(x_{k+1});\ \text{where } \phi = Q(y_{k+1} - y_{sp})^2 + R\Delta U_k^2 \tag{6}$$

here $J(x_{k+1})$ is the "cost-to-go" value starting from x_{k+1} to the setpoint, which is estimated through offline solution of Bellman equation, $J^{opt}(x_k) = \min_{u_k}(\phi(x_k, u_k) + J^{opt}(x_{k+1}))$.

The computational load in the calculation of cost-to-go values for all the points in the state space increases exponentially as the state dimension increases, which is referred to as 'curse of dimensionality'. ADP overcomes this problem by identifying smaller region in the state space through the closed loop simulation from sub-optimal controllers like MPC, PID etc and using a function approximator for the interpolation of cost-to-go values. The optimal path in reaching the set-point is assumed to lie within this identified region.

In this paper we have used nMPC as the sub-optimal controller and collected about 579 data for disturbance1 and 546 data for disturbance2 respectively by varying prediction

horizon (sampling time of 0.05 seconds is used). For the purpose of interpolating the cost-to-go values, 'K-nearest neighbour (KNN)' function approximator (with K = 4) which interpolates the cost-to-go values from K nearest neighbors based on distance weighted averaging is used.

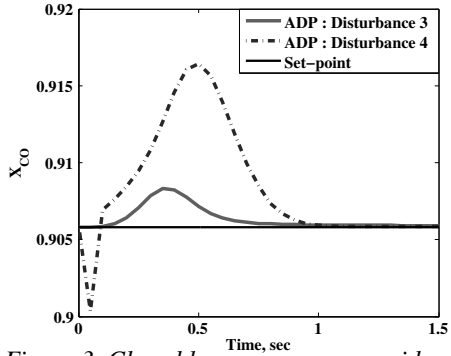

Figure 3. Closed loop response :considering fresh disturbance other than used for generating sub-optimal data

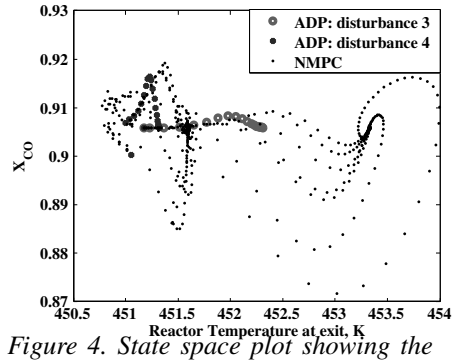

Figure 4. State space plot showing the path traced by the ADP in the operating region with two new setpoints

In order to restrict the search in the region of data density and to avoid excessive extrapolation, quadratic penalty function with Parzen density estimator is used which limits the controller from extrapolating to the region of lower density by assigning higher cost-to-go values to those points outside the region. The Parzen local density estimate for the data set Ω near the query point x_0 is defined as follows,

$$f_\Omega(x_0) = \frac{1}{N}\sum_{i=1}^{KNN}\frac{1}{2\pi\sigma^2}exp\left(\frac{-\|x_0 - x_i\|_2^2}{2\sigma^2}\right);\ \sigma \Rightarrow \text{ user defined parameter} \tag{7}$$

The quadratic penalty function is defined between $\|x_0 - x_i\|_2^2 = \sigma^2$ (with no penalty below this limit) and $\|x_0 - x_i\|_2^2 = 3\sigma^2$ (with maximum penalty, J^{max} after this limit) as follows,

$$J_{penalty}(x_0) = S.H\left(\frac{1}{f_\Omega(x_0)} - \beta\right)\left[\frac{\frac{1}{f_\Omega(x_0)} - \beta}{\beta}\right]^2 \text{ and hence } J(x_0) \Leftarrow J(x_0) + J_{penalty}(x_0) \tag{8}$$

where S is the scaling parameter, β is the threshold value and H is the Heaviside step function. The value of σ is taken as 10 for this study. For further details on the calculation of S, J^{max} and β refer Lee et al. (2006).

The cost-to-go values for the points collected from nMPC are improved by value iteration using the Bellman equation. The one step ahead prediction is obtained by simulating the discretized model equations (20 nodes) and solving the resulting set of ODEs along time in MATLAB. The optimization routine `fmincon` in MATLAB is used for the calculation of minimal cost for each of these points and this cost value is updated at every iteration. The maximum absolute difference between the cost-to-go values of subsequent iteration is monitored for convergence. The final converged cost-to-go values are then used for the online optimization.

The ADP controller is initially tested for the disturbances which was used for the generation of sub-optimal data points. The input(R) and output(Q) weight for online implementation are taken as 10 and 1000 respectively. From the closed loop simulation results

(Refer 1 and 2) and comparison of cost-to-go values (Disturbance 1: 249.83 for ADP and 365.06 for nMPC, Disturbance 2: 1034 for ADP and 1087 for nMPC), it is observed that the performance of ADP is marginally better compared to nMPC. However, the computational load for 2.5 seconds of closed loop simulation is significantly lower: Disturbance 1: 369.98 seconds for ADP and 3413.10 seconds for nMPC, Disturbance 2: 478.5 seconds for ADP and 3303.91 seconds for nMPC.

Next, closed loop performance of the ADP controller is tested for two fresh disturbances (disturbance 3: 15% step down in inlet temperature and disturbance 4: 15% step down in inlet temperature and flow rate) with the same suboptimal data obtained previously. Figures 3 and 4 indicate satisfactory closed loop performance in the presence of these disturbances. This means that given sufficient amount of data considering all the relevant disturbances, ADP could be deployed to reject disturbances in a wide range.

The performance of the ADP controller can be improved by adding relevant data points in the state space. The inclusion of additional points would result in more coverage of state space where optimal path lies and hence the estimate of cost-to-go values for online optimization would be closer to optimal. Although the computational time is considerably lower as compared to nMPC, there is still scope for reducing it further. There are several ways one could address this problem such as use of order reduction techniques, using better function approximation etc.

4. Conclusion

The control of a compact WGS reactor coupled with a heat exchanger is considered. The nonlinear nature of the process and wide operating region necessitates the use of nonlinear model for model based control of the reactor. ADP based controller has been designed for the WGS reactor for disturbance rejection and it has been found that the computational demand of ADP is considerably much smaller than corresponding MPC. Further improvement in computational time is required and the use of Method Of Characteristics (MOC) for model order reduction and prediction is under investigation.

References

Baier, T., Kolb, G., 2007. Temperature control of the water gas shift reaction in microstructured reactors. Chemical Engineering Science 62, 4602–4611.

Kim, G. Y., Mayor, J. R., Ni, J., 2005. Parametric study of microreactor design for water gas shift reactor using an integrated reaction and heat exchange model. Chemical Engineering Journal 110, 1–10.

Lee, J. M., Kaisare, N. S., Lee, J. H., 2006. Choice of approximator and design of penalty function for an approximate dynamic programming based control approach. Journal of Process Control 16, 135 –156.

Ling, C., Edgar, T. F., 1997. Real-time control of a water-gas shift reactor by a model-based fuzzy gain scheduling technique. J. Proc. Cont. 7, 239–253.

Varigonda, S., Eborn, J., Bortoff, S. A., 2004. Multivariable control design for the water gas shift reactor in a fuel processor. In: American Control Conference Proceedings. pp. 840–844.

Wright, G. T., Edgar, T. F., 1994. Nonlinear model predictive control of a fixed-bed water-gas shift reactor: An experimental study. Computers them. Engng 18, 83–102.

I.A. Karimi and Rajagopalan Srinivasan (Editors), Proceedings of the 11th International Symposium on Process Systems Engineering, 15-19 July 2012, Singapore.

Comparison of MIMO MPC and PI Decoupling in Controlling Methyl Tert-butyl Ether Process

Sudibyo, I.M. Iqbal, M.N. Murat and *N.Aziz

School of Chemical Engineering, Engineering Campus, Universiti Sains Malaysia, 14300 Nibong Tebal, Seberang Perai Selatan, Penang, Malaysia.
**E-mail: chnaziz@eng.usm.my*

Abstract

The main control objective of Methyl Tert-butyl Ether (MTBE) reactive distillation is to maintain the MTBE product purity within the desired range at the highest isobutene conversion possible. However, MTBE purity and isobutene conversion have strong interaction, hence need a multiple input – multiple output (MIMO) based control system. In this work, MIMO model Predictive control (MPC) and Proportional Integral (PI) decoupling have been implemented to control both the MTBE purity and isobutene conversion by manipulating the reboiler duty and reflux flowrate. The purity of MTBE is at 99% and the isobutene conversion is at 99.83%. Performance of both controllers are then compared in term of integral absolute error (IAE), integral squared error (ISE), integral of the time-weighted absolute error (ITAE) and settling time. The results showed that the MIMO MPC is better than the PI decoupling.

Keywords: Multivariable processes, PI decoupling, MPC, Reactive distillation; MTBE

1. Introduction

MTBE is well known chemical used as an anti-knock agent to replace tetra ethyl lead [Satyanarayana and Saha, 2005; Sharma and Singh, 2010]. Using reactive distillation, the MTBE conversion can reach up to 99% [Taylor and Krishna, 2000]. The maximum production of the MTBE process can be achieved if the reaction and separation can be kept at the optimum conditions. Therefore, the development of the MTBE reactive distillation control is important to achieve the process which can lead to high yield of MTBE production.

Controlling of this reactive distillation is a challenging task due to its process uncertainties, time delay, strong interactions, the large number of possible control configuration and the complex dynamics arising from the combination of reaction and separation [Satyanarayana and Saha, 2005; Nagya *et al.*, 2007, Kawathekar and Riggs, 2007; Sharma and Singh, 2010]. To control the reactive distillation process, choosing control configuration by selecting the best pairing of manipulated variable (MV) and control variable (CV) is very important [Satyanarayana and Saha, 2005; Nagya *et al.*, 2007]. The degree of the variable interaction and the best pairing of MV and CV can be determined by implementing a singular value decomposition (SVD) test [Luyben, 2006].

Normally, to increase the purity of MTBE and the conversion of isobutene, the reboiler duty and reflux flowrate are manipulated. However, the increase of conversion of isobutene will decrease the MTBE purity, thus this become one of major problem in controlling the MTBE reactive distillation process. PI decoupling and MPC are among

the well known control strategies that can be applied in MTBE reactive distillation control to cater the interaction of the control variables. The aim of this work is to compare the performance of both PI decoupling and MIMO MPC in controlling the MTBE purity and isobutene conversion in the MTBE reactive distillation. Prior to control implementation, the SVD test is carried out to analyze the degree of the variable interaction and also to choose the best pairing of MV and CV.

2. MTBE Reactive distillation

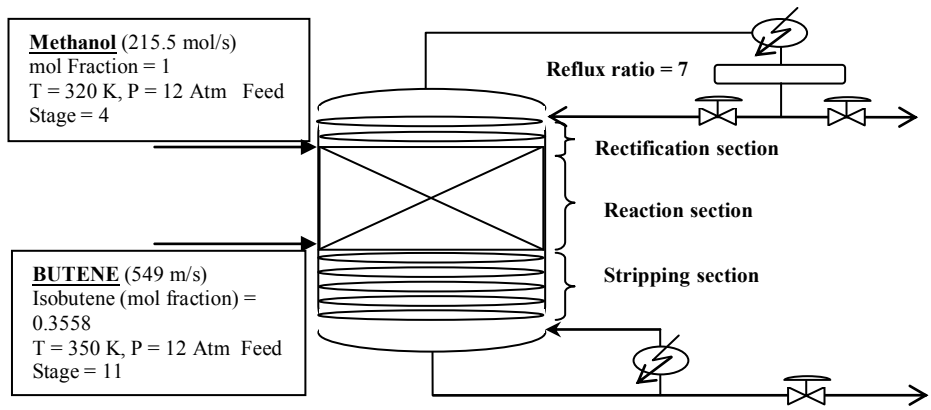

Figure 1. MTBE Reactive Distillation Column Configuration

The specification used here is similar to the specification used by Higler *et al.* [1999], except the number of passes, the pressure column and location of feed stages are different. In this work, 4 passes and 12 atm of pressure column are used while Higler *et al.*[1999] used 5 passes and 11 atm. Meanwhile, the feed, methanol and butane, are fed at stages 4 and 11, respectively. The reaction scheme to produce MTBE is:

$$i\text{-}C_4H_8 + CH_3\text{-}OH \rightleftharpoons C_5H_{12}O \quad (1)$$

In this work, the steady state Aspen simulators were used to simulate the process. Then, the model obtained is exported to Aspen dynamics using flow driven dynamic model.

3. Control Development

3.1. SVD Analysis

SVD test is used to select the best control configuration and to know the degree of interaction among the variables. For SVD test, the reflux flowrate was changed at 0.1 % while the reboiler duty was kept constant and the the reboiler duty was changed at 0.1 % while the reflux flowrate was kept constant [Luyben , 2006]. The result obtained is shown in matrix *k*. Matrix *u* show that the purity of MTBE has the largest magnitude (largest effect) due to reflux flowrate change, while the isobutene conversion has largest magnitude for reboiler duty change. Thus, both pairs of manipulated and control variables are selected. From the SVD analysis (matrix *s*), the condition number was calculated by dividing the large value (8.1×10^{-4}) with the small value (4.5×10^{-6}) of the singular matrix which resulted to 179.4. This means the variable have strong interaction and need the decoupling system to control this process.

$$k = \begin{bmatrix} -6.2764e-4 & 5.0763e-4 \\ 1.11e-5 & -3.2183e-6 \end{bmatrix}; u = \begin{bmatrix} -0.9999 & 0.0132 \\ 0.0132 & 0.9999 \end{bmatrix}; s = \begin{bmatrix} 8.1e-4 & 0 \\ 0 & 4.5e-6 \end{bmatrix}$$

3.2. PI Decoupling scheme

Fig. 2 shows the PI Decoupling scheme for the MTBE process. The decoupling for two inputs and two outputs system are shown below:

$$\begin{bmatrix} T_{1,1(s)} & 0 \\ 0 & T_{2,2\ (s)} \end{bmatrix} = \begin{bmatrix} g_{1,1(s)} & g_{1,2(s)} \\ g_{2,1(s)} & g_{2,2(s)} \end{bmatrix} \times \begin{bmatrix} D_{11(s)} & D_{12(s)} \\ D_{21(s)} & D_{22(s)} \end{bmatrix} \quad (2)$$

where T is the decoupled process matrix, G is the process matrix and D is the decoupling matrix. The input interaction in transfer function G (process) can be eliminated by introducing decoupling matrix D , as shown in figure 3 [Yaghoubi and Shahmansoorian, 2011]. $T_{1,1\ (s)}$ and $T_{2,2\ (s)}$ can be set equal to one, then the matrix D can be determined by choosing two from four element of matrix D as c_1 and c_2. Here, c_1 and c_2 are assumed equal to one. Hence, the matrix D can be obtained as shown below:

$$D = \begin{bmatrix} c_1 & -\frac{g_{12}.c_2}{g_{11}} \\ -\frac{g_{21}.c_1}{g_{22}} & c_2 \end{bmatrix} = \begin{bmatrix} 1 & -\frac{g_{12}.1}{g_{11}} \\ -\frac{g_{21}.1}{g_{22}} & 1 \end{bmatrix} \quad (3)$$

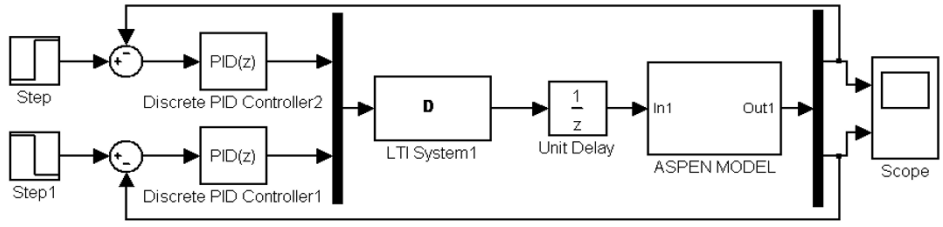

Figure 2. PI Decoupling scheme for the MTBE process

3.3. MIMO MPC Scheme

The MPC objective function (j_k) for two inputs and two outputs (2 x2) is defined as [Kawathekar and Riggs, 2007]:

$$j_k = \sum_{i=1}^{P} \left((y_{f1|k+i} - y_{sp1|k+i})^2 Q_1 + (y_{f2|k+i} - y_{sp2|k+i})^2 . Q_2 \right) + \left(\Delta u_{f1|k+i} \right)^2 . R_1 + \left(\Delta u_{f2|k+i} \right)^2 . R_2 \quad (4)$$

where y_f is a predicted future output, y_{sp} is a set point, Q is an error penalty, R is an input change penalty, Δu_f is a future input change and k is a current sampling time. In this work, for MIMO MPC, the Aspen dynamics model is used to represent the process, the state space equations as the process model and the quadratic programming as an optimizer. The MIMO MPC scheme for MTBE process is shown in figure 3.

3.4. State space model

To generate data for state space model development, two generalized multiple-level noise (GMN) signals are used as input signal to the Aspen dynamics based model which is integrated in Matlab simulink block. One third of 98% process settling time is used as the average switching time for the excitation signal [Arefi *et al., 2008*]. The GMN signal has 11 input levels from +7% to -7% of the input nominal value. In this test, the GMN generate data for 30 hours. The generated data was then used in the system identification to develop the state space model of the process. The state space model obtained is used in both PI decoupling and MIMO MPC. The state space model obtained is:

$$x(t+Ts) = A\,x(t) + B\,u(t) + K\,e(t) \quad (5)$$
$$y(t) = C\,x(t) + D\,u(t) + e(t) \quad (6)$$

where:

$$A = \begin{bmatrix} 0.73897 & -0.042774 & 0.060387 & 0.02007 \\ -0.34542 & 0.7133 & 0.31961 & 0.30447 \\ 0.24956 & 0.44335 & 0.34635 & -0.7272 \\ 0.035443 & 0.059417 & -0.11259 & 0.61541 \end{bmatrix} \quad B = \begin{bmatrix} -1.3786 & 1.5398 \\ -4.2 & 4.1893 \\ 6.4984 & -5.8288 \\ 1.1353 & -0.38649 \end{bmatrix}$$

$$C = \begin{bmatrix} 0.20528 & 0.10429 & 0.10847 & -0.11637 \\ -0.0039021 & 0.0034986 & 0.0019554 & -0.00039005 \end{bmatrix}$$

while D, u and x are matrix zero with size (2x2), (4 x 2) and (4 x 1), respectively.

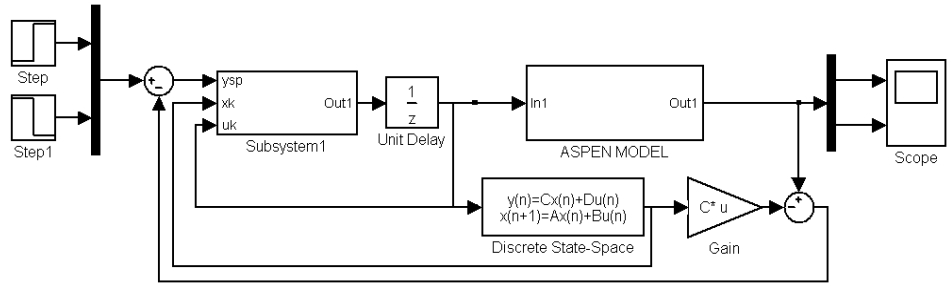

Figure 3. MIMO MPC scheme for MTBE process

4. Results and Discussion

The result of the PI and MIMO MPC tuning is shown in Table 1. CV1 is referring to MTBE purity (set point at 99%) and CV2 is referring to conversion of isobutene (set point at 99.83%). Meanwhile, figure 4 shows the response of both controllers proposed. The figure shows that when using PI decoupling, the settling time for the MTBE process is more than 2 hours from the time when the step setpoint is introduced. Meanwhile less than one hour settling time is required when MIMO MPC is used. For the CV2, the settling time given by PI decoupling and MIMO MPC are 4 and 1 hours, respectively. Table 2 tabulated the value of IAE, ISE and ITAE values for both PI Decoupling and MIMO MPC. The table shows that the MIMO MPC produces lower error value if compared to PI decoupling, thus proved that MIMO MPC better than PI decoupling.

Table 1. PI Decoupling and MIMO MPC setting after tuning

PI Decoupling :	CV 1	CV 2	MIMO MPC :	CV1	CV 2
Proportional (P)	-0.44	-173.45	Penalty error (Q)	2	3
Integral (I)	-53.045	-6446.98	Input changes penalty (R)	0.00015	0.01
			Input change constraint	±10%	±10%

Table 2. Performance of PI decoupling and MIMO MPC

PI Decoupling			MIMO MPC	
	CV1	CV2	CV1	CV2
IAE (%)	3.42	3.20×10^{-2}	0.25	7.83×10^{-3}
ISE (%)	0.10	8.39×10^{-6}	3.56×10^{-3}	6.52×10^{-7}
ITAE (%)	5.61	5.27×10^{-2}	0.47	1.56×10^{-2}
Settling Time	2 hr	4 hr	0.6 hr	1 hr

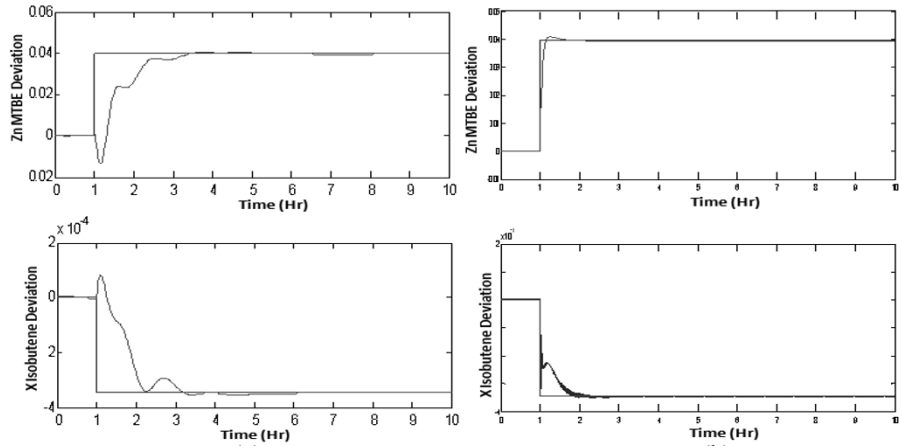

(a) (b)

Figure 4. Response of (a) PI decoupling (b) MIMO MPC

5. Conclusion

PI decoupling and MIMO MPC have successfully designed and implemented to control the MTBE reactive distillation in order to maintain the purity of MTBE at 99% and isobutene conversion at 99.83%. From the results, the MIMO MPC outperformed the PI decoupling in all performances criteria considered.

Acknowledgement

The financial support from Universiti Sains Malaysia through Research University (RU) Grant and Graduate Assistant (GA) to the first author are greatly acknowledged.

References

A.P. Higler, R. Taylor and R. Krishna, 1999, The influence of mass transfer and mixing on the performance of a tray column for reactive distillation, Chem. Eng. Science, 54, 2873-2881

D.E. Seborg, T. F. Edgar, D. A. Mellichamp and F.J. Doyle, 2011, Process dynamics and control, 3rd ed., John Wiley.

M.M. Arefi, A. Montazeri, J. Poshtan and M.R. Jahed-Motlagh, 2008, Wiener-neural identification and predictive control of a more realistic plug-flow tubular reactor, Chemical Eng. Journal, 138, 274-282.

N. Sharma and K.Singh, 2010, Control of Reactive Distillation Column: A Review, Int. J. Chemical Reactor Eng., 8, R5

R.K. Pearson, 2003, Selecting Nonlinear model structures for computer control, Journal of process control, 13, 1-26

R. Kawathekar, J.B. Riggs, 2007, Nonlinear model predictive control of a reactive distillation column, Control Engineering Practice, 15, 231–239

R. Taylor and R. Krishna, 2000, Review: Modelling reactive distillation, Chem. Eng. Science, 55, 5183-5229.

T. Satyanarayana and P. Saha, 2005, Modeling and Control Structure Selection for Reactive Distillation Process using Aspen Custom Modeler, CHEMCON – 05, New Delhi.

W. L. Luyben, 2006, Evaluation of criteria for selecting temperature control trays in distillation columns, Journal of Process Control, 16, 115–134.

Z. Yaghoubi, A. Shahmansoorian , 2011, Inverted decoupler and PID controller design for MIMO processes with time delays, Canadian J. on Electrical and Electronics Eng., 2, No. 6.

I.A. Karimi and Rajagopalan Srinivasan (Editors), Proceedings of the 11th International Symposium on Process Systems Engineering, 15-19 July 2012, Singapore

MPC for LPV systems using perturbation on control input strategy

Pornchai Bumroongsri, Soorathep Kheawhom *

Department of Chemical Engineering, Faculty of Engineering, Chulalongkorn University, Bangkok, Thailand

Abstract

In this paper, a model predictive control (MPC) algorithm for linear parameter varying (LPV) systems is proposed. The proposed algorithm consists of two steps. The first step is derived by using parameter-dependent Lyapunov function and the second step is derived by using the perturbation on control input strategy. An overall algorithm is proved to guarantee robust stability. The controller design is illustrated with a case study of continuous stirred-tank reactor. Comparisons with other MPC algorithms for LPV systems have been undertaken. The results show that the proposed algorithm can achieve better control performance.

Keywords: MPC, LPV, parameter-dependent Lyapunov function, perturbation on control input strategy, continuous stirred-tank reactor

1. Introduction

Model predictive control (MPC) is an effective control algorithm widely used in the chemical processes. At each sampling time, MPC uses an explicit process model to solve an open-loop optimization problem and implements only the first element of input sequence. MPC based on linear model is typically used because the on-line optimization problem can be formulated as the convex optimization problem by either linear programming or quadratic programming (Kothare et al. , 1996). This is a good assumption for typical processes. However, most of the chemical processes are nonlinear. Thus, when the operating conditions undergo significant changes, the performance of linear MPC can deteriorate drastically. Moreover, the stability of the control system cannot be guaranteed.

In Kothare et al. (1996), min-max predictive control strategy was presented. The nonlinear system is approximated by the polytopic uncertain system. The goal is to design a state feedback control law which minimizes the worst-case performance cost. The algorithm is proved to guarantee robust stability. However, the algorithm turns out to be conservative because the nonlinear system is approximated by the polytopic uncertain system. Moreover, the scheduling parameter is not considered in the controller synthesis. In order to reduce the conservativeness, the idea of controlling nonlinear systems by using linear parameter varying (LPV) systems has been widely investigated. At each sampling instant, the scheduling parameter is measured on-line.

In Lu et al. (2000), Quasi-min-max MPC algorithm for LPV systems was presented. The control input is computed by minimizing the quasi-worst-case performance cost. The algorithm is seen as an extension of the algorithm presented in Kothare et al. (1996) by keeping the first control input as a free decision variable. The algorithm is proved to

*soorathep.k@chula.ac.th

guarantee robust stability. However, an invariant ellipsoid constructed to guarantee robust stability is derived by using a single Lyapunov function. Thus, the conservative result is still obtained. A feedback min-max MPC algorithm for LPV systems subject to bounded rates of change of parameters was presented in Casavola et al. (2002) . The algorithm in Lu et al. (2000), where open-loop MPC scheme is limited to one step control horizon, is extended to the general case of control horizon of arbitrary length N. The perturbation on control input strategy is developed in order to improve control performance. However, this strategy cannot guarantee robust stability due to the fact that the constraint on terminal invariant set is not explicitly imposed. Moreover, robust constraint satisfaction before switching horizon N cannot be guaranteed (Ding and Huang , 2007).

In this work, the closed-loop MPC strategy for LPV systems is developed. The proposed algorithm consists of two steps. The first step is derived by using parameter dependent Lyapunov function (Wada et al. , 2006). In the second step, the perturbation on control input strategy is introduced to improve control performance. Moreover, the algorithm in the second step is developed such that it can be implemented with a state feedback gain derived by using parameter-dependent Lyapunov function, and robust stability and constraint satisfaction for the whole algorithm can be guaranteed.

2. Problem Description

The model considered here is the following discrete-time LPV system

$$x(k+1) = A(p(k))x(k) + Bu(k), \tag{1}$$

where $x(k)$ is the state of the plant. $u(k)$ is the control input. We assume that the scheduling parameter $p(k)$ is measurable on-line at each sampling time k. Moreover, we assume that $A(p(k)) \in \Omega, \Omega = Co\{A_1, A_2, ..., A_L\}$, where Ω is the polytope. Co denotes convex hull. A_j are vertices of the convex hull. Any $A(p(k))$ within the polytope Ω is a linear combination of the vertices such that $A(p(k)) = \sum_{j=1}^{L} p_j(k)A_j, \sum_{j=1}^{L} p_j(k) = 1, 0 \leq p_j(k) \leq 1$. Further, let $\chi_K^{k+i}(x(k)) = Co\{\bar{\Phi}_K(p^{k+i-1})x(k)\}$ denotes the closed convex hull of all i-steps state trajectories from x at time k under the state-feedback gain K where $\Phi_K(p(k)) = A(p(k)) + BK$ and $\bar{\Phi}_K(p^{k+i-1}) = \Phi_K(p(k))\Phi_K(p(k+1))\Phi_K(p(k+2))...\Phi_K(p(k+i-1))$.

The above sets can be computed according to $\chi_K^{k+i}(x(k)) = Co\{\Phi_K(p(k+i-1))z, \forall z \in vert\{\chi_K^{k+i-1}(x(k))\}, \forall p(k+i-1) \in P^{K+i-1}\}$, and $P^{K+1} = vert\{Co\{p(k) \pm \Delta p\}\}$, $P^{K+2} = vert\{Co\{p(k+1) \pm \Delta p\}\}$, $P^{K+i-1} = vert\{Co\{p(k+i-2) \pm \Delta p\}\}$, where Δp is the bounded parameter variation and it is assumed to be known and *vert* denotes the vertices of the polytope.

The aim of this research is to find a state feedback regulation $u(k) = g(x(k))$, which stabilizes Eq. 1 and achieves the following performance cost

$$\min_{u(k+i/k)} \max_{A(p(k+i)) \in \Omega, i \geq 0} \sum_{i=0}^{\infty} \begin{vmatrix} x(k+i/k) \\ u(k+i/k) \end{vmatrix}^T \begin{vmatrix} \Theta & 0 \\ 0 & R \end{vmatrix} \begin{vmatrix} x(k+i/k) \\ u(k+i/k) \end{vmatrix}, \tag{2}$$

where $\Theta > 0$ and $R > 0$ are symmetric weighting matrices, subject to constraints

$$|u_h(k+i/k)| \leq u_{h,max}, h = 1, 2, 3, ..., n_u, \tag{3}$$

$$|y_r(k+i/k)| \leq y_{r,max}, r = 1, 2, 3, ..., n_y. \tag{4}$$

3. The proposed MPC algorithm for LPV systems

Algorithm 3.1: Step 1: At any sampling time k, measure $x(k)$ and find $\gamma, K_j = Y_j G_j^{-1}, Q_j$ by solving the following problem (Wada et al. , 2006)

$$\min_{\gamma, Y_j, G_j, Q_j} \gamma, \tag{5}$$

$$\text{s.t.} \begin{vmatrix} 1 & * \\ x(k/k) & Q_j \end{vmatrix} \geq 0, \forall j = 1,2,...,L, \tag{6}$$

$$\begin{vmatrix} G_j + G_j^T - Q_j & * & * & * \\ A_j G_j + B Y_j & Q_l & * & * \\ \Theta^{\frac{1}{2}} G_j & 0 & \gamma I & * \\ R^{\frac{1}{2}} Y_j & 0 & 0 & \gamma I \end{vmatrix} \geq 0, \forall j = 1,2,...,L, \forall l = 1,2,...,L, \tag{7}$$

$$\begin{vmatrix} X & * \\ Y_j^T & G_j + G_j^T - Q_j \end{vmatrix} \geq 0, \forall j = 1,2,...,L, X_{hh} \leq u_{h,\max}^2, h = 1,2,...,n_u, \tag{8}$$

$$\begin{vmatrix} S & * \\ (A_j G_j + B Y_j)^T C^T & G_j + G_j^T - Q_j \end{vmatrix} \geq 0, \forall j = 1,2,...,L, S_{rr} \leq y_{r,\max}^2,$$
$$r = 1,2,...,n_y. \tag{9}$$

Step 2: Given $\gamma, K_j = Y_j G_j^{-1}, Q_j$ from step 1, find $C_{\text{opt}} = C(k+i/k)_{i=0}^{N-1}$ by solving the following problem

$$\min_{J_i, C_{\text{opt}}} \sum_{i=0}^{N} J_i, \tag{10}$$

$$\text{s.t.} \begin{vmatrix} J_N & * \\ z(k+N/k) & \gamma^{-1} Q_j \end{vmatrix}, \forall j = 1,2,...,L, \forall z(k+N/k) \in vert\{\chi_K^{k+N}(x(k))\}, \tag{11}$$

$$J_N \leq \gamma, \tag{12}$$

$$|(K_j z(k+i/k) + c(k+i/k))_h| \leq u_{h,\max}, \forall i \in \{0,1,...,N-1\},$$
$$\forall h \in \{1,2,...,N_u\}, \forall z(k+i/k) \in vert\{\chi_K^{k+i}(x(k))\}, \tag{13}$$

$$|(Cz(k+i/k)_r| \leq y_{r,\max}, \forall i \in \{0,1,...,N-1\}, \forall r \in \{1,2,...,N_y\},$$
$$\forall z(k+i/k) \in vert\{\chi_K^{k+i}(x(k))\}, \tag{14}$$

$$\begin{vmatrix} I & * & * \\ \Theta^{\frac{1}{2}} z(k+i/k) & J_i I_{n_x} & * \\ R^{\frac{1}{2}} c(k+i/k) & 0 & J_i I_{n_u} \end{vmatrix} \geq 0, \forall i \in \{0,1,...,N-1\},$$
$$\forall z(k+i/k) \in vert\{\chi_K^{k+i}(x(k))\}. \tag{15}$$

Feed the plant by $u(k) = K(p(k))x(k) + c(k), K(p(k)) = \sum_{j=1}^{L} p_j(k) K_j$.

Theorem 3.1: The control law provided by the algorithm 3.1 assures robust stability to the closed-loop system.

Proof: By applying Schur complement to Eq.11, with Eq.12, we obtain $z(k+N/k)^T \gamma Q^{-1} z(k+N/k) \leq J_N \leq \gamma$ where $Q = \sum_{j=1}^{L} p_j(k) Q_j$. This is equivalent to $z(k+N/k)^T Q^{-1} z(k+N/k) \leq 1, \forall z(k+N/k) \in vert\{\chi_K^{k+N}(x(k))\}$. Thus, the state $x(k+N/k)$ is restricted to lie in an invariant ellipsoid $\varepsilon = \{x / x^T Q^{-1} x \leq 1\}$ and the control law $u(k+i/k) = K(p(k+i))x(k+i/k), i \geq N$ is able to steer the state $x(k+N/k)$ to the origin.

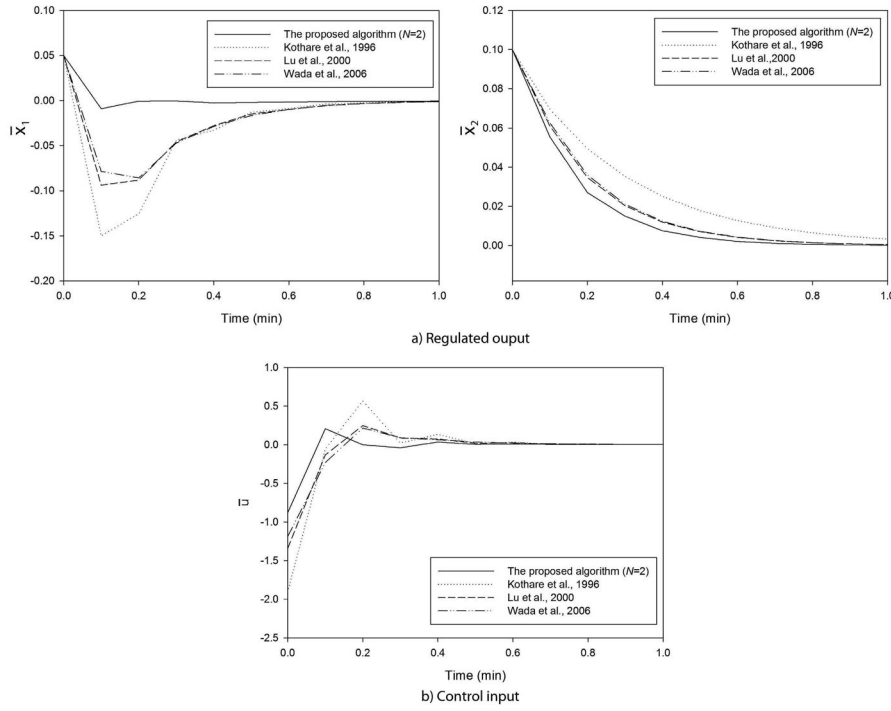

Figure 1. The closed-loop responses of nonlinear CSTR in the case study.

4. Example

The numerical simulations have been performed in Intel Core i-5 (2.4GHz), 2 GB RAM, using YALMIP (Löfberg , 2004) within Matlab R2008a environment.

Consider the following nonlinear model for CSTR where the consecutive reaction $A \rightarrow B \rightarrow C$ takes place

$$\begin{vmatrix} \dot{x_1} \\ \dot{x_2} \end{vmatrix} = \begin{vmatrix} -1-Da_1 & 0 \\ Da_1 & -1-Da_2x_2 \end{vmatrix} \begin{vmatrix} x_1 \\ x_2 \end{vmatrix} + \begin{vmatrix} 1 \\ 0 \end{vmatrix} u, \tag{16}$$

where x_1 and x_2 denote the dimensionless concentration of A and B, respectively. The control input u corresponds to the inlet concentration of A. $Da_1 = 1$ and $Da_2 = 2$ are Damkohler numbers. Here $J_\infty(k)$ is given by Eq. 2 with $\Theta = 10I$ and $R = 0.01$. The objective is to regulate the deviated states $\bar{x}_1$ and $\bar{x}_2$ from 0.05 and 0.1, respectively to the origin by manipulating $\bar{u}$. The input and output constraints are $|\bar{x}_1| \leq 2$, $|\bar{x}_2| \leq 2$ and $|\bar{u}| \leq 2.5$.

Figure 1 shows the closed-loop responses of the system. The proposed algorithm can achieve less conservative result as compared to MPC algorithms of Kothare et al. (1996), Lu et al. (2000) and Wada et al. (2006).

5. Conclusions

In this work, a model predictive control (MPC) algorithm for linear parameter varying (LPV) systems is proposed. The proposed algorithm is derived by using parameter-dependent Lyapunov function with the perturbation on control input strategy. An overall algorithm is proved to guarantee robust stability. The controller design is illustrated with a case study. The results show that the proposed algorithm can achieve better control performance as compared with existing robust MPC algorithms for LPV systems.

Acknowledgement

The authors gratefully acknowledge the financial support provided by the Higher Education Research Promotion and National Research University Project of Thailand, Office of the Higher Education Commission (EN636A)

References

Casavola, A., D. Famularo, G. Franze, 2002. A feedback min-max MPC algorithm for LPV systems subject to bounded rates of change of parameters. IEEE T. Automat. Contr. 47(7), 1147-1152.

Ding, B., B. Huang, 2007. Comments on A feedback min-max MPC algorithm for LPV systems subject to bounded rates of change of parameters. IEEE T. Automat. Contr. 52(5), 970.

Kothare, M.V., V. Balakrishnan, M. Morari, 1996. Robust constrained model predictive control using linear matrix inequalities. Automatica 32 (10), 1361-1379.

L öfberg, J., 2004. YALMIP : A toolbox for modelling and optimization in MATLAB. in Proceedings of the 2004 IEEE international symposium on computer aided control systems design, Taipei, Taiwan, 284-289.

Lu, Y., Y. Arkun, 2000. Quasi-min-max MPC algorithms for LPV systems. Automatica 36 (4), 527-540.

Wada, N., K. Saito, M. Saeki, 2006. Model predictive control for linear parameter varying systems using parameter dependent lyapunov function. IEEE T. Circuits Syst. 53(12), 1446-1450.

I.A. Karimi and Rajagopalan Srinivasan (Editors), Proceedings of the 11th International Symposium on Process Systems Engineering, 15-19 July 2012, Singapore.

Systematic Specification of a Logic Controller for a Delayed Coking Drum[1]

Stephan Fischer,[a] Herbert Teixeira,[b] Sebastian Engell[a]

[a] *Process Dynamics and Operations Group, Department of Biochemical and Chemical Engineering, TU Dortmund, 44221 Dortmund, Germany*
[b] *PETROBRAS / CENPES, Av. Horácio Macedo, 950 - Cidade Universitária, Ilha do Fundão, Rio de Janeiro, 21949-915, Brazil*

Abstract

This paper presents the results of the application of a systematic logic controller design methodology to an industrial case study, the delayed coking drum process. The design process starts from a set of semi-formal documents from which a formal specification of the control requirements is derived. The formal specification is transformed into a logic controller implemented in *Sequential Function Charts* as well as into a timed automata model of the logic controller which in turn is utilized to validate the logic controller by means of simulation and formal verification.

Keywords: Logic Controllers, Systematic Design, Formalization

1. Introduction

In chemical plants, logic controllers play an important role to realize desired sequences in batch processes as well as during start-up and shut-down of continuous plants. The design and the implementation of logic controllers have to be performed by teams of experts from different engineering disciplines: process engineers usually specify the function of the logic controller in natural-language or semi-formal documents and the controller is then implemented by automation engineers in specific programming languages as defined in the standard IEC 61131-3 (IEC (2003)). As the specifications usually are neither complete nor consistent, and often ambiguous, frequent iterations between the two sides are necessary and changes may still be required in the commissioning phase which may cause costly delays and lead to inconsistencies of the documentation and the implementation.

Many different methods for the enhancement of the design of logic controllers have been developed which can be grouped into two classes. The first class consists of methods for the formalization of the requirements or of the specification using a variety of formalisms such as Petri-nets (Ferrarini & Piroddi (2003), Klein et al. (2003)) or automata-based formalisms (Maler et al. (1995), Ramadge & Wonham (1989), and Stursberg (2005)). The formalized specification is then used to (algorithmically) derive logic controllers which are correct by design. The second class of approaches focuses on quality control of the logic controllers at the end of the design process. This class contains methods for the algorithmic generation of test cases (Provost et al. (2009)) or the verification of logic controllers using formalisms like timed automata (Stursberg & Lohmann (2005) and L'Her et al. (2001)) or Petri-nets (Fujino et al. (2000)).

[1] The research reported in this paper was (partly) funded by the European FP7 project MULTIFORM, contract number INFSO-ICT-224249, http://www.ict-multiform.eu. This support is very gratefully acknowledged.

In our recent work (see Fischer et al. (2011)), we have proposed a systematic logic controller design method that combines features of both classes. On the one hand, the design process is supported by providing a transparent and consistent formal specification that is refined into controller code in the programming language *Sequential Function Charts* (SFC) step by step. On the other hand, the final formal specification is transformed into models that are used to verify the controller.
In this contribution we report the application of this *DC/FT* design approach and of the corresponding software tool to an industrial-scale case study, an automation system of delayed coking drum plant, operated by PETROBRAS.

2. Systematic Logic Controller Design

Following industrial practice, the design starts from a set of informal, natural-language requirements that represent a coarse description of the desired behavior of the controlled process. In contrast to a manual conversion, as reported e.g. in Lucas & Tilbury (2004), of more or less structured requirements into logic controller code which is not easily comprehensible to process engineers, in the *DC/FT* approach first a structured and formalized representation of the requirements is generated. The desired functionality is represented in a modular fashion, dividing the sequences of actions into smaller parts. These parts are then further refined until all requirements have been processed and the controller is specified in detail. The approach makes use of three major principles to structure, simplify, and improve the design process:

1. Hierarchy and refinement to reflect the complexity of the controller and to deal with the large amount of information in the different phases of the design process, ranging from abstract representations of the specification and control algorithms (that are required in the early design stages) to very detailed representations in the later design stages and in the implementation phase.
2. Flexibility to be able to react to revisions of the specification that are necessary due to changes or more detailed definition on the requirements of the plant and/or of the controller.
3. Structured documentation of all design decisions to provide a consistent and intuitive representation of all (informal and formal) design parameters and decisions to the design team in all stages of the design process.

2.1. The DC/FT Formalism

The DC/FT structuring formalism consists of two coupled formalisms, the *Dependency Chart* (DC) and the *Function Table* (FT). A DC is a two-dimensional graphical representation of the conceptual design of the logic controller (see Fig. 1). It consists of a set of *Function Blocks* (symbolized by rectangular boxes) and a set of directed connections between the blocks, the *Transitions*. The DC can be seen as an extended version of the Gantt chart formalism that provides an intuitive representation of sequential processes and is used in e.g. scheduling as well as for project management tasks. Hierarchy is introduced to the DC formalism by the refinement of the function blocks of the DC. Each function block holds either a *Function Table* or one or more DCs. In contrast to the original definition of Gantt charts, the DC also supports the concepts of alternative branching (including priorities), loops, and jumps. A FT is inspired by the documentation formats that are used in industry to specify control systems. It consists of a set of *Function Table Entries* (FTE), where each FTE holds an executable action with an assigned qualifier and, if applicable, a Boolean condition that controls the execution of the action. If this condition is empty, the condition of the preceding FTE is used instead, so that two or more actions can be coupled. The conditions and actions are defined by

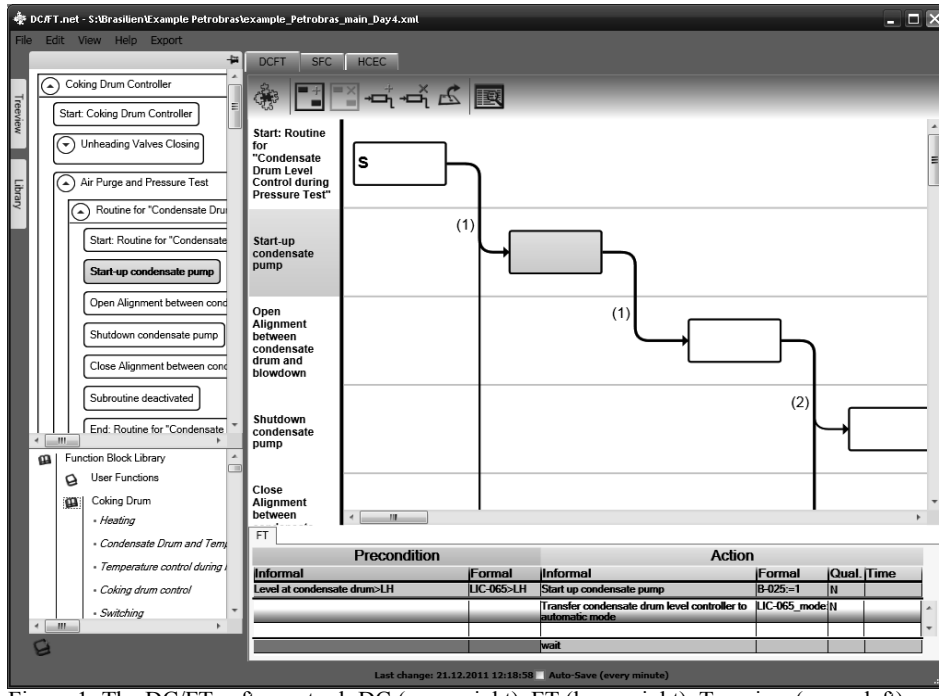

Figure 1: The DC/FT software tool: DC (upper right), FT (lower right), Treeview (upper left), and Library (lower left)

an informal description as well as by a formal specification. The qualifiers assigned to the actions are taken from the set of qualifiers defined in the IEC standard (IEC(2003)) for SFC to facilitate the coupling of DC/FT and SFC. Actions can be executed in a stored mode (qualifiers S, SL, DS, SD) which means that they remain active until the action is reset with the qualifier R, or in a non-stored mode (N, L, D) which means that they are switched off automatically when the following condition evaluates to true; a third group of qualifiers (P, P_0, P_1) executes the action as a pulse. Some of the qualifiers involve time (e.g. to delay the execution of an action). If these qualifiers (D, L, SL, SD, and DS) are assigned to an action, the time span has to be specified in the last column of the function table. The FTEs are executed sequentially without branching or repetition. For more details of the DC/FT formalism and a formal definition we refer to Fischer et al. (2011).

2.2. The DC/FT Software Tool

The *DC/FT* design process is supported by a software tool with an intuitive graphical editor (Fig. 1). The benefit of the tool-based design process is that in addition to the desired logic controller in the format of SFC, a consistent formal specification of the logic controller is obtained. The tool also provides the possibility to export parts of the formalized specification (function blocks or DCs) to a library. Several export filters, notably to the *UPPAAL* model checker (Larsen et al. (1997)) and to the *Compositional Interchange Format for Hybrid Systems* (van Beek et al. (2008)) to which many other model-based design and analysis tools are connected are integrated into the tool, which can be used for analyses of the controller (simulation, testing, formal verification).

3. Example Process

The example process (see Fig. 2), a delayed coking plant consists of pairs of reactors (drums) used for the coking of heavy-oil that are operated in batch mode. The drums are

connected to a fired heater that provides a mixture of steam and bottoms product of a heavy oil fractionator. The process is called delayed as the reaction to coke and shorter olefins is taking place in the drum while the components are mixed before in the fired heater. During operation, a drum is filled with the solid coke until it is filled completely. Since the coking drums are connected to the continuously operating fractionator (distillation column), the reactors are filled and emptied in an alternating fashion. The emptying and preparation procedure consist of the following phases:

1. Purge volatile components to the fractionator using steam
2. Cooling and drainage
3. Decoking using a water lance
4. Purging of air and pressure test
5. Heating to reach the operation temperature

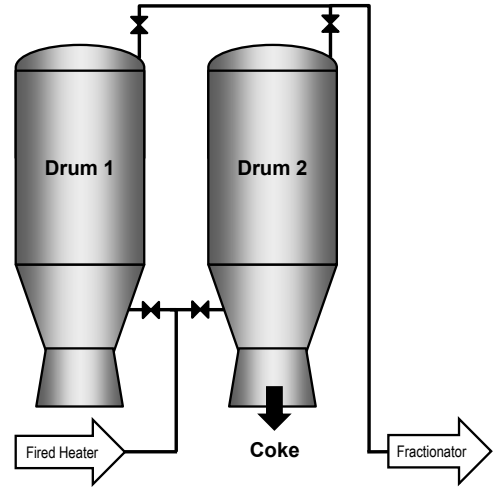

Figure 2: Delayed Coking Drum Process (simplified)

3.1. Formalization of the Control Requirements of the Example Process

At the beginning of the design process the requirements were given in a semi-formal document (~30 pages A4 paper), consisting of description of the process and the desired control system behavior, and *Piping and Instrumentation Diagrams* (PID) of the plant. The sequences of action are given as flow-charts. It was decided to split the requirements into seven function blocks according to the phases described above with one additional block for the coking (operation) and the switching procedure. Each of the blocks was refined further by means of one or more dependency charts that were again refined using function blocks and (in the end) function tables. The function block "Air Purge and Pressure Test" for instance contains three parallel DCs (purge and test sequence and in parallel pressure and condensate level control) that in turn are further refined, etc. The final formal specification consists of more than 350 function blocks on four hierarchy levels, resulting in ~250 function tables at the end of the refinement. The navigation through the large hierarchical structure is realized by means of the treeview (see Fig. 1). During the design process both relatively small parts of the specification like the opening/closing of valves or the waiting for operator permission and larger parts of the specification like the level or pressure control in the drum were frequently reused saving a lot of time and effort.

After all requirements were formalized, a SFC representation is generated which serves as a documentation of the requirements and as basis for the implementation. Parts of the specification were transformed into a *UPPAAL* (timed automata) model and were simulated and verified with regard to certain properties. Particularly, the correctness of the pressure control of the coking drum during the pressure test was verified.

4. Conclusions

By utilizing the DC/FT approach, a formalization of the specification using intuitive data formats replaces the informal and manual implementation procedure. Based on the

formalized specification, all parties involved can discuss the control logic and find possible errors in the specification as well as implementation errors. Furthermore, the hierarchical and modular structure of DC/FT is partly preserved and recognizable in the SFC. Although no real hierarchy is defined for SFC, this well-arranged structure improves the readability and maintainability of the SFC code. The DC/FT paradigm provides an intuitive and systematic approach to the design of logic controllers that covers the complete design sequence, from early specification to implementation.

The explicit documentation of knowledge and expertise of all members of the team, irrespective of their technical background and in a format that is understandable for other design team members, greatly simplifies the detection of design errors and their correction and thus ensures a high quality of the designed controller. The methodology and the prototype tool were proven to have the potential to improve the current design flows by reducing errors and facilitating later changes. The hierarchical and modular structure of the DC/FT formalism enables the designers to reuse parts of the controller code to further improve the efficiency of the development process. The controller can also be exported into the CIF (Sonntag & Fischer (2010)) to validate the controller together with an accurate plant model (including continuous plant dynamics).

References

IEC 61131-3, 2003. Programmable Controllers – Programming Languages.

Ferrarini, L. and Piroddi, L., 2003. Modular Design and Implementation of a Logic Control System for a Batch Process, Computers and Chemical Engineering, 27(7), 983-996.

Klein, S., Frey, G., and Litz, L.,2003. Designing Fault Tolerant Controllers Using SIPN and Model-Checking. Proc. IFAC-Safeprocess, 115-120.

Maler, O., Pnueli, A., and Sifakis, J., 1995. On the Synthesis of Discrete Controllers for Timed Systems. Proc. Theoretical Aspects of Computer Science, STACS'95.

Ramadge, P. and Wonham, W., 1989. The Control of Discrete Event Systems. Proc. of IEEE, 77(1), 81-98.

Stursberg, O., 2005. Supervisory Control of Hybrid Systems Based on Model Abstraction and Guided Search. Nonlinear Analysis, 65(6), 1168-1187.

Provost, J., Roussel, J.M., and Faure, J.M., 2009. Test Sequence Construction from SFC Specification. Proc. Dependable Control of Discrete Systems, 341-346.

Stursberg, O. and Lohmann, S., 2005. Analysis of Logic Controllers by Transformation of SFC into Timed Automata. Proc. CDC/ECC, 7720-7725.

L'Her, D., Le Parc, P., and Marce, L., 2001. Proving Sequential Function Chart Programs Using Timed Automata. Theoretical Computer Science, 267(1-2), 141-155.

Fujino, K., Imafuku, K., Yamashita, Y., and Nishitani, H., 2000. Design and Verification of the SFC Program for Sequential Control. Comp. and Chem. Eng., 24(2-7), 303-308.

Fischer, S.; Hüfner, M.; Sonntag, C.; Engell, S., 2011. Systematic Generation of Logic Controllers in a Model-Based Multi-Formalism Design Environment. Proc. IFAC World Congress, 12490-12495.

Lohmann, S. and Engell, S., 2008. Systematic Logic Controller Design as Sequential Function Chart Starting from Informal Specifications. Chin. Journal of Chem. Eng., 32, 43-47.

Lucas, M.R. and Tilbury, D.M., 2004. The Practice of Industrial Logic Design. Proc. American Control Conference, 1350-1355.

Larsen, K.G., Pettersson, P., and Yi, W., 1997. Uppaal in a Nutshell. International Journal on Software Tools for Technology Transfer, 1(1–2), 134-152.

van Beek, B., Reniers, M.A., Rooda, J.E., and Schiffelers, R.R.H., 2008. Concrete Syntax and Semantics of the Compositional Interchange Format for Hybrid Systems. Proc. IFAC World Congress, 7979–7986.

Sonntag, C.; Fischer, S., 2010 Translating Sequential Function Charts to the Compositional Interchange Format for Hybrid Systems. Proc. CDC, 4250-4256.

I.A. Karimi and Rajagopalan Srinivasan (Editors), Proceedings of the 11th International Symposium on Process Systems Engineering, 15-19 July 2012, Singapore

A Mixed Integer Quadratic Reformulation of the Quadratic Assignment Problem with Rank-1 Matrix

Otto Nissfolk[a] * Ray Pörn[a] Tapio Westerlund[a] Fredrik Jansson[b]

[a] *Center of Excellence in Optimization and Systems Engineering, Åbo Akademi University, Biskopsgatan 8, 20500 Åbo, Finland*

[b] *Department of Physics and Material Sciences Center, Philipps-Universität Marburg, Renthof 6, D-35032 Marburg, Germany*

Abstract

This paper focuses on the formulation and solution of certain quadratic assignment problem (QAP). A new mixed integer quadratic programming (MIQP) formulation of the QAP is presented that is especially well suited for solving instances where the flow or distance matrix is of rank-1. Computational experiments are conducted on some special generated instances as well as on some instances from the QAPLIB (Burkard et al., 1997; QAPLIB, 2012). The QAP is solved using a two-stage procedure. The objective is first simplified as a result of the rank-1 assumption and thereafter the quadratic objective is convexified. The resulting convex MIQP is then solved with a suitable solver.

Keywords: Quadratic assignment problem (QAP), mixed integer quadratic programming (MIQP), semidefinite programming (SDP), quadratic convex reformulation (QCR)

1. Introduction

This paper addresses the important task of solving certain classes of the Quadratic Assignment Problem introduced by Koopmans and Beckmann in 1957. The QAP is a problem where n facilities and n locations are given with specified flows and distances between the facilities and locations, respectively. The cost is a function of the distances and flows between the facilities and an additional cost may be associated with placing a facility at a certain location. The overall objective is to minimize the total cost of placing each facility to a certain location. In addition to facility layout problems, the QAP appears in applications such as backboard wiring (Steinberg, 1961), scheduling (Geoffrion and Graves, 1976), gray pattern generation (Taillard, 1995) and many other.

In its basic form QAP is a non-convex 0-1 quadratic program. A common approach for solving QAPs is based on using different types of linearizations. A linearization procedure overcomes the quadratic structure by introducing a set of new variables and additional linear and binary constraints. Linearization techniques can also be used to obtain bounds for QAP problems. Different heuristics have also proved to be efficient to obtain bounds, but optimality of such solutions cannot be proven (Burkard et al., 1998).

The paper is organized as follows. The different quadratic formulations are introduced in section 2. The set of testproblems and well-known linearizations are presented in section 3. Section 4 contains the solution results and section 5 concludes the paper.

*Otto.Nissfolk@abo.fi

2. Problem formulation

2.1. The Quadratic Assignment Problem

The quadratic assignment problem introduced by Koopmans and Beckmann (1957) has the following form:

$$\min_{x\in X} \sum_{i=1}^{n}\sum_{j=1}^{n}\sum_{k=1}^{n}\sum_{l=1}^{n} f_{ik}d_{jl}x_{ij}x_{kl} + \sum_{i=1}^{n}\sum_{j=1}^{n} c_{ij}x_{ij} \tag{1}$$

$$\text{where } X = \{x| \sum_{j=1}^{n} x_{ij} = 1 \quad i \in N, \sum_{i=1}^{n} x_{ij} = 1 \quad j \in N, x_{ij} \in \{0,1\} \quad i,j \in N\} \tag{2}$$

and f_{ik} is the flow between facilities i and k, d_{jl} is the distance between locations j and l, and c_{ij} is the cost of placing facility i at location j. The variable $x_{ij} = 1$ if facility i is assigned to location j, otherwise, $x_{ij} = 0$ and $N = \{1,2,\ldots,n\}$. With no loss of generality we can assume that $c_{ij} = 0$ and omit the linear term in (1). In this paper we also assume that the flow and distance matrices are symmetric.

2.2. Trace formulation

Another popular formulation of the QAP is the trace formulation (Edwards, 1980). If $\mathbf{F}$ and $\mathbf{D}$ are given flow and distance matrices and $\mathbf{X}$ the permutation matrix with elements defined by (2) the quadratic objective in (1) (with $c_{ij} = 0$) can be expressed using the trace-operator according to

$$\sum_{i=1}^{n}\sum_{j=1}^{n}\sum_{k=1}^{n}\sum_{l=1}^{n} f_{ik}d_{jl}x_{ij}x_{kl} = \text{tr}(\mathbf{DXFX}^T).$$

2.3. QAP with rank-1 flow matrix

We assume that the flow matrix (or distance matrix) is of rank-1, i.e. $\mathbf{F} = \mathbf{qq}^T$ for some vector $\mathbf{q} = (q_1,\ldots,q_n)^T$. The quadratic part of the objective function (1) can, in this case, be restated as

$$\sum_{i=1}^{n}\sum_{j=1}^{n}\sum_{k=1}^{n}\sum_{l=1}^{n} f_{ik}d_{jl}x_{ij}x_{kl} = \text{tr}(\mathbf{DXFX}^T) = \text{tr}(\mathbf{DXqq}^T\mathbf{X}^T) = \text{tr}(\mathbf{Dyy}^T) = \mathbf{y}^T\mathbf{Dy}$$

where **y=Xq**, i.e. $\mathbf{y}$ is a permutation of $\mathbf{q}$. By substituting, $y_i = \sum_{j=1}^{n} q_j x_{ij}$ we then get a quadratic problem of the form

$$\min_{x\in X, y\in\mathbb{R}^n} \mathbf{y}^T\mathbf{Dy} \tag{3}$$

$$\text{subject to } y_i = \sum_{j=1}^{n} x_{ij}q_j \quad \forall i, \quad \sum_{i=1}^{n} y_i = \sum_{j=1}^{n} q_j \tag{4}$$

Problem (3-4) is a mixed integer quadratic optimization problem with n continuous, n^2 binary variables of SOS1-type and $n+1$ linear constraints. The objective function is not necessarily convex.

2.4. Convex QAP with rank-1 flow matrix

In order to efficiently solve the quadratic formulation defined in section 2.3 we have to convexify the objective (3). The convexification can be done, for example, by adding the smallest eigenvalue to the diagonal so that $\text{Diag}(\mathbf{u}) = -\lambda_{min}(\mathbf{D})\mathbf{I}$ or by using the QCR-method (Billionnet et al., 2009). By solving an SDP problem we will get an optimal $\mathbf{u}$-vector so that the lower bounding is as tight as possible. If we add $\mathbf{u}$ to the diagonal of $\mathbf{D}$ then we have to subtract new variables $\mathbf{z}(z_i = y_i^2)$ to obtain the same objective value as in (3).

$$\min_{x \in X,\, y,z \in \mathbb{R}^n} \mathbf{y}^T(\mathbf{D} + \text{Diag}(\mathbf{u}))\mathbf{y} - \mathbf{u}^T\mathbf{z} \tag{5}$$

$$\text{subject to } y_i = \sum_{j=1}^{n} x_{ij} q_j, \quad z_i = \sum_{j=1}^{n} x_{ij} q_j^2 \quad \forall i, \quad \sum_{i=1}^{n} y_i = \sum_{j=1}^{n} q_j \tag{6}$$

Problem (5-6) is a convex MIQP with $2n$ continuous, n^2 binary variables and $4n+1$ constraints (counting SOS1-constraints). This formulation is referred to as QAP-r1. If the vector $\mathbf{q}$ contains many identical elements, an alternative formulation can be derived. Let $\{v_1, \ldots, v_m\}(m \leq n)$ be the distinct values in $\mathbf{q}$ and $\{f_1, \ldots, f_m\}$ the corresponding frequencies. This observation leads to a slightly different formulation.

$$\min_{y,z \in \mathbb{R}^n} \mathbf{y}^T(\mathbf{D} + \text{Diag}(\mathbf{u}))\mathbf{y} - \mathbf{u}^T\mathbf{z} \tag{7}$$

$$\text{s.t. } y_i = \sum_{j=1}^{m} x_{ij} v_j,\ z_i = \sum_{j=1}^{m} x_{ij} v_j^2,\ \forall i, \quad \sum_{i=1}^{n} y_i = \sum_{j=1}^{m} f_j v_j,\ f_j = \sum_{i=1}^{n} x_{ij}\ \forall j, \quad \sum_{j=1}^{m} x_{ij} = 1\ \forall i \tag{8}$$

Problem (7-8), referred to as QAP-r1-freq, is also a convex MIQP but with $2n$ continuous, nm binary variables and $3n+m+1$ constraints. Formulation (7-8) does, however, not give the optimal permutation of q only the optimal objective value. If $m << n$ the formulation QAP-r1-freq is considerably smaller than formulation QAP-r1.

3. Testproblems

The problems solved in this paper are gray-scale pattern instances (Taillard, 1995) and rank-1 approximations of all symmetric problems from the QAPLIB (2012). The problems are solved using CPLEX 12.2.0.0 on a Intel i7-930 processor with 6GB RAM running Windows 7.

3.1. Linearizations

The linearizations XYL and GLL (Zhang et al., 2012) are used as comparison to the quadratic formulations of rank-1 QAP. Both XYL and GLL have n^2 continuous variables, n^2 binary variables and $2n^2$ constraints.

3.2. Taixxc-problems

The taixxc problems found in the QAPLIB are of size 8×8 and 16×16. These problems are too large for testing so we created some smaller instances using the formula found

in (Taillard, 1995). The tai36c problem that is used in 4.2 is a grayscale problem of size 6×6. In these instances, the flow and distance matrices are defined as follows:

$$T_{rstu} = \max_{v,w \in \{-1,0,1\}} \frac{1}{(r-t+nv)^2 + (s-u+nw)^2}$$

$$f_{ij} = \begin{cases} 1 & \text{if } i \leq m \text{ and } j \leq m \\ 0 & \text{otherwise} \end{cases}, \quad d_{ij} = d_{n(r-1)+s \quad n(t-1)+u} = T_{rstu}$$

4. Results

4.1. QAPLIB-results

First all symmetric problems, 111 out of 135 in total, from QAPLIB (2012) are approximated as rank-1 problems and then solved for 1800 seconds. The solutions times for the four different formulations are the compared using performance profiles showing the solution time versus number of problems solved. As one can see from figure 1 the QAP-

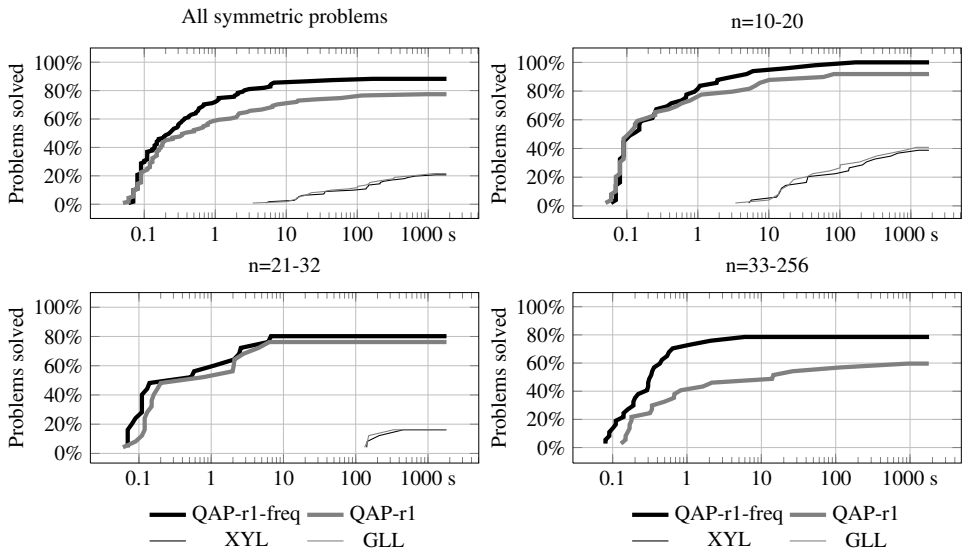

Figure 1. Percentage of problems solved within the timelimit of 1800 s

r1-freq formulation seems to be the best, solving about 90% of all problems followed by QAP-r1 formulation solving a bit over 80% of all problems. As one could expect, the linearizations are quite similar and not as good as the quadratic ones, both solving around 20% of all problems. The linearizations work on small problems but the quadratic formulations are the best approach for these problems.

4.2. Taixxc-results

In figure 2 the results for the tai36c problem are presented. The b-values on the x-axis correspond to different densities of gray where $b = 0$ is all white and $b = 36$ is all black. The timelimit for the solver is set at 1800 seconds. The solution time of instances with gray

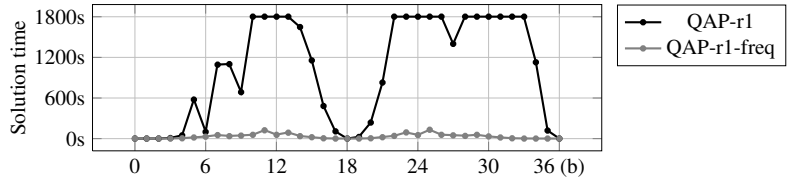

Figure 2. Solution times of the tai36c problem

density close to 50% is very low, since the gray pattern will resemble a checkerboard and therefore there are very few good solutions. Instances with gray density close to 0% and 100% are also easy since they correspond to almost all white and all black, respectively. The intermediate instances are difficult since there exists many near-optimal patterns. The QAP-r1-freq formulation is the better one for solving these problems.

5. Conclusions

In this paper two MIQP formulations of rank-1 QAPs were derived. The results show that the formulations are efficient for solving QAPs with a rank-1 flow matrix. The QAP-r1-freq formulation seems to be the most efficient approach. This is due to a model with fewer binary variables than QAP-r1. The drawback with QAP-r1-freq is that the solution only contains the objective value but no information about the permutation vector.

References

Billionnet, A., Elloumi, S., Plateau, M.-C., March 2009. Improving the performance of standard solvers for quadratic 0-1 programs by a tight convex reformulation: The QCR method. Discrete Appl. Math. 157, 1185–1197.

Burkard, R., Cela, E., Pardalos, P., Pitsoulis, L., 1998. Handbook of Combinatorial Optimization. Vol. 3.

Burkard, R. E., Karisch, S. E., Rendl, F., June 1997. Qaplib – a quadratic assignment problem library. J. of Global Optimization 10, 391–403.

Edwards, C. S., 1980. A branch and bound algorithm for the Koopmans-Beckmann quadratic assignment problem. Combinatorial Optimization II 13, 35–52.

Geoffrion, A., Graves, G., 1976. Scheduling parallel production lines with changeover costs. Operations Research 24, 595–610.

Koopmans, T. C., Beckmann, M., 1957. Assignment problems and the location of economic activities. Econometrica 25 (1), pp. 53–76.

QAPLIB, 2012. http://www.seas.upenn.edu/qaplib/inst.html.

Steinberg, L., 1961. The backboard wiring problem: A placement algorithm. SIAM Review 3 (1), 37–50.

Taillard, D., 1995. Comparison of iterative searches for the quadratic assignment problem. Location Science 3 (2), 87 – 105.

Zhang, H., Beltran-Royo, C., Ma, L., 2012. Solving the quadratic assignment problem by means of general purpose mixed integer linear programming solvers. Annals of Operations Research, 1–18.

I.A. Karimi and Rajagopalan Srinivasan (Editors), Proceedings of the 11th International Symposium on Process Systems Engineering, 15-19 July 2012, Singapore.

Uncertainty evaluation for multivariate industrial processes

Reiner Requião[a], M.A.F. Martins[a], Ricardo de Araújo Kalid[a], Rafael de Pelegrini Soares[b]

[a]*Research Group on Process Uncertainty at theFederal University of Bahia, Rua Aristides Novis, 02, Sala 6.1.18, Federação, Salvador, CEP 40210-630, Brazil*
[b]*Federal University of Rio Grande do Sul (UFRGS), Porto Alegre, Brazil*

Abstract

The paper presents a supplement for the equation-oriented process simulator EMSO - Environment for Modeling Simulation and Optimization – which automatically evaluates the uncertainty of process output variables. Two methods for the evaluation of process uncertainty in multivariate systems have been implemented, namely: MLPU (Multivariate Law of Propagation of Uncertainties) and MLPP (Multivariate Law of Propagation of Probability Density Functions). For illustrative purposes, a comparative analysis of both approaches is carried out in a typical nonlinear industrial process system: a continuous stirred-tank reactor (CSTR). The paper finally closes with a discussion which raises some issues for future work.

Keywords: Propagation of Uncertainties, Multivariate Systems, Probability Density Functions, EMSO.

1. Introduction

Modeling and simulation are common tools in the engineering field and its use often results in multivariate systems (MIMO - Multiple Input Multiple Output). These systems are usually described by implicit nonlinear equations. In general, the simulation software available does not evaluate the uncertainties associated with the variables and rarely discloses the equipment models used, which with some effort allow the calculation of these uncertainties.

On the other hand, the available specialized software for uncertainty evaluation cannot usually handle multivariate systems and are not integrated with the simulators of industrial processes. In order to overcome these limitations, we have developed a new module for the software EMSO - Environment for Modeling Simulation and Optimization – namely *Uncertainty*. This module can evaluate the uncertainties associated with variables of nonlinear multivariate models in the steady-state. EMSO is a general equation-oriented process simulator. It can handle both dynamic and steady-state models and implements its own object-oriented modeling language. The simulator comes with an extensive library of models for chemical processes and allows the user to create new equipment models. Furthermore, it is accompanied by a series of numerical packages for solving a wide range of problems and it also contains modules to perform case studies, sensitivity analysis, optimization, data reconciliation, among others (Soares & Secchi 2003).

The purpose of this paper is to present the *Uncertainty* module developed for EMSO that performs the best estimates and the covariance matrix of output variables of industrial processes through methods based on the MLPU approach - Multivariate Law

of Propagation of Uncertainty (Lira 2002) - and the MLPP approach - Multivariate Law of Propagation of Probability Density Functions (PDF) which uses a Monte Carlo method (MCM) (Martins & Kalid 2011); these two approaches are in accordance withSupplement 2 of the Guide to the Expression of Uncertainty in Measurement (GUM S2) (BIPM et al. 2011).

2. Methods

The problem addressed here consists of a multivariate process model with various output quantities Y_j related directly to several input quantities X_i through known functional relationships of the form

$$\begin{cases} h_1\left(Y_1, \dots, Y_j, \dots Y_K; X_1, \dots, X_i, \dots X_N\right) = 0 \\ \vdots \\ h_K\left(Y_1, \dots, Y_j, \dots Y_K; X_1, \dots, X_i, \dots X_N\right) = 0. \end{cases} \tag{1}$$

The set of model relations (1) is generally determined from phenomenological (conservation laws and constitutive equations) or empiric modeling. In some simple cases the equations may be solved analytically, however, a numerical solution is usually mandatory in cases of nonlinear systems. In matrix notation, (1) can be written in a more compact form as follows:

$$\mathbf{h}(\mathbf{Y};\mathbf{X}) = \mathbf{0}, \tag{2}$$

where $\mathbf{h} = (h_1, \dots h_K)^{\mathrm{T}}$, the symbol $\mathbf{0}$ stands for a column vector with all elements equal to zero. From the formulation set out above, the MLPU and MLPP approaches are outlined in the following two subsections.

2.1. MLPU approach

The MLPU approach consists of propagating the vector of input estimates ($\mathbf{x}$) and its covariance matrix ($\mathbf{U_X}$) through a first-order Taylor series approximation of the process model for evaluating the vector of estimates ($\mathbf{y}$) and the associated covariance matrix ($\mathbf{U_Y}$) of the output quantities (measurands). The key features of this approach are summarized hereafter:

(1) Set up the model process, estimates and associated covariance matrix of the input quantities, $\mathbf{x}$ and $\mathbf{U_X}$, respectively;

(2) Compute the estimates of the output quantities through the solution of multivariate model $\mathbf{h}(\mathbf{y};\mathbf{x}) = \mathbf{0}$;

(3) Compute the sensitivity matrix or both input and output quantities, evaluated at the estimates $\mathbf{y}$ and $\mathbf{x}$:

$$\mathbf{C_X} = \begin{pmatrix} \frac{\partial h_1}{\partial x_1} & \cdots & \frac{\partial h_K}{\partial x_1} \\ \vdots & \ddots & \vdots \\ \frac{\partial h_1}{\partial x_N} & \cdots & \frac{\partial h_K}{\partial x_N} \end{pmatrix} \text{ and } \mathbf{C_Y} = \begin{pmatrix} \frac{\partial h_1}{\partial y_1} & \cdots & \frac{\partial h_K}{\partial y_1} \\ \vdots & \ddots & \vdots \\ \frac{\partial h_1}{\partial y_K} & \cdots & \frac{\partial h_K}{\partial y_K} \end{pmatrix};$$

(4) Compute the covariance matrix associated with the output quantities as follows: $\mathbf{U_Y} = \mathbf{C}^{\mathbf{T}}\mathbf{U_X}\mathbf{C}$, where $\mathbf{C} = (-\mathbf{C_Y^{-1}}\mathbf{C_X})^{\mathbf{T}}$.

2.2. MLPP approach

Compared to MLPU,a more general approach is adopted by MLPP. MLPP treats the numerical evaluation of process uncertainty with a Monte Carlo method (MCM) as an

implementation of the propagation of probability density functions (PDFs). The basic idea of the MLPP approach is to draw random samples from the joint PDF assigned to the input quantities $g_{\mathbf{X}}(\boldsymbol{\xi})$ and propagate these samples through the model (2) to yield the joint PDF associated with the output quantities $\mathrm{g}_{\mathbf{Y}}(\boldsymbol{\eta})$; here the possible values of the input and output quantities are denoted respectively as $\boldsymbol{\xi} = [\xi_1, \ldots, \xi_n]^{\mathrm{T}}$ and $\boldsymbol{\eta} = [\eta_1, \ldots, \eta_K]^{\mathrm{T}}$. An algorithm for this method follows:

(1) Draw a set $\{(\xi_1^1, \ldots, \xi_N^1), \ldots, (\xi_1^M, \ldots, \xi_N^M)\}$ of M independent samples from $g_{\mathbf{X}}(\boldsymbol{\xi})$;

(2) Compute M samples for the output quantities using the model (2), at least 10^4:

$F(\boldsymbol{\eta}^r; \boldsymbol{\xi}^r) = \mathbf{0}, \quad r = 1, \ldots, M$. These samples constitutes a set of independent random deviates from $g_{\mathbf{Y}}(\boldsymbol{\eta})$.

(3) Calculate the estimates y and its covariance matrix $\mathbf{U}_{\mathbf{y}}$ according to equations:

$$y_j = \frac{1}{M}\sum_{r=1}^{M} \eta_j^r, \quad j = 1, \ldots, K \tag{3}$$

$$U_y(i,j) = \frac{1}{M-1}\sum_{r=1}^{M} (\eta_i^r - y_i)(\eta_j^r - y_j), \quad i,j = 1, \ldots, K \tag{4}$$

3. *Uncertainty* module

The *Uncertainty* module is designed to be versatile software, i.e. it allows the user to provide the estimate of the input quantities and its correlation matrix or combined uncertainty or the parameters of their PDF as well as set up the simulation parameters, such as number of simulations of the MCM, tolerance, iterations etc. A general picture of the *Uncertainty* module structure and its components (input and output data) is shown in Figure 1.

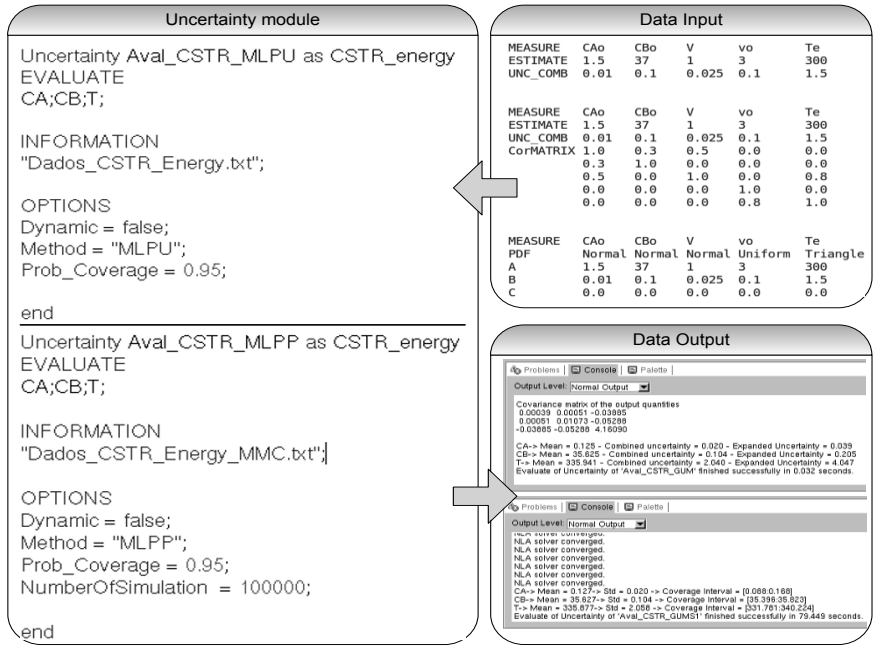

Figure 1.General vision of the *Uncertainty* EMSO module structure and its components.

To use *Uncertainty,* one needs a process model (*FlowSheet*) that runs at steady-state and then this module converts the process equations into a multivariate process model like (2) in order to evaluate the estimate and the covariance (uncertainty) matrix of all output quantities, using both the MPLU and the MLPP approaches.

4. Case Study: a CSTR

CSTR is an industrial equipment that may be described by a system of nonlinear implicit algebraic equations, obtained from mass and energy balances combined with reaction rates:

$$\begin{cases} C_A = \dfrac{v_0 . C_{A0}}{v_0 + V . k_0 . e^{-\frac{E}{R.T}}} \\ C_B = C_{B0} + \nu_2 . (C_{A0} - C_A) \\ \sum_{i=1}^{n} C_{i0} . Cp_i . (T - T_e) + (C_{A0} - C_A) . \nu_i . \left(H^{\circ}_{i,R}(T_R) . Cp_i . (T - T_R) \right) = 0, \end{cases} \quad (5)$$

where C_{i0}, Cp_i e $H^{\circ}_{i,R}$ are the initial concentration, specific heat at constant pressure and formation enthalpy at reference temperature (T_R), respectively, for each substance i; E is the activation energy; R is the universal gas constant; k_0 is the frequency factor; ν_i is the vector of reaction stoichiometric coefficients; these variables are considered parameters with negligible uncertainties. For this particular case, or for more information about reaction modeling in general see (Fogler 2002).

The volumetric flow rate (v_0), reactor volume (V), initial concentration of the reactants A (C_{A0}) and the B (C_{B0}) and inlet temperature (T_e) are input quantities of the process model. For each of these input quantities a Gaussian PDF was assigned with the expectation and standard deviation equal to the estimate and standard uncertainty presented in Table 1, respectively.

Table 1.Estimate and process uncertainties of the input quantities.

Input quantities	C_{A0}/(kmol.m^{-3})	C_{B0}/(kmol.m^{-3})	v_0/(m^3.h^{-1})	V/m^3	T/K
Estimate	1.5×10^{0}	3.7×10^{1}	3.0×10^{0}	1.0×10^{0}	3.0×10^{2}
Standard uncertainty[1]	1.0×10^{-2}	1.0×10^{-1}	1.0×10^{-1}	2.5×10^{-2}	1.5×10^{0}
PDF	Gaussian	Gaussian	Gaussian	Gaussian	Gaussian

[1] This is evaluated according to section 5.1.2 of GUM S1 (BIPM et al. 2008).

The purpose of this case is to evaluate the estimate and the covariance matrix, using the MLPU and MLPP approaches, for the following output quantities: final concentration of A (C_A) and B (C_B) and the discharge temperature (T). These results are shown in Table 2 and 3.

As can be seen for the given case study, the results of the MLPU and MLPP approaches are fairly close in this operating point. Even though the difference in the results of both methods is negligible in this example, the MLPP approach is expected to provide a more reliable uncertainty evaluation than that given by MLPU, mainly when the process model is strongly nonlinear (Martins et al. 2011). Nevertheless, MLPP requires rather more computational effort (see the processing time of both methods in Table 2 and 3), which is proportional to the size of M samples; in addition, it can accumulate numerical errors when the computational algorithm of the random numbers generator is not carefully developed.

5. Conclusions

In this paper, we presented the new *Uncertainty* module developed within the equation-oriented process simulator EMSO. This module evaluates the uncertainties for the output quantities of general process models based on methods recognized internationally for this task, namely MLPU and MLPP. The tool developed here can be used to evaluate uncertainty in process analysis, design of equipment or industrial process optimization considering measurement uncertainty. For future works, our goals for the *Uncertainty* EMSO module are: (i) to build the coverage region associated with the output quantities with support for processes composed of more than 1000 variables; and (ii) to implement other methods for the evaluation of uncertainty, such as the Bayesian and Kragten multivariate methods for either dynamic or steady models.

Table 2.Estimate and standard uncertainties of the output quantities using the MLPU approach.

Output quantities	Estimate	Standard uncertainty	Correlation		
			C_A	C_B	T
$CA/(\mathrm{kmol/m^3})$	125.0×10^{-2}	2.0×10^{-2}	1.00	0.25	-0.96
$CB/(\mathrm{kmol/m^3})$	356.3×10^{-1}	1.0×10^{-1}	0.25	1.00	-0.25
T/K	335.9×10^{0}	2.1×10^{0}	-0.96	-0.25	1.00
Processing Time		0.012 seconds			

Table 3.Estimate and standard uncertainties of the output quantities using the MLPP approach using $M = 10^5$ samples.

Output Quantities	Estimate	Standard Uncertainty	Correlation		
			C_A	C_B	T
$CA/(\mathrm{kmol/m^3})$	127.0×10^{-2}	2.0×10^{-2}	1.00	0.25	-0.96
$CB/(\mathrm{kmol/m^3})$	356.3×10^{-1}	1.0×10^{-1}	0.25	1.00	-0.25
T/K	335.9×10^{0}	2.1×10^{0}	-0.96	-0.25	1.00
Processing Time		71.388 seconds .			

References

BIPM et al., 2011. Evaluation of measurement data – Supplement 2 to the "Guide to the expression of uncertainty in measurement" – Models with any number of output quantities, Joint Committee for Guides in Metrology - JCGM 102:2011.

BIPM et al., 2008. Evaluation of measurement data — Supplement 1 to the "Guide to the expression of uncertainty in measurement" — Propagation of distributions using a Monte Carlo method 1st ed., Joint Committee for Guides in Metrology - JCGM 101:2008.

Fogler, H.S., 2002. Elementos de engenharia das reações químicas 3rd ed., Rio de Janeiro - BRA: LTC.

Lira, I.H., 2002. Evaluating the Measurement Uncertainty: Fundamentals and practical guidance 1st ed., Bristol, UK: Institute of Physics Publishing.

Martins, M.A.F. & Kalid, R.A., 2011. Métodos Clássicos para Avaliação da Incertaza de medição em Sistemas Multivariáveis. Sba: Controle e Automação Sociedade Brasileira de Automatica.

Martins, M.A.F., Requião, R. & Kalid, R.A., 2011. Generalized expressions of second and third order for the evaluation of standard measurement uncertainty. Measurement, 44(9), pp.1526-1530.

Soares, R. de P. & Secchi, A.R., 2003. EMSO: A New Environment for Modelling, Simulation and Optimisation. Computer Aided Chemical Engineering, 14(C), pp.947-952.

I.A. Karimi and Rajagopalan Srinivasan (Editors), Proceedings of the 11th International Symposium on Process Systems Engineering, 15-19 July 2012, Singapore

Frequency and Identification

Heinz A Preisig*
Dept of Chem Engineering; NTNU; Trondheim, Norway

Abstract

Process and model identification are very common operations in chemical engineering applications. Reasons are mainly that we do not have all information of the process and that we model processes only approximately. In the latter case we usually hope that the fitting of the model will smoothed out some of the modelling errors that we cannot avoid, such as approximating a distributed system by a network of lumped systems. The latter definitely implies that our models are usually not providing a good description for the high-frequency behaviour of our processes, which is not a surprise. But is it then clever to put a lot of effort into generating identification signals, excitation signals, that have a very high portion of high frequencies, such as steps, pulses and random switching / binary / multi-valued input signals? The answer is no, because indeed the high frequencies only hurt the estimate.

Keywords: dynamic system, software engineering, computational engineering

1. The issue

Modelling is central to most chemical engineering activities. If possible one uses mechanistic models that build on the conservation principles, but then many of the constituent models may not be white box models, but grey or black box models. The models, being parametrised can often be instantiated with parameters from the literature, but then not always everything is available and thus needs to be acquired through experimental means. Also, in all cases the model is not identical with the process, but is an approximate representation of the behaviour of the plant being modelled. And as such, modelling errors may make it necessary to fit the model to the plant thereby compensating for some of the modelling errors.

This paper is aiming at illustrating the latter problem, namely fitting a model, which we know has the wrong structure. Fitting the wrong model seems rather unreasonable, but it only reflects the fact that we cannot mimic the process in all details, thus we have to live with modelling errors. The objective of this paper is to provoke some thinking towards on how to choose the excitation signal for the model identification having some basic knowledge on where some modelling errors must exist. The paper does not attempt to provide theoretical answers, some of which can be found in the literature. The recent survey summarises many of the theoretical results Gevers et al. (2011). The paper focuses mainly on control. An analysis using wavelets that provides time-local frequency information is absent.

When modelling a process, we usually capture the steady-state behaviour well mainly because this is usually also a requirement, but we do not capture the fast parts accurately. This has many reasons but not at least because of the complexity associated with geometry, uniformity of material and distribution of mass and energy in the plant body.

*Heinz.Preisig@chemeng.ntnu.no

In order to fit of the model to the plant, we perform identification experiments, or experiments for regression, or calibrate the model, three terms being coined by three different communities. Each experiment injects an identification signal, a disturbance, that must be sufficiently exciting to let the process exhibit its properties. Literature coins the term "persistent excitation" (Ljung (1987); Goodwin and Payne (1977)) requesting that all modes are being excited. So the apparently save thing to do is to excite the whole spectrum, from low to high. The step input is satisfies these conditions and is often relatively easy to apply and thus a commonly applied input signal. In some communities one would also use pulse functions that are short but intensive enough to get as close as possible to an impulse. This to get the approximate impulse response, which provides the approximate residence time distribution of the analysed equipment.

Most processes exhibit the behaviour of infinite order, because natural systems are distributed. Making simple, lumped models, or approximating distributed systems as networks of lumped systems, makes it apparent, that these models do not capture the high-frequency behaviour of a the plant. A simple example is the use of overall heat transfer models for a energy being transferred from one fluid to another through a wall, for example in the form of heat: This model has no dynamics, as it assumes zero capacity effect of the physical transfer system.

Using excitation signals that cover the full range, or at least as much as possible, of the frequency range seems a save way of doing things. This contribution shows that this is not the case and that one should pay attention to the frequency range in which the model actually mimics the process relatively accurately.

2. A simple case to illustrate

2.1. The plant and the model

To illustrate the above-sketched problem, we use a nominal case, probably one of the simplest ones: For the process we use a second-order process with two time constants and for the model we use a first-order model. We use standard software, thus no particular sophisticated methods, tricks and no special conditions. The transfer function of the model and the plant are:

$$\text{plant}: \quad g_p(s) := \frac{1}{(T_1 s+1)(T_2 s+1)}, \qquad \text{with } T_1 := 1 \text{ and } T_2 := 0.1 \tag{1}$$

$$\text{model}: \quad g_m(s) := \frac{1}{(\tau_1 s+1)} \qquad \text{with } \tau_1 \text{ to be identified} \tag{2}$$

The Bode plot of the plant has two corner frequencies, one at 1 rad/s and one at 10 rad/s, whilst the model will only have one at the location we are going to identify through our identification experiments.

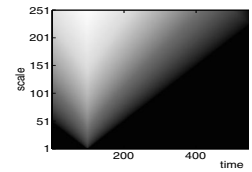

Figure 1. Haar wavelet coefficients for a step at t=100

2.2. Input signal: step

A step signal is the integral of an impulse, with the impulse exciting all the frequencies equally. The step thus also excites all frequencies. A wavelet analysis of the step clearly shows that the high frequencies are most active at the beginning of the step, which is at time 100, whilst the lower frequencies are becoming

more important later. This could also be deducted from a Fourier series representation of a pulse, where the high frequencies compensate each other in the centre of the pulse, whilst adding to form the steep ascent at the beginning and the equally steep decent at the other end.

2.3. Fitting the first-order model

It is apparent that this model, when excited with a step, will respond immediately: the slope at time zero is non-zero, whilst it is zero for our second-order plant. So in terms of the slope, the deviation is relative largest at the beginning and if one looks closer, the difference decreases later for most well-fitted models. The second effect one observes is a shift in the response, a reflection of the phase shift. Also, the extreme phase shift, at high frequencies, is double for the plant compared to the model.

The different frequencies are thus more or less "active" as time progresses when applying a step. In order to get a view on how different frequencies affect the identification, we shall use a package of well-defined frequencies to excite the system, namely a package of 8 sinusoidal functions that are logarithmically spaced in a frequency range.

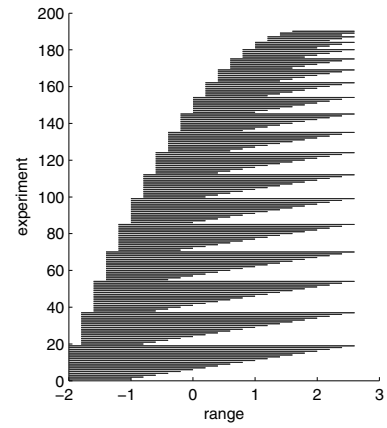

Figure 2. Frequency ranges for the 19 sets of experiments

A number of experiments are performed, whereby the range is changed and the input-output signals are used to fit a first-order model keeping the gain constant to the nominal value. Thus we only adjust the time constant in the identification focusing the dynamics.

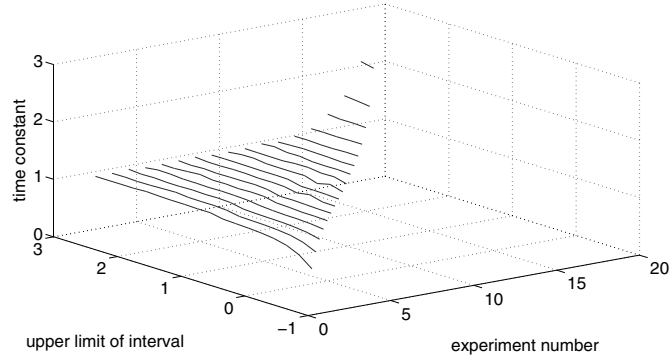

Figure 3. Experiments with packages of 8 sinusoidal. Each line is the set of experiment with range shown in Figure 2 with the upper limit changing.

The range is changed by setting a lower limit well below the first corner (1 rad/s)and extending the range step-wise at the upper end including more and more of the frequencies covering beyond the second corner (10 rad/s) up to 2.7 rad/s.

The upper limit is set to meet the Shanon condition for sampling, as the simulation of the plant is sampled at 0.001 s. Measuring the frequencies relative to the corner frequencies, the experiments begin with packages that are below the lower corner gradually increase the range including both. Next the lower limit is increased and the set of experiments is again performed until the packages cover a range up to the upper limit. The effect is that we get experiments covering only below and above the two corners and different ranges including both and one or the other.

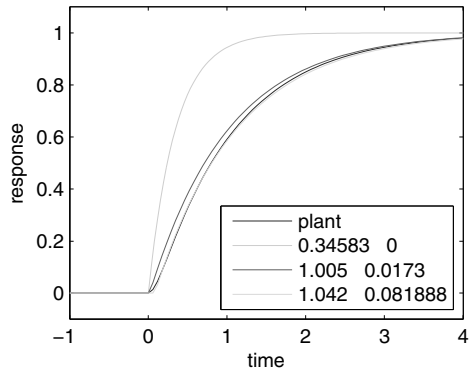

Figure 4. Step responses of different models compared with plant

Looking at the fit in the time domain, the step responses for an under-estimated, a well estimated and an over-estimated model are shown in Figure 4. The difference in the model is apparently large and most likely significant to any application. The figure also clearly reveals the second-order behaviour of the plant, specifically the zero slope at the beginning.

The frequency responses look similarly intriguing. Figure 5 shows the same three models and the plant in Bode plots.

Apparently the phase is not matched as the model's high-frequency phase shift is 90 degrees, whilst the plant has 180 degrees. Most likely, at this point control people would suggest a first-order-plus-dead-time model, which when fitted would do a better job on the phase. Indeed if we use the same experiments as above, this is the case, though only for frequency packages that are below the second time constant. Above things get hairy very quickly and the algorithms fail to provide an estimate. On the lower frequency package side nothing changes, the estimated dead time is zero. Figure 6 shows the situation in the frequency domain. for three models. The

Figure 3 shows the result. Using only a package of relative low frequencies results a time constant smaller than the dominating one. Increasing the range (see first experiment set) the estimate does change less and less, but increasingly monotonically towards the end (left end). The low estimate is due to not having the first corner frequency (located at 0) included in the range. As one moves the package range covering the two corners, the estimates get relatively constant though always increasing with the inclusion of higher frequencies. Once one is over the limit of including the lower corner frequency, which is a 1, the estimated time constant is increasing rapidly.

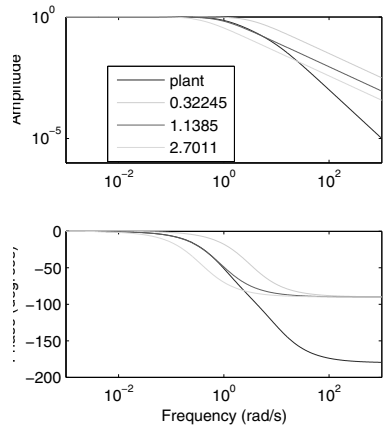

Figure 5. Step responses of different models without dead time compared with plant

three chosen experiments are the very first, thus the package clearly below the dominating time constant (green, top one), the second is the red one (second from the top, down turning in the phase plot) and the third is fitting best (third in the phase plot turning down most quickly). The step responses for the two last estimates look superb, whilst the first is equally bad as shown in Figure 4.

3. Discussion

The choice of frequencies for the excitation affects the model fidelity. The high frequencies for which the model deviates significantly from the plant, have clearly a negative effect on the estimated model parameter. The effect is most visible if one chooses the wrong frequency range. Obviously one would not use such extreme conditions. We did so because we want to make to problem visible. However, using steps or approximate steps or any other excitation signal that contains high frequencies, is not necessarily a good idea. The high frequency parts have clearly a negative effect on the estimate.

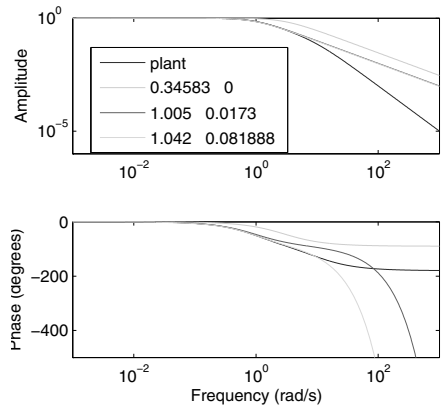

Figure 6. Step responses of different models with dead time compared with plant

Whilst this has the flavour of a negative statement, in reality this is usually quite happy news, because generating high frequency input is usually not easy to realise and in many cases inflicts quite a bit of costs. This because the state of a physical system can only be affected by the transfer of extensive quantity such as mass and energy. The flow is to be controlled with a valve or a corresponding device if it is not volume flow. Fast moving valves are usually more expensive than slow ones and similarly for tracer experiments high frequency injections are not easy to generate reproducible.

4. Conclusions

Spending effort on generating very fast changing inputs for the purpose of exciting the process for model fitting is usually not a good idea. The high frequencies, rather then adding information to the estimated model, actually usually reduce the fidelity of the model. Since we nearly always under-model our physical processes, the frequency range in which the model describes the process well, is limited and should be considered both in the identification task as well as in the utilisation of the model.

References

Gevers, M., Xavier, B., Hildebrand, R., Solari, G., 2011. Optimal design for open and closed-loop system identification. Communications in Information and Systems 11 (3), 197–224.

Goodwin, G. C., Payne, R. L., 1977. Dynamic system identification: Experiment design and data analysis. Academic Press.

Ljung, L., 1987. System Identification Theory for the User. Prentice Hall Inc. Englewood Cliffs, New Jersey.

I.A. Karimi and Rajagopalan Srinivasan (Editors), Proceedings of the 11th International Symposium on Process Systems Engineering, 15-19 July 2012, Singapore.

Real-time optimization of energy systems in sugar and ethanol facilities: a modifier adaptation approach

Fernán Serralunga, Miguel C. Mussati, Pio A. Aguirre

INGAR Instituto de Desarrollo y Diseño (CONICET-UTN), Avellaneda 3657, (S3002GJC) Santa Fe, Argentina.

Abstract

Real-time optimization (RTO) is used to operate industrial processes close to their minimum cost or maximum profit conditions. Model-based RTO needs an adaptation step to update the model under plant/model mismatch. This work proposes a novel RTO approach based on the modifier adaptation strategy, aiming to reduce the dimension of the gradient correction problem. The approach was tested in a model of a heat and power system of a sugar/ethanol facility. It could be also applied to other kind of processes. The results showed a noticeable performance improvement when compared to adaptation strategies without gradient correction.

Keywords: real-time optimization; energy optimization; sugar and alcohol industry.

1. Introduction

Sugarcane is nowadays the most efficient way to produce bioethanol at large scales. Due to improvements in process technology, sugar and ethanol plants have become energy self-sufficient, and they can export electric power by burning surplus bagasse. Optimal operating setpoints for the energy system in these plants can change along time, as result of changes in sugarcane quality, equipment performances (fouling), power price and production level. This encourages the use of real-time strategies to maximize performance or minimize energy costs. A recent work shows industrial application of computer-aided real-time tools for energy management in sugar and alcohol facilities (Mariani et al., 2009).

Real-time optimization (RTO) can be used to continuously improve the performance of an industrial process. Model-based RTO approaches need to deal with parametric and structural plant/model mismatch. Structural mismatch can make the system converge to operating points different to the real plant optimum. Some algorithms (ISOPE, modifier adaptation) have been developed to overcome this difficulty (Chachuat et al., 2009). They incorporate gradient correction terms aiming to match the Karush-Kuhn-Tucker conditions of the plant, making thus the model optimum coincident with the plant optimum, upon convergence.

Real-plant gradient estimation is not a trivial task. Some techniques make use of current and past data (Broyden methods, dual control, dynamic identification), other ones add perturbations to the plant around each steady state (finite forward differences, etc). (Mansour and Ellis, 2003, Srinivasan et al., 2011).

This work proposes a real-time optimization scheme for steam and power generation in a sugar plant with annexed ethanol production. The scheme is based on the modifier adaptation approach. It only adapts specific performance equations, such as those used for calculating boilers and turbines efficiencies and multiple-effect evaporation

coefficients. Data from current and past RTO cycles are used (Yip et. al., 2002). The algorithm is tested under different operating scenarios of the sugar/ethanol facility.

2. Real-Time Optimization

The proposed RTO approach assumes that all the parametric and structural uncertainty is included in a subset of equations, which calculate efficiencies and performances in pieces of equipment. The problem to solve can be stated as:

$$\begin{aligned} &\min_{\mathbf{u}} Q(\mathbf{y},\mathbf{u}) \\ &s.t.\ \ \mathbf{h}(\mathbf{y},\mathbf{u},\boldsymbol{\eta}) = \mathbf{0} \\ &\quad \mathbf{h}_m(\mathbf{u}) = \boldsymbol{\eta} \\ &\quad \mathbf{g}(\mathbf{y},\mathbf{u}) \le \mathbf{0} \\ &\quad \mathbf{u}_l \le \mathbf{u} \le \mathbf{u}_u \end{aligned} \tag{1}$$

where **y** are the process outputs, **u** the process inputs, **h** the process model (mass, energy and entropy balances, considered as free of uncertainty), and **g** inequality equations. $\boldsymbol{\eta}$ are performance or efficiency factors, whose functionality with process inputs is only known by an approximate model $\mathbf{h}_m(\mathbf{u})$.

In a RTO cycle *k*, after measurements validation and data reconciliation, the actual efficiency terms $\boldsymbol{\eta}_k$ can be known without the need of the uncertain equations $\mathbf{h}_m$. Therefore, equations $\mathbf{h}_m$ can be adapted to match the predicted value with the actual one. Modifier adaptation (Chachuat et al., 2009) would adapt the equations as:

$$\boldsymbol{\eta} = \mathbf{h}_m(\mathbf{u}) + \boldsymbol{\beta}_k + \boldsymbol{\lambda}_k^T(\mathbf{u} - \mathbf{u}_k) \tag{2}$$

where $\boldsymbol{\beta}_k = \boldsymbol{\eta}_k - \mathbf{h}_m(\mathbf{u}_k)$ is the so-called constraint modifier. $\boldsymbol{\lambda}_k = [\nabla\boldsymbol{\eta} - \nabla\mathbf{h}_m]_{\mathbf{u}=\mathbf{u}_k}$ is the gradient correction term. Under convergence, this approach matches a KKT point of the plant, and therefore both feasibility and optimality are guaranteed. Constraint adaptation (Chachuat et al., 2008) only includes the term $\boldsymbol{\beta}_k$ and no gradient correction; this guarantees feasibility but not optimality under structural mismatch.

This work proposes the following adaptation:

$$\eta_j = h_{m,j}(\mathbf{u}_k) + \gamma_{jk}(\mathbf{x}_j(\mathbf{u})) \qquad j = 1,2,..nj \tag{3}$$

where each efficiency η_j (being *nj* the total number of adapted equations) has an adaptation term γ_{jk}, which is a linear or quadratic function of a subset of states $\mathbf{x}_j$. Coefficients γ_{jk} are obtained from current and past data by linear regression:

$$\begin{aligned} &\min_{a_k,\mathbf{b}_k,C_k} \sum_{j=1}^{nj}\sum_{i=k-n}^{k} w_i(\beta_{ji} - \gamma_{ji})^2 \\ &s.t.\ \ \beta_{ji} = \eta_{ji} - h_{m,j}(\mathbf{u}_i) \\ &\quad \gamma_{ji} = a_{jk} + \mathbf{b}_{jk}^T \cdot \mathbf{x}_{ji} + \mathbf{x}_{ji}^T C_{ji} \mathbf{x}_{ji} \\ &\quad \mathbf{x}_{ji} = \mathbf{x}_j(\mathbf{u}_i) \\ &\quad a_j^L \le a_{jk} \le a_j^U \qquad\qquad j = 1..nj \\ &\quad \mathbf{b}_j^L \le \mathbf{b}_{jk} \le \mathbf{b}_j^U \qquad\qquad i = (k-n),\ldots,k \\ &\quad C_j^L \le C_{jk} \le C_j^U \end{aligned} \tag{4}$$

where a_{jk}, $\mathbf{b}_{jk}$ and C_{jk} are the coefficients of the regression. w_i is a weight factor that gets smaller as the data gets older and $n+1$ is the number of RTO cycles used in the regression. This allows having a data set with enough elements to eliminate the effect of noise, and at the same time to discard old data that could include different values of process disturbances. If the proposed function is a linear one, the method is similar to modifier adaptation, but using a special update method for the linear (gradient) term.

This method can be useful when each efficiency term is a function of a small subset of states. This situation can often be observed in heat and power systems as the one studied in this work. Indeed, by fixing the steam temperature and pressure, the performance of pieces of equipment like boilers and turbogenerators, is a function of the load, while process disturbances can remain approximately constant if the period analyzed is short.

3. Sugar and ethanol energy system model

A steady state model of a steam system of a sugar and ethanol facility was built. It includes two bagasse boilers, a set of turbines for cane milling, an extraction-condensing turbine for power generation, a 5-effect evaporator with vapor bleeding in the first 3 effects, and a set of steam demanding units (sugar boiling, ethanol distillation, steam deaerator). The diagram of the steam system is shown in Figure 1.

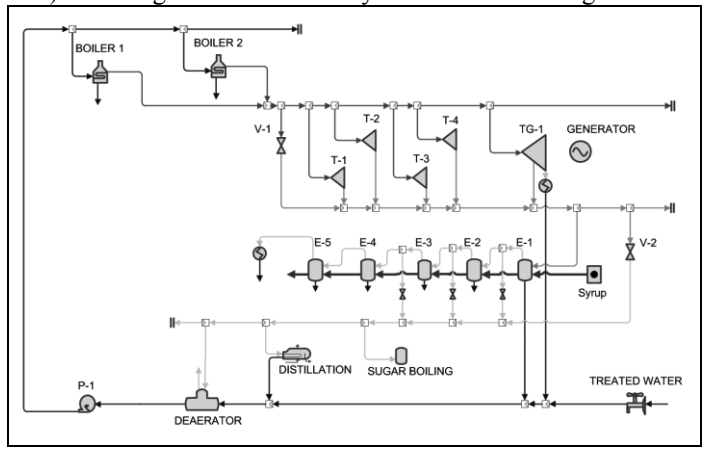

Figure 1. Diagram of the modeled steam system.

The model consists of mass, energy and entropy balances, and a set of equations that predict boiler and turbogenerator efficiencies, and evaporation coefficients in the evaporators. In order to evaluate the performance of the proposed RTO scheme, a different model (called hereafter "real plant") represents the real plant behavior. It consists of the same balance equations and a different set of equations to predict efficiencies and coefficients. Boiling point elevation in evaporator effects is calculated using correlations (Camargo, 1990) and is considered as free of error.

The real plant model is used to evaluate the evolution of the system after applying RTO results, and to provide data to the next RTO cycle. These data are used to adapt the model equations as described in the previous section. In order to simulate measurement errors and perform a data reconciliation step, the real plant simulation outputs are modified with a Gaussian noise prior to RTO calculations.

Table 1 lists RTO and real plant model equations. F_1 and F_2 are boiler steam flows, F_3 and F_4 are TG-1 admission and exhaust flows; T_3 is TG-1 extraction temperature; e is the evaporator effect. X_e and T_e are effect solids fraction and steam temperature.

Table 1. Real and RTO efficiency equations

	Real plant	RTO (h_{mj})
Boiler 1	$90-0.001(145-F_1)^2-10^{-6}F_1^3$	$92-0.005(150-F_1)^2$
Boiler 2	$91-0.001(155-F_2)^2-1.2\times10^{-6}F_2^3$	$93-0.005(150-F_2)^2$
TG-1 stage 1	$53-0.0023(120-F_3)^2+1\times10^{-6}F_3^3$	$70-0.005(130-F_3)^2$
TG-2 stage 2	$66-0.0018(50-F_4)^2+2.2\times10^{-6}F_4^3+10^{-2}T_3$	$70-0.004(41-F_4)^2$
Evaporation coefficients	$(0.0012-0.0001e)(96-X_e)(T_{e-1}-54)$ $-0.2(X_e/100)^2-0.5\exp(-(T_{e-1}-50)/100)$	$0.001(100-X_e)(T_{e-1}-54)$

Efficiency equations are adapted with second-order polynomials, which are functions of the equipment flow (even TG-1 2nd stage efficiency, which is actually also function of temperature). The quadratic terms can be different to zero only after 5 RTO cycles. Evaporation coefficients are adapted with a linear function of the live steam flow consumed in effect 1 (F_V). The optimization problem to solve in a k^{th} RTO cycle is:

$$\min_{\mathbf{u}} Q_1+Q_2-c_1W$$

$$s.t\quad \begin{cases} \mathbf{h}(\mathbf{F},\mathbf{P},\mathbf{T},\mathbf{B},W,Q_1,Q_2,\boldsymbol{\eta})=\mathbf{0} & \\ \eta_j=h_{mj}(F_j)+a_{jk}+b_{jk}F_j+c_{jk}F_j^2, & j=1\ldots4 \\ \eta_j=h_{mj}(F_j)+a_{jk}+b_{jk}F_V & j=5\ldots9 \\ \mathbf{F}_l\le\mathbf{F}\le\mathbf{F}_u & \\ \left\|F_j-F_{j,k}\right\|\le2.5 & j=1,2 \end{cases} \tag{5}$$

where **F, P** and **T** are steam flows, pressures and temperatures, W is the power produced by the turbogenerator. Q_1 and Q_2 are boiler fuel consumptions, **B** are the syrup Brix degrees in all evaporator effects. η_1 to η_4 are boiler and turbine efficiencies according to Table 1, and η_5 to η_9 are evaporation coefficients in effects 1 to 5. c_1 is the power cost. a_{jk}, b_{jk} and C_{jk} are the adaptation parameters (Eq. 4). **u** are the process inputs; in this case they are Boiler productions, TG-1 extraction and vapor bleeding in the evaporators. The last constraint is added to limit the size of changes in each RTO cycle.

4. Results

The performance of the proposed RTO scheme is analyzed under different scenarios. A starting operating point is simulated with the real plant model. After that, Gaussian noise is added to the results, and a data reconciliation step is performed using the RTO model, which allows calculating efficiencies and evaporator coefficients. The adaptation step is then performed, followed by RTO optimization. The calculated optimum inputs are used to simulate the real plant model, calculating the real cost achieved and starting the cycle again with noise addition and the data reconciliation step.

The results considering an evaporator feed of 500 m^3/h, initial and final Brix of 15 and 70, respectively, are shown in Figure 2, and compared with a constraint adaptation (CA) approach. Initial steam demand (distillation and sugar boiling) is of 200 t/h. The model parameters are $c_1=0.018$, $n=10$, $w_i=0.85^{k-i}$. The proposed adaptation shows convergence close to the real plant optimum in noise-free scenarios. When Gaussian noise is present, it shows better performance than CA for both constant and variable steam demand.

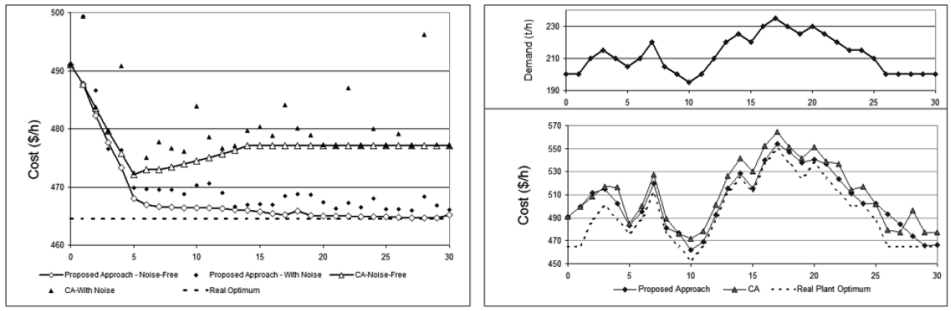

Figure 2. Cost evolution for 30 RTO cycles. Constant steam demand (left). Variable steam demand with noise (right). Gaussian noise standard deviation: Flow = 0.3 t/h, Temperature = 0.5°C, Fuel = 1 Gcal/h, Power = 25 kW.

Such performance comparisons were performed using Extended Design Cost (Zhang et al., 2000), which evaluates the distance from the real plant optimum. For constant demand, the relative costs are: CA without noise: *100*; CA with noise: *127*, proposed approach without noise: *30*, proposed approach with noise: *49*. For variable steam demand, CA: *100*, proposed approach: *62.5*.

5. Conclusions

A RTO approach based on modifier adaptation has been proposed, which has been shown to be efficient through a sugar and alcohol facility steam system. However, it could be applied straightforward to other industrial processes. The performance of the proposed scheme, which includes a correction of model gradients, was better than that using constraint adaptation, in line with theory and results of the mentioned references.
Energy systems in sugar/ethanol plants provide a wide range of opportunities for applying real-time optimization. In this line, the performance of RTO schemes under lack of instrumentation, measurement failures and non-steady behavior will be the objective of further research.

Acknowledgements: The authors gratefully acknowledge the financial support from CONICET and Soteica Latinoamérica S.A.

References

B. Chachuat, B. Srinivasan. and D. Bonvin, 2009, Adaptation strategies for real-time optimization. Computers & Chemical Engineering 33, 1557 – 1567.
B. Chachuat, A. Marchetti, and D. Bonvin, 2008. Process optimization via constraints adaptation. Journal of Process Control, 18(3-4), 244 – 257.
C. Camargo, A. Ushima, A.. Ribeiro, M. Souza, N. dos Santos, Manual de Recomendacões-Conservacão de Energia na Indústria do Açúcar e Álcool, Publicação IPT, São Paulo, 1990.
M. Mansour and J. Ellis, 2003, Comparison of methods for estimating real process derivatives in on-line optimization. Applied Mathematical Modelling 27, 275 – 291.
D. Mariani, . Kihn, and C. Ruiz, 2009. Industrial experience on the implementation of real time on line energy management systems in sugar and alcohol industry. Computer Aided Chemical Engineering, 27, 459 – 464.
B. Srinivasan, G. François and D. Bonvin, 2011, Comparison of Gradient Estimation Methods for Real-Time Optimization. Computer Aided Chemical Engineering, 29, 607-611.
W. Yip and T. Marlin, 2002. Multiple data sets for model updating in real-time operations optimization. Computers & Chemical Engineering, 26(10):1345 – 1362.
Y. Zhang, and J.F. Forbes, 2000, Extended design cost: a performance criterion for real-time optimization systems. Computers & Chemical Engineering 24, 1829 – 1841.

I.A. Karimi and Rajagopalan Srinivasan (Editors), Proceedings of the 11th International Symposium on Process Systems Engineering, 15-19 July 2012, Singapore.

On the Stability and Feasibility of Model Predictive Control

Supriyo K. Mondal,[a] Swapan Paruya,[a] S. S. Rao[b]

[a]*National Institute Technology, Durgapur 713209, India*
[b]*University of Miami, Florida 33124, USA*

Abstract

In this paper, we demonstrate the issues of feasibility, stability and performance of constrained finite receding horizon linear quadratic regulator (RHLQR) problems using primal-dual interior point (PDIP) method developed in FORTRAN. Instead of including path constraints, we have chosen sufficiently long horizon to achieve stability with finite horizon cost leading to Lyapunov function. We observed a significant improvement of stability of model predictive control using PDIP over active set method.
Keywords: feasibility, stability, performance

1. Introduction

The developments of model predictive control (MPC) deal with the existence of solution to optimal control problems. MPC for constrained linear and nonlinear systems essentially uses Lyapunov and Riccati stability theory. Feasibility, stability and performance are the important issues of MPC. It is always challenging to study the issues for making MPC more suitable in real-time applications. Survey of literature indicates that the studies on the issues began late seventy. Kwon and Pearson (1977) found cost function (J_N) to be non-increasing with length of horizon (N) by imposing an end constraints on the state (x(N)=0), which guarantees stability. Based on the exhaustive survey of literatures, Mayne et al. (2000) made generalization for ensuring closed-loop stability of MPC under terminal cost, terminal constraint set and local stabilizing controller. Primbs and Nevistic (2000) proved using the finite horizon cost (acting as a Lyapunov function) that a sufficient long horizon is required for feasibility and stability of a constrained receding horizon (RH) policy. Santos et al. (2008) demonstrated with the help of nonlinear programming techniques that constrained MPC is robustly stable for the case with modeling errors.

In this paper, we focus on the analysis of feasibility, stability and performance of constrained finite receding horizon linear quadratic regulator (RHLQR) problems adopted from published literatures. We do not consider any end constraint or terminal constraint. Instead, we suitably chose sufficiently long horizon to achieve stability with finite horizon cost leading to Lyapunov function. We show how the costly primal-dual interior point (PDIP) method for optimization makes an impact on the feasibility, stability and performance of MPC. As analyzed by Mondal et al. (2011), PDIP has a guaranteed feasibility property due to the barrier function used in PDIP. We expect to an improvement of feasibility and stability of MPC using PDIP. From the analysis, we have also determined the optimal horizon length (N^*).

The performance or cost function of MPC can be expressed as below:

$$\min \phi = [x^T(p)Px(p) + \sum_{k=0}^{p-1} x^T(k)Qx(k) + \sum_{k=0}^{m-1} u^T(k)Ru(k)] \quad (1)$$

Where p is prediction horizon, m is control/input horizon and k is the sampling time step. We consider $p = m = N$. Subject to the linear state space model constraint:

$$x(k+1)=Ax(k)+Bu(k);\ k = 0, 1, 2,\ldots\ldots, N-1 \quad (2)$$

The number of input and state variable are denoted by *ni and ns*. *A* and *B* are the system matrices with the dimension. *P* is the terminal weight and solution of the *P* is to the corresponding Lyapunov equation or discrete-time Riccati equation. *Q* and *R* are the weight matrices. X_k is a system state variable and U_k is the system control / input.

2. Criteria for feasibility and stability

We discuss here the condition related to the feasibility and stability based on which the present analysis has been made. We attempt to identify the feasible region in which the constrained optimal control problem is solvable. For a properly chosen horizon, RH policy always remains in the region. The RH policy can be shown to be capable of retaining feasibility without end constraints (Primbs & Nevistic, 2000).

We consider the following time-invariant linear system. The constraints:

$x(k+1)=Ax(k) + Bu(k),\ x(0) = x_0,$ (3)

s.t: $Ex + Fu \leq \psi$ (4)

where $x(k)\in R^n$, $u(k)\in R^m$, $\psi\in R^p$, $E\in R^{p\times n}$ and $F\in R^{p\times m}$ denote the state vector, input vector and constraints respectively.

The cost function of a linear quadratic regulator (LQR) problem may be expressed infinite or finite horizon as follow:

Infinite horizon cost function:

$$J(x_0) = \inf_{u(.)} \sum_{k=0}^{\infty} (x^T(k)Qx(k) + u^T(k)Ru(k)) \tag{5}$$

Finite horizon cost function:

$$J_N(x_0) = \inf_{u(.)} \left[x^T(N)P_0x(N) + \sum_{k=0}^{N-1} \left(x^T(k)Qx(k) + u^T(k)Ru(k)\right) \right] \tag{6}$$

Criteria are based on the following assumptions:

(i) $Q > 0, R > 0$ ($[Q^{1/2}, A]$ observable).

(ii) [A, B] controllable.

(iii) $P_0 = Q$ (J_N is monotonically non-decreasing).

(iv) There exists a neighborhood of the origin which is feasible for deadbeat and the unconstrained optimal control.

For any set *W*, let $\overset{0}{W}$ denote its interior, $\overline{W}$ its closure, and W^c its complement. Given two sets *W* and *M*, $W - M = W \cap M^c$. Let L_θ denote the θ sub-level set of the optimal infinite horizon cost J(x) i.e:

$L_\theta = \{x : J(x) \leq \theta\}$

2. 1 Computational Schemes for stability parameter

Calculate $\theta = \max_{x\in I} x^T Px$ and define the set $W = \{x: x^T Px \leq \theta\}$ and solve the following optimization problems:

$$\tau_N = \max \frac{J_{N+1}(x)}{J_N(x)} \text{ ,s.t } x \in W \tag{7}$$

and $\chi_N = \min \dfrac{x^T Qx}{J_N(x)}$, s.t. $x \in W$ (8)

$$\text{or } \xi_N = \max \frac{J_N(x(1))}{J_N(x(0))}, \text{ s.t. } x \in W \tag{9}$$

3. Numerical results

Here we consider one case study from literature in order to experience and analyse the response, feasibility, stability and performance. We also discuss the numerical results we obtain in relation to the data from the literature. CPU used in our computations is Intel(R) core(TM)2 Duo E7500@2.93 GH_Z. PDIP method and MPC algorithm were implemented using digital visual FORTRAN 5.0.

3.1 Case study 1: The problem adapted from Pistikopoulos et al.

The following discrete state-space model with sampling period of 0.1s is considered:

$$x_{k+1} = \begin{bmatrix} 0.7326 & -0.0861 \\ 0.1722 & 0.9909 \end{bmatrix} x_k + \begin{bmatrix} 0.0609 \\ 0.0064 \end{bmatrix} u(k) \tag{10}$$

$$y_k = \begin{bmatrix} 0 & 1.4142 \end{bmatrix} x_k \tag{11}$$

The constraints on input are as follows:

$$-2 \le u \le 2 \tag{12}$$

And the weight matrices,

$$Q = \begin{bmatrix} 1 & 0 \\ 0 & 1 \end{bmatrix}, R = 1$$

Initial conditions: $x(0) = [1 \quad 1]^T$, N = 2

The system (10-12) was run 40 samplings. We apply the receding horizon policy for optimal control of the system. The optimal control sequence is obtained by minimizing the cost function along with the constraint (12) and $P \geq 0$ is the solution to the corresponding Lyapunov equation which is given below:

$$P = \begin{bmatrix} 3.0485 & -2.5055 \\ -2.5055 & 12.9916 \end{bmatrix}; P \text{ is the terminal weight.}$$

Fig. 1(a) shows the system state response varying with number of sampling. Fig. 1(b) presents the variation of input (control action) with number of samplings. Both the state and the input settle at zero as expected in the regulator problem. While comparing these results with those of Pistikopoulos et al. (2002) using QP, it is observed that the results in the present studies are found to be very close to the later with improved stability with our PDIP method. The method yields faster convergence and better feasibility with continuous variations of states and input, although the number of active constraints in our study is almost equal to those obtained by them using QP method. It is noted that number of iteration for convergence is independent of the size of the problem.

3.1.1. Feasibility of the solutions

Here, we analyse the feasibility of the solution. In order to test the feasibility, we satisfy the following conditions:

$$\mu \ge J(x(0)) \ge J_N(x(0)) \ge J_{N-1}(x(1)) \ge x^T(1)Qx(1) \tag{13}$$

where μ is sub level set and $\mu = x^T P x = 11.029$ with $x(0) = [1 \quad 1]^T$

$J_N(x(0)) = 10.47$ at N = 8

$J_{N-1}(x(1)) = 6.4361$ at N=7

$x^T(1)Qx(1) = 1.5985$

We see most of the condition is fulfilling according to present theorem. So, our solution is in the feasible region.

3.1.2. Stability of the system

Following the procedure outlined in the Section 2.1, the sensitivity of stability parameter ξ_N with horizon length (N) is presented in the Fig. 2 using Eq. (9) and the relevant parameters are tabulated in the Tables 1. The variation of ξ_N is linear. One may note in the Fig. 3 that $\xi_N < 1$ for $N \geq 3$. Specifically, τ_N and χ_N were calculated using Eq. (7) and Eq. (8) respectively.

Although ω_N <1 or ξ_N < 1 determines stability of closed loop, ξ_N < 1 is less conservative than ω_N. Considering the results using ω_N, a horizon of 4 is sufficient to guarantee stability. The variation of parameters τ_N and χ_N with N are displayed in Table 1 for reference. These parameters are necessary to calculate ω_N and additionally, τ_N is needed to calculate performance parameter $\prod_N$ in conjunction with both ω_N and ξ_N.

Performance result is presented in Table 1 with the help of Eq. (14) and Eq. (15). With ω_N, a horizon length of 5 is sufficient to guarantee performance in terms of Π_N^{ω}. Similarly under ξ_N, a horizon length of 5 is sufficient to guarantee performance in terms of Π_N^{ξ}. The criteria yield similar results.

Another computation of our results using PDIP with Primbs and Nevistic(1997) shown in Fig. 3 reveals that our PDIP yields improved stability compared to SQP-active set method. ξ_N is well below unity compared to that of Primbs and Nevistic(1997), as evident in the figure. This is due to faster convergence rate and better feasibility properties of PDIP. ξ_N with PDIP appreciably decreases with N (although depending on IC) compared to active set method.

The performance Π_N^{ω} with respect to ω is given by:

$$\Pi_N^{\omega} = \left[1 + \left(\frac{\tau_{N-1} - 1}{\tau_{N-1}}\right)\frac{\omega_N}{1-\omega_N}\right] \tag{14}$$

Π_N^{ξ} with respect to ξ_N is given by:

$$\Pi_N^{\xi} = \left[1 + \left(\frac{\tau_{N-1} - 1}{\tau_{N-1}}\right)\frac{\xi_N}{1-\xi_N}\right] \tag{15}$$

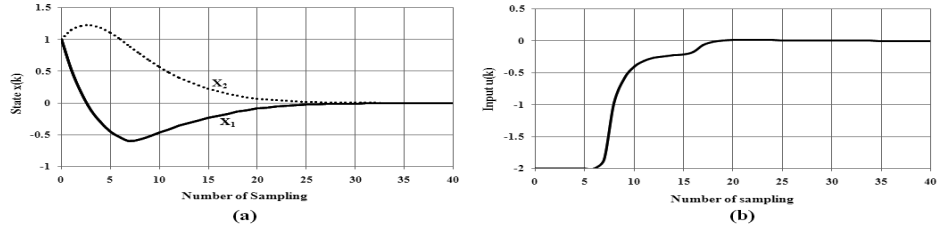

(a) (b)

Fig. 1. (a) State response with number of sampling. (b) Response of input with number of sampling.

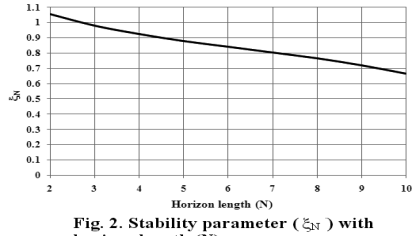

Fig. 2. Stability parameter (ξ_N) with horizon length (N).

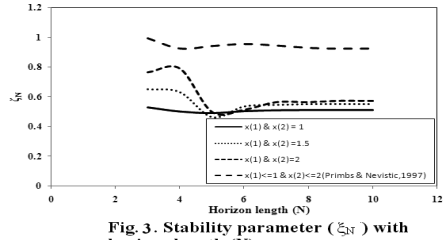

Fig. 3. Stability parameter (ξ_N) with horizon length (N).

Table 1
Stability parameter ω_N and parameters τ_N, χ_N (used to calculate ω_N) and performance results Π_N^{ω} and Π_N^{ξ} (using ω_N and ξ_N).

N	ω_N	τ_N	χ_N	Π_N^{ω}	Π_N^{ξ}
2	-	-	0.093418	-	-
3	1.008164	1.101582	0.084803	-	5.530698325
4	0.933611	1.018414	0.083270	1.25427103	1.225820551
5	0.880265	0.963535	0.086421	0.721769944	0.719103799
6	0.835272	0.921694	0.093763	0.569203025	0.542520512
7	0.792027	0.885790	0.105853	0.508973309	0.465784039
8	0.747602	0.853455	0.124029	0.491401221	0.437606066
9	0.698175	0.822203	0.150849	0.499789514	0.441232071
10	0.638368	0.789217	0.191138	0.528542373	0.471430225

4. Conclusion

We have presented one case study of constrained finite RHLQR problems from the published literature to demonstrate feasibility, stability and performance of MPC developed with FORTRAN. From the analysis, we have determined the optimal horizon length (N). However, stability parameters and performance parameters is observed to have decreased with horizon length. In the case study, we observed that the stability and the feasibility were achieved for $N \geq 3$ and the performance parameter is very close to unity. It is also found that $\xi_N < 1$ for stability seems to be less conservative than $\omega_N < 1$. PDIP method contributes to improve stability compared to active set method.

References

W.H. Kwon, A.E. Pearson, 1977, A modified quadratic cost problem and feedback stabilization of a linear system, IEEE Trans Automat Contr, 22, 838-842

S.K. Mondal, N. Goswami, S. Paruya, S.S. Rao, 2011, Primal-dual interior point (PDIP) for model predictive control – a computational experience, Submitted in J Optimiz Theory App.

L.O. Santos, L.T. Biegler, J.A.A.M. Castro, 2008, A tool to analyse robust stability for constrained nonlinear MPC, J. Process Control, 18, 383-390

J. Primbs, V. Nevistic, 1997, Constrained finite receding horizon linear quadratic control, CDS Technical Memo #CIT-CDS 97-002

J. Primbs, V. Nevistic, 2000, Feasibility and stability of constrained finite receding horizon control, Automatica, 36, 965-971

E.N. Pistikopoulos, V. Dua, N.A. Bozinis, A. Bemporad, M. Morari, 2002, On-line optimization via off-line parametric optimization tools, Comput Chem Eng, 26, 175-185

D.Q. Mayne, J.B. Rawlings, C.V. Rao, P.O.M Scokaert, 2000, Constrained model predictive control: Stability and optimality, Automatica, 36, 789-814

I.A. Karimi and Rajagopalan Srinivasan (Editors), Proceedings of the 11th International Symposium on Process Systems Engineering, 15-19 July 2012, Singapore.

Studying Various Optimal Control Problems in Biodiesel Production in a Batch Reactor under Uncertainty

Pahola T. Benavides1, [a,b] Urmila M. Diwekar, [a,b]
[a]*Department of Industrial Engineering, University of Illinois, Chicago, IL 60607 - USA*
[b]*Center for uncertain Systems: Tools for Optimization & Management (CUSTOM), Vishwamitra Research Institute, Clarendon Hills, IL 60514 – USA*

Abstract

Optimal control problems encountered in biodiesel production can be formulated using various performance indices like maximum concentration, minimum time, and maximum profit. The problems involve determining optimal temperature profile so as to maximize these performance indices. This paper presents these three formulations and analyzes the solutions in biodiesel production. We also present the maximum profit problem where the variability and uncertainties in the feed composition of soybean are considered.

Keywords: batch reactor, biodiesel, optimal control, stochastic optimal control, maximum principle, minimum time, maximum profit.

1. Introduction

Optimal control problems are defined in the time domain and their solution requires establishing a performance index for the system. Because of the dynamic nature of the decision variables encounter, optimal control problems are much more difficult to solve compared to normal optimization where the decision variables are scalars.

Optimization in batch processes can lead to different types of problems depending on the objective of the process. Some of the examples of optimal control problems in batch reactor are presented in Denbigh, 1958; Crescitelli and Nicoletti, 1973; Luus, 1999, and Aziz and Mujtaba, 2001. To solve these problems, dynamic and NLP methods are employed; however, since these types of problem are large, they require large-scale NLP solvers. In this paper, we are proposing an alternative approach that avoids the use of these large-scales NLP solvers. Moreover, we study the three optimal control problems on batch reactors: maximum concentration problem (MCP) of methyl ester, the minimum time problem (MTP), and the maximum profit problem (MPP) for biodiesel production in batch reactor. The MCP and MTP illustrated in this paper are solved using the maximum principle theory, and the approach is based on the Steepest Ascent of Hamiltonian, also shown in Diwekar, 2008. On the other hand, the MPP is solved using an algorithm that combines the maximum principle and NLP techniques. This algorithm is an efficient approach which avoids the solution of the two-point boundary value problem that results in the pure maximum principle or in the solution of the partial differential equations for the pure dynamic programming formulation.

Biodiesel is one of the most well-known examples for alternative energy and is also renewable and domestic resource with an environmentally friendly emission profile (Zhang et al., 2003). This biofuel is derived from vegetables oils produced by transesterification reaction with an alcohol (methanol). Several factors that can affect the process in terms of yield have been investigated. Among of these factors, the most relevant are the alcohol ratio, catalyst concentration, reaction temperature, and reaction time. To mention some important aspects Leung and Guo 2006 has an excellent summary. Here we present the optimal control problem where optimal temperature profile is derived using optimal control theory.

Optimal control problems become more challenging when variability in any parameter or variable is included. In biodiesel production, there are inherent uncertainties that have a significant impact on the product quantity, quality and process economic. One of the most influential uncertainties in this process is the feed composition since the percentage and type of triglycerides in biodiesel composition varies considerable (Linstromberg, 1970). This uncertainty can be modeled using probabilistic techniques, and can be propagated using stochastic modeling iterative procedures (Diwekar and Rubin, 1991). Therefore, at the end of this paper we propose a stochastic maximum profit problem (SMPP) that regards the variability in the feed composition to observe how this uncertainty affects the process economic in the batch reactor.

2. Optimal Control Problem:

Table 1 summarizes the optimization problems presented in this paper.

Table 1 Optimal Control problems in Biodiesel Production

Problem	Concentration	Batch time	Objective
Maximum concentration	Free	Fixed	Maximize C_E
Minimum Time	Fixed	Free	Minimize t_f
Maximum profit	Free	Free	Maximize profit

The kinetic model for biodiesel production presented here is based on Noureddini et al., 1997 and is used to solve the three optimal control problems.

$$F_1 = \frac{dC_{TG}}{dt} = -k_1 C_{TG} C_A + k_2 C_{DG} C_E \quad (1)$$

$$F_2 = \frac{dC_{DG}}{dt} = k_1 C_{TG} C_A - k_2 C_{DG} C_E - k_3 C_{DG} C_A + k_4 C_{MG} C_E \quad (2)$$

$$F_3 = \frac{dC_{MG}}{dt} = k_3 C_{DG} C_A - k_4 C_{MG} C_E - k_5 C_{MG} C_A + k_6 C_{GL} C_E \quad (3)$$

$$F_4 = \frac{dC_E}{dt} = k_1 C_{TG} C_A - k_2 C_{DG} C_E + k_3 C_{DG} C_A - k_4 C_{MG} C_E + k_5 C_{MG} C_A - k_6 C_{GL} C_E \quad (4)$$

$$F_5 = \frac{dC_A}{dt} = -\frac{dC_E}{dt} \quad (5)$$

$$F_6 = \frac{dC_{GL}}{dt} = k_5 C_{MG} C_A - k_6 C_{GL} C_E \quad (6)$$

where C_{TG}, C_{DG}, C_{MG}, C_E, C_A, and C_{GL} are the state variables and represent concentrations of triglycerides, diglycerides, monoglycerides, methyl ester, methanol, and glycerol, respectively. The initial conditions are: $C_i(t_0) = [C_{TG}; 0; 0; 0; C_A; 0]$ [mol/L]. The reaction constant, k_i, is expressed by the Eq.7.

$$k_i = a_i e^{-\frac{b_i}{T}} \quad (7)$$

where T is the reaction temperature (control variable), a_i is the frequency factor and $b_i = E_{ai}/R$ for which E_{ai} is the activation energy for each component i and R is the gas constant.

The objective function for the maximum profit problem is represented by Eq.8 (Kerhof and Vissers, 1978).

$$\max J^{w} = \frac{M_E P_r - B_o C_o}{t + t_s} \quad (8)$$

where M_E is the amount if product (kg), P_r is the sales value of the product ($/kg), B_o is the amount of feed F (kg), C_o is the cost of feed ($/kg), t is batch time (minutes)

and t_s is the setup time for each batch (minutes). However, this equation can be converted as:

$$\max J^{w} = \frac{(\max M_E)P_r - B_o C_o}{t+t_s} \quad (9)$$

Table 2 shows the information needed for profit function calculation. The amount of feed involves the quantity of methanol and triglycerides at the beginning of the reaction while the amount of product is the final concentration of methyl ester which is maximized by finding a temperature profile as a control variable.

Table 2 Information for maximum profit problem

Item	Data
Raw materials [a]	
Soy bean oil (Triglycerides)	\$0.62/kg
Methanol	\$0.320/kg
Product	
Biodiesel (methyl ester)	\$ 3/gallon=\$ 0.9/kg
Additional parameters	
Biodiesel density	0.88 kg/l
Triglyceride density	885.446 kg/l
Methanol density	32.04 kg/l
Setup time (t_s)	10 min
Volume	10000 l

a Chemical Market Reporter (www.icis.com), Zhang et al., 2003

For the MCP and MTP, maximum principle is used to solve the optimal control problem. On the other hand, a combination of maximum principle and nonlinear optimization (NLP) technique based on SQP algorithm is used to solve the MPP.

In the SMPP, the objective function in this problem is subject to fluctuations due to the uncertainty arising in the feedstock content. In a previous work of our group (Benavides and Diwekar, 2012), we showed the uncertainty characterization and the stochastic simulation for the feed stock composition of soybean oil. The interest of these types of problems is to determine the expected value of the maximum profit. Then, the objective function for the SMPP can be formulated as it is shown in Eq. 10.

$$\max J^{w} = E\left[\frac{(\max M_E)P_r - B_o C_o}{t+t_s}\right] \quad (10)$$

where the values of P_r, B_o, C_o and t_s are the same values shown in Table 2.

3. Result and discussion

The results of the three optimal control problems in a batch reactor for biodiesel production are analyzed in this section. Figure 1 shows the concentration profiles obtained for the three optimal control problems and two base cases. To start with, consider the concentration profile of methyl ester for the maximum concentration problem. Here, we are comparing the concentration values at constant temperature (base case 1: 315K and base case 2: 323K) with the values calculated at optimal temperature profile. It can be seen that at 100 minutes of reaction time, the concentration of methyl ester at optimal control temperature reaches its maximum value, 0.7944mol/L; while at constant temperature 315K and 323K, the maximum concentration is 0.7324mol/L and 0.7829mol/L, respectively. This change represents an increase of 8.46 % with base case 1 and 1.47% with base case 2 on the concentration of methyl ester. The increment for the second base case is not significant since the constant profile at 323K belongs to the constant optimal profiles reported in the

literature (Dennis Y.C. L et al., 2010). Moreover, if we fix the concentration at 0.7324mol/L, which is the concentration reached in base case1, the reaction time needed is 30.5 minutes which represents 69.5% less than it was at the beginning (100 minutes) after using optimal control. Compare with base case 2, the reduction on time represents 46% of the original reaction time. This improvement does not affect the behavior of the other components because after 50 minutes their concentration values remain constant. For the MTP, after fixing the concentration of methyl ester to 0.7324mol/L the minimum reaction time reached is around 30.6 minutes when optimal control approach is applied, while for base case 1 and 2 their minimum time is reached at 100 and 54 minutes, respectively. Although, the optimal control profiles shown in Figure 2 for the two optimal control problems are significantly different, their results are similar showing that this problem have multiple solutions.

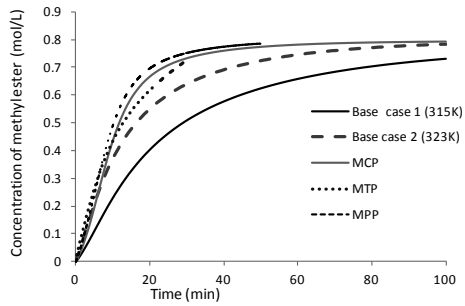

Figure 1 Concentration Profiles for the Three Problems and the Two Base Cases.

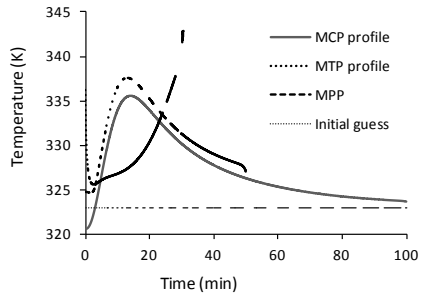

Figure 2 Optimal Temperature Profiles for the Three Problems

For the case of MCP, it can be seen that at 50 of minimum time there is an increase of methyl ester concentration of 25.56% (base case 1) and 8.50% (base case 2). Moreover, if we compute the profit values in the MCP and MTP using Eq. 9 and compare these values with the profit value found in the MPP, there is an increment of 45.32% and 355.58%, respectively; this information is summarized in Table 3.

Table 3 Comparison of the optimal control problems

Parameter	Maximum Concentration	Minimum Time	Maximum Profit
Concentration of Biodiesel (mol/L)	0.7944	0.7324	0.7802
Time (minutes)	100	30.5	50
Profit ($/hr)	103.1005	32.8868	149.8260

Finally, results of these problems regarding uncertainty in the feed composition are shown in Table 4. This table compares between the two bases cases, the deterministic and stochastic optimal control profiles in the face of uncertainties. As it is shown, in stochastic case there is an improvement of 7.69% compare to the deterministic case and a very significant improvement compare with the two base cases. In other words, the SMPP gives 11.499$/hr more than MPP (deterministic case) and 78.458$/hr and 149.67$/hr more than base case 1 and 2, respectively.

Table 4
Comparison between Constant temperature, deterministic and stochastic cases.

Parameter	Base case (315K)	Base case (323K)	Deterministic case	Stochastic case
Concentration of Biodiesel (mol/L)	0.7316	0.7767	0.7799	0.7791
Time (minutes)	100	92.653	50	44.912
Profit ($/hr)	11.197	82.409	149.368	160.867

4. Conclusions

The article presented three operation modes for optimal control problems encounter in biodiesel production. The problems involved determining optimal temperature profile so as to maximize or minimize three performance indices, namely, concentration, time, and profit. For the maximum concentration and minimum time problem, the maximum principle along with the steepest ascent of the Hamiltonian method was used as the solution technique. It was shown that the solution of these two problems results in similar equations for maximum principle and in both cases around 30.5 to 30.6 minutes of reaction time the concentration of methyl ester was the same, 0.7324mol/L. While in the maximum profit, the solution technique used was based on combining the maximum principle and NLP techniques. It was shown that applying optimal control under uncertainty (feed composition) it resulted in better reaction time to produce the same amount of biodiesel which improved the profit value of the problem.

References

Aziz, N.; and Mujtaba, I.M. Optimal control of semi-batch reactors. Computer Aided Chemical Engineering. 9 (2001) 609.

Benavides, P.; Diwekar, U. Optimal Control of Biodiesel Production in a Batch Reactor Part lI: Stochastic Control. Fuel. 94 (2012) 218.

Crescitelli, S.; and Nicoletti, B. Near optimal control of batch reactors. Chem. Eng. Sci. 28 (1973) 463.

Denbigh, K. G. Optimum temperature sequences in reactors. Chem. Eng. Sci. 8 (1958) 125.

Dennis Y.C. L.; Xuan, W.; and Leung, M.K.H. A review on biodiesel production using catalyzed transesterification. Applied Energy 87 (2010) 1083.

Diwekar U, Rubin ES. Stochastic modeling of chemical processes. Comput. Chem. Eng. 15 (1991) 105.

Diwekar, U. Introduction to Applied Optimization. Springer. Second Edition (2008).

Kerkhof, L. H. J.; and Vissers, J. M. On the profit of optimum control in batch distillation. Chem. Eng. Sci. 33 (1978) 961.

Leung, D.Y.C., and Guo, Y. Transesterification of neat and used frying oil: optimization for biodiesel production. Fuel Process Technol. 87 (2006) 883.

Linstromberg WW. Organic chemistry. MA: DC Heath and Co. Lexington. (1970) 129.

Luus, R.; Okongwu, N. O. Towards practical optimal control of batch reactors. Chem. Eng. J. 75 (1999) 1.

Noureddini H, Zhu D. Kinetic of transesterification of soybean oil. J Am Oil Chem Soc. 74 (1997) 1457.

Zhang, Y.; Dube, M.A.; McLean, D.D.; and Kates, M. Biodiesel production from waste cooking oil: 1. Process design and technological assessment. Bioresour. Technol. 89 (2003) 1.

I.A. Karimi and Rajagopalan Srinivasan (Editors), Proceedings of the 11th International Symposium on Process Systems Engineering, 15-19 July 2012, Singapore.

Neural Network Predictive Control of a Tubular Solid Oxide Fuel Cell

S. A. Hajimolana,[a] M. A. Hussain,[a] J. Natesan,[a] S. M. Tonekaboni Moghaddam[a]

[a]*Chemical Engineering Department, Faculty of Engineering, University of Malaya, Kuala Lumpur, Malaysia*

Abstract

The dynamic behavior and control of a tubular solid oxide fuel cell will be studied in this paper. The effect of fuel/air temperature and pressure will be investigated. Controlling the average stack temperature is the final objective of this study due to a high operating temperature of the system. In this case, temperature fluctuation induces thermal stress in the electrodes and electrolyte ceramics; therefore, the cell temperature distribution should be kept as constant as possible. A mathematical modeling based on first principles is developed. The fuel cell is divided into five subsystems and the factors such as mass/energy/momentum transfer, diffusion through porous media, electrochemical reactions, and polarization losses inside the subsystems are presented. Dynamic fuel-cell-tube temperature responses of the cell to step changes in conditions of the feed streams will be presented. A neural network model predictive controller (NNMPC) is then implemented to control the cell-tube temperature through manipulation of the temperature of the inlet air stream. The results show that the control system can successfully reject unmeasured step changes (disturbances) in the load resistance.

Keywords: Neural network predictive control; SOFC; cell-tube temperature.

1. Introduction

Solid oxide fuel cells (SOFCs) have shown promise in the electricity generating sector for stationary applications in the mid-term future. This is due to the fact that the energy efficiency usually achieved in a SOFC is much greater than that obtained from conventional heat engines or any other types of fuel cells. SOFCs offer high power density, low cost, scalability, fuel flexibility, and superior durability. Only few research studies are available on mathematical modelling of NH_3-SOFC (M. Ni et al., 2008). However, in all of these studies the mathematical models were based only on electrochemical models of planar SOFCs and did not cover the entire system. Besides working on fuel cell modeling, some studies on the control of fuel cell systems have been published (F. Jurado, 2006, S. A. Hajimolana et al., 2009). However, controlling the fuel cell temperature by using neural network predictive control has not been done before with these researchers.

In this work a dynamic model of an ammonia fed-tubular solid oxide fuel cell that is based on first principles is developed and presented. A NNMPC system is implemented to control the cell-tube temperature.

2. Model description

The mathematical model used in this study was previously developed by this research group (S.A. hajimolana et al., 2009). The tubular SOFC system under study here is a bank of single tubular SOFCs. Each cell has two tubes, an outer tube and an inner tube.

The outer tube is a cell tube. The outer surface of the outer tube is the anode side of the cell, and its inner surface is the cathode side. Between the anode and cathode sides (surfaces) lies the solid oxide electrolyte. The inner tube is an air injection and guidance tube, from which preheated air is injected into the bottom of the cell tube and flows over the cathode surface of the cell tube through the gap between the injection and the tubes. Fuel gas flows over the anode surface through the gap among the cell tubes. To develop a first-principles model of the SOFC system, a single tubular fuel cell is considered and divided into five subsystems (Hajimolana et al., 2011): Subsystem 1 (SS1): air inside the injection tube; Subsystem 2 (SS2): injection tube; Subsystem 3 (SS3): air inside the space between the cell and injection tubes; Subsystem 4 (SS4): cell tube; and Subsystem 5 (SS5): fuel flow channel. The assumption considered in the mathematical formulation is that the gas boundary layers are very small relative to the corresponding radius; therefore, the equations governing the diffusion processes are written in the Cartesian coordinates. Fluid velocities are averaged along the radial direction. Partial pressures, temperatures, and fluid velocities in each subsystem are uniform in every direction. The mass/momentum and energy balance inside SS1, SS3 and SS5 are given as follows, respectively:

$$L\frac{d\xi^i_j\rho^i_j}{dt} = u^i_{j_{in}}\xi^i_j\rho^i_{j_{in}} - u^i_j\xi^i_j\rho^i_j + \sum N_j M_j\left(\frac{2r_i L}{r_i^2 - r_0^2}\right) + nr_j \tag{1}$$

$$L\frac{d(u_i\rho_i)}{dt} = (u_{i_{in}})^2\rho_{i_{in}} - (u_i)^2\rho_i + \frac{\rho_{i_{in}}R^*T_{i_{in}}}{M_i} - \frac{\rho_i R^*T_i}{M_i} \tag{2}$$

$$L\frac{d(\tilde{H}^i_j\rho^i_j)}{\partial t} = \rho^i_{j_{in}}u^i_{j_{in}}H^i_{j_{in}} - u^i_j\rho^i_j\tilde{H}^i_j + \frac{2Lh_w}{r}\left(T_w - T^i_j\right) \tag{3}$$

i is air flow injection tube, air flow inside cathode side, fuel flow inside anode side, *j* is air, oxygen, nitrogen, ammonia, hydrogen, w is the wall, r_i and r_o is the inner and outer radius respectively, N_j is mass transfer by means of diffusion, *n* is the molar number and r_j is producing or consuming of the components.

This model assumes that the pressure drop caused by the pipe resistance over the distance *L* is negligible. It is also assumed that energy is transferred to the flow streams by convection only. Enthalpy of formation, heat capacities, viscosities, and conductivities of the components of air and the fuel are given in a previous work (Hajimolana et al., 2009).

Energy balance for the solid parts (SS2 and SS4) leads to:

$$m_s\tilde{C}_{p_s}\frac{dT_s}{dt} = \frac{\sigma 2\pi rL}{R_{rad}}\left(T_w^4 - T_j^4\right) + 2\pi rLh_w(T^i_j - T_w) + 2\pi rLh_w\left(T^i_j - T_w\right) + \tag{4}$$

$$\sum H_j N_j\left(\frac{2r_i L}{r_i^2 - r_0^2}\right) + 2r_{ct_o}LR_{NH_3}\Delta H_{R_{NH3}} - 0.001V_{out}I$$

The last three parts are heating transfer by means of diffusion, heating consuming by ammonia decomposition and heating supply by electrochemical reaction, respectively only in SS4. Electrochemical reaction occurs inside the fuel cell (SS4) at the triple phase boundary (*TPB*). Fuel cell voltage output is dependent on gas partial pressures and is adversely affected by concentration, activation, and ohmic losses (polarizations or irreversibilities). The electromotive force, reversible open-circuit cell voltage is given by the Nernst equation. However, the actual cell voltage (*E*) is less than its theoretical open circuit voltage because it is strongly affected by several irreversible losses

including activation losses due to irreversibility of electrochemical reactions at the *TPB*, concentration losses due to mass transport resistance in the electrodes (especially for thick anodes as in an anode-supported SOFC) and ohmic losses due to ionic and electronic charge transfer resistances. Actual voltage is thus given by:

$$E = E^o - \eta_{act_{ano}} - \eta_{conc_{ano}} - \eta_{act_{cat}} - \eta_{conc_{cat}} - \eta_{ohm} \tag{5}$$

The thermal decomposition of ammonia for hydrogen production in the porous anode is solved using the chemical model described as follows. NH_3 thermal decomposition takes place on the anode surface (fuel) channel (SS4) as this process is favored at high temperatures (G. Meng, 2007):

$$r_{NH_3} = z_r \exp\left(-\frac{E_r}{R_{kj} T_{ct}}\right) P_{NH_3} \tag{6}$$

where P_{NH3} is the partial pressure of NH_3. It's considered that the reaction rate is mainly dependent on the partial pressure of NH_3 and the operating temperature. It is assumed here that NH_3, H_2O and N_2 diffuse into the anode at a negligible rate; only H_2 gas diffuses into the anode (SS4).

3. Results and discussion

3.1.1st Model validation

Simulation was done to compare the results with the experimental data of Singhal. In this simulation, the values of fuel and air flow rates were adjusted to match the values of factors given by Singhal. The current–potential plot obtained from this simulation was compared with the experimental data and the predictions from the model developed by Ota and co-workers, 2003, as shown in Fig. 1. Excellent agreement was obtained in the low current density region in comparison to the model developed by Ota et al., 2003, which actually showed some deviation from experimental results. After validating the mathematical model developed in this work with experimental results of Singhal (2000) for H_2-SOFC, the model was improved to account for NH_3-SOFC.

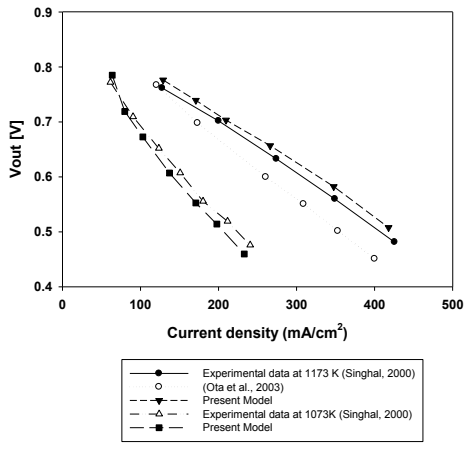

Fig. 1: Comparison of current–potential plots from the present model, model from Ota et al. 2000, and the experimental data available in the literature (Ota et al., 2003).

3.1. 2nd Open-loop Dynamic Cell Rresponses

The dynamic model of the SOFC system derived in the previous section has 20 first order ordinary differential equations, which are integrated numerically using MATLAB. Figure 2 and 3 depict the dynamic responses of the fuel cell to step changes of +5% in the temperature, pressure, and velocity of the inlet fuel and air stream respectively at time t= 100 s. Simulation results show that temperature of the inlet air stream has the strongest effect on the cell performance.

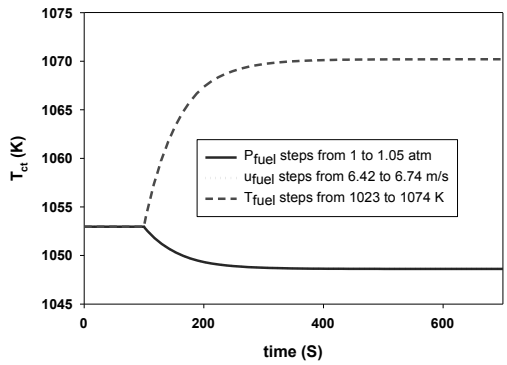

Fig. 2: Open-loop responses of the SOFC to step changes of +5% in the inlet fuel stream

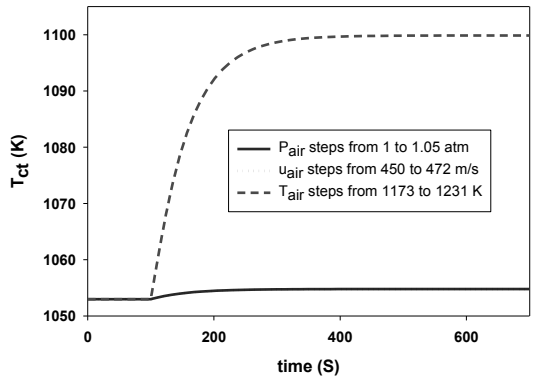

Fig. 3: Open-loop responses of the SOFC to step changes of +5% in the inlet air stream

4. Control of the SOFC System

A SOFC has a problem with regard to the durability of the ceramics used as its cell materials, because its operating temperature is very high, and its cell temperature fluctuation induces thermal stress in the ceramics. Therefore, the cell temperature distribution should be kept as constant as possible. In this case, NNMPC is used to predict future plant responses to control signals. The controller then calculates the control input that will optimize plant performance over a specified future time horizon. The first step in model predictive control is to determine the neural network plant model. Next, the plant model is used by the controller to predict future performance. MPC refers to a class of control algorithms in which a dynamic model of the plant is used to predict and optimize the future behavior of the process. The basic control strategy of the MPC is to select a set of future control horizons and minimize a cost

function based on the desired output trajectory over a prediction horizon with a chosen length. To select the manipulated input that has the strongest effects (in terms of dimensionless steady-state gain) on the controlled output, the open-loop analysis suggests that the cell tube temperature can be paired with the air inlet temperature. Figure 4 shows the performance of the NNMPC in tracking the series of setpoint changes for T_{ct} and satisfactory to reject the unmeasured disturbances.

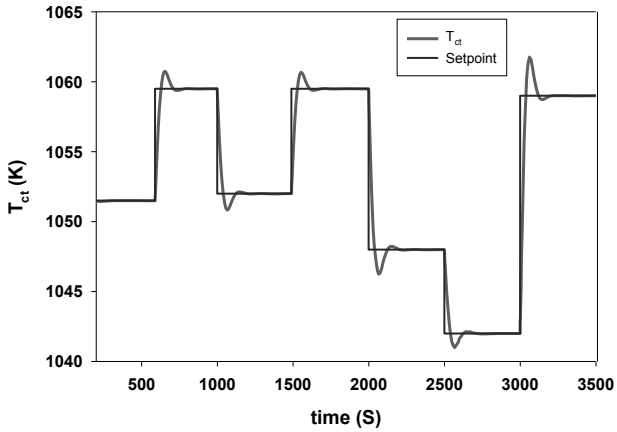

Fig. 4: The performance of the MPC

5. Conlusion

A dynamic model of a tubular solid oxide fuel cell (SOFC) was presented. Simulation results indicate that temperature of the inlet air stream has the strongest effect on the cell performance. The cell-tube temperature was regulated effectively using a NNMPC that manipulates the temperature of the inlet air stream. The performance of the control system was determined to be satisfactory to reject the unmeasured disturbances.

Acknowledgment

The authors are grateful to the University of Malaya Research Grant and the UM Bright Sparks Unit Bsp_App462/11(K) for providing financial assistance for this project.

References

Ni, M. Leung, M.K.H, 2008, Mathematical modelling of ammonia-fed solid oxide fuel cells with different electrolytes. Int. J. of Hydrogen Energy, 88, 33, 5765-5772.

Jurado, F. 2006, Predictive control of solid oxide fuel cells using fuzzy Hammerstein models. J. Pow. Sour, 11, 158, 245-253.

Hajimolana, S.A. Soroush, M, 2009, Dynamics and Control of a Tubular Solid-Oxide Fuel Cell. Ind. Eng. Chem, 23, 48, 6112-6125.

Hajimolana, S.A. , Hussain, M. A. Wan Daud, W. A. Soroush, M. Shamiri, A. 2011, Mathematical modelling of solid oxide fuel cells: A review. Renew. and Sustain. Ener. Rev. 121, 15, 1893-1917.

Meng, G. 2007, Comparative study on the performance of a SDC-based SOFC fueled by ammonia and hydrogen. J. Pow. Sour, 32, 173,189-193.

Singhal, S.C. 2003, Advances in solid oxide fuel cell technology. Sol. St. Ion, 23, 135,305-313.

Ota, T. 2003, Object-based modeling of SOFC system: dynamic behavior of micro-tube SOFC. J. Pow. Sour, 118, 125, 430-439.

I.A. Karimi and Rajagopalan Srinivasan (Editors), Proceedings of the 11th International Symposium on Process Systems Engineering, 15-19 July 2012, Singapore.

Novel MILP-based optimization method for heat exchanger network retrofit considering stream splitting

Ming Pan, Igor Bulatov, Robin Smith

Centre for Process Integration, School of Chemical Engineering and Analytical Science, The University of Manchester, Manchester, M13 9PL, UK

Abstract

This paper presents a novel optimization method for heat exchanger network (HEN) retrofit including stream splitting. A simple mixed integer linear programming (MILP) model and two iterative loops have been developed to effectively deal with the nonlinear computational difficulties associated with logarithmic mean temperature difference (LMTD) and retrofit costs for HEN retrofit problems. In case study, comparison with the existing methods illustrates the validity of the proposed approach.

Keywords: Heat exchanger network (HEN), retrofit, optimization, mixed integer linear programming (MILP), stream splitting

1. Introduction

Mathematical programming techniques have been widely studied in heat exchanger network (HEN) retrofit problems. The published work for HEN retrofit can be divided into two parts, conventional topology modifications and intensified implementation without topology modification.

The HEN retrofit problems addressing topology modifications include the strategies of restructuring heat matches (e.g. exchanger relocating, and stream repiping), adding additional heat transfer area, and installing new exchangers. Most of the relevant models involve MINLP formulations or NLP-MILP combination formulations. To deal with the non-convexities in these models, Ciric & Floudas (1990) used the Generalized Benders Decomposition techniques which can repeatedly update the values of variables in an iterative procedure (primal sub-problem to master sub-problem) until the final solution was found; while Yee & Grossmann (1991) introduced some simplifications to relax nonlinear equations, and replaced logarithmic mean temperature difference (LMTD) with arithmetic mean temperature difference (AMTD). On the other hand, stochastic optimization approaches, simulated annealing (SA) (Athier et al., 1998) and genetic algorithms (GA) (Bochenek & Jezowski, 2006; Rezaei & Shafiei, 2009), have been carried out for handling such NP-hard problems. Implementing intensified techniques in HEN without topology modifications is easily achieved in practice, due to the lower capital cost of during the retrofit in existing HEN and shorter implementation. Pan et al. (2012a, 2012b) have firstly proposed a new MILP-based iterative optimization method to intensify heat transfer in HEN without topology modifications for some literature problems, and then successfully extended the approach to large scale problems.

In this paper, the method proposed by Pan et al. (2012a) is developed to address HEN retrofit with structure modifications (including stream splitting). Distinguished from the previously proposed method, the new model addresses network topology modification and stream splitting, which is more complicated and difficult for optimization.

2. MILP-based iterative method for HEN retrofit

The optimization work is based on a potential superstructure network proposed in this section, where all potential matches are presented. Fig. 1 illustrates a HEN superstructure involving two hot streams and two cold streams. The whole stream region is divided into seven intervals, in which a stream-splitting match locates in interval 4, and no-stream-splitting matches are in the rest.

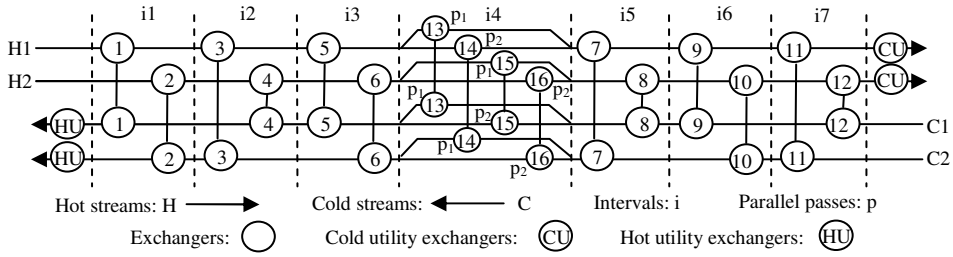

Figure 1. The superstructure network involving two hot streams and two cold streams

2.1. MILP-iteration method for structure optimization

The objective of this stage is to determine the suitable network structure for retrofit scenario. Based on the work proposed by Pan et al. (2012a), LMTD ($LMTD'_{ex}$), heat transfer (HBA_{ex} and HBB_{ex}) and energy balance (AEB_{ex} and BEB_{ex}) in no-stream-splitting matches are formulated in Eqs. (1)-(5).

$$LMTD'_{ex} = \frac{(HTI'_{ex} - CTO'_{ex}) - (HTO'_{ex} - CTI'_{ex})}{\ln[(HTI'_{ex} - CTO'_{ex})/(HTO'_{ex} - CTI'_{ex})]}, \quad \forall ex \in EX \tag{1}$$

$$HBA_{ex} \geq HFCP_{ex} \times (HTI_{ex} - HTO_{ex}) - EXA_{ex} \times U_{ex} \times LMTD'_{ex}, \quad \forall ex \in EX \tag{2}$$

$$HBB_{ex} \geq EXA_{ex} \times U_{ex} \times LMTD'_{ex} - HFCP_{ex} \times (HTI_{ex} - HTO_{ex}), \quad \forall ex \in EX \tag{3}$$

$$AEB_{ex} \geq HFCP_{ex} \times (HTI_{ex} - HTO_{ex}) - CFCP_{ex} \times (CTI_{ex} - CTO_{ex}), \quad \forall ex \in EX \tag{4}$$

$$BEB_{ex} \geq CFCP_{ex} \times (CTI_{ex} - CTO_{ex}) - HFCP_{ex} \times (HTI_{ex} - HTO_{ex}), \quad \forall ex \in EX \tag{5}$$

In stream-splitting match, stream heat-flow capacities ($HFCP_{ex}$ and $CFCP_{ex}$) are variables, thus the stream duties ($HFCP_{ex} \times (HTI_{ex}\text{-}HTO_{ex})$ and $CFCP_{ex} \times (CTI_{ex}\text{-}CTO_{ex})$) have to be linearized. Eqs. (6)-(8) show the first order Taylor series expansions of $HFTI_{ex}$ ($HFCP_{ex} \times HTI_{ex}$), where $HFTI'_{ex}$, $HFCP'_{ex}$ and HTI'_{ex} are the initial values; positive variables, $AHFTI_{ex}$, and $BHFTI_{ex}$, are remainder terms, and should be very small, which is to be formulated in the objective function.

$$HFTI_{ex} = HFTI'_{ex} + HFCP'_{ex} \times (HTI_{ex} - HTI'_{ex}) + HTI'_{ex} \times (HFCP_{ex} - HFCP'_{ex}), \quad \forall ex \in EX \tag{6}$$

$$AHFTI_{ex} \geq HFTI_{ex} - HFTI'_{ex}, \quad BHFTI_{ex} \geq HFTI'_{ex} - HFTI_{ex}, \quad \forall ex \in EX \tag{7, 8}$$

Based on Eqs. (6)-(8), the bilinear term $HFCP_{ex} \times HTI_{ex}$ has been converted into linear terms, and other bilinear terms ($HFCP_{ex} \times HTO_{ex}$, $CFCP_{ex} \times CTI_{ex}$ and $CFCP_{ex} \times CTO_{ex}$) can be linearized in the same way.

To select exchangers in the retrofitted HEN, a set of binary variables is used: $ESEX_{ex}$ is equal to 1, if exchanger *ex* exists in the retrofitted HEN; otherwise, it is 0. In no-stream-splitting matches, hot-stream temperatures are restricted in Eqs. (9)-(14), where $HSTI_{hs,i}$ and $HSTO_{hs,i}$ are inlet and outlet temperatures of hot stream in the i^{th} interval.

$$HTI_{ex} - M \times (1 - ESEX_{ex}) \leq HSTI_{hs,i} \leq HTI_{ex} + M \times (1 - ESEX_{ex}), \forall hs \in HS, i \in I, ex \in EX_{hs,i} \tag{9, 10}$$

$$HTO_{ex} - M \times (1 - ESEX_{ex}) \leq HSTO_{hs,i} \leq HTO_{ex} + M \times (1 - ESEX_{ex}), \forall hs \in HS, i \in I, ex \in EX_{hs,i} \tag{11, 12}$$

$$HSTI_{hs,i} - M \times ESEX_{ex} \leq HSTO_{hs,i} \leq HSTI_{hs,i} + M \times ESEX_{ex}, \forall hs \in HS, i \in I, ex \in EX_{hs,i} \tag{13, 14}$$

For stream splitting, the outlet temperatures of parallel exchangers ($PTO_{hs,i}$) are given:

$$HTO_{ex} - M \times (1 - ESEX_{ex}) \le PTO_{hs,i,p} \le HTO_{ex} + M \times (1 - ESEX_{ex}), \ \forall p \in P, ex \in EX_{hs,i} \quad (15, 16)$$

$$HSTI_{hs,i} - M \times ESEX_{ex} \le PTO_{hs,i,p} \le HSTI_{hs,i} + M \times ESEX_{ex}, \forall hs \in HS, \ p \in P, ex \in EX_{hs,i} \quad (17, 18)$$

Note that the heat duties of mixing streams after two parallel exchangers are normally described as bilinear terms, such as $HPTO_{hs,i,p} = HFP_{hs,i,p} \times PTO_{hs,i}$ (where $HFP_{hs,i,p}$ is the hot stream (*hs*) heat-flow capacity in the p^{th} parallel pass in the i^{th} interval), thus they can be linearized with first order Taylor series expansions similar to Eqs. (6)-(8). Then heat transfer (PHA_{ex} and PHB_{ex}) balance after two parallel exchangers is obtained:

$$PHA_{hs,i} \ge \sum_{p \in P} HPTO_{hs,i,p} - THF_{hs} \times HSTO_{hs,i}, \quad \forall hs \in HS, \ i \in I \quad (19)$$

$$PHB_{hs,i} \ge THF_{hs} \times HSTO_{hs,i} - \sum_{p \in P} HPTO_{hs,i,p}, \quad \forall hs \in HS, \ i \in I \quad (20)$$

where parameter THF_{hs} is the total heat-flow capacities of hot stream *hs*.

Hot stream inlet and outlet temperatures in each interval are presented as:

$$HSTO_{hs,i} = HSTI_{hs,i+1}, \quad \forall hs \in HS, \ i \in I \quad (21)$$

The cold-stream temperatures in each interval ($CSTI_{cs,i}$ and $CSTO_{cs,i}$) can be treated in the same manner as the hot-stream temperatures in each interval ($HSTI_{hs,i}$ and $HSTO_{hs,}$). Furthermore, Eqs. (22) and (23) show the constraints of minimum temperature difference allowed (ΔT_{min}) in each exchanger.

$$HTI_{ex} \ge CTO_{ex} + \Delta T_{\min}, \quad HTO_{ex} \ge CTI_{ex} + \Delta T_{\min}, \qquad \forall ex \in EX \quad (22, 23)$$

To maximize retrofit profit, the costs of utility consumption (*CU*) is formulated first, where *PHU* and *PCU* are price of hot utility and cold utility, EX_{hu} and EX_{cu} are the set of all hot and cold utility exchangers.

$$CU = PHU \times CFCP_{ex} \times (CTO_{ex} - CTI_{ex}) + PCU \times CFCP_{ex'} \times (CTO_{ex'} - CTI_{ex'}), \forall ex \in EX_{hu}, \ ex' \in EX_{cu} \quad (24)$$

In the structure stage, average area of the existing exchangers (*AVEXA*) is used to estimate the cost of adding exchanger area ($CEXA_{ex}$).

$$PAEXA_{ex} \ge EXA_{ex} - AVEXA, \ \forall ex \in EX \quad (25)$$

Normally, $CEXA_{ex} = \alpha \times (PAEXA_{ex})^{\beta}$, this nonlinear term can be linearized as well by using first order Taylor series expansions. Eq. (26) shows the cost of installing new exchangers (*CNEX*) estimated in the structure stage, where *FCNEX* is the fixed cost of installing new exchanger, and *NE* is the exchanger number in the initial HEN.

$$CNEX = \left(FCNEX + \alpha' \times AVEXA^{\beta'}\right) \times \left(\sum_{ex \in EX} ESEX_{ex} - NE\right) \quad (26)$$

The estimated retrofit profit (*ERP*) in the structure stage can be described as the energy saving costs (*OCU*-2×*CU*) minus the total retrofit cost (*CNEX*+$\sum$*CEXAex*). In Eq. (27), *IFY* is the interest factor in the investment years, *OCU* is the original utility cost in the existing HEN, and *ACF* is the annual cost factor.

$$ERP = IFY \times \left((OCU - 2 \times CU) - \left(CNEX + \sum_{ex \in EX} CEXA_{ex}\right) \times ACF\right) \quad (27)$$

As the HEN structure changes after retrofit, the initial and updated variables before and after solving the MILP model might be different. The objective of the new method is to find a feasible retrofit solution whereby the differences of heat transfers and energy balance, the differences between initial and updated variables, and the remainder terms in the first order Taylor series expansions are minimized close to 0 under the restriction of a certain retrofit profit value (*ERP'*), as shown in Eqs. (28) and (29).

$$ERP \ge ERP' \quad (28)$$

$$Obj = heat\ transfer\ differences + energy\ balance\ differences + variable\ differences + remainder\ terms\ in\ the\ first\ order\ Taylor\ series\ expansions \quad (29)$$

The new MILP-based model for network structure optimization consists of an objective function given in Eq. (29) and other constraints given from Eqs (1)-(28).
The iteration algorithm is mainly based on the work proposed by Pan et al. (2012a), where two iteration loops are proposed to find the optimal solutions for HEN retrofit. The first loop is to find the solution for HEN retrofit under certain retrofit profit, while the second loop is to find the maximum retrofit profit for HEN retrofit.

2.2. MILP-iteration method for investment stage

The first optimization stage is to find the suitable retrofitted structure, and then the accurate investment for retrofitted exchangers is considered in the selected network structure. In this stage, the costs of adding area, new exchanger and exchanger moving can be formulated with accurate parameters. Thus, the average area of the exchangers before retrofit (*AVEXA*) in Eqs. (25) and (26) is replayed with the exchanger area in existing HEN. Then the same iteration algorithm is executed to find the optimal solution with calculated retrofit costs.

3. Case study

A famous example reported in literature is carried out to test the new method. The existing HEN includes two hot streams (H1 and H2) and two cold streams (C1 and C2). The heat-flow capacity of each stream is 30 kW/K (H1), 15 kW/K (H2), 20 kW/K (C1), 40 kW/K (C2), and 94.95 kW/K (CW). Other information include: U = 0.8 kW/m^2·K for all exchangers, cost of area for a new exchanger ($) =1300A$^{0.6}$, cost of adding area for an existing exchanger ($) =1300ΔA$^{0.6}$, fixed cost for a new exchanger ($) =3000, cost of moving an existing exchanger ($) =300; plant life time is 3 years with 33% rate of interest. The original HEN is presented in Fig. 2(a).

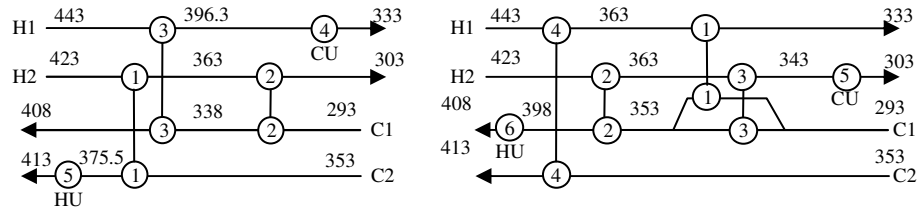

(a) Original HEN (ΔT_{min}=10K) (b) Retrofitted HEN (ΔT_{min}=10K)

Figure 2. Original HEN and retrofitted HEN (ΔT_{min} = 10K)

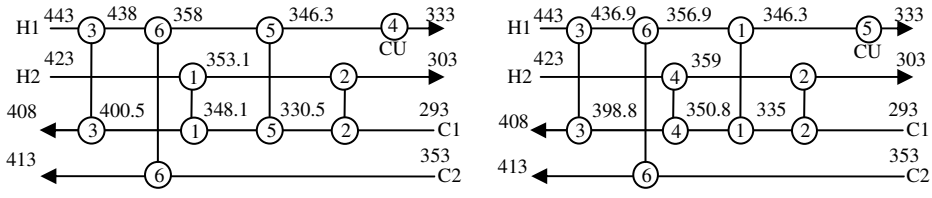

(a) Retrofited HEN (ΔT_{min}=5K) (a) Retrofited HEN (ΔT_{min}=2.7K)

Figure 3. Retrofited HEN (ΔT_{min} = 5K) and Retrofited HEN (ΔT_{min} = 2.7K)

The optimal solutions based on the proposed approach in different ΔT_{min}, such as 10 K, 5 K and 2.7 K, are shown in Fig. 2(b) and Fig. 3. Table 1 presents the retrofit and cost details of each exchanger in the optimal solutions. To prove the advantage of the new method, the solutions obtained in this work are compared with those reported in the

references, as presented in Table 2. The comparison shows that the new method can achieve higher retrofit profit than the existing methods, especially in lower ΔT_{min}.

Table 1. Exchanger details in original and retrofitted scenarios

Scenarios	Exchanger area (m^2)						Cost (10^3×$)			
	1	2	3	4	5	6	Added area	New exchanger	Exchanger moving	Utility
Original	46.7	68.7	38.3	40.2	35.0					158.0
R(10K)	52.0	68.7	15.1	164.8	32.8	5.3	27.0	6.6	1.2	28.0
R(5K)	112.7	60.8	5.2	11.2	34.8	241.4	16.1	38.0	0.6	8.0
R(2.7K)	46.7	65.6	6.3	81.1	11.3	273.4	12.0	40.7	0.9	8.0

Table 2. Comparison of the new and existing methods

ΔT_{min} (K)	Methods	Profit (10^3×$)	Utility (10^3×$)	Cost (10^3×$)			
				Total	Added area	New exchanger	Exchanger moving
10.0	**New**	**336.2**	**28.0**	**34.8**	**27.0**	**6.6**	**1.2**
	Ciric & Floudas (1990)	334.5	28.0	35.5	3.5	30.8	1.2
5.0	**New**	**453.6**	**8.0**	**54.7**	**16.1**	**38.0**	**0.6**
	Yee & Grossmann (1991)	347.7	24.7	41.5	10.1	30.8	0.6
	Athier et al. (1998)	380.9	19.4	45.9	45.3		0.6
	Bochenek & Jezowski (2006)	335.3	28.3	34.3	2.6	30.8	0.9
2.7	**New**	**455.8**	**8.0**	**53.6**	**12.0**	**40.7**	**0.9**
	Rezaei & Shafiei (2009)	442.4	8.0	59.3	58.4		0.9

4. Conclusions

In this paper, the nonlinear computational difficulties of optimizing HEN retrofit problems have been reduced efficiently with the proposed MILP-iteration method. Compared with the existing methods, the proposed approach is able to find suitable retrofitted structures, and requires less modification expense in most cases. Deeper insight on the proposed method, such as global optimization and large scale problems, will be addressed in future work.

Acknowledgement

Financial support from FP7-SME-2010-1 (262205 Intensified Heat Transfer Technologies for Enhanced Heat Recovery - INTHEAT) is gratefully acknowledged.

References

A. R. Ciric, & C. A. Floudas, 1990, A Mixed Integer Nonlinear Programming Model for Retrofitting Heat-Exchanger Networks, Ind. Eng. Chem. Res., 29, 239-251.

E. Rezaei, & S. Shafiei, 2009, Heat Exchanger Networks Retrofit by Coupling Genetic Algorithm with NLP and ILP Methods, Comput. Chem. Eng., 33, 1451-1459.

G. Athier, P. Floquet, L. Pibouleau, & S. Domenech, 1998, A Mixed Method for Retrofiting Heat-Exchanger Networks, Comput. Chem. Eng., 22, S505-S511.

M. Pan, I. Bulatov, R. Smith, & J. K. Kim, 2012a, Novel MILP-Based Iteractive Method for the Retrofit of Heat Exchanger Networks with Intensified Heat Transfer, Comput. Chem. Eng., in press, doi: 10.1016/j.compchemeng.2012.02.002.

M. Pan, I. Bulatov, R. Smith, & J. K. Kim, 2012b, Optimisation for the Retrofit of Large Scale Heat Exchanger Networks with Comprising Different Intensified Heat Transfer Techniques, Appl. Therm. Eng., in press, doi: 10.1016/j.applthemaleng.2012.04.038.

R. Bochenek, & J.M. Jezowski, 2006, Gentic Algorithms Approach for Retrofitting Heat Exchanger Network with Standard Heat Exchangers, Comput. Aided Chem. Eng., 21, 871-876.

T. F. Yee, & I. E. Grossmann, 1991, A Screening and Optimization Approach for the Retrofit of Heat-Exchanger Networks, Ind. Eng. Chem. Res., 30, 146-162.

I.A. Karimi and Rajagopalan Srinivasan (Editors), Proceedings of the 11th International Symposium on Process Systems Engineering, 15-19 July 2012, Singapore.

Simulation based Heuristics Approach for Plantwide Control of Propane Precooled Mixed Refrigerant in Natural Gas Liquefaction Process

Yuli Amalia Husnil[1], Changuk Park[2], Moonyong Lee[1]*

[1]*School of Chemical Engineering, Yeungnam University, Gyeongsan, 712-749, Korea*
[2]*Institute for Advanced Engineering, Yongin, 449-863, Korea*
**Corresponding Author's e-mail: mynlee@ynu.ac.kr*

Abstract

In this paper a simulation based heuristic approach is used to configure the control structure of propane precooled mixed refrigerant (MR) natural gas (NG) liquefaction process. The liquefaction of NG in cryogenic exchanger involves MR stream condensation and vaporization in different sections of cryogenic exchanger. This increases the interactions among MR streams as illustrated using dynamic simulation. To identify these interactions, first the sensitivity analysis of propane precooled MR was carried out and then several heuristic based on dynamic simulation were proposed for disturbance rejection and increased liquefied natural gas (LNG) production rate. Major findings from several case studies suggest that the maximization of available cold energy is possible by utilizing temperature difference between MR streams as set point for controlling LNG production rate.

Keywords: Plantwide control, Cryogenic exchanger, Heuristics, Dynamic simulation, LNG.

1. Introduction

Several Natural gas (NG) liquefaction process are available in world market and Air Products and Chemical, Inc. licensed, propane pre-cooled mixed refrigerant process (C_3MR) accounts for about 80% of worlds baseload liquefied natural gas (LNG) production capacity. Liquefaction of NG in this process is achieved by successive condensation and vaporization of MR in cryogenic heat exchanger. MR with lower boiling and higher boiling components flows in separate loops in cryogenic exchanger to achieve liquefaction. The presence of several MR loops provides difficulty in designing robust control structure which is essential for plant safety and profitable operation. Understanding the hidden nature of interaction that exists between MR loops and other plant variable can overcome the challenging task of robust control design. In this regard, dynamic simulation plays an essential role in giving the insight of inherent process dynamics. In dynamic simulation every independent variable of the plant can be changed arbitrarily to see its effect on the process plant which is not possible in real plant. However, without well structured guideline these tests will fall on the series of trials and errors and consumes a lot of time. Konda et al (2005) proposed an integrated framework of dynamic simulation and heuristics based on Luyben's work (Luyben et al., 1997). This idea is uncommon considering most of the works in plantwide control design utilize dynamic simulation to validate the control structure (Vasbinder et al., 2004). This work of configuring the control structure of C_3MR is also inspired by Luyben's work. First the main disturbances are identified and the best manipulated

variables are correspondingly paired with controlled variables that increase LNG production and plant safety. Based on extensive case studies performed on dynamic simulation of C_3MR process, several general guidelines and heuristics are proposed for robust control and are listed in section 3.6.

2. Description of C_3MR Process Plant

The dynamic model of C_3MR plant was developed in Aspen Hysys® V.7.1 platform and the schematic diagram is illustrated in *Fig 1*. Peng-robinson equation of state was used for thermodynamic property calculation. It should be noted that propane cycle which precools NG to -32.7^{o}C is ignored in this study and MR cycle is considered for control configuration. High pressure NG stream which is mainly methane enters the cryogenic exchanger at -32.7^{o}C and exchange heat with MR in Exchanger 1 & 2 (Exchanger 1 & 2 are in fact hypothetical division of main cryogenic exchanger) and exits at -146.7^{o}C which is flashed to atmospheric pressure before shipping. Other part of MR liquefaction consists of compression and cooling assembly of MR. Compressed MR is flashed and MR vapor and liquid (MRV & MRL) enters the Exchanger 1. MRL after pressure let down in Joule Thompson valve act as cold stream for the other stream in Exchanger 1. Similarly in Exchanger 2 MRV act as cold stream which subcooled and liquefy the NG gas. Compression of MR is achieved in staged compression with intermediate cooling. Presence of several MR loops provides challenge in profitable and safe operation of liquefaction plant. Hence a robust control strategy must be needed and described in section 3.4.

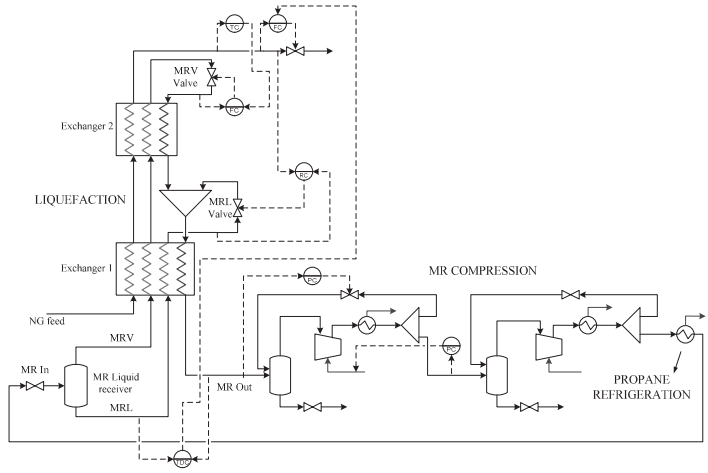

Figure 1. Process flowsheet and control configuration of C_3MR process plant

3. Dynamic Simulation and Heuristic Methods

The simulation based heuristic method is explained in this section. The original method of Konda et al. consists of 8 steps but in this work only the first four are applied with some adjustments. The rest of other steps are considered irrelevant with the respective process. The role of steady-state and dynamic simulation will be involved in most of the steps.

3.1. The Control Objectives

A plant control system can be divided into three levels of hierarchy (Hovd and Skogestad, 1993). From the lowest to the highest level, control objectives of C_3MR

process can be summarized as follows. At the level of *regulatory control* the control objective is to maintain the stability of the operation. Moving to *supervisory control*, the control structure is aimed to maintain the quality of the product and can be obtained by maintaining the temperature of LNG. At the highest level, *plantwide optimization*, the objective is to optimize the usage of cold energy available in MR. Considering above, LNG production rate in C_3MR can be adjusted according to the available cold energy in MR, instead of fixing it at certain value. The difference, between inlet and outlet temperature of MR can be utilized as indicator for the availability of cold energy in the liquefaction. The higher the difference means there is still some cold energy available that can be used to liquefy more natural gas. In contrary, if the difference getting smaller and cross the lower bound then the natural gas throughput should be decreased.

3.2. Control Degrees of Freedom (CDOF) Analysis

CDOF analysis based on Konda et al. (2006) was performed for process under study and the value of 13 variables was come out. Among those variables, flowrate of LNG, MRL, and MRV are selected as manipulated variables. The controlled and manipulated variables are listed on *Table* 1.

Table 1. List of controlled and manipulated variables

Controlled Variables	**Manipulated variables**
LNG temperature (y_1)	LNG flowrate (u_1)
Temperature Difference between inlet (MRL inlet stream) and outlet MR (y_2)	MRV flowrate (u_2)
	MRL flowrate (u_3)

3.3. Disturbances Identification & controller pairing selection

Based on simulation studies three potential sources of disturbance are identified for the process under study that are NG inlet; temperature, pressure and composition. Among the three disturbance sources, NG pressure and its composition has significant effect to controlled variables. The most interesting result obtained from series of tests in dynamic simulation is the inverse response of LNG temperature when MRV and MRL flowrate were step changed as can be seen from *Fig. 2*. Step change responses of MRL & MRV flowrate have same controller gain but give different time constant. It is expected that pairing MRL flowrate with both controlled variables would give a poor performance and should be avoided.

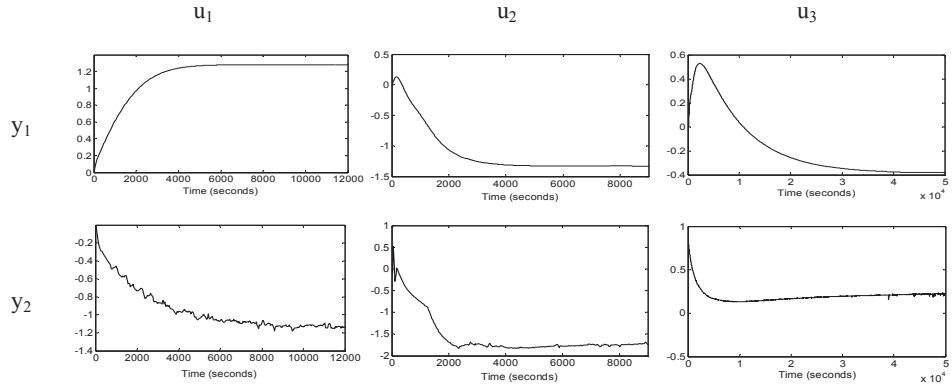

Figure 2. Open loop responses of controlled variables after step changes on manipulated variables

3.4. Selecting Best Pairings

Relative gain array (RGA) is utilized for find best pairing that corresponds to good controller performance. The steady-state gain that is used in pairing analysis purpose is obtained from closed and open loop simulation of the process. The summaries of RGA are shown in *Table 2*.

Table 2. Results from RGA analysis of three different structures

Closed-loop						Open loop					
Structure 1		Structure 2		Structure 3		Structure 1		Structure 2		Structure 3	
u_1-u_2		u_2-u_3		u_1-u_3		u_1-u_2		u_2-u_3		u_1-u_3	
0.67	0.33	0.35	0.65	11.84	-10.84	0.47	0.53	0.45	0.54	-2.71	3.71
0.33	0.67	0.65	0.35	-10.84	11.84	0.53	0.47	0.54	0.45	3.71	-2.71

RGA analysis shows inconsistent results. Closed and open loop RGA recommends different pairing for structure 1. Also, structure 3 has negative RGA in off-diagonal pairing based on closed-loop analysis while in open loop analysis the negative RGA is in diagonal pairing. Despite these contradictions, the negative magnitude of RGA in structure 3 is enough reason to screen it out. It is said earlier, based on analysis of *Fig. 2*, that utilizing MRL flowrate or u_3 as manipulated variable should be avoided because it gives relatively slow response. Since structure 2 contains u_3 as one of manipulated variables therefore this structure is also omitted.

The analysis above left structure 1 as the only candidate for control structure. However it is also not clear whether to select the diagonal or the off-diagonal pairing. Several disturbance tests on simulation studies will provide the answer of which pairing gives better control performance. In case of MRL flowrate, there are two possible ways of utilizing it. One is by utilizing MRL flowrate or MRL valve for controlling liquid level of MR receiver. Second, MRL flowrate is fixed on certain ratio with LNG flowrate using MRL valve as the control element.

Finally, four control structures are left after screening and their description is provided in *Table 3.*

Table 3. List of four final control structures

Manipulated variable	Structure 1 (S_1)		Reverse Structure 1 (RS_1)	
	S_1-LC	S_1-RC	RS_1-LC	RS_1-RC
LNG flowrate	LNG temperature	LNG temperature	Temp. difference	Temp. difference
MRV flowrate	Temp. difference	Temp. difference	LNG temperature	LNG temperature
MRL valve	Liquid level	LNG/MRL ratio	Liquid level	LNG/MRL ratio

3.5. Control Structure Assessment

S_1-RC is discarded from the structure candidate because it fails to maintain controlled variables at their respective setpoints during inlet pressure disturbance. The other three structures are able to reject the disturbance but perform differently. Screening best among the final three structures is based on IAE performance during disturbance rejection and shown in *Fig 3 & 4*. RS_1-RC has the smallest IAE compare to the other structures in both disturbance tests. Therefore, RS_1-RC is selected as the control structure for C_3MR liquefaction process. The control arrangement for RS_1-RC is presented on *Fig. 1*.

3.6. Conclusions

A robust plantwide control strategy for C_3MR process plant was developed based on dynamic simulation and RGA analysis. Preliminary selection among several candidate control configuration was based on RGA analysis. IAE performance was used to choose the best structure and finally RS_1-RC was selected. Based on simulation studies and quantitative analysis performance on C_3MR plant several heuristics are made:

i) LNG outlet temperature should always be paired with MRV flowrate.
ii) MR temperature difference is a good measure for product maximization.
iii) Simulation and quantitative analysis should be used in parallel to get the best controller configuration.
iv) IAE index is a good performance evaluation criterion in liquefaction plant control strategy development.

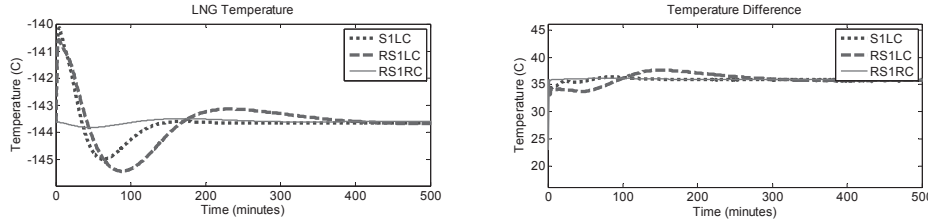

Figure 3. Responses of variables on different structures after NG inlet pressure is increased 1 bar

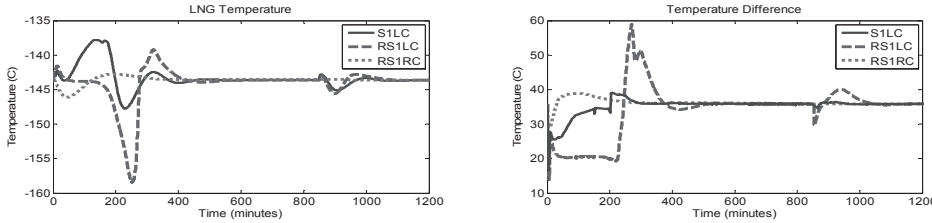

Figure 4. Responses of variables on different structures after composition of NG is changed (reducing 20% of methane and increasing 20% of ethane)

Acknowledgment

This research was supported by a grant from the Gas Plant R&D Center funded by the Ministry of Land, Transportation and Maritime Affairs (MLTM) of the Korean government

References

N. V. S. N. M. Konda, G. P. Rangaiah, P. R. Krishnaswamy, 2006, A Simple and Effective Procedure for Control Degrees of Freedom. Chem. Eng. Sci., 61, 1184-1194.

N. V. S. N. M. Konda, G. P. Rangaiah, P. R. Krishnaswamy, 2005, Plant-Wide Control of Industrial Processes: An Integrated Framework of Simulation and Heuristics, Ind. Eng. Chem. Res., 44, 8300-8313.

M. L. Luyben, B. D. Tyreus, W. L. Luyben, 1997, Plantwide control design procedure, Process Systems Engineering, 43, 3165-3174

M. Hovd, S. Skogestad, 1993, Procedure for Regulatory Control Structure Selection with Application to the FCC Process. AICHE Journal, 39, 1938-1953

E. M. Vasbinder, K. A. Hoo, U. Mann, 2004, Synthesis of Plantwide Control Structures Using a Decision-Based Methodology. In The Integration of Process Design and Control; Seferlis, P., Georgiadis, M. C., Eds; Elsevier: New York, 375-400.

I.A. Karimi and Rajagopalan Srinivasan (Editors), Proceedings of the 11th International Symposium on Process Systems Engineering, 15-19 July 2012, Singapore.

Studying the effect of feed composition variation on typical natural gas liquid (NGL) recovery processes

Mesfin Getu[a], Mohd Shariq Khan[b], Nguyen Van Duc Long[b] and Moonyong Lee[b*]

[a]Chemical Engineering Department, Curtin University of Technology, CDT 250, 98009 Miri, Sarawak, Malaysia.

[b]School of Chemical Engineering, Yeungnam University, 214-1 Dae-dong, Gyeongsan, Gyeongbuk 712-749, Republic of Korea.

*: Corresponding author: mynlee@ynu.ac.kr

Abstract- In this work, the different process schemes used for known NGL recovery methods have been studied with various feed compositions. The original turbo-expander process scheme (ISS) was considered as a base case. The GSP, CRR, RSV and RSVE process schemes are those which focus on improvement at the top of the demethanizer column, while the IPSI-1 and IPSI-2 at the bottom of the demethanizer column. All the process schemes have initially built using ASPEN HYSYS with a common set of operating criteria. Numerous simulation runs have been made later by taking various typical feed compositions classified as lean and rich. Regardless of the common operating conditions set to each process schemes, there exist different performance results obtained from the simulation. Accordingly, the reboiler duty requirement is high for the GSP, CRR, RSV and RSVE due to the need for external refrigeration. However, the IPSI-1 and IPSI-2 simulation result show relatively lower reboiler duty requirement for the self-refrigeration system applied to the systems.

Keywords: Feed composition, lean feed, process scheme, rich feed.

1. INTRODUCTION

Basic technology trends for natural gas liquid (NGL) recovery have emerged since 1970 onwards. A major leap in gas processing industries was the introduction of a turbo-expander design scheme, which is also known as an Industry-Standard Single-stage (ISS) process scheme. The ISS scheme is considered as a major leap development towards gas industry for its better performance compared to the previous oil absorption and refrigeration techniques. However, this process scheme has still certain limitation in terms of operational flexibility and overall recovery performance (Rahman et al., 20004). As a result, a number of various design schemes have evolved after that to improve the process efficiency which can contribute for higher NGL recovery. The Gas sub-cooled process (GSP) scheme was later developed by Campbell and Wilkinson (1981) to solve several problems related to the turbo-expander process scheme. The cold residue-gas recycle (CRR) was introduced in the original design of GSP by Campbell et al. (1989) to improve ethane recovery efficiency. The Recycle split-vapor (RSV) developed by Campbell et al. (1996) was another alternative process scheme for high NGL recovery. A modification of the RSV process scheme, recycle split- vapor

with enrichment (RSVE), was also developed by Campbell et al. (1999). All the GSP, CRR, RSV and RSVE process schemes mainly focus on improving of the reflux stream to the demethanizer column. Unlike those process schemes, an enhanced NGL recovery process (IPSI-1) which was introduced by Yao et al. (1999) gives a process enhancement at the bottom of the demethanizer column. The internal refrigeration for enhanced NGL recovery (IPSI-2), which is introduced recently by Lee et al. (2007), is also another process enhancement which focuses on the bottom of the demethanizer column. The condition for feed composition is an important factor since it determines what kind of process configuration to be employed for recovering NGLs (Jibril et al., 2006). It is also considered as a basic requirement for particular process scheme whether it can accommodate a range of feed composition which varies from time to time. In this work, various feed compositions were considered and characterized under the basic classification of lean and rich feeds. The original turbo-expander process scheme (ISS) is taken as a base case plant. The GSP, CRR, RSV and RSVE are those process schemes those that focus improvement on the top of the demethanizer column. The IPSI-1 and IPSI-2 are those that focus on the bottom of the demethanizer column. Accordingly, HYSYS (Aspen HYSYS V7.1) simulations were made initially for all the process schemes by setting common operating parameters as criteria in order to compare the performance of each scheme. Later, a range of typical feed compositions which are classified as lean and rich feeds are used to study the performance of each process schemes.

2. Case study

2.1. Feed composition and operating conditions

The feed composition is a very vital factor which affects the NGL recovery. Since the feed normally originates from upstream plants, there is a continuous variation of feed composition which increases the instability of the plant operation (Fleshman et al. 2005). Thus, to study the different feed composition types, a typical eight gas feeds are adapted from literatures Jibril et al. (2006) as shown in Table 1. The feeds have been arranged in accordance to increasing order of C_{5+} content (heavier hydrocarbons).

Table 1: Typical feed composition in mole percent (mol %)

Components	Feed 1	Feed 2	Feed 3	Feed 4	Feed 5	Feed 6	Feed 7	Feed 8
C_1	0.9717	0.8457	0.8400	0.8034	0.7260	0.6507	0.6539	0.5952
C_2	0.0189	0.0820	0.0760	0.0693	0.0494	0.1050	0.0504	0.0536
C_3	0.0029	0.0340	0.0200	0.0259	0.0176	0.0497	0.0297	0.0471
iC_4	0.0013	0.0058	0.0000	0.0043	0.0038	0.0095	0.0090	0.0203
C_4	0.0012	0.0086	0.0000	0.0073	0.0067	0.0187	0.0172	0.0239
IC_5	0.0007	0.0028	0.0070	0.0018	0.0031	0.0077	0.0085	0.0180
C_5	0.0005	0.0021	0.0000	0.0015	0.0031	0.0078	0.0084	0.0161
C_6	0.0004	0.0018	0.0030	0.0016	0.0046	0.0125	0.0160	0.0260
C_7	0.0024	0.0012	0.0000	0.0017	0.0167	0.0149	0.0214	0.1998
C_8	0.0000	0.0005	0.0000	0.0018	0.0000	0.0156	0.0243	0.0000
C_9	0.0000	0.0004	0.0000	0.0019	0.0000	0.0108	0.0194	0.0000
C_{10}	0.0000	0.0005	0.0000	0.0005	0.0000	0.0352	0.0652	0.0000
N_2	0.0000	0.0055	0.0540	0.0619	0.1325	0.0349	0.0464	0.0000
CO_2	0.0000	0.0091	0.0000	0.0171	0.0365	0.0270	0.0302	0.0000
Total	1.0000	1.0000	1.0000	1.0000	1.0000	1.0000	1.0000	1.0000

The first five feeds (1 to 5) are classified as lean feeds, while the remaining three feeds (6 to 8) are rich feeds. The classification for lean and rich feed is usually based on the contents of C_2 or C_3 components. Accordingly, if the C_2 content is less than 10% or the C_3 content less than 4%, the feed is considered as lean feed, otherwise it is taken as rich feed. Feed 5 is more close to lean feed property than rich feed even if it does not fulfil to the above requirement due to its large N_2 content (13.25%). It is also important to notice that feed 5 has the maximum contents of N_2 and CO_2 components. The feeds which contain the minimum N_2 content ($N_2 = 0$) are feed 1 and 8. Similarly, the feeds which contain the minimum CO_2 content ($CO_2 = 0$) are feed 1, 3 and 8.

The main step toward a good comparison of the different alternative NGL recovery method is to assess the details of the simulation for each process scheme (Lynch et al., 2007). Due the different types of additional equipment introduced on each process scheme, it may not be possible to have an exact comparison among the processes. However, by tabulating some main operating data, it is possible to identify those key process parameters which have a significant effect on the overall plant performance. The key process operating parameters which are used for comparison purpose are shown in Table 2.

Table 2: common process key parameters taken for comparison

Feed flow (kgmole/h)	5000
Plant inlet gas pressure (psia)	1040
Plant inlet gas temperature (°F)	120
Salesgas outlet pressure (psia)	730
Salesgas outlet temperature (°F)	120
Product specification (C_1/C_2 ratio)	0.02
Theoretical trays including reboiler	41
Compressor/Expander/pump efficiency (%)	75
Demethanizer pressure (psia)	337
Pressure drop across the heat exchangers, shell and tube sides (psi)	10
Property fluid package	Peng Robinson

2.2. Effect of feed composition on various process scheme

The feed energy requirement for each process scheme is shown in Fig. 1. It can be observed from the figure that the feed energy is same for a particular feed regardless of the different process schemes applied. For example, if we consider feed 1, the corresponding feed energy value is -10.56×10^4 kW for all the process schemes. The feed energy is actually obtained by multiplying the enthalpy of the feed and its flow rate. However, the feed flow rate is constant for all the feeds as shown in Table 2. The difference in feed energy for the eight feed types arises due to the variation of the feed compositions shown in Table 1, which in turn changes the values of the enthalpy. Based on Fig. 8, the rich feeds (6-8) normally requires more chilling than the lean feeds (1-5). Hence, mechanical refrigeration which consists of primarily pure refrigerant, such as propane, is mostly used as external refrigeration source especially for GSP, CRR, RSV and RSVE. In addition, a mixed refrigerant and cascade refrigeration cycle may also be used depending on the process requirement. Further cooling of those feeds is also provided by the turbo-expander with appropriate heat exchange.

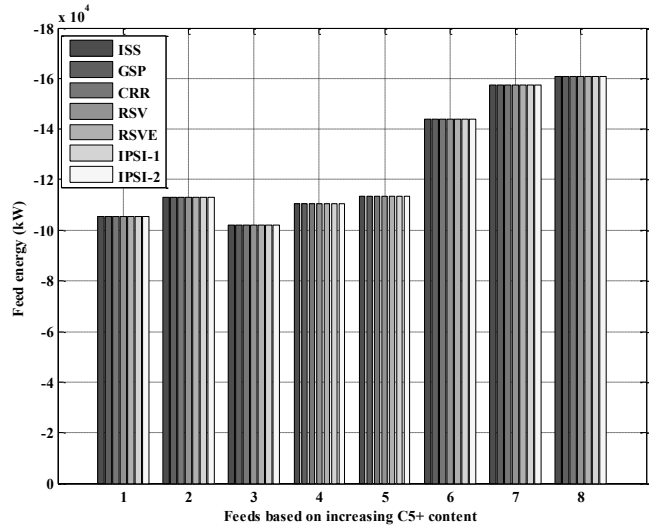

Fig. 1 Energy requirement of feed

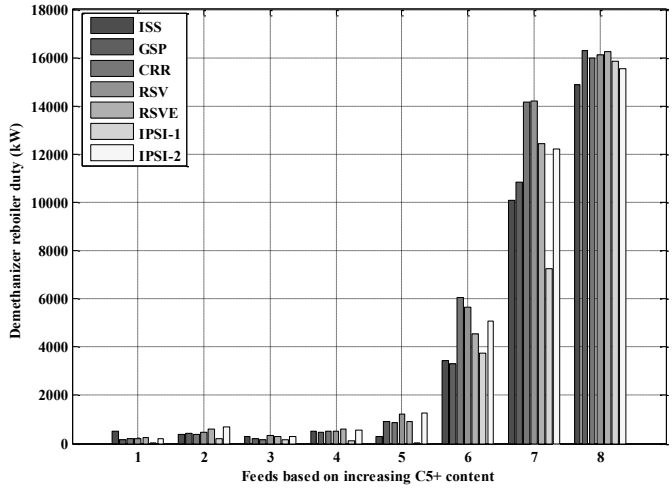

Fig. 2 Energy consumed by demethanizer reboiler

The demethanizer reboiler and salesgas compressor are the major energy consuming units in NGL recovery. The energy consumption of the demethanizer reboiler as the heavier hydrocarbon content increases is shown in Fig. 2. The leaner feeds (1-5) generally give a lower duty than those of the rich feeds (6-8). This is due to the presence of high heavier hydrocarbons (C_{5+}) components in the rich feeds. Propane refrigeration or other external sources is usually used for the rich feeds (6-8) to condense the heavier hydrocarbon (C_{5+}) components. This will maintain the low temperature profile in the demethanizer column by reducing the steam requirement. Referring to Fig.2, the IPSI-1 process scheme has the lowest reboiler duty for the lean feeds (1-5) compared to any of the other process scheme. This is mainly because the advantage of the self refrigeration system which can efficiently reduces energy for such kind of feeds. Even for the rich

feed 6 and 7, the IPSI-1 process scheme has lower reboiler duty. However, for very rich feed, such as feed 8, the IPSI-2 process scheme gives a lower reboiler duty than IPSI-1. One of the limitations of the IPSI-1 process scheme was that when a large amount of external refrigeration is needed, there seems a shortage of refrigeration that can be produced by the self refrigeration system. However, the improved self refrigeration system (open and closed refrigeration cycles) of the IPSI-2 scheme helps to reduce this limitation. Accordingly, the IPSI-2 process scheme lowers the temperature in the demethanizer column and improves the heat integration to cool the rich feed gas through reboiler. This will reduces external heating and refrigeration requirements. In addition, it also reduces the need for external reboiler heat and thereby saves both steam and refrigeration usage.

Conclusion

A simulation study for comparing representatives NGL recovery process has been made by considering a range of various feed composition classified as lean and rich feeds. The effect of feed composition variation and its impact on the economic analysis for the different process schemes have also been assessed. The ISS, GSP, CRR and RSV generally require more refrigeration for rich feeds than lean feeds. Lean feeds give a lower reboiler duty than rich feeds. The self-refrigeration system applied to the IPSI-1 and IPSI-2 has helped in reducing the reboiler duty requirement by avoiding additional external refrigeration as compared to those developments made at the top of the demethanizer column.

Acknowledgment

This research was supported by a grant from the gas plant R&D center funded by the Ministry of Land, Transport & Maritime Affairs (MTLM) of the Korean Government.

References

Campbell, R.E., Wilkinson, J.D.1981. Hydrocarbon gas processing. *U.S. Patent 4,278,45*.

Campbell, R.E., Wilkinson, J.D., Hudson, H.M., 1989. Hydrocarbon gas processing. *U.S. Patent 4,889,545*.

Campbell, R.E., Wilkinson, J.D., Hudson, H.M.,1996, Hydrocarbon gas processing. *U.S. Patent* 5,568,737.

Campbell, R.E., Wilkinson, J.D., Hudson, H.M., Pierce, M.C.,1999, Hydrocarbon gas processing. *U.S. Patent* 5,983,664.

Fleshman, J., Alderton, P., Bahnassi, E., Khori, A.R.,2005, Achieving Product Specifications for Ethane through to Pentane Plus from NGL Fractionation Plants. *Presented on AIChE annual meeting*, Cincinnati, OH.

Jibril, K.L., Al-Humaizi, A.L., Idriss, A.A., Ibrahim, A.A.,2006, Simulation study determines optimum turboexpander process for NGL recovery. *Oil and Gas Journal,* 104, 58-62.

Lee, R.J., Zhang, Y., Yao, J., Chen, J.J and Elliot, D.G.,2007, Internal refrigeration for enhanced NGL recovery. U.S. Patent 7,257,966.

Lynch, J.T., Lousberg, N.B., Pierce, C.M., 2007, How to compare cryogenic process design alternatives for a new NGL project. *Presented at the 86th annual convention of the gas processors association, Denver, Colorado*.

Rahaman, A.A., Yusof, A.A., Wilkinson, J.D., Tyler, L.D.,2004, Improving ethane extraction at the PETRONAS gas GPP-A facilities in Malaysia. *Presented at the 83rd annual convention of the gas processors association* New Orleans, Louisiana.

Yao, J., Chen, J.J., Elliot, D.G.,1999., Enhanced NGL recovery processes, *United states patent number:* 5,992,175.

I.A. Karimi and Rajagopalan Srinivasan (Editors), Proceedings of the 11th International Symposium on Process Systems Engineering, 15-19 July 2012, Singapore.

Techno-Economic Analysis for the Synthesis of Downstream Processes from the Oxidative Coupling of Methane Reaction

Daniel Salerno[a], Harvey Arellano-Garcia[a], Günter Wozny[a]

[a] *Department of Process Dynamics and Operations, Sekr, KWT-9, Berlin Institute of Technology, Strasse des 17 Juni 135, D-10623, Berlin, Germany*

Abstract

Due to the huge methane deposits worldwide and the great need for the chemical process industry to have new alternatives for olefins production, especially ethylene as starting raw material for numerous products, the direct conversion of methane to ethylene has attracted considerable interest. The main reason that motivates the realization of this new approach is to exploit the availability of un-reacted methane, coming from the exit flue gas products of the OCM reactor, and thus, design an alternative process for methanol and formaldehyde production via OCM and the co-generation of electricity that can make the process economically attractive and designed so as to be industrially implemented. The total project investment, based on total equipment cost, as well as variable and fixed operating costs, was developed based on mass and energy balance information taken from Aspen® Process Economic Analyzer simulation results. The feasibility was evaluated in terms of energy savings, CO_2-emission reductions and costs, in comparison to the separate production of methanol with conventional technology alone. Before starting the economic study of the OCM process a preliminary analysis of possible plant locations has been developed. Natural gas is a commodity which price varies strongly from one region to another. Moreover, not only the price of raw materials is affected by the location of the plant but also the costs associated with the production, namely: steam, refrigeration, electricity, fuel, wages, etc., affecting strongly the profitability of a petrochemical project. Due to low natural gas prices in Venezuela, which has the highest production potential in South America, and the highest ethylene sales for the European market, this geographical location has been chosen for economic analysis of this project. Kinetic data of the OCM reaction were taken from the experimental fluidized bed reactor values that has been build in our facilities at TU-Berlin, which reflect promising conversion, selectivity and yield values, testing different catalysts developed at the Institute of Chemistry inside the scope of the UNICAT project. This analysis suggests areas for research focus that might improve the profitability of natural gas conversion, and the results have also been used for the design of the pilot plant which is now being operational at our department.

Keywords: OCM reaction, ethylene production, methanol generation, formaldehyde production, economic evaluation.

1. Introduction

The oxidative coupling of methane (OCM), a heterogeneously catalyzed reaction, is one of the most intensively studied as a promising route for the production of ethylene by utilizing methane, the main constituent of natural gas. Despite the great efforts

dedicated to research better catalysts, so far only a few have achieved promising ethylene conversion values but it was not possible in the past 20 years to achieve yield values more than of 26% (Zavyalova, et al. 2011). There have been major research efforts to solve this problem and achieve higher methane conversions to make this process economically attractive to the industry (Kondratenko and Baerns, 2008). As oil prices rise, it becomes necessary to seek alternative sources of energy, so that for several years has become a concern for scientists to use natural gas as feedstock for the chemical industry; it is more advantageous to convert the natural gas to the useful products and transport the end product to users. Thus, several researchers are currently making great efforts to direct conversion of methane to value added products, such as ethylene (feedstock for petrochemicals), aromatics (ethyl benzene) and liquid hydrocarbon fuels (methanol). With this in mind, the development of a new process that converts directly methane into liquid fuel (e.g., gasoline), rather than through synthetic gas, has been carried out (Graf, 2008). Although great effort has been made on direct CH_4 conversion into oxygenates, the yield for desired products was below an economical value. However, the methane source is a key factor to make this oxidation process for methanol (CH_3OH) and formaldehyde (HCHO) economical achievable. The work presented here describes a feasibility study on the production of ethylene and oxygenated products (methanol and formaldehyde) and and also generation of electricity using the non-reacted methane coming from the OCM reaction.

2. Brief description of the processes

2.1. Original OCM Process

The OCM reaction is a highly exothermic process that is performed on metal oxide catalysts at temperatures between 700 and 900 °C. The process products are C_2H_6, C_2H_4, CO, CO_2, H_2 and H_2O. The COx (CO and CO_2) are formed from the complete combustion of hydrocarbons, which leads to point out the difficulties of achieving high performance in the OCM reaction process (Coronas, 1995). The complete process consists of three main sections: reaction, purification and separation section. Figure 1 shows the flowsheet for this process. The reactor is continuously fed with natural gas and oxygen. The feed gas is preheated to 700 °C, catalytic partial oxidized at pressure of 115 kPa and the reaction is carried out at 850 °C. The exothermic reaction heat has to be immediately removed using the transfer line exchanger to takeaway by vaporization of high-pressure boiler feed water, which is separated in the steam drum and subsequently superheated in the convection section to high-pressure superheated steam. The reaction products are compressed in a multi-compaction section to 1090 kPa and cooled down to 40 °C later on. In the purification section the reactor effluent gasses are cooled and then are fed into the bottom stages of a series of absorber columns that uses monoethanolamine (MEA) as absorbent solution. The MEA solvent is then regenerated in stripper columns thereby releasing the CO_2 captured in a dilute stream with water vapor product. The operation data from a pilot plant at TU Berlin were used to specify feed conditions and unit operation block specifications in the model. Finally, the ethylene separation section consists of two cryogenic distillation columns. The first one is the demethanizer and the unconsumed methane is separated from the product stream (ethylene and ethane). After the removal of light OCM gases, the next column separates the C_2+ components: ethylene at the top and ethane at the bottom.

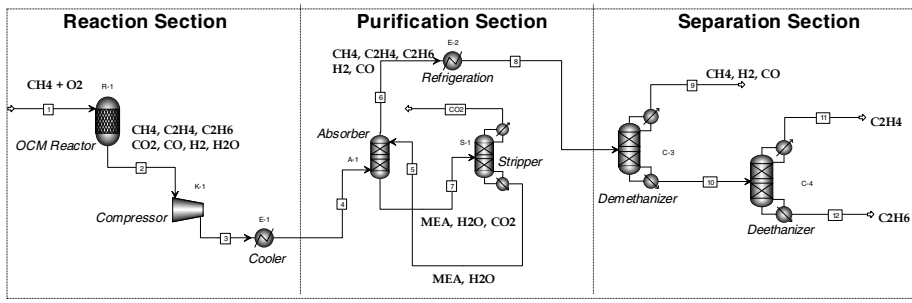

Fig. 1: Flowsheet for the Oxidative Coupling of Methane Process.

2.2. Formaldehyde and methanol process

The designed process is different from a commercial methanol plant based on autothermal reforming of natural gas. It uses the non-reacted methane from the OCM reaction process, a gas phase by-product stream composed by H_2O, CH_4, CO_2, CO and H_2. Although this is a by-products stream with low economic value for the ethylene production process, the amount of CO produced is attractive enough to be used in the production of synthesis gas. First this gases are purified by removing the components that may affect the conversion into synthesis gas (ethylene traces), before being used in the methanol process. The unreacted methane is used as raw material for the formaldehyde reaction. The reactor uses the selective oxidation of methane yielded essentially CH_2O, CO, CO_2, and H_2O, which takes into account chemical kinetics obtained from the fixed-bed reactor experiment (Yang et al. 1998). Additional oxygen as oxidant is required to fulfill the reaction conditions producing the equivalent of 117.1 metric tons of formaldehyde per day. All CH_2O formed in this reactor has been purified using two distillation columns. After the formaldehyde product separation follows the synthesis gas production using the stream coming from the top of the demethanizer column of the formaldehyde purification section. For this section the synthesis gas comes from a fixed-bed reactor for the catalytic partial oxidation of methane at conditions suitable for the production of methanol (De Smet, 2001). Addition of CO_2 (from the OCM purification process with amines) is possible in order to adjust the carbon/hydrogen ratio, which depends on the concentrations of CO and CO_2 from the non-reacted methane. The gas exiting the reformer is cooled with water generating the steam for the reformer. The synthesis gas is compressed to 30 bar by intercooled compressors before entering the synthesis reactor. The reactor operates at 250 °C and the composition of the outlet gas is calculated assuming chemical equilibrium. The chemical equations used in the production of methanol and the kinetic data were taken from Gallucci et al. (2007). The flowsheet of the process is shown in figure 2.

3. Results and discussions

The strategic implications of being able to use natural gas as a feedstock continue to provide an incentive to develop the OCM process. One way forward is to integrate the OCM process with another process, whereby through synergistic effects the combined process can be made economically attractive. The feature of the OCM process that can most obviously be exploited in this context is the large heat of reaction.

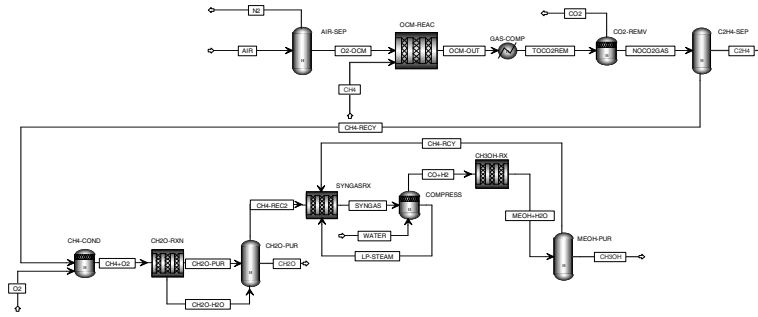

Fig. 2: Simplified flowsheet for oxygenates plant process.

Before deciding what to do with the amount of non-reacted methane in the OCM process, we performed an economic analysis to compare the costs associated with recycling of this methane. Table 1 summarizes the economic overview of this analysis. The steady state flow rates of raw materials, products and by-products streams are summarized in Table 2. Both simulated processes (OCM alone and proposed alternative) consume a 2593 t/d pure methane as feed-stock, resulting in a production of 396 t/d of 99% purity ethylene. The alternative process also produces 117.1 and 204.2 t/d of formaldehyde and methanol respectively. The difference in water production in both processes can be explained because the alternative process goes through more equipment to produce steam to be the raw material for the syngas reaction before its final use in the methanol reactor.

Table 1: OCM Process Economic Results

Investment (Millions €)	OCM Process without CH_4 Recycling	OCM Process with CH_4 Recycling
Total Project Capital Cost	170.67	183.94
Total Operating Cost	266.05	255.34
Total Raw Material Cost	83.77	81.31
Total Utilities Cost	154.89	147.71
Total Products Sales (C_2H_4)	272.40	272.40
Payout Period (Years)	12.16	10.54

4. Conclusions

This analysis shows that it is possible to produce ethylene from the OCM reaction and also oxygenated products, methanol and formaldehyde, from the non-reacted methane coming from the OCM process. The design of the process has taking into consideration the alternative production of valuable chemicals, such as methanol, giving added value to the OCM process, besides the ethylene production made with this use of natural gas. This process can be implemented to enable an optimum utilization of the methane gas based on market demand. The payout period, the expected number of years required to recover the original investment in the project, is 8 years. The process presented here shows that it should be possible to produce ethylene from the OCM reaction that is suitable to satisfy de ethylene demand worldwide as a precursor for the production of other chemicals.

Table 2: OCM and Oxygenated Process Economic Results

	OCM Process Alone	OCM & Oxygenated Process Proposed
Raw Materials	(metric ton/day)	
Methane	2593.2	2593.2
Mono Ethanol Amine	676.7	676.7
Products		
Ethylene	396.0	396.0
Formaldehyde	---	117.1
Methanol	---	204.2
Ethylene purity (mass %)	99.6	99.2
By-products		
H_2O	1438.9	229.2
C_2H_6	19.6	25.7
CO_2	1675.2	518.8
CO	126.5	1512.9
H_2	72.0	108.6
Non-reacted CH_4	1421.1	502.2

The development of integrating the OCM process technology, including reactor considerations, and a materials survey under severe OCM reaction conditions have been conducted in this project. The inclusion of alternative processes to the traditional OCM process to increase its profitability is indeed feasible. Nevertheless, a bigger capital investment is required, and the benefits obtained from this are still overcome by the margins and pay out time periods of the OCM process, due to the increase on capital expenses and operative costs.

Acknowledgment
The authors acknowledge support from the Cluster of Excellency "Unifying Concepts in Catalysis" coordinated by the Berlin Institute of Technology and funded by the German Research Foundation – Deutsche Forschungsgemeinschaft.

References

J. Coronas, 1995, Síntesis de Hidrocarburos por Acoplamiento Oxidativo de Metano. Utilización de Reactores de Membrana. Doctoral Thesis, Universidad de Zaragoza, Departamento de Ingeniería Química y Tecnologías del Medio Ambiente (in Spanish).

F. Gallucci and A. Basile, 2007, A theoretical analysis of methanol synthesis from CO_2 and H_2 in a ceramic membrane reactor, International Journal of Hydrogen Energy, 32, 5050-5058.

P. Graf, PhD Thesis, 2008, University of Twente, Enschede, Netherland.

E. Kondratenko and M. Baerns, 2008, Oxidative Coupling of Methane, Handbook of Heterogeneous Catalysis, Chapter 13, Wiley-VCH, Weinheim, p. 3010-3023.

H. De Smet, H. de Croon, R. Berger, G. Marin and J. Schoten, 2001, Design of adiabatic fixed-bed reactors for the partial oxidation of methane to synthesis gas. Application to production of methanol and hydrogen-for-fuel-cells, Chemical Engineering Science, 56, 4849-4861.

C. Yang, N. Xu and J. Shi, 1998, Experimental and Modeling Study on a Packed-Bed Membrane Reactor for Partial Oxidation of Methane to Formaldehyde. Ind. Eng. Chem. Res. 37, 2601-2610.

U. Zavyalova, M. Holena, R. Schlögl and M. Baerns, 2011, Statistical Analysis of Past Catalytic Data on Oxidative Methane Coupling for New Insights into the Composition of High-Performance Catalysts, ChemCatChem, DOI: 10.1002/cctc.201100186.

I.A. Karimi and Rajagopalan Srinivasan (Editors), Proceedings of the 11th International Symposium on Process Systems Engineering, 15-19 July 2012, Singapore

Targeting industrial heat pump integration in multi-period problems

Helen Becker, * François Maréchal
Industrial Energy Systems Laboratory, Ecole Polytechnique Fédérale de Lausanne (EPFL), Lausanne, Switzerland

Abstract

Process integration aims at optimizing industrial processes by identifying the heat recovery potential and the optimal integration of energy conversion systems. Most industrial processes especially in the food industry are non-continuous problems (batch problems) that are more difficult to tackle with process integration techniques. Process integration of multi-period problems can become complex and often the heat integration is realized by using time averaging approaches. The main disadvantages are that the sizing of equipments becomes more difficult and that the investment cost calculation is almost impossible at the targeting stage, since storage tanks are not included. This work presents a MILP method that targets simultaneously the heat recovery and the integration of energy conversion systems like heat pumps and other utilities in multi-period multi-time problems. In each time slice, the heat cascade constraints are considered together with the flows of the utility streams and the mass balances for storage, which create a link between the different operating times.

Keywords: energy integration, pinch analysis method, utility integration, industrial heat pumps, process design, multi-period, storage units

1. Introduction

Process integration was originally developed for continuous processes. But many processes have non-continuous operation tasks and therefore the approach has to be adapted for multi-period problems. Often pseudo multi-period heat integration is realized by using the time average model (TAM) or the time slice model (TSM) (Linnhoff et al., 1988). The time average model uses average values over all operating time slices. This approach is correct when it is assumed that all batch operations can take place at any time and in any order or when it is assumed that heat storage is available. On the other side, the time slice model cuts the process into several time slices where the process operations are simultaneous. Using the composite curves resulting from the TAM, Krummenacher and Favrat (2001) propose a heuristic targeting method to identify the minimum number of heat storage units for the heat recovery. According to Kemp and Macdonald (1987), the TAM or pseudo-continuous approach is too simple and may give over optimistic results, except when heat storage is available, the TAM results in the theoretical energy efficiency which can be achieved with the maximum heat storage. The authors propose analog to the graphical heat cascade the new "time cascade" to identify energy storage for batch problems. Applying mathematical programming techniques, Grossmann and Santibanez (1980) present a mixed integer linear programming (MILP) formulation for a given number of time slices with different prices and demand fluctuations. The problem

*helen.becker@epfl.ch

not only optimizes the total annual costs but also gives the optimal scheduling solution. Later, Maréchal and Kalitventzeff (2003) developed a methodology, based on the TSM for multi-time problems. The times are only linked with the usage level of utilities but there is no possibility to integrate heat storage. To integrate indirect energy storage of batch problems in the heat exchanger network, Chen and Ciou (2008) use a mixed integer non-linear programming (MINLP) formulation. The problem can become very complex, since the storage tanks are included in the superstructure. Using the TSM and total site approach, Varbanov and Klemeš (2011) integrate heat storage to manage the heat supply from renewables. A systematic approach allows heat storage between process operations but the self-sufficient pockets are not considered, which may miss opportunities for combined heat and power integration. Stoltze et al. (1995) propose a combinatorial method to include the heat storage in the heat exchanger network design. Sadr-Kazemi and Polley (1996) propose an iterative search method based on the composite curves in terms of heat quantities to define the temperature interval. Heat storage and intermediate heat transfer networks enables the process to stay independent and more flexible. As shown from the literature review, heat storage is very important to improve the energy efficiency of a non-continuous process. The TSM seems to be more realistic for integrating multi-period and storage problems, since instant heat loads can be used. The purpose of this paper is to adapt the multi-period targeting method, using the TSM and to include the possibility to integrate heat storage tanks simultaneously with energy conversion units (e.g. heat pumps) to maximize the heat recovery in multi-period problems.

2. Methodology

This paper develops a methodology based on a MILP formulation, which is able to solve multi-scenarios (without storage) and multi-time slices (with storage between time slices). Each period is defined by the operating conditions and the operating time. A multi-time slice problem consists in several successive process operations in a given period. Non-continuous processes can easily be modeled, by dividing them for example into a certain number of typical days and each day is divided into necessary time slices depending on the process schedule (e.g. 12 typical days a year and 24 time slices corresponding to one hour of operation). The approach can also be useful for other application like the optimization of large scale process or urban systems.

2.1. MILP formulation for multi-time problems

A MILP problem that targets simultaneously the heat recovery and the integration of energy conversion systems like heat pumps and other utilities in multi-time problems, is developed. For each time slice, the heat cascade constraints are considered together with the flows of the utility streams and the storage tanks. The storage equations are added and create a link between the different time slices. Utility and storage units are optimized to satisfy the process demand for all time slices simultaneously. The MILP formulation developed for heat exchange restrictions (Becker and Maréchal, 2012) is extended to the time dimension. For a given period, the objective function minimizes the yearly operating costs (e.g. OpC_p from Eq. (1)) or the total costs including the annualized investment costs.

$$min(cy_p \sum_{t=1}^{nt} d_{p,t}(\sum_{f=1}^{nf}(c^{+}_{f,p,t}\sum_{u=1}^{nu} f_{u,p,t}\dot{E}^{+}_{f,u,p,t}) + c^{+}_{el,p,t}\dot{E}^{+}_{el,p,t} - c^{-}_{el,p,t}\dot{E}^{-}_{el,p,t} + \sum_{u=1}^{nu} f_{u,p,t}c_u)) \quad (1)$$

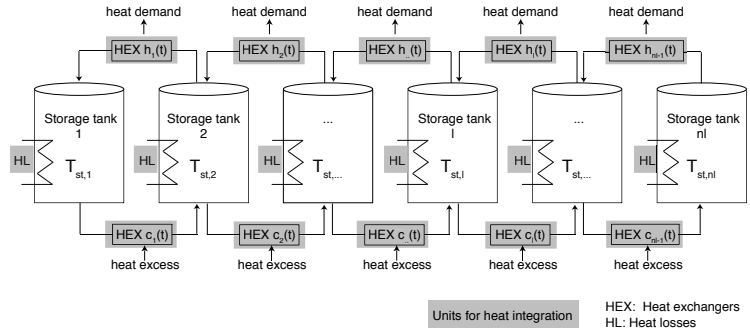

Figure 1. Definition of the storage network

nt is the number of time slices, cy_p is the number of cycles (e.g. number of days a year which can be represented by a chosen typical day), $d_{p,t}$ are the operating hours of time slice t in period p. The other terms concern the operating costs linked to fuel and electricity consumption and additional operating costs. For each time slice, the overall electricity import and the produced electricity in the process are defined. It becomes possible to take into account electricity price variations (e.g. peek hours or night prices). $f_{u,p,t}$ defines the multiplication factor of unit u in time t and period p. A unit can be a process ($f_{u,p,t} = 1$) or a utility ($f_{u,p,t}$ variable) unit. The flow rates of streams belonging to utility units are proportional to the multiplication factor. This factor is limited by a minimum and maximum value and corresponds to the usage level for a given time. The associated integer variable $y_{u,p,t}$ defines if the utility unit u is added to process ($y_{u,p,t} = 1$) or not ($y_{u,p,t} = 0$) in time t and period p. Thus, globally integrated utilities can be activated in a time slice and deactivated in another time slice.

$$y_{u,p,t} \cdot f_u^{min} \leq f_{u,p,t} \leq y_{u,p,t} \cdot f_u^{max} \tag{2}$$

Basically, the equations are extended to include the time dimension. In order to be able to integrate storage units, each time slice needs a link with its previous and next time slice.

2.2. Integration of storage tanks

Although the concept can be easily adapted to any kind of storage, only liquid (sensible) storage will be considered here. A given number of interdependent water tanks at discretized temperature levels can be integrated, as shown in Fig. 1. Water is heated up with available excess heat and will then be stored in a tank at higher temperature. In a following time slice, the water will be cooled down to satisfy a hot demand of the process. The cold water is then stored in a tank at lower temperature. The total maximal amount of water (M_{tot}) and the temperature levels of the tanks are defined as input parameters. The approach includes an estimation of heat losses which is linked to the temperature of the tank. The investment is evaluated as a function of the maximum needed storage capacity.

2.2.1. Mass balance

The overall mass balance is given as the cyclic constraint in Eq. (3), which states that the total stored mass has to be given back to the process. The water content after each time

is calculated for each tank in Eq. (4). $ds_{p,t}$ is the operating time in seconds of time slice t in period p and $\dot{M}$ is the water flow rate. Furthermore, constraints have to be added to guaranty the positive level of the tank, and that the total volume of water is not exceeded.

$$\sum_{t=1}^{nt}(ds_{p,t}\sum_{l=1}^{nl}(\sum_{h_l=1}^{ns_{h,l}} f_{u,p,t}\dot{M}_{h,l,u,p,t} - \sum_{c_l=1}^{ns_{c,l}} f_{u,p,t}\dot{M}_{c,l,u,p,t})) = 0 \tag{3}$$

$$M_{l,p,t} = M_{0,l} + \sum_{t=1}^{t}(ds_{p,t}\sum_{l=1}^{nl}(\sum_{h_l=1}^{ns_{h,l}} f_{u,p,t}\dot{M}_{h,l,u,p,t} - \sum_{c_l=1}^{ns_{c,l}} f_{u,p,t}\dot{M}_{c,l,u,p,t})) \tag{4}$$

2.2.2. Definition of thermal streams for the heat integration

The heat exchange with other process or utility units is shown on Fig. 1. The cold storage stream $c_n(t)$ is heated up by process excess heat and is going from a lower temperature tank l to tank $l+1$. Whereas the hot storage stream $h_n(t)$ corresponds to water coming from a higher temperature level and giving back heat to process units. As an example, a cold stream from tank l to tank $l+1$ is defined with the inlet temperature $T_{in} = T_{st,l}$ and the outlet temperature $T_{out} = T_{st,l+1}$. The corresponding heat amount is calculated with Eq. (5). By analogy the heat load is given for the hot stream.

$$\dot{Q}_{c,l} = f_{u,p,t} \cdot \dot{M}_{c,l,u,p,t} \cdot c_p \cdot (T_{st,l+1} - T_{st,l}) \tag{5}$$

2.2.3. Heat losses in storage tanks

Heat losses can be included, by adding a cold stream which corresponds to maintaining the temperature of each tank. The difficulty is to estimate the heat losses of each tank, especially because the size of tank is an optimization result and not known in advance. Therefore Eq. (6) has been used to estimate the heat losses in the tank. Knowing the current stored mass from Eq. (4), the heat losses can be calculated by Eq. (6).

$$\dot{Q}_{hl,l,p,t} = k_{hl} \cdot \frac{f_{hl} \cdot 4 \cdot M_{l,p,t}}{\rho \cdot d} \cdot (T_{st,l} - T_a) \tag{6}$$

ρ is the density of the considered storage fluid in the tanks in kg/m^3. In the following examples water is used. d is the diameter of the tank in m. k_{hl} is the considered heat loss coefficient and f_{hl} is a factor to account the heat losses on the top and bottom of the storage tank. To model the heat losses, new cold streams corresponding to the heat losses and the associated temperature are added to the heat cascade. The multiplication factor has been fixed to consider the calculated heat losses as heat loads. The advantage of adding the heat losses are on the one hand to make the problem more realistic and on the other side, it ensures that the storage fluid will be used as soon as possible.

3. Example and conclusions

As example, Fig. 2 gives some typical results of the presented methodology. The case study consists in one period with 15 time slices. For each time slice the storage tank levels and the optimal utility usage rates are calculated, which allows to evaluate the corresponding investment costs for new storage and utility equipments in a next step. The above method is generic and can be adapted through the definition of temperature levels, number of tanks and the maximum content. Heat pump integration benefits can be increased when integrating storage units because the heat pump working hours and their profitability can, by this way, be increased.

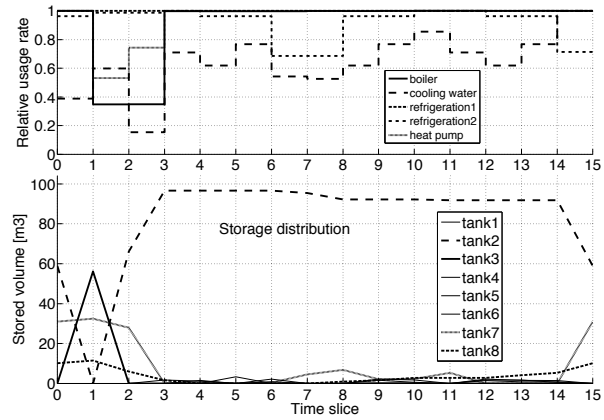

Figure 2. Storage tank distribution and relative utility utilization rate

4. Acknowledgements

The authors wish to thank ECLEER for supporting this research and collaborating in its realization.

References

Becker, H., Maréchal, F., 2012. Energy integration of industrial sites with heat exchange restrictions. Computers and Chemical Engineering 37, 104–118.

Chen, C., Ciou, Y., 2008. Design and optimization of indirect energy storage systems for batch processes. Industrial & Engineering Chemistry Research 47, 4817–4829.

Grossmann, I., Santibanez, J., 1980. Applications of mixed integer linear programming in process synthesis. Computers and Chemical Engineering 4 (4), 205–214.

Kemp, I., Macdonald, E., 1987. Energy and process integration in continuous and batch processes. IChemE Symposium Series (105), 185–200.

Krummenacher, P., Favrat, D., 2001. Indirect and mixed direct-indirect heat integration of batch processes based on pinch analysis. International journal of applied thermodynamics 4 (3), 135–143.

Linnhoff, B., Ashton, G., Obeng, E., 1988. Process integration of batch processes. IChemE Symposium Series (109), 221–237.

Maréchal, F., Kalitventzeff, B., 2003. Targeting the integration of multi-period utility systems for site scale process integration. Applied thermal engineering 23, 1763–1784.

Sadr-Kazemi, N., Polley, G., 1996. Design of energy storage systems for batch process plants. Chemical Engineering Research and Design 74 (5), 584–596.

Stoltze, S., Mikkelsen, J., Lorentzen, B., Petersen, P., Qvale, B., 1995. Waste-heat recovery in batch processes using heat storage. Journal of Energy Resources Technology, Transactions of the ASME 117 (2), 142–149.

Varbanov, P., Klemeš, J., 2011. Integration and management of renewables into total sites with variable supply and demand. Computers and Chemical Engineering 35, 1815–1826.

I.A. Karimi and Rajagopalan Srinivasan (Editors), Proceedings of the 11th International Symposium on Process Systems Engineering, 15-19 July 2012, Singapore.

Thermodynamic analysis of homogeneous non-isothermal mixing influence on the water-using networks' energy target

LUO Yiqing , LUO Sucai, YUAN Xigang

School of Chemical Engineering and Technology,Tianjin University, Tianjin 300072,China

Abstract

In order to take full advantage of non-isothermal mixing in designing a simple and energy efficient water network, this paper has divided streams into three types and has explored the effects of different mixing patterns between the three types of homogeneous streams on the water-using network' utility consumption target based on thermodynamic analysis method. The conclusions for homogeneous non-isothermal mixing in the paper can be used to analyze or optimize the heat exchanger network of a given water-using system.

Keywords: homogeneous non-isothermal mixings, thermodynamic analysis, water-using network, influence mechanism

1. Introduction

There are numerous cases where streams in industrial processes are allowed to be mixed. This is particularly the case with water networks. The energy required by water streams could be supplied indirectly through heat exchangers or directly through streams mixing. The implementation of streams mixing not only permits the reduction of the heat load exchanged in the system and therefore that of the amount and area of heat exchangers, but also changes the number of streams which exchange heat through heat exchangers. However, improper mixing would result in a penalty for energy targets because a larger temperature approach between streams causes energy degradation. Although conceptual methods [1-4] as well as mathematical programming methods [5-8] have studied more about the minimization of water and energy consumption for water-using system, they have mainly focused on network design purpose with the consideration of streams mixing opportunities, rather than understanding the mechanism of energy penalty caused by mixing and how the penalty can be eliminated or avoided. In this paper, the effect of different types of homogeneous non-isothermal mixing on system utility consumption is studied by thermodynamic analysis method, and conclusions obtained can be used to identify whether a homogeneous non-isothermal mixing is beneficial or not to the system utility consumption.

2. The classification of streams and of stream mixing

For the convenience of expression, some temperatures which characterize a stream joined in mixing are defined as follow:

T_{mix}: the temperature of the stream after mixing;

$T_{S,high}$: the supply temperature of the stream with $T_{S,high} > T_{mix}$;

Foundation item: supported by the National Natural Science Fundation of China under Grant 21176178 and the National Basic Research Program of China (973 Program) 2012CB720500

$T_{S,low}$: the supply temperature of the stream with $T_{S,low} < T_{mix}$;
T_P: the pinch temperature of a water-using system before streams mixing;
T_{target}: the temperature of a water-using unit.

Streams joined in mixing could be classified into two main groups:

Non-across-pinch stream. If T_P does not belong to the temperature range from $T_{S,high}$ (or $T_{S,low}$) to T_{mix}, the stream is a non-across-pinch stream. Non-across pinch streams can be further divided into streams above the pinch and streams below the pinch.

Across-pinch stream. If T_P belongs to the temperature range from $T_{S,high}$ (or $T_{S,low}$) to T_{mix}, the stream is an across-pinch stream.

Obviously there is a relationship $T_{S,high} > T_{mix} > T_{S,low} > T_{target}$ for hot-hot streams mixing, and $T_{target} > T_{S,high} > T_{mix} > T_{S,low}$ for cold-cold streams mixing. Therefore the mixing patterns between homogeneous streams (mixing between hot streams or mixing between cold streams) can be classified according to the position of the pinch temperature, as shown in the table 1.

Table1. Mixing patterns for homogeneous streams

Pinch position	Mixing patterns
$T_P \geq T_{S,high}$	Mixing between hot (or cold) streams below the pinch
$T_{S,high} > T_P > T_{mix}$	Mixing between a hot (or cold) stream across the pinch and a hot (or cold) stream below the pinch
$T_{S,high} > T_P = T_{mix}$	Mixing between a hot (or cold) stream above the pinch and a hot (or cold) stream below the pinch
$T_{S,high} > T_{mix} > T_P > T_{S,low}$	Mixing between a hot (or cold) stream across the pinch and a hot (or cold) stream above the pinch
$T_{S,low} \geq T_P$	Mixing between hot (or cold) streams above the pinch

3. The influences of homogeneous stream mixings on water-using network's energy target

In this paper water-using network structure is assumed to be given, and the continuous operation of water usage is considered, each water-using unit operated isothermally without water loss and heat loss, water stream data are available for mass flowrate and operating temperatures. The discharge temperature and the fresh water source are both specified as 30℃. And an equal specific heat capacity 4.2 kJ/kg ℃ for all water streams is assumed. Non-water-using operations are not included in heat recovery. A minimum temperature approach (ΔT_{min}) of 10℃ is assumed for any heat exchanger. After classifying the types of streams and mixing patterns, the influence of different kind of mixing to water-using system's energy target could be studied by thermodynamic analysis according to heat transfer and grade variation caused by stream mixing.

3.1. The mixing between homogeneous streams above the pinch ($T_{S,low} \geq T_P$)

When two hot streams join in mixing, a new stream with temperature (T_{mix}) is generated. If the mixing process is described using stream composite curve in T-H diagram, it can be found the flowrate of hot stream in the temperature range from $T_{S,high}$ to T_{mix} will decrease, and the flowrate in the temperature range of T_{mix} to $T_{S,low}$ will increase. As a result, the gradient of the hot composite curve from the temperature range of $T_{S,high}$ to T_{mix} will increase (in some cases, the hot composite curve in the temperature range may even vanish), while that from T_{mix} to $T_{S,low}$ will decrease, as the gradient of the hot composite curve is in inverse proportion with the stream mass flowrate. Therefore, it can be presumed that after the mixing, if the heat from T_{mix} to T_P (the T_P corresponding

to hot stream) can be totally recovered by cold streams in the temperature range from (T_{mix} – ΔT_{min}) to T_P (the T_P corresponding to cold stream), the system energy consumption will not change. Otherwise, the system energy consumption will increase. The reason for the increase is that part of the heat above the pinch is transferred to cold streams below the pinch after mixing, which will cause the waste of high temperature energy. Similarly, for the mixing between cold streams above the pinch, if the heat of hot streams in the temperature range between (T_{mix}+ ΔT_{min}) and T_P can't be totally recovered by the cold streams in temperature range from T_p to T_{mix}, the residual heat have to be transferred to the cold streams below the pinch, which definitely causes an energy penalty of the system. Otherwise, the hot and cold utilities consumptions of the system will keep still. An example of mixing between hot streams above the pinch with energy penalty is given in Fig.1 for detail illustration.

The water-using network is shown in figure 1a. When indirect heat exchange through exchangers is adopted for the water-using network, the cold and hot composite curves of the system are shown in the Fig. 1b. The pinch temperature is 60℃ (for hot streams) and 50℃ (for cold streams). When the mixing between the stream $F_{1,3}$ and $F_{2,3}$ is adopted, the mixing is between hot streams above the pinch. According to the mass and energy balance for the mixing, T_{mix} is 62.5 ℃. Obviously, the hot stream which can supply heat from 70℃ to 62.5 ℃ disappears, while the flow rate of hot stream supplying heat from 62.5 ℃ to 60 ℃ increases from 5 kg·s-1 to 20 kg·s^{-1}. Namely after the mixing, certain number of heat supplied originally in temperature interval from 70℃to 62.5 ℃ before the mixing now shifts to the temperature interval below 62.5 ℃. However, the heat requirement by cold stream from 50 ℃ to 52.5 ℃ does not change. Therefore after the mixing, there must be a part of the heat above the pinch now used to heat cold streams below the pinch, and the energy penalty of the system must occur. The composite curves of the system after the mixing (Fig. 1c) just demonstrate the result, the hot composite curve from 70 ℃ to 62.5 ℃ disappears after the mixing, while the gradient of the hot composite from 62.5 ℃ to 60 ℃ decreases. What's more, after the mixing the hot and cold utilities consumptions increase to 525kW and 1785kW respectively.

Example1： The mixing between hot streams above the pinch (with energy penalty)

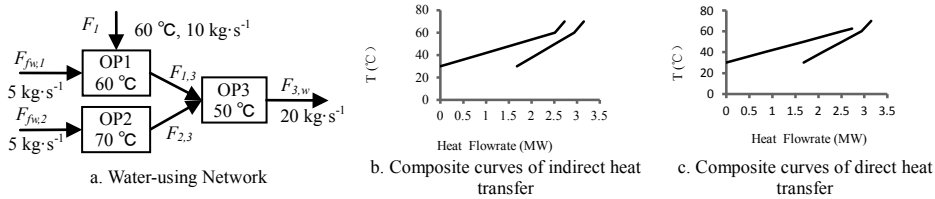

a. Water-using Network

b. Composite curves of indirect heat transfer

c. Composite curves of direct heat transfer

Fig 1. The mixing between hot streams above the pinch

3.2. The mixing between homogeneous streams below the pinch ($T_P \geq T_{S,high}$)

When the mixing between hot streams below the pinch occurs, in the temperature range from $T_{S,high}$ to T_{mix}, hot stream flowrate will decrease, which leads to the gradient of the hot composite curves in this temperature range increase; The flowrate in the temperature range from T_{mix} to $T_{S,low}$ will increase, which leads to the gradient of the hot composite curves in this temperature range decrease; Therefore, the hot composite curve will come closer to the cold composite curve after mixing. If hot streams in temperature range from T_{mix} to T_p can still supply the cold streams between (T_{mix} - ΔT_{min}) and T_p with the heat they need, the system energy consumption will not change; Or else, the system

energy consumption will increase. And the reason for the increase is also because part of heat above the pinch is transferred to cold streams below the pinch after mixing. For the mixing between cold streams below the pinch, if the heat of hot streams between ($T_{mix} + \Delta T_{min}$) and T_P can still meet the needs of cold streams from T_{mix} to T_p after mixing, the system energy performance will keep still. However, if not, the energy penalty occurs.

3.3. The others mixing patterns of homogeneous streams mixing

The other three types of hot-hot streams mixing will inevitably make some heat transferred across the pinch from up to down, and the energy punishment of the system must occur. Take the mixing between a hot stream across the pinch and a hot stream below the pinch for instance, as one of the mixing streams is across the pinch, part of the energy above the pinch will definitely be transferred to the mixing hot stream with a lower temperature below the pinch, which causes a penalty on the system energy consumption. As for the reminder mixing patterns of cold-cold streams mixing, the mixing will inevitably cause a penalty on the system utilities consumption, as part of heat will be transferred across the pinch from up to down.

3.4. Homogeneous mixing influence on water-using system utilities consumption

From analyzing all homogeneous mixing patterns, we can conclude as follows:

(1) For hot-hot steams mixing, three types of mixing will definitely cause energy penalty on water-using system energy consumption, including the mixing between a hot stream across the pinch and a hot stream below the pinch, the mixing between a hot stream above the pinch and a hot stream below the pinch and the mixing between a hot stream across the pinch and a hot stream above the pinch.

(2) For cold-cold streams mixing, three types of mixing will also cause energy penalty, including the mixing between a cold stream across the pinch and a cold stream below the pinch, the mixing between a cold stream above the pinch and a cold stream below the pinch and the mixing between a cold stream across the pinch and a cold stream above the pinch.

(3) The mixing between hot streams above the pinch and the mixing between cold streams above the pinch will cause energy penalty if the energy in the temperature range from T_{mix} to T_p cannot be totally recovered by the cold streams above the pinch, or else the system utilities consumption will keep still.

(4) The mixing between hot streams below the pinch and the mixing between cold streams below the pinch will cause energy penalty if the energy demand by cold streams from T_{mix} to T_p cannot be satisfied by the hot streams below the pinch, otherwise the system utilities consumption will keep still.

4. An application example

The water-using network of Example2 given in Fig.2 has six possibilities of streams mixing at the inlets of unit OP5, OP6, OP7, OP8, OP9 and OP 10. Fig. 3 shows that the pinch temperature of the indirect exchanger network is 100/90℃. The hot and the cold utility consumption are 1890kW and 9240kW respectively. Based on the guidance concluded in the section 3.4, the mixings at the inlet of OP5, OP6 and OP10 has no influence to the system utility consumption. For the mixings at the inlet of OP7 and OP8, they will definitely cause the energy penalty. As to the mixing at the inlet of OP9, which is between a cold and a hot stream belongs to heterogeneous non-isothermal mixing, which we will consider in our future's work. Fig. 4 shows the composite curves after the three types of mixing at the inlet of OP5, OP6 and OP10. Although the composite curves vary, the total energy target keeps still, and this testifies our results.

On the whole, there are three kinds of mixing operations out of the five types of homogeneous mixings we can make use of. Although the three mixings have no energy saving effect, they are still adoptable. Because after mixing the total number of heat exchangers will decrease, which is beneficial to the capital cost.

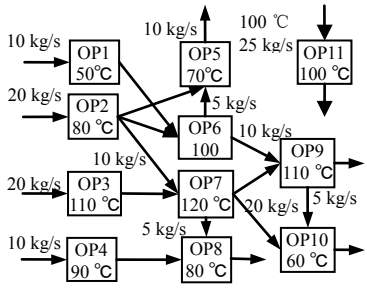

Fig. 2 Water-using Network for example 2

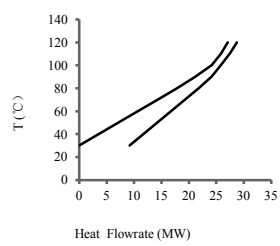

Fig. 3 Composite curves of indirect heat transfer

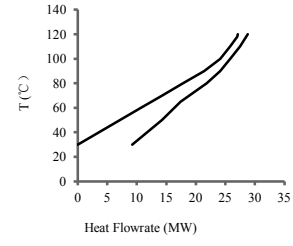

Fig. 4 Composite curves after suitable mixings

5. Conclusions

This paper has classified streams into three types, namely the stream above the pinch, the stream below the pinch and the stream across the pinch. Based on these stream classifications, mixing patterns are defined according to the position of the pinch temperature. Through thermodynamic analysis for homogeneous non-isothermal mixing on system utilities consumption, it has been found that the potential value of homogeneous non-isothermal is to reduce the equipment investment cost. And it will never have energy saving effect. The conclusions for homogeneous non-isothermal mixing in the paper can be used to analyze or optimize the heat exchanger network of a given water-using system. What is more, they may be used establishing a simple model to simultaneously optimize water consumption and energy consumption by mathematical programming method. In terms of the heterogeneous non-isothermal mixing, based on our method, we will explore it in our next work.

References

[1]L.E. Savulescu, M. Sorin, R.Smith, 2002, Direct and indirect heat transfer in water network systems. Applied Thermal Engineering, **22**(8), 981-988.

[2]M. Sorin, L.Savulescu, 2004, On minimization of the number of heat exchangers in water networks, Heat Transfer Engineering, **25**(5), 30-38.

[3]L. Savulescu, J K. Kim, R.Smith, 2005, Studies on simultaneous energy and water minimization-Part II: Systems with maximum re-use of water, Chemical Engineering Science, 60(12), 3291-3308

[4]X. Feng, Y.C Li, X.J. Yu, 2008, Improving energy performance of water allocation networks through appropriate stream merging, Chinese Journal of Chemical Engineering, 16(3):480-484.

[5]M. Bagajewicz, H. Rodera, M. Savelski, 2002, Energy efficient water utilization systems in process plants, Computers and Chemical Engineering, **26**(1), 59-79.

[6]H.G.Dong, C.Y.Lin, C.T. Chang, 2008, Simultaneous optimization approach for integrated water-allocation and heat-exchange networks, Chemical Engineering Science, **63**(14), 3664-3678.

[7]M. Bogataj, M.J. Bagajewicz, 2008, Synthesis of non-isothermal heat integrated water networks in chemical processes, Computers and Chemical Engineering, **32**(12), 3130-3142.

[8]J.Y. Kim, J.K. Kim, J.G. Kim, 2009, A simultaneous optimization approach for the design of wastewater and heat exchange networks based on cost estimation, Journal of Cleaner Production, **17**(2), 162-171.

I.A. Karimi and Rajagopalan Srinivasan (Editors), Proceedings of the 11th International Symposium on Process Systems Engineering, 15-19 July 2012, Singapore.

Optimal Process Configurations of Bioethanol Dehydration for Different Ethanol Inlet Concentrations and Throughputs

Pakkapol Kanchanalai, Matthew J Realff ,Yoshiaki Kawajiri

School of Chemical & Biomolecular Engineering, Georgia Institute of Technology
311 Ferst Drive, Atlanta, GA 30332-0100

Abstract

Purification of low concentration ethanol solutions is an energy intensive process that comprises a significant portion of the overall cost of biobased ethanol. Optimization models of two hybrid ethanol separation processes, distillation-membrane pervaporation process and vapor-compression-membrane-gas-permeation technology, are developed. These options are compared for different feed concentrations and throughputs. Different feed concentrations change the optimal separation process because the top composition of the column using vapor compression is more sensitive to feed concentration than the pervaporation case. The pervaporation annualized capital cost increases more slowly with increasing throughput, but its operating cost increases more quickly, leading to very little impact on scale on the optimal decision at any given feed concentration.

Keywords: Biofuels, ethanol, hybrid separation, optimization, superstructure

1. Introduction

Energy demands, particularly in the form of liquid fuels, have been increasing globally driven by the rise of GDP in rapidly developing countries. This, coupled with concerns about increased atmospheric CO_2 concentrations, has driven the search for other fuels that do not come from fossil hydrocarbons. Biobased ethanol has been considered as a promising and potentially sustainable fuel since it can be used as a gasoline oxygenate, both to increase the octane number and provide a cleaner combustion, as well as being produced from carbon fixed from the atmosphere over relatively short time periods (Huang et al, 2008). However, the cost of biobased ethanol production is relatively high compared to other fuel production, particularly if sourced from lignocellulosic materials. Significant efforts have been undertaken to improve and optimize the biobased ethanol production process. Fuel grade biobased ethanol is above 99 wt %, and requires separation from water above its azeotrope, increasing the energy demand of distillation processes. Beyond distillation, several separation technologies have been proposed such as adsorption and membrane gas and pervaporation separation, as well as hybrid systems with distillation. However, each process has its own advantages and disadvantages – extractive distillation is considered a highly energy intensive process, while membrane separation consumes less energy with higher capital cost (Frolkova & Raeva, 2010). Previous studies have proposed a hybrid system of distillation and membrane separation. The optimization of this hybrid process has been investigated to minimize the total annual cost of the separation process (Szitkai et al, 2002).

Optimal process selections may depend on different ethanol inlet purities which rely on the ethanol conversion process and feed conditions. In addition, the costs of alternative technologies scale differently with production flow rate. The effect of the ethanol inlet

concentration and throughput should therefore be considered to determine the optimal purification process. In this work, the combination of distillation and a membrane system are investigated for two different membrane options, pervaporation and gas permeation. The latter allows vapor compression distillation to be employed. Optimal configurations for each technology that minimize ethanol unit cost are determined for different inlet ethanol concentrations and throughputs by considering rigorous cost optimization models. Superstructures of these two technologies are formulated as mixed integer nonlinear programming (MINLP) models where numerous operating and design parameters are optimized such as the number of stages, feed location, reflux ratio, pressure, and membrane area. The cost model is applied to estimate the capital cost, operating cost and the unit cost of the biobased ethanol (Seider et al, 2010).

2. Process Description

2.1. Distillation-membrane pervaporation process

The first hybrid process considered combines a distillation column with the membrane pervaporation process. The pervaporation network is placed after the distillation column to separate the top product across the azeotropic point after an initial dehydration from the atmospheric distillation column. A superstructure of this hybrid process is obtained by integrating the superstructure of a distillation column and that of a pervaporation network shown in Figure 1a (Malik & Naidu, 2011). The superstructure of the distillation column is used to find the optimal number of theoretical stages, feed stage location, recycle stage location, and reflux ratio by applying logical constraints on binary variables (Viswanathan & Grossmann, 1993). The superstructure of pervaporation contains multiple stages of membranes arranged in series. The ethanol liquid stream from the top distillate is concentrated by partially vaporizing through the hydrophilic membrane. The driving force depends on the partial pressure difference between the liquid and vapor phase (Davis, 2002). The enthalpy of vaporization is provided by the sensible heat of the feed, and hence the driving force of the pervaporation drops along the membrane as the sensible heat converts into the heat of vaporization of the water, lowering the liquid partial pressure. Intermediate heat exchangers are therefore used to reheat the liquid feed and the intermediate streams to below the maximum membrane operating temperature. The appropriate number of membrane stages is investigated by solving several cases. Little improvement is observed when the number of stages is increased from four. Four membrane stages with four interstage heaters are therefore found to be sufficient in this work. The permeates from all stages operated under the same vacuum pressure are combined and condensed by the chilled water before being recycled to the column.

2.2. Vapor-compression-membrane-gas-permeation process

The second hybrid process, illustrated in Figure 1b (Huang et al, 2010), considers a membrane gas permeation system combined with a distillation column. The key point of this process design is that it uses the mechanical work from the compressor to increase the driving force in the membrane and also to provide heat for the vapor stream which enables energy recovery in the column reboiler. The distillation column performs an initial step of separation similar to the pervaporation process; and the membrane is used to concentrate the ethanol of the vapor from the distillate to cross the azeotropic point. The membrane for this system must be able to operate at a high temperature to maintain a vapor phase of the mixture at a high pressure. The superstructure of this system uses a similar distillation column model and integrates it with the gas permeation system. Unlike the pervaporation system, the driving force (partial pressure difference) depends

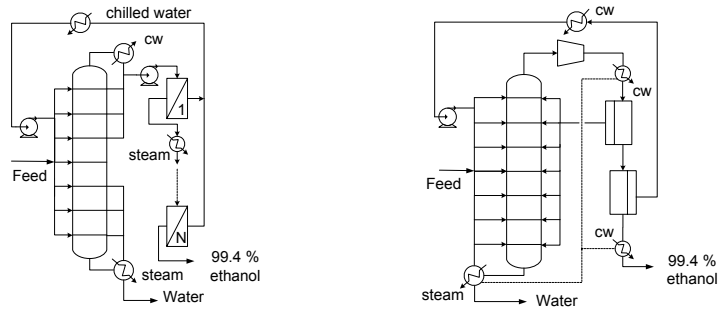

Figure 1. Superstructure of hybrid separation process (a) Distillation - Membrane pervaporation (b) vapor- compression gas permeation

on the pressure difference of vapor stream between the feed and the permeate, as well as the compositions. Therefore, the column may operate under a vacuum to increase this driving force for the membrane separation, since the permeate from the first membrane stage is returned to the column. The vapor stream from the top distillate is compressed and cooled down to below the maximum membrane operating temperature and fed to the membrane unit. This paper considers a vacuum distillation column with two membrane units which allow the system to operate with two different permeate pressures. The permeate stream from the first membrane stage is recycled back to the column and the permeate from the second membrane stage is condensed and return to the column as a reflux. Heat integration between heat exchangers is also considered in this system as shown by the dashed line in Figure 1b.

3. Results

This work uses MINLP model of the superstructure of a distillation column (Viswanathan & Grossmann, 1993) with up to 120 integer variables, and VLE model using NRTL. A high selectivity commercial polyvinyl alcohol membrane is used in the pervaporation process where the permeability correlation comes from Davis (2002), and the maximum operating membrane temperature of 90°C is assumed. In contrast, the gas permeation membrane can operate at a higher temperature, where the maximum of 120°C is used, but with a lower selectivity which is modeled by assuming constant average permeability (Huang et al, 2010). The logarithmic-mean pressure driving force is used in both membrane process (Davis, 2002). The separation costs for both technologies are minimized at different ethanol feed concentration and throughputs based on the best solution found from GAMS/SBB solver with different initial guesses. Ethanol of 99.4wt% purity with 99% recovery is produced, and the unit cost is computed using the capital cost models and all energy costs from Seider et al. (2010) with a discount rate of 7% per year, and 5 year life cycle.

3.1. Effect of ethanol feed concentration

It can be seen from Figure 2 that for both throughputs, the pervaporation technology has lower separation cost than the vapor compression process at a low ethanol feed concentration, but at approximately above ethanol feed at 0.2 w/w and 0.24 w/w for the feed of 10 Mgal/yr and 100 Mgal/yr respectively, the optimal technology switches to vapor compression. Each hybrid technology partitions the separation work between the distillation column and the membrane differently. From Figure 3, the top ethanol concentration in pervaporation is almost constant near the azeotropic point for all inlet

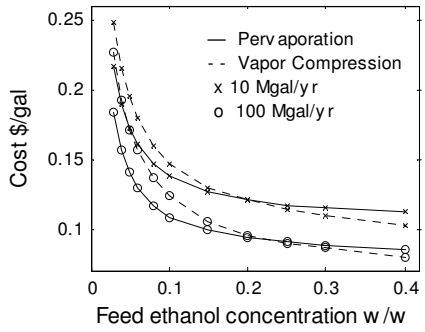

Figure 2. Ethanol cost of pervaporation and vapor compression technologies with different feed concentrations.

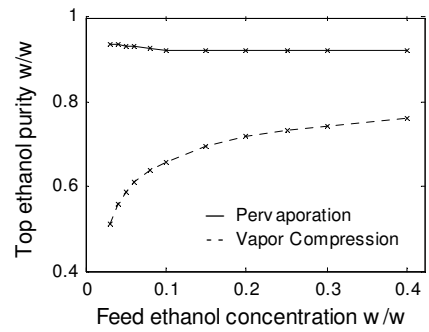

Figure 3. Ethanol concentration from the top of the distillation column with different inlet concentrations at 100 Mgal/year.

concentrations. The optimizer decides to purify the mixture mainly by the distillation column in order to reduce the expensive membrane area. In contrast, the top ethanol concentration in the vapor compression process increases with increasing ethanol feed concentration. The top purity of the distillation column relies on the purity and the liquid flow from the second membrane permeate. It requires a significantly larger membrane area to increase the purity of both the overhead vapor and the second membrane permeate. The optimizer therefore decreases the overhead ethanol content of the distillation column. This requires more membrane separation work and leads to a higher cost than the pervaporation technology at low ethanol feed concentrations.

3.2. Effect of ethanol throughputs

The result from Figure 2 shows that the concentrations at which the costs of the two technologies cross for two different capacities are slightly different – 0.2 w/w for 10 Mgal/yr and 0.24 w/w for 100 Mgal/yr. This concentration range is further investigated for more different throughputs as shown in Figure 4. At ethanol feed of 0.23 w/w, the vapor compression has cheaper separation cost than the pervaporation process at a small plant capacity. When increasing the feed flow rate, the cost of pervaporation technology becomes lower than the vapor compression at above 40 Mgal/yr. This demonstrates that the pervaporation process is slightly more sensitive to the throughputs. This is because the cost components of each technology scale differently. From Figure 5, the pervaporation process has a higher operating cost for all throughputs, but the annualized capital cost is cheaper and overcomes the effect of higher operating cost. This leads to

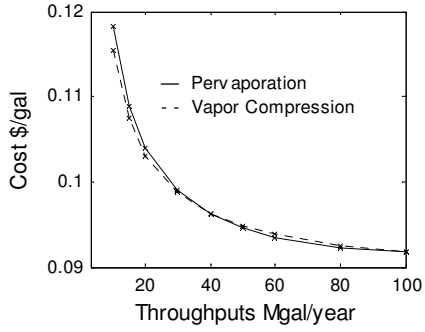

Figure 4. Cost of pervaporation and vapor compression with different feed throughputs at ethanol feed of 0.23 w/w

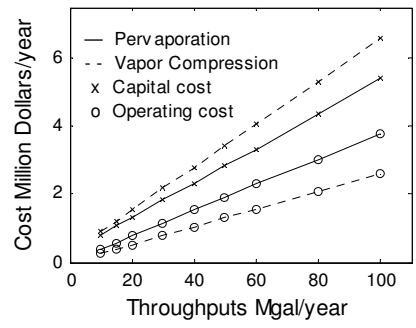

Figure 5. Annualized capital cost and operating cost of two technologies for different feed throughputs at ethanol feed of 0.23 w/w

a lower ethanol unit cost than the vapor compression technology at a higher throughput above 40 Mgal/yr. A more detailed examination of the component costs shows that the pervaporation process requires less membrane area than vapor compression, since the distillation column, a cheap separation unit, in the pervaporation technology can achieve a higher top ethanol concentration. Moreover, the compressor capital cost in the vapor compression technology is a high portion in the capital cost of separation process. The membrane and the compressor cost then increase significantly when the throughputs through the membrane increase. Furthermore, an external investigation reveals that the maximum operating temperature for the membrane also has a significant impact on the cost. These results therefore may change if different membrane is used in the process.

4. Conclusion

Two MINLP models of bioethanol hybrid separation technologies are optimized to compare the purification cost for different inlet concentration and throughputs. Pervaporation technology is optimal at a very low feed concentrations, while vapor compression process, more sensitive to the feed concentration, has a lower separation cost at a higher inlet ethanol concentration. Different throughputs also have an effect on the optimal technology in that the pervaporation process is more sensitive to the plant capacity. Because of the higher operating cost but lower capital cost, the pervaporation process is cheaper than the vapor compression technology at higher throughputs, but only marginally. From these results, the vapor compression process may benefit more from feed pretreatment because of its higher sensitivity to the inlet concentration. Different membrane permeabilities and the maximum membrane operating temperature may also change the results of optimal process configuration and technology; these impacts will be investigated in the future work.

Acknowledgements

The authors are grateful for the financial support from PTT Public Company Limited, Thailand. The second author gratefully acknowledges partial financial support from NSF grant and GOALI program, CBET 0933392.

References

Davis, R.A., Simple gas permeation and pervaporation membrane unit operation models for process simulators. Chemical Engineering & Technology, 2002. 25(7): p. 717-722.

Frolkova, A.K. and V.M. Raeva, Bioethanol dehydration: State of the art. Theoretical Foundations of Chemical Engineering, 2010. 44(4): p. 545-556.

Huang, H. J., Ramaswamy, S., Tschirner, U. W., & Ramarao, B. V., A review of separation technologies in current and future biorefineries. Separation and Purification Technology, 2008. 62(1): p. 1-21.

Huang, Y., R.W. Baker, and L.M. Vane, Low-Energy Distillation-Membrane Separation Process. Industrial & Engineering Chemistry Research, 2010. 49(8): p. 3760-3768.

Malik, R.K. and Y. Naidu, A generalized methodology for optimal configurations of hybrid distillation-pervaporation processes. Chemical Engineering Research & Design, 2011. 89(8A): p. 1348-1361.

Seider, Warren D., J. D. Seader, Daniel R. Lewin, and Soemantri Widagdo. Product and Process Design Principles: Synthesis, Analysis and Design. 3rd ed. Chichester: John Wiley, 2010.

Szitkai, Z., Lelkes, Z., Rev, E., & Fonyo, Z., *Optimization of hybrid ethanol dehydration systems.* Chemical Engineering and Processing, 2002. 41(7): p. 631-646.

Viswanathan, J. and I.E. Grossmann, Optimal Feed Locations and Number of Trays for Distillation-Columns with Multiple Feeds. Industrial & Engineering Chemistry Research, 1993. 32(11): p. 2942-2949.

I.A. Karimi and Rajagopalan Srinivasan (Editors), Proceedings of the 11th International Symposium on Process Systems Engineering, 15-19 July 2012, Singapore.

A comparison between the two balancing regimes of the natural gas market in the Netherlands

Catalin Bucura[*a], Zofia Lukszo[a]

[a]*Delft University of Technology, Faculty of Technology, Policy and Management, Jaffalaan 5, Delft, 2621BX, the Netherlands*
(c.a.bucura; z.lukszo)@tudelft.nl

Abstract

The functioning of the old and new balancing regimes of the natural gas market in the Netherlands is explored using an agent-based model. The two balancing regimes are simulated to determine the participants' cash flows under different behavioral strategies for both regimes. The total system imbalance and the costs associated to the balancing strategies are calculated. Model simulations runs and observation of shippers' cumulative penalties and rewards provide support in understanding the old and new regime.
Keywords: agent-based models, simulation, gas market, balancing regime.

1. Introduction into the Dutch gas market and its balancing regime

The third EU energy package – Third Gas Directive [1] was adopted by the European Parliament in September 2009. The goals of the directive are to increase competition and efficiency, to ensure security of supply and to ensure the freedom of choice of consumers at a fair price. The Dutch natural gas market has formed back in the 1960's when the gas field Groningen in the North of the country has been discovered, and ever since, it has been continuously going through many technical and institutional changes.

Figure 1 presents an overview of the Dutch gas market. The company that operates the gas network is Gas Transport Services B.V. (GTS), also known as the Dutch Transport Service Operator (TSO).

Figure 1: The Dutch Gas market value chain

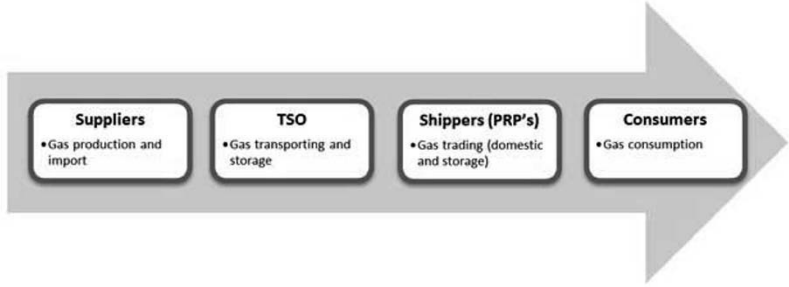

* corresponding author

2. The old and new balancing regime

At abstract level, the functioning of the gas market is fairly simple: suppliers produce the gas, traders commercialize it, customers use it, and the transporter makes sure that gas gets from one side to the other. Transportation of gas must be done according to a set of rules, and it also must be done in a safe and reliable way.

The reliable operation of the Dutch gas network requires that the TSO, maintains pressure in the network within certain limits. The system is considered to be *out of* balance if the pressure in the network falls outside those limits. If the pressure is too low, the system is *short* and *long* if the pressure is too high. The companies which trade the gas are called *shippers.*

2.1. The old balancing regime

In the old balancing regime if the network was out of balance, the first intervention in balancing was done by the TSO. Next, the shipper with contractual rights on almost all assets, took out or injected the amount needed to balance in concordance with the contracts. In case one shipper was out of balance, it had to pay penalties. Not only were those penalties excessively high, but they were applied regardless the position of the shipper (long or short). All these penalties due to the shippers' imbalance were used to pay the costs of balancing the national transport network.

In 2006, the Dutch Parliament decided to change this detrimental situation and requested improvement in the system. On the 1st of April 2011 a *new balancing regime* was adopted.

2.2. The new balancing regime

The design of the new regime relies on a market driven balancing mechanism. All the participants in the balancing system are called Program Responsible Parties (PRP's). They are now responsible for balancing any difference between their forecasted volume of gas to be transported and the actual transported volume. However, a tolerance which is related to the size of their portfolio is applied (i.e. smaller PRP's have a larger tolerance than larger ones) [2].

In the new regime the TSO provides the shippers with two real time information signals: the System Balance Signal (SBS) and Portfolio Imbalance Signal (POS). POS represents the own imbalance of a shipper, whereas the SBS represents as the name suggests, the sum of all POS's [3,4]. A responsible party whose imbalance is the opposite of the total system imbalance is called a *helper*, and respectively, a party with imbalance in the same direction is called a *causer*.

Another new component of the new Dutch gas market balancing regime is the Bid Price Ladder (BPL) mechanism, designed to purchase and sell deficit as well as excess volumes of gas. It also determines the cost of imbalance, unlike in the previous old regime where the penalties were related to the price of transactions on the virtual trading point.

3. Modeling the two balancing regimes of the natural gas market

3.1. Modeling approach

The new balancing regime has come with changes to the existing system. It is now based on penalties and incentives for the shippers. It stimulates them to participate on the market, rather than, like in the old regime, charge them for whichever type of imbalance. Balancing the network becomes now a common task for the shippers. The emergent behavior of such a complex system is not obvious, and its properties are hard

to deduce. The behavior of the whole system is different from the individual behavior of its components.

Complex adaptive systems are systems evolving over time, composed by agents which react with each other according to what the others agents do [5]. Agents are semi-autonomous entities that seek to maximize their objectives by evolving over time. Examples of such complex systems are economies, weather, traffic, social organizations, and most of the infrastructure systems that are composed of heterogeneous actors. One way to explore and understand such complex systems is represented by the use of Agent Based Modeling (ABM).

In ABM, a complex system is decomposed into agents whose actions aim to simulate the behavior of the real life actors. The aggregate behavior as a result of interaction of the individual behaviors allows analyzing the system as a whole. Creating an ABM of the old and new balancing regime aims to provide insight into the operation of this new complex system.

3.2. Goals of the model

The model aims to explore the operation of the two balancing regimes. The model replicates the operation of the gas market in the old and new balancing regime. It simulates the effects of the individual shippers' decisions on the operation of the system as a whole.

3.3. Design of the model

The model simulates the operation of the gas market composed out of several types of agents: suppliers, TSO, shippers and consumers (see Fig. 1 for the sequence). The system is in balance as long as the aggregated system position is between the predefined bounds. When the system is out of balance the TSO buys or sells gas according to the system's state.

The shippers are responsible for balancing. They have to make sure that their own portfolio is balanced and also they must ensure that the total network is balanced, too. In case the network goes out of balance, then the TSO calls the bid ladder. The bid ladder is constructed by using the volumes with their corresponding prices submitted by the PRP's, but not used in the previous transactions. At this stage, only bids that can physically be delivered are accepted. To construct the BPL, the accepted bids are sorted based on the merit order, so that those with the lowest marginal costs are the first ones to be bought. The price of the last bid that satisfies the demand is the price used for the transactions on the BPL.

3.4. Agents

Agent Based Models (ABM) approach usually consists in decomposing the complex system into autonomous agents, which interact with each other. The agents are represented using formalized concepts and definitions. This formalization is represented by the *ontology*. The use of ontologies for conceptualizing domain knowledge has been a standard practice in information science [6]. In ABM, ontology provides a shared vocabulary that can be used to model a socio-technical system: the type of objects and concepts that exist, and their properties and relations [7]. As we built the model of the (new) balancing regime, we created the ontology used later on, as a simplified conceptualization of the real system.

In our ontology, every social node has a physical node attached; every agent owns or operates a technology. The social nodes represent the agents and the physical nodes represent technologies. Agents in the model represent the decision makers in the real world: suppliers, TSO, shippers and consumers (see Fig. 1 for the sequence). Technologies in the ontology are used to describe the physical connections and reflect

the physical constraints. The model is composed of the following agents: demand (commercials, electricity producers, export, households and industry), supply, the TSO and the shippers. Trading of gas takes place, and depending on the total system position and imbalance, the TSO calls the BPL accordingly. Helpers are rewarded whereas causers are penalized according to the BPL mechanism and the settlement price. At this stage of the model, the agents do not learn from their mistakes in the past

4. Model results and insights

In this section we compare and discuss the simulations of the two balancing regimes. The two charts for both simulations - the old and new regime (Figure 2) represent the liquid assets of three types of shippers (represented in the model as 10 different shippers), i.e. with large (shippers 1, 2, 3), medium (shippers 4, 5, 6 and 7) and small portfolio (shippers 8, 9 and 10).

Comparing the two simulations from Figure 1 we observe that in the old regime all shippers pay penalties. Large shippers (2 and 3) pay the highest penalties. In the old regime, without any information about SBS and penalties paid regardless their position, shippers with larger portfolio get higher imbalance and smaller tolerance, and therefore higher penalties. Small size shippers (e.g. shipper 10) also get penalties even if their imbalance is not high. In the real life, most of the transactions were done on a bilateral market, or "over the counter", and for this reason the shippers did not get bankrupt.

In the new regime, even though there is no negotiation between the shippers, they do not always pay penalties (right side of Figure 1). Shipper 2 (blue 'x' in the graph), which has a large portfolio, has negative outcome. On the opposite, the medium size shipper 4 (black triangle in the graph) performs much better in the first half of the simulation. The explanation for this is that shipper 2 overbooks the network, and has a large portfolio which triggers a large imbalance and small tolerance. The medium size shipper 4, turns the imbalance into his own favor and due to his small overbooking, it performs well.

The three types of shippers perform rather different in the two regimes. In the old one, regardless their imbalance all paid penalties. Small shippers paid high penalties in the old regime even though their imbalance is not high. In the new regime, however, medium shippers perform better. The simulations show that for large capacity overbooking, none of the shippers performs well. This is also one of the new regime goals – more efficient capacity utilization. It should be added that we have showed that individual imbalances of a shipper are only relevant in relation to the aggregate system position. For this reason we do not treat shippers individually. [8]

5. Final remarks

In this paper we have presented agent based simulations of the old and new balancing regime of the natural gas market in the Netherlands. The new regime is rather complex and relatively difficult for shipper's operation. Every hour signaling may not be most appropriate way for presenting the system position. There is an expectation that the EU grid code will be published shortly and it will require daily balancing, with limited possibility for within-day actions. The simulations as presented in this paper can give a valuable support in understanding the consequences of the new EU grid code.

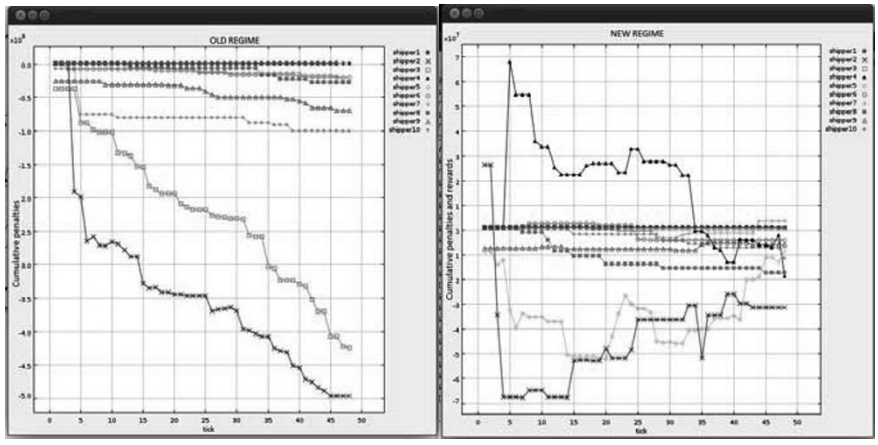

Figure 2. Cumulative penalties of shippers in the old regime (left side) and cumulative penalties and rewards in the new regime (right side)

As is the case with most agent-based models of complex systems, the process of building the model helps to conceptualize the system and to understand it. The aim of this paper is not to measure the performance of any of the two regimes, but to explore and understand them. The model is not yet in the final state. In the future research the real system data will be used and the model will be extended by adding storage facilities.

6. Acknowledgements

This research is funded by the Dutch Energy Delta Gas Research (EDGaR) program. The focus EDGaR is to understand the challenges encountered by the transition of the gas-based energy market to a more liberal, secure, affordable and sustainable state.

References

[1] Directive 2009/73/EC gas – "Third Gas Directive", [last visited on 20.01.2012] http://ec.europa.eu/energy/gas_electricity/legislation/third_legislative_package_en.htm
[2] Procedure qualifying balancing instrument gas transport services, [last visited on 20.01.2012] http://www.gastransportservices.nl/en/balancing/procedure-qualifying-balancing-instrument
[3] Shippers and traders in the Dutch gas market, [last visited on 20.01.2012] http://www.gastransportservices.nl/en/shippers
[4] About POS and SBS, [last visited on 20.01.2012] http://www.gastransportservices.nl/en/balancing/about-pos-and-sbs
[5] Dooley, K. (1996), "A Nominal Definition of CASystems," The ChaosNetwork, 8(1): 2-3.
[6] P. A. Fishwick and J. A. Miller. Ontologies for modeling and simulation: issues and approaches. Winter Simulation Conference, pages 259–264, Washington, D.C., 2004.
[7] K. van Dam. Capturing socio-technical systems with agent-based modelling. PhD thesis, Delft University of Technology, the Netherlands, 2009.
[8] C. Bucura et al., Modeling the new balancing regime of the natural gas market in the Netherlands. ICNSC - IEEE, pages 68-73, the Netherlands, April 2011

I.A. Karimi and Rajagopalan Srinivasan (Editors), Proceedings of the 11th International Symposium on Process Systems Engineering, 15-19 July 2012, Singapore

Model predictive control for BioPower combined heat and power (CHP) plant

Jukka Kortela * Sirkka-Liisa Jämsä-Jounela
Aalto University School of Chemical Technology; PL 16100, FI-00076 Aalto, Finland

Abstract

This paper presents a model predictive control (MPC) development for BioGrate boiler. Amount of fuel and moisture in the furnace are chosen as the state variables for the MPC model in order to take into account fuel quality. To this end, dynamic models for fuel decomposition and water evaporation in the furnace are used. As a result, the drum pressure can be predicted accurately and an efficient stabilization of the plant operations is possible by using the MPC. The performance of the MPC is evaluated using real industrial plant data and compared with the currently used control strategy. Finally, the results are presented, analyzed and discussed.

Keywords: biopower, combustion, biomass, fuel quality, MPC, moisture, advanced control, power plant

1. Introduction

The usage of biomass fuel for heat and power production is growing due to an increasing demand for replacing of fossil energy sources with renewable energy. The fuel is usually a blend of different batches, for example, spruce bark and dry woodchips with varying moisture content between 30% and 55% (Yin et al. (2008)). This varying moisture content of the fuel results in uncertainty in the energy content of the fuel and complicates the operation of combustors. One of the latest developed processes, which can burn biomass fuel with high moisture is BioGrate technology developed by MW Biopower. In the BioGrate system, this is achieved by feeding the fuel onto the center of a grate, thus improving water evaporation due to the heat of the surrounding burning fuel and thermal radiation from the brick walls (Wärtsilä Biopower (2005)).

An important step in the control strategy development for BioGrate boiler has been to develop a method for estimating the furnace fuel flow and combustion power, as shown in theoretical studies and practical tests by Kortela and Lautala (1981). On-line measurements of oxygen consumption were used when a new cascade compensation loop was built to optimally control the fuel flow. It was reported that the amplitude and the settling time of the response of the generator power decreased to about one third of the original.

In addition, advanced combustion control has been applied to control air and fuel. Havlena and Findejs (2005) used model-based predictive control to enable tight dynamical coordination between air and fuel to take into account the variations in power levels. The results showed that this approach enabled boiler to be permanently operated with optimum excess air, resulting in reduced O_2 and a significant increase in the boiler efficiency. Similar results have also been reported for the application of a multivariable long-range predictive control (LRPC) strategy based on a local model network (LMN) in the simulation of a 200

*jukka.kortela@aalto.fi

MW oil-fired drum-boiler thermal plant (Prasad et al. (1998)) and for a scheme presented by Swarnakar et al. (1998) for robust stabilization of a boiler, based on linear matrix inequalities (LMIs). However, there are still some challenges and unattained objectives in the development combustion power control. For example, variations in the moisture of fuel should be considered in order to correct any estimation errors of combustion power.

This paper presents a model predictive control (MPC) development of BioGrate boiler. The paper is organized as follows: Section 2 presents the process description, the MPC control strategy, and the models for the MPC controller for BioPower CHP plant. The test results of MPC control strategy are presented in Section 4, followed by the conclusions in Section 5.

2. Description of the process and model predictive control strategy for Biopower 5 CHP plant

In the BioPower 5 CHP plant, the heat used for steam generation is obtained by burning solid biomass fuel: bark, sawdust and pellets, which are fed to the steam boiler together with combustion air. Heat and flue gases generated in the result of combustion are used to produce steam which accumulates in the drum.

The aim of the control is to keep the energy production at the target level that allows to stabilize the steam pressure in the drum. The suggested MPC control strategy presented in Fig. 1 utilizes fuel flow and fuel moisture soft-sensors and furnace state estimators to handle the inherent large time constants and long time delays of the boiler. In addition, models for fuel decomposition and water evaporation are used to predict the combustion power and to stabilize the drum pressure. This results in a radical reduction of settling time of the drum pressure and enables faster steam load changes, while maintaining the stability of the boiler.

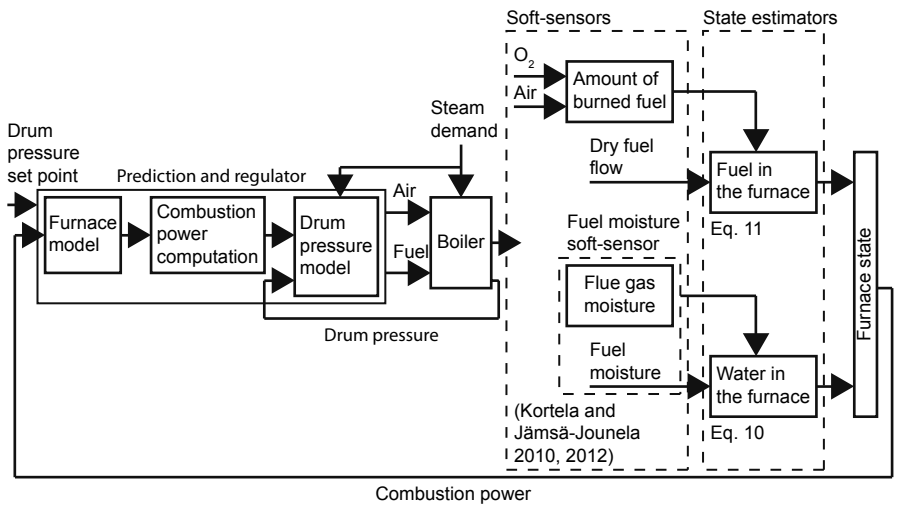

Figure 1. Model predictive control (MPC) strategy of BioGrate boiler

2.1. MPC Controller for BioGrate boiler

The MPC control is used as a master control, manipulating simultaneously set points for air and fuel flows. The configuration of the models is as follows: the fuel flow MV1 and the primary air flow MV2 are the manipulated variables; the fuel moisture DV1 is the estimated disturbance and the steam demand DV2 is the measured disturbance; and the combustion power CV1 and the drum pressure CV2 are controlled variables. The models are stacked into a linear state space system:

$$\begin{aligned} x_{k+1} &= Ax_k + Bu_k + Ed_k \\ z_k &= C_z x_k \end{aligned} \tag{1}$$

where x are the states, u are the manipulated variables (MVs), and d are the measured disturbances. z denote the controlled variables (CVs). Regularized l_2 output tracking problem with input and output constraints is formulated as (Maciejowski (2002))

$$\begin{aligned} \min \phi &= \frac{1}{2}\sum_{k=1}^{N} \|z_k - r_k\|^2_{Q_z} + \frac{1}{2}\|\Delta u_k\|^2_S \\ s.t.\, x_{k+1} &= Ax_k + Bu_k + Ed_k, k = 0,1,\ldots,N-1 \\ z_k &= C_z x_k, k = 0,1,\ldots,N \\ u_{\min} &\leq u_k \leq u_{\max}, k = 0,1,\ldots,N-1 \\ \Delta u_{\min} &\leq \Delta u_k \leq \Delta u_{\max}, k = 0,1,\ldots,N-1 \\ z_{\min} &\leq z_k \leq z_{\max}, k = 1,2,\ldots,N \end{aligned} \tag{2}$$

2.2. Modelling of BioGrate boiler for MPC

Modelling of grate combustion is of great importance, since unknown fuel flow and water evaporation result in uncertainty in the combustion power, and complicate the operation of the boiler. The model is based on two mass balances for water and dry fuel, in which both models are obtained from the literature and their parameters are defined with experimental data. Other models of the boiler include the drum, the primary air, and the secondary air models.

2.2.1. The model for amount of moisture in the furnace

According to (Bauer et al. (2010)), the rate of water evaporation is mainly independent of the primary air flow and the dynamics of the moisture in the furnace m_w is

$$\frac{dm_w}{dt} = -\alpha_{wev} * m_w + m_{w,in}(t - T_d) \tag{3}$$

where α_{wev} is a dimensionless scaling factor, $m_{w,in}$ is the moisture in the fuel feed, and T_d a constant delay.

2.2.2. The model for amount of dry fuel in the furnace

Bauer et al. (2010) showed that the overall effect of the primary air flow rate on the thermal decomposition rate is multiplicative. Therefore, the thermal decomposition of dry fuel is as follows

$$\frac{dm_{ds}}{dt} = -\alpha_{thd} * m_{ds} + m_{ds,in}(t - T_d) - \alpha_{pa} * m_{pa} \tag{4}$$

where α_{thd} is the decomposition rate coefficient of fuel flow, and α_{pa} the decomposition rate coefficient of primary air flow, $m_{ds,in}$ is the stoker speed, and T_d a constant delay.

2.2.3. Drum model

If the drum level is kept at a constant set point, the variations in the steam volume are small. Neglecting these variations, the drum model is (Åström and Bell (2000))

$$\frac{dp}{dt} = \frac{1}{e}(Q - m_f(h_w - h_f) - m_s(h_s - h_w)) \quad (5)$$

$$e \approx \rho_w V_{wt} \frac{\partial h_w}{\partial p} + m_t C_p \frac{\partial T_s}{\partial p} \quad (6)$$

where Q is combustion power (MJ/s), m is mass flow rate (kg/s), h is specific enthalpy $(MJ/kg$, ρ is specific density (kg/m^3), V is volume (m^3), m_t is the total mass of the metal tubes and the drum (kg), C_p is specific heat of the metal (MJ/kgK), and T_s temperature of steam (K). The subscripts f, w, s, refer to feed-water, water, and stem, respectively. Double subscript t denotes total system. The combustion power and fuel moisture soft-sensor are described detailed in (Kortela and Jämsä-Jounela (2010)) and (Kortela and Jämsä-Jounela (2012)).

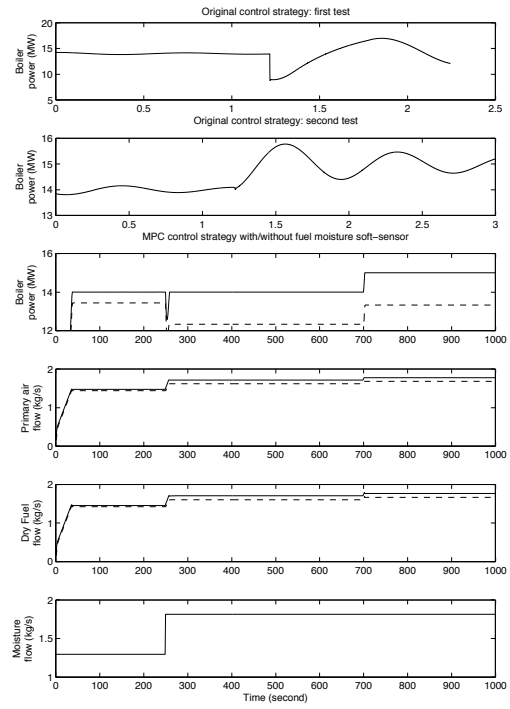

Figure 2. The test results when the MPC control estimates both states: fuel and moisture in the furnace (solid line), and the test results when the MPC control assumes that the moisture content is constant (dashed line). The top two pictures show the boiler power of the original control for the first and the second test.

2.2.4. Models for the primary air and secondary air flows

The primary air and secondary air models represent the dynamics of the regulatory layer PID control loops of air transport.

$$G_{pa}(s) = \frac{1}{\tau_{pa}s + 1} e^{-\alpha s} \quad (7)$$

$$G_{sa}(s) = \frac{1}{\tau_{sa}s + 1} \quad (8)$$

3. Test results of MPC control strategy of BioGrate boiler

The performance of the MPC control strategy was evaluated using real industrial plant data. In the first test scenario, the power demand of the boiler was kept at 14 MW while the moisture content of the fuel flow was changed from 47% to 51% at a time 300 seconds, as shown in Fig. 2. When the MPC control estimates both states: fuel and fuel moisture in the furnace, the boiler power drops by 1.5 MW for a short time. Nevertheless, the power demand and the actual power match really well. To compare, there is an offset in the results when the MPC control assumes that the moisture content in the fuel is constant. With the original plant control, the change in the moisture content caused strong oscillations. In the second scenario, the power demand was changed from 14 MW to 15 MW at a time 700 seconds. The settling time is only 2 minutes with the MPC control strategy, whereas it was about 1.5 hours with the original control.

4. Conclusions

This paper presented model predictive control (MPC) development for BioGrate boiler. The performance of the MPC was evaluated using real industrial plant data and comparison was made with the currently used control strategy. The test results show that the MPC followed power demand better compared with the currently used control strategy while maintaining stability.

References

Bauer, R., Gölles, M., Brunner, T., Dourdoumas, N., Obernberger, I., 2010. Modelling of grate combustion in a medium scale biomass furnace for control purposes. Biomass and Bioenergy 34 (4), 417–427.

Havlena, V., Findejs, J., 2005. Application of model predictive control to advanced combustion control. Control Engineering Practice 13 (6), 671–680.

Kortela, J., Jämsä-Jounela, S.-L., 2010. Fuel quality soft-sensor for control strategy improvement of the Biopower 5 CHP plant. In: Control and Fault-Tolerant Systems (SysTol), 2010. Nice, France, 6-8 October 2010, pp. 221–226.

Kortela, J., Jämsä-Jounela, S.-L., 2012. Fuel moisture soft-sensor and its validation for the industrial Biograte boiler. In: 17th Nordic Process Control Workshop. Kgs Lyngby, Denmark, 25-27 January 2012.

Kortela, U., Lautala, P., 1981. A New Control Concept for a Coal Power Plant. In: Proceedings of the 8th IFAC World Congress. Kyoto, Japan, 1981.

Maciejowski, J. M., 2002. Predictive Control with Constraints. Prentice Hal, Harlow, England.

Prasad, G., Swidenbank, E., Hogg, B. W., 1998. A Local Model Networks Based Multivariable Long-Range Predictive Control Strategy for Thermal Power Plant. Automatica 34 (10), 1185–1204.

Swarnakar, A.,Marquez, H.J., Chen, T. 2007 Robust stabilization of nonlinear interconnected systems with application to an industrial utility boiler. Control Engineering Practice 15(6), 639-654

Yin, C., Rosendahl, L. A., Kær, S. K., 2008. Grate-firing of biomass for heat and power production. Progress in Energy and Combustion Science 34 (6), 725–754.

Wärtsilä Power Plants: Bioenergy solutions. Vaasa: Waasa Graphics; 2005.

Åström, K. J. A., Bell, R. D., 2000. Drum-boiler dynamics. Automatica 36 (3), 363–378.

I.A. Karimi and Rajagopalan Srinivasan (Editors), Proceedings of the 11th International Symposium on Process Systems Engineering, 15-19 July 2012, Singapore.

Exergetic optimization of a refrigeration cycle for natural gas liquefaction

Liza Cipolato,[a] Maria C. A. Lirani,[a] Thiago V. Costa,[a] Francine M. Fábrega,[a] José V. H. d'Angelo[a.]

[a]*School of Chemical Engineering, University of Campinas, Rua Albert Einstein, 500 – Bloco A, Campinas (SP) – 13083-852, Brazil*

Abstract

Natural gas is widely use in many industries as fuel and also as raw material. Although gas pipelines present less transportation losses they become impracticable when distances are too long or when demands are highly variable. The liquefaction of natural gas is then necessary to allow its transportation in great volumes, with little loss of material. This also enables its storage in a more stable way. Natural gas consumption is continuously growing worldwide and consequently, the number of exporter terminals (liquefaction industries) and importer terminals (regasification plants) will increase. The natural gas liquefaction process is based on a sequence of refrigeration cycles, which need to work in an optimized way. The exergetic analysis is a very useful thermodynamic tool to evaluate the efficiency of these cycles. This work aims at an exergetic analysis of a multistage cascade refrigeration cycle applied to a natural gas liquefaction process. Firstly, the process was simulated using commercial software and the results obtained from the simulations were validated with literature data, showing a good agreement. After that, different operational conditions, according to a complete factorial design of experiments, were studied, in order to verify the influence of pressure in six specific points of the cycle. The response variable analyzed is the rate of total exergy destroyed in the cycle. The results showed a new set of operational condition to the refrigeration cycle in which the destroyed exergy rate was reduced by approximately 48% in comparison with literature data.

Keywords: natural gas, liquefaction, exergy, optimization, refrigeration.

1. Introduction

Natural gas consumption is growing worldwide mainly because of its good properties as a fuel. The transportation of natural gas from the producing site to the consumption site is usually done by pipelines, but when the distances are great or the sites are separated by an ocean, the transportation of natural gas in the liquid state is preferred.

Natural gas is in liquid state at temperatures around -150 ^{o}C or lower and pressures varying up to 500 kPa. In order to reach this low temperature refrigeration cycles are used. The most usual liquefaction processes are: multistage cascade liquefaction; mixed refrigerant and turbine-based. Finn *et al.* (1999) and Geist (1983) have presented in detail the advantages and disadvantages of each one of these cycles.

The classical cascade liquefaction cycle was the first one to be applied in natural gas plants. It is based on a three stage refrigeration cycles, each one operating with a different fluid: methane, ethane (or ethylene) and propane. The mixed refrigeration cycle utilizes only one refrigeration fluid using a mixture of refrigerants, which

composition is adjusted in order to have its evaporation temperature similar to the natural gas being liquefied, which can change depending on its origin.

Because of the high costs involved in construction and operation, the feasibility of an industrial site is strictly related to the efficiency of the process. One possible way of reducing thermodynamic losses of the process is to perform an exergetic analysis, to reduce exergy losses, leading to an optimal operation.

The objective of this work is to perform an exergetic analysis of a classical multistage cascade refrigeration cycle applied in the liquefaction of natural gas, in order to propose an optimal operational condition, contributing to reduce the exergy destroyed in the cycle. This analysis will consider the influence of six pressures in different points of the cycle: after the compressor and after the expansion valve of each subcycle.

2. Materials and Methods

2.1. Multistage Cascade Refrigeration Cycle

The multistage cascade refrigeration cycle presents lower energy consumption when compared to the other types, enables flexible operation, as each cycle can be independently operated, and requires smaller heat transfer area in the evaporators. This last characteristic implies in a lower thermodynamic efficiency of the process, which requires higher utilities demand. Another disadvantage is the high installation and maintenance costs, as each cycle has its own compressor and refrigeration fluid storage tank. Figure 1 shows the cascade cycle studied in this paper. For simplification of the figure, only one stage is shown per refrigeration fluid. In this cycle, natural gas is cooled and finally liquefied by a three stage process. In the real cycle, each refrigeration stage has multiple expansion and condensation steps, being each of them operated at three different evaporation temperatures. Details of this multicascade cycle can be found in Kanoglu (2002).

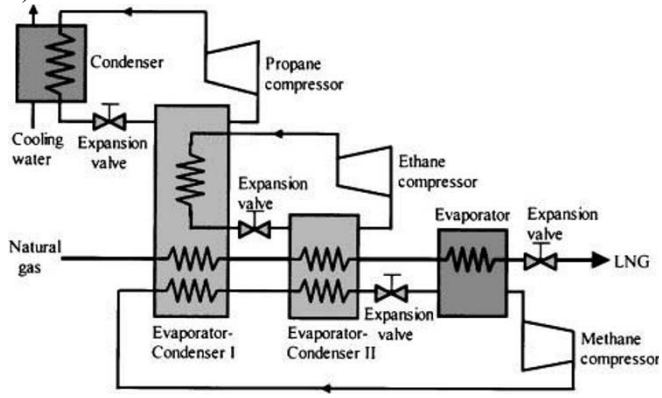

Figure 1-Multistage refrigeration cycle (Kanoglu, 2002).

2.2. Process Simulation

The multistage cascade refrigeration shown in Figure 1 was simulated using Hysys (Aspen Technology, version 3.2), based on the works of Kanoglu (2002) and Filstead (1965). The fluid package chosen to provide thermodynamic properties was the Peng-Robinson equation of state, which is adequate for the refrigerants used in the cycles. Steady state operation and adiabatic equipments were assumed in the simulations. Natural gas molar composition used in the simulation was taken from a Brazilian LNG

plant and is: 90.7% CH_4, 6.8% C_2H_6, 1.3% C_3H_8, 0.3% C_4H_{10}, 0.7% N_2 and 0.2% O_2. Refrigerants selected were: methane, ethane and propane (all 100% pure).

After validation of the simulation by comparison with literature data, obtaining a good agreement, different operational conditions were tested following a full factorial experimental planning. Finally, the results were analyzed by a statistical software, and an optimal operation condition for the process was proposed.

2.3. Exergetic Analysis

Details of how to perform an exergetic analysis may be found in Szargut (1980). The aim of this analysis is to locate and evaluate quantitatively the effect of irreversibilities which reduce thermodynamic efficiency of a process, proposing modifications in order to reduce these irreversibilities, by reducing destroyed exergy. In this work only the physical component of exergy for each process stream was analyzed using Equation (1):

$$ex = (h - h_o) - T_o(s - s_o) \quad (1)$$

where h is enthalpy and s is entropy at temperature and pressure of the process stream and the index "o" indicates the value of the variables at the reference state considered, which is T_o = 298.15 K and P_o = 101.3 kPa. The total destroyed exergy of the multistage cascade refrigeration cycle considered in this work is the sum of the destroyed exergy in each control volume of the cycle, which is obtained through an exergy balance.

2.4. Factorial Experiment Design

To evaluate the influence of pressures at six different process streams of the cycle (after the compressor and after the expansion valve of each refrigeration subcycle) over total destroyed exergy, a 2^6 factorial design was applied. Therefore, 6 factors were analyzed, being 2 levels for each one. Following the experimental design, a minimum number of simulations need to be performed for the minimization of the resulting variable, which is the total destroyed exergy of the system. The experimental design resulted in 64 simulations plus the base case, which is the one studied by Kanoglu (2002).

In the full factorial design, both the individual and the combined influence of the input factors (pressures) in the total destroyed exergy are analyzed. The basis selection for the different pressure levels for the streams was ±10% over the value of the base case. This choice is due to a limited operational range. Table 1 shows the superior and inferior levels for the tested factors. The results obtained from the full factorial experimental planning were evaluated by a statistical analysis with Minitab 15.

Table 1: Planning matrix for the tested factors (pressures, in kPa).

Stream	Description	Cycle	Base case	Inferior	Superior
7	after compressor	Methane	3337	3003	3671
10	after expansion valve	Methane	170	153	187
12	after compressor	Ethane	2069	1862	2276
14	after expansion valve	Ethane	110	99	121
16	after compressor	Propane	1344	1210	1478
18	after expansion valve	Propane	110	99	121

*streams numbers correspond to the ones used in the simulations.

3. Results and Discussion

After 65 simulations, some combinations of the variables have shown cross temperatures in some heat exchangers. In order to avoid this the pressures of the propane cycle were fixed at the base case value and a new full factorial design was constructed, being 4 factors at 2 levels (2^4), resulting in 16 experiments plus the base

case (run #17). Table 2 shows the results obtained for this new experimental design. Run #12 has presented the minimum value for the total destroyed exergy.

Table 2: Results of the full factorial design.

	Process Stream/ Pressure (kPa)				Total destroyed exergy (kJ/h)
Run	7	10	12	14	
1	3003	153	1862	99	132262
2	3671	153	1862	99	10750
3	3003	187	1862	99	250836
4	3671	187	1862	99	10290
5	3003	153	2276	99	134099
6	3671	153	2276	99	10916
7	3003	187	2276	99	254631
8	3671	187	2276	99	10461
9	3003	153	1862	121	130182
10	3671	153	1862	121	10563
11	3003	187	1862	121	246560
12	**3671**	**187**	**1862**	**121**	**10096**
13	3003	153	2276	121	131957
14	3671	153	2276	121	10723
15	3003	187	2276	121	250215
16	3671	187	2276	121	10262
17	3337	170	2069	110	19494

Figure 2 shows the main effects plot for the full factoril design 2^4. From Figure 2, one can see that the factors which individually influence the destroyed exergy are the pressures of streams 7 and 10. As the slope seen in the plot of stream 7 is higher than that of stream 10, it is possible to conclude that the influence of the pressure of stream 7 on the response variable is higher. The pressures of streams 12 and 14 are not statistically significant, when analyzed individually, as the plots of these streams show practically horizontal lines. Figure 3 is the Pareto diagram of the full factorial design and presents the influence of the factors, individually and combined, on the response variable. Figure 3 shows that the destroyed exergy was influenced by factors A, B and AB. That means that the pressures of streams 7, 10 and also the combined effect of these two pressures together influence the destroyed exergy of the cycle. The thin line at 0.05 represents the confidence interval (95%), which is the limit to the significance of the estimated effects.

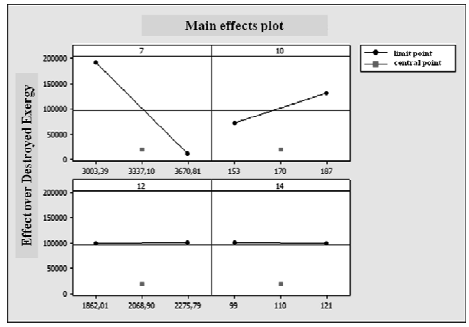

Figure 2: Main effects plot over the total destroyed exergy.

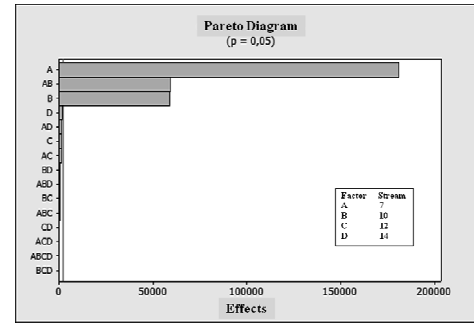

Figure 3: Pareto diagram for total destroyed exergy.

The independent variables and the interactions are statistically significant if the value of the effect is at right side of p = 0.05. Thus the significant effects are the pressures of streams 7, 10 and the combination of pressures 7 and 10.

Figure 4 shows the response surface for the relation between the total destroyed exergy and pressures of streams 7 and 10. Lower values for total destroyed exergy are achieved for high pressure values of streams 7 and 10. It is important to notice that when analyzing the independent influence of the factors on the response variable, Figure 2, one would suggest that the pressure of stream 10 should operate at its minimum value. Nevertheless, when the factors are analyzed together the combined influence of the pressures is higher than the influence of pressure of stream 10 alone, as shown in the Pareto diagram. Therefore, the influence of the pressure of stream 10 alone is disguised by the influence of combined pressures of streams 7 and 10 and as a result, the optimal operation point is at both higher points of streams 7 and 10. Using the optimization tool of Minitab 15, the optimal operation point was determined, which is the one shown in run #12 at Table 2.

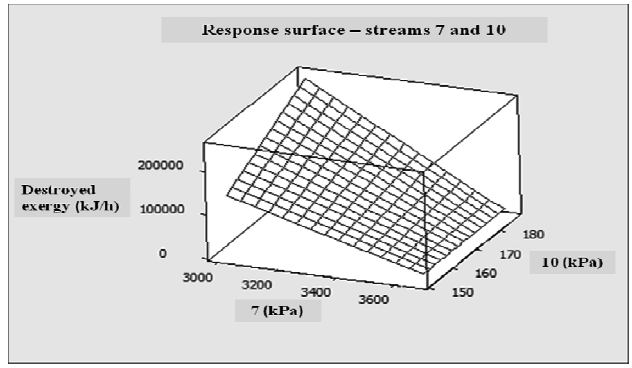

Figure 4: Response surface - relation between destroyed exergy and pressures at streams 7 and10.

4. Results and Discussion

The classical multistage cascade refrigeration cycle applied in the liquefaction of natural gas was studied using an exergetic analysis. The influence of six pressures at six different points of the cycle was evaluated: after the compressor and after the expansion valve of each refrigeration subcycle. The base case scenario has presented a rate of total destroyed exergy of 19494 kJ/h. Through a full factorial design and a statistical analysis a new set of operational conditions based on the analyzed factors resulted in a reduction of 48% of this rate, obtaining a new rate of total destroyed exergy of 10096 kJ/h. Using a thermoeconomic analysis it is possible to check the final benefit of this reduction in the total destroyed exergy. Technically, the modifications proposed are feasible.

References

C.G. Filstead, 1965, Camel LNG Plant: world`s largest, Hydrocarbon Processing, v. 44, n.7, 135-138 pp.

A.J. Finn, G.L. Johnson, T.R. Tomlinson, 1999, Gas processing developments: a special report – developments in natural gas liquefaction, Hydrocarbon Processing, v. 78, n. 4, 47-60 pp.

J.M. Geist, 1983, The role of LNG in energy supply, International Journal of Refrigeration, v. 6, n. 5, 283-297 pp.

M. Kanoglu, 2002, Exergy analysis of multistage cascade refrigeration cycle used for natural gas liquefaction, International Journal of Energy Research, v. 26, 763-774 pp.

J. Szargut, 1980, International progress in second law analysis, Energy, v. 5, 709-718 pp.

I.A. Karimi and Rajagopalan Srinivasan (Editors), Proceedings of the 11th International Symposium on Process Systems Engineering, 15-19 July 2012, Singapore.

Theoretical analysis of a multi-stage membrane reactor for oxidative coupling of methane

Sirikarn Tiraset,[a] Wisitsree Wiyaratn,[b] Suttichai Assabumrungrat,[a] Amornchai Arpornwichanop[a,*]

[a] *Computational Process Engineering, Department of Chemical Engineering, Faculty of Engineering, Chulalongkorn University, Bangkok 10330, Thailand*
[b] *Department of Production Technology Education, Faculty of Industrial Education and Technology, King Mongkut's University of Technology Thonburi 10140, Thailand*
[*] *e-mail: Amornchai.a@chula.ac.th*

Abstract

Oxidative coupling of methane (OCM) is a promising route for the production of ethylene by fully utilizing the abundance of methane feedstock. In this study, a multi-stage dense tubular membrane reactor is investigated to improve the performance of OCM. Mathematical model of the membrane reactor based on conservative equations and detailed OCM kinetic model is employed to analyze the effect of key operating parameters such as temperature and methane to oxygen feed ratio, on the efficiency of the OCM process in terms of CH_4 conversion, C_2H_4 selectivity and C_2H_4 yield. Adjustment of feed distributions at each membrane stage is also studied. The result shows that the multi-stage membrane reactor shows a better performance than the single-stage one. Moreover, a suitable feeding policy can improve the OCM performance.

Keywords: Oxidative coupling of methane, Membrane reactor, Multi-stage reactor, Feed distribution, Performance analysis

1. Introduction

An oxidative coupling of methane (OCM) to produce more valuable hydrocarbons, C_{2+} products, is an attractive technology for fully utilizing the abundance of methane feedstock. The major target product of OCM is ethylene, which is an important petrochemical feedstock. Extensive studies on OCM processes have been conducted and many different reactor concepts, therefore, have been proposed for this process. Due to its technological simplicity, a fixed-bed reactor (FBR) is widely implemented. The operation of this reactor is accidentally prone because of the large amount of heat released during the course of reaction. Furthermore, a poor heat removal from the highly exothermic reaction results in the occurrence of hot spots, affecting the reactor operation such as temperature runaway, catalyst deactivation, undesired side reactions and thermal decomposition of products. The use of a fluidized-bed reactor, which has high heat transfer capacity, shows better heat management and temperature control than a fixed bed reactor system. Talebizadeh et al. (2009) studied the OCM over $Mn/Na_2WO_4/SiO_2$ catalyst in a two-zone fluidized-bed reactor (TZFBR) and its performance was compared with a fluidized-bed reactor. Although the TZFBR gave the C_2 selectivity higher than the fluidized-bed reactor, the C_2 yield was still relatively low (< 20%).

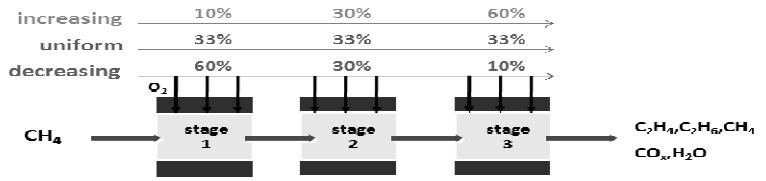

Fig. 1. Schematic diagram of a multi-stage membrane reactor.

The difficulty in the operation of OCM process lies in the fact that the intermediates and target products are higher reactive than the reactant and therefore are prone to deeply oxidize to CO_x. Thus, the oxidation of methane and C_{2+} products seems to be unavoidable when high oxygen content is present in the feed stream. The concept of using an oxygen distribution in a fixed-bed reactor was studied by Zarrinpashne et al. (2004) in order to improve the OCM performance. There are five oxygen feeding points along the reactor with precise control of oxygen flow rate at each point. However, the proposed reactor concept cannot achieve the high yield of ethylene due to the incomplete gas mixing at the oxygen feeding points. This causes high oxygen concentration zones at which the C_{2+} product is easily combusted and its selectivity falls significantly. Omata et al. (1989) initially applied a membrane reactor for the OCM process. The use of the membrane reactor to control oxygen concentration offers a possibility to achieve much higher C_2 hydrocarbons selectivity and yield. Mixed-conducting oxide membranes such as perovskite-type membranes, are well known for their abilities to separate oxygen from air. $Ba_{0.5}Sr_{0.5}Co_{0.8}Fe_{0.2}O_{3-\delta}$ (BSCFO), which was first reported by Shao et al. (2000), is a promising mixed conducting membrane with high oxygen permeability and has proven to be a good candidate for use as an oxygen distributor in the OCM reactor.

In this study, a BSCFO tubular membrane reactor is proposed to improve the performance of the oxidative coupling of methane. A multi-stage membrane reactor is considered and its performance with respect to key operating parameters such as temperature and methane-to-oxygen feed ratio is analyzed. Adjustment of feed distributions at each membrane stage is also studied. The result of applying a multi-stage membrane reactor is compared with a single-stage one.

2. Theory

2.1. Principle

The schematic diagram of a multi-stage membrane reactor is shown in Fig. 1. Three arrangements of oxygen feeding distribution are considered: (i) increased feed, (ii) uniform feed and (iii) decreased feed.

2.2. Reactor model

The mathematical model of a multi-stage membrane reactor is based on the following assumptions: (i) the reactor is under steady-state and isothermal operation, (ii) radial concentration distributions in tube and shell sides of the reactor are negligible and (iii) axial diffusion is neglected. The mass balance of component *i* can be written as:

Tube side (reaction side):

$$\frac{dN_i^t}{dz} = \frac{W}{V} A_{CS} \sum_{j=1}^{n} v_{i,j} r_j + \pi d_2 J_{O_2} \tag{1}$$

Shell side:

$$\frac{dN_{O_2}^s}{dz} = -\pi d_1 J_{O_2} \tag{2}$$

The oxygen flux (Eq. (3)), which was developed by Kim et al. (1998), is used to determine the oxygen permeation through a tubular BSCFO membrane where a bulk diffusion is the controlling step for oxygen permeation.

$$J_{O_2} = \frac{\pi L C_i D_a}{2S \ln(d_1/d_2)} \ln\left(\frac{P_1}{P_2}\right) \tag{3}$$

2.3. Kinetics of oxidative coupling of methane

A comprehensive kinetic model of OCM used in this study was developed by Stansch et al. (1997) for La_2O_3/CaO catalyst. The reaction scheme describing the network of primary reactions for the OCM involves all relevant chemical species as:

Step 1 : $CH_4 + 2O_2 \rightarrow CO_2 + 2H_2O$ (4)

Step 2 : $2CH_4 + 0.5O_2 \rightarrow C_2H_6 + H_2O$ (5)

Step 3 : $CH_4 + O_2 \rightarrow CO + H_2O + H_2$ (6)

Step 4 : $CO + 0.5O_2 \rightarrow CO_2$ (7)

Step 5 : $C_2H_6 + 0.5O_2 \rightarrow C_2H_4 + H_2O$ (8)

Step 6 : $C_2H_4 + 2O_2 \rightarrow 2CO + 2H_2O$ (9)

Step 7 : $C_2H_6 \rightarrow C_2H_4 + H_2$ (10)

Step 8 : $C_2H_4 + 2H_2O \rightarrow 2CO + 4H_2$ (11)

Step 9 : $CO + H_2O \rightarrow CO_2 + H_2$ (12)

Step 10 : $CO_2 + H_2 \rightarrow CO + H_2O$ (13)

The reaction rates for each step are given by Eqs. (14)-(19) and the kinetic parameters are listed in Tabel 1.

$$r_j = \frac{k_{0,j} e^{-E_{a,j}/RT} P_C^{m_j} P_{O_2}^{n_j}}{(1 + K_{j,CO_2} e^{-\Delta H_{ad,CO_2}/RT} P_{CO_2})^2} \qquad j = 1, 3-6 \tag{14}$$

$$r_2 = \frac{k_{0,2} e^{-E_{a,2}/RT} (K_{0,O_2} e^{-\Delta H_{ad,O_2}/RT} P_{O_2})^{n_2} P_{CH_4}}{[1 + (K_{0,O_2} e^{-\Delta H_{ad,O_2}/RT} P_{O_2})^{n_2} + K_{j,CO_2} e^{-\Delta H_{ad,CO_2}/RT} P_{CO_2}]^2} \tag{15}$$

$$r_7 = k_{0,7} e^{-E_{a,7}/RT} P_{C_2H_6} \tag{16}$$

$$r_8 = k_{0,8} e^{-E_{a,8}/RT} P_{C_2H_4}^{m_8} P_{H_2O}^{n_8} \tag{17}$$

$$r_9 = k_{0,9} e^{-E_{a,9}/RT} P_{CO}^{m_9} P_{H_2O}^{n_9} \tag{18}$$

$$r_{10} = k_{0,10} e^{-E_{a,10}/RT} P_{CO_2}^{m_{10}} P_{H_2}^{n_{10}} \tag{19}$$

Table 1. Kinetic parameters of the OCM reactions

Step	$K_{0,j}$(mol $g^{-1}s^{-1}$ $Pa^{-(m+n)}$)	$E_{a,j}$ (kJ mol^{-1})	m_j	n_j	$K_{j,CO2}$ (Pa^{-1})	$\Delta H_{ad,CO2}$ (kJ mol^{-1})	$K_{j,O2}$ (Pa^{-1})	$\Delta H_{ad,O2}$ (kJ mol^{-1})
1	0.20×10^{-5}	48	0.24	0.76	0.25×10^{-12}	-175		
2	23.2	182	1.00	0.40	0.83×10^{-13}	-186	0.23×10^{-11}	-124
3	0.52×10^{-6}	68	0.57	0.85	0.36×10^{-13}	-187		
4	0.11×10^{-3}	104	1.00	0.55	0.40×10^{-12}	-168		
5	0.17	157	0.95	0.37	0.45×10^{-12}	-166		
6	0.06	166	1.00	0.96	0.16×10^{-12}	-211		
7	1.2×10^{7} [a]	226						
8	9.3×10^{3}	300	0.97	0				
9	0.19×10^{-3}	173	1.00	1.00				
10	0.26×10^{-1}	220	1.00	1.00				

[a]Units are mol $s^{-1}m^{-3}Pa^{-1}$.

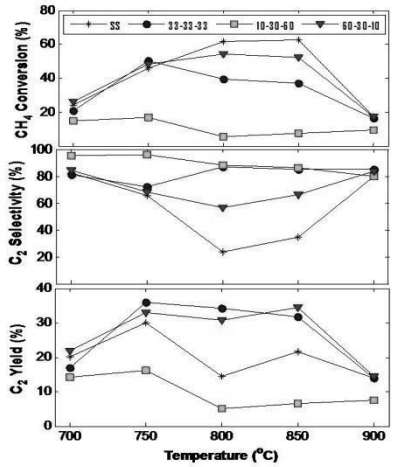

Fig. 2. Effect of operating temperatures on single- and multi-stage membrane reactors (CH_4/O_2 ratio = 1.5 and CH_4 feed flow rate = 1.6×10^{-3} mol/s).

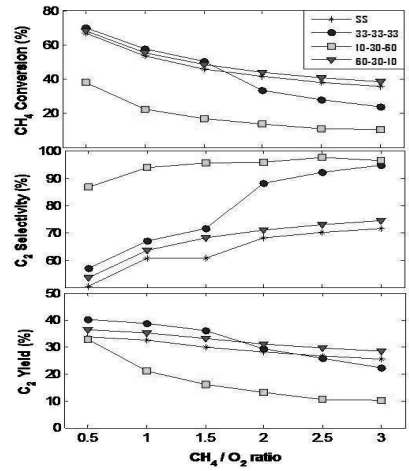

Fig. 3. Effect of CH_4/O_2 ratio on single- and multi-stage membrane reactors (T = 750 °C and CH_4 feed flow rate = 1.6×10^{-3} mol/s).

3. Results and Discussion

The effect of operating temperatures on the performance of single- and multi-stage membrane reactors for the OCM reaction is presented in Fig. 2. It is found that the multi-stage membrane reactor operated under the uniform and decreased feeding policy of oxygen shows higher selectivity and yield of C_2 than the single stage one. The conversion of methane in the single-stage membrane reactor is higher than that in the multi-stage reactor, especially at the temperature higher than 750 °C, because of a higher oxygen permeability. However, the C_2 selectivity of a single stage reactor is lower than a multi-stage reactor because a decrease in the methane partial pressure in the tube side leading to low methane and oxygen ratio (high oxygen content in the reaction side). In case of the multi-stage membrane reactor with increased feed of oxygen, due to the very low CH_4 conversion, the C_2 yield is therefore low even the highest C_2 selectivity is obtained.

Fig. 3 shows the effect of CH_4/O_2 ratio varying from 0.5 to 3 on the performance of the OCM membrane reactor. It can be seen that the performance of the single-stage membrane reactor is quite similar to the multi-stage membrane reactor with a decreased distribution of oxygen. The conversion of CH_4 and the yield of C_2 decrease with increasing the CH_4/O_2 ratio. The C_2 selectivity can be improved by using the multi-stage membrane reactor, especially at high CH_4/O_2 ratio.

Fig. 4a. shows the profiles of oxygen concentration at the tube side, which increases as more oxygen permeates from the shell side. Under the increased oxygen feeding policy, low oxygen content in the first stage of the multi-stage reactor causes relatively low CH_4 conversion and C_2 yield (Fig. 4b and Fig. 4d). The selectivity of C_2 at the outlet of each stage is given in Fig. 4c. The multi-stage membrane reactor with an increased distribution of oxygen shows higher C_2 selectivity than the others. An increase in the oxygen concentration, especially in the third stage, reduces the C_2 selectivity at the outlet due to undesired series reactions.

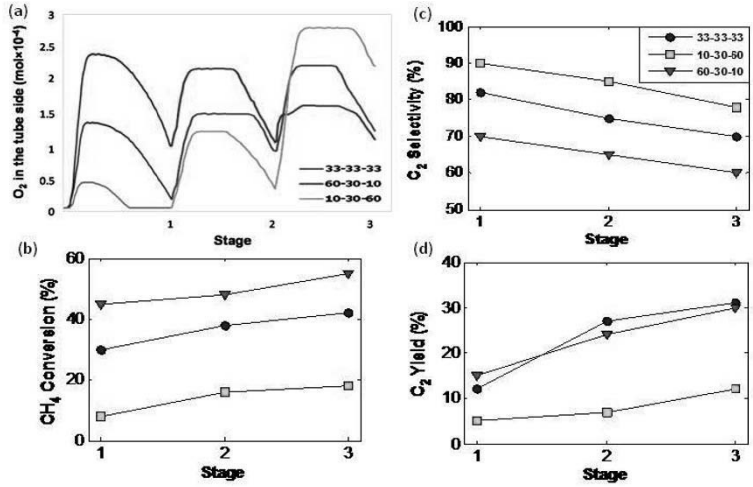

Fig. 4. (a) O_2 concentration profile at the tube side, (b) conversion of CH_4, (c) C_2 selectivity and (d) C_2 yield, at the outlet of each stage of the multi-stage membrane reactor, respectively (T = 800 °C and CH_4/O_2 ratio = 2 and CH_4 feed flow rate = 1.6×10^{-3} mol/s)

4. Conclusions

In this study, the performance of a multi-stage membrane reactor for OCM was investigated via simulation studies. The results have shown that the use of membrane as an oxygen distributor improves the OCM process. In addition, the multi-stage membrane reactor with a distributed feeding policy shows a better performance, in terms of C2 selectivity and yield, compared with a conventional single-stage membrane reactor. This is because the adjustment of oxygen feed distributions at each membrane stage avoid the formation of high oxygen concentration zones.

5. Acknowledgement

Support from the National Research Council of Thailand, the Thailand Research Fund and Commission of Higher Education is also gratefully acknowledged.

References

S. Kim, Y.L. Yang, A.J. Jacobson, B. Abeles, 1998, Diffusion and surface exchange coefficients in mixed ionic electronic conducting oxides from the pressure dependence of oxygen permeation, Solid State Ionics, 106, 189, 95.

K. Omata, S. Hashimoto, H. Tominaga, K. Fujimoto, 1989, Oxidative coupling of methane using a membrane reactor, Appl. Cat., 51, L1-L4.

Z. Shao, W. Yang, Y. Cong, H. Dong, J. Tong, G. Xiong, 2000, Investigation of the permeation behaviour and stability of a $Ba_{0.5}Sr_{0.5}Co_{0.8}Fe_{0.2}O_{3-\delta}$ oxygen membrane, J. Membr. Sci., 172, 177.

Z. Stansch, L. Mleczko, M. Baerns, 1997, Comprehensive kinetics of oxidative coupling of methane over the La_2O_3/CaO catalyst, Ind. Eng. Chem. Res., 36, 2568.

A. Talebizadeh, Y. Mortazavi, A.A. Khodadadi, 2009, Comparative study of the two-zone fluidized-bed reactor and the fluidized-bed reactor for oxidative coupling of methane over $Mn/Na_2WO_4/SiO_2$ catalyst, Fuel Proc. Tech., 90, 1319–1325.

S. Zarrinpashne, J.S. Ahari, R. Ahmadi, 2004, Development of a process for ethylene production from methane by OCM reactions and its commercialization challenges, Research Institute Of Petroleum.

I.A. Karimi and Rajagopalan Srinivasan (Editors), Proceedings of the 11th International Symposium on Process Systems Engineering, 15-19 July 2012, Singapore.

Optimal synthesis for the feed-water-heater network of a Pulverized Coal (PC) power to minimize water consumption

Juan M. Salazar, [a] Urmila M. Diwekar, [a]

[a]*Vishwamitra Research Institute: Center for Uncertain Systems, Tools for Optimization and Management, 368 56th Street, Clarendon Hills, Il 60514, USA*

Abstract

Coal-fired power plants contribute to almost 50% of the United States' total electric power production. At the same time, pulverized coal (PC) power plants are large water consumers to the point that construction and operability of PC power plants have started to be constrained by water availability in some regions of the country. Research efforts have been intensified to reduce the water usage and consumption which are closely related to the water losses associated to the cooling systems and gas purification operations. Two process systems engineering approaches have been studied to minimize the water consumption of power plants. First, a better optimization of nonlinear uncertain systems (BONUS) algorithm has provided solutions to the minimization of water consumption under uncertain atmospheric conditions. The calculated conditions for a 550 MW PC plant predicted reductions of 6.4%, 3.2%, 3.8% and 15.4% in the average water consumption for the four different seasons from fall to summer respectively. A second approach pursues the reduction of the residual heat in the steam cycle of the PC process by formulating an optimal design of the feed water heat exchange network (HEN). The proposed methodology uses Aspen Energy Analyzer (AEA) to determine the mass flowrates of the bleeding streams while generating alternative designs that can potentially reduce the water consumption by reducing the total cooling requirement. The optimization approach to process synthesis involves the selection of an optimal solution from the superstructure with a simulated annealing (SA) capability built in Aspen Plus. Results show at least a 5% reduction in water consumption for the PC power plant via this enhanced HEN synthesis technique
Keywords: Pulverized Coal power plants, water management, stochastic optimization HEN synthesis.

1. Introduction

Water consumption is one of the characteristics that need to be addressed when assessing the generation capabilities of a coal-fired power plant [1] . Makeups, blowdowns, process water and cooling water are responsible for consumption with the evaporative cooling system being the largest water consumer in power plants [2] . Comprehensive simulation models of pulverized coal (PC) power plants have been formulated in Aspen Plus to estimate the performance of the processes including its water consumption[1] . It has been reported that evaporative loses in the cooling tower are significant and they are affected by environmental conditions like air temperature and humidity and design conditions like process efficiency [2] . This implies that computational tools of process analysis should include approaches to account for the influence of uncertain parameters in the models and to improve efficiency of the process.

Stochastic modeling (process modeling under uncertainty), has been used for process analysis in power systems [3] . When including optimization techniques, the resulting non-linear stochastic programming (NLSP) can become highly computationally demanding [4] . These computational expenses have been drastically decreased with the better optimization of non-linear uncertain systems (BONUS) algorithm [4] . Heat exchange network (HEN) synthesis has been employed to improve the efficiency of power cycles [5] . Aspen Energy Analyzer (AEA) is a simulation and design tool that can be employed to generate alternative HENs with the purpose of improving the process performance [6] . In this work, BONUS algorithm has been integrated to Aspen Plus simulator via the advanced engineering co-simulator (APECS) and CAPE-OPEN interface. Also, a HEN synthesis problem is formulated by switching the roles of hot streams to hot utilities and modifying their costs to generate alternative designs with AEA. Finally, an integrated approach of process synthesis under uncertainty is proposed as an efficient alternative to minimize the water consumption of PC processes

2. Process Description

The PC power plant model studied in this paper is based on Case 11 referenced by the DOE/NETL's report on cost and performance of fossil energy plants [1] . This power plant is a re-heating cycle with feed-water heating. The process comprises a boiler section where coal is burned and the combustion heat is transferred to water generating steam, and a steam section where the high pressure steam is expanded through a train of high, intermediate and low pressure turbines. Steam is initially generated in the boiler and expanded in the high pressure (HP) turbine; then, it is re-heated at the boiler for later expansion at the intermediate (IP) and low pressure (LP) turbines. Then, exhausted steam is condensed with liquid water and returned to the boiler while heated with bleeding streams of steam from the turbines (feed-water heater). Cooling water is sent to the cooling tower where heat from the cycle is ultimately rejected to the environment by evaporative cooling.

3. Optimization under uncertainty

3.1. Stochastic Simulation

As it was previously said, water consumption is strongly affected by weather conditions like air temperature and humidity. Detailed information about air conditions for different locations within the US can be obtained from the website (http://www1.eere.energy.gov). Histograms of the frequency distributions were fitted to the appropriate probability density functions to represent the air conditions variability of an average U. S. Midwestern urban center during each of the four seasons [7] . Stochastic simulation is carried out by efficiently sampling these distributions to generate a set of scenarios under which the plant models are evaluated and a corresponding probability distribution of water consumption (output variable) is calculated.

3.2. Stochastic Optimization

Minimization of water consumption in power plants is a stochastic non-linear programming (SNLP) problem where one of the moments (expected value, standard deviation, etc.) of the water consumption's probability distribution is the objective function, the model is the set of constraints and model parameters are the decision variables. BONUS algorithm [4] is a "here and now" approach to solve this problem [8] determining the process conditions under which the expected value of the water

consumption can be reduced compared to the base case originally reported, as shown in Table 1[9] . It can be seen that the reduction on the consumption strongly depends on the season consumption during drastic weather conditions as summer can be reduced by changing some of the parameters of the process.

Table 1 Minimization of average water consumption under uncertain air conditions for a 550 MW PC power plant located at Midwestern US for four different seasons [9] .

Season	Optimal values of decision variables					Savings %
	Par 1 (%)	Par 2 ^{0}F	Par 3 Mass fraction	Par 4 pressure ratio	Par 5 pressure ratio	
Fall	38.9	1160.8	0.31	0.49	0.61	6.4
Summer	48.9	1174	0.42	0.49	0.66	15.4
Spring	35.5	1096.5	0.22	0.36	0.61	3.8
Winter	19.0	1141.9	0.30	0.49	0.79	3.2
	Base case values of decision variables					
All	20	1157	0.3	0.365	0.637	

4. Heat Exchange Network synthesis for water management

4.1. Modified HEN synthesis in AEA

Conventional methodology for the heat exchange network synthesis of the feed water heating system is based on equal enthalpy change on the liquid stream for each of the heaters. Mass flow rates of the bleeding streams are calculated based on such heat load distribution. AEA generates alternative designs with a mixed integer linear programming (MILP) algorithm. The solution of the MILP problem is based on the thermodynamic characteristics of the involved streams and on fixed mass flowrate of the bleeding streams. This approach was modified based on the early work by Linhoff [5] that proposes the employment of pinch technology to define mass flowrates from the bleeding streams for maximum heat recovery and improved cycle efficiency. This cycle efficiency is directly associated to the PC process water consumption through the amount of heat rejected by the cycle.

The main idea of this work is employing the AEA MILP algorithm to determine the mass flowrates of the bleeding streams while generating alternative designs that can potentially reduce the water consumption by reducing the total cooling requirement. For this purpose, the bleeding streams have been treated as utilities (instead of process streams) whose mass flowrates are determined by the calculated heat load assigned to them by the MILP algorithm.

4.2. Cost modification for alternative utility streams

Optimization algorithms based on process costs (as the one used by AEA) yield designs that employ mostly hot streams because they minimize heat transfer area leaving low temperature streams unused. To avoid this situation a cost penalty was assigned to bleeding (utility) streams. The approach assumes that feed water heating is expensive for the process when using high pressure steam and using low pressure steam is inexpensive to the point that some income can be generated. The main reason is that employing large amounts of high pressure steam may decrease the process productivity

and preheating the feed water with low pressure steam will increase the process efficiency. The utility costs were assigned as shown in Table 2(For the description and location within the process of bleeding streams the reader is referred to original work by Linhoff [5]). It can be seen that the highest costs (based on the cost of high pressure steam as utility) is assigned to the bleed stream "bleed 3" and the lowest value corresponds to the coldest bleed as the stream entering the last low-pressure turbine. The other values were assigned as equally spaced values yielding 4 positive values and 4 negative values.

Table 2 Assumed costs of bleeding streams as utilities for the heat integration of feed water heater network

Bleed stream	Temperature (F)	cost index/BTU
bleed 1	773	2.04E-06
bleed 2	660	4.08E-07
bleed 3	929	2.86E-06
deareator stream	720	1.22E-06
bleed 4	568	-4.09E-07
bleed 5	308	-1.23E-06
bleed 6	227	-2.04E-06
bleed 7	146	-2.86E-06
Cooling Water		4.49E-06

The drain streams are mixed and also are used to transfer sensible heat to the feed water. The costs assigned to these drains are naturally related to those shown in Table 2and reported in Table 3. It can be seen that the costs of "Drain1" and "Drain5" are equal to those of "bleed 1" and "bleed 5" respectively. The reason is that these drains are not mixed with any other so their employment as heat sources for the feed water preheating will be associated to that of the corresponding bleeds.

Table 3 Assumed costs of drain streams as utilities for the heat integration of feed water heater network

Drain stream	cost index/BTU	weights		
Drain 1	2.04E-06			
Drain 2	1.39E-06	bleed 1:0.6	bleed 2:0.4	
Drain 3	1.71E-06	bleed 3: 0.5	bleed 1: 0.3	bleed 2: 0.2
Drain 5	-4.09E-07			
Drain 6	-7.35E-07	bleed 4; 0.6	bleed5: 0.4	
Drain 7	-9.80E-07	bleed 4: 0.5	bleed 5: 0.3	bleed 6: 0.2

On the other hand the remaining drain streams are mixtures of two or three drains. Therefore their costs have been assumed to be a weighted average of their bleeding constituents having more weight the cost of the bleed that is more expensive. This formulation of the problem and its solution with AEA yielded interesting alternative designs whose cold utility consumption is lower than that of the base case as shown in Table 4 and it is expected that the water consumption will also be lower.

Table 4 Cooling requirements for designs that consider the bleed streams as utilities

Design	Cooling requirement X 10 7 BTU/h
base case	1.024
Design1	0.627
Design2	0.627
Design3	0.627

5. Conclusion

This paper presents a framework for integrated water management in power systems. It has been found that water consumption depends on the weather conditions and the uncertainties in weather affect the consumption considerably. We presented an optimization under uncertainty problem for savings water consumption. The second approach is heat integration. An algorithmic framework (Figure 1) based on simulated annealing (and OA/ER/AP MINLP) for discrete decisions, BONUS algorithm for the stochastic NLP, and Hammersley sequence sampling for the sampling saved 97% of computational time to solve this problem. Optimization under uncertainty allowed us to save up to 15% in the expected value of water consumption in a PC plant and a pinch technology approach to the heat exchange network synthesis allowed a 38% in cooling requirement which will be translated in water savings as well.

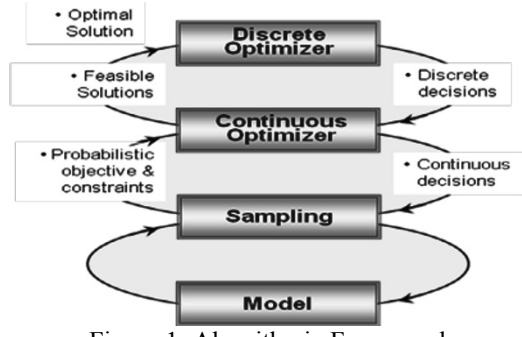

Figure 1: Algorithmic Framework

References

[1]DOE/NETL, Cost and performance baseline for fossil energy plants, (2007). DOE/NETL-2007/1281.
[2]DOE/NETL, Power plant water usage and loss study, (2007).
[3] U. Diwekar and E.S. Rubin, Comput. Chem. Eng. 15 (1991) 105-114.
[4] K. Sahin and U. Diwekar, Annals of Operations Research 132 (2004) 47-68.
[5] B. Linhoff and F.J. Alanis, ASME Advanced Energy Systems 85 (1989) 10-15.
[6] J.M. Salazar, U.M. Diwekar and S.E. Zitney, Comput. Chem. Eng. 35 (2011) 1863-1875.
[7] J.M. Salazar, U.M. Diwekar and S.E. Zitney, Energy Fuels 24 (2010) 4961-4970.
[8] U.M. Diwekar, Introduction to Applied Optimization, 2nd ed., SpringerLink, New York, 2008.
[9] J. Salazar and U. Diwekar. Energy Systems 2 (2011) 263-279.

I.A. Karimi and Rajagopalan Srinivasan (Editors), Proceedings of the 11th International Symposium on Process Systems Engineering, 15-19 July 2012, Singapore.

Techno-economic analysis of coal gasification based co-production systems

Siyu Yang, Hengchong Li, Yu Qian

School of Chemistry and Chemical Engineering, South China University of Technology, Guangzhou 510640, P.R. China

Abstract

Coal gasification based co-production systems are increasing popular in the world because they are assumed to be advantageous in energy efficiency and economic cost. However, there has been seldom researches on quantifying these advantages. In this paper, the co-prouction systems are analyzed from the technical and ecnomic point of views. During the study, the co-production system, of which the products are electricity and methanol, is modeled and simulated. For analysis, the energy analysis model and the economy analysis model are established. Results show that the co-production system has higher energy efficiency and less capital expenditure than tranditional single production systems.

Keywords: Co-production system; Techno-economic analysis; Coal gasification; Combined cycle.

1. Introduction

Coal has been broadly accepted as one of inportant alternatives of petroleum. NBS (NBS 2008) reported that coal provides 70.3% of energy in China. Similar to petroleum, the derivatives of coal include electricity, fuels, and chemicals. Traditional coal based techniques have low energy efficiency. For high energy and resource efficiency, the coal gasification based co-production systems are developed and increasing popular. However, the co-production systems are complex. Till now, there have been many researches on the systems (Yamashitaa & Barretob 2005, Rieger et al. 2008, Liu et al. 2010). However, most of them are limited on the technical analyses. The aim of this paper is to analyze the systems from technical and economic aspects.

2. Conceptual structure of the co-production system

Co-production systems are developed for high energy and resource efficiency. These systems have different configurations through selecting derivative products. The schematic of the co-production system used in this paper is shown in Figure 1.

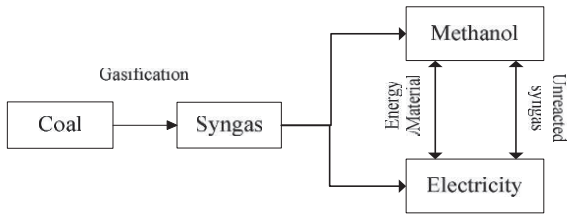

Figure 1 Structure of the co-production system

It can be seen that the co-production system consists of two parts: electricity generation and chemical production. For the former part, the combined cycle process is used due to

China's energy development tendency (i.e. clean energy). For the latter part, methanol is selected as the chemical product. The following sections brief the modeling and simulation of the co-production system.

3. Modeling and simulation of the co-production system

The co-production system (Figure 2) consists of a number of general process units: Air separation unit (ASU), Solid feed preparation and gasification (SPG), Acid gas removal (AGR), CLAUS sulfur recovery (CLAUS); Water gas shift (WGS), Heat recovery steam generation (HRSG), Combined cycle (CC), Methanol synthesis subsystem (MS).

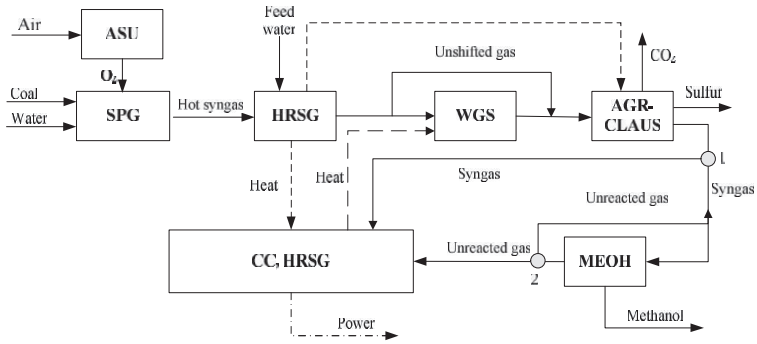

Figure 2 Schematic of the co-production system

As Figure 2 shown, coal slurry is combusted with O_2 in the gasifier to produce syngas. The syngas is cleaned in AGR-CLAUS to remove acid gas and recover elemental S. The H_2/CO ratio is adjusted in WGS by converting CO into H_2. MS is used to synthesize methanol. CC includes the gas turbine and the steam turbine to generate electricity. Heat of the gas is recovered in HRSG to generate steam. Aspen Plus software is used to model and simulate the co-production system. The operational parameters for the system are listed in Table 1.

Table 1. Reference operational parameters of the co-production system

Parameters	Value	Parameters	Value
O_2 supplied mole purity	95%	Gas turbine outlet temperature	1250K
O_2 supplied pressure	40atm	Gas turbine expansion ratio	16
Gasification pressure	42atm	High pressure	120atm
Gasification temperature	1645K	High temperature	838K
CO conversion ratio	47%	Intermediate pressure	40atm
H_2/CO ratio in syngas	0.6	Intermediate temperature	836K
Methanol synthesis temperature	545K	Low pressure	3atm
Methanol synthesis pressure	80atm	Low temperature	516K

4. Analyses of the co-production system

4.1. Energy analysis

Analysis model

In theory, exergy of a system reflects the maximum work that the system can do. Energy efficiency is calculated by using exergy theory as shown in Eq. 1.

$$\eta_{ex} = EX_{out} / EX_{in} \quad (1)$$

Where η_{ex} is the energy efficiency, EX_{out} is the output exergy of a process and EX_{in} is the input exergy of a process. In theory, exergy consists of physical exergy, chemical exergy and exergy change of mixing. Chemical exergy refers to the standard chemical exergy of chemical elements (Kameyama et al. 1982).The exergy of heat stream and work stream is calculated in Aspen Plus. The exergy loss of a process unit is the difference between the input exergy and the output exergy. Exergy loss ratio ξ for the process unit *j* is formulated as.

$$\xi_j = EX_{loss,j} / EX_{in} \quad (2)$$

The coal from Luzhou, China is used in this study. According to the work of Zhong (Zhong 1988), the exergy of raw coal is 27703.3kJ/kg.

Result and discussion

For energy analysis of the co-production system, it is compared with two single produciton sysetms (IGCC and methanol produciton system). For comparision, the co-production system is set to generate the same amount of electricity and methanol as those of the single systems. Through the comparison, the reduction of exergy loss are explored. The results are shown in Table 2.

Table 2. Energy performance of the co-production system and standalone systems

	IGCC		CMS		COME	
	kJ	Ratio (%)	kJ	Ratio (%)	kJ	Ratio (%)
Coal input	13145	100	14682	100	27703	100
Gasification	1840	14.0	1835	12.5	3851	13.9
CC	3154	25	1071	7.1	5153	18.6
WGS	-	-	88	0.6	150	0
MES	-	-	396	1.3	55	0.2
HRSG	1432	10.9	1791	12.2	2937	10.6
ASU	381	2.9	734	5.0	1039	3.75
Others	920	7	1174	8	1662	6
Sum	7729	59.7	7092	46.5	14696	53.05
Electricity	5416	41.3	-	-	5416	19.5
Methanol	-	-	7591	51.7	7591	27.5

The co-production system has the energy efficiency of 47.4% between those of IGCC (40.3%) and CMS (53.5%). Considering exergy loss of process units, it is found that SPG and CC are the main sources for exergy loss. In the gasifier, the exergy loss is caused by irreversibility in the heat transferring of exothermic reactions. In CC, the heat loss in the gas turbine and the steam turbine is the main source of exergy loss. By comparison, the co-production system needs for 27827Kj coal more than that of the single systems. The co-production system has better performance in energy utilization.

4.2. Economic analysis

The economy analysis for the co-production systems is as important as the energy analysis. Understanding their production process from economic viewpoint explores unnecessary expenditures. This paper builds an economic analysis model, in which the cost of the co-production process consists of the static investment and the operating cost.

The static investment of unit j is equal to domestic made factor γ multiplied by the sum of overnight cost $I_{OC,j}$ and the construction interest $I_{IC,j}$. I_{IC} is calculated by multiplying I_{OC} the construction period interest λ (set to 0.12). I_j^{OC} is formulated as:

$$I_{OC,\ j} = \theta I_j^b \left(S_j / S_j^b\right)^f \quad (3)$$

where θ and f indicate the regional factor and the scaling factor, S_j and S_j^b are the practical scale and the reference scale of unit j, and I^b_j is the reference investment of unit j. Depending on the researches(Huang 2008a, Huang 2008b), the above parameters of process units are determined and shown in Table 3.

Table 3. Parameters for estimating static investment

	S^b_j	f	Θ	I^b_j (million \$)	γ
ASU	21.3kg/s (O_2)	0.5	0.5	45.7	0.5
Solid preparation	27.4kg/s (Coal)	0.67	0.65	29.1	0.65
Gasification	39.2kg/s (Coal)	0.67	0.8	78	0.8
WGS	716 MW (Heat)	0.67	0.65	28	0.65
AGR-CLAUS	29.3 mol/s (S)	0.67	0.65	67.34	0.65
Gas turbine[a]	276 MW (Electricity)	0.67	1	83	1
Steam turbine	59.2 MW (Electricity)	0.67	0.65	94.7	0.65
MES	10810mol/s (syngas)	0.67	0.65	20.4	0.65

Besides the static investment, the operating cost is an important indicator to evaluate the process. In this paper, the annual operating cost is the sum of the annual investment I_{CRF} , the material charge I_{MT}, and the matainence cost I_{MC}. According to Li et al (Li et al. 2007) the annual investment is equal to the static investment multiplying the capital recovery factor (CFR), which can be formulated as

$$CRF=i(1-(1+i)^{-n}) \quad (4)$$

where n denotes the useful life and is set to 30, i means the discount rate and is set to 0.1 in this paper. The maintenance cost here is set to 4% of the overnight cost. The products of the co-production system are 263.3MW electricity and 312.9MW methanol. The annual operation time is set to 8000 hours. Prices of coal in this paper is 2 \$/GJ.

4.2.1. Result and discussion

Depending on the economic model, the investment of the co-production system for 30 years are calculated and shown in Table 4.

Table 4. Economic analysis of the co-production system (million \$)

	IGCC +CME	CFCP
I_{OC}	571	402
I_{CI}	70	49
I_{MT}	60.5	42.5
I_{MC}	84.1	74.2
I_{CRF}	22.8	16.1

As the results shown, the co-production system save 224.6 million \$ investment compared to the single systems. The save is broken down to the static investment 190 million \$ and the operating investment 34.6 million \$.

5. Conclusion

This paper analyzed the co-production systems from technical and economy aspects. The products of the system are electricity and methanol. In the technical analysis, exergy theory is used to calculate the energy efficiency. In the economic analysis, the total investment is estimated by summing the static investment and the operating cost. Comparison with single systems (IGCC and methanol production system) is used for analysis. Result shows that the co-production systems use less energy and spends less investment than single systems. China is now going through a rapid industrialization and economic growth. The demand for energy and capital is larger than ever before. The analysis in this paper is worthwhile to be expanded in other energy and chemical systems.

Acknowledgements

This work is supported by the China NSF key project (No. 21136003), National Basic Research Program (No. 2012CB720504) and Specialized Research Fund for the Doctoral Program of Higher Education (No. 20100172110016).

Reference

B. Lin, J. Liu, 2010, Estimating coal production peak and trends of coal imports in China, Energy Policy, 38 512–519.

C. Yongtaek, G. S. Harvey, 2003, Water gas shift reaction kinetics and reactor modeling for fuel cell grade hydrogen. Journal of Power Sources, 124, 432–439.

H. Huang, 2008, Economic estimation model of IGCC plant, Journal of power plant, 28(4): 633-637.

H. Huang, Estmination model of design, procurement and construction of IGCC plant, Journal of power plant, 28(3): 475-479, 2008.

H. Kameyama, K. Yoshida, S. Yamauchi, K. Fueki, 1982, Evaluation of reference exergies for the elements. Applied Energy, 11(1), 69-83.

M. Rieger, R. Pardemann, H. Rauchfuss, B. Meyer, 2009, Carbon capture and storage power plants; effects of ASU integration on IGCC performance and gas turbine operation. VGB Powertech 88 (3), 102 – 107.

National Bureau of Statistics of China (NBS), 2008 China Statistics Yearbook Beijing: China Statistic Press.

S.M. Zhong, 1989, Handbook of Water and Vapor Character Parameter with Exergy Character, Hydroelectricity Press, Beijing.

I.A. Karimi and Rajagopalan Srinivasan (Editors), Proceedings of the 11th International Symposium on Process Systems Engineering, 15-19 July 2012, Singapore.

A Process Integration Technique for Steam System Synthesis Involving Multiple Levels

[a]Sheldon G. Beangstrom, [a,b]Thokozani Majozi[*]

[a]*University of Pretoria, Lynnwood Rd, Pretoria, 0002, South Africa*
[b]*Modelling and Digital Science, CSIR, Meiring Naude Rd, Pretoria, 0002, South Africa*
[*]*corresponding author: thoko.majozi@up.ac.za*

Abstract

Recent work has shown that process integration techniques can be used to systematically reduce the flowrate of steam through a network. This is achieved by reusing hot condensate as an additional heating medium. This paper presents techniques for the application of process integration techniques to systems with multiple steam levels. The method is limited to a graphical technique as this allows the designer to interact with and guide the technique using one's knowledge of the system.

Application of these techniques to an illustrative example reduced the steam flowrate by 24% and reduced the cost of the steam network by 13%. This is advantageous in establishing new plants as well as debottlenecking old plants.

Keywords: heat exchanger network, synthesis, process integration, pinch analysis

1. Introduction

Given the steady increase in the cost of energy as well as the cost of process equipment, a great emphasis has been placed on finding techniques to reduce the capital and operating costs of a plant. Pinch analysis is well suited to help optimize processes in order to meet these demands.

Pinch analysis was first popularized by Linnhoff and Flower (1978) and Linnhoff and Hindmarsh (1983) in the form of process-process heat integration. In their method, heat is transferred from a hot process stream to a cold process stream, thereby reducing the duties of the external hot and cold utilities. The limit to the amount of energy that can be saved is seen when hot and cold composite curves are shifted together, until at some point the two curves are separated by a predetermined minimum temperature difference for heat exchange. This point is then referred to as the pinch point.

More recently, Kim and Smith (2001) have applied process integration to the optimisation of cooling water networks. Their work was inspired by evidence that the effectiveness of a cooling tower can be improved by reducing the flowrate of cooling water and increasing the return temperature of the water (Bernier, 1994). They developed a method using pinch analysis whereby cooling water is reused from one heat exchanger to another. By adding reuse streams to the Heat Exchanger Network (HEN), the flowrate of cooling water required is reduced. Since the cooling duty remains constant, the return temperature of water also increases. This in turn raises the effectiveness of the cooling tower.

Not much has been done on the topic of process integration as applied to the steam system network, particularly where the use of condensate is considered. Coetzee and Majozi (2008) proposed that the flowrate of steam can be minimised by using the sensible heat of the hot condensate to perform low temperature heating. They present the ground work for a graphical method of targeting the minimum steam flowrate, but

require a linear program to design the layout of the HEN and all the reuse streams. Their work was also limited to a single level of steam. This work was motivated by the fact that the purchase cost of boilers rise rapidly with increasing flowrate.

Price and Majozi (2010) developed a number of models that included the boiler efficiency. Their work aimed to minimise the flowrate of steam while maintaining the boiler efficiency and minimising pressure drop.

In this paper, we outline a graphical method for targeting the minimum steam flowrate and synthesizing the HEN in the presence of multiple steam levels. A method is given in which various composite curves are systematically shifted to target the minimum steam flowrate. Once the target has been determined, the HEN is synthesized using another graphical method.

2. Problem Statement

The problem which the design procedure addresses can be stated as follows.
Given:

1. a set of heat exchangers,
2. the fixed duties of the respective heat exchangers,
3. the limiting inlet and outlet temperatures of the hot utility passing through each heat exchanger,
4. the minimum global driving force ΔT_{min} for all the heat exchangers in the system,
5. the thermophysical properties of all the available steam levels from the boiler(s), and
6. the thermophysical properties and fixed flowrates of all present turbine exhaust streams.

Determine the minimum flowrate of steam required from each steam level and design the layout of the HEN that will achieve this target.

3. Flowrate Targeting

The first task to be completed is to target the minimum steam flowrate across the various steam levels. Once the desired flowrate has been targeted, the HEN can be synthesized to meet this target.

The method by which a single level of steam can be minimized is based on the work by Coetzee and Majozi (2008). First, one must determine the limiting utility profile for each process. In a counter-current heat exchanger, there exists a minimum temperature difference for heat exchange (ΔT_{min}). A hot utility that is ΔT_{min} above the process stream at all points in the heat exchanger represents a feasible lower limit on the utility. To extract this limiting data from the process data, ΔT_{min} must be added to the supply and target temperature of the cold process streams to give the minimum feasible target and supply temperatures of the hot utility respectively. This data is then used to create a limiting utility curve, similar to a composite curve but moving in the opposite direction. This curve represents a feasible boundary, as any utility line that crosses this boundary is in violation of the minimum driving force for heat transfer.

The utility line representing the steam and condensate is composed of two parts: a horizontal segment representing the latent heat, and a slanting segment representing the sensible heat. Fig.1 shows this shape.

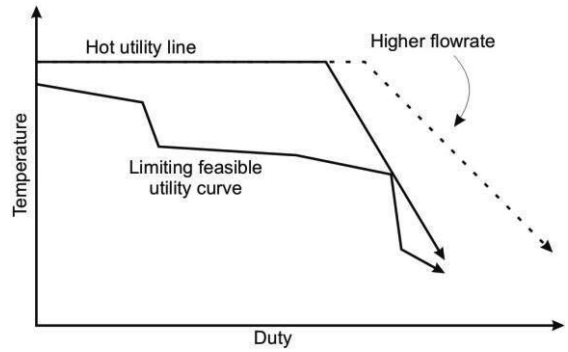

Figure 1: Limiting utility curve and a utility line representing one steam source

The hot utility line is constructed using the standard equations representing the latent and sensible heat of steam. As can be seen in Fig. 1, changing the flowrate not only makes the utility line longer or shorter, but also changes the slope of the sensible heat segment. This will cause a pinch to form at the minimum flowrate. Coetzee and Majozi (2008) show that this represents the minimum feasible steam flowrate that is capable of heating the system. Thus, to target the minimum possible steam flowrate, one needs only to reduce to flowrate until a pinch is observed between the two curves.

To extend this approach to multiple steam level systems, one needs to follow a two-step approach. In the first step, the original limiting utility curve is divided between the intervals created by the different steam level temperatures. The above technique is applied individually to each interval to initially minimize the flowrate of each individual steam level.

The second step involves identifying opportunities for further reductions. This begins in the highest temperature interval and moves downwards. Fig. 2(a) shows the utility lines of two steam levels that have been minimized inside their respective intervals. The highest steam level has been extended into the infeasible region. Where the line crosses the boundary, it is broken and shifted to the right to form a new pinch. The flowrate of the lower steam level can then be minimised further over the unheated region that remains, as shown in Fig 2(b).

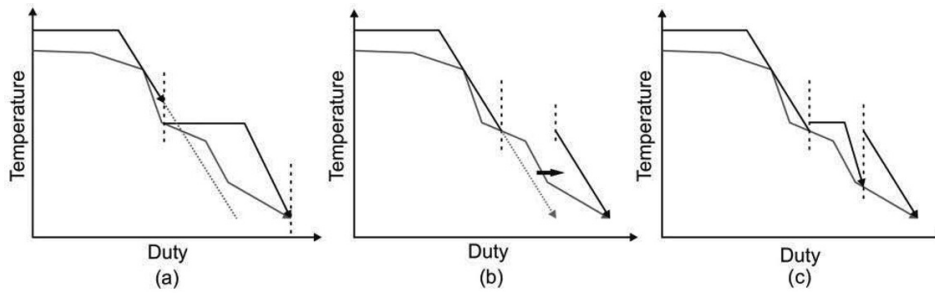

Figure 2: Producing further reductions in steam flowrate. (a) original curves, (b) shifting a segment of the higher steam level curve to form a new pinch, (c) minimising the lower steam level between the new boundaries.

By doing this, the flowrate of the lower level is reduced at no cost to the higher level. This procedure must be repeated over all the lower temperature intervals. Once this is

done, the designer can use these flowrates to specify the size of the boilers, or relax them as needed.

4. HEN Layout

Having targeted the various steam flowrates, the focus is turned to synthesizing the HEN that corresponds to these flowrates, with each steam level requiring its own network. Since both sensible and latent heat is being utilized, the networks will have two distinct regions, as seen in Fig. 3. The set of heat exchanges utilizing latent heat are arranged in parallel. After that, the condensate is passed to the heat exchangers utilizing sensible heat, where series and reuse connections may be required to maintain the flowrate whilst meeting the constraints.

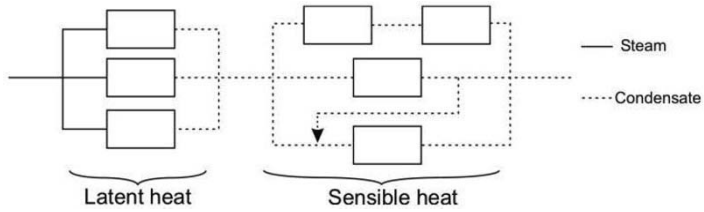

Figure 3: The two regions of a typical HEN for minimum flowrate.

Several mathematical modeling methods exist which can be used to design the layout of the sensible heat region. In this work, an adaptation of the "water mains" method developed by Kim and Smith (2001) is used.

5. Illustrative Example

An illustrative example is presented to demonstrate the targeting and synthesis procedure and to highlight its benefits. A grassroots design must be created for the hot utility system using multiple steam levels. Table 1 gives the limiting minimum supply and target temperatures of a hot utility, based on the supply and target temperatures of 11 cold process streams. A ΔT_{min} of 10 °C was applied to the data. A boiler produces superheated steam at 200 °C, part of which will be used to run a small turbine and the remainder throttled to saturation conditions to heat the process streams. A stream of saturated exhaust steam is produced at 130 °C with a flowrate of 42.2 tons per hour, which acts as a second steam level. Steam tables were used for the thermophysical properties of the water and steam.

The heating network was designed using the conventional design procedures and also using the technique outlined above. In the conventional design, 142.7 ton/h of steam was required. In the new design, only 108.4 ton/h of steam was required, and no cooling water. The minimum steam flowrate obtained using the new technique was confirmed to be the minimum by comparing it to the results obtained using the Mixed Integer Linear Program developed by Price and Majozi (2010). This represents a 24% reduction in steam flowrate. Furthermore cost estimates were used to compare the increase in cost due to additional heat exchangers versus the decrease due to a smaller boiler. The reduction in the steam flowrate resulted in a 57% increase in the heat exchanger costs and a 31% decrease in the boiler cost, giving a total cost reduction of 13%.

Table 1: Limiting hot utility temperatures and duties

Stream	1	2	3	4	5	6	7	8	9	10	11
Supply temp (°C)	106	174	164	142	102	76	106	154	78	194	142
Target temp (°C)	64	174	135	89	71	76	53	30	35	106	64
Duty (kW)	414	15610	5811	912	358	12923	4312	14239	941	13980	3585

6. Conclusion

A graphical method has been presented for targeting the steam flowrate and designing the HEN in the presence of multiple steam levels. Designing a HEN for minimum steam flowrate by reusing hot condensate has a number of advantages. In an existing plant, the technique can be used to debottleneck the boiler and avail steam for use in increased production rates. With a grassroots design, application of this new method can reduce the capital cost of the steam system and allow for a smaller and more efficient boiler to be purchased.

An example is presented to illustrate the use of the new synthesis method, as well as to demonstrate its advantages. A process with 11 cold streams that required heating is used. A boiler supplied steam for heating, as well as to a power generation turbine. By comparing the new design with the traditional design, it was shown that the flowrate of steam could be reduced by 24%, which reduced the capital cost of the network by 13%. The results of the graphical technique were compared with a mathematical programming technique in the open literature, and were found to be accurate. It is concluded that the new synthesis procedure has significant economic benefits.

References

MA Bernier, 1994, Cooling tower performance, *ASHRAE Trans:Reshearch*, 100, 114-121.

WAS Coetzee, T Majozi, 2008, Steam system network synthesis using process integration, *Industrial and Engineering Chemistry Research*, 46(13), 4405-4413.

JK Kim , R Smith, 2001 Cooling water system design, *Chemical Engineering Science*, 56(12), 3641-3658.

B Linnhoff, JR Flower, 1978, Synthesis of heat exchanger networks, *AIChE Journal*, 24(4), 633-654.

B Linnhoff, E Hindmarsh, 1983, The pinch design method for heat exchanger networks, *Chemical Engineering Science*, 38(5), 745-763.

T Majozi, T Price, 2010, On synthesis and Optimization of Steam system networks 1: Sustained boiler efficiency, *Industrial and Engineering Chemistry Research*, 49, 9143-9153.

T Price, T Majozi, 2010, On synthesis and Optimization of Steam system networks 2: Multiple steam levels, *Industrial and Engineering Chemistry Research*, 49, 9154-9164.

T Price, T Majozi, 2010, On synthesis and Optimization of Steam system networks 3: Pressure drop consideration, *Industrial and Engineering Chemistry Research*, 49, 9165-9174.

R Sinnott, G Towler, 2009, *Coulson & Richardson's Chemical Engineering Design,* UK, Butterworth-Heinemann.

I.A. Karimi and Rajagopalan Srinivasan (Editors), Proceedings of the 11th International Symposium on Process Systems Engineering, 15-19 July 2012, Singapore.

Modeling the dissolution of carbonate minerals utilized in Flue Gas Desulfurization scrubbers. A stepwise titration technique applied to low Grashof-Reynolds ratio.

Cataldo De Blasio[a], Claudio Carletti[b], Kurt Lundqvist[b], Loay Saeed[a], Tapio Westerlund[b], Carl-Johan Fogelholm[a].

[a]*Department of Energy Technology, Aalto University, P.O. Box 17800 FI-00076 Aalto, Finland.*
[b]*Department of Chemical Engineering, Åbo Akademi University, Biskopsgatan 8, 20500 Turku, Finland.*

Abstract

Every year a significant amount of Sulfur Dioxide (SO_2) is discarded in the atmosphere. SO_2 can cause indirect ozone depletion, it leads to the formation of acidic rains and a large number of diseases are provoked by contact with sulfur dioxide. Limestone ($CaCO_3$) is widely utilized in Flue Gas Desulfurization (FGD) processes because of its ability to capture the sulfur and precipitate as solid gypsum. The correct evaluation of limestone reactivity is a key aspect for FGD wet scrubbing process design and plant operation. In the present study results from tests to a particular group of samples classified as Sedimentary Limestone and Sedimentary Dolomite are reported.

Keywords: Gas Desulfurization, Limestone Reactivity, Mathematical Modeling, Transport Phenomena.

1. Objective

The sedimentary rocks in our possession are numerous and from different regions of the world, the project aims to classify and evaluate the reactivity of a large amount of samples with a great suitability for wet Flue Gas Desulfurization. A stepwise titration method and a mathematical model for non-steady state conditions allow the very accurate estimation of limestone's reaction rate constant and mass transfer coefficient. The dynamic conditions of an actual Holding Tank in a FGD wet scrubbing process were simulated by a Batch Stirred Tank Reactor (BSTR), in addition the fluid dynamic conditions for complete re-suspension of the solid particles were accurately evaluated.

2. Modeling

The sedimentary rocks were tested in diluted concentrations of hydrochloric acid in order to simulate the acidic conditions of the actual industrial process. The main reaction steps involved in a Limestone-HCl system are described in literature (S. Kiil *et al.,* 1998) where four stages have been considered with final formation of CO_2 and H_2O. The reaction rate for limestone has been reported as proportional to the H^+ ions activity to the first power for *pH* values less than four (Plummer *et al.,* 1978). The general mass balance (macro) for pseudo first order chemical reaction and related to the dissolving component is expressed in Eq.(1):

$$\frac{dC_a}{dt} = -k_r \cdot C_a + \frac{\langle k_c \rangle \cdot S}{V} \cdot \left(C_{ai} - C_a\right), \tag{1}$$

where C_a is the concentration of the carbonate ions (mol/dm^3), V is the reactor volume (dm^3), S represents the surface of reaction (dm^2), k_r and k_c are respectively the reaction rate constant (1/s) and the mass transfer coefficient (dm/s). Dividing the first and second term of Eq.(1) by the concentration value at saturation C_{ai}, it is possible to use a convenient non-dimensional form for the concentration, C_a^*. With the substitution $\tau = V/(\langle kc \rangle \cdot S)$ after integration over the time and C_a^*, the general solution becomes:

$$C_a^* = -\frac{\left(-1+e^{(-k_r - 1/\tau)\,t}\right)}{\tau\left(k_r + 1/\tau\right)}. \tag{2}$$

The first order chemical kinetic describes accurately the dissolution of limestone (Fig. 2) while dolomite dissolution is well modelled by a first order model only for the first period of the titration steps (Fig. 3, left). A second order model, where the term $(C_a^*)^2$ is used as the multiplier for k_r instead of C_a^* in Eq.(1), approximates the dissolution of dolomite for the entire duration of the titrations (Fig. 3, right). The analytical solution for the second order model is reported as follows:

$$C_a^* = \frac{-B+\sqrt{B}\sqrt{4k_r+B}\,Tanh\left[\frac{1}{2}\left(\sqrt{B}\sqrt{4k_r+B}\,t+2\,ArcTanh\left[\frac{\sqrt{B}}{\sqrt{4k_r+B}}\right]\right)\right]}{2k_r}, \tag{3}$$

where $B = 1/\tau$. In order to estimate the re-suspension of all solid particles belonging to a determinate Particle Size Distribution (PSD), a relation between non-dimensional numbers, Eq.5, is obtained by combining a balance of forces at incipient lift of the particles with the friction velocity as follows (O. Molerus, 1987):

$$\frac{\pi d_p^2}{4}\tau_w = (\rho_s - \rho_F)\frac{\pi d_p^3}{6} g \quad \longleftarrow \quad u_\tau = \sqrt{\frac{\tau_w}{\rho_F}}, \tag{4}$$

in the equations above, d_p is the mean particle's diameter, ρ_s and ρ_F the particle's and the fluid mass density (kg/m^3), g the gravity acceleration (m/s^2) and τ_w the wall shear stress (N m^{-2}). Eqs.4 lead to:

$$\mathrm{Re}_\tau^2 = \left(\frac{d_p u_\tau}{\nu}\right)^2 = \frac{2}{3}\frac{d_p^3 \cdot g}{\nu}\frac{\rho_s - \rho_F}{\rho_F} = \frac{2}{3}Ar, \tag{5}$$

where Re is the Reynolds number, Ar is the Archimedes number, ν is the kinematic viscosity (m^2/s) of the fluid and u_τ is the shear stress velocity (m/s) evaluated by:

$$u_\tau = 0.182\frac{\nu^{0.1} u_\infty^{0.9}}{D^{0.1}}; \tag{6}$$

D is the diameter of the vessel, and u_∞ is defined as the reference velocity evaluated at a distance "large enough" from the center of the vessel. The reference velocity is evaluated as $u_\infty = KD_s\omega$, where D_s is the stirrer diameter, ω is the angular velocity (s^{-1}) and K is a non-dimensional constant which is a function of the system's geometry. The method described above demonstrate that the particles in our experiments were completely immersed in the viscous sub-layer since Re_τ is between 0 and 5, for $0.117 < K < 1$; this is in accordance with O. Molerus in (O. Molerus,1987).

3. Materials and methods

3.1. Analyzed samples with compositions

The samples analyzed in the present study are a part of a series of 25 samples coming from different locations of the world. The samples were crushed and ground in three different size fractions (63-106 μm, 106-150 μm and 150-250 μm). Detailed images were obtained by using a Scanning Electron Microscope (SEM). Figure 1 gives a SEM image of one selected sample and the design of the experimental setup. Table 1 shows the description of four samples, their provenience and bulk composition measured with x-ray fluorescence (XRF).

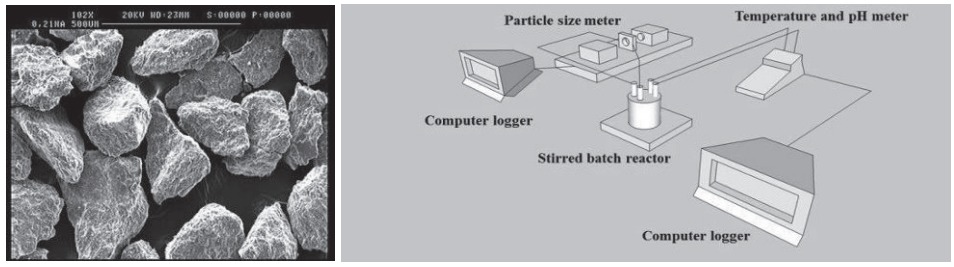

Figure 1. Left: SEM image of Limestone LJJ-27C for the size fraction 150-250 μm. Right: experimental setup.

Table 1. Sample description, provenience, XRF bulk composition for CaO, MgO and SiO_2 (wt%).

Sample	Description/Age	Provenience	CaO %	MgO%	SiO2%
LJJ-27C	Limestone, (416-360Ma)	Röngu, Estonia	53.0	0.52	2.6
LJJ-28C	Dolomite, (416-360 Ma)	Otepää, Estonia	30.8	19.9	1.3
LJJ-29C	Dolomite, (461-444 Ma)	Kore, Estonia	30.8	19.7	1.5
LJJ-30C	Limestone, (444-416 Ma)	Tallin-Tartu, Estonia	52.6	2.5	0.27

3.2. Experimental settings

The experimental set-up consists of a Batch Stirred Tank Reactor (BSTR), a laser diffractometer (Malvern 2600C), a fast electrode *pH* meter with temperature measurement for adjustment (EDT Micro 2) and two computer logger for data collection (Fig. 1, right). The procedure consisted in a step by step titration (J. Ahlbeck *et al.* 1993), a variable amount of particles between 1 – 2.8 g were added to the reactor creating a suspension suitable for particle size distribution measurements.

4. Results and discussion

Following the method described previously the mass transfer rate can be expressed by a parametric function of the constants *kr* and *kc*. The parametric evaluation has been performed for ten titration steps, for each experiment and for all the samples considered by using an implemented software procedure which handles thousands of *pH* values and more than fifty particle's size ranges. The Ca^{2+} concentration over time was evaluated by using *pH* data and the surface of reaction was evaluated considering spherical particles and taking into account the cumulative frequency function obtained from the PSD measurements; the titration stages were performed in sequence for each experiment.

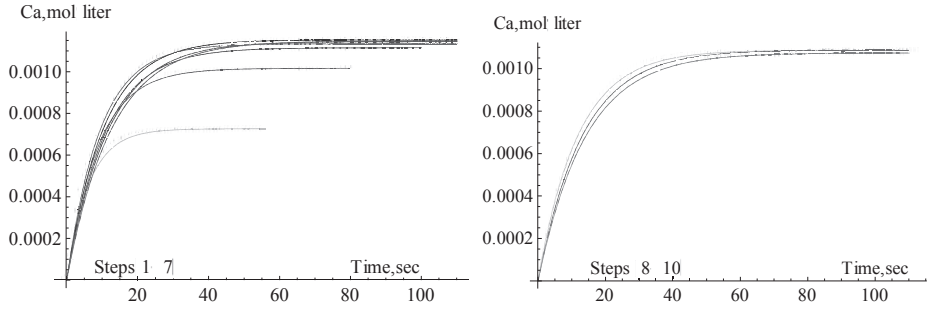

Figure 2. Eq.2 (line) and experimental data (dots) for limestone sample Ljj-27c, titration steps [1-7] (Left) and steps [8-10] (Right).

The following figure shows experimental results concerning the dolomite sample Ljj-28c.

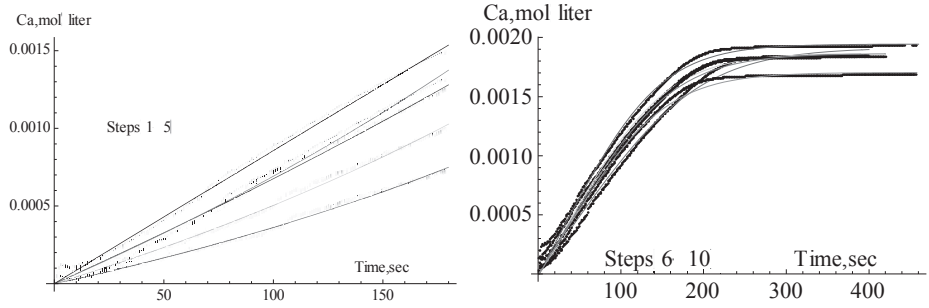

Figure 3. Left: Eq.2 (lines) and experimental data (dots) for dolomite, steps [1-5]. Right: Eq.3 (lines) and experimental data (dots) for dolomite, steps [6-10].

A stabilization of the values for *kr* and *kc* can be observed for both dolomite and limestone, this is in agreement with our expectations since a graining phenomenon can be experimentally observed for the first titration steps and for this reason the surface of reaction is altered, this phenomenon disappears when proceeding with the experiment giving more stable results. The mean reaction rate constant for the sedimentary rocks listed in Table 1 and the particle size distribution versus particle size (μm) for sample Ljj-27c and ten titration steps are reported in the following figure.

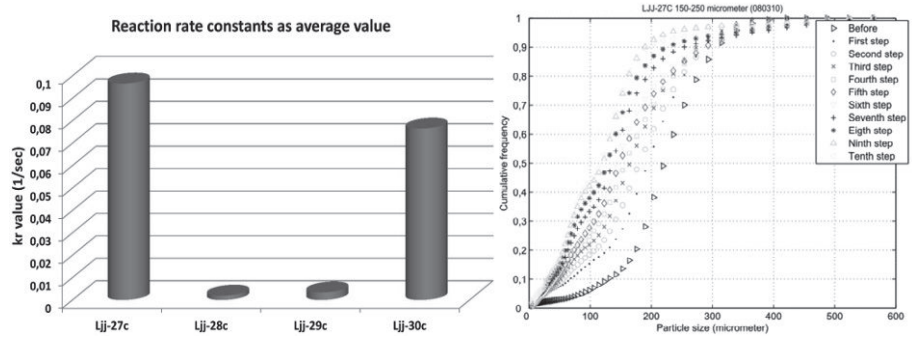

Figure 4. Left: overall reaction rate constants for limestone (Ljj-27,30c) and dolomite (Ljj-28-29c). Right: particle size distribution versus particle size (μm) for LJJ-27C-150-250 μm.

The mean values of the reaction rate constants are evaluated considering a period of three minutes from the titration's start, (Fig.4). In this time range both limestone and dolomite follow a first order model which allows for a suitable comparison of their reactivity. The experimental data related to the limestone samples were fitted by the model (Eq.2) in a really accurate manner (Fig.2). Great difference can be observed between the CaO and MgO content (Tab.1); dolomite is belonging to the Rhombohedral class with a different arrangement for Mg atoms compared to limestone belonging to the Hexagonal Scalenohedral class, hence the different dissolution behavior. The rate of reaction of limestone with hydrochloric acid was much greater than in the case of dolomites in accordance with previous studies (K. Lund *et al.,* 1973). As expected, the reactivity of the dolomite samples was much smaller. Values for the saturation concentration of carbonic ions where taken from literature (Manahan *et al.,* 2005).

5. Conclusions

Since more than one phase is present, the mass transport from phase to phase must be considered in the rate equation (O. Levenspiel, 1999). Thus the rate expression in general will incorporate mass transfer terms in addition to the usual chemical kinetics term, hence the meaning of k_r and k_c. The stepwise titration method allows for a more accurate determination of the above mentioned parameters since more sets of data are obtained for each experiment and for the same sample. The more pure limestone follows a first order model with respect to k_r, while dolomite dissolution is well approximated by a first order model only in the beginning of the titration steps (Fig. 4, left). A second order model, (Fig. 4, right), approximates in a better way the dissolution of dolomite for the entire duration of the titration steps, this is in accordance with previous studies (Chou *et al*., 1989) where is stated that the existence of successive reactions may lead in ideal cases to a reaction order with respect to H^+ of one or two, but not less than one. The obtained values for k_r and k_c for limestone are well in agreement with the case of semi-slow reaction regime (Sharma *et al.*,1984).

6. Acknowledgements

The authors sincerely acknowledge the Laboratory of Energy Engineering and Environmental Protection at Aalto University, the Process Design and Systems Engineering Laboratory and the Department of Geology at Åbo Akademi University in Finland. The CARETECH project under the Akademi of Finland's Sustainable Energy Program (SusEn). M.Sc. Lauri Järvinen is highly acknowledged for his collaboration.

References

S.Kiil, M.L. Michelsen and K. Dam-Johansen. 1998. Ind.Eng.Chem.Res.,37,2792-2806.

Plummer, L.N., Wigley, T.M.L., Parkhurst, D.L., 1978, American Journal of Science, Vol. 278, pp. 179-216.

O. Molerus, 1987, Chem. Eng. Sci. Vol.42, No.6, pp. 1423-1430.

Alhbeck, J., Engman, T., Fältén, S., Vihma, M., 1993, Chemical Engineering Science, Vol. 48, No 20, pp. 3479-3484.

K.Lund, H.S. Fogler, C.C. McCune., 1973. Chem. Eng. Sci, Vol. 28, pp.691-700.

S.E.Manahan, 2005, Environmental Chemistry,8th Edition, Sections 3.7-3.8, CRC Press.

O. Levenspel,1999,Chemical Reaction Engineering,3rd Edition, J.Wiley & Sons.

Chou L., Garrels R. M., and Wollast R., 1989. Comparative study of the kinetics and mechanisms of dissolution of carbonate minerals. Chemical Geology, vol. 78, pp. 269-282.

L. K. Doraiswamy, M.M. Sharma, 1984. Heterogeneous Reactions Analysis Examples and Reactor Design (vol2). United States : John Wiley & Sons. ISBN:0-471-05367-8.

I.A. Karimi and Rajagopalan Srinivasan (Editors), Proceedings of the 11th International Symposium on Process Systems Engineering, 15-19 July 2012, Singapore.

Optimal Multi-Objective Planning of Distributed Biorefinery Systems Involving Economic, Environmental and Social Aspects

José Ezequiel Santibañez-Aguilar,[a] J. Betzabe González-Campos,[a] José María Ponce-Ortega,*[a] Medardo Serna-González[a] and Mahmoud M. El-Halwagi[b,c]

[a]*Universidad Michoacana de San Nicolás de Hidalgo, Morelia 58060, México*
[b]*Texas A&M University, College Station 77843, USA*
[c] *Adjunt faculty at the King Abdulaziz University, Jeddah, Saudi Arabia*

Abstract

This work presents a multi-objective optimization model based on a mathematical programming formulation for the optimal planning of distributed biomass conversion systems. The model considers the optimal selection of feedstocks, processing technologies and products while considering a time horizon. The multi-objective optimization problem simultaneously considers the profit maximization, the environmental impact minimization, as well as the maximization of the social impact benefit through the generation of jobs in rural areas. The economic objective function takes into account the availability of bioresources, processing limits and demand of products, as well as the cost of feedstocks, products and processing routes. The environmental impact is measured through the eco-indicator-99 based on the life cycle analysis methodology. The social impact is measured through the number of jobs generated. This formulation considers the variation of parameters over time. For instance, time-based profiles for raw-material availability and product demand are considered. Although the economic and environmental objectives may contradict each other with an influence on the social impact, by means of the proposed methodology is possible to obtain a set of Pareto curves that identify the set of optimal solutions for each objective. Each Pareto curve shows the compromise between the objectives and enables a better decision about the processing of biomass. The proposed methodology is applied to a case study for planning the production of a biorefinery system in Mexico, where several scenarios that compensate the economic, social and environmental objectives are identified.

Keywords: Biorefineries, Biofuel Supply Chain, Biomass, Environmental Impact, Social Impact, Sustainable Process.

1. Introduction

Nowadays the increasing demand of energy around the world has incremented the demand of petroleum to be used as fuel, increasing its cost and, at the same time, decreasing the proved reserves; consequently, its currently use as fuel will not be feasible in the future. In addition, petroleum fuels have drastically deteriorated the global environment through the huge greenhouse gas emissions (GHGE).This has promoted the research for renewable energy sources to satisfy economically, environmentally and socially efficiently the energy demanded around the world. In this context, biomass as feedstock for energy production has gained great attention because

*jmponce@umich.mx

it has interesting characteristics including: 1) Renewable resource –to guarantee a sustainable production; 2) Significant reduction in the life cycle of GHGE –to guarantee the sustainability for the environment; 3) Competitive costs –to compete with the use of petroleum; 4) Huge abundance in the planet –to guarantee the generation of jobs in marginal areas; and 5) Flexibility to produce a lot of products. In addition, because the flexibility of the biomass to produce several products (biofuels, polymers, specialty chemicals, etc.), the biorefineries have gain a lot of attention. A biorefinery is an industrial facility similar to the petroleum-based refinery, but this uses biomass as feedstock instead of petroleum.

Recently, several papers have been reported for the optimization of supply chain for biofuels production (see, for examples, Aksoy et al., 2008; Sammons et al., 2007; Bowling et al., 2011; Santibañez-Aguilar et al., 2011). However, these methodologies include some drawbacks: a) they have not considered the variation of the availability of the feedstock year-round (a very important fact in countries where the weather drastically changes through the year); b) the interaction between the economic, environmental and social impacts have not been taken into account; and c) the simultaneous consideration for the economies of scales has not been properly considered. Therefore, to overcome these drawbacks, this paper proposes a new multi-objective optimization approach for the optimal planning of a biorefinery system considering the seasonality variation for the feedstock availabilities and product demands as well as the economic, environmental and social objectives. The economic objective considers the total net profit associated to the biorefinery based on a distributed system and considering the economies of scale, while the environmental impact includes the global impact measured through the eco-indicator99 based on the life cycle assessment, this methodology is damage oriented and considers the impacts to the human health, the ecosystem and the resources, and finally the social impact is measured through the jobs generated for the implementation of the biorefinery supply chain.

2. Problem Statement

Figure 1 shows schematically the problem addressed in this paper, which is described as follows. Given are: A set of available bioresources in specific places with given characteristics. It should be noted that the amount available for each bioresource depends on the season of the year and the location. Each bioresource has associated a unit cost, as well as unit environmental and social impacts. Also, there is a set of places where the bioresources can be stored. This work considers a set of processing plants to produce several products through different technologies from several bioresources, these technologies have given conversion factors and unit costs, as well as unit environmental and social impacts. Furthermore, there is a set of storages for products, a set of consumers located in different places with given demands through the year and a set of transportation methods. The objective is to determine the optimal configuration for the planning system that considers the seasonality and simultaneously compensates the economic, environmental and social objectives, identifying the used bioresources, location for production for each season of the year, the products produced as well as the consumers; and the transportation and storage requirements. To account for the economies of scale the formulation presented considers a distributed systems that includes central and hubs processing facilities.

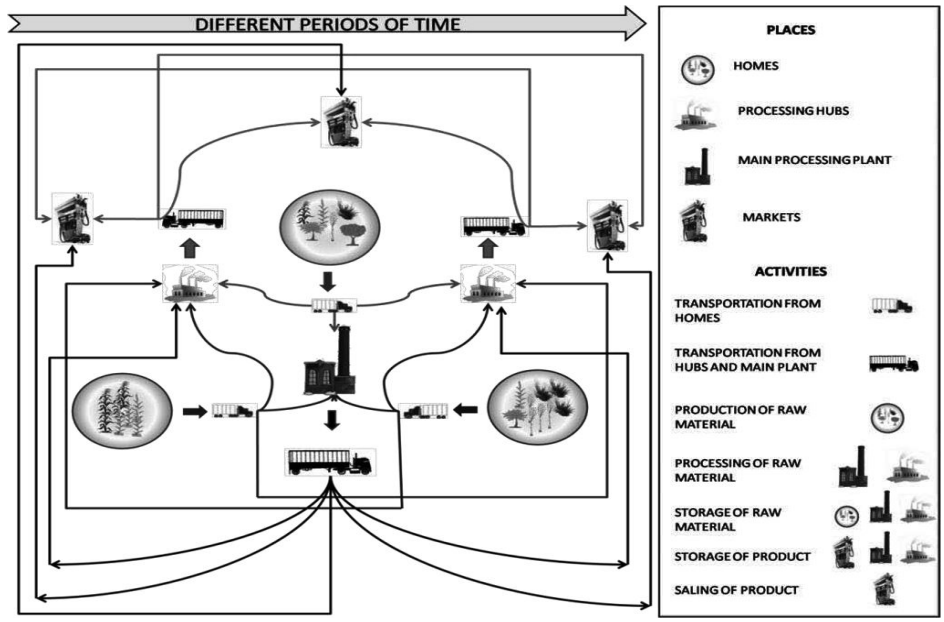

Figure 1. Representation of the addressed problem.

3. Model Formulation

The model is based on a state-task network representation for distributed systems, where the states are represented by the materials in the different places. In this approach, each state such as feedstock in home, feedstock in processing facilities, product in hubs and product in markets is different each other (i.e., each material depends on the location). On the other hand, the tasks are the different activities that consume a given time and divide the states (i.e., sugar cane after harvesting is transported to produce sugar cane in processing plant). Each activity has a binary variable associated because they are time depended; in addition, each activity has associated different economic, environmental and social impact. This way, the model considers mass balances in the homes for the feedstock, mass balances in the hubs, and in the main plants for the feedstock and products, mass balances in the storage, relationships for transportation and processing, and availability constraints. The economic objective function consists in the maximization of the net profit, taking into account the income for the sale of products minus the cost for the processing, transportation, storage and production of raw materials. This economic objective function is stated as follows:

Net Profit=Profit for Sales-Cost for [Processing Hubs+Processing Centralizers+Storage raw materials+Storage product-Transportation raw materials+Transportation product+Raw material production]

Also, there is an environmental objective function that incorporates the environmental impact through the eco-indicator99 considering the life cycle assessment. This function considers the eco-indicator99 for the raw material production, processing, transportation and use of products. This is stated as follows:

Environmental Impact =Eco-indicator for use of products+Eco-indicator for production of raw materials+Eco-indicator for processing in central and hub facilities+Eco-indicator for transportation

Furthermore, the model presented takes into account the social impact through the number of jobs generated for the raw material production, transportation and processing (notice that additional social impacts like the competitive use of bioresources can be included). This objective is difficult to consider because the jobs produced do not impact in the same form; for instance, the jobs generated in the field are different of the jobs for the transportation. However, this objective is very important because it gives a different vision for the biorefinery production. This social objective function is stated as follow:

Social Impact =Jobs production of raw materials+Jobs processing in central and hub facilities+Jobs transportation

To solve properly this problem and to generate a set of Pareto solutions that compensate these objectives, the e-constraint method is implemented. This way the problem is solved for the maximization the net profit for given constraints for the environmental impact and satisfying given requirements for the number of jobs generated.

4. Case Study

To test the proposed approach, a case study for the biofuels production in Mexico is presented. The data for this case were taken from the reports of the Mexican Agriculture Commission accounting for the seasonal variability and dividing the country in 6 regions. The example considers 9 bioresources available in Mexico, 2 products (bioethanol and biodiesel) and several technologies. The economic and environmental data were taken from Santibañez-Aguilar et al. (2011). This example was solved using different constraints for the objectives considered and the Pareto curves are shown in **Figure 2**. The curves represent the set of Pareto solutions for different cases, the upper is the curve without penalty and others have a penalty for the unsatisfied demand. Notice in this figure the interesting relationships between the profit and the environmental impact: for low environmental impact the associated profit is small, whereas for moderate environmental impact the associated profit is high. It is noteworthy that for high environmental impact the associated net profit does not increase significantly. In addition, for this case study, the higher the number of jobs, the higher the environmental impact; also, the number of jobs increases when the net profit increases. These interesting relationships between these contradict objectives allow the decision makers to choose the solution that shows the best compromise between them. It is noteworthy that each point of the Pareto curve represents different bioresources used and product produced in different places and considering the season of the year; for the case that maximizes the profit without considering the environmental and social impacts the main raw materials used are wood chips, african palm and jatropha; whereas for the case where the environmental impact become important the raw materials used are sorghum and sugar cane, with a little amount of wood chips, african palm and jatropha. Finally, the season of the year is very important in the example presented because the used raw materials change drastically through the year, for example the main raw material used in January is sorghum whereas in July it is sugar cane. Each point on the Pareto curves have different value of environmental and economic impacts as well as number of jobs, that is because the selection of different raw materials and places on the time horizon. For example, the number of jobs for point A is 2686, where

these jobs are mainly for the production of raw materials (sugar cane and sorghum), this point A also shows a moderate environmental impact with a huge annual profit.

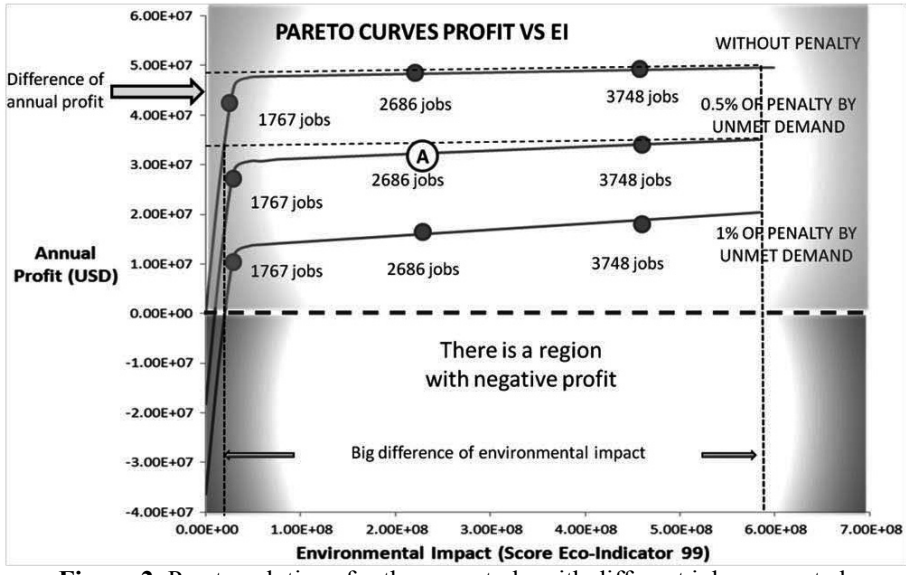

Figure 2. Pareto solutions for the case study with different jobs generated.

5. Conclusions

This paper proposes a new optimization model for the supply chain optimization of biorefinery systems. The proposed approach simultaneously considers the economic, environmental and social objectives; in addition, it allows to take into account the seasonal dependence for the feedstock as well as the economies of scale considering the installation of a distributed systems that includes preprocessing hubs and central facilities. The application of the proposed approach to a case study from Mexico, allows to identify the interaction between these contradict objectives, and gives the opportunity to the decision maker to choose the solution that best satisfy the specific requirements. Finally, the proposed approach is useful to identify the governmental incentives required to yield a given social benefit though the jobs generated in given marginal places.

References

B. Aksoy, H.T. Cullinan, Jr.N.E. Sammons, R.M. Eden, 2008. Identification of optimal poultry litter biorefinery location in Alabama through minimization of feedstock transportation cost. Environmental Progress, 27(4), 515-523.

I.M. Bowling, J.M. Ponce-Ortega, M.M. El-Halwagi, 2011. Facility location and supply chain optimization for a biorefinery. Industrial and Engineering Chemistry Research, 50(10), 6276-6286.

Jr.N. Sammons, R.M. Eden, W. Yuan, H. Cullinan, B. Aksoy. 2007. A flexible framework for optimal biorefinery product allocation. Environmental Progress, 26(4), 349-354.

J.E. Santibañez-Aguila, J.B. González-Campos, J.M. Ponce-Ortega, M. Serna-González, M.M. El-Halwagi, 2011. Industrial and Engineering Chemistry Research, 50 (14), 8558-8570.

F. You, L. Tao, D.J.Graziano, S. W. Snyder, 2011. Optimal design of sustainable cellulosic biofuel supply chains: Multiobjective optimization coupled with life cycle assessment and input–output analysis. AIChE Journal, In press, DOI: 10.1002/aic.12637.

I.A. Karimi and Rajagopalan Srinivasan (Editors), Proceedings of the 11th International Symposium on Process Systems Engineering, 15-19 July 2012, Singapore.

Bi-objective MINLP optimization of an industrial water network via benchmarking

Hella Tokos,[a] Zorka Novak Pintarič,[b] Yongrong Yang[a]

[a] *State Key Laboratory of Chemical Engineering, Department of Chemical and Biochemical Engineering, Zhejiang University, Hangzhou, 310027, P.R. China*
[b] *University of Maribor, Faculty of Chemistry and Chemical Engineering, Smetanova 17, SI–2000 Maribor, Slovenia*

Abstract

This paper presents an approach to water system retrofitting by estimating both the economic and environmental impacts of the water network design using bi-objective optimization. The environmental impact is evaluated via benchmarking. By using benchmarking, the decision maker could obtain insight not only into the environmental impact of a certain design belonging to the Pareto optimal solutions, but also into the competitiveness of the design within a particular production sector. The economic criterion used is the total cost of the water network and involves the freshwater cost, annual investment costs of the storage tank, piping and local treatment unit installation, and wastewater treatment cost. This approach uses a mixed-integer nonlinear programming (MINLP) model that enables water re-use and regeneration re-use in batch and semi-continuous processes. The Pareto front is generated using the Normal-Boundary Intersection (NBI) method. The proposed approach can be used for the separate integration of production sections, but also for joint integration of the sections via temporal decomposition. The proposed approach was applied to an industrial case study in a brewery.

Keywords: bi-objective; retrofit; economic criteria; environmental impact; MINLP.

1. Introduction

Due to increasing awareness about the effects of industrial activities on the environment, along with an ever more demanding legal enforcement, it has become necessary to take into consideration both, the economic and environmental impacts of production sites. Typically, traditional process design and optimization are based on economic objectives, such as capital investment, net present value (NPV), operating cost, and payback period. Water network synthesis is used to minimize the flow rate and cost of freshwater in the water supply systems of industrial plants, by maximizing water reuse and regeneration re-use. Two main approaches are generally used for addressing the issue of freshwater demand minimization within total water networks, i.e. the graphical approach (Liu et al., 2009; Ng and Foo, 2009), and the mathematically-based optimization approach (Li et al., 2010; Tan et al., 2008). The environmental aspect of water networks has recently become more important in water network synthesis, in order to enhance their environmental performances. Process flow diagram (PFD)-based life cycle assessment (LCA) (Lim and Park, 2007), and sustainable process index (Ku-Pineda and Tan, 2006) have been employed to evaluate the environmental impacts of water networks. Also, multi-objective optimization has been studied in order to minimize the total annualized cost and environmental impacts (Erol and Thöming, 2005). A streamlined mathematical

optimization model has been proposed for practically synthesizing an environmentally-friendly water network, by Lim and Park (2008).
In this paper, a bi-objective optimization method is presented that uses the environmental sustainability index to evaluate the environmental impacts of the obtained water networks, and the total annual water network cost as the economic criterion. The proposed approach is used for separate and joint integration of the production sections within a brewery via temporal decomposition.

2. Benchmarking in bi-objective optimization

A given set of indicators provides no information on a company's progress towards sustainable development in relation to other companies within the sector, unless a reference value, such as a benchmark is assigned to each indicator. According to this, the decision maker who uses benchmarking would gain insight, not only into the environmental impact of certain design from the set of Pareto optimal solutions but also into the competitiveness of the design compared to other companies within the production sector. In bi-objective optimization of a water network, the environmental sustainability index is used as the first objective function, with the total cost of the water network as the second objective function. The proposed environmental sustainability index is calculated over four steps:

1) Defining the indicators and benchmarks: The selection of a suitable set of indicators should always be performed in close cooperation with the industry, using for example Global Reporting Initiative (GRI) guidelines. The benchmark values of the selected indicators should be determined based on the values of the best available techniques (BAT), measurements and standards within the company, local legal regulations, GRI reports for specific production sectors, and other relevant documents.
2) Judging the importance of indicators and their normalization: Normalization is necessary for integrating the selected indicators into a composite index, as they are usually expressed in different units. Regarding their influence on the sustainable development, the indicators are divided before normalization into the group of indicators, the increasing values of which have a positive impact on sustainable development (I^+), e.g. water re-use, and those indicators the increasing values of which have negative impact (I^-), e.g. toxic releases into water. When applying distance to a reference method the normalized value is calculated as a ratio between the indicator and the benchmark:

$$I_{N_i}^{+} = \frac{I_i^{+}}{I_i^{Benchmark}} \qquad \forall i \in I \tag{1}$$

$$I_{N_i}^{-} = \frac{I_i^{Benchmark}}{I_i^{-}} \qquad \forall i \in I \tag{2}$$

3) Determination of the indicator weights: The budget allocation process was used to determine the indicator weights. This method calculates the indicator weights based on expert opinion. In order to establish a proper weighting system, it is essential to bring together experts representing a wide spectrum of knowledge and experience, e.g. experts from different production sectors and management within the company.
4) Aggregation of the indicators into the environmental sustainability index: The environmental sustainability index, I_{ES}, is determined by linear aggregation, which is based on summation of weighted and normalized individual indicators:

$$I_{ES} = \sum_i I_{N_i}^{+} \cdot w_i + \sum_i I_{N_i}^{-} \cdot w_i \qquad \sum_i w_i = 1,\ w_i \geq 0 \tag{3}$$

The applied mixed-integer nonlinear programming (MINLP) model is given in Tokos and Pintarič (2009) and enables water re-use and regeneration re-use in batch and semi-continuous processes for known and fixed operating schedules. The Pareto front is generated using the NBI method. This method solves a bi-objective optimization problem by constructing sub-problems with an aggregated objective function using the solution obtained in the previous sub-problem. The proposed approach can be used for the separate integration of water networks within each production section, and for joint integration of water networks within several sections via temporal decomposition. The joint integration is performed in two steps: firstly, both strategies perform simultaneous retrofit of the integrated water system for each working day by identifying the daily water re-use and regeneration re-use connections among water consumers within all sections. At the second step of the first strategy, the design of integrated water system is performed over the entire working week for each section by fixing the identified daily matches between sections. In the second strategy, the freshwater upper and wastewater lower bounds of the integrated processes are modified, and retrofit performed for each production section over the entire working week. More detail about the decomposition method can be found in Tokos et al. (2012).

3. Case study

The described bi-objective optimization strategy was applied to a brewery case study. The environmental sustainability index used as the environmental objective function consisted of five indicators: volume ratio of freshwater consumed to beer production, volume ratio of wastewater discharged from production to beer produced, indirect emission of CO_2 by electricity generation per volume of beer produced, indirect emission of CO by electricity generation per volume of beer produced, indirect emission of NO_x by electricity generation per volume of beer produced (the emissions were calculated based on the electricity needed for pumping water from the wells to/within the production site). The benchmarks for the selected indicators were 3.7 m^3/m^3, 2.89 m^3/m^3, 2.05 kg/m^3, 0.019 kg/m^3 and 0.0067 kg/m^3, respectively. The indicators' weights determined by the budget allocation method were 0.63 for freshwater consumption, 0.1 for wastewater discharge and 0.09 for greenhouse gas emissions. The economic criterion used was the total cost of the water network.

3.1. Separate integrations of the production and the packaging sections

The optimal water network for the weekly schedule in the packaging area at an increasing weight of the environmental criterion would include: wastewater re-use between the can rinser and the pasteurization process, water re-use between the rinser for non-returnable glass bottles and the washer for returnable glass bottles, wastewater re-use from the pasteurization process to the washer for returnable glass bottles, wastewater re-use from the washer for returnable bottles and the crate washer, and water re-use between the rinser for non-returnable glass bottles and the crate washer. Several water networks exist with the same sustainability index but different total costs because in the model formulation, the water consumptions of the operations can vary between the lower and upper bounds. The weekly freshwater consumption could be reduced from 2,233 t to 1,493 t. The environmental sustainability index improved from 0.911 to 0.952. The total annual network cost was between 223,162 €/a (at the environmental criterion weight of 0), and 514,833 €/a (at the environmental criterion weight of 1).

The optimal water network for the weekly schedule in the production area at an increasing weight of environmental criterion would include: re-use of wastewater from filtration as water for pouring the batch material in the cellar or in the brewhouse, regeneration re-use of wastewater from pouring operation in CIP systems. The wastewater purification is carried out by nanofiltration technology. The weekly freshwater consumption could be reduced from 2,592 t to 1,861 t. The environmental sustainability index improved from 0.829 to 0.928. The total annual network cost is between 334,804 €/a (at the environmental criterion weight of 0), and 1,072,521 €/a (at the environmental criterion weight of 1). In case of the highest total annual network cost both batch and semi-continuous local treatment units are included in the water network.
The environmental sustainability index of all networks in the packaging and production sections is lower than 1. This problem can be solved by investing in new technologies with lower freshwater consumption. For example, new washers for returnable glass bottles have lower freshwater consumption, and/or the tunnel pasteurizers could be replaced by flash pasteurizers. Another possibility is joint integration of the production and packaging sections.
The size of the MINLP model was approximately 6,600 constraints, 3,300 continuous variables, and 1,500 binary variables in the case of the packaging area, and approximately 21,500 constraints, 10,500 continuous variables, and 4,600 binary variables for the production area. The model was solved by the GAMS/DICOPT solver using 218 seconds of CPU time at the PC (P4, 2.6 GHz and 512 MB RAM) in the case of the packaging area, and 3,884 seconds in the case of the production area.

3.2. *Joint integration of production and packaging sections*

In the first step of joint integration, the water networks of the production and the packaging sections are simultaneously integrated for each working day by identifying the daily water re-use and regeneration re-use options. By changing the weight coefficient of the environmental criterion between 0.0 and 0.6, one connection is identifiable between the sections, i.e. wastewater from pasteurization in the packaging area is re-used as pouring water for batch material in the brewhouse. A storage tank would be needed for wastewater re-use between the sections. The capacity of the storage tank would be 105 t. Two connections between the sections can be found at higher weight coefficients (0.8 and 1.0): re-use of wastewater from pasteurization in the packaging area as pouring water for batch material in the brewhouse and the cellar. The required storage tank capacity is 210 t.
Two analyses are performed during the second step. A water re-use connection between pasteurization in the packaging area and batch material pouring in brewhouse is fixed in the first evaluation. The optimal water network in the production and the packaging areas contains water re-use and regeneration re-use options as in the case of separated integration. The weekly freshwater consumption could be reduced from 4,725 t to 2,882 t. The environmental sustainability index improved from 0.993 to 1.093. The total annual network cost is between 560,434 €/a (at the environmental criterion weight of 0), and 3,428,927 €/a (at the environmental criterion weight of 1).
Both of the identified connections are fixed in the second evaluation. The optimal water networks include the same connections as in case of separated integration of the production sections. The weekly freshwater consumption could be reduced from 4,725 t to 2,847 t. The environmental sustainability index increases from 1.013 to 1.106. The total annual network cost is between 739,887 €/a, and 4,911,839 €/a.
According to the results, the environmental sustainability index is slightly higher than 1, except in the optimal water network obtained by fixing only one connection at the

environmental criterion weight equal to 0. This means that the company can perform better than the assigned benchmarks by applying one of the obtained optimal water networks.

The size of the MINLP model was up to 16,900 constraints, 8,300 continuous variables and 3,800 binary variables in the case of the first step and the model was solved by the GAMS/DICOPT solver using up to 2,245 seconds of CPU time at the PC (P4, 2.6 GHz and 512 MB RAM). In the case of the second step the model had up to 39,000 constraints, 18,600 continuous variables, and 8,400 binary variables, which were solved using up to 10,907 seconds of CPU time.

4. Conclusion

This paper presented the bi-objective optimization method for retrofitting total water networks, which evaluates the economic and environmental impacts of a water network. The environmental impact is evaluated via benchmarking. The economic criterion used is the total cost of the water network. The approach uses a mixed-integer nonlinear programming (MINLP) model which enables water re-use and regeneration re-use in batch and semi-continuous processes. The Pareto front is generated using the NBI method. The proposed approach was applied to an industrial case study in a brewery. The results obtained show that the benchmark cannot be reached by the individual integrations of two sections, and investment in new technologies with lower freshwater consumption would be needed. The environmental sustainability index rose to slightly above 1 by integrating water networks of the production and the packaging sections, which means that the brewery can achieve better performance than its competitors by using the results of process integration.

References

P. Erol, J. Thöming, 2005, ECO-design of reuse and recycling networks by multi-objective optimization, Journal of Cleaner Production, 13, 15, 1492–1503.

GAMS Beta 22.4. The Solver Manuals. Washington: GAMS Development Corporation. 2007.

V. Ku-Pineda, R. R. Tan, 2006, Environmental performance optimization using process water integration and Sustainable Process Index, Journal of Cleaner Production, 14, 18, 1586–1592.

L-J. Li, R-J. Zhou, H-G. Dong, 2010, State-Time-Space Superstructure-Based MINLP Formulation for Batch Water-Allocation Network Design, Industrial & Engineering Chemistry Research, 49, 1, 236–251.

S-R. Lim, J. M. Park, 2007, Environmental and economic analysis of a water network system using LCA and LCC, AIChE Journal, 53, 12, 3253–3262.

S-R. Lim, J. M. Park, 2008, Synthesis of an environmentally friendly water network system, Industrial & Engineering Chemistry Research, 47, 6, 1988–1994.

Z-Y. Liu, Y-M. Li, Z-H. Liu, Y-J. Wang, 2009, A Simple Method for Design of Water-Using Networks with Multiple Contaminants Involving Regeneration Reuse, AIChE Jounal, 55, 6, 1628–1633.

D. K. S. Ng, D. C. Y. Foo, 2009, Automated Targeting Technique for Single-Impurity Resource Conservation Networks–Part 1 and 2, Industrial & Engineering Chemistry Research, 48, 16, 7637–7661.

R. R. Tan, K. J. Col-long, D. C. Y. Foo, S. Hul, D. K. S. Ng, 2008, A methodology for the design of efficient resource conservation networks using adaptive swarm intelligence, Journal of Cleaner Production, 16, 7, 822–832.

H. Tokos, Z. Novak Pintarič, 2009, Synthesis of batch water network for a brewery plant, Journal of Cleaner Production, 17, 16, 1465–1479.

H. Tokos, Z. Novak Pintarič, Y. Yang, Z. Kravanja, 2012, Multilevel strategies for the retrofit of large-scale industrial water system: a brewery case study, AIChE Journal, 58, 3, 884–898.

I.A. Karimi and Rajagopalan Srinivasan (Editors), Proceedings of the 11th International Symposium on Process Systems Engineering, 15-19 July 2012, Singapore.

A Graphical Approach to Optimal Source-Sink Matching in Carbon Capture and Storage Systems with Reservoir Capacity and Injection Rate Constraints

Raymond R. Tan[a], Raymond Ooi[b], Dominic C. Y. Foo[b], Denny K. S. Ng[b], Kathleen B. Aviso[a], Santanu Bandyopadhyay[c]

[a]*Chemical Engineering Department, De La Salle University, 2401 Taft Avenue, 1004 Manila, Philippines*
[b]*Department of Chemical & Environmental Engineering/Centre of Excellence for Green Technolgies, The University of Nottingham, University of Nottingham, Malaysia, Selangor 43500, Malaysia*
[c]*Department of Energy Science and Engineering, Indian Institute of Technology, Bombay, Powai, Mumbai 400076, India*

Abstract

Carbon capture and storage (CCS) is regarded as an important interim technology for the reduction of carbon dioxide (CO_2) emissions from large industrial facilities such as power plants and refineries. CCS involves capture of concentrated CO_2 streams from industrial flue gases, followed by subsequent secure storage in an appropriate natural reservoir. Such reservoirs include various geological formations such as depleted oil or gas wells, inaccessible coal seams and saline aquifers. In practice, such storage sites will have limitations on both CO_2 storage capacity and injection rate, subject to geological characteristics. In this work, a graphical methodology is proposed for optimally matching multiple CO_2 sources and storage sites or sinks within a predefined geographical region. The technique is developed based on analogies with existing graphical pinch analysis approaches for the synthesis of industrial resource conservation networks. A hypothetical case study is shown to illustrate the methodology. In addition, generalized principles for optimal CO_2 source-sink matching based on pinch analysis insights are discussed.

Keywords: Pinch analysis, carbon capture and storage, source-sink matching.

1. Introduction

In addition to strategies involving energy efficiency enhancement and increased use of low-carbon energy sources, CO_2 capture and storage (CCS) is widely considered as an essential technology for mitigating climate change by reducing industrial greenhouse gas emissions. CCS entails capturing relatively pure CO2 streams from point sources through techniques such as flue gas scrubbing, pre-combustion capture through gasification-based combined cycles and oxy-fuel combustion. The CO_2 may then be stored in various reservoirs such as depleted oil wells, inaccessible coal seams, saline aquifers and other geological structures (Davison et al., 2001). Various systems engineering techniques have been proposed for the planning of the deployment of CCS on a large scale, including insight-based analysis (Tan et al., 2009; Shenoy and Shenoy,

2012), rule-based algorithms (Kazmierczak et al., 2009) and mathematical programming models (Turk et al., 1987; Benson and Ogden, 2003; Middleton and Bielicki, 2009; Pekala et al., 2010; Tan et al., 2010; Fimbres Weihs et al., 2011; Tan et al., 2012a; b).

From a systems standpoint, one key problem in planning the deployment of CCS is matching CO_2 sources with the appropriate sinks. This problem is structurally analogous to the synthesis of resource conservation networks (RCNs). The specific graphical procedure used in this work is the material recovery pinch diagram (MRPD) which was developed independently by El-Halwagi et al. (2003) and Prakash and Shenoy (2005) for targeting of maximum material recovery. However, there are various pinch techniques are described in a recent review by Foo (2009) which are equivalent to MRPD, and may thus be used as alternative solution techniques. Such insight-based approaches have been shown to be an effective complement to mathematical programming based strategies, especially for decomposing difficult problems into computationally tractable subproblems. A formal problem statement is given, followed by a description of the methodology and an illustrative case study. Finally, conclusions and prospects for future work are given.

2. Problem Statement

The formal problem statement addressed in this work is as follows:

- The CCS system is assumed to be comprised of m CO_2 sources, n CO_2 sinks, all of which are available at the start of the planning horizon.
- Each CO_2 source i (i = 1, 2, …, m) is characterized by fixed captured CO_2 flowrate that corresponds to the maximum removal from the plant's flue gas. Furthermore, the operating life of each source i is also defined.
- Each CO_2 sink j (j = 1, 2, …, n) is characterized by an upper limit for CO_2 storage capacity; the maximum rate at which CO_2 may be injected into each sink is also given. Both of these characteristics are based on the geological characteristics of the storage site.
- The objective is to determine the minimum amount of unutilized CO_2 storage capacity by matching CO_2 sources and sinks, given these specified temporal and physical constraints.

3. Methodology

The targeting procedure used in this work is based on the MRPD approach (El-Halwagi et al., 2003; Prakash and Shenoy, 2005), and is hereby referred to as the CO_2 capture and storage pinch diagram (CCSPD). As with all pinch-based techniques, it requires that each source and sink be characterized in terms of "quantity" (amount of CO_2 associated with the source or sink, typically measured in megatons or Mt) and "quality" (the reciprocal of the lifespan of the source or sink, measured in 1/year or y^{-1}). The main steps are as follows:

- The sources are first ranked in order of ascending numerical value of their quality indices. Since the quality index is simply the inverse of duration, the CO_2 with the longest lifespan is ranked first, and the rest are listed based on progressively shorter operating lives.
- The "load" for each source is calculated by multiplying the "quantity" and "quality" index. Note that the resulting value is measured in Mt/y, and is thus actually the CO_2 flow rate of the source.

- The *source composite curve* is drawn using the cumulative "quantity" index as the horizontal axis and the "load" index as the vertical axis. Each segment of this composite curve corresponds to one source. The sources are plotted end to end, in the same manner as with graphical summation of vector quantities.
- These three steps are repeated for the sinks, to generate the *sink composite curve*.
- The relative positions of the two composite curves then provide the basis to determine the system target. The source composite curve must be below and to the right of the sink composite curve. If this geometric condition is not met, then the current solution is infeasible. The target may be determined by shifting the source composite curve horizontally to the right, until the condition is just met. As a result, the two composite curves will be tangent to each other at a pinch point (in some instances there may be multiple pinch points). The distance by which the source composite curve was shifted is the minimum unutilized CO_2 storage capacity in Mt.

The procedure is illustrated in the next section with a simple case study.

4. Case Study

In this example, there are four CO_2 sources and two CO_2 sinks with relevant data as shown in Table 1, respectively. Note that the sources generate a combined 800 Mt of CO_2 throughout the entire planning period, while the combined storage capacity of the sinks is 1,000 Mt. Thus, it may seem at first that it will be possible to capture and store all of the CO_2 in the system.

Table 1. Quantity, quality and load indices of CO_2 sinks and sources

Source	Amount of CO_2 (Mt)	1/Lifespan (y^{-1})	CO_2 Flowrate (Mt/y)
1	200	0.025	5
2	300	0.033	10
3	200	0.04	8
4	100	0.05	5
Total	800		
Sinks	Amount of CO_2 (Mt)	1/Lifespan (y^{-1})	CO_2 Flowrate Limit (Mt/y)
1	750	0.02	15
2	250	0.1	25
Total	1,000		

Following the first four steps described in the previous section results in the CCSPD shown in Figure 1. It can be seen that the relative positions of the composite curves indicate that this is an infeasible solution. An optimal solution may be found by shifting the source composite curve to the right to give a target of 250 Mt, which corresponds to the minimum unutilized storage capacity for the system (Figure 2). As the sinks have a combined 1,000 Mt of storage capacity, this solution implies that 750 Mt of CO_2 can be captured and stored. Note that this targeted amount of CO_2 is 93.75% of the 800 Mt of CO_2 from the sources. Thus, there is 50 Mt of CO_2 which may not be stored in these available sinks. It can be seen that Sources 1 and 2 are below and to the left of the pinch point, while Sources 3 and 4 are above and to its left. The source-sink matching can thus be solved by inspecting the above- and below-pinch regions separately, either by inspection or through the *nearest neighbor algorithm* (Prakash and Shenoy, 2005). The resulting optimal allocation for this system is given in Table 3. This result illustrates

that, below the pinch point, there is surplus storage capacity, and the main bottleneck for CCS is the injection rate limit into the sinks in this region. On the other hand, above the pinch point there is surplus injectivity and, in this case, insufficient storage capacity such that only half of the CO_2 from Source 4 can be stored. One possible interpretation is that Source 4 may be linked to Sink 2 during its first 10 years of operation while an alternative storage site is developed for the remaining 50 Mt to be stored in the final 10 years of the life of this plant.

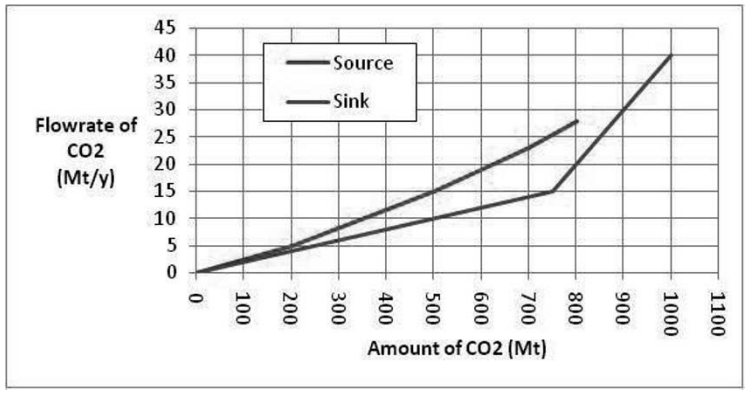

Figure 1. CCSPD showing infeasible initial solution

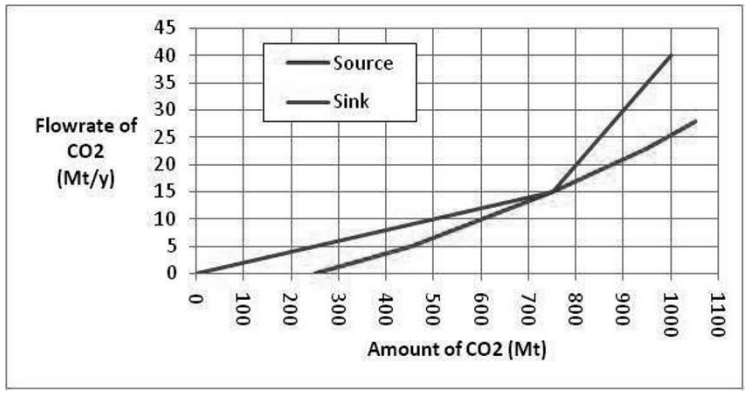

Figure 2. CCSPD showing optimal solution

Table 3. Optimal CO_2 allocation network

	Sink 1	Sink 2	Uncaptured CO_2
Source 1	200	0	0
Source 2	300	0	0
Source 3	0	200	0
Source 4	0	50	50

5. Conclusion

A graphical approach to optimal matching of CO_2 sources and sinks in CCS systems has been developed. This technique is based on pinch analysis methods developed for generic resource conservation networks, and as with such insight-based strategies, allows system targets to be determined based on the physical characteristics of the sources and the sinks. Furthermore, pinch-based insights can be used for problem decomposition to determine general guidelines for the synthesis of the CO_2 network. A simple case study has been used to demonstrate the methodology. In this paper, geographical distances, and hence pipeline costs, between various sources and sink are neglected. Future research works directed to address this issue. Extensions of the methodology developed here will also address uncertainties encountered in CCS planning, such as storage capacity of reservoirs and operating lives of sources and sinks.

References

Benson, H. Y. and Ogden, J. M. (2003). Mathematical programming techniques for designing minimum cost pipeline networks for CO_2 sequestration. Proceedings of the 6th International Conference on Greeenhouse Gas Control Technologies (October 1 – 4, 2002, Kyoto, Japan) p. 627 – 632.

Davison, J., Freund, P. and Smith, A. (2001). Putting carbon back into the ground. International Energy Agency Greenhouse Gas R&D Programme, Cheltenham.

El-Halwagi, M. M., Gabriel, F. and Harrel, D. (2003). Rigorous graphical targeting for resource conservation via material recycle/reuse networks. Industrial & Engineering Chemistry Research 42: 4319 – 4328.

Fimbres Weihs, G. A., Wiley, D. E. and Ho, M. (2011). Steady-state optimisation of CCS pipeline networks for cases with multiple emission sources and injection sites: south-east Queensland case study. Energy Procedia 4: 2748 – 2755.

Foo, D. C. Y. (2009). State-of-the-art review of pinch analysis techniques for water network synthesis. Industrial & Engineering Chemistry Research 48: 5125 – 5159.

Kazmierczak, T., Brandsma, R.,Neele, F. and Hendriks, C. (2009). Algorithm to create a CCS low-cost pipeline network. Energy Procedia 1: 1617 – 1623.

Middleton, R. S. and Bielicki, J. M. (2009). A scalable infrastructure model for carbon capture and storage: SimCCS. Energy Policy 37: 1052 – 1060.

Pekala, L. M., Tan, R. R., Foo, D. C. Y. and Jezowski, J. (2010) Optimal energy planning models with carbon footprint constraints. Applied Energy 87: 1903 – 1910.

Prakash, R. and Shenoy, U. V. (2005). Targeting and design of water networks for fixed flowrate and fixed contaminant load operations. Chemical Engineering Science 60: 255 – 268.

Tan, R. R., Ng, D. K. S. and Foo, D. C. Y. (2009). Pinch Analysis Approach to Carbon-Constrained Planning for Sustainable Power Generation. Journal of Cleaner Production 17: 940 – 944.

Shenoy, A. U. and Shenoy U. V. (2012). Targeting and design of energy allocation networks with carbon capture and storage. Chemical Engineering Science 68: 312 – 327.

Tan, R. R., Ng, D. K. S., Foo, D. C. Y. and Aviso, K. B. (2010). Crisp and fuzzy integer programming models for optimal carbon sequestration retrofit in the power sector. Chemical Engineering Research and Design 88: 1580 – 1588.

Tan, R. R., Aviso, K. B., Bandyopadhyay, S. and Ng, D. K. S. (2012a). Optimal Source-Sink Matching in Carbon Capture and Storage Systems with Time, Injection Rate and Capacity Constraints. Environmental Progress and Sustainable Energy, DOI: 10.1002/ep.11630.

Tan, R. R., Aviso, K. B., Bandyopadhyay, S. and Ng, D. K. S. (2012b). A Continuous-Time Optimization Model for Source-Sink Matching in Carbon Capture and Storage Systems. Industrial and Engineering Chemistry Research, DOI: 10.1021/ie202821r.

Turk, G. A., Cobb, T. B., Jankowski, D. J., Wolsky, A. M. and Sparrow, F. T. (1987). CO_2 transport: A new application of the assignment problem. Energy 12: 123 – 130.

I.A. Karimi and Rajagopalan Srinivasan (Editors), Proceedings of the 11th International Symposium on Process Systems Engineering, 15-19 July 2012, Singapore.

Fugitive Emission Reduction through Optimization

A-Jalil, S.[a*], Hashim, H.[a], Hassim, M. H.[a], Johari, A.
[a]*Process System Engineering Centre(PROSPECT), Faculty of Chemical Engineering, Universiti Teknologi Malaysia, 81310, UTM JB, Johor, Malaysia*

Abstract

Fugitive emissions (FE) nowadays become a great concern around the world due to their negative impacts on productivity, environment and health. This paper presents a mathematical model for reducing fugitive emissions from piping equipment. The problem is formulated as mixed integer linear programming and coded in General Algebra Modeling System (GAMS). The MILP model proposed in this work can be used to identify the most appropriate technologies for fugitive emissions reduction as well as maximize the profit. . Application of this model on the case yields a significant FE reduction up to 82.2 percent, illustrating the effectiveness of the technique.

Keywords: *fugitive emissions, mitigation, valve, GAMS, optimization*

1. Introduction

Fugitive emissions (FE) are spurious leak in an industrial site that comes from the equipment such as valve, pump, pipeline etc. (Lipton and Lynch, 1994). The emissions are not only an environmental and economy issue, but also a concern to health. Despite being very small and mostly invisible, FE are the main sources of the continuous background exposure to workers. It also leads to a substantial impact on global warming problem. Even though the impact on the daily life is a small, but it still can affect if the problem is not resolve from now. The study on the FE has been done widely especially in the United States and Europe country in term of the estimation or quantifying. The regulation regarding this matter had been implemented in both countries.(Kakaiya, S.,1999) However, for the research on the FE mitigation, the research is still few and not much done by the researchers nowadays.

It was found that valve contributed to the higher FE than the other piping equipment. Most of the study conducted by past researcher is related to strategies to overcome the leakage from the valve. They carried out a study on the properties of sealing material used for the valve and also the valve type and maintenance that may be the factor of the leakage (Kakaiya, 1999, Onat, 2008). According to the Cornelsen (2006), there are two problems from valve that causes the emissions which are from the body to bonnet joint which was readily solved and also from the valve stem packing. . It can be concluded that material technologies is the important element for solving the problem. Regardless the study on the sealing material and the successfulness of it to reduce the FE, due to the highly cost of maintenance and services to change the equipment, most of the industry do not see the important of it as the loss on cost is invisible and can be neglected (Szweda, 2000).

According to the report from Australian Government, Department of Climate Change and Energy Efficiency the amount of FE will rapidly growth from 2010 onwards where the projection showed 7 percent of FE is increasing each year. This amount can be reduced if the steps on the reduction are taken now for all the industry around the world.

2. Development of fugitive emissions mitigation model

There are certain technologies that had been developed by certain company in order to comply the regulation from the authorities (Cornelsen, 2006 and Vogel,. 2007) Even though the technologies are successes, due to the cost, most of the companies neglected it and make no change with the reduction of FE. Table 1 shows the relative life cycle cost for potential valve seal types compared with the impact on environment as total emission level (Ellis, 2004).

Table 1: Relative life-cycle cost for potential valve seal types compared with impact on the environment as total emissions level.

Packing types / Parameters	Standard packings	Die-formed packing rings sets	Fugitive emissions packing sets with/without spring loaded gland	Bellows seals with safety packing	Packing sets with lantern rings for leakage collection
Packing System cost	Low	Low to average	Average to high	High	High
Installation efforts/costs	Average	Low	Low to average	Average	High
Maintenance frequency/costs	Average	Average	Low to average	Low	High
Leakage performance	ISO 15848-1 Class B or C	ISO 15848-1 Class B or C	ISO 15848-1 Class A or B, TA-Luft	ISO 15848-1 Class A or TA-Luft	ISO 15848-1 Class A or TA-Luft
Life expectancy (service life)	Low to average	Average	Average to high	High	Average

From the table, it can be seen that the better leakage performance, the higher the cost of the systems. Therefore, in order to find the optimal solution that will satisfy the cost and also the environment regulations, a systematic technique for mitigate the FE which takes in to account cost as the main objective had been developed.

2.1. Superstructure Model and parameter data

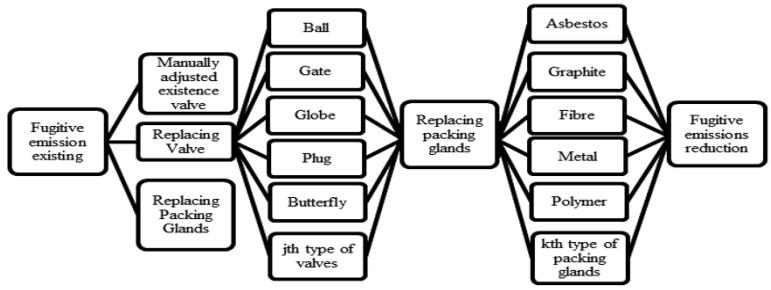

Figure1: The superstructure model describes the methods and the steps for the reductions of fugitive emissions.

There are three available mechanisms that can be implemented for FE reduction as illustrated in Figure 1. These include (i) manually adjusted valve, (ii) replacing valve and (iii) replacing packing glands. Manually adjusted valve is not preferable method as it needs a consistently monitoring on the valve. By replacing the valve and packing glands with the new technologies of valve and packing glands for the minimal emission leakage, it will reduce the emission in the industry. Table 2 shows the data of emission control, maximum operating condition and the cost for each type of valve and packing

glands which will be the constraints for the selection while Table 3 is the data input from the industries.

Table 2: Emission Control, Operating Condition and Cost of each type of valve and packing glands

Type of Valve(jth)	*Emission Control (ppm)*	*T Max (oC)*	*P Max (bar)*	*Cost (RM)*	*Type of Packing(kth)*	*Emission Control (ppm)*	*T Max (oC)*	*P Max (bar)*	*Cost (RM)*
Ball	70	190	20	100	Asbestos	150	200	25	250
Gate	200	200	25	400	Graphite	90	250	30	150
Globe	100	170	15	300	Polymer	100	180	12	300
Butterfly	150	300	20	200	Metal	400	300	20	200
Plug	250	250	30	500	Fibre	250	220	30	450

Table 3: Input data of the current fugitive emission, operating condition and budget provided for each stream from chemical plant.

	Stream 1	*Stream 2*	*Stream 3*	*Stream 4*	*Stream 5*	*Total*
Current FE (ppm)	600	900	1000	600	400	3500
Operational Temperatute, T(°C)	150	120	160	200	200	
Operational Pressure, P(bar)	12	15	25	18	10	
Budget, RM	500	800	900	700	1000	3900

Table 4: List of Variables

Variables	Description
C_{equip}	Cost due to the replacement of each equipment in pipeline
C_m	Cost due to the maintenance/services
C_b	Maximum Budget prepared for the replacement
FE_{ex}	Estimation of currents fugitive emissions in the plant
FE_{red}	Emission control by the equipment (jth, kth)
T^{max}	Maximum temperature of each equipment
p^{max}	Maximum pressure by each equipment(jth, kth)
T^{opt}	Operational temperature in the plant
p^{opt}	Operational pressure in the plant

2.2. Mathematical Modeling

There are 5 main steps involve obtaining the optimal solution for FE reductions where the variables described in table 4 above:

Step 1: Specify or Evaluate the Fugitive Emission Quantification

The fugitive emission (FE) quantification should be known. It can be measured /calculated from existing plant or at the design stage by using the tool of FE quantification. Summation of the fugitive emission from piping equipment i^{th} is the total of FE at the plant.

$$\sum_i FEex(i) = \text{Total FE at the plant} \quad (1)$$

Step 2: Specify Design Operational Condition Constraints

This constraint indicates that the replacement of new equipment such as valves and packing glands must satisfy the operational condition. Two operational conditions that need to be considered are the operational temperature and pressure.

$$T^{\max}(j,k) \geq T^{opt}(i) \quad (2) \qquad P^{\max}(j,k) \geq P^{opt}(i) \quad (3)$$

The above equations indicates that the maximum temperature and pressure of the new equipment $j^{th}$and k^{th} must be higher than the operational temperature and pressure at the piping line i^{th}. This constraint is important as to ensure the equipment will not be harmed if the operational temperature and pressure are higher that the allowable maximum temperature and pressure of the equipment.

Step 3: Specify the Limitation of the Budget for Installation New Equipment

The cost of replacement, maintenances and other services must be lower than the budget provided by the company.

$$\sum_i \sum_j \sum_k C_{equip} + C_m \leq C_b \quad (4)$$

Step 4: Calculate the Maximum Saving Cost After Installation

Equation (5) represents the objective function to maximizing the saving cost of the plant after the installation of the new equipment and also reducing the FE at the plant.

$$\max cost(RM) = \sum [(FEex(i) - FEred(j,k)) * P - (Cequip(j,k) + Cm)] * y(a) * x(b) \quad (5)$$

The choice of the equipment which is valve and packing glands are depends on the target and limitation. From above equation, i^{th} indicates the equipment at the pipe line which consist the FE while j^{th} and k^{th} indicates the new equipment of valve and packing glands which can reduce the existing FE at the plant. The FE which is measure in concentration or part per million(ppm) at the i^{th} can be reduce after installing the new valve and packing glands jth and kth and give a saving cost of emission reduction after multiply by the cost of chemical/substance produce by the plant, *P (RM/ppm). FEred (ppm)* represent the quantity of FE after the installation of the new equipment.

Cost of the equipment chosen after meet the satisfied operational condition and budget limitation will affect the maximum cost. So, the maximum saving cost for this equation is based on the equipment chosen after satisfying the operational condition, budget limitation and will give the minimum cost of replacement/installation compare to other equipment listed.

Step 5: Calculate the Percentage of Emission Reduction

The percentage of emission reduction can be calculated as follows:

$$\%\text{emission reduction} = \frac{\text{Total Existing Emission - Total Emission after installation (ppm)}}{\text{Total Existing Emission (ppm)}} \quad (6)$$

where, total existing emission is the summation of emission at the piping equipment for the whole plant, $\sum FEex(i)$ and total emission after installation is the emission after replacing the chosen equipment at the piping equipment, $\sum FEred(j,k)$

3. Results and Discussions

Figure 2 represents the cost savings analysis and the percentage reduction of FE for each stream while table 4 shows type of valves and packing glands for stream 1. . It is observed that, by replacing t ball valve with graphite can leads to the cost savings up to RM 65750 with 73.3% emission reduction.

The valve and packing glands selected are varies depending on the operating condition for each stream. The results shows that, for the same type of valve and packing glands for stream 1 and 2 , provides about RM110750 profit and 82.2% reductions forFE. . For stream 4, butterfly valve with fibre packing is recommended for the replacement. This is due to the higher temperature of stream 4.

Table 5: Optimal Solution for Valve and Packing Glands for stream 1

	Type of Packing/ Type of Valve	*Asbestos*	*Graphite*	*Polymer*	*Fibre*	*Metal*
STREAM 1	Ball	0	1	0	0	0
	Gate	0	0	0	0	0
	Globe	0	0	0	0	0
	Butterfly	0	0	0	0	0
	Plug	0	0	0	0	0

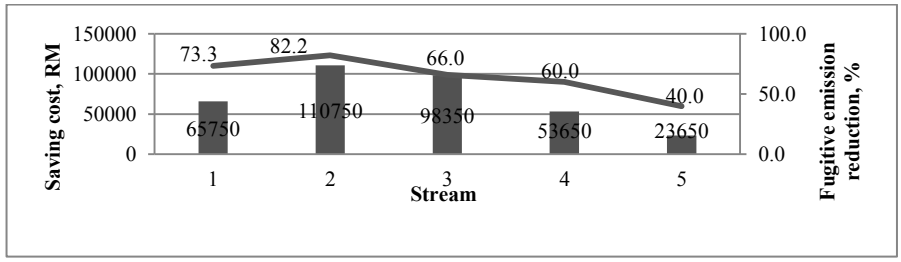

Figure 2: Graph on maximum saving cost (RM) and percentages of emission reduction for each stream in chemical process industry.

4. Conclusion

The systematic technique to determine the best technologies to reduce the FE as well as maximised profits to the industries is developed. This proposed technique is highly in need as it can be used to design the chemical process with more sustainable features through fugitive emissions reduction. It can be used by all the chemical process industry in order to comply the regulation from the authorities and at the same time give a significant cost savings to the process plant.

Acknowledgement

Special thanks to Universiti Teknologi Malaysia and Ministry of High Education for sponsoring my research under Research University Grant (vot: Q.J130000.7125.01H52)

References

Australia's emissions projection 2010. http://www.climatechange.gov.au/publications/projections/australias-emissions-projections/emissions-projection-2010.aspx

Cornelsen, D., (2006). The development of effective fugitive emissions control fro valves. Valve World, February 2006, pages 49-53

Ellis, B. (2004). Developments in EU environmental legislation and the ESA guidance note. Sealing Technologies, Volime 2004, Issues 10, Octover 10, pages 6-8

Kakaiya, S. (1999). Valve fugitive emissions: the challenge ahead. Sealing Technologies, Volume 1999, Number 71, November 1999, Pages 7-9.

Lipton, s. And Lynch, J.(1994). Hnadbook of Health Hazard citrol in Chemical Process Industry. John Wiley and Sons, New York.

Onat, A. (2008). The effects of sealing materials on elimination of fugitive emissions. Material and Design (2008), pages 533-538.

Szweda, R. (2000). Fugitive emissions: The matter of imperfect seals. Sealing Technologies, Volume 2000, Number 83, November 2000, pages 9-11.

Vogel, R., Danner, S., Smith, B. (2007). Fugitive emissions: Guidelines for successful valve upgrades. Valve World, June 2007, pages 80-85

I.A. Karimi and Rajagopalan Srinivasan (Editors), Proceedings of the 11th International Symposium on Process Systems Engineering, 15-19 July 2012, Singapore.

Process modeling and economic analysis of microalgal systems for CO_2 capture and production of chemicals

Rui Vogt Alves da Cruz, Claudio Augusto Oller do Nascimento
Chemical Engineering Department - Escola Politécnica da Universidade de São Paulo, Av. Prof. Luciano Gualberto, trav. 3, n. 380, CEP 05508-900 São Paulo, Brazil

Abstract

The use of microalgae and cyanobacteria for the production of biofuels and other substances of commercial interest has been widely advertised as an extremely promising sustainable technology, due to the high areal productivity, potential for fixation of CO_2, possibility of using non-arable land and alternative sources of nutrients such as brackish water and agricultural and industrial effluents. The commercial production of cyanobacteria in open raceway ponds was studied through the combination of a mathematical model for the algal growth with technical, economical and sustainability evaluations. A macromodel was developed to simulate the ponds, and it was used to assess the impact of environmental variables, such as light and temperature, and to optimize the process conditions for operation and harvesting. A detailed economic analysis demonstrated the impact of capital, operation costs and energy consumption, also highlighting the importance of revenue from high value products to process viability, considering the current technology. The sensitivity analysis and evaluation of both technology improvements and alternative business models enabled the prioritization of future research areas, based on economic and environmental impact.

Keywords: Algae. Economic Analysis. Process Modeling.

1. Introduction

The use of microalgae and cyanobacteria for the production of biofuels and renewable feedstocks has been regarded as an extremely promising sustainable technology [1]. Some of the key advantages are the high areal productivity and lipid content [2], the potential for CO_2 fixation (ca. 1.8 kg CO_2 per kg of biomass produced) [3], the possibility of using non-arable land and the number of high value substances that can also be extracted.

However, there are still challenges for the large scale implementation of this technology, such as, high capital, operation costs and energy consumption, seasonal variations in productivity and contamination risks when using open ponds. The harvesting and extraction steps represent one of the main areas for improvement, accounting for up to 30% of the capital costs [3] and 90% of the total energy demand. A number of studies have described the economic analysis for open and closed systems, describing the current challenges related to economic viability and the dependence on the revenue for high value added products [4].

The mathematical modeling of growth in photobioreactors and open ponds is another challenging task which is extremely important for designing the system, predicting process efficiency and optimizing and controlling operation conditions. Several authors have developed mechanistic and hybrid models for growth of microalgae and cyanobacteria in photobioreactors, or using neural networks or response surface models. However, the development of macromodels for prediction and control of algal growth in open ponds has been much less frequently studied [5-7]. Guterman, Vonshak and Ben-Yaakov [5] developed a model for growth of *Spirulina platensis* in open raceway ponds, capable of simulating the biomass productivity, pH, and growth rate as function of light intensity, temperature, nutrients and other parameters.

2. Model Development and Analytical Methodology

The production system used for the development of the model and subsequent analysis is based in a farm of open raceway ponds, with concrete walls and compacted earth bottoms. The reference system was a total area of 500 ha, split in 80,000 m^2 ponds, 0.4 m deep. The suspension is harvested periodically to an intermediate tank, being afterwards transferred to a cluster of continuous centrifuges and concentrated to 22% solids. The culture medium is recycled to a buffer tank, where nutrients and additional water are made up. The resulting sludge is then dried in belt dries, followed by solvent extraction with n-hexane, extracting the algal oils. The solvent is recycled and the remaining solid biomass goes through a finishing step to remove the residual solvent.

The algal growth model used to simulate the open ponds is based on the equations developed by Guterman, Vonshak and Ben-Yaakov [5] for *Spirulina platensis*, growing in a low cost culture media based on fertilizers and industrial grade salts [8], and was developed in MATLAB R2007b (The Mathworks, Natick, MA). The biomass growth components of the model are summarized by the equations below.

$$\frac{dC(t)}{dt} = \mu_e C(t)$$

$$\mu_e = \mu_p - \mu_r$$

$$\mu_p = \frac{qI_0}{2{,}3OD(t)H}\left[1 - e^{(-2{,}3OD(t)H)}\right]$$

$$\mu_r = \begin{cases} a \cdot T + b, & 15 < T \leq 40^oC \\ 0, & 15^oC \end{cases}$$

Where C(t) is the concentration of algal biomass at a given time, μ_e the effective growth rate, μ_f is the photosynthesis growth rate, μ_r is the respiration growth (consumption) rate, q is the light conversion rate, I_o the light intensity at the surface of the pond, OD(t) the optical density of the suspension at a given time, H the depth of the pond, and a and b are the linear regression parameters for respiration rate as function of temperature.

CO_2 is supplied by dispersors disposed in sumps along the ponds. The reference case considers the use of flue gas from a thermoelectric power plant as the source of CO_2. Figure 1 summarizes the system used in the development of the models and economic analysis.

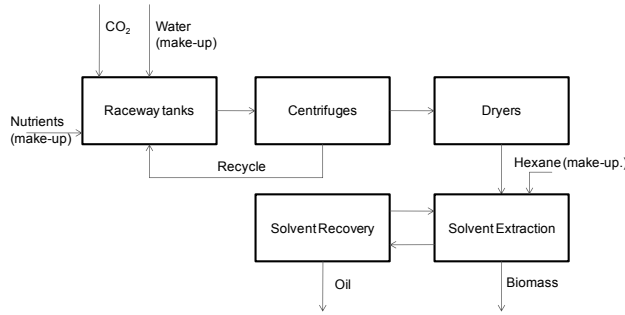

Figure 1 – Block diagram for reference system

The mass balance for water used empirical relations proposed by EPA [9] to estimate typical losses with evaporation. The mass balance for CO_2, biomass and nutrients was based on the stoichiometric relations measured for *Spirulina platensis* by Cornet et al [10]. The cost of equipment, construction and energy demand of unit operations was based in specific equipment specs and quotes or estimated using the charts by Peters, Timmerhaus and West [11]. The additional capital costs (installation, instrumentation, engineering, etc) and the operation costs were calculated using the estimates proposed by Peter, Timmerhaus and West [11] and representative data on labour and utilities costs for a plan in Texas, USA. For each case studied the net present value (NPV) and internal rate of return (IRR) were calculated.

3. Results and Discussion

3.1. Mathematical model for growth in raceway ponds

The model developed was initially used for the study of the main process parameters in growth rate and productivity. The considerable decrease of μ_e for increasing concentrations is a consequence of the light attenuation by the algal suspension (Figure 2). Temperature also has an important effect on the effective growth rates, impacting both the photosynthesis rate but also the respiration rate in the dark zones of the pond (Figure 3). Figure 4 describes the combined effect of pond depth and initial cell concentration in daily areal productivity. The understanding of those effects allows the determination of design and process conditions in order to maximize productivity. It also supports the evaluation of potential locations for the production of microalgae and cyanobacteria, based on the daily and seasonal variation of light and temperature.

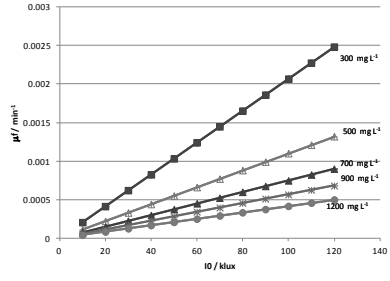

Figure 2 – Effect of light intensity and cell concentration in growth rate

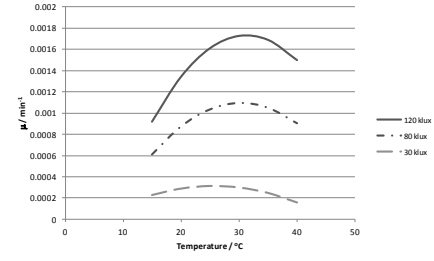

Figure 3 – Effect of temperature and light intensity in growth rate

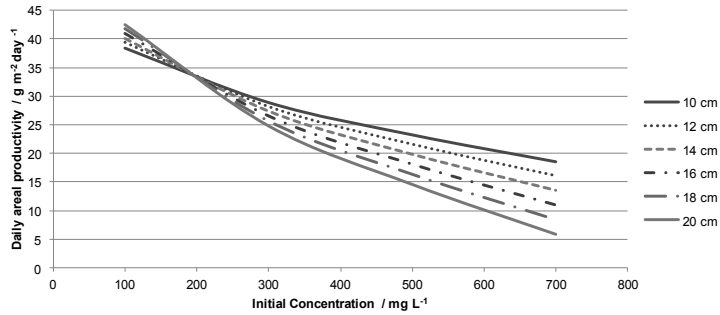

Figure 4 – Effect of pond depth and initial cell concentration in daily areal productivity

The model was also used to optimize operational conditions, especially the maximum concentration before harvesting and the renewal rate (% of total pond volume harvested and replaced by fresh culture medium). Table 1 describes the results of a designed experiment using the model to optimize the above mentioned process parameters. Higher productivities were obtained for higher renewal rates and lower harvesting concentrations, in agreement with experiments in batch photobioreactors [12].

Table 1 – Results of experiment to optimize process conditions. The productivity is calculated for a 1000 m^2 pond, 0.2 m deep, and reported in kg day^{-1}

Harvesting concentration / g L^{-1}	Renewal Rate					
	20%	30%	40%	50%	50%	70%
0.4	31.5	33.4	35.6	36.4	37.8	39.8
0.5	28.5	32.6	31.2	33.2	33.2	37.9
0.6	26.8	28.0	29.0	31.9	32.1	32.8

3.2. Economic analysis

A sensitivity analysis of the simplified economic model is summarized in Figure 5. The main variable impacting the IRR are capital costs and productivity. A detailed analysis, taking into consideration specific equipment costs and consumption of utilities, also highlights the cost of nutrients (30% of operation costs), and energy (up to 14% of operation costs, for electricity and natural gas).

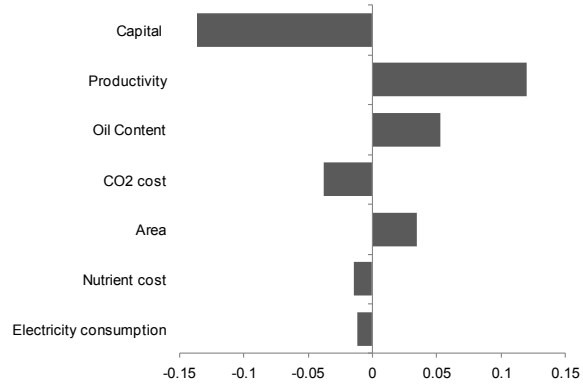

Figure 5 – Normalized effects of variables in the internal rate of return

The detailed economic analysis has also showed the importance of high value products to the total revenue and economic viability, based on the currently available technology. The only alternative cases studied with positive NPVs and an IRR above 15% were based on the sale of a high value specialty apart from the algal oil and biomass. The use of alternative nutrient sources (to reduce operation costs) and the development of improved technologies for harvesting and separation (to reduce capital and energy consumption) were identified as key priorities to improve the economics of microalgae related products.

4. Conclusions

The development of reliable and robust models for the production of microalgae and cyanobacteria in open ponds is critical for designing improved systems and optimizing and controlling process conditions. A detailed economic analysis demonstrated the impact of capital, operation costs and energy consumption, also highlighting the importance of revenue from high value products to process viability, considering the current technology. The sensitivity analysis and evaluation of both technology improvements and alternative business models enabled the prioritization of future research areas, based on economic and environmental impact.

References

[1] Greenwell HC. Laurens LML. Shields RJ. Lovitt RW. Flynn KJ. Placing microalgae on the biofuels priority list: a review of the technological challenges. J R Soc Interface 2010;7:703-26.

[2] Chisti Y. Biodiesel from microalgae. Biotechnol Adv 2007;25:294-306.

[3] Benemann JR. Oswald WJ. Systems and economic analysis of microalgae ponds for conversion of CO2 to biomass. Final report to the Department of Energy. Pittsburgh: Pittsburgh Energy Technology Center; 1996.

[4] Stephens E. Ross IL. King Z. Mussgnug JH. Kruse O. Posten C. Borowitzka. MA. Hankamer B. An economic and technical evaluation of microalgal biofuels. Nat Biotech 2010;28:126-28.

[5] Guterman H. Vonshak A. Ben-Yaakov S. A macromodel for outdoor algal mass production. Biotechnol Bioeng 1990;35:809-819.

[6] Sukenik A. Levy. RS. et al. Optimizing algal biomass in an outdoor pond: a simulation model. J App Phycol 1991; 3:191-201.

[7] James SC. Boriah V. Modeling algae growth in an open-channel raceway. J Comp Biol 2010; 17:895-906.

[8] Raoof V. Kaushik. BD. Prasanna R. Formulation of low-cost medium for mass production of Spirulina. Biomass Bioen 2006; 30:537-542.

[9] EPA. Technical Guidance for Hazard Analysis. U.S. EPA. 1987. http://www.epa.gov/OEM/docs/chem/tech.pdf.

[10] Cornet JF. Dussap. CG. et al.. A structured model for simulation of cultures of cyanobacterium Spirulina platensis in photobioreactors: II. Indentification of kinetic parameters under light and mineral limitations. Biotechnol Bioeng 1992;40:826-834.

[11] Peters M. Timmerhaus K. West R. Plant design for chemical engineers. 5 ed. New York: McGraw-Hill. 2003.

[12] Reichert CC. Reinehr CO. Costa AV. Semicontinous cultivation of the cyanobacterium Spirulina platensis in a closed photobioreactor. Braz J Chem Eng 2006;23:23-28.

I.A. Karimi and Rajagopalan Srinivasan (Editors), Proceedings of the 11th International Symposium on Process Systems Engineering, 15-19 July 2012, Singapore.

Sustainability Assessment of CO2 Capture Process in the Preliminary Process Design: Selection of Solvents

Namjin Jang, [a] Hae-jin Moon, [a] Inhyck Choi,[a] En Sup Yoon [a]

[a] *Seoul National University, Gwanak st. 1, Gwansk-gu, Seoul 154-742, Korea*

Abstract

The sustainable process is drawing attention as the upcoming frontier and alternative works. Sustainable developments of chemical process are one of the core activities to launch the production of chemical materials in the chemical process industries. We introduce a set of indicators that can be used to measure the sustainability performance of chemical process, such as net present value, material intensity, energy intensity, CO2 capture efficiency, global warming, and inherent safety, etc. The evaluation was done by using the 6th alternative of solvents for post-compustion in CO2 capture technologies as a case study. Sustainability in chemical process design can be applied to product and process design to improve sustainable developments that is economic, environmental, and social aspects. Also, it can be considered in order to counteract multidisciplinary change such as environmental responsibility, social concerns, and economic uncertainty, etc.

Keywords: Sustainabiltiy, CO2, post-combustion, solvents, CCS.

1. Introduction

The concept of sustainability was first mentioned in scientific literature by the German Miner Hans Car von Carlowitz referring to sustainable forestry in "Sylvicultura oeconomica" in 1713. Especially, sustainability have recently interested and studied both the society at large and micro scale of process. In this sense, the sustainable process is drawing attention as the upcoming frontier and alternative works. Development of sustainable chemical process is one of the core activities to launch the production of chemical materials in the chemical process industries. Especially, process design and synthesis is the essential engineering activity based on the mathematics, basic science, engineering science, economics, safety, reliability, and social consideration, etc. in the whole process design phases (Kim, 2010; Sigiyama, 2007). Generally, there are three major facets considered in sustainability, such as economic, environment and society/safety to assess sustainability. In the preliminary process design phase, sustainability of alternative process needs to be studied to evaluate improvement options, strategies for development, innovations of process and inherent safety design, etc (Azapagic, 2006).

Removal of carbon dioxide (CO2) is an important industrial operation. CO2 is produced in large quantities by many important industries such as fossil-fuel-fired power plants, steel production, chemical and petrochemical manufacturing, cement production, and natural gas purification. The reasons for the CO2 removal are traditionally technical and economic concerns. Also, environmental concerns, such as global warming, climate change, etc., are now focused as one of the most important and

challenging environmental issues facing the world community (Ma'mun, 2006; Wang et al., 2011).

Carbon dioxide capture by an absorption process is one of the most common industrial technologies today. Recent economic studies (IEA GHG, 2006; Desidere and Corbelli, 1998; Zahraa et al., 2011) indicate that the process will also remain competitive in the future. One of the key improvements under development is new, faster and more energy–efficient absorbents. A chemical to be used as a commercial absorbent must have high net cyclic capacity, high absorption rate for CO2, and good chemical stability. For example, alkanolamines are the most commonly used chemical absorbents for the removal of acidic gases today.

In this paper, we are focused on the chemical absorption process (Zahraa et al., 2011 ; Husebye et al., 2011). Over ten absorbents are developed and researched in the world including alkanolamines, methanol, K2CO3, Ammonia, etc. as represented in Table 37. Especially, we evaluated six absorbents, which is 2-amino-2-methyl-1-propanol (AMP), diethanolamine (DEA), potassium carbonate (K2CO3), monoethanol amine (MEA), methanol and ammonia since these absorbents has studied in pilot plant. Actually, chemical absorption process consists of two mainly equipment which are absorber and stripper. Here, Figure 1 is a flowsheet diagram representing the pilot plant at the University of Texas at Austin for CO2 capture by MEA and the unit operations. The absorber and stripper data for the CO2 capture process by various absorbents.

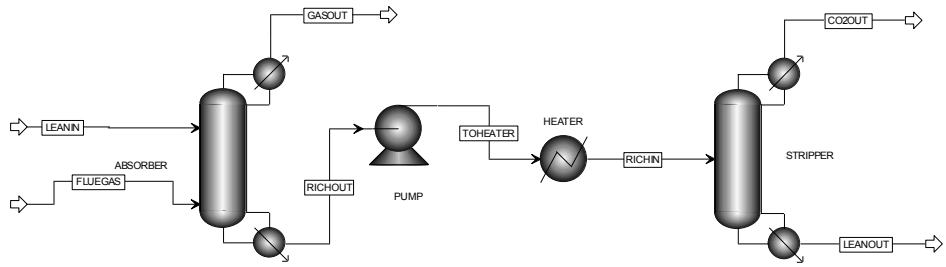

Figure 1. Simple schematic of the CO2 capture process using MEA.

2. Sustainability Assessments

In this paper, we are focused on the three indicators to evaluate sustainability of CO2 capture process, which are CO2 removal efficiency with capital and operating cost as an economic indicator, environmental impact as environmental indicator and inherent safety impact as a safety and social indicator. Here, first of all, we need to identify alternatives and define scope of sustainability. And then, the database is constructed including capital costs, production costs and simulated the process information. Finally, sustainability will be drawn by using graph.

2.1. Economic Impact Assessments

As an economic aspect, in this paper, we proposed efficiency analysis based on cost of production by removing CO2 in the process. It is accounted for costs of raw materials (absorbents) and utilities used in the reaction, separation, waste treatments, etc. of the alternatives based on the CO2 removal quantity in the cost using Eq. (1)

$$Ecc = (AR\_CO2 \times C\_CO2)/TPE \quad (1)$$

Where,

E_{CC} = Cost of Production for CO2 removing

AR_CO2 = CO2 absorption rate [kg/hr]
C_CO2 = Price of CO2 [kg/$]
TPE = Total Product Expense [$/hr]

ECC means the ratio of total product expense to remove CO2 quantity in the process. Also, ECC is normalized using Eq. (2) in order to compare with other indicators in sustainability. Actually, small value of ECC means more economic. We can use this factor, when expense is greater than profit, excluding social benefits.

$$\textit{Cost of Production factor} = \log10\ (1/E_{CC}) \quad (2)$$

Table 1 represents the results of economic analysis of absorbents. Methanol is ranked as a high efficiency material. Also, It means that to remove same quantity of CO2, methanol-based process require small methanol as an absorbent and spend small heat duty for cooling and heating in the absorber and stripper during plant operation time compared with other absorbents-based process. Also, ammonia, MEA and DEA based process is ranked in high efficiency compared with other absorbents.

Table 1. Results of economic analysis of absorbents

	AMP	DEA	K2CO3	MEA	MeOH	NH3
CO2 removal efficiency	2.55	1.79	3.22	1.80	1.17	1.34
Rank	5	3	6	4	1	2

2.2. Environmental Impact Assessments

Environmental impact is one of the key parameter for evaluating sustainability in not only world societies but also chemical process industries. In the environmental analyses, we can evaluate energy consumption, waste generation, global warming effect, and environmental and health impact based on the chemical and physical properties.

M. H. Hassim (Hassim and Ali, 2009) proposed health and environmental criteria such as material state, volatility, chronic toxicity and adverse impact as a health impact and terrestrial toxicity as an environmental impact. In order to show results, the index values are normalized to the same magnitude range of 0 to 10. The absorbents are ranked by their environmental and health index as shown in Figure 2.

The index calculations indicate that the ammonia has the largest potential hazard from environmental and health aspects because ammonia evaporate easily and is very toxic material. K2CO3, on the other hands, is ranked as the best absorbent based on the environmental and health index. K2CO2 existed by dissolved in water. Therefore, K2CO3 has low volatility and toxicity scores in the process.

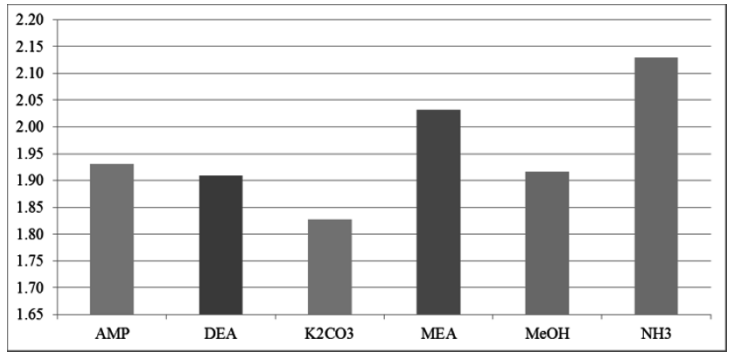

Figure 2. Results of environmental impact of CO2 absorbents.

2.3. Social and safety Impact Assessments

To evaluate inherent safety of absorbents, first of all, we simulate CO2 capture process using Aspen Plus to get process conditions and material data. Also, chemical and physical properties were obtained from Material Safety Data Sheet (MSDS) or literature reports. Results of inherent safety for absorbents are showed in Figure 3. In the results, ammonia, AMP, MEA is determined high ranking in general because of low operating temperature and pressure. In risk-standard rule (fifty-fifty rule), AMP ranks top (1.98) material among the alternatives. And then, NH3 ranked (2.12). However, in risk-aversion rule, the rank is changed. NH3 (2.69) ranks top and then MEA (3.06) ranked. AMP (3.26) is ranked in third.

This result is not quantitative assessment. However, these trends of CO2 absorbents can recommend the inherently safer material to design of chemical process. Also, in the next section, we will evaluate sustainability of CO2 absorbents including economic impact and environmental impact. It can be possible guide to adequate decision to improve sustainability.

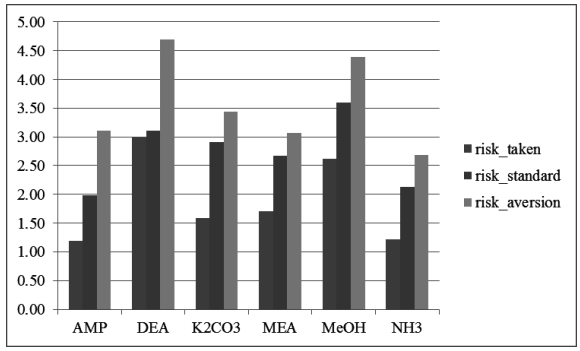

Figure 3. Result of inherent safety evaluation of CO2 absorbents.

2.4. Results of Sustainability Assessments

Figure 4 represents the comparison results of sustainability indicators for CO2 absorbents in normalized value of range 0 to 10. Here, the inherent safety result was based on the risk-standard rule. In the graph, the low value means better process compared with other. In the results, ammonia is ranked in high priority in the aspect of sustainability. And then AMP and MEA have been ranked in second and third. Especially, methanol has low tendency in economic and environmental aspect except for social and safety impact.

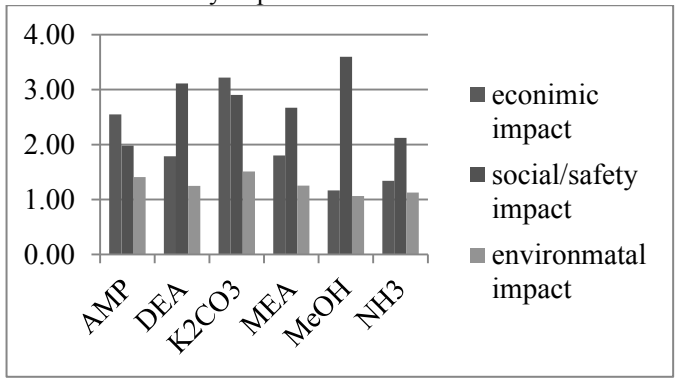

Figure 4. Comparison results of sustainability indicators for CO2 absorbents.

3. Conclusions

The sustainable process is drawing attention as the upcoming frontier and alternative works. Sustainable developments of chemical process are one of the core activities to launch the production of chemical materials in the chemical process industries.

In this paper, the evaluation was done by using the 6th alternative of solvents for post-compustion in CO2 capture technologies as a case study. Here we proposed the framework for sustainability study in the process design. In the case study, we used CO2 capture efficiency based on the Cost of Production analysis of process as an economic aspect. Environmental and health impact study is used as an environmental aspect. Finally, we use inherent safety performance index for evaluating inherent safety of process of case study regarding social and safety aspects.

Sustainability in chemical process design can be applied to product and process design to improve sustainable developments that is economic, environmental, and social aspects. Also, it can be considered in order to counteract multidisciplinary change such as environmental responsibility, social concerns, and economic uncertainty, etc.

References

A. Azpagic, A. Millington and A. Collett, 2006, A Methodology for Integrating Sustainability Considerations into Process Design, Chemical Engineering Research and Design, 84, 439 – 452.

U. Desideri, R. Corbelli, 1998, CO2 Capture in Small Size Cogeneration Plants: Technical and Economic Considerations, Energy Convers. Mgmt., 39, 857–867.

M. H. Hassim and M. W. Ali, 2009, Screening Alternative Chemical Routes based on Inherent Chemical Process Properties Data: Methyl Methacrylate Case Study, Journal the Institution of Engineers, Malaysia, 70, 2-9.

Jo Husebye, Rahul Anantharaman and Stein-Erik Fleten, 2011, Techno-economic Assessment of Flexible Solvent Regeneration & Storage for Base Load Coal-Fired Power Generation with Post Combustion CO2 Capture, Energy Procedia 4, 2612-2619.

IEA Greenhouse Gas R&D Programme (IEA GHG), January, 2006, Estimating future trends in the cost of CO2 capture technologies, 2006/5.

H. S. Kim, 2010, Study of Multiobjective Process Synthesis Based on Generalized Disjunctive Programming and Process Simulator, Doctoral thesis, Seoul National University.

Sholeh Ma'mun, 2006, Selection and Characterization of New Absorbents for Carbon Dioxide Capture", Doctoral thesis, Department of Chemical Engineering, Norwegian University of Science and Technology, Norway.

Hirokazu Sugiyama, 2007, Decision-making Framework for Chemical Process Design including Different Stages of Environmental, Health and Safety (EHS) Assessment, Doctoral thesis, ETH Zurich, Diss. ETH No. 17186.

M. Wang, A. Lawal, P. Stephenson, J. Sidders, and C. Ramshaw, 2011, Post-combustion CO2 capture with chemical absorption: A state-of-the-art review", Chemical Engineering Research and Design, 89, 1609-1624.

Mohammad R. M. Abu Zahraa, Eva Sanchez Fernandezb, Earl L. V. Goetheerb, 2011, Guidelines for Process Development and Future Cost Reduction of CO2 Post-Combustion Capture, Energy Procedia 4, 1051-1057.

Acknowledgement

This paper was supported by the Engineering Research Institute and ASRI (Automation and Systems Research Institute) in Seoul National University.

I.A. Karimi and Rajagopalan Srinivasan (Editors), Proceedings of the 11th International Symposium on Process Systems Engineering, 15-19 July 2012, Singapore.

Characterization of moisture and free air space effects and the optimal operation of a composting process for minimal waste and energy use

Gi Hoon Hong[a], Bettar El Hady[a], Ki Don Joo[a], Dongil Shin[a]

[a]*Department of Chemical Engineering, Myongji University, Yongin 449-728, Korea*

Abstract

Since composting of organic material releases a high amount of CO_2, which is known as a greenhouse gas, it is needed to reduce CO_2 emission to protect our planet from the global warming; in this study we have managed to reduce CO_2 by 23% compared to the previous study. We optimized the quality of compost by changing only one parameter and letting the other parameters be fixed, which permitted us to handle the composting process in easier way. In this work, a new dynamic model of composting process was developed and optimized using SuperPro Designer and Matlab. We studied the influence of air flow rate on oxygen concentration, CO_2, moisture and degradation of volatile solid. It was observed that those parameters depend strongly on air flow rate; for air flow rate at 2,000 kg/hr the temperature and oxygen showed the optimum results.

Keywords: Mathematical modeling, optimization, composting process, reactor modeling, SuperPro Designer.

1. Introduction

Composting is a biological decomposition and stabilization of organic substrates, under conditions that allow development of thermophilic temperatures as a result of biologically-produced heat, to produce a final product that is stable, free of pathogens and plant seeds, and can be beneficially applied to land. This is a largely satisfactory definition, although omission of the high solids aspect of composting means that this description might apply equally to liquid phase aerobic digestion [1]. However, the product stability criterion would not be met in the latter case, since the biological solids produced remain very wet, and thus prone to subsequent anaerobic biological activity. Composting is also a very important element in the successful operation of the recycle and reuse process of valuable resources out of municipal collection of garbage. Since the municipal garbage contains lots of biodegradable materials, proper treating through composting enables easy handling and separation of reuse materials. This research investigates on a dynamic modeling, simulation and optimization of a composting process operated mainly for this purpose (see Fig. 1).

2. Process Description

The most commonly-used type of equipment for composting process is a reactor; before the raw material to be sent to the reactor it is mixed with air in a mixer to upgrade the concentration of oxygen in the raw material. After the reaction is occurred, the product is flowed to a conveyer. By using the conveyer we can transport the reactor output to a centrifuge where we can separate substrates based on their size. Substrates that have size less than 30 mm are mixed with air in mixer, before being sent to generic procedure

where the second reaction occurs [1]. From the high outlet of generic procedure we have the gases and from the second outlet we have the final products; 10% of the products will be recycled and used as an amendment for raw material and the 90% is sent for storage or sold.

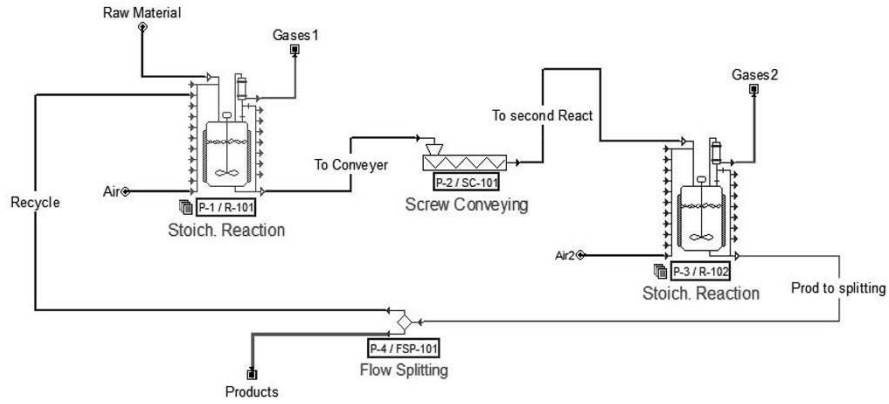

Fig. 1 Schematic diagram of the composting process being simulated

2.1. Raw material

Biodegradable waste is a type of waste, typically originating from plant or animal sources, which may be degraded by other living organisms. Wastes that cannot be broken by other living organisms are called non-biodegradable. Biodegradable waste can be commonly found in municipal solid waste (sometimes called biodegradable municipal waste, or BMW) as green waste, food waste, paper waste and biodegradable plastic.

2.2. Temperature and volatile solid

Because of the strong relationship of temperature with decomposition, temperature provides an important indicator of composting process efficiency [3]. Flow rate of 2,000 kg/h was able to reach the maximum temperature faster than the other flow rates, presumably because increased aeration minimized the oxygen limitation common in the initial phases of composting. The temperature and air flow profiles obtained for control strategy based on air flow regulation from temperature measure are shown in Fig. 2. According to previous studies [8,9], the sensing was placed at a middle layer matrix. It was necessary to begin the simulation with the oxygen controller until the thermophilic temperatures were achieved. Shortly before the third day of process, the maximum air flow rate was applied.

The effect of temperature on the substrate has been adjusted by the KT; the main factors affecting the BVS biodegradation were organic matter component and microorganism succession. During first 14 hr, BVS degradation accumulation was 0.026 kg which was about 0.7% of the total accumulation, so microorganism succession should be the main factor affecting the degradation. The slow degradation rate may be attributed to the inactivity of aboriginal microbes in the raw material when the temperature is rising. At 17 hr, mesophilic bacteria began to grow quickly. Decreasing volatile solid (VS) continued throughout the composting process as microbes degraded the organic material in mixture (see Fig. 3). Decomposition kinetics depends on a variety factors including moisture, oxygen and temperature in ranges appropriate to

support microbial activity [2]. The volatile solid decreased more rapidly at flow rate equal to 2000 kg/h than the other flow rates in the latter half of the composting process. This difference likely resulted from the more optimal moisture at the optimum flow rate at that stage of the process. The relatively high oxygen concentration of the optimum flow rate reactors may also have a positive influence on volatile solid degradation.

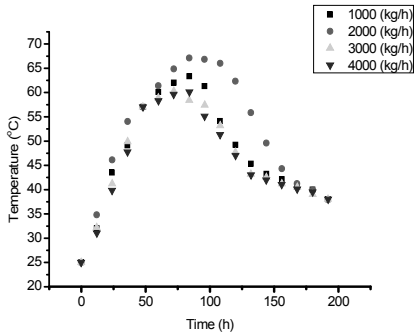

Fig. 2 Profile of substrate temperature with different initial airflow rate

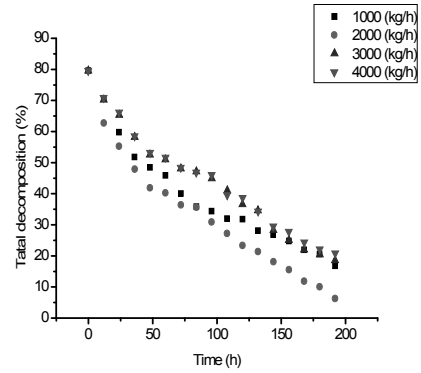

Fig. 3 Profile of substrate VS with different initial airflow rate

2.3. Output of reactors

The simulation results showed that most compost indexes decreased during the composting process. Because the high energy released from the reaction is exothermic, the temperature increases rapidly at the early stage. The oxygen concentration kept stable, showing that function of air supply in this period was mainly cooling compost. As we can see here, an increase in airflow rate led to low temperature and slows the degradation of substrate. Oxygen concentration in the exit gas did not fall below 5% which is the boundary for anaerobic condition. The output values examined were the total material reduction, the total percent reduction, and the maximum biomass concentration in products. For better description of the process, the effect of carbon nitrogen ratio should be included in the model kinetics. Evolved carbohydrate can stay in the solution in form of liquid or gas. Modeling of all possible ways is a very complicated task. For better prediction of carbohydrate we need to use different percentage of both moisture and oxygen concentration [4-7].

3. Emission of Exhaust Gases

3.1. CO_2 emission

Predicted percentages of CO_2 and oxygen in exhaust gas mixture follow qualitatively the simulation results. The deviations found could be explained by opening of the reactor during sampling periods, and they could also be attributed to the variation of the liquid-gas transfer rate as the material is dried. The water soluble fraction is mineralized to CO_2 through a first order reaction at K_{aq} rate. The mineralization rate of water soluble carbon is not expected to be rate-limiting. Therefore, an infinite value can be used for the C_{eq} mineralization rate constant to reflect rapidity of this stage. A fraction of the water-soluble carbon is assumed to convert to CO_2, while the rest is converted to microbial biomass, which is also part of the total solid carbon sink. Due to endogenous decay, a fraction of the microbial biomass is ultimately converted to CO_2 yield coefficient, as used in the model, referring to the mineralization carbon that will be

ultimately converted to CO_2, regardless of the pathway followed. Therefore, this yield coefficient is taken equal to 1, indicating that all initial mineralization carbon will be eventually converted to CO_2.

3.2. Oxygen concentration

Oxygen levels within the pile can also be used as an indicator of how the composting process is developing. As aerobic activity increases, the oxygen consumption should also increase causing the oxygen levels to decrease. Measuring oxygen levels to monitor the composting process is not as accurate as measuring temperatures. Oxygen monitoring is most useful to show that stability has been reached. Oxygen levels remain low during the active composting period. However, as the pile reaches maturity and microbial activity begins to slow, oxygen levels rise. Because CO_2 is a product of aerobic respiration, it can also be used as an indicator of microbial activity. The CO_2 levels should increase as microbial activity develops and decrease as the composting process approaches maturity.

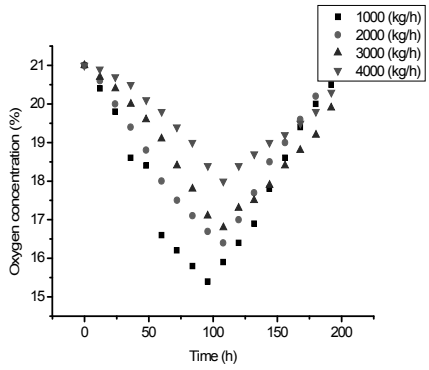

Fig. 4 Oxygen concentration in exhaust gas

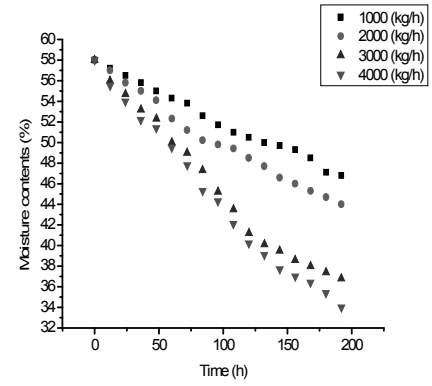

Fig. 5 Moisture contents of substrate with different airflow rate

3.3. Moisture

The measurement of moisture in both initial substrate and composted material allowed the determination of the amount of water accumulated during the composting treatment. Finally, gas monitoring enabled the determination of vapor flow in the incoming and outgoing gas [10,11]. Then, conducting a water balance allowed the calculation of the amount of water produced through bio-degradation of organic matter. As a first approximation, considering that biodegradable organic matter could be described as $C_xH_yO_z$, neglecting nitrogen content, the conversion of biodegradable organic matter during composting can be assumed by its oxidation, then transformation of biodegradable organic matter. Fig. 5 shows the variation of moisture content during the process in both reactors, initial moisture contents of about 62% wet basis decreased during the composting process, heat neglected by biological metabolism and the convective air flow increased water evaporation in the reactors. The compost moisture content in the high flow rate decreased more rapidly than in the low flow rate, in the high flow rate reactor led to low moisture content less than 40%, for 2,000 kg/h the moisture contents is at its optimum, around 46%.

4. Conclusion

This study provided a quantitative explanation for the current experience-based operation of a commercial composting plant for municipal waste and demonstrated the complex interactions which occur in composting processes. Variations of compost indexes, such as volatile solid degradation, temperature fluctuation, moisture exchanges and oxygen concentration were simulated; the decay rate and quality of compost were good due to reaching thermophilic phase in less than 48 hr and the process kept in it for 5 days. In this study, the percentage of cell mass in the mass composition of products was increased to 63% which can give high stability and desired products. The two-reactor system produces more stable compost than a single reactor in less composting time. Internal recirculation of air in the first reactor leads to more homogeneous temperature distribution throughout the composting mass as compared to no-recirculation, resulting in improved organic matter degradation. The model was developed based on several assumptions and simplifications, it could be further improved in the future when the complex reaction among and within the three phases are allowed (this work assumed that the raw materials have high moisture contents and high C/N ratio and free air space is enough to assure the circulation of air). To improve the robustness of the simulation model further studies on the complex transactions are required.

Acknowledgment

This work was supported by the Energy Efficiency & Resources program of the Korea Institute of Energy Technology Evaluation and Planning (KETEP) grant funded by the Korea Government Ministry of Knowledge Economy (*No. 2011T100200023*).

References

1. I.G. Mason, “Mathematic modeling of the composting process: A review”, *Waste Management*, 26, 3-21 (2006).
2. N. Bongochetsakul and T. Ishida, “A new analytical approach to optimizing the design of large scale composting systems”, *Bioresource Technology*, 99, 1630-1641 (2008).
3. A. Vlyssides, S. Mai and E.M. Barampouti, “An integrated mathematical model for composting of agricultural solid wastes with industrial waste water”, *Bioresource Technology*, 100, 4797-4806 (2009).
4. D.P. Komilis, “A kinetic analysis of solid waste composting at optimal conditions”, *Waste Management*, 26, 82-91 (2006).
5. M. Baptista, F. Antunes, M. S. Goncalve, B. Morvan and A. Silveira, “Composting kinetics in full-scale mechanical-biological treatment plants”, *Waste Management,* 30, 1908-1921 (2010).
6. H. Zhang and T. Matsuto, “Mass and element balance in food waste composting facilities”, *Waste Management*, 30, 1477-1485 (2010).
7. I. Petric and V. Selimbasic, “Development and validation of mathematical model for aerobic composting process”, *Chemical Engineering*, 139, 304-317 (2008).
8. M.E. Lang and R.A. Jager, “Evaluation of composting feasibility for regional implementation”, *Waste Management*, 35, 138-145(2009).
9. B. Puyuelo, T. Gea and Antoni Sanchez, “A new control strategy for the composting process based on the oxygen uptake rate”, *Chemical Engineering*, 165, 161-169 (2010).
10. P. Beuno, R. Tapias, F.Lopez and M.J. Diaz, “Optimization composting parameters for nitrogen conservation in composting”, *Bioresource Technology*, 99, 5069-5077 (2008).
11. H.K. Ahn, T.L. Richard and H.L. Choi, “Mass and thermal balance during composting of a poultry manure-wood shavings mixture at different aeration rates”, *Process Biochemistry*, 42, 215-223 (2007)..

I.A. Karimi and Rajagopalan Srinivasan (Editors), Proceedings of the 11th International Symposium on Process Systems Engineering, 15-19 July 2012, Singapore.

Post-Combustion CO_2 Capture Process with Aqueous MEA: An Advanced MEA Process using a Phase Separation Heat Exchanger

Jaeheum Jung[a], Yeong Su Jeong[a], Ung Lee[a], Youngsub Lim[a], Seeyub Yang[a], Chi Seob Lee[b], Jaehyung Kim[b], Chonghun Han[†a]

[a]*School of Chemical and Biological Engineering, Seoul National University, Gwanak-ro 599, Gwanak-gu, Seoul 151-742, South Korea*
[b]*KEPCO Engineering & Construction Company, INC., 2354 Yonggudaero, Giheung-gu, Yongin-si, Gyeongi.do, South Korea*

Abstract

A CO_2 capture process using MEA (Monoethanolamine) scrubbing has been considered a leading technology in the early phase of the CCS (Carbon Capture & Storage) market due to its high CO_2 capture capacity and feasibility of use with existing power plant facilities. In spite of these advantages, this process has a disadvantage of requiring high energy for solvent regeneration in the stripper. For this reason, various improved solvents and process alternatives have been developed to reduce the solvent regeneration energy. This paper suggests an advanced MEA scrubbing process with a PSHE (phase separation heat exchanger) and shows its energy reduction effect using a commercial simulator. The main idea of the PSHE process is to reduce the reflux ratio of the stripper by sacrificing a part of the sensible heat recovery in the heat exchanger. In order to mitigate this sensible heat recovery loss, the PSHE process uses a phase separation heat exchanger. As a result, the PSHE process saves 123MJ/hr of condenser cooling energy while losing 51MJ/hr of sensible heat recovery in the phase separation heat exchanger. Consequently, the net energy reduction is 72 MJ/hr, and the ton CO_2 capture energy decreases about 14%, from 3.31 GJ/ton CO2 to 2.86 GJ/ton CO_2.

Keywords: CO_2 Capture Process, Post Combustion CO_2 Capture, MEA Scrubbing, Split Flow Configuration, Phase Separation Heat Exchanger

1. Introduction

The CO_2 capture process using MEA (Monoethanolamine) scrubbing has been considered as one of the most promising technologies to reduce CO_2 emissions. The MEA process is suitable for treating the flue gas from large CO_2 emission sources because of its high CO_2 capture capacity and feasibility for use with existing coal-fired power plant facilities. This MEA process, however, consumes a lot of heat energy for solvent regeneration in the stripper. In order to overcome this problem, various process alternatives have been developed such as absorber intercooling(Reddy, Johnson et al. 2008), lean vapor compression(Reddy, Johnson et al. 2008), staged feed of the stripper(Le Moullec and Kanniche 2011), split-flow configurations(Chang and Shih 2005), and integration of the power plant and amine scrubbing(Alie, Douglas et al. 2006). This paper suggests an advanced CO_2 capture process using the PSHE (phase separation heat exchanger), which inhibits water vaporization at the top of the stripper.

2. Typical CO_2 Capture Process using Aqueous MEA

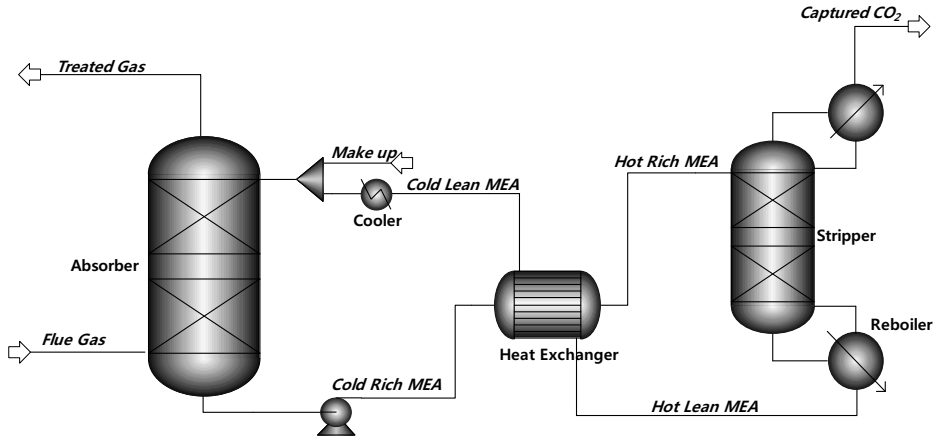

Figure 1. Process flow diagram of the reference process

The typical CO_2 capture process using MEA scrubbing is composed of an absorber and a stripper as indicated in Figure 1. The SO_x free flue gas enters at the bottom of the absorber (Flue gas) and cold lean solvent enters at the top of the absorber (Cold Lean MEA). In the absorber, the lean solvent selectively absorbs CO_2 by exothermic reaction and drains out at the bottom of the absorber (Cold Rich MEA). The remaining flue is purged out the top of the absorber (Treated Gas). The cold rich solvent is preheated by passing through the heat exchanger and enters at top of the stripper (Hot Rich MEA). In the stripper, the hot rich solvent desorbs CO_2 by endothermic reaction at the high temperature condition and drains out at the bottom of the stripper (Hot Lean MEA). The detached CO_2 is cooled by passing through the condenser and is captured at the top of the stripper (Captured CO_2). The hot lean solvent is cooled through the heat exchanger and cooler, and recycled at the top of the absorber to absorb CO_2 in the flue gas. Since the reboiler is the most energy intensive unit in this process, most of advanced MEA scrubbing processes target the reduction of the reboiler heat energy.

Table 1. Main stream information in Reference Process

Stream	Variable	Specification
Flue gas	CO2 composition	0.184 mol%
	Flow rate	18.46 kmol/hr
Solvent	MEA concentration	30 wt%
	Flow rate	2219 kg/hr
	Lean a (mol CO_2/ mol MEA)	0.27

3. Advanced MEA Process using a Phases Separation Heat Exchanger

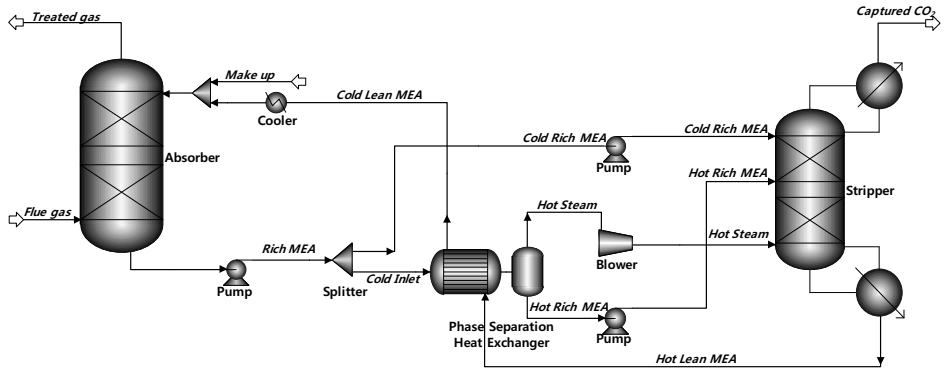

Figure 2. Process flow sheet of the phase separation heat exchanger process

The main idea of the PSHE process is to prevent water vaporization at the top of the stripper by reducing the temperature. In order to reduce this temperature, the cold inlet stream (Rich MEA) is split before it passes through the heat exchanger, as indicated in Figure 2. One of the split streams (Cold Rich MEA) directly enters and cools the top of the stripper. Consequently, this split cold stream prevents water vaporization, which simultaneously reduces both condenser and reboiler heat energy. This split flow configuration, however, diminishes sensible heat recovery in the heat exchanger because the cold stream's heat capacity is decreased by splitting the stream. In order to increase the cold stream's heat capacity, this PSHE process operates a phase separation heat exchanger in low pressure conditions. The cold stream is heated and vaporized in the phase separation heat exchanger. As a result, the cold stream heat capacity increases rapidly, which is increasing the amount of heat recovery in the phase separation heat exchanger. In the flash drum, the vaporized stream (Hot Steam) enters the bottom of the stripper as an energy source after it passes through the blower. The hot liquid (Hot Rich MEA) enters the middle of the stripper after it passes through the pump. As indicated in Table 2, 25% of the cold stream enters and cools the top of the stripper and 75% of the cold stream enters the phase separation heat exchanger for recovering sensible heat.

Table 2. Main process variables in the phase separation heat exchanger process

Unit	Variable	Specification
Heat exchanger	Cold side pressure drop	1.6atm to 1.2atm
Blower	Discharge pressure	2.1atm
Splitter	Split ratio to the top of the stripper	0.25
	Split ratio to the heat exchanger	0.75

4. Simulation Results

The main effect of the PSHE process is to cool the top of the stripper using the split cold stream. Consequently, the temperature at the top of the stripper is reduced from 101°C to 52 °C. Corresponding to this temperature drop, the condenser cooling energy is reduced from 136 MJ/hr to 13 MJ/hr, as indicated in Table 3. On the other hand, the PSHE process recovers less sensible heat in the heat exchanger compared with reference data. The amount of heat recovery loss is 51 MJ/hr which is about 10% decrease. It is commendable performance because only 75% of the cold stream recovers 90% of the sensible heat using the phase separation heat exchanger. Consequently, the net energy reduction is about 72 MJ/hr, and this value is reflected in the regeneration energy. The regeneration energy is summation of blower energy and reboiler energy. In order to convert electrical energy to thermal energy, 10 MJ/hr of blower electrical power is converted to 20 MJ/hr of heat energy. The regeneration energy in the PSHE process is lower than that in the reference process by 61 MJ/hr. The ton CO_2 capture energy decreases about 14%, from 3.31 GJ/ton CO_2 to 2.86 GJ/ton CO_2.

Table 3. Summary of the energy recover and consumption in each unit

	Heat exchanger heat recovery [MJ/hr]	Condenser cooling duty [MJ/hr]	Blower power [MJ/hr]	Reboiler heat duty [MJ/hr]	Ton CO_2 Capture Energy [GJ/ton CO_2]
Reference Process	539	136	-	446	3.31
PSHE Process	488	13	10	365	2.86

5. Conclusion

The MEA scrubbing CO_2 capture process has been considered as one of the most promising techniques to reduce CO_2 emissions. However, this process has a disadvantage of requiring high energy for water vaporization in the stripper, which is a common issue when using aqueous solvent. To overcome this problem, this paper suggests an advanced MEA scrubbing CO_2 capture process, the PSHE process. In the PSHE process, one of the split cold rich streams is fed into the stripper to reduce the reflux ratio, and the other split cold rich stream recovers sensible heat in the phase separation heat exchanger. As a result, the condenser heat energy saving is about 123 MJ/hr, and the sensible heat recovery loss is about 51 MJ/hr. Consequently, the net energy reduction is about 61 MJ/hr, and the ton CO_2 capture energy decreases about 14% compared with the reference process.

6. Acknowledgement

This research was supported by the second phase of the Brain Korea 21 Program in 2012, Institute of Chemical Processes in Seoul National University, Strategic Technology Development and Energy Efficiency & Resources Development of the Korea Institute of Energy Technology Evaluation and Planning (KETEP) grant funded by the Ministry of Knowledge Economy (MKE) and grant from the LNG Plant R&D Center funded by the Ministry of Land, Transportation and Maritime Affairs (MLTM)

of the Korean government.

References

Alie, C., P. Douglas, et al. (2006). Simulation and optimization of a coal-fired power plant with integrated CO2 capture using MEA scrubbing.

Chang, H. and C. M. Shih (2005). "Simulation and Optimization for Power Plant Flue Gas CO2 Absorption-Stripping Systems." Separation science and technology **40**(4): 877-909.

Le Moullec, Y. and M. Kanniche (2011). "Optimization of MEA based post combustion CO2 capture process: Flowsheeting and energetic integration." Energy Procedia **4**: 1303-1309.

Reddy, S., D. Johnson, et al. (2008). Fluor's Econamine FG Plus SM Technology for CO2 Capture at Coal-fired Power Plants.

I.A. Karimi and Rajagopalan Srinivasan (Editors), Proceedings of the 11th International Symposium on Process Systems Engineering, 15-19 July 2012, Singapore.

A superstructure model of water-using network synthesis with multiple contaminants for batch processes and its solution

Xia YANG, Jincai YUE, Shiqing ZHENG

Research Center for Computer and Chemical Engineering, Qingdao University of Science and Technology, Qingdao 266042, China

Abstract

The key contaminant component (KCC) is defined to establish a superstructure model of water-using network synthesis for batch process with multiple contaminants, which uses storage tanks to eliminate the time limitations for water reuse or recycle, and its mathematic programming model is established and solved by nonlinear programming (NLP) method by a two-step solution strategy. Finally, an example is illustrated to show the efficiency of this method.

Keywords: water-using network; multiple contaminants; superstructure model; batch process

1. Introduction

Since Wang and Smith (1994) addressed the minimization of wastewater in the process industries, water-using network synthesis (WNS) targeted for freshwater and/or wastewater minimization in these industries has become an urgent task because these industries not only consume enormous fresh water, but discharge enormous wastewater containing many kinds of dangerous contaminants.

Over decades lots of techniques of WNS for process industries are developed, but it is much less for batch process than for continuous process as batch process is not steady and must be described by (partial) differential equations. R.Grau et. al.(1996) developed a mathematical technique for waste minimization with emphasis on waste generated during changeover. M.Almato´(1999) adopted a mathematical programming to optimize the network and get the assignment coefficient between tank and operation. Yao and Yuan (2000) developed a discrete time mathematical model by optimizing production campaigns. J.K Kim and R. Smith(2004) considered time constraints and the network design and systematically identified minimum cost. D.C. Foo etc.(2005) developed a new two-stage approach to synthesize a batch maximum water recovery network based on pinch technology. T. Majozi.(2005) developed a continuous-time mathematical formulation using central reusable water storage in batch wastewater minimization. Cheng (2007) presented a mathematic programming model for batch WNS with single contaminant, and Yang (2007) developed a time-purity two dimensional graph method to design water network for batch. E. Dogaru and V. Lavric (2011) took a water network for a batch process as a dynamic structure which changes its topology at fixed time intervals delimited by events. M. Bagajewicz (2000) and J. Jezowski (2010) both gave a detailed overview on the subject.

This paper presents a superstructure model of water-using network synthesis for batch process with multiple contaminants (BMWNS) and develops a two-step strategy of solution, the detail is as followed.

2. Model Establishment and Solution

2.1. Key contaminant component definition

Though there are multiple contaminants for a water-using unit j (WU_j), only one contaminant affect the fresh water usage of WU_j, so the key contaminant component (KCC) of the unit, which is denoted as key can be written by the following formula:

$$M_{f,j,key} = \frac{m_{j,key}}{c^{\max}_{j,key,out}} = \max_{i=1}^{C}\left(\frac{m_{i,j}}{c^{\max}_{i,j,out}}\right) \tag{1}$$

In which, M stands for water mass flowrate, ton; m for contaminant mass transfer, kg; C and c stands for the number of contaminants and contaminant concentrations (ppm) respectively, the subscrip f stands for fresh water, and the subscript out stands for the outlet of WU_j.

2.2. Superstructure model establishment

All water-using units (WUs) are sorted firstly according to their water-using starting time, if the WUs with the same starting time are taken as the same sequences; then the KCC of every units are determined by Eq.(1), and by which water sources are determined for every units according to their water-using time sequences. Figure 1 describes partial superstructure of unit j, the cylinders stand for storage tanks, cylinder 0 storages fresh water, cylinder w storages waste water; WU_j has three water sources (including fresh water), its outlet water is used as water sources by two units and the rest is discharged.

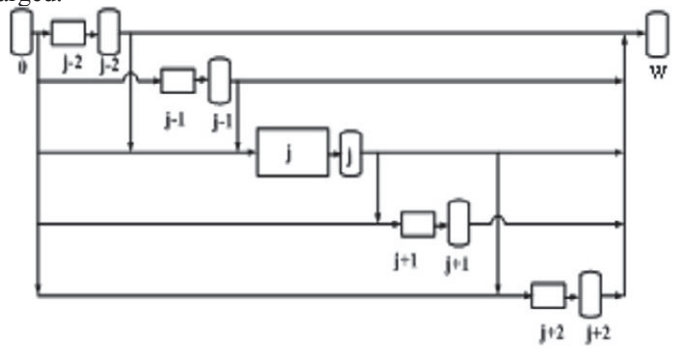

Fig.1 the partial superstructure of WU j for batch

2.3. mathematical model

A double layer mathematical model is developed to describe the superstructure of water-using network for batch, which includes the inner model and the outer model: the former is to find the minimum freshwater of unit j in the current water-using period, and the latter is to find the minimum freshwater of all units in the current water-using period. During a water-using process with N units, there are p ($p \le N$) water sources for WU_j, and its discharged outlet water is taken as q ($q \le N$)water sources. The mathematical model is written as equations from (2) to (14). In which, F stands for water mass flowrate, ton/h, t for water-using time, hour; the superscript $surplus$ for the surplus water in storage tank; and the superscript e, s and new for starting time and end time of the WUs, the new data of the next cycle respectively. It is clear that equation (6) and (7) are not linear so the model is a nonlinear problem (NLP).

Outer model: min $z = \sum_{j=1}^{N} M_{f,j}$ (2)

$$\text{s.t. } M_{f,j,surplus}^{new} = M_{f,j,surplus} - \sum_{j=1}^{N} M_{f,j} \quad (3)$$

Inner model: min $z = M_{f,j}$ (4)

$$s.t.\ M_j = M_{f,j} + \sum_{ij=1(ij\neq j)}^{p} M_{j,ij} \quad (5)$$

$$m_{j,key} = M_j \cdot (c_{j,key,out} - c_{j,key,in}) \quad (6)$$

$$M_j \cdot c_{j,key,in} = \sum_{ij=1(ij\neq j)}^{p} M_{ij,j} \cdot c_{j,key,out} + M_{f,j} \quad (7)$$

$$\sum_{i=1}^{q} M_{j,i} \le M_{j,surplus} \quad (8)$$

$$M_{j,surplus}^{new} = M_{j,surplus} - \sum_{i=1}^{q} M_{j,i} \quad (9)$$

$$M_i = F_i(t_i^e - t_i^s) \quad (10)$$

$$M_{j,i} = F_{j,i}(t_i^e - t_i^s) \quad (11)$$

$$M_{f,i} = F_{f,i}(t_i^e - t_i^s) \quad (12)$$

$$0 \le c_{j,key,in} \le c_{j,key,in}^{\max} \quad (13)$$

$$0 \le c_{j,key,out} \le c_{j,key,out}^{\max} \quad (14)$$

2.4. model solution strategy

2.4.1. the first step

In the first step, time constraints are not considered in the model, so there are only concentration variables for every WUs. The minimum limiting flowrate is introduced as equation (15).

$$F_j^{\min} = \max_N \left(\frac{c_{j,key,out}^{\max} - c_{j,key,in}^{\max}}{c_{j,key,out}^{\max}} \cdot F_j^{\max}\right) \quad (15)$$

The obtained result is an optimum water-using network with only concentration consideration for batch, since a storage tank is connected with every water unit, the obtained water-using structure could be the target network for the problem.

2.4.2. the second step

Time constraints are taken into the model, and the main task is to design storage tanks before the network steady. The water-using network with time consideration is designed in terms of the target network from the first period to the next until the network reaches its steady state.

3. Case study

A water-using process with 3 contaminants and 3 water-using units is illustrated here to demonstrate the practicability of the established model and the efficiency of the presented solution methods, water-using data are listed in table 1. It is seen from table 1 that the total fresh water usage is 128.3ton before WNS, and the original water-using network is as figure 2.

Table 1 Water using data of the case

j	i	$C_{i,in}^{max}$ 10^{-6}	$C_{i,out}^{max}$ 10^{-6}	t^s h	t^e h	m kg
	1	100	400			30
1	2	200	400	1	1.5	20
	3	50	200			15
	1	0	200			8
2	2	0	100	1	1.5	4
	3	0	50			2
	1	100	200			2.5
3	2	50	100	0	0.5	1
	3	50	150			2

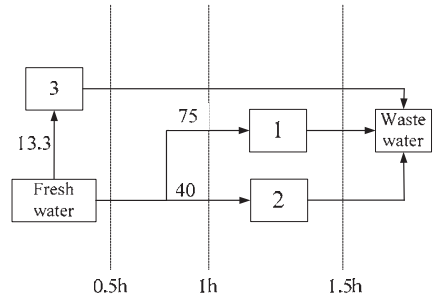

Fig.2 Original network for the case

According to the presented method above, firstly WNS problem is regarded as a pseudo-continuous process without time constraints consideration, the, the optimum water-using network is seen as figure 3, and which is the target network for the case, the minimum fresh water usage is 102.5 ton.

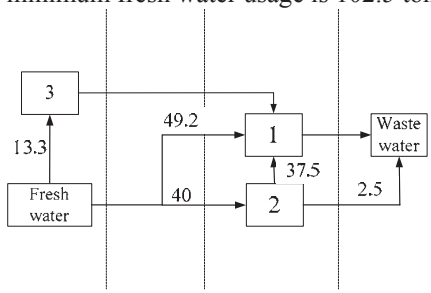

Fig. 3 The target network for the case

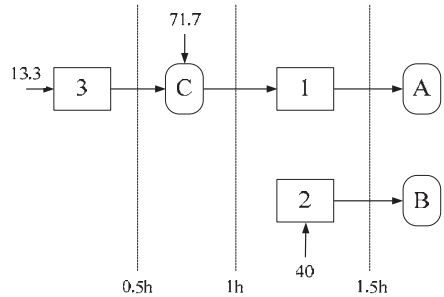

Fig. 4 Water network in the first period

Secondly, time constraints are considered in the model. In the first period, every water-using units are not steady, and no outlet water could be reused, so water sources are only fresh water, so unit 3 could be only use fresh water during 0-0.5h; during 1.0-1.5h, unit 2 is not steady so that its outlet water could not be reused, so unit 2 could only be used fresh water, however unit 1 as the last water-using unit it could be used the outlet water of unit 3; the outlet water of unit 1 and 2 are fed into storage tank A and B respectively, therefore the first period finished and the obtained network is shown as figure 4.

It could be seen that unit 2 and unit 3 are steady by comparison figure 4 with figure 3, but unit 1 is not steady, so the second period must be calculated, and the obtained network is shown as figure 5.

It could be seen that all units are steady by comparison figure 5 with figure 3, so the network is steady and also reached the target fresh water usage 102.5 ton, which reduces 20% compared with the original 128.35 ton.

The final optimum water network is obtained by more optimizing the location and number of storage tanks, which is shown as figure 6.

4. Conclusions

A superstructure model for water-using network synthesis with multiple contaminants for batch process is established in the paper, in which the key contaminant component is defined and adopted. Because of time characteristics of batch the model reduction rules are put forward and a two-step solution method is presented, the first step is to determine the target network for the problem by not considering time constraints, and the second step is to determine the final optimum water-using network by optimizing the storage tanks in terms of the obtained target network. At last, a case is introduced, the calculation results show the model is practical and the solution method is efficient.

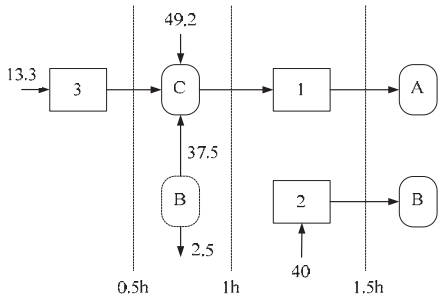

Fig. 5 Water network in second period

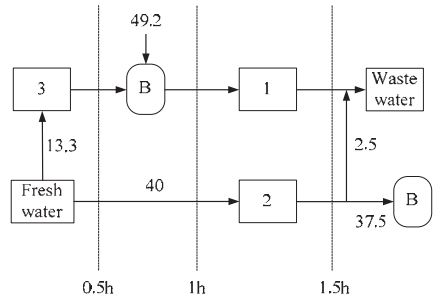

Fig. 6 Final water using network

References

D.C.Y. Foo, Z. A. Manan and Y. L. Tan., 2005, Synthesis of maximum water recovery network for batch process systems. Journal of Cleaner Production, Volume 13, Issue 15, Pages 1381-1394

E. Dogaru,V. Lavric, 2011, Dynamic Water Network Topology Optimization of Batch Processes, Ind. Eng. Chem. Res. Volume 50, Issue 7, Pages 3636–3652

H. N. Cheng, 2007, Fresh water minimization for batch process with single contamination based on linear programming. Journal of Chemical Industry and Engineering (China), Volume 58, Issue 2, Pages 417-424

J. Jezowski, 2010, Review of Water Network Design Methods with Literature Annotations, Ind. Eng. Chem. Res. 2010, Volumn 49, Issue 10, Pages 4475–4516

J.K Kim, R. Smith,2004, Automated design of discontinuous water systems. Transactions of the Institute of Chemical Engineers, Part B, 82(B3), Pages 238-248.

M. Bagajewicz, 2000, A review of recent design procedures for water networks in refineries and process plants, Computers and Chemical Engineering, Volumn 24, Issue 9, Pages 2093–2113

M. Almató, A. Espuña, L. Puigjaner., 1999, Optinization of water use in batch process Industries. Computers and Chemical Engineering, Volume 23, Pages 1427-1437

R. Grau, M. Graells, J. Corominas, A. Espun˜a & L. Puigjaner, 1996, Global strategy for energy and waste analysis in scheduling and planning of multiproduct batch chemical processes. Computers and Chemical Engineering, Volume 20, Pages 853–868.

T. Majozi., 2005, Wastewater minimisation using central reusable water storage in batch plants .Computers & Chemical Engineering, Volume 29, Issue 7, Pages 1631-1646

X. Yang, J.C. Yue, R.S. Bi, et. al., 2007, Single contaminant water network design for batch processes, Journal of Chemical Industry and Engineering(China), Volume 58, Issue 1, Pages 161-167

Y.P. Wang, R. Smith, 1994, Wastewater minimisation. Chemical Engineering Science, Volumn 49, Issue7, Pages 981-1006.

Z. L. Yao, X.G. Yuan, 2000, An approach to optimal design of batch processes with waste minimization. Computers and Chemical Engineering, Volume 24, Pages 1437–1444.

I.A. Karimi and Rajagopalan Srinivasan (Editors), Proceedings of the 11th International Symposium on Process Systems Engineering, 15-19 July 2012, Singapore.

Effects of greenhouse gas emission on decentralized wastewater treatment and reuse system

Hyunjoo Kim[a], Yujin Cheon[a], Ho-Kyung Lee[b] and In-Beum Lee[a]

[a]*Department of Chemical Engineering, POSTECH, Pohang, Kyungbuk 790-784, Republic of Korea*
[b] *LG Chem, Ltd / Research Park, Daejeon 305-380, Republic of Korea*

Abstract

There are growing concerns on greenhouse gas (GHG) emission from wastewater treatment. It is generally known that decentralized treatment of wastewater allows industrial sectors to increase wastewater reuse rate, meanwhile usually consume more energy resulted additional GHG emissions. Therefore the optimized wastewater reuse system can be largely differed when GHG emissions are considered.
We optimized industrial wastewater reuse networks considering GHG emissions. We constructed a mathematical model of wastewater reuse network including intermediate treatment facilities and a final treatment plant. Amount of emission was calculated then converted to monetary terms via carbon price and cost minimization was performed.
An industrial sector with four types of plants was selected as a case study. We figured out changes in the system when installation of intermediate facilities was allowed. If decentralized treatment and reuse were adopted the amount of freshwater consumption were decreased to 65% of the base case; when GHG emissions were considered as additional cost, the freshwater consumption increased to 87%, which is a drawback from the former case. Sensitivity analyses on the GHG expenses were performed which showed importance of pricing scheme on the network formation.

Keywords: wastewater reuse, greenhouse gas, decentralized treatment

1. Introduction

As greenhouse gases (GHG) from human activities are believed to be a main reason of climate change, estimating GHG emission draws strong interests in various fields these days. Water and wastewater treatment is not an exception; water and wastewater plants have been known as one of the most common minor source of GHG emission. In consequence there are growing numbers of researches estimating GHG emission and its impacts in water treatment and utilization. (Shahabadi et al. 2009; Fine and Hadas 2011)
It is generally known that introducing decentralized wastewater treatment encourages industrial sectors as well as urban water systems to increase water reuse ratio with shorter pipe length and easier source/effluent quality control.(Orth 2007) However, decentralized treatment facilities designed for wastetewater recycling and/or reuse usually adopt advanced treatment methods which require relatively more energy. Therefore the optimized wastewater reuse system with decentralized treatment can be largely differed when GHG emissions are considered.
In this research we optimized industrial wastewater reuse networks considering GHG emissions. We constructed a mathematical model of wastewater reuse network including intermediate treatment facilities and a final treatment plant. A wastewater network of an industrial sector was optimized as a case study and results were discussed.

2. Methodology

2.1. GHG emissions in wastewater reuse

GHG emissions from wastewater treatment are generally classified into two categories: (1) direct emissions from biological degradation (2) indirect emissions from energy usage, mainly electricity. While typical secondary treatment facilities show higher direct emission ratio, major part of emissions in advanced treatment methods are from their electricity use since their general aim is to remove metals and recalcitrant organics which do not discharge biological GHGs like methane when removed. (Environment Agency 2009)

2.2. Mathematical formulation of wastewater reuse network

Figure 1 shows general configuration of water network in an industrial sector adopted in this research. The network includes four types of unit process; manufacturing processes, decentralized (intermediate) treatment facilities, final treatment center and reclamation unit as its annex. Flow and mass balance equations were developed and listed in Table 1.

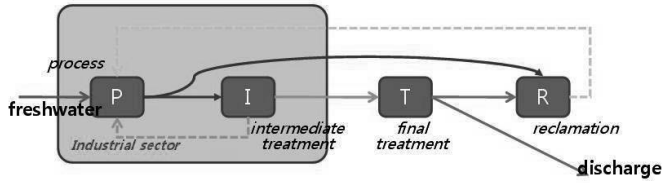

Figure 1. General wastewater reuse network

Table 1. Flowrate and mass balance equations

	Flowrate balance	Mass balance
Manufacturing process	$fw_p + \sum_i rg_{i,p} + rc_p \geq fpin_p$, $fpout_p = \sum_i wwi_{p,i} + wwt_p$	$Cfw_p fw_p + \sum_i Crg_{i,p} rg_{i,p} + Crc_p rc_p \leq Cfpin_p (fw_p + \sum_i rg_{i,p} + rc_p)$, $Cfpout_p = Cwwi_{p,i} = Cwwt_p$
Intermediate treatment	$\sum_p wwi_{p,i} = fiin_i$, $fiin_i = fiout_i$, $fiout_i = \sum_p rg_{i,p} + wwd_i$	$\sum_p Cwwi_{p,i} wwi_{p,i} = Cfiin_i fiin_i$, $Cfiin_i = \chi \cdot Cfiout_i$, $Cfiout_i = Crg_{i,p} = Cwwd_i$
Final treatment	$\sum_p wwt_p = ftin$, $ftin = ftout$, $ftout = wwr + dc$	$\sum_p Cwwt_p wwt_p = Cftin \cdot ftin$, $Cftout = Cwwr = Cdc$
Reclamation unit	$wwr + \sum_i wwd_i = frin$, $frin = frout$, $frout = \sum_p rc_p$	$wwrCwwr + \sum_i Cwwd_i wwd_i = frinCfrin$, $Cfrout = Crc_p$

2.3. Economic evaluations

In developing wastewater reuse network economic evaluation is a must, since cost reduction is one of the main reasons of wastewater reuse. We calculated total annual

expenses of the network with capital and O/M cost including charges for water consumption and wastewater discharge and individual treatment facility operation cost if introduced.
In this research we dealt with different expensing schemes for direct and indirect GHG emissions. For emissions from electricity use from pumping and freshwater consumption a fixed carbon tax was imposed. In the case of emissions from treatment facilities carbon credit method was introduced.

3. Case Study

3.1. System descriptions
We carried out a case study with the mathematical model and optimization strategy. A South Korean industrial sector with 15 plants discharging highly contaminated wastewater with metals and chemicals was selected as a case study. The plants were categorized into four business types (general, cements, chemicals, textile) and standard concentration values were assigned for each category if not specified.

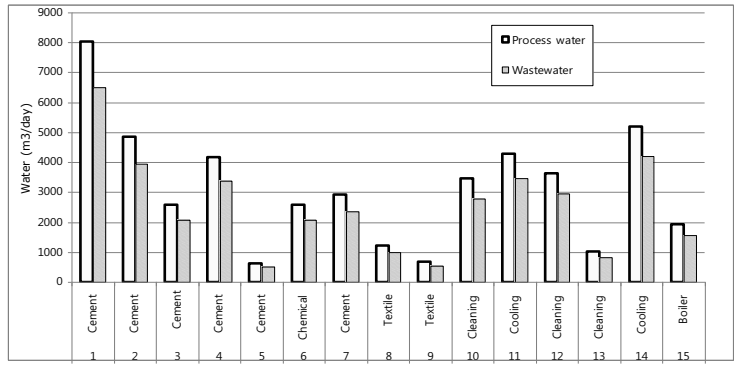

Figure 2. Water/wastewater characteristics of plants in the sector

Two types of intermediate treatment facilities, reverse osmosis (RO) and microfiltration (MF), were considered. Their cost, treatment efficiencies as well as GHG emission were presented in Figure 3.
Cost minimization was performed (1)considering decentralized treatment facilities, without GHG expenses (2) under cost objective function with GHG expenses. Then the results were compared and analyzed.

3.2. Results
While a wastewater reuse network can be formulated without intermediate treatment center, decentralized facilities gave more reuse oppotunities to the system. Amount of wastewater reuse decreased when additional expense from GHG emissions was included. The reuse amount reduction in the latter case was mainly due to the additional GHG expenses, since total GHG emission of the system was decreased to 25% of the second case(9,812,000 to 2,514,000 kgCO_2/day).
As shown in Figure 5, RO was favored in both cases. Better treatment efficiency of RO was the major reason of the preference despite of the higher capital cost. It was also noticeable from figure 4 and 5 that reclaimed water from intermediate facilities was much preferred when GHG emissions were considered.

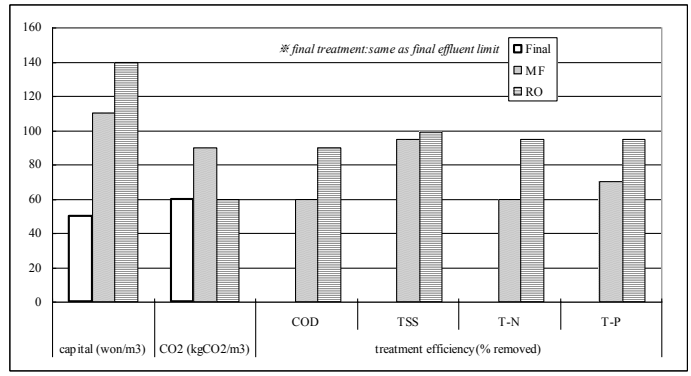

Figure 3. Characteristics of treatment facilities

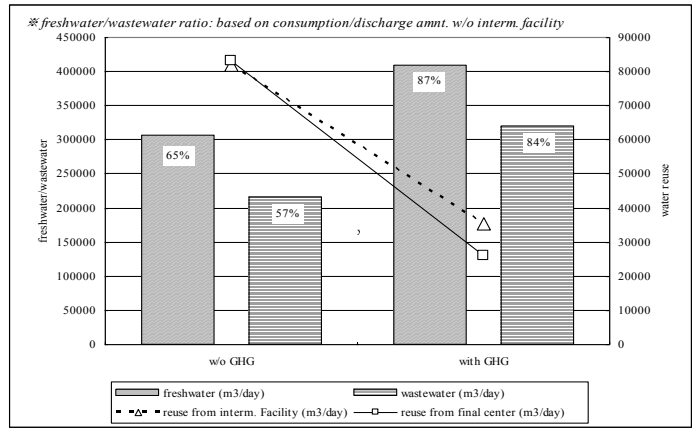

Figure 4. Amount of water consumption/discharge and reuse under different obj. functions

To figure out effects of GHG expense to the system we performed a couple of sensitivity analysis on GHG price. When GHG tax on freshwater increased, amount of reuse was increased to some extent then remained on the same. In the case of carbon capping for facilities, as carbon tax increased amount of reuse from intermediate facilities were decreased.

Based on the sensitivity analyses the pricing rule which enabled maximun amount of reuse can be derived. While the result cannot be adopted directly because of the lack of data validation, it shows that a proper GHG pricing scheme is necessary for developing effective reuse networks.

4. Conclusions

Wastewater reuse network with decentralized treatment facilities were developed and optimized considering GHG emissions from both direct and indirect sources. While decentralized facilities increased reuse potential within the system, additional expenses from GHG emission gave negative effects on wastewater reuse. By modifying GHG pricing scheme the reuse network can be evolved into more efficient one.

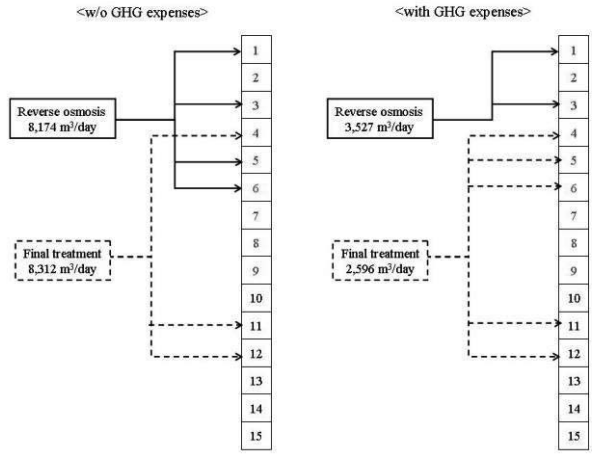

Figure 5. Reclaimed water usage

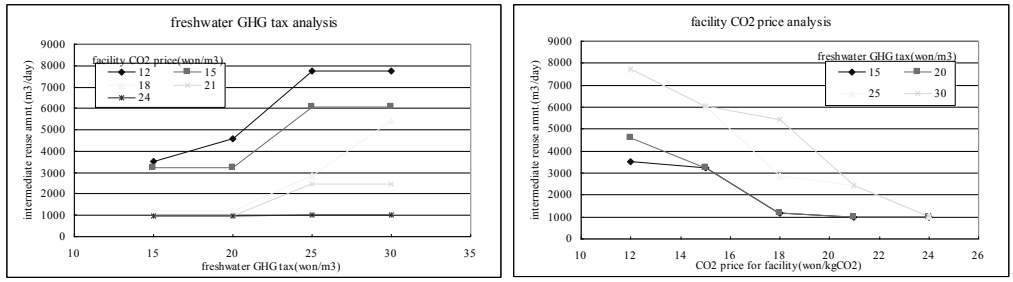

Figure 6. Total freshwater consumptions under different GHG pricing schemes

Nomenclature

p: manufacturing process ; i: intermediate treatment facility ; fw_p: freshwater into process p
$rg_{i,p}$: reclaimed water from intermediate facility i to process p
rc_p: reclaimed water from final reclamation unit to process p
$wwi_{p,i}$: wastewater from process p to intermediate treatment facility i
wwt_p: wastewater from process p to final treatment center
$fiin_i$: wastewater into intermediate facility i ; $fiout_i$: reclaimed water from intermediate facility i
wwd_i: reclaimed water from intermediate facility i to reclamation unit
ftin: wastewater into final treatment center ; ftout: reclaimed water from final treatment center
wwr: reclaimed water from final treatment center to reclamation unit ; dc: discharged water
frin: reclaimed water into reclamation unit ; frout: reclaimed water from reclamation unit

References

M. B. Shahabadi , L. Yerushalmi, F. Haghighat, Impact of Process Design on Greenhouse Gas Generation by Wastewater Treatment Plants, Water Research, 43,10, 2009, 2679-2687

P. Fine, E. Hadas, Options to Reduce Greenhouse Gas Emissions During Wastewater Treatment for Agricultural Use, Science of The Total Environment, 2011, Article in press

Environment Agency, Transforming Wastewater Treatment to Reduce Carbon Emissions, 2009

H. Orth, Centralised versus decentralised wastewater systems?, Water Science & Technology, 56,5, 2007, 259-266

I.A. Karimi and Rajagopalan Srinivasan (Editors), Proceedings of the 11th International Symposium on Process Systems Engineering, 15-19 July 2012, Singapore.

Optimal Membrane Desalination Network Synthesis with Detailed Water Quality Information

Sabla Y. Alnouri, Patrick Linke

Department of Chemical Engineering, Texas A&M University at Qatar, Education City, PO Box 23874, Doha, Qatar,
sabla.alnouri@qatar.tamu.edu; patrick.linke@qatar.tamu.edu

Abstract

This work builds on a previously developed superstructure optimization approach for SWRO desalination network design, and expands the richness of the representation by accounting for multiple water quality parameters, including boron. This involves replacing conventionally-simplified feed solution assumptions, and incorporating multiple water quality parameters into the SWRO network optimization problem. In doing so, simple correlations capable of predicting RO membrane performance, according to salt rejection characteristics, is carried out by exploiting numerical simulation data via the specialized commercial membrane design software such as ROSA Filmtech (Reverse Osmosis Systems Analysis). A number of additional degrees of freedom are introduced into the problem, such as the pH level, since it considerably affects the boron removal efficiency. Moreover, the superstructure representation has been extended to include multiple membrane element choices for the different SWRO units within the network, rather than strictly limiting the network design to a single membrane type, thus allowing the assessment of several choices of membrane types within a single optimization. Moreover, enhanced economic and environmental assessment procedures are adapted, that capture more genuine and accurate design performance predictions. The method is illustrated through a case study example involving a typical seawater feed.

Keywords: *desalination; reverse osmosis; process design; multiple water quality parameters; boron removal*

1. Introduction

Membrane-based water desalination technologies have become increasingly attractive, as well as globally utilized in order sustain the rapid increase in demand for potable water [1]. The design of such desalination processes resembles a network synthesis problem, for which the utilization of a superstructure optimization approach is employed to identify plausible design candidates, given certain desirable performance conditions and constraints. However, it is often realized that many previous approaches, although capable of capturing rich sets of process configurations, generally lack the ability to handle detailed water quality information as part of the process synthesis and optimization problem [2, 3]. This usually presents inconsistency in terms of the richness of the solutions obtained since detailed information is often essential when assessing important operational and product constraints. Handling multiple water quality parameters are of preeminent importance, especially within a desalination network design problem, due to the variable scaling tendency of certain seawater components. Therefore, it is essential to capture multiple water quality parameters when solving a

SWRO network design problem, as opposed to adopting the standard assumption of two pseudo components, i.e. “water” and “total dissolved solids”. This would enable the design impact of important phenomena to be addressed, most importantly membrane scaling and, boron removal.

2. Synthesis Approach

This work adopts a well-defined SWRO network synthesis strategy representation introduced previously [4], that involves two main steps:

2.1. Targeting: The performance target of the system is determined through global optimization of full superstructures, in which the best performing design is extracted and subsequently used as a benchmark whilst assessing different design alternatives.

2.2. Development of Alternative Designs: Reduced superstructures resembling fundamentally distinct design classes are globally optimized, such that design alternatives of increasing complexity can be identified. Therefore, insights for potential performance advantages, any complex designs offer over more simple designs can be analyzed.

3. Accounting multiple water quality parameters

The prediction of membrane desalination process performance in relation to a reflective multiple water quality nature within the network is of imminent importance, since the presence of turbidity and high concentration levels of hardness ions, such as calcium and magnesium, tend to degrade a SWRO plant performance [1]. Therefore, effective knowledge regarding the concentrations of the various sweater components (especially dissolved ions which are usually lumped together as a Total Dissolved Solids “TDS” category) would drastically improve understanding of the behavior of such components in a SWRO network optimization problem. Simplified analytical relations that provide technical membrane performance information, in terms of salt rejection capacities of individual ions are developed accordingly. Such water quality parameter information is extracted from available membrane commercial simulators, such as ROSA Filmtech (Reverse Osmosis Systems Analysis) [5]. All data extracted are in the form of simple linear relationships relating ion-specific rejection characteristics to temperature, and such relevant information pertaining to membrane performance, serve with relatively sufficient accuracy over typical variations in operating conditions.

4. Accounting for boron removal requirements

Standard boron removal techniques, that would effectively achieve low boron levels in the permeate have been previously presented and adopted [6-8]. Therefore, models that predict boron removal efficiency within a SWRO network optimization problem are very imperative for an accurate determination of plausible designs. Operating parameters such as the temperature and pH, affect the levels of boron removed from the permeate stream. Thus, in order to enable accurate predictions for the purpose of screening the various boron removal options, simplified analytical relations are developed for multiple membrane element choices. This enables the superstructure optimization to determine SWRO networks that feature different types of membrane elements in different parts of the network, targeting the removal of specifically important water quality parameters. For each membrane element choice, correlations are using the combined effects of temperature and pH onto boron rejection, as well as all other ions constituting the feedwater, for a number of commercial membrane elements:

BW30-2540, SW30HRLE-4040, SW30-2540 and SW30HRLE-400i. The information regarding these modules has been extracted from ROSA, in order to capture the observed membrane element performance.

5. Enhanced economical assessment considerations

To enable the extraction of meaningful solutions, we have formulated a comprehensive economic objective function, so as to capture the multiple fixed and variable costs associated with real SWRO plants. This is implemented through the use of a thorough cost breakdown assessment procedure, consisting of computations for the Total Annualized Cost (TAC) as function of an annualized form of Total Capital Investment (TCI), involving Direct Capital Costs (DCC), Soft Costs (SC) as well as a Contingency Cost (CC) factor, all added to the Total Operating Cost (TOC) of the system, both Variable O&M Costs (VOC), and Fixed O&M Costs (FOC). [1, 9-13]. A Lang Factor (LF) and a Depreciation (D) value were assumed to be associated with the total capital investment term, over the useful plant lifetime.

6. Mathematical Formulation & Implementation

The problem formulation involves a performance assessment criterion as an objective, relating various operational and capital cost elements to the design variables. System constraints involving mass balance calculations around the inlet process splitter, outlet process mixers, mixers and splitters associated with individual membrane units in the system (both reject and permeate) are formulated. The resulting optimization problem takes the form of a Mixed Integer Non Linear Program (MINLP), in which the aim was to minimize the total annual cost (TAC), subject to process equality and inequality constraints. Given these conditions, the optimization problem is solved using "*what'sBest"* LINDO Mixed-Integer Global Solver for Microsoft Excel [14], so as to keep the implementation simple and user friendly.

7. Case Study

A seawater desalination case study example is carried out using the modified representation, which has been introduced in previous work [4]. The capability of extracting multiple water quality information, boron removal efficiency, and assessing the performance of several membrane element types within the optimization problem is implemented. Table 1 summarizes some of the input parameters for the case study using a typical seawater feed (salinity 34.39 g/L). Figure 1 illustrates an optimal solution example attained using superstructure optimization for a design that incorporates three units, where both exiting streams from first RO unit are treated using both a subsequent stage and pass simultaneously. The solution was obtained in 74s of CPU time on a on a desktop PC (Intel® Core ™ i7-2620M, 2.7 GHz, 8.00 GB RAM). Table 2 summarizes the water quality information extracted, for the network reject and permeate. Therefore, the example illustrates how detailed insights into water quality dependent problem features can be explored within reasonable CPU times using the proposed approach. The total annual cost of the design illustrated was found to be \$0.574/m^3, with an annual fixed cost of \$0.107/ m^3, and an operating cost of \$0.466/m^3 of water produced.

Table 1- Case Study Input Data

Parameter	*Value*
Total inlet feedwater flowrate into the network (m^3/day)	40,000
Minimum permeate flow required in the network (m^3/day)	12000
Maximum allowable TDS in the permeate (ppm)	450
Maximum allowable boron concentration in the permeate (ppm)	0.5
Pressure drop in RO unit j (bar)	1.3
Maximum allowable feed pressure using SW RO elements (bar)	70
Maximum allowable feed pressure using BW RO elements (bar)	15.5
Temperature (^oC)	25
Number of Skids	1
Lang Factor	5
Depreciation (yr)	20
Power Cost ($/kWh)	0.05

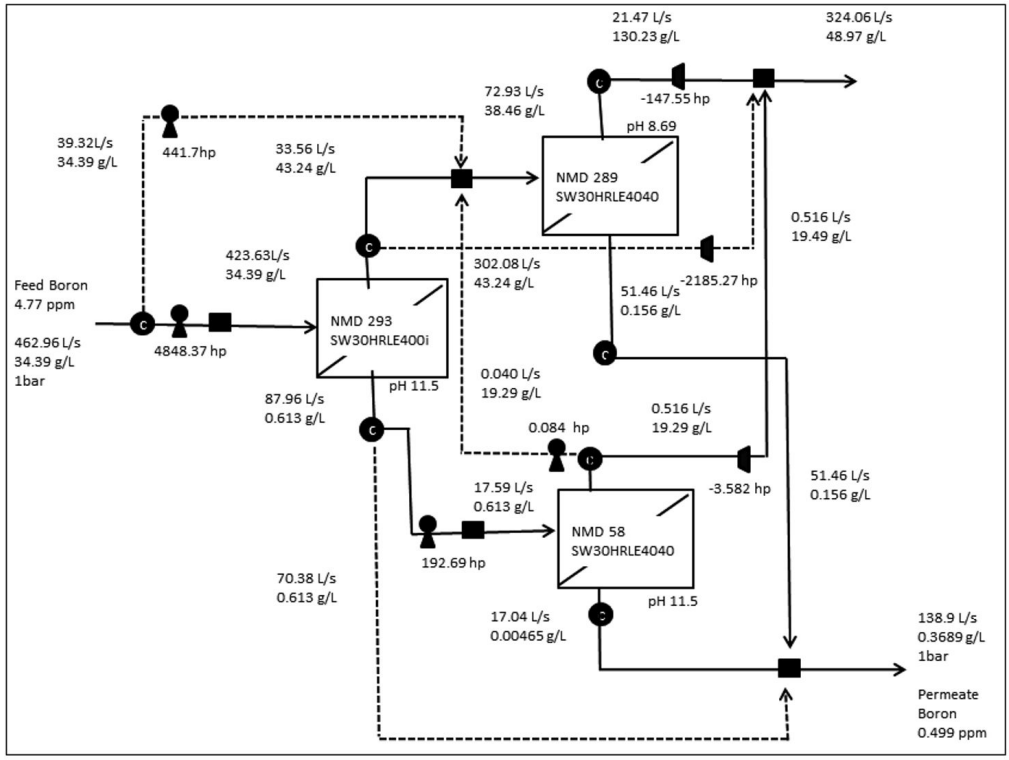

Figure 1. Typical seawater feed, optimal solution example involving a three-unit design case

Table 2. Water quality information extracted

Ions	*Feed (mg/L)*	*Permeate (mg/L)*	*Reject (mg/L)*
K	380	10.68	538.27
Na	10556	246.75	14974
Mg	1262	7.07	1799.8
Ca	400	2.21	570.47
Sr	13	0.07	18.54
HCO3	140	3.20	198.62
SO4	2649	56.91	3760
Cl	18985	42.58	27103
Boron	4.77	0.499	6.60
TDS	34390	368.95	48970

7. Conclusions

This paper involves the utilization of a superstructure optimization approach, and expands the proposed representation so as to incorporate additional water quality parameters, including boron considerations, as well as multiple membrane element choices into the SWRO network optimization problem. Data extracted for various membrane elements, that predict water quality parameters using commercial membrane software, are employed. A case study that illustrates the various features of the problem is demonstrated, and it was shown that the solutions extracted become a lot richer, within reasonable CPU computational timings.

References

1. A. Cipollina, G. Micale, L. Rizzuti, Seawater Desalination Conventional and Renewable Energy Processes (2009), Springer-Verlag Berlin Heidelberg
2. M. El-Halwagi, AIChE Journal, 38 (8) (1992) 1185-1198.
3. Y. Saif, A. Elkamel, M. Pritzker, Ind. Eng. Chem. Res. 47 (1) (2008) 3060-3070.
4. S. Alnouri, P. Linke (2012). Reliable and Efficient Targeting for Optimal Design of SWRO Desalination Processes. In I.D.L. Bogle and M. Fairweather (eds), Proceedings of the 22nd European Symposium on Computer Aided Process Engineering, 17 - 20 June 2012, London, Elsevier
5. http://www.dowwaterandprocess.com/support_training/design_tools/rosa.htm
6. P. Glueckstern, M. Priel, Desalination 156 (1–3) (2003) 219–228.
7. N. Nadav, M. Priel, P. Glueckstern, Desalination 185 (1–3) (2005) 121–129.
8. L.F. Greenlee, et al., Water Research 43 (9) (2009) 2317–2348.
9. M. Wilf, The Guidebook to Membrane Desalination Technology: Reverse Osmosis, Nanofiltrartion and Hybrid Systems: Process Design, Application and Economics (2007), Balaban Desalination
10. S. Frioui, R. Oumeddour, Desalination 223(1) (2008) 457–463
11. I.C. Karagiannis, P.G Soldatos, Desalination 223(1) (2008) 448–456
12. R.T.Vicente, G.R, Lourdes, Desalination 181(1) (2005) 43-59
13. S.C, McCutcheon, J.L, Martin, T.O, Barnwell, Handbood of Hydrology: Water Density as a Function of Temperature and Concentration (1993)
14. http://www.lindo.com/index.php?option=com_content&view=articleReferences

I.A. Karimi and Rajagopalan Srinivasan (Editors), Proceedings of the 11th International Symposium on Process Systems Engineering, 15-19 July 2012, Singapore.

Modeling and Simulation of CO_2 Absorption with Amine Component Solvent

Yanjie Chen[a,b], Yuehua Yao[a,b], Xiangping Zhang[b,*], Chunshan Li[b], Haifeng Dong[b] , Ying Huang[b], Baozeng Ren[a]

[a]*School of Chemical Engineering and Energy, Zhengzhou University,450001,Zhengzhou, China*
[b]*Institute of Process Engineering, Chinese Academy of Sciences, 100190, Beijing, China*

Abstract:Blended amine solvent has been shown unique and predominant performance while used to capture CO_2 compared with the single amine solvent. Calculations were compared with experimental solubility measurements of CO_2 in aqueous ternary and quaternary systems of H_2O, MEA and AMP. Electrolyte non-random two liquid (ENRTL) theory was employed to fit solubility data in three ternary systems CO_2–H_2O–MEA and CO_2–H_2O–AMP. The binary interaction energy parameters for the ionic species were obtained by regression of the experimental solubility data of the ternary systems. A good agreement between the calculated values and the experimental data was achieved. Process simulation for CO_2 removal using an equilibrium approach was performed with newly fitted parameters. The simulation results have been compared with the pilot plant experimental data.

Keywords: CO_2 capture; Blended amine; Electrolyte-NRTL model; Simulation

1. 1 Introduction

The application of CO_2 capture and subsequent geological storage (CCS) is a promising option to significantly reduce the greenhouse gas emissions of coal-fired power plants[1]. In a post combustion CO_2 capture process, CO_2 is separated from the flue gas of the power plant.Recently the use of blended amines (a solution of two or more amines in varying compositions) in gas-treating processes is a subject of potentially major industrial importance.The blended amines, which contain a combination of the absorption characteristics of the amines, such as higher loading capacity and faster reaction rate, brings about a considerable improvement in absorption and a great savings in energy requirements. Over the past two decades, extensive data for the ternary systems CO_2–H_2O–MEA and CO_2–H_2O–AMP have been collected. Many thermodynamic models were proposed in order to reproduce experimental data[2,3].The Electrolyte Non-Random Two Liquid (NRTL) model is a versatile model for the calculation of activity coefficients. Using binary and pair parameters, the model can represent aqueous electrolyte systems as well as mixed solvent electrolyte systems over the entire range of electrolyte concentrations,so the Electrolyte-NRTL model is used in this paper.

This paper focuses on CO_2 capture from flue gas by absorption with mixed amines of monoethanolamine (MEA) and 2-amino-2-methyl-1-propanol (AMP), which appears to be an attractive new blended amine solvent for the gas treating processes. Electrolyte-NRTL equations for equations for electrolytic mixed-solvent solution were applied also and the equilibrium model of gas absorption in the system of CO_2-MEA-AMP-H_2O was established. The parameters in Electrolyte-NRTL equations were carefully selected and

* Corresponding authors. E-mail addresses: xpzhang@home.ipe.ac.cn(X.P. Zhang)

obtained through regression. With the parameters generated from gas absorption equilibrium data, solubilities of CO_2 in the mixed amine solutions can be directly predicted. The process simulation was also carried out with the thermodynamic model. The simulation results are compared with measured data from pilot plant.

2. Thermodynamic Model

2.1. Electrolyte-NRTL model

The CO_2-MEA-AMP-H_2O quaternary system involving different ionic species, the activity coefficient of any species is calculated from the partial derivative of the excess Gibbs energy with respect to the mole number, i.e.

$$\ln\gamma_i = \frac{1}{RT}\left[\frac{\partial(n_t g^{ex})}{\partial n_i}\right]_{T,P,n_{j\neq i}} \tag{1}$$

The electrolyte NRTL model uses the infinite dilution aqueous solution as the reference state for ions[4,5]. The excess Gibbs energy of a mixed solvent electrolyte system can be written as the sum of two contributions; local ion–molecule, ion–ion and molecule–molecule interactions that exist in the immediate neighborhood of any species and long-range ion–ion interactions.

$$g^{ex} = g^{ex,LR} + g^{ex,local} \tag{2}$$

The first term on the right hand side of Eq.(3) is the original Pitzer-Debye-Hu¨ ckel equation while the second term is the Born expressions for excess Gibbs energy:

$$\frac{g^{ex,LR}}{RT} = -\left(\sum_k x_k\left(\frac{1000}{M_s}\right)^{0.5}\left(\frac{4A_\phi I_x}{\rho}\right)\ln\left(1+\rho\sqrt{I}\right)\right) + \frac{e^2}{2kT}\sqrt{\left(\frac{1}{D}-\frac{1}{D_w}\right)}\left(\sum_i \frac{x_i z_i^2}{r_i}\right)\times 10^{-2} \tag{3}$$

The local-composition electrolyte NRTL expression for excess Gibbs energy is given as follows，

$$\frac{g^{ex,local}}{RT} = \sum_m X_m \frac{\sum_j X_j G_{jm}\tau_{jm}}{\sum_k X_k G_{km}} + \sum_c X_c \sum_{a'}\left(\frac{X_{a'}}{\sum_{a''} X_{a''}}\right)\frac{\sum_j X_j G_{jc,a'c}\tau_{jc,a'c}}{\sum_k X_k G_{kc,a'c}} + \sum_a X_a \sum_{c'}\left(\frac{X_{c'}}{\sum_{c''} X_{c''}}\right)\frac{\sum_j X_j G_{ja,c'a}\tau_{ja,c'a}}{\sum_k X_k G_{ka,c'a}} \tag{4}$$

The different terms in Eq.(4), are computed using the following expressions:

$$G_{jm} = \exp(-\alpha_{jm}\tau_{jm}),\ G_{jc,ac} = \exp(-\alpha_{jc,ac}\tau_{jc,ac}),\ G_{ja,ca} = \exp(-\alpha_{ja,ca}\tau_{ja,ca})$$

$\tau_{ca,w}$，$\tau_{w,ca}$，binary interaction parameters are expressed as a function of temperature:

$$\tau_{ca,w} = C_{ca,w} + \frac{D_{ca,w}}{T} \quad \tau_{w,ca} = C_{w,ca} + \frac{D_{w,ca}}{T}$$

The data regression system (DRS) in Aspen Plus allows the use of user experimental data to estimate the model parameters. In this work, the following interaction parameters are fitted from experimental data available in literature. H_2O–$MEACOO^-MEAH^+$, $MEACOO^-MEAH^+$–H_2O, H_2O–HCO_3^-MEAH+ , HCO_3^-MEAH+–H_2O, H_2O–HCO_3^-AMPH+, $HCO_3^-MEAH^+$–H_2O.

2.2. Experimental results

Experimental data are important for the regression of interaction parameters, so the reliability of the data is important. In this work, VLE data of CO_2 in MEA were form

the literature Jou et al[6]. The data has sufficiently covered temperature from 0℃to150℃,CO_2 partial pressure from 0.001-2000 kPa. The VLE data source of CO_2-AMP comes from Seo and Hong, and it covers the blends of MEA and AMP, including the ratio of MEA and AMP is 18 wt%/12 wt%(1:1 in mole)[7].

2.3. Results and discussion

In this work, interaction parameters were fitted using data regression to determine the parameter values was performed using an algorithm reported by Britt and Luecke[8]. The objective function is formulated based on the maximum likelihood principle. Table 1 shows new parameters for the Electrolyte-NRTL. All parameters obtained for the ternary systems, were used for in the quaternary systems.

Table 1 Interaction parameters estimated using Aspen Plus

Value	$C_{w,ca}$ /$C_{ca,w}$	$D_{w,ca}$ /$D_{ca,w}$
H_2O-$MEAH^+$-HCO_3^-	5.3467128	964.48626
$MEAH^+$-HCO_3^- -H_2O	-4.0754512	-11.071867
H_2O- $MEAH^+$-$MEACOO^-$	9.8773762	10.809863
$MEAH^+$-$MEACOO^-$ -H_2O	-4.9595131	0.062485124
H_2O-$AMPH^+$-HCO_3^-	22.531087	-4296.8954
$AMPH^+$-HCO_3^- -H_2O	-11.374142	2248.5915

The model parameters generated from the single amine experimental data were used to predict CO_2 loading in MEA–AMP mixtures without further regression. The model predictions are compared with the experimental values for mixtures of 12 wt%-18 wt%. Fig.1 shows the solubility of CO_2 in the aqueous of MEA and AMP (1:1 in mole) solution at 40℃, and the results are in good agreement with the experimental data.

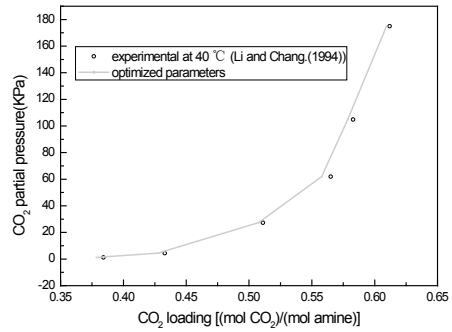

Fig.1 VLE figure of CO_2–blended amine–H_2O with E-NRTL model at 40 ℃.

3. Process simulation

3.1. Pilot plant experiment

The experimental equipment of CO_2 capture by reactive absorption was designed and set up in our laboratory, and the capacity of the gas treatment is $1m^3$/hr. The detailed parameters of the equipments are listed in table 2.

Table 2 Data of the absorber and the desorber in our pilot plant

Parameter	Absorber	Desorber
Diameter (m)	0.05	0.05
Packing height(m)	1.6	1.4
Packing type	Θring 5×5	Θring 5×5
Operation pressure(bar)	<15	<10

The simulated flue gas are made through mixing N_2 and CO_2.The CO_2 gas mixture, with the flow rate of about 0.5 m^3/h and the CO_2 volume concentration about 9%, entering the absorber from the bottom, and the amine solution, with the flow rate of around 3 kg/h and after cooled to 40℃by the cooler, entering the absorber from the top. After absorbing the CO_2 in the flue gas, the purified gas leaves at the top of the absorber. The rich amine solution is pre-heated to 95 °C by the heat exchanger, entering into packed desorber from the top. After heating, the amine solution evaporates and has the liquid-gas mass exchange in the desorber, achieving the desorption process. Consequently, after reaching the steady state, this experimental procedure system is acompletely closed loop system.The experimental run 48 hours, except the data recorded by the computer ,liquid samples were collected from the absorber feed and the outlet to check for CO_2 loading .

3.2. Process simulation for CO_2 absorption with mixed amines

A simulation program was established to simulate the capture and desorption process with software Aspen Plus. The thermodynamic model Electrolyte-NRTL and parameters regressed in this work are used. An equilibrium-stage model was adopted in this work in view of its lesser complexity. The simulation results will be compared with the pilot plant measurement data.

Table 3 Comparison between simulation results and experimental data of absorption column

Item	Value of simulation	Value of experiment
Inlet gas/$Nm^3.h^{-1}$	0.5	0.5
Inlet lean solvent/$l.h^-$	3	3
Flue gas inlet temp/℃	30	30
Outlet gas temp/℃	40	40.1
Lean solvent feed temp/℃	40	39.9
Top pressure/bar	1.1	1.2
Bottom pressure/bar	1.15	1.18
Rich CO_2 loading ($molCO_2$/mol MEA)	0.35	0.34
CO_2 at outlet (mol% wet)	0.7	1

CO_2 recovery(%)	92.9	89.8

Table 4 Comparison between simulation results and experimental data of desorption column

Item	Value of simulation	Value of experiment
Outlet CO_2 gas/$Nm^3.h^{-1}$	0.042	0.40
Inlet rich solvent/$l.h^-$	3	3
Outlet gas temp/℃	40	40.1
Rich solvent feed temp/℃	40	39.9
Top pressure/bar	1.1	1.1
Bottom pressure/bar	1.15	1.12
Lean CO_2 loading (molCO_2/mol MEA)	0.16	0.15

It can be seen from Table3-4 that the predictions of the model are in good agreement with the experimental data. A difference of less than 7% between the models prediction and the pilot plant experimental data has been obtained.

4. Conclusions

Thermodynamic models have been established for calculation of gas solubility of CO_2 in aqueous amine solution with electrolyte-NRTL model equations as the activity coefficient model. The electrolyte-NRTL model parameters generated in the single amine MEA and AMP can be used to predict CO_2 solubility in the mixed amine solutions. The process simulation software is established based on gas solubility thermodynamic models. Simulation prediction results are in good agreement with pilot plant experimental ones. This work will provide some instructions in rational design and simulation of the gas treating units involving blended amine solvent.

References

[1] Hongqun Yang, 2008, Progress in carbon dioxide separation and capture: A review. Journal of Environmental Sciences. 20, 14–27.

[2] Ying Zhang, 2009, Rate-Based Process Modeling Study of CO_2 Capture with Aqueous Monoethanolamine Solution. Ind. Eng.Chem.Res. 48, 9233–9246.

[3] B. P. Mandala, 2001, Removal of carbon dioxide by absorption in mixed amines: modelling of absorption in aqueous MDEA/MEA and AMP/MEA solutions. Chemical Engineering Science. 56, 6217–6224.

[4] M.K. Aroua, 2002, Modelling of carbon dioxide absorption in aqueous solutions of AMP and MDEA and their blends using Aspenplus. Separation and Purification Technology. 29, 153–162.

[5] Yunda Liu, 1999, Representing Vapor-Liquid Equilibrium for an Aqueous MEA-CO_2 System Using the Electrolyte Nonrandom-Two-Liquid Model. Ind. Eng. Chem. Res. 38, 2080-2090.

[6] Fang-Yuan Jou, 1994, Vapor-Liquid Equilibrium of Carbon Dioxide in Aqueous Mixtures of Monoethanolamine and Methyldiethanolamine. Ind. Eng. Chem. Res. 33, 2002-2005.

[7] MengHui Li,1994, Solubilities of Carbon Dioxide in Water+Monoethanolamine +2-Amino-2-methyl-1-propanol. J.Chem. Eng. Data. 39, 448-452.

[8] Aspen Physical Property System,V7.2. Aspen Technology, Inc:Burlington, MA,2010.

I.A. Karimi and Rajagopalan Srinivasan (Editors), Proceedings of the 11th International Symposium on Process Systems Engineering, 15-19 July 2012, Singapore.

Life cycle assessment of coal-based methanol

Hengchong Li, Siyu Yang, Yu Qian

School of Chemistry and Chemical Engineering, South China University of Technology, Guangzhou 510640, P.R. China

Abstract

This paper analyzes the environment impact of methanol production from both product life cycle and process life cycle. Four indicators, global warming, acidification, photochemical oxidant formation and human toxicity, are used for assessment. According to the analysis, the periods that have significant impacts on environmental performance are explored. Several suggestions are provided at the end.

Keywords: Process life cycle; Product life cycle; LCA; Environmental impact.

1. Introduction

Life cycle environmental assessment (LCA) is the cradle to grave analysis. It investigates environmental impacts of a system, a process, or a product. Application of LCA is now expanded and its techniques are used in the evaluation of economic and technical performance. The methodological framework of LCA includes goal and scope definition, inventory analysis, impact assessment and interpretation.

In this paper, LCA is used to assess the environmental impact of the process of coal producing methanol. The reason for selecting this process is due to the dominance of coal in China's energy structure. Methanol is an important platform chemical and can be used to synthesize a large range of derivatives, methanol gasoline and formaldehyde, dimethyl ether, etc. In China, the demand for methanol is increasing. However, the production process of methanol gives environmental impacts. This impact is increasingly worse as the production scale increases. It is therefore important to assess this impact. This paper uses LCA to analyze the production process from both product life cycle and process life cycle. The combination of these two gives a comprehensive assessment on environmental performance of the production process.

2. Goal and scope definition

Four indicators for environmental assessment are used in this paper. They are global warming, acidification, photochemical oxidant formation and human toxicity. As for defining the boundaries, the product life cycle and the process life cycle are considered separately. For the product life cycle, five periods, coal mining, coal transportation, methanol production, methanol utilization and waste disposal, are defined. For process life cycle, there are five periods, building materials production, building materials transportation, factory construction, plant operation and factory disposal. The boundaries are shown in Figure 1. It can be seen that the methanol production period in the product life cycle is equivalent to the plant operation period in the process life cycle.

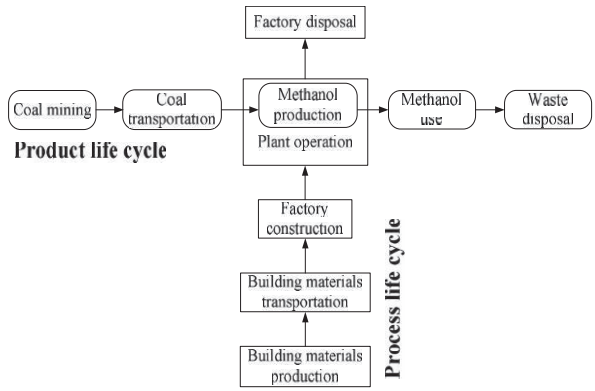

Figure 1. Life cycle boundaries of methanol production processes

3. Inventory analysis

Inventory analysis is the most important step in LCA because of its significant affect on final results. In this paper, eight general pollutant emissions (PM10, SO_X, CO, CO_2, VOC, CH_4, NOX, and N_2O) are collected for inventory. For the methanol utilization period, methanol is used as fuel (M100, Methanol solution without additives) for vehicles. The emitted gases from vehicles are not recycled so there is no waste disposal period in this paper. The production process of methanol involves a large number of material flows and heat flows. It is therefore difficult for data collection for the production period. Aspen Plus is used for modeling and simulating the process. The relevant parameters refer to the Handbook of Modern Coal Chemical Technologies (Xie, 2006). Emissions of the production period are obtained from the simulation results.

For inventory of the process life cycle, we assume that the location of the plant is in Guangzhou, China. We also assume that the building materials are transported from Foshan (40km away from Guangzhou) by diesel trucks. The emissions in the production process of these building materials refer to the literatures (Marono, 2001; Liu, 1998). Data for plant construction and plant disposal was found in Ecoinvent Database (Althaus, 2007). Life length of the plant is set to 30 years. Emissions in the coal mining period are calculated depending on Chinese year book (National Bureau of Statistics of China, 2011). Emissions of the methanol fuel are calculated by GREET model, which is developed by Argonne National Laboratory of US (Wang, 1999). Emissions of the different life cycle periods are listed in Table 1. Depending on this table, Figure 1 is drawn for better showing the distribution of the emissions.

Table 1 Emission of the different life cycle periods ($kg \cdot kg^{-1}$ Me.)

Emission factors	PM10	SO_X	CO	CO_2	CH_4	NO_X	N_2O	VOC
Coal mining	2.65E-03	2.14E-04	7.67E-06	2.48E-02	5.68E-03	1.05E-04	2.50E-06	1.90E-04
Coal transportation	7.05E-07	5.11E-06	4.36E-06	8.58E-04	1.93E-07	3.59E-07	5.12E-06	8.68E-08
Methanol production	0.00E+00	1.10E-05	1.95E-05	1.95E-02	1.63E-04	9.70E-07	0.00E+00	2.67E-07
Methanol use	1.01E-04	8.08E-06	1.06E-02	1.20E+00	2.61E-06	1.54E-05	1.74E-06	1.09E-03
Process life cycle	6.99E-06	1.17E-05	1.35E-06	1.00E-03	5.37E-06	3.05E-06	1.19E-07	1.13E-07
Total	2.76E-03	2.50E-04	1.06E-02	1.25E+00	5.85E-03	1.25E-04	9.48E-06	1.28E-03

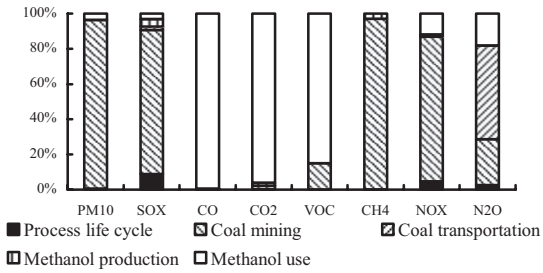

Figure 2. Emission distribution of different life cycle stages

It can be seen that CO, CO_2 and VOC are mainly emitted in the methanol utilization period. In the coal mining period, the emissions are PM10, SO_X, CH_4, and NO_X. Large amount of N_2O is emitted in the coal mining period, the coal transportation period and the methanol utilization period. The emissions of the methanol production period are CO_2, SO_X, and CH_4. Compared to the emissions in the product life cycle, the emissions in the process life cycle are much less.

4. Impact assessment

A three-step model for impact assessment is used in this paper, which includes classification, characterization and quantification. There are many environmental indictors, generally including depletion of nonrenewable resources, biological resources depletion, global warming, ozone depletion, photochemical smog, human toxicity, eco-toxicity, acidification and eutrophication. Four indicators are used in this paper, global warming, acidification, photochemical smog and the human toxicity.

4.1. Global warming

Emission of greenhouse gas (GHG) is the main factor for global warming. The general GHG are CO_2, CH_4, CO, and N_2O. For calculating the global warming potential (GWP) of GHG except for CO_2, the characterized factor model is used and shown as Eq. 1. This model is developed by Intergovernmental Panel on Climate Change (IPCC) (Siebenhuner, 2003). 50 years' average data are used for the calculation,

$$GWP_i = E_i \times CF_{CO_2} \qquad (1)$$

where *i* indicates GHG, *E* denotes the emission quantity and CF_{CO2} means the CO_2 characterized factor.

Table 2. GWP of the methanol life cycle

GHG	CF (kg $CO_{2\text{-eq}}$)	Emission (kg•kg^{-1}Me.)	GWP (kg $CO_{2\text{-eq}}$•kg^{-1}Me.)	Proportion (%)
CO_2	1	1.25E+00	1.25E+00	87.23
CH_4	21	5.85E-03	1.23E-01	8.58
CO	2	1.06E-02	2.12E-02	1.48
NO_X	310	1.25E-04	3.88E-02	2.71
Total	—	—	1.43E+00	100.00

As shown in Table 2, GWP of the methanol life cycle is 1.39kg $CO_{2\text{-eq}}$•kg^{-1}Me. It is mainly aroused by CO_2. Depending on the inventory analysis in Chapter 3, it is known that most of CO_2 is produced in the production period and utilization period. Besides, CO is produced by the incomplete combustion of methanol in the utilization

period. CH_4 is emitted in the coal mining periods. NO_X is mainly emitted in the coal mining period and the methanol utilization period.

4.2. Acidification

Acidification is mainly aroused by the emission of acidic gases. The acidic gases usually contain elements, N, S, and P. They damage soil, change the pH value of water, and finally destruct the living environment of plants and fishes. In LCA of methanol, emitted acidic gases are SO_X and NO_X. Similar to GWP, the calculation of acidification potential (AP) uses SO_2 as the base. The model refers to the report of EPA (EPA, 2000) and is shown in Eq. 2 where CF_{SO2} refers to the SO_2 characterized factor.

$$AP_i = E_i \times CF_{SO_2} \quad (2)$$

Table 3. AP of the methanol life cycle

Acidic gas	CF (kg $SO_{2\text{-eq}}$)	Emission (kg•kg^{-1}Me.)	AP (kg $SO_{2\text{-eq}}$•kg^{-1}Me.)	Proportion (%)
SO_X	1	2.50E-04	2.50E-04	74.10
NO_X	0.7	1.25E-04	8.73E-05	25.90
Total	—	—	3.37E-04	100.00

As shown in Table 3, the total AP is 3.37E-4kg $SO_{2\text{-eq}}$ • kg^{-1}Me. This AP has 74.10% from SO_X and 25.90% from NO_X. According to the inventory analysis, most of these two acidic gases are generated in the consumption of fuel for mining tools in the mining period.

4.3. Photochemical smog

Photochemical smog is produced by photolysis of pollutants in atmosphere. The smog mainly consists of CH_4, SO_X, NO_X and VOC. We use photochemical oxide creation potential (POCP) to assess the impacts of photochemical smog. The calculation of POCP is based on the quantity of photochemical smog made by the C_2H_4 (Yan, 2005) and is calculated in Eq. 3 where CF_{C2H2} refers to the C_2H_4 characterized factor.

$$POCP_i = E_i \times CF_{C_2H_4} \quad (3)$$

Table 4. POCP of the methanol life cycle

Photochemical smog gas	CF (kg $C_2H_{4\text{-eq}}$)	Emission (kg•kg^{-1}Me.)	POCP (kg $C_2H_{4\text{-eq}}$•kg^{-1}Me.)	Proportion (%)
CH_4	0.006	5.85E-03	3.51E-05	6.02
SO_X	0.048	2.50E-04	1.20E-05	2.06
NO_X	0.028	1.25E-04	3.50E-06	0.60
VOC	0.416	1.28E-03	5.32E-04	91.31
Total	—	—	5.83E-04	100.00

As shown in Table 4, we find that 91.31% of POCP is aroused from the emission of VOC. This is because VOC is made up by low-carbon hydrocarbons and low-carbon aldehydes. They are the main components of photochemical smog. Depending on the inventory analysis, VOC is mainly emitted in the methanol utilization period.

4.4. Human toxicity

Human toxicity (HT) includes Human Toxicity Potential by Ingestion (HTPI) and Human Toxicity Potential by Inhalation or Dermal Exposure (HTPE). According to Table 1, SO_X, NO_X, CO, and PM10 are classified as the human toxicity substances. The calculation of HT is based on 1, 4-dichlorobenzene (Yan, 2005). The HT of the methanol life cycle is calculated by Eq. 4 where $CF_{1,\ 4\text{-}C6H4Cl2}$ means the 1, 4-$C_6H_4Cl_2$ characterized factor.

$$HTP_i = E_i \times CF_{1,4-C_6H_4Cl_2} \quad (4)$$

Table 5. HTP of the methanol life cycle

HT substances	CF (kg 1,4-$C_6H_4Cl_{2\text{-eq}}$)	Emission (kg•kg^{-1}Me.)	HTP (kg 1, 4-$C_6H_4Cl_{2\text{-eq}}$•kg^{-1}Me.)	Proportion (%)
SO_X	0.096	2.50E-04	2.40E-05	0.94
NO_X	1.2	1.25E-04	1.50E-04	5.85
CO	0.012	1.06E-02	1.27E-04	4.96
PM10	0.82	2.76E-03	2.26E-03	88.25
Total	—	—	2.56E-03	100.00

As shown in Table 5, PM10 occupies 88.25% of HTP. NO_X and CO have the small percentage of HTP. According to Table 1, we can find PM10 mainly generated in the coal mining period.

5. Conclusion

This paper assessed the environmental impact of the coal-generated methanol from the product life cycle and the process life cycle. Four indicators, global warming, acidification, photochemical oxidant formation and human toxicity, were used for the assessment. The substances that affect these indicators are explored. In the result analysis, we identify environmental impacts of the different life periods and their percentages. Due to the importance of coal chemical industry, people are increasingly concerned with LCA of coal-generated chemicals. The analysis results of this work are worthwhile for further researches of other coal-generated chemicals.

Acknowledgements

This work is supported by the National Natural Science Foundation of China (No. 21136003), National Basic Research Program of China (973 Program, No. 2012CB720504) and Specialized Research Fund for the Doctoral Program of Higher Education (No. 20100172110016).

References

Y. He. 2006, Handbook of Modern Coal Chemical Technology, Beijing: Chemical Industry Press.

H. Althaus, M. Chudacoff, S. Hellweg. 2007, Life Cycle Inventories of Chemicals, Ecoinvent Data v2.0, http://www.pre.nl/

S. Liu, Z. Lin, X. Zhang. 1998, Life cycle assessment of portland cement, *China Environmental Science*, 18(4), 328-332.

J. J. Marano, J. P. Ciferno. 2001, Life-cycle Greenhouse-gas Emissions Inventory for Fischer-Tropsch Fuels, National Renewable Energy Laboratory, http://www.netl.doe.gov/technologies/coalpower/gasification/pubs/systems_analyses.html

National Bureau of Statistics of China, 2011, China Statistical Yearbook of 2010, Beijing: China Statistics Press.

M. Wang. 1999, GREET 1.5 Transportation Fuel-Cycle Model Volume II: Appendices of Data and Results, http://greet.anl.gov/publications.html

B. Siebenhuner. 2003, The changing role of nation states in international environmental assessment-the case of the IPCC, *Global Environmental Change*, 13(2), 113-123.

EPA (Enviromental Protection Agency), 2000, Using life cycle assessment to evaluate preferability of product. Framework for responsible environmental decision making, http://www.epa.gov/nrmrl/std/sab/lca/lca_fred.htm.

Z. Yan. 2005, Chemical Product Life Cycle Evaluation of Integrated Environmental and Economic Performance, Guangzhou: South China University of Technology.

I.A. Karimi and Rajagopalan Srinivasan (Editors), Proceedings of the 11th International Symposium on Process Systems Engineering, 15-19 July 2012, Singapore.

Information integration: From P&I diagrams to functional models

Manuel Rodríguez[a], José L. De la Mata[a], M. Eugenia Alvarez

[a]*Autonomous System Laboratory, Universidad Politécnica de Madrid, José Gutierrez Abascal 2, Madrid 28006, Spain*

Abstract

Information integration is a very important topic. Reusing the knowledge and having common and exchangeable representations have been an active research topic in process systems engineering. In this paper we deal with information integration in two different ways, the first one sharing knowledge between different heterogeneous applications and the second one integrating two different (but complementary) types of knowledge: functional and structural. A new architecture to integrate these representation and use for several purposes is presented in this paper.

Keywords: Process representation, functional models, structural models.

1. Introduction

Information integration and exchange has been and still is a very important topic (see ISO standards like 10303-221, 231 or AP233). In the past decades ontologies have got an important role in information representation, some of them have been developed for process systems, as OntoCape (Morbach et al., 2007) and some neutral model formulations have also been presented (as CapeOpen). But these approaches deal only with structural models and with the problem of merging and using information from different software applications (Wiesner et al., 2011). In this paper we present an architecture to integrate the information coming from the structural and the functional views of a single system. The remaining of the paper is organised as follows, section 2 introduces the D-higraph functional modeling methodology, the third section presents the developed tool for the integrated use of structural and functional models, section four shows an application of the proposed architecture and finally section five presents the conclusions of this work.

2. D-higraph functional modeling methodology

This section briefly presents the D-higraph methodology. For further information and deeper understanding of the methodology, the reader is encouraged to have a look at De la Mata & Rodríguez (2010b).

2.1. D-higraph: Dualization of Higraphs

Higraphs are a general kind of diagramming objects well suited to the behavioral specification of complex concurrent systems, presented by Harel (1987). Higraphs consist of two basic elements called blobs (denote states) and edges (denote transitions) connecting the blobs. However, higraphs original formulation is not suited for process systems specifications. Rodríguez & Sanz (2009) first presented D-higraphs as a functional modeling technique that merges functional and structural information of the system modeled.

D-higraphs come from the dualization of Higraphs: blobs representing transitions and edges representing states. Disjoint blobs imply an AND relation, i.e., both transitions between states take place. Orthogonal blobs represent an OR relation, i.e., only one of the transitions takes place.

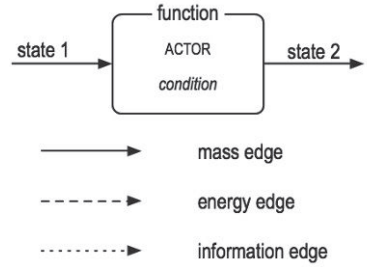

Figure 1. Basic blobs and types of edges

2.2. Main components

Blobs represent functions (transitions) and they include the ACTOR of the function and an optional condition for the transition to fire. As a result a new state is generated. The states are represented by edges coming in or out of a blob. Edges represent flows of mass, energy or information, which are responsible of all of the interactions in a process system (Lind, 1994). Mass, energy and information edges are depicted differently, as shown in the bottom of Fig. 1. However, the type of flow does not affect the behavior of the model, it is a visual aid to represent more information. An additional end of an edge is a hollow arrow which means that the state has influence on the blob pointed by the arrow (although the flow is in the opposite direction).

2.3. Properties

• *Blob connection.* An edge always links two blobs. Under certain conditions one of the blobs can not be represented (elliptic blob) but it exists.

• *Blob inclusion.* Blobs can be included inside of other blobs. This means that the inner blob performs a function that is necessary for the function of the outer blob. This is how hierarchical functions are represented and how structural and functional information is integrated.

• *Partitioning blobs.* A blob can be partitioned into orthogonal components, establishing an OR condition between the partitions.

The main objective of D-higraphs is not only the representation of knowledge about process systems. De la Mata & Rodríguez (2010a,b) provide a series of causation rules that allow to track the evolution and propagation of failures across the system. This rules combined with sensor data of the process enables the possibility of performing FDI analysis using D-higraphs models.

3. Information integration tool

3.1. P&I representation

The available P&I diagram of a process is translated to a steady state model, in this case to an Aspen Plus model. This initial translation is performed manually. The generated model is converted to a dynamic model (Aspen Dynamics / Aspen Custom Modeler). This completes the structural representation of the process.

3.2. D-h tool

The steady state model is automatically translated to a D-higraphs model, additional information regarding the functionality of the different units is provided to the API to perform the creation of the model. The developed tool, Álvarez (2010), allows a visual representation of the goals of the process.

3.3. CLIPS

The D-higraph representation is automatically translated to production (rule based) system (CLIPS, 2011) that will be used to conduct fault diagnosis and HAZOP analysis.

3.4. Architecture

Figure 2 shows all the components of the architecture. The communication between the structural (dynamic) model and the functional one is through an access extension coded as a dll. This dll allows bidirectional communication between the simulation and the functional representation, allowing to study the effects of a fault on the whole process.

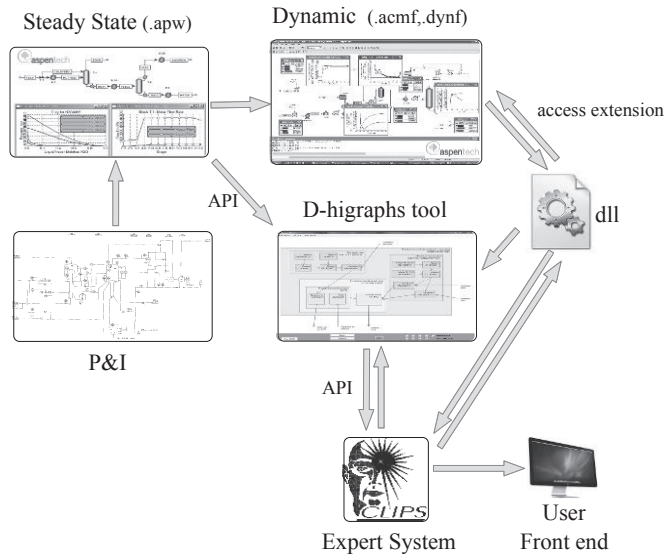

Figure 2. Structural-functional information integration architecture

There are different uses of this environment from conventional simulation to fault diagnosis, sensor validation, control reconfiguration or HAZOP analysis.

4. Application

Amine gas treating is a process that uses an aqueous solution of an amine to remove H_2S and CO_2 from gases. In this case we consider the treatment of an off-gas from a secondary absorber of a FCC in an oil refinery using an aqueous solution of diethanolamine (DEA). In the absorber the DEA solution absorbs H_2S and CO_2 from the incoming off-gas producing a sweetened gas stream and a DEA solution rich in the absorbed acid gases. The sweet gas is sent to the high-pressure gas system of the refinery while the rich amine is routed to the regenerator.

The regenerator is a stripper with a reboiler where the rich amine desorbs H_2S and CO_2 producing a lean amine stream that is recycled to the absorber for reuse. The reboiler is fed with steam to vaporize the DEA solution. The acid gas is sent to a Claus process

while the lean DEA is recycled to the absorber. A make-up DEA stream is needed to keep the amine inventory. The P&ID of the process is shown in Fig 3

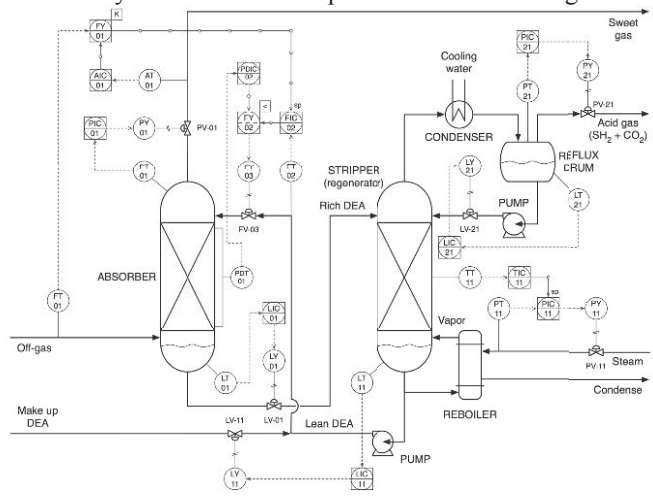

Figure 3. Piping and instrument diagram of the amine gas treating process

For this P&I a steady state model as well as a dynamic model has been created. A functional model has also been generated using the D-higraph tool. Figure 4 shows the D-higraph of a small part of the process, the reflux section of the stripper and the dynamic model generated using Aspen Dynamics.

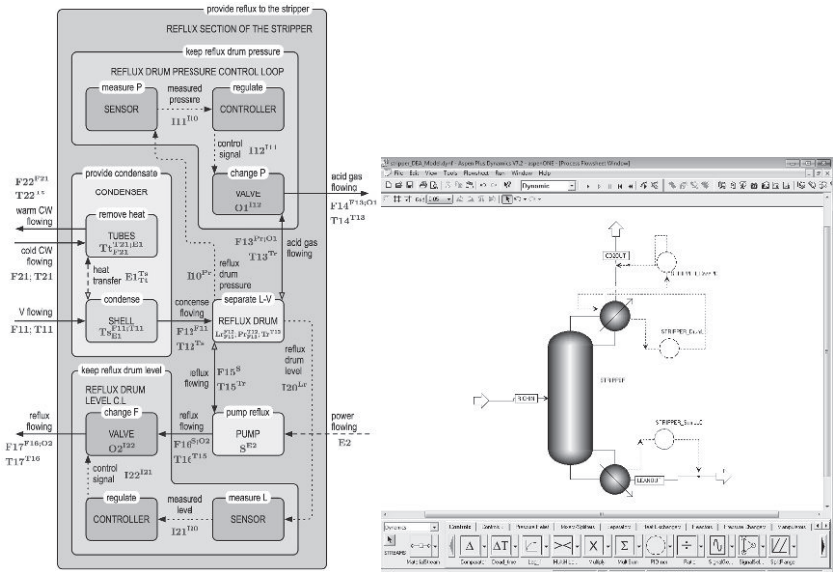

Figure 4. Functional model of the stripper reflux section (left) and the dynamic model (right)

For the first test we have a dynamic model for the stripper, which receives actual input data from the plant. Using the dynamic model, a fault has been identified following De la Mata & Rodríguez (2011). This fault has been input to the functional model, which generates a tree with the consequences of the fault. For the second test a fault has been observed and the functional model has generated the tree of possible causes. The

generated fault is produced in the pressure sensor. Figure 5 shows the set of possible causes (it produces as a possible cause the sensor fault I11 signal in the tree) and the simulated model used to validate and quantify the deviations provided by the functional model.

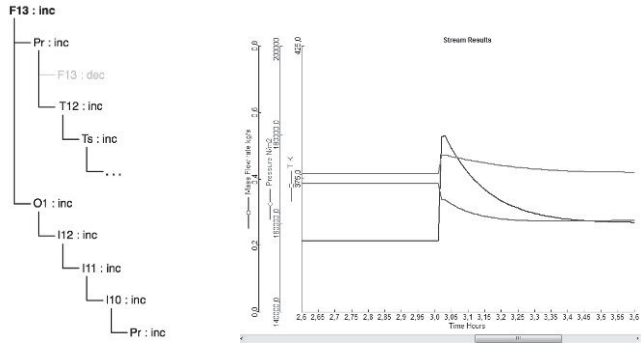

Figure 5. Causal tree and dynamic simulation of the sensor fault

5. Conclusions

In this paper a new architecture to integrate structural as well as functional information has been presented. Functional models are represented using the D-higraphs formalism and its exploitation is made using a production system. Structural (steady state and dynamic) models are generated using the AspenTech software. Communication between both representations is made using a dll component which can control the simulation or generate events for the functional representation. This approach has been tested on an industrial process with satisfactory results. It can be used in many different ways as to validate and quantify functional models, to validate sensors and alarms or to provide control reconfiguration. Future research is being focused on automating all the procedure (including adding functional information directly on the Aspen models) and on testing and creating a procedure for automatic control reconfiguration.

References

Álvarez, M. E. (2010). Diagnosis de fallos en procesos químicos mediante modelos D-higraph. *Final Project, Department of Chemical Engineering, Technical University of Madrid.*

CLIPS (2011). *CLIPS, A Tool for Building Expert Systems.* March, 13, 2011. http://clipsrules.sourceforge.net/

De la Mata, J. L., Rodríguez, M. (2010a). Abnormal Situation Diagnosis Using D-higraphs. *Computer Aided Process Engineering (ESCAPE 20),* pp. 1477-1482.

De la Mata, J. L., Rodríguez, M. (2010b). D-higraphs. *ASLab Report.* http://www.aslab.org

De la Mata, J. L., Rodríguez, M. (2011). Self-learning of fault diagnosis identification. *Proc. of the 21th European Symposium on Computer Aided Process Engineering (ESCAPE 21)*., pp. 885-889

Harel, D. (1987). Statecharts: A Visual Formalism for Complex Systems. *Sci. Comput. Program, 8 (3),* pp. 231-274.

Lind, M. (1994). Modeling Goals and Functions of Complex Industrial Plant. *Applied Artificial Intelligence, 8 (2),* pp. 259-283.

Morbach, J., Yang,A., Marquardt, W. (2007). OntoCAPE-A large-scale ontology for chemical process engineering. *Engineering Applications of Artificial Intelligence*, 20 (2), pp. 147-161.

Rodríguez, M., Sanz, R. (2009). Development of Integrated Functional-Structural Models. *Computer Aided Process Engineering, 27,* pp. 573-578.

Wiesner, A., Morbach, J., Marquardt, W. (2011). Information integration in chemical process engineering based on semantic technologies. *Computers & Chem. Eng.*, 55 (4), pp. 692-708

I.A. Karimi and Rajagopalan Srinivasan (Editors), Proceedings of the 11th International Symposium on Process Systems Engineering, 15-19 July 2012, Singapore

Nonlinear Design of Stimulus Experiments for Optimal Discrimination of Biochemical Systems

Robert J. Flassig,[a*] Kai Sundmacher,[ab]

[a] *Otto-von-Guericke University, Process Systems Engineering, Universitätsplatz 2, D-39106 Magdeburg, Germany*

[b] *Max Planck Institute for Dynamics of Complex Technical Systems, Sandtorstr. 1, D-39106 Magdeburg, Germany*

Abstract

Biochemical reaction networks in the form of coupled ordinary differential equations (ODEs) provide a powerful modeling tool to understand the dynamics of biochemical processes. During the modeling process a pool of competing nonlinear models is generated, from which the most plausible set has to be selected, given distributed model parameters and hence distributed model prediction. At this point, robust (=taking distributed model responses into account) model-based stimulus experiments can be used, to find experimental conditions at which models show maximal dissimilarities to focus experimental efforts. Response variabilities are typically obtained from linearization. Here we compare this method to the nonlinear Sigma-Point approach for a nonlinear, multi-stable model and show its advantage for model discrimination, especially for large parameter variances.

Keywords: optimal stimulus design; nonlinear model discrimination; sigma point method

1. Introduction

Mechanistic ODE models can help to find missing links based on dynamic features of hypothesized mechanisms. However, large biological variability and measurement noise lead to distributed model parameters, which in combination with several hypotheses render model-based prediction highly uncertain. Model-based experimental stimulus design can be used to optimize new experimental data for (i) parameters estimation and/or (ii) model discrimination. Most of the work on optimal experimental stimulus design (OESD) for biochemical systems focuses on parameter estimation. Here, the origin of distributed parameters is solely attributed to suboptimal parameter sensitivities and measurement noise. Natural parameter variations and potentially associated multi-stable states are excluded. For (bio)chemical systems, there exists also work on OESD for model discrimination, e.g., Chen and Asprey (2003); Apgar et al. (2008). As has been illustrated by Chen and Asprey (2003), the consideration of model response variabilities strongly improves discrimination designs. Here, linearization has been used to estimate model response variabilities. However, by using the Sigma-Point method (Julier et al. (2000)), Heine et al. (2008); Schenkendorf et al. (2009) show that a linear OED for best parameter estimation is suboptimal for nonlinear systems. In the case of OESD aimed at model discrimination, we have shown in (Flassig and Sundmacher, 2012), that the Sigma-Point method outperforms linearization with respect to accuracy and discriminative power at same computational costs for nonlinear models. In this work we analyze the behavior of both methods in the presence of multiple stable states using the Schlögl model.

*flassig@mpi-magdeburg.mpg.de

2. Approach

2.1. Modeling

In many situations, the dynamics of a biochemical system with internal states $\mathbf{x}(t,\mathbf{u}(t),\theta_x) \in \mathbb{A}_\mathbf{x} \subset \mathbb{R}^{n_x}$ can be described by the solution of an initial value problem of the form

$$\frac{\mathrm{d}}{\mathrm{d}t}\mathbf{x}(t) = \mathbf{f}(\mathbf{x}(t),\mathbf{u}(t),\theta_\mathbf{x}); \qquad \mathbf{y}_{sim}(t,\theta) = \mathbf{g}(\mathbf{x}(t,\theta_\mathbf{x}),\theta_\mathbf{y}) \tag{1}$$

with initial system state $\mathbf{x}(t_0) = \mathbf{x}_0$ and right hand side function $\mathbf{f}(\mathbf{x}(t),\mathbf{u}(t),\theta_\mathbf{x})$ describing biological interaction mechanisms, which depends on the system states $\mathbf{x}(t)$, (multiple) stimuli $\mathbf{u}(t)$, and kinetic parameters $\theta_\mathbf{x}$. The response signal is determined by the function $\mathbf{g}(\mathbf{x}(t,\theta_\mathbf{x}),\theta_\mathbf{y})$, relating the system states to the readouts of the experiment. All modeling parameters may be lumped to the model parameter vector $\theta = [\theta_\mathbf{x},\theta_\mathbf{y}]^\mathrm{T}$, with redefined $\theta_\mathbf{x} \equiv [\theta_\mathbf{x},\mathbf{x}_0]^\mathrm{T}$. The dynamic model defined by Eq. (1) represents a nonlinear mapping from model parameter space $\mathbb{A}_{\theta_\mathbf{x}} \times \mathbb{A}_{\theta_\mathbf{y}} = \mathbb{A}_\theta \subset \mathbb{R}^{n_\theta}$ to model output space $\mathbb{A}_\mathbf{y} \subset \mathbb{R}^{n_\mathbf{y}}$. Assuming the model parameters to be distributed according to $\rho_\Theta(\theta)$, $\mathbf{y}_{sim}(t,\theta)$ represents a time dependent, distributed variable $\mathbf{Y}$, which can be described by a model response distribution (MRD) $\rho_{m_\mathbf{Y}}(\mathbf{y},t)$.

2.2. Design criterion for model discrimination

The shape of an MRD is determined by the underlying ODEs and applied stimuli. OESD seeks stimuli that minimize similarities of competing MRDs. Similarities of two MRDs, referred to as model overlap, can be measured by the scalar product

$$\Phi(t,\mathbf{u}(t)) = \int_{\mathbb{A}_\mathbf{y}} \rho_{A_\mathbf{Y}}(\mathbf{y},t,\mathbf{u}(t))\rho_{B_\mathbf{Y}}(\mathbf{y},t,\mathbf{u}(t))\mathrm{d}\mathbf{y}. \tag{2}$$

From this, the average model overlap of the time course is

$$O = \langle\Phi(\mathscr{D})\rangle_t = \frac{1}{n_t}\sum_{k=1}^{n_t}\Phi(t_k,\mathbf{u}(t_k)), \tag{3}$$

where $\mathscr{D} \in \mathbb{D} = \mathbb{T}\times\mathbb{U}\times\mathbb{Y}$ represents the experimental design, encompassing for instance selection of discrete measurement time points $t_k \in \mathbb{T}$, stimulus design $\mathbf{u}(t) \in \mathbb{U}$ and readout design $\mathbf{g} \in \mathbb{Y}$. An optimal model discrimination design $\mathscr{D}_\dagger$ minimizes Eq. (3). When approximating the MRD by $\rho_{\mathbf{Y}|m}(\mathbf{y},t,\mathbf{u}(t)) \simeq \mathscr{N}(\mu_{\mathbf{y}|m}(t,\mathbf{u}(t)),\Sigma_{\mathbf{y}|m}(t,\mathbf{u}(t)))$, the integration in Eq. (2) can be performed to yield an analytic expression of the approximate overlap in terms of $\mu_{\mathbf{y}|m}(t,\mathbf{u}(t)),\Sigma_{\mathbf{y}|m}(t,\mathbf{u}(t)))$. For details see Jebara et al. (2004).

2.3. Estimation of the response distribution

If we approximate the parameter distribution $\rho_\Theta(\theta)$ by its first two statistical moments, $\mathbf{E}[\theta]$ and $\mathbf{C}[\theta]$, we can apply the linearization or Sigma-Point method to estimate the first two statistical moments of the resulting time dependent MRD.

Linearization: Applying the chain rule to the readout function in Eq. (1) yields

$$\mathbf{y}^\mathscr{L}(t,\theta) = \mathbf{y}_{sim}(t,\mathbf{E}[\theta]) + \mathbf{S}(t,\mathbf{y})^\mathrm{T}\big|_{\theta=\mathbf{E}[\theta]}(\theta - \mathbf{E}[\theta]), \tag{4}$$

with response sensitivity matrix $\mathbf{S}(t,\mathbf{y}) = \frac{\partial\mathbf{y}_{sim}(t,\theta)}{\partial\mathbf{x}}\mathbf{S}_\mathbf{x}(t,\mathbf{x}) + \frac{\partial\mathbf{y}_{sim}(t,\theta)}{\partial\theta}$ and state sensitivity matrix $\mathbf{S}_\mathbf{x}(t,\mathbf{x}) = \frac{\partial\mathbf{x}}{\partial\theta}$. Then, the linear estimates of expectation and variance-covariances

of the MRD can be calculated as

$$\mathbf{E}_t^{\mathscr{L}}[\mathbf{y}] = \mathbf{y}_{sim}(t, \mathbf{E}[\theta]); \qquad \mathbf{C}_t^{\mathscr{L}}[\mathbf{y}] = \mathbf{S}(t,\mathbf{y})\,\mathbf{C}[\theta]\,\mathbf{S}(t,\mathbf{y})^{\mathrm{T}}. \tag{5}$$

These local estimates may miss parameter dependent coexisting stable states. Further, for nonlinear models, the estimate of the expectation is typically biased, i.e., $\mathrm{Bi} = \mathbf{E}_t^{\mathscr{L}}[\mathbf{y}] - \mu_{\mathbf{y}} \neq \mathbf{0}$. The computational effort is of order $\mathscr{O}(n_{\theta_{\mathbf{x}}})$.

Sigma-Point: According to Julier et al. (2000), the first two statistical moments of nonlinear transformed distribution can be estimated by the following procedure:
1. Select $2n_\theta + 1$ Sigma Points in the original domain according to

$$\theta^{(0)} = \mathbf{E}[\theta]; \qquad \theta^{(i)} = \theta^{(0)} \pm \sqrt{n_\theta + \lambda}\sqrt{\mathbf{C}[\theta]}^{(i)}, \tag{6}$$

2. Propagate these through the model $\mathbf{y}_t^{(i)} = \mathbf{y}_{sim}(t, \theta^{(i)})$.
3. Estimated expectation and variance-covariance of the MRD are given by

$$\begin{aligned}\mathbf{E}_t^{\mathscr{S}}[\mathbf{y}] = \sum_{i=-n_\theta}^{n_\theta} w^{(i)}\mathbf{y}_t^{(i)}; \quad \mathbf{C}_t^{\mathscr{S}}[\mathbf{y}] =& (1-\alpha^2+\beta)\left(\mathbf{y}_t^{(0)} - \mathbf{E}_t[\mathbf{y}]\right)\left(\mathbf{y}_t^{(0)} - \mathbf{E}_t[\mathbf{y}]\right)^{\mathrm{T}} + \\ &+ \sum_{i=-n_\theta}^{n_\theta} w^{(i)}\left(\mathbf{y}_t^{(i)} - \mathbf{E}_t[\mathbf{y}]\right)\left(\mathbf{y}_t^{(i)} - \mathbf{E}_t[\mathbf{y}]\right)^{\mathrm{T}}\end{aligned} \tag{7}$$

with weights $w^{(0)} = \frac{\lambda}{n_\theta+\lambda}$, $w^{(\pm i)} = \frac{1}{2(n_\theta+\lambda)}$ and $\lambda = \alpha^2(n_\theta + \kappa) - n_\theta$. In the case of nonlinear systems, this provides higher order information without any need of derivative information. We may use this method as a Monte-Carlo surrogate to compare the linear estimates of expectation and covariance to, Flassig and Sundmacher (2012). The computational effort is of order $\mathscr{O}(2n_\theta + 1)$.

3. Numerical Analysis

The Schlögl model is a canonical example of a biochemical system exhibiting bi-stability, Schlögl (1972). It describes an autocatalytic, tri-molecular reaction, that occurs in biochemical system such as cell metabolism or signaling. Two model alternatives for the rate of concentration change of specie x are given by

$$\frac{\mathrm{d}}{\mathrm{d}t}x_m(t) = k_1\, a\, s_m(u(t))x_m^2(t) - k_2 x_m^3(t) - k_4 x_m(t) + k_3 b, \tag{8}$$

$$s_A(u(t)) = u(t) \quad \text{or} \quad s_B(u(t)) = \frac{1}{2}(u(t) + u^2(t)) \tag{9}$$

and distributed initial condition $X_0 \propto N(\mathrm{E}[x_0], \eta\mathrm{E}[x_0])$. The model alternatives differ in the input layer $s_m(u(t))$. Parameters a and b represent the concentration of two reaction partners a and b of specie x, which both are assumed to be in constant exchange with a material bath. The parameter values are taken from Vellela and Qian (2009). For an initial, suboptimal experiment with stimulus $u(t) = 1$, models A and B cannot be distinguished, given $y_m(t) = x_m(t) + \theta_\varepsilon$ to be the response signal. Additionally to a distributed initial

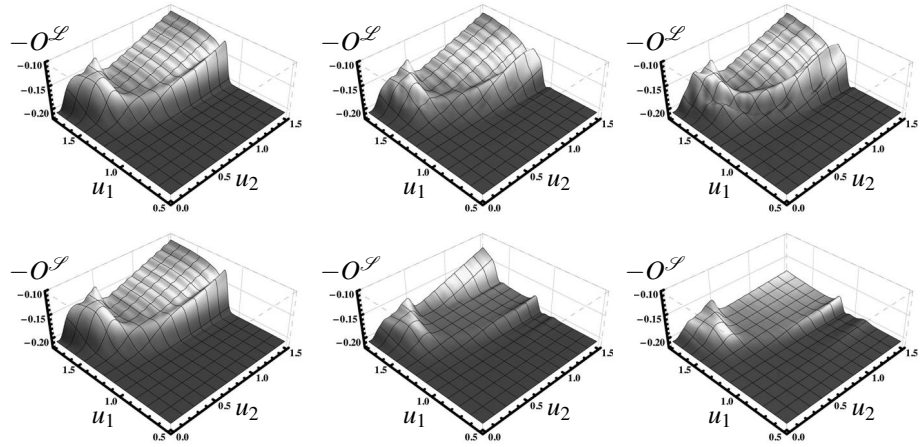

(a) $\eta = 0.01$ (b) $\eta = 0.3$ (c) $\eta = 0.6$

Figure 1: Design $\mathscr{D} = [u_1, u_2]^{\mathrm{T}}$ dependent overlap landscape for three different levels of parameter variances.

condition x_0, we assume a constant additive measurement noise with zero mean and $\sigma_\varepsilon^2 = 0.1$. We parameterize the stimulus as

$$u(t) = u_1 \left(\Theta[u_2 - t] + (1 - \Theta[2u_2 - t]\Theta[3u_2 - t])\right); \quad \Theta[t] = \begin{cases} 1, & \text{if} \quad t \leq 0 \\ 0, & \text{else,} \end{cases} \tag{10}$$

which allows to analyze the overlap landscape as a function of u_1 and u_2. Both parameters are subjected to box constraints mimicking experimental limitations, i.e., $u_{i|lb} \leq u_i \leq u_{i|ub}$. In Fig. 1 we show the design dependent overlap landscape, i.e., Eq. 3 for $n_t = 30$ and different levels of parameter variances derived from $\sigma_{x_0} = \eta \mathrm{E}[x_0]$. For small parameter variances both methods estimate the same overlap landscape, thus same optimal design $\mathscr{D}_\dagger^{\mathscr{E}}$. For $\eta = 0.6$ the best design points $= \max(-O^{\mathscr{E}})$ differ for both methods, i.e., $\mathscr{D}_\dagger^{\mathscr{L}} \neq \mathscr{D}_\dagger^{\mathscr{S}}$. In Fig. 2 we show time courses of the estimated moments (thick/thin lines expectation/std. deviation) for each best designs $\mathscr{D}_\dagger^{\mathscr{E}}$ based on linearization $\mathscr{E} = \mathscr{L}$ and Sigma-Points $\mathscr{E} = \mathscr{S}$. Evaluating the overlap of the optimal linear design with the Sigma-Points reveals a larger expected overlap $O_\dagger^{\mathscr{L}\mathscr{S}} > O_\dagger^{\mathscr{L}\mathscr{L}}$, as linearization misses the spread of the variance and the location of the expected response due to the existence of a second stable state (Fig. 2 (b) vs. (c)). The optimal Sigma-Point design minimizes the overlap by "switching" optimally between the two states while keeping the variance minimal (Fig. 2 (f)). We also see that $O_\dagger^{\mathscr{S}\mathscr{S}} < O_\dagger^{\mathscr{L}\mathscr{S}}$, i.e., the linear design is suboptimal.

4. Conclusion

The behavior of linear and Sigma-Point estimations of nonlinear transformed statistical Gaussian moments, has been analyzed in the framework of OESD in the presence of multiple stable states. As we illustrate, due to the non-local estimation property of the Sigma-Point method, the optimizer can use the bistability for optimal discrimination. Further, the estimated variances of the Sigma-Point method encompass both stable states, whereas the estimated expectation lies between the stable states. In contrast, linearization captures only one of the states, which results into underestimated variances, biased expectation

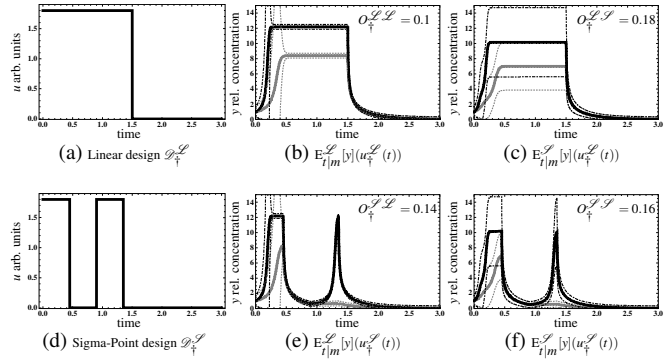

(a) Linear design $\mathscr{D}^{\mathcal{L}}_{\dagger}$ (b) $\mathrm{E}^{\mathcal{L}}_{t|m}[y](u^{\mathcal{L}}_{\dagger}(t))$ (c) $\mathrm{E}^{\mathcal{S}}_{t|m}[y](u^{\mathcal{L}}_{\dagger}(t))$

(d) Sigma-Point design $\mathscr{D}^{\mathcal{S}}_{\dagger}$ (e) $\mathrm{E}^{\mathcal{L}}_{t|m}[y](u^{\mathcal{S}}_{\dagger}(t))$ (f) $\mathrm{E}^{\mathcal{S}}_{t|m}[y](u^{\mathcal{S}}_{\dagger}(t))$

Figure 2: Time course estimates of both models (A gray, B black) for $\eta = 0.6$.

estimates and suboptimal OESD. As both method have the same computational effort, we conclude that the Sigma-Point method provides a powerful estimation method, when designing discrimination experiments for complex, nonlinear biochemical ODE models having widely distributed parameters and associated multiple stable states.

References

Apgar, J. F., Toettcher, J. E., Endy, D., White, F. M., Tidor, B., 2008. Stimulus Design for Model Selection and Validation in Cell Signaling. PLoS Comput Biol 4 (2).

Chen, B. H., Asprey, S. P., 2003. On the Design of Optimally Informative Dynamic Experiments for Model Discrimination in Multiresponse Nonlinear Situations. Industrial & Engineering Chemistry Research 42 (7), 1379–1390.

Flassig, R. J., Sundmacher, K., 2012. Optimal design of stimulus experiments for robust discrimination of biochemical reaction networks. Bioinformatics *submitted*.

Heine, T., Kawohl, A., King, R., 2008. Derivative-free optimal experimental design. Chemical Engineering Science 63 (19), 4873–4880.

Jebara, T., Kondor, R., Howard, A., Bennett, K., Cesa-bianchi, N., 2004. Probability product kernels. Journal of Machine Learning Research 5, 819–844.

Julier, S., Uhlmann, J., Durrant-Whyte, H. F., 2000. A new method for the nonlinear transformation of means and covariances in filters and estimators. IEEE Transactions on Automatic Control 45 (3), 477–482.

Schenkendorf, R., Kremling, A., Mangold, M., 2009. Optimal experimental design with the sigma point method. IET Systems Biology 3 (1), 10–23.

Schlögl, F., 1972. Chemical reaction models for non-equilibrium phase transitions. Zeitschrift für Physik A Hadrons and Nuclei 253, 147–161.

Vellela, M., Qian, H., 2009. Stochastic dynamics and non-equilibrium thermodynamics of a bistable chemical system: the schlögl model revisited. Journal of The Royal Society Interface 6 (39), 925–940.

I.A. Karimi and Rajagopalan Srinivasan (Editors), Proceedings of the 11th International Symposium on Process Systems Engineering, 15-19 July 2012, Singapore.

Multi-scale modeling for prediction of distributed cellular properties in response to substrate spatial gradients in a continuously run microreactor

Rita Lencastre Fernandes[a], Ulrich Krühne[a], Ingmar Nopens[b], Anker D. Jensen[c], Krist V. Gernaey[a]

[a]*Center for Process Engineering and Technology, Technical University of Denmark, 2800 Kgs. Lyngby, Denmark*
[b] *BIOMATH, Department of Mathematical Modelling, Statistics and Bioinformatics, Ghent University, Coupure Links 653, 9000 Ghent, Belgium*
[c] *Center for Combustion and Harmful Emission Control, Department of Chemical and Biochemical Engineering, Technical University of Denmark, 2800 Kgs. Lyngby, Denmark*

Abstract

In large-scale fermentors, non-ideal mixing leads to the development of heterogeneous cell populations. This cell-to-cell variability may explain the differences in e.g. yields for large- and lab-scale cultivations. In this work the anaerobic growth of *Saccharomyces cerevisiae* in a continuously run microbioreactor is simulated. A multi-scale model consisting of the coupling of a population balance model, a kinetic model and a flow model was developed in order to predict simultaneously local concentrations of substrate (glucose), product (ethanol) and biomass, as well as the local cell size distributions.

Keywords: Population Balance Model, Computational Fluid Dynamics, yeast, microreactor, fermentation

1. Introduction

A heterogeneous microbial population consists of cells in different states, which implies a distribution of activities (e.g. respiration, product efficiency), as well as different responses to extracellular stimuli. The existence of a heterogeneous cell population may explain the lower productivities obtained for cultivations in large-scale reactors, where substrate and oxygen gradients are observed, in comparison to cultivations in well-mixed bench scale reactors (Enfors et al, 2001).

Population balance models (PBM) have been used in various applications (e.g. crystallization, granulation, flocculation, polymerization processes, etc.) to predict distributions of certain population properties including particle size, mass or volume, molecular weight,... Similarly, PBM allow for a mathematical description of distributed cell properties within microbial populations (Lencastre Fernandes et al, 2011).

Phenotypic heterogeneity arises as a result of the variability inherent to the metabolic mechanisms of single cells. Cell size is a key feature affecting cellular design, fitness and function (Jorgensen and Tyers, 2004). In fact, cell growth and division are tightly coupled, and this is reflected in the cell's capability of adjusting its growth rate to nutrients' availability (Enfors et al, 2001; Jorgensen and Tyers, 2004). Cell total protein content distributions (a measure of cell size) have been observed to provide a dynamic

picture of the interplay between the cells and surrounding extracellular environment (Alberghina et al, 1998).
The work hereby presented focuses on modeling the development of a microbial population growing in a continuous microbioreactor. The dynamics of single cell total protein content are described by a PBM, the consumption of substrate and production of ethanol are described by simple kinetics (unstructured model), and the transport of the species throughout the reactor is described by a computational fluid dynamics (CFD) model.

2. Case Study

The anaerobic fermentation of *Saccharomyces cerevisiae* in a continuous microreactor is used as case study. As above mentioned, cell growth and division are tightly coupled, and are modulated according to the substrate availability. The regulation of growth ensures that cells attain a critical size before initiating the division process (Rupeš, 2002; Porro et al, 1995). In the particular case of *S. cerevisiae*, two critical sizes corresponding to the regulation points START (committing to budding, or budding transition) and division have been identified. A schematic representation of the cells transition through the cell cycle and the associated cell growth (i.e. size increase) is presented in Fig. 1.
Using cell size as population descriptor allows, thus, for describing the distribution of cellular states. Moreover, a better description of the cellular state is obtained by determining the distribution of cells in cell cycle phases, i.e. by measuring DNA distributions (Alberghina et al, 1998). It was thus found desirable to use a PBM based on cell size as model variable, which is applied to different stages (i.e. subpopulations) corresponding to the non-budding and budding (cell cycle) phases.

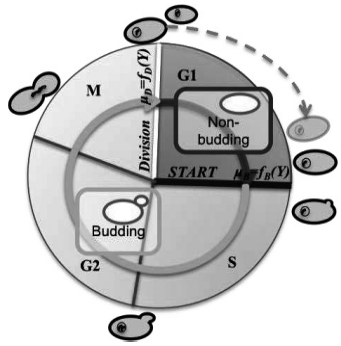

Figure 1 - Schematic representation of the cell cycle during exponential growth. The dark arrow (inside the circle) corresponds to the duration of the non-budding stage (G1phase). Due to their bigger size, G1 phase is shorter for mother cells than for daughter cells (dashed arrow). The *START* point represents the regulation point that defines the inititation of the DNA replication and budding process, i.e. transition to the S phase. The division point corresponds to the completion of the mitotic process and separation of a budding cell into two non-budding ones.

The microreactor consists of a sequence of spherical chambers connected in the center by a channel (Fig. 2). An inlet mass flow rate of $1x10^{-9}$ kg/s, containing glucose (20 g/l), was applied. The ethanol and biomass concentrations at the inlet are 0 g/l. The hydraulic retention time is 783 s.

3. Model Description

Aiming at both describing the distributions of single-cell sizes for the two cell size stages (non-budding and budding), a population balance model was coupled to an unstructured model describing the extracellular environment.

3.1. Population Balance Model

The PBM developed for this study is based on a multi-stage model reported in the literature (Hatzis and Porro, 2006). In this work, the segregated model consists of two

population balance equations (PBE), which describe cell growth, initiation of the budding process, cell division and birth, for both the non-budding and budding stages (Eq. 1 and 2), as well as the corresponding initial and boundary conditions.

$$\frac{\partial N^{NB}(m,t)}{\partial t}+\frac{\partial}{\partial m}\left[r_m(m,Y)N^{NB}(m,t)\right]=-\Gamma_B(m|Y)N^{NB}(m,t)+2\int_m^{\infty}\Gamma_D(m'|Y)P(m,m'|Y)N^B(m',t)dm' \quad \text{(Eq. 1)}$$

$$\frac{\partial N^{B}(m,t)}{\partial t}+\frac{\partial}{\partial m}\left[r_m(m,Y)N^{B}(m,t)\right]=-\Gamma_D(m|Y)N^{B}(m,t)+\Gamma_B(m|Y)N^{NB}(m,t) \quad \text{(Eq. 2)}$$

Here $N^{NB}dm$ and $N^{B}dm$ represent the number of cells in the cell size interval *[m, m+dm]* for the non-budding and budding stages, respectively, *m* is the cell total protein content or cell size (in arbitrary units), and *Y* designates the extracellular environment. The budding and division transitions, Γ_{NB} and Γ_B, are mathematically described as hazard functions (Eq. 3 and 4, for the budding transition) where the probability that a cell of mass *m* initiates the budding process, i.e. transitions to the budding stage, or divides into two new cells is described by a Gaussian probability density function with mean μ_B and μ_D, respectively. The standard deviation was assumed to be the same for the two transition functions and constant along the cultivation.

$$\Gamma_{NB}(m|Y)=r_m(m,Y)\frac{h_{NB}(m|Y)}{1-\int_{m_0}^{m}h_{NB}(m')dm'} \quad \text{(Eq. 3)}$$

$$h_{NB}(m|Y)=N(\mu_{NB}(Y),\sigma_{NB}) \quad \text{(Eq. 4)}$$

$$r_m(m,Y)=k_G m\cdot\lambda(Y) \quad \text{(Eq. 5)}$$

Generally, the link to the extracellular environment is accounted for by including substrate dependency in the growth function as well as transition functions (budding and division) for each of the stages: (i) the growth rate of single cells (r_m, *Eq. 5*) depends on the mass of each cell (first-order kinetics) and on the available concentration of glucose. The substrate factor, λ(Y), can be regarded as a single cell specific growth rate and it is derived from the unstructured model describing the consumption of glucose and formation of ethanol; (ii) concerning the budding and division transitions, the critical transition cell sizes (μ_B and μ_D) are function of the locally available substrate concentration, and mathematically described by Monod type expressions. A mother and a daughter cell are generated upon division, where the ratio of the mother cell size to the daughter cell size is defined by the partitioning function, *P(m,m'| Y)*. This function consists of a symmetrical beta probability density function. The dependence of the partitioning function on the substrate was neglected for this case study.

3.2. Unstructured Model: Description of the extracellular environment

The unstructured model describes the fermentation of glucose (substrate) to ethanol. The local consumption rate is estimated based on an averaged yield of biomass on substrate and the concentration of biomass present at a given location in the microreactor and a given time point. The rate of formation of ethanol is estimated in a similar fashion. This concentration of biomass is calculated as the zeroth moment of the total cell size distribution. The updated concentrations of glucose and ethanol are used for recalculating the substrate factor λ(Y), which serves as input to the PBM.

3.3. Solution methods

The fixed-pivot technique (Kumar and Ramkrishna, 1996) was used to discretize the PBE, using an evenly distributed grid with 20 pivots. The commercial software by ANSYS® CFX (v. 12.1) was used, and PBM was implemented using the expression language (CEL). The geometry was defined with ICEM CFD 12.1, and a hexahedral

mesh with 32159 elements and 36535 nodes was generated. Diffusion was not considered in the simulations.

4. Results and Discussion

The glucose supplied at the inlet is transported through the reactor, allowing for the biomass to grow. The biomass is suspended, and thus is also transported throughout the reactor until it exits the system. The spherical structures allow for a higher retention of the biomass within the reactor in comparison to a plug-flow configuration, preventing a complete wash out of the biomass. The steady-state profiles for glucose, total biomass and ethanol profiles are presented in Figure 2.

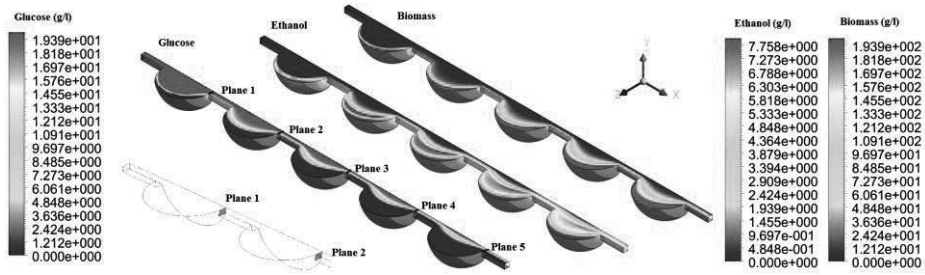

Figure 2 – Glucose, total biomass and ethanol profiles obtained at steady-state. As the reactor is symmetrical along the x- and y-axis, only a quarter of the reactor was simulated and illustrated. The total length of the reactor is 8 mm. The inlet of the reactor is located at the nearest to Plane 1.

The glucose concentration is highest at the inlet and decreases along the reactor. Therefore, the biomass growth rate is highest close to the inlet. The biomass formed in the first compartments is transported along the flow streamlines towards the outlet (Fig. 2). This results in a higher biomass concentration in the compartments closest to the outlet, although the growth rate here is virtually zero. Ethanol cannot be consumed by the cells due to the lack of oxygen. Its concentration is highest at the interface of glucose and the biomass is accumulated in each compartment.

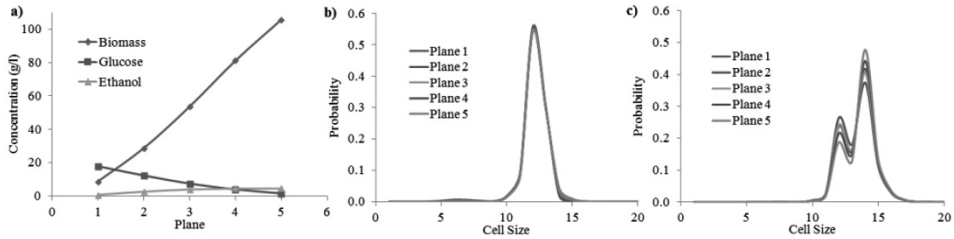

Figure 3 – Comparison of average concentrations and cell size probability density distributions for different location planes in the reactor: a) average concentrations of total biomass, glucose and ethanol b) distribution for the non-budding stage c) distribution for the budding stage. Arbitrary units are used for cell size.

Four different location planes were selected corresponding to the outlets of the spherical compartments (Fig.2) . The average glucose, ethanol and total biomass concentrations corresponding to each location plane are presented in the Figure 3. Additionally, the cell size distributions for the two stages for each of the locations are compared (Fig. 3). While the difference in the distributions is not significant for the non-budding stage, this difference is rather noticeable for the budding stage. If cells were imobilized in the

different compartments, it would be expected that the population in the compartment closest to the inlet (experiencing higher glucose concentration) would contain a higher fraction of bigger cells. Experimentally, the cell size distributions shifts towards smaller sizes when entering stationary phase (Werner-Washburne et al., 1993). This is however not observed in the simulation results, where cells are transported through the reactor. The coupling of a segregated biological model with the fluid dynamic model, increases the complexity of the problem and challenges the interpretation of the results. Different control tests, e.g. continuity check and mass balance closure, have been performed. Further investigation, both *in silico* and experimentally, is required in order to assess the validity of these results.

5. Conclusions

In this case study, a PBM describing the distribution of cell size for cell cycle stages, and its dependence on the available substrate concentration, was coupled to a fluid dynamic model that describes the transport of the supplied substrate and the biomass throughout the reactor. The interpretation of the results is challenging as the transport of the cells along the fluid streams has to be considered together with biological phenomena (growth, budding and division) taking place locally. The study is, nonetheless, a contribution to the development of modeling tools for successful prediction of the dynamic behavior of total protein content distributions of a yeast population under non-ideal mixing conditions, as found in large-scale fermentors as well. In the future a comparison of this more detailed model with simpler ones (e.g. lumped models) should be performed in order to identify the situations where the use of more complex models such as the proposed one is adequate and justifiable.

Acknowledgments

The Danish Council for Strategic Research is acknowledged for financial support in the frame of project number 09-065160.

References

S.-O. Enfors, M. Jahic, A. Rozkov et al. 2001. Physiological responses to mixing in large scale bioreactors. Journal of Biotechnology, 85, 175-185

R. Lencastre Fernandes, M. Nierychlo, L. Lundin et al. 2011. Experimental methods and modeling techniques for description of cell population heterogeneity. Biotechnology Advances, 29, 575-599

L. Alberghina, H.V. Westerhoff eds. 2005. Systems biology. Berlin/Heidelberg: Springer-Verlag. Vol. 13.

L. Alberghina, C. Smeraldi, B.M. Ranzi, D. Porro. 1998. Control by nutrients of growth and cell cycle progression in budding yeast, analyzed by double-tag flow cytometry. Journal of Bacteriology, 180, 3864-3872.

P. Jorgensen, I. Rupeš , J.R. Sharom et al. 2004. A dynamic transcriptional network communicates growth potential to ribosome synthesis and critical cell size. Genes & Development, 18, 2491 -2505.

I. Rupeš. 2002. Checking cell size in yeast. Trends in Genetics, 18, 479-485.

D. Porro, F. Srienc. 1995. Tracking of individual cell cohorts in asynchronous saccharomyces cerevisiae populations. Biotechnology Progress, 11, 342-347.

C. Hatzis, D. Porro. 2006. Morphologically-structured models of growing budding yeast populations. Journal of Biotechnology, 124, 420-438.

S. Kumar, D. Ramkrishna. 1996. On the solution of population balance equations by discretization—i. a fixed pivot technique. Chemical Engineering Science, 51,1311-1332.

M. Werner-Washburne, E. Braun, G.C. Johnston , R. A. Singer. 1993. Stationary phase in the yeast Saccharomyces cerevisiae. Microbiology and Molecular Biology Reviews, 57, 383-401

I.A. Karimi and Rajagopalan Srinivasan (Editors), Proceedings of the 11th International Symposium on Process Systems Engineering, 15-19 July 2012, Singapore.

Development of an integrated model for cobalt solvent extraction using Cyanex 272

Heather A Evans[a], Linh Vu[a], Parisa A Bahri[a] and Keith R. Barnard[b]

[a] *Murdoch University – School of Engineering, South Street, Murdoch, 6150, Australia*
[b] *CSIRO Process Science and Engineering, PO Box 7229 Karawara,WA 6152, Australia*

Abstract

A model of metal extraction based on pH isotherms was generated and applied to a cobalt solvent extraction (SX) circuit. Cyanex 272 (*bis*-(2,4,4-trimethylpentyl) phosphinic acid) was used as the organic extractant due to its selectivity for cobalt over nickel in the extraction process. Experiments were conducted for cobalt, nickel and magnesium extraction, with the latter two representing impurity elements in Co SX. The methods for determining metal extraction incorporated the effects of temperature, solution composition and pH on the equilibrium constant *k*, and hence on the overall extraction extent. This information was applied to a multi-stage mixer-settler model consisting of integrated extraction units. The initial mathematical model for cobalt, which was built in Matlab can be further developed to include the impurity elements and incorporate the scrubbing and stripping units. Future work will focus on using the model for process optimisation.

Keywords: cobalt, solvent extraction, modelling, equilibrium constant, Cyanex 272

1. Solvent Extraction modelling background

1.1. Solvent extraction

Solvent Extraction (SX) is a hydrometallurgical process used to purify and concentrate metal ions of interest from an aqueous phase. It has been used on commercial scale since the 1950's (Sole et al., 2005). Selective extraction of cobalt typically from nickel-rich sulfate solutions using SX became widely possible in the 1980's with the introduction of the organic extractant Cyanex 272, which contains *bis*(2,4,4-trimethyl pentyl) phosphinic acid ('phosphinic acid') as its active component (Bourget et al., 2011). Cobalt SX using this reagent, diluted in a suitable diluent (solvent), is an equilibrium process whereby cobalt is selectively extracted from an aqueous feed solution onto the organic phase, typically by using a series of mixer-settler units. Cobalt loaded onto the organic phase is subsequently recovered by stripping with an acidic aqueous solution. The aqueous cobalt concentration can be increased by judiciously varying the aqueous to organic ratio in both the extraction and stripping stages. Cobalt extraction follows the general form of Equation 1, where RH represents the phosphinic acid.

$$Co^{2+}{}_{(aq)} + 2(RH)_{2\ (Org)} \leftrightarrow Co(R_2H)_{2(org)} + 2H^{+}{}_{(aq)} \quad (1)$$

A typical flowsheet for cobalt recovery using Cyanex 272 as the extractant is shown in Figure 1. The evaluated flowsheet consisted of three stages of counter-current extraction in mixer-settlers to effectively separate the cobalt from the pregnant leach solution (PLS). As the reaction proceeds, hydrogen ions are released from the extractant into solution, lowering the pH of the solution (Equation 1). As the reaction is highly pH dependent, alkali (base) is added to neutralise the hydrogen ions and maintain the desired pH. To minimise the risk of any entrained organic extractant being transferred to the downstream circuit, the aqueous solution leaving the last extract stage (E3) is washed with fresh diluent in the diluent wash (DW) mixer-settler. The cobalt-rich loaded organic (LO) phase leaving the first extract stage (E1) is scrubbed (Sc) to remove any co-extracted impurities such as nickel and calcium, before entering the strip circuit. Cobalt is then progressively stripped from the organic using a combination of aqueous lean electrolyte and acid to produce the loaded strip liquor (LSL) from which Co is recovered. The stripped organic is then washed with water to dilute any entrained cobalt and acid, prior to returning to the extraction circuit. For the purpose of this paper, only the extraction circuit has been modelled in detail.

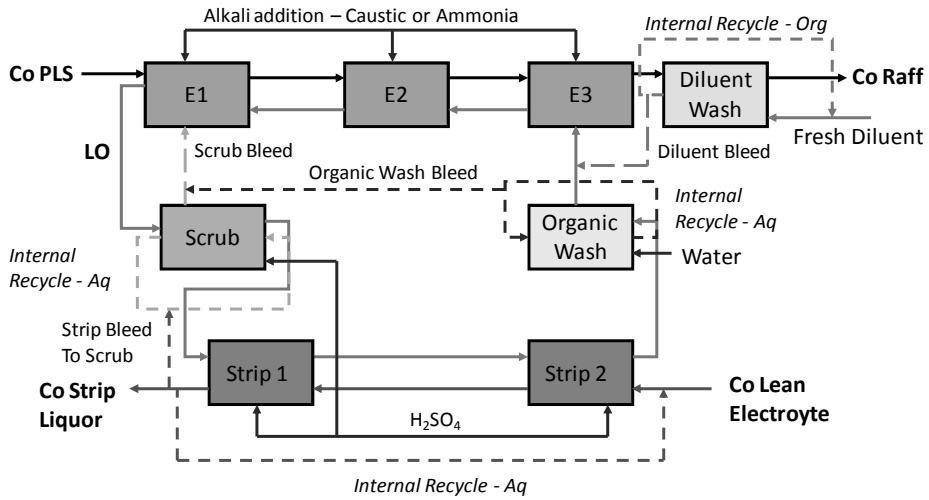

Figure 1: Flowsheet for cobalt solvent extraction using Cyanex 272

1.2. Modelling

Flowsheet modelling is an important area in the metallurgy/chemical engineering disciplines due to the high cost of new metallurgical plants and more complex processing routes being used. Engineers designing new plants and optimising existing circuits need to have a good understanding of the process and what is likely to happen if any of the input variables change during operation. While initial bench scale and pilot scale testwork can provide valuable information regarding the chemistry of the system, the long term testing required is very expensive. Therefore the use of flowsheet modelling to assist in project evaluation is becoming more widespread. The commercial modelling packages are continually being updated as new computational techniques are developed and more is known about the unit operations being modelled.

From the SX perspective, the most developed models are the proprietary modelling packages owned and operated by the reagent suppliers, the most common of which are the Isocalc™ TM (total metallurgy) and and MINCHEM® computer simulation packages developed by Cognis (formally Henkel) and Zeneca (now Cytec) respectively, as tools to assist in simulating copper solvent extraction (CuSX) processes involving sulfuric acid leaching followed by copper extraction using a phenolic oxime extractants. These modelling packages are used to develop circuit layouts, flow options, recovery options, reagent inventory and make-up requirements. Both packages rely on extensive isotherm libraries developed over a number of years covering an extremely wide range of feed and reagent combinations. Outputs from these models include McCabe-Thiele plots, calculations of stage efficiencies and final rich electrolyte and raffinate copper concentrations. These can be used to model alternate plant configurations. Inputs required are stripped organic copper concentration, feed rate and concentration and reagent concentration. However these can be varied to achieve a desired output concentration. These programs are helped by the high selectivity these phenolic oximes show for copper over other metal ions. In recent years Cytec has been adapting the MINCHEM® software for use in cobalt solvent extraction using Cyanex 272 (Bourget et al., 2011). However, this is a challenging task as this reagent can extract multiple cations besides cobalt, and exhibits variable complex stoichiometry.

2. Experimental

To generate the data required for model construction, some experimental work was undertaken. This involved the construction of pH-extraction isotherms for cobalt, nickel and magnesium extraction with Cyanex 272 under various operating conditions (refer Figure 2). The experimental procedure has been discussed elsewhere (Evans et al., 2008), and only the key results will be included here.

2.1. Relationship between log k and extraction extent for cobalt, nickel and magnesium

It is known that cobalt and magnesium tend to form tetrahedrally co-ordinated complex with phosphinic acid and nickel forms a hydrated octahedral complex (Tati, 1993; Badrul et al., 2007). As shown elsewhere (Evans et al., 2008) for the purpose of this work, we can express the extraction extent (ε%) for each metal, which can be readily measured directly, in terms of its equilibrium constant (k) and the free or available phosphinic acid (RH). Based on the resulting coordination complexes for cobalt and magnesium we use Equation 2 and for nickel we use Equation 3.

$$\varepsilon\% = \frac{k[\overline{(RH)_2}]^2}{k[\overline{(RH)_2}]^2+[H^+]^2} \quad (2)$$

$$\varepsilon\% = \frac{k[\overline{(RH)_2}]^3}{k[\overline{(RH)_2}]^3+[H^+]^2} \quad (3)$$

The equilibrium constant was determined for each metal using the experimental data and using least squares regression techniques to solve for log k. Examples of the experimental and calculated isotherms for the three metals are shown in Figure 2.

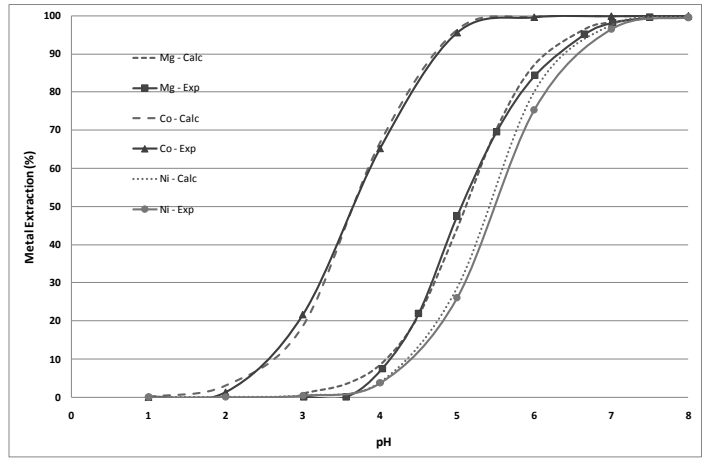

Figure 2: Experimental and calculated isotherms for cobalt, nickel and magnesium as extracted from single metal systems with 20%v/v Cyanex 272 at 35 °C.

3. Model Construction

The steady state model developed for the 3-integrated extraction units is based on the total and component mass balances around the whole system and each unit. For the purpose of the extraction model, each unit has three inlet streams: aqueous phase (A), organic phase (O) and ammonia hydroxide solution (B) used for pH neutralisation. It is assumed that B is soluble in the aqueous phase and no tertiary phases are generated, so that there are only two outlet streams A and O.

Inputs to the model are the feed composition of the aqueous phase (pH, Co, Mg and Ni concentrations), the composition of the barren organic (available RH, any residual loaded metal values Co, Mg and Ni), extraction unit pH, the temperature of the system (in K) and organic and aqueous flow rates (m^3/h). For the purpose of the initial model it is assumed that the mass flowrate of the organic phase does not change throughout the extraction stage. For the three metals studied, it was found that the Arrhenius relationship (Equation 4) could be used to determine the effect of temperature (T) on the equilibrium constant (k).

$$Ln\, k = \frac{A}{T} + B \qquad (4)$$

The two constants A and B were determined for each metal individually and the results are shown in Table 1. The high correlation (R^2) for cobalt and magnesium show that the equilibrium constants for these metals does indeed follow the Arrhenius relationship. However, the R^2 for nickel was significantly lower, indicating that nickel extraction with Cyanex 272 was relatively independent of temperature.

The model also calculates the mass of ammonia hydroxide solution to be added to each unit to maintain the pH of the reaction at a desired set-point, e.g. pH 5.5. If ammonia is not added to the mixer, the pH will drop during the extraction reaction, which lowers the overall metal extraction for the process. If too much ammonia is added, then more impurity metals will be co-extracted, and the risk of metal precipitation also increases.

Table 1: Values for constants A and B determined as a function of operating temperature

Metal	A	B	R^2
Cobalt	-8330.5	10.509	0.9892
Magnesium	-9670.9	9.252	0.9677
Nickel	-2233.4	-18.115	0.6632

The available information and the model equations were applied to develop a steady state model in Matlab code. Using the constants A and B with the temperature of the system allows the determination of the equilibrium constant for each metal. This together with the input values previously mentioned, eg pH, allows the calculation of the available RH and metal content of each stream leaving the extraction unit. As the Matlab solver can only sequentially solve the model equations, the extraction efficiency for units E1, E2 and E3 must be known to recalculate the concentration of RH in the organic phase leaving each unit. The initial model focused only on cobalt extraction using the assumption that $\varepsilon 1 = \varepsilon 2 = \varepsilon 3$. The value of $\varepsilon 3$ can be calculated directly from the pH, initial RH concentration and k as per Equation 2. After the first simulation is performed, $\varepsilon 1$, $\varepsilon 2$ and $\varepsilon 3$ must be back-calculated. If their values are significantly different from $\varepsilon 3$, the second simulation with updated values for $\varepsilon 1$, $\varepsilon 2$ and $\varepsilon 3$ must be performed and back-calculated until insignificant change in values of ε is achieved.

The initial cobalt only model assumed a feed of 0.5 g/L cobalt at pH of 5.5 with a flow rate of 300 m^3/h, at an O:A ratio of 1. At the high extraction efficiency of 95%, only 2 stages were required to extract the cobalt producing a raffinate of 0.01 g/L Co.

4. Future work

The Matlab model will be updated to include nickel and magnesium. The mathematical model will be transferred to Aspen Custom Modeller (ACM), which with its object oriented features will provide the ability to build a more efficient flowsheet incorporating recycle streams to more accurately reflect a commercial operation. This will then be used for trialling different process configurations and operating parameters leading to the optimisation of the process.

The authors would like to thank the Parker Centre for the initial project funding and CSIRO and Murdoch University for ongoing support.

References

IM Badrul, HM Zahurul, IM Shamsul, 2007, Studies on Cyanex 272 complexes of Mg(II), Ca(II) and Fe(III), Bangladesh Journal of Scientific and Industrial Research, 42, 1, pp 475-482.

C Bourget, M Soderstrom, S Donegan, J Morrison, 2011, Design optimisation of a Cyanex 272 solvent extraction circuit, Proceedings of ISEC 2011, pp 1-9.

Cognis Mining Chemicals Technology, Blue Line Technical Bulletin, www.cognis-us.com access date 31/12/2011.

HA Evans, PA Bahri, JA Rumball & KR Barnard, 2008, Modelling cobalt extraction with Cyanex 272, Proceedings of ISEC 2008, pp 459-466

KC Sole, AM Feather, PM Cole 2005, Solvent extraction in southern Africa: An update of some recent hydrometallurgical operations, Hydrometallurgy, 78, pp52-78.

BK Tait, 1993, Cobalt-nickel separation: the extraction of cobalt(II) and nickel(II) by Cyanex 301, Cyanex 302 and Cyanex 272, Hydrometallurgy, 32, pp 365-372.

I.A. Karimi and Rajagopalan Srinivasan (Editors), Proceedings of the 11th International Symposium on Process Systems Engineering, 15-19 July 2012, Singapore.

Fast simulation of annual optical efficiency of solar tower power plant

Fei Xie, Yuhong Zhao, Lifang Zhou

Department of Control Science & Engineering, Zhejiang University, Hangzhou 310027, China

Abstract

The simulation of annual optical efficiency is important for the design of a solar tower power plant. The acceleration of the efficiency computation is investigated in this paper. An efficient implementation is presented using a Graphics Processing Unit (GPU) for the optical analysis of the heliostat field in the tower power plant and a new code is developed. The efficiency and the general applicability of the proposed method to different field arrangements are verified by the numerical simulations. The speedup of the calculation on a GPU with respect to that on a CPU is significant.
Keywords: solar tower power plant, optical efficiency, GPU computing

1. Introduction

The solar tower power plant is the most economical way to produce solar electricity in large scale. It employs an array of mirrors called heliostat field to focus the sunlight upon a receiver to concentrate solar thermal energy. The heliostat field is an important subsystem because it provides the reflected energy and contributes almost half of the total plant cost. Therefore the optical efficiency needs to be calculated repeatedly to evaluate the performance of the heliostat field during the design and optimization of the heliostat field layout. Although some codes and methods have been developed to simulate the optical efficiency of the heliostat field (Garcia et al., 2008), none of them has a good performance on accuracy, computing speed and versatility simultaneously due to the large amount of computation which is difficult to be handled with CPU.

On the other hand, Graphics Processing Unit (GPU) has become an integral part of today's mainstream computing systems for the purpose of high performance computing since NVIDIA released the Compute Unified Device Architecture (CUDA) toolkit in 2006. With the help of CUDA, GPU can be easily used for general-purpose computing and numerous scientific papers have been published showing moderate to impressive improvements in performance of codes on a GPU over a CPU (Bleichrodt et al., 2011).

CUDA programming model allows programmers to define a C function, called kernel, which can be executed in parallel on a set of GPU threads. The threads are organized into groups called thread blocks. One or more than one blocks consist of a grid. This provides a more efficient architecture with two parallel levels in a kernel function: the coarse-grained parallel (blocks in a grid) and fine-grained parallelism (threads in a block). A detailed introduction to CUDA can be found in NVIDIA, 2011.

In this paper, a new acceleration method for the computation of the optical efficiency of the heliostat field is proposed by exploring the parallel processing capabilities of GPU. The model and the numerical methods adopted are introduced in Section 2. In Section 3, the implementation on CUDA is described in detail. In Section 4, the simulation results are given and the performance of two codes is compared. Finally, conclusions are drawn and the future research is indicated in Section 5.

2. The numerical model of the optical efficiency

The optical efficiency is to measure the energy loss of the heliostat field which is about 47% annually. The loss mainly comes from five parts: the cosine loss (23.4%), the mirror reflectance loss (10%), the atmospheric attenuation loss (6%), the shading and blocking (s&b) loss (5.6%) and the receiver spillage loss (2%) (Wei et al., 2010).
In general, the optical efficiency of the field $\eta_{optical}$ can be given by

$$\eta_{optical} = \rho_{Mirror} \cdot \eta_{cos} \cdot \eta_{Atmosph.Att} \cdot \eta_{s\&b} \cdot \eta_{spillage} \quad (1)$$

where ρ_{Mirror}, η_{cos}, $\eta_{Atmosph.Att}$, $\eta_{s\&b}$ and $\eta_{spillage}$ are the mirror reflectance efficiency, the cosine efficiency, the atmospheric attenuation efficiency, the s&b efficiency and receiver spillage efficiency respectively, which is equivalent to 1 minus the corresponding loss. Since the mirror reflectance loss depends on the heliostat reflective rate, ρ_{Mirror} can be considered as a constant ($\rho_{Mirror} = 0.9$ is adopted in this work). The heliostats are assumed to be perfectly flat and the sunlight is supposed to be parallel in this paper, therefore the receiver spillage loss was not taken into consideration, namely $\eta_{spillage} = 1$. As a result, three types of efficiency need to be computed to determine the optical efficiency.
In fact, in order to obtain the annual optical efficiency of the field, which is based on the hourly performance of each heliostat on certain days during a year (Pitz-Paal et al., 2011), these three efficiencies have to be simulated at hundreds of solar positions (the azimuth angle and the elevation angle of the sun) for thousands of heliostats leading to a large amount of computation and then a long running time. Hence, a parallel computing method is presented to accelerate the procedure of the efficiency calculation.
The calculation method of the three efficiencies for a single heliostat called calculated heliostat which is represented by H with center $O_H(x_{OH},y_{OH},z_{OH})$ is described in this section. The other heliostats can be calculated similarly.

2.1. The cosine efficiency, η_{cos}

The amount of insolation reflected by the heliostat is proportional to the amount of sunlight intercepted. The reflected power is proportional to the cosine of the angle between the heliostat normal and the incident sun rays. Let S be the unit vector with the opposite direction of the incident ray and R be the unit vector of reflected ray of H. Because the angle between S and R is twice of the angle between the heliostat normal and S, the cosine efficiency can be expressed as follows:

$$\eta_{cos} = cos\left[\frac{1}{2} arccos(S \cdot R)\right] \quad (2)$$

2.2. The atmospheric attenuation efficiency, $\eta_{Atmosph.Att}$

Some of the energy of the reflected rays is scattered and absorbed by the atmosphere. This effect is referred to as the atmospheric attenuation loss. The atmospheric attenuation efficiency can be calculated simply as a function of the distance between heliostat and receiver d_{HR} in meter for a visual range of about 40 km (Wei et al., 2007):

$$\eta_{Atmosph.Att} = \begin{cases} 0.99321 - 0.0001176 * d_{HR} + 1.97 * 10^{-8} * d_{HR}^2 & (d_{HR} \leq 1000m) \\ e^{-0.0001106 \times d_{HR}} & (d_{HR} \geq 1000m) \end{cases} \quad (3)$$

2.3. The shading and blocking efficiency, $\eta_{s\&b}$

The shading loss is the part of the reflective area which shadowed by other heliostats. The blocking loss is the fraction of the reflected radiation hitting the back of other heliostats. The s&b loss is mainly caused by adjacent heliostats. Before computing the

s&b efficiency, the heliostats that may cause s&b loss to the calculated heliostat H must be decided. First two rectangles are generated with O_H located at the midpoint of one side of each rectangle as shown in Fig. 1 and the other pair of sides parallel with the incident ray (for judging shading loss) and the reflected ray (for judging blocking loss) separately. The side lengths depend on the relative position of H, the receiver and the sun. The calculation is omitted due to space limitation.

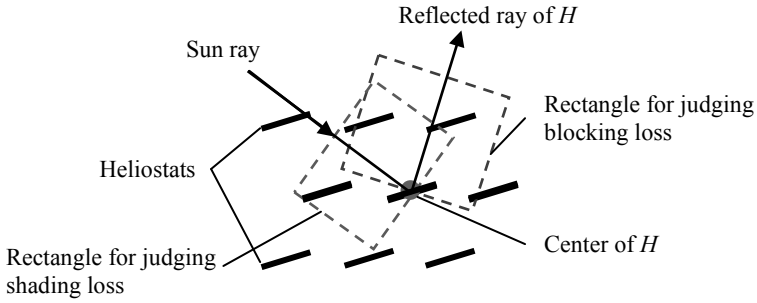

Fig. 1 Diagram of determining the heliostats that may cause shading and blocking loss (from top view in the ground coordinate system)

All the heliostats whose centers locate in the rectangle margin are called projecting heliostats, which may cause s&b loss to H. A projection parallelogram can be formed for each projecting heliostat by projecting the vertices of the projecting heliostat to the plane spanned by H along the direction of the incident ray or the opposite direction of the reflected ray and transforming the results into the coordinate system of H, which is depicted as Fig. 2.

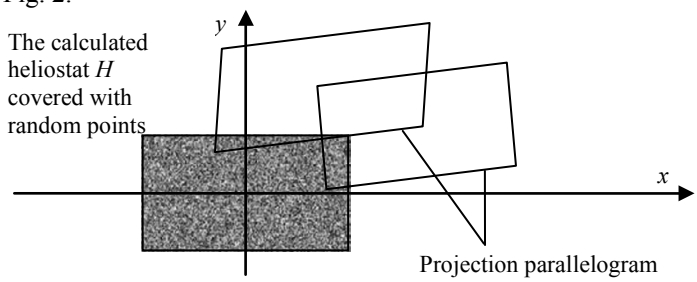

Fig. 2 Diagram of computing the s&b efficiency

The s&b efficiency is the ratio of the area of H that is not covered by any projecting parallelogram to the area of H. Since it is difficult to calculate this irregular area analytically, Monte Carlo method is adopted. Numerous random well-distributed points are generated to cover H. Count the points which are not in any parallelogram and the s&b efficiency can be represented by the ratio of the counter to the total number of random points. The total number determines the accuracy of the derived efficiency.

3. Implementation details

The method described in Section 2 is implemented on CPU and GPU respectively. The main parts of both codes are written in MATLAB. The difference is that the GPU code calls CUDA through the parallel computing toolbox in MATLAB when computing the most computationally intensive part, $\eta_{s\&b}$.

The inputs for both codes are the coordinates in the ground coordinate system of the heliostats and the receiver and the solar position. The unit vectors of the incident ray, the reflected ray and the normal of each heliostat are computed first, followed by η_{cos},

$\eta_{Atmosph.Att}$ and the coordinates of the vertices of each heliostat, and finally $\eta_{s\&b}$ of each heliostat is calculated as following steps:
1) Decide the projecting heliostats;
2) Compute the coordinates for the vertices of the projection parallelogram;
3) Judge the points that are not in any projection and calculate the s&b efficiency.
The key issues of step 1 and 3 are the same, which is to identify whether a point is inside a quadrilateral or not. Different methods are adopted on GPU and CPU to make use of their advantages. As CPU is good at logical affair and serial computing while GPU performs well implementing highly threaded parallel processing tasks, a coordinate judgment method with more logical affair is used on CPU and the Helen Theorem method exhibiting more computationally intensive is used on GPU to achieve the fastest running speed on both codes. The former judges the position relationship between the point and the four vertices of the parallelogram, while the latter computes the areas of the four triangles which are formed by the point with every two adjacent vertices of the parallelogram and compares their sum with the area of the parallelogram. By exploiting the two-level parallel architecture of GPU, each block is used to calculate the efficiency of a different heliostat and the threads in each block are in charge of the related calculation of the same heliostat.

4. Simulation Results

The numerical simulations are implemented on an Inter® Core™ i5-2300 CPU @2.80GHz and a NVIDIA's GTX 570 GPU. The performance comparisons between the codes on CPU and GPU are illustrated in Fig. 3. Both codes are applied to calculate the optical efficiency of a corn-field heliostat field with similar heliostat size and field arrangement to the eSolar's plant at an individual solar position (Schell, 2011). Fig. 3(a) shows the running time comparisons between two codes at different field scales and with different accuracy which is defined as the reciprocal of the number of the random points covering a heliostat. The Grid size used in the GPU code is 10000, which is the product of the block number and the number of threads in each block. In Fig. 3(b), the speedup of the calculation on the GPU with different Grid size with respect to that on CPU is plotted for different field scales with same accuracy of 0.0001. The results manifest that the proposed method behaves much better on GPU than on CPU especially with the increasing of the computation if the Grid size is big enough.

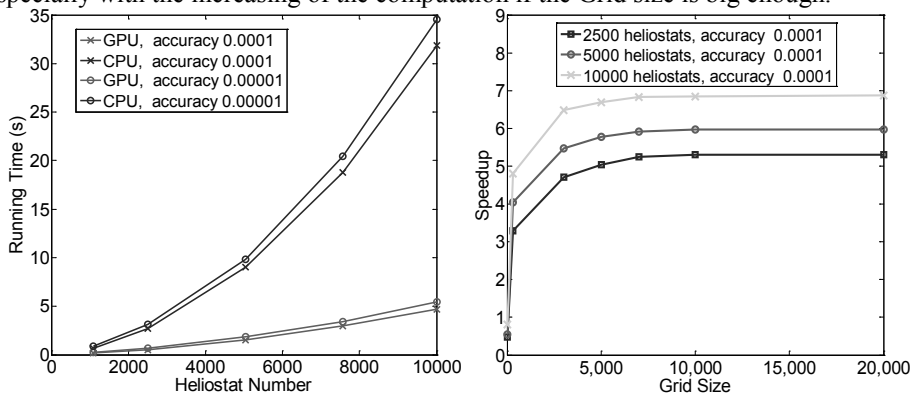

(a) Running time at a solar position on GPU and CPU (b) Speedup of GPU compared to CPU

Fig. 3 Performance comparisons of GPU and CPU

Moreover, the proposed method can be applied to various arrangements. The annual optical efficiencies of two different fields are depicted as Fig. 4. Fig. 4(a) indicates the

result of a corn-field heliostat field consisting of 10000 heliostats and 4(b) indicates the result of a radiate heliostat field consisting of 554 heliostats with an area of $80m^2$(10m*8m) (Siala et al., 2001). The accuracy of both simulations is 0.0001, and the running time is 4.69 seconds for the corn-field heliostat field and 0.52 seconds for the radiate heliostat field at one solar position.

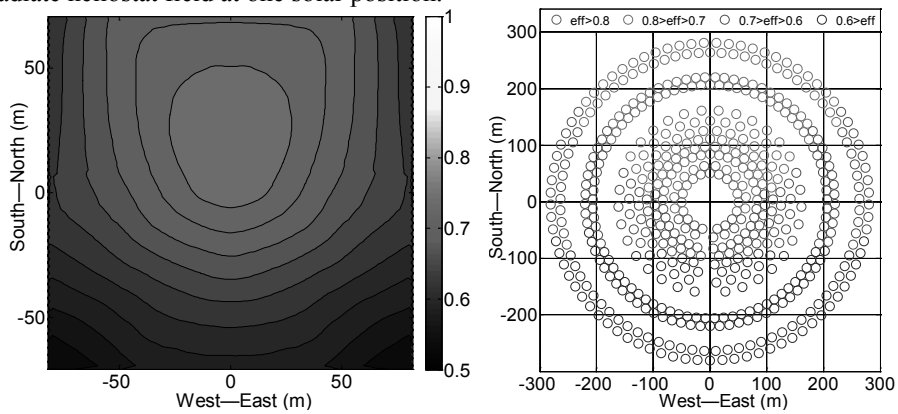

(a) Corn-field heliostat field (b) Radiate heliostat field

Fig. 4 Simulation results of the heliostat fields

5. Conclusion

A new parallel simulation method of the optical efficiency of the heliostat field in a solar tower power plant is presented on GPU using a CUDA implementation. The method is applicable to various field arrangement and scale. The simulation results demonstrate that the speedup compared with the CPU method is significant under the same accuracy. However, the efficiency model used is somewhat simplified and the GPU code is not optimized to be more efficient. The further work will be focused on how to develop a more effective algorithm and a more efficient GPU code considering more practical effects.

Acknowledgements

The authors gratefully acknowledge the financial support of NSFC (61173128, 60974007) and 973 Program of China (2012CB720500).

References

F. Bleichrodt, H.B. Rob, A.D. Henk, 2011, Accelerating a Barotropic Ocean Model Using a GPU, Ocean Modelling, 41, 16–21.

P. Garcia, A. Ferriere, J.J. Bezian, 2008, Codes for Solar Flux Calculation Dedicated to Central Receiver System Applications: A Comparative Review, Solar Energy 82, 189–197.

NVIDIA, 2011, NVIDIA CUDA C Programming Guide, Version 4.0.

R. Pitz-Paal, N.B. Botero, A. Steinfeld, 2011, Heliostat Field Layout Optimization for High-temperature Solar Thermochemical Processing, Solar Energy 85, 334–343.

S. Schell, 2010, Design and Evaluation of eSolar's Heliostat Fields, Solar Energy 85, 614–619.

F.M.F. Siala, M.E. Elayeb, 2001, Mathematical Formulation of a Graphical Method for a No-blocking Heliostat Field Layout, Renewable Energy 23, 77–92.

X.D. Wei, Z.W. Lu, Z. LIN, 2007, Optimization Procedure for Design of Heliostat Field Layout of a 1MWe Solar Tower Thermal Power Plant, Proc. of SPIE 6841, 684119-1–684119-10.

X.D. Wei, Z.W. Lu, W.X. Yu, 2010, A New Code for the Design and Analysis of the Heliostat Field Layout for Power Tower System, Solar Energy 84, 685–690.

I.A. Karimi and Rajagopalan Srinivasan (Editors), Proceedings of the 11th International Symposium on Process Systems Engineering, 15-19 July 2012, Singapore.

A Numerical Analysis for Total Site Sensitivity

Peng Yen Liew[1], Sharifah Rafidah Wan Alwi[1*], Petar Sabev Varbanov[2], Zainuddin Abdul Manan[1], Jiří Jaromír Klemeš[2]

[1]*Process Systems Engineering Centre (PROSPECT), Faculty of Chemical Engineering, Universiti Teknologi Malaysia, 81310 Skudai, Johor, Malaysia.*
[2]*Centre for Process Integration and Intensification – CPI[2], Research Institute of Chemical and Process Engineering, Faculty of IT, University of Pannonia, Egyetem u. 10, H-8200 Veszprém, Hungary. Email: [*]shasha@cheme.utm.my*

Abstract

Total Site Heat Integration (TSHI) is an established method for analysis and mapping of heat sources and sinks of multiple processes linked via a centralised utility system. The TSHI method is very beneficial for analysing a total site's sensitivity to plant maintenance shutdown and production changes that affect integrated heat sources and sinks. This paper presents the Total Site Sensitivity Table (TSST) as a systematic approach for exploring the effects of plant shutdown or production changes. TSST can be used hand in hand with TSHI graphical approaches (Grand Composite Curve, Total Site Profile and Site Composite Curve) or numerical approach (Total Site Problem Table Algorithm). The graphical approach provides better insights while the numerical approach provides faster, easier and accurate calculations. Both approaches have its advantages and disadvantages and it is up to the engineers which approach they prefer or complement. The use of TSST allows a design engineer to clearly see the sensitivity of Total Site (TS) towards operational changes. The best setting for different operation condition in total site context can be selected by exploiting this tool. The worst case scenario can also be explored for the integrated TS system through the use of TSST. This information is useful for exploring the individual plant operational flexibility. Decision for having a backup heat exchanger network according to TSST would increase the energy saving for various TS operating conditions. TSST can be used to consider various *'what if'* scenarios. They allow the determination of the optimum size of utility generation system and backup piping needed to be designed, external utilities that need to be bought and stored. Application of this technique on a case study demonstrates with the assistance of TS-PTA, TSST clearly pinpoint the effects of plant shutdown or production changes on heat distribution and utility generation systems of a Total Site.

Keywords: *Total Site Heat Integration; Pinch analysis; Total Site Problem Table Algorithm (TS-PTA); Total Site Sensitivity Table (TSST); plant sensitivity*

1. Introduction

Total Site Heat Integration (TSHI) is an inter-processes integration method linked by a common site utility system. The concept was first introduced by Dhole and Linnhoff (1993) and Raissi (1994) and further extended by Klemeš et al. (1997) in the form of

designing software. This integration method offers a greater energy saving opportunity compared to single processes integration. Perry et al. (2008) has conceptually extended TSHI to reduce carbon footprint by integrating large community servicing and corporate building as additional heat sinks, and renewable energy as heat sources. However, the variability of heat supply and demand has increased the difficulty in handling and controlling the system. Varbanov and Klemeš (2011) has later introduced Time Slices with heat storage system for solving the variable supply and demand problem in TSHI. Other researches in TSHI include the development of cogeneration targeting by Bandyopadhyay et al. (2010) and Kapil et al. (2011). Varbanov et al. (2012) also revisited the minimum temperature difference (ΔT_{min}) and new software module for TSHI.

In previous methods, the site utility targets are typically obtained from graphical approach, e.g. Total Site Profile (TSP) and Site Composite Curve (SCC). Just recently, Liew et al. (2012) has introduced an alternative approach based on numerical method known as Total Site Problem Table Algorithm (TS-PTA) to target TSHI. This method is easier to construct and gives faster, easier and accurate results as compared to graphical approach which have the tendency of graphical error due to curve shifting.

In this paper, a new tool for exploring TS sensitivity - a Total Site Sensitivity Table (TSST) - is introduced. This tool can be used hand in hand with either the graphical (Dhole and Linnhoff, 1993; Klemeš et al, 1977) or numerical TSHI approaches (Liew et al., 2012). This method allows the effect of process disruption within a TS to be analysed and contingency plans and actions to be taken to avoid affecting other processes. Process disruptions may include shutdowns of one or more plants, scheduled maintenance, production changes or emergency cases. The worst case scenario for the integrated plants can also be determined using TSST, for operational flexibility of the individual plants in the TS system.

2. Methodology

The proposed methodology of TSST is defined as follows:

STEP 1: Determine TS utility requirement using the TSP (Dhole and Linnhoff, 1993; Raissi, 1994; Klemeš et al., 1997) or TS-PTA (Liew et al., 2012) for various 'what if' scenarios e.g. when there are one or more plants shutdown. To do this, the source and demand data of the plant being shut down are omitted in the construction of TSP or TS-PTA.

STEP 2: Construct TSST to show the variation of utility requirement in the TS for the different scenarios.

i. The requirements for different types of utilities during different scenario are recorded in the TSST. All values are stated in positive values for both hot and cool utilities.
ii. The variations between normal operations and the various operating conditions are calculated by subtracting the utility requirements in normal operations from the utility requirements under different operating conditions according to utility types. A positive variance indicates that there is excess utility, while a negative variance represents the deficit of external utility.

iii. If there is excess utility (positive variance), it can be cascaded down to the lower utility level with negative variance to form the "variance after cascade". If there is still excess utility, it could be sold, cooled down or the utility generation can be reduced.

iv. A summary can be made according to the results for each scenario:
- The maximum requirement for each type of utility can be computed by adding the absolute value of the most negative number in the "variance after cascade" with the utility requirement at normal operation. If there are no negative values, the maximum utility requirement is equal to the normal operation utility.
- The minimum utility requirement for each type of utility can be calculated by deducting the most positive value of "variance after cascade" from the utility requirement at normal operation.

3. Demonstration Case Study

The construction of TSST is illustrated using a demonstration case study with four process units - Processes A, B, C and D (see Table 1). The minimum temperature difference between process streams ($\Delta T_{min,pp}$) of 20 °C and the minimum temperature difference between process streams and utility ($\Delta T_{min,up}$) of 10 °C are assumed for the system. The existing available utilities are high pressure steam (HPS) at 270 °C, medium pressure steam (MPS) at 179.93 °C, low pressure steam (LPS) at 199.59 °C and cooling water (CW) at 15-20 °C.

An example of TS-PTA under normal operation is shown in Table 2. Column 8 shows the utility requirement for normal operation of this Total Site. Total Site Pinch is located at between LPS and CW. Total heating and cooling requirement for the system are 4,807 kW and 3,085 kW respectively. Multiple utility targeting at TS-PTA shows that the system requires 1165kW of HPS, 645.5 kW of MPS and 2,996.5 kW of LPS as heating utility for the whole TS. 3,085 kW of CW is required as cooling utility. These values are recorded in the second column of TSST as shown in Table 3.

Table 1: Stream data for Processes A, B, C and D

Stream	T_S (°C)	T_T (°C)	ΔH (kW)	Cp (kW/°C)	T_S' (°C)	T_T' (°C)
Process A						
A1 Hot	200	100	2,000	20	190	90
A2 Hot	150	60	3,600	40	140	50
A3 Cold	50	220	-2,550	15	60	230
A4 Hot	150	130	1,000	50	160	140
Process B						
B1 Hot	200	100	2,000	20	190	90
B2 Cold	50	120	-4,900	70	60	130
B3 Cold	50	200	-750	5	60	210
Process C						
C1 Hot	200	50	450	3	190	40
C2 Hot	200	119	1,863	23	190	109
C3 Cold	30	200	-680	4	40	210
C4 Cold	130	150	-300	15	140	160
Process D						
D1 Hot	240	100	210	1.5	230	90
D2 Cold	50	250	-400	2	60	260
D3 Cold	40	190	-1,500	10	50	200

D4 Cold	109	140	-186	6	119	150

Table 2: TS-PTA at normal operation.

1	2	3	4	5	6	7	8
Utility	Heat Source (kW)	Heat Sink (kW)	Heat Requirement (kW)	Initial Cascade (kW)	Final Cascade (kW)	MU Cascade (kW)	Utility Requirement (kW)
				0	4,807	0	
HPS		1,165	-1,165				1165
				-1,165	3642	0	
MPS	50	695.5	-645.5				645.5
				-1810.5	2,996.5	0	
LPS	1,549	4,545.5	-2996.5				2,996.5
				-4,807	0	0	**Pinch**
CW	3,085		3085				-3085
				-1,722	3,085	0	

The TS utility requirements and THU for various scenarios involving process shut downs and production changes are evaluated using TS-PTA and recorded into TSST. The variances between normal operation and the various scenarios of TS utilities requirement are then determined. For example, when Plant A is run at half of its production rate, the system has extra HPS and CW and requires more MPS and LPS as shown in scenario 3 of Table 3(a).

Table 3(a): Total Site Sensitivity Table (TSST)

Scenario		**1**			**2**			**3**		
Utility	Normal (kW)	A shut down (kW)	Variance (kW)	Variance after cascade (kW)	B shut down (kW)	Variance (kW)	Variance after cascade (kW)	½ A shut down (kW)	Variance (kW)	Variance after cascade (kW)
HPS	1165	565	600	0	1065	100	100	865	300	0
MPS	6,45.5	695.5	-50	0	645.5	0	0	670.5	-25	0
LPS	2,996.5 pinch	4,511.5 pinch	-1,515	-965	pinch 553.5	2,443	2,443	3,754 pinch	-757.5	-482.5
CW	3,085	0	-3,085	-3,085	3085	0	0	1,542.5	1,542.5	1,542.5

Table 3(b): Total Site Sensitivity Table (TSST) (continue)

Scenario		**4**			**5**			**Summary**	
Utility	Normal (kW)	BC shut down (kW)	Variance (kW)	Variance after cascade (kW)	BCD shut down (kW)	Variance (kW)	Variance after cascade (kW)	Maximum requirement (kW)	Minimum requirement (kW)
HPS	1165	885	280	280	600 pinch	565	565	1165	600
MPS	645.5	545.5 pinch	100	100	50	595.5	595.5	645.5	50
LPS	2,996.5 pinch	519.5	2477	2477	1,515	1,481.5	1,481.5	3,961.5	519.5
CW	3,085	3,085	0	0	3085	0	0	3085	1,542.5

After analysing the various 'what if' scenario, the total site integration for the demonstration case study requires a boiler that can produced a maximum capacity of 1,165 kW of HPS, 645.5 of MPS and 3,961.5 kW of LPS, giving a total 5,772 kW of steam production compared to 4,807 kW of steam required during normal operation. A

backup boiler may be a good option to cater for this production changes or the steam requirement can be obtained externally. In worst case, the minimum steam requirement for the system is 1,169.5 kW (summation of each steam types minimum requirement). Normally a boiler would require a turn down ratio of not lower than 50%. Hence assuming the boiler lowest capacity is 2,403.5 kW. It would mean the remaining 1,269 kW of steam needs to be cooled down using cooling water or sold to other plants. Another alternative is to divert the excess steam production for Combined Heat and Power (CHP) system to generate more power.
For cooling water, the maximum capacity required is 3,085 kW and minimum capacity is 1,542.5 kW.

4. Conclusion

The TSST is a simple and systematic tool for accessing the TS sensitivity towards the plant operational changes due to schedule maintenance or emergency shutdown. The tool can be used for both TS-PTA and TSP to develop utility system planning such as determining the maximum boiler size, turn down ratio, backup piping system planning and the heat to be bought or sold. The tool is also able to detect the worst case scenario in the integrated TS system for plants' operational flexibility.

Acknowledgement

The authors would like to thank MOHE (Ministry of Higher Education) Malaysia and UTM in providing the research fund for this project under Vote No. Q.J130000.7125.00H22.

References

A. Kapil, I. Bulatov, R. Smith, J. Kim, 2011, Site-wide low-grade heat recovery with a new cogeneration targeting method. Chemical Engineering Research and Design. doi:10.1016/j.cherd.2011.09.001

J. Klemeš, V. R. Dhole, K. Raissi, S. J. Perry, L. Puigjaner, 1997, Targeting and Design Methodology for Reduction of Fuel, Power and CO_2 on Total Site, Applied Thermal Engineering, vol. 7 , 993–1003.

K. Raissi, 1994, Total Site Integration, PhD Thesis, UMIST, Manchester, U.K.

P. Varbanov, J. Klemeš, 2011, Integration and Management of Renewables into Total Sites with Variable Supply and Demand. Computers & Chemical Engineering, 35(9), 1815-1826.

P. S. Varbanov, Z. Fodor, J. J. Klemeš, 2012, Total Site Targeting with Process Specific ΔT_{min}. Energy. doi: 10.1016/j.energy.2011.12.025

P. Y. Liew, S. R. Wan Alwi, P. S. Varbanov, Z. A. Manan, J. J. Klemeš, 2011, A Numerical Technique for Total Site Sensitivity Analysis, Applied Thermal Engineering. doi: 10.1016/j.applthermaleng.2012.02.026

S. Bandyopadhyay, J. Varghese, and V. .Bansal, 2010, Targeting for Cogeneration Potential Through Total Site Integration, Applied Thermal Engineering, Vol. 30, 6-14.

S. Perry, J. Klemeš, I. Bulatov, 2008, Integrating Waste and Renewable Energy to Reduce The Carbon Footprint of Locally Integrated Energy Sectors, Energy, 33, 1489-1497.

V. R. Dhole, B. Linnhoff, 1993, Total Site Targets for Fuel, Co-generation, Emission and Cooling. Computers and Chemical, 17, S101–S109.

I.A. Karimi and Rajagopalan Srinivasan (Editors), Proceedings of the 11th International Symposium on Process Systems Engineering, 15-19 July 2012, Singapore.

Study on a New type of Gas-Liquid Cyclone used in COIL

BI Rong-shan[a*], WANG Zhen-xing[a], LI Yu-gang[a], TAN Xin-shun[a] , ZHENG Shi-qing[a], LIU Zhen-dong[b], CHEN Wen-wu[b]

[a]*Research Center for Computer and Chemical Engineering, Qingdao University of Science and Technology, Qingdao and 266042,China;*
[b]*Dalian Institute of Chemical Physics, Chinese Academy of Science, Dalian and 116023, Liaoning, China*

Abstract

In order to separate the gas-liquid products from new ejector singlet oxygen generator (SOG) effectively, we designed a new type of gas-liquid cyclone. The classical Muschelknautz cyclone model method, the improved method and computational fluid dynamics (CFD) code's discrete phase model (DPM) and eddy diffusion concept (EDC) were used for the new type separator's calculation and simulation. The results show that: (1) Compared with classical Muschelnautz model, the improved Muschelknautz model can predict the cyclone's separation performance more accurately; (2) On the design conditions, the smaller droplets have more complex trajectories. For droplets larger than 3 μm, their separation efficiency is over 80% in the new separator; (3) The droplets' entrance locations affect the droplets' trajectories and separation efficiency, (4) The residence time which CFD predicts ranges from 1 to 50 ms and decreases with the droplets size increasing (5) The loss of $O_2(^1\triangle)$ in the gas phase is less than 1% and it loses primarily on the gas-liquid contact reaction.

Keywords: gas-liquid cyclone Muschelknautz Model CFD $O_2(^1\triangle)$

1. Introduction

Chemical oxygen-iodine laser (COIL)[1-3] generator can efficiently use the chemical energy and has scale-up effects. With the development of technology, there are bubble-type $O_2(^1\triangle)$ generator, rotating disk $O_2(^1\triangle)$ generators, jet $O_2(^1\triangle)$ generator and uniform droplet generator in the form types[4]. Our team developed a new type of ejector singlet oxygen generator. Because the products from ejector singlet oxygen generator have the characteristic of great gas-liquid ratio, and in order to reduce the separation process of quenching reaction, the droplets residence time in separator should be as short as possible. Besides, we designed a new type of gas-liquid cyclone, as shown in Fig. 1.

Muschelknautz model is based on Professor W. Barth[5](1956)'s research. In the past thirty years, Muschelknautz model has been becoming a perfect model to perform the actual situation of cyclone separator[6], however the gas-liquid transfer is completely different from the gas-liquid's, Muschelknautz model is rarely used for gas-liquid cyclone. The improved Muschelknautz model modified the two-phase fraction factor and limit-loading concentration[7-9]. The classical Muschelknautz cyclone model method,

* Corresponding author. Tel.: +86 532 84022515;
E-mail address: birongshan@163.com

the improved method and DPM and EDC were used for the new type of gas-liquid cyclone's calculation and simulation.

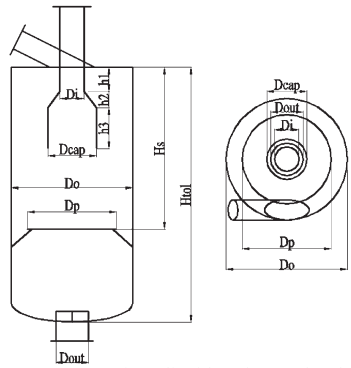

Fig. 1 New type of gas-liquid cyclone's sketch

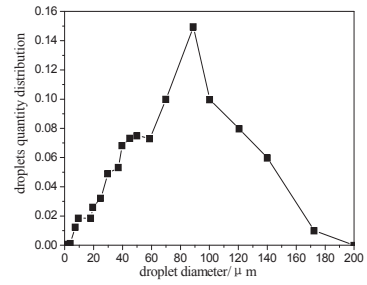

Fig. 2 Droplet diameter distribution

2. Device structure and simulation conditions

2.1. Device structure

In order to take the advantages of Muschelknautz model, the complex gas-liquid cyclone structure was simplified as following:

(1) The declination inlet tube would be a horizontal one, (2) The circular inlet would be a rectangular inlet with the same area, (3) Complex vortex finder would be a simple straight pipe and the new diameter would take the average of the original sizes, (4) Don't study the flow field below the baffle and the gap between the baffle and the wall is the liquid outlet.

2.2. Simulation conditions

The inlet boundary condition is mass-flow-inlet at the mass flow rate of 0.075kg/s. The injection type of particle phase is surface at the inlet. The outlet pressure at the top of vortex finder is 20000kpa. Discrete phase model (DPM)[10-11] was used to simulate the movement of liquid droplets and the particles' size distribution (PSD) can be presented as shown in Fig. 2. The mass rate of liquid phase is 2.6kg/s. The CFD simulation was performed with a Pentium Dual-Core E5300, 2GB RAM-memory, and 250GB hard-disc memory.

3. Result and discussion

3.1. Pressure drop

Fig. 3 shows the pressure drop of new gas-liquid cyclone CFD simulation. The static pressure decreases radically from wall to the cyclone center, and the minimum pressure appears near the top of vortex finder. The greater pressure gradient is below the vortex finder, because of the effect of the quasi-forced vortex. There is little change in static pressure field along the axis below the wide segment of the vortex finder. Besides, a sharp pressure drop appears near the narrow segment in the vortex finder, as the static pressure converts into dynamic pressure rapidly.

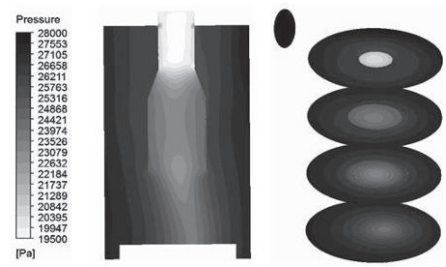

Fig. 3 contours of static pressure calculated using CFD

3.2. Grade efficiency

In this study, similar grade efficiency curves were obtained by using different calculation methods as shown in Fig. 4. The deviations of the cyclone grade efficiency between improved mathematic model and CFD are much smaller than the classic model. When the particle size is over 3μm, the grade efficiency has almost no change. The new gas-liquid cyclone can effectively remove the liquid droplets larger than 5μm and the grade efficiency is almost 100%. However, the new gas-liquid can't effectively remove the liquid droplets less than 5μm which account for a very small mass fraction; this means the new type of gas-liquid cyclone can effectively separate the gas-liquid mixture.

It also can be seen in Fig. 4 that the grade efficiency calculated by improved Muschelknautz model is better than the classic one. This is because the classic Muschelknautz model's total friction factor doesn't suit gas-liquid mixture, which can get an inaccurate tangential velocity at the cylindrical surface.

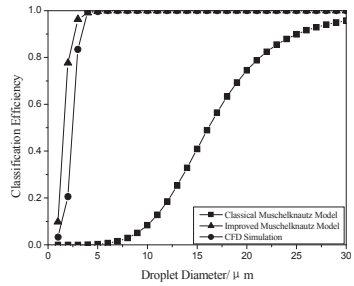

Fig. 4 Classification Efficiency at different models

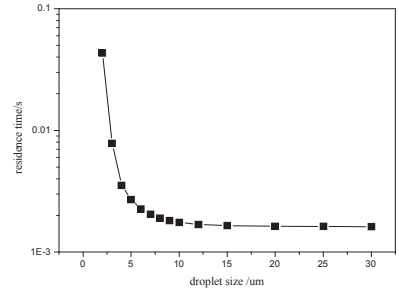

Fig. 5 the residence time of different droplets sizes

3.3. Droplets residence time

In the gas-liquid cyclone separation process, the gas-liquid mixture feeding the cyclone enters though some upstream piping where droplets coalesce into bigger one which is different from solid particles. Professor Wendy Zhang and Silney Nagal[12-13] studied the process of droplets hitting a surface under different surrounding pressure. The results show that the presence of gas is a decision condition to form droplets splashing. The design pressure of ejector singlet oxygen generator is 20kPa which is very similar with the Wendy Zhang's experiment's 17.2kPa. When the droplets hit the wall, they will form a uniform film without serious splash and shed along the wall. The time for droplets reaching the wall was considered the residence time of droplet for the loss of $O_2(^1\triangle)$ mainly happening in the gas-liquid transfer process. Fig. 5 shows the residence time of different droplets sizes calculated by CFD. The residence time which CFD predicts ranges from 1 to 50 ms and decreases with the droplets size increasing, which are in keeping with practical experience and previous laboratory studies. As the droplet size distribution tested by PDPA shown in Fig. 2, most of the droplets residence time is about 1.6ms.

3.4. Particles trajectories

The calculated particles' trajectories with different sizes are shown in the Fig. 6. As shown in the figures, the increase of liquid droplets size raises the collection efficiency since the effect of larger centrifugal force causes a larger advance distance. The particles with larger scale, such as 4μm and 5μm, can quickly spin down along the wall to reach the new separator's baffle. For small particles, the centrifugal force will be less than the drag force between air and droplets, which will make the small particles reach the wall difficultly and do many rotations below the bottom of vortex finder. As for critical particles, 3μm particles has a strong random. If they enter the irregular flow field at the

bottom of gas-liquid cyclone, they have a great chance to escape from the vortex finder.

The droplets' entrance locations can significantly affect the droplets' trajectories and separation efficiency. As shown in Fig. 6's 3μm(b), two 3μm particles enter the new separator from the top of inlet surface. Because the roof affects the top flow field of gas-liquid cyclone, the particles do rotations with almost parallel way at the top of separator. Compared with the 3μm(a) particles can be easily caught, the 3μm(b) particles have more complex trajectories and the less efficiency.

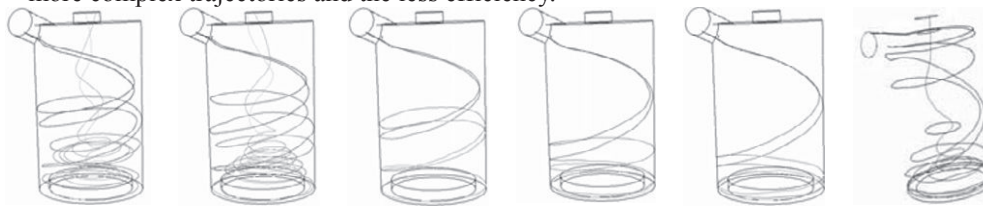

Fig. 6 the track of droplets with different sizes

4. Reaction research

4.1. $O_2(^1\triangle)$ quenching reaction in gas phase

In order to study the details of $O_2(^1\triangle)$ quenching reaction in gas phase, Eddy-Dissipation-Concept(EDC) was used for CFD simulation. The inlet feed is composed of $O_2(^1\triangle)$, Cl_2, He, H_2O(vapor), and their mole fractions are 0.3846, 0.01, 0.6044, 0.001. Fig. 7 shows the mole fraction of $O_2(^1\triangle)$ in the axial section and radial sections with different heights. At the inlet of gas-liquid cyclone separator, the concentration of $O_2(^1\triangle)$ is the highest, with the gas-liquid separation process carrying through, quenching reactions become more and more severe; the bottom of gas-liquid cyclone separator is the position where $O_2(^1\triangle)$ concentration is lowest; when the gas coming from bottom enters into the vortex finder, they mix with the fresh gas from inlet which causes an apparent high level. However, the $O_2(^1\triangle)$ quenching in gas phase is little, just from 38.46% to 38.28%. Most of the quenching occurs in the gas-liquid contact reaction.

4.2. p-τ of gas-liquid cyclone separator

p-τ value was experimentally proved to be a key parameter for the chemical efficiency of the chemical oxygen-iodine laser (COIL). In our COIL device with ejector singlet oxygen generator and chlorine flow rate of 0.5mol/s, the $O_2(^1\Delta)$ absolute yield and p-τ have a good correlation. Here, the $O_2(^1\Delta)$ absolute yield is defined as the converting efficiency from chlorine and measured by PS method[14].

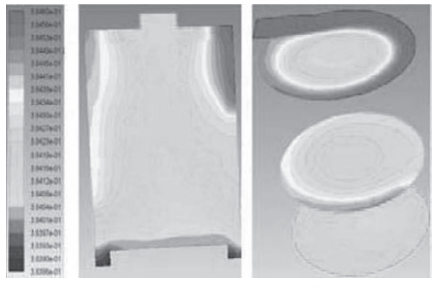

Fig. 7 the mole fraction of $O_2(^1\triangle)$

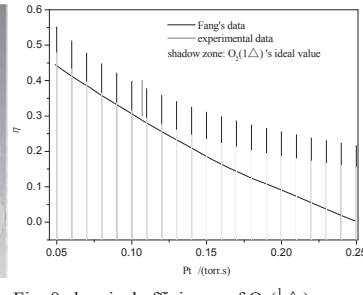

Fig. 8 chemical efficiency of $O_2(^1\triangle)$ vs p-τ value

Fig. 8 shows the relationship between chemical efficiency of $O_2(^1\triangle)$ and p-τ value. Red line is our experimental data obtained in the pilot test system. Compared with Fang's data[15], in the same p-τ value, chemical efficiency of $O_2(^1\triangle)$ is higher than Fang's device ; so it is better than Fang's device. Shadow area is obtained by calculating the chemical efficiency of $O_2(^1\triangle)$ using Fang's empirical formula. As the shadow area is basically on the top of the Fang's data, the new gas-liquid cyclone separator of ejector SOG system is reliable and feasible.

5. Conclusion

In this paper, we designed a new gas-liquid cyclone separator for separating the gas-liquid products from new ejector SOG effectively. The classical Muschelknautz cyclone model, the improved cyclone model, CFD and experiment was used to study the new gas-liquid cyclone separator's performance. The results show that: (1) the improved Muschelknautz cyclone model is very similar to the CFD simulation results; (2) droplet size and inlet position can significantly affect the droplet's separation efficiency; (3) the droplet residence time is inversely proportional to the size of droplets; (4) the loss of $O_2(^1\triangle)$ in the gas phase is less than 1% and it loses primarily on the gas-liquid contact reaction; (5) compared with Fang's experimental data, the new SOG system is reliable and feasible.

References

[1] J.Vetrovee, 1996, Prospects for an industrial chemical oxygen-iodine laser, Proc. SPIE, 3092: 723-726.
[2] W. C. Solomon and D. L. Carroll, 2000, Commercial applications for COIL, Proc. SPIE, 3887: 137-151.
[3] W. P. Latham, K. R. Kendrick and B. Quillen, 2000, Applications of the chemical oxygen-iodine laser, Proc. SPIE, 3887:170-178.
[4] SANG Feng-ting, JIN Yu-qi, DUO Li-ping, 2006, Chemical laser and its application, Chemical Industry Press, Beijing.
[6] Hoffmann A C,Stein L E. 2004, Gas cyclone and swirl tubes: principles, design and operation. Chemical Industry Press, Beijing.
[7] Muschelknautz E,Trefz M. Design and calculation of higher and highest loaded gas cyclones. Proceedings of Second World Congress on Particle Technology[C], Japan,52-71.
[8] Trefz M, Muschelknautz E., 1993, Extended cyclone theory for gas flows with high solids concentration, Chem Eng Techn, 16(3):153-160.
[9] Muschelknautz E,Dahl H D, 1994, Cyclone as Droplet Separators, Chem Ing Techn, 66(2), 223-229.
[10] Elsayed K, Lacor K, 2010, Optimization of the cyclone separator geometry for minimum pressure drop using mathematical models and CFD simulations, Chem Eng Sci, 65(8): 6048-6058.
[11] Fluent Inc., 2003, FLUENT User's Guide, Fluent Inc.
[12] L. Xu, W. Zhang, S. R. Nagel, 2005, Drop Splashing on a Dry Smooth Surface, Phys. Rev. Lett., 94, 184505.
[13] Michelle M. Driscoll, Cacey S. Stevens, and Sidney R. Nagel, 2010, Thin film formation during splashing of viscous liquids, Phys. Rev. E 82, 036302.
[14] Duo L P, Cui T J, Wang Z Q, 2001, Absolute $O_2(^1\Delta)$ concentration measurement in singlet oxygen generator by using the piston source method, Journal of Physical Chemistry A, 105: 281-284.
[15] FANG Ben-jie, WEI Ling-yun, etc, 2002, Experiment investigation of the influence of *p-τ* on COIL, High Power Laser and Particle Beams, 14(1):26-28.

I.A. Karimi and Rajagopalan Srinivasan (Editors), Proceedings of the 11th International Symposium on Process Systems Engineering, 15-19 July 2012, Singapore.

Trend analysis for studies of knowledge flow in research on polymeric materials

Sitarz R.[a,b*], Heneczkowski M. [b], Kraslawski A. [a,c].

[a]*Department of Chemical Technology, Lappeenranta University of Technology, POBox 20, 53851 Lappeenranta, Finland.*
[b]*Faculty of Chemistry,, Rzeszow University of Technology Al. Powstancow Warszawy 6, 35-959 Rzeszów, Poland.*
[c] *Faculty of Process and Environmental Engineering, Technical University of Lodz, Poland*

Abstract

Dynamics of research trends and patenting activity in a given period of time are important factors influencing the composition of the portfolio of the research projects. This article introduces the methods for identification of thematic clusters, determination of their development dynamics and prediction of the short-term trends in a specific research domain. The research on polymeric materials: composites, nanocomposites and blends has been analyzed in this paper. The presented method of structuring is based on clustering of word sets. The financial analysis techniques are applied to identification of dynamics and trend development in the analyzed field of research. The presented analyse is limited to the research papers found in Science Direct database in 1980-2010. The diversified development trends of the identified clusters have been identified e.g. strong development trend of the cluster "Biomedical application", or visible decline of the cluster "Structure of nanocomposites"

Keywords: blends, nanocomposites, composites, technology forecasting, trend analysis

1. Introduction

The assessment of development trends in the given branch of technology is important factor influencing decisions on R&D funding (Zapata et al. 2008, Rajapakse et al. 2005). The number of scientific publications and patents is indirect indicator of importance and growth potential of the specific area of expertise (Fabry et al. 2006). The changing number of publications and patents is an important information facilitating the prediction of the development trends in the analyzed field of research.
This paper analyses the following aspects of research on composites, nanocomposites and blends:

- identification of thematic clusters
- determination of research dynamics
- prediction of the short-term development trends

* Corresponding Author e-mail: robs@prz.edu.pl

2. Method

The identification of the thematic clusters and prediction of the development trend in a given research field is based on the method presented by Sitarz et al. (2010). The structure of the method is given in Fig. 1.

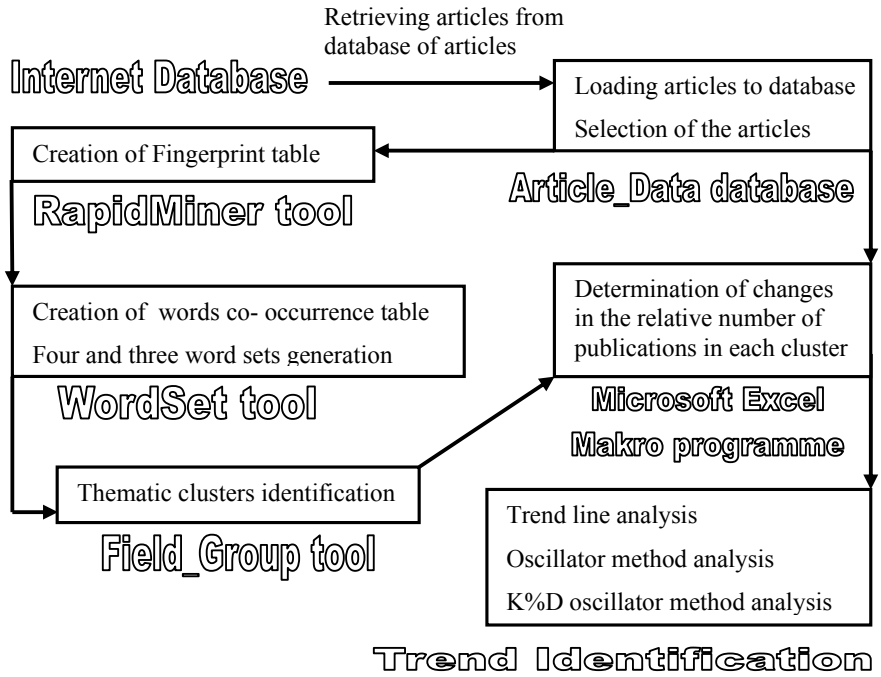

Figure 1. The structure of the method for identification of development trends in a given field of research

The creation of fingerprint table is realized using a dedicated tool: a Rapidminer with TextInput operator (Mierswa et al. 2006). The fingerprint of each paper consists of the set of characteristic words that constitute the meaning of a given paper. The table is created using the statistical analysis of the text and removal of non-specific "stop-list" words, such as "the", "be", "can". The next tasks are realized applying "WordSet" tool. It creates the word co-occurrence table (Ding et al. 2001) and generates four- and three-word sets (Sitarz et al. 2010). The columns and rows of the co-occurrence table are composed of the fingerprint words. The value in each cell shows how many times a given column-row word pair co-occurs. The four-word sets, which determine the seeds of thematic clusters, are generated by checking every possible four-word combination. The combinations satisfying the conditions presented below are selected (Sitarz et al. 2010):

$$D_{wi} \cap D_{wj} \cap D_{wk} \cap D_{wl} \geq ThrA \quad ; \frac{D_{wi} \cap D_{wj} \cap D_{wk} \cap D_{wl}}{\frac{1}{4}\left(D_{wi} + D_{wj} + D_{wk} + D_{wl}\right)} \geq ThrB \qquad (1)$$

where: D_{wi} – number of articles where word wi occurs; ThrA, ThrB – threshold values.

The values of ThrA and ThrB affect the number of word sets. There should be a minimal number of the articles that is greater than ThrA in order to identify only the essential thematic clusters as well as emerging ones. However, only the significant words should be considered, it means characterized by high word co-occurrence between words constituting the same thematic field. In the next step, the four- and three-word sets are grouped into thematic fields by the "Field_Group" tool, applying the agglomerative clustering method (Voorhees 1986).

The similarity between cluster pair (e.g. X and Y) is calculated as follow:

$$MIN\left[\left(\frac{D_{Si} \cap D_{Sj}}{MIN(D_{Si}, D_{Sj})}\right), For \quad i = 1..I, j = 1..J\right] \tag{2}$$

where: Si denotes the word sets belonging to the cluster X, Sj denotes the word sets belonging to the cluster Y, D_{Si} - number of the articles where word set Si co-occurs, I-number of the word sets in the cluster X, J - number of the word sets in the cluster Y,
In the next step, the determination of the yearly distribution of the relative number of the papers belonging to every thematic cluster is performed using Microsoft Excel Makro programme (Sitarz et al. 2010).

The last block, trend identification, is composed of three methods used in the technical analysis of the financial markets (Murphy 1999). The application of the methods (trend line method, oscillator method and K%D stochastic oscillator method) was presented in Sitarz et al. 2010.

3. Results

There were analyzed 17431 papers published in 1980- 2010 and found in Science Direct database using the search query: "blend and (composite or nanocomposite) and polymer". In the next step of the analysis, 13828 papers with the published abstracts were selected. Rapidminer has generated the fingerprint table for 7287 fingerprint words. 1050 four-word sets were identified for ThrA equal 14 and ThrB set as 0.13. The "Field_Group" tool identified 318 thematic clusters for the previously generated word sets for a C threshold value equal to 30%.
Due to the limited space, only the most representative examples are selected to present the most typical trends. Fig. 2 presents the change in the relative number of the papers belonging to the clusters "Biomedical application" and "Sources of electricity – batteries" published between 1980 and 2010, as well as the trend line method (solid lines I, II and III). Fig. 3 and 4 present the results of two oscillator methods for the clusters. On the left side of the figures the oscillator method is presented for x parameters equal 4 (oscillator 4) and 2 (oscillator 2). On the right side of the figures the results of K%D oscillator method are given (%K line for a y parameter equal 4), Murphy 1999.

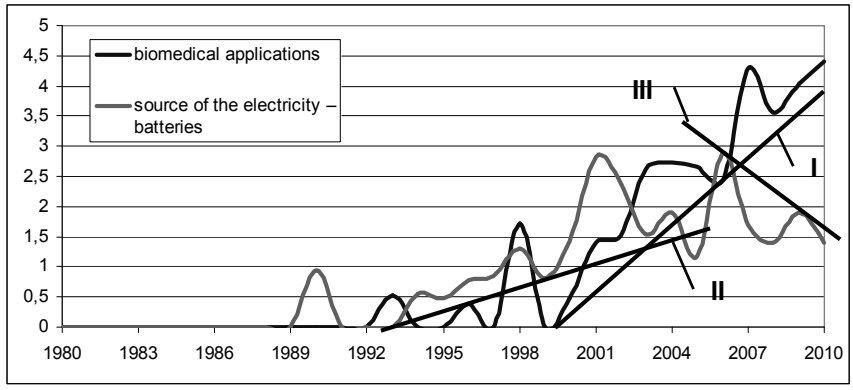

Figure 2. Relative number of publications and trend line method for the clusters "Biomedical application" and "Sources of electricity – batteries"

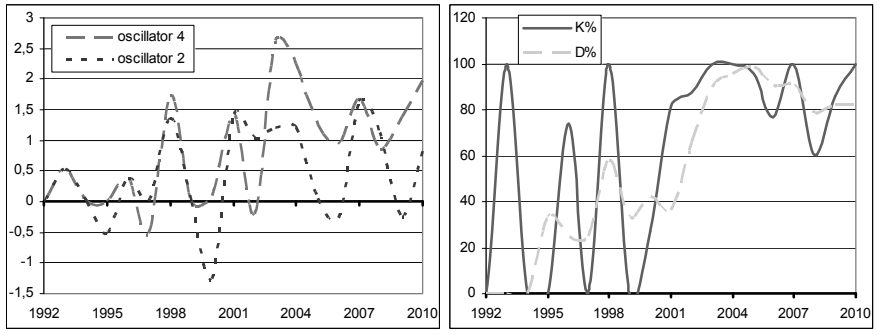

Figure 3. Oscillator and K%D methods for the cluster "Biomedical application"

For the cluster "Biomedical application" an increasing trends from 1999 can be identified, Fig. 2 and Fig. 3. It is illustrated by the increasing trend line I, positive momentum values of both oscillators after 1999, as well as intersection %K and %D lines in 2000.

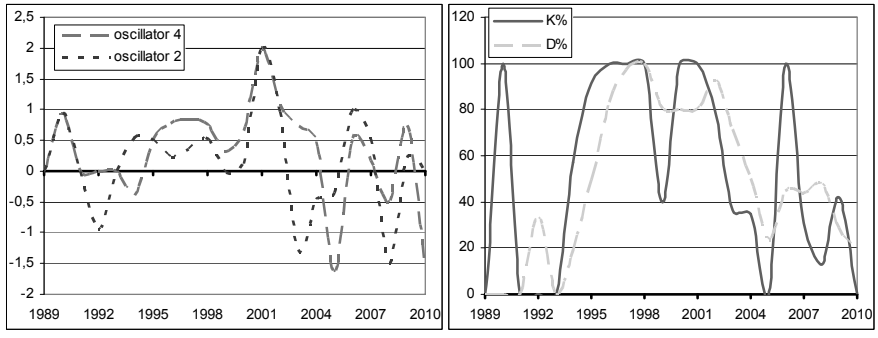

Figure 4. Oscillator and K%D methods for the cluster "Sources of electricity – batteries"

For the second analyzed cluster, the trend line method suggested an increasing trend from 1993 to 2004 (trend line II in Fig. 2), and next the increase of the relative number of publication toward 2006, and the decreasing trend toward 2010 (trend line III in Fig. 2). The momentum values of both oscillator methods were positive between 1994 and 2004, confirming the increasing trend for this period. Afterwards, the momentum values intersected at the zero line several times, forming the increasing trends from 2005 to 2007 and 2009-2010 as well as decreasing trend between 2004 and 2005 and from 2007 to 2009. The intersection of the zero line in 2010 by both momentum lines is a signal of future decreasing trend.
The first presented cluster "Biomedical application" is still developing, but the second one "Sources of electricity – batteries" seems to be declining, despite the peak activity in 2001 and 2006.

4. Summary

The identified clusters have shown the diversified patterns of development. Some clusters, e.g. "Biomedical application", "Carbon nanotubes", "Carbon nanofibers", "Photovoltaic cells", exhibited the increasing trend. The others, e.g. "Structure of nanocomposites", "Thermal resistance", "Hybrid polymers" have shown the signs of decline. The other ones, e.g. "Sources of electricity – batteries", "Fracture and stress cracking", "Tribological properties", have exhibited the long stagnation period.
The presented method identifies potentially interesting areas of research, worth of investments, for which development is forecasted. The method is universal and can be adopted to various research disciplines. The authors have analyzed several research field using the presented method (e.g distillation, filtration) with good predictive performance.

References

Y. Ding, G.G. Chowdhury, S. Foo, 2001, Bibliometric cartography of information retrieval research by using co-word analysis, Information Processing and Management, 37, 817 – 842.
B. Fabry, H. Ernst, J. Langholz, M. Köster, 2006, Patent portfolio analysis as a useful tool for identifying R&D and business opportunities—an empirical application in the nutrition and health industry, World Patent Information, 28, 3, 215-225.
I. Mierswa, M. Wurst, R. Klinkenberg, M. Scholz, T. Euler, 2006, YALE: Rapid Prototyping for Complex Data Mining Tasks, in Proceedings of the 12th ACM SIGKDD International Conference on Knowledge Discovery and Data Mining (KDD-06).
J.J. Murphy, 1999, Technical Analysis of the Financial Markets, New York Institute of Finance.
A. Rajapakse, N.J. Titchener-Hooker, S.S. Farid, 2005, Modelling of the biopharmaceutical drug development pathway and portfolio management, Computers & Chemical Engineering, 29, 1357-1368.
R. Sitarz, A. Kraslawski, J. Jezowski, 2010, Dynamics of Knowledge Flow in Research on Distillation, Computer Aided Chemical Engineering, 28, 583-588.
E.M. Voorhees, 1986, Implementing agglomerative hierarchic clustering algorithms for use in document retrieval, Information Processing & Management, 22, 465-476.
J.C. Zapata, V.A. Varma, G.V. Reklaitis, 2008, Impact of tactical and operational policies in the selection of a new product portfolio, Computers & Chemical Engineering, 32, 307-319.

I.A. Karimi and Rajagopalan Srinivasan (Editors), Proceedings of the 11th International Symposium on Process Systems Engineering, 15-19 July 2012, Singapore.

Multidimensional Monte Carlo Cell Population Dynamics in Virus Replication Systems

Andreas Voigt[a]

[a]*Process Systems Engineering, Otto-von-Guericke-University Magdeburg, Universitätsplatz 2, 39106 Magdeburg, Germany*

Abstract

We present a kinetic Monte Carlo simulation of a discrete cell population model. The model takes into account internal cell properties related to the viral RNA translation and replication. These dynamical changes can be compared to new available experimental data obtained with quantitative real-time reverse transcription PCR. In combination with the virus release from the cells into solution the model couples the internal and external cell environment in one single ansatz. This kind of high dimensional population balance modeling has already shown promising results in other areas of process systems technology, for example particulate processes. Here its application for applied biosystems technology is key to a better understanding of the process as a whole and to possibilities of process optimization and experimental design.

Keywords: Kinetic Monte Carlo Simulation, Cell Population, Virus Replication

1. Introduction

A biotechnological process of virus production using Madin-Darby canine kidney cells (MDCK) has been studied experimentally and theoretically (see e.g. [1,2]). A thorough understanding of the complex interaction of the cell population and the virus replication is important in order to optimize and improve the established process technology. Measurements of different continuous process parameters as well as measurements of internal cell properties enable options to model the complex interaction between the cells and the virus and also the replication mechanism inside the cells [3,4]. One already established model approach is based on the representation of the cell population as a discrete population balance and the simulation with a kinetic Monte Carlo Ansatz [5]. This type of stochastic modeling is well suited for such a system as it is an easy approach to take inot account a larger number of cell properties leading to a high dimensional population model where analytical and differential solvers run often into numerical difficulties. Also the kinetic Monte Carlo approach is typically developed in a modul-like fashion and therefore easy the extend in order to take into account new theoretical ideas or new experimental results. A last but important aspect of the kinetc Monte Carlo Ansatz is the use of a random factor which reflects especially here the underlying variability of any cell population. Recent studies using quantitative real time reverse transcription PCR of the process enables a new and improved validation of the model formulation of the internal dynamics of the virus replication inside cells [6,7,8]. Using this data one is now able to improve the qualitative level of description of the whole process. One can now combine both the internal as well as the external dynamics of the virus replication in the vaccine production. Here we want to present a first model formulation together with qualitative simulation as a starting point for further experimental as well as theoretical analysis of the technical virus production.

2. Model Formulation

Our kinetic Monte Carlo model will consider a population of cells, N, studied dynamically under the influence of a virus infection. Based on previous work, one is interested in the external dynamics, for example the number of virus, replicated throughout the complete process. In order to understand the time evolution of this process property, one would like to know, how cells change internally during the replication cycle. The virus number can be monitored with a hemagglutination assay (HA); the overall internal replication of virus inside a cell can be measured using flow cytometry [4]. More information on the internal replication is now available with a new quantitative real-time reverse transcriptase polymerase chain reaction assay (RT-qPCR). This information will be modeled here by taking into account three different internal cell properties, namely the amount of viral genomic RNA (vRNA), the amount of viral messenger RNA (vmRNA) and the amount of viral complementary RNA (cRNA). These specific molecules were analyzed in [6] even for specific viral segments. The current model will as a starting point only take into account an overall change of these three molecule species. In [7] it has been shown the qualitative time course of the dynamics for the specified segments is comparably similar. For our model formulation we therefore present every cell as a compartment with 3 internal variables, M_{vRNA}, M_{vmRNA} and M_{cRNA}. The dynamical evolution of these three basic molecules leads finally to a situation where the cell internally produces all necessary components for a new virus. Once a sufficient amount of virus components has been accumulated inside a cell, virus is released from a cell and can be observed in the external solution with the HA assay.

In our internal cell model we start with an infection where at first vRNA is initiated from the attacking virus inside the cell. This molecule is either used in a transcription step to produce vmRNA or used for a replication step to produce cRNA. From cRNA more vRNA can be replicated. The change of the molecule numbers of these components is modeled here. Inside the cell more steps for the production of certain virus proteins are taken (see e.g. [3]). The number of M_{vRNA}, M_{vmRNA} and M_{cRNA} can be followed with our model and qualitatively compared to the data from [7] as well as to fluorescence and HA data (for example from [1,2]). The number of accumulated molecules of M_{vRNA}, M_{vmRNA} and M_{cRNA} corresponds to virus proteins numbers and are therefore connected to the ability of the cell to release virus. Keeping track of these numbers on can estimate the time point where virus release will happen from a particular cell.

The internal model dynamics of every cell *i* consist of three basic steps:

1. Replication of cRNA: $M_{cRNA}(i,k+1) = M_{cRNA}(i,k) + p_{cRNA} \cdot M_{vRNA}(i,k)$
2. Transcription of vmRNA: $M_{vmRNA}(i,k+1) = M_{vmRNA}(i,k) + p_{vmRNA} \cdot M_{vRNA}(i,k)$
3. Replication of vRNA: $M_{vRNA}(k+1) = M_{vRNA}(k) + p_{cRNA} \cdot M_{cRNA}(k)$

The internal biological variation of every individual cell is taken into account by a random factor. Each individual step 1-3 is carried out for every cell *i* only with a chance of 0.5 at every time step.

The external dynamic of virus numbers in solution is connected to the internal cell property via a release step once a certain threshold, $p_{release}$, of $M_{vRNA}(i,k)$ molecule numbers has been reached in a given cell *i*:

4. If$(M_{vRNA}(i,k) > p_{release})$: $Vir(k+1) = Vir(k) + rand \cdot (M_{vRNA}(i,k) - p_{release})$

This step 4 decreases the number of M_{vRNA} molecules inside the cell with a certain variability given by a random factor. This release number leads to an external change in the system, namely a corresponding increase of virus in solution. From the experimental

data is deduced, that the release step is connected to a similar release and degradation of certain numbers of M_{vmRNA} and M_{cRNA} molecules inside a cell. We reflect this by including step 5 with a random decrease of p_{deg} molecules of M_{vmRNA} and M_{cRNA}:

5. If($M_{vRNA}(i,k)>p_{release}$): $M_{vmRNA}(i,k) = M_{vmRNA}(i,k) - \text{rand}\cdot(p_{deg}\cdot M_{vmRNA}(i,k))$
   $M_{cRNA}(i,k) = M_{cRNA}(i,k) - \text{rand}\cdot(p_{deg}\cdot M_{cRNA}(i,k))$

For the simulation of the model a MatLab simulation has been developed, where the different steps are represented by discrete time steps of the whole cell population. In the beginning an array for the cell population of size N is defined. As in a typical kinetic Monte Carlo Ansatz at every single time step every cell will change according to the given model rules. Here for every time step, all cells are simulated according to the random internal change of the molecule numbers via steps 1-5. In particular a random number is generated with a selected random number generator provided by MatLab (i.e. Marsaglia, Twister or Congruential) and compared to the specific probability factors. If the random number exceeds the factor, the change of the internal state in the cell is made and recorded in the cell array. Throughout the whole simulation we monitor any change in the internal cell property and calculated from that selected averaged data for the whole cell population. Also a display of different cell property distributions is possible. In order to compare to experimentally available data we select specific average numbers and cell property distributions in the result section.

3. Simulation Results

The new model will be used for a first qualitative comparison to the new information about internal changes of the cells, available from the RT-qPCR data in [7]. We will here address a similar situation within this new model approach.

All simulation results have been checked for statistical validity by varying cell numbers from 100 to 10^4, extended statistics over 10-20 runs and variations of the used random number generators. No significant statistical deviations have been observed and we show therefore typically overlay data for 1000 cells and of 5 runs in order to show the statistical error of the method.

In [7] the experiment has been carried out for MDCK cell where initially a very high multiplicity of infection (MOI=6) was used. This approach was applied in order to ensure that already in the beginning all cell are infected. Therefore our simulation starts with the same situation. All cell are infected at time point t=0 and therefore contain one M_{vRNA} molecule. Now every cell will develop according to the steps 1-5. In Fig. 1 we show the time evolution of our model system for 10 hours. Our simulation time step is 3min; the simulation respectively runs for 200 Monte Carlo steps. The parameters p_{vmRNA}=0.8, p_{cRNA}=0.6 and p_{vRNA}=0.6 reflect the experimental observation qualitatively so that the average molecules numbers $M_{vRNA}(k)$, $M_{vmRNA}(k)$ and $M_{cRNA}(k)$ per cell can be compared to Fig. 1 from [7] qualitatively. If $p_{release}$=1000 is reached (also obtained from [7]) step 4-5 set in. Now cells randomly release virus (and decrease M_{vRNA} respectively) and randomly degrade M_{vmRNA} and M_{cRNA} with p_{deg}=0.05.

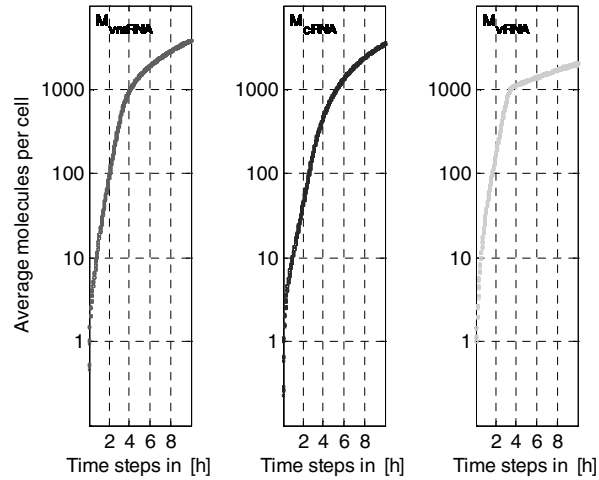

Fig. 1: Time evolution of average molecule numbers of vmRNA, cRNA and vRNA per cell from 5 statistical runs from a population of 1000 cells.

Of interest and may be to be compared with fluorescence measurements are the corresponding cell property distributions. In Fig. 2 we show the molecule number distribution of $M_{vRNA}(i,k)$, $M_{vmRNA}(i,k)$,$M_{cRNA}(i,k)$ at two time points. Time point t=3h (Fig.2, left) corresponds to the situation where no virus has been released yet, according to the HA assay from [7]. At time point t=6h (fig.2, right) virus is released and this is reflected especially in pronounced changes in the M_{vRNA} distribution.

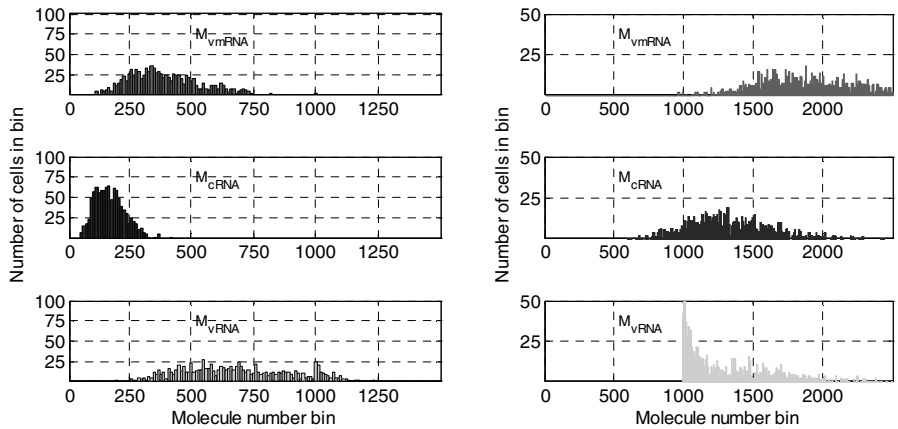

Fig. 2: Molecule number distribution of the cell population at a time point t=3h (left) and (t=6h) for vmRNA, cRNA and vRNA, collected into molecule number bins of width of 10 molecules.

With all the options for data calculation the model can be used to extract cell property distribution, its dynamics, the virus release numbers as well as other quantities of interest. More data from experiments, RT-qPCR, fluorescence data or HA assays, can now be compared in order to judge on the validity of the model representation. Model variations and parameter estimations are another important step for further investigations.

4. Conclusion

We have presented a new model approach to simulate a cell population in a virus production process based on infection of MDCK cells with influenza virus. New data from quantitative real-time reverse transcription PCR enables a comparison of internal cell dynamics from this model with experimental data. The simulation is carried out within a discrete kinetic Monte Carlo method where every cell behaves slightly differently according to given probabilities of cell changes. These changes represent steps in the virus replication cycle where virus RNA is transcribed and replicated so that finally new virus particles can be release by the given cell. A first qualitative analysis shows the applicability of the model approach. The parameters have been adjusted so that a qualitative agreement between data from an experiment (see Fig. 1 from [7]) and model data is achieved. The model can be used to track other properties or to monitor for example certain cell property distributions. These results will help in experimental design and improved understanding of the process. The long term goal should be the simultaneous application of model simulation and experiments in order to improve reliability and efficiency of this technologically very important virus production process.

References

[1] Kalbfuss, B. et al, Monitoring influenza virus content in vaccine production: precise assays for the quantification of hemagglutination and neuraminidase activity, *Biologicals* 36, p.145 (2008).

[2] Schulze-Horsel, J. et al, Infection dynamics and virus induced apoptosis in cell culture based influenza vaccine production flow cytometry and mathematical modeling, *Vaccine* 27, p.2712 (2009).

[3] Sidorenko, Y. and Reichl, U., Structured model of influenza virus replication in MDCK cells, *Biotechnol. Bioeng.* 88, p.1 (2004).

[4] Sidorenko, Y et al, Stochastic population balance modeling of influenza virus replication in vaccine production processes, *Chemical Engineering Science* 63, p. 157 (2008).

[5] Diaz et al, Modeling the Innate Immune Responses of Cells for Vaccine Production, *Chemical Engineering Science* 66, p.3954-3961 (2011).

[6] Robb, N. et al, NS2/NEP protein regulates transcription and replication of the influenza virus RNA genome *J. Gen. Virol.,*90, p.1398-1407 (2009).

[7] Vester, D. et al, Real-time RT-qPCR assay for the analysis of human influenza A virus transcription and replication dynamics, *Journal of Virological Methods* 168, p. 63-71 (2010).

[8] Kawakami, E. et al, Strand-specific real-time RT-PCR for distinguishing influenza vRNA, cRNA and mRNA, *Journal of Virological Methods* , 173, p.1-6 (2011).

I.A. Karimi and Rajagopalan Srinivasan (Editors), Proceedings of the 11th International Symposium on Process Systems Engineering, 15-19 July 2012, Singapore.

CFD Analysis of Cavitation in a Crude Oil Pipeline to an Oil Tanker

Woohyun Kim[a], Munkyu Yoon[b], Moonyong Lee[b], Sunwon Park[a]

[a]*Department of Chemical and Biomolecular Engineering, Korea Advanced Institute of Science and Technology (KAIST), Daejeon, Republic of Korea*
[b] *School of Chemical Engineering, Yeungnam University, Gyeongsan, Republic of Korea*

Abstract

Emission of volatile organic compounds (VOCs) during loading crude oil to oil tankers has become a particularly critical issue because it does not only cause environmental problems but also economic loss. Since a pipeline from a terminal to an oil tanker has a long vertical drop line, the acceleration of the pipe flow by the gravity may cause a sudden pressure drop that stimulates cavitation, the evaporation of the VOCs in crude oil. To analyze the amount of vaporized VOCs and the fluid dynamic behaviors of the two-phase pipe flow, experiments have been conducted with a pilot-scale pipeline and a computational fluid dynamic (CFD) model have been developed based on the experimental result. As crude oil is the complex mixture of various hydrocarbons, a phase transition model based on crude oil assay data has been developed and included in the CFD model. This developed model is capable of predicting the amount of vaporized VOCs and the fluid dynamic behaviors of the pipe flow with different operating conditions, e.g. flow rate, pump pressure, type of crude oil, etc. Thus, it is expected that the model will contribute to analyzing the amount of VOC emission during loading crude oil onto an oil tanker.
Keywords: computational fluid dynamic model; cavitation; crude oil; oil tanker; volatile organic compound

1. Introduction

Emission of volatile organic compounds (VOCs) during loading crude oil to oil tankers has become a particularly critical issue with the growth of maritime transport since it does not only cause environmental problems but also economic losses (Husain et al., 2003). Crude oil is a mixture of various hydrocarbons and VOCs in crude oil generally refers to some light end components that range from C1 to C10. These components can evaporate during loading, transportation, or discharging processes because pressure changes can accelerate evaporation. The amount of VOCs emitted during loading is found to be in the range of 0.08 - 0.15 % of the total volume loaded in an oil tanker (web site of Hamworthy).

In terms of environmental impacts of VOC emission, it is reported that VOCs emitted from crude oil contribute to global warming. Especially, methane in the evaporated VOCs has a strong effect on global warming and various international regulations are imposed and reinforced these days (Endresen et al., 2003).

The VOC emission also causes adverse economic losses. A 130,000-deadweight-ton oil tanker discharging oil 40 times per year emits approximately 5,000 tons of VOCs per year. Since the oil price is around $ 110/bbl, the economic loss of the evaporated crude oil is expected to be about $ 4,000,000, assuming that price and specific gravity of VOCs are equivalent to ones of crude oil.

One of the main causes of the VOC emission is pressure drop along the loading pipe line (Rudd & Hill, 2001). Since a gravity-driven pipe flow runs through the pipe line, a sudden pressure drop can occur. Thus, negative pressure may appear in the oil loading system and it obviously accelerates the vaporization of the VOCs in crude oil.

To design a system to reduce the amount of the VOC emission, a high-fidelity model predicting the phase-transition phenomena will be necessary so we have developed a computational fluid dynamic (CFD) analysis method which is capable of analyzing the amount of vaporized VOCs and the fluid dynamic behaviors of the two-phase pipe flow in this work. Therefore, experiments corresponding to an actual oil loading system have been carried out and a phase transition model based on crude oil assay data has been developed for the accurate CFD model

2. Experiment

2.1. Theoretical Background

Since crude oil contains various organic compounds, light compounds can naturally boil off at ambient temperature and pressure. Plus, if negative pressure, meaning pressure lower than ambient pressure, appears in the oil loading system, the pressure accelerates the evaporation of VOCs, causing cavitation. In this section, physical phenomena of gravity-driven pipe flow and the volatility of crude oil are discussed.

A loading system of an oil tanker has long vertical pipe lines which are generally longer than 20 m (*see* Figure 1). When crude oil running through a horizontal pipe line starts to fall into the vertical drop line, the fluid is suddenly accelerated by the gravity. This acceleration results in drastic decrease in static pressure along the pipe line. This phenomenon is same as the principle of a siphon. Consequently, the low static pressure stimulates the evaporation of VOCs in crude oil so cavitation occurs in the pipe flow.

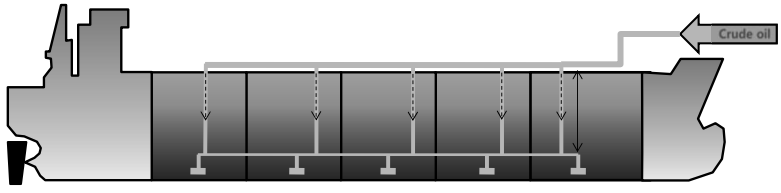

Figure 1. Conceptual design of oil loading pipe lines

To predict the amount of vaporized VOCs, the volatility of crude oil should be analyzed. It is obviously found that the composition of the components in crude oil varies depending on the types of crude oil. When oil with higher content in light components is transported, more amount of VOC emission is expected. Thus, a model based on assay data of crude oil is necessary to predict the phase transition phenomena of crude oil. In this work, we have calculated the vapor volume fraction of crude oil at equilibrium using assay data and Aspen PLUS and the calculated data is used to develop the phase-transition model for the CFD analysis. The calculation procedure is explained as follows:

(1) Gathering assay data of crude oil: Assay data includes average molecular weight, true boiling point (TBP) data, light end components, viscosity, etc.
(2) Calculating vapor volume fraction: Using the assay data, the vapor volume fraction of crude oil at given temperature and pressure can be calculated in Aspen PLUS. Based on the calculated data, we can develop function to predict vapor volume fraction with respect to pressure. This function is combined with the phase transition model in the CFD model.
In the experiment, a pipe line has been designed to observe the fluid dynamic behaviors of the gravity-driven flow and CFD analysis has been carried out based on the experimental data.

2.2. Details of Experiment

In the experiment, we have designed 20-m-high pipe line (see Figure 2). The line is composed of 40A steel pipes.

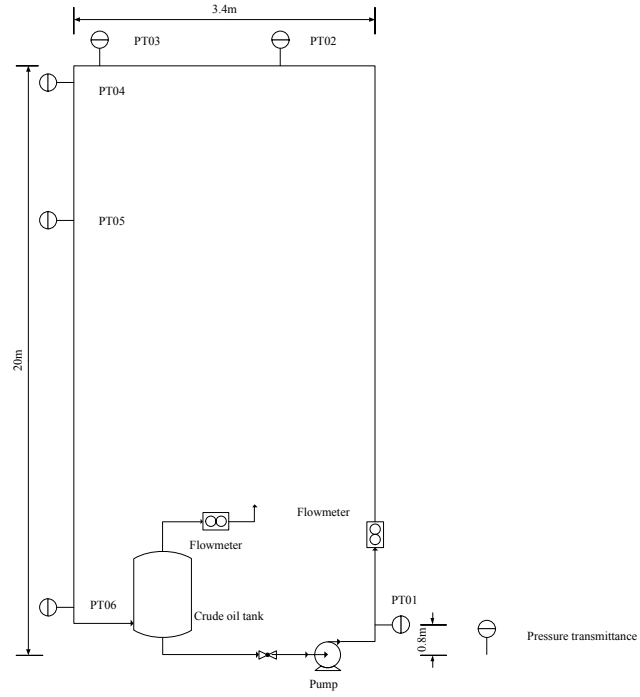

Figure 2. The P&ID chart of the experimental facility

We have tested several cases in the experiment varying the flow rate. The CFD simulation results of the pressure profiles are compared with the experimental data for the model validation. In the experiment, pressure profile is measured by the pressure transmittances (see Figure 2 and Table 1) and vapor flow, which means the amount of vaporized VOCs, is measured by the flow meter located at the top of the tank.

Table 1. The locations of the pressure transmittances

	Pressure transmittances					
	PT01	PT02	PT03	PT04	PT05	PT06
Altitude from the bottom	0.8m	20m	20m	19.9m	13.5m	0.88m
Length from the pump	0.8m	22m	23.1m	23.5m	28.9m	42.4m

3. CFD Analysis

3.1. Phase Transition Model of Crude oil

We have modified an evaporation-condensation model for describing the phase transition phenomena in crude oil with respect to pressure. Since saturated temperature and pressure cannot be determined for mixture, we have used equilibrium vapor volume fraction, which is calculated in Aspen PLUS using the assay data of crude oil. In this model, mass flux between phases is determined based on deviation from the equilibrium vapor volume fraction at given pressure and temperature. The mathematical expression of the model is shown below.

$$\dot{m}_{l\to v} = c_1 \cdot \alpha_l \cdot \rho_l \frac{\alpha_l - \alpha_{l,eq}}{\alpha_{l,eq}} \qquad \text{(1) mass flux from liquid to vapor: vaporization}$$

$$\dot{m}_{v\to l} = c_2 \cdot \alpha_v \cdot \rho_v \frac{\alpha_v - \alpha_{v,eq}}{\alpha_{v,eq}} \qquad \text{(2) mass flux from vapor to liquid: liquefaction}$$

c_1 and c_2: mass flux coefficient
α_l and α_v: current volume fraction of liquid and vapor (subscript *eq* means equilibrium.)

The essential coefficients, c_1 and c_2, are adjusted to make CFD simulation results similar to experimental data. To determine these parameters, we have used the assay data of the crude oil we have used in the experiments. This model is developed as a user-defined function in FLUENT and combined with the momentum balance equation and the continuity equation of the CFD model.

3.2. CFD Model

In this work, we have used FLUENT for CFD analysis. Since the pipe flow has two phases, vapor and liquid, we have selected the mixture model of FLUENT. A turbulent model is also selected because the Reynolds number is high enough. Thus, the k-ε model is used in this work. The standard k-ε model in ANSYS FLUENT is one of the most practical engineering flow calculations. It is a semi-empirical model and the derivation of the model equations relies on phenomenological considerations and empiricism. This model is combined with the momentum balance equation of each phase. In this simulation, we have prepared a 2-D model for fast calculation. Since the system we have analyzed consists of simple pipes without considerable 3-D changes in flow direction, 2-D analysis is assumed to be reasonable. All the simulations are carried out in an Intel Core2 Quad Q9550 processor machine with 4.0 GB RAM.

4. Results

As we observed in the experiment, the lowest static pressure is calculated around the location where the oil starts to fall along the vertical drop line.

Table 2.Comparison between the CFD simulation results and the experimental data

Flow rate		Static pressure measured at each pressure transmittance					
		PT01	PT02	PT03	PT04	PT05	PT06
17 m^3/h	experiment	2.80 bar	-0.24 bar	-0.24 bar	-0.23 bar	-0.06 bar	0.02 bar
	simulation	2.80 bar	-0.15 bar	-0.21 bar	-0.18 bar	-0.10 bar	0.02 bar
15 m^3/h	experiment	2.40 bar	-0.42 bar	-0.44 bar	-0.43 bar	-0.26 bar	0.03 bar
	simulation	2.40 bar	-0.40 bar	-0.42 bar	-0.43 bar	-0.30 bar	0.03 bar

Table 2 shows the comparison between the experimental data and the simulation result in the two different cases. According to the table above, the CFD model is considered to be acceptable.

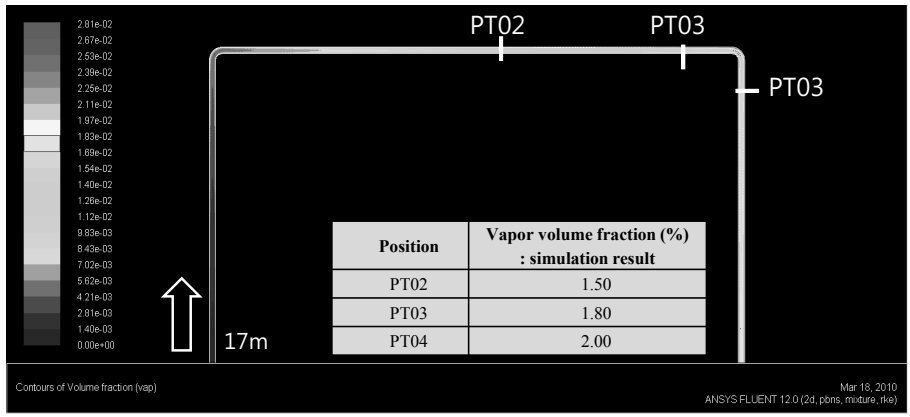

Figure 3. Profile of vapor volume fraction (Flow rate: 15 m^3/h)

Figure 3 shows the predicted vapor volume fraction along the pipe line. In the simulation result, it is observed that the vaporized VOCs are partially liquefied at the bottom of the vertical drop line since the static pressure at the bottom is almost same as the atmospheric pressure. The amount of the vaporized VOCs is predicted as approximately 0.09 % by weight when the flow rate is 15 m^3/h and it is similar to the experimental data (0.1 - 0.12 % by weight). This value is also similar to the amount of crude oil loss in the actual loading process of an oil tanker caused by VOC emission.

5. Conclusions

To analyze the amount of vaporized VOCs and the fluid dynamic behaviors of the two-phase oil flow driven by the gravity, the experiments have been conducted and the CFD model have been developed based on the experimental result. The experiments have been carried so that the negative pressure and the vaporization of VOCs are experimentally observed. The proposed CFD model, which can predict the amount of the vaporization and condensation of the VOCs based on the property data of the crude oil, is also considered to be acceptable since the simulation results of the pressure profiles and the amount of VOC emission have been compared with experimental data. Thus, the model can be used to analyzing the amount of VOC emission during loading crude oil onto an oil tanker under different operating conditions. This modeling approach will contribute to designing a system to reduce the VOC vaporization.

References

Endresen, Ø, Sørgård, E, Sundet, J.K., Dalsøren, S.B., Isaksen, I.S.A., Berglen, T.F., Gravir, G. (2003). Emission from international sea transportation and environmental impact. Journal of Geophysical Research, 108, 4560.

Web site of Hamworthy: http://www.hamworthy.com/Products-Systems/Hamworthy-Marine/Gas-System/VOC-recovery/

Husain, M., Hunter, H., Altshuller, D., Shtepani, E., Luckhardt, S., Lemley, N. W., Daidola, J. C., Aabo, K. and Hirst, D. (2003). Crude oil under negative pressure and hydrocarbons emission containment. Transactions-Society of Naval Architects and Marin Engineers, 111, 584.

Rudd, H.J., Hill, N.A. (2001). AEA TECHNOLOGY Report: Measures to reduce emission of VOCs during loadign and unloading of ships in EU. (Available on the web: http://ec.europa.eu/environment/air/pdf/vocloading.pdf)

I.A. Karimi and Rajagopalan Srinivasan (Editors), Proceedings of the 11th International Symposium on Process Systems Engineering, 15-19 July 2012, Singapore

Utilisation of Computer Science Design Patterns in Chemical Engineering

Heinz A Preisig, and Tore Haug-Warberg
Dept of Chem Engineering; NTNU; Trondheim, Norway

Abstract

Keywords: dynamic system, software engineering, computational engineering

1. Computational chemical engineering

Computer-aided process engineering has been the main source for computational tools that make it possible to experiment with processes, explore and test any scenarios without having to fool around with real processes and their limitations. The tools are essential for our community and their position and usage is only going to grow. Naturally Chem Eng has been focusing on its interests: the project and problems the community have and want to solve whilst benefiting from the increasing computing power and increasing possibilities to polish the user interfaces. This left little room for adjusting the underlying structure whilst in the meantime, computer science also made progress driven by a large growth and diversification of the application market. This should also affect on the structure of our tools.

2. Software considerations

The concept of *design patterns* in computer science is a loosely defined term which addresses the fact that many tasks in object oriented programming (OOP) are quite standard when viewed as semantic operations Gamma et al. (2009, c1995). The implementation into a specific programming language will differ and they are not standard at the syntactic level, but they are mostly independent of the programming language and implementation details. A design pattern is therefore not an algorithmic description of a certain mathematical operation but is more akin to a pattern of programmatic behaviour. This is an interesting observation that lends more to psychology and philosophy than it points to hard evidences in natural sciences. To put it short it can be argued that design patterns in OOP must be lifted from the existing pool of computer programs and that they in some sense are the common denominators of how we organize, structure and solve certain tasks that over the years have become standard in the software industry. Seen from this perspective it is clear that design patterns are not inventions of the human mind but are rather representatives of human nature. Design patterns are therefore not limited in number; new ones will emerge and old ones may die out. Some important patterns (like e.g. the *iterator* pattern) will find their way into the programming languages and become part of the languages themselves or the standard libraries. This process has already become visible in several open source OOP languages like e.g. C++, Perl, Python and Ruby.

The first question is how, or if, the design patterns are useful to software enterprises in mathematics, physics and chemistry. The answer to this question is definitely positive because design patterns conserve somehow the way human thinks. The next question that

pops up is what design patterns we would need to solve our programming tasks connected to: formulation, calculus, analysis, exportation, execution and interfacing.

From what was said above—that design patterns reflect they way we tend to solve routine programmatic problems—we might argue that we have in fact identified six patterns here. Philosophically this is true but not practically. We have not yet reached the abstraction level there it is sufficient to say *model formulation* and let this be instructive for how we choose to implement the model. It may therefore be instructive to see what the computer scientists have come up with over the years and, if this looks promising, borrow their terms to describe our own activity. Design patterns in OOP are currently classified into *creational* (C), *structural* (S) and *behavioural* (B) patterns, see Gamma et al. (2009, c1995). There are at least 23 patterns suggested of which we think around a dozen are sufficiently important to help us describing our task:

C: Factory (creating objects from textual information), Builder (factory for building objects incrementally), Singleton (one-to-one factory for single objects)

S: Decorator (in-situ extension of objects), Adapter/wrapper (interface adaptation) Composite (internal nodes and leave nodes have the same basic interface), Facade (interface to group of objects), Bridge (kind of driver)

B: State (changing behaviour when internal state changes), Interpreter (parsing text according to a grammar), Iterator (accessing objects sequentially)

The process of generating e.g. a thermodynamic run-time library can now be described on a very high level of abstraction. The description is sufficiently accurate to indicate what complexity we are talking about, yet it is insufficient to tell anything about the actual implementation. However, it tells very accurately that any programming language covering the ?? design patterns mentioned above will be adequate for the actual implementation. The answering of that question alone is so important that it by itself "rettferdiggjÃÿr" the design pattern idiom. Looking into the past there are countless examples of engineering software projects that have stranded because the "wrong language" was used. Choosing the right language from the outset is in fact a premise for success in this context.

2.1. Factory

Creates objects without specifying the exact class of objects that it creates.

The factory pattern has a direct application in modelling involving flowsheets that commonly use specific thermodynamic material models and kinetic models. An object-oriented implementation the material model could be equipped with a symbolic and numerical solution engine. It will also have to know the material's composition, specifically what species make up the material and consequently must be modelled. Similarly for the object of a reaction: it requires a kinetic model, and the knowledge of what intensive properties it depends on, not at least the species composition and the relevant intensive quantities, primarily the temperature and pressure. The symbolic and numerical procedures may be taken from different places, whilst the dependencies are likely provided by an ontology.

2.2. Builder

Separate the construction of an object from its representation.

The thermodynamic model are often very complex and in order to capture this complexity we build them recursively as tree structures. This requires the objects to be built incrementally. Typically, one line of code is needed per line of input taken from the textbook description of the model. This one-to-one relationship between programming and textual formatting is important for two reasons: Firstly, it reduces the likelihood of mistakes in the code because the generation of the code line is a linear translation. Secondly, it makes the documentation and maintenance easier because the textbook model can be directly utilised as explanation for the code. A self documenting code is of course the ultimate goal. Whilst it is probably not quite realistic to reach this goal absolutely, tailor-made languages are very helpful auxiliary tools (see discussion of the *Interpreter* below).

2.3. Singleton

Restrict instantiation of a class to one object.

This concept is suitable to capture the basic structures as they are formulated in the associated ontology. In our applications typical elements are conservation equations, transport and kinetics.

2.4. Decorator

Add behaviour to an existing object dynamically.

The decorator is a handy feature when generating different target output. Models may be written in different target languages for there consequent utilisation. The purposes are numerous including: LaTeX for generating automatic documentation; C, C++, Fortran and Matlab for numeric calculations; DOT for visualizing the model hierarchy; and Ruby and Python for object oriented programming and not at least any type of model exchange format such as the mock-interface language currently developed in the Modelica community Modelisar (2012). There are virtually endless options here and for any application, it is essential that the exportation is open to enable interactions with other software components. The structure should be such that the programming effort increases linearly with the number of exported languages. To achieve this goal the decorator pattern is very useful. For example, using abstract syntax trees for the representation of expressions and equations, or for that matter any such information having a tree structure, it is sufficient to renew the definition of one single method called `_fu`) in each of the classes of which the leave nodes are instances. The decorator pattern is a dynamic feature and thus happens at run-time such that several languages can be exported from the same tree. The tree itself respond to a method called) that invokes the leaf-nodes sequentially using the *Iterator* pattern described below and execute `_fu`) on each of the node objects. The tree itself is not touched, just the leaf-nodes. In this way it is possible to export the model into any kind of language that does not require external information beyond what can reasonably be supplied as default, or at run-time, values or is already stored in the model graph. The code exportation is basically a linearisation technique in that it takes a complicated tree structure and writes it out as a linear program. A second thought will soon reveal a possible caveat: Not all programming languages are linear in the sense that the information generated by the node objects all go into one place. In LaTeX documents for instance there is a heavy mix of information that goes into the individual parts, chapters and sections.

2.5. State

Considering the fact that executing software is an automaton, it has also a state. The concept *state* can be used exactly the same way as we use state in physics and engineering. It has applications as state of the software but also as state of the process one has implemented in software as well as the abstract state of a model, for example.

2.6. Interpreter

Specifies how to evaluate sentences in a language.

We use this technology in several places in our modelling software. It has a direct application for the implementation of algebraic expression built from basic objects variables and operators, whereby the object variable is extended to various classes such as physical variables. The approach is also used to build and analyse composite type definitions that are utilised by the graphical model editor Preisig (2010, 2011).

The language RGrad Løvfall (2008) was invented by our group to describe the thermodynamic models (or any other models relying on multi-dimensional inner product rules) on a symbolic level. Rather that defining a stand-alone parser for RGrad it was decided to write it as an extension to the Ruby language. In this way we could rely on the rich syntax of the Ruby parser and focus on modelling issues instead. The decision turned out to be highly successful and time–cost effective.

2.7. Iterator

Travers a data container and access the individual elements.

Constructing and storing models makes extensive use of graphs: trees for algebraic expressions, for typing using hierarchical attributes, species in different state of aggregation, reaction schemes, etc. All these containers will have an iterator associated enabling the traversing of the data container.

2.8. Wrapper

Translate one interface for a class onto a compatible interface.

The application is apparent: make software written in one language available in another. The CAPE-OPEN project is a classic representative of this approach. The fact that the wrapped software modules may be binary, enables the utilisation of compiled and proprietary software in different environments. This may be models at various levels, where the physical property calculations are of particular interest in model-supported computational engineering. But also models with built-in solvers are interesting applications.

2.9. Composite

A group of objects are to be treated in the same way as a single instance.

The graphical interface module for the hierarchical tree of systems with the leave nodes being simple control volumes, this concept is directly applicable to handling the tree itself, but also the associated graphics.

2.10. Facade

Provide a simplified interface to e.g. a class library

A typical application is material models. There exists several hundred equations of state, which can be grouped. Putting these models into a library, where groups of models are being realised as packages, with a facade providing a common interface.

2.11. Bridge

Decouples an abstraction from its implementation so that the two can vary independently.

3. Conclusions

The concept or paradigm of "Program to an 'interface', not an 'implementation'." Gamma et al. (2009, c1995) (Gang of Four 1995:18) has been very useful in the generation of high-level modelling software, specifically model structure editor and thermodynamic factory and computational engine.

Many of the OOP design patterns are extremely useful for the implementation of such tools and have certainly made the realisation easier and more structured yielding a much more flexible framework that is easy to maintain given the level of complexity. In general it has been observed that the for any particular problem or need there exists a suitable pattern for the implementation.

References

Gamma, E., Heim, R., Johnson, R., Vlissides, J., 2009, c1995. Design patterns: elements of reusable object-oriented software. No. 37th printing. Addison-Wesley, Boston. 2, 3

Løvfall, B. T., 2008. Computer realisation of thermodynamic models using algebraic objects. Ph.D. thesis, Norway: NTNU. 2.6

Modelisar, 2012.
URL www u l ku 2.4

Preisig, H. A., 2010. Constructing and maintaining proper process models. Comp & Chem Eng 34(9), 1543–1555. 2.6

Preisig, H. A., 2011. A multi-layered ontology for physical-chemical-biological processes. ESCAPE 21 (2011), Porto Carras, Chalkidiki, Greece 1, ISBN 978-0-444-53711-9 (ISBN 978-0-444-53711-9), 101–105. 2.6

I.A. Karimi and Rajagopalan Srinivasan (Editors), Proceedings of the 11th International Symposium on Process Systems Engineering, 15-19 July 2012, Singapore.

NGL Recovery from CO_2–EOR Streams

Maíra C. Barbosa[a], José Luiz de Medeiros[a], Ofélia Q. F. Araújo[a], Giovani Cavalcanti Nunes[b]

[a] *Departament of Chemical Engineering, Escola de Química da Universidade Federal do Rio de Janeiro. Av. Horácio Macedo, 2030, Bloco E - Centro de Tecnologia, Ilha do Fundão, CEP: 21949-900, Rio de Janeiro, Brazil.*
[b] *ENGP/IPP/PMF, Petrobras, Rio de Janeiro, Brazil.*

Abstract

The need to reduce concentration of greenhouse gases has promoted the use of technologies for CO_2 destination. Of particular interest is the use of CO_2 present in natural gas streams in the context of the Brazilian pre-salt fields. This motivation guides the development of CO_2 based processes that attribute extra revenue to the oil and gas production therefore reducing the penalty posed by CO_2 capture. In this work, a feasibility analysis is performed on the process of recovering Natural Gas Liquids (NGL) from CO_2 rich streams used in Enhanced Oil Recovery (EOR). For this purpose, a waste stream from synthetic natural gas production reported in the literature was analyzed. The proposed process arrangement employs natural gas processing techniques to recovering NGL from EOR streams rich in CO_2. Among the technologies available, three are approached and applied to recover propane (C_3), butane (C_4) and natural gasoline (C_{5+}) fractions: (a) Joule Thomson Process, (b) Turbo Expander Process and (c) Cryogenic Process. The comparative study presented includes process simulation in the environment UNISIM DESIGN (Honeywell), and sizing of main equipment for economic analysis, which includes calculation of capital and operational expenditures (CAPEX and OPEX). The study indicates the Cryogenic Process as the most feasible. Based on its superior performance, this process is applied to a case study concerning Tupi Pilot field, belonging to the Brazilian pre-salt layer, even though large uncertainties surround the actual data from the pre-salt reservoirs. With further consideration of revenues from Carbon Credits, the three processes and the case study are found to be economically feasible.

Keywords: greenhouse gases, EOR, pre-salt, NGL Recovery.

1. Purpose

The purpose of the work is to study the technical and economic feasibility of different Natural Gas Liquids (NGL) Recovery Processes from CO_2 rich streams for use in Enhanced Oil Recovery (EOR).

2. Introdution

With the intensification of global climate changes due to global warming associated to increased emissions and consequent atmospheric buildup of Greenhouse Gases (GHG), sustainable processing of oil reserves should pursue GHG emissions reduction targets. Among the various greenhouse gases, CO_2 is identified as the main contributor to global warming.
In Brazil, the environmental concern tends to worsen after the announcements of the discoveries made by Petrobras for oil in the Brazilian Pre-Salt. The oil found in this region is

light, and the associated natural gas presents large amounts of CO_2: preliminary studies indicate an approximate percentage of 10% to 15% CO_2 in these fields (Formigli, 2007).
The projections of the graph in Figure 1 show that, in 2030, this increase in emissions could reach 55% of emissions in 2004:

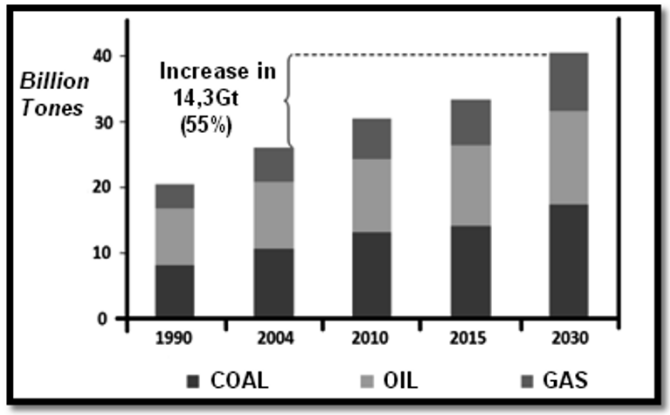

Figure 1: CO_2 emissions in billion tones. SOURCE: Costa, 2009 - adapted by the author

Carbon Capture and Storage (CCS) is currently the most promising solution to the long-term and widespread storage of CO_2, with some projects already underway (Costa, 2009). The technique is characterized by the injection of a liquid or the supercritical CO_2 in geological formations, in order to isolate it from the atmosphere.
Undoubtedly, the alternative of geologic sequestration increases operating costs of production. In this case, uses of CO_2 that generates revenues should hence be prioritized. In this respect, the application of CO_2 in EOR is attractive. In order to minimize even more the cost of CO_2 destination, this study evaluates three processes for NGL recovery from these CO_2 rich streams.
The result of evaluation of NGL recovery process technically and economically feasible for acid gas rich streams is then applied to a case of interest to the Brazilian Oil Sector. Thus, because of the importance of the Tupi Pilot field for history, it was chosen as a case study for this work.

3. Methods

At first glance for process analysis a CO_2 rich stream from synthetic natural gas is adopted as feed to compare NGL Recovery Process.
This waste stream came from the Great Plains Synfuels Plant operated by Dakota Gasification Company which is used for EOR purposes in *Weybum* and *Midale* fields, located in Saskatchewan, Canada (Vargas, 2010).
Among the existing NGL Recovery Process, were evaluated and compared three of them:

1) **Joule Thomson** – this process has the lowest cost but has restricted use because it does not guarantee the sale specification for the Natural Gas (NG) according to ANP. This is basically a process for setting the dew point of the NG. The temperature decreases when the system expands freely while maintaining constant enthalpy. In an industrial plant, this expansion is accomplished in a isenthalpic pressure control valve;

2) **Turbo Expander** – this process is similar to the Joule Thomson procedure but in lieu of being a pressure control valve the expansion takes place in a turbine, which releases energy that is used in the present process. It`s more expensive than the previous process since it has more critical equipment, such as the turbine;
3) **Cryogenic** – this process is more complex than the two previous ones, since it necessarily have a propane refrigerant cycle to decrease the temperature. This has a moderate investment and is capable of generating GN with the sale specification required by ANP.

Figures 2A, 2B and 2C show schematic diagrams of these processes:

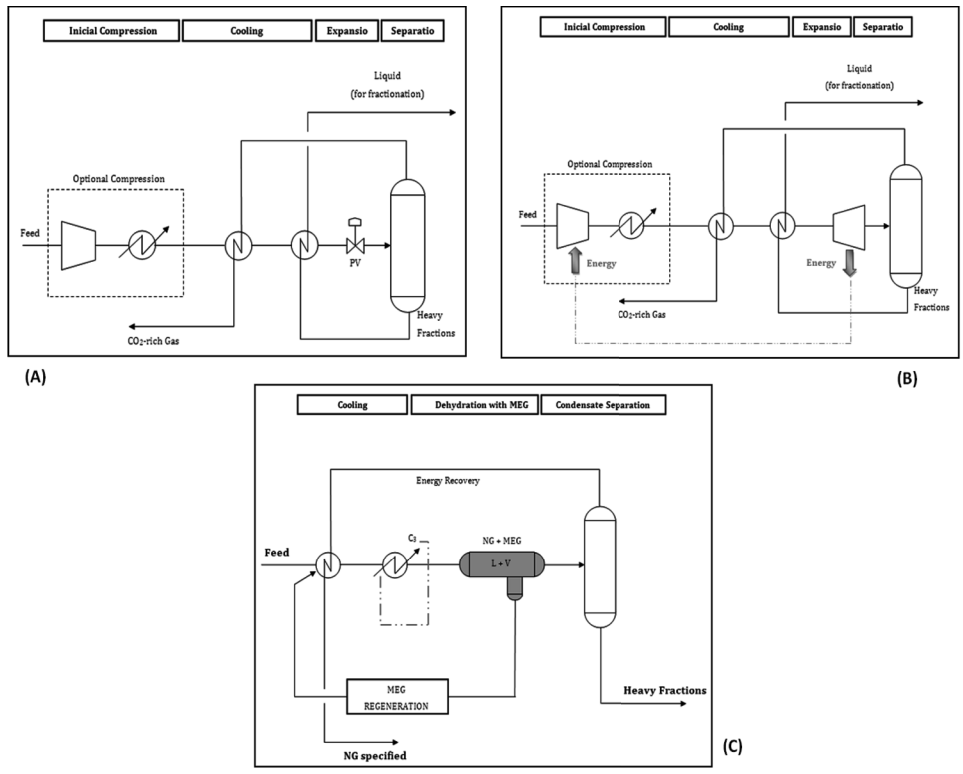

Figure 2: **(A)** Joule Thomson Process; **(B)** Turbo Expander Process; **(C)** Cryogenic Process.
SOURCE: Vaz et al. 2008 - adapted by the author

The proposed flow diagrams in the environment UNISIM DESIGN (Honeywell) include three sections:

a. *Initial Section*, where one of the components of the gas stream migrates to the liquid phase for later recovery. This migration occurs when the process stream is subjected to very low temperatures, around -30°C;
b. *Fractionation Section*, where the liquid fraction obtained in the previous step is directed to a battery of distillation columns, to separate streams for future injection (CO_2 and light components, as C_1 and C_2) and streams for market (C_3, C_4 and C_5^+);
c. *Compression and Injection Section*, where the flow of CO_2 and light components obtained in the previous step is compressed into three stages of compression and then is sent by pipeline to the oil well head.

The processes are simulated using UNISIM DESIGN and the main equipment sizing is performed to calculate capital costs (CAPEX) and operational costs (OPEX).
The methodology used for economic analysis (Turton et al., 2009) sought a preliminary estimate of the cost, which is indicated for comparison of alternatives of the same process, the focus of this work.
The estimated cost of a plant may be done in two ways: from a similar existing plant, for example, in the case of a REVAMP, or can also be made for a new plant ("Grass Roots ").
In the case of an existing plant, the cost of the new plant should be update in relation to the nominal capacity and the date of construction. This update date use Economic Indexes presents in the literature, for example, the CEPCI ("Chemical Engineering Plant Cost Index") or M&S ("Marshall & Swift Equipment Cost Index"). Otherwise, for a new plant, the total capital cost "Grass Roots" is calculated by the cost associated with its main equipment.
In this study, the Guthrie technique introduced in the late 60's and recognized as the best estimate for capital expenditures was used. It calculates the cost in a baseline condition and employs correct factors (adapting the material of construction, pressure, etc.) to find the installed cost of the module (CM).
The last step in this economic analysis is the Cash Flow. The method used was the Discounted Cash Flow (DCF), which is one of the main methods used for economic evaluation. The approach used by the method determines the value of the company through a projected cash flow, discounted by a rate that reflects the risk associated with investment.
The DCF calculated for the three processes are evaluated and then compared on an economic basis for determining the most attractive alternative.
The winner process was applied to the case study of the Tupi Pilot field.

4. Results

The three cases showed very similar mass flow rates for the sale streams and for the injection streams (EOR), which indicates that their recovery efficiencies are equivalent. Two approaches are used for the economic analysis. The first one is a more rigorous analysis, considering NGL sale as the only process revenue. In this analysis, the most profitable process is the Cryogenic alternative, with an investment return around 8 years of operation (figure 3A).
The second analysis accounts for the environmental cost associated with power consumption. In addition, the analysis also considers carbon credits associated with the CO_2 emissions avoided as extra revenue to the LGN sale. Finally, the increased productivity of the well with the activity of EOR is also included in the analysis. In this case, the three cases appear to be attractive, with an investment return occurring within the first 3 years of plant operation (figure 3B).

Figure 3: **(A)** Cash Flow only with NGL sale; **(B)** Cash Flow with new revenues and NGL sale.

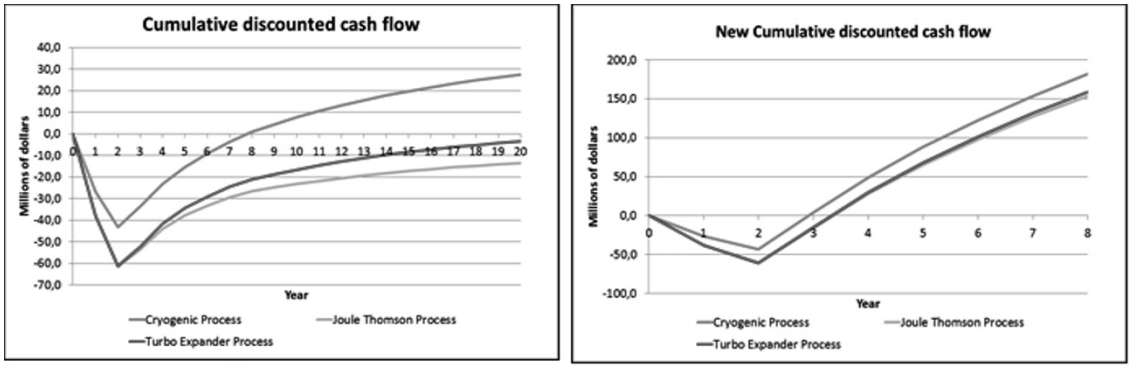

(A) (B)

For the study case with the cryogenic process, the same two approaches are used for the economic analysis. In the first analysis the process was not feasible but in the second analysis the process proved to be profitable with an investment return around 3 years of operation.

5. Conclusions

In the comparative study the economic analysis indicated similar performance in relation to the product flows obtained for the three simulated cases. In a first approach to economic analysis, the cryogenic process showed the best discounted cash flow. However, in a second and more complete analysis, considering carbon credits, the three cases shown to be feasible and attractive.

Finally, for the study case of the Tupi Pilot field the Cryogenic process is feasible only when the carbon credits associated with the CO_2 and the increased productivity of the well with the activity of EOR where considered.

Acknowledgment

Financial support of MCT/FINEP/CTPETRO, Grant No.2460-06 is kindly acknowledged.

References

I. V. L. Costa, 2009, “Análise do Potencial Técnico do Seqüestro Geológico de CO_2 no Setor de Petróleo do Brasil”, Dissertação de Mestrado. Rio de Janeiro, RJ, Brasil : UFRJ - COPPE.

J. Formigli, November 2007, “Pre-Salt Reservoirs Offshore Brazil: Perspectives and Challenges”, Energy Conference, Miami, USA.

IPCC, 2005, “Special Report on Carbon Dioxide Capture and Storage”, United Kingdom and New York: Cambridge University Press.

C. E. M. Vaz, J. L. P. Maia, W. G. Santos, 2008, “Tecnologia da Indústria do Gás Natural”. São Paulo: Blucher.

R. Turton *et al.*, 2009, “Analysis, Synthesis, and Design of Chemical Processes”. Prentice Hall, 3rd. Edition.

K. J. Vargas, 2010, “Refrigeration provides economic process for recovering NGL from CO2-EOR recycle gas”, Oil & Gas Journal. Canada : Falcon EDF Limited.

I.A. Karimi and Rajagopalan Srinivasan (Editors), Proceedings of the 11th International Symposium on Process Systems Engineering, 15-19 July 2012, Singapore.

Integrated Platform at ICES Kilo-Lab for Process Quality by Design

Suat-Teng Tan, David Wang, Iskandar Halim, Soo Khean Teoh, Paul Sharratt, Gabriel Loh, Run Ling Wong, Steven Mun Chun Yee, Chien Ying Loke, Wee Chew*

*Institute of Chemical and Engineering Sciences (ICES), Agency for Science, Technology and Research (A*STAR), 1 Pesek Road, Jurong Island, Singapore 627833, Singapore*

Abstract

The paradigm shift that is attempting to change the way pharmaceutical manufacturing is undertaken in the 21st century has raised practical challenges for the adoption and implementation of the Process Analytical Technology (PAT) framework initiated by the U.S. Food and Drug Administration (FDA). The motive is to engender a science-oriented pharmaceutical manufacturing that is along FDA's pharmaceutical product quality by design (QbD) ideology. One such challenge revolves around the integration of PAT technologies such as varied process analytics (e.g. sensors, spectrometry, chromatography, etc.), multivariate analyses, knowledge management, and process control under a common information exchange and data-logging platform. Such an integrated platform was recently installed and commissioned at the Kilo-Lab in the Institute of Chemical and Engineering Sciences (ICES). Its efficacy was demonstrated through synthesizing 4-D-erythronolactone at kilo-scale using a four-phase hybrid process.

Keywords: Process Analytical Technology (PAT), Quality by Design (QbD), Process Raman Spectroscopy, Supervisory Control and Data Acquisition (SCADA), Multivariate Data Analysis and Management

1. Introduction

With the introduction of two key FDA guidance documents in 2004 along the themes of 21st century pharmaceutical current good manufacturing practice (cGMP) [1] and Process Analytical Technology (PAT) [2], there has been a paradigm shift that is brewing within the pharmaceutical industry and related fields, including R&D carried out in academia and research institutions. The drive is towards achieving innovation in pharmaceutical manufacturing unit operations through process understanding along the FDA ideology of "quality by design" (QbD) [1]. Moreover, the undergirding thrust of process analytical technology (PAT) purports an *integrated systems approach* in the implementation of QbD in PAT pharmaceutical processes [2]. These two FDA initiatives essentially revolve around the tripartite guidelines Q8(R2), Q9 and Q10 by the ICH (International Conference on Harmonisation of the Technical Requirements for Registration of Pharmaceuticals for Human Use), which respectively expound details on pharmaceutical development, risk assessment and quality system [3]. The ICH guidelines are also drawn upon by other deliberations from pharmaceutical professional societies, e.g. ASTM committee E55 documents [4] and Product Quality Lifecycle Implementation (PQLI) roadmap of ISPE (International Society for Pharmaceutical

* chew_wee@ices.a-star.edu.sg

Engineering) [5]. In effect, the aforesaid publications from FDA, ICH, ASTM committee E55 and ISPE PQLI espouse the translation of a cadre of manufacturing philosophy and methodological concepts related to the PAT framework and process innovation [6], e.g. systems approach, risk and knowledge management, quality by design, etc., into practical steps realizable for actual processes within the envisioned 21st century science-based pharmaceutical cGMP.

As with all paradigm shifts, there are gaps and teething issues to overcome in changing the way pharmaceutical manufacturing is carried out [6]. One major hurdle in realizing the aforesaid innovation pharmaceutical manufacturing is the lack of an integrated approach to bridge the various *sub-disciplines* (e.g. process chemistry development, process analytical chemistry, process engineering and design, multivariate chemometrics, chemical process systems and control engineering) and *enabling technologies* (e.g. in situ process analytics, multivariate numerical software, SCADA and expert systems) [6]. Second, the PAT framework suggested four essential tools, namely: (i) multivariate tools for design, data acquisition and analysis, (ii) process analyzers, (iii) process control tools, and (iv) continuous improvement and knowledge management tools [2]. As such, the process data and information communication under this PAT framework is both multi-dimensional and voluminous, and it happens in real-time between (i) in- or on-line process analytics that monitors the state of processes with (ii) supervisory control and data acquisition software (SCADA), and (iii) numerical software handling multivariate data analyses, process models and control strategies. The aforesaid two challenges circumscribe a technological gap to be bridged before PAT validated 21st century pharmaceutical cGMP scenarios can be easily implemented. This void also impacts the real-time release of drugs and time-to-market of new chemical entities or drug formulations.

This contribution describes the use of an *integrated platform* that brings together varied software, process units and IT technologies that can help to resolve the aforesaid impasse. Such an integrated platform was tested on the synthesis of 4-D-erythronolactone (4-DEL) through a four-phase hybrid process (i.e. with batch and continuous processing units) [7].

2. Methodological Framework for Integrated Platform

Implicit in the aforesaid strive towards achieving innovative 21st century pharmaceutical cGMP along the ideology of QbD and the PAT framework is the necessity of reliable and timely process information. This process information, as implied in various professional guidelines and documents, will be multi-dimensional and mixed-type in nature; that is the information contains scalar, arrays (vectors and matrices), and even hyperspectral data types [6]. As such, it is considerably more complex than the usual scalar (univariate) process data, e.g. pH, temperature, flow rates and pressure. Thus, a practical methodological framework had to be conceptualized so as to capture the *intrinsically data-rich information environment* within which the aforesaid integrated platform architecture is to interface and function. Figure 1 schematically shows the scenario of a typical QbD/ PAT validated process (unit operation) that needs to be integrated. It consists of (i) various manual controls and automation (valves, pumps, temperature control, etc.) to regulate process conditions, and (ii) data transmission between analytical instrumentation (sensors, spectroscopic probes, etc.) and the supervisory control and data acquisition (SCADA) or distributed control system (DCS) for monitoring and controlling the process state. However, as the real-time data is intrinsically multi-dimensional and complex, it had to be analyzed using multivariate

analyses (chemometrics models) before returning critical process parameters (e.g. chemical concentrations, abstract principal components information, etc.) to the control algorithms residing in the SCADA/ DCS for initiating process control strategies. Third party numerical software might also be invoked to execute specialized mathematical procedures to aid the process analyses and control.

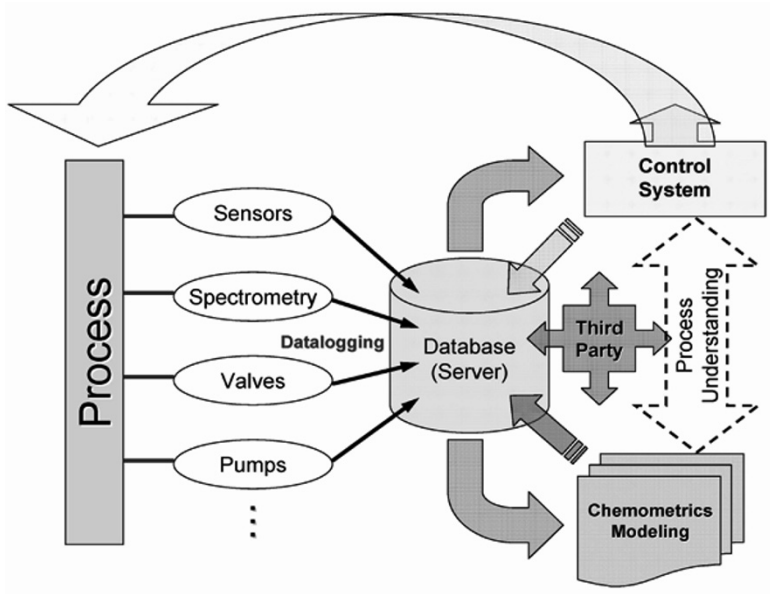

Figure 1 ICES Kilo-Lab vessels and equipment utilized for Integrated Platform

Furthermore, in a science-oriented regulated process scenario described by the FDA PAT guidance [2] and also the ISPE PQLI initiative [6], process analytics, data analysis and control are to be well described within the *design space* and *control strategy* of the process/ unit operation. This implies a *flexible integrated platform* to allow for (i) automated datalogging of process analytical and parameter data, (ii) a secured database server (or historian) that records and maintains the integrity of all data (raw and calculated), and (iii) a flexible software architecture that facilitates the retrieval and inter-exchange of pertinent data from varied software that perform data analyses (e.g. through chemometrics modelling), process modelling (obtained through laboratory and simulation studies), and process control. Modern SCADA/ DCS are able to achieve parts (i) and (ii), with their analytical process measurements and control primarily based on univariate sensors such as temperature, pH, etc. A segment of part (iii), particularly the link between spectroscopic measurements, multivariate chemometrics numerical packages and some form of process control, is presently under development and testing in actual manufacturing facilities by major players in the process system integration and automation industry [6], e.g. ABB Industrial^{IT} eXtended Process Analytical Technology (xPAT) platform, GE Intelligent Platforms Proficy® Process Systems, and Siemens SIPAT™ PAT software that works in conjunction with their SIMATIC WinCC software package. All data flow, analyses and feedback must be governed by science-based process understanding along the QbD ideology, and also compliant to regulatory stipulations (e.g. FDA's 21 CFR electronic records [8]). To the best of our knowledge, such a flexible infrastructure is currently rare, if ever one actually exists, in both industrial and academic R&D facilities; and a full and seamless integration of all

aspects of (i)-(iii) is presently unheard of [6]. Therefore, the ability to set up such a platform would mean a significant step forward to realizing product quality by design (QbD) envisioned by the pharmaceutical fraternity.

3. Implementing an Integrated Platform at the Kilo-Lab Facility of the Institute of Chemical and Engineering Sciences (ICES)

The Kilo-Lab at ICES is the first of its kind within academic research institutions in Southeast Asia. It is geared towards developing new process research techniques and to solve problems of scale-up and manufacturing for the pharmaceutical and specialty chemicals industry sector. The Kilo-Lab is equipped with batch reactor systems and has been building up its continuous processing facilities over the recent few years. Before installing Siemens technologies for the aforementioned integrated platform, the batch process equipment is managed using the GE iFIX SCADA system, whilst the continuous processing skids are separately controlled by the ABB 800xA DCS. To test the integrated platform, a kilo-scale four-phase hybrid processing of 4-DEL was implemented at the ICES Kilo-Lab, which involves (i) salt formation using D-isoascorbic acid and sodium carbonate solutions, (ii) batch oxidation using hydrogen peroxide and (iii) continuous operation of salt formation and oxidation, and (iv) acidification using hydrochloric acid to induce ring closure [7].

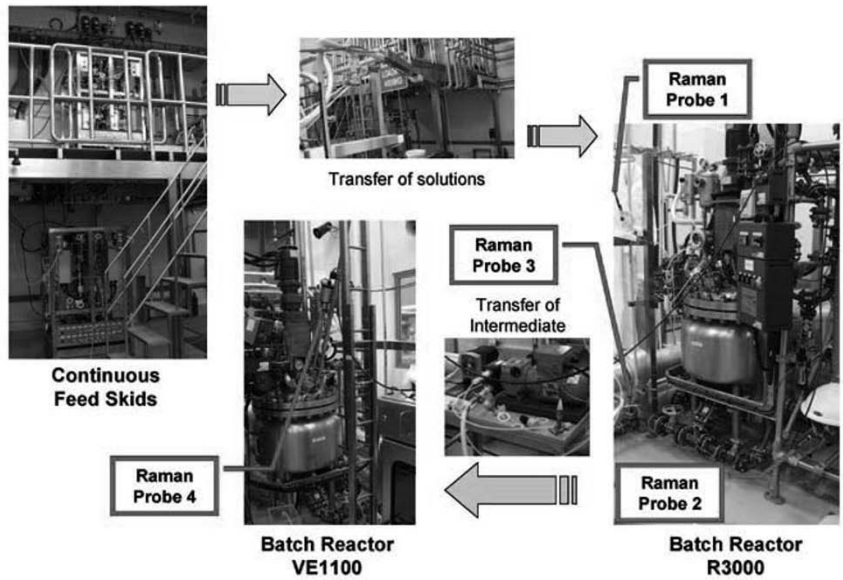

Figure 3 ICES Kilo-Lab vessels and equipment utilized for Integrated Platform

As shown in Figure 3, the kilo-scale implementation of the 4-DEL synthesis involves the use of continuous mobile skids that transfers initial reagents of D-isoascorbic acid, sodium carbonate, hydrogen peroxide in either batch or continuous fashion into the two Hastelloy batch reactors (R3000 and VE1100) that act as either reactors or receivers for different phase of operations. The hydrochloric acid solution (ca. 18% strength) used for ring closure was dosed into VE1100 vessel using a separate pump. The integrated platform is realized through combining Siemens WinCC SCADA and PAT (SIPAT) software technologies, with communication hardwiring using Ethernet lines and the data-exchange through the OLE for Process Control (OPC) protocol. Data acquisition and process control was achieved from the WinCC-SIPAT integrated platform via the

two legacy ABB DCS and GE SCADA systems to control the programmable logic controls (PLCs) of the continuous feed skids and batch reactors.

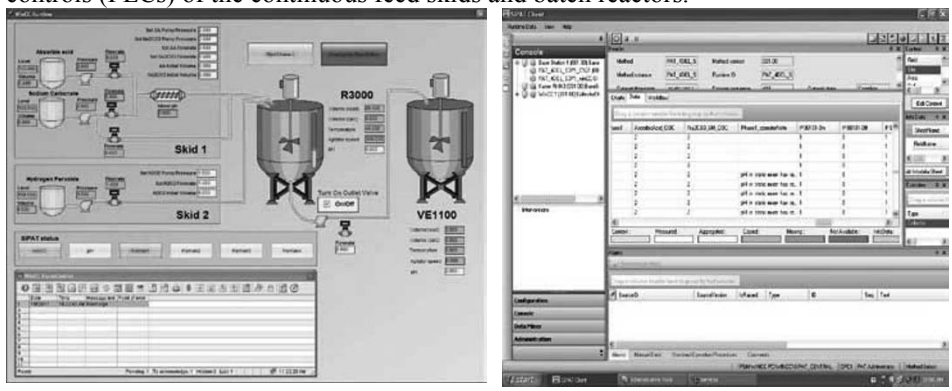

Figure 4 Typical WinCC Graphical User Interface and SIPAT in 4-DEL kilo-scale synthesis

The integrated platform is also directly linked through OPC tags and Ethernet protocol to the in situ Kaiser RamanRXN3 with four multiplexing probes, multivariate chemometrics analyses through MATLAB® and Gensym's G2 monitoring system for real-time process data acquisition and multivariate analyses. In addition, the process understanding acquired from laboratory-scale experimentation was incorporated through programmable scripts in C language for triggering operation logic automation during the kilo-scale operations for all four phases of 4-DEL synthesis. Graphical user interfaces (GUI) for all four phases of operations were also created for simple operator-level command and control with SIPAT displaying real-time process information (e.g. Figure 4). All SIPAT methods development, kilo-scale 4-DEL synthesis runtime data and information such as critical process parameters (CPPs), process alarms, multivariate Raman spectroscopic data and real-time estimates of chemical species concentrations were automatically data-logged into a secured SQL database in compliance to FDA 21 CFR Part 11 requirements.

This successful implementation of the integrated platform at the ICES Kilo-Lab, tested by a four-phase hybrid processing of 4-DEL kilo-scale synthesis, demonstrates great promise as a flexible plug-and-play methodology for facilitating the development and implementation of PAT validated processes.

References

[1] U.S. Food and Drug Administration, September 2004, Pharmaceutical cGMPS for the 21st Century – A Risk-Based Approach (Final Report).
[2] U.S. Food and Drug Administration, September 2004, Guidance for Industry, PAT – A Framework for Innovative Pharmaceutical Development, Manufacturing, and Quality Assurance.
[3] http://www.ich.org/products/guidelines/quality/article/quality-guidelines.html.
[4] http://www.astm.org/COMMIT/COMMITTEE/E55.htm.
[5] T. Garcia, G. Cook, R. Nosal, 2008, PQLI Key Topics - Criticality, Design Space, and Control Strategy, *Journal of Pharmaceutical Innovation*, 3, 60-68.
[6] Chew W. and P. Sharratt, *Analytical Methods* 2 (2010) 1412–1438.
[7] L.L. Wong, R.L. Wong, G. Loh, P.E.W. Tan, S.K. Teoh, S.M. Shaik, P.N. Sharratt, W. Chew, S.T. Tan, D. Wang, Multi-Kilo Synthesis of 4-D-Erythronolactone via Batch and Continuous Processing, *submitted manuscript*.
[8] U.S Food and Drug Administration (FDA), August 2003, Guidance for Industry Part 11, Electronic Records; Electronic Signatures – Scope and Application.

I.A. Karimi and Rajagopalan Srinivasan (Editors), Proceedings of the 11th International Symposium on Process Systems Engineering, 15-19 July 2012, Singapore.

Multiphase CFD simulation of an F-T airlift external loop slurry reactor

Zhenxing Zhu，Jie Yang，Qing Bian

SINOPEC Research Institute of Petroleum Processing，No.18, Xueyuan Road, Haidian District, Beijing, 100083，China

Abstract

F-T Synthesis is a hot spot in the development of new resource. Because of its simple structure and effective heat removal, Slurry bed becomes a most promising technology for F-T Synthesis. But because of its complex hydrodynamics, the reactor is difficult to design and enlarge. Based on the airlift external-loop slurry reactor's cold model, CFD simulations were taken to optimize the gas distributor in a gas-liquid system. Then a study on a gas-liquid-solid system was carried out to observe the flow and distribution of each phase.

Keywords: CFD, F-T Synthesis, Slurry bed, Multiphase Main Text

1. 1. Introduction

As a route converting synthesis gas to liquid fuels or chemical feedstocks, Fischer-Tropsch synthesis (FT Synthesis) has been an interesting topic in reactor design as well as process scale-up.[1] Understanding the flowing status in the designed reactor is of great importance for the design of a specified F-T process because of the complex multiphase flow in FT Synthesis reactor. The flowing status may dramatically change with operation condition and reactor structure.[2] It is well-known that the flow field (such as velocity, pressure, volume fraction of each phase) is closely related to the type of reactor. There are many types of reactors can be used in F-T Synthesis process, such as fixed bed reactor, fluidized bed reactor and slurry bed reactor, among which slurry bed reactor is superior to other beds in many fields, such as heat transfer performance, investment and product yield. Because of the simple structure and effective ability of heat removal, the airlift external-loop slurry bed reactor has been regarded as the most promising technology for F-T synthesis.

The flow in an airlift external-loop slurry bed reactor is quite complicated, because there are three phases inside it, namely gas, liquid and solid. In such fluidization system, bubble dynamics plays a key role in dictating the transport phenomena and ultimately affects the overall rates of reactions. It has been recognized that the bubble wake, when it is present, is the dominant factor governing the system hydrodynamics (Fan and Tsuchiya, 1990).[3] A proper holdup and volume fraction distribution of gas, which is mostly depend on the structure of gas distributor, may be quite important to the process. On the other hand, the existence of solid may be an intractable influence on flowing behavior inside reactor. Unfortunately, the solid motion can not be described directly from experiments because of the lack of measuring instruments.

There are various approaches to the mathematical and physical modeling of multiphase flows. The most widely used methods for CFD are the Eulerian-Eulerian[4] and the Eulerian-Lagrangian approach[5]. In the Eulerian method, both the continuous and dispersed phase(s) are mathematically modeled as interpenetrating fluids, represented by sets of mass, momentum and energy balances. In the Lagrangian approach, a large

number of particles are tracked individually, while the liquid phase is treated as a continuum. The interaction between the particles and the liquid shows up as a source term in the momentum equations. The advantage of the Eulerian method above the Lagrangian way is the void fraction of the dispersed phase is high. While the computational time in the latter approach depends highly on the number of particle trajectories to be calculated, in the Eulerian method the number of equations to be solved remains the same. Interaction terms describing drag, virtual mass and elects of lift forces appear in momentum balances of both phases.[6] Turbulence modeling in three-phase flow is done using the same approach as in single-phase flow.
Two CFD causes using Eulerian method was involved in this article, a simulation of gas-slurry system to optimize the gas distributor and a simulation of gas-liquid-solid system to gain the flowing field and volume fraction of each phase. Both of them was based on and had been verified with a cold model test.

2. 2. Setup and CFD-Approach

In this paper, an Eulerian-Eulerian approach is presented to study the flow in a three-phase external-loop airlift slurry bed reactor. The reactor is shown schematically in Fig. 1. The airlift consists of a riser that is a cylinder tower (H=3000mm, D=280mm) filled with water. A circulating tube (H=2000mm, D=70mm) create a down comer beside the riser. Gas is injected via a distributor on the bottom of the riser. At first, the system is treated as a pseudo-two-phase: the carrier-phase contains liquid with small solid particles, which is modeled as a pseudo single-phase to reduce the calculating time. The gas enters directly into the riser (see Fig. 1) as a dispersed phase. A Reynolds stress models, including source terms due to coupling of the phases, is used for the turbulence and solved simultaneously with the mass and momentum balances. The turbulent kinetic energy and dissipation rate of the dispersed phase are obtained by algebraic relation and are functions of turbulent kinetic energy and dissipation rate of the continuous phase. In the present simulations, interest is merely in steady-state solutions of the two-fluid formulations, throw which the gas distributor may be optimized and the velocity distribution of each phase can be obtained. Then, a gas-liquid-solid system can be simulated by using the information of the two-phase calculation.

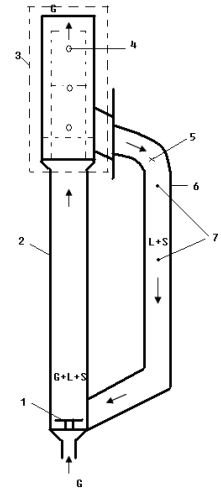

Fig. 1 schematic diagram of external-loop airlift slurry bed reactor

3. 3. Optimization of gas distribution

Through long term experiments, the gas should be better injected down into the reactor. The diameter and the open porosity of gas holes on the distributor were considered in this section. When the average volume fraction of solid is 0.2, the superficial velocity of gas is 0.144m/s, the diameter of gas hole is 2mm, the holdup and velocity distribution of gas at a horizontal plane which is 619mm above the distributor with deferent open porosity can be obtained (see Fig. 2). Under the same conditions, the holdup and velocity distribution of gas at the plane with deferent diameter of gas holes can be obtained by fixing the open porosity on 0.2 (see Fig. 3).

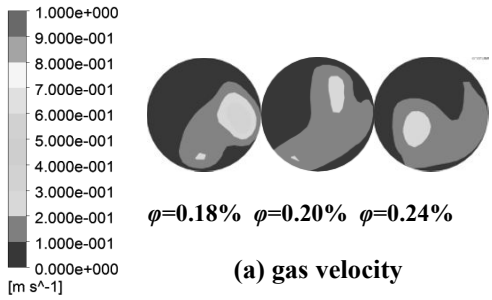

Fig. 2 Velocity and holdup distribution of gas with deferent open porosity

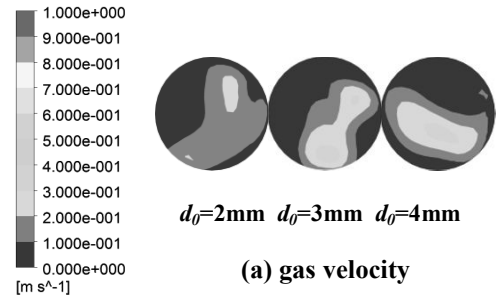

Fig. 3 Velocity and holdup distribution of gas with deferent diameter

It can be found from Fig. 2 and Fig. 3 that gas was distributed uniformly, when the open porosity was 0.2 and diameter is 2mm. It can be inferred that the slurry was also distributed uniformly under the same conditions. Furthermore, the variance of the flowing field of each phase at a horizontal plane which is 619mm above the distributor with deferent open porosity and deferent diameter of gas holes was involved to verify the conclusions (see Table 1 and Table 2). When the open porosity was 0.2 and diameter was 2mm, the variance of gas velocity, slurry velocity and holdup was minimum, which indicated that the most uniform flow was provided.

Table 1 The variance of the flowing field with deferent open porosity

Open porosity of gas holes	φ=0.18%	φ=0.20%	φ=0.24%
Gas velocity	4.78E-03	3.14E-03	3.71E-03
Slurry velocity	1.89E-02	3.25E-03	6.42E-03
Holdup	2.81E-03	2.83E-03	2.88E-03

Table 2 The variance of the flowing field with deferent diameter

Diameter of gas holes	d_0=2mm	d_0=3mm	d_0=4mm
Gas velocity	3.14E-03	6.53E-03	9.03E-03
Slurry velocity	3.25E-03	1.32E-02	4.25E-03
Holdup	2.83E-03	3.40E-03	5.59E-03

4. 4. Gas-liquid-solid CFD simulation

To describe the flow of each phase in details, a gas-liquid-solid CFD simulation was carried out with the results of former section, for example, the gas velocity via holes. The volume fraction of each phase in the reactor can be calculated (see Fig. 4), when the average volume fraction of solid is 0.1, the superficial velocity of gas is 0.054m/s.

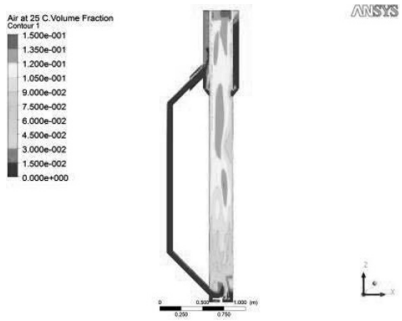

（a）Holdup in ZX plane

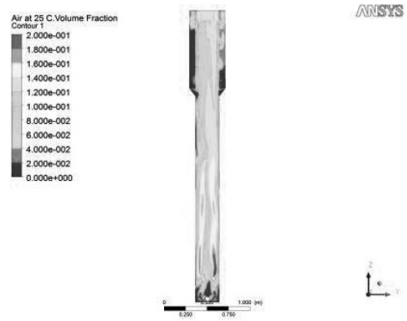

（b）Holdup in ZY plane

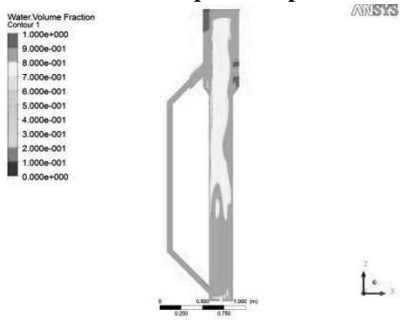

（c）Volume fraction of liquid in ZX plane

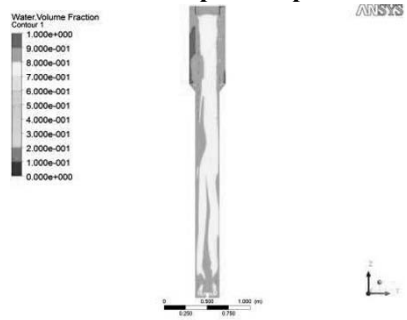

（d）Volume fraction of liquid in ZY plane

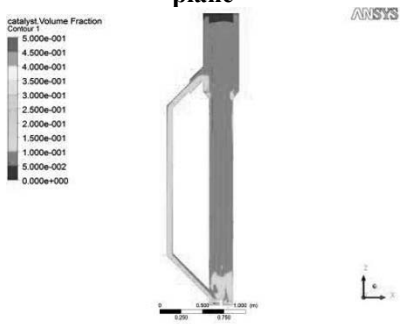

（e）Volume fraction of solid in ZX plane

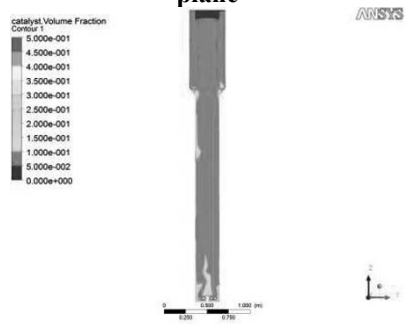

（f）Volume fraction of solid in ZY plane

Fig. 4 The volume fraction distribution of each phase in reactor

It can be seen that the volume fraction distribution of solid and liquid showed a good agreement, a slurry had been formed by these two phases. All of the three phases distributed symmetrically in the view of ZY plane, by which the effects of gas distributor could be confirmed.

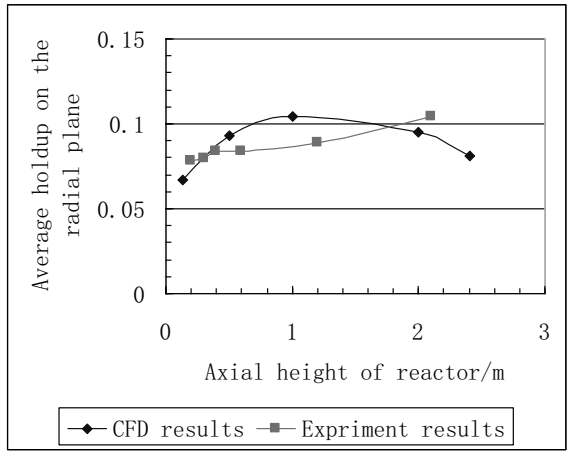

Fig. 5 Average holdup along the axis of reactor

The average gas holdup of radial planes along the axis of reactor was involved to verify the simulation through the results of a cold model test (see Fig. 5). There is a good agreement between simulation and experiment, by which the simulations was proved to be correct. The tiny errors may be cased by neglecting the Coalescence and breakup of bubbles, or gas expansion in reactor.

5. 5. Conclusion

An Eulerian-Eulerian approach was presented to simulate the flow in a multiphase external-loop airlift slurry bed reactor. The gas distributor inside the reactor was optimized by a two-phase simulation. Then, a gas-liquid-solid CFD simulation was performed to observe the flow inside the reactor extensively. The simulation was reasonable through a comparison of the calculating results and the experimental results. Many useful information can be provided from the CFD simulations, according to which, the further researches on the design and scale up of F-T slurry beds must be stepped deeply.

References

[1] R.Krishna, J. M. V.Baten, M. I.Urseanu, J.Ellenberger, 2001, Design and scale up of a bubble column slurry reactor for Fischer-Tropsch synthesis. Chem. Eng.Sci. 56, 537.
[2] B. H. Davis, 2002, Overview of reactors for liquid phase Fischer-Tropsch synthesis. Catal. Today 71, 249.
[3] L.S. Fan, K. Tsuchiya, , 1990. Bubble Wake Dynamics in Liquids and Liquid–Solid Suspensions. Butterworth-Heinemann, Stoneham, MA.
[4] A. Sokolichin, , G. Eigenberger, 1999. Application of the standard k-ε model to the dynamic solution of bubble columns. Chemical Engineering Science, 54, 2273-2284.
[5] S. Lain, S. D. Broder, M. Sommerfeld, 1999. Experimental and numerical studies of the hydrodynamics in a bubble column. Chemical Engineering Science, 54, 4913-4920.
[6] R. T. Jr. Lahey, D. A. Drew, 1992. On the development of multidimensional two-fluid models for vapor/liquid two-phase flows. Chemical Engineering Committee, 118, 125-139.

I.A. Karimi and Rajagopalan Srinivasan (Editors), Proceedings of the 11th International Symposium on Process Systems Engineering, 15-19 July 2012, Singapore.

Multi-scale process and supply chain modelling: from feedstock to process and products

Seyed Ali Hosseini[a] , Atiyeh Abedpour[a], Mingyen Yu[a]

[a]*Center for Process and Information Systems Engineering, University of Surrey, Guildford, GU2 7XH, UK*

Abstract

There is a large body of literature regarding the choice and optimization of different processes for converting feedstock to bioethanol and bio-commodities; moreover, there has been some reasonable technological development in bioconversion methods over the past decade. However, the eventual cost and other important metrics relating to sustainability of biofuel production will be determined not only by the performance of the conversion process, but also by the performance of the entire supply chain from feedstock production to consumption. Moreover, in order to ensure world-class biorefinery performance, both the network and the individual components must be designed appropriately, and allocation of resources over the resulting infrastructure must effectively be performed. The goal of this work is to describe the key challenges in bioenergy supply chain modelling and then to develop a framework and methodology to show how multi-scale modelling can pave the way to answer holistic supply chain questions, such as the prospects for second generation bioenergy crops.
Keywords: Supply chain management, Optimization, Renewable energy

1. Introduction

Although the main global concerns about biofuel are currently limited to sustainability, energy security and prices, each specific bioethanol production plant also faces a wider range of uncertainties, such as which of different processes to choose, which feedstock will be best for the plant, and even the best location for the plant, since all these factors are the main factors that determine cost. In addition to direct cost-determining factors, there are number of indirect effects, such as the effect of the production site and feedstock fields on local communities and the social economy. There is a large body of literature about choice and optimization of different processes for converting feedstock to bioethanol and bio-commodities; however, there is no single best process for all the different feedstocks, and based on the source and composition of the feedstock; there may be several feasible processes. The availability of the right feedstock for the plant is a spatial function of crop production yields, land availability, rainfall, and even the political decisions of local governments. These all imply that all the determining factors for any specific biorefinery are interlinked, and that obtaining the maximum profit for a production site and the maximum benefit for the social economy is only possible by realizing the holistic nature of all the factors and their interrelationship at different scales. These all imply that the eventual cost of biofuel production will be determined not only by the performance of the conversion process, but also by the performance of the entire supply chain from feedstock production to consumption. These relationships can be explained through multiscale modelling.

2. Multiscale Process Modelling and the Supply Chain

There is a large body of literature regarding the choice and optimization of different processes for converting feedstock to bioethanol and bio-commodities; moreover, there has been some reasonable technological development in bioconversion methods over the past decade (Hosseini and Shah, 2009a and 2009b). However, a question that has gone unconsidered in the literature is how technological developments in processing technologies and the life cycle of bioethanol feedstocks will affect the structure of the supply chain. In order to ensure world-class biorefinery performance, both the network and individual components must be designed appropriately, and allocation of resources over the resulting infrastructure must effectively be performed. Shah (2005) has divided all supply chain problems into three categories: (i) supply chain infrastructure (network) design; (ii) supply chain analysis and policy formulation; (iii) supply chain planning and scheduling. Regarding bioenergy, there is a lack of methodology on how to incorporate all the available knowledge into one interconnected network to answer important supply chain questions.The key goal of this work is to develop a framework and methodology to show how multiscale modelling can pave the way to answer holistic supply chain questions; this is illustrated in the figure below.

2.1. Supply Chain Network Design

The bioenergy supply chain network is a direct medium for engaging the end users of bioethanol derivatives and the suppliers of the feedstock; thus, at first glance, the main data required for designing such a network is spatial distribution of biomass supply and energy (fuel, electricity and heat) demand. A great deal of the PSE literature deals with how to handle demand uncertainty, mainly for consumer products (Tsiakis, Shah and Pantelides, 2001a); however, current global biofuel production, specifically in the EU, is much smaller than the desired target. Consequently, at this stage, research focussed on demand forecasting is irrelevant as supply is far lower than current demands. In modelling terms, the authors believe that at this stage, demand should be treated as a deterministic temporally growing spatial function, and not as stochastic.

Classically, location-allocation problems have tended to focus only on logistical aspects (Geoffrion and van Roy, 1979); however, in the process industry supply chain, greater benefits could be achieved by considering logistic and processing aspects simultaneously. The first step in the biofuel supply chain network design should be listing all the possible bioconversion methods for any given biomass. Then, for any specific bioconversion method, a multiperiod spatial optimisation can be built to maximise the total net profit of global network and/or GHG and/or energetic efficiency. This type of model is usually based on technology capital and operating cost as well as distance, capacity and costs of biomass and ethanol; the table below shows one example of the decision spaces for two processing options and three feedstocks. If there are a number of different types of objective functions and trading off between these objectives is difficult, a multi-objective optimisation procedure should be used. Considering these elements together provides opportunities for systems involving distributed pre-processing coupled with centralised processing (Dunnett et al, 2008).

In the optimisation problem, key decision variables can be: mode of transport at each stage, operating mode of equipment in each time period, production and supply of products, number of echelons, number of components in each echelon, and the

connectivity between components in adjacent echelon. The choice of deciding factors usually depends on the availability of data and the complexity of the network; nevertheless, a larger number of decision factors usually lead to more robust network structures, although it makes the optimisation problem more complex. In general, there exists a trade-off between models' precision and complexity; thus, a modeller's skill lies in choosing the right combination. Having developed optimisation problems for each specific biomass and any possible bioconversion methods, one can then easily compare these networks based on metrics such as cost, GHG, capacity, products, etc. In this way, a supply chain network design can be a valuable tool for decision-making.

2.1.1. Fundamental Bioenergy Supply Chain Network

Most of the literature on bioenergy supply chains assumes a given fundamental structure for the network in terms of suppliers, manufacturing plants, warehouses, distribution centres and customers. Thus the design procedure mainly focuses on the number of echelons and the connectivity between adjacent echelons. This is mainly due to the relative youth of the field of supply chain management (SCM), as most of the companies with established supply chain networks traditionally used SCM techniques to increase the efficiency of their already-established network. However, at this stage of development of biofuel production, the fundamental structural elements of the bioenergy supply chain have not yet been established; since these are important aspects of overall efficiency, one of the key challenges in the field is to integrate the different components of supply chains without any prior assumptions about the fundamental structure of the network (e.g. allowing distributed pre-processing).

Tsiakis *et al*. (2001b) addressed this problem in general, and proposed a general framework using the concept of flexible nodes. These nodes can be located at any one of a set of candidate locations, produce one or more products using one or more shared resources, hold inventories of the products as well as of any other materials in the network, and exchange material with other nodes. The functions of these nodes are therefore not specified a priori, and no flow network is superimposed. Consequently, the node functionalities and the flows between nodes are determined as part of the optimisation. Authors believe that applying this methodology to the bioenergy supply chain may result in a leaner network, where storage capacity is only established when necessary. Furthermore, this method provides the possibility of taking advantage of economies of scale in transportation that can result in huge financial savings due to the low energy value of biomass.

2.1.2. Integration of Process Model to Supply Chain Model

It should be mentioned that in the field of operational research and PSE, a very large amount of work has been undertaken to address both the infrastructure network design problem and optimisation of established networks. However in most of the work to date, the potential benefit of including more detail in the manufacturing process has not been established. Since there is huge uncertainty regarding the efficiency of each bio-refining process option in its mature state, at this stage of development these uncertainties should be captured in the global network model, to direct the research in way that most benefits the global network. For example, Hosseini and Shah (2009a) showed that optimising the biomass chip size in a dilute acid pretreatment process achieves average savings equivalent to a 5% improvement in the yield of the biomass-to-ethanol

conversion process. This kind of improvement in processing efficiency can lead to completely different result in global network optimization results; therefore, it is of utmost importance to formulate a methodology incorporating process uncertainty in the global supply chain network.

Although multiscale modelling is a promising technique for integrating all processing aspects at different scales into the biofuel supply chain, computational efficiency is also an intellectual challenge in the PSE area, as computation usually increases exponentially with problem size (Grossmann and Westerberg, 2000). One practical way to address this challenge would be to use conceptual process models from the molecular level up to the unit operation level in order to predict the possible range of operation and efficiency at each unit of operation, and then, in the supply chain model, consider the overall process as a combination of different outcomes, i.e. scenarios from process models at all scales. In other words, it would use characteristic models to run detailed dynamic simulations for each unit operation, and then use the results of these simulations (as "metamodels") in the global network model offline. In this way, it would be possible to consider uncertainty at a process level in the supply chain model; moreover, since these uncertainties are determined by conceptual models, it would be possible to find the root of the uncertainties. For example, if the model predicts a rising cost-purity curve for a specified unit of operation, then it would be possible to integrate this into the supply chain model and chose the appropriate purity for that specific unit of operation in order to maximize overall network efficiency. Therefore, in this approach, instead of considering the process as a black box, it would be possible to consider the process as a set of black boxes (unit operations) with a range of inputs and outputs for each unit of operation. Indeed, this approach would aid in optimizing the interactions between all available unit operations so that opportunities for new flowsheet configurations are facilitated.

2.2. Supply Chain Simulation

As stressed in the previous section, characteristic models are of utmost importance since they are the closest representation of reality and provide a way to find the root of uncertainties at any level. Therefore characteristic models are the most appropriate method for designing a fundamental bioenergy supply chain network. However, simulation models can be used to study the detailed dynamic operation of a fixed configuration under operational uncertainty, and can be used to evaluate expected performance measures for the fixed configuration to a high level of accuracy.Therefore, model-based simulations can have great significance for policy makers, as they can identify the potential socioeconomic effects of the bioenergy supply chain under different operating policies, ahead of actual implementation of any one policy.

2.3. Supply Chain Planning and Scheduling

Supply chain planning starts immediately after designing an infrastructure network and considers a fixed infrastructure over a certain time period, usually up to one year, and seeks to find the best network configuration to respond to forecast supply and demand in an economically efficient manner. In most of the works to date, the focus of researchers has been on identifying the best way to design the best network configuration based on demand uncertainty. However, as discussed earlier, there is not going to be a huge variation in ethanol demand; the main problem will be the variation of biomass supply due to seasonality. Therefore, the main issue for bioenergy supply

chain planning will be finding the best network configuration, using different feedstocks throughout the year to meet constant demand. At this stage of development, most of processes are designed for specific biomass types; it should be emphasized that for a bioenergy network to be economically efficient, biorefineries should be able to use different feedstocks with only minimum changes made to their overall process. For example, processes should be flexible enough so that different operating conditions (i.e., different residence time or temperature in a bioreactor) are enough to process different types of feedstock, and it is not necessary to change the overall process configuration. It should be possible to get the same result from different feedstocks in an economically feasible manner. To conclude, authors believe process intensification –developing processes which are more responsive to market needs whilst responding to changes in process parameters in seconds, rather than several minutes or hours – is essential to designing an efficient global bioenergy network.

3. Conclusion

Over the past few years there has been huge body of literature published addressing challenges for commercial bioenergy production ranging from feedstocks to processes and products. However, there is lack of methodology on how to incorporate all the available knowledge into one interconnected network to answer key supply chain questions holistically. Thus, in this work we have described the key challenges in modelling the bioenergy supply chain and then developed a framework and methodology to show how multi-scale modelling can pave the way to answer holistic supply chain questions, such as how to design fundamental bioenergy supply chain and incorporate process models into supply chain models. The important next steps involve modellers working alongside scientists engaged in fundamental experimental work on biomass production and conversion, ensuring that there is a good fit between the needs of whole systems modelling and the generation of empirical data.

References

Dunnett, A. J, C. S Adjiman, and N. Shah. “A spatially explicit whole-system model of the lignocellulosic bioethanol supply chain: an assessment of decentralised processing potential.” *Biotechnology for biofuels* 1 (2008): 13.

Geoffrion, A. M., & van Roy, T. J. (1979). Caution: Common sense planning methods can be hazardous to your corporate health. *Sloan Management Review*, *20*(4), 31–42.

Grossmann, I. E, and A. W Westerberg (2000). “Research challenges in process systems engineering.” *AIChE Journal* 46, no. 9 (2000): 1700–1703.

Hosseini, Seyed Ali, and Nilay Shah (2009a) . “Multiscale modelling of hydrothermal biomass pretreatment for chip size optimization.” *Bioresource Technology* 100, no. 9 (May 2009): 2621-2628.

Hosseini, Seyed Ali, and Nilay Shah (2009b). “Multiscale modelling of biomass pretreatment for biofuels production.” *Chemical Engineering Research and Design* 87, no. 9 (September 2009): 1251-1260.

Shah, N “Process industry supply chains: Advances and challenges (2005).” *Computer Aided Chemical Engineering* 18 (2004a): 123–138.

Tsiakis, P., Shah, N., & Pantelides, C. C. (2001a). Design of multi-echelon supply chain networks under demand uncertainty. *Industrial and Engineering Chemistry Research*, *40*, 3585–3604.

Tsiakis, P., Shah, N., & Pantelides, C. C. (2001b). Optimal structures for supply chain networks. In *Presented at AIChE annual meeting*.

I.A. Karimi and Rajagopalan Srinivasan (Editors), Proceedings of the 11th International Symposium on Process Systems Engineering, 15-19 July 2012, Singapore.

Performance Assessment of Water Gas Shift Membrane Reactors by a Two-dimensional Model

Marcello De Falco[a], Vincenzo Piemonte[a], Angelo Basile[b]

[a]*Faculty of Engineering, University Campus Bio-Medico of Rome, via Alvaro del Portillo 21, 00128 Rome, Italy*
[b]*CNR-ITM, c/o University of Calabria, Via Pietro Bucci, Cubo 17/C, 87030 Rende (CS,)Italy.*

Abstract

There is currently a large world effort towards developing hydrogen power as the next generation of clean energy for both the transportation and the electricity sectors.
Water gas shift (WGS) is a thermodynamically limited reaction which has to operate at low temperatures, reducing kinetics rate and increasing the amount of catalyst required to reach valuable CO conversions.
It has been widely demonstrated that the integration of hydrogen selective membranes is a promising way to enhance WGS reactors performance: a Pd-based membrane reactor (MR) operated successfully overcoming the thermodynamic constraints of a traditional reactor (TR) thanks to the removal of hydrogen from reaction environment.
In this work, the effect of hydrogen removal in membrane water gas shift reactors will be investigated by a two-dimensional, non-isothermal model in order to analyze the WGS reactor performance.
Keywords: WGS, Mathematical Modeling, Computer Simulations, Hydrogen.

1. Introduction

The water gas shift (WGS) reaction is an important step of hydrogen production in industrial cycles for upgrading H_2 rich streams by CO conversion present in syngas mixtures. In the last few years, significant developments in membrane science and the vision of process intensification by multifunctional reactors have stimulated the academic and industrial research focused on membrane reactor application to chemical processes (Mendes et al., 2010). From these works, the increase of the CO conversion above the equilibrium values appears to be possible when hydrogen is removed through the membrane. The membrane integration inside the WGS reactor leads to two main advantages: firstly, by allowing operation at optimum temperatures, MR improves reaction rates and reduces the need for excess water, improving plant efficiency. Secondly, by providing both reaction and product separation in one process step, a MR can potentially reduce the plant size and thus capital costs.
Membranes integrated in WGS reaction environment are usually dense metallic membranes composed by a Pd-alloy selective layer and a ceramic or Porous Stainless Steel (PSS) support. Composite dense Pd-based membranes are extremely selective and allow the separation of an ultra-pure hydrogen stream from the reaction environment. On the other hand, composite Pd-based membranes suffer for thermal stability problems due to the adherence between selective layer and support, which imposes a temperature constraints (operating temperature < 500°C, Bredesen, 2008). However, it is a worth assessment that the membrane temperature threshold would be coherent with the typical

WGS operating temperature (250-450°C). In this work, a Matlab model was developed to analyze and predict the performance of a WGS membrane reactor for H_2 production.

2. Mathematical Model

The WGS reaction is described as follow:

$$CO + H_2O \Leftrightarrow CO_2 + H_2 \quad (1)$$

The membrane reactor (MR) is composed by a reaction zone, where a catalyst is packed in order to support the WGS reaction, and a permeation zone where a carrier gas is fed to carry out the hydrogen permeated through the Pd-based dense membrane. Therefore, to describe the MR by a mathematical model, mass, energy and momentum balances have to be imposed both in reaction and permeation zones.

The 2D non-isothermal model has been developed by the following assumptions: steady-state conditions; negligible axial dispersion and radial convection; ideal gas behavior; pseudo-homogenous condition inside the reactor; perm-selective of Pd-Ag membrane towards hydrogen 100%; negligible radial dispersion and isobaric conditions in permeation zone.

The model equations, together with boundary conditions, are reported as follows:

2.1. Mass balances

Reaction zone:

$$\frac{\partial(\tilde{u}_z\tilde{c}_i)}{\partial\tilde{z}} = \frac{d_p \cdot L}{Pe_{mr} \cdot r_{i,o}{}^2} \cdot \left(\frac{\partial^2(\tilde{u}_z\tilde{c}_i)}{\partial\tilde{r}^2} + \frac{1}{\tilde{r}} \cdot \frac{\partial(\tilde{u}_z\tilde{c}_i)}{\partial\tilde{r}}\right) - \frac{\rho_{bed} \cdot L}{u_{z,in}c_{CO,in}} \cdot \eta \cdot R_i \quad (2)$$

where $\tilde{u}_z$ and $\tilde{c}_i$ are the dimensionless gas mixture velocity and mole concentration of component i, $u_{z,in}$ and $c_{CO,in}$ inlet velocity and inlet CO concentration, $\tilde{z}$ and $\tilde{r}$ dimensionless axial and radial coordinates, d_p the catalyst particle diameter, L and $r_{i,o}$ reactor length and catalytic bed tube radius respectively, ρ_b is the packed bed density, η and R_i are the effectiveness factor and the intrinsic rate for component i, expressed according to (Criscuoli et al., 2010) and Pe_{mr} is the mass effective radial Peclet number given by (Kulkarni and Doraiswamy, 1980) for Reynolds number greater than 1000.

Permeation zone:

$$\frac{dY_{H_2}}{d\tilde{z}} = \pm\frac{N^m_{H_2} \cdot 2\pi \cdot r_{o,i}}{u_{z,in} \cdot c_{CO,in}} \quad (3)$$

where $Y_{H_2} = \frac{F_{H_2,perm}}{F_{CO,in}}$ is the hydrogen recovered per mole of inlet carbon dioxide, $r_{o,i}$ is the membrane radius and $N^m_{H_2}$ is the hydrogen flux permeating through the membrane, evaluated by the Richardson's law for dense membranes when the limiting step is the diffusion of atomic hydrogen in the metallic layer:

$$N^m_{H_2} = \frac{P_H}{\delta} \cdot \left(p^{0.5}_{H_2,reac} - p^{0.5}_{H_2,perm}\right) \quad (4)$$

where δ is the Pd-based membrane thickness (20 μm in this work), $p_{H_2,reac}$ and $p_{H_2,perm}$ are hydrogen partial pressures in the reaction and permeation zone, respectively, and P_H is the membrane permeability, depending on temperature and

membrane composition (Shu et al., 1994). The sign + or – in is related to co-current or counter-current sweeping gas configuration.

2.2. Energy balances

Reaction zone:

$$\frac{\partial \tilde{T}_R}{\partial \tilde{z}} = \frac{\lambda_{er} \cdot L}{(u_z c_{tot}) \cdot c_{p,mix} \cdot r_{i,o}^{\ 2}} \cdot \left(\frac{\partial^2 \tilde{T}_R}{\partial \tilde{r}^2} + \frac{1}{\tilde{r}} \cdot \frac{\partial \tilde{T}_R}{\partial \tilde{r}}\right) + \frac{\rho_b \cdot L \cdot \eta \cdot R \cdot (-\Delta H)}{(u_z c_{tot}) \cdot c_{p,mix} \cdot T_{R,in}} \quad (5)$$

where $\tilde{T}_R$ and $T_{R,in}$ are the dimensionless reaction zone temperature and the inlet temperature, $c_{p,m}$ is the specific heat of gas mixture, c_{tot} is the total gas concentration, R is the reaction rate of reaction, (-ΔH) is the enthalpy of reaction and λ_{er} is the effective radial thermal conductivity of packed bed and gas mixture, considered as a pseudo-homogeneous phase and calculated according to (Elnashaie and Elshishini, 1993).

Permeation zone:

$$\frac{d\tilde{T}_P}{d\tilde{z}} = \frac{L}{F_{P,tot} \cdot c_{p,perm}} \cdot \frac{1}{T_{R,in}} \cdot \left[U_1 \cdot 2\pi \cdot r_{i,i} \cdot (T_R - T_P) + N_{H_2}^m \cdot \pi \cdot r_{o,i} \cdot (h_{H_2,reac} - h_{H_2,perm})\right] \quad (6)$$

where $\tilde{T}_P$ is the dimensionless permeation zone temperature, $c_{p,perm}$ is the specific heat of gas mixture in permeation zone, $F_{P,tot}$ the total flow-rate, $r_{i,i}$ the membrane internal radius, $h_{H_2,reac}$ and $h_{H_2,perm}$ hydrogen enthalpies in the reaction and permeation zone and U_1 the overall heat transfer coefficient between reaction and permeation zone.

2.3. Momentum balances

In the reaction zone, the momentum balance is described by the well-know Ergun equations for packed beds. In the permeation zone, the pressure drop is negligible.

2.4. Boundary conditions

If the co-current MR configuration is imposed, the boundary conditions have to be fixed in the inlet section and at external and internal tubes. The PDEs set will be solved by a numerical method. On the other hand, if the counter-current configuration is imposed, the permeation zone equations boundary conditions will be fixed at $\tilde{z} = 1$ and the problem is a BVP (Boundary Value Problem), to be solved by a shooting method.

3. Results and Comments

In figure 1 the reactor conversion versus the gas hourly space velocity (GHSV) at T=550 - 600 K is reported. The hydrogen conversion both in membrane and conventional reactors decreases increasing space velocity. Moreover, at low space velocities the reactor conversion growth is more evident due to the membrane presence inside the WGS reactor: indeed a higher hydrogen flow crosses the reaction zone towards the permeation zone. Furthermore the reactor conversions are very close to equilibrium conditions for operating temperature of 600 K, while, due to kinetic rate reduction, the reactor conversions obtained at 550 K are far from equilibrium also for low values of the GHSV.

Figure 2 shows the effect of inlet reaction zone temperature on CO. At 600 K there is a maximum on the reactor conversion. It can be seen that, with temperature increasing, the conversions are reduced but drawing ever nearer to equilibrium. At temperatures

above 675 K, the conversion of the membrane reactor appears to be greater than the equilibrium conversion, while the conversion of the traditional reactor (TR) moves toward equilibrium.

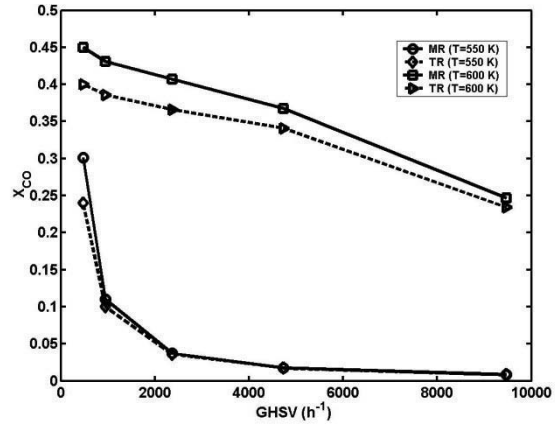

Figure 1 - CO conversion vs GHSV at 550 – 600 K (Reaction pressure = 10 bar, permeation pressure = 1 bar, H2O/CO = 1.1, Equilibrium conversion at 550 K = 0.6, Equilibrium conversion at 600 K = 0.45)

Figure 3 reports the reactor temperature profiles vs. the reactor axial coordinate: at low space velocities, initially there is a large increase of temperature because the reaction is very fast. When the reaction slows, T is reduced because there is a greater amount of outgoing heat due to the ΔT with the wall temperature (outlet temperature is set equal to the inlet temperature, i.e. 600 K) with respect to the amount of heat generated by the reaction.

4. Conclusions

A two-dimensional model was developed to analyze and predict the performance of a WGS membrane reactor for H2 production.

The main advantages of membrane reactors in WGS processes are CO conversion larger than in TR due to hydrogen removal during reaction. The model highlights the effect of the main operating parameters:

• at higher mixture GHSV the CO conversion decreases but the catalyst productivity increases;

• CO conversion profiles in function of operating temperature shows a maximum at 600 K about.

References

R. Bredesen, 2008, Thin Pd-23w%Ag membranes for hydrogen separation, CASTOR workshop, Lyon 22 – 24 January 2008.

A. Criscuoli, A. Basile, E. Drioli, 2000, An analysis of the performance of membrane reactors for the water-gas shift reaction using gas feed mixtures, Catalysis Today, 56 , 53-64.

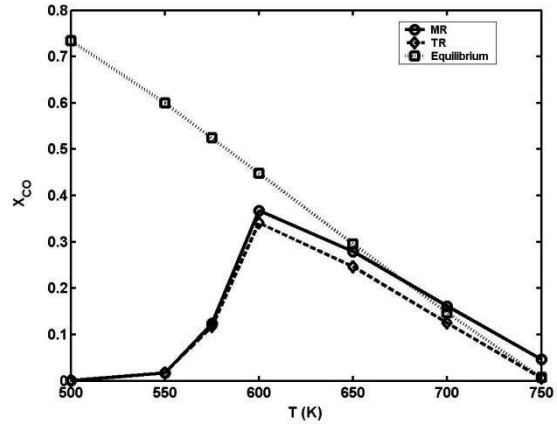

Figure 2 - CO conversion vs T (GHSV = 4750 h^{-1}, Reaction pressure = 10 bar, permeation pressure = 1 bar, H2O/CO = 1.1)

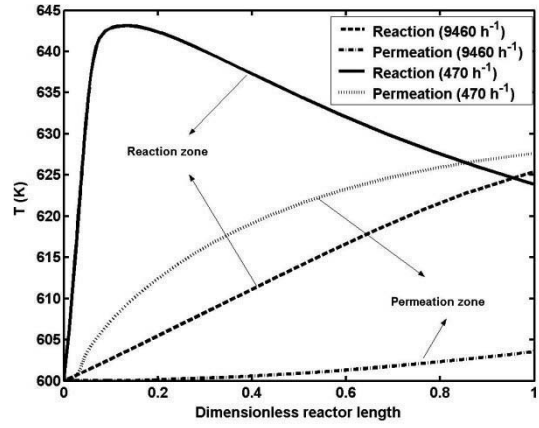

Figure 3 - T vs reactor length (GHSV = 4750 h-1, Reaction pressure = 10 bar, permeation pressure = 1 bar, H2O/CO = 1.1) (De Falco, 2011).

M. De Falco, V. Piemonte, A. Basile, 2011, Simulation of Water Gas Shift Membrane Reactors by a Two-dimensional Model, 21st European Symposium on Computer Aided Process Engineering – ESCAPE 21, in press.

S. Elnashaie, S. Elshishini, 1993, Modelling, simulation and optimization of industrial fixed bed catalytic reactors, Vol. 7 of Topics in Chemical Engineering, Gordon and Breach Science Publisher.

B.D. Kulkarni, L.K. Doraiswamy, 1980, Estimation of effective transport properties in packed bed reactors, Catalysis Reviews: Science and Engineering, 22, 3, 431-483.

D. Mendes, A. Mendes, L.M. Madeira, A. Iulianelli, J.M. Sousa, A. Basile, 2010, The Water-Gas Shift Reaction: From Conventional Catalytic Systems to Pd-based Membrane Reactors – a Review, Asia-Pacific Journal of Chemical Engineering on Membrane Reactors, 5, 111-137.

J. Shu, B. Grandjean, S. Kaliaguine, 1994, Methane steam reforming in asymmetric Pd and Pd-Ag porous SS membrane reactors, Appl. Catal. A: General, 119, 305-325.

I.A. Karimi and Rajagopalan Srinivasan (Editors), Proceedings of the 11th International Symposium on Process Systems Engineering, 15-19 July 2012, Singapore.

A Hybrid Meta-heuristic Method for Optimizing Logistic Networks Subject to Operational Conditions in Practice

Yoshiaki Shimizu and Syota Tsuchiya

[a]*Department of Mechanical Engineering, Toyohashi University of Technology, 1-1 Hibarigaoka, Ten-paku-cho, Toyohashi 441-8580, Japan*

Abstract

Under agile and global manufacturing environment, importance of logistics as a core of supply chain management has been acknowledged increasingly. In this study, we provide a practical hybrid method for a hierarchical logistic network optimization belonging to a tactical level. Since the problem is made of different kinds of NP-hard combinatorial optimization problems, its rigid solution is almost impossible for practical scale problems. Hence, to cope with the problem in practice, we have developed a three-level method in terms of the modified insertion method for VRP with time windows. It is deployed on a basis of Ton-Kilo (load (ton) multiply distance (km)) based evaluation instead of the conventional Kilo (distance only) based one. It also includes a new mechanism that enables us to engage in multi-objective analysis between economics and service of delivery. Validity of thus developed method is examined through numerical experiments.

Keywords: Global combinatorial optimization, Logistics, Vehicle routing, Hybrid method, Tabu search, Insertion method.

1. Introduction

To improve business efficiency for agile and global manufacturing, importance of logistics as a core of supply-chain management has been acknowledged increasingly. Noticing a similarity of hierarchy of decision level, which is popularly classified as long-term, middle-term and short term levels in production planning, this study provides a practical hybrid method for a hierarchical logistic network optimization belonging to a middle-term or a tactical level. Following this category, we classify traditional location problems (Melo, Nickel and Saldanha-da-Gama, 2009) into the long-term planning while vehicle routing problems (VRPs; Yeun, et al., 2008) into the short-term planning. Then the middle-term tries to consider a location problem and VRP at the same time.

Since thus defined problem is made of different kinds of NP-hard combinatorial optimization problems, we have developed a new hierarchical method so as to commonly evaluate transportation cost throughout the levels. For this purpose, we try to develop a modified insertion method that derives a near optimal solution for VRP on a basis of Ton-Kilo (load multiply distance) cost accounting instead of the conventional Kilo basis (only distance). It also includes a new mechanism that enables us to engage in multi-objective analysis between economics and service represented by the term associated with due dates of delivery. Thus developed solution method provides a unique integrated method amenable to practical applications at tactical level.

2. Problem Statements and Basic Idea for Solution

Let us consider a logistics network composed of plants, depots and customers as shown in Fig.1 (left). Then the present problem tries to optimize the selection of available depots, shuttle paths between plants and depots and circular routes covering the client customers of every depot. This problem is formulated as a mixed integer programming problem with an objective function composed of transportation costs, fixed changes of opening depots and serving vehicles, shipping cost at plants and handling cost at depots. As a tactical delivery condition that will link to a certain service, we consider a time window or an admissible delivery interval for every customer.

Conventionally, transportation costs of location problems are counted on a basis both of distance and load (Ton-Kilo base) while just on distance (Kilo base) in VRP. We can claim that the Ton-Kilo base is more realistic than Kilo base since the transportation cost depends not only distance but also weight of loads. Hence, in order to keep consistency of cost accounting for both problems, it makes sense to follow the Ton-Kilo base (Shimizu, 2011). Though thus formulated problem is not only consistent but also practical in cost accounting, such idea has never been considered in previous location-routing problems.

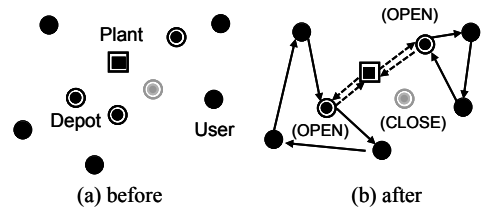

Fig. 1: Logistics network model in concern

Moreover, since the resulting problem refers to an integrated NP-hard problem, it becomes almost impossible to directly solve the mathematical programming model with real-world size. Then, we try to extend our two-level hybrid method of the location problem (Shimizu and Wada, 2004) as shown in Fig.2. The deployed idea is a three-level method and the third level VRP problem starts with searching the circular routes based on the solution of the second level location problem. Letting the customers served by the depot be its clients, we can cope with the multi-depot VRP problems practically. Below, key components of the proposed procedure will be described.

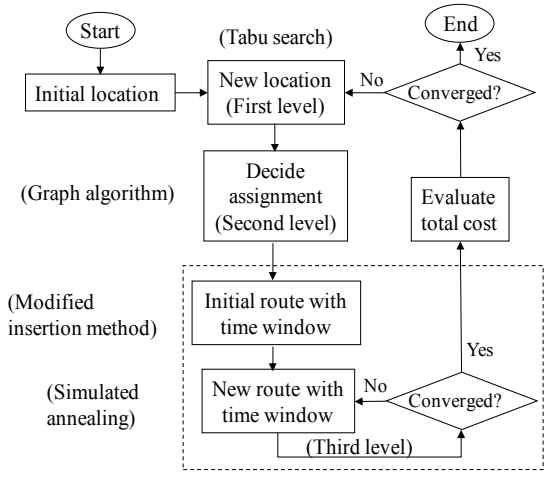

Fig. 2: Flow chart of the algorithm

3. Modified VRP Method with Time Window

3.1. Insertion Method for Ton-Kilo based VRP

Insertion method (Solomon, 1987) has been known as an effective approximation method of VRP together with saving method. For the present Ton-Kilo based case, we extended the original procedure as follows.

Step 1: Select randomly seed customers till the numbers of truck.

Step 2: Decide initial routes by round trip between the depot and each seed customer (Fig.3(a)).
Step 3: List the remaining customers in the descending order of $d_{0k}w_k$ for all k except for the seeds customers, and select one for the next step from the top of the list, in turn.
Step 4: Insert customer k between the node i and j for which Δ_{ij}^k $(=\Delta c_{ij}^k)$ becomes minimum for $\forall i, j$ as long as such insertion will not violate the admissible condition (upper bound for payload of truck) (Fig.3(b)).

$$\Delta c_{ij}^k = w_k(d_{01} + d_{12} + \cdots + d_{i-1,i} + d_{ik}) + (w_j + \cdots + w_n + q)(d_{ik} + d_{kj} - d_{ij}) \qquad (1)$$

where d_{ij}, w_k, q denote distance between nodes i and j (0 means depot), demand at customer k and weight of truck.
If customer k is selected, delete it from the list. Otherwise, go back to Step 3.
Step 5: Repeat the above procedures (Fig.3(c)) until the list becomes empty.
Step 6: Letting the above result as an initial guess, improve it based on simulated annealing (SA) until a certain convergence criterion has been satisfied.

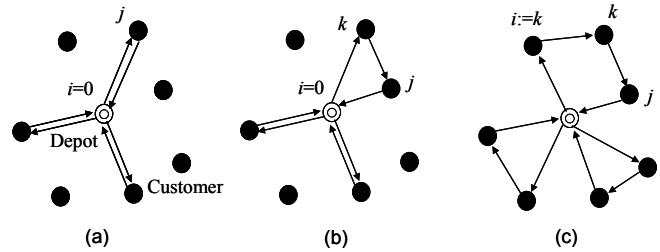

Fig.3: Scheme of insertion method

3.2. Time Window as for Describing Customer Service

To deliver products just on time is one of the essential customer service required for the today's tactical delivery. The idea is deployed as the time window in VRP. Accordingly, besides the payload requirement in Step 4, we must add the one whether the arrival time is on time or not as another admissible condition (hard condition) (See Fig.4). On the other hand, regarding the waiting time for the earlier delivery, we view it as a soft condition and modified the computation in Eq.(1) as Eq.(2).

$$\Delta_{ij}^k = \Delta c_{ij}^k + \alpha \cdot \Delta t_{ij}^k \qquad (2)$$

where Δt_{ij}^k denotes the increment of waiting time at node j when customer k is inserted between node i and j. Moreover, α is a weighting factor between the delivery cost and the waiting time. Generally speaking, shorter waiting time transport needs longer trip distance and spends more vehicles. Since those will increase the cost, and vice verse, there exists a trade-off between them. By solving the problem with a set of weighting factor α, we can engage in the trade-off analysis.

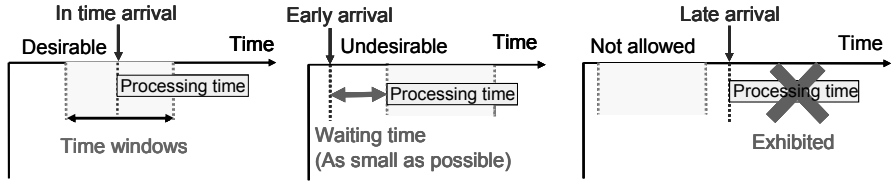

Fig.4: Scheme on time window condition

4. Numerical Experiment

We carried out a numerical experiment for the problem with 5 plants, 10 depots and 100 customers to illustrate the proposed procedure.

Table 1 show the system parameters employed here. Regarding the tuning parameters of SA, we set the initial temperature as 100 and annealing factor as 0.9. The algorithm is applied by using four methods for generating neighbors such as insert, swap, cross exchange and 2-opt operations (See Fig.5) under 50 outer iterations and 100 inner iterations.

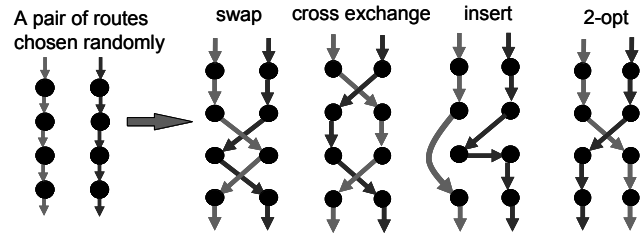

Fig.5: Employed operations for neighbourhoods generation

To validate the performance, we compared the results among three variants of application as shown in Fig.6. The first method is the expedient since none of the previous methods can cope with such a consistency that is considered here in cost accounting. Deriving the circular routes from the conventional or the Kilo-based method, we re-account the cost in terms of the Ton-Kilo basis and continue the solution procedure. Regarding the variants of the proposed approach, the method 2 skips the additional search at VRP by SA. Hence according to the ascending order, the accuracy of solution will increase.

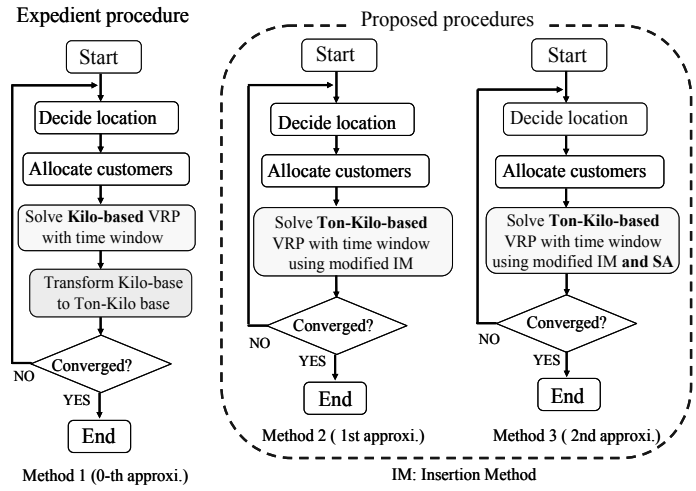

Fig.6: Comparison of applied procedures

In Fig.7, we compare the results by solving each problem with various values of α. Since making α larger means shorter waiting time is more preferred, each solution moves on in southeast direction. Eventually, we can observe the trade-off between the cost and the waiting time, and know the method 3 outperforms the others as expected since its Pareto front sticks out most to the direction of origin.

Table 1 Employed parameter values

Plant	Number = 5	Available supply	[0, 1000]
DC	Number = 10	Holding capacity	[250, 300]
Customer	Number = 100	Demand	[10, 20]
		Earliest time	[8:00, 16:00]
		Latest time	[9:00, 17:00]

Moreover, we can confirm the adequateness of the result if we compare the specified results shown in Fig.8. The route that weights the total cost (Fig.8(a)) will make the travel distance shorter or the cost cheaper while another extreme neglects such effort to reduce the total waiting time.

5. Conclusion

To improve business efficiency for agile and global manufacturing, this study has developed a practical method for a logistic network optimization at a tactical level. Thereat a Ton-Kilo based hybrid method for VRP with time window is proposed so that it can concern with multi-objective analysis between economics and service of delivery. Presenting a general formulation and giving its algorithm, we provided numerical experiments to examine the validity through comparison of multi-objective analysis among the variant applications. Future studies should be devoted to apply the method to real-world problems concerning with multi-objective optimization and parallel computing (Shimizu and Ikeda, 2010) to enhance the solution speed.

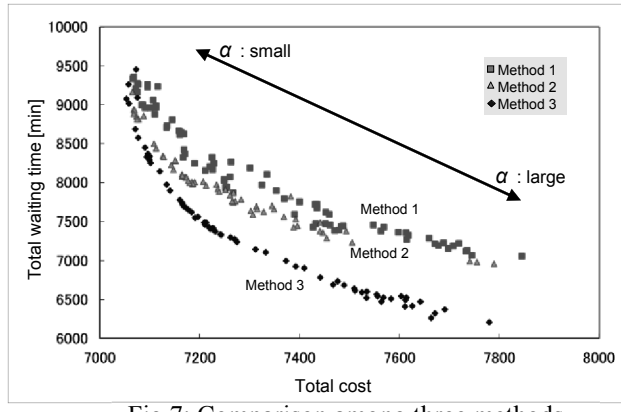

Fig.7: Comparison among three methods

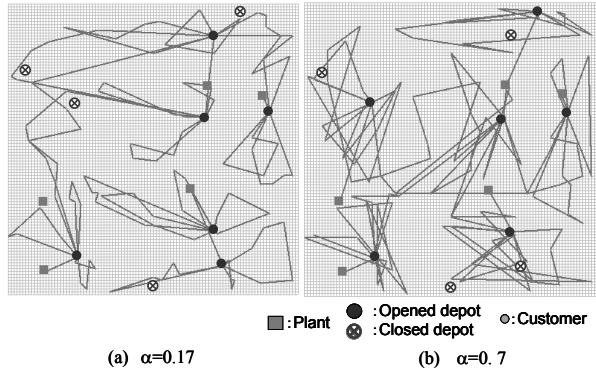

Fig.8: Comparison of routes for the specific α

References

M. T. Melo, S. Nickel and F. Saldanha-da-Gama, 2009, Facility location and supply chain management-A review, European Journal of Operational Research, 196, 401-412

Y. Shimizu, and T. Wada, 2004, Hybrid Tabu Search Approach for Hierarchical Logistics Optimization, Transactions of the Institute of Systems, Control and Information Engineers, 17, 6, 241-248

Y. Shimizu and M. Ikeda, 2010, A Parallel Hybrid Binary PSO for Capacitated Logistics Network Optimization, Journal of Advanced Mechanical Design, Systems, and Manufacturing, 4, 3, 616-626

Y. Shimizu, 2011, A Meta-heuristic approach for variants of VRP in terms of generalized saving method, Transactions of the Institute of Systems, Control and Information Engineers, 24, 12, 287-295

M. M. Solomon, 1987, Algorithms for the Vehicle Routing and Scheduling Problems with Time Window Constraints, Operations Research, 35, 254-265

L. C. Yeun, W. R. Ismail, K. Omar, and M. Zirour, 2008, Vehicle Routing Problem: Models and Solutions, Journal of Quality Measurement and Analysis, 4, 1, 205-218

I.A. Karimi and Rajagopalan Srinivasan (Editors), Proceedings of the 11th International Symposium on Process Systems Engineering, 15-19 July 2012, Singapore.

Application of bee colony algorithm for optimization of CCR reforming process

Majid Sa'idi, Navid Mostoufi , Rahmat Sotudeh-Gharebagh

Oil and Gas Processing Centre of Excellence, School of Chemical Engineering, College of Engineering, University of Tehran, PO Box 11155-4563, Tehran, Iran

Abstract

Swarm intelligence is a member of exploration calculations which is used in different industrial, commercial and engineering fields due to its wide range of applications, easy implementation and capability of reaching the absolute optimum. The bee colony optimization (BCO) algorithm is one of the most recent and efficient swarm intelligence based algorithms which simulates the foraging behavior of honey bee colonies. In this work, BCO algorithm is introduced and used for optimizing continuous catalytic regeneration (CCR) reforming process. The CCR optimization leads to non linear programming that contains non-linear quality constrains such as octane number and coke concentration on catalyst particles. The non-linear optimization problem with process constraints was used to improve the process performance and maximize unit profitability. The BCO algorithm performance was compared with genetic algorithm (GA) for optimizing the CCR process. Modeling and optimization results of the model were validated by industrial data.

Keywords: Bee Colony Optimization algorithm, Genetic algorithm, Kinetic model.

1. Introduction

Continuous catalytic regeneration (CCR) is one of the main refinery and petrochemical process for converting low-octane hydrocarbons to high-octane. According to modes of catalyst regeneration, reforming processes are generally classified into three types: semi-regenerative, cyclic and continuous regenerative process. Nowadays due to high catalyst activity, higher aromatic content and high hydrogen purity, applying of CCR units are very common respect to other type of reforming process.

In this work, Bee Colony Optimization (BCO) algorithm was used for optimizing operating conditions of the reactors of the CCR process. Artificial bees represent agents, which collaboratively solve complex combinatorial optimization problem. The artificial bee colony behaves to some extent similar and to some extent in a different way from bee colonies in nature. They explore through the search space looking for the feasible solutions. In order to discover superior solutions, artificial bees cooperate with each other and exchange information. Therefore, the BCO algorithm can be used as an effective optimization algorithm applying to multi objective engineering problems.

2. Bee Colony Optimization Algorithm

BCO is a bottom-up approach to modeling where special kinds of artificial agents are created by analogy with bees. High speed convergence, independent of the initial solutions, low number of algorithm parameters and accurate solution with lower evaluation of the objective function is characteristics of this algorithm. Colony of artificial bees collaboratively searches for the optimal solution of a given problem. Each

artificial bee generates a solution to the problem. In strategy of finding solution, there are two alternating phases, forward pass and backward pass, constituting single step in the BCO algorithm. Forward pass expresses the process of a forager bee leaving the beehive and flying towards a food source while backward pass denotes the process of a forager bee returning to the beehive and sharing the food source information with other forager bees (role change). In the algorithm, the length of each forward move is determined by NC which represents the number of solution components which is visited by each bee in each forward pass. In a forward movement, the forager bee may evaluate the profitability of every partial route during a foraging trip and in the backward pass upon a return to a hive from a food source, the forager bee must release the food (scheduling solution) and share the food source information with other forager bees. When the bees obtained new partial solutions, they start the backward pass and meet their nest mate in the hive. After evaluating all solutions and according to the quality of solutions, each bee decides whether to abandon its food source and search for another promising flower patch which was selected by her nest mate, continue to forage at the new food source or perform the waggle dance to recruit nest mates. According to above rule, in BCO algorithm, there are two types of bees, scout bee and follower bee. If the profitability of the solution found by the forager bee in the forward move is greater than the expectations of the bee colony, its role would be as a scout in this round and advertises its solution. If the profitability of the solution found by the forager bee in the last forward move is smaller than the expectations of the bee colony, its role would become a follower (Teodorovi, 2009; Davidovic et al. 2011).

For producing initial food source sites according to range of the boundaries of the parameters, the following random function was used:

$$x_{i,j} = x_j^{lowerbound} + rand(0,1)\left(x_j^{upperbound} - x_j^{lowerbound}\right) \tag{1}$$

where i =1... B and j =1... D. B and D are the number of bees and number of optimization parameters respectively. Roulette wheel method was used for producing the initial solutions of bees. As mentioned above, NC determines the number of constructive moves during a forward pass.

$$\text{Number of Forward Passes} = {}^{D}\!/_{NC} \tag{2}$$

Each bee is associated with only one food source site and produces a modification on the solution in its memory depending on its neighboring food source and local information according to:

$$x_{ij}^{'} = x_{ij} + \alpha_{ij}\left(x_{ij} - x_{kj}\right) \tag{3}$$

where k =1... D. In the above function, x_{ij} is a component of solution, x_{kj} is a neighbor of a component and x'_{ij} is a modified value for x_{ij}. If the modified value produced by this operation exceeds its boundaries, the component can be set to an acceptable value, the boundary itself in this work. After producing x'_{ij} within the boundaries, fitness value for a minimization problem can be assigned to the solution x'_{ij} by using equation (4). A greedy selection is applied between x_{ij} and x'_{ij}, then the better one is selected depending on fitness values of the complete solution.

$$fitness\ i = \begin{cases} \dfrac{1}{1+(object\ \ value)_i} & if\ \ (object\ \ value) \geq 0 \\ 1+abs\left[(object\ \ value)_i\right] & if\ \ (object\ \ value) < 0 \end{cases} \tag{4}$$

After completing all solution, the solutions with low fitness values must be identified by using equation (5) and final improvement will be done by Eq. (3) again.

$$p_i = \frac{fitness_{\max} - fitness_i}{fitness_{\max} - fitness_{\min}} \tag{5}$$

3. CCR process modeling

The most common feed to the catalytic reforming unit is the straight-run naphtha, distilled to obtain a narrower cut to be reformed. The most important reactions in the catalytic reforming are dehydrogenation, dehydrocyclization, isomerizatiom, hydrocracking, hydrodealkilation and catalyst deactivation. The hydrocarbon stream flows in the redial direction and the catalyst moves along the axial direction of the reactor. Consequently, conversion of hydrocarbons occurs in the radial direction while the catalyst becomes deactivated while moves down the reactor. Therefore, mass and heat balance equations for each reactor was written for a limited length of the reactor, L, in which the reaction rates ($r_{i,n}$) were assumed to be constant in axial direction (Ancheyta and Villafuerte, 2000).

$$\frac{dF_i}{dR} = (2\pi R\rho_b)\sum_{n=6}^{n=9}\sum_{j=1}^{12}\left(r_{j,n}\nu_{i,j}\right)L, \qquad i = 1\ to\ 26 \tag{6}$$

$$\frac{dT}{dR} = (2\pi R\rho_b)\frac{\sum_{n=6}^{n=9}\sum_{j=1}^{12}\left(-\Delta H_{j,n}r_{j,n}\right)}{\sum_{i=1}^{26}\left(F_i C_{p_i}\right)}L \tag{7}$$

R, ρ_b and $v_{i,j}$ are reactor radius, catalyst bed density and stoichiometic coefficient respectively. The effect of catalyst deactivation is simulated by defining catalyst deactivation factor (η_j).

$$r_j = \eta_j . r_j^0, \qquad 0 \leq \eta_j \leq 1 \tag{8}$$

$$\eta_j = \exp\left(-\alpha_j C_c\right) \tag{9}$$

$$r_c^0 = \frac{dC_c}{d\tau} = \left(k_p P_p + k_A P_A\right) p_{H_2}^{n_1} C_c^{n_2} e^{-k_c C_c} \tag{10}$$

In the above equations Cc is coking content on catalyst particles, n1 and n2 are constants and P_P, P_A and P_{H2} are paraffin, aromatic and hydrogen vapor pressures (Raeev, 2003; Froment, 2001). For parameter estimation the following objective function was minimized by the genetic algorithm and model validation is carried out by another set of industrial data.

$$\text{Objective function} = \sum_{k=1}^{26}\left[\frac{\left(x_{k,model} - x_{k,Ind}\right)}{x_{k,Ind}}\right]^2 + \sum_{m=1}^{4}\left[\frac{\left(T_{m,model} - T_{m,Ind}\right)}{T_{m,Ind}}\right]^2 \tag{11}$$

4. CCR process optimization

For process optimization, there are different viewpoints leading to different objective functions. In this work, the objective function is minimizing energy consumption per unit reformate production and inlet temperature of the reactors were decision variables. The objective function and mole flow rate of fuel consumption were defined as below:

$$F = \min\left[F_{fuel} \Big/ F_{reformate} \right] \tag{14}$$

$$F_{fuel} = \frac{q}{(Eff \times NHV)} \tag{15}$$

Furnace efficiency was considered to be 85% and the net heat value of fuel (NHV) was 40480 (kJ/kmol) in this case. Characterization and parameters of the BCO and the Genetic Algorithm (GA) considered in this work are given in Table 1.

Table1. BCO and GA characterizations

Algorithm	BCO	GA	
Algorithm Parameter Characteristic	B=100	Population=100	Random Selection
	D=4	Single Point Crossover = 0.8	Mutation and Elite units
	NC=4	Stochastic Uniform	Forward Migration
	Number of Evaluation<80000		

5. Results and discussion

Three sets of industrial data were used for determining kinetic model parameters and model validations. The modeling results are compared with an industrial CCR plant data in Table 2 in terms of outlet temperature of reactors. This table indicates that the modeling results are in appropriate agreement with the industrial plant data.

Table2. CCR process modeling results

	Model outlet Temp. (K)	Industrial outlet Temp. (K)	Error
Reactor 1	665.62	661.35	0.65%
Reactor 2	712.14	712.95	0.11%
Reactor 3	739.37	731.45	1.08%
Reactor 4	744.29	744.15	0.02%

Product mole Percent	Model's data	Industrial's data
Paraffins	12.16	11.89
Naphtenes	1.03	0.58
Aromatics	12.30	11.39
Light Components	9.99	9.32
Hydrogen	64.51	66.82

The BCO algorithm optimization results were compared with the values obtained by the GA. According to table 3, the optimum inlet temperature of reactor 1 is higher than the existing industrial value. In contrast, inlet temperature of the fourth reactor should be lower than the existing industrial value. Since the reaction in the first reactor is endothermic, higher reactor inlet temperature increases the rate of reactions. On the contrary, in the fourth reactor, due to occurrence of the exothermic reaction, lower reactor inlet temperature is required.

Table3. Energy function optimization results

	Plant Data	BCO	GA
Reactor1 inlet temperature (K)	776.55	784.3	784.42
Reactor2 inlet temperature (K)	774.25	769.87	788.16
Reactor3 inlet temperature (K)	781.25	764.87	772.31
Reactor4 inlet temperature (K)	781.15	773.67	771.34
RON	98.3	99.01	98.82
Reformate (kmol/hr)	943.97	965.41	949.92
Fuel consumption (kmol/hr)	1285	1159.8	1196.9
Fuel consumption/ Reformate(kmol/ kmol)	1.36	1.20	1.26

As indicated in Table 3, by using BCO and GA, the ratio of fuel consumption to reformate production decreases from 1.36 to 1.20 and 1.26, respectively, while the reformate production rate is increased. Figure 1 represents the performance of BCO and GA in energy optimization. The optimum value of the objective function in the BCO algorithm is reached faster and to a better value with respect to the GA.

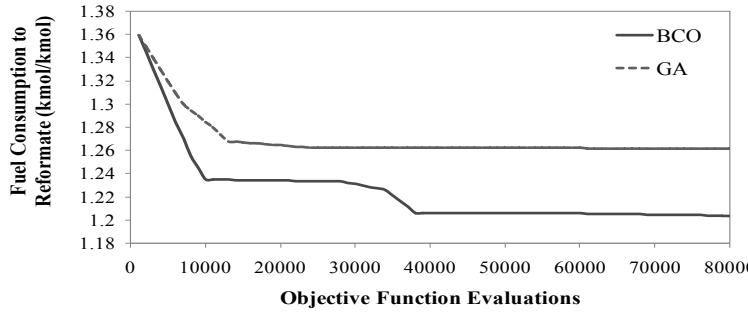

Figure1. CCR process optimization

6. Conclusion

The BCO algorithm was introduced as a new and powerful optimization algorithm for optimizing the chemical processes. The process considered in this work was CCR reforming process and its model is consisted a set of mathematical relations which simulates the kinetics of reforming process based on 48 reactions network and 26 pseudo components and implemented by catalyst deactivation derived from literature. In the process optimization, the fuel consumption in the furnaces per flow of reformate was minimized. Optimization was performed with both BCO and GA. It was shown that the BCO algorithm leads to a significant improvement of the optimum value with respect to the GA and it was found to be considerably faster than the GA. Finally the BCO algorithm can be used for optimizing the other chemical engineering problems.

References

D. Teodorovi, 2009, Bee colony optimization (BCO), Innovations in Swarm Intelligence, 39-60.

G. Froment, 2001, Modeling of catalyst deactivation, APPL CATAL A-GEN. 212, 117-128.

J. Ancheyta, E. Villafuerte, 2000, Kinetic modeling of naphtha catalytic reforming reactions, Energy Fuels. 14, 1032-1037.

S. Raeev, 2003,Thermal and catalytic processes in petroleum refining, marcel Dekker, New York.

T. Davidovic, D. Ramljak, M. Selmic, D. Teodorovic, 2011, Bee colony optimization for the p-center problem, COMPUT OPER RES, 38, 1367-1376.

I.A. Karimi and Rajagopalan Srinivasan (Editors), Proceedings of the 11th International Symposium on Process Systems Engineering, 15-19 July 2012, Singapore.

A scatter search algorithm for the twin roll caster scheduling problem in aluminum industry

Qingxin Guo, Lixin Tang[a,b]

[a]*The Logistics Institute, Northeastern University, Shenyang, 110819, China*
[b]*Liaoning Key Laboratory of Manufacturing System and Logistics, Northeastern University, Shenyang, 110819, China*

Abstract

This paper investigates the scheduling problem in the aluminum twin roll casting process. The ultimate goal is to determine the sequence of aluminum coils considering the sequence-dependent setup cost caused by alloy, width, thickness of the adjacent coils and the orders' specifications. A mixed integer linear programming model considers both the makespan and total tardiness is proposed to describe the problem. Since this problem and the mathematical model are very complex, a scatter search based heuristic is designed to solve the problem. Computational experiments show that the proposed method could get better solutions than the CPLEX software package.

Keywords: twin roll caster scheduling, sequence-dependent setup, makespan and total tardiness, scatter search

1. Introduction

The twin roll caster is a common unit of aluminum production process. In twin roll caster, molten aluminum alloy is fed onto water-cooled rolls, where it solidifies and is then rolled into aluminum coils with various widths and thicknesses. These coils are then rolled to the desired dimensions and properties through cold milling, annealing, surface processing and cutting operations according the customers' orders.

Strip casting using the twin roll caster has many advantages. First of all, the twin roll caster is a very simple process with low equipment cost and low space requirements. Also, the energy consumption of twin roll caster is only 40% of conventional casting method. However, the twin roll caster is not suitable for some aluminum alloys with wide freezing range. Another drawback of the technique is its low productivity due to the low casting speed of the roll caster. So managers are most concerned about how to better preparation of the alloy composition and improve the productivity.

The twin roll caster scheduling problem can be described as follows. There are N orders to be produced by a twin roll caster. The orders have different alloy compositions, due dates, widths, thickness and weights. The task is to decide the scheduling of the orders and the objective is to minimize both the makespan and total tardiness. Because the processing time of an order is only depended on its weight, so the makespan is mainly related with the setup times between two consecutive orders.

The setup time for twin roll caster includes the furnace cleaning and shutdown to adjust the export flow of the shaper. The furnace cleaning may be required while there is an alloy change between two consecutive orders. Specifically, the cleaning is not required to process an order with more composite alloy after an order with pure alloy. But the furnace must be cleaned thoroughly if an order with pure alloy is to be cast after an order with composite alloy. A significant shutdown must be required to adjust the export flow of the shaper if the width or thickness change occurs between two

consecutive orders. In general, it is expected that the cleaning and shutdown occur infrequently since they are both costly and time consuming.

There has been less research on scheduling related to aluminum production process. Bowers et al (1995) proposed a two-phase model for scheduling the aluminum ingot casting process to reduce ingot misapplication/import and maintains low inventory levels. Gravel et al (2002) proposed an ant colony optimization algorithm for the scheduling problem in an aluminum casting center. Prasad et al (2006) present a mixed-integer linear programming model for the optimization of aluminum smelter casthouse operations. Ladurantaye et al (2007) studied the integrated homogenizing furnaces and the mill scheduling problem in aluminum hot rolling mill. Duman et al (2008) presented a mathematical formulation for scheduling casting lines jobs to minimize setup time on production lines for a given time period while balancing workload between production lines to accommodate potential new orders.

The single machine scheduling problem has been extensively studied, but the setup times in our problem are more sophisticated and we consider both makespan and total tardiness in the objective function. The motivation of this paper is to study single machine scheduling problem deeply, the more important is to solve actual aluminum twin roll caster scheduling problem that did not find research works. The remainder of the paper is organized as follows: Section 2 describes the mix-integer linear programming model is formulated. A scatter search algorithm is proposed in Section 3. Section 4 reports the experimental results of the scatter search algorithm compared with the CPLEX solver. Finally, conclusions are stated in Section 5.

2. Mathematical model

We formulate the scheduling problem for the twin roll caster as a mixed-integer linear programming model as follows:

Parameters are described as follows, the set of orders is N (N=$\{0,1,\ldots,n\}$), for each order i or j ($i, j \in N$), the release time of order i is r_i, the alloy composition of the molten aluminum in order i is p_i, the width of order i is w_i, the thickness of order i is g_i, the due date of order i is d_i, the weight of order i is c_i, the processing time of unit weight order is t, the time of hot cleaning is t_w, the adjustment time for the width change is t_c ($t_c < t_w$).

Auxiliary variable

$$P_{ij} = \begin{cases} 1, & \text{if } p_i \neq p_j \\ 0, & \text{otherwise} \end{cases} \qquad W_{ij} = \begin{cases} 2, & (w_i \neq w_j) \wedge (g_i \neq g_j) \\ 1, & (w_i \neq w_j) \vee (g_i \neq g_j) \\ 0, & (w_i = w_j) \wedge (g_i = g_j) \end{cases}$$

Decision variables

$$x_{ij} = \begin{cases} 1, & \text{if order } j \text{ is produced directly after order } i \\ 0, & \text{otherwise} \end{cases}$$

s_i The start time of order i.
e_i The completion time of order i.
$C_{\max}$ makespan.
T_i The tardiness time of order i.

Let λ_1, $\lambda_2 \in [0,1]$ be two preset constants such that $\lambda_1+\lambda_2=1$. Using the above symbols, the model is constructed as follows:

$$\text{Min} \quad \lambda_1 C_{\max} + \lambda_2 \sum_i T_i \tag{1}$$

s.t. $\sum_{i=0}^{n} x_{ij} = 1 \qquad j = 0,\ldots,n$ (2)

$\sum_{j=0}^{n} x_{ij} = 1 \qquad i = 0,\ldots,n$ (3)

$e_i = s_i + c_i t_i \qquad i = 0,\ldots,n$ (4)

$T_i \geq e_i - d_i \qquad i = 0,\ldots,n$ (5)

$s_j = \max\{r_j, e_i\} + \sum_{i=1}^{n} \max\{P_{ij} t_w, W_{ij} t_c\} \cdot x_{ij} \qquad i = 0,\ldots,n \qquad j = 0,\ldots,n$ (6)

$C_{\max} \geq e_i \qquad i = 0,\ldots,n$ (7)

$x_{ij} \in \{0,1\} \qquad i = 0,\ldots,n \qquad j = 0,\ldots,n$ (8)

$s_i \geq r_i, e_i \geq 0 \qquad i = 0,\ldots,n$ (9)

In this model, objective function (1) consists of two components, the first one is the makespan and the second one is the total tardiness. Constraints (2) ensure that exactly one order is produced before order *j*. Constraints (3) guarantee that exactly one order is produced after order *i*. Constraints (4) mean that the completion time of each batch is equal to its start time plus its processing time. Constraints (5) represent the tardiness of order *i*. Constraints (6) guarantee that two orders can not be produced at the same time; the order *j* can be produced only after its release time is reached and its previous order *i* is completed, the starting time of order *j* equals to the maximum time between its release time and the completion time of order *i* plus the possible wash furnace (width-modulated) time. Constraint (7) detects the maximum completion time. Constraint (8) and (9) impose the binary and nonnegative restrictions on the decision variables.

3. The proposed scatter search algorithm

Scatter search (SS) is an evolutionary method in which solutions are intelligently combined to yield better solutions. Our proposed SS is described in the following discussion.

3.1. Diversification generation method

To guarantee a diversified population of solutions, we use three types of heuristic strategies to construct a subset P of p initial solutions. The first heuristic randomly selects orders from the orders set until it is empty. The orders are sorted as the selection sequence. The second one randomly selects an order for the first position, and then the order with the smallest difference for the second position is chosen from the remaining order set. This process is repeated until the set is empty. And the third one is based on the earliest due-date (EDD) rule which generates one trial solution.

3.2. Improvement method

In scatter search, an improvement method is introduced to transform a trial solution into one or more enhanced trial solutions. In this paper, we use a local search that is a combination of the insert and swap neighborhood. The insert move means removing an order from current position and inserting it into another position. The swap move of two orders means swapping two orders between two positions.

3.3. Reference set update method

The scatter search algorithm builds a reference set (*Refset* for short) of solutions that containing high evaluation to generate new solutions to replace less promising solutions

in the implementation process. A straightforward way to create a reference set *Refset* consists of selecting the two subsets, the first set with high quality solutions and the second set with diverse solutions by selecting the solution that differs by the greatest amount from the current reference set.

As a diversity measure we define $div(s_1, s_2)$ to be the diversification value between two solutions s_1 and s_2 and calculate the value of $div(s_1, s_2)$ as the number of edges in scheduling sequence by which the two solutions differ from each other. Based on the above diversity measure formula, the candidate solutions are included in $Refset_2$ according to the *Maxmin* criterion that maximizes the minimum distance of each candidate solution to all the solutions currently in the reference set.

3.4. Subset generation method

The subset generation method is to operate on the reference set, to produce a subset of its solutions as a basis for creating combined solutions. The most common subset generation consists of creating a list of all pairs (i.e., all 2-element subsets) of reference solutions for which at least one of the solutions is new. A reference solution is new means that it hasn't been used by the combination method. In our work, all possible 2-element subsets are adopted.

3.5. Solution Combination Method

The solution combination method generates one or more new trial solutions for every subset generated in the previous step. In this paper, we adopt directly the first and the third combination methods from the Campos' (2005) ten and also a crossover operator similar to the first method. These methods generate one new trial solution from the combination of two reference solutions.

3.6. The Stopping Criteria

While the iteration of the best solution can not be improved reaches the given maximum consecutive iterations or the computing time reaches the given maximum time, the whole scatter search terminates.

4. Computational experiments

To test the performance of the model and algorithm described in Sections 2 and 3, computational experiments have been conducted on randomly generated problem instances. For the test instances, the parameters are given as follows: the number of orders is chosen from {5, 6, 7, 8, 9, 10, 11, 12, 13, 14, 15, 16, 17, 18, 19}, p_i is randomly generated from uniform distributions of which range was set to be [99.53%, 99.99%]. The range of w_i, g_i and c_i are set to be [900mm, 1100mm], [6mm, 10mm] and [1.25t, 1.55t] by the uniform distributions, respectively. The range of r_i and d_i are set according to the number of orders and the total processing time of these orders. The parameters t, t_w and t_c are taken as 0.2h, 2h and 1h, respectively.

The testing results of scatter search algorithm and CPLEX software are given in Table 1. The first column is the number index of problem instance; the second column is the number of orders; the third column is the objective function value of CPLEX; the fourth column is the objective function value of scatter search; the fifth column is the computation time of CPLEX and the sixth column is the computation time of scatter search. Note that the values of the table are the ratios between the scatter search and CPLEX (taking the values of CPLEX as the divisor).

From table 1, it can be seen that both scatter search and CPLEX can obtain optimal solutions with short computation time for small size instances. As the problem size increases, the computation time of CPLEX increases rapidly and the results of CPLEX

are deteriorated. The scatter search can also obtain satisfactory solutions for large size instances with reasonable computation time.

Table 1 Comparison results between scatter search and CPLEX

Instance	n	Computation results		Computation time (s)	
		CPLEX	Scatter search	CPLEX	Scatter search
1	5	1.0000	1.0000	0.500	1.719
2	6	1.0000	1.0000	1.000	1.547
3	7	1.0000	1.0000	1.760	1.672
4	8	1.0000	1.0000	15.320	1.875
5	9	1.0000	1.0000	34.110	2.062
6	10	1.0000	1.0000	31.890	2.421
7	11	1.0000	0.9968	23.560	2.593
8	12	1.0000	0.9437	25.860	2.781
9	13	1.0000	0.9122	48.360	2.984
10	14	1.0000	0.7620	48.120	3.187
11	15	1.0000	0.7930	54.040	3.562
12	16	1.0000	0.7329	1000	3.797
13	17	1.0000	0.6470	1000	4.125
14	18	1.0000	0.6961	1000	4.407
15	19	1.0000	0.6565	1000	4.687

5. Conclusions

In this paper, we proposed a mixed integer linear programming model for the scheduling problem in the aluminum twin roll casting process. The model considers the actual production constraints as well as both the makespan and total tardiness as the objective function. A scatter search based heuristic is implemented to solve the problem. Computational experiments show that the proposed method outperforms the CPLEX software package.

Acknowledgements

This research is partly supported by State Key Program of National Natural Science Foundation of China (71032004), the Fundamental Research Funds for the Central Universities (N090104002, N100704002)

References

M.R. Bowers, L.A. Kaplan and T.L.Hooker, 1995, A two-phase model for planning the production of aluminum ingot, European Journal of Operational Research, 81(1): 105-114.

M. Gravel, W.L. Price and C. Gaqné, 2002, Scheduling continuous casting of aluminum using a multiple objective ant colony optimization metaheuristic, European Journal of Operational Research, 143(1): 218-229.

P. Prasad, C.T. Maravelias and J. Kelly, 2006, Optimization of aluminum smelter casthouse operations, Industrial & Engineering Chemistry Research, 45: 7603-7617.

D.Ladurantaye, M. Gendreau and J.Y. Potvin, 2007, Scheduling a hot rolling mill, Journal of the Operational Research Society, 58: 288-300.

Duman, E., Yildirim, M.B. and Alkaya, A.F., 2008, Scheduling continuous aluminium casting lines. International Journal of Production Research, 46(20): 5701-5718.

V. Campos, M. Laguna and R. Martı′, 2005, Context-independent scatter and tabu search for permutation problems, INFORMS Journal on Computing, 17(1): 111-122.

I.A. Karimi and Rajagopalan Srinivasan (Editors), Proceedings of the 11th International Symposium on Process Systems Engineering, 15-19 July 2012, Singapore.

Hydrogen Network Integration with both Pressure and Impurity Constraints

Qiao Zhang,[a] Xiao Feng[b*]

[a]*Department of Chemical Engineering, Xi'an Jiaotong University, Xi'an 710049, China*
[b]*College of Chemical Engineering, China University of Petroleum, Beijing 102249, China*

Abstract

For refineries, the minimization of fresh hydrogen consumption is significant to minimize operation cost and maximize profit. To get such effect, in addition to the flow rate and purity of hydrogen sources and sinks, the main constraints are pressure and impurities based on the operation requirements. Based on the existing hydrogen network, by introducing pressure cascade use and impurity diverted path corresponding to pressure and impurity constraints, this paper presents an experiential method for hydrogen network optimization. As complement to integration methodology, the reduction of fresh hydrogen is reliable and attainable. Finally, a refinery case study is used to illustrate the method.

Keywords: hydrogen network, optimization, pressure cascade use, impurity diverted path

1. Introduction

Hydrogen is an expensive utility to oil refineries. In recent years, increasing strictly environmental regulations and the change of crude oil to high-sulfur and/or heavier oil both require increasing processing depth of hydrogen-consuming crafts, resulting in huge deficiency of fresh hydrogen. Thus, effective use and conservation of fresh hydrogen is significant to the profit of petrochemical industries.

For the minimization of fresh hydrogen, process integration is an effective way in refinery hydrogen network optimization. Pinch-based conceptual methods and mathematical programming have been widely used to analyze and optimize the whole network performance. Pinch-based methods have clear concepts and insights to the optimization. Alves and Towler(2002) put forward hydrogen surplus diagram to identify the pinch and minimum fresh hydrogen demand. Successively, material recovery pinch diagram(El-Halwagi et al., 2003; Zhao et al., 2006), and other visual solutions(Agrawal and Shenoy, 2006; Bandyopadhyay, 2006; Foo et al., 2006; Zhang et al., 2011) are also developed to address the fresh hydrogen target and/or network design. Compared to pinch-based methods, mathematical programming is able to deal with complex hydrogen systems and various constraints. Hallale and Liu(2001) put forward a fundamental superstructure with flow rate, hydrogen purity, pressure and purifiers, as well as economic consideration. After this work, Van den Heever and Grossmann(2003), Liu and Zhang(2004), Khajehpour et al.(2009), and Liao et al.(2011a,b) set up respective superstructures and mathematical models, in which important factors, such as purifiers selection, reactive scheduling, production planning, utility system, costs etc., are taken into consideration.

* Corresponding author. Tel.:+86 10 89703991. E-mail address: xfeng@cup.edu.cn.

For hydrogen network retrofit, experiential observation may be very important to give effective guideline in a simple way. In this paper, an experiential method based on observation of pressure cascade use and impurity diverted path is proposed, so as to discover possible direct reuse of hydrogen sources, for pressure and impurity are two main factors influencing on the hydrogen network optimization. Its solution is reliable and easily to be determined.

2. The Method with Pressure Cascade Use and Impurity Diverted Path

2.1. Background

Figure 1 is a typical hydrogen network. In this flow sheet, the X coordinate is the increasing impurity purity direction, and the Y coordinate is the lifting pressure direction. Hence, streams locate at left top position are the highest quality streams both in hydrogen purity and pressure. Conversely, streams locate at the right bottom is the lowest quality streams. Firstly, the fresh hydrogen is with low pressure and high hydrogen purity, so it locates at the left bottom. When pressure is lifted to the required high levels by compressors 1, 2 and 3, it rises to respective high positions (sources 1, 2 and 3). Such high pressure gradually drops as the fresh hydrogen go through the reactors (sinks 1, 2 and 3), separators (1, 2 and 3), purification unit etc. Meanwhile, streams with high hydrogen purity are devalued to low hydrogen purity, accompanied by the stepwise accumulation of impurities, as internal sources (1 and 2) and tail gas generated. In order to reuse the considerable internal sources, a purification unit is introduced to concentrate hydrogen and remove harmful impurities. The purified product is near to fresh hydrogen in quality and returned to the left bottom. For sinks 1, 2 or 3, the thick solid lines with arrows compose such a cycle.

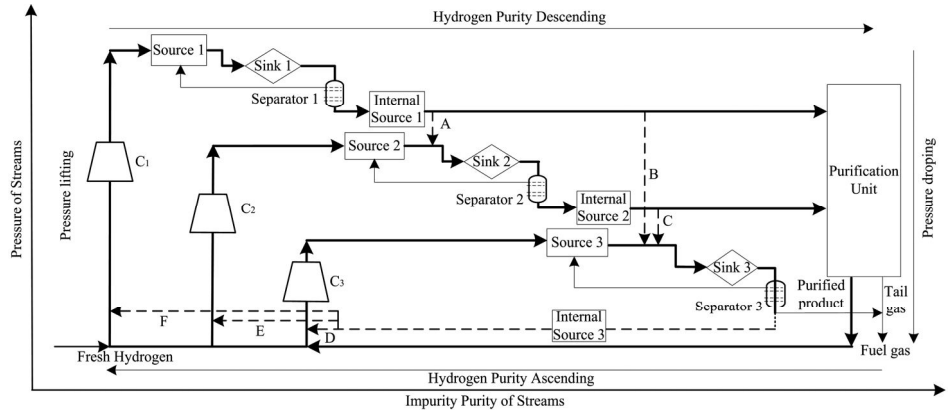

Figure 1. A typical flow sheet of refinery hydrogen network

2.2. Pressure cascade use and impurity diverted path

2.2.1. Pressure cascade use

From Figure 1, internal sources 1 and 2 have high pressure, but they are sent to purification unit. Because the pressure of the purified product is dropped in purification process, it should be lifted again. Such depressurization and repressurization processes result in waste of compressing work. From this point, the sources with high pressure should be directly reused at maximum extent.

Pressure cascade use means that each high pressure internal source is possible to supply hydrogen for all sinks with lower pressures. For an existing hydrogen network, it is probably that some such cascade uses are not included, and should be discovered.

For example, internal source 1 has higher pressure than sinks 2 and 3, and internal source 2 has higher pressure than sink 3. Thus, the three dotted arrows A, B and C are all possible pressure cascade uses which are not included in the hydrogen network. After such complement, the possible pressure cascade uses are complete, and feasible ones can be determined according to practice consideration.

2.2.2. Impurity diverted path

Purification causes not only pressure drop, but also hydrogen loss in terms of tail gas, which is discharged to the fuel gas system. Hence, unnecessary purification should be avoided.

Reasonable mix can increase direct reuse. Impurity diverted path is a way to mix internal sources with each other or fresh hydrogen, which has low purity in any impurity. In this way, internal sources with high impurity purities can be diluted by other sources with low purities of corresponding impurities, so as to make the sources with high impurity purities feasible for direct reuse.

For example, if part of internal source 1 can be mixed with source 2 or source 3 to dilute some impurities, then such part of internal source 1 can be directly sent to sink 2 instead of sent to purification reuse. Similarly, the mixture of internal source 2 and source 3 sent to sink 3 could also be such case.

In addition, there are still some other internal sources, which cannot be directly sent to sinks after mix because of low pressure, such as internal source 3. As there is no other sinks with lower pressure than that of internal source 3, it can only be mixed with fresh hydrogen and then get direct reuse after pressurized by compressors.

Thus, A, B, C, D, E and F are all possible impurity diverted path and feasible ones can be determined according to practice consideration.

With both pressure cascade use and impurity diverted path, the possible direct reuse of hydrogen sources can be taken into consideration, and the fresh hydrogen consumption can be reduced.

3. Case study

This is a refinery case, and the current flow sheet and network is shown in Figure 2(a). The data are extracted and shown in Table 1. This hydrogen network contains eight sources and three sinks, three impurities, H_2S, N and C, six compressors. SR1 is the fresh hydrogen, and its current minimum flow rate is 15385 Nm^3/h.

For this case, all impurity purities of sources are given, and the limiting impurity purities of sinks are also listed. SR3 has high pressure with high purity of impurity C, and thus 3000 Nm^3/h is sent to purification unit. The purified product is suitable to SK3 in pressure and so allocated to it. Although the pressure of SR7 is high enough to direct reuse, the impurity purities restricts the reuse.

By observation, SR3 to SK2 and SR4 to SK3 are two feasible pressure cascade use. For impurity diverted path, the mixture of SR2 and SR3 to supply for sink 2, the mixture of SR3 and SR4 to supply for sink 3, and the mixture of SR6 and fresh hydrogen to supply for all three sinks, are all possible cases.

With the observed pressure cascade use and impurity diverted path, after calculation for flow rate, hydrogen purity and impurity purities requirements, the feed of 3000 Nm^3/h to purification unit and SR6 can both be directly reused completely, and the membrane separation can be eliminated.

After the retrofit, the high quality internal source of 3000 Nm^3/h, 7.0MPa is sent to sink 2 instead of sent to membrane separation, part of SR4 (3000 Nm^3/h, 4.5MPa) is sent to

sink 3, and SR6 is intercepted to three streams, which are separately mixed with fresh hydrogen and then directly reused after pressurization by compressors.
After the improvement of experiential guidelines, the minimum fresh hydrogen demand is reduced from 15385 Nm^3/h to 14500 Nm^3/h.

Table 1. The Current Data of a Refinery Case

Streams	Flow rate (Nm^3/h)	Purity (mol%)	H_2S (ppm)	N (ppm)	C (ppm)	Pressure (Mpa)
Sources (SR1 is the fresh hydrogen)						
SR1	15385	99.9	0	0	0	2.1
SR2	2615	95	2	0	10	2.5
SR3	27000	92.0	10	0	60	7.0
SR4	10000	90.0	30	0	30	4.5
SR5	6000	88.0	70	50	35	2.2
SR6	500	80.0	100	150	100	2.1
SR7	385	71.7	143	0	400	5.0
SR8	1000	60.0	1000	2000	3000	0.5
Sinks						
SK1	36000	≧93.0	≦15	/	/	17.5
SK2	15000	≧90.0	/	/	≦30	6.8
SK3	10000	≧88.0	/	≦50	/	3.8
(/ no requirement)						

The modified flow sheet is shown in Figure 2(b), in which the dotted line shows the difference to Figure 2(a). After modification, 885 Nm^3/h fresh hydrogen, taking up 5.75% of the current demand, can be reduced; only some pipelines and streams interception are needed; membrane separation, an expensive purifier, is eliminated; the inlet flow rate of compressors does not increase. From the retrofit of the network, it can obviously be seen that the improvements are very cost-efficient.

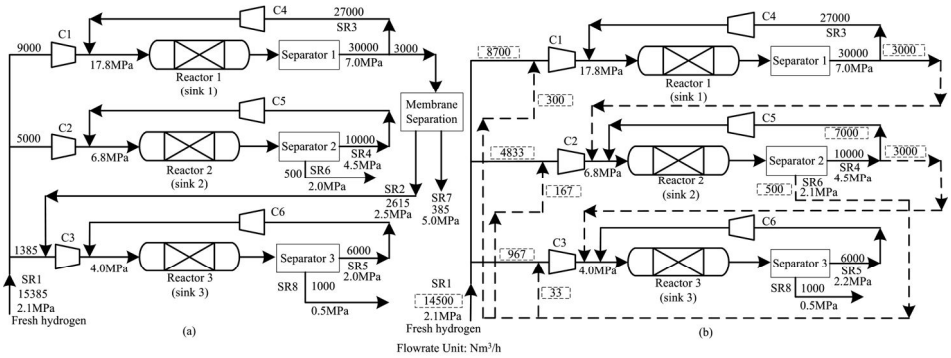

Figure 2. The optimization results. (a) The current network; (b) The modified network.

4. Conclusion

This paper presents an experiential approach to reduce the fresh hydrogen consumption of hydrogen networks with both pressure and impurity constraints. Based on a refinery hydrogen network, experiential rules of pressure cascade use and impurity diverted path are developed to give a simple way to deal with hydrogen network synthesis.

This method is for hydrogen network retrofit. The modification involves the placement of only additional pipelines and the elimination of expensive membrane separation. The reduction of fresh hydrogen is 5.75% of current demand, and thereby the retrofit is very cost-efficient. Although the method is experiential and based on a refinery case, it is more practical, and can probably be extended to a systematic methodology in future work.

Acknowledgement

The financial support for this research provided by the National Basic Research Program of China (973 Program: 2012CB720500) and the National Natural Science Foundation of China under Grant 20936004 is gratefully acknowledged.

References

Agrawal V., Shenoy U.V., 2006, Unified conceptual approach to targeting and design of water and hydrogen networks. *AIChE Journal*, 52 (3), 1071-1082.

Alves J.J., Towler G.P., 2002, Analysis of refinery hydrogen distribution systems, *Industrial & Engineering Chemistry Research*, 41 (23), 5759-5769.

Bandyopadhyay S. Source composite curve for waste reduction. *Chemical Engineering Journal.* 2006;125(2):99-110.

El-Halwagi M.M., Gabriel F., Harell D., 2003, Rigorous graphical targeting for resource conservation via material recycle/reuse networks, *Industrial & Engineering Chemistry Research*, 42 (19), 4319-4328.

Foo D.C.Y., Kazantzi V., El-Halwagi M.M., Manan Z.A., 2006, Surplus diagram and cascade analysis technique for targeting property-based material reuse network, *Chemical Engineering Science*, 61 (8), 2626-2642.

Hallale N., Liu F., 2001, Refinery hydrogen management for clean fuels production. *Advances in Environmental Research*, 6 (1), 81-98.

Khajehpour M., Farhadi F., Pishvaie M.R., 2009, Reduced superstructure solution of MINLP problem in refinery hydrogen management, *International Journal of Hydrogen Energy*, 34 (22), 9233-9238.

Liao Z.W., Rong G., Wang J.D., Yang Y.R., 2011, Rigorous algorithmic targeting methods for hydrogen networks—Part I: Systems with nohydrogen purification, *Chemical Engineering Science*, 66 (5), 813-820.

Liao Z.W., Rong G., Wang J.D., Yang Y.R., 2011, Rigorous algorithmic targeting methods for hydrogen networks—Part II: Systems with one hydrogen purification unit, *Chemical Engineering Science*, 66 (5), 821-833.

Liu F., Zhang N., 2004, Strategy of purifier selection and integration in hydrogen networks, *Chemical Engineering Research & Design*, 82 (A10), 1315-1330.

Van den Heever S., Grossmann I., 2003, A strategy for the integration of production planning and reactive scheduling in the optimization of a hydrogen supply network, *Computers & Chemical Engineering*, 27 (12), 1813-1839.

Zhang Q., Feng X., Liu G.L., Chu K.H., 2011, A novel graphical method for the integration of hydrogen distribution systems with purification reuse, *Chemical Engineering Science,* 66 (4), 797-809.

Zhao Z.H., Liu G.L., Feng X., 2006, New graphical method for the integration of hydrogen distribution systems, *Industrial & Engineering Chemistry Research*, 45 (19), 6512-6517.

I.A. Karimi and Rajagopalan Srinivasan (Editors), Proceedings of the 11th International Symposium on Process Systems Engineering, 15-19 July 2012, Singapore.

Modeling and Solving Batch Scheduling Problems with Various Storage Policies and Operational Policies using Timed Automata

Christian Schoppmeyer [a], Subanatarajan Subbiah [a], Sebastian Engell [a]

[a]*Process Dynamics and Operations Group, Department of Biochemical and Chemical Engineering, Technische Universität Dortmund, 44221 Dortmund, Germany*

Abstract

In this contribution we present the conceptual ideas on modeling deterministic batch scheduling problems with various storage policies and operational policies using timed automata (TA) and on solving them using reachability analysis for TA. We propose a new reduction technique to improve the efficiency of the search algorithm for scheduling problems with non-intermediate storage policy. The performance of the proposed modeling approach and the reduction technique is evaluated by investigating it on benchmark instances from OR literature and on typical batch scheduling problems. The comparative study shows that the proposed modeling approach handles the crucial aspects of the storage policies and operational policies in straightforward way and the new reduction technique increases the overall performance of the solution algorithm.

Keywords: Batch scheduling, storage policies, operational policies, timed automata.

1. Introduction

In multi-product batch processing plants, efficient scheduling of the scarce resources can have a substantial impact on the economic performance of the plant. The availability of storage units and their functional limitations in the plant can have a major impact on the feasibility of schedules and therefore they should be modeled precisely. The state-of-the-art approach to address this type of scheduling problems is to model them as MILP or MINLP and to solve them using solution techniques such as branch-and-bound or cutting-plane methods. The authors in Ferrer-Nadal et al. (2008) demonstrated that several MILP models which either simplify or neglect the storage policies or material transfer times compromise on the feasibility of the schedules and proposed a MILP formulation to address the problem of handling various storage policies. However the efficiency of the solution approach was not quantitatively illustrated.

An alternative approach to handle batch scheduling problems is to model them using timed automata (TA) and to apply the technique of reachability analysis for TA to compute schedules, see Subbiah et al. (2011a). Model building using TA is relatively straightforward due to the graphical nature of the formalism and the modular definition of the elements of the problem. In this contribution, the modeling of scheduling problems with various storage policies and operational policies as TA is discussed, and a new reduction technique is introduced to improve the efficiency of the search algorithm for problems with non-intermediate storage policy.

2. Timed Automata Based Modeling

Fig 1. shows a modular TA model for an example process where two products A and B have to be produced using processing units U_1 and U_2. The operational sequence and the

durations for product A are $(op_1,U_1,5)$ followed by $(op_2,U_2,7)$. Similarly, for product B they are $(op_3,U_2,6)$ followed by $(op_4,U_1,3)$. Details on the modeling procedure and on the solution algorithm using reachability analysis can be found in Subbiah et al. (2011a, 2011b).

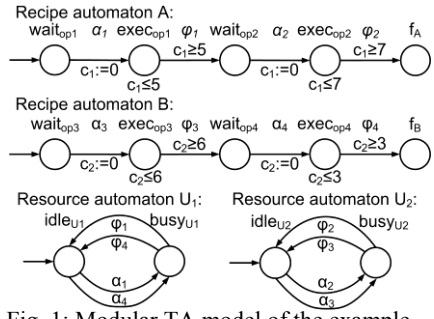

Fig. 1: Modular TA model of the example problem

3. Modeling Storage Policies

Based on the presence of storage units between the process stages the storage policy can be classified into two main categories namely "With intermediate storage (WIS)" and "Non-intermediate storage (NIS)". The WIS policy can be further classified into "Dedicated intermediate storage (DIS)" where the storage unit is allowed to store only one type of material and "Common intermediate storage (CIS)" where the storage unit is allowed to store more than one material. Both the DIS and the CIS are further classified based on their storage capacities.

3.1. Modeling the dedicated-intermediate storage policy

The idea of how to model the dedicate-intermediate storage (DIS) policy is explained by extending the example process by a dedicated storage unit $U_{str\text{-}A}$ to store the intermediate material Int_A of the product A. The modular TA model for the example problem is extended by creating a separate *storage automaton* for the storage unit. The TA for the storage unit $U_{str\text{-}A}$ is shown in Fig. 2. The storage automaton for unit $U_{str\text{-}A}$ consists of a location *empty* $U_{str\text{-}A}$ representing that the storage unit is empty and a location *filled* $U_{str\text{-}A}$ representing that the storage unit is filled with the material Int_A. Draining the material Int_A to the storage unit after finishing the operation op_1 in the upstream unit U_1 is represented by a transition from the location *empty* $U_{str\text{-}A}$ to *filled* $U_{str\text{-}A}$. Pumping the material Int_A from the storage unit to the downstream unit U_2 is represented by a transition from the location *filled* $U_{str\text{-}A}$ to *empty* $U_{str\text{-}A}$. These transitions are synchronized with the corresponding transitions of the recipe automaton. A shared variable S_A is introduced to model the amount of intermediate material Int_A present in the storage. Guards on the transitions of the storage automaton ensure that the amount of material drained to the storage unit $b_{in,A}$ does not exceed the maximum capacity $max(S_A)$ and that the storage automaton switches back to the location *empty* $U_{str\text{-}A}$ when the entire amount of material is pumped to the downstream unit. Additional transitions from the *filled* $U_{str\text{-}A}$ location to itself model the change in the amount of material present in the storage when more than one batch of a product is produced.

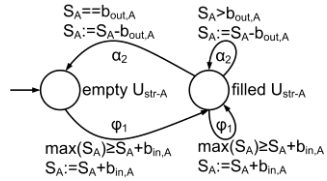

Fig. 2: TA model for the storage

3.2. Modeling the common-intermediate storage policy

The idea of how to model the common-intermediate storage (CIS) policy is explained by extending the example process by a common storage unit shared among both intermediate materials Int_A and Int_B. The modular TA model for the example problem is extended by creating a common *storage automaton*. The TA for the common storage unit is shown in Fig. 3. The storage automaton consists of one

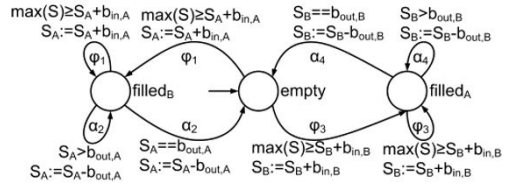

Fig. 3: TA model for the common intermediate storage

empty location representing that the storage unit is empty and one *filled*$_l$ location for each intermediate product $l \in \{Int_A, Int_B\}$ which can be stored in the storage unit representing that the storage unit is partly or completely filled with the corresponding intermediate material. For each intermediate product a shared variable is introduced. The guards and the actions on the corresponding synchronized transitions model the amount of material present in the storage.

3.3. Modeling the non-intermediate storage policy

The idea of how to model the non-intermediate storage policy (NIS) is explained by extending the example process such that no storage units exist in the plant. For each processing unit U_k a shared variable S_k is introduced to model the occupancy of the unit. Each shared variable is initialized with a value of 0 indicating that the unit is not occupied and with a value of 1 if it is holding any amount of processed material. Guards on the shared variables in the recipe automata ensure than an operation can start only if the corresponding unit is unoccupied. The state of the unit is updated by actions on the shared variables when the corresponding transition is taken. The extended TA models for the recipes *A* and *B* are shown in Fig. 4. In production environments with NIS policy a phenomenon called *blocking* may occur when an upstream unit has finished an operation and the downstream unit is busy or occupied then the upstream unit is not allowed to release the material till the downstream unit is free thus blocking the upstream unit.

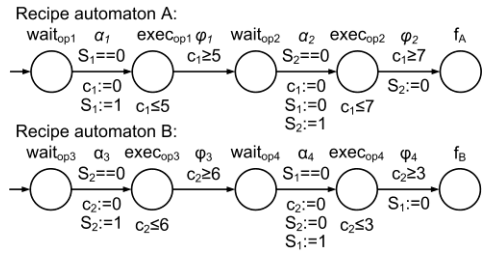

Fig. 4: TA models for the recipes *A* and *B* of the example problem with NIS policy

4. Blocking Reduction

The first part of the reachability tree of the example process with NIS policy is shown in Fig. 5. It can be seen from the figure that there exist four traces that lead to leaf nodes which are not target nodes but deadlocks. These leaf nodes represent partial schedules in which both recipes *A* and *B* have finished the first operation op_1 and op_3, respectively. In this state, neither of the recipes can start the second operation since the needed resource is occupied and thereby blocked by the other recipe. This is known as *mutual blocking*. The computational effort is wasted by exploring traces that lead to mutual blocking and demands for efficient reductions schemes to prune such traces in the search tree. The idea is to compare the sequence of the resources of a recipe order with the sequence of the resources in other recipe orders for which the latter is a swap of the former and to avoid starting an operation that would lead to mutual blocking. The blocking reduction schemes are explained below.

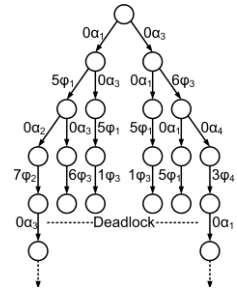

Fig. 5: Reachability tree

4.1. α-φ Reduction

In the reachability tree given a node q with outgoing timed transitions $\tau_1\varphi_i$ and $\tau_2\alpha_j$ where $\tau_1\varphi_i$ denotes finishing of operation i after τ_1 time units and $\tau_2\alpha_j$ denotes starting of operation j after τ_2 time units, the transition $\tau_2\alpha_j$ is removed and all successor nodes are pruned if all the following conditions are satisfied: (1) Operation i and j are not the last operations of their respective recipes, (2) the resource currently executing operation i is the same resource required by the operation $j+1$ where $j+1$ is the operation immediately

succeeding *j* with respect to the recipe it belongs to, and (3) the resource allocated to execute operation *j* is the same resource required by the operation *i+1* where *i+1* is the operation immediately succeeding *i* with respect to the recipe it belongs to.

4.2. α-α Reduction

In the reachability tree given a node *q* with outgoing timed transitions $\tau_1\alpha_i$ and $\tau_2\alpha_j$ where $\tau_1\alpha_i$ denotes starting of operation *i* after τ_1 time units and $\tau_2\alpha_j$ denotes starting of operation *j* after τ_2 time units, the transition $\tau_1\alpha_i$ is removed and all successor nodes are pruned if all the following conditions are satisfied: (1) Operation *i* is not the last operation to be performed to complete the recipe it belongs to and operation *j* is not the first operation to be performed to start the recipe it belongs to, (2) both operations *i* and *j* bid for the same resource, and (3) the resource in which operation *j-1* was executed is the same resource required by operation *i+1* where *j-1* is the operation immediately preceding *j* with respect to the recipe it belong to and *i+1* is the operation immediately succeeding *i* with respect to the recipe it belongs to.

5. Modeling Operational Policies

The different operational policies that are observed in chemical process industries can be classified into three main categories namely "Infinite waiting (IW)", "Finite waiting (FW)" and "Zero waiting (ZW)".

5.1. Modeling finite waiting

The idea of modeling the FW operational policy is explained by extending the example process such that the intermediate material Int_A of recipe *A* has a finite waiting period. The material Int_A has to be stored for at least A_{min} time units before it can be processed in unit U_2 and is allowed to be stored for at most A_{max} time units. The $wait_{op2}$ location of the recipe automaton *A* is extended by an invariant restricting the residence time of Int_A to $A_{max,}$ the outgoing transition α_2 is extended by a guard ensuring a minimum residence time of A_{min}, and the clock is reset on transition φ_1. The extended recipe automaton is shown in Fig. 6.

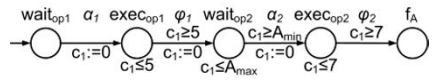

Fig. 6: TA model of recipe A with FW policy

5.2. Modeling zero waiting

The idea of modeling the zero waiting policy (ZW) is explained by extending the original example process with the ZW policy for the intermediate product Int_A of recipe *A*. The $wait_{op2}$ location of the recipe automaton *A* is marked as an *urgent* location forcing the automaton to leave the location immediately once it is active (i.e. the automaton is not allowed to stay more than 0 time units in the location). Due to the zone abstraction technique used in the reachability analysis, however, the optimal solution for problems with ZW policy may not be found, see Subbiah et al. (2011a).

6. Numerical Results

The blocking reduction schemes were implemented in the TA-based scheduling tool TAOpt developed at our group. The search algorithm chosen is a combination of a depth-first and a best-first search strategy. The reduction techniques safe non-laziness, safe sleep-set method and the MRPT scheme are used in the tests, see Subbiah et al. (2011a, 2011b). The computation equipment used is a Linux machine with 2x2.4 GHz speed and 16GB memory. In order to investigate the performance of the blocking reduction a series of problems with NIS policy were generated using the benchmark instance generator; see Demirkol et al. (1998). Table 1 shows the number of nodes explored and

the computation times required to prove the optimality of the best solution obtained in the reachability analysis for the different reduction techniques The results show that when the number of recipes increases, for the same number of units the search space increases substantially due to an increase in the possible degrees of freedom. Since the search space increases, the computation time also increases. The blocking reduction (BR) reduces the search space for all instances tested compared to the algorithm without the BR. The MRPT-based bounding scheme is efficient in comparison to the BR as the number of nodes explored is less. For all instances tested the MRPT-based bounding in combination with BR could explore the complete search space with minimal computation time. Three case studies proposed in Ferrer-Nadal et al. (2008) are considered for investigation. Table 2 shows the number of nodes explored and the computation times required to prove the optimality of the best solution obtained with different reduction techniques for the case studies. For the cases with ZW policy the optimal solutions could not be found due to the zone abstraction technique, however feasible solutions close to the optimal solutions were found.

Table 1: Comparison results on the generated job-shop instances.

EN – number of nodes explored to prove optimality; T_{CPU} – computation time in CPU seconds required to prove optimality; None – without blocking reduction and bounding scheme; BR – blocking reduction; MRPT – MRPT-based bounding scheme.

Res.	Recp.	None		BR		MRPT		MRPT+BR	
		EN	T_{CPU}	EN	T_{CPU}	EN	T_{CPU}	EN	T_{CPU}
6	4	16775	0.37	14877	0.32	2159	0.19	1867	0.16
	5	136649	3.32	120634	2.89	21296	1.17	17993	1.61
	6	1018063	26.40	917328	24.02	178504	18.13	154398	15.99
	7	5064805	150.47	4485761	135.33	479783	63.18	396756	52.02
7	4	50038	1.26	44621	1.12	4255	0.39	3710	0.36
	5	511087	13.15	466325	12.53	51922	5.72	448361	4.90
	6	3934306	118.32	3462821	103.92	432144	61.32	360107	49.48
	7	10mio*	322.39*	10mio*	323.49*	2354210	376.330	1960728	319.38

* - sub-optimal solution – node limit of 10 million reached.

Table 2: Comparison results on the case studies from Ferrer-Nadal et al. (2008).

EN – number of nodes explored to prove optimality; T_{CPU} – computation time in CPU seconds required to prove optimality; None – without blocking reduction and bounding scheme; BR – blocking reduction; MRPT – MRPT-based bounding scheme.

CS	Policy	None		BR		MRPT		MRPT+BR	
		EN	T_{CPU}	EN	T_{CPU}	EN	T_{CPU}	EN	T_{CPU}
1	UIS	11807	0.23	-	-	699	0.03	-	-
	NIS	6530	0.11	6045	0.10	1071	0.05	983	0.03
2	UIS	1684	0.01	-	-	176	0.01	-	-
	NIS	1283	0.11	1036	0.02	863	0.03	681	0.03
3	UIS	10mio*	468.41	-	-	27600	0.79	-	-
	NIS	10mio*	392.40	5989973	214.19	69421	6.93	38378	3.90

* - sub-optimal solution – node limit of 10 million reached.

7. Conclusions

The conceptual ideas of modeling batch scheduling problems with various storage policies and operational policies have been presented. Furthermore, a new blocking reduction technique was introduced and tested on batch scheduling problems with NIS policy. The results show that the reduction technique increases the efficiency of the reachability algorithm in terms of the number of nodes explored and the computation time required to prove optimality or to find the best schedule. Current work includes the extension of the zone abstraction technique to problems with ZW policy and building a reactive scheduling framework for the TA-based approach.

References

Ferrer-Nadal, S., Capon-Garcia, E., Mendez, C. A., Puigjaner, L., 2008. Material Transfer Operations in Batch Scheduling. A Critical Modeling Issue. Ind. & Eng. Chem. Res. 47(20), 7721-7732.

Subbiah, S., Schoppmeyer, C., Engell, S., 2011a. An Intuitive and Efficient Approach to Process Scheduling with Sequence-Dependent Changeovers Using Timed Automata Models. Ind. & Eng. Chem. Res. 50(9), 5131-5152.

Subbiah, S., Schoppmeyer, C., Engell, S., 2011b. Efficient Scheduling of Batch Plants Using Reachability Tree Search for Timed Automata with Lower Bound Computations. In Proceedings of European Symposium on Computer Aided Process Engineering, 930-934.

Demirkol, E., Mehta, S., Uzsoy, R., 1998. Benchmarks for Shop Scheduling Problems. European Journal of Operations Research 109(1), 137-141.

I.A. Karimi and Rajagopalan Srinivasan (Editors), Proceedings of the 11th International Symposium on Process Systems Engineering, 15-19 July 2012, Singapore.

Optimal design of batch-storage network under sporadic operating time loss

Gyeongbeom Yi[a], Bomsock Lee[b], Euy Soo Lee[c]

[a]*Pukyong National University, 100 San Yongdang-Dong Nam-Gu, Busan 608-739, Korea*
[b]*Kyung hee University, 1732 Dugyoungeaero Gyhung-Gu Yonginsi, Kyunggi 446-701, Korea*
[c]*Dongguk University, 26 3-Ga Pi-Dong Jung-Gu, Seoul 100-715, Korea*

Abstract

The purpose of this study is to find the analytic solution of determining the optimal capacity(lot-size) of batch-storage network to meet the finished product demand under periodic or sporadic operating time losses. Batch processes are bound to random but infrequent operating time losses. Two common remedies for these failures are duplicating another process or increasing process and storage capacity, which are very costly. An optimization model minimizing total cost composed of setup and inventory holding costs as well as the capital costs of constructing processes and storage units is pursued with the framework of batch-storage network of which flows are susceptible to periodic or sporadic operating time losses. The superstructure of the plant consists of a network of serially and/or parallel interlinked batch processes and storage units. The processes transform a set of feedstock materials into another set of products with constant conversion factors. A novel production and inventory analysis method, PSW(Periodic Square Wave) model, is applied. The advantage of PSW model comes from the fact that the model provides a set of simple analytic solution in spite of realistic description of the material flow between processes and storage units. The resulting simple analytic solution can greatly enhance the proper and quick investment decision at the early plant design stage confronted with diverse economic situations.

Keywords: Optimal Lot Size, Process-Inventory Network, Periodic Shutdown, Sporadic Shutdown.

1. Introduction

Periodic or sporadic shutdowns are very common in batch chemical processing. A certain class of production shutdowns caused by planned preventive maintenance such as inspection or replacement of rapidly aging parts and periodic switching of operation mode as well as seasonal production commonly occur in periodical (and sometimes sporadic) pattern. Processes are also susceptible to infrequent random processing failures as well as intentional shutdowns. Random processing failures are usually originated from equipment damage, operator mistakes and process troubles, and irregular and insufficient feedstock delivery or sudden sales fluctuation in the product market. Such failures incur emergency corrective maintenance and therefore sporadic shutdowns. The periodic or sporadic shutdowns cause periodic or sporadic loss of operation or business times as well as maintenance cost. In spite of such operation or business time losses, the customer demand of final products should be satisfied. In

order to supply the customer demand during shutdown or failure period, duplicated processes and/or increased storage capacity are unavoidable. On the contrary, duplicating processes or increasing storage capacity is not easy task any more. It is no doubt that the design and construction cost of the chemical processes is substantially increasing with respect to their total capacities. Nowadays, even the storage facilities are growingly expensive because of increased land value, environmental concern and severe quality control requirement. Moreover, modern plant design concept such as JIT (Just-In-Time) strongly pursues to reduce storage capacity. Therefore, the storage capacity in conjunction with process capacity should be selected carefully to consider the operational characteristics such as frequent or sporadic shutdowns.

In this study, the plant structure is composed of a batch-storage network that can cover most supply chain components, for example raw material purchasing, production, transportation and finished product demand. PSW(Periodic Square Wave) model has been successfully used to find the analytical solution of optimal design of batch-storage network including uncertainty and waste streams[1]. In this study, we modified the previous PSW model to incorporate the periodic shutdowns and sporadic shutdowns. We would not use an ordinary probabilistic analysis of random failures. Instead, we will use a judicious graphical method to find the upper and lower bound of the flows under periodic or sporadic shutdowns. Specially, we focus on obtaining a compact set of analytical solutions with minimally given shutdown information.

2. Problem Formulation

Figure 1 shows two typical flows of periodic shutdown $F(t)$ and sporadic shutdown $\mathbf{F(t)}$.

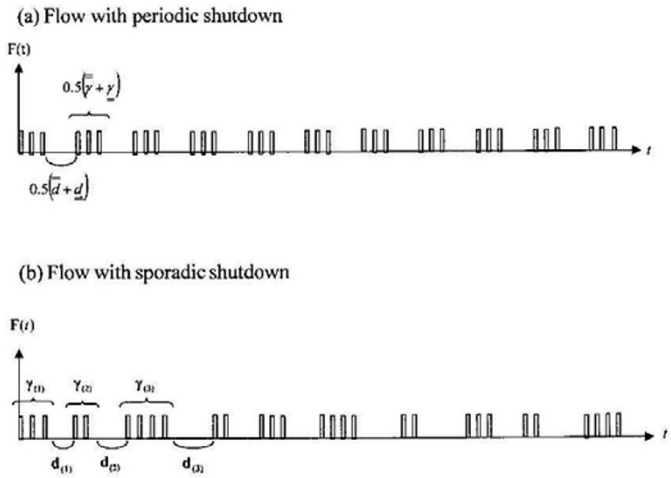

Figure 1. Definition of Uncertainty in Sporadic Shutdown.

The sporadic shutdowns have random characteristics. The random properties of sporadic shutdown are characterized by two random variables $\boldsymbol{\gamma}_{(l)}$ and $\mathbf{d}_{(l)}$ as are shown in Figure 1(b) where subscript **(l)** represent the sequence of occurrence. It is not

necessary to know the exact distribution functions of $\boldsymbol{\gamma}_{(l)}$ and $\mathbf{d}_{(l)}$. We assume that $\boldsymbol{\gamma}_{(l)}$ and $\mathbf{d}_{(l)}$ have symmetrical distribution function with $\underline{\underline{\gamma}} \le \boldsymbol{\gamma}_{(l)} \le \overline{\overline{\gamma}}$ and $\underline{\underline{d}} \le \mathbf{d}_{(l)} \le \overline{\overline{d}}$. That is, the maximum and minimum values of random variables are already known. The mean values of $\boldsymbol{\gamma}_{(l)}$ and $\mathbf{d}_{(l)}$ are $0.5\left(\underline{\underline{\gamma}} + \overline{\overline{\gamma}}\right)$ and $0.5\left(\underline{\underline{d}} + \overline{\overline{d}}\right)$ respectively. Note that $\underline{\underline{\gamma}}, \overline{\overline{\gamma}}$ and $0.5\left(\underline{\underline{\gamma}} + \overline{\overline{\gamma}}\right)$ are all integer values. For $0.5\left(\underline{\underline{\gamma}} + \overline{\overline{\gamma}}\right)$ to be integer, both $\underline{\underline{\gamma}}$ and $\overline{\overline{\gamma}}$ should be odd or even numbers. Suppose that $\boldsymbol{\gamma}_{(l)}$ and $\mathbf{d}_{(l)}$ have identical independent distribution functions with respect to **(l)**. For a given convergence limit $0 < \varepsilon_1, \varepsilon_2 << 1$ and confidence level $0 < \delta_1, \delta_2 << 1$, the weak law of large numbers says that there exists an integer η such that $P\left\{\left|\frac{1}{\eta}\sum_{l=1}^{\eta} \boldsymbol{\gamma}_{(l)} - 0.5\left(\underline{\underline{\gamma}} + \overline{\overline{\gamma}}\right)\right| < \varepsilon_1\right\} \ge 1 - \delta_1$ and $P\left\{\left|\frac{1}{\eta}\sum_{l=1}^{\eta} \mathbf{d}_{(l)} - 0.5\left(\underline{\underline{d}} + \overline{\overline{d}}\right)\right| < \varepsilon_2\right\} \ge 1 - \delta_2$. From Tchebycheff's inequality, $\eta \ge \frac{Var\left(\boldsymbol{\gamma}_{(l)}\right)}{\delta_1 \varepsilon_1^{\,2}}$ and $\eta \ge \frac{Var\left(\mathbf{d}_{(l)}\right)}{\delta_2 \varepsilon_2^{\,2}}$, that is, $\eta = \max\left\{\text{int}\left[\frac{Var\left(\boldsymbol{\gamma}_{(l)}\right)}{\delta_1 \varepsilon_1^{\,2}}\right], \text{int}\left[\frac{Var\left(\mathbf{d}_{(l)}\right)}{\delta_1 \varepsilon_1^{\,2}}\right]\right\} + 1$ if the least integer is chosen.[1] η, called occurrence number, should be an even number in order for 0.5η to be an integer value. The long cycle time in the sporadic shutdown case is different from that in the periodic shutdown case. The time interval during which η number of shutdowns occur is defined as a long cycle time $\tilde{\omega}$. Because the sample means of $\boldsymbol{\gamma}_{(l)}$ and $\mathbf{d}_{(l)}$ converge to their mean values during a long cycle time according to the weak law of large numbers, total number of batches and total shutdown duration during a long cycle time are $0.5\left(\underline{\underline{\gamma}} + \overline{\overline{\gamma}}\right)\eta$ and $0.5\left(\underline{\underline{d}} + \overline{\overline{d}}\right)\eta$ respectively. And thus, $\tilde{\omega} = 0.5\eta\left[\left(\overline{\overline{\gamma}} + \underline{\underline{\gamma}}\right)\omega + \overline{\overline{d}} + \underline{\underline{d}}\right]$. Here, the long cycle time has the meaning of the least period within which all random effects diminish with given confidence level. We note that the flow with sporadic shutdowns has a constant average flow rate $D = \frac{\left(\overline{\overline{\gamma}} + \underline{\underline{\gamma}}\right)B}{\left(\overline{\overline{\gamma}} + \underline{\underline{\gamma}}\right)\omega + \overline{\overline{d}} + \underline{\underline{d}}}$ measured during a long cycle time. This means that in spite of the randomness, the total quantity processed during a long cycle time is a constant. In order to make the optimization formulation, what we need is the upper/lower bound and average inventory level of storage units under sporadic shutdowns. The upper bound of inventory level will be used to compute the storage size; the lower bound of inventory level will be used in the optimization constraint that ensures the inventory level is always nonnegative; and the average inventory level will be used to compute the inventory holding cost of the optimization problem. Two extreme cases of the flow with sporadic shutdowns; (a) Upper bound case and (b) Lower bound case, exist. The

upper bound case has 0.5η times of minimum shutdown duration $\underline{\underline{d}}$ with maximum batch frequency $\overline{\overline{\gamma}}$ and then 0.5η times of maximum shutdown duration $\overline{\overline{d}}$ with minimum batch frequency $\underline{\underline{\gamma}}$ within repeated long cycle times. The lower bound case has 0.5η times of maximum shutdown duration $\overline{\overline{d}}$ with minimum batch frequency $\underline{\underline{\gamma}}$ and then 0.5η times of minimum shutdown duration $\underline{\underline{d}}$ with maximum batch frequency $\overline{\overline{\gamma}}$ within repeated long cycle times. Figure 2 shows the cumulative flow functions of the two cases.

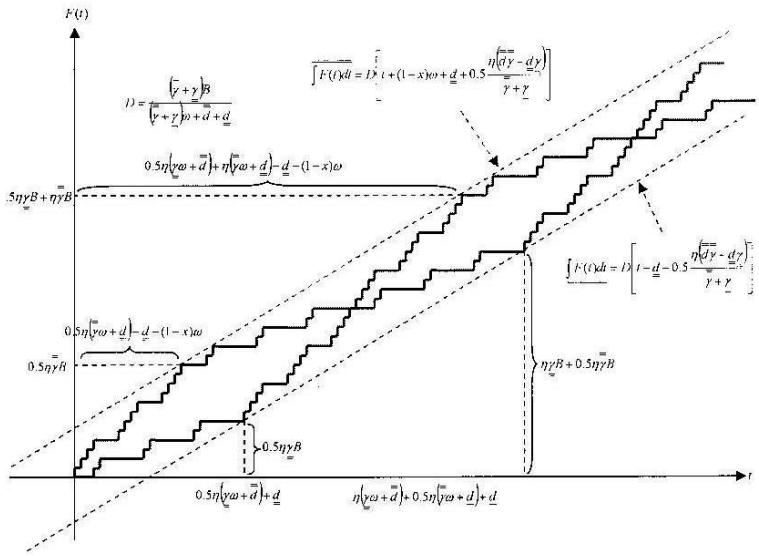

Figure 2. Cumulative Flow Function for Two Extreme Cases.

The dotted lines are the upper and lower bounds of the two extreme cases. All integrals of flows with sporadic shutdowns $\int_0^t \mathbf{F}(t)dt$ exist between the dotted lines whose equations are given in Figure 2.

$$D\left[t+(1-x)\omega+\underline{\underline{d}}+0.5\frac{\eta\left(\overline{\overline{d}}\,\overline{\overline{\gamma}}-\underline{\underline{d}}\,\underline{\underline{\gamma}}\right)}{\overline{\overline{\gamma}}+\underline{\underline{\gamma}}}\right] \geq \int_0^t \mathbf{F}(t)dt \geq D\left[t-\underline{\underline{d}}-0.5\frac{\eta d\left(\overline{\overline{d}}\,\overline{\overline{\gamma}}-\underline{\underline{d}}\,\underline{\underline{\gamma}}\right)}{\overline{\overline{\gamma}}+\underline{\underline{\gamma}}}\right]$$

The upper bound of the inventory level, $\overline{\overline{V^j}}$, is computed by adding the upper bounds of all incoming flow integrals and subtracting the lower bounds of all outgoing flow integrals from the initial inventory. The lower bound of the inventory level, $\underline{\underline{V^j}}$, is computed by adding the lower bounds of all incoming flow integrals and subtracting the upper bounds of all outgoing flow integrals from the initial inventory. Incoming flows are raw material purchase flows and product discharging flows from production

processes. Outgoing flows are feed flows to production processes and finished product demand flows. We can find the upper and lower bounds of inventory level. Note that the overall material balance around a storage unit, still holds for the case with sporadic shutdowns. The average inventory level is highly dependent on the random properties of failures. The exact value of it cannot be obtained without defining the probability distribution function of all random variables, which is a nontrivial work. In this study, we will take an intuitive approach. The average of $\overline{\int_0^t \mathbf{F(t)}dt}$ is selected as the line equidistant from the upper and lower bounds. [1]

$$\overline{\int_0^t \mathbf{F}(t)dt} = D\left[t + 0.5(1-x)\omega\right]$$

The average inventory level of a storage unit is is computed by adding the average of all incoming flow integrals and subtracting the average of all outgoing flow integrals from the initial inventory. The objective function for the design of the batch-storage network is to minimize the annualized expectation of total cost, which consists of the setup cost of processes, the inventory holding cost of storage units, and the capital cost of the processes and storage units at a given minimum/maximum shutdown duration, minimum/maximum batch frequency and occurrence number in a long cycle time of each process.

$$TC = \sum_{j=1}^{|J|}\sum_{k=1}^{|K(j)|}\left[\frac{0.5\eta_k^j\left(\overline{\overline{\gamma}}_k^j + \underline{\underline{\gamma}}_k^j\right)A_k^j}{\tilde{\omega}_k^j} + a_k^j B_k^j\right] + \sum_{i=1}^{|I|}\left[\frac{0.5\eta_i\left(\overline{\overline{\gamma}}_i + \underline{\underline{\gamma}}_i\right)A_i}{\tilde{\omega}_i} + a_i B_i\right]$$
$$+ \sum_{j=1}^{|J|}\left[H^j\overline{V^j} + b^j\overline{\overline{V^j}}\right]$$

The constraints of optimization are no depletion of all storage units, $0 \le \underline{\underline{V^j}}$. Optimal cycle times are:

$$\omega_k^j = \sqrt{\frac{A_k^j}{D_k^j\Psi_k^j}} - \frac{\overline{\overline{d}}_k^j + \underline{\underline{d}}_k^j}{\left(\overline{\overline{\gamma}}_k^j + \underline{\underline{\gamma}}_k^j\right)}, \qquad B_k^j = \sqrt{\frac{A_k^j D_k^j}{\Psi_k^j}}$$

$$\omega_i = \sqrt{\frac{A_i}{D_i\Psi_i}} - \frac{\overline{\overline{d}}_i + \underline{\underline{d}}_i}{\left(\overline{\overline{\gamma}}_i + \underline{\underline{\gamma}}_i\right)}, \qquad B = \sqrt{\frac{A_i D_i}{\Psi_i}}$$

References

1. Yi G. 2008 Optimal design of batch-storage network under joint uncertainties. *AIChE J.* 54 p2567

This work was supported by the Pukyong National University Research Fund in 2011(C-D-2011-0197).

I.A. Karimi and Rajagopalan Srinivasan (Editors), Proceedings of the 11th International Symposium on Process Systems Engineering, 15-19 July 2012, Singapore.

Steady-state optimization of an industrial high-density polyethylene slurry process based on an equation-oriented molecular weight distribution model

Zhiliang Zhan[a], Zhijiang Shao[a], Xi Chen[a], Yuhong Zhao[a], Xueping Gu[b], Zhen Yao[b], Lianfang Feng[b]

[a] *Department of Control Science and Engineering, Zhejiang University, Hangzhou, Zhejiang, 310027, P. R .China*
[b]*State Key Laboratory of Chemical Engineering, Department of Chemical and Biological Engineering, Zhejiang University, Hangzhou, Zhejiang, 310027, P. R. China*

Abstract

High-density polyethylene (HDPE) has been widely used as the main material in the film, pipe, and container industries. An equation-oriented molecular weight distribution (MWD) model is developed for an industrial HDPE slurry process using the method of moments and Flory's distribution. The Kriging method is used to establish a surrogate model for the thermodynamic properties. A completely simultaneous approach is proposed to optimize the steady-state process and achieve products with expected MWDs. Two HDPE grades with different MWDs are discussed.
Keywords: High-density polyethylene slurry process; Equation-oriented; Kriging; Optimization; Molecular weight distribution.

1. Introduction

The slurry polymerization process is widely used to produce high-density polyethylene (HDPE). Its major advantages include mild operating conditions, ease of heat removal, high monomer conversion, and relative ease of processing (Hakim and Moballegh 2006; Hakim, Nekoomanesh et al. 2008). Molecular weight distribution (MWD) is a key quality index for polymers, measurement and optimization of MWD is of considerable importance since the microstructural properties determine its mechanical and rheological properties. However, MWD optimization in a polymerization process is always a challenging task because of the large-scale features. Population balances and the method of moments are usually used to describe the mass conservation of polymer components in polymer systems (Soares 2001). On the basis of the moment models, Flory's most probable distribution can be used to describe the instantaneous chain length distribution (CLD) in ethylene polymerization in each reactor (Soares 2001). Changing CLD into MWD is easy by using two simple mathematical transformation steps (Alghyamah and Soares 2009). In the present project, a large-scale, equation-oriented (EO) model with over 140,000 variables is developed for an industrial HDPE slurry process. A simultaneous approach that optimizes the process and produces of different HDPE grades with expected MWDs is then presented.

2. Model development

Fig. 1 shows the flowsheet of an industrial HDPE slurry process with two reactors in a series. A five-site Ziegler-Natta catalyst, with titanium tetrachloride ($TiCl_4$) as the

primary catalyst and triethyl aluminum ($Al(C_2H_5)_3$) as the co-catalyst, is used. The modeling work consists of thermodynamics, kinetics, MWD calculation, and process unit models that include reactors, flash drums, coolers, compressors, and pumps. Unit models other than the reactors are formulated using the general approach and will not be described in detail because of space constraints.

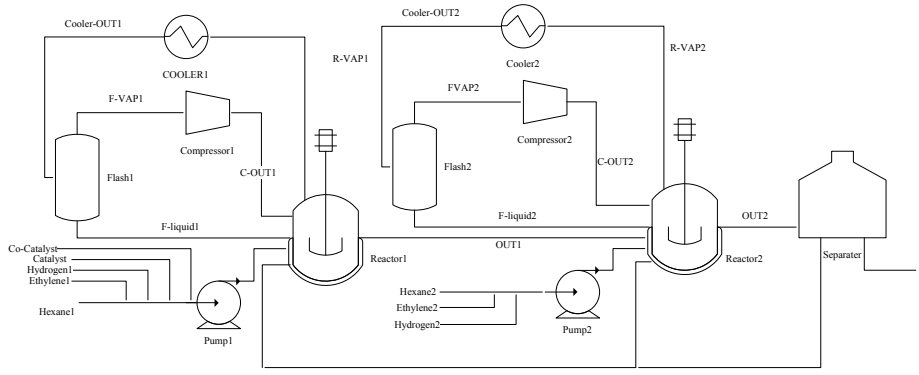

Fig 1. Flow chart of ethylene slurry polymerization process

2.1. Thermodynamic properties based on Kriging

Equation-of-state models are usually used to calculate the thermodynamic properties of polymer systems, among which, the perturbed-chain statistical associating fluid theory (PC-SAFT) is the most accepted one for the polyethylene system (Gross and Sadowski 2001). Given the complexity of the PC-SAFT model, developing an EO model for PC-SAFT is very difficult. To fully exploit the advantages of simultaneous EO optimizations, surrogate models based on the Kriging technique are proposed and developed to describe the relationship between the physical conditions (temperature, pressure, and mole fraction) and the properties (fugacity coefficients, enthalpy, entropy, and density). Kriging models are a family of reduced models that have been used as metamodels (Palmer, Realff 2002). They have also been used in process optimizations (Gomes, Bogle et al. 2006, 2008).

Given the inputs $x=[x_1,x_2,\cdots,x_n]$ and the responses $y=[y_1,y_2,\cdots,y_m]$, the model $\hat{y}(x)$ expresses the deterministic response for an input x as a sum of a regression model and a random function (Lophaven, Nielsen et al. 2002).

$$\hat{y}(x)=f(x)^{\mathrm{T}}\beta^{*}+r(x)^{\mathrm{T}}\gamma^{*} \tag{1}$$

where $f(x)$ is the regression model, $r(x)$ is the correlation model, β^{*} is the regression parameter, and γ^{*} is the correlation parameter. Unlike PC-SAFT, which works for a wide range of conditions, deriving a surrogate model that also covers a wide range is difficult. Considering the features of the simultaneous approach and the huge differences between the streams, a strategy that divides the process into several subsystems and establishes a Kriging model for each subsystem is proposed. In practice, each stream and unit is set as a subsystem. The regression data were generated using the Aspen Property software with PC-SAFT. Up to 3000 data were collected for regression and 10,000 other data for verification. The dimension of the Kriging model is highly related to the data number. Therefore, the surrogate models derived for the thermodynamic properties are in considerably large scales. However, they will not add difficulty in solving the procedure because only direct calculations are involved. The

verification shows that the average errors between the Kriging model and PC-SAFT for all systems in the process model are less than 0.1%, and the maximum relative errors are less than 0.5% for the non-polymer system and 2% for the polymer system. The maximum errors in the properties of the main streams (F-VAP, F-LIQUID, OUT, and VAP) are shown in Table 1. The physical conditions are the inputs to the models for the calculation of these properties, including the enthalpy (H), density (ρ), entropy (S), and fugacity coefficients (φ). The subscript A denotes the co-catalyst. The results prove that the Kriging model can approximate the PC-SAFT for each subsystem well.

Table 1. The regressive results of properties for main streams of both reactors

Stream	Physical conditions	Properties	Max error %	Stream	Physical conditions	Properties	Max error %
F-VAP	T	H	0.224	F-LIQUID	T	H	0.005
	P	φ_{H2}	0.072		P	φ_{H2}	0.191
	x_{H2}	φ_{C2H4}	0.054		x_{H2}	φ_{C2H4}	0.182
	x_{C6H14}	φ_{C6H14}	0.082		x_{C6H14}	φ_{C6H14}	0.265
		S	0.158	R-VAP	T	ρ	0.053
OUT	T	ρ	0.092		P	H	0.035
	P	H	0.007		x_{C2H4}	φ_{H2}	0.034
	x_{H2}	φ_{H2}	1.789		x_{C6H14}	φ_{C2H4}	0.017
	x_{C2H4}	φ_{C2H4}	0.821			φ_{C6H14}	0.057
	x_A	φ_{C6H14}	1.072				
	x_{HDPE}						

2.2. Moment model for polymerization reactor

The reactors are assumed to be continuous stirred tank reactors (CSTR). The kinetics of the polymerization reaction includes catalyst activation, initiation, propagation, transfer, and deactivation. The kinetic parameters can be found in the report by Gu et al. (2008). Population balances and the method of moments are used to describe the mass conservation of the polymer components. The moments of the chain length distribution are calculated for both living and dead polymers.

2.3. The method of instantaneous distribution

The method of instantaneous distribution relies on the assumption that the time-scale for the life of a polymer chain is several times smaller than that for dynamic phenomena taking place. The average lifetime of a polymer chain is in the order of seconds, whereas the time-scale for the reactor and particle dynamics during ethylene polymerization under realistic conditions is generally in the order of several minutes up to hours (Soares 2001). Hence, the use of the method of instantaneous distribution for the HDPE process is fully justified. Associated with the reaction kinetics and the moments of the polymer, the instantaneous CLD for ethylene polymerization at site j is given by a single-parameter equation , Flory's distribution, as follows:

$$w_j(n) = n\tau_j^2 \Big/ (1+\tau_j)^{n+1} \tag{2}$$

where $w_j(n)$ is the weight chain length distribution of the polymer chains with length n, τ is the ratio of all the chain transfer rates to the propagation-rate (calculated from the kinetic model), and j is the site number. Transformations (Alghyamah and Soares 2009) are further performed to convert CLD to MWD in the logarithmic scale, as follows:

$$w_j\left(\log MW\right) = \ln 10 \times MW^2 \left(\tau_j / mw\right)^2 \left(1+\tau_j\right)^{-\left(\frac{MW}{mw}+1\right)} \tag{3}$$

The entire instantaneous distribution of the molecular weight for each reactor can be obtained using the weighted superposition of Flory's distribution for each site.

$$W\left(\log MW\right)=\sum_{j=1}^{Ns} w_j\left(\log MW\right)mf_j \tag{4}$$

where mf_j is the mass fraction of the polymer at site *j*. The MWD of the final product is a combination of the two instantaneous distributions in each reactor, as follows:

$$W_{com}\left(\log MW\right)=\left(m_1W_1\left(\log MW\right)+m_2W_2\left(\log MW\right)\right)/\left(m_1+m_2\right) \tag{5}$$

where m_1 and m_2 are the polymer masses in the first and second reactors, respectively, and can be calculated from the moment models.

3. Results and discussion

Given a designed MWD curve of HDPE as the product quality requirement, an optimization problem can be formulated to minimize the error between the given and predicted distributions by adjusting the process operation conditions, as follows:

$$\begin{aligned}
&\min_{z} \sum_{k=1}^{N_{point}}\left[W_{exp}\left(\log MW^k\right)-W_{com}\left(\log MW^k\right)\right]^2\\
&\text{s.t.}\quad h\left(W_{com}\left(\log MW^k\right),\tau_i,mf_i\right)=0\\
&\qquad g\left(z,\tau_i,mf\right)=0\\
&\qquad z_{lb}\le z\le z_{ub}
\end{aligned} \tag{6}$$

where $W_{exp}\left(\log MW\right)$ is the expected MWD, N_{point} is the curve sampling number (100 in the current project), MW^k is the molecular weight at a discrete point, and *z* is the optimized operational conditions, including the reactor temperatures and pressures and the feed flowrates of hydrogen, ethylene, and hexane in both reactors.

Two MWD curves, one with two peaks and the other with a single peak, are plotted for the optimization. The complete EO model consists of more than 141,101 variables, most of which are the intermediate variables in the Kriging models. The simultaneous approach is used for the optimization using the interior point optimizer (IPOPT) as the solver. Fig. 2 shows that the expected MWDs can be achieved in both cases. The optimized and expected MWDs almost overlap each other. The instantaneous MWDs of the first and second reactors are also shown in the figure. The composite MWD can be very different in shape as a result of the combination of the two reactors. The optimal operation conditions for each case are presented in Table 2.

Table 2. The operation conditions from the optimization

		T(°C)	P (Mpag)	L (%)	H_2 (Nm^3/h)	C_6H_{14} (t/h)	C_2H_4 (t/h)
Twin Peaks	Reactor 1	91.98	0.4516	70.05	49.55	280.23	3.21
	Reactor 2	78.73	0.25	73.36	54.29	23.91	6.82
Single Peak	Reactor 1	80	0.6574	52.34	58.08	80.74	1.3
	Reactor 2	82.1	0.1187	69.66	49.55	282.52	2.32

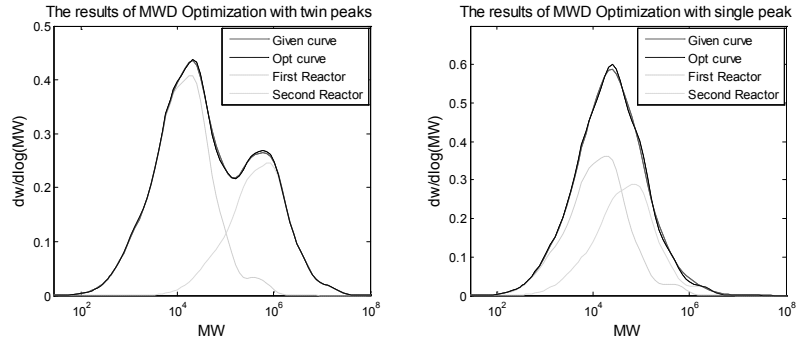

Fig.2 Comparison between MWD optimization results and given curve

4. Conclusion

A steady-state MWD model for the polymerization of ethylene in the slurry process is developed in the present paper. A simultaneous approach is used to optimize the operational conditions and produce polymers with expected MWDs. The optimization results show that good performance can be achieved for different shapes of the MWD curves, thereby providing potential applications in product design.

Acknowledgment

We gratefully acknowledge the financial support of 973 Program (No.2009CB320603), National Natural Science Foundation of China (No. 61074148) and the Fundamental Research Funds for the Central Universities.

References

A. A. Alghyamah, J. B. P. Soares, 2009, Simultaneous Deconvolution of the Bivariate Distribution of Molecular Weight and Chemical Composition of Polyolefins Made with Ziegler-Natta Catalysts, Macromolecular Rapid Communications, 30, 4-5, 384-393

K. Palmer, M. Realff, 2002, Optimization and Validation of Steady-State Flowsheet Simulation Metamodels, Trans IChemE Part A - ChERD, 80, 7, 773-782

J. B. P. Soares, 2001, Mathematical Modelling of the Microstructure of Polyolefins Made by Coordination Polymerization: a Review, Chemical Engineering Science ,56, 13, 4131-4153

J. Gross, G. Sadowski, 2001, Perturbed-chain SAFT: An Equation of State Based on a Perturbation Theory for Chain Molecules, Industrial & Engineering Chemistry Research, 40, 4, 1244-1260

M.V.C.Gomes, I.D.L.Bogle, et al., 2006, An Application of Metamodels for Process Optimisation, Proceedings of the 16th European Symposium on Computer Aided Process Engineering, 1449

M. V. C.Gomes, I. D. L. Bogle, et al., 2008, Using Kriging Models for Real-time Process Optimisation, Computer Aided Chemical Engineering, 25, 361-366

S.Hakim, L. Moballegh, 2006, Simulation of a Series of Industrial SlurryReactors for HDPE Polymerization Process Using Deconvolution of the GPC Graph of Only the First Reactor, Iranian Polymer Journal, 15, 8, 655-666

S. Hakim, M. Nekoomanesh, et al. , 2008, Investigating the Behaviour of a Bi-Supported SiO2/TiCl4/THF/MgCl2 Catalyst in Slurry Ethylene Polymerization: Activity and Molecular Weight, Iranian Polymer Journal, 17, 3, 209-216

S. N.Lophaven, H. B. Nielsen, et al., 2002, DACE: A Matlab Kriging Toolbox, Technical Report IMM-TR-2002-12

X. Gu, L. Feng, et al., 2008, Simulation for Grade Transition of Ethylene Slurry Polymerization Process, Sciencepaper online, 3, 12

I.A. Karimi and Rajagopalan Srinivasan (Editors), Proceedings of the 11th International Symposium on Process Systems Engineering, 15-19 July 2012, Singapore.

Cyclic Scheduling of Cracking Furnaces System with Real Operational Characters

Lijie Su, Lixin Tang,

The Logistics Institute, Northeastern University, *Shenyang 110819*, *Liaoning*, *China*

Abstract

The cyclic scheduling of cracking furnaces is investigated with the practical operational characters, which are concurrent or serial cracking different raw materials in one furnace between its two adjacent decoking operations. This paper presents two mixed-integer nonlinear programming (MINLP) formulations respectively for the two scheduling problems based on a continuous time representation. Valid inequalities and linearization techniques are used, and an improved Outer Approximation (OA) algorithm with parallel strategies is designed for solving the formulations. Numerical experiments demonstrate the efficiency of the models and solution strategies. [1]

Keywords: Cyclic Scheduling, Ethylene Cracking Furnace, MINLP, Outer Approximation

1. Introduction

Ethylene production is multi-stage continuous process with parallel cracking units as illustrated in Figure 1, which operate multi-feedstock and produce few final popular products. Cracking furnaces would need periodical decoking in order to assure the conversion of final products, protect furnace pipes and save fuel. The cyclic scheduling of the process would determine assignment, processing times, and number of subcycles of various feeds on different units during a optimal production cycle. Jain and Grossman(1998) presented a pseudo-convex MINLP formulation for one general scheduling problem. The work of Liu et al(2010) considered the non-simultaneous cleanup constraints. Those two papers are assumed that only one kind of raw materials is processed in one subcycle, and the length of subcycle is between lower and upper bounds dependent on cracked raw materials. However, concurrent or serial cracking different raw materials during one subcycle of same furnace often occurs in practical production. This two operation ways could increase the flexibility of process, ease the shortage of raw materials and avoid shutting down.

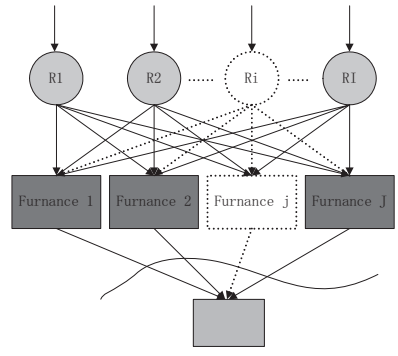

Figure 1 Cracking Process of Ethylene Production

With the concerns of practical operation, this paper presents two formulations for the cyclic scheduling of cracking furnaces with new operational characters. The

This research is partly supported by State Key Program of National Natural Science Foundation of China (71032004), the Fundamental Research Funds for the Central Universities (N090104002，N100704002).

linearization and valid inequalities are designed to reformulate the models. And an improved OA algorithm with some parallel strategies is designed to solve the model. Some cases would demonstrate the efficiency of the presented formulations and improved algorithm.

2. Problems Statement

With non-simultaneous cleanup constraints, the cyclic scheduling problem would also determine decoking times of each furnace during one cycle in order to maximize the net profit value per time. Here, assume (1) regressed cracking yield model based on plant data is reliable; (2) The conversion to final products are assumed as Jain and Grossman(1998). Based on our investigation of real Ethylene plants, two kind of cracking operation for one furnace in one subcycle which would not be considered before often occur.

2.1. Concurrent cracking problem

The minimal producing unit is pipe group in one cracking furnace. For example, there are 4-6 pipe groups in the SRT types. And different pipe groups could operate different feeds with similar cracking condition. For these groups belong to one furnace, the starting and ending times of the subcycles are same, and cleanup must be simultaneous.

2.2. Serial cracking problem

The subcycle length is about 50-80 days in real production. Therefore, processing one kind of feeds in single subcycle must assume sufficient feedstock supply, which is often unavailable in practical process. For one furnace, serially cracking different feeds during one subcycle would relax the strong assumption. Here, assume one raw materials be processed continuously in one subcycle. The processing rate of furnace could be adjusted in some scope, which be considered as a constant before.

3. MINLP Formulations

Two MINLP formulations are presented for the cyclic scheduling problem with different operating rules as described. The definition of production cycle is composed of complete subcycles with their cleanup durations. Continuous-time representing method are applied to determine the boundaries of every subcycle. Distinctive constraints are described as follow and others which are described in Jain and Grossman(1998) or Liu etc(2011) are omitted here, which include some general assignments, integrality, mass balance, non-simultaneous cleanup constraints and objective functions.

3.1. Concurrent cracking model

Except indices of feeds, furnace and subcycle, number of pipe groups in one furnace is introduced as one index. The definition of binary variable X_{ijgk} is that whether assign feed i to the pipe group g of furnace j in subcycle k. Those pipe groups included in one furnace must work synchronously, which lead to the following constraint:

$$|G| \cdot \sum_{i} X_{ijgk} \geq \sum_{i,g} X_{ijgk} \quad \forall j,g,k \tag{1.1}$$

The subcycles must be front closely, that is if one subcycle of a furnace is empty, the following subcycles of that cracking unit should be empty.

$$\sum_{i,g} X_{ijgk} \geq \sum_{i,g} X_{ijgk+1} \quad \forall j, k < K \tag{1.2}$$

The continuous variables Ts_{jk} , Tp_{jk} represent the starting time and duration for subcycle k of furnace j, and Tr_{ijgk} is the duration of feed i cracked in pipe group g of furnace j during its subcycle k. Then constraints (1.3) and (1.4) would insure that pipe groups in one furnace operate synchronously.

$$Tr_{ijgk} \leq Tp_{jk} \quad \forall i, j, g, k \tag{1.3}$$

$$\sum_{i,g} Tr_{ijgk} = |G| \cdot Tp_{jk} \quad \forall g, k \tag{1.4}$$

Cleanup duration of each subcycle for one furnace Tcl_{jk} would be equal to the maximum cleanup one of cracked feeds.

$$\tau_{ij} \cdot X_{ijgk} \leq Tcl_{jk} \quad \forall i, j, g, k \tag{1.5}$$

There are minimal demand rates for different kind of final product.

$$\sum_{i,j,g,k} F_{ijg} \cdot \left[c_{ijl} \cdot Tr_{ijgk} + \frac{a_{ijl}}{b_{ijl}} \left(e^{b_{ijl} \cdot Tr_{ijgk}} - 1 \right) \right] \geq Q_l \cdot T_{cycle} \quad \forall l \tag{1.6}$$

3.2. Serial cracking model

Here, sequence of feeds in one subcycle of a furnace is introduced as one additional index. The sequence in subcycle also is front closely.

$$\sum_{i} X_{ijks} \geq \sum_{i} X_{ijks+1} \quad \forall j, k, s < I \tag{1.7}$$

Using F_{ijk} represents the processing rate, and T_{ijk}^{SC} represents the processing duration of feed in subcycle, which are continuous variables here. Through introducing an auxiliary variable FT_{ijk} and four additional constraints, the mass balance constraint could be linearization, which would avoid the bilinear term in the model. T^L , T^U are lower and upper bounds of continuous processing time of one kind of feeds.

$$FT_{ijk} \geq T^L \cdot F_{ijk} + F_{ij}^L \cdot T_{ijk}^{SC} - T^L \cdot F_{ij}^L \quad \forall i, j, k \tag{1.8}$$

$$FT_{ijk} \geq T^U \cdot F_{ijk} + F_{ij}^U \cdot T_{ijk}^{SC} - T^U \cdot F_{ij}^U \quad \forall i, j, k \tag{1.9}$$

$$FT_{ijk} \leq T^U \cdot F_{ijk} + F_{ij}^L \cdot T_{ijk}^{SC} - T^U \cdot F_{ij}^L \cdot \sum_{s} X_{ijks} \quad \forall i, j, k \tag{1.10}$$

$$FT_{ijk} \leq T^L \cdot F_{ijk} + F_{ij}^U \cdot T_{ijk}^{SC} - T^L \cdot F_{ij}^U \cdot \sum_{s} X_{ijks} \quad \forall i, j, k \tag{1.11}$$

The summation of serial processing durations for different feeds in each subcycle equals to the length of subcycle.

$$\sum_{i} T_{ijk}^{SC} = Tp_{jk} \quad \forall j, k \tag{1.12}$$

The product of coking-velocity coefficient γ_{ij} and cracking duration of one feed stock T_{ijk}^{SC} is described as the cleaning up duration of this feed. Assume the decoking duration of one subcycle Tcl_{jk} is equal to the accumulation of cleaning up duration of some feeds, which are cracked in this subcycle.

$$Tcl_{jk} = \sum_{i} \gamma_{ij} \cdot T_{ijk}^{SC} \quad \forall j,k \tag{1.13}$$

Using lower and upper bound of decoking time determines the length of subcycle.

$$\tau^{L} \cdot \sum_{i} X_{ijks} \le Tcl_{jk} \le \tau^{U} \quad \forall j,k,s=1 \tag{1.14}$$

In order to define the beginning processed time of feed i in subcycle k of furnace j, that is $\tilde{T}s_{ijk}$, introduce another auxiliary variable TX_{ijks} and linearization constraints

$$TX_{ijks} \le T^{U} \cdot X_{ijks} \quad \forall i,j,k,s \tag{1.15}$$

$$TX_{ijks} \le T_{ijk}^{SC} + M \cdot \left(1 - X_{ijks}\right) \quad \forall i,j,k,s \tag{1.16}$$

$$TX_{ijks} \ge T_{ijk}^{SC} - M \cdot \left(1 - X_{ijks}\right) \quad \forall i,j,k,s \tag{1.17}$$

Then

$$\tilde{T}s_{ijk} \ge \sum_{i' \ne i} \sum_{s' < s} TX_{i'jks'} - M \cdot \left(1 - X_{ijks}\right) \quad \forall i,j,k,s \tag{1.18}$$

$$\tilde{T}s_{ijk} \le \sum_{i' \ne i} \sum_{s' < s} TX_{i'jks'} + M \cdot \left(1 - X_{ijks}\right) \quad \forall i,j,k,s \tag{1.19}$$

With the beginning processed time, the ending time could be easily given.

$$\tilde{T}e_{ijk} = \tilde{T}s_{ijk} + T_{ijk}^{SC} \quad \forall i,j,k \tag{1.20}$$

The objective of the cyclic scheduling problem would maximize the average profit。

$$Max\ z = \sum_{i,j,k,l} \begin{pmatrix} PR_{l} \cdot [c_{ijl} \cdot FT_{ijk} + F_{ijk} \cdot a_{ijl} \left(e^{b_{ijl}\tilde{T}e_{ijk}} - e^{b_{ijl}\tilde{T}s_{ijk}} \right) / b_{ijl}] \\ -(CR_{i} + CP_{j}) \cdot FT_{ijk} - CC_{j} \cdot Tcl_{jk} \end{pmatrix} / TC \tag{1.21}$$

Based upper bound of coking thickness and coefficient of coking velocity, the upper bound of subcycle length could be calculated. Therefore, the maximum kind of raw materials which could be processed in one subcycle could be gotten.

$$\sum_{i,s} X_{ijks} \le \frac{\tau^{U}}{\min_{i}\left\{\gamma_{ij}\right\} \cdot T^{L}} \quad \forall j,k \tag{1.22}$$

The proposed models are both MINLP with nonlinear objective function and linear constraints.

4. Solution Algorithm

There are four-index binary variables and more big-M constraints in our models. As one of general algorithms for MINLP, an improved Outer approximation(OA) algorithm with parallel strategy is designed for the presented models in order to decrease the

iterations. With the description of general OA from Grossmann(2002), a simplified description of the algorithm is as follows.
Step 1, Initialization: solve the relaxed NLP1 of primal MINLP, getting the lower bound of the problem, then solve constructed master MILP based on the solution of NLP1;
Step 2, Construct several NLP2 with the different collected integer solutions of MILP, then solve these problems concurrently, get few solutions of NLP2;
Step 3, Construct MILP master problem based on these solutions of NLP2, then solve the master problem. If the terminal condition would be not satisfied, collect few solutions of MILP, return to step 2, else stop.
The presented model is formulated with GAMS(Brooke etc, 1992). The improved OA is also programmed on GAMS platform.

5. Computational Results

One example is considered respectively for the two formulations. It is desired to determine a cyclic schedule to process three different feeds A, B, C in a furnace. Other part of related parameters are from Jain and Grossman(1998). The predefined number of subcycles is 7, and the lower bound of total cyclic length is set 135 days.
For the concurrent cracking model, the number of pipe groups is 3, An optimal solution is shown in Figure 2. Concurrent operation based on pipe-groups could release the shortage of feeds. For the serial cracking model, an optimal solution is shown in Figure 3.
Data experiments demonstrates that the presented improved OA algorithm could decrease whole iterations.

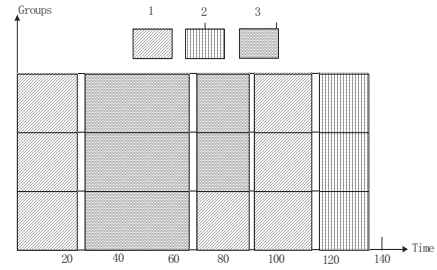

Figure 2 Optimal scheduling solution for concurrent cracking model

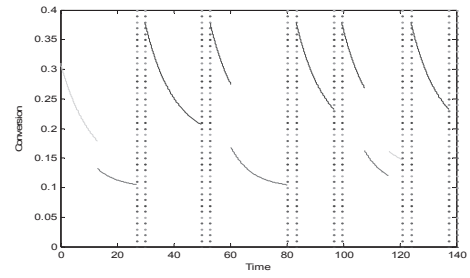

Figure 3 Optimal scheduling solution for serial cracking model

6. Conclusions

The characters of concurrent and serial operations are considered in the cyclic scheduling for multiple cracking furnaces. Continuous-time representation method, linearization and valid inequalities are used to reformulate two MINLP models. The improved OA algorithm is designed to solve the problems. Results could reflect the flexibility of production process, and better mass balance.

References

V. Jain, I. E. Grossmann, 1998, Cyclic Scheduling of Continuous Parallel-Process Units with Decaying Performance, AIChE Journal, Vol. 44, No. 7, 1623-1636.
C.W. Liu, J. Zhang, Q. Xu, K. Y. Li, 2010, Cyclic scheduling for best profitability of industrial cracking furnace system, Computers and Chemical Engineering, Vol. 34 544-554.
I. E. Grossmann, 2002, Review of nonlinear mixed-integer and disjunctive programming techniques. Optimization and Engineering, Vol.3, 227–252.
A. Brooke, D. Kendrick, A. Meeraus, 1992, GAMS: A user's guide. Palo Alto, CA: Scientific Press.

I.A. Karimi and Rajagopalan Srinivasan (Editors), Proceedings of the 11th International Symposium on Process Systems Engineering, 15-19 July 2012, Singapore.

Thermodynamic analysis and modeling for typical feed-preheating and fractionating processes in delayed cokers

Yang Lei, Bingjian Zhang, Qinglin Chen*

School of Chemistry and Chemical Engineering/Key Lab of Low-carbon Chemistry & Energy Conservation of Guangdong Province, Sun Yat-Sen University, Guangzhou 510275, China

Abstract

Delayed coking is one of the main processes for heavy oil processing with higher energy consumption in refineries. The present analysis includes the energy and exergy balance of the de-superheating section, the heat exchanging process of the feeds, etc. An approach to optimize the heat exchanger network through integrating the fractionating process is illustrated. A much higher feed temperature is usually considered better for an energy-use optimization retrofit. However, considering the limit of the energy integration within the whole plant, determining the feed preheating temperature is usually an optimization problem. Finally, a model is built that the annual cost is set as an objective function which is subject to the restrictions mentioned above.

Keywords: delayed coker; modeling; optimization; thermodynamic analysis

1. Introduction

To efficiently lower the energy consumption of a delayed coking unit (DCU), it is crucial to increase the efficiency of the coking furnace, to reasonably use the heat of the main fractionator within the unit (Chen et al., 2004). In DCUs, there exist special energy-use characteristics for the heat exchanger network (HEN) and fractionating processes (Rodriguez-Reinoso et al., 2011). So far, the existing heat integration methods are mainly based either on pinch analysis techniques or on mathematical programming (Morar et al., 2010). Most researches and engineering retrofits mainly focused on the heat integration between different plants (Plesu et al., 2003; Zhang et al., 2011). For a single plant, Al-Riyami et al. (2007) analyzed the heat integration of a HEN in a fluid catalytic cracking plant. However, it is seldom considered how to optimize the HEN of DCUs through simultaneously integrating the fractionating processes. Consequently, thermodynamic analysis results are presented for three typical processes of DCUs. Then an optimization approach is proposed in which the integration between HEN and fractionating processes is considered. An optimal model is established for the optimal feed preheating temperature.

2. Comparison and thermodynamic analysis of three processes

A conventional DCU generally consists of three sections, i.e. coking, oil and gas separation and heat exchanging. Three typical flowsheets with different feed preheating and fractionating processes are sketched in Fig. 1, in which the primary difference is within the section of preheating/steam generation. The three processes presented above

* Correspondence author, email: chqlin@mail.sysu.edu.cn.

are all simulated by using software PRO/Ⅱ.

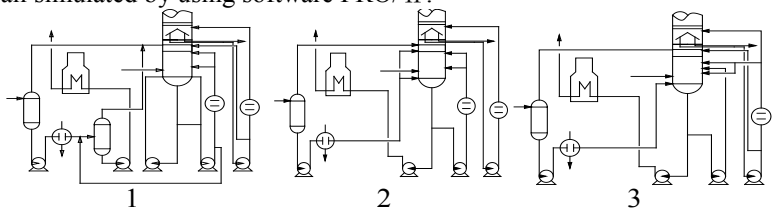

Fig. 1 Schematic representation of typical DCUs

Coking section The inlet temperature of the residual oil to the coking furnace (T_{inlet}) via energy conservation exists:

$$T_{inlet,1} < T_{inlet,3} < T_{inlet,2} \quad \text{(Eqn. 1.)}$$

Separation section The pump-around heat removal in the main fractionator is different:

$$\left(\frac{Q_t + Q_d}{Q_{all}}\right)_1 < \left(\frac{Q_t + Q_d}{Q_{all}}\right)_3 < \left(\frac{Q_t + Q_d}{Q_{all}}\right)_2 \quad \text{(Eqn. 2.)}$$

The exergy losses of the factionators are different, which is affected by the heat transfer temperature difference in the de-superheating section:

$$Ex_{loss,1} < Ex_{loss,3} < Ex_{loss,2} \quad \text{(Eqn. 3.)}$$

Heat exchanging section It is assumed that the heat exchanging sequence is same. The temperature of the preheated feed (T_{feed}) in three processes is different:

$$T_{feed,2} < T_{feed,3} < T_{feed,1} \quad \text{(Eqn. 4.)}$$

3. HEN optimization principle through integrating fractionating processes

To address the problem of the HEN optimization through integrating the fractionating process, the following strategies are presented.

1.1. Heat integration strategies

(1) All streams' data should be collected firstly. When the ratio of Q_t and Q_d to Q_{all} is less than C1 which is defined by heuristic rules, the heat removal should be changed. Thus, in the premise of Q_{all} is constant, the process simulation should be applied to increase the heat removal of the intermediate and gas oil pump-arounds. By combining with the practical operation experiences, simulations should be carried out repeatedly to make sure the optimal heat recovery.

(2) All the new hot and cold streams data must be defined. The corresponding pinch diagram can be drawn by means of ASPEN PINCH in which the minimum utility requirement can be estimated. If the difference between the actual hot utility and minimum hot utility is less than C2 which is defined by the tradeoff between the capital and energy costs involved, the HEN is optimal. Otherwise, the HEN is not the best and there exist optimization potentials.

(3) If there is a potential for HEN retrofit, there are three design objectives for HEN retrofit. The first one is to maximize the T_{feed}. So the theoretically maximum T_{feed} should be defined by pinch diagram in which the radiation oil heated by the coking furnace, and the deaerated water should not be included. The second one is to generate the maximum steam through process streams within the units. In the pinch analysis, the radiation oil is not included. The deaerated water for steam generation should be heated possibly by using hot process streams. The third one is to consider the tradeoff between the T_{feed} and the quantity of generated steam.

(4) In objective 1, or 2, three pinch principles should be carried out to retrofit the HEN.
(5) In the objective 3, to define the best HEN through calculating minimum *TAC* model.

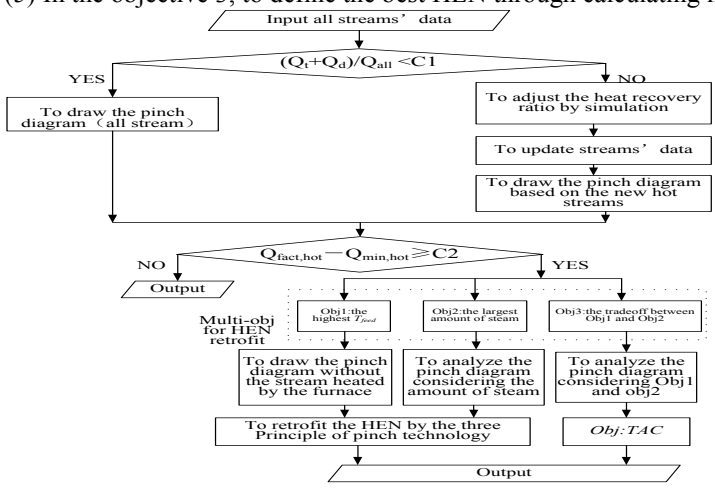

Fig. 2 Flowchart of steps for HEN optimization by integrating the fractionating process

1.2. TAC model

HEN superstructure: For the objective 3, Fig. 3 shows a superstructure with seven stages for a one-cold and four-hot stream synthesis problem. It is assumed that there is no split for feed. The order of the hot streams is defined by comparing the temperature levels. *TAC* is used as the objective function to be minimized which includes the annualized capital costs and operating costs. (Douglas JM, 1988).

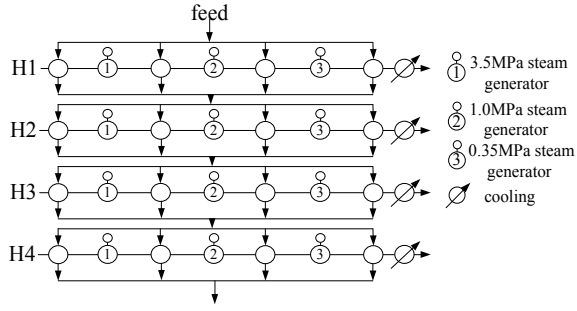

Fig. 3 HEN superstructure

Minimum TAC:

$$\frac{\sum_{j\in J}\sum_{k\in k1} Z_{jk}SS+\sum_{j\in J}\sum_{k\in k2} Z_{jk}CS+\sum_{j\in J} Z_{cuj}CS}{Payback\ period}+\sum_{j\in J} Z_{cuj}C_w+C_{hu}-\left(\sum_{j\in J} Z_{j2}C_{3.5s}+\sum_{j\in J} Z_{j4}C_{1.0s}+\sum_{j\in J} Z_{j6}C_{0.35s}\right) \quad \text{(Eqn. 5.)}$$

Overall heat balance:

$$F_j\left(T_{j,in}-T_{j,out}\right)=\sum_{k\in K} q_{jk}+q_{cuj}\ ,\ F_{feed}\left(T_{feed}-T_{f,in}\right)=\sum_{j\in J} q_{j1}+\sum_{j\in J} q_{j3}+\sum_{j\in J} q_{j4}+\sum_{j\in J} q_{j7} \quad \text{(Eqn. 6.)}$$

Assignment of superstructure inlet temperature and monotonic decrease in temperature:

$$t_{j,k}=T_{j,in},\ T_{f,in}=T_{f,1},\ T_{feed}=T_{f,out}=T_{f,5}t_{j,k}\le t_{j,k+1}\ ,j\in J,k\in K,\ t_{f,j}\le t_{f,j+1}\quad j\in J \quad \text{(Eqn. 7.)}$$

Heat loads of hot and cold utilities:

$$Q_c=F_j\left(t_{j,8}-T_{j,out}\right)\ ,\ Q_f=F_f\left(500-T_{feed}\right) \quad \text{(Eqn. 8.)}$$

Approach temperature and logical constraints:

$$d_{tjk} \geq \Delta T_{\min} \quad d_{tcuj} \geq \Delta T_{\min}, q_{j,k} \leq \alpha_{zjk} \quad q_{cuj} \leq \alpha_{zcuj} \tag{Eqn. 9.}$$

$$Z_{j1} + Z_{j3} + Z_{j5} + Z_{j7} \leq 1 \quad j \in J \tag{Eqn. 10.}$$

Internality conditions and bound limitations:

$$Z_{jk}, Z_{cuj} = 0,1 \quad j \in J \quad , \quad T_{j,out} \leq t_{j,k} \leq T_{j,in} \quad T_{f,in} \leq t_{f,j} \leq T_{feed} \quad j \in J, \ k \in K \tag{Eqn. 11.}$$

$$q_{jk} \geq 0, \ q_{cuj} \geq 0 \quad j \in J, \ k \in K \tag{Eqn. 12.}$$

4. Case study

A DCU is taken as an example to study for introducing objective 1. In Fig. 4a, the curve which includes all streams indicates that the pinch point is at T_p=149℃.

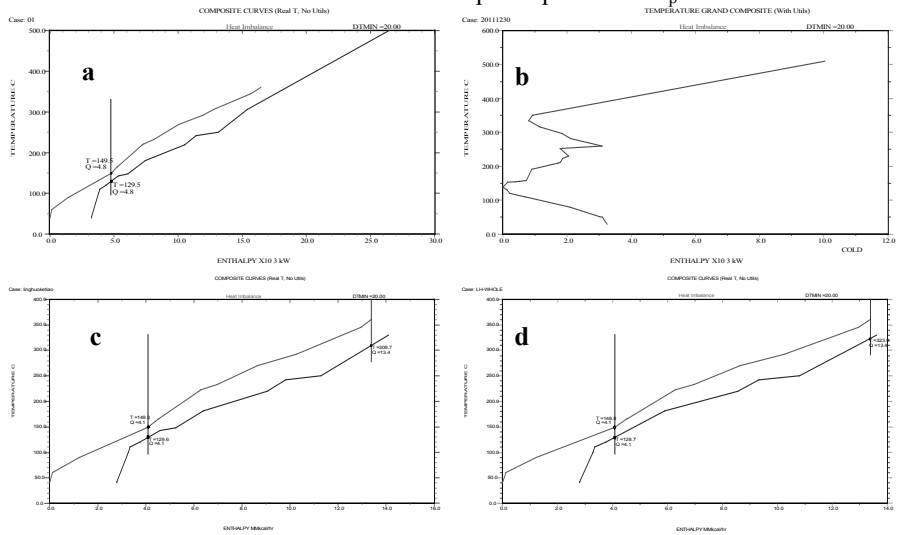

Fig. 4 DCU representation as composite and grand composite curves

From Fig. 4b, we can find that a pocket above 140℃ until 334℃ exists. The corresponding pinch diagram is shown in Fig. 4c for keeping the generated steam constant. Thus the deaerated water for steam generating is included in the streams. However, the residual oil heated by the coking furnace is used to heat the feed, so it is not included in the pinch analysis. Furthermore, a new pinch diagram is presented in Fig. 4d in which the cold streams don't include the deaerated water. On this figure, the maximum feed temperature T_{feed} is nearly 323℃. The current and new topology is presented in Fig. 5. After retrofit four heat exchangers are added, and 1435kW of hot utility can be saved. The steam generated with pressure of 1.0MPa decreased by 2.34 t/h. It is remarkable that the T_{feed} is near to the theoretical temperature.

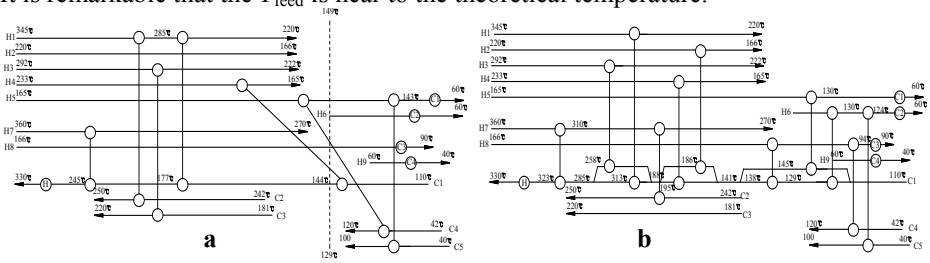

Fig. 5 Structure of the heat exchanger network of DCU

5. Conclusions

Based on a thermodynamic analysis presented for three typical flowsheets with different heat exchange and fractionating processes, the energy-use retrofit potentials are identified. An approach for retrofit design of the HEN through integrating the fractionating process in DCUs is proposed by considering the limitation of the energy integration within the whole plant, the temperature at the bottom of the main fractionator and the quantity of steam generated, etc. Three design objectives of the maximal feed preheating, the maximum quantity of steam generated and the minimum annual cost are taken for energy-use optimization of the unit. A practical delayed coker is analyzed and optimized to illustrate the performance of the design approach so as to make the feed temperature of the coking furnace T_{feed} maximal through integrating the energy-use improvement of the main fractionator. The results obtained demonstrate that the HEN of a delayed coker can be improved feasibly in accordance with the requirements of the whole unit.

Acknowledgement

The authors gratefully acknowledge the financial support from the National Natural Science Foundation of China (No. 20906016, 21076233) and the Major Science and Technology R&D Program of Guangdong Province (No. 2010A080801003).

References

Q. L. Chen, Q. H. Yin, S. P. Wang, B. Hua, 2004, Energy-use analysis and improvement of delayed coking units, Energy, 29, 12-15, 2225-2237.

F. Rodriguez-Reinoso, P. Santana, E. R. Palazon, M. -A. Diez, H. Marsh, 1998, Delayed coking: industrial and laboratory aspects, Carbon, 36, 1, 105-116.

M. Morar, P. S. Agachi, 2010, Review: Important contributions in development and improvement of the heat integration techniques, Comput. Chem. Eng., 34, 1171-1179.

V. Plesu, G. Bumbac, P. Lancu, I. Ivanescu, D. C. Popescu, 2003, Thermal coupling between crude distillation and delayed coking units, Appl. Therm. Eng., 23, 1857-1869.

B. J. Zhang, X. L. Luo, Q. L. Chen, C. W. Hui, 2011, Heat integration by multiple hot discharges/feeds between plants, Ind. Eng. Chem. Res., 50, 18, 10744-10754.

B. A. Al-Riyami, J. Klemes, S. Perry, 2007, Heat integration retrofit analysis of a heat exchanger network of a fluid catalytic cracking plant, Appl. Therm. Eng., 21, 13-14, 1449-1487.

J. M. Douglas, 1988, Conceptual design of Chemical process, McGrawHill, New York.

Nomenclature

CS--cost for lower *T* (≤200 ℃) heat exchanges

SS--cost for lower *T* (⩾ 200 ℃) heat exchanges

F--heat capacity flowrate

α-- an upper bound for heat exchange

ΔT_{min}--minimum approach temperature

Subscripts

all--total pump-around heat removal

d--diesel pump-around heat removal

j--hot stream, set $J=\{j \mid 1,2,3,4\}$

k--index for stage, and temperature location, set $K=\{k \mid 1,2,3,4,5,6,7\}$

t--top pump-around heat removal

s--steams

w--cooling water

Positive, continuous variables

d_{tjk}--temperature approach for (j, $=k$) at the hot end

$t_{j,k}$ --temperature of stream j at the hot end of k

d_{tcuj}-- temperature approach for (j, *cu*)

t_{fj} -- temperature of stream feed at the hot end heat exchanging with stream j

q_{jk} -- heat exchange between (j, *feed*) in k

q_{jcu} --heat exchange between (j, *cu*) in k

Binary variables

Z_j--existence of unit for march(j,f) in stage k

Z_{cuj}--existence of unit for march(j,*cu*)

I.A. Karimi and Rajagopalan Srinivasan (Editors), Proceedings of the 11th International Symposium on Process Systems Engineering, 15-19 July 2012, Singapore.

On an Operational Model and a Computer Support Environment for Batch Plants Based on Adaptive Scheduling –Application of simulators to obtain initial conditions for rescheduling–

Hisaaki Yamaba, Shigeyuki Tomita

University of Miyazaki, 1-1, Gakuen Kibanadai-nishi, Miyazaki, Japan

Abstract

Scheduling is one of the most important features in production management. Production systems are operated according to schedules in order to minimize production costs and complete the production of given demands by their due dates. However, production cannot be often carried out as scheduled because of problems or accidents such as reactor malfunctions and tardiness of chemical reactions. Even in such situations, production activities must continue while modifying the original schedules. In the present study, an operational model of a production system, which is used to continue production under uncertainties, was considered. A series of experiments was carried out using a computer-aided environment developed based on an object-oriented approach in order to evaluate the performance of the proposed method for various parameters.

Keywords: Batch plant, rescheduling, object-oriented

1. Introduction

In order to minimize production costs and complete production on time, production systems are operated according to a schedule. However, production cannot be carried out on a given schedule because of problems or accidents such as malfunctioning reactors or tardiness of chemical reactions. Even under such circumstances, production activities must continue while modifying the original schedule. At present, such modifications of schedules are carried out based on human experience. Therefore, a rational manner of dealing with problems and accidents is needed.

In the present study, an operational model of a production system that continues production activities under production environments with various uncertainties is considered. Concretely, the following features are of interest:

1. How to determine whether rescheduling should be performed.
2. How to determine which jobs should be rescheduled and which jobs should be processed according to the original schedule.
3. How to process jobs that should be processed according to the original schedule, which no longer works well.

These factors should be fixed depending on the configurations of target plants. In order to determine the three factors described above, a simulation-based approach was adopted. A computer-aided environment that consists of simulators and schedulers is developed based on an object-oriented approach. In the present study, a series of experiments is carried out using this environment in order to evaluate the performance of the proposed method for various parameters.

2. Basic Concept of the Operational Model

Figure 1 shows the basic concept of the operational model proposed herein.
(1) First, a scheduler makes an original schedule for a given demand. The plant starts production as scheduled. However, when it becomes difficult to continue production under the current schedule because of problems or accidents, rescheduling is carried out and the production is shifted from the original schedule to another schedule after a given switching time.
(2) In order to make out a modified schedule, the progress of production in the target time window is needed as the initial condition for the rescheduling. In order to obtain the information, a plant simulation system is introduced. The simulator works according to the conditions of the plant with the operational policy of the plant.
(3) The simulation results (e.g., the working conditions of the plant) are fed to the scheduler of the support environment. Using the information as the initial condition, the scheduler makes out a modified schedule that starts from the switching time point.
(4) By switching to the new modified schedule at the switching time, the target plant can continue seamless production.

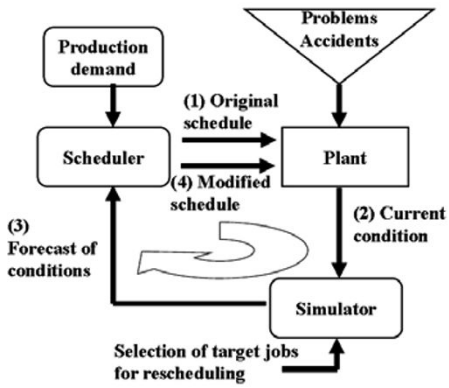

Figure 1. Concept of the proposed support method of production.

3. Class of Target Production System

In the present study, a job refers to a single process in a sequence of processes required for each final product. Production demands are sent to the plant in a periodic fashion. A schedule of demands given in the *i-1*th period is made in the *i*th period, and the demands are processed in the *i+1*th period. The productive capacity of the target plant is assumed to be balanced with the production load of given demands. Therefore, a schedule of the *i*th period has to be created under the condition that some jobs in the schedule of the *i-1*th period are pushed to the *i*th period. The concept of adaptive scheduling (Tomita 1991a) was proposed in order to cope with such production systems by iterative scheduling.

4. Operational Method

In the present study, as an example of a concrete problem, the tardiness of the operation is considered.
The basic concept of the proposed method is shown in Figure 2. In the Gantt charts for each machine, the lower rows represent schedules, and upper rows represent the corresponding progress.

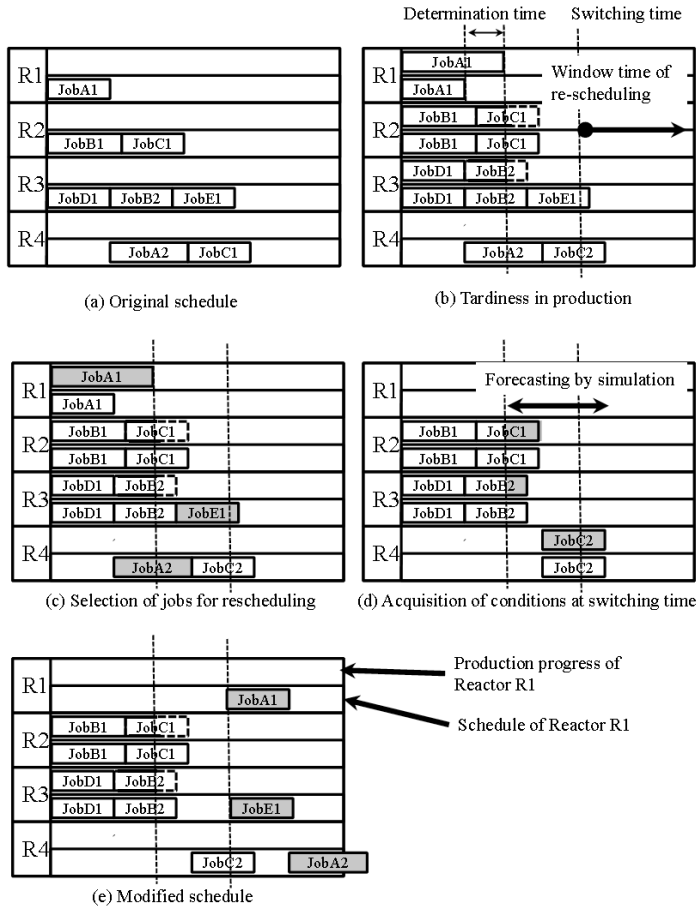

Figure 2. Proposed operational method.

1. First, the original schedule is given (Figure 2(a)).
2. When the progress of production is not in agreement with the original schedule because of problems or accidents, the plant operator must decide whether to modify the current schedule. This determination is made when a job does not end within a fixed time from the scheduled end time for the job. This fixed length of time is hereinafter referred to as the determination time (Figure 2(b)).
3. If rescheduling is performed, the switching time, which is the start time of the schedule window of the rescheduling, is first decided. In the present study, the modified schedule will start *n* time units after the determination time (Figure 2(b)).
4. Next, jobs that have not been completed are divided into two groups: jobs that are the target of rescheduling and jobs that are performed according to the current schedule. In the present study, jobs that do not start at the determination time are selected as targets for rescheduling (Figure 2(c)).
5. The jobs in the former group are performed under the policy described later in step 8.
6. A modified schedule is generated for the jobs belonging to the latter group. The target schedule span is from the switching time to the end time of the current production period. In order to create a feasible schedule, the condition of the plant in the target scheduling span must be given. A plant simulator is used to forecast the condition. (Figure 2(d)).

7. After the switching time, the plant is operated according to the new schedule (Figure 2(e)).
8. During the period from the decision time to the switching time, production is carried out according to the original schedule. However, the start time of each job is delayed according to the tardiness of the schedule. In particular, in order to synchronize the time to transfer materials between an upper reactor and a lower reactor, an additional waiting operation must be included in the process flow

The appropriate determination time and time span from the determination time to the switching time are considered to depend on the features of each production environment and each plant. In the present study, these times are decided through simulation experiments. In the next section, the performances of several candidate determination times are investigated under various production environments.

5. Experiments

The operation support environment for production systems that consists of schedulers Bpos (Tomita 1991b) and simulators was developed based on the above-described operation model using an object-oriented approach (Yamaba 2008). A series of experiments was carried out in order to evaluate the influence of the above-mentioned operational parameters on the performance of a model plant.

5.1. Conditions

The production period of the model batch plant was one day. A single experiment involved a series of seven-day simulations. The switching time was set to 30 time units after the time at which it was decided to perform rescheduling. The purpose of the experiments is to investigate the influence of the length of the determination time on the productive performance of a plant. Four delay generation environments were introduced for three candidate determination times. The results were evaluated as the total delay time of jobs that were not completed on the scheduled day. One delay was generated in one day. A delayed operation was selected at random. The duration of the delay was calculated according to the regular distributions listed in Table 1. The three candidate determination times were 50 time units, 100 time units, and never rescheduling.

Table 1. Delay generation environments

	Average	Distribution
1	30	50
2	80	50
3	100	50
4	200	50

5.2. Experimental Results

The experiments were carried out for 15 combinations of the three determination times and the four delay generation environments. Seven-day simulations were repeated five times for each set of 15 experiments. Figure 3 plots the average total delay times obtained in the experiments. In the experiments using delay generation environments 3 and 4 (respective average delay times: 100 and 200 time units), the shortest delay time was obtained when the decision time was 50 time units. Under the condition in which rescheduling was not performed, the total delay time was the longest, which means that rescheduling was effective in delay generation environments that generate longer delays. On the other hand, in environment 1 (average delay time: 30 time units), no job was delayed under the condition in which rescheduling was not executed. Moreover, some jobs were delayed when the decision time was set to 50 or 100 time units.

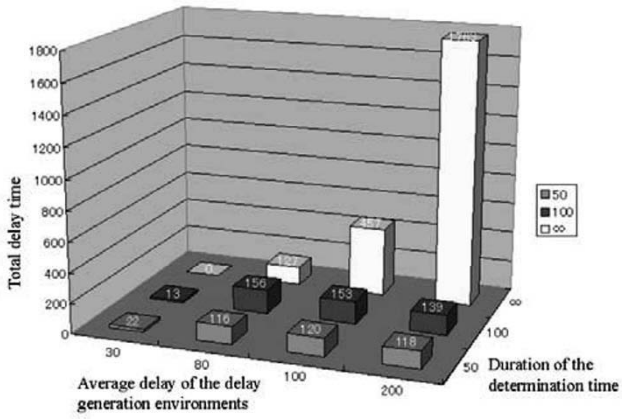

Figure 3. Experimental results.

In general, some of the jobs selected for rescheduling may have been scheduled to be processed between the determination time and the switching time in the original schedule. Since the new start times of such jobs must be postponed until after the switching time in the modified schedule, the modified schedule tends to be tight, which means that the rescheduling results in lower performance when the expected average delay time is shorter. However, for the case in which the expected delay time is longer, earlier determination of rescheduling reduces the delay in production. The boundary of the average delay time to determine whether rescheduling should be performed is indicated to be 80 time units under the conditions of the experiments.
Since the validity of knowledge obtained based on these results is limited to the conditions used in these experiments, the support environment was confirmed to be useful for obtaining the parameters of the proposed management method.

6. Conclusions

In order to manage a batch type chemical plant under uncertain conditions, a management support method was introduced along with a computer-based support system, which consists of simulators and schedulers. A series of experiments was carried out using this environment in order to evaluate the performance of the proposed method for various parameters. The experimental results demonstrate the effectiveness of this environment.

References

S. Tomita, H. Yamaba, E. O'shima, 1991a, On an Intelligent Scheduling System for a Parallel Distributed Process of Multi-Product - An attempt of developing an 'Adaptive scheduling' system -, Proceeding of 4th International Symposium on Process Systems Engineering (PSE '91), II, 19.1-19.15.

S. Tomita, H. Yamaba, E. O'shima, 1991b, Development of an intelligent Scheduling System for Managing Multipurpose Chemical Batch Plant - An attempt to exploit heuristic rules for developing an 'Adaptive' scheduling system - (In Japanese), Kagaku Kogaku Ronbunshu, 17, 740-749.

H. Yamaba, M. Hirosaki, S. Tomita, 2008, An Operational Model and a Computer Support Environment for Batch Plants Based on Adaptive Scheduling, Proceedings of 12th International Conference on Knowledge-Based and Intelligent Information and Engineering Systems, III, 33-40.

I.A. Karimi and Rajagopalan Srinivasan (Editors), Proceedings of the 11th International Symposium on Process Systems Engineering, 15-19 July 2012, Singapore.

A Comparison Study of Adjoint-Based Gradient Search Technique and Mathematical Programming for Optimal Well-Placement

R.Y. Toh[1], M.S. Tavallali[1], W.X. Leow[1], I.A. Karimi[1*]

[1]*Department of Chemical & Biomolecular Engineering*
National University of Singapore
4 Engineering Drive 4, Singapore 117576

Abstract

Optimal well placement in petroleum fields has an immense techno-economical importance. It is vital to choose the correct mathematical tool to address this important problem. Therefore, in this study we compare the adjoint-based gradient search method with a mathematical programming approach in terms of the efficiency and solution quality when addressing well placement problems.

Keywords: Adjoint-Based Gradient Search Technique, Mathematical Programming, Optimal Well Placement

1. Introduction and Previous Research

Worldwide energy demand has been steadily increasing. In order to meet energy challenges of the future, optimal recovery from all marginal, mature and any possible new hydrocarbon fields is necessary. Well placement can clearly affect the efficiency of petroleum recovery and is therefore of utmost importance.

Multiphase flow in porous media of reservoirs is represented via a set of coupled PDEs. The numerical simulators use its discrete format due to their limitations. Since wells are presented only in the cells that accommodate them (and not other grids), the problem becomes non-differentiable with respect to well location. Hence, optimal well placement is often treated as a discrete problem which will render the solutions computationally very expensive. It is therefore important to choose the right mathematical tool to solve this complicated problem.

Evolutionary methods, as the first option, are simple to use but yet are very time-consuming (Yeten et al, 2003). Gradient based approach as the second option, requires converting the problem into their compatible format and subsequently the adjoint gradient method can efficiently provide gradient information (refer to Jansen (2011)). Researchers such as Zandvliet et al. (2008) and Forouzanfar (2010) have employed pseudo well approach for this purpose. Finally, mathematical programming as the third option, has not considered the dynamic behavior of the system in details. Recently, Tavallali et al (2011) and Leow et al (2012) have modeled the dynamic well placement problem as a mixed integer nonlinear programming problem and modified the outer approximation, with equality relaxation and augmented penalty (OA/ER/AP) algorithm to solve the model.

Cleary there are both advantages and disadvantages associated with using any of above methods. This paper uses the mathematical model of Leow et al. (2012) as the

[1*] Corresponding author: Tel.: +65 6516-6359, Fax: +65 6779-1936, Email – cheiak@nus.edu.sg

main platform and solves that by both OA/ER/AP and (after customizing the model) by the pseudo-well approach of Zandvliet et al. (2008). The remaining parts of this paper are organized as follows: we start with the problem definition and formulation; we present a case study and finally provide a description of both algorithms and qualitatively compare both approaches.

2. Problem Definition

Given an oil reservoir with existing wells, the goal is to expand the production by infill drilling of new wells. Relevant petro-physical data and economical data such as projected demand curve, drilling costs, discount rate, as well as operational data such as water-cut limits, production and injection capacity expansion plan for surface facilities are also provided beforehand. It is assumed that the reservoir is a horizontal 2D plane with water and oil phases and the main driving mechanism is water-drive injection.

The objective of the mathematical programming model is to maximize the net present value (NPV) of oil production over a fixed planning horizon through the determination of new well locations.

3. Formulation

As per Tavallali et al. (2011) and Leow et al. (2012) we include the equations describing multiphase flow in a reservoir with spatial and implicit time discretization. These include water and oil mass balances and mobilities in equality form. A series of inequalities provide more information regarding the physical and operational relations and they include, ratio of water and oil flow rates, pipe flow relation for producers and injectors, water cut, demand and capacity constraints. For more information refer to the aforementioned papers. We use their MINLP model for the mathematical programming approach and for the gradient based search we slightly customize that by removing the binary variables and defining well set. A concise representation of that is as follows:

Sets:

t : Discrete time domain; n: Discrete spatial domain; W: All wells

Variables:

x_n^t : State variables (Pressure, saturation); m_n^t : Intermediate variables (Phase mobility)

u_n^t : Control variables (Total well flow rate, +ive for producer and –ive for injectors)

q_n^t : Output variables (Oil flow rate)

Objective Function: $\min \sum_{t\geq 2}\sum_{n\in W} J_n^t(u_n^t, q_n^t)$ NPV (1)

Subject to:

System Equations: $g_n^t(u_n^t, q_n^t, x_n^t, x_n^{t-1}, m_n^t) = 0;$ Mass balance (2)

Initial Conditions: $x_n^1 = \breve{x}_n^1$ Initial state (3)

Intermediate Constraints: $c_n^t(x_n^t, m_n^t) = 0$ Mobility (4)

Output Constraints: $h_{n\in W}^t(u_n^t, x_n^t, q_n^t, m_n^t) \leq 0$ Pipe flow (5)

Other Inequality Constraints: $d_n^t(u_n^t, q_n^t, m_n^t) \leq 0$ Water Cut, etc (6)

4. Algorithm

4.1. Gradient based search

Figure 1-a presents this algorithm. Given a set of proposed injectors and producers (an initial guess), Zandvliet et al. (2008) introduced a set of pseudo-wells with negligible flow rate into the eight adjacent grid-blocks of each proposed well. Their flow rates should have minimal impact on reservoir states. The gradient of the objective function over the simulation time with respect to flow rate of each pseudo-well can be determined via adjoint gradient calculation approach. Each potential well would then move into the pseudo-well grid-block with the largest value among the eight adjacent cells. This process is repeated for the new potential well location until selected wells alternate between two different positions. There are no binary variables in this method.

To use the adjoint gradient calculation method, Euler-Lagrange function is constructed with all constraints being adjoined to the objective function. A forward simulation (reservoir production simulation) provides the value of gradient of each constraint with respect to different variables and a backward LP simulation calculates the Lagrangian multipliers and the targeted derivative. For more information about this method, refer to the review paper of Jansen (2011).

4.2. Mathematical Programming and Outer approximation

Figure 1-b shows this approach. As before, the master MILP problem is responsible for the search and the primal NLP problem evaluates the proposed solution. However, method of Tavallali et al (2011) adds few steps to the outer approximation, with equality relaxation and augmented penalty (OA/ER/AP) algorithm. Firstly, considering the dynamic nature of the problem, they solve the primal problem sequentially by marching into the time domain. Secondly, before terminating the search procedure, they perform series of local searches to partially check the local optimality.

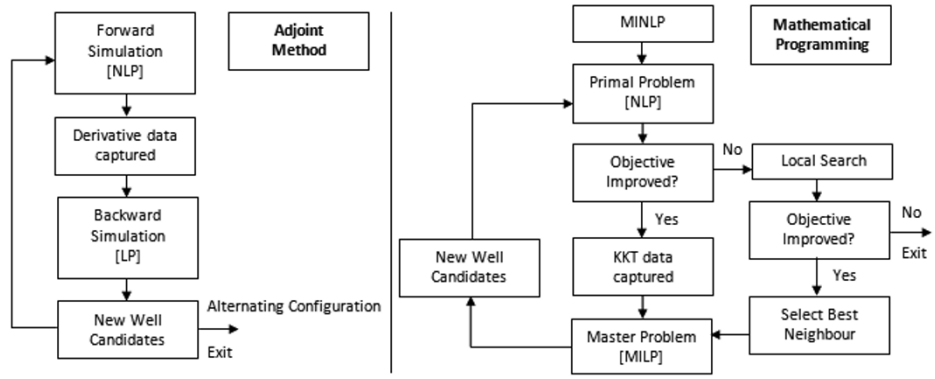

Figure 1-a. Adjoint-based technique flowchart Figure 1-b. Mathematical Programming flowchart

5. Case Study

Considering a 20x20 reservoir with 3 existing producers and 2 existing injectors labeled as “PRO” and “INJ” in figure 2. Computation was performed in an identical manner as described by Leow (2012) with the addition of the CPLEX solver for the backward simulation. The goal is to locate the best drilling site for a new producer in this oil field. To do the gradient dependant search, we had to develop our own in-house adjoint gradient evaluator tool box that can consider the inequality constraints. For this purpose we used the value of slack variables and only considered the binding inequalities.

A brute force search was conducted by introducing new producers at every possible location with the exclusion of the existing wells; the heat map of Figure 2 denotes its outcome. Both mathematical programming and adjoint-based gradient search technique approaches were utilized by identical initial guesses and in the diagram above we present 2 sets of them. The numbered configurations represent the steps that the gradient search method takes from an initial guess "1"; termination involves alternating configurations represented by the curved arrows. Additionally, the straight black arrows denote the initial and final well location as determined by the OA/ER/AP algorithm from the same initial guesses. Convergence criteria as described by Zandlivet et al. (2008) involved alternating between two well configurations. This was shown to be the case for the majority of our tests (the pair of curved arrows). However, there are instances where cycling would occur. The unpaired curved arrows denote such an occurrence. For example the initial guess at [4,11] would result in a series of new well candidates that would eventually return [4,11] and thus repeatedly cycle. Cycling can be easily dealt with by storing all previous well candidates and terminating if any candidate is selected twice. With suitable initial guesses both methods converge to their global optimal location as determined by the brute force search.

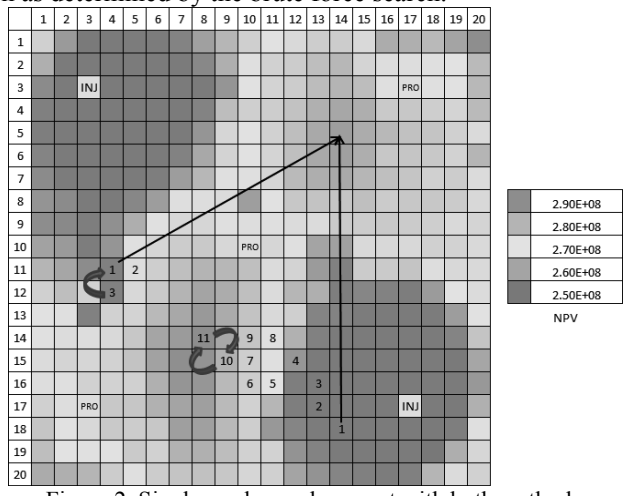

Figure 2. Single producer placement with both methods

To our knowledge there is no comparison of these two approaches, specifically for optimal well placement problem in literature. Therefore, based on both available literature and mainly our own experience, we provide a comparison both approaches:

Table 1. Comparison between Mathematical Programming and Adjoint-Based Gradient Search Technique for well placement problem

	Mathematical Programming	**Gradient Method**
Problem type	Primal – NLP	Forward – NLP
	Master – MILP	Backward – LP
Preliminary preparation	MILP model preparation	Backward LP preparation
Inequality handling	Simple	Might be difficult
Information collected from Reservoir Sim.	Values of all variables and Lagrangian multipliers	Values of all variables (and slack variables if required)

Search engine	Master MILP section	LP backward and steepest ascent method
Reducing number of wells	By setting the well binary variable to zero	By merging two or more wells into a same cell
Optimum no. of wells	Can check, but maximum number should be specified	Can check, but maximum number should be specified
Well configuration constraints	The background MINLP model handles implicitly	The algorithm should intervene during iterations
Initial guess	Important	Very important
Objective value improvement	Is assured	Not guaranteed
Cycling	Integer-cut prevents that	Can happen
Termination criteria	Heuristic, deterioration of objective value	Alternating or cycling heuristic
Search time duration	Longer, keeps increasing per each iteration	Shorter, may decrease per iteration as two well merge

6. Conclusion

In this paper we provided a qualitative comparison between mathematical programming and an adjoint-based gradient search method for optimal well placement. Both approaches are currently at research stage and require improvement to be able to handle uncertain and large size problems. However, in a general comparison with evolutionary search methods, they are faster and might be able to handle more detailed problem such as scheduling the drilling order, and simultaneous well placement and well optimal control.

7. Acknowledgements

We would like to extend our gratitude to Schlumberger for the provision of the VFPi software to aid us in our work.

References

Forouzanfar Fahim**,** Gaoming Li & A.C. Reynolds (2010): A two-stage well placement optimization method based on adjoint gradient , 2010 SPE Annual Technical Conference and Exhibition , Florence, Italy

Jansen, J.D. (2011). "Adjoint-based optimization of multi-phase flow through porous media – A review." Computers & Fluids **46** (1): 40-51

Leow, W.X., Tavallali, M.S., Karimi, I.A., & Teo, K.M. (2012). Simultaneous Optimal Placement of Injector and Producer Wells Using Mathematical Programming. 11th International Symposium on Process Systems Engineering, Singapore.

Tavallali, M.S., Karimi, I.A., & Teo, K.M. (2011). Dynamic Optimal Well Placement In Oil Reservoirs. Annual Meeting of AICHE. Minneapolis, USA.

Zandvliet, M.J., Handels, M., van Essen, G.M., Brouwer, D.R. & Jansen, J.D. (2008). Adjoint-based well-placement optimization under production constraints. SPE Journal **13** (4): 392-399.

Yeten B., Durlofsky, L.J., & Aziz, K. (2003). Optimization of Nonconventional Well Type, Location, and Trajectory. SPE Journal **8** (3): 200-210.

I.A. Karimi and Rajagopalan Srinivasan (Editors), Proceedings of the 11th International Symposium on Process Systems Engineering, 15-19 July 2012, Singapore.

Minimization of storage requirement in a batch process using pinch analysis

Nitin Dutt Chaturvedi* and Santanu Bandyopadhyay

Department of Energy Science and Engineering, Indian Institute of Technology Bombay, Powai, Mumbai 400 076, INDIA
**corresponding author's E-mail: nitin.chaturvedi@iitb.ac.in*

Abstract

In this paper an algebraic algorithm, based on the concepts of pinch analysis, is proposed to determine the minimum storage requirement for a batch process, while satisfying the minimum resource requirement. The proposed algorithm can be applied to any fixed flow rate and fixed scheduled batch process involving single quality. The proposed algorithm is proved for optimality on basis of rigorous mathematical arguments and also provides physical insight to the problem.

Keywords: batch process; pinch analysis; storage optimization; resource minimization.

1. Introduction

In recent years, significant research efforts are directed to minimize resources (such as: energy, freshwater, cooling water, hydrogen, raw materials, etc.) in batch processes. Most of the work is directed towards water minimization (Gouws et al., 2010). The methods are often categorized as mathematical based optimization (Almató et al.,1999; Majozi, 2005; Chen et al., 2010) and pinch based optimization (Wang and Smith, 1995; Kim, 2011). Recently, a hybrid approach, known as automated targeting technique, has been developed by Foo (2010). Although networking is considered as more important than targeting part but still in batch process it is less focused. Optimizing the storage requirement is also an important aspect considering network complexity, space limitation as well as capital investment. In this paper a mathematically rigorous algorithm is proposed to determine the minimum storage requirement to satisfy the minimum resource requirement for a single batch process The methodology is based on concepts of pinch analysis so provides physical insight understanding of problem.

2. Problem definition

A general problem to determine the minimum storage requirement, for a batch process satisfying the minimum resource requirement, may be given as follows: (i) A set of internal demands is given. Each demand requires a defined flow at a given maximum allowable quality for a fixed interval of time. (ii) A set of internal sources is also given. Each source produces a fixed flow at a given quality for a fixed interval of time, which can be used in internal demands appearing during or after the availability of source flows. (iii) An external source, called resource, is also available to satisfy the requirement of internal demands, at a given quality (q_{rs}). (iv) The objective is to determine the minimum storage requirement while satisfying the minimum resource requirement.

3. Minimum storage algorithm (MSA)

The following algorithm is proposed to determine the minimum storage requirement

while satisfying the minimum resource requirement.

1. Divide the entire time horizon of batch process into several time intervals (say T_1, T_2, T_3, ..., T_n) considering start and end time of each source and demand.
2. Integrate the sources and demand within each interval to calculate pinch location and waste profile (maximum possible flow available at each source quality after integration) of each interval.
3. Add the waste profile from time interval T_1 as sources to next time interval T_2. Recalculate resource requirement, waste profile, and pinch location (say end pinch location, q_{Pte2}) at the end of interval T_2 .Calculate the storage requirement as the wastes of time interval T_1 utilized in time interval T_2 as follows:
   Storage requirement at given quality level can be calculated using Equation (1).
   $$Storage\ \ requirement = W_T - W_{ie} \quad (1)$$
   W_T is the waste transferred at that quality level from other intervals and W_{ie}, is the net waste generated after the transfer in interval T_i at a given quality level. It may be noted that if $W_T - W_{ie}$ is negative than storage is considered to be zero.
4. Repeat Step 3 and 4 to calculate individual pinch location (q_{PTi}), waste profile at the end of the time interval and the end pinch location (q_{PTei}) for all the subsequent time intervals.
5. Apply the following three rules to reduce the storage requirement:
   Rule 1: Waste transfer is to be carried out directly from interval T_i and T_{i+1} to T_{i+2} for the case where $q_{PT_{i+2}} \geq q_{PT_{i+1}} \geq q_{PTe_i}$, till the overall resource requirement till T_{i+2} is unaffected.
   Rule 2: For the cases where waste transfer only leads to its redistribution into higher and lower qualities but does not affect the resource requirement, then this redistribution is skipped if it does not give any resource reduction on transferring to subsequent time intervals.
   Rule 3: For the cases where, $q_{PTe_{n-l}} \geq q_{PT_{n-l+1}} \geq ..... \geq q_{PT_n}$ any indirect waste-transfer is not required.
6. List out storage requirement at each quality level and its duration. Select the highest value of storage requirement on same quality level having completely different duration of requirement of storage. Sum up individual storage requirements to get total storage requirement.

It may be noted that source composite method (Bandyopadhyay et al., 2006) is used to calculate minimum resource requirement and waste profile.

4. Mathematical proof

Mathematical induction method is used to prove minimum storage algorithm (MSA). For any resource allocation network it is proved by Pillai and Bandyopadhyay (2007), that minimization of the external resource requirement (R) is equivalent to the minimization of the total waste generation (W). Therefore, it is sufficient to minimize the overall waste generation to minimize the overall resource requirement. To calculate the change in waste flow, expression for the minimum waste generation, as derived by Pillai and Bandyopadhyay (2007), is utilized in this paper. However, detailed calculations are not shown for brevity.

A batch process containing only two time intervals (T_1 and T_2) is considered first. Let q_{PT1} and q_{PT2} be the individual pinch qualities respectively, when these time intervals are solved without integration. Let δ amount of flow is transferred (at a quality of q_{si}) from interval T_1 to interval T_2 such that the pinch qualities of both the time intervals

remain same. The changes in overall waste generation for all possible cases are expressed as follows:

$$\Delta W = \begin{cases} 0 & \text{when } q_{si} \geq q_{PTt1}, q_{PT2} \\ \delta \dfrac{q_{PT1} - q_{si}}{q_{PT1} - q_{rs}} & \text{when } q_{PT1} \geq q_{si} \geq q_{PT2} \\ -\delta \dfrac{q_{PT2} - q_{si}}{q_{PT2} - q_{rs}} & \text{when } q_{PT2} \geq q_{si} \geq q_{PT1} \\ \delta(q_{si} - q_{rs}) \dfrac{(q_{PT1} - q_{PT2})}{(q_{PT1} - q_{rs})(q_{PT2} - q_{rs})} & \text{when } q_{PTt1}, q_{PT2} \geq q_{si} \end{cases} \quad (2)$$

It may be concluded that change in waste (ΔW) is negative (implies a reduction in overall waste generation) only when q_{PT1} is less than q_{PT2} which is Rule 3 of MSA.

A batch process containing three time intervals is considered now. There could be two options for transferring the waste: sequentially or directly. In sequential transfer, wastes of interval T_1 are transferred to interval T_2 and then combined wastes at the end of interval T_2 are transferred to interval T_3. In direct transfer, wastes of interval T_1 and T_2 are directly transferred to interval T_3. Let δ_{T1} amount of flow from pinch quality source (q_{PT1}) of interval T_1 and δ_{T2} amount of flow from pinch quality source (q_{PT2}) of interval T_2 are transferred to interval T_3 using both of these options. The change in waste generation, are calculated for sequential (ΔW_S) and direct transfer (ΔW_D) and their differences are summarized as follows:

$$\Delta W_S - \Delta W_D = \begin{cases} 0 & \text{Case 1}: q_{PT3} \geq q_{PT2} \geq q_{PT1} \\ -\delta_{T1} q_{PT1} \left(\dfrac{q_{PT2} - q_{PT3}}{(q_{PT2} - q_{rs}(\,))(q_{PT3} - q_{rs})} \right) & \text{Case 2}: q_{PT2} \geq q_{PT3} \geq q_{PT1} \\ -\delta_{T1} \left(1 - \dfrac{q_{PT2} - q_{PT1}}{q_{PT2} - q_{rs}} \right) & \text{Case 3}: q_{PT2} \geq q_{PT1} \geq q_{PT3} \\ 0 & \text{Case 4}: q_{PT1} \geq q_{PT2} \geq q_{PT3} \end{cases} \quad (3)$$

Therefore, sequential waste transfer always leads to the minimum resource requirement. Cases 1 and 4 bring about Rule 1 and Rule 3 of MSA, respectively. There are two more cases to be considered: Case 5 ($q_{PT1} \geq q_{PT3} \geq q_{PT2}$) and Case 6 ($q_{PT3} \geq q_{PT1} \geq q_{PT2}$). In these cases, there is a possibility of waste profile change without any change in overall waste generation. Let δ_{T1} amount of flow (q_{PT1}) gets distributed in two different sources: a flow δ_u is added to higher quality source (q_u) and δ_l flow is added to lower quality source (q_l). The differences of the waste flows are expressed as follows:

$$\Delta W_S - \Delta W_D = \begin{cases} 0 & \text{Case 5a}: q_u, q_l \leq q_{PT3}, q_{PT3} \geq q_{PT1} \geq q_{PT2} \\ 0 & \text{Case 5b}: q_u, q_l \geq q_{PT3}, q_{PT3} \geq q_{PT1} \geq q_{PT2} \\ -\delta_u \left(\dfrac{q_u - q_{PT3}}{q_{PT3} - q_{rs}} \right) & \text{Case 5c}: q_l \leq q_{PT3} \leq q_u, q_{PT3} \geq q_{PT1} \geq q_{PT2} \\ 0 & \text{Case 6a}: q_u, q_l \leq q_{PT3}, q_{PT1} \geq q_{PT3} \geq q_{PT2} \\ 0 & \text{Case 6b}: q_u, q_l \geq q_{PT3}, q_{PT1} \geq q_{PT3} \geq q_{PT2} \\ -\delta_u \left(\dfrac{q_u - q_{PT3}}{q_{PT3} - q_{rs}} \right) & \text{Case 6c}: q_l \leq q_{PT3} \leq q_u, q_{PT1} \geq q_{PT3} \geq q_{PT2} \end{cases} \quad (4)$$

This signifies that when waste is redistributed across the pinch quality of interval T_3 (q_{PT3}) then sequential transfer leads to more or same reduction in waste as compared to direct transfer. These cases result in Rule 2 of MSA.

The MSA is assumed to be true for a batch process involving 'n' time intervals. Let us consider a batch process with '*n+1*' time intervals. There are two possible cases for $n+1^{\text{th}}$ time interval. For case A ($q_{PTe_n} \geq q_{PT_{n+1}}$) by our assumption, MSA guarantees the minimum storage requirement to satisfy resource requirement up to time interval T_n. This reduces our problem to an equivalent batch process involving only two time

intervals T_n and T_{n+1}. So as discussed in earlier section there is no reduction in resource requirement via waste transfer which is included in MSA via Rule 3. For case B ($q_{PTe_n} \le q_{PT_{n+1}}$), the role of the time interval prior to n^{th} time interval have to be investigated. For $n\text{-}1^{th}$ time interval again there could be two possible cases, for the case $q_{PTe_{n-1}} \le q_{PT_n}$, where the problem reduces to case 1 of batch process containing three intervals and such cases are included in Rule 1 of MSA. For the other case $q_{PTe_{n-1}} \ge q_{PT_n}$ the problem essentially reduces to case 5 and case 6 of the batch process having three intervals which are included in Rule 2. This proves the result.

5. Illustrative example: batch water network

Limiting water data for this example are given in Table 1. All the sources and demands are segregated into six time intervals T_1,T_2, T_3,T_4, T_5 and T_6 (0-1h, 1-2h, 2-3h, 3-4h, 4-5h and 5-6h) based on their start and end time points. Initially sources and demands lying within each time interval are integrated and individual pinch location (q_{PTi}) and waste generation (W_i) are calculated. Then, resource requirement and waste generation are for each interval is recalculated considering waste up to preceding interval as additional sources (Table 2) and storage requirement is calculated as 72.83 t using Equation (1).

Table 1: Limiting water data for the example

Source	Flow rate (t/h)	Conc. (ppm)	Duration (h)	Demand	Flow rate (t/h)	Conc. (ppm)	Duration (h)
S1	5	25	0.0-1.0	D1	10	0	0.0-1.0
S2	5	15	0.0-1.0	D2	40	27.5	1.0-2.0
S3	51.34	37.5	1.0-2.0	D3	5	15	1.0-3.0
S4	20	93.75	2.0-3.0	D4	5	25	2.0-3.0
S5	12.5	150	3.0-4.0	D5	100	84.375	3.0-4.0
S6	90	75	3.0-4.0	D6	100	33.75	3.0-4.0
S7	12.5	60	3.0-5.0	D7	35	10	4.0-5.0
S8	90	30	3.0-4.0	D8	20	5	5.0-6.0
S9	50	10	5.0-6.0				

Table 2: Storage calculation using sequential transfer

C (ppm)	W_1	W_2	W_3	W_4	W_5	W_6	W_1	W_{2e}	W_{3e}	W_{4e}	W_{5e}	W_{6e}
150	0	0	0	0	0	0	0	0	0	5	5	5
93.75	0	0	17.87	0	0	0	0	0	20	0	0	0
84.375	0	0	0	0	0	0	0	0	0	0	0	0
75	0	0	0	2.5	0	0	0	0	0	17.5	17.5	17.5
60	0	0	0	0	6.67	0	0	0	0	5	17.5	17.5
37.5	0	20	0	0	0	0	0	25.33	20	0	0	0
30	0	0	0	2.5	0	0	0	0	0	17.5	0	0
25	5	0	0	0	0	0	5	0	0	0	0	0
15	5	0	0	0	0	0	5	0	0	0	0	0
10	0	0	0	0	0	40	0	0	0	0	0	40
Cum. FW(t)	-	-	-	-	-	-	10	19	23.7	23.7	45.8	55.8
Storage								10	5.33	40	17	**Tot. 72.8**

Rule 1 ($q_{PTe1} \le q_{PT2} \le q_{PT3}$) of MSA is applicable to first three intervals (step 6). Hence, individual waste generation of interval T_1 and T_2 can be transferred directly to the interval T_3 instead of sequential supply from T_1 to T_2 and then to T_3 to reduce the storage requirement. Note that the cumulative resource requirement up to interval T_3 is unaffected while this transfer. Total 40 t of waste is generated (20 t at each 37.5ppm

and 93.75 ppm) at the end of third time interval. It can be observed from Table 2 that both wastes get redistributed when transferred to fourth interval without affecting resource requirement. But according to Rule 2 of MSA the transfer of 20 t at 93.75 ppm is not required as its distribution does not affect the overall resource requirement when transferred subsequent interval while skipping the waste redistribution of other one gives a penalty of 1.83 ton in resource requirement. The pinch at the end of time interval T_5 is higher than the pinch location of interval T_6. Hence, according to Rule 3 of MSA waste transfer from interval T_5 to T_6 is not required. Therefore, minimum 47.5 t of storage is required to satisfy the minimum resource requirement. (see Table 3).

Table 3: Storage calculation using MSA

C(ppm)	W_1	W_2	W_{3e2}	W_{4e2}	W_{5e2}	W_{6e2}
93.75	0	0	***20***	***20***	***20***	20
84.375	0	0	0	0	0	0
75	0	0	0	2.5	2.5	2.5
60	0	0	0	5	17.5	17.5
37.5	0	20	20	0	0	0
30	0	0	0	17.5	0	0
25	5	0	0	0	0	0
15	5	0	0	0	0	0
10	0	0	0	0	0	40
Cum FW	10	23.7	23.7	23.7	45.8	55.8
storage			10	20	17.5	**Tot. 47.5**

6. Conclusion

An algorithm is proposed to determine minimum storage requirement while satisfying targeted minimum resource requirement for a fixed flow rate and fixed scheduled batch process with single quality. The algorithm based on pinch analysis and proved rigorously using mathematical results therefore, guarantees the optimum solution. The methodology is applicable when single batch operation is carried out and cannot be applied when operation is carried out in cyclic mode. Such aspect is addressed as future work.

References

Almató, M.; Espuña, A; Puigjaner L. Optimisation of water use in batchprocess industries. Computers and Chemical Engineering, 1999 23, 1427-1437.

Bandyopadhyay, S.; Ghanekar, M.D.; Pillai, H.K. Process water management. Ind Eng Chem Res 2006 45, 5287-5297.

Chen, C.L; Lee, J.Y.; Ng, D.K.S.; Foo, D.C.Y. A unified model of property integration for batch and continuous processes. AIChE J. 2010 56, 1845-1858..

Foo, D.C.Y. Automated targeting for batch process integration. Ind. Eng. Chem. Res. 2010 49 (20), 9899-9916.

Gouws, J.F.; Majozi, T; Foo, D.C.Y.; Chen, C.L; Lee, J.Y. Water Minimization Techniques for Batch Processes, Ind Eng Chem Res 2010 49, 8877-8893.

Kim, J.K. Design of discontinuous water using systems with a graphical method. Chemical Engineering Journal 2011 172 799– 810.

Majozi, T. Wastewater minimization using central reusable storage in batch plants. Comput. Chem. Eng. 2005 29, 1631–1646.

Pillai, H.K.; Bandyopadhyay, S. A rigorous targeting algorithm for resource allocation networks. Chem. Eng. Sci. 2007 62, 6212–6221

Wang, Y.P., Smith, R. Time pinch analysis. Transaction of the Institute of Chemical Engineers 1995 73 Part A, 905—914.

I.A. Karimi and Rajagopalan Srinivasan (Editors), Proceedings of the 11th International Symposium on Process Systems Engineering, 15-19 July 2012, Singapore.

Targeting Minimum Heat Transfer Fluid Flow for Multiple Heat Demands

Mukund H. Bade* and Santanu Bandyopadhyay

Department of Energy Science and Engineering, Indian Institute of Technology Bombay, Powai, Mumbai 400 076, INDIA
**corresponding author's E-mail: mukundbade@gmail.com*

Abstract

In this paper, an algorithmic procedure, called resource targeting algorithm (RTA), is proposed to target the minimum flow rate of heat transfer fluid (HTF) used to supply heat from a single heater to multiple heat demands. The proposed methodology is based on the principles of pinch analysis. The applicability of RTA is demonstrated through an illustrative example.

Keywords: Pinch analysis; Targeting; Heat transfer fluid; Indirect heating

1. Introduction

Heat transfer fluid (HTF) is primarily used as an intermediate fluid to transfer heat from a heat source to other heat demands (or cold streams). Single heater can provide heat to any number of cold streams through HTF. The HTF is recirculating fluid that transfers heat through heat exchangers to cold streams and returns to the heat source (heater). Selection of HTF is based on the type of industrial applications, stable temperature range for safe operation and life of the HTF (Guffey 1997; Krishanan, 2005). Mckechnie (1927) proposed the design and manufacturing guidelines for HTF system. Design and operating problems of HTF system have been the main attention of manufacturers and process engineers. However, research related to HTF focused on individual components and not on the overall system. Traditionally, heat exchangers are arranged in parallel and hence, the inlet temperature of HTF is same in all the exchangers (Stoecker, 1989). However, such a parallel arrangement of heat exchangers need not guarantee the minimum flow rate of the circulating HTF. Determination of the minimum circulating HTF flow rate is important as the capital cost of the HTF can be reduced significantly. Use of HTF for process heating application may reduce number of fired heaters (Varghese and Bandyopadhyay, 2012). In this paper, an algorithmic methodology, called resource targeting algorithm (RTA), is proposed to target the minimum HTF flow rate to supply heat from single heater to multiple heat demands.

2. Minimum HTF flow rate targeting

The methodology to target the minimum HTF flow rate is analogous to the methodologies for analyzing cooling water system (Kim and Smith, 2001) and water management systems (Wang and Smith, 1994). Similar to cooling duties (Kim and Smith, 2001), all heat demands do not require HTF to supply at maximum stable temperature of HTF. This allows to change the heat exchanger network from parallel to

a series-parallel arrangement in most cases. A series-parallel arrangement of heat exchangers allows reuse of HTF so that the circulation flow rate of HTF can be reduced significantly. Sahu and Bandyopadhyay (2010) proposed an energy recovery algorithm (ERA) to target minimum hot and cold utilities requirement for heat integrated water network problems where the effects of contaminants can be neglected. ERA is suitably modified in this paper to target the minimum flow rate of HTF.

Capacity rate of HTF is the product of mass flow rate and specific heat at constant pressure. In this paper, specific heat of HTF is assumed constant and thus, minimizing mass flow rate is equivalent to minimizing capacity rate of HTF. Minimum temperatures of HTF for each process stream are determined by adding minimum approach temperature ($\Delta T_{\min}$) to the respective temperatures of cold fluids.

Steps of the proposed RTA are given as follows:

Step 1: Convert all cold streams temperatures (T_i) to minimum temperature for HTF by adding suitable minimum approach temperature ($\Delta T_{\min}$).

Step 2: Tabulate temperature of all the streams, including the maximum stable temperature of HTF, in decreasing order in the first column. If particular temperature occurs more than once, the same need not to be repeated. Without loss of generality, it can be said that a temperature for i^{th} row is denoted as T_i such that

$$T_1 > T_2 > \cdots > T_i > \cdots > T_n \tag{1}$$

Typically, T_1 represents the maximum stable temperature of the HTF (T_{rs}). The HTF is heated up to this temperature in the heater.

Step 3: Tabulate net capacity rates (i.e., product of mass flow rate and specific heat) in the second column. Consider capacity rate of inlet stream as negative and outlet stream as positive. As the HTF capacity rate is not known a priori, capacity rate for T_1 is assigned as zero in the second column. For i^{th} row, net capacity rate ($C_{i\text{Net}}$) at T_i may be expressed as:

$$C_{i\text{Net}} = \sum C_{\text{in}T_i} + \sum C_{\text{out}T_i} \tag{2}$$

Step 4: Tabulate the cumulative capacity flow rates in the third column. Summation of net capacity flow rates for all previous rows $(C_{Ti} = \sum_{l=1}^{i} C_{l\text{Net}})$ denotes the cumulative capacity flow rate for i^{th} row. Last entry in this column gives zero, as mass flow rates are conserved and specific heats are assumed constant in this algorithm.

Step 5: First entry in the fourth column is assigned zero. For all subsequent rows in the fourth column, heat load (Q_i) for temperature interval (i, i-1) can be calculated using Equation 3.

$$Q_i = \begin{cases} 0 & for \quad i = 1 \\ (T_i - T_{i-1}) \sum_{l=1}^{i-1} C_{l\text{Net}} & for \quad \text{i} > 1 \end{cases} \tag{3}$$

Step 6: Cumulative heat loads are addition of heat loads for all previous rows $\left(\sum_{l \le i} Q_l\right)$ and tabulated in the fifth column. Using Equation 3, cumulative heat load till i^{th} row may be expressed as (Equation 4).

$$\sum_{l=1}^{i} Q_l = \begin{cases} 0 & for \quad i = 1 \\ \sum_{l=1}^{i-1} \left[(T_i - T_l) C_{l\text{Net}} \right] & for \quad i > 1 \end{cases} \tag{4}$$

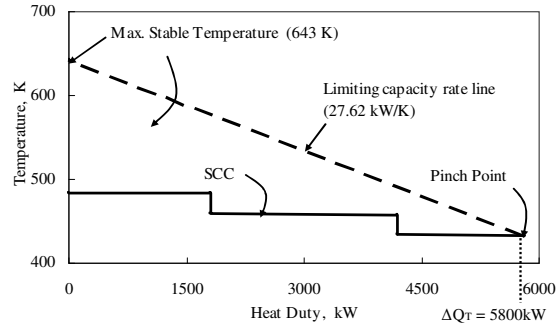

Figure 1: Resource targeting algorithm for minimum HTF flow rate (ΔTmin = 10K)

Now, cumulative heat load may be plotted against temperature to obtain source composite curve (SCC) as shown in Figure 1. Physically, SCC is equivalent to grand composite curve (GCC) in heat-exchanger synthesis. Bottom entry in the fifth column signifies total heat load (ΔQ_T) to be supplied by the heater through HTF.

$$\Delta Q_T = \sum_{l=1}^{n} Q_l = \sum_{l=1}^{n-1} (T_n - T_l) C_{l\text{Net}} \tag{5}$$

Step 7: Capacity rate of HTF is calculated using Equation 6:

$$C_i = \frac{\sum_{l=1}^{i} Q_l}{T_{rs} - T_i} \qquad for \quad T_i < T_{rs} \tag{6}$$

Largest entry in the sixth column is the minimum capacity rate of HTF required for the problem. This procedure can be explained geometrically as follows.

Any line with a negative slope on temperature (T) versus heat load (ΔQ) diagram, passing through a point (0, T_{rs}), represents a capacity rate line. Equation for capacity rate line is

$$\Delta Q = \Delta Q_T - C_T (T_{rs} - T) \tag{7}$$

Note that slope of capacity rate line is inversely proportional to mass flow rate of HTF. It should also be noted that at any point, capacity rate line cannot cross SCC i.e., it cannot transfer more heat load than required (as given by SCC or cumulative heat load available at any given temperature). Therefore, the minimum flow rate can be targeted by rotating a capacity rate line with (0, T_{rs}) as the pivot point such that it just touches the SCC. A point at which, capacity rate line touches the SCC denotes the pinch point (see Figure 1) and the line may be called the limiting capacity rate line (Figure 1). Temperature corresponds to the minimum capacity rate represents the pinch temperature.

3. Illustrative example

A simple example from Stoecker (1989) is used to demonstrate methodology of the RTA. The heating system (Figure 2) has three different reboilers using HTF to heat three process fluids. The heat duty, heating temperature and minimum temperatures of HTF for all process fluids are given in Table 1 (Stoecker, 1989). The heat evolved by the combustion of fuel in fired heater is transferred to reboilers through HTF (Figure 2). HTF is heated in fired heater up to the maximum stable temperature of 643K and then it is passed through reboilers transferring heat to process fluids. Subsequently it is circulated back to the fired heater at a lower temperature. The objective is to minimize the capacity rate of HTF (or equivalently the mass flow rate of the HTF).
Table 2 summarizes step-by-step calculation procedure given for RTA. The minimum approach temperature ΔT_{min} is assumed as 10 K for this problem. Process temperatures are converted to minimum inlet/outlet temperatures for HTF and arranged in descending order (column 1, Table 2). As process fluids are heated at constant temperature, 1 K temperature difference between inlet and outlet temperatures is considered to avoid the problem of infinite capacity rate. For example, the stream 1 is heated at 473 K by HTF in reboiler, so the minimum temperatures for HTF at inlet and outlet are calculated as 484 K and 483 K respectively. Similarly, temperatures of all the process streams are converted to HTF temperatures (column 3, Table 1). First entry in column 1 of Table 2 is the maximum stable temperature of HTF (i.e., 643 K). Column 2 gives cumulative heat capacity for a particular temperature interval.

Table 1: Process data given in Illustrative Example (Stoecker, 1989)

Reboiler No.	Duty, kW	Temperature of fluid being heated, K	Minimum approach temperature of HTF ΔT_{min} = 10 K	
			T_i K	T_o K
1	1800	473	484	483
2	1600	423	434	433
3	2400	448	459	458

In Table 2, last entry of column 3 is zero, as explained validation of mass conservation. Last entry of fifth column suggests that 5800 kW of total heat load is to be supplied by fired heater (ΔQ_T = 5800 kW). Column sixth of Table 2 gives minimum HTF capacity rate 27.62 kW/K at a pinch temperature of 433 K.

Table 2: RTA to target minimum Capacity applied to Example

Temperature K	Heat Capacity kW/K	Cumulative Heat Capacity kW/K	Heat Flow kW	Cumulative Heat Flow kW	Heat Capacity kW/K
643	0	0	0	0	0
484	-1800	-1800	0	0	0
483	1800	0	1800	1800	11.25
459	-2400	-2400	0	1800	9.78
458	2400	0	2400	4200	22.70
434	-1600	-1600	0	4200	20.096
433	1600	0	1600	5800	**27.62**

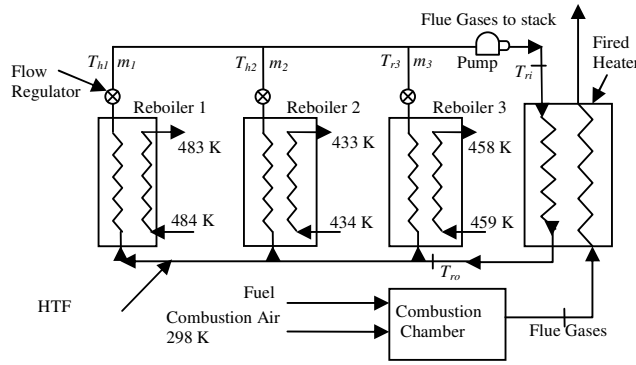

Figure 2: Heating system containing reboilers, fired heater and HTF

A source composite curve (SCC), temperature Vs. heat duty (Table 2, column 1 vs. column 5) is plotted as shown in Figure 1. The limiting capacity rate line shown in Figure 1, dictates minimum HTF capacity rate. For the same problem and data, instead of series-parallel configuration of reboilers, parallel configuration is used then HTF capacity rate can turn out to be 31.84 kW/K. Thus total HTF capacity rate is least for series-parallel configuration. This is targeted before actual design of reboilers.

4. Conclusions

Pinch technology, initially proposed as a thermodynamics-based approach to energy conservation, has evolved over the years to become a powerful tool for process integration and resource optimization. The tools of pinch technology are extended to target the minimum HTF flow rate. As the pinch analysis recognizes the importance of setting targets before design, similarly it sets the minimum HTF capacity rate target using RTA. The proposed RTA for the minimum HTF capacity rate shows 15.3% less capacity rate than the parallel configuration for 10 K approach temperature. Future work focuses on the overall optimisation of the HTF system by integrating radiator and heat exchangers.

References

Guffey E.G. II. 1997. Sizing up heat transfer fluids and heaters, Chemical Engineering, 126- 131.
Kim J.K. and Smith R. 2001. Cooling water system design, Chemical Engineering Science 56(12), 3641-3658
Krishnan S. 2005. Get the Most from High-temperature Heat-transfer-fluid Systems, Chemical Engineering, 46- 50.
Mckechnie A.B. 1927. Industrial Heating by Oil Circulation, Industrial & Engineering Chemistry 19(6), 691-693.
Sahu G.C. and Bandyopadhyay S. 2010. Energy Conservation in Water Allocation Networks with Negligible Contaminant Effects, Chemical Engineering Science 65(14), 4182-4193.
Stoecker W.F. Design of thermal systems, 1989, Third Edition, McGraw-Hill Company, New York.
Varghes J. and Bandyopadhyay S. 2012. Fired heater integration into total site and multiple fired heater targeting, Applied Thermal Engineering, In press.
Wang Y.P. and Smith R. 1994. Wastewater minimization, Chemical Engineering Science, 49(7), 981-1006.

I.A. Karimi and Rajagopalan Srinivasan (Editors), Proceedings of the 11th International Symposium on Process Systems Engineering, 15-19 July 2012, Singapore.

A Study of Complex Distillation Arrangements for Improved Depropanizing, Debutanizing and Deisobutanizing Fractionation of NGL

Youngmi Jung, Nguyen Van Duc Long, Mesfin Getu Woldetensay, Moonyong Lee†

School of Chemical Engineering, Yeungnam University, Gyeongsan 712-749, South Korea

Abstract

The depropanizing, debutanizing and deisobutanizing fractionation steps of processing natural gas liquids were improved through studying complex distillation arrangements, including the double dividing wall column arrangement (DDWC), the sequence including a dividing wall column (DWC) and a bottom DWC (BDWC) and the sequence including a DWC and a BDWC with top vapor recompression heat pump. These arrangements offer benefits by decreasing reboiler and condenser power consumption. Reducing the number of columns and their diameters can potentially reduce construction costs. The result also showed that operating cost could be reduced most significantly through novel combinations of internal and external heat integration: bottom dividing wall columns employing a top vapor recompression heat pump.

Keywords: Dividing wall column; DWC; Heat pump; NGL recovery.

1. Introduction

The uses and processing of natural gas (NG) are still evolving since their early twentieth century origins in the United States. Although its primary use is as a fuel, NG is also a source of hydrocarbons for petrochemical feed stocks and a major source of elemental sulfur, an important industrial chemical (Kidnay, 2006). Its clean burning and ability to meet stringent environment requirements ensure demand for natural gas (Elliot *et al.*, 2005). Recovery of natural gas liquids (NGL) has become increasingly economically attractive as a number of its components are often isolated and sold separately. Consequently, numerous methods exist to increase NGL recovery from a feed gas, with potential enhancements involving integrated processes (Elliot *et al.*, 2005; Mak, 2006).

Distillation is the primary separation process used in industrial chemical processing. While it has many advantages, a drawback is its large energy requirement (Schultz *et al.*, 2002), which can significantly influence overall plant profitability. Increasing energy costs deter energy consumption as do tighter environmental regulations regarding fossil fuel use, leading to research into new and more efficient separation methods (Knapp and Doherty, 2005; Malinenand and Tanskanen, 2009).

Ternary separations typically involve either direct or indirect sequences with two conventional columns. Although the control and operation of conventional columns are simple, their use is inefficient in terms of energy due to the mixing entropy by irreversible split (Aspiron, 2010). Therefore, various methods have been developed to improve the energy efficiency of such distillation systems. Many studies confirm that the Fully Thermally Coupled Distillation System (FTCDS) or the Petlyuk column can reduce energy consumption (Halvorsen and Skogestad, 2004; Jiménez *et al.*, 2003). The

Petlyuk column allows reversible splits, with no part of the separation being performed twice (Figure 1), which gives superior separation energy efficiency over other column configurations (Poth *et al.*, 2004).

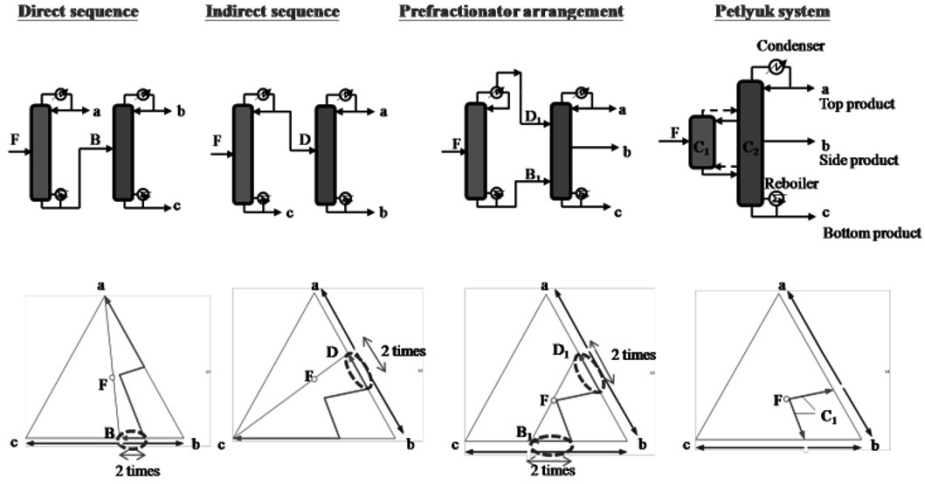

Figure 1. The ternary systems of direct sequence, indirect sequence, prefractionator arrangement, and the Petlyuk system.

Instead of having an external prefractionator, the prefractionator can be incorporated into a single shell arrangement by installing an internal wall, which divides the column into the prefractionator and the main section. This dividing wall column (DWC) is conceptually similar to the Petlyuk column, given their thermodynamically equivalent arrangements (Amminudin *et al.*, 2001), and is expected to give a similar energy saving. However, the dividing wall column requires less capital expenditure and space. Its single shell feature, single reboiler and condenser can typically reduce capital expenditure by 30% compared with conventional two column sequences. The design of the dividing wall column is more complex than a simple column because there are more degrees of freedom that need to be specified. Key variables and parameters such as the number of trays of the column, the liquid and vapor splits each side of dividing wall, and the feed and side tray locations must be established. These degrees of freedom all interact with each other and need to be simultaneously optimized to obtain the best design. Since number of stages is an integer variable, column optimization falls into a class of mixed integer non-linear programming problems (MINLP) (Dejanović *et al.*, 2010), which cannot be solved by commercially available process simulators.
Integrating three columns, whose operating pressures are so different, in such ways is impractical (Long and Lee, 2012). At least two columns are needed. This work aims to find a configuration suitable for improving the performance of the depropanizing, debutanizing and deisobutanizing fractionation steps of NGL processing.

2. Conventional column sequence

Liquid hydrocarbons recovered from NGL are typically separated into relatively pure ethane (C_2), propane (C_3), isobutane (iC_4), normal butane (nC_4), and gasoline products (C_{5+}). This is conventionally done by distilling C_2, C_3 and C_4 from gasoline in sequence

and then distilling iC_4 from nC_4. Because of the large energy consumption, there are numerous configurations and methods known to increase NGL recovery from a feed gas. The difference of operating pressures complicates columns' integration and directly affects energy consumptions and the use of refrigeration.

The depropanizer, possessing 34 theoretical trays, is operated at 17.50 bar as commercial propane can be condensed with cooling water at this pressure, as seen in Figure 2a. The debutanizer and deisobutanizer columns, with 40 and 92 trays, respectively, are operated at 3.50 and 4.40 bar, respectively (Manley, 1997; Amminudin and Smith, 2001). The final distillation of iC4 from nC4 is energy and capital intensive because these compounds' small relative volatility (Manley, 1998). Simulations were performed using the simulator Aspen HYSYS V7.1. The Peng-Robinson equation of state that supports the widest range of operating conditions and the greatest variety of systems was used to predict the vapor-liquid equilibria of these simulations (Aspen Technology, 2009). The base case simulation shows that the energy consumptions of the depropanizer, debutanizer and deisobutanizer are 21.54, 10.48 and 23.80 MW, respectively.

(a) (b)

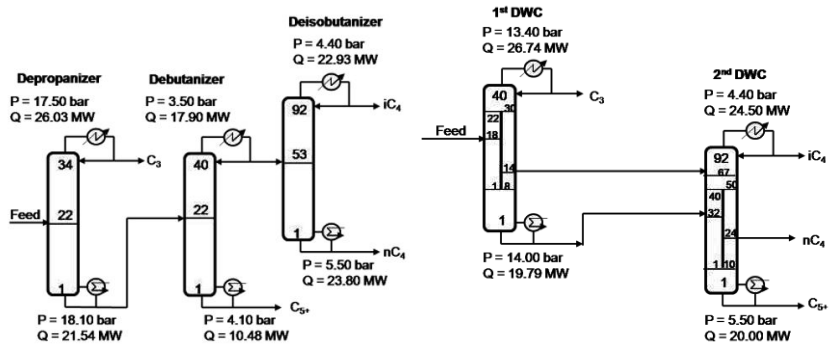

Figure 2. Simplified flow sheet illustrating (a) the separation train of three conventional columns and (b) the DDWC system.

3. Proposed base sequence

3.1. Integration by DWC and bottom dividing wall column (BDWC)

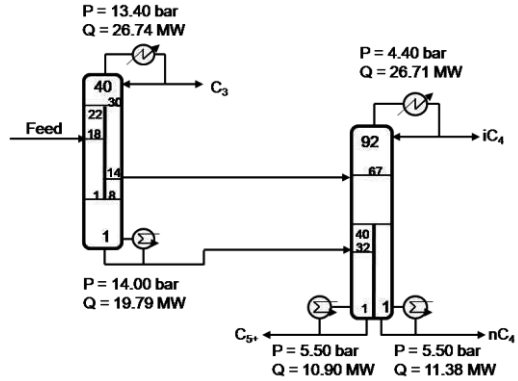

Figure 3. Simplified flow sheet illustrating the DWC and BDWC arrangement.

A double dividing wall column (DDWC) sequence was used to improve energy efficiency in NGL recovery process (Figure 2b) (Long and Lee, 2012). Instead of using the 2nd DWC, a bottom dividing wall column (BDWC) can be used as shown in Figure 3. This BDWC is created by moving the dividing wall down to the bottom of the column to separate the column to three sections: one is prefractionator section for the feeding the mixtures with its own reboiler to produce C_{5+}, another is the top section upper the divided wall, and the last is the divided wall section. Compared to the DWC, the BDWC has one more reboiler causing more investment cost. Using one DWC and one BDWC sequence could save 24.63% in terms of energy consumption. BDWC shows less advantage as compared to DWC because this kind of column could not be adjusted in terms of vapor split ratio (R_v). However, it gives a potentiality with the assistance of heat pump.

3.2. Integration by DWC and BDWC with top vapor recompression heat pump

In the former, instead of using a separate condenser and reboiler, the top product can be compressed to a higher pressure and then condensed in the reboiler of the column. As a result, the condensed vapor provides heat needed for vapor generation at the bottom of the column in the heat exchanger. Then the top outlet stream must be further cooled before being divided to two streams, which including one is recycled back the column as reflux, another is the final top products as shown in Figure 4. Note that the pressure of outlet compressor was adjusted to obtain a minimum approach in the heat exchanger of 5°C. It is possible to save 45.02% in terms of reboiler energy. But that is not the only advantage of this arrangement because, by using a heat pump, the CO_2 footprint could be reduced (Díez *et al.*, 2009). Hence, there is an environmental advantage which could become more important if CO_2 quotas are enforced by governments.

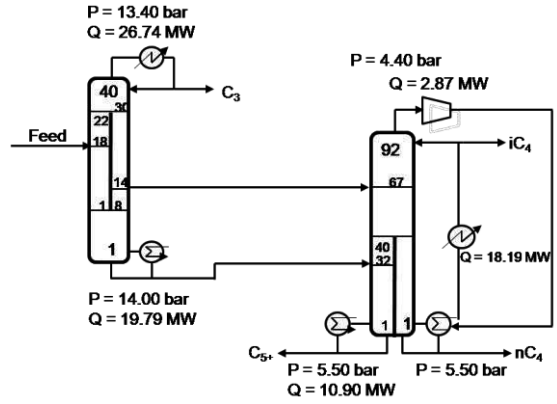

Figure 4. Simplified flow sheet illustrating the DWC and BDWC with top vapor recompression heat pump arrangement.

4. Conclusions

Complex distillation sequences were studied to improve the performance of the depropanizing, debutanizing and deisobutanizing fractionation steps of NGL processing. The sequence including a DWC and a BDWC was shown to reduce energy requirement considerably compared with conventional distillation sequence. Furthermore, operating cost could be reduced most significantly through novel combinations of internal and external heat integration: bottom dividing wall columns

employing either a top vapor recompression heat pump. Furthermore, these sequences, with a decreased number of smaller columns, could reduce investment costs. The reduced numbers of columns and reboilers could also make a plant more compact.

Acknowledgments

This research was supported by a grant from the Gas Plant R&D Center funded by the Ministry of Land, Transportation and Maritime Affairs (MLTM) of the Korean government.

References

Amminudin, K. A.; Smith, R.; Thong, D. Y. C.; Towler, G. P. Design and Optimization of Fully Thermally Coupled Distillation Columns: Part 1: Preliminary Design and Optimization Methodology. Trans. IChemE. 2001, 79 (Part A), 701-715.

Amminudin K. A., R. Smith. Design and optimization of fully thermally coupled distillation columns. Part 2: application of dividing wall columns in retrofit Trans. IChemE., 2001; 79, 716-724.

Aspen Technology. Aspen HYSYS Thermodynamics COM Interface, version number V7.1, January 2009.

Asprion N., G. Kaibel. Dividing wall columns: Fundamentals and recent advances, Chem. Eng. Process., 2010; 49, 139-146.

Dejanović I., Lj. Matijašević, Ž. Olujić. Dividing wall column-a breakthrough towards sustainable distilling, Chem. Eng. Process., 2010; 49, 559-580.

Díez E., P. Langston, G. Ovejero, M. D. Romero. Economic feasibility of heat pumps in distillation to reduce energy use, App. Ther. Eng., 2009; 29, 1216-1223.

Elliot, D.; Qualls, W. R.; Huang S.; (Roger) Chen J. J. Benefit of Integrating NGL Extraction and LNG Liquefaction Technology. AIChE Spring National Meeting, 5th topical conference on Natural Gas Utilization (TI) Session 16c-Gas, 2005.

Halvorsen I. J., S. Skogestad. Shortcut analysis of optimal operation of Petlyuk distillation, Ind. Eng. Chem. Res., 2004; 43, 3994-3999.

Jiménez A., N. Ramírez, A. Castro, S. Hernández. Design and energy performance of alternative schemes to the Petlyuk distillation system, Trans. IChemE., 2003; 81 (Part A), 518-524.

Knapp J.P., M.F. Doherty. Thermal integration of homogeneous azeotropic distillation sequences, AIChE J., 1990; 36, 969-984.

Kidnay, A. J.; Parrish W. R. Fundamentals of Natural Gas Processing; Taylor and Francis: Baca Raton, 2006.

Long, N. V. D.; Lee, S. H.; Lee, M. Y. Design and Optimization of a Dividing Wall Column for Debottlenecking of the Acetic Acid Purification Process. Chem. Eng. Process. 2010, 49, 825-835.

Long N. V. D.; Lee M. Y. Improvement of Natural Gas Liquid Recovery Energy Efficiency through Thermally Coupled Distillation Arrangements, Asia Pac. J. Chem. Eng., In Press, 2012.

Manley, D. B. Deethanizer/Depropanizer Sequences with Thermal and Thermo-Mechanical Coupling and Component Distribution. U.S. patent 5,673,571, 1997.

Manley, D. B. Multiple Effect and Distributive Separation of Isobutane and Normal Butane. U.S. patent 8,806,339, 1998.

Mak J. Configurations and methods for improved NGL recovery, U.S. Patent 7,051,552, 2006.

Malinenand I., J. Tanskanen. Thermally coupled side-column configurations enabling distillation boundary crossing. 1. An overview and a solving procedure, Ind. Eng. Chem Res., 2009; 48, 6387-6404.

N. Poth, D. Brusis, J. Stichlmair. Minimaler energiebedarf von trennwandkolonnen, Chem. Ing. Tech., 2004; 76, 1811–1814.

Schultz M.A., D.G. Stewart, J.M. Harris, S.P. Rosenblum, M.S. Shakur, D.E.O'Brien. Reduce costs with dividing wall columns, CEP, 2002, 64-71.

I.A. Karimi and Rajagopalan Srinivasan (Editors), Proceedings of the 11th International Symposium on Process Systems Engineering, 15-19 July 2012, Singapore.

Water condensate collection system by using MINLP model

Anita Kovac Kralj, [a] Jernej Hosnar[a]

[a]*Faculty of Chemistry and Chemical Engineering, University of Maribor, 2000 Maribor, Slovenia*

Abstract

This paper presents a retrofitted procedure for wastewater, or more specifically, water condensate's separate collection, using an intermediate mathematically-programmed heating design based on a MINLP (mixed-integer nonlinear programming) model. The existing separate condensate collection using an intermediate heating system may no longer be optimal; the basic intention being that minimal changes in the system can efficiently improve the separate collections of low and high-temperature condensates, and the use of available heat. This water condensate collection process was tested on an existing methanol process, by using a MINLP model, which allowed for more effective and additional 5 % water condensate collection system for steam generation.
Keywords: water condensate, MINLP-model, energy saving

1. Introduction

Water minimization within the process industry is becoming increasingly important as environmental legislation becomes more stringent, and awareness increases about the impact of industrial activities on the environment. Extensive work was carried out by Bagajewicz (2000) and Foo (2009) on water-minimization during continuous processes. They developed methodologies for wastewater minimization during continuous processes, mainly using pinch-analysis techniques.

Water condensate collection is very important during real chemical processes because it can reduce raw materials, energy-losses, and costs, and can improve the operations of energy and process systems (Richter, 1993). Water is amongst the more important raw materials and utilities, therefore, it is reasonable to collect water during the process industries' activities.

This paper presents the separate collection of low and high-temperature condensates using an intermediate heating by the mathematical techniques - MINLP model.

2. Water condensate collection with an intermediate heating by using MINLP model

Water is amongst the more important raw materials and utilities, therefore it is reasonable to collect water from process industries.

Their goal is to minimize the amount of wastewater, or more specifically reuse condensates by using a MINLP model. Condensate, as produced during a process, could be separately collected, heated, and utilized for steam-generation.

The MINLP approach deals with both continuous and discrete variables, simultaneously (Biegler et al., 1997). Whilst continuous variables are defined for the continuous optimization of parameters (mass flow-q, heat flow rate-Φ, temperatures-T, specific heat capacity-cp costs, etc.). The basic structural binary variable (y) determines the location of an exact condensate (c) into an exact reservoir (r; eq. 1). Each condensate

has the possibility of entering into any reservoir, and this selection can be determined by the binary variables. If the value is one, it means, that the condensate is selected for a particular reservoir, if zero, and then it is not selected (eq. 1).

$$\sum_{r} y_{c,r} = 1 \qquad r = 1. \ldots R \qquad c = 1, \ldots C \tag{1}$$

Different temperature condensates could be collected more efficiently with separated collections for high-temperature and low-temperature condensate collection reservoirs, according to the minimum energy-loss.

When the different temperature condensates are separately collected within a variety of different lower and higher temperature reservoirs and then followed by heating, the allocation choice for various condensates is very important.

This system of separated lower and higher temperature condensates' (c = 1, …C) collection with intermediate heating, includes different numbers of reservoirs (r = 1, …R) and heaters (h = 1,…H) using mass balance equations (Fig. 1). The mass balance for reservoir number 1 (eq. 2) includes all inlet (fresh water - q_{in} and condensates - $q_{c,r}$) and outlet streams (q_r; eqs. 2, 3):

$$q_{in}\, cp_{in}\, T_{in} + \sum_{c}(\, q_{c,r}\, y_{c,r}\, cp_c\, T_c) = [\sum_{c}(q_{c,r}\, y_{c,r}) + q_{in}]\, cp_r\, T_r \qquad c = 1, \ldots C \quad r = 1 \tag{2}$$

$$q_r = \sum_{c}(q_{c,r}\, y_{c,r}) + q_{in}] \qquad c = 1, \ldots C \quad r = 1 \tag{3}$$

The outlet stream from reservoir number 1 is the same as the stream into heat-exchanger number 1:

$$q_r = q_h \qquad r = 1 \qquad h = 1 \tag{4}$$

Mass balance of reservoir number two is:

$$q_h\, cp_h\, T_h + \sum_{c}(\, q_{c,r}\, y_{c,r}\, cp_c\, T_c) = [\sum_{c}(q_{c,r}\, y_{c,r}) + q_h]\, cp_r\, T_r \qquad c = 1, \ldots C \quad r = 2 \quad h = 1 \tag{5}$$

$$q_r = \sum_{c}(q_{c,r}\, y_{c,r}) + q_h] \qquad c = 1, \ldots C \qquad r = 2 \qquad h = 1 \tag{6}$$

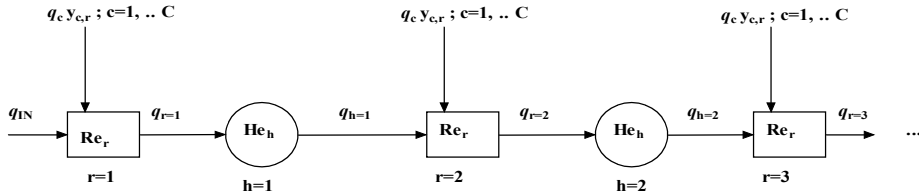

Figure 1: Collection of condensates.

General mass balance of reservoir r is:

$$q_h\, cp_h\, T_h + \sum_{c}(\, q_{c,r}\, y_{c,r}\, cp_c\, T_c) = q_r\, cp_r\, T_r \qquad c = 1, \ldots C \qquad r = 1, \ldots R \qquad h = 0, 1 \ldots H \tag{7}$$

The energy balance for the heater h is:

$$\Phi_h = q_r \,.\, (cp_r + cp_h)/2 \,.\, (T_h - T_r) \qquad r = 1, \ldots R \qquad h = 1 \ldots H \tag{8}$$

The objective function (OBF, eq. 9) of the MINLP model was to maximize the output temperature from reservoir number 2 by saving (C_{sav} = 100 EUR/K):

$$OBF = C_{sav}\, T_{r2} \tag{9}$$

Many constrained engineering and industrial optimization problems can be modelled as mixed integer nonlinear programming (MINLP) problems.

3. Case study

The existing methanol production had a condensate collection system using two reservoirs. The efficiency of the collection was tested using an MINLP (mixed-integer nonlinear programming) model.

During the methanol process, all the condensates (c=K1−K5) were collected as utilities for 37 bar steam-generation (Fig. 2). The collected condensates were added to the freshly- demineralization water ($q_{FR\text{-}W}$ =19791 kg/h) within the reservoir (R1). The fresh-water and condensates were heated in a heat-exchanger (E111=he-1), followed by another collection of condensates into the reservoir (R2), pumped using a pump (P1) at 50 bar, and then heated in heat-exchangers (E110, E102, REA2, E107, E104, E103). The necessary heat flow rates for the heating of a steam-generation system were obtained from synthesis gases (E111, E110, E107), the furnace-channel (E102, E104, E103), and the REA-2 reactor.

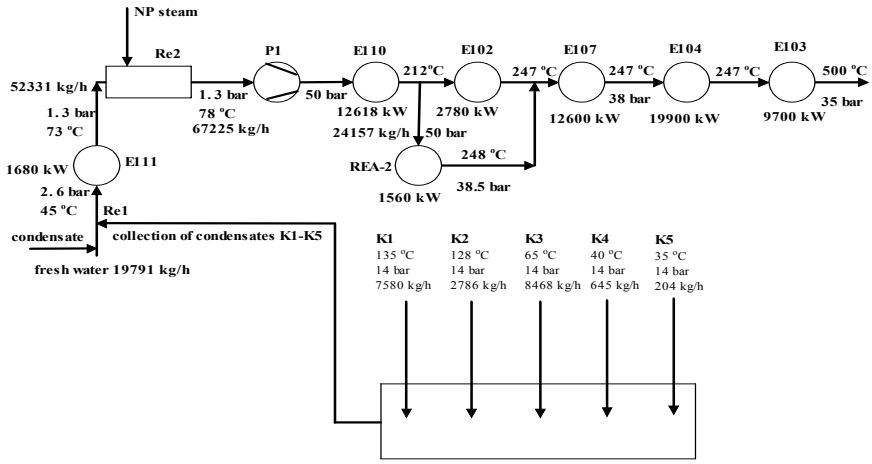

Figure 2: The existing steam-generation.

The existing steam preparation system had been modified by using an Aspen Plus simulator (Aspen Plus, 1996) without a mathematical method. The existing steam preparation system was newly-optimized by using mathematical methods. The optimal modification can be obtained by the mathematical MINLP method by using GAMS optimization tool with execution time of 4.9 s (GAMS with DICOPT, 1992). The MINLP model includes equations from 10 to 18.

Five condensates (c=K1−K5) with different constant temperatures (T_c) and mass flow rates (q_c) were collected within reservoirs (r = R1, R2). Each condensate (c=K1−K5) could be collected in reservoirs 1 or 2, but not in both (eq. 10):

$$\sum_{r} y_{c,r} = 1 \qquad r = R1, R2 \qquad c = K1, K2, K3, K4, K5 \tag{10}$$

Mass balance for the reservoir number 1 is:

$$\sum_{c}(q_{c,r1}\, y_{c,r1}\, cp_c\, T_c) + (q_{FR\text{-}W} + q_{add})\, cp_{FR\text{-}W}\, T_{FR\text{-}W} = [\sum_{c}(q_{c,r1}\, y_{c,r1}) + q_{FR\text{-}W}]\, cp_{r1}\, T_{r1} \tag{11}$$

$$q_{m\,r1} = [\sum_{c}(q_{c,r1}\, y_{c,r1}) + q_{FR\text{-}W}] \quad c = K1, K2, K3, K4, K5 \tag{12}$$

Parameter $q_{FR\text{-}W}$ denotes the heat-flow rate of the fresh water with constant inlet temperature (T_c) and heat-capacity (cp_c), which is only entering reservoir number 1. Parameter q_{add} denotes the additional heat-flow rate of the fresh water with constant

parameters (T_c, cp_c), and with an upper-limit of 3700 kg/h. This is an upper-limit where the system is not too overloaded. All existing units remain the same without additional modifications.

E111 heater (he-1= E111), which heats the outlet from reservoir number one. The energy balance for the heater is:

$$\Phi_{\text{he-1}} = q_{\text{m r1}} (cp_{\text{r1}} + cp_{\text{he-1}})/2 \ (T_{\text{he-1}} - T_{\text{r1}}) \quad (13)$$

The heat flow rate ($\Phi_{\text{he-1}}$) can be calculated using known-values for the inlet and outlet heat capacities (cp_{r1}, $cp_{\text{he-1}}$) and temperatures ($T_{\text{he-1}}$, T_{r1}) of heat exchanger number 1, by using equation 13.

Mass balance for reservoir number 2 is:

$$\sum_{c}(q_{\text{c, r2}} y_{\text{c, r2}} \ cp_c T_c) + q_{\text{h-w}} \ cp_{\text{h-w}} T_{\text{h-w}} + q_{\text{m r1}} cp_{\text{r1}}, T_{\text{r1}} = [\sum_{c}(q_{\text{c,r2}} y_{\text{c, r2}}) + q_{\text{h-w}} + q_{\text{m r1}}] \ cp_{\text{r2}} \ T_{\text{r2}} \quad (14)$$

Variables T_{r1} and T_{r2} are the denoting outlet temperatures from reservoirs 1 and 2. Parameter $q_{\text{h-w}}$ denotes the heat-flow rate of the hot water-stream with constant inlet temperature ($T_{\text{h-w}}$) and specific heat capacity ($cp_{\text{h-w}}$), which is only entering reservoir number 2. Parameter $q_{\text{m r1}}$ is the sum of all the mass-flow rates, into reservoir 1 (eq. 12), which then further enters the next reservoir number 2. All the condensates (c=K1−K5) have a constant mass-flow rate (q_c), temperature (T_c) and heat-capacity (cp_c) and, therefore, can be multiplied by the binary parameters ($y_{\text{c, r}}$).

The specific heat-capacity ($cp_{\text{c,r}}$) regarding reservoirs 1 and 2, can be calculated by using linear equation 15, depending on the outlet temperature from the tank (T_r). The parameters of specific heat capacity (a_r b_r) are known values (0.0093, and 1.1067 kJ/(kg K)) for water.

$$cp_r = a_{,r} \ T_r + b_r \qquad r = R1, R2 \quad (15)$$

Specific heat-capacity ($cp_{\text{c,r}}$) after heating in heater he-1, can be calculated by using linear equation 16 depending on the outlet temperature from heater ($T_{\text{he-1}}$).

$$cp_{\text{he-1}} = a_{\text{, he-1}} \ T_{\text{he-1}} + b_{\text{he-1}} \qquad \text{he} = \text{he-1} \quad (16)$$

An equation similar to the eighteenth can be used for a further heat-exchanger, by considering the additional mass-flow:

$$\Phi_{\text{he}} = (q_{\text{m he}} + q_{\text{add}})(cp_{\text{he-in}} + cp_{\text{he-out}})/2 \ (T_{\text{he-out}} - T_{\text{he-in}}) \quad \text{he} = \text{E110, E102, E107, E104, E103} \quad (17)$$

The objective function (OBF, eq. 18) of the MINLP model maximized additional profit. The reconstruction did not include many modifications, and thus costs. The process did not operate at 100 % capacities, and so the existing process could be used without additional modification. The basic additional cost of reconstruction ($C_{\text{add-fw}}$ = 0.02 EUR/kg) was the cost of additional fresh water mass-flow rate (q_{add}), including the contingencies cost. The additional income accounted for the additional price of steam-generation ($P_{\text{st-gen}}$ = 0.1 EUR/kg). The maximum additional mass-flow rate of steam generated would be increased by 3700 kg/h (an upper-limit), including 40 % efficiency. The operational time (O) was 8000 h/a.

$$\text{OBF} = P_{\text{st-gen}} \ q_{\text{add}} \ 0.4 \ O - C_{\text{add-fw}} \ q_{\text{add}} \ O \quad (18)$$

3.1. Retrofitted system of condensate collection

The existing steam-generation system, including all hot and cold streams (Fig. 3) during the methanol process could be optimized by using MINLP.

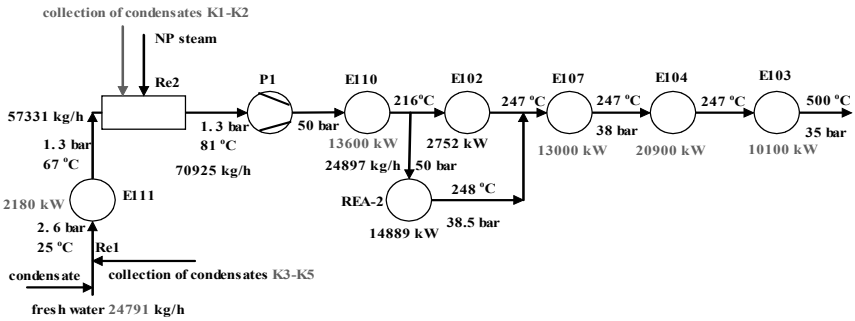

Figure 3: The retrofitted steam-generation.

The optimal result of the objective function was the selection of separate condensate collections (Fig. 3). Low-temperature condensates K3–K5 could be collected within a Re1 reservoir containing fresh-water. The high-temperature condensates K1–K2 could then be collected within a Re2 reservoir. Selection was the same as for the first objective function. The additional heat-flow rate of fresh water (q_{add}) was 3700 kg/h, which was within the lower-bound. The loss of heat-flow rate into the air-cooler was distributed into E111 and E110 heat-exchangers heated with 500 and 1000 kW higher heat-flow rates for the demineralization water, and the inlet temperature of the air-cooler was reduced to 101 °C. The demineralizated water was evaporated in E107 and E104 with additionally-available heat within the furnace-channel, followed by overheating into E103.

The reconstruction of the steam-generation-system could be more effective, as all the available-heat was used during the process. 5 % more steam could be produced by the existing system, which does not work at 100 % capacity.

4. Conclusions

The optimal allocation of condensate collection could be optimized by using a mathematical method, as such the MINLP model. The MINLP model enables both the low and high-temperature condensates to have the possibility of entering into any reservoir, and this choice of selection can be determine by the binary variables.

The existing condensate collection during the methanol process was modified in order to collect low and high-temperature condensates, separately. By modifying the existing process, very little change would be needed for a better preparation of overheated-steam, as used in steam-turbines for producing electricity. The additional profit from the retrofitted steam production system was 590 kEUR/a.

References

Aspen Plus (1996). User Guide, Cambridge.

M.J. Bagajewicz, (2000), A review of recent design procedures for water networks in refineries and process plants, Computers and Chemical Engineering 24, pp. 2093–2113.

L. T. Biegler, Grossmann I. E. and Westerberg A. W., (1997), Systematic methods of chemical process design, Prentice Hall, Upper Saddle River, New Jersey, pp. 1–408.

A Brooke., D. Kendrick and A Meeraus. (1992). GAMS: A User's Guide, Palo Alto, Scientific Press.

D. C. Y. Foo, (2009), A state-of-the-art review of pinch analysis techniques for water network synthesis, Ind. Eng. Chem. Res. 48, pp. 5125– 5159.

H.J Richter., (1993),Thermodynamics and the design, analysis and improvement of energy systems 1993, HTD-Vol. 266 ASME, New York.

I.A. Karimi and Rajagopalan Srinivasan (Editors), Proceedings of the 11th International Symposium on Process Systems Engineering, 15-19 July 2012, Singapore.

Pressure Drop Consideration in Cooling Water Systems with Multiple Cooling Towers

Khunedi V. Gololo[a,b], Thokozani Majozi[a]

[a]*Department of Chemical Engineering, University of Pretoria, Pretoria, South Africa*
[b]*Council for Scientific and Industrial Research, Advanced Modelling and Digital Science, Pretoria, South Africa*

Abstract

Pressure drop consideration has shown to be an essential requirement for synthesis of cooling water network where reuse/recycle philosophy is employed. This is due to an increased network pressure drop associated with additional reuse/recycle streams. This paper presents a mathematical technique for pressure drop optimization in cooling water systems consisting of multiple cooling towers. The proposed technique is based on the Critical Path Algorithm (CPA) and the superstructural approach. The CPA is used to select the cooling water network with minimum pressure drop whilst the superstructure allows for cooling water reuse. This technique which was previously used in a cooling water network with single source is modified and applied in a cooling water network with multiple sources. The mathematical formulation exhibits a mixed integer nonlinear programming (MINLP) structure. The cooling tower model is used to predict the exit conditions of the cooling towers, given the inlet conditions from the cooling water network model.

Keywords: Cooling water system, Pressure drop, Critical Path Algorithm, Optimization

1. Introduction

Cooling water systems are used in many industries to remove waste heat from the process to the environment. Research in this area has focused mostly on optimization and synthesis of cooling water systems in which the technique of recycle and reuse is explored. In most cases the synthesized cooling water network is more complex thus resulting in a higher pressure drop. Kim and Smith (2001) used the graphical technique to debottleneck a cooling water system with single source. Ponce-Ortega *et al.* (2010) also presented a mathematical model for synthesis of cooling water networks that was based on a stage wise superstructural approach. This work included the cooling tower model and the pressure drop for each cooler was considered. Panjeshahi and Ataei (2008) extended the work of Kim and Smith (2001) on cooling water system design by incorporating a comprehensive cooling tower model. Different approach was taken by Majozi and Moodley (2008) who developed a mathematical model for optimization of cooling water systems with multiple cooling towers. This work was later improved by Gololo and Majozi (2011) by incorporating the cooling tower model.

In all the abovementioned work the topology of cooling water network was more complex thus prone to higher pressure drop than the conventional parallel design. Kim and Smith (2003) presented a paper on retrofit design of cooling water systems in which pressure drop was taken into consideration. The authors used graphical technique to

target the minimum circulating water flowrate and mathematical technique to design a cooling water network. This work was limited to one cooling source.
This paper presents a mathematical technique for pressure drop optimization in cooling water systems consisting of multiple cooling towers. The proposed technique is based on the Critical Path Algorithm (CPA) and the superstructural approach. The CPA is used to select the cooling water network with minimum pressure drop whilst the superstructure allows for cooling water reuse. This technique was previously used by Kim and Smith (2003) to synthesize cooling water network with single source. However in this paper CPA is adapted for a cooling water network with multiple sources. Furthermore, the detailed cooling tower model is also incorporated.

2. Model development

A two-step approach is employed to synthesize and optimize the cooling water system with multiple cooling towers considering pressure drop. The first step involves targeting of the minimum circulating water flowrate and in the second step the CPA is incorporated to synthesize the cooling water network with multiple cooling sources.
The cooling tower model developed by Kröger (2004) is used to predict the outlet conditions of the cooling towers and the overall cooling towers effectiveness. The cooling water network model by Gololo and Majozi (2011) is improved by incorporating the modified heat exchangers and pipes pressure drop correlations of Nie and Zhu (1999) shown in Eq. (1) and Eq. (4) respectively. In this paper the correlation of Nie and Zhu (1999) is expressed in terms of mass flowrate.

$$\Delta P = N_{t1} m^{1.8} + N_{t2} m^2 \tag{1}$$

where $$N_{t1} = \frac{1.115567 \mu^{0.2} {n_{tp}}^{2.8} A}{\pi^{2.8} \rho N_t^{2.8} d_o d_i^{4.8}} \tag{2}$$

$$N_{t2} = \frac{20 {n_{tp}}^3 \rho}{\pi^2 N_t^2 d_i^4} \tag{3}$$

The line pressure drop is calculated from Eq. 4 (Kim and Smith, 2003).

$$\Delta P = N_p \frac{1}{F_p^{0.36}} \tag{4}$$

where $$N_p = \frac{188.318 \rho^{0.176} \mu^{0.2} L}{\pi^{1.8}} \tag{5}$$

The CPA is used to select the cooling water network with minimum pressure drop. Kim and Smith (2003) used the superstructure shown in Fig. 1(a). The superstructure is based on single source cooling water network. By modifying the superstructure for single source cooling water systems, a multiple sources superstructure is shown in Fig. 1(b). The CPA used by Kim and Smith (2003) is based on finding a path from source to sink with maximum pressure drop. The maximum pressure drop path is then minimized during optimization to obtain the network with minimum pressure drop. Eq. (6) is used to identify the maximum pressure drop path between the source and sink.

$$P_m - P_n \geq \Delta P_{mn} \tag{6}$$

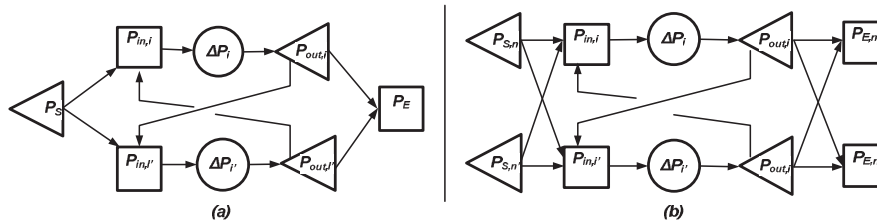

Figure 1: Cooling water system superstructure; (a) Single source (b) Multiple sources

To cater for multiple sources and sinks, the superstructure in Fig. 1(b) is modified by using single imaginary source and sink as shown in Fig. 2. Eq. (7) is then used to define the pressure of source node *n* from the imaginary source node.

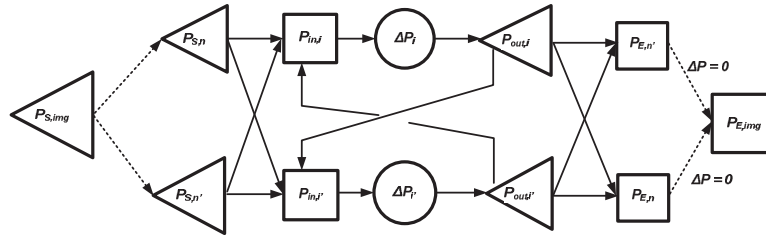

Figure 2: Multiple sources cooling water system superstructure

Eq. (8) to (11) represent the CPA adapted from Kim and Smith (2003). Eq. (12) defines the pressure at the imaginary sink node. From this equation the imaginary sink node will assume a value from all sink nodes with minimum pressure thus identifying a path with maximum pressure drop. The pressure drop of this critical path is then minimized to synthesize a cooling water network with minimum pressure drop.

Sets

$i = \{ i \mid i$ is a cooling water using operation$\}$

$n = \{ n \mid n$ is a cooling tower$\}$

$$P_{S,img} - P_{S,n} = \Delta P_{img,n} \tag{7}$$

$$P_{S,n} - P_{in,i} + LV\left(1 - x_{n,i}\right) \geq \Delta P_{n,i} \tag{8}$$

$$P_{out,i'} - P_{in,i} + LV\left(1 - y_{i',i}\right) \geq \Delta P_{i',i} \tag{9}$$

$$P_{in,i} - P_{out,i} = \Delta P_i \tag{10}$$

$$P_{out,i} - P_{E,n} + LV\left(1 - z_{i,n}\right) \geq \Delta P_{i,n} \tag{11}$$

x, y and z are a binary variables indicating the existence of stream from any source *n*/ operation *i*' *to* operation i/sink *n*. *LV* is a large value.

$$P_{E,n} - P_{E,img} \geq \Delta P_{n,img} \tag{12}$$

The network topology with minimum pressure drop is then synthesized by minimizing the pressure drop between the imaginary source and sink shown in Eq. (13).

$$P_{S,img} - P_{E,img} = \Delta P \tag{13}$$

A case study is considered which involves a cooling water system with dedicated cooling water sources and sinks. This implies that a set of heat exchanger can only be supplied by one cooling tower. No pre-mixing or post-splitting of cooling water return is allowed. However, reuse of water within the network is still allowed (Majozi and Moodley, 2008). The developed mathematical model consists of bilinear terms and binary variable thus rendering the models MINLP.

3. Solution Procedure

The solution procedure involves linearization of nonlinear terms and using results from linearized model as a starting point for the exact MINLP. The bilinear terms in the cooling water network model are linearized using the Reformulation Linearization technique by Sherali and Alameddine (1992) as shown in the paper of Gololo and Majozi (2011). However, a different technique is used to linearize the pressure drop equations. Functions are first plotted within the operating range of the heat exchangers and the piecewise linearization is then used to approximate the nonlinear function (Kim and Smith, 2003).

4. Case Study

Fig. 3 shows a cooling water system consisting of three cooling towers each supplying a set cooling water using operations. The total circulating water flowrate is 31.94 kg/s and the overall cooling towers effectiveness is 90%.

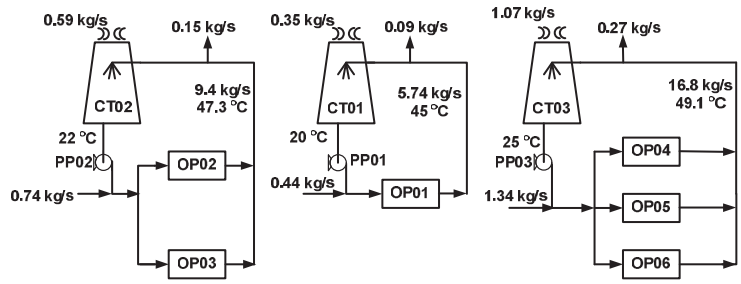

Figure 3: Cooling water system with multiple cooling towers (Majozi and Moodley, 2008)

Fig. 4 shows synthesized cooling water system after the application of the proposed technique. The total circulating cooling water decreased by 22% due to the exploitation of reuse opportunities. The overall increase in cooling tower return temperature associated with decrease in overall circulating water flowrate resulted in a 4%

improvement in effectiveness. The proposed methodology does not only debottleneck the cooling water system but also generate the network topology with the least pressure drop. This has a potential to minimize pumping cost associated with additional reuse/recycle streams. The pressure drop between sources and sinks $\Delta P_{S1,E1}$, $\Delta P_{S2,E2}$ and $\Delta P_{S3,E3}$ is 19 kPa, 31 kPa and 43 kPa respectively.

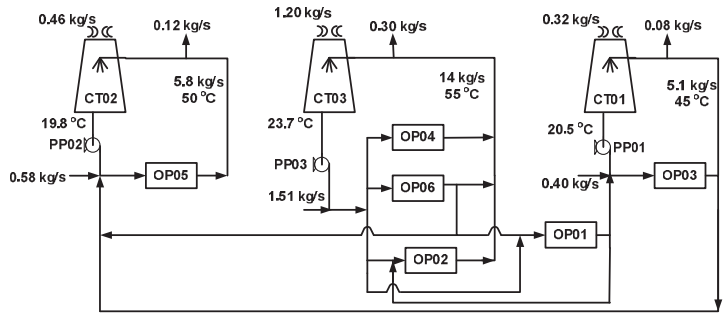

Figure 4: Debottlenecked cooling water system with the minimum pressure drop

5. Conclusion

The mathematical model for synthesis and optimization of cooling water systems with multiple cooling sources which takes into account the pressure drop is presented. The proposed technique is based on the CPA and the superstructural approach. The mathematical formulation developed yields MINLP structure. The case study showed a 22% decrease in circulating water flowrate due to the exploration of reuse opportunities. The return cooling tower temperature was increased which resulted in 4% improvement in the overall effectiveness. The proposed technique offers the opportunity to debottleneck the cooling water system with multiple cooling towers while maintaining minimum pressure drop and maximizing the overall cooling tower effectiveness.

References

J.K. Kim, & R. Smith, (2001), Cooling water system design, Chem. Eng. Sci., 56, 3641-3658

J.M. Ponce-Ortega, M. Serna-González, & A. Jiménez-Gutiérrez, (2010), Optimization model for re-circulating cooling water systems, Comput. Chem. Eng., 34, 177-195

M.H. Panjeshahi, & A. Ataei, (2008), Application of an environmentally optimum cooling water system design in water and energy conservation, Int. J. Environ. Sci. Technol., 5(2), 251-262

T. Majozi, & A. Moodley, (2008), Simultaneous targeting and design for cooling water systems with multiple cooling water supplies, Comput. Chem. Eng., 32, 540-551

K.V. Gololo, & T. Majozi, (2011), On synthesis and optimization of cooling water systems with multiple cooling towers, Ind. Eng. Chem. Res., 50,(7), 3775-3787

J.K. Kim, & R. Smith, (2003), Automated retrofit design of cooling water system, AICHE J. ,Vol 49, No 7, 56, 1712-1730

D.G. Kröger, (2004), Air-cooled heat exchangers and cooling towers: mass transfer and evaporative cooling, Penn Well Corporation, USA

X. Nie, & X.X. Xhu, (1999), Heat exchanger retrofit considering pressure drop and heat transfer enhancement, AICHE J., 45, 1239-1254

H.D. Sherali, & A. Alameddine, (1992), A new reformulation-linearization technique for bilinear programming problems, J. Global Optim., 2(4), 1992, 379-410

I.A. Karimi and Rajagopalan Srinivasan (Editors), Proceedings of the 11th International Symposium on Process Systems Engineering, 15-19 July 2012, Singapore.

New method for large-scale heat exchanger network synthesis

Christopher Brandt,[a] Georg Fieg,[a] Xing Luo,[b] Ole Engel[c]

[a]*HamburgUniversity of Technology, 21073 Hamburg, Germany*
[b]*Helmut Schmidt University, 22043 Hamburg, Germany*
[c]*XRG Simutlation GmbH, 21073 Hamburg, Germany*

Abstract

For the synthesis of large-scale heat exchanger networks a new method based on a hybrid genetic algorithm is proposed. It uses subnets in order to improve the resulting network structures and the calculation time. The application of the new method on an example from literature yielded a HEN structure with reduced total annual costs by 14% and a decreased calculation time by a factor of 18.

Keywords: heat exchanger network synthesis, genetic algorithm, MINLP.

1. Introduction

Production processes in chemical industry usually come along with a large energy consumption. Therefore, the integration of a heat exchanger network (HEN) can have a major impact on energy consumption and sustainability of a production plant. With increasing heat recovery the energy costs are decreasing whereas the investment costs are increasing. Thus, the design of a cost optimal HEN can be considered as a classical optimization problem.

Due to availability of special software and the strong sequential procedure, the most common used method for HEN synthesis is the well-known pinch design method (Linnhoff & Flower, 1978). Recent research activities have shown that specially tailored genetic algorithms are very capable of finding even better HEN structures (Luo et al., 2009), though. However, because of the large number of optimization variables the computation time is very high especially for large-scale HEN. In order to overcome this disadvantage a new method has been developed by the Institute of Process and Plant Engineering of the Hamburg University of Technology. This new method is based on the idea of subnets. A subnet represents a part of the whole network that does not have any contact to other parts of the HEN. Thus, it can be considered and treated like a single subproblem, which therefore can be easily solved by the genetic algorithm. Further, in order to increase the quality of the result, single subnets are combined and then solved again by the genetic algorithm. The application of this innovative method on industrial relevant problems yielded very promising results.

2. Formulation of the optimization problem

For structural representation of a HEN a simple stage-wise superstructure is used. This method was first introduced be Yee et al. in 1990. With this representation a wide range of theoretically possible network structures is covered. Fig. 1 illustrates the fundamental principle for an example with four hot process streams and three cold process streams.

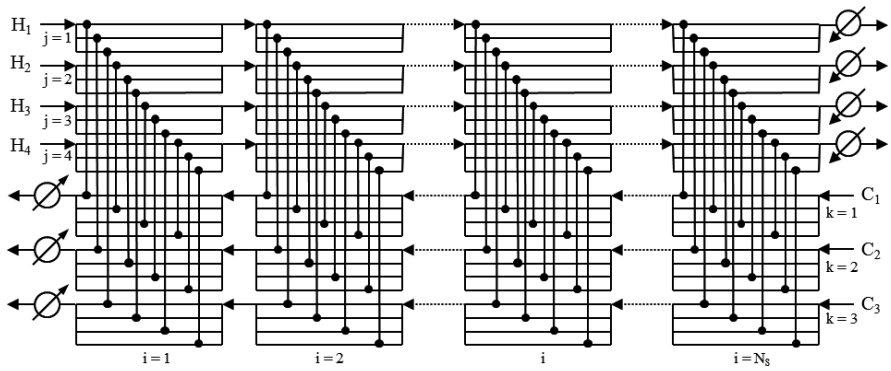

Figure 1: Stage-wise superstructure

Within a stage *i* each hot stream *j* is connected to every cold stream *k* once. The number of stages is proposed as either the amount of hot process streams or the amount of cold process streams, depending which of them is higher (Fieg et al., 2009).
The actual number of series connections of one stream to other streams in an optimal structure is usually rather small. Thus, the number of stages could be smaller. With less amount of stages valuable computational time can be saved.
With a fixed arrangement of the variables *i*, *j*, and *k* every heat exchanger (HX) in the structure has its explicit index that can be calculated by Eq. (1). The HX *ijk* in a given structure connects the hot stream *j* with the cold stream *k* in stage *i*.

$$ijk = (i\text{-}1)N_hN_c + (j\text{-}1)N_c + k \tag{1}$$

The synthesis problem of heat exchanger networks is typically given as a set of N_h hot process streams and N_c cold process streams. These streams are defined by their heat capacity flow rates $\dot{W}$, the overall heat transfer coefficients h and the supply temperatures t_{in} and the target temperatures t_{out}, respectively. For any additional heating and cooling of process streams utility streams are needed. A utility stream is defined by its inlet and outlet temperatures, heat transfer coefficient and a heat load dependent cost factor.
The given task is then to determine the network structure, which produces the minimum total annual costs. Therefore, a HEN is characterized by the heat transfer areas and heat capacity flow rates of the hot and cold streams of each existing heat exchanger within the structure. Thus, the variables to be optimized are the areas A_{ijk} and the heat capacity flow rates $\dot{W}_{h,ijk}$ and $\dot{W}_{c,ijk}$ of the stage-wise superstructure.
The total annual costs are considered as the sum of the investment costs of the heat exchangers and the costs caused by utility usage. In order to avoid binary variables it is stipulated that a positive value for a heat exchanger area indicates an existing HX within the network structure. For the calculation of the investment costs of a HX a typical area dependend approach is used:

$$C_{HX} = a + bA^c \tag{2}$$

This approach considers the fixed costs a of a HX and an area depending part bA^c. For temperature calculation an explicit analytical solution is used (Chen at al., 2007; Fieg et

al. 2009). With this method it is possible to calculate all temperatures within the network as well as the outlet temperatures of the network. In order to meet the postulated target temperatures of the process streams the excessive use of utilities proposed by Lewin et al. in 1998 is applied. A process stream that doesn't reach its target temperature at the outlet of the stage-wise superstructure will be cooled down or heated up by utility anyway. Cold utility is used if the exit temperature of this stream is higher than its target temperature and hot utility is used if its target temperature is below the exit temperature, no matter if it is a hot or a cold process stream. With this method applied the feasibility of any randomly generated HEN is ensured. The necessary heat load for additional heating or cooling is then used to calculate the costs for the utility usage. Therefore, the heat load Q_U that has to be provided by the respective utility U is linked to a cost factor c_U. The costs of each utility are calculated by:

$$C_U = c_U Q_U \tag{3}$$

Thus, the objective function is defined as the sum of the investment costs of all heat exchangers present in the HEN and the costs for the complete utility usage.

3. New synthesis method

3.1. Concept

As mentioned above specially tailored genetic algorithm are very capable of cost optimal HEN synthesis. The combination of heuristic approaches and a genetic algorithm improved the solving characteristics even further (Brandt et al., 2011). Yet, the computational time can get very high for large-scale problems. This is because of the immense amount of structural and continous variables to be optimized. Good large-scale HEN structures consist of many subnetworks, though. The main positive effect is the increasing stability of the process with increasing amount of subnetworks. Occasionally appearing disturbances like temperature changes of single process streams can only effect the respective subnetwork. Therefore, it is not necessary to optimize the whole problem in one single step. Based on this idea the concept of the new method was built up. The new algorithm decomposes the problem into as many subproblems as possible. Each of these subproblems can then be easily solved by the genetic algorithm.

3.2. The new algorithm

In a process without any heat integration each process stream can be considered as a single subnetwork. This is the starting point for the new algorithm. From this set few hot and cold streams are randomly selected to form a new subproblem definition. This subproblem is then optimized by the genetic algorithm presented in the work of Brandt et al. in 2011. From this optimization step the resulting structure is implemented back into the network. Afterwards a novel search algorithm investigates the complete HEN structure for new subnetworks and identifies them. This search algorithm is based on the depth first search method from graph theory. This ensures that all subnetworks will be identified without the need of much calculation time. The result of the search algorithm is a new set of subnetworks. From this set some subnetworks are randomly picked again in order to build a new subproblem definition for the genetic algorithm. This procedure ist carried out until the total annual costs of the complete network can not be reduced over 30 iteration steps. In order to guarantee the HEN synthesis is carried out entirely, two additional constraints are defined. The first constraint ensures that every stream has been used at least once within the optimization procedure. The

second constraint defines the minimum size of a subproblem. Each subproblem formed by several independent subnetworks must consist of more than three process streams.
In order to improve the performance of the new method further, some characteristics of the genetic algorithm are utilized. It turned out that the structural search ability of the genetic algorithm is considerable higher in comparison to the optimization of the continuous variables. Therefore, the new synthesis method runs through two stages, that mainly differs in the parametrisation of the genetic algorithm. In the first stage a rough structural search is carried out. This is to find the most promising combinations of hot and cold process streams. For this task it is reasonable to reduce the population size of the genetic algorithm. Half the size of the population compared to the normal application of the algorithm is enough for finding good first structures. Within the second stage the optimization of the subproblems is carried out more intensively. That means that at this stage the continous variables are optimized as well. Here the parametrisation is the same as for the normal application of the genetic algorithm, see Brandt et al..

3.3. Case study

In this section we demonstrate the improvement of the new method and compare the results to these from literature. For this matter we took one of the largest published examples. It was first presented in the work of Kefeng in 1998 and describes an Ethylene production plant. This example contains 55 process streams and 11 utility streams. In the respective literature a new HEN design was proposed with a claimed total annual cost of 33.1E6 $/a. However, the explicit structure of the HEN was not given. Therefore, this result has to be considered warily.
The HEN synthesis for this example was carried out ten times using the genetic algorithm introduced by Brandt et al. and ten times using the new synthesis method. The results are presented in Table 1. For each calculation run the HEN structure with the lowest total annual costs is considered. For a more practical point of view the process to process heat exchangers and the amount of subnets within these structures are presented, as well.
In order to demonstrate the improvement regarding the calculation effort the average calculation times are presented in Table 1, also. All calculations were carried out on a personal computer with an Intel Xeon 2.8 GHz CPU.

Table 1. Results for case study

	Literature	Genetic Algorithm	New Method
min. costs [$/a]	33,100,000	7,899,968	6,775,277
Number of HX [-]	51	38	32
Amount subnetworks [-]	n.a.	17	23
avg. calc. time [min]	n.a.	1,322	74

Compared to literature the results from the genetic algorithm are considerably better. Especially the costs could be reduced dramatically. On the other hand, the practicability seems also to be improved by the genetic algorithm. Although, the actual structure from literature is unknown, this is strongly indicated by the reduced number of HX. A HEN with less heat exchangers is more likely to have a higher amount of subnetworks. Furthermore, the risk of remixing of process streams due to leakages is reduced by the presence of fewer heat exchangers. Finally, by the application of the new synthesis

method these results could be improved even further. The found structure shows more subnetworks, less heat exchangers and decreased total annual costs by 14 %. A noticable reduction in the calculation time could also be observed. In comparison to the simple application of the genetic algorithm the new synthesis method is about 18 times faster.

4. Conclusion

In this work a new synthesis method for large-scale HEN was introduced. This method uses subnetworks in order to improve the solving characteristics of a genetic algorithm. The application of this method on a large scale problem with 55 process streams yielded very promising results. Compared to the simple application of a genetic algorithm the new method was 18 times faster and a HEN structure was found with 14% less total annual costs. In addition, the practicability could also be improved. The application of the new method yielded a structure with more subnetworks and less process to process heat exchangers.

References

C. Brandt et al., 2011, Efficient synthesis of heat exchanger networks combining heuristic approaches with a genetic algorithm, Heat Mass Transfer, Volume 47, Issue 8, 1019-1026

D.-Z. Chen et al., 2007, An explicit solution for thermal calculation and synthesis of superstructure heat exchanger networks, Chinese Journal of Chemical Engineering, Volume 15, Issue 2, 296-301

G. Fieg et al., 2009, A monogenetic algorithm for optimal design of large-scale heat exchanger networks, Chemical Engineering and Processing: Process Intensification, Volume 48, Issues 11-12, 1506-1516

W. Kefeng, 1998, Model and algorithm for optimal synthesis of large scale heat exchanger networks without stream splitting, Journal of south China University of Technology, Volume 26, Issue 11, 52-61

D. R. Lewin et al., 1998, A generalized method for HEN synthesis using stochastic optimization – I. General framework and MER optimal synthesis, Computers and Chemical Engineering, Volume 22, Issue 10, 1503-1513

B. Linnhoff, J. R. Flower, 1978, Synthesis of heat exchanger networks: I. Systematic generation of energy optimal networks, AIChE Journal, Volume 24, Issue 4, 633-642

X. Luo et al., 2009, A hybrid genetic algorithm for synthesis of heat exchanger networks, Computers and Chemical Engineering, Volume 33, Issue 6, 1169-1181

T. F. Yee et al., 1990, Simultaneous optimization models for heat integration – I. Area and energy targeting and modeling of multi-stream exchangers, Computers and Chemical Engineering, Volume 14, Issue 10, 1151-1164

I.A. Karimi and Rajagopalan Srinivasan (Editors), Proceedings of the 11th International Symposium on Process Systems Engineering, 15-19 July 2012, Singapore.

Dynamic characteristics of self-heat recuperative distillation process

Yasuki Kansha, Akira Kishimoto, Atsushi Tsutsumi

Collaborative Research Center for Energy Engineering, Institute of Industrial Science, The University of Tokyo, 4-6-1, Komaba, Meguro-ku Tokyo 153-8505, Japan

Abstract

Recently, self-heat recuperation technology has been developed. In this technology, whole process heat is recirculated in the process without heat addition, leading to the drastic energy saving for the process. Although the process based on this technology can achieve drastic energy saving at steady state, the dynamics of the process have not been investigated. Therefore, operators of the process have to manually switch the conventional operation mode to the operation mode by self-heat recuperation at reaching steady-state. Two stream lines for each operation mode are required and increase the capital cost. Thus, in this paper, the dynamic characteristics of the self-heat recuperative process for distillation have been investigated to design operation systems such as controllers for further energy saving and stability of this process during operation.

Keywords: Energy, modeling, self-heat recuperation, dynamics, exergy

1. Introduction

Distillation has been widely used for separation in industries owing to the simplicity of their process. Simultaneously, it is well-known process for consuming a large amount of energy, because of large latent heat between liquid and vapor phases. So far, many innovative distillation processes for energy saving purpose have been developed. A vapor recompression (VRC, Annakou and Mizsey, 1995) technology is one of the most famous technologies, in which the top vapor stream is compressed and the heat of the stream is exchanged with the heat of the bottom liquid stream in the column to recover the heat of condensation to the heat of vaporization. Another famous technology is a heat integrated distillation column (HIDiC, Huang et al., 2006). In this technology, the distillation column can be divided into two parts and the condensation heat is exchanged with the vaporization heat between these two parts by using pressure difference. However, both VRC and HIDiC are only focused on heating by the reboiler in the distillation column and are not interested in the heating of feed stream to the distillation. Recently, by incorporating compressors and heat exchangers, the authors have developed another attractive technology to reduce the energy consumption of chemical processes (Kansha et al. 2009) and applied it to the distillation process (Kansha et al. 2010a,b). In this technology, a process unit is divided into functions to analyze the process required heat and all of the self-heat of process stream is recirculated in the process without any external heat source. As a result, the energy consumption and exergy destruction of the process can be greatly reduced in the steady state. Although this technology achieved reduction of energy consumption in the steady state, only few investigations of process dynamics and operation methods for the self-heat recuperative process have been performed. Thus, to apply this technology to actual industrial processes, it is necessary to design the operation system. In fact, there is a pilot self-heat

recuperative distillation process for ethanol production in Japan. This process achieves drastic energy reduction in the steady state. However, operators are switching the operation mode and stream lines when it reaches steady state condition.
Thus, we investigated the dynamic characteristics of the self-heat recuperative process especially distillation, to design the operation systems for the process, achieve further energy savings and investigate the stability of the process during operation in this research.

2. Self-Heat Recuperative Separation Process

To Apply the self-heat recuperation technology to separation processes (Kansha et al. 2010a,b), a system including not only the separation process itself but also the preheating/cooling section, is divided on the basis of their functions, namely separation and heat circulation modules in which the heating and cooling loads are balanced, as shown in Fig. 1. This figure shows the case which has one feed and two products. The enthalpy of inlet stream (feed) is equal to that of the summation of outlet streams (products) in each module. Then, the cooling load in each module is recuperated by compressors and exchanged with the heating load by following the self-heat recuperation technology. As a result, the heat of the process stream (self heat) is perfectly circulated without any heat addition in each module, the perfect internal heat circulation in a whole separation process can be obtained.

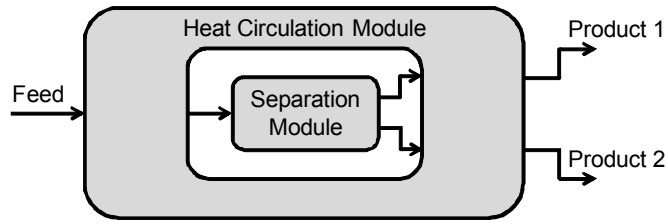

Fig. 1. Conceptual figure of Self-Heat Recuperative Separation

2.1. Self-heat recuperative distillation

To prevent the emission of CO2 by following the self-heat recuperation technology (Kansha et al. 2010b), distillation process can be divided into two sections, namely the preheating and distillation sections, on the basis of their functions. The heating and cooling load are balanced by performing enthalpy and exergy analysis, and the self-heat recuperation technology is applied in these two sections. In the preheating section, one of the streams from the distillation section is a vapor stream and the stream to the distillation section has a vapor–liquid phase. It is necessary to balance the enthalpy of the feed streams and that of the effluent streams in the section, namely heat circulation and distillation module. In balancing the enthalpy of the feed and effluent streams in the heat circulation module, the enthalpy of the streams in the distillation module is automatically balanced. Thus, the reboiler duty is equal to the condenser duty of the distillation column. Therefore, the vapor and liquid sensible heat of the feed streams can be exchanged with the sensible heat of the corresponding effluent streams and the vaporization heat can be exchanged with the condensation heat in each module as shown in Fig. 2.
Figure 2 (a) shows the structure of a self-heat recuperative distillation process consisting of two standardized modules, namely, the heat circulation module and the distillation module. Note that in each module, the summation of the enthalpy of the feed

streams and that of the effluent streams are equal. Figure 2 (b) shows the temperature and heat diagram of the self-heat recuperative distillation process. Both the sensible heat and the latent heat of the feed stream are subsequently exchanged with the sensible and latent heat of effluents in a heat exchanger. The vaporization heat of the bottoms from the distillation column is exchanged with the condensation heat of the distillate from the distillation column in the distillation module. The heat of streams are recuperated by the compressors and exchanged with the heat in the module. It can be seen that all the self-heat is exchanged. As a result, the exergy loss of the heat exchangers can be minimized and the energy required by the distillation process is reduced to 1/6–1/8 of that required by the conventional heat exchanged distillation process. Finally, to examine the feasibility of the simulation when applied to the industrial processes in petrochemical industry, Matsuda et al. (2011) provided it with practical industrial data and modified the stream lines to be suitable for the practical processes. The energy required, exergy destruction and economical efficiency are examined. From these studies, it can be concluded that the self-heat recuperative distillation process is a very promising process for energy saving.

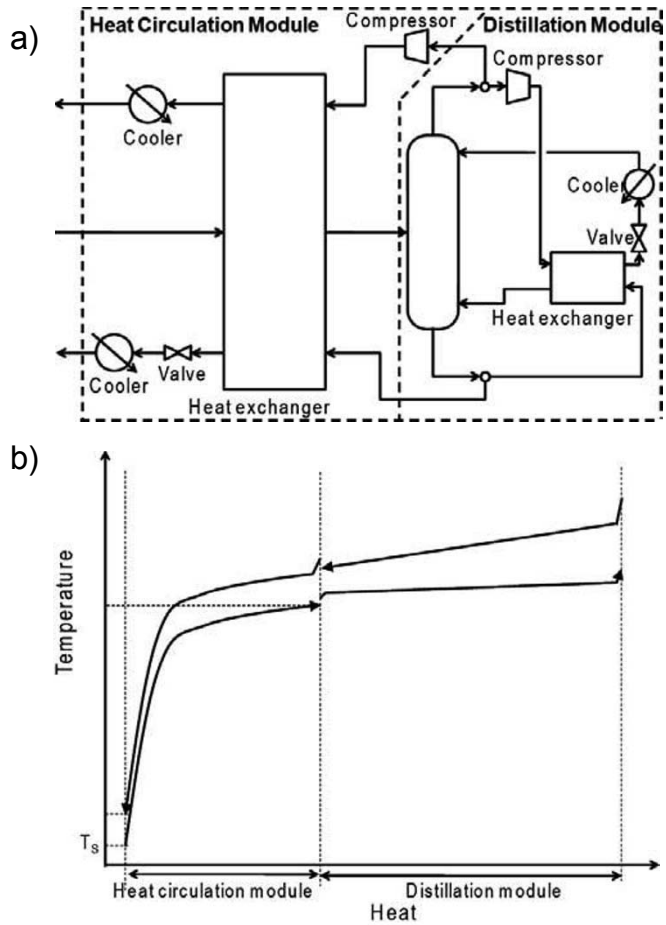

Fig. 2. A Schematic Image of Self-Heat Recuperative Distillation

3. Dynamic Characteristics of Self-Heat Recuperative Process

To investigate the dynamic characteristics of a self-heat recuperative process, step response test was conducted by HYSYS Ver. 7.3 (ASPEN Tech.). The schematic flow diagram for gas stream is shown in Fig. 3. As a real fluid, butane was used for the gas stream. The stream 1 was heated from 25 ^{o}C to a set temperature 100 ^{o}C, and the flow rate of the stream was 100 kmol/h at the initial steady state and ±10 % step changes of the flow rate were introduced to investigate the dynamics. The Soave-Redlich-Kwong (SRK) was used for the state equation. The minimum temperature difference for heat exchange was assumed to be 6 K. The efficiency of the heat exchanger and the adiabatic efficiency of the compressor were 100% (i.e., no heat loss) and 80%. A type of heat exchanger and TEMA type were assumed shell and tube and AFL. Overall heat transfer (UA) in the heat exchanger was 1.216×10^{5} kJ/K^{-1}h^{-1}. The pressure drops of both streams in this heat exchanger are 0.69 kPa. The stream pressures among the compressor are 100.6 and 120.8 kPa. Figure 4 shows the representative response curves of stream temperatures (stream 2 and 4) when the flow rate 10% increase is introduced. It can be seen that the stream temperature of stream 2 cannot reached to the set temperature (100 ^{o}C) due to the increased flow rate. This means that in the case of gas streams, this process cannot naturally keep the equal enthalpy of the feed streams to that of the effluent streams in the module without any adequate operation system under dynamic condition.

As well as the case study with gas stream, the simulation using water as a vapor/liquid stream to close the distillation process was conducted. In this simulation, water must be liquid at standard condition. Thus, it is easy to understand that this process requires the heater to produce vapor initially. Although the heater to initially heat the process stream was introduced, the super heated steam cannot be produced and vapor/liquid mixture was produced in this dynamic simulation. The feed water transforms the phase from liquid to vapor in the heat exchanger in steady state simulation. However, the hold-up in the heat exchanger is required in dynamic simulation and it cannot perfectly transform the phase in this ordinal heat exchanger. Thus, it requires other suitable heat exchanger to produce the super heated steam.

To realize the ideal heat circulation module, it is required to balance the enthalpy of the feed streams to that of the effluent streams. However, this observed phenomena caused by hold-up in the heat exchanger seem to be preferable in respect of design of the heat circulation module in the self-heat recuperative distillation, because the void fraction and enthalpy of feed stream are possible to be controlled by controlling the hold-up level in the heat exchanger.

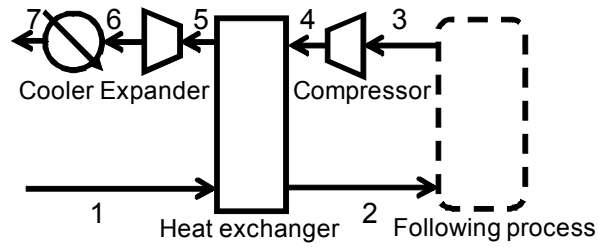

Fig. 3. Flow Diagram for Gas Stream Using Self-Heat Recuperation

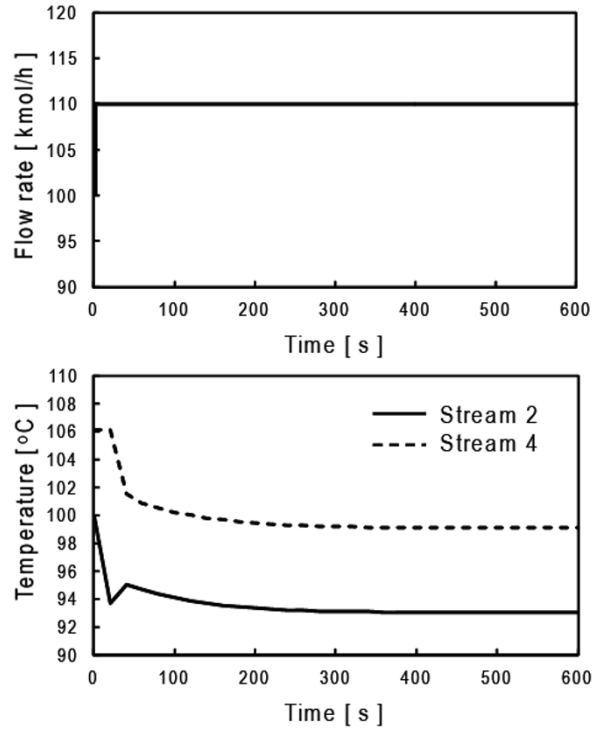

Fig. 4. Step Change of Flow Rate from 100 to 110 kmol/h and Response of Stream Temperature

4. Conclusion

The dynamic characteristics of the self-heat recuperative process to design the operation systems for the process to achieve further energy saving and to investigate the stability of the process during operation are investigated in this paper. To realize the self-heat recuperative distillation, it requires balancing the enthalpy of the feed streams to that of the effluent streams. According to these simulations, it is necessary to design the suitable operation system with further investigation to automatic operation. However, it can also be seen that this process has some potential for further energy saving.

References

O. Annakou, P. Mizsey, 1995, Rigorous Investigation of Heat Pump Assisted Distillation, Heat Recovery Syst. CHP, 15, 241–247

K. Huang, K. Matsuda, T. Takamatsu, M. Nakaiwa, 2006, The Influences of Pressure Distribution of Ideal Heat-Integrated Distillation Column (HIDiC), J. Chem. Eng. Japan, 39, 652–660

Y. Kansha, N. Tsuru, K. Sato, C. Fushimi, A. Tsutusmi, 2009, Self-Heat Recuperation Technology for Energy Saving in Chemical Processes, Ind. Eng. Chem. Res., 48, 7682–7686

Y. Kansha, N. Tsuru, C. Fushimi, K. Shimogawara, A. Tsutsumi, 2010, An Innovative Modularity of Heat Circulation for Fractional Distillation, Chem. Eng. Sci., 65, 330–334

Y. Kansha, N. Tsuru, C. Fushimi, K., A. Tsutsumi, 2010, Integrated Process Module for Distillation Processes Based on Self-Heat Recuperation Technology, J. Chem. Eng. Jpn., 43, 502–507

K. Matsuda, K. Kawazuishi, Y. Kansha, C. Fushimi, M. Nagao, H. Kunikiyo, F. Masuda, A. Tsutsumi, 2011, Advanced Energy Saving in Distillation Process with Self-Heat Recuperation Technology, Energy, 36, 4640-4645

I.A. Karimi and Rajagopalan Srinivasan (Editors), Proceedings of the 11th International Symposium on Process Systems Engineering, 15-19 July 2012, Singapore.

Model-Based Optimal Design of Experiments for Determining Reaction Network Structures

M. D. Hoang[a*], G. Wozny[a], Y. Brunsch[b], A. Behr[b], J. Markert[c], C. Hamel[c], A. Seidel-Morgenstern[c], H. Arellano-Garcia[a]

[a] *Chair of Process Dynamics and Operation, TU Berlin, Str. des 17. Juni 135, 10623 Berlin, Germany*

[b] *Technische Chemie A, TU Dortmund, Emil-Figgestr. 66, 44227 Dortmund, Germany*

[c] *Chemische Verfahrenstechnik, OvGU Magdeburg, 4120, 39016 Magdeburg, Germany*

Abstract

A new approach for optimal experimental design has been developed to support the work of chemists and process engineers in determining reaction kinetics of complex reaction networks. The methodology is applied on sub-networks of the hydroformylation process of 1-dodecene with a Biphephos-modified rhodium catalyst in a DMF-decane thermomorphic solvent system (TMS). The isomerization and hydrogenation sub-networks are systematically analyzed with respect to parameter estimability. They are determined in a sequential approach using model-based optimal experimental design via perturbations with respect to temperature and synthesis gas pressure, and subsequently used to build up the reaction network. The focus of this contribution is the parameter estimation procedure at the very early investigation stage where model uncertainties are high. Sensitivities of sensitive parameters are increased while others are suppressed, which are carried over from the estimated sub-networks or structurally more difficult to determine. This subsequently leads to more reliable parameter estimations.

Keywords: optimal experiment design, model discrimination, parameter estimation, hydroformylation, 1-dodecene

1. Problem Statement

The German Collaborative Research Centre/Transregio 63 is engaged in the development of efficient production processes based on integrated chemical processes in liquid multiphase systems (InPROMPT). Currently, the hydroformylation process of 1-dodecene with a Biphephos-modified rhodium catalyst in a DMF-decane TMS-system is investigated. The proposed complete hydroformylation reaction network is quite complex. It is well known, that side reactions can occur in the hydroformylation reaction like isomerization and hydrogenation of 1-dodecene and its isomers. These side reactions have a negative influence on the product distribution. Hower, side or subsequent reactions leading to adols, alcohol and acids have not been observed in all our experiments leading to a reaction network as proposed in Fig. 1:

* Corresponding author Tel.: +49-30-314-26901; Fax: +49-30-314-26915; E-mail: duc.hoangminh@mailbox.tu-berlin.de

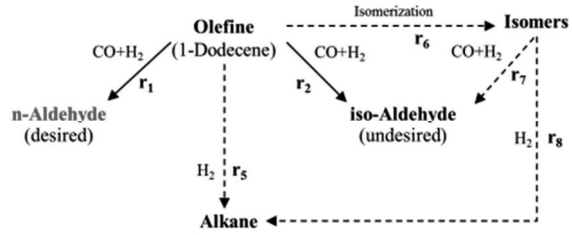

1: investigated hydroformylation reaction network

The hydroformylation network involves a large number of parameters so that it could not be estimated in an *all-in-one* approach. Therefore, an investigation series of sub-networks is suggested in order to achieve an accurate estimation of the kinetic parameters. The crucial idea is to avoid simply putting the estimated sub-networks together but to regard their estimated parameter sub-sets as uncertainties. Moreover, regarding the parameter estimation of complex reaction networks, it is usually necessary to fix some parameters in order to estimate the free parameters properly. However, most of the experimental design approaches aim at maximizing sensitivities of all parameters. It is rather recommendable to hold the sensitivities of those parameters, which are going to be held constant, as low as possible.

In both cases, the goal is to ensure an acceptable performance of the parameters to be estimated for all possible values of uncertain parameter subsets. A new robust experimental design method is proposed to implement this idea (see 2.2.2).

Notation

c_i	concentration of component i	$c^{L,I}$	g-l-interphase concentration
k_{eff}	effective mass transport coefficient	p	partial pressure
H	Henry coefficient	$\mathrm{H_{ads}}$	adsoprtion enthalpie
r	reaction rate	k_r	reaction rate coefficient
k_{ref}	normalized frequency factor	k_{eff}	effective mass transfer coefficient
c_{Cat}	catalyst concentration	z	state variable (concentrations,…)
s	sensitivity ($\partial z/\partial\theta$)	s^*	sensitivity to be suppressed
u	control variable	h	element length (OC on FEM)
N_e	number of elements(OCFEM)	N_n	number of states
N_θ	number of parameters	N_{sp}	number of sampling points
K	order of OC on FEM	Q	weighting matrix
q_r	diag. element of Q w.r.t. the r-th state	E_a	activation energy

Greek letters

θ_i	i-th parameter	ψ	polynomial base of degree K

2. Methodology

2.1. Model building

By dividing the main network into sub-networks, one can determine the parameters step by step. The isomerization and hydrogenation sub-networks are shown in figure 2a and 2b.

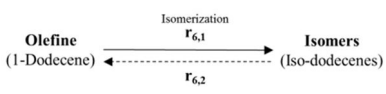

2a: Isomerization sub-network

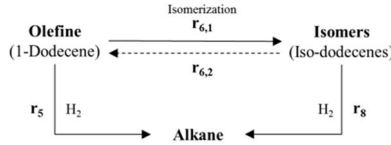

2b: Hydrogenation sub-network

The mass transfer of hydrogen through the gas-liquid interface is modeled as:

$$\dot{N}_{H_2} = k_{eff,H_2}\left(c_{H_2}^{L,I} - c_{H_2}^{L}\right)$$

Using the Henry's Law with the Van't Hoff temperature dependency, the interfacial concentration on the liquid side can be described as follows

$$c_{H_2}^{L,I} = \frac{p_{H_2}}{H_{H_2}(T)}, \qquad H_{H_2}(T) = H_{0,H_2}\, exp\left(\frac{H_{ads}}{RT}\right)$$

The ractionrate for the isomerization and hydrogenation reaction are as follows

$$r_{6_1/6_2} = c_{Cat} k_{r,6_1/6_2}\, c_{Doce/IsoDoce}^{L}, \qquad r_{5/8} = c_{Cat} k_{r,5/8} c_{H_2}^{L} c_{Doce/IsoDoce}^{L}$$

The temperature dependency of the reaction rate coefficients are described as proposed by Buzzi-Ferraris et al. [2009]:

$$k_{r,i} = k_{ref,i} ex\, p\left(-\frac{E_{a,i}}{R}\left(\frac{1}{T} - \frac{1}{T_{ref}}\right)\right)$$

2.2. Estimability analysis

If it is not possible to estimate all parameters in an *all-in-one* approach, then one would like to know, which one has to be held constant in the first estimation loops. In this step, the parameter estimability analysis proposed by Franceschini and Machietto [2008] is applied. If the rank of the estimability matrix P_E is equal to the number of parameters N_θ, then all model parameters are estimable. If not, the analysis of the P_E-matrix will give us the information of which parameter sensitivity must be taken out of the analysis. This is equivalent to identify those parameters, which must be held constant in the subsequent parameter estimation. The idea is to push the sensitivities of those parameters to zero. This aims for ensuring an acceptable performance of the "estimable" parameters for all possible values of the discarded parameters.

2.3. Optimal Experimental Design

The main idea of maximizing the divergence of competing model candidates for model discrimination or maximizing the information content of designed experiments for precise parameter estimation are the main methods of the model based experimental design community. In this work, a simultaneous approach for optimal experimental design is proposed based on the simultaneous optimization approach of Biegler et al. [1991]. Moreover, a new A_R-criterium for robust parameter estimation is discussed.

2.3.1. Problem Formulation

The defined problem (Espie and Macchietto, [1989]) can generally be written as an optimal control problem consisting of the objective function:

$$\varphi(z(t), s(t), u(t), \theta) = \sum_{l=1}^{N_{sp}} \Phi_l(z(t_l), s(t_l), u(t_l), \theta)$$

which is to be maximized, subject to a process model:

$$0 = f(z(t), s(t), u(t), \theta), \qquad 0 = g(z_{t0}, s_{t0}, u_{t0}, \theta)$$

where $0 = g(...)$ is the general formulation of the initial state conditions. Furthermore the system has to follow the constraints of states and controls:

$$z_L \le z \le z_U, \qquad u_L \le u \le u_U$$

2.3.2. Robust Experimental Design Criterion

Applying the simultaneous approach with orthogonal collocation on finite elements on the A_R-criterion, one obtains:

$$\max_{u_{ik},z_{ik},s_{ik}} \varphi(u_{ik},z_{ik},s_{ik}) = \sum_{m=1}^{N_{sp}} \left(\frac{\sum_{r=1}^{N_n}\sum_{s=1}^{N_\theta} q_r \cdot (s_{ik}^{rs})^2}{\exp\left(\sum_{r=1}^{N_n^*}\sum_{s=1}^{N_\theta^*} q_r \cdot \left(s_{ik}^{*,rs}\right)^2\right)} \right)_m$$

Where x_{ik} are the fully discretized state variables, $x := [z, s]$. The equality and inquality constraints of the process model are:

$$0 = \sum_{k=0}^{K} x_{ik}\dot{\psi}_k(\tau_j) - h_i f(x_{ij}, u_{ij}, \theta), \qquad i = 1, \dots, N_e; j = 1, \dots, K$$

$$x_{10} = x_{t_0}, \qquad x_{l0} = x_{l-1K}, \qquad l = 2, \dots, N_e$$

$$x_L \le x_{ij} \le x_U, \qquad u_L \le u_{ij} \le u_U$$

In order to maximize the objective function φ, the sensitivities of the discarded parameters $s_{ik}^{*,rs}$ are suppressed.

3. Results

The methodology is described by an experimental design example for robust parameter estimation of the hydrogenation sub-network.

It is very common to identify the solubility of the gas educts separately without the reactions. Those thermodynamic parameters are fixed afterwards for the determination of the reaction kinetics parameters. Nevertheless they still represent uncertainties because of their high sensitivities towards the reaction rates and so make the kinetic parameter estimation unreliable. Now, one would like to have an experimental design which suppresses the sensitivities of the solubility parameters making the kinetic measurements more robust towards mass transfer effects.

As shown in figure 3a the sensitivity of solubility parameters could be reduced upto 50%. On the other hand the designed experiment still yields high sensitivities for the wanted kinetic parameters (fig. 3b). The difference with respect to control trajectories between classical and robust experimental design can be seen in figure 4.

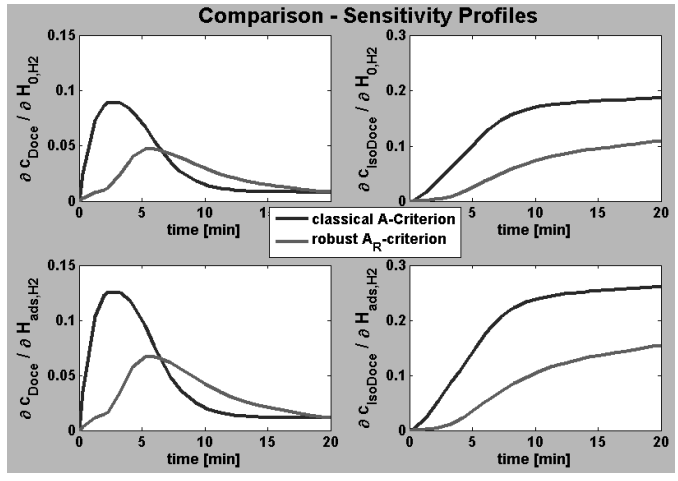

3a: sensitivities with respect to solubility parameters

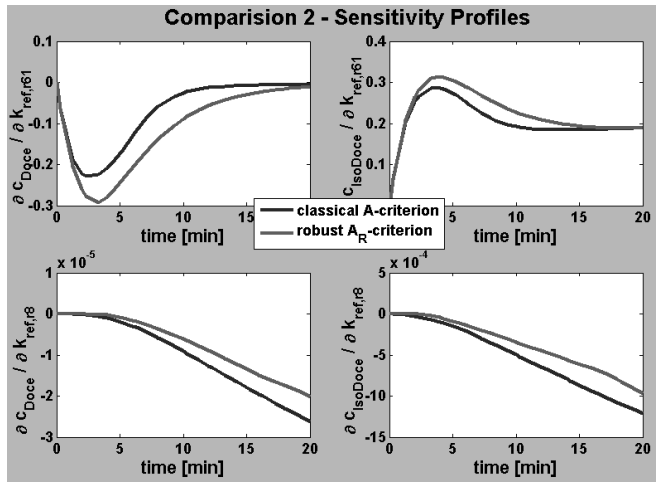

3b: sensitivities with respect to kinetic parametres

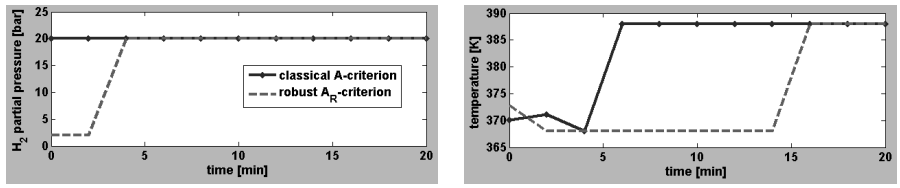

4: sensitivities with respect to kinetic parametres

4. Conclusion

The solution strategy aims at dividing a complex reaction network into sub-networks, in particular, if an *all-in-one* parameter estimation approach is not possible. The determination of the sub-networks provides parameter subsets which are transfered to the main reaction network and treated as uncertainties. The new method aims for a robust optimal experimental design which ensure an acceptable performance of the new parameters for all possible values of the carried over parameter-subsets. This subsequently leads to more reliable kinetic parameter estimations.

Acknowledgement: This work is part of the Collaborative Research Centre "Integrated Chemical Processes in Liquid Multiphase Systems" coordinated by the Technische Universität Berlin. Financial support by the Deutsche Forschungsgemeinschaft (DFG) is gratefully acknowledged (TRR 63).

References

Behr A., Obst D., Turkowski B., 2004 Isomerizing Hydroformylation of *trans*-4-octene to *n*-nonanal in Multiphase Systems: Acceleration Effect of Propylene Carbonate, Journal of Molecular Catalysis A: Chemical 226, 215–219

Biegler T. L., Tjoa B., 1991, Simultaneous Solution and Optimizazion Strategies for Parameter Estimation of DAE Systems, Ind. Eng. Chem. Res., 30, 376-385

Buzzi-Ferraris G., Manenti F., 2009, Kinetic models analysis, Chem. Eng. Sience, 64, 1061-1074

Espie D., Macchietto S., 1989, The Optimal Design of Dynamic Experiments, AIChE J., 35, 2, 223-229

Franceschini G., Macchietto S., 2008, Model-based design of experiments for parameter precision: SotA, Chem. Eng. Science, 63, 4846-4872

Koeken C.J. A., v. d. Broeke J.P.L., Deelman B., Keurentjes T.F. J., 2011,Full kinetic description of 1-octene hydroformylation in a supercritical medium. Journal of Molecular Catalysis A: Chemical, 346, 1-11

I.A. Karimi and Rajagopalan Srinivasan (Editors), Proceedings of the 11th International Symposium on Process Systems Engineering, 15-19 July 2012, Singapore.

A continuous hydroformylation process in a mini-plant scale: equipment design for the separation of three liquid phases

Michael Müller[a,*], Yasemin Kasaka[b,*], David Müller[a,*], Reinhard Schomäcker[b,*], Günter Wozny[a,*]

[a]*Chair of process Dynamics and Operation, Sekr. KWT9*
[b]*Department of Chemistry, Sekr. TC8*
[*]*Berlin Institute of Technology, Straße des 17. Juni 135, D-10623, Germany*

Abstract

A novel process concept for the hydroformylation of long chain olefins in micro emulsions is investigated and developed within the framework of a Collaborative Research Centre in Germany. In this process, the liquid feed material (C12 olefin) is brought in contact with a hydrophilic rhodium-ligand-complex, which is dissolved in an aqueous phase while forming a micro emulsion system under the use of non-ionic surfactants. The hydroformylation reaction is started by adding syngas (H_2&CO) into a continuously stirred tank reactor (CSTR). Due to phase separation into an aqueous phase (catalyst-rich) and an organic phase (product-rich), the valuable rhodium catalyst can be retrieved and recycled. This key separation step is challenging and crucial for the technical and economic feasibility of the overall process concept and plant design.

Depending on the temperature the mixture decomposes into two or even three liquid phases. Preliminary investigations have shown that product and catalyst separation in a continuous process is only attainable in the three phase state, given the required separation time and quality. However, due to the lack of thermodynamic data for micro emulsion mixtures, the design of the phase separation unit strongly depends on experimental data. Consequently, a systematic experimental approach has been developed to identify potential operating conditions and relevant design parameters. In order to classify and find these, a set of systematic experimental set-ups have been investigated to characterize impact factors on the phase separation such as type of surfactant, different concentrations of surfactant, olefin, product, and water. With the information gained through the observations the relevant composition of the investigated mixture and the separation temperature are determined for the operating conditions. Finally, necessities with regards to plant and process design are revealed.

Keywords: Hydroformylation, micellar catalysis, phase separation, process design

1. Introduction

Hydroformylation represents an important application in the field of homogenous catalysis. For short olefins, hydroformylation has already been established as a standard process in order to produce aldehydes. Due to the decreasing solubility of alkenes with an increasing length of carbon chains in the aqueous phase, hydroformylation of higher olefins is not yet performed in industry. Therefore, non-ionic surfactants are applied to

increase the miscibility of the oil- and the catalyst-containing water phase. In order to increase yield and selectivity even under mild reaction conditions, a water-soluble, hydrophilic rhodium-ligand-complex is employed. The resulting multiphase system offers the possibility to separate the valuable rhodium catalyst comparatively easy from the organic product (Bode et al., 2000). Figure 1 shows the novel process concept for the hydroformylation of long chain olefins in a micellar multiphase system.

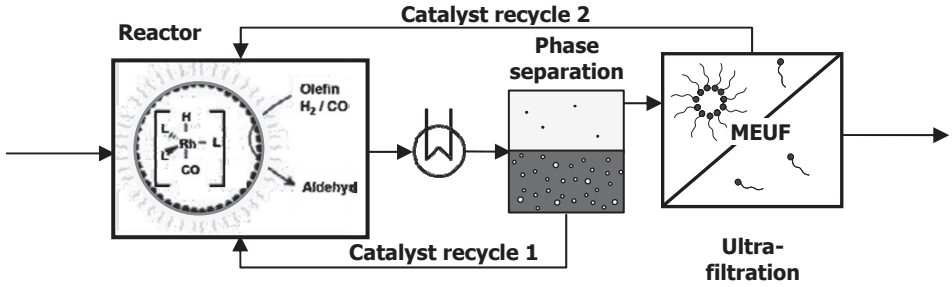

Figure 1: Novel process concept for the hydroformylation of long chain olefins

The first step is the hydroformyltion reaction of C12 olefins in a CSTR according to Figure 2. Secondly, the valuable catalyst is retrieved by means of phase separation and subsequently recycled to the reactor. Due to high catalyst costs a second separation step through ultra filtration is required to reduce the catalyst loss to a minimum (lower 1ppm) and to ensure economic feasibility.

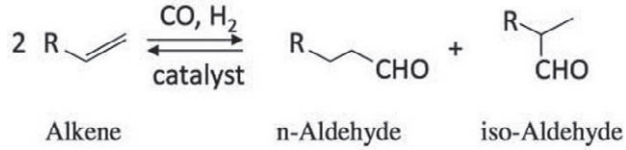

Figure 2: Basic concept of the hydroformylation reaction equation (Kupka, 2006)

The initial catalyst removal takes place in the phase separation unit (decanter), in which most of the rhodium is drawn into the aqueous phase. Preliminary investigations have shown that this is quite challenging. Phase separation itself as well as separation quality and time strongly depend on the type of surfactant and its concentration (γ, Eq. 1), on temperature, on the amount of water (α, Eq. 2), and product (λ, Eq. 3). The following three equations are employed to represent the respective concentrations after the reaction.

$$\gamma = \frac{m_{\text{surfactant}}}{m_{\text{olefin}} + m_{\text{water}} + m_{\text{surfactant}}} \tag{1}$$

$$\alpha = \frac{m_{\text{olefin}}}{m_{\text{olefin}} + m_{\text{water}}} \tag{2}$$

$$\lambda = \frac{m_{\text{aldehyde}}}{m_{\text{aldehyde}} + m_{\text{olefin}}} \tag{3}$$

2. Systematic analysis of the micro emulsion mixture for process and equipment design

Due to the lack of thermodynamic data for micro emulsion mixtures and a lack of reliable simulations, the design of the phase separation unit strongly depends on experimental data. Therefore, a systematic experimental approach is developed so as to identify potential operating conditions and relevant design parameters.

2.1. General phase separation behavior

In a first step, the general phase separation behavior is determined. There are four potential states, which depend on temperature and conversion rate. These are depicted in Figure 3 in the form of Kahlweit´s fish (Kahlweit et al., 1983) for a given composition.

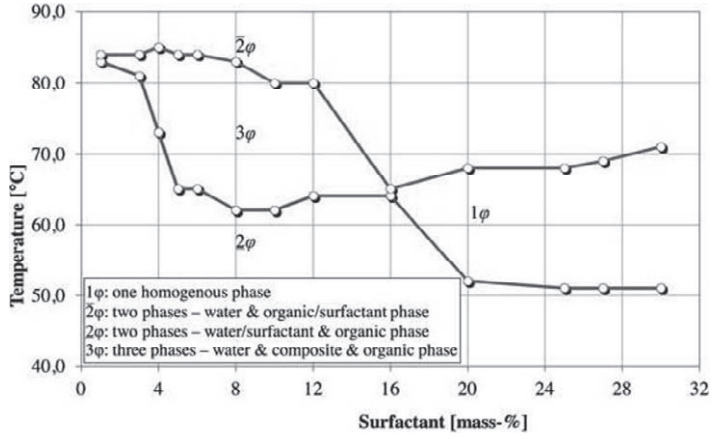

Figure 3: Kahlweit's fish for Marlophen NP9, α=0.5 and λ=0.5 conversion

Preliminary investigations of a mixture consisting of Marlophen NP9, water, and dodecene show that product and catalyst separation in a continuous process are only attainable in the three phase state, given the required separation time and quality. Hence, the initial aim is to identify the three phase region to find potential operating conditions.

2.2. Dynamics of phase separation & quality classification

In a second step the separation dynamics and quality of the three phase state has to be determined. Therefore, the mentioned composition is mixed in a tempered measuring glass and the separation progress of each single phase is recorded. In Figure 4 two graphs are shown for the dynamic separation behavior at 71°C and 74°C.

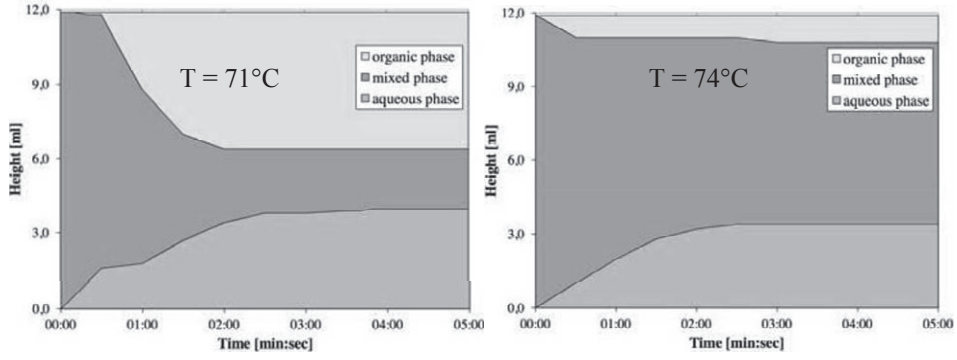

Figure 4: Dynamic phase separation behavior for γ=0.05, α=0.5, λ=0.5 at 71°C and 74°C

For 71°C the separation occurs comparatively fast, reaching a quasi steady state after around three minutes. All of the three phases appear transparent, which signifies a complete separation of the micro emulsion. A further quality criterion is a small mixed phase in comparison to the other two phases. These observations imply a qualitatively good separation. On the other hand, the graph for 74°C shows that the separation of the organic phase is poor and most of the product remains in the mixed phase. This is an example for an undesired phase separation behavior. The comparison of these two examples illustrates the difficulty in handling this multiphase system, because of the strong temperature dependency. Even within the three-phase-state, the separation quality of each phase differs strongly for small temperature changes, in this case, 3 K. This necessitates a flexible and fast temperature control.

2.3. Continuous separation

Since adequate and potential process parameters were found by means of the dynamic investigations of the mixture, the next step is the demonstration of the general applicability in a continuous separation process. Figure 5 shows the PFD-diagram and a picture of the applied experimental test set-up. The mixture consisting of γ=0.05, α=0.5, λ=0.5 is heated and stirred in the composite storage tank and pumped into the heated glass decanter, which is designed referring to the required retention time. Here, both of the heavier phases, the catalyst rich aqueous and the surfactant rich middle phase, are removed together. The lighter organic product phase is removed separately. The experimental results show that the separation of a three phase micellar multiphase system is possible for a continuous process.

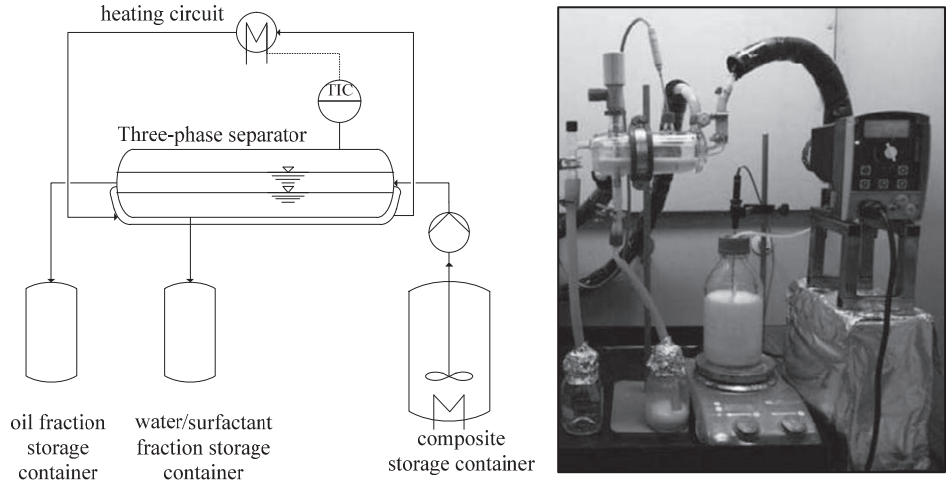

Figure 5: PFD diagram and a picture of the experimental test set-up for the continuous separation of a three phase micellar multiphase system

3. Mini-plant Design

The systematic approach discribed so far aids in designing a mini-plant to test the viability of the process concept and at the same time shows opportunities to optimize the yield of the almost pure organic product phase. The observations of the dynamic separation behavior highlight the necessity of a temperature control system in both

reactor and decanter of the mini-plant. Thus, the temperature for an optimal phase separation with respect to quality and time can be maintained. Furthermore, the results obtained during the continuous separation allow for the sizing of the actual decanter in relation to the reactor volume. The instability of the phase separation dynamics with regards to the temperature influence imply the implementation of an additional quality control of the product phase to ensure and ascertain the composition. This is achieved through an online HPLC which can be used to modify and control feed and recycle streams of the mini-plant.

To proceed, the afore mentioned investigation of the phase separation dynamics may aid in improving the control concept through the development of a short-cut model predicting the phase sizes in the decanter. This requires extensive experimental investigations of the stand-alone decanter for various temperatures and concentrations.

4. Conclusion

The removal of the valuable rhodium catalyst for recycling by means of phase separation is vital for the economical and technical feasibility of the proposed novel process concept for the hydroformylation of long chain olefins. To identify potential process and design parameters for a micellar multiphase system, a systematic approach has been successfully developed and established in three steps. First of all the general phase separation behavior was determined. Then, the dynamics of the phase separation were investigated, which basically provide information to evaluate and classify potential process parameters and to enable the design of a decanter. In the last step, the applicability of a continuous phase separation was demonstrated by means of an experimental test set-up. This systematic approach now offers the possibility to adapt the decanter operation of the mini-plant towards new developments concerning the micellar multiphase mixture and contributes to improve and develop the novel process design systematically.

Acknowledgement: The authors acknowledge the support from the Collaborative Research Center SFB/TR 63 InPROMPT “Integrated Chemical Processes in Liquid Multiphase Systems” coordinated by the Berlin Institute of Technology and funded by the German Research Foundation.

References

1. G. Bode, M. Lade, R. Schomäcker, 2000, The Kinetics of an Interfacial Reaction in Micro-emulsions with Excess Phases, Chem. Eng. Technol. 23, 405-409.
2. J. A. Kupka, 2006, Hydroformylierung von 1-Octen in Mikroemulsion, Diss. Technische Universität Braunschweig.
3. M. Kahlweit, R. Lessner, R. Strey, 1983, Influence of the Properties of the Oil and the Surfactant on the Phase Behavior of Systems of the Type H_2O-Oil-Nonionic Surfactant, J. Phys. Chem. 87, 5032-5040.

I.A. Karimi and Rajagopalan Srinivasan (Editors), Proceedings of the 11th International Symposium on Process Systems Engineering, 15-19 July 2012, Singapore.

A generic process template for continuous pharmaceutical production

Ravendra Singh,[a] Raquel Rozada-Sanchez,[b] William Dean,[b] Jacob Perkins,[b] Frans Muller,[b] Andy Godfrey,[b] Krist V. Gernaey,[a] Rafiqul Gani,[a] John M. Woodley[a]

[a]*Department of Chemical and Biochemical Engineering, Technical University of Denmark (DTU), DK-2800 Kgs. Lyngby, Denmark*

[b]*AstraZeneca Limited, Charter Way, Silk Road Business Park, Macclesfield, Cheshire SK10 2NA, UK*

Abstract

In the work reported here, a conceptual generic continuous process *template* for pharmaceutical production is presented. The template is demonstrated on a nitro reduction case study that should in principle be generic such that it can handle a series of substrates with similar molecular functionality. To assist in adoption of different substrates, a systematic substrate adoption methodology (SAM) has also been developed. The objective of the generic process *template* together with the SAM is to provide flexibility as well as increased efficiency to continuous processes while reducing inventory for safer operations (from 50 to 100 L in batch or 3 to 5 L in continuous processes). It is shown that the use of the template together with SAM can lead to potential savings in product development times through flexible and efficient production of Kg amounts of product material for clinical trials and other analyses.

Keywords: process template, API, substrate adoption, methodology, pharmaceutical.

1. Introduction

Identification of an effective and safe pharmaceutical product is based on success in clinical trials. Often, several candidate APIs (active pharmaceutical ingredients) targeting the same disease area are tested in order to identify efficacious products. This involves the manufacture of small quantities of compounds in early delivery campaigns. Of these candidates only a few are successful for which, further development is required to scale–up the process. Conventionally, for each candidate API, a whole new manufacturing system (process, reagents, process conditions etc.) needs to be developed, which is costly in terms of time and resources. One solution is to develop a generic process 'template' (a common manufacturing platform) that can be adapted for the production of a series of similar APIs for their early delivery campaigns, resulting in a reduction of time, early manufacturing cost and resource consumption.

2. A conceptual generic nitro reduction process template

A conceptual generic nitro reduction process *template* has been designed (see Figure 1). The template consists of several route alternatives as well as generic process equipments. The nitro compound (C_N) is dissolved in a solvent (S) in a stirred tank, prior to filtration to remove any un-dissolved material before feeding to the reactor. The reducing agent (R_A) can be mixed with C_N, with the catalyst or fed directly to the reactor. The suspension of catalyst may also be prepared in a stirred tank prior to being

continuously fed to the reactor. A slurry plug-flow micro-reactor is used to perform the reaction in continuous mode. The outlet stream from the reactor contains product (P_N, representing, for example, an amino compound), catalyst, any un-reacted R_A and by-product(s), P_B. The subsequent steps are to separate catalyst, reducing agent, products (P_N and P_B) and solvent.

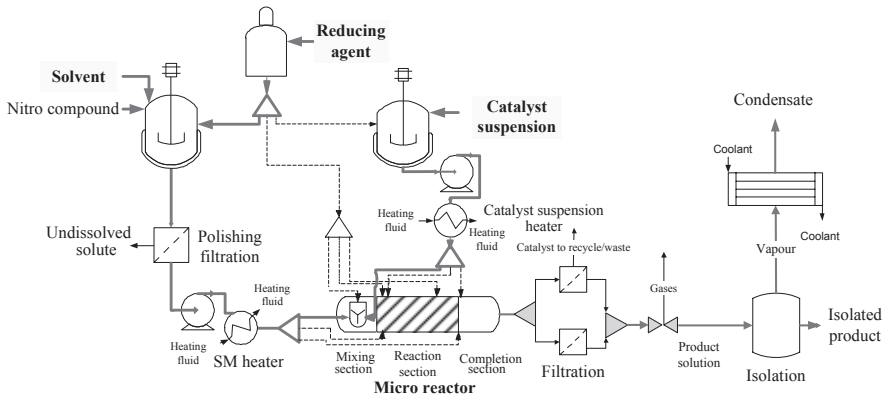

Figure 1. Nitro reduction process template (one route is highlighted)

A generic form of the nitro reduction reaction is given in Scheme 1. Through this reaction, an aromatic nitro compound (C_N) is reduced to the corresponding amine (P_N). The reducing agent, solvent and catalyst are the key materials which need to be selected for a given substrate. By-product(s) depend on the type of reducing agent used. The number of alternatives because of R and reducing agent is potentially very high.

$$R\text{-}NO_2 \quad + \quad \text{Reducing agent} \quad \xrightarrow[\text{Solvent}]{\text{Catalyst}} \quad R\text{-}NH_2 \quad + \quad \text{By-product(s)}$$

Scheme 1. Generic nitro reduction forming an amine

3. Substrate Adoption Methodology (SAM)

To adopt any new substrate in the generic process template, SAM employs 6 hierarchical steps as shown in Figure 2. In step-1 the aim is to check whether the substances involved in the process are hazardous. In step-2 a preliminary solvent list, suitable for dissolving the substrate and product is generated. The reducing agent and catalyst are selected in step-3 through reactivity and selectivity assessments. In step-4, an appropriate process flowsheet is generated from the process template and the corresponding process conditions are identified. The feasibility of the generated process is analyzed in step-5. On the basis of the outcomes of steps-1 to -5, reducing agent, catalyst, solvent, process flowsheet and the process operating conditions necessary for a new product synthesis are summarized (step-6). These can then be further validated through experiments. The data sources needed and the corresponding output from the methodology are also given in Figure 2. Each step of the methodology is described in a publication by Singh et al. (2011) – the SAM related work-flow is new.

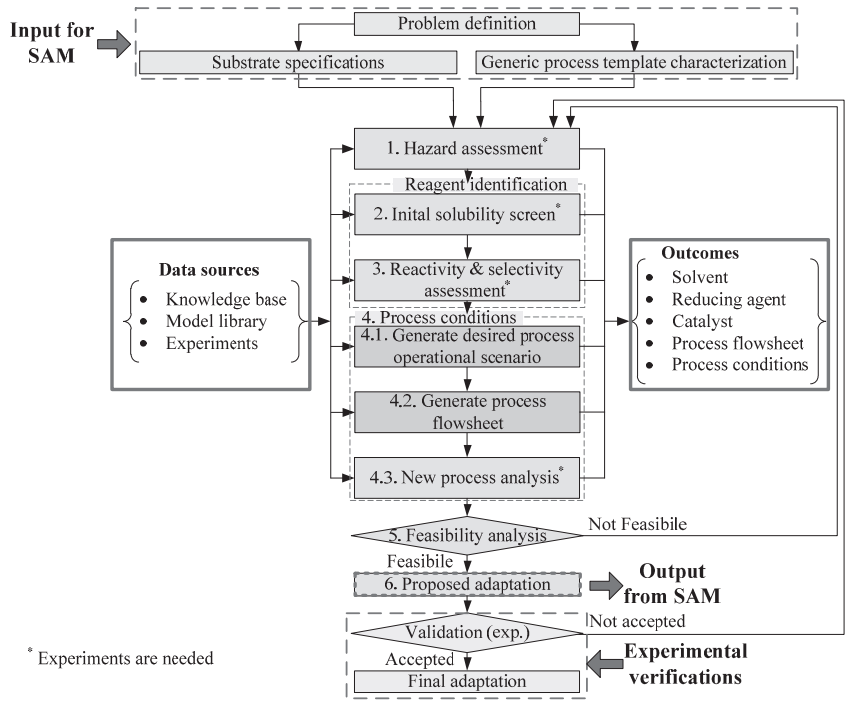

Figure 2. Substrate adoption methodology (SAM)

4. Conceptual case study

Problem definition: To adapt a generic nitro reduction process template for the production of P_N (a multi-functional organic chemical with C, H, N & O atoms) through transfer hydrogenation (for reasons of confidentiality, the actual names of the chemicals cannot be disclosed). The reaction scheme is similar to that shown in Scheme-1.

Substrate specifications: The reactant (substrate) is CN (also a multi-functional organic chemical with C, H, N & O atoms).

Generic process template characterization: Based on experimentation and analysis of several nitro compounds and the nitro reduction process template, some common information & data is generated, which are expected to be applicable to a series of nitro compounds. For example potential reducing agent candidates (e.g.: triethylammonium formate and ammonium formate), catalyst candidates (e.g. Pd/C, Pt/C) and solvent candidates (THF, IPA, NMP) are identified.

4.1. Hazard assessment (step-1)

The substrate is subjected to a hazard assessment methodology. For the purpose of this example, we will assume that based on experimental results, it was concluded that this substrate could be considered for adoption with appropriate safety measures.

4.2. Initial solubility screen (step-2)

The solubility of reactant and product in different solvent candidates is predicted using the UNIFAC group contribution model to select the appropriate solvent. For the purpose of this demonstration, the solubility order found is THF >IPA>NMP.

4.3. Reactivity and selectivity assessment (step-3)

A number of reducing agents and catalyst candidates can be used to carry out this reaction. Based on our existing knowledge, only one reducing agent candidate (for example, triethylammonium formate), one catalyst candidate (for example, Pd/C) and three solvent candidates (THF, IPA and NMP) are considered for further analysis (see Figure 3). Figure-3 shows an example of the type of information that could be generated in this step of the methodology. In the case of THF as solvent, the yield increases rapidly at first but after a certain reaction time the yield decreases, meaning that the reaction is fastest in this case but it also leads to the highest over-reduction. However, the maximum yield achieved with triethylammonium formate, Pd/C and THF is satisfactory meaning that these could be considered as reagents. Furthermore, the use of continuous reaction technology allows a better control of reaction time compared to batch operation and therefore an adaptation is proposed for this reaction with these reagents.

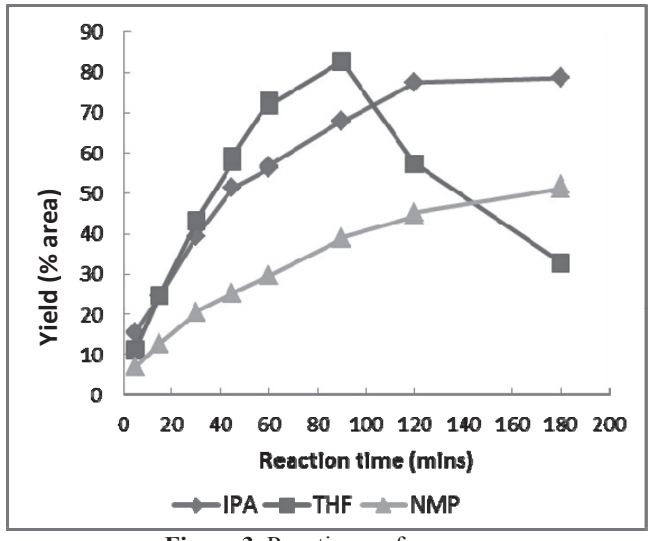

Figure 3. Reaction performance

4.4. Process conditions (step-4)

For the purpose of this demonstration, a process flowsheet is generated (indicated by the highlighted part of Figure 1) from the generic process template. The process is then analyzed and operating conditions are generated. The reactor operating window is shown in Figure 4 as an example.

4.5. Feasibility analysis (step-5)

In this step plant feasibility, operational feasibility and reagents feasibility are analyzed and could be considered satisfactory for the purpose of this demonstration.

4.6. Proposed adaptation (step-6)

On the basis of the outcomes of steps-1 to -5, the necessary reagents, process flowsheet and operating conditions are proposed as a demonstration example.

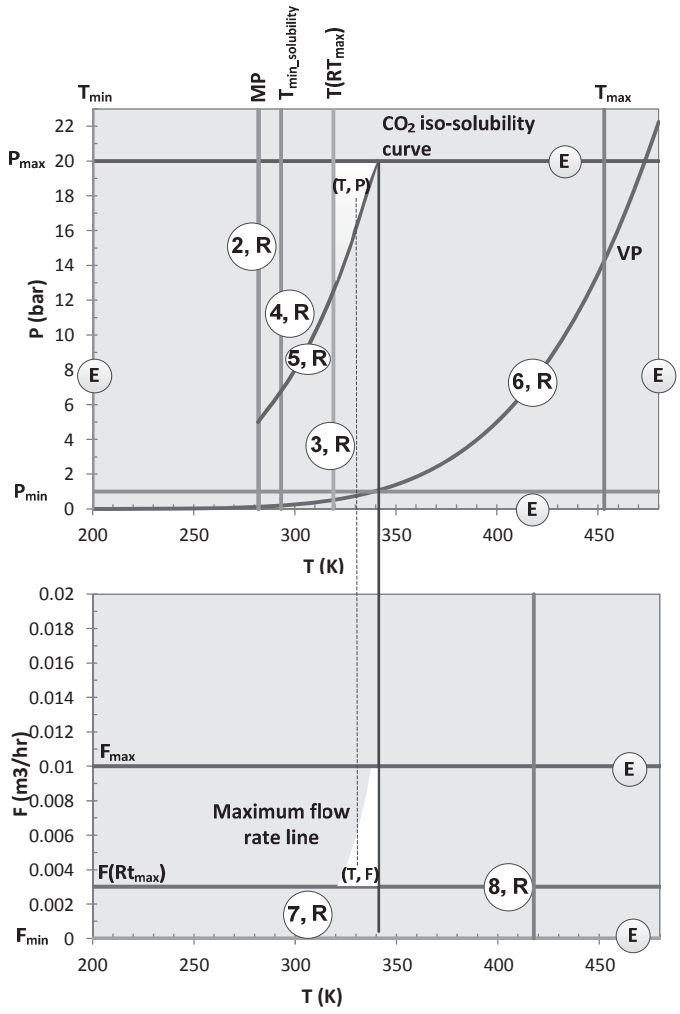

Figure 4. Reactor operating window (R: reaction dependent, E: equipment dependent)

5. Conclusions

In this paper, a generic nitro reduction process template has been reported. To assist in adaptation of the process template, a systematic substrate adoption methodology (SAM) has also been developed. The scope and significance of the process template and SAM has been demonstrated through a conceptual case study. The practical implementation of the template will now follow. The rapid and easy adaptation of the process template results in potential savings of time and resources.

Reference

R. Singh, R. Rozada-Sanchez, T. Wrate, F. Muller, K. V. Gernaey, R. Gani, J. M. Woodley, 2011, A retrofit strategy to achieve "Fast, Flexible, Future (F^3)" pharmaceutical production processes, Computer-Aided Chemical Engineering, 29, 291-295.

I.A. Karimi and Rajagopalan Srinivasan (Editors), Proceedings of the 11th International Symposium on Process Systems Engineering, 15-19 July 2012, Singapore.

Probabilistic design approach to build the litheness in an integrated process scheme

Shyamal Gondkar [a] [b], *Edwin Zondervan* [a], *Sivakumar Sreeramagiri* [b], *Andre.B. de Haan* [a], *Jan Meuldijk* [a]

[a] Eindhoven University of Technology (TU/e), Eindhoven, The Netherlands

[b] GE India Technology Centre Pvt. Ltd., Innovative Plastics Lab, Bangalore, India

Abstract

Flexibility in manufacturing processes is essential not only to handle a variety of feed stocks or to produce multiple product grades but also to accommodate process or catalyst inventions to improve productivity or quality. While designing in litheness we should ensure the robustness of the process output. In this paper, through a case study of biodiesel manufacturing, we summarize a novel technique which uses a probabilistic design approach using meta-models to evaluate the process intensification/integration scheme in a bio-refinery context.

In our methodology first we develop individual process models for a number of processes intensification alternatives where waste or non-edible vegetable oil are converted to biodiesel. These alternatives include the use of reactive distillation and a supercritical process. We integrate these process intensification schemes along with other necessary process steps to establish a plausible manufacturing process. Simultaneously we formulate high fidelity meta-models to describe the various responses of the reactive distillation column w.r.t the changes in the process conditions (or decision variables) in a given design space as an example. This simplification allows us to setup a probabilistic design using commercially available meta-heuristic optimization tools.

Keywords: process integration, reactive distillation, meta-model, probabilistic design

1. Introduction

There have been various efforts worldwide for more efficient conversion of biomass into syn-gas, chemicals, fuels etc. to overcome certain technical challenges leading to better process economics and operations. Biomass is a promising resource having lower carbon footprint compared to the existing non-renewable energy sources such as coal or petroleum based feedstocks. The areas of ongoing research include biomass pre-treatment e.g. biochemical or thermochemical routes such as biomass gasification or pyrolysis, gas treatment and cleaning, biogas to liquid conversion such as Fischer-Tropsch synthesis, transformation of bio-oil or vegetable oil into biodiesel by transesterification and esterification, fermentation of biomass to ethanol or other products, use of biogas in fuel cell for electric power. Each process or technology has its own advantages, for example, in a thermochemical path-way most of the biomass including lignin can be converted into added value chemicals, which is difficult using biochemical treatment. With the availability of many technologies and the ongoing

developments for converting variety of biomass to more useful products, integrating these technologies or processes in the most economical way has become equally important. Generally bio-refinery is referred as a facility capable of converting various types of bio-feedstock into biofuels, chemicals and energy in a sustainable way. In such a scenario, flexibility of the manufacturing unit is essential not only to handle multiple feed stocks or multiple products but also to accommodate process inventions to improve overall economics and sustainability of an integrated scheme. Our work mainly focuses on developing a tool which will enable to assess various process integration alternatives for biomass conversion. In our previous paper (Gondkar *et al.*, 2011) we discussed various types of uncertainties encountered in process engineering problems. Probabilistic design allows to quantify the fitness of a given process or component by providing a probability (likelihood) that the same will survive the operating conditions. In this paper first we discuss a case-study *i.e.* a process integration alternative for manufacturing of biodiesel and then derive a framework for probabilistic design. For this purpose we used the literature reported kinetics as mentioned in the next section. We demonstrate the power of this design with an example where the meta-model is used for optimization of a reactive distillation case.

2. Case Study

A case study for manufacturing of fatty acid alkyl esters (FAAE) of non-edible or waste vegetable oil feedstock containing higher amount of free fatty acids is investigated. In a typical heterogeneous catalytic transesterification and esterification process a fixed bed reactor is fed with a mixture of oil and methanol at a given molar ratio. Excess methanol and water formed due to esterification is removed at the exit of the reactor by partial evaporation. Esters and glycerol are separated in a settler. The reaction products are further purified and methanol can be reused after removing water. Solid acid catalysts and amphoteric metal oxides based on zinc or lanthanum are promising candidates. It is a well-known fact that heterogeneous catalyst for such reactions result in much slower volumetric reaction rates as compared to homogeneous catalysts. There is also a possibility of significant catalyst deactivation, leaching or blocking of porous solid catalyst because of its use. It is possible to overcome such limitations by further optimization of the reaction conditions, by minimizing mass transfer limitations or by carefully designing the catalyst architecture.

First we investigated the possibility of a process intensification alternative for fatty acid methyl esters (FAME) manufacturing comprising a reactive distillation using a heterogeneous catalyst. Here the oil containing higher fatty acid is continuously fed in the upper section of the distillation column containing a heterogeneous catalyst and the methanol is fed at a location a few stages above the reboiler. The bottom product obtained from the reboiler contains FAME, unreacted oil *i.e.* mixture of glycerides, glycerol and water. It is not necessary to have catalyst in the bottom stages to avoid hydrolysis. Methanol is distilled at the top which is either refluxed or recycled to the column. This concept avoids the use of a separate column to separate water and methanol and also possibly helps to improve mass transfer because of the presence of vapors bubbling on each stage. We developed Aspen Plus steady-state models for these processes. Dortmund modified UNIFAC property method is used. For the reactive distillation case we used the pseudo-homogenous catalytic reaction kinetics for tranesterification and esterification, as an approximation to demonstrate the concept. We derived the apparent kinetics from the published work of Qing *et al.,* (2011) for carbon

based solid acid catalyst as an example. Simulation results suggest that the reactive distillation alternative is useful to convert free fatty acids into esters and partial conversion of triglycerides at moderate process conditions (<125^0C). At higher temperatures the reaction would be more sensitive to solid-liquid mass transfer and requires a higher operating pressure for the reactive distillation column.

The other process intensification option we considered is a heterogeneous catalytic supercritical process. It uses CO_2 as a solvent along with methanol in a fixed bed catalytic reactor at elevated temperatures (approximately 200^0C) which needs much shorter residence times. For this case, the pseudo homogenous kinetics are derived from the reported experimental results (Macaira *et al.*, 2011) for a solid acid catalyst, Nafion SAC-13. One of the advantages of this process is that liquid to solid mass transfer under super-critical condition is so high that the reaction is still in the kinetically controlled regime. The downside of such a process is a need to separate water from the recovered solvents, which makes it energy intensive. Our simulation results suggest that if there is no water present in the recovered mixture of CO_2 and methanol, the energy requirement can be considerably reduced. So this process requires either using a feed free from fatty acids or a solvent dewatering scheme such as molecular sieves.

In order to leverage the best of both processes, it is possible to integrate the reactive distillation with the supercritical process. Reactive distillation is useful to convert free fatty acids into esters and realize partial conversion of triglycerides at moderate process conditions. The supercritical methanol and CO_2 based catalytic process is suitable for further conversion of glycerides at reasonable energy consumption. The flow-sheet of the integrated scheme is shown in Figure-1. When such processes are integrated the design and operation of individual unit are critical to obtain the optimum performance of an integrated shceme. In the next section the design philosophy is discussed using reactive distillation as an example.

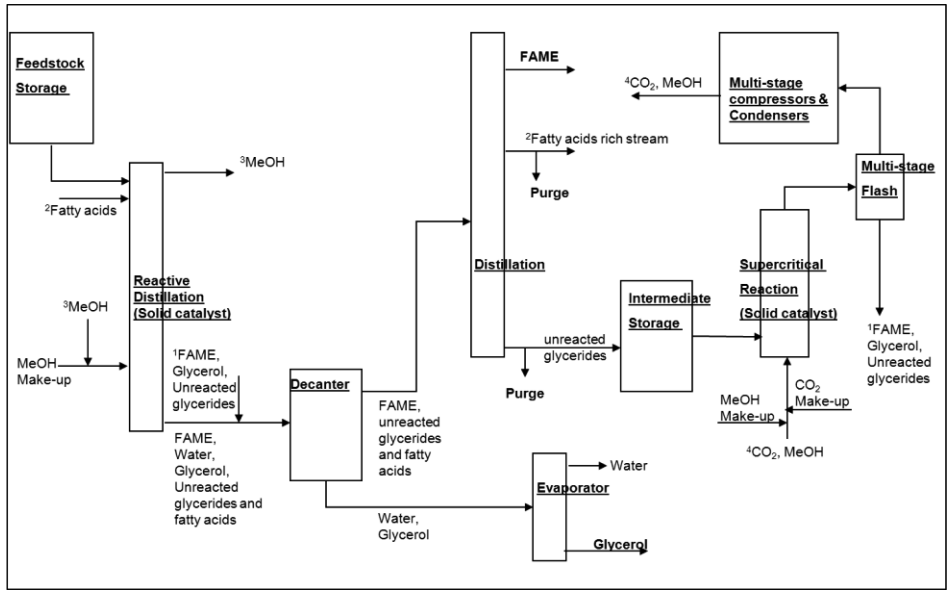

Figure-1: Integrated process (simplified block diagram)

3. Probabilistic Design

In our previous work (Gondkar *et al.,* 2011) for optimization of process intensification, we attempted the use of classical response surface methodology (C-RSM) based on a center composite design (CCD), but the errors associated with these simplified models (linear or quadratic) were resulting in wider error range on the predictions. We also directly coupled a commercially available meta-heuristic optimizer with a process simulator such as Aspen Plus. The results were satisfactory but the simulations were computationally intensive, i.e. long CPU times. This prompted us to look for an alternative methodology for model simplification. The use of meta-models is reported in structural engineering or mechanical design, but their application is very limited in process engineering (Palmer & Realff, 2002; Caballero & Grossmann, 2008; Henao & Maravelias, 2011). In the following section we will discuss the results from C-RSM and the meta-modeling exercise and the subsequent optimization of the reactive distillation for the kinetics derived from recent work by Qing *et al.,* 2011. In this example for illustration purposes, we selected 2 variables (methanol feed rate and reflux ratio), 7 responses (FAME rate, reboiler duty, condenser duty, methanol losses, liquid flow rate, gas flow rate and liquid hold-up) and the objective was set to maximize the product rate i.e. FAME rate with certain design requirements or constraints derived from the other responses.

C-RSM simulations were run at CCD design points (i.e. factorial points, center point and star points – alpha=1.41421)suggested by Design Expert software. As expected from our previous work (Gondkar *et al.,* 2011) the models suggested have very poor R^2. The diagnostic plots (*e.g.* Actual vs. Predicted) for two of the responses are shown in Figure 2. Such large residuals of the model predictions do not justify further optimization.

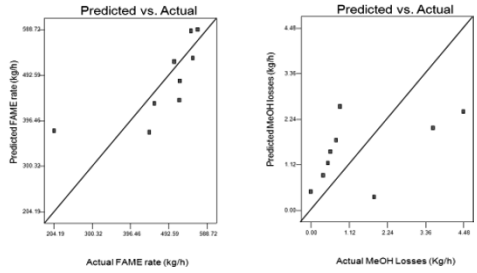

Figure 2: C-RSM model predictions (for CCD design) for reactive distillation

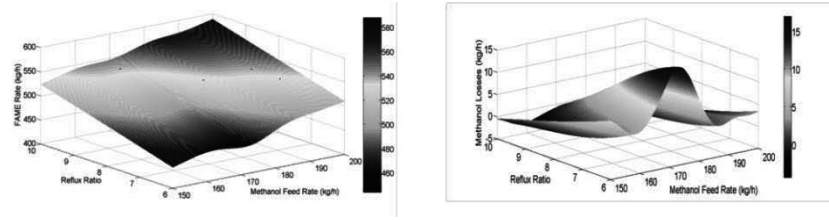

Figure 3: Response surface obtained using Kriging meta-model.

For the purpose of meta-modeling a Latin Hypercube sampling technique was preferred by keeping the same sample size as that of C-RSM and simulations were run at these points. For the fitting of the meta-models for all the responses, the Kriging toolbox implemented by Lophaven, Nielsen and Sondergaard (Nielsen, 2002) was used. The

meta-model parameters are estimated to minimize root mean squared error (RMSE). The response surface obtained using Kriging interpolation are given in Figure-3 for FAME rate and methanol losses.

For probabilistic optimization we developed a framework as follows: Crystal Ball, a spreadsheet based application is used for sampling probability density functions of decision variables as well as running simulations using above mentioned meta-models. For optimization OptQuest a meta-heuristic commercial optimization software is used. In this example for the decision variables i.e. methanol feed rate and reflux ratio standard deviation of 2% and 3% are specified to obtain the distribution of these variables at a given point. For the objective function defined and the design requirements specified the results obtained from this optimization exercise are given in Table 1. These results are further validated using Aspen Plus model.

		Objective	Requirements					Decision Variables	
		Maximize P99.87 Percentile	Certainty of 2.75-3.75 >= 95%	Certainty of 250.00-425.00 >= 95%	Certainty of 0.00-0.75 >= 95%	Certainty of -0.75-0.00 >= 95%	Certainty of 0.00-20.00 >= 95%		
Rank	Solution #	FAME rate *Kg/h*	Liquid rate *M^3/h*	Gas rate *M^3/h*	Reboiler duty per 1000 Kg FAME *Gcal/h*	Condenser duty per 1000 Kg FAME *Gcal/h*	MeOH losses per 1000 Kg FAME *kg/h*	Reflux ratio	MeOH rate *kg/h*
1	113	509.74	100.00%	95.50%	100.00%	100.00%	95.51%	8.75	173.94
2	190	509.33	100.00%	97.83%	100.00%	100.00%	100.00%	8.75	173.67
3	33	508.99	100.00%	98.16%	100.00%	100.00%	96.65%	8.72	173.94

Table 1: Results obtained from optimization for reactive distillation example for 1000 kg/h of oil feed.

4. Conclusions and Path Forward

In our case study for evaluating a possible process intensification alternative it was found that highly non-linear responses can be described by high fidelity meta-models. This simplification allowed us the probabilistic design, which otherwise was difficult using classical response surface methodology because of large error, or by integrating process model with an optimizer. The methodology discussed here can be used to design an industrial system comprising of multiple processes and products. This will be accomplished using a multi-layer hierarchical framework (Zondervan *et al.,* 2008).

References

S. Gondkar *et al.*, (2011). Chemical Engineering Transactions, 24, 355-360. Towards the assessment of robustness in an industrial process system.

S. Qing *et al.*, (2011). Chinese Journal of Chemical Engineering, 19(1), 163-168. Reaction Kinetics of Biodiesel Synthesis from Waste Oil Using a Carbon-based Solid Acid Catalyst

J. Macaira *et al.,* (2011). Fuel, 90, 2280–2288. Biodiesel production using supercritical methanol/carbon dioxide mixtures in a continuous reactor.

K. Palmer & M. Realff (2002). Chem. Eng. Res. Des., 80(7), 760-772. Metamodeling approach to optimization of steady-state flowsheet simulations: Model generation.

J. Caballero & I. Grossmann (2008). Computer Aided Chem. Eng. 25, 551- 556. Rigorous flowhseet optimization using process simulators and surrogate models.

C. Henao & C. Maravelias (2011). AIChE, 57(5), 1216-1232. Surrogate-based superstructure optimization framework.

H. Nielsen (2002). "DACE, A MATLAB Kriging toolbox", http://www.imm.dtu.dk/hbn/dace/.

E. Zondervan *et al.*, (2008). FOCAPO, 397. Flexible optimization of industrial process systems.

I.A. Karimi and Rajagopalan Srinivasan (Editors), Proceedings of the 11th International Symposium on Process Systems Engineering, 15-19 July 2012, Singapore.

Integrated optimization of the adsorption of theaflavins from black tea on macroporous resins

Miguel Monsanto, [a], Edwin Zondervan, [a] O. Trifunovic, [a] Peter M.M. Bongers [a],[b].

[a] *Eindhoven University of Technology, the Netherlands*

[b] *Unilever, Vlaardingen, the Netherlands*

Abstract

In this work the adsorption and desorption parameters for the separation of theaflavins from tea are determined. The obtained data is used for a preliminary selection of the resin with the best adsorption capacity and desorption ratio. From the four tested resins the hydrophobic A-DVB resin has the best characteristics. In addition, the data was used to fit the adsorption isotherms at different temperatures to two theoretical models. The isotherms form the basis of a more extensive model that can be used to optimize the sorption separation yield. The selected resin will be used in a follow up study to determine the optimal operating conditions of the system, using design of experiments and analysis of variance.

Keywords: macroporous resin, adsorption, food industry, polyphenols, tea.

1. Introduction

Tea polyphenols are associated with many health benefits, such as prevention of heart, inflammatory and neurological diseases, as well as cancer prevention. While in green tea mostly catechins can be found, black tea is the source of several types of polyphenols formed by enzymatic polymerisation of catechins, including theaflavins, which can only be found in black and oolong teas [1,2].

The conventional approach for large-scale polyphenols separation is solid-liquid extraction followed by column adsorption chromatography as a purification step. Although this process is not very efficient from an energy requirement and reagents consumption point of view [3], today there is no established alternative to it. Macroporous adsorption resins are economically attractive and have a large surface area combined with a hollow and layered structure [4]. The purification mechanism is based on differences in polarity, hydrophobicity, molecular size and the shape of the different solutes for adsorbent resin. While the literature reports some investigation about suitable resins for green tea polyphenols adsorption [5], information about black tea polyphenols (namely theaflavins) adsorption is scarce.

The first step in designing any adsorption system is to acquire knowledge about adsorption equilibria, kinetics and capacity for target compounds on the selected ligand. The capacity of the adsorbents is usually characterized by isotherms, where Langmuir [6] and Freundlich [7] isotherms are most often applied for phenolic compounds:

Langmuir: $$Q_e = \frac{K_L C_e}{1 + a_L C_e} = \frac{Q_m a_L C_e}{1 + a_L C_e} \quad (1)$$

Freundlich: $$Q_e = K_F C_e^{1/n} \quad (2)$$

where K_L(l/g) is the solute adsorptivity, a_L(l/mg) is a Langmuir constant that represents the ratio between the adsorption and desorption rate constants, Q_m(mg/g) is another Langmuir constant that represents the maximum adsorption capacity, K_F (l/g) is the

Freundlich constant that represents the adsorption capacity and $1/n$ (dimensionless) is an empirical constant that represents the magnitude of the adsorption driving force [8,9].

In this study both the adsorption and the desorption parameters for the separation of theaflavins from black tea were determined. Adsorption data has been analyzed with both types of isotherms to determine the best experimental fit. The results obtained will be used further as a basis for characterization and optimization of a suitable system for purifying the theaflavins from the black tea on the large scale.

2. Experimental

2.1. Reagents and adsorbents

Acetonitrile and ascorbic acid were analytical grade obtained from Sigma – Aldrich. Glacial acetic acid (HPLC grade) and ethanol absolute were purchased from Merck KGaA. Individual theaflavins standards were obtained from Unilever NV. The deionized water (< 18,2 MΩ) used in the experiments was Milli-Q gradient (Millipore). Freeze-dried dry black tea powder was supplied by Unilever R&D.

The resins used in this work and their characteristics are presented in Table 1. Prior to the adsorption-desorption experiments, all resins were pre-treated to remove the monomers and preservative agents. The resin was subsequently dried at 70°C in the oven during 24 hours. Weighted amounts of resin where then washed with ethanol and subsequently a second thorough wash with deionized water was done [10,11].

Table 1: Screened macroporous resins physical properties (manufacturer data)

Resin matrix	Surface area (m^2/g)	Particle size (mm)	Pore volume (ml/g)	Polarity
Polymethacrylic acid ester (AAE)	370	0.25-0.84	1.14	Moderate polar
Aromatic divinylbenzene copolymer (A-DVB)	700	0.6-0.75	1.4	Non polar
Styrene-divinyl benzene (S-DVB)	600	0.25-0.85	1.30	Non polar
Formophenolic (F-PHE)	150-250	0.56-0.76	0.95-1.18	Polar

2.2. Static adsorption and desorption experiments

The tea solutions used for the resin screening and for the adsorption isotherms were prepared by dissolving tea powder in 20% aqueous acetonitrile solution. The starting concentration of theaflavins used in the resin screening tests was around 0.4 mg/ml and for the isotherms experiments the theaflavins concentration range was 0.11-0.62 mg/ml.

For the desorption on the A-DVB resin at different water ethanol solutions, the tea solutions were prepared by dissolving tea powder in water (with stirring). This change in the solution preparation method was made to achieve similar properties to the tea at the process level. All future tests will be done using tea aqueous solutions.

For the static adsorption tests, the hydrated resin (with a dry weight of 1.5 g) was placed in an Erlenmeyer with a lid and 25 ml of black tea solution was added to it. The Erlenmeyer was shaken at 100 rpm at 25°C in a temperature controlled IKA KS 4000i Control Orbital Shaker, during 4 hours. After achieving the adsorption equilibrium, a desorption test was initiated by placing the resin in another Erlenmeyer and adding 25 ml of eluent. The Erlenmeyer was again shaken at 100 rpm and 25°C during 4 hours. Based on the results obtained by Huang *et al.* [12] we decided to use a 50 % (v/v) ethanol solution in this preliminary screening study. In another experiment the ethanol-water ratio was varied to study it's effect in the desorption ratio.

The adsorption capacity (Qe, in mg/g) and adsorption ratio (E, in %) of the theaflavins in the tested resins were calculated according to the following equations:

$$Q_e = \frac{(C_0 - C_e)V_i}{W} \quad (3)$$

$$E = \frac{(C_0 - C_e)V_i}{C_0} \times 100\% \quad (4)$$

where C_0 (g/l) and C_e (g/l) were the initial and equilibrium concentration of the solute in solution, respectively, V_i (l) was the volume of initial solution and W (g) was the weight of dry resin. Desorption ratio (D, in %) was calculated according to:

$$D = \left[\frac{C_d V_d}{(C_0 - C_e)V_i}\right] \times 100\% \quad (5)$$

where C_d (g/l) is the concentration of the solute in the desorption solution and V_d (l) is the volume of desorption solution.

2.3. Analytical methods: HPLC analysis of theaflavins

Individual theaflavins concentrations were determined by HPLC analysis on a Varian HPLC equipped with a Varian Prostar 310 UV Detector and on a Waters 2695 equipped with a 2487 wavelength detector. The analysis was performed in a C18 column, by isocratic elution with acetic acid/water/acetonitrile solutions. The exact method was supplied by Unilever R&D. The total amount of theaflavins was determined by a summation of the four theaflavins (theaflavin, theaflavin 3 monogallate, theaflavin 3' monogallate and theaflavin digallate).

3. Results and discussion

3.1. Static adsorption

The adsorption process during the first hour exhibits an almost linear increase (Figure 1) for all tested resins, followed by a slow increase until the equilibrium plateau was reached. The maximum adsorption capacities, adsorption and desorption ratios at room temperature can be found in Table 2. The polar F-PHE resin consistently showed

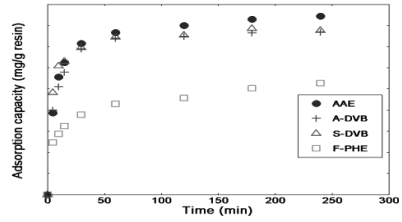

Figure 1:Adsorption kinetic curves for total theaflavins

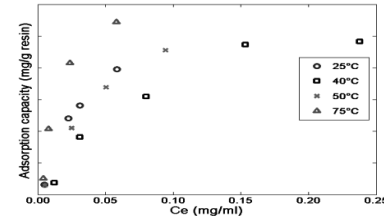

Figure 2: Adsorption isotherms of theaflavins on a A-DVB resin

lower adsorption capacity, probably due to slightly hydrophobic nature of theaflavins. Gogoi *et al.* [5] noticed a completely opposite trend when testing tea catechins adsorption capacities of different resins, where the most polar resin had the best performance. Similar results were reported for polyphenol adsorption on microporous non-ionic aliphatic ester resin by Silva *et al.* [12], where hydrogen bonding between studied polyphenols and resin active sites was the most probable adsorption mechanism. This is not surprising as the theaflavins, which are dimers of green tea catechins, are expected to have a reduced polarity compared to their monomers, i.e. hydrophobic interactions are expected to have a predominant effect for adsorption. However, a straightforward conclusion why a certain resin behaves better than the other is difficult to make at this stage, as their active surface areas (Table 1) are quite different: Although the F-PHE resin has approximately three times lower surface area when comparing to both DVB resins, it only has a ~50 % lower adsorption capacity (Table 2).

Table 2: Adsorption capacity and ratio of adsorption and desorption for theaflavins at 25 °C

Resin	Q_e (mg/g resin)	E (%)	D (%)
AAE	8.44	82	38
A-DVB	7.69	81	71
S-DVB	7.76	71	61
F-PHE	5.26	49	78

According to Table 2 the resin with the best combined adsorption and desorption characteristics was the highly hydrophobic A-DVB resin. This resin was further used to determine parameters for both isotherms. Figure 2 shows the adsorption isotherms for the theaflavins on A-DVB resin at four different temperatures. To calculate the values for both adsorption models, Eq. 1 and Eq. 2 were re-written into their linear forms:

$$\frac{1}{Q_e} = \frac{1}{K_L C_e} + \frac{1}{Q_m} \quad (6)$$

$$\log Q_e = logK_F + \left(\frac{1}{n}\right) logC_e \quad (7)$$

The parameters of the two isotherms are summarised in Table 3. The correlation coefficients are very high for the Langmuir isotherm model at all the tested temperatures and for the Freundlich isotherm model at 25°C and 50°C, suggesting that both models fit very well to the experimental data. The Langmuir model shows a better fitting than the Freundlich model and the highest correlation coefficient is obtained at 25°C for the Langmuir equation (R^2 = 0.9961). The constant (1/n) in the Freundlich equation is the degree of favorability in the adsorption. Since the value is always between 0.1 and 1, the adsorption of theaflavins on the A-DVB resin was considered to be favorable. For a value above 1 it would be very difficult for the adsorption to occur [13].

Table 3: Langmuir and Freundlich adsorption values for theaflavins on A-DVB resin

Temperature (°C)	Langmuir model	R^2	Freundlich model	R^2
25	Ce/Qe=0.0745 Ce+0.0016	0.9961	Qe= 50.81 $Ce^{0.5520}$	0.9872
40	Ce/Qe =0.0693 Ce+0.0013	0.9925	Qe= 26.91 $Ce^{0.4908}$	0.9598
50	Ce/Qe=0.0713 Ce+0.0019	0.9873	Qe= 38.48 $Ce^{0.5058}$	0.9954
75	Ce/Qe=0.0607 Ce+0.009	0.9914	Qe= 65.83 $Ce^{0.5284}$	0.9202

3.2. Static desorption on A-DVB resin

Theaflavins are soluble in water, ethanol, methanol, acetone and ethyl acetate [14]. Since the possibility of food grade operations is to be tested, the desorption study was performed with different concentrations of ethanol-water solutions.

According to Figure 3, the normalized desorption ratio (to 100% ethanol) of theaflavins increases with increasing ethanol concentrations until it reaches a maximum at 70% (v/v). At higher ethanol concentrations the desorption ratio decreased again.

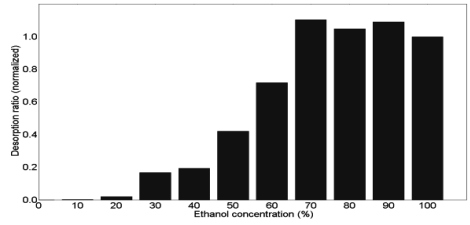

Figure 3: Normalized desorption ratio of theaflavins on A-DVB resin with different ethanol–water solutions

This ethanol-water desorption ratio is in accordance with the result obtained by Yi *et al.* [15] for eluting purified theaflavins. This is explained by a higher hydrophobicity of the theaflavins when comparing to other components present in black tea, e.g. catechins or caffeine, which have higher desorption rates at lower ethanol concentrations.

4. Future work

The selected resin will be used in a follow up study to identify the operational conditions (temperature, flow, etc.) that significantly affect the adsorption and desorption behavior of the resin. To capture the nonlinear behavior between the influence factors and the response factors a surface response methodology will be used. In addition, polynomial models can be generated from the data which can be used for optimization purposes.

5. Conclusions

Four commercial macroporous resins ranging from polar to non-polar were tested for their theaflavins adsorption characteristics from real aqueous black tea extracts. Among all resins studied, the most apolar A-DVB resin was found to have the best adsorption and desorption characteristics, probably due to chemical nature of the adsorbent. The desorption process was strongly influenced by the water content of the alcoholic solvent, as theaflavins will partition in the alcoholic phase only if their energy requirement for that phase is lower than for their sorption on the resin. The adsorption equilibrium exhibited a slightly better fit with the Langmuir model for all resins studied.

This work is the first step for a more detailed characterization and modeling study of the theaflavins adsorption process.

Acknowledgements

This work was supported by the Institute for Suistainable Processing Technology (ISPT) consortium.

References

[1] M.E. Harbowy, D.A. Balentine, (1997), *Critical Reviews in Plant Sciences*. 16(5), 415.
[2] C. S. Yang, J. Y. Chung, G.Yang, S. K. Chhabra and M.J. Lee, (2000), *J.Nutr.* 130, 472S.
[3] Y. J. Fu, Y. G. Zu, W. Liu, T. Efferth, N. J. Zhang, X. N. Liu, Y. Kong, (2006), *Journal of Chromatography A*, 1137, 145.
[4] F.Shahidi, (2007), Nutraceuticals and Functional Foods in Health Promotion and Disease Risk Reduction. Shanghai: Based on Keynote presentation at IUFoST Conference held in conjunction with Fi Asia/China.
[5] P. Gogoi, N.Dutta, P.Rao, (2010), *Indian Journal of Chenical Tecnology*, Vol.17(5),337-3.
[6] I. Langmuir, (1918), *The Journal of the American Chemical Society*.40 (9), 1361.
[7] H. Freundlich, (1907), *Z Phys Chem*, 57, 385.
[8] E.M. Silva, D.R. Pompeub, Y. Larondelle, (2007), *Sep. Purif. Technol.* 53, 274.
[9] X.L. Du, Q.P. Yuan, J.S. Zhao, (2007), *J. Chromatogr. A* 1145, 165.
[10] R.S. Juang, J.Y. Shiau, (1999), *J. Hazard. Mater*. B 70, 171.
[11] M. Scordino, A.D. Mauro, A. Passerini, (2003), *Agric. Food Chem.* 51, 6998.
[12] R. Q. Huang, N. H. Li, S.Y. Huang, (2011), Advanced Materials Research, 2957,236-238.
[13] R.E. Treybal, Mass-Transfer Operations. third ed., McGraw-Hill International, 1981.
[14] M. Naczk, F. Shahidi, (2004), J. Chromatogr. A 1054, 95–111.
[15] X. Yi, J. Yuxia, W. Yuanyuan, T. Youying, (2010), *Journal of Liquid Chromatography & Related Technologies*, 33:20, 1791.

I.A. Karimi and Rajagopalan Srinivasan (Editors), Proceedings of the 11th International Symposium on Process Systems Engineering, 15-19 July 2012, Singapore.

Influence of the organic phase fraction in the biphasic organic-aqueous reactor feed stream on the enzymatic hydrolysis of FAME in a packed bed

Przemyslaw Krause, Georg Fieg

Hamburg University of Technology, Institute of Process and Plant Engineering, Schwarzenbergstrasse 95 C, 21073 Hamburg, Germany, p.krause@tu-harburg.de

Abstract

The behavior of a differential packed-bed reactor element was investigated regarding the impact of the organic phase fraction on the reaction rate of an enzymatic hydrolysis with biphasic reactant flow. Wetting of the catalyst particles played an important role for this reaction system, and an assumed packed-bed flow pattern was examined. To cover the entire operation range varying from biphasic flow with high water excess to singular organic phase flow an integrated approach consisting of experiments and simulation was chosen. With the developed method wetting of the catalyst particles only by one liquid phase could be confirmed for the entire operation range.

Keywords: packed bed, enzyme, multiphase reactors, modeling

1. Introduction

For the development of production processes in the biochemical industry quantitative information about the behavior of reaction systems is decisive. Their knowledge enables the transfer of imaginable processes, already working in laboratory scale, to concepts suitable for production scale. The present work deals with a systematic investigation of a biotechnological reaction system. To ensure practical relevancy the procedure was developed on the basis of a model system, so that this work may be seen as an exemplary case study. The findings were obtained from knowledge-based assessment and modeling of the enzymatic hydrolysis of short-chain fatty acid (C_6–C_{10}) methyl esters using *Candida antarctica* lipase B (Novozym®435). The reacting methyl esters and water formed two liquid phases. The reaction was performed as batch run in a recycle packed-bed reactor assembly containing swollen catalyst particles. Fatty acids and methanol were obtained as products.

2. Theoretical Approach

The reaction behavior of the packed-bed element was determined from experiments and their model based analysis. For this purpose the usage of a phenomenological model based upon a decomposition of the observed reaction behavior into singular contributions was required. A mathematical model for the aforementioned hydrolysis reaction was developed by Krause and Fieg (2011) and utilized for the present study. This model assumed a pseudo-homogeneous reaction in the organic phase, whereas the kinetic expression used thermodynamic activities. The approach applied a UNIQUAC model for description of the liquid-liquid phase behavior. The biochemical reaction occurring at the active sites of the catalyst depended on the transport of the reactants and products between the bulk phase and the particles. The bulk phase composition was obtained from macroscopic balances of the entire experimental assembly. The

macroscopic balances constituted the connection between the actual (intrinsic) reaction and the observed reaction behavior. To limit the complexity of the modeling approach simplifying assumptions were made. All simplifications were justified by choosing adequate reaction conditions, e.g., to warrant ideal mixing or excluding mass transfer limitations by choosing appropriate superficial velocities.
The examination of the flow patterns showed that both liquid phases occupied the same pores of the particle bed, whereas the particles were enclosed by the organic phase. Hence, wetting of the catalyst particles only by the organic phase was assumed. The schematic representation of the determined flow pattern at biphasic flow is depicted in Fig. 1. Fig. 1 shows a strong simplification of the observed flow pattern, which exhibited a dynamic change of the flow channel positions and geometries.

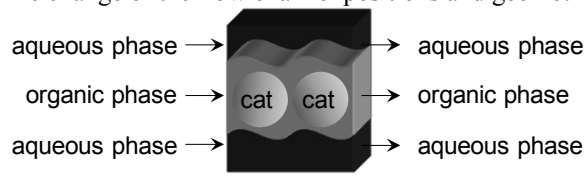

Figure 1: Schematic representation of the determined flow pattern in the packed-bed reactor at biphasic flow. (cat = catalyst particle)

At absence of mass transfer limitations a differential reaction step in the assembly can be subdivided in two separate imaginary steps (Krause and Fieg (2012)): (1) differential reaction progress in the bed element, and (2) attainment of the phase equilibrium. Assuming that for step 1 only the organic phase is required, both imaginary steps can be sterically separated from each other without the change of the observed global reaction behavior in the apparatus. From this decomposition two operation modes resulted, which could be compared: the two-phase flow operation mode in which both phases were passed through the packed bed vs. the singular phase flow operation mode with only organic phase flow through the reactor, in which the liquid-liquid phase mass transport exclusively occurred outside the reactor. In both operation modes only differential conversion per pass through the reactor was presumed.

3. Experimental Procedure

The kinetic experiments were performed in a so-called batch recycle packed-bed reactor assembly (Krause and Fieg (2011)). The schematic representation is given in Fig. 2. A similar setup was used, for example, by Kosugi and Tomizuka (1995), however without following the above described differential reactor concept. The assembly exhibited one circuit to provide the feed stream from the mixing vessel to the packed-bed reactor. To realize the decomposition of the reaction steps the experimental assembly could be run in two operation modes: either biphasic flow through the packed bed or singular phase flow. In the biphasic flow operation mode a homogeneous emulsion generated in the mixing vessel was passed through the reactor circuit. In the singular phase flow operation mode only the organic phase was passed from the mixing vessel to the reactor circuit. The liquid-liquid phase equilibrium was subsequently achieved in the mixing vessel. Within the experiments the impact of high water excess was investigated in the two-phase flow operation mode, whereas the singular phase flow operation mode was additionally used to confirm the model validity. The experimental assembly operated in the singular phase flow operation mode is depicted in Fig. 3. Fig. 3 shows that at the appropriate stirrer speed it was possible to achieve an o/w-emulsion in the aqueous phase while a clear organic phase layer on top of the emulsion was obtained.

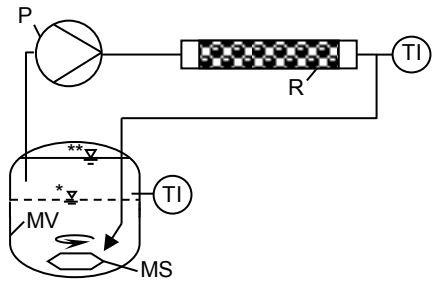

Figure 2: Schematic representation of the used reactor assembly. (MV = mixing vessel with 600 ml volume, MS = magnetic stirrer, P = circulation pump, R = 8 cm long packed-bed reactor with 1 cm i.d. containing Novozym®435 particles, TI = temperature indication, **▽ = liquid level at both operation modes, *▽ = phase boundary between the continuous organic phase layer on top of the aqueous phase in the singular phase flow operation mode)

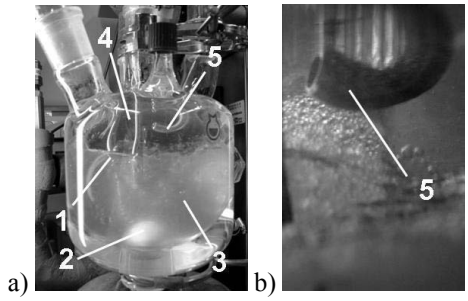

Figure 3: a) Mixing vessel in the singular phase flow operation mode. b) Magnification of the intake pipe. ((1) liquid-liquid phase boundary, (2) stirrer, (3) aqueous phase (o/w-emulsion in the mixing zone), (4) organic phase, (5) intake pipe of the reactor circuit)

4. Results and Discussion

4.1. Operation at low organic phase fractions

All kinetic parameters were determined on the basis of experimental conversion courses X_i obtained in the two-phase flow operation mode with organic phase total mass fractions of approximately 0.3, corresponding to an initial water to methyl ester mass ratio of $A_{H2O} = 2.3$. The determination of the kinetic parameters in this operation range provided advantages in the experimental procedure and a simplified mathematical evaluation. The main benefit was that the entire assembly could be treated as a stirred tank because of the comparatively small conversion per pass through the reactor, while still a sufficiently high final total conversion of the methyl esters was obtained despite the strong limitation by the reaction equilibrium (Krause et al. (2010)). From experimental runs it was found that the initial reaction rate was independent of the aqueous phase fraction and constant for a constant organic phase to catalyst ratio.

For decreasing organic phase fractions in the emulsion the conversion per pass through the packed bed increased when flow velocity and bed length remained unchanged. This caused an increasing deviation of the assembly behavior from the stirred tank assumption. The reason for not reducing the bed length was to maintain exactly the same catalyst bed throughout one experimental series. Hence, for low organic phase fractions the packed bed could not be treated as a differential reactor in the modeling

approach. To consider the integral character of the bed it was treated as a plug flow reactor.

Measuring the conversion courses X_i on the basis of the organic phase compositions was impossible at low organic phase fractions without significantly interfering with the observed system behavior. However, the reaction could be tracked by following the methanol mass fraction in the aqueous phase $w_{MeOH,aq}$, which was an adequate method to compare the experimentally determined and modeled reaction courses. For this purpose the absence of mass transfer limitations and a reliable description of the methanol distribution between the phases were required. The comparison of the obtained experimental and calculated courses is given in Fig. 4. For the cases (1) to (4) the overall methyl ester conversion increased from $X \approx 0.5$ to 0.8 (the temperature had no decisive influence). Because of the decreasing total amount of methyl ester and the increasing water excess the methanol content of the aqueous phase decreased.

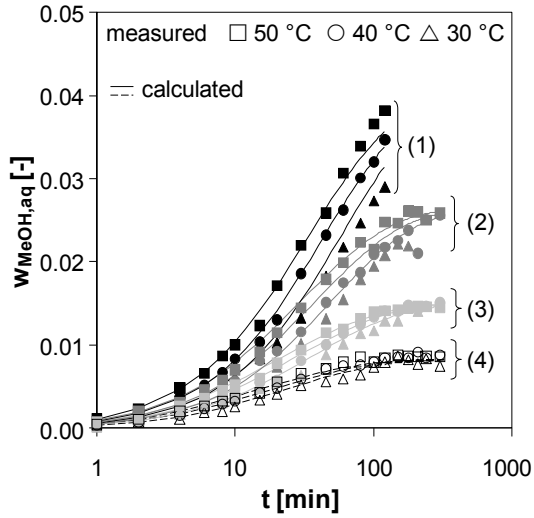

Figure 4: Influence oft the initial water to methyl ester (A_{H2O}) and catalyst to methyl ester (A_{cat}) mass ratios on the conversion course during the hydrolysis of methyl octanoate at constant total reactant mass and a packed bed superficial velocity of 0.07 m/s. (1) $A_{H2O} = 2.3$, $A_{cat} = 7\times10^{-3}$; (2) $A_{H2O} = 4.4$, $A_{cat} = 12\times10^{-3}$; (3) $A_{H2O} = 9.8$, $A_{cat} = 23\times10^{-3}$; (4) $A_{H2O} = 20.6$, $A_{cat} = 46\times10^{-3}$. Comparison of calculated and measured methanol mass fractions $w_{MeOH,aq}$ in the aqueous phase.

Within the mathematical model wetting of the entire particle bed by the organic phase irrespective of A_{H2O} and direct proportionality between the reaction rate and the catalyst mass were assumed. From the good agreement between the calculated and measured courses shown in Fig. 4 it can be concluded that the modeling assumptions were correct up to a water excess of 20:1 g/g for temperatures ranging from 30 to 50 °C.

4.2. Direct comparison of the operation modes

In section 2 the decomposition of the reaction in two steps was suggested. The purpose of the decomposition was to prove the validity of the assumptions regarding the catalyst wetting applying the sterical separation of reaction and liquid-liquid mass transfer. A direct comparison between calculated and measured courses for both operation modes is shown in Fig. 5. The calculated courses were based upon the parameter determination from two-phase flow experiments as described in section 4.1. The successful separation of both elementary steps enabled the examination of the impact of the catalyst wetting on the reaction rate from the direct comparison of experiments performed in both

operation modes for a fixed value of A_{H2O}. From the comparison it can be concluded that both operation modes gave nearly identical conversion courses, which confirmed that in both cases the same amount of catalyst was active. Thus, wetting of the entire particle bed by the organic phase at two-phase flow could be assumed.

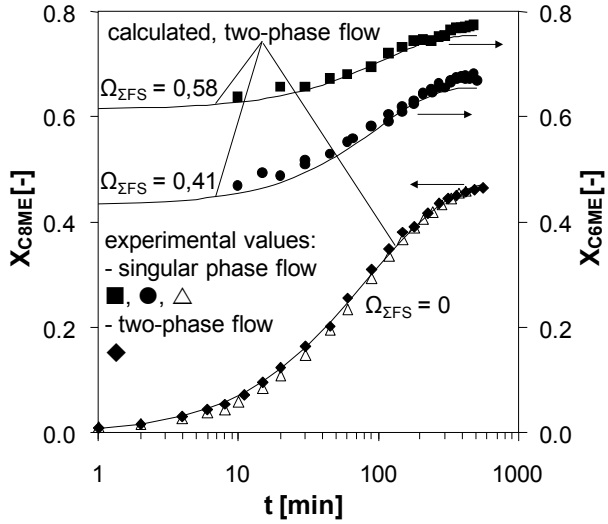

Figure 5: Comparison of experimental and calculated conversion courses obtained in the singular and two-phase flow operation mode at A_{H2O} = 2.3 exemplarily given for four independent experimental runs. (X_{C6ME}, X_{C8ME} = methyl hexanoate or methyl decanoate conversion; $\Omega_{\Sigma FS}$ = initial fatty acid to (fatty acid + methyl ester) mass ratio).

5. Conclusions

For this type of equilibrium limited reactions multistage extractive-reaction processes provide an alternative concept for shifting the equilibrium conversion toward the products (Krause et al. (2010), Samant and Ng (1998)). Either high water to methyl ester mass ratios resulting in a comparatively small number of equilibrium stages, or a moderate water excess resulting in a comparatively high number of stages are applicable. Both strategies lead to different requirements in respect of the process design. Using the suggested examination method a reliable calculation model necessary for the simulation of process alternatives was obtained.

References

Y. Kosugi, N. Tomizuka, 1995, Continuous lipolysis reactor with a loop connecting an immobilized lipase column and an oil-water separator, JAOCS, 72, 1329-1332

P. Krause, R. Macias, G. Fieg, 2010, Applicability of a Countercurrent Enzymatically Catalyzed Multistage Extractive Reaction Process for the Hydrolysis of Methyl Octanoate, Ind. Eng. Chem. Res., 49, 3217-3222

P. Krause, G. Fieg, 2011, Experiment based model development for the enzymatic hydrolysis in a packed-bed reactor with biphasic reactant flow, Chem. Eng. Sci, 66, 4838-4850

P. Krause, G. Fieg, 2012, Applicability of a simple laboratory setup for the extractive hydrolysis using immobilized enzymes, Chem. Eng. Process., submitted

K.D. Samant, K.M. Ng, 1998, Design of Multistage Extractive Reaction Processes, AIChE J., 44, 12, 2689-2702

I.A. Karimi and Rajagopalan Srinivasan (Editors), Proceedings of the 11th International Symposium on Process Systems Engineering, 15-19 July 2012, Singapore.

Statistical Monitoring of Water Systems

Marco Cedeño Viteri,[a] Leandro Rodriguez Aguilar,[a] Mabel Sánchez[a]

[a]*Planta Piloto de Ingeniería Química (UNS- CONICET,) Camino La Carrindanga Km 7, (8000) Bahía Blanca, Argentina*

Abstract

In this work a new statistical control methodology that works in the original variable space is presented. The study is focused on the performance of the detection stage, which applies the 2-order Mahalanobis distance as statistical test. Its critical-value is estimated using a kernel density estimation technique. The identification stage uses the concept of the nearest in control neighbor to calculate the variable contributions to the inflated statistic and employs the same distance measure. Application results are provided for a waste water treatment plant.

Keywords: Statistical Process Control, Mahalanobis Distance, Waste-Water Treatment Plants.

1. Introduction

Multivariate Statistical Process Control (MSPC) techniques have been widely applied for turning data into information since they are suitable to develop empirical descriptions of the process behavior based on measurements. Most of them work in latent-variable spaces. In the spirit of developing new approaches that could provide new features and capabilities to those techniques, little attention has been paid to the fact that some strategies which work in the original measurement space could also perform well when monitoring a process (Alvarez et al., 2010).

From the monitoring standpoint, determining whether the process can be considered as in-control at a given time t is just one step in the procedure, called the detection stage. The MSPC approaches that work in the space of measurements make use of the Hotelling (T^2) statistic, which is a measure of the linear Mahalanobis Distance (MD), for this purpose. Whenever one observation is believed to show an abnormal behavior, all the effort must be oriented towards finding what the root cause of the deviation is. The activities related to isolating the variable(s) that indicate(s) the faulty state conform what is known as the identification stage, which is frequently performed by calculating the variable contributions to the inflated statistic. The main purpose of evaluating those contributions is to compare the relative influence of each measured variable on the final T^2-statistic value. It is considered that those having the largest contributions reveal the faulty state. In this sense, Mason and Young (2002) presented a combinatorial strategy to decompose the T^2-statistic into the contributions of each variable. It has the limitation that a great number of possible decompositions are obtained, increasing the complexity of the identification procedure. Then a straightforward method to decompose the T^2 statistic as a unique sum of variable contributions, called OSS, was developed by Alvarez et al. (2007). Recently, Alvarez et al. (2010) proposed a new MSPC strategy for batch process monitoring, called OSSBP, based on that decomposition. For the analyzed case studies, the proposed strategy has comparable abilities regarding the detection of process failures with respect to the ones presented by the most popular latent variables-based approaches (Westerhuis et al., 2000; Ramaker et al., 2005; Yoo et al., 2004).

Moreover, identification performance indexes show better results for the OSSBP. Its satisfactory behaviour may be attributed to the fact that the number of variables involved in this type of processes is moderate and the strong non-linear relationships among them prevent the measurements from being linear combinations. These facts prevent the data correlation matrix to be singular.

When the T^2-statistic is applied for the detection stage of a MSPC procedure, it is generally assumed that measurement vectors are independent and follow a multivariate normal distribution. In this case, the T^2-statistic follows a $[J(I^2-1)/(I^2-IJ)]F_{J,I-J,\alpha}$ distribution where, $F_{N,I-N,\alpha}$ is the value of the F distribution for a level of significance α with J and $(I-J)$ degrees of freedom, I represents the number of samples in the reference population and J is the number of measurements. No assumption about the probability density function (*pdf*) is required when the threshold value T^2_C is determined as the $(1-\alpha)$ quantile of the T^2 *pdf*, which can be estimated using well-known kernel density estimation (KDE) methods. Although the computational effort increases, the extra calculations are performed offline, thus no application restrictions during the online monitoring stage arise due to the extra computational burden (Alvarez et al, 2010).

Because the OSS methodology has a comparable ability for fault detection with respect to the existing latent-variable procedures, the use of a different distance measure to indicate the out of control state is analyzed in this work. The same type of distance between the nearest in control neighbour (NICN) and the current observation (Alvarez et al., 2009) is used to determine the contribution of each variable to the out of control state. Those variables whose distance measures exceed a certain threshold value are considered as suspicious. The coordinates of the NICN are obtained by solving a minimization problem. In this work, the Polynomial Mahalanobis distance of order 2 is selected for both stages of the proposed MSPC.

The rest of the paper is structured as follows. In Section 2 the methodology is presented. Results corresponding to its application for the detection of faults in a waste water treatment plant (WWTP) benchmark are provided in Section 3. A Conclusion section ends this work.

2. Methodology

The Mahalanobis distance is a common metric that attempts to capture the non-isotropic properties of a J-dimensional feature space. It weights the distance calculation according to the statistical variation of each component using the covariance matrix of the observed sample. Grudic and Mulligan (2006) have shown that the MD may not tightly follow a learning data set, and substituted it by the Polynomial Mahalanobis distance (PMD), which is obtained by mapping the measurement space into high order polynomial terms. They use the PMD for classifying path regions in images of natural outdoor environments.

Those authors formulated the q-order PMD (q-PMD) as follows. Given a set of $\mathbf{x}_k$ observation vectors (k=1,..,I) of dimension J, the q-PMD between vectors $\mathbf{x}_i$ and $\mathbf{x}_j$ is calculated by first mapping each $\mathbf{x}_k$ into all polynomial terms of order q or less, which are included in vector $\mathbf{z}_k$, and then calculating the MD between $\mathbf{z}_i$ and $\mathbf{z}_j$ using the covariance matrix obtained from the reference population of polynomial term mappings. In this way they attempt to describe more sophisticated and nonlinear relations among feature vectors.

The T^2- statistic applied in MSPC procedures is a measure of the MD between an observation and the population mean. An out-of-control state of the process is indicated

if the T^2- statistic value exceeds the critical one. This is calculated using a KDE technique when the OSS procedure is used.
In this work a new MSPC procedure is devised whose detection stage makes use of the 2-order PMD (PMD^2) between an observation and the population mean as statistic test. That PMD^2 is formulated following the work by Grudic and Mulligan (2006) and the critical value of the statistic PMD^2_C is calculated using the KDE technique.
Regarding the identification stage, the knowledge about how far the faulty observation is from an in-control allocation gives us an idea of the directions whose distances explain the anomalous situation. This information is obtained by finding the nearest neighbour of the observation point that is in statistical control ($\mathbf{x}_{NICN}$). An optimization problem is formulated whose objective is to minimize the PMD^2 between $\mathbf{x}_{NICN}$ and the measured point $\mathbf{x}$, subject to the constraint that the PMD^2-value for $\mathbf{x}_{NICN,}$ is equal to the critical one (PMD^2_C). The comparison of the absolute difference between x_{NICN} and x for each variable j with a threshold value τ, which is obtained by simulations for a given Number of Precise Identifications (Alvarez et al., 2010), allows to identify the suspicious measurements.

3. Application Results for the WWTP Benchmark

In this section application results of the proposed strategy for the detection and identification of faults associated to a WWTP benchmark are presented. The plant layout, model equations and control strategy are not included for the sake of brevity but they are described in detail online [http://www.ensic.u-nancy.fr/COSTWWTP]. For the present study, plant layout combines nitrification with predenitrification, which is the most commonly used method for nitrogen removal. The plant is designed to treat an average flow of 20,000 m^3/day with an average biodegradable chemical oxygen demand concentration of 300 mg/l. The plant is made up of five-compartment biological tanks and a secondary settler. The first two compartments of the bioreactor are not aerated whereas the others are aerated. The nonreactive secondary settler is modeled with a series of 10 layers. There are two internal recycles: the nitrate internal recycle from the last tank to the first tank, and the activated sludge recycle from the underflow of the secondary settler to the front end of the plant. In Figure 1 a schematic diagram of the simulation benchmark is shown.

Fig 1: WWTP Layout

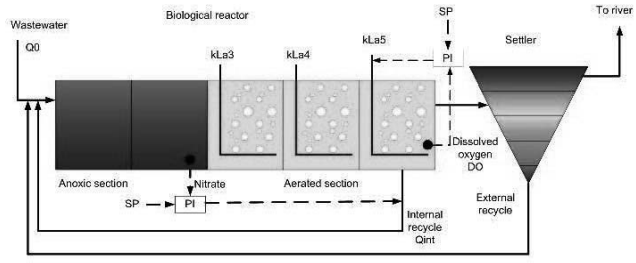

The training model is based on a normal operation period of 1-week of dry weather and a 1-week data set is used for validation. The sampling time is 15 min; therefore 96 samples are taken each 24-hour period. The data used are the influent file and outputs with noise suggested by the benchmark. The following eight variables are selected to build the monitoring system: influent ammoniac concentration, influent flow rate, total

suspended solids in reactor 4, effluent total suspended solids, dissolved oxygen concentration in reactors 3 and 4, oxygen transfer coefficient in reactor 5, and nitrate concentration in reactor 2.

In this work, three scenarios describing real situations are considered for the analysis. The first external disturbance takes the form of a storm event. It originates that the influent flow rate exceeds the maximum standardized value for normal operating conditions, which is equal to 2.67, during the following time intervals (848-857), (1049-1086), (1095-1103). The second external disturbance is the increment of the influent flow rate due to rain. This flowrate exceeds its maximum normal-operating value from samples (807-906). The third fault is a mean change in the nitrate concentration sensor noise. This fault is introduced at the beginning and maintained until the end of the simulation.

Regarding the detection capabilities of the proposed strategy, the evolution of T^2-statistic and PMD^2-statistic in time is analyzed. Both statistics are compared to their corresponding critical values obtained using a KDE technique. For a significance level α= 0.06, their values are: 16.85 for T^2, and 120.11 for PMD^2. A failure is declared after three consecutive warnings.

For the storm disturbance, the T^2-statistic gives alarms at samples 849 and 1051, and the PMD^2-statistic indicates a fault condition at samples 849 and 1049. Both statistics point out the abnormal situation for a long time. This shows the effect of the influent flowrate increment on internal variables persists in time. The evolution of the influent flowrate, the T^2-statistic and PMD^2-statistic in time is displayed in Figure 2 for the storm event.

Fig 2: Storm Events

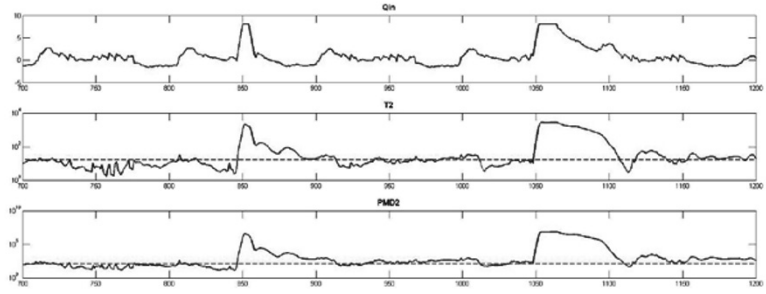

Fig 3: Rain Event

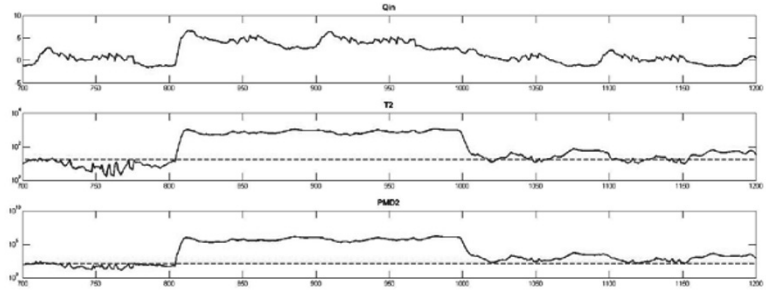

For the rain event, both the T^2-statistic and PMD^2-statistic give an alarm at sample 807, that also persist in time. The time evolution of the statistics for this event is shown in Figure 3. The next figure reports the same information for the third fault, which is

associated with a mean change of the concentration nitrate sensor noise. The T^2-statistic gives an alarm at sample 47, after 3 consecutive warnings are obtained. In contrast the PMD^2-statistic provides the first alarm signal at sample 3 and it is repeated many times during the operation. Variable contributions to the inflated statistics are obtained that properly indicate the faulty variables. Contribution plots are not included for the sake of brevity.

Fig 4: Mean change in sensor noise

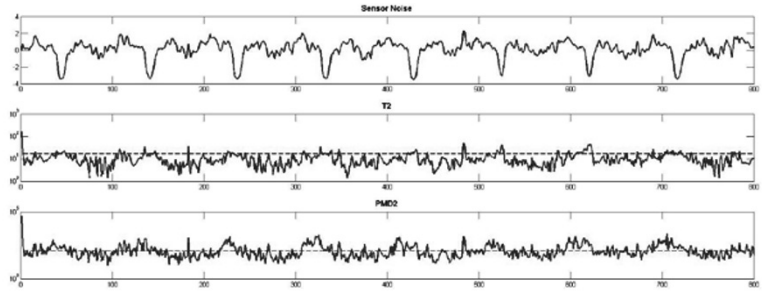

4. Conclusions

In this paper a new MSPC methodology that works in the original variable space is presented and applied for WWTP fault diagnosis. A different distance measure, the *q order-PMD*, is used as test statistic for the detection stage and to determine the variables that signal the fault.

For the fault scenarios of the WWTP analyzed in this work, the PMD^2 has shown better capabilities for fault detection with respect to the T^2-statistic. Also it has a rewarding performance with respect to the statistics used in the latent variable space methodologies reported in literature when the action to signal time is considered for comparison purposes.

The computational load of the identification stage ensures real-time results for the tested faults. Future work involves the selection of the polynomial order.

References

C. Alvarez, A. Brandolin, M. Sánchez, 2007, On the Variable Contributions to the D-statistic, Chemom. & Intell. Lab. Syst., 88, 2, 189-196.

C. Alvarez, A. Brandolin, M. Sánchez, 2009, A Neighbour in Control Technique for Batch Process Monitoring", Comp. Aided Chem. Eng. Elsevier, 27, C, 1581-1586.

C. Alvarez, A. Brandolin, M. Sánchez, 2010, Batch Process Monitoring in the Original Measurement's Space, J. of Process Control, 20, 6, 716-725.

G. Grudic, J. Mulligan, 2006, Outdoor Path Labeling Using Polynomial Mahalanobis Distance, Proceedings of Robotics: Science and Systems II, MIT Press, Cambridge, Massachusetts.

R. Mason, J. Young, 2002, Multivariate Statistical Process Control with Industrial Applications, ASA SIAM, Philadelphia.

H. Ramaker, E. Van Sprang, J. Westerhuis, A. Smilde, 2005, Fault Detection Properties of Global, Local and Time Evolving Models for Batch Process Monitoring, J. of Process Control, 15, 7, 799-805.

J. Westerhuis, S. Gurden, A. Smilde, 2000, Generalized contribution plots in multivariate statistical process monitoring, Chemom. & Intell. Lab. Syst., 51, 1, 95-114.

C. Yoo, J. Lee, P. Vanrolleghem, I. Lee, 2004, On-Line Monitoring of Batch Processes Using Multiway Independent Component Analysis, Chemom. & Intell. Lab. Syst., 71, 2, 151-163.

I.A. Karimi and Rajagopalan Srinivasan (Editors), Proceedings of the 11th International Symposium on Process Systems Engineering, 15-19 July 2012, Singapore.

Next-Generation, Integrated Fire Detection and Diagnosis Built Upon the Recent Advances in the Abnormal Situation Management

Kijun Lee[a], Seong-Hwan Han[a], Tae-Ok Kim[a], Dongil Shin[a]

[a]*Department of Chemical Engineering, Myongji University, Yongin 449-728, Korea*

Abstract

Process fault monitoring, detection and diagnosis, and fire detection and isolation technologies have many common characteristics between them, and the amount of technological overlapping is being increased. This paper compares and discusses our works in the areas of conventional abnormal situation management (ASM) as well as fire alarm generation management, as a try to show how the ASM technologies would contribute in developing next-generation fire detection and management technologies and improve the safety of process plants and the public. And the lessons from the fire detection research that could be applied for better monitoring, detection and diagnosis of processes are also discussed.

Keywords: Fire Detection, Process Monitoring and Diagnosis, Industrial Applications, Process and Public Safety, Computational Methods

1. Introduction

Fire is one of the oldest hazards and has been around the human beings with the start of the history. Process fault monitoring, detection and diagnosis and fire detection and isolation technologies have been developed separately and have rich histories individually, but there has been no study of the commonality of the both. There are many sharing characteristics between them and the amount of technological overlapping is being increased: Mitigation of sensor failures, context sensitivity, and minimization of Type I, II errors are important problems. Use of wireless sensors and merge of heterogeneous information are getting the focus en route to the next-generation technologies. This paper discusses how the abnormal situation management technologies, studied in the process systems engineering perspective, would contribute in developing next-generation fire detection and management technologies and improve the safety of process plants and intelligent buildings as well. The next sections show our works in the area of conventional abnormal situation management as well as fire alarm generation management.

2. Fault Detection, Monitoring and Diagnosis System for CNG Stations

2.1. Necessity of the Research

The compressed natural gas (CNG) among the eco-friendly energy sources already accounts for more than 10 percent of domestic energy consumption of Korea. CNG vehicles and also the gas stations are being increased. However, more than nine large and small accidents of CNG vehicle and gas stations have occurred in the past five years, which makes us aware of the need for the study for the safety and safe operations of CNG stations. A lot of non-repetitive transition sections exist during the ordinary operation of CNG gas stations. Therefore, fault detection and diagnosis are limited with

the current monitoring methods, and the advanced maintenance before failures is almost impossible and even the alarms exceeding the specified upper and lower thresholds are ignored as nuisant [1,2].

2.2. Using PCA

In this study, we developed a system (see Fig. 1) to build a monitoring model for the CNG station and perform the real-time monitoring and diagnosis using Principal Component Analysis (PCA), which is suitable for processing large amounts of multi-dimensional data for multivariate statistical analysis [3].

2.2.1. Filtering and Scaling

Filtering and scaling processes are conducted prior to the model construction and application. As shown in Fig. 2, data during the start-up and shut-down are removed from the 7 pressure sensor and 5 temperature sensor data collected per second, and the remaining data of ordinary charging operation are used for model development [4,5,7].

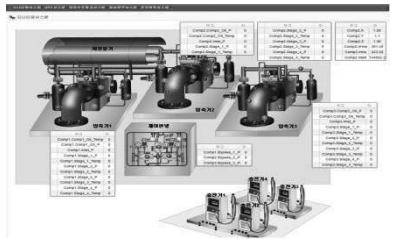

Fig. 1. Screenshot of the developed system

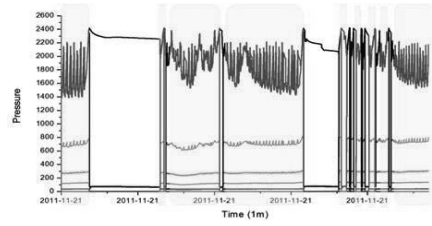

Fig. 2. Filtering of the pressure data

2.2.2. Modeling

We built the PCA model in Fig. 3 by the calculation of the new characteristics variables, called as the major component, finding the factors representing the trend of unsteady process operation. Fig. 4 represents Q residuals of model data [6].

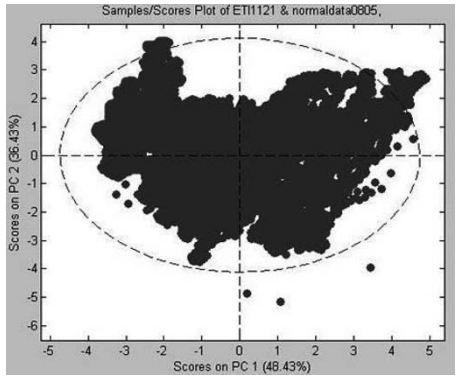

Fig. 3. Score plot of PCA model

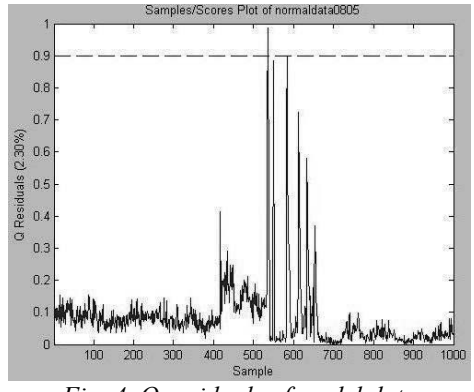

Fig. 4. Q residuals of model data

2.3. Result

The performance of real-time monitoring was measured against the data of process operations already stored in the real-time database. As a result of conducting the off-line monitoring in order to improve the accuracy of the system and verification, all data in the normal operation were distinguished as normal. And when an abnormal

phenomenon was tested by reflecting the abnormal process data, the cause of abnormality could be refined by detecting abnormality as in Fig. 5 and by tracking main contributing variables as in Fig. 6.

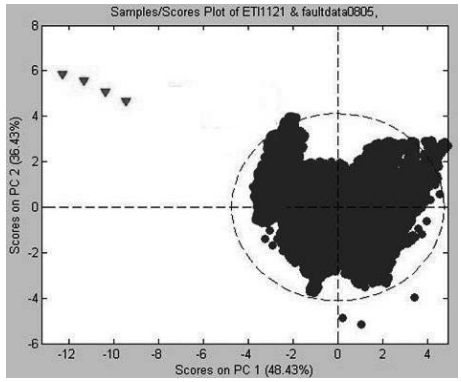

Fig. 5. Plot of detecting abnormality

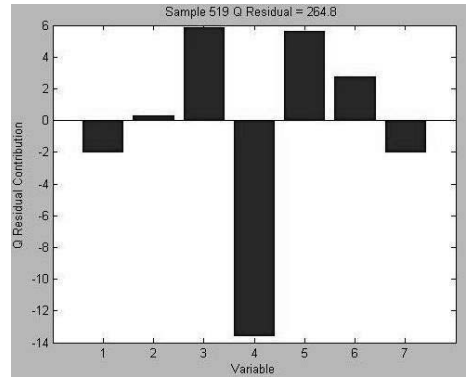

Fig. 6. Diagnosing cause of abnormality

Even though the training data of abnormal operations are rare, the proposed system is able to efficiently cope with the abnormality in process through fault detection and diagnosis with the development and building of the monitoring system for CNG gas stations using PCA. It is estimated that the optimized operation of the facility would be possible by the real time comparison of the current state of facility to the normal state of the past.

3. Fire Detection System Design Based on Multi-sensor Information for Improved Reliability

3.1. Necessity of the Research

The fire detector is used to sense and alarm the danger in an emergency, and the time it takes from the outbreak of fire and detecting the danger and its accuracy are considered critical [8]. For existing detectors, such as mechanical method (on-off), single sensor-based (heat, smoke, or flame), or dual sensor (HR combination system), malfunctions as false-positive alarms not going off in case of fire or false-negative alarms ringing when there is no fire occur frequently [9].

3.2. Improved Detection Algorithm

This study suggested an improved algorithm that senses fire by using three types of information of heat detector, smoke detector, and concentration detector, and has established a fire detecting testbed on LabVIEW, and verified algorithm by using the testbed [12]. Simulation was carried out by using the measured sensor data according to the experiments provided by Fire Research Division of NIST, and was able to verify if a fire occurs or not for a given set of data [10,11].

3.2.1. Fire Detection Algorithm

This study determined whether the temperature, smoke, or carbon monoxide values exceeded the critical value, and suggested an integrated fire detecting algorithm that determines cases of emergency based on the results as shown in Fig. 7.

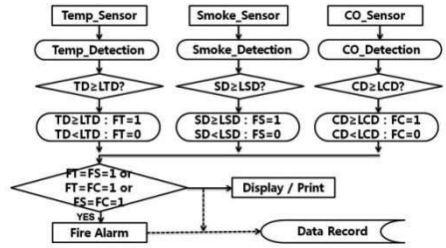

Fig. 7. Fire detection based on multiple information

3.2.2. Simulation

As shown in Fig. 8, the testbed was established on LabVIEW, implementing the suggested algorithm, and simulation was carried out by using the sensor measuring data according to the situation of Home Smoke Alarm Tests performed by the Fire Research Division of NIST from 2004 to 2008. A test scenario among Home Smoke Alarm is as shown in Table 1, and the simulation process is as shown in Fig. 9 [12].

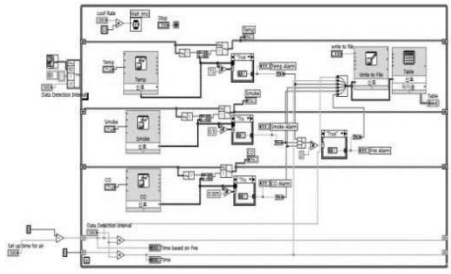

Fig. 8. Testbed implemented

Table 1. Fire place and a source of ignition [12]

Situation	Test	Ignition	Fuel Package	Fire Location
Fire	SDC02	Flaming	Chair	Living Area
	SDC05	Flaming	Mattress	Bedroom#2
	SDC08	Smoldering	Mattress	Bedroom#2
	SDC11	Smoldering	Chair	Living Area
	SDC15	Flaming	Chair	Living Area
	SDC39	Flaming	Mattress	Bedroom#2
	SDC41	Heating	Cooking Oil	Kitchen Area
Non-fire	MHN30	14 g (1 tbls) butter, cast iron pan, fan on		
	MHN31	14 g (1 tbls) butter, cast iron pan, fan off		
	MHN40	Smoldering PU foam block, fan off, (flamed)		

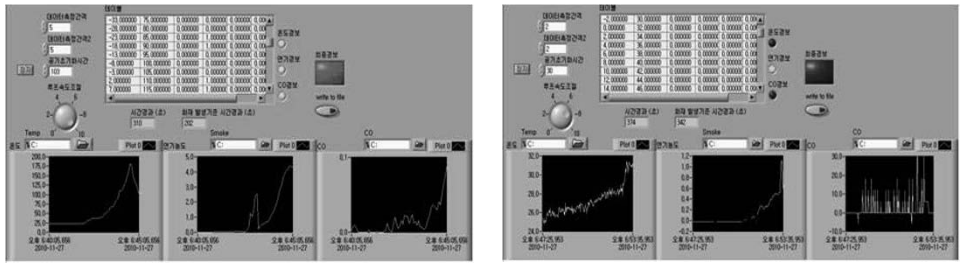

Fig. 9. Simulation: Minimization of false negative and positive errors (Scenario SDC05 at 202sec : Detected false positive / Scenario SDC05 at 342sec : Detected false negative)

3.3. Result

As a result, the elapsed time until the very first integrated generation of warning and alarm operation was identified as shown in Tables 2 and 3. Every fire emergency except for Test SDC41 was detected, and the integrated alarm method worked successfully for all non-fire situations.

The integrated fire detection system based on multiplexed information of three independent measuring data improved the accuracy of diagnosing the real and non-fire situations than the existing fire detecting systems based on single or dual information.

Improvement in more collection of quantitative data, which consider both accuracy and time of detection, and advanced algorithm built upon the recent advances in the abnormal situation management are considered to make contribution in a development of next-generation fire detection system. Performance evaluation of fire detection system which was actually restricted other than actual fire experiments is considered to be possible by expanding the suggested testbed.

Table 2. Detected all fire situations

Test	Ignition	Fuel Pkg.	Fire Location	Fire Alarm (s)	Temp Alarm (s)	Smoke Alarm (s)	CO Alarm (s)
SDC02	Flaming	Chair	Living Area	110	146	110	0
SDC05	Flaming	Mattress	Bedroom#2	117	117	67	192
SDC08	Smoldering	Mattress	Bedroom#2	3721	3721	3721	3809
SDC11	Smoldering	Chair	Living Area	4289	4303	773	3549
SDC15	Flaming	Chair	Living Area	327	313	327	417
SDC39	Flaming	Mattress	Bedroom#2	128	108	128	-
SDC41	Heating	Cooking Oil	Kitchen Area	-	-	1206	-

Table 3. Detected all non-fire situations

Test	Nuisance Sources	Fire Alarm (s)	Temp Alarm (s)	Smoke Alarm (s)	CO Alarm (s)
MHN30	14 g (1 tbls) butter, cast iron pan, fan on	-	-	324	-
MHN31	14 g (1 tbls) butter, cast iron pan, fan off	-	-	310	40
MHN40	Smoldering PU foam block, fan off, (flamed)	-	-	-	470

4. Conclusion: Integrated fire detection and diagnosis

Process fault monitoring, detection and diagnosis and fire detection and isolation technologies have many common characteristics between them, and the amount of technological overlapping is being increased: Mitigation of sensor failures, context sensitivity, and minimization of Type I, II errors are important problems. This paper discussed how the abnormal situation management technologies, shown for the case of fault detection, monitoring and diagnosis system for CNG stations, would contribute in developing next-generation fire detection and management technologies and improve the safety of process plants and public safety for the realization of better sustainable society.

References

[1] David M. Himmelblau, *Fault Detection and Diagnosis in Chemical and Petrochemical Processes*, Elsevier (1978)

[2] Kourti, T. and MacGregor, J. F., "Process Analysis, Monitoring and Diagnosis Using Multivariate Projection Methods", *Chemometrics and Intelligent Laboratory System* 28(1), 3-21 (1995)

[3] ChangKyoo Yoo, et al., "Recent Research Trends of Process Monitoring Technology: State-of-the Art", *Korean J. Chem. Eng*., 46(2), 233-247 (2008)

[4] Manabu Kano, et al., "A New Multivariate Statistical Process Monitoring Method Using Principal Component Analysis", *Computers and Chemical Engineering,* 25, 1103-1113 (2001)

[5] Jong-Min Lee, et al., "Fault detection of batch processes using multiway kernel principal component analysis", *Computers and Chemical Engineering,* 28, 1837-1847 (2004)

[6] Barry M. Wise, *PLS_Toolbox 3.5 Manual*, Eigenvector Research (2004)

[7] Hyosung Corporation, *CNG compressor package manaul system*: V1.03

[8] Mark Hunter, "False alarm reduction by use of new technology", *International fire protection,* 55-58 (2006)

[9] M. Thuillard, "New Methods for Reducing the Number of False Alarms in Fire Detection Systems", *Fire Technology J.*, 30(2). 250-268 (1984)

[10] J.A. Milke, L.A. Cestari and W. Clarence, "Advanced Fire Detection Algorithms Using Data from the Home Smoke Detector Project", *Fire Safety J*., 40(1) 1-28 (2005)

[11] A. Scheidweiler, "The Distribution of Intelligence in Future Fire Detection Systems", *Fire Safety J*., 6, 209–214 (1983)

[12] NIST, Home Smoke Alarm Tests, http://smokealarm.nist.gov/

I.A. Karimi and Rajagopalan Srinivasan (Editors), Proceedings of the 11th International Symposium on Process Systems Engineering, 15-19 July 2012, Singapore

Hierarchical proficiency evaluation system of plant operation for effective operator training

Taketoshi Kurooka,[a] * Masaki Yasuda,[b] Haruyuki Okuda,[b]
Hironobu Arakawa,[b] Hideki Manako,[b]

[a] *Department of Life Sciences & Bioengineering, Faculty of Engineering, University of Toyama, Gofuku 3190, Toyama-shi, Toyama 930-8555, Japan*
[b] *System Advanced Solutions Department, Project Division II, Mitsubishi Chemical Engineering Corporation, 4-2-8 Shibaura, Minato-ku, Tokyo 108-0023, Japan*

Abstract

We have developed a new method to evaluate plant operators' proficiency. In this method, an operating procedure is hierarchically analyzed so that the method can be applied to complicated operations. Furthermore, the method was evaluated with indices based on Levenshtein distance. The proposed method was applied to simulator training on the start-up operation of a distillation column. The results demonstrate the utility and effectiveness of the proposed method.

Keywords: Proficiency metric, Plant operation, Skill assessment, Skill transition, Simulator training

1. Introduction

Recently, plant operation has become highly complicated, and thus inexperienced operators must often learn new operational procedures in complex plants. Additionally, in Japan, many veteran operators have been retiring in recent years, forcing younger operators to assume more of a leadership role. Therefore, effective training systems are required to train inexperienced operators more efficiently and quickly. For this purpose, training simulators are often used. Training simulators have been significantly improved, and their level of realism has been greatly enhanced (Jeong et al., 2002; Barrero et al., 2003) . In particular, Mitsubishi Chemical Engineering Corporation has been developing a simulator training system called MECTRNR ®. This system is equipped with advanced functions that can evaluate an operator's proficiency and perform PKYK (Process-Kiken-Yochi-Kunren; "process risk assessment by operators" in Japanese) through simulator training. These functions are useful for developing ideal operating ability. In this paper, we present a newly developed proficiency evaluation method and apply it to the function of assessing operators' capabilities.

For effective simulator training, it is necessary to evaluate how far the operator's skill has progressed in order to check his or her present skill level and to design effective training programs. This proficiency assessment is usually done with a subjective measure such as trainers' observation records or trainees' self-evaluations such as NASA-TLX or SWAT (Hart and Staveland, 1988; Reid and Nygren, 1988; Nishitani et al., 1997). However, subjective evaluation results vary according to the judgement of the assessor. As objective measures, physiological signals, such as an electroencephalogram or heart rate, are often

*kurooka@eng.u-toyama.ac.jp

used (Kurooka et al., 1998, 2001, 2003). However, measuring physiological signals imposes a strain on subjects. Recently, a new proficiency evaluation method was proposed, which uses an operating procedure index and a process stability index, and it was shown that the method can evaluate a simple operation (Kurooka et al., 2008). However, it is still necessary to develop a proficiency evaluation method that can be applied to a complicated operation in a large-scale plant. For this purpose, we developed a hierarchical system that can analyze and evaluate an operator's proficiency in a large-scale plant.

2. Hierarchical proficiency evaluation

2.1. Operational data for evaluation

We used a message summary that consists of two types of information: "when and what kind of alarm occurs and stops" and "when and what kind of operation is executed." These data, i.e. a message summary, can be easily obtained through a distributed control system (DCS) included in the training simulator system.

2.2. Evaluation procedure

The proposed evaluation procedure is carried out as follows:

Step 1 Constructing the hierarchical structure of a standard operating procedure: :
Based on a standard operating procedure, a hierarchical structure is built as shown in Fig. 1. This is done by decomposing tasks into sub-tasks or by grouping small tasks that have the same sub-goal. For example, the activity of starting up a distillation column can be decomposed into tasks of starting feed, starting reboil-up, and so on. On the other hand, some elementary tasks, such as setting MV of FC101 and setting SV of PC103, could have the same goal, i.e. starting feed.

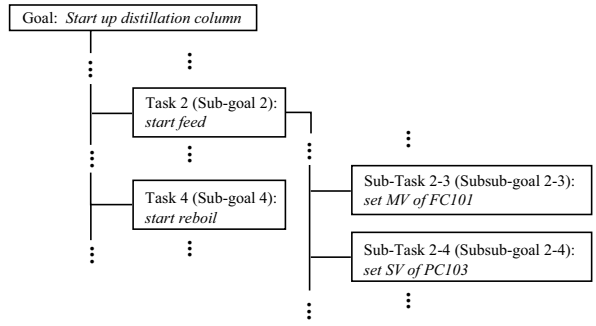

Figure 1. Example of an operation's hierarchical structure

Step 2 Building the hierarchical dictionary of a standard operating procedure: :
After constructing the hierarchical structure of a standard procedure, each task is symbolized and a layered task dictionary, i.e. a hierarchical dictionary, is built.

Step 3 Obtaining and symbolizing a trainee's operational data set:
Once the hierarchical dictionary is made, it is possible to hierarchically evaluate an operation. When a trainee is engaged in the target task on the training simulator, an alarm summary and an operating log are obtained through the distributed control system (DCS).

The obtained operating procedure is symbolized by referring to the symbols in the lowest sub-task level of the dictionary.

Step 4 Identifying higher-level tasks and calculating the task scores:
The obtained symbols of the trainee's operating procedure are divided into groups that are identified as higher-level tasks by referring to the dictionary. To identify the tasks, similarity indices are calculated. We adopted two types of similarity indices. When the sub-tasks of a task must be done in order, Levenshtein distance (*LD*) (Levenshtein, 1966) is calculated and similarity r is estimated by the following equation:

$$r = \frac{n - LD}{n} \times 100 \tag{1}$$

Here, n is the number of sub-tasks of the target task in the dictionary, and *LD* is the smallest number of insertions, deletions, and substitutions required to change one string into another, and it is applied in various areas such as spell checking, speech recognition, and DNA analysis. Through the process of calculating *LD*, we can not only analyze the extent of the difference between the trainee's operation and the standard operation but also identify the sub-tasks which produce the difference. When the sub-tasks of the task can be done in any order, r is estimated by the following equation:

$$r = \frac{n_d}{n} \times 100, \tag{2}$$

where n_d is the number of sub-tasks that are done by the operator as elements of the target task in the dictionary, and n is the total number of sub-tasks of the target task in the dictionary. The calculated r is recorded as the task score.

Step 5 Hierarchical identification:
Step 4 is done at the higher levels and repeated to the highest level of the hierarchy of the dictionary.

Step 6 Evaluating the operation:
We can evaluate and analyze the operation by observing the scores and the identification results from the highest level to the lower levels step by step.

3. Example

We applied the proposed proficiency evaluation system to actual simulator training. The target operation is starting up the distillation column shown in Fig. 2. Start-up is one of the plant's complicated operations and has many variations. The following four cases of this operation were performed by a trainee and then the results were evaluated:

Case 1) Operation according to standard operating procedure (changing the load in several steps)
Case 2) Operation while ignoring standard operating procedure
Case 3) Operation mostly according to standard operating procedure but drastically changing the load in one step
Case 4) Operation mostly according to standard operating procedure but changing the load in two steps

The evaluation results at the top of the hierarchy (Fig. 3) show that the ideal task sequence is listed in accordance with the dictionary made in Step 2. Here, r_{mean} and r_{max} are the mean and maximum values of the similarity indices of the identified sub-tasks.

More specifically, the evaluation results show that:

1) The overall scores r of operations in cases 1 and 4 indicate that those operations are similar to the standard (ideal) operation in outline.
2) The subtask scores r_{min} of case 4 are smaller than those of case 1 for task Nos. 8 and 9, which relate to loading up.
3) The overall score r of performing the operation in one's own way (case 2) is very poor.

These results are reasonable. As shown in result 2), the difference between cases 1 and 4 can be found by using a hierchical approach. If we want to analyze the difference in more detail, we can examine the lower-level evaluation results in sequence.

The r of case 1 does not show 100 due to the identified location of task No. 6. This is because the standard operation cannot describe the entire set of operations in full detail, and thus task No. 6 was difficult to identify in this example.

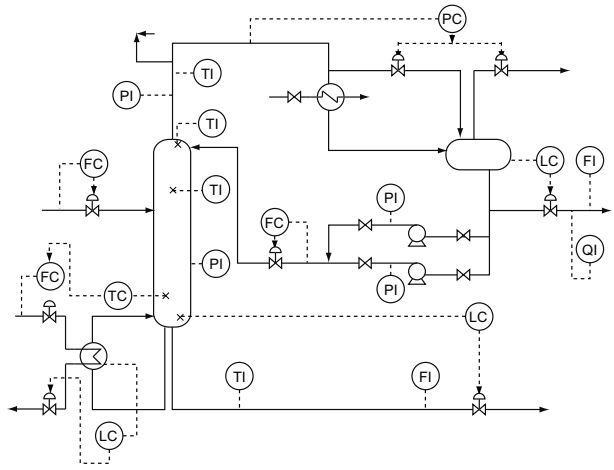

Figure 2. Example target plant

4. Conclusions

The proposed proficiency evaluation method can hierarchically evaluate and analyze an operation. This evaluation method was adopted in the simulator training system called MECTRNR, and the system was applied to a distillation column's start-up operation as an example. The results of trial evaluations show that the proposed method is useful in evaluating proficiency.

References

Barrero, L., Canales, R., Juárez-Romero, D., Mendoza, Y., Ruiz, G., Santoyo-Gutiérrez, S., 2003. Systematic building-testing of dynamic models for training simulators. Computers & Chemical Engineering 27 (10), 1421–1430.

Ideal task sequence at highest level

task No.	1	2	3	4	5	6	7	8	9

Case 1) r = 78

task No.	1	2	6	3	4	5	7	8	9
r_{mean}	87.5	15.0	10.1	40.0	40.0	50.0	3.7	54.4	40.8
r_{max}	100.0	100.0	66.7	40.0	40.0	50.0	50.0	100.0	55.6

Case 2) r = 33

task No.	1	2	6	9	7	4	5
r_{mean}	75.0	14.0	8.7	39.6	50.0	20.0	11.1
r_{max}	75.0	100.0	66.7	50.0	50.0	40.0	50.0

Case 3) r = 44

task No.	1	2	4	6	9	5	7	8
r_{mean}	87.5	12.5	40.0	9.1	40.8	50.0	50.0	83.3
r_{max}	100.0	100.0	40.0	66.7	55.6	50.0	50.0	100.0

Case 4) r = 78

task No.	1	2	6	3	4	5	7	8	9
r_{mean}	87.5	12.1	7.1	40.0	40.0	50.0	50.0	40.0	37.6
r_{max}	100.0	100.0	33.3	40.0	40.0	50.0	50.0	100.0	47.6

Figure 3. Results of evaluation at highest level

Hart, L. A., Staveland, L., 1988. Development of the NASA Task Load Index (TLX) : Results of empirical and theoretical research. Elsevier Science Publishers, Amsterdan, North-Holland, pp. 139–184.

Jeong, K. S., Kim, K. R., Jung, W. D., Ha, J. J., 2002. Development of severe accident management advisory and training simulator (SAMAT). Annals of Nuclear Energy 29, 2055–2069.

Kurooka, T., Hoshi, I., Yamashita, Y., Nishitani, H., Aug. 24-29 2003. Cascade estimation model for thinking state monitoring using plural physiological signals. In: In Proceedings of the International Ergonomics Association XVth Triennial Congress (IEA2003) and the 7th Ergonomics Society of Korea/Japan Ergonomics Society Joint Conference. Seoul, KOREA,, pp. Session HP–03–2.

Kurooka, T., Inoue, H., Watanabe, Y., June 29-July 18 2008. A new metric for evaluation of plant operators' proficiencies. In: In Proceedings of Computer-Aided Process Operations (FOCAPO 2008). Boston Massachusetts, USA.

Kurooka, T., Kisa, M., Yamashita, Y., Nishitani, H., Sept. 16-18 1998. Application of mind state estimation to plant operators. In: In Proceedings of 7th IFAC/IFIP/IFORS/IEA Symposium on Analysis, Design and Evaluation of Man-Machine Systems (IFAC-MMS'98). Kyoto, Japan, pp. 539–544.

Kurooka, T., Yamakawa, M., Yamashita, Y., Nishitani, H., 2001. Real-time monitoring of a plant operator's thinking state. Journal of Chemical Engineering of Japan 34 (11), 1387–1395.

Nishitani, H., Kurooka, T., Kitajima, T., 1997. Evaluation method of human interface in crt operation using protocol analysis. The Journal of the Society for Industrial Plant Human Factors of Japan 2 (1), 16–25.

Reid, G. B., Nygren, T. E., 1988. The Subjective Workload Assessment Technique: A scaling procedure for measuring mental workload. Elsevier Science Publishers, North-Holland, pp. 185–218.

I.A. Karimi and Rajagopalan Srinivasan (Editors), Proceedings of the 11th International Symposium on Process Systems Engineering, 15-19 July 2012, Singapore.

Simulation study of alternatives for the efficient start-up of dividing-wall distillation column sequences

Maria A. Vargas,[a] Georg Fieg[a]

[a]*University of Technology, Schwarzenbergstraße 95c,Hamburg 21071, Germany*

Abstract

The increasing interest in the use of dividing wall distillation columns demands procedures for its optimum operation. The start-up is a complicated process that requires the simultaneous and coordinated manipulation of multiple variables to take an empty column at ambient conditions to the required operation point. In the present research work is studied the start-up of a dividing-wall distillation column system (DWCSys) for the separation of a multicomponent mixture into five products using two different strategies. The implemented alternatives in the DWCSys are examined and evaluated according to the start-up time, energy consumption and accumulation of out of spec products. The results depict the influence of impurities and changes in the concentration of the feed stream on the start-up behavior of the column system. At the same time it was proven the robustness of the simulation model and the stability of the solution method to solve a very complex system of algebraic and differential equations with discontinuities that are commons in a start-up process.

Keywords: start-up, dividing-wall column, distillation sequence.

1. Introduction

The competiveness of today's market demands quality products at lower prices and thus it is required the implementation of more efficient processes. A clear example to diminish energy usage and at the same time reduce investment costs in a thermal separation process is the technology of dividing-wall distillation column (DWC). It consists of a column shell with a partition wall that separates the middle section of the column into two parts, the prefractionator and the side segment. This partition wall avoids the radial mixing of the internal vapor and liquid fluids in the prefractionator and main column, allowing the production of three pure components in a single column shell.

In recent years there have been a considerable growing interest in DWCs for industrial implementation. It demands clear procedures for the design and optimum but safe operation of the column, spanning the startup, production and shutdown periods. Numerous scientific publications have dealt with the design and control of DWCs but only few refers to the start-up process.

Start-up is a complex operation generally characterized by a long and unproductive duration. In this period, an empty column passes from ambient conditions to the required operation point. Non-specification products are produced and high amounts of energy are consumed. The economical and ecological interest to minimize the time of this non-productive period creates the necessity of developing time optimal start-up strategies which guarantee its feasibility, safety and easy implementation in columns of industrial scale. Additionally, the understanding of the process behaviour, avoids wrong

manipulations which could even retard more the start-up and create hazardous situations.
Rigorous simulation studies can be used to prepare adequate strategies and to plan a proper start-up procedure for operators.
In the simulation study of this work, start-up strategies are implemented in a dividing-wall column system (DWCSys). The system separates a mixture of linear alcohols in a direct sequence of two DWCs of industrial scale. The rigorous mathematical model used for this investigation was subject of an extensive experimental validation in a previous research in the Institute of Process and Plant Engineering (PAT) in the Hamburg University of Technology (*Niggemann et al.*). The implemented alternatives in the DWCSys are examined and evaluated according to the start-up time, energy consumption and accumulation of out of spec products.

2. Dividing-wall distillation column system

To separate a mixture into five products, three combinatorial possibilities of DWC arrangements (direct, side and indirect sequence) are feasible and the optimal column configuration is sought. The case study of this work consist of a mixture with equal mass concentration of the lineal alcohols, n-hexanol (C6), n-octanol (C8), n-decanol (C10), n-dodecanol (C12) and n-tetradecanol (C14). In a previous work from *Vargas et al.* was found that the direct connection results in the alternative with the lowest annualized total costs. A saturated liquid feed enters to the system with a mass flow rate of 5000 kg/h and is separated in products with a mass concentration > 0.99 wt.-/wt (Fig. 1). The two columns operate with a top pressure of 40 mbar which guaranteed a temperature in the condenser to cool with water and an enough low temperature in the bottom to avoid degradation.

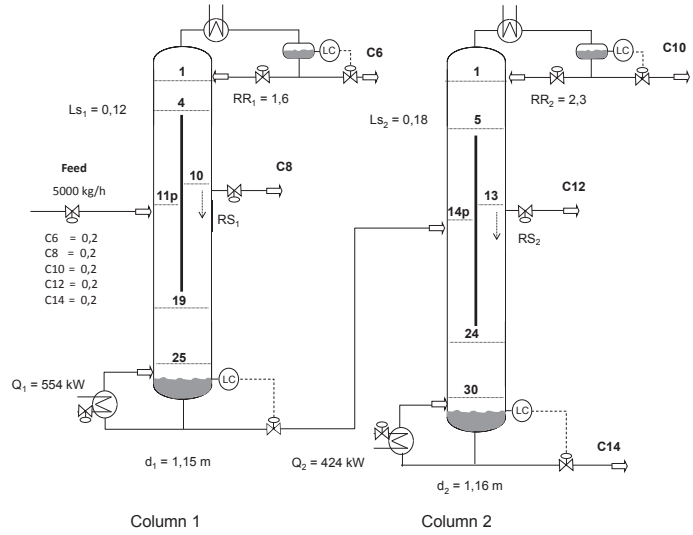

Figure 1. Dividing-wall distillation column system for five products separation.

The level in the reflux drum of both columns is controlled with the distillated stream, while the bottom level is controlled with the bottom stream respectively. The proportional controllers are set to have in the reflux drum 5 min retention time during normal operation and 5 min retention time in the bottom column. However, during the

start-up process the set point in the bottom column is doubled to avoid the dried up of the columns. Both columns are designed with Montz packing type B1-500. The column shell is of stainless steel with thickness of 0.012 m, determined according the standards AD 2000.

3. Simulation of the start-up process

A rigorous mathematical model built in the Institute of PAT capable of simulate the complete start-up process from an empty dividing-wall column at ambient temperature to steady state conditions is used. The model is composed of a system of differential and algebraic equations result of MESH balances in a column discretized in theoretical stages. Periphery equipments as reboiler, condenser and reflux drum are also integrated in the model. The simulation model also includes special features of DWCs as self adjustment of the vapour split by equalization of pressure drop in both sides of the dividing wall and heat transfer across the dividing wall.

The model is set according the column sequence design previously described, including all the design parameters, e.g., mass of packing, mass of column shell and liquids hold up which are required to simulate the heating up and filling of the column during the start-up process. Physical properties of the multicomponent mixture are determined with UNIQUAC activity coefficient model.

Typically the aim in a start-up process is to minimize the time required to achieve the steady state conditions and the production of off spec products. Several process variables can be manipulated in the attempt to speed up the process: feed flow rate, reboiler heat duty, reflux ratio, product flow rate and liquid split. These variables can vary during the start-up process within the constraints and set to the steady state value at the end of the process. In addition, during the start-up of a column system the time at which the columns are connected could have a major effect on the results.

In this work a conventional start-up strategy is implemented in the column system, in which the process variables are set to their steady state value as soon as feasible. Following the sequence of steps performed during the start-up operation:

- $t=t_0$: Begin feed input
- $t=t_1$: The liquid level set point in the bottom column is reached. Activation of reboiler (Q_i) and set to the steady state heat input.
- $t=t_2$: The boiling temperature is reached in the bottom column and the vapor starts to ascends until it reaches the condenser.
- $t=t_3$: The liquid level set point in the reflux drum is reached. The reflux ratio (RR_i), side split ratio (RS_i) and liquid split (Ls_i) are set to the steady state value.

The sequence of steps is equally performed in the two columns of the arrangements. However, during the start-up process the feed conditions to column 2 (e.g. flow rate, component concentration) may undergo changes until the stedy state conditions are reched in column 1. Two different start-up alternatives are evaluated. In the first alternative the feed to column 2 starts once the bottom product of column 1 is produced (simultaneous start-up strategy) and in the second alternative the feed to column 2 starts only after the steady state conditions in the connecting stream are reached (sequential start-up strategy).

3.1. Simultaneous start-up strategy

In the simultaneous start-up strategy the feed to column 2 starts as soon as feasible (t=0.34 h). At this moment the connecting stream (feed to column 2) still faces continues changes in composition, flow rate, temperature and pressure. Fig. 2(a) depicts

the concentration profile of the key components in the two columns of the sequence. In the first column the top and side products reach the steady state concentration relatively fast at t=1.34 h and t=1.37 h respectively (0.1 % of deviation from steady state value is accepted), but it is only at t=7.28 h when the steady state concentration is attained in the bottom stream. On the other hand in column 2, the steady state concentration of key components takes relatively longer to be reached. The low rate of increment of C10 in column 2 is mainly due to the presence of C8 impurities in the feed stream to column 2. The total start-up time of the column system is t=12.75 h limited by the bottom stream in column 2.

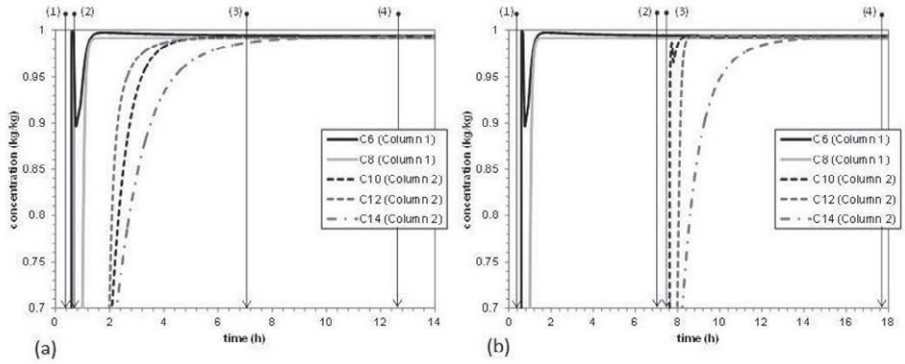

Figure 2. Concentration of key components during the (a) simultaneous and (b) sequential start-up of the dividing-wall column system, with (1) activation of reboiler (Q_1) in column 1, (2) activation of reboiler (Q_2) in column 2, (3) steady state in column 1 and (4) steady state in column 2.

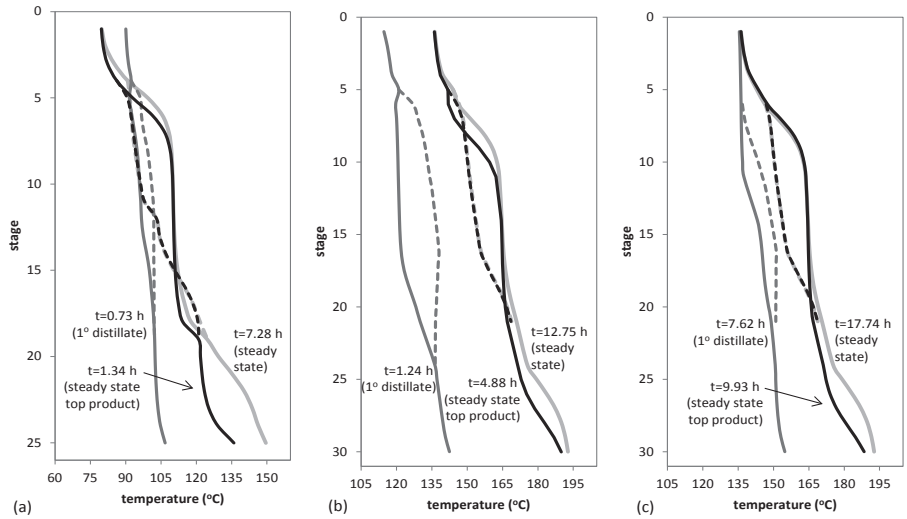

Figure 3. Temperature profile in (a) column 1 and column 2 during the (b) simultaneous and (c) sequential start-up of the dividing-wall column system. Prefractionator (- - - - -) and main column (——).

3.2. Sequential start-up strategy

In this strategy the connecting stream (feed to column 2) is deviated to a storage tank until it reaches the steady state conditions (t=7.28 h) . The concentration profile of key

components in column 2 (Fig. 2(b)) shows now a very similar behavior to the concentration profile of key components in column 1. The steady state concentrations in top and side products are reached relatively fast, once the reboiler is activated. The total start-up time of the system is t=17.74 h limited by the concentration of the bottom product in column 2.

The temperature profile during the start-up in the two columns of the sequences also reveals the consequence of impurities in the feed stream to column 2 (Fig. 3(b)). At the point the first drop of distillate is produced in column 2 with the simultaneous strategy, the temperature profile still very far from the steady state values. However, on the other hand, with both strategies is evident that after the steady state concentration in the distillate stream is reached, only in the lower segments of the column 1 and 2 there is a considerable difference with the steady state temperature profile (Fig. 3).

4. Comparison of start-up strategies

By only observing the start-up time, the simultaneous start-up strategy (t= 12.75 h) would results in the preferable alternative when compared to the sequential start-up strategy (t=17.74 h). However the total energy usage of the sequential strategy is around 13 % lower but with a higher amount of off spec product accumulation (Table 1). It evidence that in the development of start-up strategies the main objectives must be clearly define.

Table 1. Accumulated off spec products and waste energy during the start-up of the dividing wall column system.

			Strategy	
			Simultaneous	Sequential
Column 1	Accumulated off spec product, (kg)	Distillate	540	540
		Side	421	421
		Bottom	-	21253
		Q_1, (kW h)	404	404
Column 2	Accumulated off spec product, (kg)	Distillate	3475	2161
		Side	3409	574
		Bottom	13090	10882
		Q_2, (kW h)	5010	4341
	Total	Product, (kg)	20935	35831
		Q, (kW h)	5414	4745

5. Conclusion

Two different alternatives for the start-up of a direct sequence of two dividing-wall distillation columns have been presented. The results serve as the bases for the further development of optimum start-up strategies for DWCSys. In addition, it was evidenced the robustness of the model and the stability of the solution method to simulate the complex start-up process of two columns.

References

Niggemann, G., Gruetzmann, S. and Fieg, G., 2006. Distillation Startup of Fully Thermally Coupled Distillation Columns: Theoretical Examinations, In E. Sørensen, ed. Distillation and Absorption 2006 (Symp. Series No. 152). London: IChemE, 800-808.

Vargas, M. and Fieg, G., 2009. Dynamic modeling and simulation of dividing-wall distillation column systems, 10th International Symposium on Process Systems Engineering: Part A – PSE2009 (Computer Aided Chemical Engineering), Volume 27, 639-644.

Ian David Lockhart Bogle and Michael Fairweather (Editors), Proceedings of the 22nd European Symposium on Computer Aided Process Engineering, 17 - 20 June 2012, London.

Model-based system identification and PI controller tuning using closed-loop set-point response

Nataliya Baran[a], Günter Wozny[a], Harvey Arellano-Garcia[a]

[a]*Chair of Process Dynamics and Operation, Berlin Institute of Technology, Sekr. KWT-9, Straße des 17. Juni 135, D-10623 Berlin, Germany, nba@zmms.tu-berlin.de*

Abstract

In this work, a new approach to model identification and PI controller tuning based on model-based experimental design is presented. In the proposed strategy, system identification relies on a closed-loop set-point response. For this purpose, experiments are first exemplarily executed with a P-controller. Therefore, in this specific case only one design variable is considered that is represented by the controller gain. Additionally, we use the results achieved in the system identification step for the calculation of controller settings. In order to validate our approach and demonstrate the benefits of the proposed strategy, different scenarios are simulated.

Keywords: controller tuning, closed-loop, set-point response, PI controller, model-based design of experiments, model identification, parameter estimation

1. Introduction

In the chemical industry, PI controllers are widely used because of their simplicity and robust structure. However, it is still difficult to find good controller settings even though PI controllers only have a few adjustable parameters (Shamsuzzoha and Skogestad, 2010). There are basically two different methods for the calculation of controller settings. One of them is based on open-loop experiments whereas the other one uses closed-loop tests. Most tuning methods are based on information about process dynamics obtained from open-loop experiments. However, this strategy is usually time-consuming and expensive. Therefore, in this work, we focus on the determination of experimental conditions using closed-loop set-point response for the estimation of system model parameters with maximum statistical quality. For this purpose, we use a model-based optimal experimental design approach (Bauer et al., Franceschini and Macchietto, Barz et al.). The optimal experimental design strategy (OED) enables us to select experimental conditions for which the resulting data yields maximum information with respect to model parameters. The challenge of our approach is the need for model identification by closed-loop experiments. According to the concept of optimal experimental design, parameter estimation is applied in order to match the model to a real process. Therefore, our calculation of controller settings consists of two steps. First, we identify the system behavior using closed-loop set-point response and after that, we calculate the controller settings using an optimization strategy.

2. Problem Statement

We assume that a given process can be described by a set of differential-algebraic equations (DAEs) (Bauer et al., 2000)

$$\dot{y}(t) = f(t, y(t), p, u_{ED}(t)), \;\; y(t_0) = y_0(p), \tag{1}$$

where $\boldsymbol{t}$ represents the time, $\boldsymbol{y}$ denotes state variables, $\boldsymbol{p}$ is a set of parameters to be determined and $\boldsymbol{u_{ED}}$ represents the set of time-varying control variables, which are later used as design variables to plan experiments. Parameter estimation is done by fitting the results of the model simulation $\boldsymbol{y^{calc}}$ to the measured data $\boldsymbol{y^{meas}}$. We assume that measurement errors $\boldsymbol{\xi^{y}}$ are independent, normally distributed and can be characterized by a measurement-covariance matrix $\boldsymbol{MV}$. The parameter estimation is based on the minimization of a weighted least square functional

$$min_p \sum_{k=1}^{N_{exp}} \left(y_k^{meas} - y_k(u_{ED,k}, p)\right)^T \cdot MV^{-1} \cdot \left(y_k^{meas} - y_k(u_{ED,k}, p)\right). \tag{2}$$

The model-based experimental design strategy aims to maximize the accuracy of the parameter estimation that is mathematically represented by the variance-covariance matrix of the model parameters $\boldsymbol{C}$ and characterizes the statistical uncertainty of parameter estimation.

$$\min_{u_{ED}} \varphi(C)$$

$$s.t.\ \ f(\dot{y}(t), y(t), u_{ED}, p, t) = 0 \tag{3}$$

$$y(t_0) = y_0(p)$$

$$u_{ED}^{min} \leq u_{ED}(t) \leq u_{ED}^{max}$$

Statistical uncertainty is represented by the confidence region. Thus, decreasing the size of the confidence region for each model parameter leads to the minimization of the variance-covariance matrix C. The size of the confidence region (the amount of the matrix C) determines the expected information content that can be extracted from the measurement data. The form of the functional $\boldsymbol{\varphi}$ characterizes the chosen optimal criterion. Common design criteria are so-called A-, D- and E-optimal criteria whose definition can be found in (Franceschini and Macchietto, 2008). In the following we use the A-optimal criterion that represents the trace of the variance-covariance matrix and minimizes the mean parameter standard deviations.

$$\varphi(C) = \frac{trace(C)}{dim\ (C)} \tag{4}$$

The covariance-variance matrix is determined as inverse of the Fisher information matrix.

$$C = F^{-1} = \left(\sum_{k=1}^{N_{Exp}} F_k\right)^{-1} \tag{5}$$

We consider a sequential strategy, so, according to (Galvanin et al., 2007), the information matrix after N_{exp} experiments can be calculated as follows

$$F = \sum_{k=1}^{N_{exp}-1} F_k + F_{N_{exp}}\left(p, u_{ED,N_{exp}}\right) = F_C + F_{N_{exp}}\left(p, u_{ED,N_{exp}}\right) \tag{6}$$

where $\boldsymbol{F_c}$ represents a constant part of the Fisher information matrix calculated by the previous $N_{exp} - 1$ experiments. In eq. (6) only the vector $u_{ED,N_{exp}}$ can be varied during the optimization.

For one single experiment, the Fisher matrix is calculated based on the sensitivities coefficients for each estimated model output

$$F_k(p, u_{ED,k}, y) = Q_k^T MV_k^{-1} Q_k, \tag{7}$$

where $\boldsymbol{MV_k}$ represents the measurement-covariance matrix and $\boldsymbol{Q_k}$ characterizes the matrix of the sensitivities. Model parameters have often very different dimension. Therefore, it is convenient to use normalized sensitivity coefficients as defined in eq. (8) (Barz et al., 2010).

$$\overline{Q_k} = \left[\frac{\partial y_k(t_i)}{\partial p_j} p_j\right];\ \forall j \in N_p, \forall i \in N_{sp} \tag{8}$$

Based on these considerations, the normalized sensitivity coefficients are applied throughout this work.

3. New system identification strategy

Controller tuning requires a good process model. Therefore, our controller tuning strategy consists of two steps (s. Fig. 1). In the first step, we identify the process behavior experimentally by using closed-loop set-point response. After this, based on the results achieved in the first step, we numerically calculate the controller settings.

We assume that each process can be described by a first or second order with time delay model (Skogestad, 2003). That means that we have three or four model parameters that have to be determined. These are the process gain $\boldsymbol{K}$, the time constants $\boldsymbol{T_1}$, $\boldsymbol{T_2}$ and the time delay, $\boldsymbol{\tau}$.

Usually, an open-loop experiment is used to identify the process behavior. In the proposed strategy, we use a closed-loop set-point response (Fig. 1) for system identification. Here an experiment is executed with just a P-controller. By this method, we are able to reduce the experimental time and decrease the number of necessary experiments as well as the required amount of measured data.

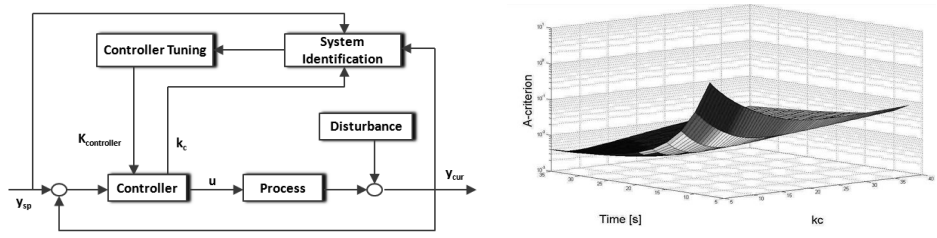

Figure 1. Controller tuning strategy (left), where $K_{controller} = [k_c, T_i]$; object function for OED over the design variable k_c for different measurement times (right)

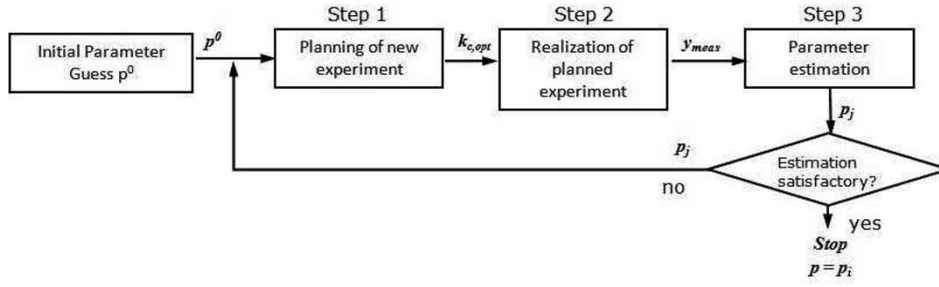

Figure 2. Model-based system identification strategy using closed-loop response

For a closed-loop system the experimental conditions are represented by controller gain $\boldsymbol{k_c}$. Here, by using the approach of OED we aim to determine the optimal value of the

controller gain $\boldsymbol{k_{c,opt}}$ for which the experimental data yields maximum information with respect to model parameters. According to the concept of OED, in the first step, the experiment is planned. Here, the optimal value of the control gain throughout the experiment is determined. Next, the planned experiment is executed and the measured data is analyzed. In the last step, the quality of the model is validated and a new set of model parameters is calculated (s. Fig. 2). These three iteration steps are executed sequentially without interruption until the required model accuracy is achieved. Important is here, that the design of a new experiment is based on the current information about model structure and parameter set obtained in the prior experiments.

4. Case Study

The strategy discussed in the previous section is applied to the first order plus time delay process (FOPTD). Based on the model reduction rule of Skogestad (Skogestad, 2003), we approximate FOPTD process with a second-order model. Here, we describe the second-order model by a model with a damping factor.

$$G_1(s) = \frac{K}{T^2 s^2 + 2dT\, s + 1} \tag{9}$$

Based on the assumed model, three model parameters have to be estimated during the model-based design. These are the process gain *K*, the time constant *T*, and the damping factor *d*. In this case study, we generate experimental data from the simulation and add a normally distributed measurement noise with the variance $\sigma^2 = 0.05$. Our goal during the parameter estimation was to get a model accuracy of 7% based on parameter standard deviations. In order to achieve the required accuracy, three experiments were executed. In the first experiment, the so called pre-experiment, the initial guess of the model parameters was identified. This experiment is unplanned and was executed with $k_c = 5$, whereas the next two experiments were designed. Table 1 shows that only two designed experiments are necessary in order to achieve the required accuracy of less than 7% for each model parameter. In addition, Fig. 3 shows the closed-loop set-point response for second designed experiment.

N_{exp}	Experimental conditions $k_{c,opt}$	Estimated parameters			Parameter standard deviations [%]		
		p_1	p_2	p_3	σ_{p1}	σ_{p2}	σ_{p3}
pre-exp	5	1.05	5.47	2.95	12.4	8.4	16.8
1st exp	15.3	0.96	5.19	2.75	7.5	4.5	7.9
2nd exp	**9.5**	**0.95**	**5.29**	**2.67**	**6.0**	**3.6**	**6.2**

Table 1. Parameter estimated during the model-based design of experiments

Once the model parameter estimation is finished, we numerically calculate the controller settings. The goal of the controller tuning is to achieve a good set-point response. Thus, our optimization problem is to minimize the overshoot while making sure that there is no undershoot. Here, the model dynamics is also represented by a second order process with a damping factor.

$$\min_{K_c, T_i} M$$
$$s.t.\ |\Delta y_s - \Delta y_u| \leq C, \tag{10}$$

where $\boldsymbol{M}$ represents the overshoot, $\boldsymbol{\Delta y_u}$ is the first minimum (undershoot), $\boldsymbol{\Delta y_s}$ denotes the set-point change and $\boldsymbol{C}$ is a constant. By solving of optimization problem (s. eq. (10)), we obtain the optimal controller settings that are represented by $k_c = 7.27$ and $T_i = 27.2$. Fig. 3 shows the closed-loop set-point response with the optimal controller parameters.

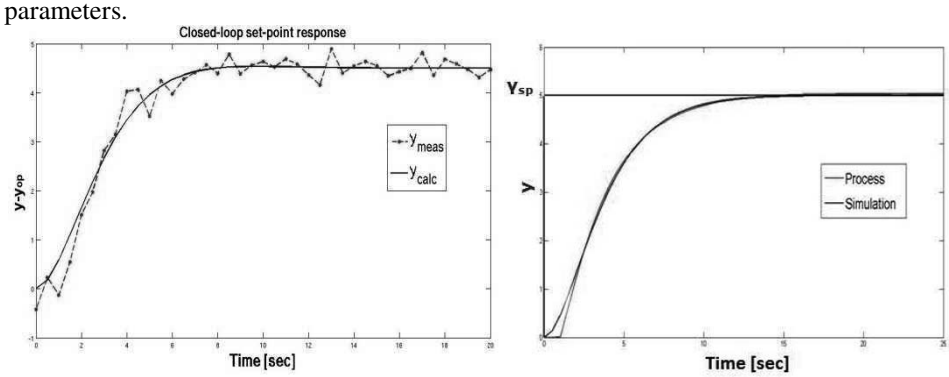

Figure 3. Closed-loop set-point response for the second designed experiment (left), where y_{op} is the operation point; closed-loop set-point response with the optimal controller settings (right).

5. Conclusions

The proposed strategy consists of two steps. In the first step, we identify the process behavior using a closed-loop set-point response. For this purpose, we first run experiments with just a P-controller. In the proposed procedure, the design variable for the optimal experimental design is represented by the controller gain k_c. After this, we calculate the controller settings by using an optimization strategy. Here, we use the model achieved in the first step for the calculation of optimal controller parameters. As the results of the case study show, one can use the second order model for calculation of the controller settings for a first order with time delay process.

Usually, a very time consuming part of the controller tuning procedure is the process identification. Here, using closed-loop set-point response leads to shorter experimental time compared to open-loop experiments. Furthermore, well designed experiments enable us to reduce the system identification effort even more. In summary, the sum of both benefits leads to reduced commissioning time in comparison to conventional methods.

References

T. Barz, H. Arellano-Garcia, G. Wozny, 2010, Handling uncertainty in model-based optimal experimental design, Ind. Eng. Chem. Res., 49, 5702-5713.

I. Bauer, H. G. Bock, S. Körkel, J. P. Schlöder, 2000, Numerical methods for optimum experimental design in DAE systems, Journal of Computational and Applied Mathematics 120, 1-25.

G. Franceschini, S. Macchietto, 2008, Model-based design of experiments for parameter precision: State of the art, Chemical Engineering Science, 63, 4846-4872.

F. Galvanin, S. Macchietto, F. Bezzo, 2007, Model-based design of parallel experiments, Ind. Eng. Chem. Res., 46, 871-882.

S. Skogestad, 2003, Simple analytic rules for model reduction and PID controller tuning, J. Process Control, 13, 291-309.

M. Shamsuzzoha, S. Skogestad, 2010, The setpoint overshoot method: A simple and fast closed-loop approach for PID tuning, J. Process Control, 20, 1220-1234.

I.A. Karimi and Rajagopalan Srinivasan (Editors), Proceedings of the 11th International Symposium on Process Systems Engineering, 15-19 July 2012, Singapore.

Optimization and control of polystyrene batch reactor using hybrid based model

Mohammad Anwar Hosen* and Mohd Azlan Hussain

Chemical Engineering Department, University of Malaya, Malaysia

Abstract

The effects of operating conditions such as initiator and monomer concentration as well as reactor temperature of polymerization reactors have been studied in this work. A recently developed hybrid model for polystyrene batch reactor was utilized in simulation study. The simulation results revealed the sensitivity of polymer properties and conversion to variation of these operating conditions. Furthermore, the study deals with the optimization of batch polymerization reactors. The optimization problem involving minimum time optimal temperature policy has been formulated and solved. Different numerical techniques have been tested and compared. The online control works were performed to validate the optimal temperature profiles. The experimental studies reveal that the calculated optimal policies were able to reduce the batch time keeping the same polymer quality.

Keywords: Polymerization reactors; Optimization; Polystyrene; Batch reactor.

***Corresponding Author,** anwar.buet97@gmail.com

1. Introduction

Recently, the use of process optimization in the control of batch reactors has received much attention in the literature (Kiparissides, 1996). This provides a useful tool for operating batch reactors efficiently and optimally. In batch polymerization, the optimization problem is identified as the time dependent control actions which maximize product quality and minimize production time(Amrehn, 1977). Different techniques have been suggested (Kiparissides, 2006) and applied to calculate and control to the optimal trajectories. Method of Pontryagin's Minimum Principle PMP) was heavily used in work of styrene polymerization in a solution batch reactor. For past seven years, researchers used solely the PMP to solve their optimal control problem (Özkan et al., 2001, Özkan et al., 2006, AltInten et al., 2003, Altinten et al., 2006, AltInten et al., 2008a, Zeybek et al., 2004, Zeybek et al., 2006, Özkan et al., 2009). The objective of optimal problem in their solution problem was to produce 50% conversion and 500 number average chain length with minimum reaction process. The temperature optimal profiles were generated using Pontryagin's Maximum Principle without any initial guess of initial costate variable. Therefore, no iteration of costate variable was initialized to obtain the time optimal temperature.

In the present work, we have considered of interest to carry out the dynamic study for a batch styrene free radical polymerization reactor theoretically and find out which variables are more effective for polymerization reactor. Later, optimization problem of minimum time optimal temperature policy has been formulated and solved for batch reactor for the solution polymerization of styrene. Finally, The generated optimal temperature profiles was used to study closed-loop control using advanced control technique which can track the process variable along the developed open-loop optimal temperature trajectory.

2. Modeling of polystyrene batch reactors.

The success of optimization efforts depends very much upon the accuracy of the process models. It has been a trend to use the simplified process models for determining the optimal control profiles, as the complexity of the process models is restricted by the methods used to determine the optimal control profiles. In this work, a simple mechanistic modelling strategy (see the AltInten et al., 2008 for details model) were used to develop optimal temperature profile (AltInten et al., 2008). However, a hybrid model (first principle-Neural network model) was used to design the controller to implement the optimum temperature profile.

Psichogios and Ungar have introduced the idea of using first principles-neural network methodology for modeling chemical processes. Such a methodology attempts to utilize all accessible process knowledge possible by implementing black-box correlations for predicting process parameters. A similar methodology was considered in the recent work of Hosen et al. (2011) for modeling the polystyrene batch reactor. In this work, the six kinetic parameters were calculated from pre-trained ANNs with high prediction capabilities (see the Hosen et al., 2011 for details hybrid model). This hybrid model was used to study the dynamic behaviour as well as to develop the advanced controller to control the polystyrene reactor.

3. Results & Discussion

First of all the simulation study was performed to study the dynamic behavior by using previously developed hybrid model (Hosen et al, 2011) and conduct the response of reactor outputs with different initial operating conditions. Secondly, developed the optimum temperature profiles based on reliable simple mathematical model (Altinten et al., 2008). Finally, an advanced controller was developed to track the optimum temperature profile.

3.1. Dynamic Open Loop Behaviour

The following simulations are performed in order to verify the sensitivity of the control system and calculate the appropriate control and system parameters. Among the simulation are:

i. Different initial initiator concentration loading to reactor (0.013, 0.016 and 0.019 mol/ltr)
ii. Different heat input to reactor system with reaction
iii. Different cooling water flow rates in cooling jacket chamber (0.5, 0.7 & 0.9 g/s).

In order to simulate these studies, the values of physical and chemical parameters used are as given in Table 1

Table 1: Operating conditions and reactor specifications

Name of the parameters	*Value*	*Units*
Reactant specific heat (C_p)	1.96886	J/g.K
Coolant specific heat (C_{pc})	4.29	J/g.K
Heat of reaction, exothermic (H)	-57766.8	J/g.K
Coolant flowrate (m_c)	0.51	g/s
Gas constant (R)	8.314	J/mol.K
Coolant inlet temperature (T_{ji})	303.14	K
Overall heat transfer coefficient (U)	55.1	W/(m^2.K)
Reactor volume (V)	1.2	ltr
Reactor jacket volume (V_c)	1	ltr
Coolant density (ρ_c)	998.00	g/ltr
Reactant density (ρ_r)	983.73	g/ltr

3.1.1. Reactor Dynamics with Different Initiator Loading

One of the control objectives in controlling the batch polymerization reactor is to control the exothermic behaviour due to the extent of reaction as the initiator is introduced to the monomer and solvent mixture in the polymerization system. It is obvious that one needs to monitor the release of heat in order to control the target specification. Moreover, the heat release may break the glass reactor depending on the temperature it can withstand. Three conditions of polymerization were used with initial initiator concentration of 0.013, 0.016 and 0.019 mol/l for this study. Each starting condition has to be maintained at fixed steady state condition. Fig. 1 represents the time trend of temperature change in terms of different initial initiator load (mol/ltr). In this case, polymer quality (X_n) highly depends on the initial initiator concentration but the conversion (X) is little affected by it.

3.1.2. Reactor Dynamic with Different Heat Loading

In the second task, the initial initiator is fixed at a value of 0.013mol/l. Five different heat input simulated the reaction in the reactor with a fixed steady state temperature at 364K. Table 2 illustrates the conversion achieved when temperature reached the steady state after high release of heat upon initiation. In addition, Fig. 2 illustrates clearly the transient behaviour of reactor temperature. As can be seen from the figure, the reactor with highest amount of heat input attains the highest overshoot. The temperature ascends from 364K to a maximum temperature of 416K and starts descending to the steady state of 403.8K completely after 500min at a heat input 150watt. In addition, it can be seen in Fig. 2 that the final polymer quality highly depends on the heat input. At lower heat input the NACL and conversion is higher than at high heat input though it requires more reaction time.

Table 2: Results of different heat input simulation

Heat, Q	Final conversion (%)	T- highest	T_{ss}
150	34.17	416	403.8
120	40.61	411	386.2
100	48.46	401	376.4

3.1.3. Reactor Dynamic with Different Jacketed Flow Rate

In the third task, the jacketed flowrate were varied three times (0.5 g/s, 0.7g/s & 0.9g/s) with the other variables kept the same as Table 1 to observe the reactor dynamics. It can be seen in Fig. 3, that the final polymer quality (NACL) highly depends on the jacketed flow rate. At lower jacketed flow rate, the NACL and conversion are higher than at higher flow rate though it requires more reaction time.

For all three conditions it can be seen that the reactor temperature profile change significantly with changing initial operating conditions or inputs. Based on these results more attention will be taken for setting the values of these operating variables at the time of experimental work. Variation in this reactor may serve as disturbances to the reactor operation.

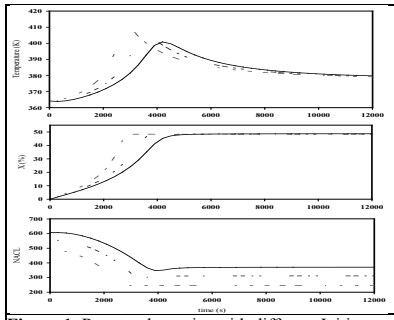

Figure 1: Reactor dynamics with different Initiator concentration. (——) at 0.013mol/ltr, (- - -) at 0.016mol/ltr and (·—·—·) at 0.019mol/ltr.

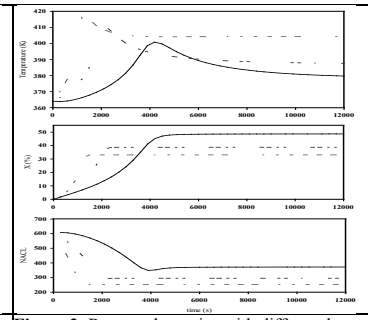

Figure 2: Reactor dynamics with different heat input. (——) at 100 watt, (- - -) at 120 watt and (·—·—·) at 150 watt.

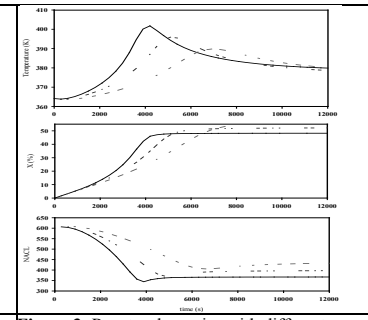

Figure 3: Reactor dynamics with different jacketed flow rate. (——) at 0.5g/s, (- - -) at 0.7g/s and (·—·—·) at 0.9g/s.

3.2. Minimum Time Optimal Temperature Profile

Recently, the offline or open loop minimum time optimal control policies were applied for the simulation of styrene polymerization in batch reactors (Altinten et al., 2008b, Zeybek et al., 2004, Zeybek et al., 2006). In this work, the optimization problem involving minimum time optimal temperature policy has been formulated and solved for a batch reactor for the solution polymerization of styrene based on previous work (Sata, 2007). This optimal temperature profile was used as set point for controller study.

The objective of optimization problem is to calculate the optimal temperature policy for a given initial initiator and monomer concentration that minimizes the reaction time, t_f, required to achieve a desired final monomer conversion, X_d. The performance target of a closed loop control minimum time optimal temperature tracking is to produce polystyrene with the specification of X_d =50% and **NACL,** $\boldsymbol{X_n}$ =500.

In order to obtain the operating conditions for minimum polymerization end-time, polymerization temperature and initiator concentration are employed as control variables. Since the temperature can be used to infer the end-quality of polymer, this work is devoted to produce specified polymer quality within the minimum time. The governing equation (Altinten et al., 2008b) for the optimal temperature profile is expressed as follows:

$$T = \frac{-(E_p + E_d/2 - E_t/2)/R}{\ln\left[E_d \Big/ \left(p_2 I^{0.5} M A_p \left(\frac{2fA_d}{A_t}\right)^{0.5} \left(E_p - \frac{E_d}{2} - \frac{E_t}{2}\right)\right)\right]} \tag{1}$$

The results of calculation for X= 50% and X_n =500 with optimal temperature T* is shown in Fig. 4. In this work, the value for initial initiator, I_0 has to be basically guessed. The procedure can determine any feasibility of the guessed value. In this study, it is found that the optimal initial initiator concentration for the initial monomer concentration of M_o=6.089 mol/l is I_o=0.016 mol/l. These optimal values are achieved within the reaction time of 138 minutes. It can be noted that the reaction time (t_f) increases with increasing I_0. Therefore, it is concluded that the optimal I_0 can be obtained by successively reducing the value of I_0 until a limiting value was reached below which the desired conversion can never be reached. Furthermore, as can be seen from the figure, as the I_0 is decreased, the gradient of the optimal temperature T* becomes more steep. The optimal temperature profile for I_0 = 0.016 will be used for tracking the set point in the control study.

3.3. Controller Design

In this work, an advanced neural network based model predictive controller (NN-MPC) was used to control the polystyrene reactor. The neural network is trained to represent the forward dynamics of the process. The experimental data of the

manipulated variable (heat load Q) and plant output (reactor temperature T) at t with two time delay units were used as inputs while the plant output reactor temperature at t+1 was used as outputs for training the neural network. The Levenberg–Marquardt method is used to train the NN based on a minimizing cost function. The mean square error (MSE) is used here as cost function. It is expressed mathematically as:

$$\mathrm{MSE} = \frac{1}{n}\sum_{k=1}^{n}\left(T_{\mathrm{tg}}(k) - T_{\mathrm{N}}(k)\right)^2 \tag{2}$$

where n is the number of training data, T_{tg} is the target/desired reactor temperature and T_{N} is the neural network output. Based on the minimizing of MSE error values, it was found that 10 hidden nodes achieve the minimum MSE value of $5.36\text{x}10^{-6}$. The design specifications for neural network model are given in Table 3.

Table 3: Design specifications of neural network model

No. of input nodes	6	
No. of hidden layer nodes	10	
No. of output nodes	1	
Total sample size	10000	
Training function	Levenberg-Marquardt Method	
	Sample size	Mean square error
Training data	5000	5.36×10^{-6}
Testing data	2500	4.13×10^{-6}
Validation	2500	4.69×10^{-6}

Before implementing the MPC controller in real time, its tuning parameters should be optimized to achieve best performance. For designing a good MPC controller it's important to specify the following controller parameters:

In this work, the developed hybrid model was utilized to determine the sampling interval and prediction and control horizon. Marlin (Marlin, 1995) general rule was used to determine the sampling interval of MPC. The prediction and control horizon were determined by trial and error method (see Dougherty and Cooper, 2003 for more details).

The performance of the controlled variable i.e. reactor temperature, was observed for a sufficient span of process dynamics time to determine the value of the prediction & control horizon. It was observed that the prediction horizon of 24 sample interval and the control horizon value of 4 sample interval provide satisfactory control performance. The other parameters of the NN-MPC controller are given in Table 4.

Table 4: Design specification of MPC

Prediction Horizon (N_2)	24
Control Horizon (N_u)	4
Control weight factor (M)	0.09
Move suppression factor(Λ)	0.003
Minimization routine	Backtracking Optimization

3.4. On-line optimal control of polystyrene reactor

In this study, the concentration of 0.016 mol/l and 6.089 mol/l for initiator and monomer loading were chosen to produce the desired target. It is noted that the benzoyl peroxide and styrene loading can produce the number average chain length (NACL) of 500 and monomer conversion of 50% at the end of 183 minutes polymerization period.

The experimental results of optimal setpoint tracking of polystyrene polymerization using NN-MPC are shown in Fig. 5. As we can see from the figure, when the initiator is introduced, the mixture temperature fell below the setpoint profile at nearly 2K. The response was realized by the controller and it acted back to increase the heat input (Q). As a result, the temperature overshot at maximum 2K and it later decayed away in decreasing oscillatory manner in 730 sec. An offset can be noted at less than .5K. This is attributed by the high exothermic load during the early course of polymerization. Nevertheless, the temperature controller performance performed well in tracking the temperature setpoint profile at the later stage of polymerization. Fig. 5 also shows the transient response of manipulated variable of heater. The regulation was smooth. It is worth mentioning that the heater regulation was initially at Q=150 Watt and it increased gradually until 200 Watt at the end of the batch-run. The final NACL and conversion can be found 496 and 52.8% respectively which is almost same as desired values.

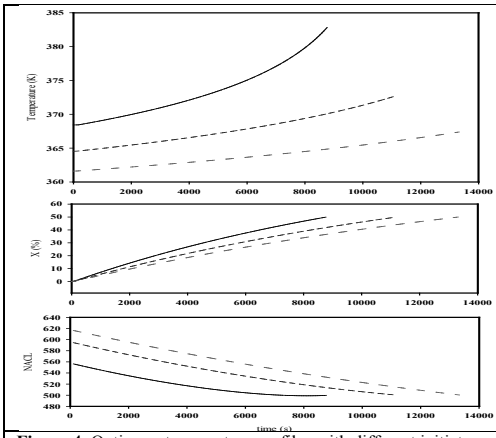

Figure 4: Optimum temperature profiles with different initiator concentration (I_o = 0.013 mol/l (—), I_o = 0.016 mol/l (- - -), I_o = 0.019 mol/l (·—·—·)

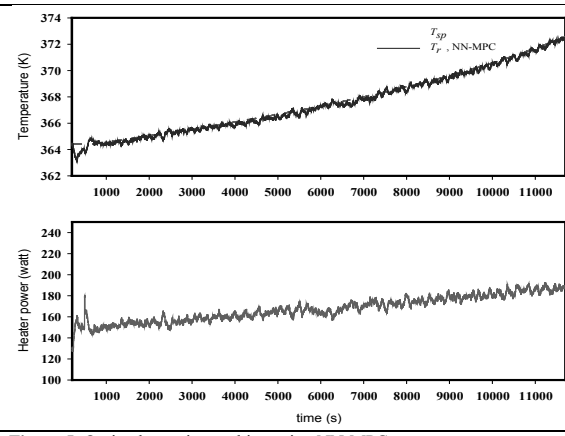

Figure 5: Optimal setpoint tracking using NN-MPC

4. Conclusion

In this work, the first principle-NN model is utilized in Matlab Simulink environment to study the dynamic behaviour of the polystyrene batch reactor. The effect of operating conditions on the properties of final product has been investigated. An optimization algorithm (Sata, 2007) was applied to optimize the reactor temperature profile based on minimal time operation. The conversion and number average chain length (NACL) was considered here as the target output for optimization. The optimized minimal time temperature profile was used as setpiont tracking for control study. An advanced controller named NN-MPC were designed and tuned for styrene polymerization batch reactor to track the optimum setpoint point experimentally. From the experimental results it can be concluded that the developed optimal temperature profile can give the desired polymer quality & quantity with the help of advanced controller.

References

ALTINTEN, A., ERDOGAN, S., HAPOGLU, H., ALIEV, F. & ALPBAZ, M. 2006. Application of Fuzzy Control Method with Genetic Algorithm to a Polymerization Reactor at Constant Set Point. *Chemical Engineering Research and Design,* 84 (11), 1012-1018.

ALTINTEN, A., ERDOGAN, S., HAPOGLU, H. & ALPBAZ, M. 2003. Control of a polymerization reactor by fuzzy control method with genetic algorithm. *Computers & Chemical Engineering,* 27 (7), 1031-1040.

ALTINTEN, A., KETEVANLIOGLU, F., ERDOGAN, S., HAPOGLU, H. & ALPBAZ, M. 2008. Self-tuning PID control of jacketed batch polystyrene reactor using genetic algorithm. *Chemical Engineering Journal,* 138 (1-3), 490-497.

AMREHN, H. 1977. Computer control in the polymerization industry. *Automatica,* 13 (5), 533-545.

DOUGHERTY, D. & COOPER, D. 2003. A practical multiple model adaptive strategy for multivariable model predictive control. *Control Engineering Practice,* 11**,** 649-664.

HOSEN, M. A., HUSSAIN, M. A. & MJALLI, F. S. 2011. Hybrid modelling and kinetic estimation for polystyrene batch reactor using Artificial Neutral Network (ANN) approach. Asia-Pacific Journal of Chemical Engineering, 6, 274-287.

KIPARISSIDES, C. 1996. Polymerization reactor modeling: A review of recent developments and future directions. *Chemical Engineering Science,* 51**,** 1637-1659.

KIPARISSIDES, C. 2006. Challenges in particulate polymerization reactor modeling and optimization: A population balance perspective. *Journal of Process Control,* 16**,** 205-224.

MARLIN, T. E. 1995. *Process control: design processes and control systems for dynamic performance,* Columbus, OH 43272, McGraw Hill Inc.

ÖZKAN, G., HAPOGLU, H. & ALPBAZ, M. 2006. Non-linear generalised predictive control of a jacketed well mixed tank as applied to a batch process--A polymerisation reaction. *Applied Thermal Engineering,* 26**,** 720-726.

ÖZKAN, G., ÖZEN, S., ERDOGAN, S., HAPOGLU, H. & ALPBAZ, M. 2001. Nonlinear control of polymerization reactor. *Computers & Chemical Engineering,* 25**,** 757-763.

ÖZKAN, G., TEKIN, Ö. & HAPOGLU, H. 2009. Application of experimental non-linear control based on generic algorithm to a polymerization reactor. *Korean Journal of Chemical Engineering,* 26**,** 1201-1207.

SATA, S. A. 2007. *Simulation and on-line control of polystyrene production in a batch reactor* PhD, University of Malaya.

ZEYBEK, Z., ÇETINKAYA, S., HAPOGLU, H. & ALPBAZ, M. 2006. Generalized delta rule (GDR) algorithm with generalized predictive control (GPC) for optimum temperature tracking of batch polymerization. *Chemical Engineering Science,* 61**,** 6691-6700.

ZEYBEK, Z., YÜCE, S., HAPOGLU, H. & ALPBAZ, M. 2004. Adaptive heuristic temperature control of a batch polymerisation reactor. *Chemical Engineering and Processing,* 43**,** 911-920.

I.A. Karimi and Rajagopalan Srinivasan (Editors), Proceedings of the 11th International Symposium on Process Systems Engineering, 15-19 July 2012, Singapore.

Modeling and stochastic dynamic optimization for optimal energy resource allocation

Go Bong Choi. Seok Goo Lee. Jong Min Lee*

School of Chemical and Biological Engineering, Institute of Chemical Processes, Seoul National University, 1 Gwanak-ro, Gwanak-gu, Seoul, 151-744, Korea

Abstract

With ever-growing global demand for energy and severe environmental regulations, optimal management of energy distribution system and policy is becoming an important problem for many countries. We present a stochastic dynamic model that describes energy resource allocation under uncertainty and derive an optimal policy for long-term investments in novel energy technologies. Probabilistic model based on Markov chain that balances the demands and supplies are developed considering the city boundaries and electric power system in South Korea. We propose an algorithmic strategy based on the framework of approximate dynamic programming and demonstrate its efficacy using a prototypic example with the available data

Keywords: Energy planning, Markov decision chain, Approximate dynamic programming.

1. Introduction

Faced with the recent challenge of meeting soaring global energy demand without damaging the environment, there has been increasing interest in a strategic approach to determining which energy sources to use and how to supply energy to demand points at optimal cost under environmental and other federal regulations. However, obtaining an optimal policy for such problems is complicated by the inherent uncertainties in demand, fuel prices, stored amount of fuels, etc. Hence, a robust dynamic optimization problem needs to be formulated and solved for deriving a meaningful optimal policy in these applications. Dynamics of such systems are stochastic because the successor state is given by a probability distribution rather than a fixed deterministic point given a current state.

When only the bounds of uncertainties are known, worst-case optimization problem set-up is introduced. If the probabilistic behavior of uncertainties can be further assumed or found from intuition or historical data, stochastic dynamic optimization problem can then be formulated.

Markov decision process (MDP) is a useful framework for modeling the problem in that it is sufficient to consider the present state only, not the past history (Puterman, 1994) and is often used to formulate most scheduling problems under uncertainty. A universal solution approach to obtain the optimal solution for MDP is dynamic programming (DP), which involves calculation of the cost-to-go value for all possible states (Bellman, 1957; Bertsekas, 2000). The main bottleneck in application of DP for

*Corresponding author. Tel. +82-2-880-1878 Email. jongmin@snu.ac.kr

practical problems is the curse of dimensionality, which refers to the exponential increase of the number of states in the state dimension. Recently, a new body of theories called Reinforcement Learning (RL) (Sutton, 2000) or approximate dynamic programming (ADP) (Powell, 2007) has attracted much attention in field of operations research due to its ability to circumvent the curse of dimensionality. The main idea of these approaches is to use closed-loop simulation with initial policies, though they may not be an optimal one, and identify relevant regions in the state space. For these identified states, Bellman's optimality equation is iteratively solved in the form of policy iteration or value iteration (Bertsekas & Tsitsiklis, 1996). In this work, we propose a Markov chain model for energy management of capital region of South Korea and apply an ADP approach to derive a nearly optimal energy management policy starting from closed-loop simulations with simple heuristics.

2. Problem description and model formulation

The objectives of this study are to develop an energy supply chain network model for the energy distribution system of capital region in South Korea and to derive an optimal policy for energy resource allocation, storage, and construction of new power plants and storage/processing facilities under demand uncertainty.

The system is composed of three types of nodes (storage, demand, and conversion nodes) and material flows. It manages energy resource flows from storage nodes (e.g., harbor, storage facility, etc.) to demand nodes such as households and corporations. It is necessary to make proper plans and minimize total cost incurred while respecting constraints. Various types of resources can be divided into primary resources and secondary resource. Resource can be carried from storage node too demand nodes directly or via conversion nodes. In this study, electricity is the only type of energy considered as the secondary energy resource and is assumed to be generated from coal, oil, natural gas, and renewable energy resources. To represent the capital region of South Korea properly, the system has two storage nodes, two conversion nodes, and three demand nodes. The data of the past 10 years on power plant constructions and consumption of energy resources in the region were obtained from KESIS (Korea Energy Statistics Information System). A prototypic energy supply chain network that represents the region is shown in Figures 1 and 2 and the details of the model are presented in the following section and summarized in Table 1.

2.1. State variable

The state vector consists of two types of variables. The first is a subset of controllable state variables that can be regulated by actions but not totally due to the existence of uncertainty. It includes the amounts of resources in the storage, the power production capacity, and the storage capacity. The second is a subset of disturbance state variables, meaning that even if it starts from the same state, its successor state cannot be always the same given the same action. The demand is only disturbance state variable in this study. Though we cannot control the demand, it is necessary to include this variable in the state vector because actions should be computed to meet the demand. The demand scenarios are constructed based on the historical data available from KESIS.

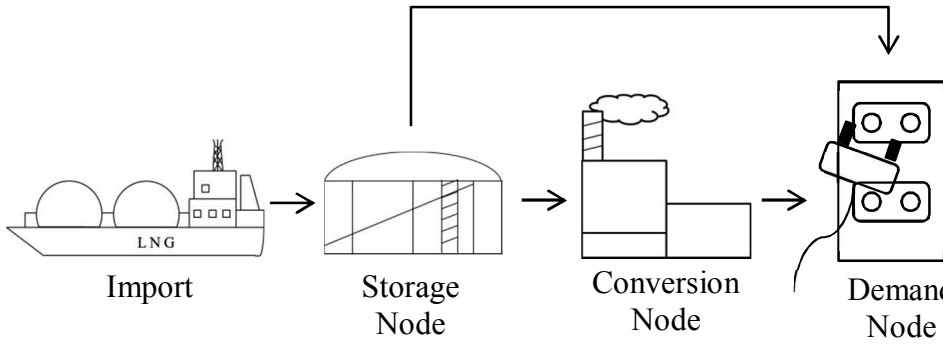

<Figure 1. Genral energy resource transit from import to demand node>

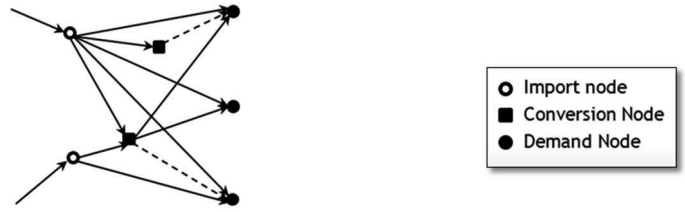

<Figure 2. Energy node network of the capital region in South Korea>

2.2. Decision variable

The decision variables are energy resource flows and capacity extension of resource facilities. The amounts of resources are divided into annual import volume and dispatch to power plants from the harbors. If the dispatch amounts are determined, the total amounts of electricity to be generated can be determined. With the assumption that all the demands should be met due to the national policy the resource flows to the households and businesses are the same with the predicted nominal demands. Capacity extension means that all the activities related to adding capacities to the current energy resource facilities. The energy resource facility has two types: power plant and storage/processing facility. Power plant capacity is defined as the maximum production of electricity from power plant for a year. Storage/processing facility capacity is the maximum volume of resources that can be stored and processed.

2.3. Objective function

The objective is to convert the available energy resources and supply the energy to meet the demand at a minimal cost. This can be cast as a stochastic dynamic optimization problem with a discounted infinite horizon cost as follows:

$$\min_{u_t} E\left(\sum_{t=0}^{\infty} \alpha^t \emptyset(x_t, u_t)\right) \quad (1)$$

$$\emptyset(x_t, u_t) = C(x_t, u_t) + X(x_t, u_t) \quad (2)$$

, where E denotes the expectation operator and the stagewise cost $\emptyset(x_t, u_t)$ involves resource and construction expenses ($C(x_t, u_t)$) and extra cost for each resource ($X(x_t, u_t)$). For instance, the extra cost term can include costs for extra risk management in nuclear power plants.

2.4. State transition rule

State transition rule indicates how state evolves over one sample time given the current state and action. The state transition equation is given by simple balance equations as in

Table 1 for the controllable part. The disturbance part of the system is represented by the nominal demand scenario with additive noise based on the historical data for the capital region of South Korea from 2001 to 2010

2.5. Uncertainty

Demand is the only uncertain state variable. We represent the demand uncertainty as the fluctuation in the storage due to the constraints of meeting the demand as much as possible.

2.6. Constraints

Energy resource reservation plan is the only explicit constraint in this model. It is derived from the petroleum reservation program that a certain amount of petroleum should be secured in preparation for difficult situations to import. We assume that amount of stockpiles is bigger than a quarter of expected demand.

<Table 1.component of energy distribution model>

	Symbol	Description
State	$D_{r,t}$	Demand of resource
	$S_{r,t}$	Storage of resource
	$C_{r,t}$	Resource storage capacity of resource t
	$C_{r,t,e}$	Power plant capacity using resource
Action	$I_{r,t}$	Import of resource
	$E_{r,t}$	Extension of resource storage capacity
	$E_{r,t,e}$	Extension of power plant capacity
	$Di_{r,t}$	Dispatch to power plant of resource
State transition rule	$S_{r,t+1}$	$S_{r,t+1} = S_{r,t} + I_{r,t} - D_{r,t} - Di_{r,t}$
	$C_{r,t+1}$	$C_{r,t+1} = C_{r,t} + E_{r,t}$
	$C_{r,t+1,e}$	$C_{r,t+1,e} = C_{r,t,e} + E_{r,t,e}$
Uncertainty	$\widehat{D_{r,t}}$	
Constraint-Explicit	$S_{r,t+1} \geq \frac{1}{4} D_{r,t}$	reserves in preparation for energy crisis

2.7. Heuristics

In this study, we sample a subset of state points by performing closed-loop simulations with two simple heuristics. The first heuristic constructs a coal-fired power plant with the first priority and the nuclear and renewable energy plants are considered as a second choice. The second heuristic mainly constructs natural gas power plant. All these heuristics use a fixed value for the energy dispatch.

3. ADP-based approach for deriving an optimal policy

With the sampled state points and a function approximation scheme such as local averaging (Lee et al., 2006), the Bellman's optimality equation is solved iteratively as in Eq. (3)

$$J^{i+1}(x) = \min_{u \in U} E[\emptyset(x,u) + \alpha \tilde{J}^{i}(\mathrm{x})] \quad (3)$$

where *i* denotes the iteration index, J^{i+1} is the vector of calculated cost-to-go values for sampled state space, $\tilde{J}^{i}$ is the estimated value of cost-to-go for the successor state form the function approximator of the i^{th} iteration. The iteration is continued until (Use the infinite norm convergence criterion here. After how much iteration did you say it is converged with what criterion?) all the *J(x)* values are converged

The total number of possible state points is 1.53×10^{14} and the total number of action values is1.024×10^{7}. The number of visited state points in the proposed scheme is 1.95×10^{7}. Figure 3 shows the comparison between the converged ADP policy and two initial heuristics in terms of expected cost over five years in the future, and it shows significant performance improvement under uncertainty. The iteration scheme converged within an error tolerance $\left\| (J^{i+1} - J^{i})/J^{i} \right\|_{\infty} < 0.05$ after 2th iteration.

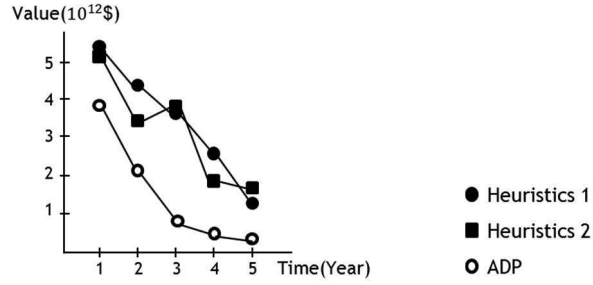

<Figure 3. Value on scenario of Heurstics and ADP>

4. Concluding Remarks

In this paper, we propose a Markov chain model for optimal energy management problem and solved it using ADP. In the revised manuscript, more comprehensive analyses and comparisons will be provided.

Acknowledgement

This subject is supported by Korea Ministry of Environment as "Projects for Developing Eco-Innovation Technologies (GT-11-G-02-001-3)".

References

Bellman, R.E. (1957). Dynamic programming. New Jersey : Princeton University Press

Bertsekas, D.P. (2000). Dynamic programming and optimal control(2nd ed.).Belmont, MA: Athena Scientific

Bertsekas, D.P., & Tsitsiklis, J.N. (1996). Neuro-dynamic programming. Belmont, Massacheusetts: Athena Scientific.

De Faria, D.P., & Van Roy, B. (2003). The linear programming approach to approximate dynamic programming. Operation Research, 51(6), 850-865

KESIS, Korea Energy Statistics Information System, from http://www.kesis.net

Lee.J.M., Kaisare, N. S., &Lee, J. H. (2006). Choice of approximator and design of penalty function for an approximate dynamic programming based control appraoch . Journal of Process Controal, 16(2), 135-156

Powell, W.B. (2007) Approximate dynamic programming : Solving the curses of dimensionality. John Wilely & Sons, Hoboken, NJ.

Puterman, M.L. (1994). Markov decision processes. New York, NY: Wiley.

Sutton, R., McAllester, D., Singh, S., & Mansour, Y. (2000). Policy gradient methods for reinforcement laernign with function approximation . In S. A. Sollar, T.K. Leen & K.-R. Muller (Eds.), Advances in neural information processing systems: 12, (pp. 1057-1063). MIT Press.

I.A. Karimi and Rajagopalan Srinivasan (Editors), Proceedings of the 11th International Symposium on Process Systems Engineering, 15-19 July 2012, Singapore.

Seawater Desalination Processes: Optimal Design of Multi Effect Evaporation Systems.

Paula Druetta[a] , Sergio Mussati[a], Pio Aguirre[a]

[a]*lNGAR - Instituto de Desarrollo y Diseño, Avellaneda 3657, Santa Fe (3000),Argentina*

Abstract

This is the first paper of a series of articles that deals with the modeling and optimization of dual-purpose desalination plants which combine thermal desalination processes and combined heat and power systems, specifically solid oxide fuel cell SOFC electricity generators. This paper presents preliminary results obtained for the multi effect evaporation (MEE) process (stand alone process). The steady state performance of the MEE system is described by a simplified and no linear programming (NLP) model. Optimal operating conditions including profiles of temperature, flow-rate and heat transfer area along the evaporator are analyzed. In addition, the influence of the effect number on the evaporation efficiency is also investigated.

Keywords: Multi-effect desalination; Optimal design; Non-Linear Programming (NLP)

1. Introduction

In many countries the most pressing issue for water security is in meeting basic provision of fresh water supply and sanitation. Sea-water desalination plays and will play in the future an important role in contributing to the provision of fresh-water since the global requirements for fresh water are increasing rapidly as the global population.

The following are the main desalination processes: a) Thermal: multi stage flash (MSF) and multi effect (MEE) distillation, vapor compression (VC) and b) reverse osmosis (RO), electrodialysis (ED), membrane distillation (MD). The thermal desalination processes are energy intensive (which global requirement is also increasing) and the efficiency is greatly improved when they are integrated with heat-power plants (co-generation power desalting plants, CPDP). Thus, the waste heat of the power plant is used as thermal source to produce fresh-water. The main drawback of such plants, however, are the high consumption of fossil fuel and high CO_2 emissions which lead to global warming and inevitable climate changes. It is essential therefore to look for cost-effective and sustainable processes that combine alternative energy sources (wind, geothermal and solar energy, fuel cells and others) with desalination technologies.

The use of high temperature fuel cells [molten carbonate fuel cells (MCFC) and solid oxides fuel cells (SOFC)] has emerged as a suitable technology for cogeneration. Certainly, electricity can be generated in a cleaner and more efficient way than with conventional technologies. In addition, the temperature of the flue gases is high enough to produce high-temperature steam to be used as heating medium in energy intensive processes.

Fig. 1 shows a schematic and feasible flow-sheet which integrates fuel cell and desalination process. The mathematical model to be presented in this work is the first basic step of a more ambitious project aimed at determining the optimal synthesis and design of the integrated process including desalination processes and SOFCs.

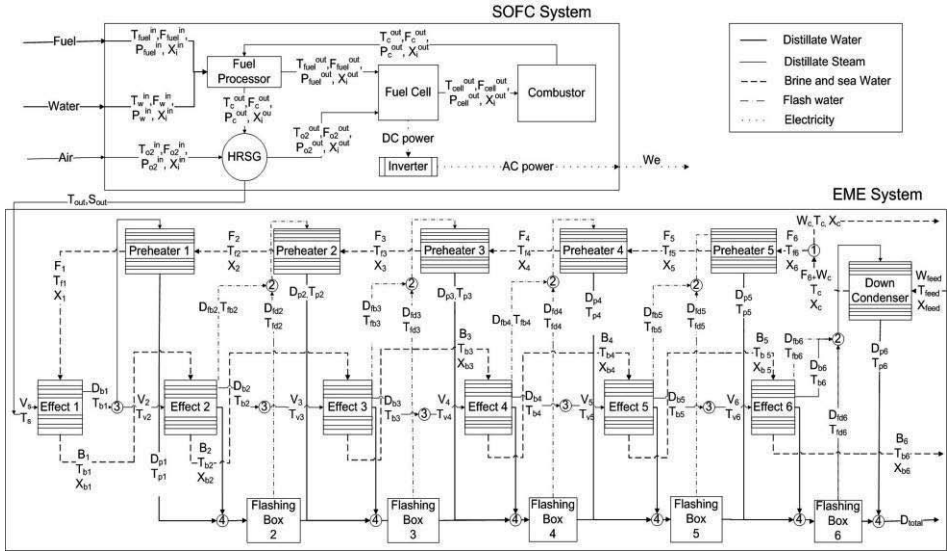

Fig. 1 Integration of SOFC and Multi-Effect Evaporation (MEE) process.

The MEE desalination system illustrated in Fig 1, which is the aim of this paper, is named "forward feed flow arrangement. As shown, each one of the effects involves a pre-heater, an evaporator and a distillate flash chamber. Feed seawater enters to the system and is preheated in the down condenser by the vapor formed in the last effect. A part of the seawater is then discharged to the sea. In the first effect, part of the vapor formed by evaporation of the brine is condensed outside the tubes of the pre-heater to heat the feed and the remaining the vapor is used in the second effect to evaporate part of the brine coming from the first effect. From the second to the last effect, the vapor formed by flashing of the brine and distillate is used to pre-heat the feed while the fresh vapor formed by evaporation is used to evaporate part of the brine in the next effect. This cycle of evaporation, condensing and heating is repeated at each effect until the last effect. The first and last stages need external heating and cooling respectively. The amount of heat removed from the last stage must nearly equal the amount of heat supplied to the first stage (Q). For sea water desalination purpose, the first stage is typically operated at a temperature below 70 °C in order to avoid scale formation.

2. Optimization Problem

The proposed optimization problem can be stated as follows. Given the sea-water conditions (composition, temperature and flow-rate), the goal is to determine the optimal operating conditions and the heat exchange values for the different heat exchangers in order to minimize the total heat transfer area in satisfying the fresh-water demand. The problem is solved for the following two cases: a) equal heat transfer areas (HTA) in all pre-heaters and evaporation effects and b) variation of HTA along the pre-heaters and evaporation effects. The output results are compared in detail. Finally, the influence of the number of effects and the steam temperature supplied in the first effect (heating utility) on the total heat transfer area is also analyzed. For this analysis, the optimization problem is systematically solved by varying both parameters.

3. Assumptions and mathematical model

The following are the main assumptions used to develop the mathematical model.

- Heat losses, non-equilibrium allowance (NEA) and Non-condensable gases effects are neglected.
- A mean value is adopted for the heat capacity coefficients (Cp), the latent heat of vaporization (λ), the overall heat transfer coefficients (U) and for the boiling point elevation of the brine (BPE), neglecting the effect of the chamber geometry, temperature, pressure and the fluid properties.
- The vapor form by flashing in the effects and the flashing boxes is used to heat the feed.
- The heat transfer equations model the HTA in each evaporator as the sum of the area for brine heating (A_b) and an area for evaporation (A_e).

3.1. Equations and computational aspects

The MEE system is represented as a No Linear Programming (NLP) model. This model consists in a set of mass and energy balances, and design equations used to compute heat transfer areas and physical-chemical properties of each one of the streams. There is mass and energy balances for each one of the pre-heaters, effects and flashing chambers. The logarithmic mean temperature difference (LMTD) is used to compute the HTA in pre-heaters. The model also includes non equality constraints which are used to avoid temperature crossover. In addition, lower and upper bounds have been imposed for each one of the variables in order to facilitate the model convergence.

The model involves non-linear constraints and bilinear terms which lead to local optimal solutions and therefore, global optimal solutions can not be guaranteed. In order to solve the optimizations, a feasible solution taken from Darwish's (2006) has been used to solve the first optimization problem. Then in order to solve the next optimization problem where some model parameters are varied, the previous solution is used as initialization. Thus, a sequence of several optimization problems is efficiently and systematically solved.

4. Results

The optimization problem described in section 3 is solved using the parameter values listed in Table 1. As mentioned earlier, the fresh-water demand (D), steam temperature (T_s), steam flow-rate (S) and seawater conditions [(X_{feed}), (T_{feed})] are given. In addition, an upper bound for the rejected brine salinity is imposed for environmental restrictions (XUp). The down condenser eject temperature (Tc) is also assumed as given.

Table 2 and Fig. 2, 3 and 4 compare the output results obtained by considering either uniform or non uniform distributions of heat transfer areas in pre-heaters and evaporation effects along the MEE system. In Table 2 are also compare same widely used variables to measure the system efficiency: the performance ratio (PR), the conversion ratio (CR), the specific total HTA (sHTA) and the specific cooling water ratio (sCWR).

Table 2 clearly shows that despite the cooling water flow-rate and the HTA in down condenser for non uniform area are greater than those required for uniform area, the total HTA required in pre-heaters and effects is considerably smaller than that required for uniform area. Fig. 2 compares the distribution of the HTA in pre-heater and evaporation effect along the MEE system (8 stages). It is possible to observe that the non uniform distribution of the HTA leads to the minimum total HTA of the process.

Fig. 3 compares the corresponding distribution of the driving force and the fresh water production in each one of the effects for both cases. It clearly shows that from the first to fifth effect the driving forces are similar in both cases and then in the last three effects the driving force for non uniform area is greater than the corresponding to

uniform distribution. In both cases, the total fresh-water production which is fixed is similarly distributed along the desaltor.

Fig. 4 compares the distribution of the temperatures in pre-heater and evaporation effect along the MEE system (8 stages) for both situations.

Table 1. Parameter values

Parameters	
Cp [KJ/Kg ºC]	4
D [Kg/s]	2500
BPE [°C]	1
λ [KJ/Kg]	2333
T_{feed} [°C]	26
T_c [°C]	40
T_s [°C]	70
X_{feed} [ppm]	45978.9
X_{Up} [ppm]	72000.0
U [kW\ m^2 ºC]	3
N	8
S [Kg/s]	600

Table 2. Optimal values

	Non uniform HTA	Uniform HTA
sHTA [m^2/Kg/s]	252.76	285.36
PR (D/S)	4.16	4.16
sCWR (Wc/D)	5.91	4.93
CR (F/D)	2.77	2.77
Cooling Water Flow [Kg/s]	14785.22	12325.65
Down Condenser HTA [m^2]	36009.02	21540.53
Total HTA [m^2]	631901.21	713408.13

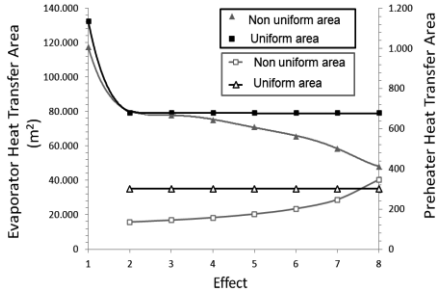

Fig. 2. Heat transfer areas vs. effect

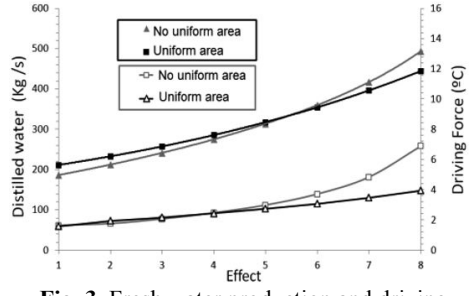

Fig. 3. Fresh water production and driving force vs. effect

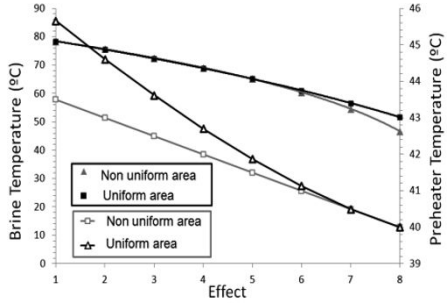

Fig. 4. Brine and preheaters temperature vs. effect

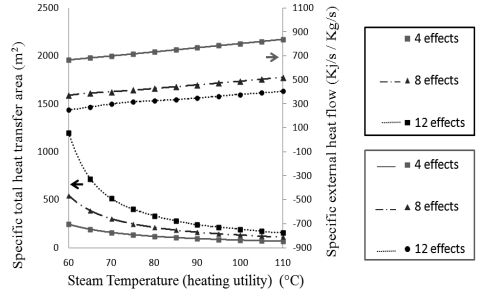

Fig. 5. Total HTA and heating utility vs. effect

The impact of the number of effects and the steam temperature used for heating utility on the total HTA and consumption of the heating utility is shown in Fig. 5. The illustrated results were obtained by minimizing the total HTA considering uniforms HTA in pre-heaters and effects and a given fresh water demand. In addition, in this case, the heating utility consumption was considered as a variable. Fig. 5 exhibits a similar behavior to those obtained via simulation by El-Dessouky (2002), instead of simultaneous optimization as is here used. As is shown, both the total HTA and heating

utility consumption are strongly influenced by the number of effects and steam temperature. The total HTA for N = 4 is not strongly influenced by the steam temperature. However, the total area is significantly increased as the number of effects increases and the steam temperature decreases. Certainly, for Ts = 65 ºC and N = 4, the total specific HTA is 192.17 m2/Kg/s, while for same steam temperature but N=12 the total specific HTA increases to 717.72 m^2/Kg/s, a 525 % higher.
By the other side, the heating utility consumption decreases as the number of effects increases and the steam temperature decreases. Certainly, for Ts = 65 ºC and N = 4, the total specific heating utility is 682.78kJ/s/Kg/s, while for same steam temperature but N=12 the total heating utility decreases to 273.57 kJ/s/Kg/s, a 59.93 % lower.

5. Conclusions and future work

A deterministic NLP mathematical model by effects for the MEE system was presented. Optimal temperature, salinity, areas dimensions and flow-rate evolutions through the equipment are obtained in order to satisfy a given fresh water demand. The proposed resulting model is a valuable tool not only to optimize the process but also to simulate the desalting process if the degree of freedom of the equation system is zero. After validation, several optimization problems using different criteria have been examined concluding that the total HTA require can be decreased a 11.4% by allowing HTA taking a non uniform distribution. It was verified that the minimization of the total HTA by fixing the fresh water demand and external heat, is equivalent to the minimization of the external heat by fixing the total HTA and fresh water demand. The effect of the number of effects and team temperature on the optimal solutions has been also investigated, obtaining similar results to those obtained by other authors. HTA and heating utility consumption are strongly influenced by the number of effects and steam temperature: the total HTA increased as the number of effects increases and the steam temperature decreases, while the heating utility consumption decreases as the number of effects increases and the steam temperature decreases.
At present, the proposed model is being expanded in order to consider the number of effects as an additional model variable (discrete decision), as well as the inclusion of the geometry, pressure drop, BPE, NEA and non-condensable gases. The coupling between the MEE system with SOFT cells and the minimization of the investment and operating costs of the entire process will be further investigated in detail. Finally, the application of a global optimum algorithm to solve the resulting model will be also addressed.

References

S. A1-Hallaj, Fuad Alasfour, Sandeep Parekh, Shabab Amiruddin, J. Robert Selman, Hossein Ghezel-Ayagh, 2004, Conceptual design of a novel hybrid fuel cell/desalination system, Desalination, 164, 19-31

M.A. Darwish, F. Al-Juwayhel, H. K. Abdulraheim, 2006, Multi-effect boiling systems from an energy viewpoint, Desalination, 194, 22–39.

H.T. El-Dessouky, I. Alatiqi, S. Bingulac, H.M. Ettouney, 1998, Steady-state analysis of the multiple effect evaporation desalination process, Chem. Eng. Technol, 21, 15±29.

H.T. El-Dessouky, H.M. Ettouney, 2002, Multiple Effect Evaporation, Fundamentals of Salt Water Desalination, Capitulo 4.2.3, ELSEVIER SCIENCE B.V., 202-205.

H.T. El-Dessouky, H.M. Ettouney, 1999, Multiple-effect evaporation desalination systems: thermal analysis, Desalination, 125, 259-276.

H.M. Ettouney, 2006, Design of single-effect mechanical vapor compression, Desalination, 190, 1–15.

P. Lisbona, J. Uche, L. Serra, 2005, High-temperature fuel cells for fresh water production, Desalination, 182, 471–482.

I.A. Karimi and Rajagopalan Srinivasan (Editors), Proceedings of the 11th International Symposium on Process Systems Engineering, 15-19 July 2012, Singapore.

An Inverse Optimization Approach to Inducing Resource Conservation in Eco-Industrial Parks

Raymond R. Tan, Kathleen B. Aviso

Chemical Engineering Department/Center for Engineering and Sustainable Development Research, De La Salle University, 2401 Taft Avenue, 1004 Manila, Philippines

Abstract

The exchange of wastes among plants within an eco-industrial park (EIP) creates potential for significant gains in sustainability through efficient use of resources and reduction of environmental discharges. If the establishment of such resource conservation networks (RCNs) is not economically optimal, intervention of an EIP authority will be necessary in order to induce companies to act in an environmentally responsible manner. This conflict of interest between the EIP authority and the industrial plants results in a Stackelberg game, which may be represented as a bi-level optimization model. In this work, a bi-level linear integer programming model for optimizing waste exchange in an EIP is developed. Then, an inverse optimization approach is used to solve it. An auxiliary model is used to determine the best set of incentives and disincentives to induce the plants in the EIP to form an optimal RCN. The methodology is demonstrated using an illustrative case study.

Keywords: Resource conservation, industrial ecology (IE), eco-industrial park (EIP), Stackelberg game, bi-level programming, inverse optimization.

1. Introduction

The concept of industrial ecology (IE) was first proposed by Frosch and Gallopolous (1989) as a means of enhancing the sustainability of manufacturing by emulating the cyclic structures of natural ecosystems. In particular, eco-industrial parks (EIPs) have been shown to be effective in developing resource conservation schemes through waste exchange and reuse. There have been significant attempts to use process systems engineering tools to provide more rigorous decision support in the design of EIPs. For example, optimal design of inter-plant water networks using mathematical programming was first proposed in the late 1990s (Keckler and Allen, 1999; Nobel and Allen, 2000); in these early models, each plant in the EIP was modeled as a "black box." Subsequent models used more detailed models describing processes within the plants themselves (Lovelady and El-Halwagi, 2009; Chew et al., 2008; Chew et al., 2010a, b; Aviso et al., 2011). Further refinements of such models were later proposed to account for potential conflicts of interest among companies (Lou et al., 2004; Singh and Lou, 2006; Piluso and Huang, 2009; Chew et al., 2009; Aviso et al., 2010a; Aviso et al., 2011; Tan, 2011; Taskhiri et al., 2011b). While many of these works have focused on water reuse, it has also been shown that the basic modeling approach may be readily extended to other streams once relevant material and energy balance considerations have been identified (Lou et al., 2004; Piluso and Huang, 2009; Aviso et al., 2011). Game theory has been proposed for resolving conflicts of interest in EIPs (Lou et al., 2004; Chew et al., 2009). In particular, some approaches have explored the role of the EIP authority (e.g.,

government) in facilitating the emergence of sustainable resource conservation networks involving different plants through incentives or disincentives (Aviso et al. 2010b; Chew et al., 2011; Tan et al., 2011a). The interaction between the EIP authority (i.e., the leader, which seeks to maximize total public good) with industry (i.e., the follower, which in turn seeks to maximize profit) results in a Stackelberg game (Aviso et al., 2010b; Tan et al., 2011a). Such games can be modeled as bi-level mathematical programs (Bard, 1998). In practice, the problem for the leader is to induce environmentally responsible behavior in the follower, despite the fact that the latter is motivated predominantly by profit. Inducement can be achieved through incentives (e.g., subsidies) or disincentives (e.g., taxes). An optimal set of incentives can then be determined, for example via inverse optimization (Ahuja and Orlin, 2001). In this work, a bi-level linear integer programming model is developed for conservation of multiple resources in an EIP. An inverse optimization solution procedure is then proposed. The methodology is demonstrated using a simple case study. Finally, conclusions and prospects for future work are given at the end of the paper.

2. Problem Statement

The formal problem statement addressed in this work is as follows:

- The EIP is assumed to be comprised of m sources, n demand, and p streams. Any given plant within the EIP can act either as a source or a demand, or both.
- Each source i (i = 1, 2, …, m) is characterized by a non-negative flowrate S_{ik} of each stream k (k = 1, 2, …, p), while each demand j (j = 1, 2, …, n) is characterized by a non-negative flowrate D_{jk} of each stream k (k = 1, 2, …, p).
- The opportunity for reuse of an given stream k between any source-demand pair is given by a constant, R_{ijk}. The decision whether or not to activate a particular link is denoted by the binary variable x_{ijk}.
- The total cost borne by industry to implement resource conservation in the EIP is assumed to be a linear function of x_{ijk}. Note that the cost may be negative.
- The total cost to the EIP authority or government to implement resource conservation in the EIP is likewise assumed to be a linear function of x_{ijk}. In general, since this cost includes externalities (e.g., monetized cost of pollution), the authority's cost function will not be the same as that of industry. However, as in the latter's case, the cost may assume negative values as well.
- Both the EIP authority and industry seek to minimize their respective cost functions, resulting in a Stackelberg game. The leader then seeks to modify both cost functions, through incentives and disincentives, so that the optimal solutions of the two decision-makers coincide. The objective is to determine the optimal set of such interventions.

3. Model

The bi-level optimization model is:

$$\min \Sigma_i \Sigma_j \Sigma_k (A_{ijk} - \alpha_{ijk} + \beta_{ijk}) R_{ijk} x_{ijk} \quad (1)$$

subject to:

$$\min \Sigma_i \Sigma_j \Sigma_k (B_{ijk} + \alpha_{ijk} - \beta_{ijk}) R_{ijk} x_{ijk} \quad (2)$$

subject to:

$$\Sigma_j R_{ijk} x_{ijk} \leq S_{ik} \qquad \forall i, k \quad (3)$$

$$\Sigma_i R_{ijk} x_{ijk} \leq D_{jk} \qquad \forall j, k \quad (4)$$

$$x_{ijk} \in \{0, 1\} \qquad \forall i, j, k \quad (5)$$

where A_{ijk} and B_{ijk} are the unit costs incurred by the leader and follower, respectively, to implement reuse of resource k between source i and demand j; α_{ijk} and β_{ijk} are the specific incentive and disincentive for the reuse of resource k from source i to demand j; R_{ijk} is the maximum amount of resource k that can be reused from source i to demand j; x_{ijk} is the binary variable denoting the decision to implement reuse of resource k between source i and demand j; S_{ik} is the amount of resource k available from source i; and D_{jk} is the amount of resource k needed by demand j. The leader's objective function is to minimize the total cost (including external costs corresponding to monetized environmental damage) associated with implementing resource reuse in the EIP (Eq. 1); likewise, the follower seeks to minimize the total cost or resource reuse (Eq. 2). The costs given by Eq. 1 and 2 may assume negative values, indicating net benefit. Source and demand balances are given by Eq. 3 and 4, while Eq. 5 restricts x_{ijk} to binary values. It can be seen that $R_{ijk} = \min(S_{ik}, D_{jk})$. Furthermore, the leader and follower will clearly have identical solutions when the terms of Eq. 1 and 2 are proportionate. Thus, when the ratio A_{ijk}/B_{ijk} is a positive constant, the leader and follower will agree on a common solution even with $\alpha_{ijk} = \beta_{ijk} = 0$. However, such a condition will rarely arise in practice, and thus it is necessary to determine what the incentives should be.

Assume that the leader seeks a set of incentives which requires the least deviation from the original cost coefficients, as proposed by Ahuja and Orlin (2001). The following auxiliary model results:

$$\min \Sigma_i \Sigma_j \Sigma_k (\alpha_{ijk} + \beta_{ijk}) \tag{6}$$

subject to:

$$\lambda (A_{ijk} - \alpha_{ijk} + \beta_{ijk}) = (B_{ijk} + \alpha_{ijk} - \beta_{ijk}) \quad \forall i, j, k \tag{7}$$

$$\lambda \geq 0 \tag{8}$$

$$\alpha_{ijk} \geq 0 \quad \forall i, j, k \tag{9}$$

$$\beta_{ijk} \geq 0 \quad \forall i, j, k \tag{10}$$

where λ is the variable proportionality ratio. Note that there are bilinear terms in Eq. 7. The procedure is illustrated in the next section with a simple case study. The optimization software Lingo 12.0 with a branch-and-bound based global optimization toolbox for non-linear models (Gau and Schrage, 2004) is used to solve the example.

4. Case Study

Consider a hypothetical EIP with three plants (i.e., a power plant, a palm oil mill and a biorefinery) and two streams (i.e., waste heat and waste biomass). The power plant may export its waste heat to the palm oil mill or the biorefinery; on the other hand, the palm oil mill generates waste biomass, which can be co-fired in the power plant or used as feedstock for the production of value-added goods in the biorefinery. The relevant stream data are shown in Table 1.

Table 1. EIP Data for Case Study

	Waste heat output (MW)	Heat demand (MW)	Waste biomass output (t/h)	Waste biomass demand (t/h)
Power plant	100	0	0	12
Palm oil mill	0	25	10	0
Biorefinery	0	20	0	5

Cost coefficients for the reuse of streams from both EIP authority and industry standpoints are given in the second and third rows of Table 2. Note that these coefficients will cause the leader and follower to seek different optimal solutions, mainly because the leader's cost coefficients account for the externalities (i.e., effects of resource conservation or pollution reduction in monetary terms).

Table 2. Cost Coefficients for Case Study

	Waste heat reuse ($/MWh)	Waste biomass reuse ($/t)
EIP Authority	−10	−1.5
Industry	2	0.2
Incentive	2	0.2

Solving the auxiliary model (Eq. 6 – 10) gives the optimal set of incentives in the last row of Table 2. The incentives in this case are just sufficient to offset the costs of implementing resource reuse, so that the industrial coalition becomes willing to accept the solution preferred for implementation by the EIP authority. Substituting these values into the main model (Eq. 1 – 5) then gives the optimal resource reuse network as shown in Table 3. The power plant exports waste heat to the two other plants for a combined recovery of 45 MW, and receives all of the available biomass (10 t/h) from the palm oil mill for co-firing.

Table 3. Optimal EIP Resource Reuse Scheme for Case Study

Source/Demand	Power plant	Palm oil mill	Biorefinery
Power plant	0	25 MW	20 MW
Palm oil mill	10 t/h	0	0
Biorefinery	0	0	0

5. Conclusion

An inverse optimization approach to inducing resource conservation in eco-industrial parks has been developed. This approach involves formulating a bi-level integer programming problem, where the EIP authority or government assumes the role of the upper-level decision maker, while the coalition comprised of participating plants acts as the lower-level decision maker. An inverse optimization strategy can be used to determine the set of incentives/disincentives that the authority should impose in order to induce the companies within the EIP to participate in resource conservation. A simple case study involving has been used to demonstrate the methodology; the model may also be tested on more complex examples in the future.

References

Ahuja, R. K. and Orlin, J. B., 2001. Inverse Optimization. Operations Research 49: 771 – 783.

Aviso, K. B., Tan, R. R., Culaba, A. B., 2010a, Designing Eco-Industrial Water Exchange Networks Using Fuzzy Mathematical Programming. Clean Technologies and Environmental Policy 12: 353 – 363.

Aviso, K. B., Tan, R. R., Culaba, A. B., Cruz, J. B., 2010b, Bi-Level Fuzzy Optimization Approach for Water Exchange in Eco-Industrial Parks. Process Safety and Environmental Protection 88: 31 – 40.

Aviso, K. B., Tan, R. R., Culaba, A. B, Foo, D. C. Y., Hallale, N., 2011, Fuzzy optimization of topologically constrained eco-industrial resource conservation networks with incomplete information. Engineering Optimization 43: 257 – 279.

Bard, J. F., 1998, Practical bilevel optimization. Algorithms and applications. Kluwer Academic Publishers, Dordrecht.

Chew, I., Tan, R. R., Ng. D. K. S., Foo, D. C. Y., Majozi, T., Gouws, J., 2008, Synthesis of direct and indirect inter-plant water network. Industrial and Engineering Chemistry Research 47: 9485 – 9496.

Chew, I. M. L., Tan, R. R., Foo, D. C. Y., Chiu, A. S. F., 2009, Game theory approach to the analysis of inter-plant water integration in an eco-industrial park. Journal of Cleaner Production 17: 1611 – 1619.

Chew, I. M. L., Foo, D. C. Y., Ng, D. K. S., Tan, R. R., 2010a, A new flowrate targeting algortihm for inter-plant resource conservation network - Part 1: unassisted integration scheme." Industrial and Engineering Chemistry Research 49: 6439 – 6455.

Chew, I. M. L., Foo, D. C. Y., Tan, R. R., 2010b, A new flowrate targeting algortihm for inter-plant resource conservation network - Part 2: assisted integration scheme." Industrial and Engineering Chemistry Research 49: 6456 – 6468.

Chew, I. M. L., Thillaivarna, S. L., Tan, R. R., Foo, D. C. Y., 2011, Analysis of inter-plant water integration with indirect integration schemes through game theory approach – Pareto optimal solution with interventions. Clean Technologies and Environmental Policy 13: 49 – 62.

Frosch, R. A., Gallopolous, N. e. 1989, Strategies for manufacturing. Scientific American 261: 94 – 102.

Gau, C.-Y. and Schrage, L. E., 2004. Implementation and testing of a branch-and-bound based method for deterministic global optimization: operations research applications. In: Floudas, C. A. and pardolos, P. M. (eds.), Frontiers in Global Optimization, p. 145 – 164, Kluwer, Dordrecht.

Keckler, S. E., Allen, D. T., 1999, Material reuse modeling; A case study of water reuse in an industrial park. Journal of Industrial Ecology 2: 79 – 92.

Lou, H., Kulkarni, M., Singh, A., Huang Y. 2004. A game theory based approach for emergy analysis of eco-idustrial systems under uncertainty. Clean Technologies and Environmental Policy 6: 151 – 161.

Lovelady, E.M. and El-Halwagi, M. M. 2009. Design and integration of eco-industrial parks for managing water resources. Environmental Progress and Sustainable Energy 28: 265 – 272.

Nobel, C. E., Allen, D. T. 2000, Using geographic information systems (GIS) in industrial water reuse modeling. Process Safety and Environmental protection 78, 295 – 303.

Piluso, C., Huang, Y., 2009, Collaborative profitable pollution prevention: An approach for the sustainable development of compex industrial zones under uncertain information. Clean Technologies and Environmental Policy 11: 307 – 322.

Singh, A., Lou, H. H. 2006, Hierarchical Pareto optimization for the sutainable development of industrial ecosystems. Industrial & Engineering Chemsitry Research 45: 3265 – 3279.

Taskhiri, M. S., Tan, R. R., Chiu, A. S. F., 2011b, Emergy-Based Fuzzy Optimization Approach for Water Reuse in an Eco-Industrial Park. Resouces, Conservation & Recycling 55: 730 – 737.

Tan, R. R., 2011, A fuzzy optimization model for source-sink water network synthesis with parametric uncertainties. Industrial and Engineering Chemistry Research 50: 3686 – 3694.

Tan, R. R., Aviso, K. B, Cruz, J. B., Culaba, A. B., 2011a, A note on an extended fuzzy bi-level optimization approach for water exchange in eco-industrial parks with hub topology. Process Safety and Environmental Protection 89: 106 – 111.

I.A. Karimi and Rajagopalan Srinivasan (Editors), Proceedings of the 11th International Symposium on Process Systems Engineering, 15-19 July 2012, Singapore.

Techno-economic analysis of ethanol production from marine biomass

Peyman Fasahati, Geongbum Yi, Jay Liu*

[a] *Department of Chemical Engineering, Pukyong National University, Busan 608-739, South Korea*

Abstract

The purpose of this study is techno-economic analysis of ethanol production from marine biomass (macroalgae), based on 10-year time frame for plant operation. This study is different from previous similar studies considering following facts: (1) Biomass considered in this study is macroalgae or seaweed, to which technologies available for conversion of biomass to fuels have been applied in limited ways. (2) This study does not provide production cost of ethanol, but target biomass cost for macroalgae production through large-scale cultivation that is a key factor for success of macroalgae as a biomass feedstock.

Currently high seaweeds price greatly limits the applicability of seaweeds as feedstocks for bioethanol production plant. To solve this issue a reduction of feedstock price seems the only option. This study develops a techno-economic model to analyze the economy of an ethanol production plant processing 100,000 MT/year (dry basis) brown algae. This study effectively defined maximum dry seaweed price (MDSP) that must be covered by large-scale seaweed production to reach a Return-On-Investment (ROI) break-even point after 10 years plant operation. The MDSP will act as target biomass cost for large-scale cultivation of macroalgae. Plant scale ups were also performed to examine the effects of plant capacity on MDSP.

Keywords: Techno-economics, Ethanol, Seaweed, Biomass, Macroalgae.

1. Introduction

Over the past 50 years, the world's population has more than doubled, coupled with an expectation of a higher standard of living and an ever-increasing economic output. This has resulted in a large increase in primary energy consumption, particularly the use of fossil fuel derived energy (BP Global, 2011).

Bio-fuels are environmentally friendly and carbon neutral, and can play a prominent role in an energy portfolio. However, if the bioenergy industry is to be successful, enough supply of biomass feedstock should be available at a low cost and on a very large scale (Antizar & Turrion, 2008).

The main obstacle of bio-energy development is stable supply of raw materials on a large scale. More than 60% of the cost for bioenergy is feedstock cost (Liu & Gu, 2008), which is a major constraint on the commercialization of algal biofuels (Johnson & Wen, 2010). It is the goal of this study to evaluate the economics of ethanol production from marine biomass, i.e., macroalgae or seaweeds (brown algae), and to calculate the maximum feed stock price based on 10-year time frame for plant operation so that industrialization of plant be economically possible. In addition, to identify most significant opportunities to decrease production costs.

* jayliu@pknu.ac.kr

An ethanol production plant from brown algae, based on a 100,000 MT/year dry feed, simulated using Aspen Plus® in order to obtain more accurate mass balance information than what typically assumed (Fasahati & Liu, 2011). Furthermore, the Aspen Plus model was used to estimate key parameters affecting the economy of the plant. Using the resulting flow rates, sizing and cost of each process unit estimated based on Aspen Process Economic Analyzer to determine the cost of bioethanol production plant. It is important to note at the outset that algal biofuel technology is still at the lab-scale or at the very early pilot stage of development; as such, the estimated cost of production may vary based on future developments on process condition and parameters change.

2. Process description

As shown in Figure 1, the simulated ethanol production process consists of three major units, feed pretreatment, simultaneous saccharification and fermentation (SSF), and finally purification. Feedstock for this plant is Saccharina Japonica, one type of brown algae, which is extensively cultivated in Korea, China, and Japan. Chemical composition for this seaweed derived from literature data (John et al., 1998; Horn S. G., 2000; Rioux et al., 2007; Jang et al., 2011). Total carbohydrates of this seaweed sum up to 66 percent of dry matter (Jang et al., 2011).

A pretreatment section carried out in two stages: The first stage is to heat up the feed stream by adding steam and H_2SO_4 for thermal acid hydrolysis. The second stage is to use enzymes for saccharification and SSF.

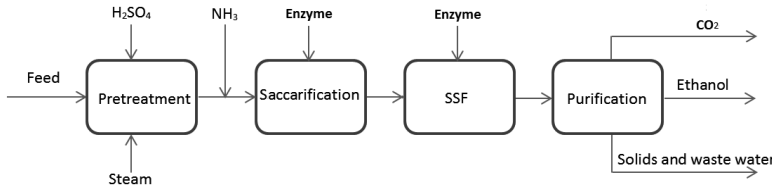

Figure 1. A simplified process flow diagram for bioethanol production plant

Slurry received from the pretreatment section first neutralized with Ammonia. Then it goes to saccharification vessels for further saccharification. Saccharified slurry, which has a reduced viscosity, goes to saccharification and fermentation vessels for SSF. Operating conditions are given in Table 1.

Table 1. Summary of plant operation conditions (Jang et al., 2011)

Unit	Condition
Thermal acid hydrolysis	10% (w/v) S. japonica, 40mM H_2SO_4, 121 °C, 60 min,
Biological saccharification	1 g dcw/L Bacillus sp. JS-1, 30 °C, 7.5 days
SSF	0.39 g dcw/L Bacillus sp. JS-1,0.45 g dcw/L P. angophorae, 30°C, 64 hr

A purification section separates the fermentation broth into water, anhydrous ethanol, and solids. Distillation and molecular sieve adsorption used to recover ethanol from the raw fermentation liquid and to produce 99.5% ethanol. Distillation accomplished in two columns. The first column, a water remover column, removes dissolved CO_2 and most of the water. The second column, an azeotropic column, concentrates ethanol from the first column to a near azeotropic composition. At the azeotropic condition ethanol products from this column goes to molecular sieves to reach 99.5 % purity. Overall process yield for ethanol production from dry seaweed is 0.25 (kg ethanol)/(kg dry seaweed).

3. Materials and methods

A list of assumptions common to all process scenarios includes the following:

- Plant base capacity is 100,000 MT/year of dry seaweed.
- Publicly available and experimentally validated literature data on reaction conversions and parameters are used.
- Equipment, chemical, and labor costs indexed to 2011 dollars.
- Contingency 18% of total project cost.
- Capital costs depreciated over 10 years of plant operation.
- Working capital 5% of total capital expense per year.
- Tax rate 24.75% per year.
- 15% internal rate of return (IRR).

The production costs include variable operating costs (such as process chemicals, bacteria, nutrients, etc.) and fixed operating costs (employee salaries, overhead, maintenance, and insurance). The chemical prices obtained from literature data and public available data such as ICIS chemical business (ICIS, 2011). Bacteria and yeast used in the process are not commercially available at a scale needed for the production plant, and this makes it difficult to obtain information needed for calculating operating costs. It is assumed that all the bacteria and enzyme will be delivered from outside to the plant and there is no onsite production. Table 2 shows material prices used in this study. CO_2 also selected as a selling material. Since this plant is capable of producing CO_2 at purity higher than 96%. We considered it as a product that can be sold.

Table 2. Raw material and product unit prices

Raw material	Cost (US$/kg)	Source
Ammonia	0.392	Humbird et al., 2011
Sulphuric acid	0.093	Humbird et al., 2011
Yeast and enzyme	0.340	Aden, 2008*
HP Steam @ 165 PSI	0.0179	Aspen utility specification
Nutrient	0.786	Aden, 2008*
Products	**Selling Price (US$/kg)**	**Source**
Ethanol 99.5%	0.891	ICIS, 2011
CO_2	0.040	Davis et al., 2011

* Nutrient and enzyme prices calculated for 2011 dollars using consumer price index, (CPI USA, 2011)

4. Results and discussions

4.1. Maximum dry seaweed price

The process model developed in Aspen Plus was sent to Aspen Process Economic Analyzer for economical evaluations. The total project capital cost is considered to depreciate, via a straight-line depreciation method, over the 10 years of economic Life of the facility. To reach a ROI break-even point after 10 years of operation, dry seaweed cost increased until net present value in 10^{th} year equals to zero. The maximum price for dry seaweed obtained was 160 $/Ton for the base case of 100,000 MT/year of dry seaweeds. Table 3 shows resulting production costs at this break-even point. Figure 2 shows a pie chart of the distribution of operating costs in 10^{th} year. From the chart, it can be seen that the raw materials constitute 68.5% of the total operating costs, and 18% of the operating cost is for utilities. This is in accordance with high raw material costs

associated for ethanol production plants using fermentation processes from biomass (Liu & Gu, 2008).

Table 3. Production costs (US$) at a ROI break-even point

Total Project Cost	12,901,300
Total operating labor and maintenance cost per year	1,466,000
Total raw material cost per year	16,302,200
Total product sales per year	26,783,400
Total utilities cost per year	4,449,870

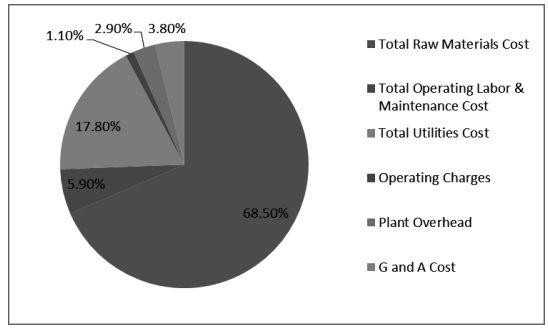

Figure 2. Operating costs break down at 10th year of plant operation

4.2. Effects of plant capacity

In order to examine the effect of plant capacity on production costs, a plant scale up from 50% to 700% of the base case (100,000 MT/Year of dry seaweeds) was performed using Aspen Process Economic Analyzer. It was found out from this study that plant economy can be improved at larger capacities. This allowed us to have increased MDSP at 10th year. Figure 3 shows the trend of MDSP changes as a function of plant capacity.

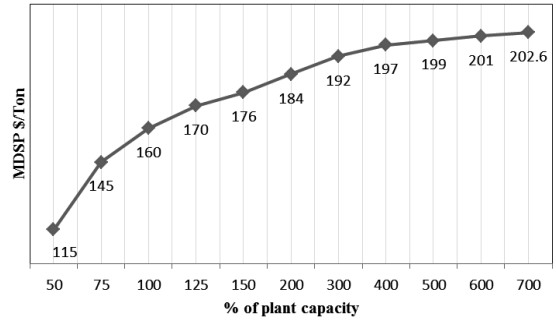

Figure 3. MDSP trend as a function of plant scale

As Figure 3 shows MDSP converge to 203 $/MT at the boundary and maximum quantity happened for plant scale up equal to 700%. Further scale ups did not affect MDSP very much and it remained constant at this value.

4.3. Conclusion

As the results of this study shows, this plant would be more economical if we can increase its capacity to five or six times of that of the base case. However, as the plant capacity increases, more biomass is needed for feed. Total production of Saccharina Japonica in South Korea in December 2011 was 43,651 MT in which 22,955 MT used

as food. This amount is much less than feedstock needed for the base case simulation. Currently, seaweeds mostly are used for food industry. Current market wholesale price of dry seaweed in South Korea is 5,622 US$/MT (December 2011) and wet seaweed price at cultivation sites is 393 US$/MT (AFL news.co.kr, 2011). Most of the seaweed available in market is wild and naturally cultivated. However, Large-scale artificial cultivation of seaweed will reduce this price. Results of this study show the necessity to perform a comprehensive study in the near future on seaweed mass cultivation procedures and efficiencies. Further technological advancements like increased conversions and process integration can further improve the plant economy and let the plant be economical even at higher seaweed prices.

Acknowledgement

This work was supported by the Ministry for Food, Agriculture, Forestry and Fisheries, and by Basic Science Research Program through the National Research Foundation of Korea (NRF) funded by the Ministry of Education, Science and Technology (2010-00003056).

• References

A. Aden, 2008, Biochemical Production of Ethanol from Corn Stover: 2007 State of Technology Model, National Renewable Energy Laboratory, NREL/TP-510-43205, Golden, CO.

BP Global: BP Energy Outlook 2030, 2011, London, UK, (www.bp.com)

L. B. Antizar and G.J.L. Turrion, 2008, Second-generation biofuels and local bioenergy Systems, Biofuels Bioprod. Bioref. 2, 455-469.

G.S. Liu and W.B. Gu, 2008, Advances in research on germplasm resources and molecular biology of the energy plants sweet sorghum, In: The proceeding of China–US workshop on bioenergy consequences for global environmental change, pp. 47-48.

M.B. Johnson and Z. Wen, 2010, Development of an attached microalgal growth system for biofuel production, Appl. Microbiol. Biotechnol. 85, 525-534.

D. Humbird, R. Davis, L. Tao, C. Kinchin, D. Hsu, A. Aden, P. Schoen, J. Lukas, B. Olthof, M. Worley, D. Sexton, and D. Dudgeon, 2011,Process Design and Economics for Biochemical Conversion of Lignocellulosic Biomass to Ethanol, In: Technical Report, National Renewable Energy Laboratory, NREL/TP-5100-47764.

R.P. John,G.S. Anisha, K.M. Nampoothiri, A. Pandey, 2011, Micro and macroalgal biomass: a renewable source for bioethanol, Bioresour Technol, 102:186–93.

P. Fasahati, J. Liu, 2012, Process simulation of bioethanol production from brown algae, ADCHEM, International Federation of Automatic Control (IFAC), Singapore.

S.J. Horn, 2000, Bioenergy from brown seaweeds, In: PhD Thesis, Norwegian University of Science and Technology, Department of Biotechnology.

L.E. Rioux, S.L. Turgeon, M. Beaulieu , 2007, Characterization of polysaccharides extracted from brown seaweeds. Carbohydrate Polymers, 69, 530–537.

S. John, T. Dunahay, J. Benemann, P. Roessler, 1998, A Look Back at the U.S. Department of Energy's Aquatic Species Program- Biodiesel from Algae, In: National Renewable Energy Laboratory, Golden, Colorado 80401-3393.

J.S. Jang, Y. Cho, G.T. Jeong and S.K. Kim, 2011, Optimization of saccharification and ethanol production by simultaneous saccharification and fermentation (SSF) from seaweed, Saccharina japonica. Bioprocess and biosystems engineering, 35, 11-18.

ICIS Chemical Business, 2011, Asia Price Report, Chemical pricing information, ICIS Pricing, 29/06/2011, Lester Teo, Lester.Teo@icis.com

AFLnews.co.kr, 2011, http://aflnews.co.kr/aflnews/news/news_contents.asp?news_code=2011011303102&c_code=0304

consumer price index, United states department of labor, 2011, Bureau of labor statistics, www.bls.gov/cpi/

R. Davis, A. Aden, P.T. Pienkos, 2011, Techno-economic analysis of autotrophic microalgae for fuel production, Applied Energy 88, 3524–3531

I.A. Karimi and Rajagopalan Srinivasan (Editors), Proceedings of the 11th International Symposium on Process Systems Engineering, 15-19 July 2012, Singapore.

Modeling and Simulation of Ship Transport of CO_2

Seok Goo Lee, Go Bong Choi, En Sup Yoon, Chonghun Han, Jong Min Lee*

School of Chemical and Biological Engineering, Institute of Chemical Processes, Seoul National University, 1 Gwanak-ro, Gwanak-gu, Seoul 151-744, Korea

Abstract

With growing concern about greenhouse gas emission, previous carbon capture and storage (CCS) research has mainly focused on efficient capture methods. However, there is a relative lack of studies on ship transport and offshore unloading. The available guidelines, if any, are simply suggested without a systematic analysis from the viewpoint of the optimal transport chain system. Thus, this study addresses the issue by modeling the ship-based transport network of CO_2. In particular, liquefaction, boil off gas (BOG) reliquefaction and offshore unloading processes are investigated to provide essential guidelines in terms of an optimal thermodynamic state (pressure-temperature: P-T). Optimal compression ratio and pressure-enthalpy flash are implemented on each compression-intercooling-separation stage, and a conceptual model for BOG reliquefaction process is also proposed.

Keywords: carbon capture and storage (CCS), CO_2, ship transport, optimal operating condition, modeling, simulation

1. Introduction

In recent years, there has been increasing demand for a significant reduction of CO_2 emissions from industrial sources to alleviate the global warming problem. Although several alternatives such as bio, wind, and solar energy are being studied to meet the huge energy demand, large amount of CO_2 emission seems to be inevitable in near future. Under the present conditions, carbon capture and storage (CCS) is considered to be the most practical approach for mitigation of CO_2 emission.

CCS technology consists of capture, transport and storage. Whereas a variety of researches have been conducted for CO_2 capture, research on systematic guidelines and technologies for transport and storage is still at its infancy.

Large amount of CO_2 can be transported via pipelines or ships. The technologies for CO_2 pipelines have been well established for many years, however this study is focused on ship transport of CO_2 due to its flexibility compared to the regional constraints of pipelines and wide range of applications. Despite the current limited knowledge and experience on ship-based CO_2 transport, there is much technical information available in the field of liquefied petroleum gas (LPG) and food grade CO_2 industries.

In order to ship CO_2, pressured-type or semi-refrigerated ship should be used for dense liquid phase conditions. Since CO_2 is in gas or solid phase at atmospheric pressure, depending on temperature, lowering the temperature at atmospheric pressure cannot liquefy CO_2 (IPCC, 2005). Hence, liquefaction of CO_2 requires a P-T condition between the triple point (T.P., 5.2 bar and -56.6 °C) and the critical point (C.P., 73 bar, 31 °C).

A key to the design for ship transport chain of CO_2 is to determine optimal P-T conditions of CO_2 because this significantly affects the system performance including liquefaction process, boil-off rate in the tank, hydrate and dry ice formation, etc. As

*Corresponding Author Tel.: +82-2-880-1878, E-mail: jongmin@snu.ac.kr

thermodynamic condition is close to the T.P., the amounts that can be transported are increased as the density rises. However, more compression energy is required for lowering the pressure for liquefaction and the amount of BOG can be increased with the temperature difference between inside and outside of the tank. If the pressure goes below the T.P., dry ice will not be necessarily formed immediately. In addition, the solubility of water in CO_2 gas decreases with higher pressure and lower temperature (Aspelund et al., 2006). For all these trade-offs, thermodynamic (P-T) conditions for liquefied CO_2 should be investigated systematically for each process.

Thus, this study systematically investigates the optimal operating condition by modeling and simulation of the major three processes, i.e., liquefaction, BOG reliquefaction, and offshore unloading.

2. Description of ship transport chain of CO_2

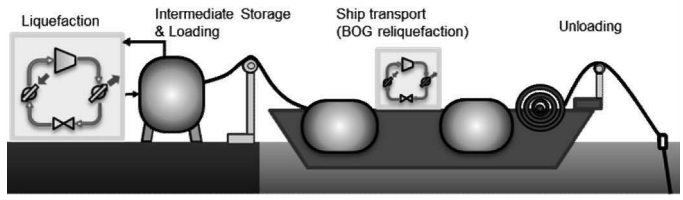

Figure 1. The ship transport chain of CO_2

As shown in Figure 1, the ship transport chain of CO_2 is divided into four parts: liquefaction, intermediate storage and loading, ship transport, and unloading. Liquefaction using Carnot cycle for volume reduction and intermediate storage tank are necessary at a terminal because CO_2 is continuously captured at the plant on shore. A loading arm or insulated flexible hose is placed between intermediate storage tank and ship. Furthermore, BOG reliquefaction process on the ship is considered in spite of much uncertainty in the amount of BOG. As the last stage, CO_2 is directly unloaded to aquifer via flexible riser (hose) which is mainly used in the field of oil/gas loading.

2.1. Liquefaction process

In the ship transport chain of CO_2, liquefaction process has the most significant influence on total cost and energy. Liquefaction of CO_2 can be classified into three categories according to the refrigeration system and refrigerant. The first is an absorption refrigeration system using NH_3. This method has the advantage of high specific heat capacity of NH_3, but is not suitable for this case due to environmental problems. The second is the method primarily used in the liquefied natural gas (LNG) industry, which lowers the temperature of CO_2 by compression-expansion loop using C_3 series refrigerant. This method has disadvantages in terms of efficiency and refrigerant cost. The last method, considered as the best, is an open cycle using the CO_2 feed as refrigerant by itself. Compared to conventional refrigerants, the most remarkable property of CO_2 is the low critical temperature of 31 °C. This means that the compression system operating at normal ambient temperatures thus works close to and even above the critical pressure of 73 bar. This leads to trans-critical cycle of CO_2 for liquefaction with favourable conditions for high compressor efficiency. In addition, most of the heat rejection at each stage takes place by air/seawater cooling instead of condenser. In other words, the refrigerant can be cooled to a few degrees above the entering coolant (air, seawater) temperature, and this contributes to the performance improvement (Neksa et al.).

As mentioned earlier, P-T condition has the most significant influence on performance for liquefaction process. This study investigates an alternative condition, which is 20 bar and -20 °C in the product stream, unlike the existing cases (7 bar, -50 °C) in the literature (Aspelund et al., 2006, 2007 & Decarre et al., 2010). Although the 20 bar and -20 °C condition may have disadvantages of high capital production cost of pressurized tank with a large volume due to the difference in density, liquefaction energy and BOG generation are smaller than the existing case (7 bar, -50 °C). This is an important problem of finding an economic optimal trade-off. However, 7 bar and -50 °C condition is unquestioningly applied to many previous studies (Aspelund et al., 2006, 2007 & Decarre et al., 2010). This study provides systematic guidelines for computing an optimal operating condition based on 20 bar and -20 °C condition.

2.2. BOG(Boil-Off Gas) reliquefaction process

With increasing fuel price, BOG reliquefaction technique has made much progress in the field of LNG transport. BOG reliquefaction for CO_2 transport is not yet reported, and there is much uncertainty about its necessity and technology. This is because there exists many difficulties in determining boil-off rate in CO_2 tank due to the uncertainties in its sensitivities with respect to insulation material and thickness, the number and size, structural shape, sloshing phenomena, impurities, etc. In addition, desirable simulation and/or experimental data for BOG reliquefaction of CO_2 has not been developed in the previous studies. Thus, to circumvent these difficulties, existing approaches in the LNG industry are applied in this study. Even though boil-off rate is determined by many variables, N_2 content is considered as a major factor in this modeling and simulation. This is because vapor-liquid equilibrium is largerly changed with N_2 content in BOG. The other variables such as insulation, surface area, and the number and size are assumed to be considered in the tank design as an economic trade-off. In addition, since N_2 is non-condensable in reliquefaction process, the amount of N_2 in BOG increases during the voyage. Thus, excessive amount of N_2 in BOG must be investigated and controlled by reliquefaction process and purge gas.

2.3. Offshore Unloading Process

There are two possible options for unloading process: indirect or direct unloading. Indirect unloading methods use a platform installed with buffer storage tank and injection facilities. Among them are submerged turret loading (STL) system and scaled-down platform (Aspelund et al., 2006). Although indirect methods can stand up to harsh condition on the sea, there are critical drawbacks that energy source for utilities on platform cannot be supplied by itself and relocation for scattered aquifers is relatively difficult.

The second method is to unload directly to aquifer without any buffer tank on ship instead of the platform. This method equips a pipeline at the bottom of ship (IPCC, 2005) or a flexible hose on the top of ship for injection. Compared with the indirect method, the direct method has many advantages such as flexibility for scattered aquifers, change of schedules and dynamic positioning. Though there are still uncertainties in choosing the best way between indirect and direct options according to given conditions, this study will focus on direct unloading methods with its economic advantages.

3. Simulation Results and Discussions

The suggested models are synthesized on process flow sheet simulator, Aspen HYSYS v7.2, and physical properties of the components were calculated by Soave-Redlich-Kwong (SRK) equation of state.

3.1. Liquefaction process

Table1. Specification of streams

	Component	Mole fraction	P-T condition	Mass flowrate
Feed gas stream	CO_2	0.95	1.1 bar, 35 °C	500 tonCO_2/hr
	H_2O	0.05		
Product stream (liquefied CO_2)	CO_2	0.9999	20 bar, -19.28 °C	475 tonCO_2/hr
	H_2O	0.0001		

Table1 shows feed flow of 500 tonCO_2/hr is used, which was determined by the thermal power plant of a unit grade 500 MW in South Korea, Boreyong city. The feed component mole fractions and P-T conditions were taken from (Aspelund et al., 2007)

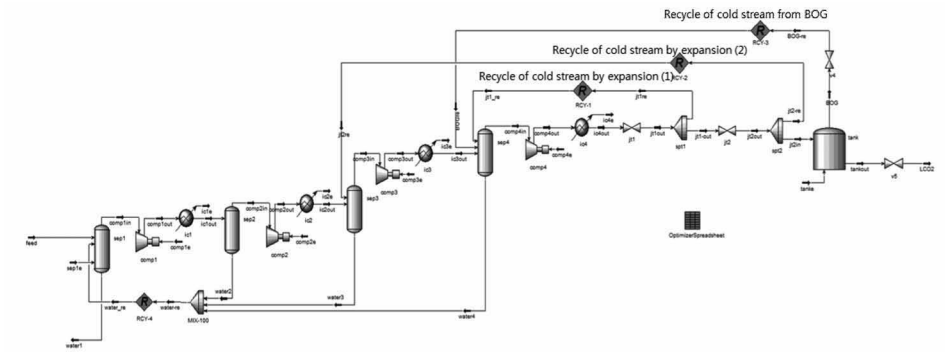

Figure 2. Process Flow Diagram of liquefaction process

For mechanical feasibility and thermodynamic efficiency, multistage compression-intercooling-separation processes are applied to increase the pressure for trans-critical cycle as shown in Figure 2, and then the liquid CO_2 is expanded over two stages to reach final specifications. The cold stream is generated by two-stage expansion and BOG from intermediate storage tank. This cold stream is recycled to pre-saturation for reducing compression power at 3 and 4 stages. Furthermore, compression pressure ratio is optimized via simulation tool satisfying mechanical constraints (i.e., in general compression ratio cannot exceed 5). As a results, the required compression power was computed as 103.42 KWh/tonCO_2. This is much more improved value compared to the previous studies (Aspelund et al., 2007 & Decarre et al., 2010). In addition, hydrate formation utility does not occur in simulation because water content is reduced to 100 ppm level in the product stream by the recycle. There are available results concerning the hydrate formation (Jakobsen et al., 2011). Hydrate will be formed at 20 bar, -20 °C when water content is contained more than 500 ppm. Thus this case does not have a problem for hydrate formation.

3.2. BOG reliquefaction process

N_2 content in the feed is contained to 500 ppm. N_2 content has a significant effect on vapor-liquid equilibrium in BOG. The boiling point of pure CO_2 at 20 bar is -19.27 °C. However the boiling point is changed to -24.35 °C when BOG contain 500 ppm N_2 content according to the SRK equation of state. The sphere tank volume and liquid volume flowrate are 10,000 m^3 and 10,000 m^3/hr, respectively. Overall heat transfer area is 2245 m^2. Heat ingress to storage tank is calculated as 64656 kJ/hr with the

overall heat transfer coefficient of 0.72 kJ/m^{2}·hr·°C. BOG massflow rate is 117.4 kg/hr containing 12 mole% N_2 content and 88 mole% CO_2 contained in BOG in the tank.

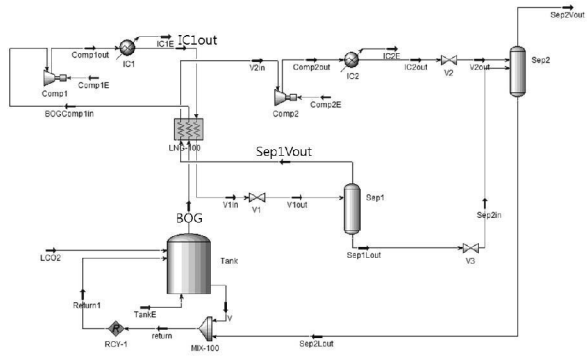

Figure 3. Process Flow Diagram of BOG reliquefaction process

Similarly, in the liquefaction process, design is proposed using CO_2 as a refrigerant by itself and two-stage compression-intercooling-expansion loop is shown in Figure 3. BOG and Sep1Vout as a cold stream pass through the multi-stream heat exchanger with hot IC1out stream after one-stage compression-intercooling. After that, the stream reliquefies via one more compression-intercooling-expansion in the last stage. Separated liquid stream containing 0.8 mole% N_2 content and 99.2 mole% CO_2 returns to the tank. It should be noted that, recovery rate is only 43%.

4. Concluding Remarks

By optimizing the compression ratio for each stage and integrating cold energy generated by expansion, the liquefaction process has been developed with 103.42 KWh/tonCO_2 of power for compression and the water content of 100 ppm level. BOG reliquefaction model for CO_2 storage tank is newly proposed to estimate the boil off rate.

Acknowledgement

This work was supported by the Industrial Strategic technology development program, 10038671, Development of Cargo Tank, Gas Dome Design, and Loading/Unloading System for CO_2 Carrier funded by the Ministry of Knowledge Economy (MKE, Korea).

References

A. Aspelund, M. J. Molnvik, G. De Koeijer, 2006, Ship transport of CO_2 - Technical solutions and analysis of costs, energy utilization, exergy efficiency and CO_2 emissions

A. Aspelund, K. Jordal, 2007, Gas conditioning - The interface between CO_2 capture and transport, International Journal of Greenhouse Gas Control, 1, 3, 343-354

The Intergovernmental Panel on Climate Change and Cambridge University, 2005, IPCC Special Report on Carbon Dioxide Capture and Storage

H. Li, J. Jakobsen, J. Stang, 2011, Hydrate formation during CO_2 transport: Predicting water content in the fluid phase in equilibrium with the CO_2-hydrate, International Journal of Greenhouse Gas Control, 5, 3, 549-554

S. Decarre, J. Berthiaud, N. Butin, J. L. Guillaume-Combecave, 2010, CO_2 maritime transportation, International Journal of Greenhouse Gas Control, 4, 5, 857-864

P. Neksa, J. Pettersen, G. Skaugen, SINTEF, CO_2 Refrigeration, Air Conditioning and Heat Pump Technology

I.A. Karimi and Rajagopalan Srinivasan (Editors), Proceedings of the 11th International Symposium on Process Systems Engineering, 15-19 July 2012, Singapore.

Design Modification Study on DME direct synthesis technology

Ik Hyun Kim, Byung Joon Kang, En Sup Yoon

School of Chemcial and Biological Engineering, Institute of Chemical Processes, Seoul National University, 1 Gwanak-ro Gwanak-gu, Seoul, 151-744, South Korea

Abstract

Korea Gas Corporation(KOGAS) has developed a process in which syngas is produced from natural gas and converted to dimethyl ether(DME) using a single-step reactor. We had conducted the study on the scale-up of the plant based on the operation experience of demo-scale plant and the numerical analysis result of the pilot-scale fixed-bed tubular reactor. Those studies didn't pay attention to the improvement of the process performance, but tended to center around the simulation of the plant with respect to development and validation of the model. In this study, we have conducted the simulation reflecting the result of a reactor modeling and the real operation data of demo-scale plant. And based on this simulation result, we make some modifications of the conceptual design of commercial-scale plant to improve its performance.

Keywords: Dimethyl-ether, One-step DME production, Conceptual Design

1. Introduction

Korea Gas Corporation(KOGAS) has developed a process in which syngas is produced from natural gas in proprietary auto-thermal reformer(Tri-Reformer) and then converted to DME in a single reactor. Based on the study of lab and pilot scale plant, KOGAS had constructed demo-scale plant since 2004 and has operated it. Scale-up study on DME plant has been carried out with the operation data of the demo plant.

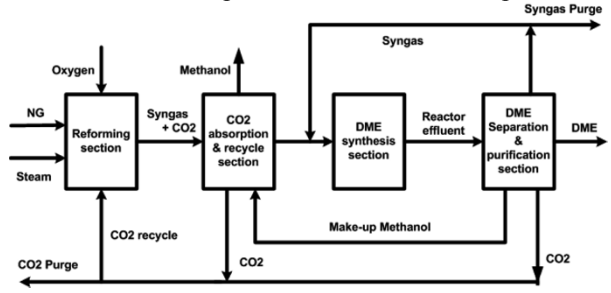

Fig.1 Simple process block diagram of one-step production of DME

The Tri-Reformer in the reforming section is an adiabatic auto-thermal reformer that is based on KOGAS' own technology. The pre-reformed natural gas (primarily methane), steam, oxygen, and carbon dioxide react to produce syngas containing the correct amount and ratio of carbon monoxide and hydrogen. The ratio of hydrogen to carbon monoxide in the Tri-Reformer outlet is set to be 1.2~1.3 to provide the correct H_2:CO ratio in the mixed feed into the DME reactor.

CO_2 absorption and recycle section uses chilled methanol as a solvent for absorbing CO_2 and serves two purposes; it removes CO_2 and water from the syngas stream going

to the DME synthesis reactor and it provides a CO_2 recycle stream being fed back to the Tri-Reformer.

The DME synthesis reactor is a tubular fixed-bed reactor with boiling water in jacket using KOGAS' catalyst. The inlet to the reactor is set to 230 C and 6.101 MPa. Given the specified feed composition and condition, the DME reactor is expected to achieve a 68% conversion of CO and provide the product profile specified by KOGAS.

DME separation and purification section is a single train that takes the combined output streams from the DME synthesis reactor, removes CO_2 to be sent back to the Tri-Reformer, recycle unreacted syngas (CO and H_2) to the DME reactor feeds, separates DME from the byproduct methanol and provides a DME product stream with the specified purity.

For the simulation of DME production plant, a commercial steady-state process simulator, Aspen Plus, has been used to model the KOGAS DME process. The previous simulation of process reflects only conceptual design of demo scale DME plants based on the pilot plant data. The revision of this simulation model should proceed for the purpose of more accurate analysis and studies.

In this paper, we have conducted simulations improved to reflect the data of experimental vapor-liquid equilibrium in the literature and the test operation data of the KOGAS' demo scale plant. And more reasonable and efficient alternatives are suggested by the modification of process.

2. Process Simulation Details

2.1. (Case1) Simulation changes by Demo plant operation data

Before this study, the simulation model had only reflected the pilot plant operation data. It should be revised to reflect the operation data of demo plant so that the simulation result of commercial plant could be correct in order for the simulation to be a useful tool for process design.

Major change from the demo plant operation is the feed and product composition changes of Tri-Reformer. This change is to increase CO_2 and O_2 composition in Tri-Reformer feed and to decrease steam demand.

This is for reasonable performance of Tri-Reformer, especially secure H_2/CO ratio in the effluent stream. As a result of this change, the demand of inlet natural gas and the flow rate of CO_2 purge stream increase since increasing demand of inlet natural gas also leads to increasing CO_2 effluent.

HP steam for supplying feed of Tri-Reformer is also serves as a preheating source of natural gas feed stream. So decreasing steam demand as a feed of Tri-Reformer causes the decreasing temperature of natural gas feed stream. As a result, the operation temperature of Sulfur Guard Bed which is required for absorbing sulfur contents in natural gas and protecting the downstream process is decreased by 10℃. Reactor performance and CO_2 absorber specification are also changed to reflect the operation data of demo plant.

2.2. (Case2) Improvement of Productivity

In the Case1, KOGAS DME plant produces DME and methanol simultaneously. KOGAS assumes that methanol produced in the DME reactor cannot be recycled due to the performance of reactor. So they allowed that the methanol needs to be purified to commercial grade and sold as a byproduct. But this means that the total capital cost and operation cost include the cost of production for not only DME but also methanol. This is not reasonable process with respect to productivity of DME.

The production of byproduct methanol also has implications for the Tri-Reformer. The amount of methanol byproduct produced impacts the H2:CO ratio required in the syngas produced by the Tri-Reformer. Methanol(CH_3OH) has an H:C ratio of 4 while DME(CH_3OCH_3) has an H:C ratio of 3. This means that as more methanols are produced, the H_2:CO ratio required in the makeup syngas will also have to increase.

To solve this problem, we added a separated methanol dehydration reactor(Fig.2). The underflow from DME separation column contains primarily methanol and water. This is sent to the primary methanol dehydration column. The reflux of methanol dehydration column is controlled so that the water content in the overhead methanol stream is maintained at 5wt%. This needs to be specified to match the feed specification for the methanol dehydration reactor. The methanol dehydration reactor is represented by a stoichiometric reactor model which converts 80% of the methanol to DME and H_2O. The reactor is assumed to be adiabatic.

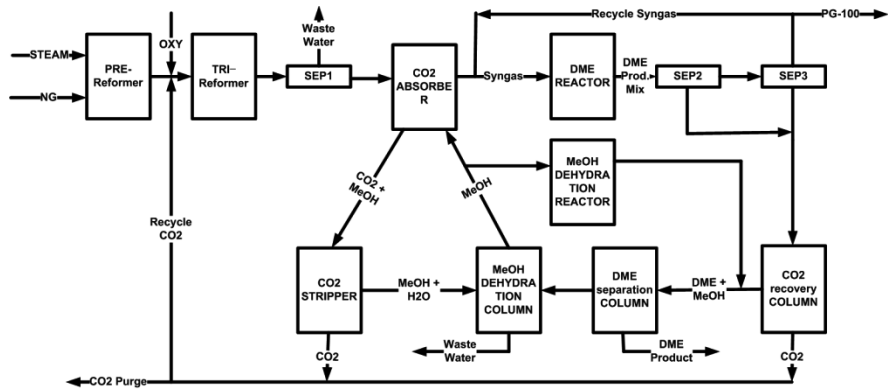

Fig. 2 Modified block diagram for Case2.

In addition, DME CO_2 absorber located between SEP3 and CO_2 recovery column in the previous cases is removed in this case. DME CO_2 absorber in DME separation and purification section is for absorbing CO_2 in the unreacted syngas recycle flow. But it seems to be unnecessary unit by the test operation of demo plant. So deleting DME CO_2 absorber from the separation process has no critical impact on the process-side streams but has an impact on the reduction of ISBL(Inside Battery Limits) and OSBL(Outside Battery Limits) fixed capital costs.

2.3. (Case3) Improvement of energy efficiency

Throughout the simulation model in the previous cases, Aspen Plus HEATER block are used to represent the process side heating and cooling. The utility side(e.g. refrigeration or steam) is not represented. In cases where process-process heat exchanger is taking place, this is represented by two HEATER blocks connected by a heat stream.

In the aspect of local energy integration, opportunities for minimizing heating and cooling utility requirements by matching hot and cold process streams were taken in all simulation cases. But the global (heat pinch type) energy integration is not conducted for 'first of a kind' plant.

In Case1 and 2, two heat exchanger blocks exist for calculating the steam generation rate in fired-heater. The fired-heater is for supplying heat duty to increase temperature of natural gas feed to 350℃. It is useful for start-up of plant, but could be substituted with an alternative reforming process scheme with respect to heat integration.

3. Result

3.1. Equipment Costs

Table 1. Equipment list in Case 1~3

	Case1	Case2	Case3
Fired-Heater	O	O	X
DME CO2 Absorber	O	X	X
Methanol Dehydration Reactor	X	O	O

The major difference of equipment costs is caused by fired heater as a reformer feed heater, DME CO_2 absorber as a CO_2 absorber in unreacted syngas recycle, and methanol dehydration reactor as an additional production of DME from byproduct methanol.

Fired-heater is the most expensive equipment but methanol dehydration reactor is the cheapest one. We can expect that Case3 can reduce about hundreds of thousands dollars of equipment cost against Case1.

3.2. Feedstock Costs

The difference of feedstock in each case is shown in Table2. Even if we only consider a natural gas feedstock, $948,000 per day can be reduced in Case3. The cost of natural gas assumed 2.0$/kg.

Table 2. Comparison of feedstock (Unit: metric ton per day)

	Case1	Case2	Case3
Natural Gas	3998	3524	3524
Oxygen	5665	4946	4946
Steam (High Pressure)	3510	3039	3162
Steam (Superheated)	1320	1193	-

3.3. Utility Costs

Table 3. Comparison of electric power requirement (Unit: kWh)

Section	Block	Case1	Case2	Case3
CO_2 Absorption and Recycle	C-2001	37087.9	34817.2	34817.2
	P-2001	3247.2	2803.0	2803.1
DME separation and purification	C-4001	1116.8	616.3	616.3
	P-4001	448.6	-	-
	P-4002	39.6	-	-
	P-4003	225.9	168.4	168.4
	P-4004	0.025	0.008	0.008
Total Costs ($/day)		50,599	46,086	46,086

Table 3 shows the electric power consumption of the whole process. Prefix ‘C’ means the compressor and ‘P’ means the pump. Case2 and Case3 consume the same electric

power which is decreased by 9% against Case 1. If the cost of electric power is 0.05 $/kWh, then the saving cost would be 4,513 $/day.

The steam requirement for reforming section is most remarkable change. This is caused by adopting methanol dehydration reactor(Case2) and deleting fired-heater from reforming section(Case3).

Table 4. Comparison of steam requirement in reforming section

Steam	Condition	Case1	Case2	Case3
SHP Steam	4.3 MPa @ 380℃	1320	1193	-
HP Steam	4.3 MPa @ Saturated vapor	3510	3039	-
HP Steam	4.3 MPa @ saturated liquid	-	-	3162

4. Conclusion

The process simulation of the commercial DME plant, which has the capacity of 3,000 metric ton per day, has been completed. The previous study on the design basis of demo plant only reflects the pilot scale plant data, but in this paper the improvement for scale-up of the commercial plant is achieved. Remarkable improvements are mainly reduction of capital costs and operating costs. This is due to adopting methanol dehydration reactor to convert the byproduct methanol to DME, removing the fired-heater as a reformer feed heater, and DME CO_2 absorber for recovery CO_2 in the syngas recycle flow. But this change of process could be influence the feasibility of operation or control. Therefore the verification of this suggestion should be performed by experiences of demo plant operation.

References

Ik Hyun Kim, Seunghyok Kim, Wonjun Cho, En Sup Yoon, Simulation of commercial dimethyl ether production plant, 2010, 20th European Symposium on Computer Aided Process Engineering

Daesung Song, Wonjun Cho, Gibaek Lee, Dal Keun Park, and En Sup Yoon, Numerical Analysis of a Pilot-scale Fixed-Bed Reactor for Dimethyl Ether(DME) Synthesis, Ind. Eng. Chem. Res, 2008, 47(13), 4553-4559.

Seung-Ho Lee, Wonjun Cho, Taekyoung Song and Young-Jun Ra, Scale up study of DME direct synthesis technology, 2009, World Gas Conf., [Pap.], 24th, WOC1

Soren Dahl, Aage Fredenslund, and Peter Rasmussen, 1991, The MHV2 Model: A UNIFAC Based Equation of State Model for Prediction of Gas Solubility and Vapor-Liquid Equilibria at Low and High Pressure, Ind. Eng. Chem. Res., 30, 1936-1945

Takashi Katayama, Kazunri Ohgaki, Goro Maekawa, Motojiro Goto, and Tamon Nagano, 1975, Isothermal vapor-liquid equilibria of acetone-carbon dioxide and methanol-carbon dioxide systems at high pressure, Journal of Chemical Engineering of Japan, Vol. 8, No. 2

Torben Laursen and Simon Ivar Anderson, 2002, High-Pressure Vapor-Liquid Equilibrium for Nitrogen+Methanol, J. Chem. Eng. Data, 47, 1173-1174

Elaine Chang, Jorge C.G. Calado, and Willian B. Streett, 1982, Vapor-Liquid Equilibrium in the System Dimethyl Ether/Methanol from 0 to 180 C and at Pressure to 6.7 MPa, J. Chem. Eng. Data, 27, 293-298

E. Brunner, W. Hultenschmidt, and G. Schlichtharle, 1987, Fluid mixtures at high pressures; Ⅳ.Isothermal phase equilibria in binary mixtures consisting of (methanol+hydrogen or nitrogen or methane or carbon monoxide or carbon dioxide), J. Chem. Thermodynamics, 19, 273-291

I.A. Karimi and Rajagopalan Srinivasan (Editors), Proceedings of the 11th International Symposium on Process Systems Engineering, 15-19 July 2012, Singapore.

Simulation of an Off-shore Natural Gas Purification Process for CO_2 Removal with Gas-Liquid Contactors Employing Aqueous Solutions of Ethanolamines

José L. de Medeiros [a], Wilson M. Grava [b], Jailton F. Nascimento [b], Ofélia de Q. F. Araújo [a], Andressa Nakao [a]

[a]*Chemical Engineering Department, School of Chemistry, Federal University of Rio de Janeiro. Av. Horacio Macedo, 2030, Bloco E, Sala E-201, CT, Cidade Universitária – Ilha do Fundão, CEP: 21949-900, Rio de Janeiro, RJ - Brazil*
[b]*Petrobras, S.A. CENPES, Ilha do Fundão Qd. 07 - Rio de Janeiro , RJ - Brazil*

1. Abstract

Brazilian Pre-Salt oil reserves present associated natural gas (NG) exhibiting high concentrations of CO_2 which requires gas purification processes for compliance with specifications imposed by the local Regulatory Agency. Due to its recognized small footprint as compared to amine based absorption route, membrane equipment show considerable potential for offshore applications. Of particular interest is the use of contactors, which combines membrane permeation with facilitated transport via liquid absorption. Process design and optimization of such innovative alternative demand flexible models to predict equipment performance at a variety of process conditions. This work presents a mathematical tool for analyzing CO_2 separation with hollow-fiber membrane contactors, using aqueous solutions of ethanolamines. The model is applied to assess the technical feasibility of offshore CO_2 separation with membrane contactors.

The developed simulator is based on rigorous principles of thermodynamics, fluid mechanics, heat transfer and mass transport. Chemical absorption modeling is approached as a typical application of the well known Chemical Theory, which aims to model chemically and/or physically complex equilibrium systems via a set of chemical equilibrium processes involving real and fictitious species. Vapor-Liquid Equilibria of real species are superimposed on the multi-reaction chemical equilibria for formation of fictitious species – non-ionic and non-volatile complexes. A process flowsheet is simulated to assert technical feasibility of this technology to offshore installations.

Keywords: CO_2 Removal, Hollow-fiber Membrane, Ethanolamines, Natural Gas Conditioning

2. Introduction

Global warming effects associated to CO_2 emissions cause societal concerns and give rise to increasing demands for clean technologies to improve sustainability of the world economy through efficient and safe usage of raw materials, and decreased CO_2 emissions (Dovi *et al*, 2009). According to Rivera-Tinoco and Bouallou (2010), among the technologies proposed to reduce CO_2 emissions, the most relevant are

associated to CCS Technologies. Ebner and Ritter (2009) state that the CO_2 removal market is dominated by amine based absorption processes. However, the authors recognize that membrane technology offers competitive advantages such as not requiring separating agent nor involving phase changes (reduced regeneration costs), which is claimed to have positive cost impacts and small footprints compared to alternative processes. Nevertheless, they state that membranes for large-scale recovery of CO_2 from natural gas are a relatively recent development.

A more innovative alternative employs gas-liquid membrane contactors for CO_2 removal from natural gas, which offers the advantages of both membrane technology and absorption processes. This hybrid-type process combines membrane separation and chemical absorption (Keshavarz *et al.,* 2008a), where the solvent (CO_2 absorbing liquid) is responsible for the selectivity of the process (typical of absorption technology) while the membrane stands as a selective barrier between the gas and the liquid. Further advantages are listed by Zhang et al. (2006), such as independent liquid and gas flow rate manipulation, much larger gas-liquid interfaces and the flexibility to scale up or down.

Differently from traditional membrane separation processes, microporous membranes used in membrane contactors are not required to be selective. The liquid phase that flows in one side of the fiber absorbs gas components physically and chemically, enhancing mass transfer therefore reducing the demand for high process pressures (Keshvarz et al, 2008b). Keshavarz and co-workers (2008a) report that the advantages depend in gas-liquid systems, types of membranes employed and applied operating conditions. The design and optimization of this innovative process suffer from a relative unavailability of experimental data and reliable mathematical representation of the impact of operational variables on process performance.

To meet this need, the present work presents a model for CO_2 separation from natural gas in membrane contactors with aqueous blends of ethanolamines. Specifically, the model treats a hollow fiber contactor configuration, based on principles of thermodynamics, fluid mechanics, heat transfer and mass transport. The tool is further applied to a conceptual process to verify the feasibility to meet natural gas CO_2 specifications.

3. Model Description

The model treats the separation of CO_2 from a stream of natural gas employing aqueous solutions of ethanolamine. Figure 1a shows the transport of the diffusing component of interest (CO_2 rich natural gas) from the gas phase through the microporous membrane into the liquid phase (aqueous amine solution) in a gas-liquid membrane contactor. The liquid absorbent flows in the lumen of the membrane while the gas mixture flows countercurrently in the shell side, configured as a fluid envelope around the hollow fiber (Figure 1b). Interaction among fibers is neglected.

Considering that the CO_2 diffusivity in the gas phase is much higher than in the liquid phase, it is reasonable to assume the gas to exhibit plug flow regime, which implies that the gas velocity and concentration distributions in the radial direction can be ignored in the shell side (Zhang et al, 2006).

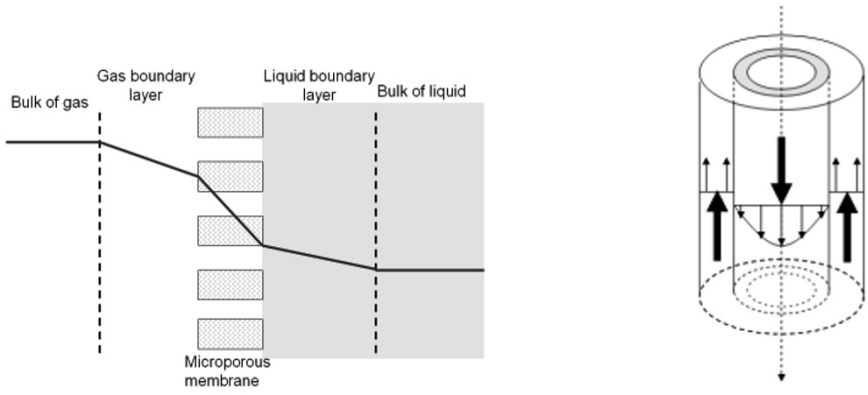

Figure 1 – Membrane Contactor. (a) mass transfer regions in membrane contactors for CO_2 absorption, (b) liquid and gas flows in a hollow fiber.

Peng-Robinson equation of state (PR EOS) has become the most popular EOS for natural gas systems (*e.g.,* Nagy and Shirkovskiy, 1982; Alfradique and Castier, 2007). The model applies rigorous thermodynamics with PR EOS to predict temperature changes associated with Joule-Thomson and dissolution effects, in a wide range of pressure, temperature and composition of multi-component gas feed stream. Chemical absorption of CO_2 in the liquid phase is represented by the *Chemical Theory* (*CT*, Prausnitz et al., 1986), which aims to model chemically and/or physically complex equilibrium systems via a set of equilibrium chemical reactions involving real and fictitious species (amine-CO_2 complexes). In the liquid compartment, multi-reactional chemical equilibria form complexes, as shown in Eqs. 1a through 1d, confined into the liquid phase, while vapor-liquid equilibria (VLE) of real species is applied.

$$CO_2 + H_2O + MEA \xleftrightarrow{K_1} CO_2 \cdot MEA \cdot H_2O \quad \text{(1-a)}$$

$$CO_2 + H_2O + MDEA \xleftrightarrow{K_2} CO_2 \cdot MDEA \cdot H_2O \quad \text{(1-b)}$$

$$H_2S + H_2O + MEA \xleftrightarrow{K_3} H_2S \cdot MEA \cdot H_2O \quad \text{(1-c)}$$

$$H_2S + H_2O + MDEA \xleftrightarrow{K_4} H_2S \cdot MDEA \cdot H_2O \quad \text{(1-d)}$$

Chemical equilibrium constants associated to the *CT* model (K_1 to K_4) were estimated via the Maximum Likelihood Criterion over VLE data of CO_2 with aqueous blends of ethanolamines (Barbosa *et al.,* 2011). The approach allows prediction of formation properties for the complexes, enthalpies and thermal effects. Barbosa *et al.* (2011) proposed an equilibrium approach for CO_2 absorption with aqueous solutions of ethanolamines using a large set of vapor-liquid CO_2/MEA/MDEA equilibrium data from the literature. The *CT* compartment was validated against the extensive databank (Barbosa *et al*, 2011) prior to application to the liquid phase of the contactor.

The *CT* model was added to the permeation model developed by Medeiros (2008), which describes the gas permeation process across a hollow-fiber membrane, with an outstanding performance when compared to the referred data bank. The combination of the two models – *CT* model and permeator model - allows investigating the performance of membrane contactors applied to CO_2 removal from natural gas. Figure 3 presents the scheme of the gas permeation module (Figure 3a) and contactors (Figure 3b). The developed contactor model is capable of describing CO_2 removal

processes using gas-liquid contactor with aqueous solutions of ethanolamines, at different process configurations.

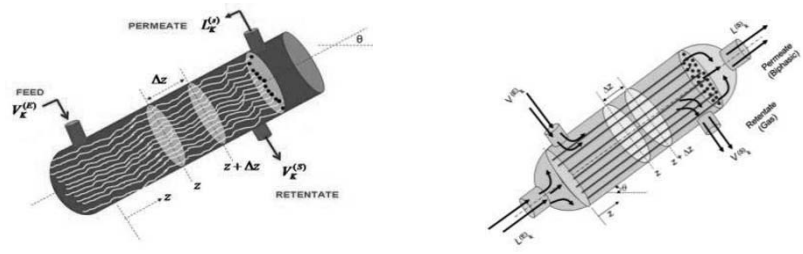

(a) (b)

Figure 3 – Equipment Schemes. (a) gas permeation module (b) gas-liquid contactor

4. Model Performance Evaluation

A process flowsheet - GN_CONTACT_1 - is used to illustrate the contactor simulator performance, shown in Figure 4, where MR1 and MR2 stand for Reacting Mixer and CGL is the gas-liquid contactor.

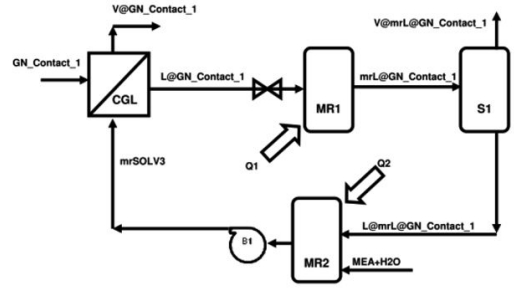

Figure 4 – CO_2 separation with Contactors

The feed stream GN_CONTACT_1 is Natural Gas with 10% of CO_2 to be purified with mrSOLV3, a stream containing an aqueous blend of MEA and MDEA. Table 1 shows a summary of stream inputs based in reported values by Formigli, 2008).

Table 1 - Summary of stream specifications and calculations for flowsheet GN_CONTACT_1

VARIABLES	STREAMS					
	GN_Contact_1	mrSOLV3	V@ GN_Contact_1	L@ GN_Contact_1	V@mrL@ GN_Contact_1	L@mrL@ GN_Contact_1
T(°C)	27	27	38.8	38.8	100.51	100.51
P(bar)	50	5	49.88	4.88	1.0	1.0
kg/h	42635	17651	33737	26549	13835	12714
MMNm³/d	1.000	---	0.829	---	0.291	---
%molCO2	10.19	0	3.49	0.437	24.895	0.096
%molCH4	73.22	0.024	76.52	0.02	33.616	0.021
%molC2H6	9.091	0.003	10.957	0.00	0.024	0.00
%molMEA	---	19.99	---	15.957	3.857	35.362
%molMDEA	---	19.99	---	11.171	0.07	49.444
%molH2O	---	59.98	---	50.595	37.523	14.482
%mol CO2H2OMEA	---	0.004	---	8.51	---	0.575
%mol CO2H2OMDEA	---	0.017	---	13.31	---	0.02
PROCESS VARIABLES						
MR1 - Q_1 (kW)	*MR2 – Q_2 (kW)*		*Make-up H2O (kg/h)*	*Make-up MEA (kg/h)*		
4300	-460		3675.3	1284.2		

Stream V@ GN_CONTACT_1 shows that the natural gas (NG) leaving the contactor meets specification on CO_2 content. Simulation results illustrate additional outputs that could support process design and optimization. Furthermore, results of the model, within a solid phenomenological framework suggest feasibility of innovative membrane contactor processes in meeting specifications of CO_2 removal from NG.

5. Conclusions

This work presents a tool to simulate processes based on innovative membrane contactors for CO_2 removal from natural gas streams. A process flowsheet employing gas-liquid contactor fed with gas stream compatible with the scenario of the Pre-Salt Pole of the Santos Basin in Brazil is presented. Simulation results show technical feasibility of this technology to offshore installations. The computational tool can be used for experimental design of pilot units to provide data for model calibration, to allow subsequent process design and optimization.

Acknowledgment

Financial support of MCT/FINEP/CTPETRO, Grant No.2460-06 is kindly acknowledged.

References

M.F. Alfradique, M. Castier, 2007, Calculation of Phase Equilibrium of Natural Gases *with the* Peng-Robinson and PC-SAFT Equations of State, Oil &Gas Science and Technology – Rev. IFP, Vol. 62, No. 5, pp. 707-714

L. C. Barbosa,; de Medeiros, J.L. ; Araujo, O. Q. F., Equilíbrio de Absorção de CO_2 e H_2S em Soluções Aquosas de Etanolaminas. Boletim Técnico da Petrobrás, v. 52, p. 21-37, 2011.

V.G. Dovi; F. Friedler; D. Huisingh; J.J. Klemes, 2009, Cleaner energy for sustainable future, J. Cleaner Production, v.17, p.889-895

A. D. Ebner, J. A. Ritter, 2009, State-of-the-art Adsorption and Membrane Separation Processes for Carbon Dioxide Production from Carbon Dioxide Emitting Industries, Separation Science and Technology, 44: 1273–1421.

J.Formigli, 2008, O Pólo Pré-Sal da Bacia de Santos – Desafios Tecnológicos para a Área de Engenharia,PETROBRAS, 2008.

P. Keshavarz, S. Ayatollahi, J. Fathikalajahi, 2008a, Mathematical modeling of gas–liquid membrane contactors using random distribution of fibers, J. Membrane Science, 325, p. 98–108.

P. Keshavarz; J. Fathikalajahi, S. Ayatollahi, 2008b, Analysis of CO_2 separation and simulation of partially wetted hollow fiber membrane contactor, J. Hazerd. Mater.,v. 152, p. 152, p. 1237-1247.

J.L. Medeiros. O. Q.F. Araujo. B. M. Versiani, 2008, Relatório 1 - Project Contact, Escola de Química, Universidade Federal do Rio de Janeiro, Brazil

Z. Nagy, A. Shirkovskiy, 1982, Mathematical Simulation of Natural Gas Condensation Processes Using the Peng-Robinson Equation of State, SPE Annual Technical Conference and Exhibition, 26-29 September 1982, New Orleans, Louisiana. 12 pages.

J.M.Prausnitz. R.N. Lichtenthaker. E.G. Azevedo, 1986, Molecular Thermodynamics of Fluid-Phase Equilibria. Englewood Cliffs, N.J., USA. 2° Edition, Prentice-Hall.

R. Rivera-Tinoco, C. Bouallou, 2010. Comparison of absorption rates and absorption capacity of ammonia solvents with MEA and MDEA aqueous blends for CO_2 capture, J. Cleaner Production, article in press.

H.Y.Zhang; R.Wang; D.T. Liang; J.H. Tay, 2006, Modeling and experimental study of CO_2 absorption in a hollow fiber membrane contactor. J. Membr. Sci., v. 279,p. 301-310.

I.A. Karimi and Rajagopalan Srinivasan (Editors), Proceedings of the 11th International Symposium on Process Systems Engineering, 15-19 July 2012, Singapore.

A Comparative Economical Analysis of Technologies for CO_2 Removal from Offshore Natural Gas

Tatiana S. Gadelha[a], Aline R. S. Guimarães[a], Andressa Nakao[a], Ofélia de Q. F. Araújo[a], José Luiz de Medeiros[a]

[a]*Departament of Chemical Engineering, Escola de Química da Universidade Federal do Rio de Janeiro. Sala R-201, Bloco E, Centro de Tecnologia, Ilha doFundão, CEP: 21949-900, Rio de Janeiro, Brazil*

Abstract

In the scenario of the Brazilian Pre-Salt fields, where associated Natural Gas (NG) shows high concentration of CO_2, gas conditioning comes out as one of the main challenges. Among the possible capture technologies available, three alternatives stand out for CO_2 sequestration: (A) gas permeation through membranes, (B) absorption columns using aqueous blends of ethanolamines and (C) application of hybrid - membrane modules in series with amine absorption and regeneration columns.

The main objective of this work is to investigate the technical and economical feasibility of applying these three separation processes on offshore platforms, given the stringent constraints on footprint and equipment weight, and for minimizing NG production and transportation costs. The methodology involves: (i) development of cases based on the Brazilian Pre-Salt gas composition. NG streams with CO_2 molar concentrations ranging from 8 to 18% are applied; (ii) Simulations of three process flowsheets, corresponding to each one of chosen technologies - A, B and C; (iii) Equipment sizing; and (iv) Analysis of economic performance through calculation of capital (CAPEX) and operational (OPEX) costs.

Keywords: CO_2, Natural Gas, Absorption, Gas Permeation

1. Introduction

In the scenario of the Pole Pre-Salt of the Santos Basin (Brazil) it has been discovered a large reserve of Natural Gas (NG) containing an expressive content of CO_2 (range: 8 to 18% mol) (Formigli, 2008). This concentration must be reduced to minimize the emission of CO_2 and to meet the National Agency of Petroleum and Biofuel (ANP) standards of marketing of NG in Brazil.

Currently, the main technologies used in industry are membrane modules and absorption equipments employing aqueous solutions of ethanolamines. Absorption of CO_2 with weak alkaline solvents is a well established technology in the chemical industry. The basic principle is a reversible chemical reaction occurring in the liquid phase between a weak alkali and the solutes (CO_2). The reaction is first impelled to solute consumption (i.e. absorption) capturing it from the raw gas stream. In the second step, the reaction is reversed releasing the separated solutes (i.e. stripping) as a gas product stream. This process involves the continuous operation of two interlinked (packing or tray) columns. The first column – the absorber – contacts the gas stream with lean solvent at moderately high pressures and moderately low temperatures. The

rich solvent (in terms of CO_2) goes to a second column – the stripper – where at expenses of lower pressures, higher temperatures and contact with a stripping agent (e.g. steam), acid gases are liberated in the top vapor product, while the lean solvent is recovered as bottom product and returned to the absorber after some cooling and making-up (Barbosa, 2010).

For gas separation in offshore platforms, membranes offer comparative advantages over other technologies – e.g. absorption and adsorption - such as: (i) process is simple requiring no heating for change in either phase, (ii) units are compact, low weight; and (iii) the modularity of membrane makes the process a flexible technology (Baker et al, 2008). These characteristics make the technology in permeation membranes more appropriate to the capture of CO_2 in offshore pre-salt conditions. However, a main obstacle to the use of membranes is the outstanding scale of separation processes required in Pre-Salt oil and gas offshore platformes, where it is possible that membrane processes lose selectivity due to high flows transfer.

This work presents a comparative economical analysis applying three separation processes on offshore platforms: (A) gas permeation through membranes, (B) absorption columns using aqueous blends of ethanolamines and (C) application of hybrid - membrane modules in series with amine absorption and regeneration columns, shown in Figures I, II and III respectively.

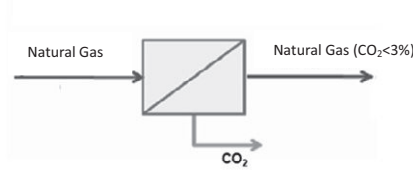

Figure I - Permeation system

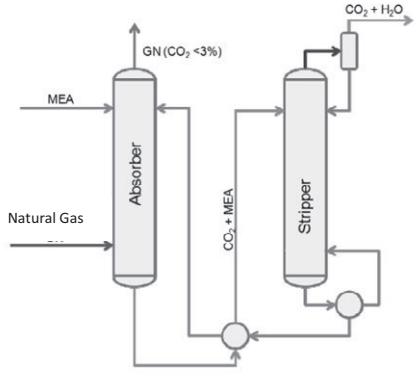

Figure II - Absorption Columns

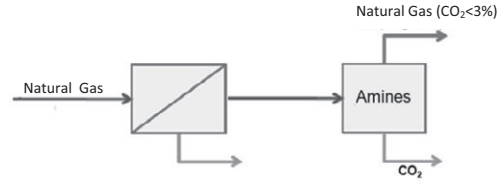

Figure III - Hybrid Process

2. Methodology

The methodology in this work deals with the following scenario:

- Development of three cases using NG streams with distinct CO_2 contents: Case 1: 8%; Case 2: 18%; and Case 3: 21%;
- Main goal of obtaining a NG stream with less than 3% of CO_2 (the standard of Brazilian Regulatory Agency);
- Operation flow is 50MMscfd;
- Three different technologies for CO_2 removal: Absorption using MEA; Membrane Permeation; and Hybrid process (Figure I, II and III);
- Processes simulations with a commercial simulator, employing a permeation module add-in developed by the Laboratory H2CIN, at Escola de Química, Universidade Federal do Rio de Janeiro, Brazil - The SPM2010 (Nakao, 2010);
- Equipment sizing.
- Calculation of Capital Expenditures (CAPEX) and Operational Expenditures (OPEX).

The economical analysis preformed is based on Turton *et al.* (2009), which was developed for chemical processes, therefore not including specifics features of the offshore environmental as modular equipments (skids), and restrictions of area and weight of these modules. However, it is emphasized that the goal of this work is the economical analysis and it is not the absolute quantification of the associated investments of each technology.

3. Results and Discussion

Compared to the absorption using amines, the hybrid process is a technology more flexible to different feeds conditions, as two different separation processes are employed.

For Cases 2 and 3, which have a process feed stream with higher CO_2 content, Baker and Lokhandwala (2008) recommend the hybrid process. In Case 1, with a feed stream with a lower concentration of CO_2, it is recommended the application of absorption column using amines. Because of this, hybrid process, in case 1, wasn't simulated.

These suggestions have been validated through the economical analysis of these three cases in this work, whose results are presented in Figure IV. The analysis shows that the flow rate and the CO_2 content have a direct influence in the technology selection for CO_2 removal.

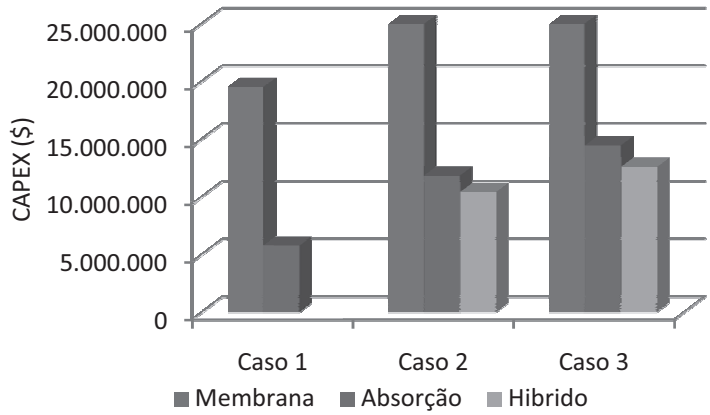

Figure IV - Capex results

Baker and Lokhandwala (2008) proposed a scheme, shown in Figure V, to guide the choice of CO_2 removal technology, based on the NG flow rate to be treated and the CO_2 content. In accordance to this scheme, this paper has conducted a preliminary economic analysis of these technologies for CO_2 removal.

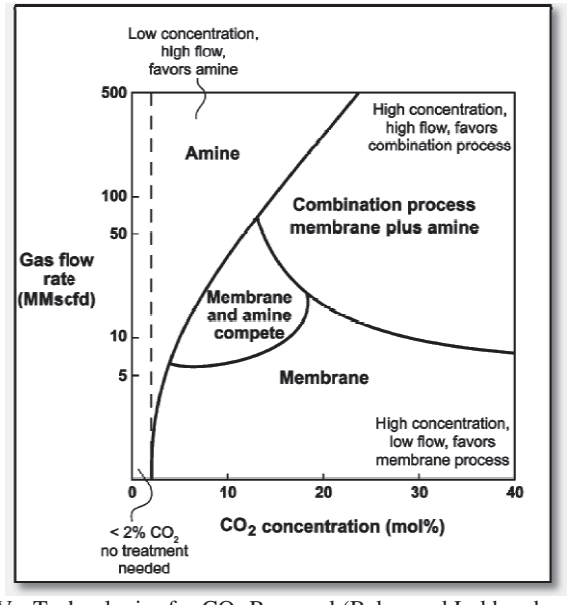

Figure V - Technologies for CO_2 Removal (Baker and Lokhandwala, 2008)

4. Conclusions

Absorption with amines showed the best results for streams with lower CO_2 content (Case 1), while hybrid process achieved better economical performance for NG streams with high concentrations (Case 2 and Case 3). These results arouse the interest in this process for the NG treatment, as proposed by Baker and Lokhandwala (2008).

5. References

R.W. Baker, K. Lokhandwala, 2008, Natural Gas Processing with Membranes: An Overview, Ind. Eng. Chem. Res., 47, p.2109-2121

L.C. Barbosa, 2010, Captura de CO_2 e H_2S com Soluções Aquosas de Alcanolaminas via Destilação Reativa; Ph.D. Thesis, Escola de Química,Universidade Federal do Rio de Janeiro.

J.M.Campbell, 2011, Gas Conditioning and Processing. Volume 2: The equipment Modules. Oklahoma: John M.Campbell and Company, 8th ed.

J.Formigli, 2008, O Pólo Pré-Sal da Bacia de Santos – Desafios Tecnológicos para a Área de Engenharia,PETROBRAS, 2008.

A. Nakao, 2010, Modelagem de Contactores Gás-Líquido para Separação de CO2 de Gás Natural com Solução Aquosa de Etanolaminas. Dissertação de Mestrado, TPQB, Universidade Federal do Rio de Janeiro

R.Turton, R. C,Bailie, W. B. Whiting, J.A. Shaeiwitz Analysis, 2002, Synthesis and Design of Chemical, Process, Prentice Hall, 2 edition

6. Acknowledgement

This work was done with the financial support from IBP - Brazilian Petroleum, Gas and Biofuels Institute and BG Group. The authors O.Q.F.Araujo and J. L. Medeiros kindly acknowledge MCT/FINEP/CTPETRO, Grant No.2460-06.

I.A. Karimi and Rajagopalan Srinivasan (Editors), Proceedings of the 11th International Symposium on Process Systems Engineering, 15-19 July 2012, Singapore.

A Systematic Approach for Optimization of an Algal Biorefinery Using Fuzzy Linear Programming

Aristotle T. Ubando[1a,c], Alvin B. Culaba[2a,c], Raymond R. Tan[3b,c],

Denny K.S. Ng[4d]

[a]*Mechanical Engineering Department, De La Salle University, Philippines*
[b]*Chemical Engineering Department, De La Salle University, Philippines*
[c]*Center for Engineering and Sustainable Development Research, De La Salle University, Philippines*
[d]*Department of Chemical & Environmental Engineering/Centre of Excelllence for Green Technologies, University of Nottingham, Malaysia*

[1]aristotle.ubando@dlsu.edu.ph, [2]alvin.culaba@dlsu.edu.ph, [3]raymond.tan@dlsu.edu.ph, [4]denny.ng@nottingham.edu.my

Abstract

In order to efficiently convert microalgae into value added products, a sustainable integrated algal biorefinery is needed. Generally, conversion of microalgae into biofuel involves several processing steps: cultivation, harvesting, dewatering, drying, oil extraction, and biofuel production. One of the main challenges in designing and optimizing an integrated algal biorefinery is determining the configuration which meets the requirements for key outputs as well as environmental and resource limits. In this work, a systematic fuzzy linear programming (FLP) approach for design and optimization of an integrated algal biorefinery which considers water footprint, land footprint, and carbon footprint is presented. A hypothetical case study is presented to illustrate the proposed approach.

Keywords: Microalgae, biofuel, biorefinery, fuzzy optimization, and process design.

1. Introduction

One of the most promising systems to convert microalgae into value-add products is the integrated algal biorefinery (IAB). An IAB combines multiple conversion pathways of microalgae to generate a range of products, such as biofuels and biochemicals (Taylor, 2008; Subhadra, 2010; Subhadra and Edwards, 2011; Tay et al., 2011a;). Such multiple pathways provide opportunities for effective utilization of process residues, thus enhancing the overall efficiency and sustainability of the biorefinery (Tan et al., 2009). Given the growing global demand for biofuels, it is necessary to assess the design of an IAB through three main environmental performance metrics: water foot print, land foot print, and carbon footprint (De Benedetto and Klemeš, 2009; Tan et al., 2009; Čuček et al., 2012). This paper presents an optimization approach for synthesis of an IAB using a fuzzy linear programming (FLP) model which considers the three main environmental performance metrics simultaneously.

2. Fuzzy Linear Programming

Fuzzy mathematical programming is used in optimization problems wherein bands of partially acceptable ranges of different objective values are considered (Zimmermann, 1978). FLP models have been used to solve multi-objective optimization problems for bioenergy systems footprint (Tan et al., 2008, Tan et al., 2009, Tay et al., 2011b). Unlike the conventional approach of identifying the Pareto optimal curve, FLP has the advantage of giving a unique solution. In this particular study, FLP approach is adapted to optimize an IAB which solves conflict of multi-objectives.

The optimization objective is to maximize the level of satisfaction (λ) of the fuzzy footprint goals:

$$\text{maximize } \lambda \tag{1}$$

Subject to:

$$\mu_i = [(f_i(x) - f_i^u) / (f_i^l - f_i^u)] \geq \lambda,\ i = 1, 2, 3 \tag{2}$$

$$f_i(x) = \boldsymbol{c_i}^T \boldsymbol{y},\ i = 1, 2, 3 \tag{3}$$

$$\boldsymbol{Ax} = \boldsymbol{y} \tag{4}$$

$$\boldsymbol{y^l} \leq \boldsymbol{y} \leq \boldsymbol{y^u} \tag{5}$$

where μ_i = degree of satisfaction of footprint goal i, $f_i(x)$ = footprint functions, i = individual footprint (i.e., water footprint, $f_1(x)$; land footprint, $f_2(x)$; and carbon footprint, $f_3(x)$), Besides, f_i^u and f_i^l are the lower and upper limits of the individual footprint i. $\boldsymbol{c_1}^T$ = water footprint coefficient vector, $\boldsymbol{c_2}^T$ = land footprint coefficient vector, $\boldsymbol{c_3}^T$ = carbon footprint coefficient vector, $\boldsymbol{A}$ is the input-output matrix , $\boldsymbol{x}$ is the process scaling vector, $\boldsymbol{y}$ is the net output vector, $\boldsymbol{y^l}$ is the lower limit for fuzzy net output vector, $\boldsymbol{y^u}$ is the upper limit for fuzzy net output vector.

The variable λ provides control to the model objective constraints which are described by the water, land, and carbon footprint that corresponds to the max-min aggregation principle (Zimmermann, 1978). The max-min aggregation ensures the optimal value of λ is the least satisfied considering the objective constraint. A value of $\lambda = 0$ indicates a state of minimum satisfaction, while a value of $\lambda = 1$ signifies a state of complete satisfaction. Partially acceptable values of λ lie in the range $0 \leq \lambda \leq 1$ as defined by the linear membership functions (Eq. 2) (Zimmermann, 1978; Lai and Hwang, 1992). Often used in a life cycle assessment, a modeling framework is used in this study based on a linear input-output (Eq. 3) (Heijungs and Suh, 2002).

Note that, unlike in Tan et al. (2008) and Tan et al. (2009); all values of $\boldsymbol{y}$ within the given limits are considered equally satisfactory for an IAB as indicated by Eq. (5). The values of the net output vector $\boldsymbol{y}$, which represents the production level of each of the outputs of the IAB, are flexibly set given a lower and upper limit.

3. Case Study

An IAB which produces biodiesel as the main product and methanol, glycerol, electricity as well as steam as by-products is used as a case study. Due to space constraints, the case study has been simplified. As biodiesel is taken as the main product, the algal residues are then separated and reprocessed to produce the by-products.

Environmental Metrics

Table 1 shows the water, land, and carbon footprint coefficients for the case study.

Table 1. Environmental metrics for the case study.

Environmental Metrics	Values
Water Foortprint	78 kg per kWh eletricity; 12,775 kg per kg algal biomass
Land Footprint	1.98×10^{-5} ha-y/ kg algal biomass
Carbon Footprint	1 kg per kWh electricity; 0.17 kg per kg steam; 3.5 kg per kg natural gas

Integrated Algal Biorefinery

The IAB can be divided into the following sections: A – Oil Extraction (including the microalgae cultivation, harvesting, and dewatering processes); B – Transesterification; C – Combined Heat and Power (CHP); D – Steam Methane Reforming (SMR); E – Residue Separator (which separates the liquid residue from the solid residue); F – Anaerobic Digester; G – Gasifier; and H – Methanol Synthesis.

In this case study, integrated algal biorefinery system consists of cultivation, harvesting, dewatering, and oil extraction of microalgae in Process A. Processes A and B can be used to extract algal oil for transesterification process to produce biodiesel. Note that a by-product glycerol is also generated in Process B. To simplify the model, these two processes can be taken as a single process unit. Process E then separates the liquid and solid residue fraction from the total algal residue from Process A. The liquid residue fraction is then processed in anaerobic digester (Process E) to produce methane which is fed into the combined heat and power (Process C) to generate electricity and steam. On the other hand, the solid residue fraction is fed into the gasifier (Process G) to produce syngas. Process D which is steam methane reforming also recycles part of the methane produced from Process E to produce syngas. The syngas produced in both Process G and D is then fed to methanol synthesis (Process H). Meanwhile, Processes G, D, and H were also combined to represent as a single cluster in the input-output matrix producing methanol from solid residue fraction of the microalgae.

Table 2. Algal Biorefinery Input-Output Coefficient Matrix.

y's	Input-Output Matrix	A-B	E	F	C	G-D-H
y_1	Microalgae (kg)	-4	0	0	0	0
y_2	Electricity (MJ)	-171	-1	-2.37	15	0
y_3	Steam (kg)	-161	-0.5	0	12.5	-0.74
y_4	Total Residue (kg)	3	-3	0	0	0
y_5	Solid Residue Fraction (kg)	0	0.6	0	0	-1
y_6	Liquid Residue Fraction (kg)	0	2.4	-2.4	0	0
y_7	Biodiesel (kg)	1	0	0	0	0
y_8	Glycerol (kg)	0.1	0	0	0	0
y_9	Methane (kg)	0	0	1.08	-1	-0.76
y_{10}	Methanol (kg)	-0.1	0	0	0	1.25

Table 2 shows the input-output coefficients of matrix A as derived from various literature sources (Singh and Gu, 2010; Khoo et al., 2011; Razon and Tan, 2011; Subhadra and Edwards, 2011; Tay et al., 2011a). Each column represents material and energy balances for a given process or cluster as discussed previously.

In the column vector, the negative values indicate the process inputs while the positive values are process outputs. For example, Figure 1 shows Process F in column vector form. The numbers indicate that 2.4 kg of liquid residue and 2.37 MJ of electricity are needed to generate 1.08 kg of methane for Process F.

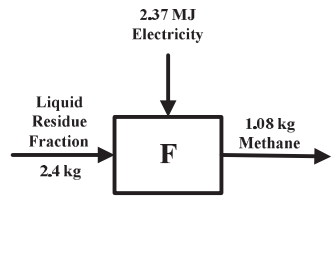

$$(A)\begin{pmatrix} 0 \\ -2.37 \\ 0 \\ 0 \\ 0 \\ -2.4 \\ 0 \\ 0 \\ 1.08 \\ 0 \end{pmatrix}$$

Figure 1. Example of column vector representation of a process.

4. Case Study Results and Discussion

Solving Eqn. (1) subject to Eqns. (2) – (5), the maximum λ is found as 0.95. Table 3 shows the optimized values for each desired outputs.

Table 3. Balanced process table for the optimal biorefinery configuration.

y's	Resulting Matrix	A-B	E	F	C	G-D-H	Net Outputs
y_1	Microalgae (kg/h)	-4,630	0	0	0	0	-4,630
y_2	Electricity (MJ/h)	-197,917	-1,157	-2,743	254,481	0	52,664
y_3	Steam (kg/h)	-186,343	-579	0	212,067	-514	24,632
y_4	Total Residue (kg/h)	3,472	-3,472	0	0	0	0
y_5	Solid Residue Fraction (kg/h)	0	694	0	0	-694	0
y_6	Liquid Residue Fraction (kg/h)	0	2,778	-2,778	0	0	0
y_7	Biodiesel (kg/h)	1,157	0	0	0	0	1,157
y_8	Glycerol (kg/h)	116	0	0	0	0	116
y_9	Methane (kg/h)	0	0	1,250	-16,965	-528	-16,243
y_{10}	Methanol (kg/h)	-116	0	0	0	868	752

As shown, it is noted that 4,630 kg/h of microalgae is used to produce 1,157 kg/h of biodiesel (via Processes A and B). On the other hand, the anaerobic digester (Process F) produces 1,250 kg/h of methane, which is then converted to electricity and steam in the combined heat and power system (Process C). Note that as the internally produced methane is insufficient to support the biorefinery, thus additional input of external methane (as natural gas) is needed. This external fossil-fuel supply adds to the IAB carbon footprint. Meanwhile, the resulting values of the water footprint, land footprint, and carbon footprint for the optimum case are 4.77×10^8 t/y, 792 ha-y, and 0 t/y; respectively. Note also that the resulting carbon footprint for the optimum case is 0 t/y since the negative carbon footprint from the export of electricity and steam offsets the carbon footprint required of the methane.

5. Conclusion

A fuzzy linear programming model has been developed to optimize the design of an integrated algal biorefinery. The model has been demonstrated for the case of an integrated algal biorefinery which produces biodiesel, glycerol, and methanol; as well as electricity and steam. Further work needs to be done in the future to include economic potential in the optimal design of IAB. Furthermore, fuzzy mixed integer linear programming approach with additional value-added products from microalgae such as bioethanol, biogas, and nutrient based-products are proposed for future studies.

Acknowledgement

The financial support of the University Research Coordinating Office of De La Salle University (Grant # 04 RPW AY11-12) and the Faculty Development Program of De La Salle University support of Ph.D. studies of the first author are gratefully acknowledged.

References

L. Čuček, J. Klemeš˘, Z. Kravanja, 2012, A Review of Footprint analysis tools for monitoring impacts on sustainability, Journal of Cleaner Production, (in press) DOI: 10.1016/j.jclepro.2012.02.036.

L. De Benedetto, J. Klemeš˘, 2009, The Environmental Performance Strategy Map: an integrated LCA approach to support the strategic decision-making process, Journal of Cleaner Production, Volume 17, pp. 900-906.

R. Heijungs, S. Suh, 2002, The Computational Structure of Life Cycle Assessment. (Kluwer, Dordrecht).

H.H. Khoo, P.N. Sharratt, P. Das, R.K. Balasubramanian, P.K. Naraharisetti, S. Shaik, 2011, Life cycle energy and CO2 analysis of microalgae-to-biodiesel: Preliminary results and comparisons, Bioresource Technology, Volume 102, pp. 5800–5807.

Y.J. Lai, C.L. Hwang, 1992, Fuzzy Mathematical Programming Methods and Applications, (Springer-Verlag, New York).

L.F. Razon, R.R. Tan, 2011, Net energy analysis of the production of biodiesel and biogas from the microalgae: *Haematococcus pluvialis* and *Nannochloropsis*, Applied Energy, Volume 88, pp. 3507-3514.

J. Singh, S. Gu, 2010, Commercialization potential of microalgae for biofuels production, Renewable and Sustainable Energy Reviews, Volume 14, pp. 2596-2610.

B. Subhadra, M. Edwards, 2011, Coproduct market analysis and water footprint of simulated commercial algal biorefineries, Applied Energy, Volume 88, pp. 3515-3523.

B. Subhadra, 2010, Sustainability of algal biofuel production using integrated renewable energy park (IREP) and algal biorefinery approach, Energy Policy, Volume 38, pp. 5892-5901.

R.R. Tan, A.B. Culaba, K.B. Aviso, 2008, A fuzzy linear programming extension of the general matrix-based life cycle model, Journal of Cleaner Production, Volume 16, pp. 1358-1367.

R.R. Tan, J.B. Ballacillo, K.B. Aviso, A.B. Culaba, 2009, A fuzzy multiple-objective approach to the optimization of bioenergy system footprints, Chemical Engineering Research and Design, Volume 87, pp. 1162-1170.

D.H.S. Tay, D.K.S. Ng, H. Kheireddine, M.M. Ell-Halwagi, 2011a, Synthesis of an integrated biorefinery via the C-H-O ternary diagram, Clean Technologies and Environmental Policy, Volume 13, pp. 567-579.

D.H.S. Tay, D.K.S. Ng, N.E. Sammons, M.R. Eden, 2011b, Fuzzy optimization approach for the synthesis of a sustainable integrated biorefinery, Industrial and Engineering Chemistry Research, Volume 50, pp. 1652-1665.

G. Taylor, 2008, Biofuels and the biorefinery concept, Energy Policy, Volume 36, pp. 4406-4409.

H.-J. Zimmermann, 1978, Fuzzy Programming and Linear Programming with Several Objective Functions, Fuzzy Sets and Systems, Volume 1, pp. 45-55.

I.A. Karimi and Rajagopalan Srinivasan (Editors), Proceedings of the 11th International Symposium on Process Systems Engineering, 15-19 July 2012, Singapore.

Process Analysis Using *Umberto Carbon Footprint* Tool

Pedro Chainho[a], Henrique A. Matos[a]

[a]*CPQ, Department of Chemical Engineering, Instituto Superior Técnico, Av. Rovisco Pais, 1049-001, Lisboa, Portugal*

Abstract

The software Umberto Carbon Footprint calculates CO_2 footprint of products or activities. It is based on analysis of primary and secondary footprints during the product lifecycle. It uses the ecoinvent database to analyse individual contribution of the resources consumption required for the footprint of the final product.

Umberto Carbon Footprint was applied to two processes where the streams and resources were characterized using the process simulator Aspen Plus: A) production of cumene from benzene and B) production of acetone from IPA (Isopropyl alcohol). The analysis was carried out for each process at two different scenarios (with and without simplified energetic integration).The results show an improvement on the carbon footprint value for the scenarios with energetic integration and a good agreement with ecoinvent database values

Umberto Carbon Footprint was also applied at one Portuguese chemical company to a formaldehyde process (patent Perstorp Formox®). Real industrial data was used on the streams and resources characterization. The carbon footprint obtained for F-100 (maximum production system scenario) shows a relative deviation of 1.8% comparing to ecoinvent database value.

Keywords: Modeling, Carbon Footprint, Umberto software, Industrial Process.

1. Introduction

Carbon footprint is a relative measurement of the amount of CO_2 release on the environment during the life cycle of a product or activity. Normally it's calculated from the analyses of direct and indirect emissions of resources consumed on a certain process. All streams of the industrial process must be previously characterized by a process simulation or using the industrial data. This tool could help in the discussion of different operating conditions scenarios, such as raw material diversity, process integration degree, utilities type, among others.

Nowadays this issues is has become increasingly important, and big supermarkets chains in UK and USA were wondering about putting the CO_2 footprint on the products descriptions labels, granting to the consumer the option of a more responsible choice in terms of ecologic matter.

The methodologies for carbon footprint calculations are still growing and it is emerging as an important tool for sustainability analysis. The concept of carbon footprinting has permeated and is being commercialized in all the areas of life and economy, but there is little coherence in definitions and calculations of carbon footprints among the studies. Carbon footprint is intended to be a tool to guide the relevant emission cuts and verifications, its standardization at international level are therefore necessary. Pandey et al. (2011) made a review where they describe the prevailing carbon footprinting

methods and raise the related issues. Some studies are being made as calculation of the corporate carbon footprint of the cement industry by MC3 methodology by Cagiao, et al. (2011). Yuttitham, et al., (2011) determined the carbon footprint of sugar produced from sugarcane in eastern Thailand. Graphical representation of carbon footprint reduction for chemical processes was applied by Tjan et al. (2010).
In this paper the carbon footprint calculation and analysis of chemical products with the application of software Umberto for Carbon Footprint using simulation and real industrial data.

2. Process simulator approach

2.1. Cumene process
Cumene is produced from a reaction in gas phase between benzene and polypropylene, with a main reaction (1) and parasite one (2):

$$\text{Propylene} + \text{Benzene} \longrightarrow \text{Cumene} \quad (1)$$

$$\text{Propylene} + \text{Cumene} \rightarrow \text{P} - \text{diisopropil benzene} \quad (2)$$

It was considered a minimum annual production of 120 kton of cumene with a specification of 99% in molar purity without any kind of heat integration (Scenario 1).

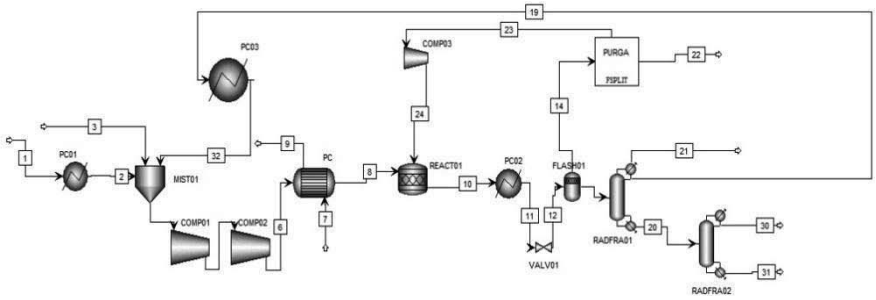

Figure 1: Cumene Process diagram in AspenPlus®. (Scenario 1)

An alternative diagram was tested with a simple energy integration of reactor effluent as hot fluid on exchanger named PC (Scenario 2).The hot utility used in Figure through stream 7 was removed.

Table 1: CO_2 Footprint and main contributions for the cumene process

Carbon Footprint (kg CO2 eq.)	
Scenario 1	Scenario 2
3.74	3.48

Contributions for the footprint			
Scenario 1		Scenario 2	
Benzene	65%	Benzene	70%
Propylene/ Propane	21%	Propylene/ Propane	22%
Others	14%	Others	8%

As expected it was noted an improvement of the CO_2 footprint of the process with simple energy integration that corresponds to a decreasing of 7% of the CO_2 footprint. The contribution of field "Others" (table 2) was smaller in the integrated process because this field includes the consumption of energetic resources that were reduced with the energetic integration.

2.2. Acetone process

The process of production of acetone from IPA contains a main reaction (3) and 2 other parasite ones (4) and (5).

$$\text{Isopropanol} \rightarrow \text{Acetone} + \text{Hydrogen} \quad (3)$$

$$\text{Isopropanol} \rightarrow \text{Propylene} + \text{water} \quad (4)$$

$$\text{Propylene} + \text{Hydrogen} \rightarrow \text{Propane} \quad (5)$$

It was considered a minimum annual production of 120 kton of acetone with a specification of 99% in molar purity (Scenario 1).

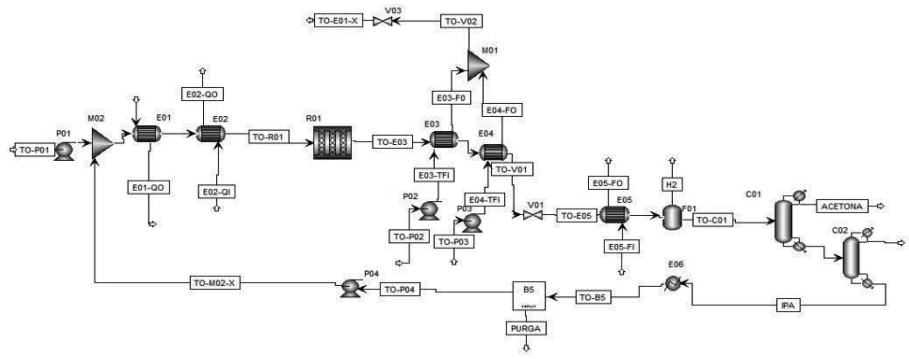

Figure 2: Acetone process diagram in AspenPlus®. (Scenario 1)

Also an alternative scenario was tested with simple energy integration. It was produced steam on the exchangers E03 and E04 and was recirculated to E01 (Scenario 2).

Table 2: CO_2 Footprint and main contributions for the acetone process

Carbon Footprint (kg CO_2 eq.)	
Scenario 1	Scenario 2
3.11	2.95

Contributions for the Footprint			
Scenario 1		Scenario 2	
IPA	77%	IPA	81%
Net steam	14%	Net steam	15%
Others	9%	Others	4%

The result is analogous of the previous process. It was verified a footprint decreasing of 5%.

3. Chemical Plant Data aproach

The carbon footprint calculation using the software Umberto for Carbon footprint is also applied to a real chemical plant data, instead of the previous approach where data was obtained by simulation with a process simulator.

This approach was applied to a process of production of formaldehyde type Perstorp Formox® of a Portuguese chemical industry. The formaldehyde production occurs on a fixed bed reactor through the partial oxidation of methanol.

The main reaction is strongly exothermic, and the heat of reaction is used to produce steam in exchanger E-2/1. The units E-18, E-22 and E-15/1 constitute the emission control system (ECS) which control the gas emissions to the atmosphere.

The equipment and streams before T-1 and T-2 are double and work in parallel, system-1 (S-1) and system-2 (S-2). The main product (F-50) is collected in T-2 and the Product F-30 on T-1.

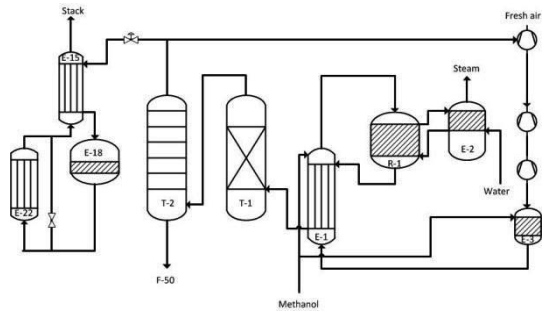

Figure 3: Simplified formaldehyde process diagram based on the Industrial site analysed.

Several production scenarios were tested:

- Scenario **3500-0**: Minimum production status, S-1 with a fresh methanol consumption of 3500 kg/h and S-2 stopped with only F-100.
- Scenario **0-4900** : S-2 with a fresh methanol consumption of 4900 kg/h and S-1 stopped;
- Scenario **3500-3500 :** S-1 with a fresh methanol consumption of 3500 kg/h and S-2 with a fresh methanol consumption of 3500 kg/h;
- Scenario **4900-4600:** S-1 with a fresh methanol consumption of 4900 kg/h and S-2 with a fresh methanol consumption of 4600 kg/h.

The scenarios with higher productions rates are the ones with smaller footprint. The carbon footprint is analysed by kg of product produced and is strongly dependent of the raw-materials utilization, and consequently in terms of process efficiency, so is expectable smaller footprints for those scenarios because they are the most efficient ones (also in observed in economical terms).

Table 3: CO_2 footprint of formaldehyde process – F100 and F-30

Methanol Consumption				
Scenario	S-1 (kg/h)	S-2 (kg/h)	CO_2 footprint (kg CO_2 eq.) F-100	CO_2 footprint (kg CO_2 eq.) F-30
3500-0	3500	0	1.11	-
0-4900	0	4900	1.22	9.91
3500-3500	3500	3500	1.07	13.45
4900-4600	4900	4600	1.09	16.49

It is predicted by ecoinvent 2.2 a carbon footprint for a formaldehyde process type Perstorp Formox® of 1.11 kg CO2 eq., for a maximum production system. Comparing this one with the value for scenario 4900-4600 is observed a relative deviation of 1.8%. The cause of deviation is explained by some differences in the calculation by ecoinvent and this one:

- Input values in ecoivent are from literature and project predicted values of several European production units.

- The ecoinvent footprint considers the contribution of final product transportation and in this project the formaldehyde was for own consumption.
- Ecoivent value uses input values from another process patent (silver catalysis) in addition to the patent Perstorp Formox®.
- Contribution of catalyst for the footprint is higher in ecoinvent because of a more regular replacement is used on the units analyzed.

Table 4: Individual contributions of Carbon footprint : F-100 and F-30

Contributions for the footprint								
Scenario	**3500-0**		**0-4900**		**3500-3500**		**4900-4600**	
	F-100	F-30	F-100	F-30	F-100	F-30	F-100	F-30
Methanol	73.3%	-	78.8%	78.9%	82.7%	83.2%	84.7%	84.5%
Electricity	3.5%	-	5.0%	4.3%	5.2%	4.2%	5.6%	6.0%
Chemical plant infrastructure	8.3%	-	6.1%	6.9%	5.2%	5.1%	3.4%	3.9%
Stack emissions	13.3%	-	9.1%	9.6%	6.9%	7.2%	5.1%	5.4%
Others	1.5%	-	1.1%	0.3%	0.1%	0.3%	1.2%	0.3%

Other causes of deviation lies on some approximations used in the footprint calculations as the assumption of CO_2 stack emissions similar for all scenarios tested and on the estimation of cooling water flows. In the future a deeper analysis will be done to overcome some practical difficulties encountered.

4. Conclusions

The Umberto for Carbon Footprint allows two different approaches for calculation of chemical processes footprints. With auxiliary data obtained for instance in a process simulator or plant data, the software becomes very easy and quick to use. The results obtained in this work show a good agreement with the ones from ecoinvent data base. In the future this contribution could be integrated with SustainPro® tool (Carvalho et al., 2008) to provide a more reliable sustainability analysis. It seems to be also an important tool to compare different process design scenarios.

References

http://www.ecoinvent.org/database/, accessed in 18/08/2011

Cagiao J., Gómez, B., Doménech, J. L., Mainar, S. G., Lanza, H. G., Calculation of the corporate carbon footprint of the cement industry by the application of MC3 methodology, Ecological Indicators, 11(6), 2011, 1526-1540

Carvalho, A., Matos, H. A., Gani. R., Design of Sustainable Chemical Processes: Systematic Retrofit Analysis Generation and evaluation of alternatives, Process Safety and Environmental Protection, 86, 2008, 328–346

Pandey, D., Agrawal, M., Pandey, J.S., Carbon footprint: current methods of estimation, Environmental Monitoring Assessment 178, 2011, 135–160

Tjan W., Tan, R. R., Foo, D.C.Y., A graphical representation of carbon footprint reduction for chemical processes, Journal of Cleaner Production, 18 (9) 2010, 848-856

Yuttitham, M., Gheewala, S. H., Chidthaisong, A., Carbon footprint of sugar produced from sugarcane in eastern Thailand, Journal of Cleaner Production, 19(17-18) , 2011, 2119-2127

I.A. Karimi and Rajagopalan Srinivasan (Editors), Proceedings of the 11th International Symposium on Process Systems Engineering, 15-19 July 2012, Singapore.

Efficient configuration/design of solvent-based post-combustion carbon capture

Zhengxiong Li, Rajab Khalilpour, Ali Abbas*

School of Chemical and Biomolecular Engineering,
The University of Sydney, Sydney, Australia
**Tel: +61 2 9351 3002; Fax: +61 2 9351 2854; E-mail: ali.abbas@sydney.edu.au*

Abstract

In this study, we analyze two design configurations for post-combustion carbon capture (PCC) namely inter-stage cooling and split flow. The results show that inter-stage cooling configuration has notable impact on improving PCC performance. It is found that, for a flue gas with 13.0 mol% of CO_2, and with objective of capturing 90% of CO_2 at purity of 98%, base case configuration imposes a 4.7GJ/ton-CO_2 reboiler duty. This energy burden decreases (about 34.8%) to 3.1 GJ/ton-CO_2 with single-stage cooling configuration. Two-stage-cooling configuration further improves the efficiency but only incrementally. Similarly, split flow design configuration shows considerable improvement in efficiency (3.8GJ/ton-CO_2 vs. 4.7GJ/ton-CO_2 for base case).

Keywords: Post-combustion carbon capture (PCC), inter-stage cooling, split flow.

1. Introduction

Solvent based PCC was evaluated by Metz et al. (2005) and described as the most mature technology for commercial scale industrial carbon capture from power plants' flue gas. The standard carbon capture process is illustrated in *Fig.1*. A stream of amine solution is continuously recycled between absorption and desorption units where the lean stream removes the CO_2 from the bulk flue gas in an absorber column and the rich stream is regenerated in the stripper column.

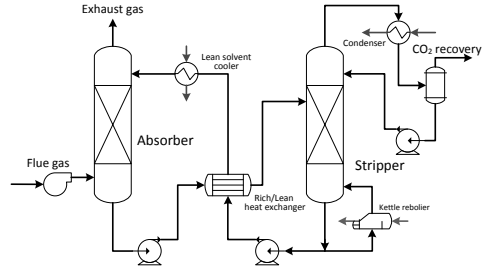

Fig.1: Schematic of standard post-combustion carbon capture process.

Despite recent progress in solvent-based PCC, the implementation of this technology still burdens a notable energy penalty mainly due to solvent regeneration. The energy penalty though varies by the type of power plant and by different techno-economic studies, is estimated to be above 20% (Khalilpour and Abbas 2011). This inevitably leads to a significant reduction in the power plant's load. The critical parameters influencing the efficiency are solvent type, solvent concentration, operating conditions

of absorption/desorption columns, percentage of CO_2 avoided, captured CO_2 purity and amount of regeneration. There are extensive research to study the impact of these parameters and their potential process improvements.

Configuration of absorption-desorption processes is also an important factor. In a conventional PCC scenario, gas enters at the bottom of the column and exists from the top. This traditional design does not exploit potential heat integration possibilities of the exothermic/endothermic absorption/desorption operation. Therefore, application of conventional simple column coupling configurations results in inefficient performances of both absorber and desorber. This leads to higher capital and operating costs. Recent studies see great potential for energy savings by introducing flow sheet innovations. Cousins et al. made an overview of several proposed configurations for PCC (Cousins et al. 2011). The purpose of this paper is to assess two improved flow schemes: Inter-stage cooling and split flow, validating their potential in relieving the energy penalty on a basis of 30wt% MonoEthanolAmine (MEA) being employed as the absorbent. Process flow diagrams of inter-stage cooling and split flow are presented in *Fig.2*. Aspen HYSYS V7.1 is used in this study.

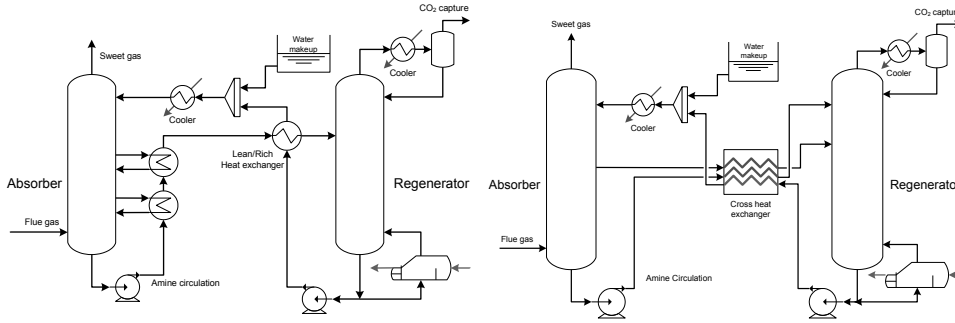

Fig. 2: Process flow diagram for (left) inter-stage cooling scheme, and (right) split flow scheme.

2. Process simulation

2.1. Fluid package

A reliable fluid package is the basis of simulation and its competency can be verified by comparing the predicted solubility of CO_2 with experimental data. Jou et al. (1995) experimentally measured the solubility of CO_2 in 30 wt% MEA solution by relating the CO_2 loading to its partial pressure. Case studies of CO_2 solubility were carried out using Amine pkg, Electrolyte NRTL respectively.

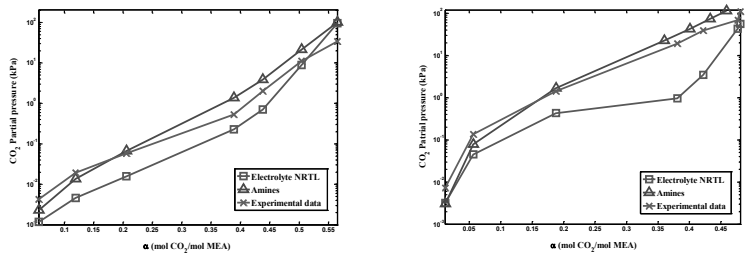

Fig.3: Validation of simulation fluid packages in terms of CO_2 solubility in 30 wt% MEA solution at (left) 60°C, and (right) 100°C.

2.2. Base case specification

The base case model was designated to achieve 90% of CO_2 removal and 98% purity of CO_2 captured. The critical operating conditions and equipment parameters are listed in *Table 1*. The composition of flue gas was set to be 12.99 mol%, after Khalilpour and Abbas (2011).

Table 1: Absorption/desorption column specifications.

Absorber		
Item	**Value**	**Reference**
Tray No.	10	
Tray Efficiency (%)	25	(Øi 2007)
Temperature (°C)	50	(Cousins, Wardhaugh et al. 2011)
Pressure (kPa)	101.3	
Stripper		
Item	**Value**	**Reference**
Tray No.	6	
Tray Efficiency (%)	50	(Øi 2007)
Reboiler pressure (kPa)	200	(Abu-Zahra, Schneiders et al. 2007)
Feed position	2	
Feed condition	Saturate liquid	

2.3. Inter-stage temperature control

The optimal temperature range for CO_2 absorption is 40-60°C since the reaction rate is highest within this range for 30 wt% MEA (Cousins et al. 2011). However the exothermic effect can raise this temperature beyond 70°C and away from the theoretical equilibrium limits, thus lowering the absorption capacity of MEA. Maintaining the temperature along the column within its optimal range could enhance the absorption performance. This idea can be realized by withdrawing a hot stream out of the column's top section (say at the third plate) and cooling it with the bottom product which is around 54°C. The cooled stream is then returned to a position below the withdrawal location (say at the fourth plate). This brings the bottom lean stream closer to the feed condition of the stripper. A temperature control strategy can further enhance the process by implementing multi-stages of cooling. In this simulation work, the side draw streams are extracted from the third and sixth trays separately and sent back to the fourth and seventh trays, respectively, after being cooled down.

2.4. Split flow

A split flow configuration provides a reduced flow to the lower section of the stripper where it can be recycled to a lower CO_2 content with the same energy input. The semi-lean solution extracted from the mid-section of the stripper removes the bulk CO_2 passing through the lower section of the absorber where partial pressure of CO_2 is sufficiently high to provide a large driving force. A side draw stream, the semi-rich amine, is extracted from the fifth plate of the absorber and sent to a cross heat exchanger where it is heated up by stripper bottom product as well as the lean amine stream from the bottom of the absorber. Then, the semi-rich amine is fed to the stripper at the fourth plate. The flow rate and the tray position where side stream is drawn from the absorber were determined by trial and error. The properties of concerned amine streams are tabulated below.

Table 2: Properties of the main process streams.

Stream properties in standard flow sheet				
	Flow rate	Temp. before HX	Temp. after HX	Loading
	tonne/hr	°C	°C	mole CO_2/mole MEA
Rich	5209	52.3	108	0.448
Lean	4980	121.3	165.5	0.241
Stream properties in split flow configuration				
	Flow rate	Temp. before HX	Temp. after HX	Loading
	tonne/hr	°C	°C	mole CO_2/mole MEA
Rich	3875	37.1	95	0.508
Semi-rich	1197	67.4	100	0.310
Lean	4843	120.7	73.6	0.252

3. Simulation Results

3.1. Temperature profile along the absorber

From *Fig.*4, it is observed that the inter-stage cooling configuration significantly levels the parabola-shaped temperature profile of the base case. It extends almost horizontally throughout the first four plates since the hot solution to be cooled down is withdrawn from the third plate. The process target is to achieve 90% of carbon capture and the ratio of amine solution to flue gas (L/G) in wt./wt. was set to be around 20. Similarly, but not as significant as inter-stage cooling, implementation of split flow also relieves the high temperature within the column (*Fig.*4).

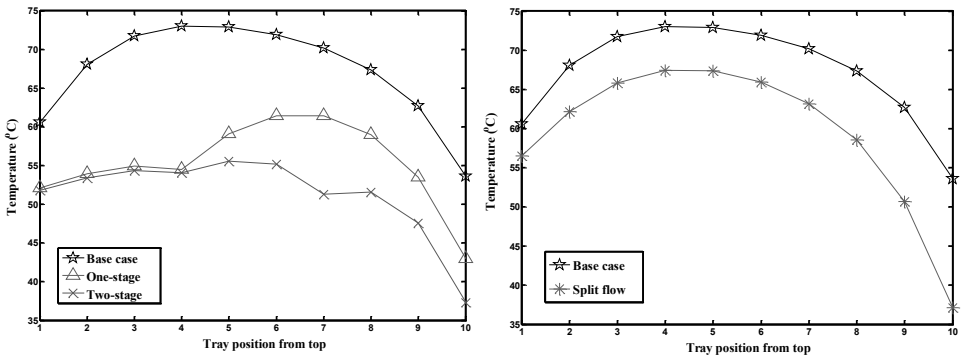

Fig.4: Temperature profile for (left) inter-stage cooling, and (right) split flow.

3.2. Improved performance in energy savings

Intensive reboiler energy consumptions in terms of GJ per tonne-CO_2-captured for base case and the new configurations were compared on a consistent basis. From Table 3, one-stage temperature control has effectively reduced the energy penalty for amine regeneration by 34.8% and split flow 18.5%.

Table 3: Reboiler duties for base case, inter-stage cooling and split flow configurations.

	L/G (tonne/tonne)	Carbon capture (%)	**Reboiler duty(GJ/tonne)**
Base Case	20.25	90.09	**4.696**
One-stage inter-cooling	20.27	90.04	**3.062**
Split Flow	20.27	90.07	**3.828**

*Fig.*4(left) shows that two-stage cooling allows a better temperature control where it has been kept below 55°C. The performances of one-stage and two-stage in terms of carbon capture with equivalent reboiler duty are compared in Table 4. With the implementation of multi-stage cooling, it yielded around 1% higher carbon capture rate with the same reboiler duty than that of single stage. These results agree well with the predicted temperature profile of *Fig.*4.

Table 4: Carbon capture rates of one-stage and two-stage inter-cooling.

	L/G (tonne/tonne)	Reboiler duty (GJ/tonne)	**Carbon capture (%)**
One-stage inter-cooling	20.25	3.008	**91.06**
Two-stage inter-cooling	20.24	3.015	**92.32**

4. Conclusion

Alternative process flowsheet models were simulated and analyzed for PCC operations. The performances with and without design changes were evaluated and analyzed on a consistent basis (90% of CO_2 removal and 98% purity of CO_2 captured). From the simulation results, we found great potential for reducing the energy consumption in PCC via the process design configurations of inter-stage cooling and split flow. Compared to the base case, both inter-stage cooling and split flow schemes successfully relieve the exothermic effect during the reaction process within the column and therefore enhance the absorption. One-stage cooling reduces the reboiler energy consumption by 34.8% while split flow reduces 18.5%. A two-stage cooling configuration was also simulated to study the performance of multistage cooling and showed 1% rise in carbon capture rate under equivalent energy consumption.

References

M. R. M. Abu-Zahra, , L. H. J. Schneiders, et al., 2007, CO2 capture from power plants. Part I. A parametric study of the technical-performance based on monoethanolamine, International Journal of Greenhouse Gas Control 1,1, 37-46.

A. Cousins, L. T. Wardhaugh, et al., 2011, A survey of process flow sheet modifications for energy efficient CO2 capture from flue gases using chemical absorption, International Journal of Greenhouse Gas Control, 5,4, 605-619.

F.Y. Jou, A. E. Mather, et al., 1995, The solubility of CO2 in a 30 mass percent monoethanolamine solution, The Canadian Journal of Chemical Engineering, 73, 1, 140-147.

R. Khalilpour, A. Abbas, 2011, HEN optimization for efficient retrofitting of coal-fired power plants with post-combustion carbon capture, International Journal of Greenhouse Gas Control, 5, 2, 189-199.

B. Metz, O. Davidson, et al., 2005, IPCC special report on carbon dioxide capture and storage, Cambridge, Cambridge University Press, for the Intergovernmental Panel on Climate Change.

L. E. Øi, 2007, Aspen HYSYS Simulation of CO2 Removal by Amine Absorption from a Gas Based Power Plant, SIMS2007 Conference, Gothenburg, Sweden.

I.A. Karimi and Rajagopalan Srinivasan (Editors), Proceedings of the 11th International Symposium on Process Systems Engineering, 15-19 July 2012, Singapore.

Effect of the microfiltration phase on pervaporation of ethanol produced from banana residues

Roger H. Bello, Ozair Souza, Noeli Sellin, Sandra H. W. Medeiros, Cintia Marangoni

University of Joinville Region (UNIVILLE) - Chemical Engineering Department, Rua Paulo Malschitzki 10 Zona Industrial, Joinville-SC 89219-710, Brazil;

Abstract

The objective of this paper is to investigate the use of microfiltration as a process of suspended solids separation in the pervaporation of bioethanol produced by banana culture residues. The composition of the fermentative broth influences on the separation, and the use of different substrates lead to a revaluation of the process, even if this is well established. Therefore, the ethanol pervaporation was studied by using polydimethylsiloxane membranes with binary mixtures (ethanol and water) as well as with fermentative broth. The fermentative broth pretreatment through microfiltration was compared to its centrifugation. It was possible to observe the reduction of the permeate flow rate, however the increasing in parameters such as the enrichment factor and the ethanol concentration in the permeate was also seen when the microfiltration was employed, comparing to the centrifugation as well as to the binary mixture.

Keywords: bioethanol, microfiltration, pervaporation, lignocellulosic residues.

1. Introduction

The need to amplify the offer of raw material for the production of ethanol without causing damage the planted areas for food, is the main factor of the development of researches using different residues for the ethanol production [1,2]. Several studies approach the use of agricultural or forest waste for the ethanol production [3]. Known as residual biomass, sugarcane bagasse and straw, or corn stover and fiber, wheat and rice straws, eucalyptus wood and residues of culture of fruits like bananas, grapes and apples are good examples. In the case of banana, although they are few, the applications are through the use of the fruits, leaves and other residues such as the stem [4].

Although the researches using banana residues show the viability of the fermentation process and consequent production of alcohol, it is important to emphasize that they are focused on the study of the hydrolysis [5] and a few of the others phases are evaluated, such as the ethanol recuperation. The use of distillation is a challenge due to its cost and the high energetic expenses [4,6]. In this context, the process of separation through pervaporation presents many advantages, because of the simplicity of its operation, use of low amounts of energy, low operational cost besides reducing the inhibition of ethanol on the fermentation [7].

Continuous fermentation processes with distillation through membranes have stood out due to the fact that they are, energetically speaking, more advantageous processes when compared to the traditional ones [8]. In this area, in the past few years pervaporation has became an alternative because of the possibility of being used coupled to the

fermentation [9,10]. However, the integrated process of fermentation and separation of the ethanol through pervaporation demands a phase of cell separation which is commonly carried out through microfiltration. There are many difficulties associated to this coupled design, related to low flows and selectivity because of the pore obstruction of the microfiltration membranes and to the swelling of the pervaporation membranes due to the presence of solids of the broth [11].
In addition, the composition of the fermentative broth influences on the separation and, the use of different substrates leads to the need of reevaluation of the process, even if it is already well established [12]. Therefore, a study of the separation of the bioethanol obtained from the residues of banana culture, employing pervaporation with commercial membranes of polydimethylsiloxane (PDMS) is proposed, aiming to evaluate the effect of the microfiltration phase as a process of separation of the solid material.

2. Materials and methods

In order to evaluate the proposal of this paper, preliminary experiments were conducted with an ethanol-water model binary mixture. This mixture was used as a pattern to analyze the results. Then, tests with the fermentative broth produced from the residues of banana pulp as a substrate were carried out. The amount of ethanol obtained in the broth was approximately 3% in mass. Two processes were compared for the cell and particulate material separation prior to the pervaporation: centrifugation and microfiltration.
The pervaporation process performance was expressed in terms of selectivity of the membrane (α) and mass flow of the permeate (J), according equations 1 and 2, where, W is the mass (g) of the permeate, A is the membrane´s effective area (m²) and, τ is the time interval (h) of the pervaporation process; y_i and y_j are the mass fractions of ethanol and water on the side of the permeate and x_i and x_j are the mass fractions of ethanol and water on the feed respectively.

$$\propto_{EtOH} = \frac{{}^{y_i}/_{y_j}}{{}^{x_i}/_{x_j}} \qquad \textit{Eq.}\ (1)$$

$$J = \frac{W}{A.\tau} \qquad \textit{Eq.}\ (2)$$

Another parameter used consisted of the enrichment factor - β_{EtOH} (Equation 3) which investigates the influence of other components on the ethanol enrichment in the permeate comparing to the feed. Yet, the index of separation through pervaporation – PSI (Equation 4) is determined by the properties of the membranes permeation and selectivity. $W_{EtOH,p}$ is the ethanol mass fraction in the permeate and $W_{EtOH,f}$ in the feed; J is the mass total flow (g/m².h) and, α the membrane´s selectivity.

$$\beta_{EtOH} = \frac{W_{EtOH,p}}{W_{EtOH,f}} \qquad \textit{Eq.}\ (3)$$

$$PSI = J.\alpha \qquad \textit{Eq.}\ (4)$$

2.1. Pervaporation

The pervaporation unit consists of a permeation removable module in PVC, with hollow membranes made of poly(dimethylsiloxane) - PDMS (PAM-PV S 0.01/PAM-Membranes), containing 50 capillaries with area of 0.04 m². The fermented broth or the model solution at approximately 22 ºC was fed with flow rates of 20 $L.h^{-1}$ from a 1 L reservoir, positioned upward the membrane, through a gear pump FE 611 (B. Braun). The vacuum pump DV 142N 250 (J/B Industries), on the permeate side, provided the pressure drop for the bioethanol vaporization (permeate pressure was lower than 5 mmHg). The vapor of permeate was collected into a reservoir refrigerated by cryogenic bath at -196 ºC, containing liquid nitrogen, for condensation. The simplified scheme of the pervaporation unity is shown in Figure 1.

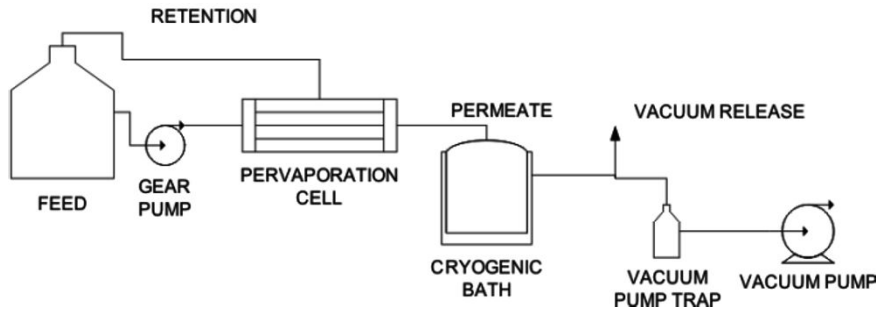

Figure 1 – Pervaporation process scheme.

The tests were carried out in duplicate, and the results presented consist on their averages. From each test, feed samples at the beginning and at the end of each experiment were taken, as well as the permeate in order to quantify the ethanol concentrations in gaseous chromatograph (GC).

2.2. Microfiltration

In natura fermented broth at environment temperature was fed from a 1 L reservoir, positioned before the membrane, by a gear pump FE 611 (B. Braun) at 90 $L.h^{-1}$. The concentrated returned to the feed in the whole microfiltration process. The microfiltration module is also made of PVC (membranes PAM) and has poly(imide) hollow membranes, with a 0.08 m^2 membrane area.

3. Results and discussion

The results obtained for the pervaporation of the ethanol and water binary model mixture are shown in Table 1. In Figure 2 the results of the flow parameters, enrichment factor and ethanol mass concentration in the permeate when centrifugation and microfiltration were used as a pretreatment are presented.

When analyzing the permeate flow, it is possible to observe that the experiments carried out with the centrifuged broth produced better results, even when they were compared to the model mixture. Those superior values can be attributed to the influence in the presence of fermentation subproducts and/or the presence of cells. In microfiltration, suspended particles may settle on the membrane surface, thus blocking feed channels and increasing friction losses (pressure drop) across the system. The result is a lower flux.

Table 1. Results of the efficiency of the separation of the ethanol and water mixture in pervaporation module with PDMS membrane

Parameter	Value
Mass Flow ($g.m^{-2}.h^{-1}$)	3.57
Selectivity (α)	8.31
Enrichment Factor (β)	7.56
PSI	29.71
Permeate Ethanol Mass Fraction % (wt/wt)	10.24

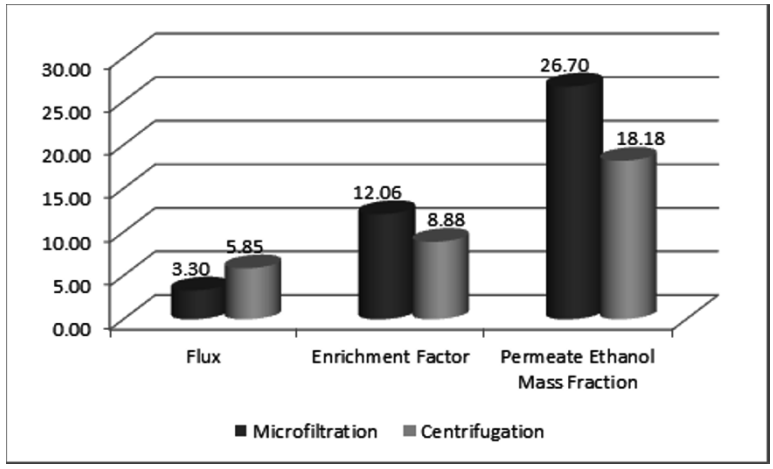

Figure 2. Comparison of the pervaporation results when the microfiltration and centrifugation processes were used as pretreatment.

On the other hand, it is possible to observe that better results for the enrichment and concentration factor of permeate were obtained when the microfiltration as pretreatments in the fermented broth cell separation was used. It was also possible to observe a 26.4% increase for the enrichment factor and 32% for the permeate ethanol mass concentration, which shows a higher potentiality in this treatment related to centrifugation. In fact, some authors [11] observed that the most used separation method for the cell segregation to be used as feed in the pervaporation process is the microfiltration, because centrifugation is widely used in liquid-solid separations at industries that produce ethanol and use distillation to recover this component.

4. Conclusions

The use of the microfiltration process coupled to the pervaporation in order to recover bioethanol from the fermentative broth produced from the lignocellulosic residues used in the banana cultivation showed itself as a very attractive alternative. The pretreatment of the fermentative broth through microfiltration presented a higher potentiality related to the centrifugation in the remaining solids separation step as well as for retaining some subproducts originated from the alcohol fermentation that influence on the pervaporation process.

References

[1] N. Sarkar; S.K. Ghosh; S. Bannerjee; K. Aikat, K., 2012Bioethanol production from agricultural wastes: An overview, Renewable Energy. *In press*.
[2] J. Swana; Y. Yang; M. Behnam; R. Thompson, 2011, An analysis of net energy production and feedstock availability for biobutanol and bioethanol, Bioresource Technology, 102, 2112-2119.
[3] M.A. Schulz, 2010, Bioethanol production from banana culture residues: Banana pulp and pell, Dissertation (Process Engineering) – UNIVILLE, Joinville, SC (In Portuguese).
[4] A.B.M.S. Hossain; S.A. Ahmed; M. A. Ahmed; M.A. Faris; M.S.M. Annua; M. Hadeel; H. Norah, 2011, Bioethanol fuel production from rotten banana as an environmental waste management and sustainable energy, African Journal of Microbiology Research, 5, 586-598.
[5] F. Lipnizki, 2010, Membrane process opportunities and challenges in the bioethanol industry, Desalination, 250, 1067-1069.
[6] R. Arumugam and M. Manikandan, 2011, Fermentation of Pretreated Hydrolyzates of Banana and Mango Fruit Wastes for Ethanol Production, Asian Journal of Experimental Biological Sciences, 2, 246-256.
[7] M. Nomura; 2002, Selective ethanol extraction from fermentation broth using a silicalite membrane, Separation and Purification Technology, 27, 59–66.
[8] M. Gryta, 2001, The fermentation process integrated with membrane distillation. Separation and Purification Technology, 24, 283–296.
[9] D.J. O'Brien; G.E. Senske; M.J. Kurantz; J.C. Craig Jr, 2004, Ethanol recovery from corn fiber hydrolysate fermentations by pervaporation, Bioresource Technology, 92, 15-19.
[10] M. Lewandowska and W. Kujawki, 2007 Ethanol production from lactose in a fermentation/pervaporation system, Journal of Food Engineering, 79, 430-437.
[11] L.M. Vane, 2005, A review of pervaporation for product recovery from biomass fermentation processes, Journal of Chemical Technology and Biotechnology, 80, 603–629.
[12] S. Chovau; S. Gaykawad; A.J.J. Straathof; B. Vand Der Bruggen, 2011, Influence of fermentation by-products on the purification of ethanol from water using pervaporation, Bioresource Technology, 102, 1669–1674.

I.A. Karimi and Rajagopalan Srinivasan (Editors), Proceedings of the 11th International Symposium on Process Systems Engineering, 15-19 July 2012, Singapore.

Virtual and Augmented Reality as Viable Tools to Train Industrial Operators

Davide Manca, Roberto Totaro, Salman Nazir, Sara Brambilla, Simone Colombo

Dipartimento di Chimica, Materiali e Ingegneria Chimica "Giulio Natta", Politecnico di Milano, Piazza Leonardo da Vinci 32, 20133 Milano, Italy

Abstract

The sensitivity and significance of operator training increased profoundly with the increase in automation of industrial plants. The paper proposes and discusses the use of Virtual Reality and Augmented Virtual Reality to train industrial operators. A detailed and immersive 3D model of the plant allows the operators understanding the details of equipment and operating conditions. Both the dynamic behavior and the control strategies of the process can be reproduced with a 3D immersive virtual environment by implementing and coupling a dynamic process simulator and a dynamic real-time accident simulator. The AVR feature enhances the VR by adding further information and analysis that result in better understanding of operators that work either in control room or in the field. The proposed training methodology allows achieving significant improvements in reliability, cost effectiveness, environmental friendliness, and process safety.

Keywords: Virtual Reality; Augmented Virtual Reality; Operator training; Dynamic process simulation; Accident simulation.

1. Introduction

The increase in complexity, technological improvement, automation, and environmental and safety constrains in the process industry, are tightly interconnected to the following demanding features:

- Retrofitting and revamping of chemical processes;
- Operators retiring and lack of viable tools to preserve their expertise, skill, experience, and knowledge without dispersing the know-how;
- Training of new operators that do not have any experience of the process since they come from different jobs and therefore are practically unaware of the specific plant features;
- Meeting quality, safety, and environmental requirements, which are difficult to achieve and preserve dynamically;
- Optimization of plant productivity, with respect to both law and process constraints.

Operator Training Simulators (OTSs) can play a major role in addressing these challenges and allowing companies to remain competitive and updated in terms of workforce. OTSs comprise both hardware devices and software tools that allow simulating the dynamic evolution of the plant and therefore allow training the operators before going on-line in the real plant. Conventional OTSs are mainly focused on replicating the control room environment by means of a mock-up of the Distributed Control System (DCS). Consequently, such OTSs (see also Figure 1) allow training

control-room operators (CROPs) whilst field operators (FOPs) are rather neglected and not looked after satisfactorily.

Figure 1: A conventional session of Operators Training.

According to the Authors, current OTSs can be expanded into three main directions:

1. Extend and improve the participation of FOPs. This allows increasing the knowledge of the field and allows facing unexpected process conditions in the shortest time while preserving the operators' safety.
2. Simulate accident events and their consequence and interaction with the plant equipment. This feature allows increasing the operator responsiveness and effectiveness (of both FOPs and CROPs) when facing real accidents.
3. Use OTSs for both business decisions and plant management to improve process performance and enhance overall safety.

These open issues are quite challenging not only in terms of single pieces of software but also in terms of effective tools to improve the skill and understanding degree of both FOPs and CROPs. Actually, one of the main objectives of modern OTSs is improving the situation awareness of operators and assessing quantitatively the training level (Endsley and Garland, 2000).

2. OTS extension to FOPs through virtual reality

The field operator section in conventional OTS is either absent or relegated to an approximated and simplified adaptation respect to the core module of the control room. Consequently, the training of FOPs, in most cases, is done on the job, *i.e.* in the real plant where the novice FOP is trained by a more experienced colleague. However, this procedure appears to be limiting, since the novice is trained to operate usually under normal operating conditions. Most of the transients (*e.g.*, startups, shutdowns, and grade changes), abnormal conditions, alarms, failures, and accidents are not easily replicable in a real plant. Actually, these scenarios are quite rare and it may happen that working in real conditions a field operator does not attend or take part to any of previous events for years.

The training of FOPs by means of a specifically designed and properly developed OTS represents a promising, and challenging solution to the aforementioned problems. However, such a feature requires the development of dedicated tools, whose function consists in building and improving the knowledge, concerning not only the process principles, but also the plant and equipment characteristics, as well as their position in the field and the interaction with the sub-assemblies, devices, valves, switches that complete the physical structure of the plant. As far as the FOP's training is concerned,

learning the plant structure means knowing not only the signs and symbols, but also the location of the equipment and devices, together with the operating procedures to run the plant under normal conditions as well as startups, shutdown, transients.
FOPs work in a complex reality where the main senses, especially sight and hearing, are called to capture every single operating detail. FOPs are able to decide and set the appropriate actions by projecting the expected results based on their choices.
In order to achieve this goal, it is recommended creating an environment based on a virtual plant, which is virtually identical to the real one. In this environment, the operator can be trained adequately without any risks for his/her safety and that of his/her colleagues. This allows avoiding any risks of economic losses and any impacts on buildings, population, and environment in case of errors done during the training session.
In order to build such a virtual environment, VE, the following features are recommended if not mandatory:

- Each process unit and device must be reproduced in the VE by using appropriate 3D editors to reconstruct its exact geometry and location. The required 3D data can be retrieved from either plant CAD drawings or laser scans of the real plant.
- A detailed photographic recognition on the plant is necessary, to achieve an accurate reconstruction of the details of the equipment in terms of external skin and usage degree. By accomplishing this step, the operator can recognize the plant as perfectly realistic. Through this measure, the gap between physical reality and the virtual one can be reduced and even dissolved.
- The operator should recognize the plant not only through the sense of sight but also of hearing. Therefore, it is advisable to implement a spatialized audio system that reproduces the surround sounds of the real plant. Using appropriate audio systems allows the operator identifying the proper source distance and the noise power.
- To increase the participation of the FOP to the VE it is possible to surround the FOP with the plant by exploiting the concept of stereoscopy, thereby, creating an immersive environment. Appropriate 3D glasses for stereoscopic vision allow the trainee to live the perception of being immersed in what s/he is observing. Using large screens allows increasing the immersivity and the sense of participation of the FOP to the training session.
- In order to increase the usability and the realism of the solution, some simple and intuitive interaction devices must be used to recognize the movements and actions done by the FOP within the chemical plant (*e.g.*, walking, looking around, climbing a vertical ladder, opening a valve, selecting and pressing a button). These devices (also known as natural interfaces) are connected to the 3D graphics engine, and present the advantage of not altering significantly the interaction between the FOP and the plant.

These recommended features of a VE represent a necessary but not sufficient condition for the training of industrial operators. Actually, the ultimate goal of a training tool is to transfer the operator a deep knowledge and understanding of the chemical process, not just to drive him/her inside an environment that is similar to the real one. To bring the OTS to a higher level of realism, the VR solution must be connected to a simulation tool capable of reproducing the dynamics of the plant. Both process and accident features should complement the simulation tool so to be able to reproduce either normal or abnormal/accident conditions. By coupling a dynamic accident simulator to a dynamic process simulator, it is possible to simulate the causes, evolution, and consequences of an accident on the equipment, the FOPs, and the environment (see also Figure 2).

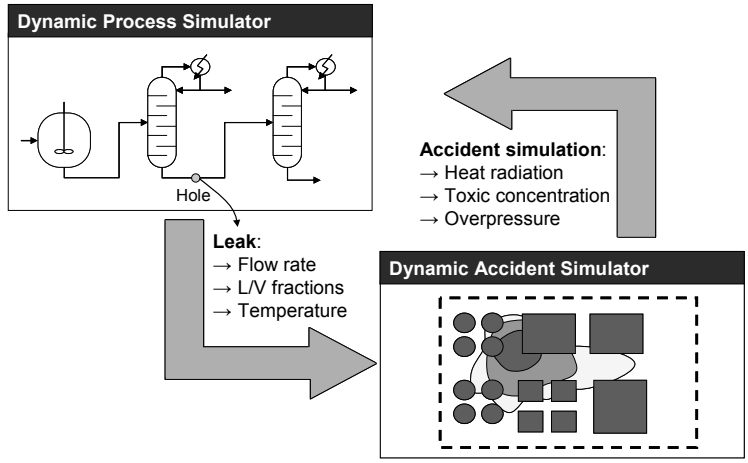

Figure 2: Two-way interaction between dynamic process and dynamic accident simulators.

3. Accident events simulation in OTS

To increase the situation awareness of operators respect to possible accident events, it is advisable to couple a dynamic process simulator to a real-time dynamic accident simulator (Brambilla and Manca, 2009). This two-way interaction was effectively implemented in an OTS for training of both CROPs and FOPs (Brambilla and Manca, 2011). The accident simulator can assess, as a function of the process variables evaluated by the process simulator, the event dynamics, which has some feedback effects on both the plant response and the FOPs' actions. The accident simulator can manage a wide range of accident scenarios, using literature models whose computation time is lower than the wall-clock time. The two-way dynamic interaction between the process and the accident simulators is carried out by considering the output variables of the process simulator (*e.g.*, flowrate) as input variables for the accident simulator, and *viceversa* (*e.g.*, the heat flux emitted by a pool fire that radiates to the surrounding equipment). In order to increase the situation awareness of FOPs about accidents, it is useful to provide the trainee(s) with some pieces of information that otherwise could not be easily visualized and understood. These details and variables fall under the realm of Augmented Virtual Reality (AVR).

4. Augmented Virtual Reality

In order to increase the operators' understanding of the process and also the effects and consequences of possible industrial accidents it can be of real help to show some additional bits of information during the training session. These bits of information are usually unavailable in real conditions but can augment the virtual reality scene by showing precious values that otherwise could not be quantified. This concept can be summarized by the AVR acronym that stands for Augmented Virtual Reality.

All the process and accident data evaluated by the corresponding dynamic simulators can be shown (according to the trainer decision) to the trainee so to increase the depth of understanding and supply statistics and records that otherwise would remain unknown. For instance, the AVR feature allows displaying the process variables that characterize the plant equipment (*e.g.*, temperatures, pressures, compositions, flowrates). The AVR feature allows also presenting the data related to the simulated accident (*e.g.*, pool diameter, jet length, cloud concentration, radiative flux, fire length, flame tilt, thermal

load, inhaled dose). These data can be shown by means of dynamically changing values, diagrams, schematics of the equipment (as shown in Figure 3). The combination of VR and AVR within the 3D VE is appealing and promising. For the sake of example, the proposed enhanced OTS (also named Plant Simulator, PS) can reproduce a process malfunction that may lead to a severe accident. Such accident event may imply the release of a liquid jet that forms a pool that spreads on the ground and that may either evaporate or be ignited with a subsequent pool fire. The PS allows displaying not only the physical features such as the liquid jet, the pool, and the fire (that are shown in the VR environment) but also the additional variables of AVR such as the radiative heat flux, the thermal load, and the consequences on the exposed FOP(s) in terms of time to reach the I, II, and III degree burns and eventually the death (Figure 3).

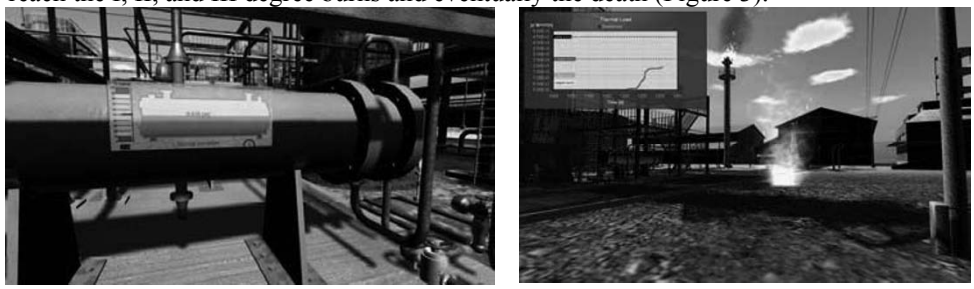

Figure 3: Two examples of AVR showing variables from the process simulator (left, reboiler level and corresponding alarms) and from the accident simulator (right, thermal load with I, II, and III degree burns).

While VR replaces the real plant, AVR is added to VR and represents a valid tool for training and increasing the conscience of operators which also refers to situation awareness. It is worth underlining that during assessment procedure, in order to make the training session consistent with what is available in the reality, the AVR tool is removed.

6. Conclusions

The challenging task of modern industrial OTSs was presented and discussed. Both VR and AVR were proposed as practical tools to improve the training level of operators and increase their situation awareness. The positive effects of an enhanced OTS and specifically of a PS consist in experimenting rather rare events such as startups, shutdowns, process transients, alarms, abnormal situations, and possible accidents. These features allow reducing the impact of human errors and human factors when running a plant by increasing the process understanding and conscience of both CROPs and FOPs.

References

Brambilla S., D. Manca, 2009, "Accidents Involving Liquids: a Step Ahead in Modeling Pool Spreading, Evaporation and Burning", Journal of Hazardous Materials, 161, 1265-1280.

Brambilla S., D. Manca, 2011, "Recommended features of an industrial accident simulator for the training of operators", Journal of Loss Prevention in the Process Industries, 24, 4, 344-355.

Coleman M.J., 1994, "Industry, school, government cooperate in model training for operators", Tappi Journal, 77, 3, 113-114.

Endsley M., D. Garland, (Eds.), 2000. Situation awareness analysis and measurement. Mahwah, NJ: LEA.

I.A. Karimi and Rajagopalan Srinivasan (Editors), Proceedings of the 11th International Symposium on Process Systems Engineering, 15-19 July 2012, Singapore.

Semantic similarity for case-based reasoning in the context of GMP

Yuske Tsujioka[a], Suriati Akmal[a], Yukihiko Takada[a], Hirofumi Kawai[b], and Rafael Batres[a]

[a]*Toyohashi Tech, Tempaku-cho, Toyohashi 441-8580, Japan*
[b]*Tokyo Institute of Technology, Nagatsuta-cho, Yokoyama 226-8503, Japan*

Abstract

The use of incident information in GMP-regulated manufacturing environments has been impeded by the lack of an effective approach to extract information. Case-based reasoning provides opportunities to extract incident information by considering an incident and its resolution as a case. Case-based reasoning relies on good similarity measures which have largely been proposed for numerical similarities. However, little has been reported for semantic similarities that can be used in case-based reasoning systems that represent part of its information using ontologies. This paper investigates semantic similarity measures based on the comparison of classes in a taxonomy by using attribute information obtained with formal concept analysis.

Keywords: semantic similarity, case-based reasoning, GMP, ontologies

1. Introduction

Good Manufacturing Practice (GMP) regulations apply to pharmaceutical, medical device, and food manufacturers to ensure that their products are processed reliably, repeatedly, consistently, safely and to a high quality. Current GMP regulations (CGMPs) require manufacturers to investigate near-misses, and other incidents that have an impact on the product quality and safety. GMP requires the result of an incident-investigation to be reported with data about the incident, including the materials and equipment involved in the incident (e.g. process lines, products, batches and raw materials), possible or actual consequences, possible causes, products made prior to and during the event and corrective or preventive actions. However, as incident reports are stored in text-form, it becomes difficult to extract information that can be used to avoid similar incidents while improving product quality and productivity.

One approach to extract information is to use case-based reasoning (CBR) in which problems are solved "by using or adapting solutions to old problems". In CBR, a case is both a representation of the problem and a solution to that problem. In this paper, a case is made up with information contained in an incident report. Incident reports are stored in a case base where incident information follows a predefined structure based on domain ontologies. When a new problem arises (for example when new incident occurs), the information that is available about this target incident is entered to retrieve similar cases from which the best matching case is selected.

Case-based reasoning uses similarity measures to identify cases which are more relevant to the problem to be solved. Approaches such as the Euclidian distance are used to evaluate the similarity of numerical attributes. Traditionally, syntax-based approaches such as the Levenshtein distance are used to calculate the similarity between

character strings. However, syntax-based similarity measures often fail to produce good matches when confronted with the meaning associated to the words they compare. For example, although pump and compressor are objects that are semantically close, a low degree of similarity is obtained.

Class hierarchies can be used in similarity measures that are based on semantics as a way to overcome the limitations of syntactic similarity measures. Thus, the similarity between two objects is based on the comparison between the classes to which the object belongs.

Unfortunately, lacking systematic approaches for their design, class hierarchies are often developed in an ad-hoc manner. Consequently, the resulting taxonomies lack the justification of the decisions that led to their creation.

To remediate this problem, we employ Formal Concept Analysis (FCA) during the taxonomy development. FCA is an analysis technique for knowledge processing based on applied lattice and order theory. FCA works by processing a collection of objects and their properties to identify hidden relationships.

2. Semantic similarity

Semantic similarity is the similarity between two classes of objects in a taxonomy (Lin, 1998). A class C_1 in the taxonomy is considered to be a subclass of C_2 if all the members of C_1 are also members of C_2. Therefore, the similarity between two classes is based on how closely they are related in the taxonomy. Wu and Palmer (1994) proposed the following similarity measure based on use of subclass links between classes:

$$\mathrm{sim}(C_1, C_2) = \frac{2N_3}{N_1 + N_2 + 2N_3} \tag{1}$$

where N_1 and N_2 are the number of subclass edges from C_1 and C_2 to their closest common superclass; N_3 is the number of subclass edges from the closest common superclass of C_1 and C_2 to the root class in the taxonomy. Note that the measure of Wu and Palmer fails when the closest common ancestor of both classes happens to be the root class.

3. Proposed approach

Based on the concept of ontology (Sowa, 2000), a class is considered to be equivalent to another class if both classes have exactly the same attributes. Similarly, for a given class *C*, all attributes of *C* are also attributes of any subclass of *C*. Therefore, similarity measures can be developed based on the number of common attributes that are shared between two classes.

However, for any taxonomy-based similarity, the correctness of a given similarity between two classes depends on the structural correctness of the taxonomy. This statement equally applies to ontologies, in which the taxonomy is a fundamental part. Here we propose the use of Formal Concept Analysis (FCA) as a way of designing the ontology as it is based on attribute information.

Equations (2)-(6) represent some attribute-based similarity measures. These equations were obtained by combining the equations given by van der Weken *et al.* (2004) but replacing fuzzy sets with attribute sets.

$$\mathrm{sim}_{Union}(C_1, C_2) = \frac{|A_1 \cap A_2|}{|A_1| + |A_2|} \tag{2}$$

$$\mathrm{sim}_{Max}(C_1, C_2) = w_1 \frac{|A_1 \cap A_2|}{|A_1| + |A_2|} + w_2 \frac{|A_1 \cap A_2|}{\max(|A_1|, |A_2|)} \quad (3)$$

$$\mathrm{sim}_{CMax}(C_1, C_2) = w_1 \frac{|A_1 \cap A_2|}{|A_1| + |A_2|} + w_2 \frac{|A_1' \cap A_2'|}{\max(|A_1'|, |A_2'|)} \quad (4)$$

$$\mathrm{sim}_{Min}(C_1, C_2) = w_1 \frac{|A_1 \cap A_2|}{|A_1| + |A_2|} + w_2 \frac{|A_1 \cap A_2|}{\min(|A_1|, |A_2|)} \quad (5)$$

$$\mathrm{sim}_{CMin}(C_1, C_2) = w_1 \frac{|A_1 \cap A_2|}{|A_1| + |A_2|} + w_2 \frac{|A_1' \cap A_2'|}{\min(|A_1'|, |A_2'|)} \quad (6)$$

where A_1 and A_2 are the sets of attributes of classes C_1 and C_2, $|A_1 \cap A_2|$ is the total number of attributes shared by C_1 and C_2, $|A_1|$ and $|A_2|$ represent the number of attributes of C_1 and C_2, A_1' and A_2' are the complements of sets A_1 and A_2 respectively. w_1, and w_2 are weights.

4. Case Study

The case study focuses on comparing the similarity measures presented in the previous section for equipment used in therapeutic protein processes.

4.1. Taxonomy construction

The equipment-class taxonomy was developed using FCA. The attributes in the context table were selected based on: (1) the behavioral characteristics of each device, (2) type of components in the device, (3) materials used or transformed by the device. ConExp (2009) was used to generate the concept lattice which is shown in Fig. 1. After analyzing and correcting the lattice, the resulting lattice and attribute information were converted to OWL format and then used in the similarity calculations. The nodes labeled with *A*, *B*, *C* and *D* represent classes obtained by the FCA analysis, which are identified by their attributes. For example, *B* represents a class of devices that contain semi-permeable membranes.

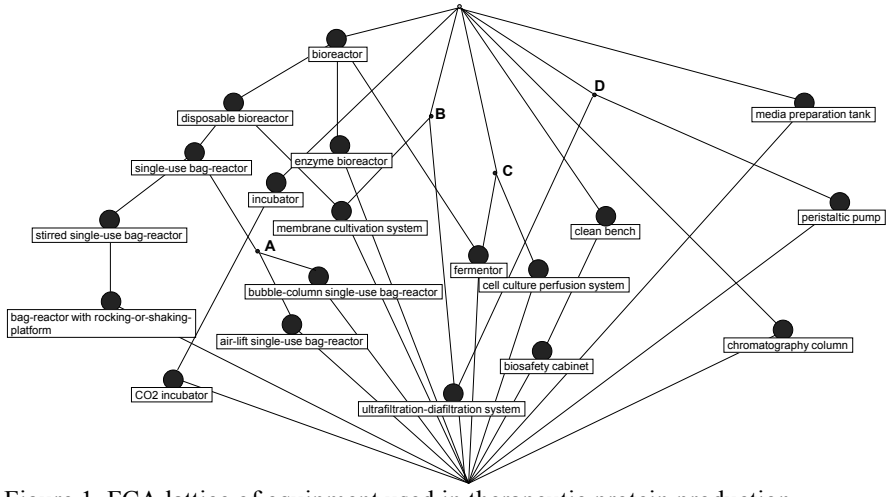

Figure 1. FCA lattice of equipment used in therapeutic protein production

4.2. Similarity calculation

A program was developed in Java to calculate similarities using the proposed approach. The program reads the OWL file and calculates the similarity between classes using equations (4) to (8). Calculations were carried out for several values of w_1, and w_2. Specifically, we focused on the similarity between *enzyme bioreactor* with the rest of the equipment classes.

Table 1. Semantic similarity measures and their correlation against human judgment

Object pair	Human judgment	Wu & Palmer	Eq. (2)	Eq. (3)	Eq. (4)	Eq. (5)	Eq. (6)
air lift single use bag reactor	0.67	0.44	0.50	0.40	0.93	0.67	0.97
Bioreactor	1.00	0.80	0.80	0.67	0.98	1.00	1.00
bioreactors with rocking or shaking platform	0.56	0.44	0.50	0.40	0.93	0.67	0.97
biosafety cabinet	0.28	0.33	0.18	0.13	0.83	0.33	0.94
bubble column single use bag reactor	0.61	0.44	0.57	0.50	0.95	0.67	0.98
cell culture perfusion system	0.72	0.33	0.25	0.20	0.90	0.33	0.95
chromatography column	0.17	0.40	0.33	0.33	0.95	0.33	0.95
clean bench	0.22	0.40	0.25	0.20	0.90	0.33	0.95
CO_2 incubator	0.44	0.29	0.18	0.13	0.83	0.33	0.94
disposable bioreactor	0.89	0.57	0.80	0.67	0.98	1.00	1.00
Fermentor	0.94	0.67	0.50	0.40	0.93	0.67	0.97
Incubator	0.39	0.33	0.22	0.17	0.88	0.33	0.95
media preparation tank	0.33	0.40	0.40	0.33	0.95	0.50	0.98
membrane cultivation system	0.50	0.57	0.50	0.40	0.93	0.67	0.97
peristaltic pump	0.06	0.33	0.22	0.17	0.88	0.33	0.95
single use bag reactor	0.83	0.33	0.80	0.67	0.98	1.00	1.00
stirred single use bag reactor	0.78	0.29	0.57	0.50	0.95	0.67	0.98
ultrafiltration diafiltration system	0.33	0.22	0.17	0.88	0.33	0.95	0.22
Correlation with human judgment	1.000	0.57	0.79	0.76	0.59	0.81	0.77

In the analysis of the results, we utilized the method proposed by Lin (1998) who compares semantic similarity measures by correlating their similarity scores with assessments made by human subjects. For this purpose, we relied on the evaluation that was carried out by a plant engineer who is knowledgeable about the use and characteristics of all the devices considered in this case study.

The results are shown in Table 1. The calculated similarities are also compared against the similarity of Wu and Palmer. Equation (5) yielded the highest correlation with a correlation coefficient of $r = 0.81$ ($w_1 = 0$, $w_2 = 1$). Using traditional statistics, it was found that the similarities against *cell culture perfusion system*, *CO_2 incubator*, *fermentor*, and *stirred single use bag reactor* performed poorly in all similarity measures, possibly due to missing attributes in the FCA analysis. This observation was also corroborated with hierarchical clustering which was carried out on both the results obtained with equation (5) and the reference data (Figure 2). The comparison of the results of the clustering analysis shows that the same four similarities are clustered differently. For example, with the propose similarity measure the similarity between *enzyme bioreactor* and *fermentor* is put closer with the similarity of the pair *enzyme bioreactor – air lift single use bag reactor* while the human expert perceives it as being closer to the similarity of the pair *enzyme bioreactor – disposable bioreactor*. After omitting these points a much higher correlation coefficient $r = 0.95$ ($w_1 = 0$, $w_2 = 1$) is obtained.

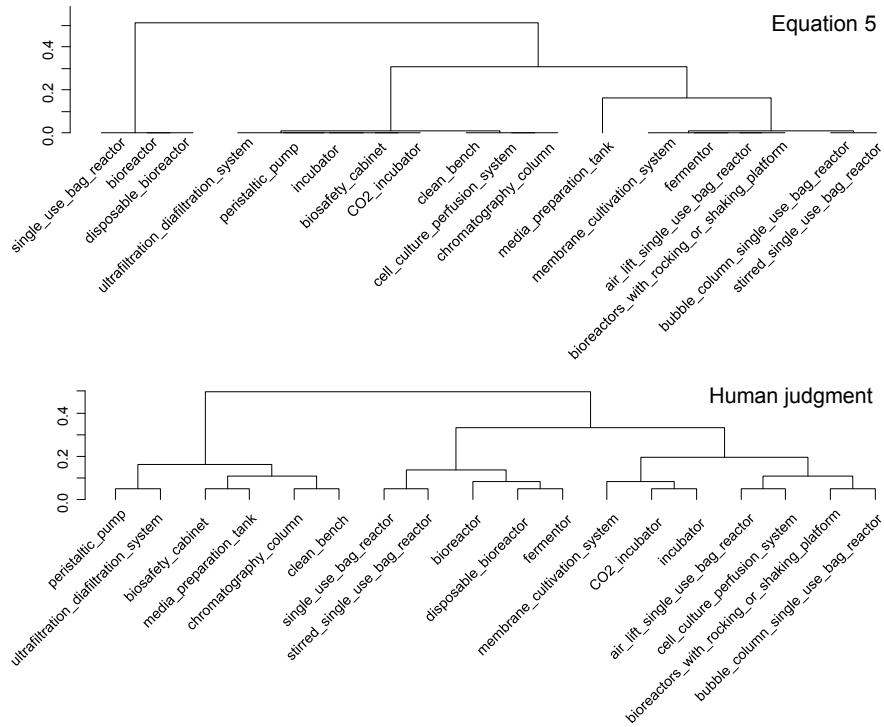

Figure 2. Comparison of the clustering of the two similarity results

5. Conclusions

This paper presented semantic similarity measures based on ontology to determine the degree of similarity of two classes. The results of the experiment show that the cardinality of the intersection between the sets of attributes of the two classes divided over the minimum cardinality performs better when compared against other semantic similarity measures. Furthermore, while Wu-Palmer's similarity is only defined for trees, our approach can be applied to taxonomies containing a class with multiple direct-superclasses (multiple-inheritance). This is because the proposed similarity measures are not only based on the taxonomy but also on the properties that characterize each class in the ontology.

References

D. Lin, (1998), An information-theoretic definition of similarity," in Proc. 15th International Conference on Machine Learning, Morgan-Kaufmann: Madison, WI, pp.296-304

J. F. Sowa, (2000), Knowledge Representation: Logical, Philosophical, and Computational Foundations, Brooks Cole Publishing Co.

D. Van der Weken, M. Nachtegael, and E. E. Kerre, (2004), Using similarity measures and homegeneity for the comparison of images, Image and Vision Computing , pp.695-702

Z. Wu and M. Palmer, (1994), Verbs semantic and lexical selection, in Procs. of the 32nd Annual Meeting of the Associations for Computational Linguistics, pp. 133-138, New mexico

S. Yevtushenko, (2009), Concept Explorer, Open source java software. (Release 1.3.) [Online]. Available: http://sourceforge.net/projects/conexp

I.A. Karimi and Rajagopalan Srinivasan (Editors), Proceedings of the 11th International Symposium on Process Systems Engineering, 15-19 July 2012, Singapore.

Computational Fluid Dynamics at work – Design and Optimization of Microfluidic Applications

Ulrich Krühne,[a] Vijaya K. Bodla,[a] Jacob Møllenbach,[b] Steen Laursen,[b] Naseem Theilgaard,[c] Leif H. Christensen,[d] Krist V. Gernaey[a]

[a] *Center for Process Engineering and Technology, Department of Chemical and Biochemical Engineering, Technical University of Denmark (DTU), DK-2800 Kgs. Lyngby, Denmark, corresponding author ulkr@kt.dtu.dk.*
[b]*Smart Biosystems ApS, Hvildkildevej 48, DK-2400 Copenhagen NW, Denmark*
[c]*Danish Technological Institute, Center of Plastics Technology, Gregersensvej 1, DK-2630 Høje Taastrup, Denmark*
[d]*Danish Technological Institute, Center of Microtechnology and Surface analysis, Gregersensvej 1, DK-2630 Høje Taastrup, Denmark*

Abstract

Computational Fluid Dynamics (CFD) is presented as a powerful tool to support design and optimization of microfluidic reactors. This is demonstrated by means of three case studies. First a three-dimensional scaffold for tissue engineering purposes is investigated using a combination of CFD and a simple biological model. The result is a suggestion of an improved geometry design. In the second case study a microfluidic cartridge of a novel automated in vitro fertilization device is presented, where the CFD model has supported the fluidic design of the microfluidic network in which the stem cells are grown. In the last case study a biocatalytic microfluidic reactor design is presented in which the material characteristics of substrates and products of the catalytic reaction can be investigated. As model system the transaminase catalyzed formation of methylbenzylamine (MBA) from acetophenone is investigated and it is demonstrated how the experimental investigation along with the CFD model can be used for the characterisation of the performance of the reactor system.

Keywords: computational fluid dynamics (CFD), microfluidics, biocatalytic reaction, in vitro fertilisation, optimisation

1. Introduction

Computer aided process engineering has many potential applications. One of the most eloquent ways of applying computational tools is to predict the performance of systems and to use the predictions for optimization of future designs. This can for instance be the configuration of single unit operations or complex process plant designs. Computational fluid dynamics (CFD) has throughout the last decades undergone a breathtaking development and is used increasingly in industrial applications. The prediction quality has indeed reached such a level of maturity that many scientific and industrial users increasingly apply the method for a broad range of applications. Often the companies are performing virtual investigations rather than experiments, or at least they are trying to reduce the number of experiments as much as possible. Typical application areas are for instance the automotive industry [1], the ship building industry [2 and 3] or turbine optimization [4]; where often the improvement of a fraction of a percent of the efficiency is guaranteeing a multimillion Euros return on investment.

A well suited field of application for CFD supported design or analysis is in the area of fluid dynamic conditions with low Reynolds numbers. Typical applications can be found where the flow channel geometries are in the range of micrometers, giving the field the name microfluidics. From a mathematical point of view the equation system is reduced to the Navier Stokes equation and hence no turbulent terms have to be implemented. Therefore the prediction quality of the CFD models is expected to supply excellent qualitative and quantitative results for such systems. In this article three different case studies of the use of CFD in designing microfluidic systems are presented.

2. Materials and Methods

2.1. Software and Modelling

In all presented cases the CFD simulations have been performed by using the ANSYS CFX software. For meshing of the geometry ICEM CFD has been used for the generation of structured hexahedral meshes. In the first case a simple biological model has been implemented with help of the CFX Command Language (CCL). This model is described in [5]. The model considers the growth of biomass with help of a Michaelis Menten kinetic and involves the growth of biomass based on the consumption of substrates and oxygen respiration. Furthermore an additional weight factor is considered in which the existence of a specific shear strain rate (SSR) will have a positive influence on the growth rate of the biomass.

2.2. Scaffold 3D Geometry Design and Optimization

The main hypothesis in this case study is that a biological model is known, which can describe the growth of autologous bone stem cells in an artificial support scaffold in which cells are cultivated in a perfusion type reactor. Besides the material transport of the substrates, the oxygen and the biomass it is assumed that a certain physiological stress level due to the laminar flow around the cells will be beneficial and is known. This assumption is made in order to consider the ongoing discussion in the medical community working in this field [6] and giving therewith the opportunity to design an optimal scaffold from a theoretical point of view.

With help of this model an automatic procedure is started in which a geometry is simulated and a cost function is calculated which is basically the squared sum of the deviation of the actual SSR from the optimal SSR. Then a change of the geometry is proposed and the new value of the cost function is calculated. If the new result is more optimal this geometry will be stored and will serve as the basis for proposing a new change to the geometry again. Otherwise the new solution will be discarded and the old version will still serve as the starting point for the search. This procedure is placed in a loop, programmed with help of a *Practical Extraction and Report Language* (PERL) routine and is automatically actuated over a specified number of runs (ca. 500). A similar evolutionary strategy has been used and is described in [7].

2.3. CFD as software sensor

In the second example a new microfluidic in vitro fertilisation chip [8] is investigated with help of a CFD model. In this chip a series of cultivation chambers are connected by means of a microfluidic channel. An automated flow is generated in this channel due to a hydrodynamic height difference between a medium reservoir and the outlet chamber, where a piston pump is removing the surplus cultivation medium with help of a capillary. A second medium reservoir can be actuated by opening and closing of an equilibration inlet. This system has been modelled by the introduction of an additional

component to the fluid which has a diffusion coefficient of $0.67 \cdot 10^{-9} m^2 s^{-1}$, corresponding to glucose in water.

2.4. The design of a microfluidic biocatalytic reactor

In this last example a biocatalytic reaction has been chosen for a microfluidic reactor system. As model system the transaminase catalyzed formation of methylbenzylamine (MBA) from acetophenone is investigated. This reaction is in detail described in [9] and is expected to be inhibited by the formed MBA or by material transport limitations of the substrate acetophenone. A reactor design in which the produced MBA can be removed simultaneously along with its formation will be desirable, and hence a simulation study of an interdigitated channel system was performed, where short diffusion distances will contribute to the fast product removal. In most cases the material characteristics such as diffusion velocities, solubilities or reaction rates are not documented. It is therefore desirable to have a mathematical tool to design experiments for verification of such key information. Similar to *2.3,* different reaction components have been modelled as additional components with different diffusion coefficients. The performance of a first experimental setup was investigated with the help of dyes, which are mixed with the different flows.

3. Results and Discussion

3.1. The optimal 3D scaffold geometry

As a starting point of the simulation it was expected that the resulting optimal geometry would be a tubular system with the corresponding diameter, which will induce the appropriate SSR at all points of the tubular wall system. In Figure 1a the starting geometry is presented with a gradient surface plot of the SSR. Figure 1b shows an intermediate result of the simulations, where it can be observed that the SSR has already considerably changed. In Figure 1c the final geometry is illustrated as a 3D surface and it can be seen that the optimal geometry is not a tubular system, as anticipated. It is rather a tube, which is squeezed in the middle and then again squeezed twice in the start and the end in a direction that is perpendicular to the first diameter reduction. In this way a larger surface is obtained along with the appropriate SSR at this increased surface area.

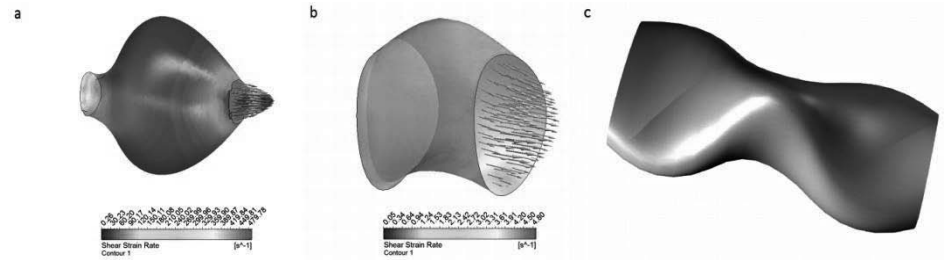

Figure 1.a. Starting geometry with SSR plot; b. intermediate result; and, c. the final 3D geometry in the optimized form.

3.2. CFD as software sensor

In this case study the IVF Chip [8] has been modelled and a transient simulation has been performed. In Figure 2a the qualitative concentration is shown in the middle plane of the flow channels and cultivation chambers. It can be seen that the upper part of the fluid domain is filled rather quickly, while the lower part, where the cells are located will not be filled as fast as the compartments above. A visual experiment with help of image analysis, shown in Figure 2b, cannot be used for the determination of the

concentration level at different depths of the system. In Figure 2c the streamlines of the flow through a cultivation compartment are presented and the worst case scenario for the placement of the embryo cell is indicated as a red cross. Finally the transient concentration profile of the averaged outlet concentration is presented in Figure 2d along with the concentration profile corresponding to the location indicated by the red cross on Figure 2c in the most downstream well. It can be seen that the transient build up of new medium at the bottom of the last well behaves much more sluggish than the outlet average concentration. But after approximately 12 minutes also the worst case placement of the cell has reached a concentration level corresponding to 95% of the desired concentration.

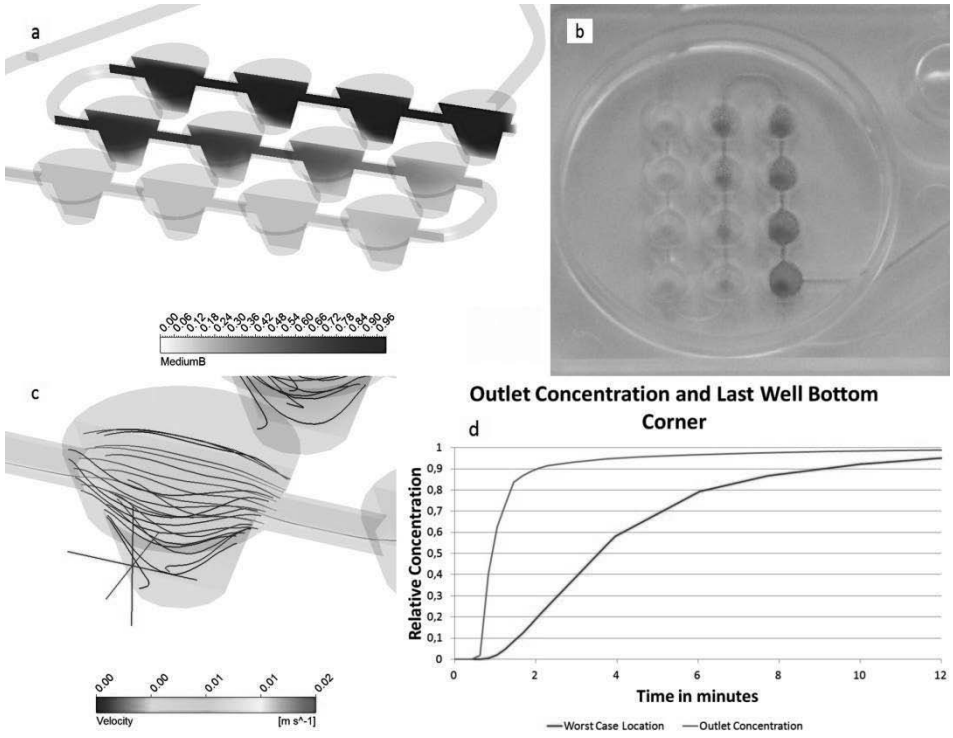

Figure 2.a. intermediate concentration profile; b. photograph of a medium change experiment with a blue dye; c. streamlines in the last cultivation chamber with the worst case placement of the cells (red cross); and, d. the transient dimensionless concentration at the outlet (averaged) and worst case placement (red cross)

3.2.1. Design of a biocatalytic reactor

In the presented simulation results in Figure 3.a the diffusion pattern of two substrate streams are shown which result from introducing alternating flows into a flow reactor (on the right hand side of figure 3a). It can be seen that the mixing due to fast diffusion coefficients ($2 \cdot 10^{-9} m^2 s^{-1}$) leads to a relatively equilibrated concentration profile already after a short distance. When performing the experimental investigation in an experimental setup with red and blue dyes with a much slower diffusion coefficient no mixing can be observed (Figure 3b). This information can be used consequently for a detailed investigation of the material properties which are predicted and observed, yielding new reactor designs, mathematical tools and simulation experiments for

optimisation of the biocatalytic reaction. Even though this result is only for demonstration purposes, the subsequent extraction of side streams at different positions of this reactor system combined with subsequent HPLC analysis will yield the exact concentration levels of the respective components. The latter will then result in a more detailed understanding of material characteristics, reaction kinetics or other information that is relevant for the specific biocatalytic reaction.

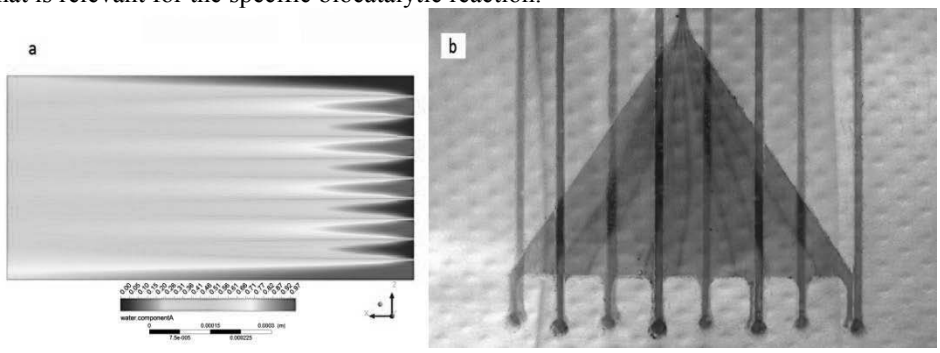

Figure 3.a. Simulation of the interdigitated fluidic array (fast diffusion coefficients for both media); b. Experimental setup with dyed liquid streams.

4. Conclusions

CFD has been demonstrated as a powerful tool for development of new theoretical qualitative insight or quantitative understanding of difficult measurable key components in microfluidic applications. Due to the lack of turbulent flow conditions in miniaturized systems the CFD results have a high predictive quality and can be obtained with relatively small effort.

Acknowledgements The work was partly financed by the Danish Research Council for Technology and Production and the 'AUTOBONE' Strep RTD project supported by the EC under the 6th Framework Programme under contract number 505711-1.

References

[1] R.Tilch et. al., 2008, Combination of body-fitted and embedded grids for external vehicle aerodynamics, Engineering Computations, 25 (1), 28-41.
[2] R. Leidenberger and K. Urban, 2011, Automatic differentiation for the optimization of a ship propulsion and steering system: a proof of concept, Journal of Global Optimization, 49 (3), 497-504.
[3] I.M. Viola, 2009, Downwind sail aerodynamics: A CFD investigation with high grid resolution, Ocean Engineering, 36 (12-13), 974-984.
[4] Y. Li et al., 2012, Dynamic overset CFD simulations of wind turbine aerodynamics, Renewable Energy 37 (1), 285-298.
[5] U. Krühne et. al., 2010, A transient 3D-CFD model incorporating biological processes for use in tissue engineering, Micro and Nanosystems, 2 (4), 249-260.
[6] C.V. Gemmiti and R. Guldberg, 2009, Shear stress magnitude and duration modulates matrix composition and tensile mechanical properties in engineered cartilaginous tissue, Biotechnology and Bioengineering, 104 (2), 809-820.
[7] D. Schäpper et. al., 2010, Topology optimized microbioreactors, Biotechnology and Bioengineering, 108 (4), 786-796.
[8] www.smartbiosystems.com
[9] P. Tufvesson et. al., 2011, Process considerations for the asymmetric synthesis of chiral amines using transaminases, Biotechnology and Bioengineering, 108 (7), 1479-1493.

I.A. Karimi and Rajagopalan Srinivasan (Editors), Proceedings of the 11th International Symposium on Process Systems Engineering, 15-19 July 2012, Singapore.

Modeling the Superovulation stage in IVF

Kirti M. Yenkie, [a,b] Urmila M. Diwekar, [a,b] Vibha Bhalerao [c]

[a]*Department of Bio Engineering, University of Illinois, Chicago, IL 60607 - USA*
[b]*Center for uncertain Systems: Tools for Optimization & Management (CUSTOM), Vishwamitra Research Institute, Clarendon Hills, IL 60514 – USA*
[c]*Jijamata Hospital, Nanded, Maharashtra, India*

Abstract

In-vitro fertilization (IVF) is the most common technique in assisted reproductive technology and in most cases the last resort for infertility treatment. It has four basic stages: superovulation, egg retrieval, insemination/fertilization and embryo transfer. Superovulation is a drug induced method to enable multiple ovulation per menstrual cycle. The success of IVF majorly depends upon successful superovulation, defined by the number and similar quality of eggs retrieved in a cycle. Hence, modeling of this stage in terms of distribution of eggs (oocytes) obtained per cycle involving the chemical interactions of drugs used and the conditions imposed on the patient during the process would provide a basis for predicting the possible outcome. This is the focus of current endeavor. The model will be made more robust by considering uncertainties; like the response of a patient depending upon previous medical history, suitability of medicine and type of protocol used. This model will then be used to decide optimal drug delivery so as to maximize good quality egg formation. Thus, a phenomenon currently based on trial and error will get a strong base. It will help the patient to decide whether to undergo superovulation or start the IVF from donor eggs, which in turn would save the patient from financial loss as well as emotional distress.

The aim of crystallization is to get maximum crystals of similar size and purity, while superovulation aims at eggs of similar quality which include the properties of size and number of chromosomes to enlist a few. The rate of crystallization and superovulation are both dependent on the process conditions and varies with time. Thus, model formulation for multiple ovulation will be on parallel lines to crystal formation in a batch process and will be modeled such.
Keywords: superovulation, batch crystallization, protocol, infertility treatment

1. Introduction

Around 80 million people in the world are suffering from infertility issues. The rate of fertility is constantly declining in the developed nations due to late marriages, postponed childbearing and primary infertility. On the contrary, in the developing world the reasons for infertility involve prevalence of sexually transmitted diseases, infections increasing the rate of secondary infertility. Childlessness is often stigmatized and leads to profound social suffering for women in the developing nations. In 1995, United Nations included rights of men and women to choose the number, timing and spacing of their children by calling reproductive health programs to include prevention and treatment of infertility (de Melo Martin, 1998).

In most countries cost is a major hurdle for access of infertility services. Most centers offering treatment for infertility operate outside of government financed health facilities. The treatment is only accessible to elites who can afford to pay for such high tech therapies. Even in a country like United States, the cost for an IVF cycle amounts

to 20% of the total annual income of a median American family. In developing nations, the cost of an IVF cycle is about 50% of the total annual income (Pennings, 2008).

2. In-vitro fertilization:

It is a process by which oocytes or egg cells are fertilized by a sperm outside the body in a laboratory simulating similar conditions in the body and then the fertilized eggs are implanted back in the uterus for full term completion of pregnancy.

2.1. Four stages in IVF:

1. Superovulation: It is method to retrieve multiple eggs using drug induced stimulation. In normal female body only one egg is ovulated per menstrual cycle, but with the use of fertility drugs and hormones, more number of eggs can be ovulated per cycle.
2. Egg collection (retrieval): On the maturation of the multiple eggs produced in the previous stage, the eggs are retrieved through special techniques like ultrasonically guided transvaginal oocyte retrieval.
3. In vitro fertilization (inseminaton/fertilization): This stage is accomplished in the IVF laboratory. Fertilization is done in the incubator using the retrieved oocytes and sperms. The conditions are maintained so as to mimic the invivo environment.
4. Embryo transfer: It takes place after several days of oocyte retrieval and after the fertilization stage is successful. The fertilized embryos are implanted into the uterus via a non-surgical technique using ultrasound guidance.

IVF treatment is an expensive treatment. There are a lot of complications associated with each stage and hence the success is highly unpredictable. The major cost of IVF is associated with the superovulation stage where expensive drugs are used and almost daily monitoring is required. Success of this stage in terms of number and quality of eggs affects the outcome of IVF and hence is a very important stage. In this work, we concentrated on modeling this stage and the approach is presented in the next section.

3. Superovulation:

In this work, we follow the analogy between batch crystallization and superovulation.

3.1. Analogy between Superovulation and Batch crystallization:

The moment model for follicle number and size is adapted from the concept of batch crystallization (Q. Hu. et. al., 2005) based on the analogy between batch crystallization and superovulation presented in Table 1.

Table 1: Analogy between batch crystallization and IVF superovulation stage

Batch Crystallization	Superovulation (IVF stage I)
Production of multiple crystals	Production of multiple oocytes or eggs
Crystal quality is determined in terms of size distribution and purity	Oocyte quality is determined in terms of no abnormalities, similar size.
The rate of crystallization or crystal growth varies with time and process conditions	The rate of ovulation or oocyte growth varies with time and drug interactions
Process is affected by external variables like agitation, and process operating variables like temperature, pressure, etc.	Process is affected by externally administered drugs and body conditions of the patient undergoing the process

The superovulation follicle growth model in general resembles greatly to the growth of seeded batch crystals. The aim of seeded batch crystallization is to allow the

seeds added to the solution to grow to desired shape and size and truncate the process of nucleation by maintaining certain process conditions. The numbers of seed added to the solution are constant and hence the zeroth moment of seeded batch crystals which corresponds to its number is constant. Similarly, when we look at superovulation, the number of follicles activated during an IVF cycle is constant. Thus, the moment model for both the processes remain the same the growth term which is a function of process variables like temperature and supersaturation in batch seeded crystallization will become a function of medicinal dosage in case of superovulation process.

4. Model details

Due to ovarian stimulation using externally injected hormones the number of follicles activated to enter into the ovulation stage are more in number as compared to a single follicle in a normal menstrual cycle. From the current data on successful superovulation for patient 1, organized in Table 2; it can be observed that during FSH dosage regime, as the time progresses the size of the eggs increase.

Table 2: Variation of Follicle size (diameter) with time and FSH dose

Sr. No	Size range (mm) ↓ / Days →	Day 1	Day 2	Day 5	Day 7	Day 9
1.	0-4	15	8	6	0	0
2.	4-8	3	6	4	2	0
3.	8-12	0	4	10	14	4
4.	12-16	0	0	0	2	11
5.	16-20	0	0	0	0	3
	FSH dose	0	300	300	300	225

4.1. Model Assumptions:

The rate expression for follicle growth is dependent on FSH administered. Thus, we can write the growth term as;

$$G=kC_{fsh}{}^{\alpha} \quad (1)$$

Assuming moment model, we consider the first six moments; zeroth moment corresponding to follicle number, the first moment corresponding to follicle size and the other 4 moments. Since, we have assumed follicle number to be a constant, hence the zeroth moment will have a constant value. Also, 1st to 5th moments are being used since they help in recovering the size distributions more precisely as against lower number of moments.

4.2. Model equations (Q. Hu. et. al., 2005):

$$\mu_0=\text{constant} \quad (2)$$

$$\frac{d\mu_1}{dt}=G(t)\mu_0(t) \quad (3)$$

$$\frac{d\mu_2}{dt}=2G(t)\mu_1(t) \quad (4)$$

$$\frac{d\mu_3}{dt}=3G(t)\mu_2(t) \quad (5)$$

$$\frac{d\mu_4}{dt}=4G(t)\mu_3(t) \quad (6)$$

$$\frac{d\mu_5}{dt} = 5G(t)\mu_4(t) \qquad (7)$$

Conversion of the data available on follicle number and size to moment using the expression given in literature by Flood, 2002:

$$\mu_i = \sum n_i(r,t) r_i^n \Delta r_i \qquad (8)$$

Here, $\mu_i = i^{th}$ moment

$n_i(r,t)$ = number of follicles in bin of mean radius 'r' at time 't'.

r_i = mean radius of i^{th} bin

Δr = range of radii variation in each bin

4.3. Moment evaluation:

Table 3: Experimental moments evaluated using equation 8

Sr. No	Time (day)	μ_0	μ_1	μ_2	μ_3	μ_4	μ_5	FSH	Cumulative FSH
1.	2	36	92	324	1340	5988	27932	300	300
2.	5	36	146	584	2728	13160	64456	300	1200
3.	7	36	180	932	4980	27428	155700	300	1800
4.	9	36	248	1764	12920	97188	749048	225	2025

5. Results:

We integrate the equations 2-7 for predicting the kinetic constants in the follicle growth expression. Later we use non-linear optimization algorithm to predict the values of these kinetic constants along with the integration constants obtained after integrating the set of moment equations. The moment values obtained from the model equations and the experimentally evaluated moments are compared and it is observed that the lower moments show some deviations, while the fit is much better for higher moments. In real practice, the model will be calibrated with the first two days of data and then used for prediction of the complete cycle.

5.1. Model Validation:

The current moment model predicts the moment values, however our final output desired is the follicle size distribution, thus in model validation the approach to obtain follicle size distribution from moment values are shown. For predicting the size distribution it is essential to have atleast 5 orders of moments to be known. The method is adapted from the literature by Flood 2002; where he shows the method to recover particle size distribution from moments in batch crystallization. Using the model predicted moment values we evaluate $n(r,t)$ and compare with the actual data to check the model accuracy. We plot the follicle size distribution for four patients for various days. The experimental size distribution is shown by symbols while the continuous curve shows the model predicted values after using the inversion method. It can be seen that the predicted values are close to experimental size distribution.

6. Conclusion

The moment model developed for IVF superovulation predicts the follicle size distribution which is in well agreement with the actual size distribution seen in the IVF cycle data. The model can be used to predict the outcome. This will reduce the almost daily requirement of testing. The model can also provide a basis for predicting the optimum dosage for the desired outcome from the superovulation stage. The model used

here is a very basic model and the complexities present in the patient are not considered. Later, we aim to include these complexities and model the system uncertainties, using more data for analysis, modeling and validation.

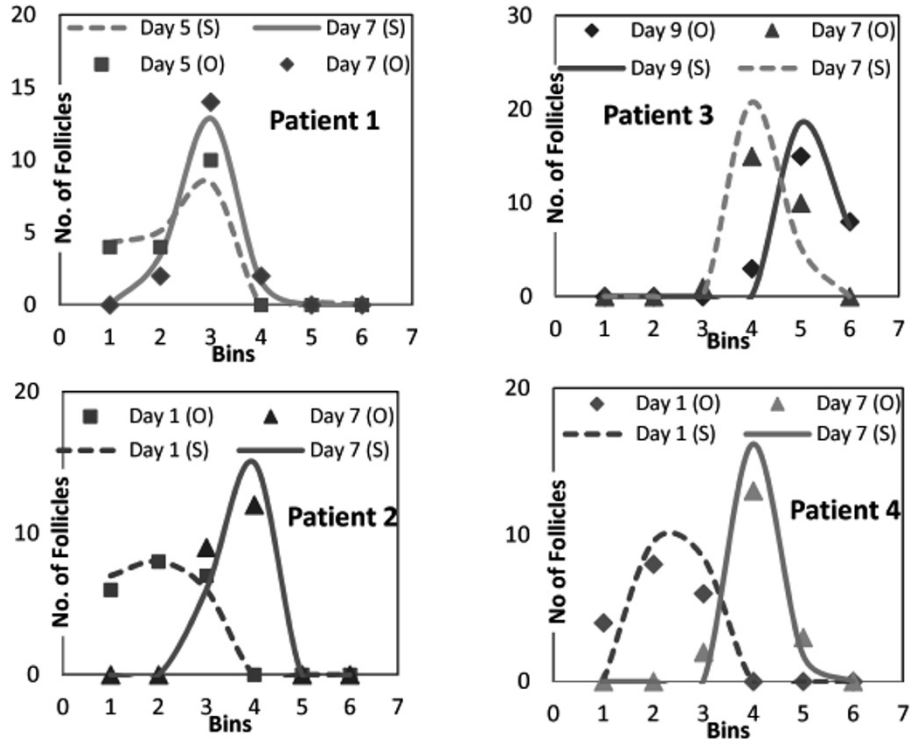

Fig 1. Follicle size distribution for four patients for various days

References

Nachtigall, R. D., 2006. "International disparities in access to infertility services", *Fertility and Sterility,* Vol. 85, No. 4, pp. 871-875.

Ombelet, W., Cooke, I., Dyer, S., Serour, G., and Devroey, P., 2008. "Infertility and the provision of infertility medical services in developing countries" *Human Reproduction Update,* Vol. 14, No. 6, pp. 605-621.

Pennings, G., 2008. "Ethical issues of infertility treatment in developing countries." *European Society of Human Reproduction and Embryology,* pp. 15-20.

Flood, A. E., 2002. "Thoughts on recovering particle size distributions from the moment form of the population balance." *Dev. Chem. Eng. Mineral Process,* Vol. 10, No. 5/6, pp. 501-519.

Commentary: The importance of fertility treatment in the developing world, 2005. *BJOG: an International Journal of Obstetrics and Gynaecology,* Vol. 112, pp. 1174 - 1176.

Baird, D. T., 1987. "A model for follicular selection and ovulation: Lessons from Superovulation." *J. steroid Biochem,* Vol. 27, No. 1-3, pp. 15-23.

Q. Hu, S. Rohani, A. Jutan, 2005. "Modelling and optimization of seeded batch crystallizers" *Computers and Chemical Engg.* Vol. 29, pp. 911-918.

de Melo-Martin, I., 1998. "Ethics and Uncertainty: In Vitro Fertilization and Risks to Women's Health" Risk: Health, Safety & Environment 201.

I.A. Karimi and Rajagopalan Srinivasan (Editors), Proceedings of the 11th International Symposium on Process Systems Engineering, 15-19 July 2012, Singapore.

Computational fluid dynamics simulation of the feed distribution system of a falling film distillation device

Joel G. Teleken,[a] Leandro O. Werle,[b] Iaçanã G. B. Parisotto,[b] Cintia Marangoni,[c] Ana P. Meneguelo,[d] Ariovaldo Bolzan,[b] Ricardo A. F. Machado[b]

[a]*Campus Palotina, Parana Federal University, Mail Box: 5153, Palotina-PR, Brazil, ZIP CODE 85950-000*
[b]*Department of Chemical Engineering, Santa Catarina Federal University, Mail Box: 476, Florianópolis-SC, Brazil, ZIP CODE 88040-970*
[c]*Process Engineering Master Program, University of the Joinville Region, University Campus, Bom Retiro, Joinville-SC, Brazil ZIP CODE 89219-905*
[d]*Federal University of Espírito Santo, Univ Center North of Espírito Santo, Department of Eng and Computing, km 60, BR101, São Mateus-ES, Brazil ZIP CODE 29932-540*

Abstract

This paper addresses the analysis of a distillation process by descending liquid film, more specifically the feed distribution system. This system offers simple construction, low resistance to liquid flow high capacity and. In this new equipment configuration the feed distribution system directly influences the efficiency of the separation. The objective of this study is to determine the best configuration of the feed distribution system through Computational Fluid Dynamics (CFD) simulations. The results obtained for this system indicate the formation of a thin liquid film on the walls of the distillation tube. The observed flow pattern oscillates between intermittent and gush, with a predominance of intermittent. Results were also obtained for the same geometry but with rotational movement.

Keywords: falling film, CFD, feed distribution system.

1. Introduction

Distillation by falling liquid film is a process with a low residence time and simple structure when compared to conventional distillation. It basically consists of a vertical unit, through which the liquid flows downwards, creating a film. Also, when the construction details are optimized, it is possible to obtain high heat and mass transfer rates [1]. However, this is an inherently non-equilibrium process, where the effect of the vapor generated by the liquid has almost no influence on the separation factor and rate. Due to the non-existence of convection by ebullition, the distillated flow is extremely limited, requiring frequent renovation. However, the process presents a simple construction, low resistance to the liquid discharge and high separation ability. As a consequence of the construction and phenomenological characteristics of this process, its effectiveness is intrinsically related to the feeding system.

In recent years, there has been considerable academic and industrial interest in the use of computational fluid dynamics (CFD) to model two phase flows in some chemical engineering processes. The volume-of-fluid (VOF) technique can be used for an initial determination of multiphase flows on structured packing. Szulczewska et al. [2] simulated the gas-liquid counter-current flow on plate-type structured packing. Gu et al.

[3] developed a two-phase flow CFD model using the VOF method to predict the hydrodynamics of falling film flow in structured packing. Ataki et al. [4] simulated the liquid flow structure in a structured packing element and liquid redistribution at the node of structured packing with the VOF model.
The hydrodynamics of the liquid-vapor contact has an essential function in the falling liquid film distillation design, since it determines the column fluid dynamics limits and controls the mass transfer rates. Computational fluid dynamics (CFD) has been used successfully to model the multiphase discharge in many chemical engineering systems [5-7]. It has become a powerful tool for the design and analysis of chemical processes. Due to the characteristics of the falling film distillation process, it is necessary to use feeding devices that allow a uniform distribution and adequate formation of a liquid film on the entire wall area of the unit. The simulations carried out allowed the evaluation of two different systems, one static and another with rotational movement using two rotation frequencies. The aim of this study is to evaluate the influence of the feeding system (rotational or static cone) on the film formation. The CFD technique was used as an auxiliary design tool due to its notable ability to represent systems. It is important to note that in this study only the flow of the water/air system will be analyzed. However, this is sufficient to characterize the flow as a whole, where the liquid mixture is represented by water vapor and the gas mixture is represented by air. Thus, an analysis of the fluid dynamics of the gas/liquid flow was carried out. The mass and heat transfer will the subject of a future study.

2. Methodology

This section is divided into three subsections. The first contains a brief description of the pilot distillation unit; the second describes the mathematical model used in these simulations; and the third presents the boundary conditions.

2.1. Geometric Characteristics of the System

The geometry for the feeding distribution system was proposed based on a study by Batistella [1]. Figure 1 shows the experimental apparatus which consists of a vertical tube and a mesh. Figure 1 (a) shows the liquid inlet at the top of the distillation tube and the design initially used to run the experimental tests with the rotational and static cones. The distribution system consists of a hollow steel cone which promotes a liquid film near the glass tube wall. Gas flows up through the inner part from the base.

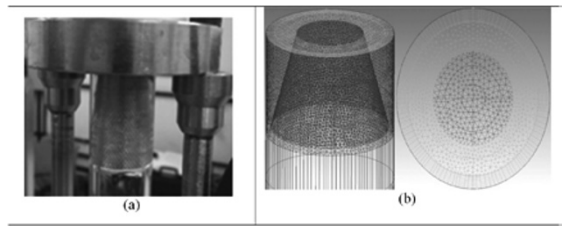

Figure 1. (a) Distribution and feeding part and (b) Hybrid mesh.

Figure 1(b) shows a hybrid mesh (with tetrahedral and prismatic volumes) built to represent the equipment and power distribution system used to perform the simulations. It should be noted that this mesh configuration gave the best numerical results with respect to convergence and time required to perform the simulations. It was built with a refined hybrid mesh comprising the prismatic walls of the distillation tube since this is the region of greatest interest in the study, *i.e.*, the area where formation of the film occurs.

2.2. Mathematical Model

The model considers the flows of gas and liquid in a Eulerian-Eulerian framework, where the phases are treated with transport equations. The equations used to solve this problem were the mass continuity and momentum equations. In order to solve these the equation of momentum flow was also required [7]. It was considered that the fluctuation (turbulence) consists of the formation and dispersion of small swarms of bubbles, and that the Reynolds stresses can be linearly related to the mean velocity gradients (eddy viscosity hypothesis), as in the case of the relation between the stress and strain tensors in laminar Newtonian flow. The shear stress transport (SST) turbulence model for multiphase flow was assumed [6].

2.3. Boundary Conditions

Dirichlet boundary conditions were used in these simulations, as follows:

1) Liquid inlet: Inlet conditions, with normal flow to the surface. A uniform liquid inlet velocity profile is recommended. Only liquid enters through the liquid inlet area, so the liquid volume fraction is taken as unity;

2) Liquid outlet: outlet condition, with normal flow to the surface. The liquid outlet boundaries were specified as pressure boundaries with volume fraction specifications. The specifications assumed that only liquid or gas leaves the simulation geometry;

3) Opening of the upper part of the cone: open condition, that is, it allows the air and/or liquid to enter and exit at the top of the cone. Entry/exit is determined by the pressure equalization;

4) Wall: All walls for the two phases are specified as no-slip wall boundaries;

5) The values of the variables of interest, such as liquid volumetric fraction, and air and water superficial velocities, were investigated at three different heights of the distillation unit and horizontal lines were drawn for this purpose. Considering the lower base of the feeding cone as zero (0) the lines were drawn at 10, 65 and 165 mm from the cone bottom. The studies were focused on the analysis of the water volumetric fraction, liquid film uniformity and thickness and formation of dry points throughout the distillation unit. The simulation conditions analyzed in this paper are listed in Table 1.

Table 1. Simulation Conditions

	Mixture water/air		
Mass Flow	50 ($kg.h^{-1}$)	50 ($kg.h^{-1}$)	50 ($kg.h^{-1}$)
Rotational Speed	-	750 rpm	1000 rpm
Wall Temperature	25ºC	25ºC	25ºC

The code used to model the computational fluid dynamics was CFX 12.0. The finite volume numeric method was used for the discretization of the equations, with a high-order interpolation scheme (high resolution) in order to avoid problems of oscillation and numerical diffusion. The pressure-velocity coupling was obtained using the phase-coupled SIMPLE algorithm. The total number of unstructured cells within the computational space was 1135238 and these are shown in Figure 1(b). Air and water were used as the gas and liquid phases, respectively, at ambient pressure. The time step was 0.01 s and the convergence criterion adopted was an average error of 10^{-5}.

3. Results and Discussions

In this section the main results obtained in the simulations carried out using the CFX 12.0 software will be reported. In Figure 2 the development of the liquid volumetric fraction profiles across the entire radius for the three height levels is shown.

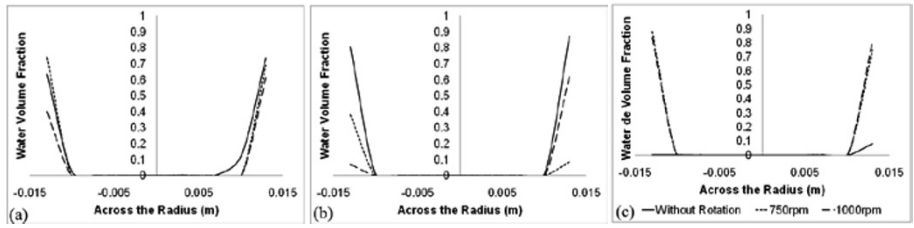

Figure 2. Liquid volumetric fraction profiles (a) 10 mm (b) 65 mm and (c) 156 mm below the feeding cone for a 50 (kg.h^{-1}) mass flow with tetrahedral mesh, cone with 750 and 1000 rpm rotation.

As can be observed in Figure 2, there were no significant differences between the liquid volumetric fractions, that is, the profiles followed a pattern formation related to the liquid volumetric fraction on the walls. On further analyzing Figure 2 it can be observed that the thickness of the film formed varies as the discharge takes place.
Figure 3 shows the Reynolds values found for each of the simulations with the power supply off and rotating at 750 and 1000 rpm.

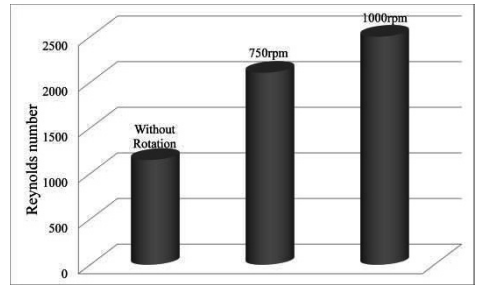

Figure 3. Average Reynolds number for each of the simulations.

It can be observed in Figure 3 that the Reynolds number increases on moving from a stationary power system to a rotation of up to 1000 rpm. This occurs because the liquid undergoes a centripetal acceleration due to the rotation of the cone and the flow has a greater velocity when in contact with the walls of the distillation tube. Figure 4 shows the volume fraction of the liquid on the distillation tube wall, over its entire length for the three simulated cases. Observing the volume fraction of the liquid on the walls of the tube distillation shown in Figure 4 (a, b and c), there is the formation of some preferential paths and also some dry spots as previously observed in experimental studies.

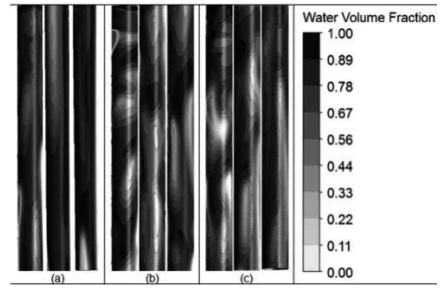

Figure 4. Profile of the volume fraction of liquid on the walls of the distillation tube for a feed flow rate of 50 (kg.h^{-1}), (a) cone without rotation, (b) cone rotating at 750 rpm and (c) cone rotating at 1000 rpm.

The formation of dry spots is not desirable from the standpoint of the distillation process by descending liquid film, because in places where there is no evaporating liquid film in contact with the steam that rises inside the tube the processes of heat and mass transfer will not occur. From the liquid volumetric fraction on the distillation unit walls in Figure 4 a slight difference can be perceived between the distributions in different parts of the unit. However, it is not possible to state that the rotational system provided a significant gain or improvement in the film formation on the distillation unit walls, and thus its use cannot be recommended.

4. Conclusions

In a rotational system the film formation is more uniform throughout the distillation unit compared with a static system. However, the formation of dry spots occurs in a similar way in both the static and rotational systems. Thus, we can conclude that this system has an impact on the film renovation. This difference becomes more evident in the case of viscous fluids. For a system with the characteristics of an air/water mixture the feeding carried out through the static device was found to be more appropriate. Studies are being carried out in order to evaluate the use of this feeding distribution system for a highly viscous mixture. The processes of heat and mass transfer through distillation using a falling liquid film are also currently being analyzed. With respect to the flow regime, two regimes were observed in full flow with a transition in the range of turbulent flow which, according to the literature, is good for the process as mass transfer can occur in a laminar flow because the film is stagnant. Regarding the maintenance of the film, it is not possible to state that the use of a rotational system substantially improved the quality of the film.

5. Acknowledgements

The authors are grateful for the financial support of the CNPq (Brazil).

6. References

[1] C.B. Batistella, (1999), Tecnologia da destilação molecular: da modelagem matemática à obtenção de dados experimentais aplicada a produtos de química fina. 216 f. (Tese de Doutorado) – Faculdade de Engenharia Química, Universidade Estadual de Campinas.
[2] B. Szulczewska, I. Zbicinski, A. Gorak, (2003), Liquid flow on structured packing: CFD simulation and experimental study, Chem. Eng. Technol., 26, 580–584.
[3] F. Gu, C. J. Liu, X. G. Yuan, G.C. Yu, (2004), CFD simulation of liquid film flow on inclined plates, Chem. Eng. Technol., 27, 1099–1104.
[4] A. Ataki, H. J. Bart, (2006), Experimental and CFD simulation study for the wetting of a structured packing element with liquids, Chem. Eng. Technol., 29, 336–347.
[5] D. Noriler, H. F. Meier, A. A. C. Barros, M. R. Wolf Maciel, (2008), Thermal fluid dynamics analysis of gas–liquid flow on a distillation sieve tray, Chem. Eng. Journal, 136, 133-143.
[6] M. R. K. Nikou, M. R. Ehsani, (2008), Turbulence models application on CFD simulation of hydrodynamics, heat and mass transfer in a structured packing, International Communications in Heat and Mass Transfer, 35, 1211-1219.
[7] X.G. Li, D. X. Liu, S. M. Xu, H. Li, (2009), CFD simulation of hydrodynamics of valve tray. Chemical Engineering and Processing: Process Intensification, 48, 145-151.

Author Index